Nonequilibrium Superconductivity: Part I

Yury Holubeu *

December 4, 2025

This draft is not aimed for distribution.

Contents

Preface 11

I Nonequilibrium Superconductivity in a Nutshell 12
0.1 Main Formulas and Ideas (?) . . . 12
0.1.1 Quantum quench phase diagrams of an s-wave BCS-BEC condensate by Yuzbashyan, Dzero, Gurarie, Foster . . . 12
0.1.2 Dynamical vanishing of the order parameter in a fermionic condensate by Yuzbashyan, Dzero . . . 12
0.1.3 Onset of superconductivity in a voltage-biased NSN microbridge by Serbyn, Skvortsov . . . 12
0.1.4 Relaxation and persistent oscillations of the order parameter in the non-stationary BCS theory by A. Yuzbashyan, Tsyplyatyev, Altshuler . . . 12
0.1.5 Solitons and Rabi Oscillations in a Time-Dependent BCS Pairing Problem by Barankov, Levitov, Spivak . . . 12
0.1.6 Synchronization in the BCS Pairing Dynamics as a Critical Phenomenon by Barankov, Levitov . . . 12

II My Theory of Nonequilibrium Superconductivity 13

III Examples and Solved Problems 14

1 Problems about Creation of a Model of Non-equilibrium Phenomena 14

2 Problems about Transformation in Derivations 14

3 Problems about Non-equilibrium Phenomena 14

4 Questions about Non-equilibrium Phenomena for Different Cases in Life 14
4.0.1 Questions to Check Knowledge . . . 14

IV Well-known and Important Theories 15

5 Quantum quench phase diagrams of an s-wave BCS-BEC condensate 15
5.1 Introduction . . . 15
5.1.1 Models and approximations . . . 18
5.1.2 Ground state . . . 21
5.1.3 Quench setup and initial conditions . . . 24
5.1.4 Main results . . . 25
5.2 Method . . . 37
5.2.1 Integrability and Lax vector construction . . . 37
5.2.2 Reduced solutions . . . 39
5.2.3 Matching integrals of motion . . . 43
5.2.4 Asymptotic solution for the quench dynamics . . . 43

*https://yuriholubeu.github.io/, yuri.holubev@gmail.com

5.3 Quench phase diagram and asymptotic spin distribution for the 2-channel model . . . 54
5.3.1 2d . . . 60
5.3.2 3d . . . 65
5.4 One channel model . . . 69
5.4.1 Quench phase diagram . . . 70
5.5 Transient Dynamics: Linear analysis . . . 72
5.5.1 Asymptotic $\Delta(t)$ and spins . . . 72
5.5.2 Normal modes and finite size dynamics . . . 73
5.5.3 Continuum limit . . . 78
5.5.4 Validity of the few spin conjecture . . . 80
5.5.5 Weak coupling limit . . . 80
5.5.6 Long time behavior of $\Delta(t)$: BCS side . . . 81
5.5.7 Long time behavior of $\Delta(t)$: BEC side . . . 82
5.5.8 Long time behavior of spins . . . 83
5.5.9 Short time behavior . . . 84
5.6 Approach to the asymptote in the nonlinear case . . . 85
5.6.1 Regime II . . . 86
5.6.2 Regime II' . . . 86
5.6.3 Gapless regime . . . 87
5.7 Experimental signatures . . . 88
5.8 Conclusion . . . 90
5.9 Pair-breaking rates . . . 92
5.9.1 Steady state molecular production . . . 93
5.9.2 Two-particle collisions . . . 95
5.10 Finite size corrections to the roots . . . 95
5.11 Identities . . . 97

6 Dynamical vanishing of the order parameter 98

7 Onset of superconductivity in a voltage-biased NSN microbridge 104

8 Relaxation, oscillations of order parameter in non-stationary BCS 112

9 Solitons, Rabi Oscillations in a Time-Dependent BCS 121
9.1 Theory . . . 121
9.2 My Notes about the article "Solitons, Rabi Oscillations in a TD BCS" . . . 131

10 Synchronization in the BCS Pairing Dynamics as a Critical Phenomenon 131
10.1 Theory . . . 131
10.2 My Questions about Synchronization in the BCS Pairing Dynamics . . . 137

11 Nonequilibrium dynamics of weakly and strongly paired SC by Gurarie 137

12 Theory of Anderson pseudospins with Higgs mode in SC by Tsuji, Aoki 143
12.1 Introduction . . . 144
12.2 Phenomenological time-dependent Ginzburg-Landau theory . . . 145
12.3 Microscopic theory for Anderson pseudospin resonance . . . 148
12.4 Response function for Anderson pseudospin resonance . . . 152
12.5 Effect of electron-electron scattering . . . 155
12.6 Summary . . . 157

13 Higgs Mode in Superconductors by Shimano, Tsuji **163**
13.1 Introduction and a Brief Historical Overview . . . 163
13.2 Nonlinear Light-Higgs Coupling . . . 165
13.2.1 A phenomenological view . . . 165
13.2.2 A microscopic view . . . 168
13.2.3 Impurity and phonon assisting . . . 170
13.2.4 Further developments . . . 171
13.3 Experiments . . . 171
13.3.1 Higgs mode in a superconductor with CDW . . . 171
13.3.2 Higgs mode in a pure s-wave superconductor . . . 173
13.3.3 Higgs mode in high-T_c cuprates . . . 177
13.3.4 Higgs mode in the presence of supercurrents . . . 179
13.4 Future Perspective . . . 180

V Old, Fundamental Theories **182**

14 Experiments on charge imbalance in superconductors by Clarke **182**
14.1 1. Introduction . . . 182
14.2 2. Theory of charge imbalance . . . 183
14.2.1 2.1. Quasiparticle charge and charge imbalance . . . 183
14.2.2 2.2. Tunneling generation and detection of charge imbalance . . . 185
14.2.3 2.3. Charge imbalance relaxation via electron-phonon scattering . . . 187
14.3 3. Experiments on tin . . . 189
14.4 4. Experiments on aluminum . . . 191
14.4.1 4.1. Charge relaxation via elastic scattering from non-magnetic impurities . . . 191
14.4.2 4.2. Inelastic scattering in aluminum . . . 194
14.5 5. Charge relaxation in the presence of magnetic impurities or a supercurrent . . . 195
14.5.1 5.1. Elastic scattering from magnetic impurities . . . 195
14.5.2 5.2. Elastic scattering in the presence of a supercurrent . . . 198
14.6 6. Resistance of the normal metal-superconductor interface . . . 200
14.7 7. Phase-slip centers . . . 206
14.8 8. Charge imbalance induced by a temperature gradient . . . 209
14.8.1 8.1. Thermoelectric generation of charge imbalance at a NS interface . . . 209
14.8.2 8.2. Spatial dependence of charge imbalance induced by a temperature gradient near a superconducting boundary . . . 211
14.8.3 8.3. Supercurrent-induced charge imbalance in the presence of a temperature gradient . . . 212
14.9 9. Dynamical charge imbalance . . . 214
14.1010. Concluding summary . . . 216

15 Nonequilibrium Phenomena in Superconducting Weak Links by Aslamazov, Volkov **229**
15.1 1. Introduction . . . 229
15.1.1 1.1. Josephson effect in systems with direct Ohmic contact . . . 229
15.1.2 1.2. Methods for studying nonequilibrium phenomena in weak links . . . 232
15.2 2. Stimulation of superconductivity in bridges of length $2L > \eta(T)$ . . . 233
15.2.1 2.1. General expressions for the order parameter and electron distribution function in contacts . . . 234
15.2.2 2.2. Stimulation of the critical current of the bridge for low-power microwave radiation . . . 235
15.2.3 2.3. Superconductivity stimulation at high irradiation powers . . . 240
15.2.4 2.4. Superconductivity stimulation in bridges by direct current . . . 242
15.3 3. Short bridges, $2L < \eta(T)$ . . . 246

15.3.1 3.1. Small voltages, $V \ll \Delta_0$; temperatures close to T_c . . . 247
15.3.2 3.2. The form of the distribution functions . . . 251
15.3.3 3.3. High voltages, $V > \Delta_0$; arbitrary temperatures . . . 252
15.3.4 3.4. Bridges with low impurity content (pure case) . . . 253
15.4 4. Discussion . . . 255
15.5 Appendix 1 . . . 256
15.6 Appendix 2 . . . 258
15.7 A2.1. Retarded (advanced) Green functions . . . 258
15.8 A2.2. The Green function $\hat{G}_1$. Distribution functions . . . 260

16 Time-Dependent Superconductivity in SNS Bridges: An Example of TDGL Theory by De Lozanne, Beasley 262
16.1 1. Introduction . . . 262
16.2 2. SNS Microbridges . . . 263
16.2.1 2.1. Bridge structure . . . 263
16.2.2 2.2. Model . . . 263
16.3 3. TDGL theory and results . . . 264
16.3.1 3.1. The TDGL equations , . . . 264
16.3.2 3.2. Applicability of the TDGL equations to planar SNS bridges . . . 268
16.3.3 3.3. Results of TDGL . . . 268
16.4 4. Comparison with experiments . . . 271
16.5 5. Conclusions . . . 273

17 Pair Breaking in Nonequilibrium Superconductors by Beyer, Pethick, Rammer, Smith 273
17.1 1. Introduction . . . 273
17.2 2. Densities and currents . . . 274
17.2.1 2.1. The quasiparticle method . . . 274
17.2.2 2.2. The Green function method . . . 276
17.3 3. Pair-breaking effects . . . 280
17.3.1 3.1. Scattering by magnetic impurities and phonons . . . 281
17.4 4. Impurity scattering in the presence of a supercurrent. Effects of a temperature gradient 288
17.4.1 4.1. Dirty limit . . . 290
17.4.2 4.2. Intermediate case . . . 291
17.4.3 4.3. Clean limit . . . 293
17.5 5. Conclusion . . . 294

18 Experimental Study of Enhanced Superconductivity by Dmitriev, Gubankov and Nad 299
18.1 1. Introduction . . . 299
18.2 2. Discovery of microwave-enhanced superconductivity . . . 300
18.3 3. Microwave-enhanced superconductivity in uniform superconductors . . . 303
18.4 4. Superconductivity enhancement by phonons and tunnel effect . . . 312
18.5 5. Superconductivity enhancement and nonequilibrium phenomena in weakly coupled superconductors . . . 314
18.6 6. The excess current effect . . . 319
18.7 7. Conclusion . . . 322

19 Theory of Superconductivity Stimulation by Eliashberg, Ivlev 333
19.1 J. Introduction . . . 333
19.2 2. Derivation of equations . . . 334
19.3 3. Superconductivity stimulation by electromagnetic field . . . 339
19.4 4. Superconductivity stimulation by acoustic waves . . . 352
19.5 5. Superconductivity stimulation by tunnel injection . . . 354

19.6 6. Investigation of stability of nonequilibrium states created by microwave radiation $\omega < 24$ near T_c. 360

20 Dynamical Effects in Nonequilibrium Superconductors: Some Experimental Perspectives by Kadin, Goldman 362
20.1 1. Introduction 362
20.2 2. Basic theory of nonequilibrium superconductors 364
20.2.1 2.1. Quasiparticle distributions and self-consistency equations 364
20.2.2 2.2. Dynamical equations and relaxation times 369
20.2.3 2.3. Charge imbalance dynamics and the transmission-line picture 376
20.3 3. Pair-field susceptibility and Josephson tunneling 380
20.3.1 3.1. Introduction and experimental configuration 380
20.3.2 3.2. Pair-field susceptibility for $T > T_c$ 383
20.3.3 3.3. Pair-field susceptibility for $T < T_c$ 387
20.4 4. Phase-slip centers and microbridges 391
20.4.1 4.1. Phase-slip centers 391
20.4.2 4.2. Superconducting microbridges 400
20.4.3 4.3. Interactions between microbridges or phase-slip centers 404
20.5 5. Discussion and conclusions 407

21 Nonequilibrium Properties of Superconductors by Aronov et al. (!!!!!!) 416
21.1 1. Introduction 416
21.2 2. The full set of equations describing transport 418
21.3 3. Different kinds of perturbation and different nonequilibrium phenomena 426
21.4 4. Stationary nonequilibrium distribution under pumping 427
21.5 5. Energy conservation and entropy production 430
21.6 6. Hydrodynamical approach 433
21.7 7. Thermoelectric phenomena 437
21.8 8. Acoustical properties of superconductors 439
21.8.1 8.1. Deformational perturbations 439
21.8.2 8.2. Nonlinear acoustic phenomena in superconductors 440
21.8.3 8.3. Acousto-electric current and field 445
21.9 9. Derivation of the transport equations for slowly varying external fields 447
21.1010. Conclusion 452

22 The Kinetic Theory of Superconductors with Excess Quasiparticles by Galitskii, Elesin, Kopaev (!!!!!!) 452
22.1 Introduction 452
22.2 1.1. The dynamic and kinetic equations in Single-band approximation 456
22.2.1 1.1.1. The order parameter equation 456
22.2.2 1.1.2. The kinetic equation for the quasiparticle distribution function 457
22.2.3 1.1.3. Sources of nonequilibrium quasiparticles 459
22.2.4 1.1.4. The kinetic equation for phonons 460
22.2.5 1.1.5. The kinetics of quasiparticles in superconductors 461
22.3 1.2. Superconductors with a wide quasiparticle source. Optical pumping and tunnel injection at high voltages in Single-band approximation 461
22.3.1 1.2.1. The distribution function of excess quasiparticles 461
22.3.2 1.2.2. The order parameter 469
22.3.3 1.2.3. The number of superconducting electrons and magnetic properties 473
22.3.4 1.2.4. The critical power of optical pumping 475
22.3.5 1.2.5. Current-voltage characteristics of tunnel junctions 476
22.3.6 1.2.6. Stability analysis. Coherent instability under optical pumping 478
22.3.7 1.2.7. Diffusion instability 480
22.3.8 1.2.8. Inhomogeneous states in the E-model 481

22.3.9 1.2.10. The inhomogeneous state of superconductors with tunnel injection . . . 484
22.3.10 1.2.11. Comparison of theory and experiment. Conclusion . . . 485
22.3.11 1.3. Superconductors with a narrow quasiparticle source. Threshold electromagnetic pumping and tunnel injection in Single-band approximation . . . 489
22.3.12 1.3.1. The quasiparticle distribution function . . . 489
22.3.13 1.3.2. The order parameter . . . 490
22.3.14 1.3.3. Threshold instability . . . 491
22.3.15 1.3.4. Inhomogeneous states . . . 492
22.3.16 1.3.5. Comparison with experiment. Conclusion . . . 493
22.4 2. Effect of electromagnetic field on superconductors in the two-band approximation . 493
22.4.1 2.1. The electron spectrum of a crystal in a strong electromagnetic field . . . 493
22.4.2 2.2. The quasiparticle distribution function . . . 494
22.4.3 2.3. The decay and spectrum of interacting quasiparticles . . . 496
22.4.4 2.4. The effect of a strong electromagnetic field on the properties of superconductors 497
22.4.5 2.5. Superconductivity in systems with repulsion and inverse quasiparticle distribution . . . 499

23 Kinetic Equations in Superconducting Thin Films by Chang 507
23.1 1. Introduction . . . 507
23.2 2. Basic equations . . . 508
23.2.1 2.1. Injection rates . . . 508
23.2.2 2.1.1. Quasiparticle tunneling injection . . . 508
23.2.3 2.1.2. Microwave irradiation . . . 510
23.2.4 2.1.3. Heat pumping and light irradiation . . . 512
23.2.5 2.2. Relaxations . . . 512
23.2.6 2.2.1. Electron-phonon collisions . . . 513
23.2.7 2.2.2. Electron-impurity interactions . . . 514
23.2.8 2.2.3. Phonon escape . . . 515
23.2.9 2.3. Summary on the kinetic equations . . . 516
23.2.10 2.4. Modified gap equation . . . 516
23.3 3. Systems near equilibrium . . . 517
23.3.1 3.1. Microscopic lifetimes: calculation . . . 518
23.3.2 3.1.1. Quasiparticle lifetimes . . . 518
23.3.3 3.1.2. Phonon lifetimes . . . 520
23.3.4 3.2. Microscopic lifetime: measurement . . . 522
23.3.5 3.3. Macroscopic lifetimes . . . 524
23.3.6 3.3.1. The quasiparticle density relaxation time . . . 524
23.3.7 3.3.2. Quasiparticle charge relaxation time . . . 527
23.4 4. Systems far from equilibrium . . . 527
23.4.1 4.1. Narrow band phonon generation . . . 528
23.4.2 4.2. Enhancement of superconductivity . . . 530
23.4.3 4.3. Analytical models and instability . . . 534

24 Vortex Motion in Superconductors by Larkin, Ovchinnikov 535
24.1 1. Introduction . . . 535
24.2 2. Equation of flux line motion in inhomogeneous superconductors . . . 536
24.2.1 2.1. Phenomenological derivation . . . 536
24.2.2 2.2. Microscopic derivation of the equation of motion . . . 538
24.3 3. Conductivity of superconductors in a mixed state . . . 540
24.3.1 3.1. Temperatures close to T_c . . . 540
24.3.2 3.2. Fields close to H_{c2} . . . 542
24.3.3 3.3. Low temperatures . . . 544
24.4 4. Nonlinear effects in the motion of vortices in superconductors . . . 546
24.4.1 4.1. Nonlinear conductivity . . . 546

24.4.2 4.2. Emission of monochromatic phonons in the motion of vortices 549
24.5 5. Elasticity of a vortex lattice 551
24.5.1 5.1. Elastic moduli 551
24.5.2 5.2. Space dispersion of elastic moduli 551
24.5.3 5.3. Absence of long-range order in a vortex lattice 553
24.6 6. Pinning 555
24.6.1 6.1. Critical current 555
24.6.2 6.2. I-V characteristic 558
24.7 7. Conclusion 562
24.8 Appendix. Kinetic equation for dirty superconductors 562

25 Theory of the Resistive State in Narrow Superconducting Channels by Galaiko, Kopnin 571
25.1 1. Introduction 571
25.1.1 1.1. Basic experimental results 573
25.2 2. The general picture of the resistive state. Phase slip centers 574
25.3 3. The phenomenological theories of the resistive state 578
25.3.1 3.1. Fluctuation-induced phase slip centers 578
25.3.2 3.2. Spontaneous formation of phase slip centers 582
25.4 4. The microscopic theory: results of numerical solutions of timedependent superconductivity equations 585
25.4.1 4.1. Time-dependent superconductivity equations 585
25.4.2 4.2. Numerical results 587
25.5 5. The microscopic theory: results of analytical solutions of timedependent superconductivity equations 590
25.5.1 5.1. The stability analysis of the current-carrying normal state 590
25.5.2 5.2. The structure of the phase slip centers 592
25.5.3 5.3. The current-voltage characteristic 595
25.5.4 5.4. The upper boundary of the resistive state 599
25.6 6. Voltage steps in the current-voltage characteristics of superconducting channels with finite length 600
25.7 7. Conclusions 603

26 Collective Modes in Superconductors by Shon 603
26.1 1. Introduction 603
26.2 2. Review of collective sound-like modes 605
26.2.1 2.1. Two-fluid hydrodynamics of helium II 605
26.2.2 2.2. Hydrodynamic description of superfluid Fermi systems 606
26.2.3 2.3. Collisionless modes 606
26.2.4 2.4. The Bogoliubov-Anderson mode 607
26.2.5 2.4.1. The problem of gauge invariance in superconductors 607
26.2.6 2.4.2. Uncharged Fermi systems 607
26.2.7 2.4.3. Superconductors 608
26.2.8 2.5 The Carlson-Goldman mode 608
26.3 3. The microscopic theory 611
26.3.1 3.1. Some remarks 611
26.3.2 3.2. Dirty limit theory 611
26.3.3 3.3. Linearized theory 614
26.4 4. The order-parameter structure factor 616
26.4.1 4.1. The formal solution 616
26.4.2 4.2. Analytic expressions 618
26.4.3 4.3. Results 620
26.4.4 4.4. Comparison with experiment* 623
26.5 5. Extensions and further collective modes 627

26.5.1 5.1. Space and time dependent conversion . . . 627
26.5.2 5.2. The "neutral" superconductor . . . 629
26.5.3 5.3. Low temperatures . . . 630
26.5.4 5.4. Further theoretical work on the Carlson-Goldman collective mode . . . 632
26.5.5 5.5. Manifestation of the Carlson-Goldman collective mode . . . 634
26.5.6 5.6. Amplitude oscillations and further collective modes . . . 635
26.6 6. Conclusions . . . 637
26.7 Appendix. Correction terms in the description of the CarlsonGoldman mode . . . 638

27 Resistive States of Type-I Superconductors by Dolgopolov 640
27.1 1. Introduction . . . 640
27.2 2. Resistive phenomena in the intermediate state . . . 641
27.2.1 2.1. The dynamic intermediate state . . . 641
27.2.2 2.2. Macroscopic electrodynamics of the intermediate state . . . 644
27.2.3 2.3. Propagation of electromagnetic waves and hydrodynamic effects in the intermediate state . . . 646
27.2.4 2.4. On the structure of the intermediate state under the destruction of superconductivity by a current . . . 648
27.3 3. Two-dimensional mixed state of type-I superconductors . . . 655
27.3.1 3.1. Introductory remarks . . . 655
27.3.2 3.2. The tm state in hollow cylinders . . . 656
27.3.3 3.3. Paramagnetic effect in type-I superconductors . . . 659
27.3.4 3.4. Study of the tm state in a longitudinal magnetic field . . . 660
27.3.5 3.5. The tm state under non-stationary external conditions . . . 661
27.3.6 3.6. Discussion of theoretical models . . . 665

28 Collisionless relaxation of the energy gap in superconductors by Volkov, Kogan 674
28.0.1 1. Introduction . . . 674
28.0.2 2. Derivation of the Fundamental Equations . . . 675
28.0.3 3. Collisionless Evolution of Perturbations in a Superconductor . . . 679
28.0.4 My questions about work by Volkov, Kogan . . . 683

29 Coherent Excited States in the Theory of Superconductivity by Anderson 683
29.0.1 I. Introduction . . . 683
29.0.2 II. Commutators and Energies of Coherent States . . . 685
29.0.3 III. Relationship of Sum Rules and Electromagnetic Properties; Comparison of Normal and Superconducting Cases . . . 690
29.0.4 IV. Plasma Considerations . . . 693
29.0.5 V. Conclusion . . . 696
29.0.6 Appendix. Computations of Commutators . . . 696

30 TDGL Equation and its Application to the Problem of Resistivity in the Mixed State 698
30.0.1 I. Introduction . . . 699
30.0.2 II. A Time Dependent Ginaburg-Landau Equation . . . 700
30.0.3 III. The Energy Theorem . . . 705
30.0.4 IV. The Resistivity of Type II Superconductors . . . 707

31 Stability of nonequilibrium Fermi distributions with respect to Cooper pairing by Aronov, Gurevich 713
31.0.1 1. Introduction . . . 714
31.0.2 2. Derivation of the Kinetic Equation . . . 716
31.0.3 3. The Two-Particle Green's Function and the Conditions for Stability . . . 720
31.0.4 4. Examples of the Investigation of Stability . . . 725

32 The Behavior of a Superconductor in a Variable Field by Gor'kov, Eliashberg 726
32.0.1 1. Introduction . . . 727
32.0.2 2. Pippard Superconductors ($\kappa \ll 1$) . . . 728
32.0.3 A. Boundary of a Bulk Superconductor . . . 729
32.0.4 B. Superconducting Plates . . . 732
32.0.5 3. London Superconductors (Alloys with $\kappa \gg 1$) . . . 735

33 Inelastic Electron Collisions and Nonequil. Stationary States in SC by Eliashberg 738
33.0.1 1. Choice of Model . . . 738
33.0.2 2. Dynamic Equations in the Phonon Model . . . 741
33.0.3 3. Kinetic Equations . . . 745
33.0.4 4. Scattering by Impurities . . . 747
33.0.5 5. Electron-Electron Interaction . . . 748
33.0.6 6. Charge and Current Densities. Electroneutrality Condition . . . 751
33.0.7 7. Thin Films in a High-Frequency Field . . . 752

VI Special Effects: Useful, Selected Articles 756

VII Experiments: Main Articles about Superconductors 757

VIII Experiments: Main Articles about Simulators, Not Superconductors 758

34 Observing Dynamical Phases of BCS Superconductors in a Cavity QED Simulator by Young et al. 758
34.1 Introduction . . . 759
34.2 Experimental setup and model system . . . 762
34.3 Phase I to phase II . . . 767
34.4 Phase II to phase III . . . 769
34.5 Scan across three dynamical phases . . . 771
34.6 Methods . . . 771
34.6.1 Experimental setup: phase I to phase II transition . . . 771
34.6.2 Experimental setup: cuts through phase III . . . 772
34.6.3 Readout . . . 773
34.6.4 Dynamical phase diagram . . . 774
34.6.5 Phase III dynamics: the case of a continuous single-particle dispersion . . . 776
34.6.6 Numerical simulations . . . 776
34.6.7 Higgs-like behaviour in short-time phase II dynamics . . . 778
34.7 Dynamical phase diagram . . . 779
34.7.1 Homogeneous model . . . 779
34.7.2 Inhomogeneous model . . . 782
34.7.3 Experimental control of dynamical phases . . . 783
34.8 Short-time signatures of dynamical phases . . . 784
34.8.1 Phase I: fast decay . . . 784
34.8.2 Phase II: Higgs oscillation . . . 785
34.8.3 Transition to phase III: frequency dip . . . 785
34.8.4 Frequency dip in the two-spin BCS model . . . 786
34.9 Axial Motion . . . 788
34.10Questions about "Observing Dynamical Phases .." by Young et al. . . . 791

Bibliography **792**
34.11Bibliography from Old, Fundamental Artiles 792
34.12Bibliography from Well-known, Important Artiles 821
34.13Bibliography from Other Artiles 844

Preface

Examples and Solved Problems

Well-known and Important Theories

Old, Fundamental Theories (starts with articles from Larkin, Landenberg)

Special Effects: Useful, Selected Articles

Amazing facts

(I'll reveal it later)

Puzzles for motivation

(I'll reveal it later)

Part I
Nonequilibrium Superconductivity in a Nutshell

0.1 Main Formulas and Ideas (?)

0.1.1 Quantum quench phase diagrams of an s-wave BCS-BEC condensate by Yuzbashyan, Dzero, Gurarie, Foster

Main ideas and formulas

(??)

0.1.2 Dynamical vanishing of the order parameter in a fermionic condensate by Yuzbashyan, Dzero

Main ideas and formulas

(??)

0.1.3 Onset of superconductivity in a voltage-biased NSN microbridge by Serbyn, Skvortsov

Main ideas and formulas

(??)

0.1.4 Relaxation and persistent oscillations of the order parameter in the non-stationary BCS theory by A. Yuzbashyan, Tsyplyatyev, Altshuler

Main ideas and formulas

(??)

0.1.5 Solitons and Rabi Oscillations in a Time-Dependent BCS Pairing Problem by Barankov, Levitov, Spivak

Main ideas and formulas

(??)

0.1.6 Synchronization in the BCS Pairing Dynamics as a Critical Phenomenon by Barankov, Levitov

Main ideas and formulas

(??)

Part II
My Theory of Nonequilibrium Superconductivity

Part III
Examples and Solved Problems

1 Problems about Creation of a Model of Non-equilibrium Phenomena

(this is very important, since the first big question is what is going on??)

2 Problems about Transformation in Derivations

(a lot of articles use it, so I'll write it here)

3 Problems about Non-equilibrium Phenomena

(real problems)

4 Questions about Non-equilibrium Phenomena for Different Cases in Life

4.0.1 Questions to Check Knowledge

(there are a lot of them, I'll write later)

Part IV
Well-known and Important Theories

5 Quantum quench phase diagrams of an s-wave BCS-BEC condensate by Yuzbashyan, Dzero, Gurarie, Foster

(I am not sure that this article is useful)

We study the dynamic response of an s-wave BCS-BEC (atomic-molecular) condensate to detuning quenches within the two channel model beyond the weak coupling BCS limit.

At long times after the quench, the condensate ends up in one of three main asymptotic states (nonequilibrium phases), which are qualitatively similar to those in other fermionic condensates defined by a global complex order parameter.

(which ones????)

In phase I the amplitude of the order parameter vanishes as a power law, in phase II it goes to a nonzero constant, and in phase III it oscillates persistently.

(why these are phases? just regimes: zero gap, nonzero gap, oscillations (???? what does it mean physically??))

We construct exact quench phase diagrams that predict the asymptotic state (including the many-body wavefunction) depending on the initial and final detunings and on the Feshbach resonance width.

Outside of the weak coupling regime, both the mechanism and the time dependence of the relaxation of the amplitude of the order parameter in phases I and II are modified.

Also, quenches from arbitrarily weak initial to sufficiently strong final coupling do not produce persistent oscillations (in which regime??) in contrast to the behavior in the BCS regime.

The most remarkable feature of coherent condensate dynamics in various fermion superfluids is an effective reduction in the number of dynamic degrees of freedom as the evolution time goes to infinity.

(how is it???)

As a result, the long time dynamics can be fully described in terms of just a few new collective dynamical variables governed by the same Hamiltonian only with “renormalized" parameters.

(how is it???)

Combining this feature with the integrability of the underlying (e.g. the two channel) model, we develop and consistently present a general method that explicitly obtains the exact asymptotic state of the system.

5.1 Introduction

The problem of a superconductor driven out of equilibrium by a sudden perturbation goes back many decades. Early studies[Anderson(1958), Galaiko(1972), Volkov and Kogan(1973), Galperin et al.(1981), Littlewood and Varma(1982), Shumeiko(1990)] addressed small deviations from equilibrium using linearized equations of motion. (add formulas, how exactly??? where was the linearization?)

An important result was obtained by Volkov and Kogan [Volkov and Kogan(1973)], who discovered a power law oscillatory attenuation of the Bardeen-Cooper-Schriffer (BCS) order

parameter for non-equilibrium initial conditions close to the superconducting ground state. (add formulas, how exactly??? not clear, what the setup is?)

In the last decade it was realized that even large deviations from equilibrium are within the reach of appropriate theoretical methods. Recent studies, motivated by experiments in cold atomic fermions, focused on quantum quenches – nonequilibrium conditions created by a sudden change in the superconducting coupling strength.

Barankov et. al. [Barankov et al.(2004)] in a paper that set off a surge of modern research in this long-standing problem [Amin et al.(2004), Andreev et al.(2004), Barankov and Levitov(2004), Szymanska et al.(2005), Warner and Leggett(2005), Yuzbashyan et al.(2005a), Yuzbashyan et al.(2005b), Yuzbashyan et al.(2005c), 19, Barankov and Levitov(2006), Yuzbashyan and Dzero(2006), Dzero et al.(2007), Barankov and Levitov(2007), Tomadin et al.(2008), Nahum and Bettelheim(2008), 36, Faribault et al.(2009)] (which problem authors mean???) in the context of quantum gases, found that for initial conditions close to the unstable normal state, the order parameter exhibits large unharmonic periodic oscillations. (think about their paper!)

Subsequently, Yuzbashyan et. al.[19] developed an analytical method to predict the state of the system at large times based on the integrability of the underlying BCS model. (write to the first part, what this method is?)

This work extended Volkov and Kogan's result (write, how exactly extended???) to large deviations from equilibrium and showed that the oscillation frequency is twice the *nonequilibrium* asymptotic value of the order parameter, a conclusion confirmed by recent terahertz pump pulse experiments in $Nb_{1-x}Ti_xN$ films [Matsunaga et al.(2013), 46]. (how exactly? analyze these articles)

Later studies [Barankov and Levitov(2006), Yuzbashyan and Dzero(2006)] mapped out the full quantum quench "phase diagram" for weakly coupled s-wave BCS superconductors finding that three distinct regimes occur depending on the strength of the quench: Volkov and Kogan like behavior, persistent oscillations, and exponential vanishing of the order parameter. (analyze this paper! write the connection to Volkov, Kogan's article!)

Most recent research[Papenkort et al.(2007), Papenkort et al.(2009), Krull et al.(2013), 77] fueled by experimental breakthroughs[98, Beck et al.(2013), Matsunaga et al.(2013)] investigates non-adiabatic dynamics of s-wave BCS superconductors in response to fast electromagnetic perturbations. (this is something that I don't understand at all. why nonadiabatic??? a lot of articles are here...)

Closely related subjects developing in parallel are exciton dynamics[Brierley et al.(2011)], collective neutrino oscillations[Pehlivan et al.(2011), Raffelt et al.(2013)], quenched p-wave superfluids[Foster et al.(2013), Foster et al.(2014)] etc. (have no idea what are they?)

Most existing work addressed the dynamics in the BCS regime and, in particular, quenches such that the interaction strength is weak both before and after the quench. This was so that the system always remains in the BCS regime, since the physics of the condensate beyond this regime was not sufficiently well understood. (strange statement, beyond BCS regime depends on a model, since BCS is just an approximation. how at all people are assured that in cold atoms, there is indeed the BCS regime???)

However, a superfluid made up of cold atoms can be as well quenched from the BCS to the Bose-Einstein Condensation (BEC) regime (how exactly?), or within the BEC regime. With few exceptions [36, Foster et al.(2013), Foster et al.(2014)], these types of quenches are not adequately studied in the existing literature. (I don't know, hot is is related to quenches before? this paper answers this question)

Our paper aims to close this gap and analyze all possible interaction quenches throughout the BCS-BEC crossover in a paired superfluid, including BCS to BEC, BEC to BCS and BEC to BEC quenches.

We fully determine the steady state of the system at large times after the quench – the asymptote of the order parameter as well as the approach to the asymptote, the many-body wave function, and certain observables, such as the radio-frequency absorption spectrum and the momentum distribution (momentum distribution?).

In the BCS limit, we recover previous results. Beyond this limit the dynamics is quantitatively and sometimes qualitatively different.

For example, the power law in the Volkov and Kogan like attenuation changes in the BEC regime, exponential vanishing is replaced with a power law, and persistent oscillations first change their form and then disappear altogether after a certain threshold for quenches from any initial (e.g. arbitrarily weak) to sufficiently strong final coupling. (write below, how exactly? we can compare these results, from this article and from VK-s.)

We believe an experimental verification of the predictions of this work is within a reach of current experiments in cold atomic systems. (why??)

The long time dynamics can be determined explicitly due to a remarkable reduction mechanism at work (???), so that at large times the system is governed by an effective interacting Hamiltonian with just a few classical collective spin or oscillator degrees of freedom.

In a sense, the system "flows in time" to a much simpler Hamiltonian.

This observation combined with the integrability of the original Hamiltonian (see below) lead to a method originally proposed in Ref. [19] for obtaining the long time asymptote (steady state) of integrable Hamiltonian dynamics in the continuum (thermodynamic) limit.

Here we improve this method as well as provide its comprehensive and self-contained review including many previously unpublished results and steps. We do so in the context of the s-wave BCS (one channel) and inhomogeneous Dicke (two channel) models (what is a Dicke model??), but with some modifications the same method also applies to all known integrable pairing models [Gaudin(1983), Richardson(2002), Ibanez et al.(2009), Dunning et al.(2010), Rombouts et al.(2010), Dukelsky et al.(2004), Ortiz et al.(2005)] , such as $p+ip$ superfluids[Foster et al.(2013), Foster et al.(2014)], integrable fermion or boson pairing models with nonuniform interactions[J. Dukelsky(2001), L. Amico(2001)], Gaudin magnets (central spin models), and potentially can be extended to a much broader class of integrable nonlinear equations. (is it really applicable?? sounds that I'll not be able to connect them, but I can check later)

The purpose of this paper is therefore twofold. First, it serves as an encyclopedia (I am not sure that there are results from all old important papers. or at least they are in different formalism) of quantitatively exact predictions, new and old, for the quench dynamics of real s-wave BCS-BEC condensates in two and three spatial dimensions.

Readers primarily interested in this aspect of our work will find most of the relevant information in the Introduction, Sect. 5.7, and Conclusion.

In particular, Sect. 5.1.4 concisely summarizes our main results and provides a guide to other sections that contain further results and details.

Our second goal is to develop and thoroughly review a method for determining the far from equilibrium dynamics in a certain class of integrable models. We refer readers interested in learning about the method to Sect. 5.2. Also, from this viewpoint, Sects. 5.3 and 5.4 should be considered as applications of our approach and Sect. 5.5 as a related development.

A major experimental breakthrough with ultracold atoms was achieved in 2004, when they

were used to emulate s-wave superconductors with an interaction strength that can be varied at will [Regal et al.(2004), Zwierlein et al.(2004)]. (read these papers!)

Experimental control parameter is the detuning ω – the binding energy of a two fermion bound state (molecule). This parameter determines the strength of the effective interaction between fermions and can be varied both slowly and abruptly with the help of a Feshbach resonance. Moreover, it is straightforward to make time resolved measurements of the subsequent evolution of the system. Thus cold atoms provide a natural platform to study quenches in superfluids and in a variety of other setups[Calabrese and Cardy(2006), Kollath et al.(2007)].

At large ω we have fermionic atoms with weak effective attraction that form a paired superfluid, an analog of the superconducting state of electrons in a metal. As ω is decreased, the atoms pair up into bosonic molecules which then Bose condense. It was argued for a long time that both the paired superfluid and the Bose-condensed molecules are in the same phase of the fermionic gas, named the BCS-BEC condensate [Leggett(1980), Nozières and Schmitt-Rink(1985)]. As ω decreases, the strength of the effective interaction (coupling) between fermions increases from weak to strong and the system undergoes a BCS-BEC crossover. At $\omega \gg 2\varepsilon_F$, where ε_F is the Fermi energy, the system is deep in the BCS regime, while at large negative ω it is deep in the BEC regime. It is not known how to recreate such a crossover in a conventional solid-state superconductor since the interaction strength cannot be easily adjusted.

In a quantum quench setup the system is prepared in the ground state at a detuning ω_i. At $t = 0$ the detuning is suddenly changed, $\omega_i \to \omega_f$. At $t > 0$ the system evolves with a new Hamiltonian $H(\omega_f)$. The main goal is to determine the state of the system at large times, $t \to \infty$.

5.1.1 Models and approximations

We consider two closely related models in this paper in both two and three dimensions. The first one is the well-known two channel model that describes two species of fermionic atoms interacting via an s-wave Feshbach resonance (what is Feshbach resonance???)

$$\hat{H}_{2\text{ch}} = \sum_{\mathbf{p},\sigma=\uparrow,\downarrow} \epsilon_{\mathbf{p}} \hat{a}^\dagger_{\mathbf{p}\sigma} \hat{a}_{\mathbf{p}\sigma} + \sum_{\mathbf{q}} \left(\omega + \frac{q^2}{4m}\right) \hat{b}^\dagger_{\mathbf{q}} \hat{b}_{\mathbf{q}} + g \sum_{\mathbf{pq}} \left(\hat{b}^\dagger_{\mathbf{q}} \hat{a}_{\frac{\mathbf{q}}{2}+\mathbf{p},\uparrow} \hat{a}_{\frac{\mathbf{q}}{2}-\mathbf{p},\downarrow} + \hat{b}_{\mathbf{q}} \hat{a}^\dagger_{\frac{\mathbf{q}}{2}-\mathbf{p},\downarrow} \hat{a}^\dagger_{\frac{\mathbf{q}}{2}+\mathbf{p},\uparrow} \right). \quad (5.1)$$

(derive this model in another note!! I don't know how to do it)

It is convenient to think of the two types of fermions of mass m and energy $\epsilon_{\mathbf{p}} = p^2/2m$ as spin up and down, created and annihilated by operators $\hat{a}^\dagger_{\mathbf{p}\sigma}$ and $\hat{a}_{\mathbf{p}\sigma}$.

The interaction term converts two fermions into a bosonic molecule and vise versa at a rate controlled by the parameter g.

Molecules are created and annihilated by $\hat{b}^\dagger_{\mathbf{q}}$ and $\hat{b}_{\mathbf{q}}$ and have a binding energy ω.

The parameter g is set by the type of atoms and the specifics of a particular Feshbach resonance and cannot be changed in a single experiment; ω can be varied at will by varying the magnitude of the magnetic field applied during the experiment.

This model describes atoms in the BCS regime when ω is large, which undergo a crossover to the BEC regime as ω is decreased.

A parameter with dimensions of energy important for our analysis of this model is $g^2\nu_F$, where ν_F is the bulk density of states (proportional to the total volume) at the Fermi energy ϵ_F. A well known parameter

$$\gamma = \frac{g^2 \nu_F}{\epsilon_F} \quad (5.2)$$

controls whether the resonance is narrow $\gamma \ll 1$ or broad $\gamma \gg 1$. (why?) This parameter is the dimensionless atom-molecule interaction strength or, equivalently, the resonance width.

A very convenient feature of the narrow resonance is that regardless of the regime of the system, controlled by ω, the system is adequately described with mean field theory [Gurarie and Radzihovsky(2007)] (why??). This is already clear from the form of the Hamiltonian: small γ implies that interaction g is small.

Broad resonances on the other hand correspond to large g. Under those conditions it is possible to integrate out the molecules $\hat{b}_{\mathbf{q}}$ to arrive at a simpler Hamiltonian [Gurarie and Radzihovsky(2007)] (how??) describing fermions interacting via a short range attractive interaction with variable strength

$$\hat{H}_{1\mathrm{ch}} = \sum_{\mathbf{p},\sigma=\uparrow,\downarrow} \epsilon_{\mathbf{p}} \hat{a}^{\dagger}_{\mathbf{p}\sigma} \hat{a}_{\mathbf{p}\sigma} - \frac{\lambda}{\nu_F} \sum_{\mathbf{p}\mathbf{p}'\mathbf{q}} \hat{a}^{\dagger}_{\frac{\mathbf{q}}{2}-\mathbf{p},\downarrow} \hat{a}^{\dagger}_{\frac{\mathbf{q}}{2}+\mathbf{p},\uparrow} \hat{a}_{\frac{\mathbf{q}}{2}+\mathbf{p}',\uparrow} \hat{a}_{\frac{\mathbf{q}}{2}-\mathbf{p}',\downarrow}, \tag{5.3}$$

where

$$\lambda = \frac{g^2 \nu_F}{\omega} = \frac{\gamma \varepsilon_F}{\omega}. \tag{5.4}$$

This is the single (one) channel or BCS model, which is the second model we analyze in this paper. It also describes the BCS-BEC crossover (what is crossover?) as ω is decreased (λ is increased). However, while in the BCS and (to some extent) in the BEC regimes corresponding to large and small λ, respectively, mean field theory holds in equilibrium, for the intermediate values of λ (neither large nor small) the mean field theory is known to break down.

A special value of λ in the middle of the regime unaccessible to the mean field theory already in equilibrium is called the unitary point. It corresponds to the interaction strength where molecules are about to be formed. Non-condensed molecules play an important role in the description of the unitary point and its special properties are a subject of many studies in the literature[Nozières and Schmitt-Rink(1985), Burovski et al.(2006)].

Just as earlier work on the far from equilibrium superconductivity, we analyze the quench dynamics in the mean field approximation where no molecules are transferred into or out of the BCS-BEC condensate after the quench, i.e. the dynamics of the condensate is decoupled from the non-condensed modes. We analyze the validity of this approximation for nonequilibrium steady states produced by quenches in two channel model in Appendix 5.9. We find that the situation is similar to that in equilibrium [Gurarie and Radzihovsky(2007)]. In the case of a broad Feshbach resonance, mean field is expected to hold for quenches where both initial and final detunings are far from the unitary point. A quench into the unitary point is a very interesting problem addressed by some publications before [Bulgac and Yoon(2009)], but the method we employ here is not applicable to this case.

Nevertheless, a variety of quenches are still accessible to our description even when the resonance is broad, including BCS→ BCS, BCS → BEC, BEC → BCS, and BEC → BEC, where BCS and BEC stand for the value of the interaction strength far weaker or far stronger than that at the unitary point. In the case of BCS-BEC superfluids formed with interactions generated by narrow Feshbach resonances, the mean field theory treatment is valid even at the threshold of the formation of the bound state and throughout the BCS-BEC crossover. Here we consider quenches of the detuning ω for both narrow and broad resonances within mean field. Note that in the case of the one channel model we expect the mean field on the BEC side to be valid only in the far BEC limit where the ground state essentially consists of non-interacting Bose condensed molecules[Levinsen and Gurarie(2006)].

In the mean field treatment the condensate is described by the $\mathbf{q} = 0$ (I have no idea, why is it so???) part of the Hamiltonian (5.1), which is decoupled from $\mathbf{q} \neq 0$ terms in this approximation. The Hamiltonian therefore becomes

$$\hat{H}_{2\text{ch}} = \sum_{\mathbf{p}} 2\epsilon_{\mathbf{p}} \hat{s}^z_{\mathbf{p}} + \omega \hat{b}^\dagger \hat{b} + g \sum_{\mathbf{p}} \left(\hat{b}^\dagger \hat{s}^-_{\mathbf{p}} + \hat{s}^+_{\mathbf{p}} \hat{b} \right), \tag{5.5}$$

where

$$\hat{s}^-_{\mathbf{p}} = \hat{a}_{\mathbf{p}\uparrow} \hat{a}_{-\mathbf{p}\downarrow}, \;\; \hat{s}^z_{\mathbf{p}} = \frac{1}{2} \left(\hat{a}^\dagger_{\mathbf{p}\uparrow} \hat{a}_{\mathbf{p}\uparrow} + \hat{a}^\dagger_{-\mathbf{p}\downarrow} \hat{a}_{-\mathbf{p}\downarrow} - 1 \right) \tag{5.6}$$

are Anderson pseudospin-1/2 operators [Anderson(1958)] and

$$\hat{b} = \hat{b}_{\mathbf{q}=0}.$$

(okay, maybe if I think for 10 min, I'll derive it...)

Hamiltonian (5.5) is also known as inhomogeneous Dicke or Tavis-Cummings model. In a quantum quench problem we need to solve Heisenberg equations of motion for this Hamiltonian for given initial conditions

$$\begin{aligned} \frac{d\hat{\vec{s}}_{\mathbf{p}}}{dt} &= \hat{\vec{B}}_{\mathbf{p}} \times \hat{\vec{s}}_{\mathbf{p}}, \quad \frac{d\hat{b}}{dt} = -i\omega \hat{b} - ig \hat{J}_-, \\ \hat{\vec{J}} &= \sum_{\mathbf{p}} \hat{\vec{s}}_{\mathbf{p}}, \quad \hat{\vec{B}}_{\mathbf{p}} = 2g \hat{\vec{b}} + 2\epsilon_{\mathbf{p}} \hat{\mathbf{z}}, \end{aligned} \tag{5.7}$$

where $\hat{\vec{b}} = \hat{b}_x \hat{\mathbf{x}} + \hat{b}_y \hat{\mathbf{y}}$, $\hat{b}_x$ and $-\hat{b}_y$ are Hermitian and anti-Hermitian parts of the operator $\hat{b} = \hat{b}_x - i\hat{b}_y$, and $\hat{\mathbf{x}}, \hat{\mathbf{y}}, \hat{\mathbf{z}}$ are coordinate unit vectors.

The second step in the mean field treatment of the two-channel model is to replace Heisenberg operator $\hat{b}(t)$ in the first equation of motion in (5.7) with its time-dependent quantum mechanical average, $\hat{b}(t) \to \langle \hat{b}(t) \rangle \equiv b(t)$, which is expected to be exact in thermodynamic limit as long as the $\mathbf{q} = 0$ state is macroscopically occupied at all times.

This replacement can be shown to be exact in equilibrium using the exact solution for the spectrum of inhomogeneous Dicke model [Richardson(1977), Gaudin(1983)] and numerically for the time dependent problem [Sträter et al.(2012)] (to understand why is it so, I need to read these articles for 3 days at least).

Upon this replacement equations of motion become linear in operators and taking their quantum mechanical average, we obtain

$$\begin{aligned} \dot{\vec{s}}_{\mathbf{p}} &= \vec{B}_{\mathbf{p}} \times \vec{s}_{\mathbf{p}}, \quad \dot{b} = -i\omega b - igJ_-, \\ \vec{J} &= \sum_{\mathbf{p}} \vec{s}_{\mathbf{p}}, \quad \vec{B}_{\mathbf{p}} = 2g\vec{b} + 2\epsilon_{\mathbf{p}} \hat{\mathbf{z}}, \end{aligned} \tag{5.8}$$

where $\vec{s}_{\mathbf{p}} = \langle \hat{\vec{s}}_{\mathbf{p}} \rangle$. These are Hamiltonian equations of motion for a classical (what is meant by "classical") Hamiltonian

$$H_{2\text{ch}} = \sum_{\mathbf{p}} 2\epsilon_{\mathbf{p}} s^z_{\mathbf{p}} + \omega \bar{b} b + g \sum_{\mathbf{p}} \left(\bar{b} s^-_{\mathbf{p}} + b s^+_{\mathbf{p}} \right), \tag{5.9}$$

which describes a set of angular momenta (classical spins or vectors) coupled to a harmonic oscillator. Here, $\bar{b}$ denotes the complex conjugate of b. These dynamical variables obey the following Poisson brackets:

$$\left\{ s^a_{\mathbf{p}}, s^b_{\mathbf{k}} \right\} = -\varepsilon_{abc} \delta_{\mathbf{pk}} s^c_{\mathbf{p}}, \quad \{b, \bar{b}\} = i, \tag{5.10}$$

where a, b, and c stand for spatial indecies x, y, and z.

Similar steps in the case of the single channel model (5.3) lead to a classical spin Hamiltonian

$$H_{1\text{ch}} = \sum_{\mathbf{p}} 2\epsilon_{\mathbf{p}} s^z_{\mathbf{p}} - \frac{\lambda}{\nu_F} \sum_{\mathbf{p},\mathbf{p}'} s^-_{\mathbf{p}} s^+_{\mathbf{p}'} \tag{5.11}$$

together with the corresponding equations of motion.

An important characteristic of the system both in and out of equilibrium is the superfluid order parameter or the gap function defined in the two channel model as

$$\Delta(t) = -g\langle \hat{b}(t)\rangle = -gb(t) \equiv \Delta_x(t) - i\Delta_y(t). \tag{5.12}$$

In the one channel limit this expression turns into

$$\Delta_{1\text{ch}}(t) = \frac{\lambda}{\nu_F} \sum_{\mathbf{p}} \langle \hat{a}_{\mathbf{p}\uparrow}(t)\hat{a}_{-\mathbf{p}\downarrow}(t)\rangle = \frac{\lambda}{\nu_F} \sum_{\mathbf{p}} s^-_{\mathbf{p}}. \tag{5.13}$$

The magnitude $|\Delta(t)|$ of the order parameter is known as the Higgs or amplitude mode for its similarity with the Higgs boson[Pekker and Varma(2014), Barankov and Levitov(2007)] (I don't still understand this relation to Higgs boson. I am not sure that there are answers in these articles, but once I'll try to find it out) and its time-dependent phase represents a Goldstone mode. Note however that out of equilibrium the gap function does not entirely determine the state of the system. It specifies the effective magnetic field acting on each spin according to Eq. (5.8), but there is still a certain freedom in how the spin moves in this field. For example, even for a constant field the spin can precess around it making an arbitrary constant angle with its direction.

In above models we took a free single particle spectrum, $\varepsilon_{\mathbf{p}} = p^2/2m$ and labeled states with momenta $\mathbf{p}$. This choice is not essential for our analysis. We can as well consider an arbitrary spectrum ε_i. The pairing is then between pairs of time reversed (time reversed) states[Anderson(1959), Kurland et al.(2000)], see also the first two pages in Ref. [Yuzbashyan et al.(2005a)] for more details.

For example, in Hamiltonian (5.5) this results in relabeling $\hat{\vec{s}}_{\mathbf{p}} \to \hat{\vec{s}}_i$, $\hat{a}_{\mathbf{p}\uparrow}\hat{a}_{-\mathbf{p}\downarrow} \to \hat{a}_{i\uparrow}\hat{a}_{i\downarrow}$, $\hat{a}^\dagger_{\mathbf{p}\uparrow}\hat{a}_{\mathbf{p}\uparrow} \to \hat{a}^\dagger_{i\uparrow}\hat{a}_{i\uparrow}$ etc., where the state $|i\downarrow\rangle$ is the time reversed counterpart of $|i\uparrow\rangle$.

(suddenly index i appears, is it the same momenta index??)

Our results below depend only on the density of the single particle states $\nu(\varepsilon)$ (why??)in the continuum limit regardless of whether these states are characterized by momenta $\mathbf{p}$ or any other set of quantum numbers i.

5.1.2 Ground state

In the ground state

$$\Delta(t) = \Delta_0 e^{-2i\mu t}, \tag{5.14}$$

where the magnitude Δ_0 is time-independent. Apart from an overall rotation about the z-axis with frequency 2μ (why 2μ?), the ground state is a static solution of the equations of motion that minimizes $H_{2\text{ch}}$. The minimum is achieved when each spin is directed against its effective magnetic field, i.e. (check it, I don't see it yet)

$$s^-_{\mathbf{p}} = \frac{\Delta_0 e^{-2i\mu t}}{2E(\varepsilon_{\mathbf{p}};\Delta_0,\mu)}, \quad s^z_{\mathbf{p}} = -\frac{\varepsilon_{\mathbf{p}} - \mu}{2E(\varepsilon_{\mathbf{p}};\Delta_0,\mu)}, \tag{5.15}$$

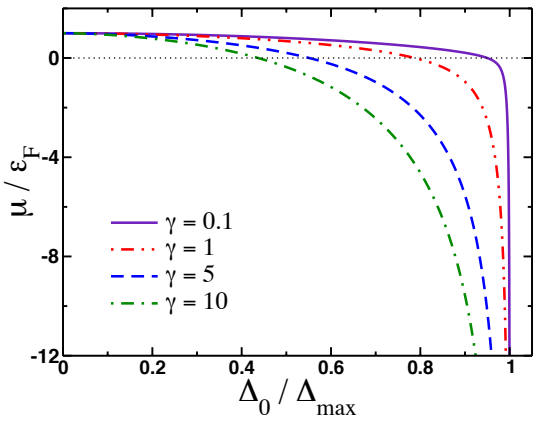


Figure 5.1: Ground state chemical potential μ (I am very confused, I thought it is fixed always. read about it a lot!) for two channel model in 3d in units of the Fermi energy ε_F as a function of the ground state gap Δ_0 for various resonance width γ. $\mu(\Delta_0)$ is calculated from Eqs. (5.25) and (5.26). Note that in the two channel model Δ_0 is bounded from above by $\Delta_{\max}$.

where

$$E(\varepsilon;\Delta,\mu) \equiv \sqrt{(\varepsilon-\mu)^2+\Delta^2}. \tag{5.16}$$

Note that the length of the spin $s_{\mathbf{p}} = 1/2$. This is because the ground state is a tensor product of single spin-1/2 wave functions and $\vec{s}_{\mathbf{p}} = \langle \hat{\vec{s}}_{\mathbf{p}} \rangle$.

The equation of motion (5.8) for b yields (check it, but maybe it is easy)

$$|J_-| = \frac{(\omega-2\mu)\Delta_0}{g^2}, \tag{5.17}$$

which implies a self-consistency equation for Δ_0

$$\frac{(\omega-2\mu)}{g^2} = \sum_{\mathbf{p}} \frac{1}{2E(\varepsilon_{\mathbf{p}};\Delta_0,\mu)}. \tag{5.18}$$

Further, the Hamiltonian (5.9) conserves

$$n = \bar{b}b + \sum_{\mathbf{p}} \left(s^z_{\mathbf{p}} + \frac{1}{2} \right), \tag{5.19}$$

which is the average total number of bosons and fermion pairs. This number is related to Δ_0 and the chemical potential μ as

$$2n = \frac{2\Delta_0^2}{g^2} + \sum_{\mathbf{p}} \left(1 - \frac{\varepsilon_{\mathbf{p}}-\mu}{E(\varepsilon_{\mathbf{p}};\Delta_0,\mu)} \right). \tag{5.20}$$

(why? Did I miss the derivation?)

The Fermi energy ε_F is the chemical potential of the fermionic atoms at zero temperature in the absence of any interaction, when only fermions are present. It provides an overall energy scale and it is convenient to measure all energies in units of the Fermi energy. Thus, from now on, we set everywhere below

$$\varepsilon_F = 1. \tag{5.21}$$

Below we often switch from discrete to continuum (thermodynamic limit) formulations. (I don't understand these two pictures, for me it is one picture. I'll think more about it later)

In the former version, there are N discrete single-particle energy levels $\varepsilon_{\mathbf{p}}$ with certain degeneracy each.

Any quantity $A_{\mathbf{p}}$ we consider in this paper depends on $\mathbf{p}$ only through $\varepsilon_{\mathbf{p}}$, $A_{\mathbf{p}} = A(\varepsilon_{\mathbf{p}})$ (why???).

For example, all spins $\vec{s}_{\mathbf{p}}$ on a degenerate level $\varepsilon_{\mathbf{p}}$ are parallel at all times and effectively merge into a single vector. There are N such vectors, so we count N distinct classical spins.

In thermodynamic limit, energies $\varepsilon_{\mathbf{p}}$ form a continuum on the positive real axis, i.e. are described by a continuous variable ε with a density of states $\nu(\varepsilon)$ that depends on the dimensionality of the problem

$$\nu(\varepsilon) = \nu_F f(\varepsilon), \tag{5.22}$$

where ν_F is the *bulk* density of states (proportional to the system volume) at the Fermi energy, $f(\varepsilon) = 1$ in 2d, and $f(\varepsilon) = \sqrt{\varepsilon}$ in 3d. Summations over $\mathbf{p}$ turn into integrations,

$$\sum_{\mathbf{p}} A_{\mathbf{p}} \to \nu_F \int_0^\infty A(\varepsilon) f(\varepsilon) d\varepsilon. \tag{5.23}$$

With only fermions present, the total particle number is

$$2n = \int_0^1 2\nu(\varepsilon) d\varepsilon = \frac{4}{d}\nu_F, \tag{5.24}$$

where $d = 2, 3$ is the number of spatial dimensions. Interaction redistributes this number between fermions and bosons as in Eq. (5.20). Combining Eqs. (5.20) and (5.24) and taking the continuum limit, we obtain

$$\frac{4}{d} = \frac{2\Delta_0^2}{\gamma} + \int_0^\infty \left(1 - \frac{\varepsilon - \mu}{\sqrt{(\varepsilon-\mu)^2 + \Delta_0^2}}\right) f(\varepsilon) d\varepsilon, \tag{5.25}$$

where γ is the dimensionless resonance width defined in Eq. (5.2).

Similarly, Eq. (5.18) becomes in the thermodynamic limit

$$\frac{2\omega - 4\mu}{\gamma} = \int_0^{\varepsilon_\Lambda} \frac{f(\varepsilon) d\varepsilon}{\sqrt{(\varepsilon-\mu)^2 + \Delta_0^2}}, \tag{5.26}$$

where ε_Λ is the high energy cutoff. In 3d it can be eliminated by an additive renormalization of the detuning ω, see e.g. Ref. [Gurarie and Radzihovsky(2007)]. This however does not affect our results for the quench dynamics as they depend on the difference between the initial and final values of the detuning.

Eqs. (5.25) and (5.26) contain two independent parameters not counting the cutoff. For example, we can choose γ and ω and determine μ and Δ_0 from these equations, or choose γ and Δ_0 and determine μ and ω etc., see Fig. 5.1 for a plot of $\mu(\Delta_0)$ for various γ in 3d. Note also that $\Delta_0^2 = g^2 \bar{b} b$ is proportional to the number of bosons and is therefore limited by the total number of particles. Eq. (5.25) implies

$$\Delta_0 \le \sqrt{\frac{2\gamma}{d}} = \Delta_{\max}. \tag{5.27}$$

5.1.3 Quench setup and initial conditions

In a quantum quench setup we prepare the system in a ground state at a certain detuning ω_i, i.e. the initial state is

$$\begin{aligned} s^-_{\mathbf{p}}(t=0) &= \frac{\Delta_{0i}}{2E(\varepsilon_{\mathbf{p}};\Delta_{0i},\mu_i)}, \\ s^z_{\mathbf{p}}(t=0) &= -\frac{\varepsilon_{\mathbf{p}}-\mu_i}{2E(\varepsilon_{\mathbf{p}};\Delta_{0i},\mu_i)}, \end{aligned} \tag{5.28}$$

where Δ_{0i}, μ_i are the ground state values determined by Eqs. (5.25) and (5.26) with $\omega = \omega_i$. We then quench the detuning $\omega_i \to \omega_f$ and evolve the system with the two-channel Hamiltonian (5.9) starting from the initial state (5.28) at $t = 0$.

The state of the system is fully determined by the many-body wavefunction, which in the mean field treatment is at all times a product state of the form

$$|\Psi(t)\rangle = |\psi(t)\rangle \otimes \left(\hat{b}^\dagger\right)^{n(t)}|0\rangle, \tag{5.29}$$

where $n(t) = |b(t)|^2$ and $|\psi(t)\rangle$ is the fermionic part of the wave function:

$$|\psi(t)\rangle = \prod_{\mathbf{p}} \left[\overline{u}_{\mathbf{p}}(t) + \overline{v}_{\mathbf{p}}(t)\hat{a}^\dagger_{\mathbf{p}\uparrow}\hat{a}^\dagger_{-\mathbf{p}\downarrow}\right]|0\rangle. \tag{5.30}$$

Bogoliubov amplitudes $u_{\mathbf{p}}(t), v_{\mathbf{p}}(t)$ obey the Bogoliubov de Gennes (BdG) equations

$$i\frac{\partial}{\partial t}\begin{pmatrix} u_{\mathbf{p}}(t) \\ v_{\mathbf{p}}(t)\end{pmatrix} = \begin{pmatrix} \epsilon_{\mathbf{p}} & \Delta(t) \\ \bar{\Delta}(t) & -\epsilon_{\mathbf{p}}\end{pmatrix}\begin{pmatrix} u_{\mathbf{p}}(t) \\ v_{\mathbf{p}}(t)\end{pmatrix}, \tag{5.31}$$

with the normalization condition $|u_{\mathbf{p}}|^2 + |v_{\mathbf{p}}|^2 = 1$. Apart from an overall time-dependent phase (which is important for certain observables), these equations are equivalent to the classical spin equations of motion (5.8) and spins are related to the amplitudes as

$$\frac{s^-_{\mathbf{p}}}{s_{\mathbf{p}}} = 2u_{\mathbf{p}}\overline{v}_{\mathbf{p}}, \quad \frac{s^z_{\mathbf{p}}}{s_{\mathbf{p}}} = |v_{\mathbf{p}}|^2 - |u_{\mathbf{p}}|^2, \tag{5.32}$$

where $s_{\mathbf{p}}$ is the length of the spin. For quench initial conditions $s_{\mathbf{p}} = 1/2$, as explained below Eq. (5.16).

Each quench is uniquely characterized by three parameters – the resonance width $\gamma = g^2\nu_F$, the initial ω_i and final ω_f values of the detuning in units of the Fermi energy. Indeed, ω_i and γ determine Δ_{0i} and μ_i and thus the initial condition, while the equations of motion (5.7) in the thermodynamic limit depend only on ω_f and γ. To see the latter, note that model parameters enter the equation of motion for spin $\vec{s}_{\mathbf{p}} \equiv \vec{s}(\varepsilon_{\mathbf{p}})$ only through $\Delta = -gb$, while the equation of motion for the bosonic field b can be equivalently written as

$$\dot{\Delta} = -i\omega_f\Delta + i\gamma\int_0^\infty s^-(\varepsilon)f(\varepsilon)d\varepsilon. \tag{5.33}$$

Instead of ω_i, ω_f we find it more convenient to characterize the quench by Δ_{0i}, Δ_{0f} – the ground state gaps corresponding to these values of the detuning. As discussed below Eq. (5.26), for a given γ, the detuning ω uniquely determines Δ_0 and vice versa. Note that Δ_{0f} has nothing to do with the time-dependent gap function $\Delta(t)$ and in particular with the large time asymptote $\Delta(t \to \infty)$. Whenever $\Delta(t)$ goes to a constant at large times, we denote this constant Δ_∞.

5.1.4 Main results

Our main result is a complete description of the long time dynamics of two and one channel models (5.9) and (5.11) in two and three spatial dimensions following a quench of the detuning $\omega_i \to \omega_f$ (coupling $\lambda_i \to \lambda_f$ in the one channel model) in the thermodynamic limit. A key effect that makes such a description possible is a drastic reduction in the number of effective degrees of freedom as $t \to \infty$. It turns out that the large time dynamics can be expressed in terms of just a few new collective spins plus the oscillator in the two channel case that are governed by the same Hamiltonians (5.9) and (5.11) only with new effective parameters replacing $\varepsilon_{\mathbf{p}}$ and ω. The number of collective spins is $m = 0, 1$ or 2 and $m = -1, 0$ or 2 for one and two channel models, respectively, depending on the quench. The difference is due to the presence of the oscillator degree of freedom in the latter case. For example, $m = -1$ means that the effective large time Hamiltonian $H_{\rm red}$ not only has no spins, but also the oscillator b is absent, i.e. $H_{\rm red} = 0$. This reduction effect combined with integrability of classical Hamiltonians (5.9) and (5.11) allows us to determine the state of the system (its many-body wave function) at $t \to \infty$. We explain this method in detail in Sect. 5.2. This subsection provides a summary of main results obtained with the help of this method.

In Sects. 5.3 and 5.4, we construct exact quench phase diagrams shown in Figs. 5.2 - 5.5. Depending on the values of ω_i and ω_f either system reaches one of three distinct steady states labeled by I, II (including subregion II') and III that can be thought about as nonequilibrium phases with second order phase transition lines between them ($t \to \infty$ limit of the order parameter $\Delta(t)$ is continuous along lines separating different regions). These steady states correspond to $m = 0, 1$ or 2 collective spins, respectively, for one channel model and to $m = -1, 0$ or 2 in the case of two channels.

Each point in the quench phase diagrams represents a particular quench specified by a pair of values $(\Delta_{0i}, \Delta_{0f})$. Here Δ_0 is the gap that the system would have in the ground state at detuning ω, which is a known function of ω. Values Δ_{0i} and Δ_{0f} – ground state gaps for $\omega = \omega_i$ and ω_f, respectively – uniquely determine ω_i and ω_f at fixed resonance width γ. Note that Δ_{0f} is *not* the magnitude of the actual steady state gap function $|\Delta(t)|$. Each quench $\omega_i \to \omega_f$ (or $\lambda_i \to \lambda_f$) therefore maps to a single point $(\Delta_{0i}, \Delta_{0f})$ and vise versa.

Steady states I, II, and III reached by the system at $t \to \infty$ can be described in terms of the superfluid order parameter $\Delta(t)$. In region I of phase diagrams in Figs. 5.2 - 5.5 the gap function vanishes at large times, $\Delta(t) \to 0$, see Fig. 5.6.

In region II (including subregion II') the magnitude of the order parameter asymptotes to a nonzero constant Δ_∞ as illustrated in Fig. 5.7,

$$\Delta(t) \to \Delta_\infty e^{-2i\mu_\infty t - 2i\varphi}, \tag{5.34}$$

where $\Delta_\infty, \mu_\infty$ are functions of ω_i, ω_f (or, equivalently, of Δ_{0i} and Δ_{0f}), and γ to be determined below, and φ is a contstant phase. Plots of Δ_∞ and μ_∞ as functions of Δ_{0f} for fixed Δ_{0i} are shown in Figs. 5.9, 5.18, and 5.19. The quantity μ_∞ plays the role of the out-of-equilibrium chemical potential. Subregions II and II' of region II correspond to $\mu_\infty > 0$ and $\mu_\infty < 0$, respectively.

In region III of quench phase diagrams the amplitude of the order parameter oscillates persistently at large times as shown in Fig. 5.8,

$$\Delta(t) \to \sqrt{\Lambda^2(t) + h_1} e^{-i\Phi(t)}, \tag{5.35}$$

where

$$\Lambda(t) = \Delta_+ \mathrm{dn}\left[\Delta_+(t - t_0), k'\right], \quad k' = \frac{\Delta_-}{\Delta_+}, \tag{5.36}$$

dn is the Jacobi elliptic function and t_0 is an integration constant. The magnitude of the order parameter oscillates periodically between $\Delta_b = (\Delta_-^2 + h_1)^{1/2}$ and $\Delta_a = (\Delta_+^2 + h_1)^{1/2}$. The phase contains linear and periodic parts[not(a)]

$$\Phi(t) = 2\mu t - \int \frac{\kappa dt}{\Lambda^2(t) + h_1}. \tag{5.37}$$

Constants $h_1, \Delta_+, \Delta_-, \mu$, and κ are known functions of Δ_{0i}, Δ_{0f} (or ω_i, ω_f), and γ to be specified below, see also Figs. 5.9 and 5.10 and refer to Sect. 5.2.4 for more information about the periodic solution.

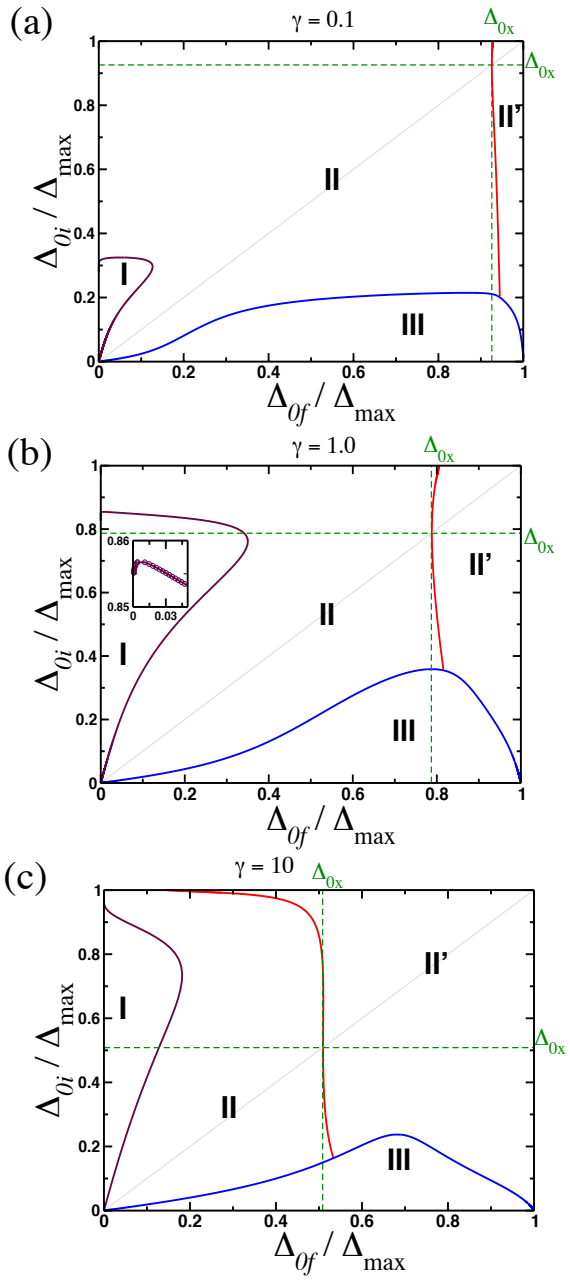


Figure 5.2: Detuning quench phase diagrams for two-channel model (5.1) in 2d for an assortment of resonance widths γ. Each point represents a single quench labeled by Δ_{0i} (vertical axis) and Δ_{0f} (horizonal axis) – pairing gaps the system would have in the ground state for initial and final detunings. At large times the system ends up in one of three steady states shown as regions I, II (including II'), and III. For quenches in region I the order parameter vanishes, $\Delta(t) \to 0$. In II $\Delta(t) \to \Delta_\infty e^{-2i\mu_\infty t - 2i\varphi}$ and in III $|\Delta(t)|$ oscillates persistently. Subregions II and II' differ in the sign of μ_∞ (out of equilibrium analog of the chemical potential): $\mu_\infty > 0$ in II and $\mu_\infty < 0$ in II'. The diagonal, $\Delta_{0i} = \Delta_{0f}$, is the no quench line. To the left of it are strong to weak coupling quenches, to the right – weak to strong. $\Delta_{\max} = \varepsilon_F\sqrt{\gamma}$ in 2d is the maximum possible ground state gap and $\Delta_{0\times}$ is the ground state gap corresponding to zero chemical potential, i.e. $\Delta_{0\times}$ is given by Eq. (5.25) for $\mu = 0$.

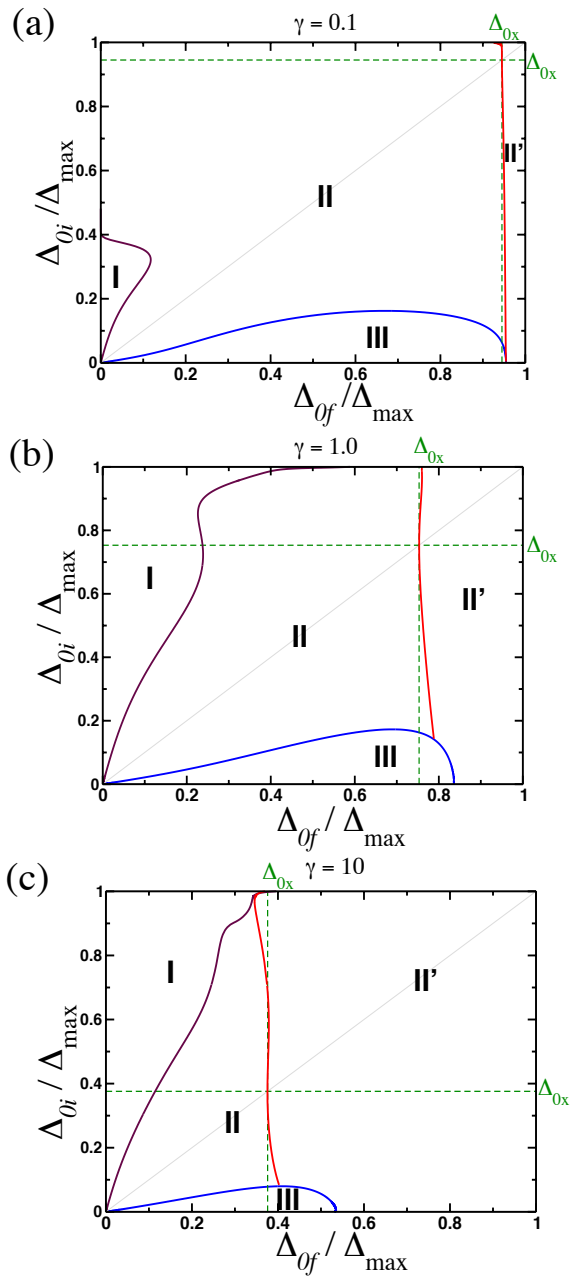


Figure 5.3: Same as Fig. 5.2 but in three spatial dimensions.

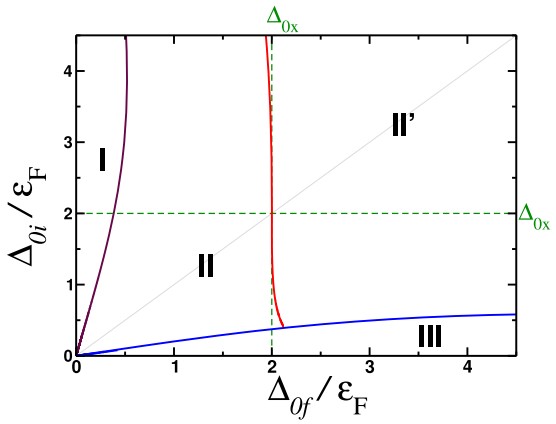


Figure 5.4: Interaction (λ) quench phase diagram for one-channel model (5.11) in two dimensions. Otherwise same as Fig. 5.2

.

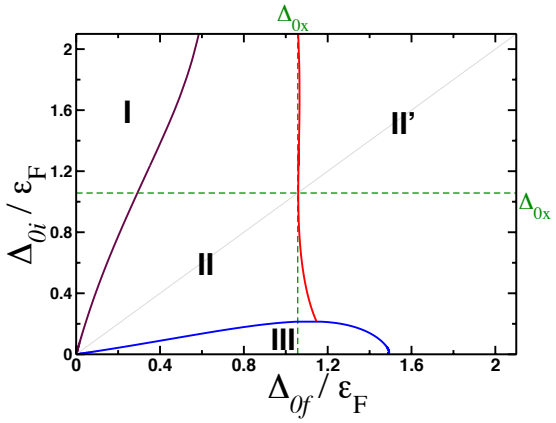


Figure 5.5: Interaction quench phase diagram for one-channel model (5.11) in 3d. Otherwise same as Fig. 5.2. Consider e.g. quenches from fixed infinitesimal coupling λ_i (small Δ_{0i}) to various final couplings λ_f. Increasing λ_f (Δ_{0f}) we move through gapless (I), gapped (II), then oscillating (III) steady states. As λ_f increases further oscillations disappear and we again end up in a steady state characterized by constant asymptotic $|\Delta(t)|$ (II').

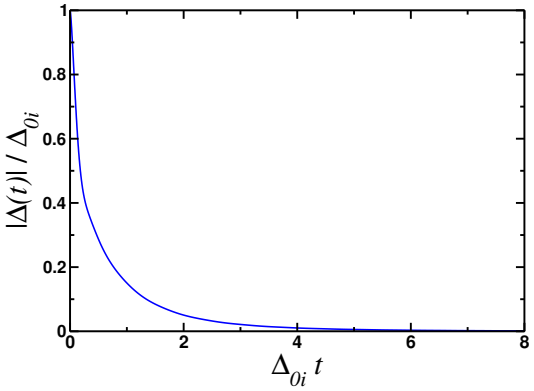


Figure 5.6: $|\Delta(t)|$ in region I for 3d two-channel model, $\gamma = 1$, obtained from numerical evolution of $N = 5024$ spins following a detuning quench $\omega_i \to \omega_f$. Here $\Delta_{0i} = 0.27\Delta_{\max}$, $\Delta_{0f} = 4.30 \times 10^{-2}\Delta_{\max}$ [cf. Fig. 5.3(b)]. From these two values all other parameters obtain, e.g. $\mu_i = 0.90\varepsilon_F$, and $\omega_f - \omega_i = 1.97\varepsilon_F$.

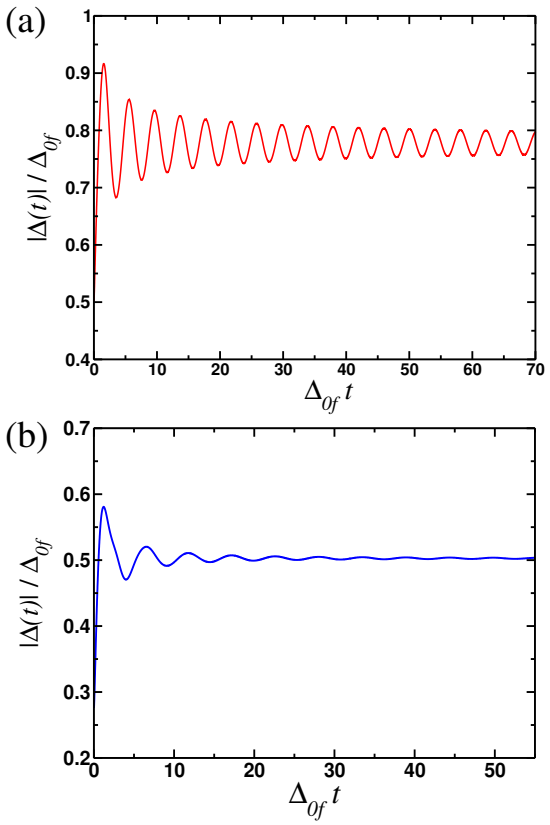


Figure 5.7: $|\Delta(t)|$ in regions II (top) and II' (bottom) for 3d two-channel model, $\gamma = 1$, obtained from numerical evolution of $N = 5024$ spins after quenching the detuning ω. $\Delta_{0i} = 0.27\Delta_{\max}, \mu_i = 0.90\varepsilon_F$ in both panels, same as in Fig. 5.6. The final detuning corresponds to: (a) $\Delta_{0f} = 0.56\Delta_{\max} = 2.07\Delta_{0i}$ and (b) $\Delta_{0f} = 0.97\Delta_{\max} = 3.59\Delta_{0i}$. See also Fig. 5.3(b).

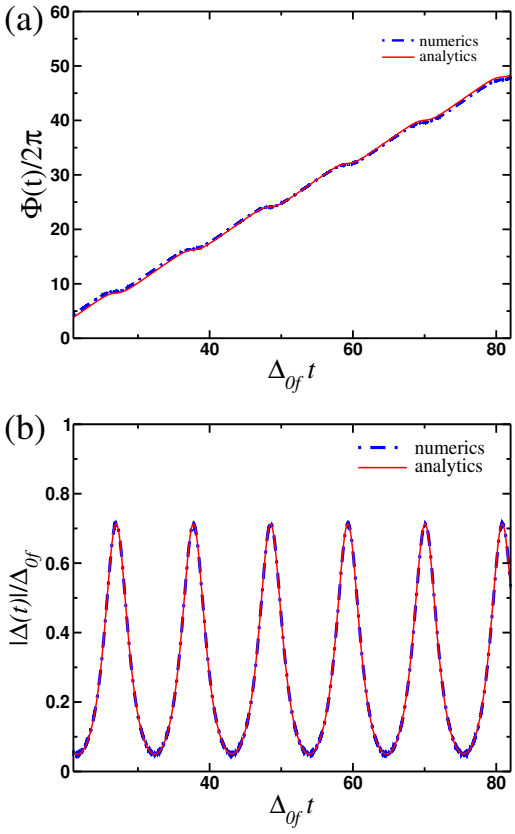


Figure 5.8: Amplitude (Higgs mode) and phase $\Phi(t)$ of the order parameter $\Delta(t)$ in region III of Fig. 5.3(c) after detuning quench from deep BCS to BEC in 3d two-channel model for $\gamma = 10$. Numerical evolution with 5024 spins vs. Eqs. (5.35) and (5.37). $\Delta_{0i} = 3.20 \times 10^{-3}\Delta_{\max}$, $\Delta_{0f} = 0.45\Delta_{\max}$, and $\delta\omega = -5.86\gamma$.

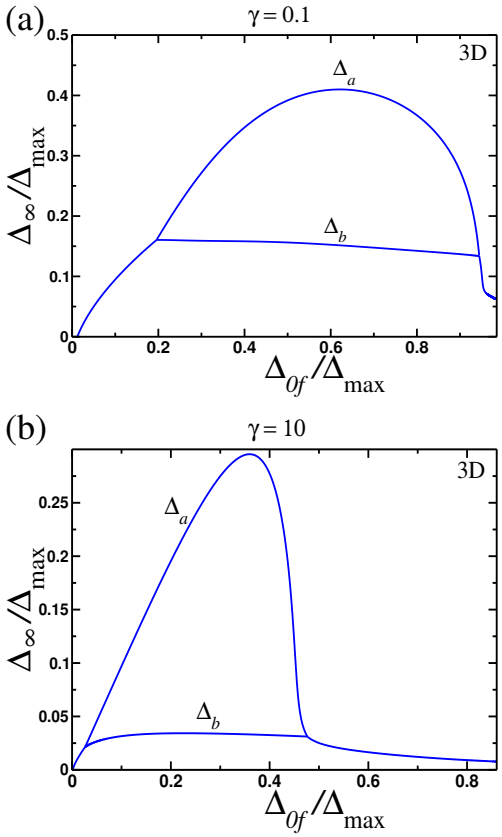


Figure 5.9: Limiting values of $|\Delta(t)|$ for 3d two-channel model at large times after a detuning quench as functions of Δ_{0f} (or, equivalently, of final detuning ω_f) at fixed small $\Delta_{0i} = 0.05\Delta_{\max}$ (fixed initial detuning deep in the BCS regime). This corresponds to moving along a horizontal line (not shown) in Fig. 5.3(a) and (c) going through regions I where $|\Delta(t)| \to 0$, II where $|\Delta(t)| \to \Delta_\infty > 0$, III where $|\Delta(t)|$ oscillates periodically between Δ_a and Δ_b, and into region II' where again $|\Delta(t)| \to \Delta_\infty > 0$. Note that persistent oscillations appear and then disappear again as we decrease $\omega_f - \omega_i$ (i.e. increase Δ_{0f} at fixed Δ_{0i}). The same behavior is observed in the 3d one-channel model, see Fig. 5.5.

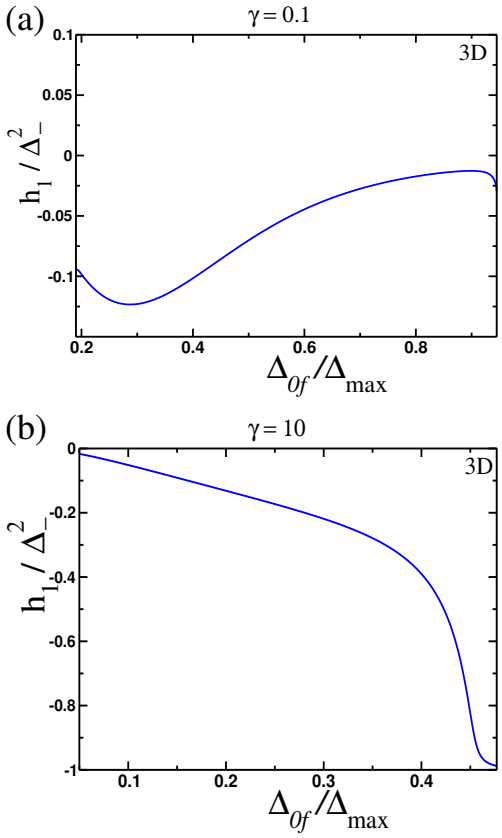


Figure 5.10: Parameter h_1 in Eq. (5.35) for asymptotic $|\Delta(t)|$ in phase III as a function of Δ_{0f} at fixed small $\Delta_{0i} = 0.05\Delta_{\max}$, same as in Fig. 5.9. For quenches within weak coupling limit $h_1 = 0$, so nonzero h_1 quantifies deviations from this limit. Note that one must have $h_1 \geq -\Delta_-^2$, so that the expression under the square root in Eq. (5.35) is nonnegative.

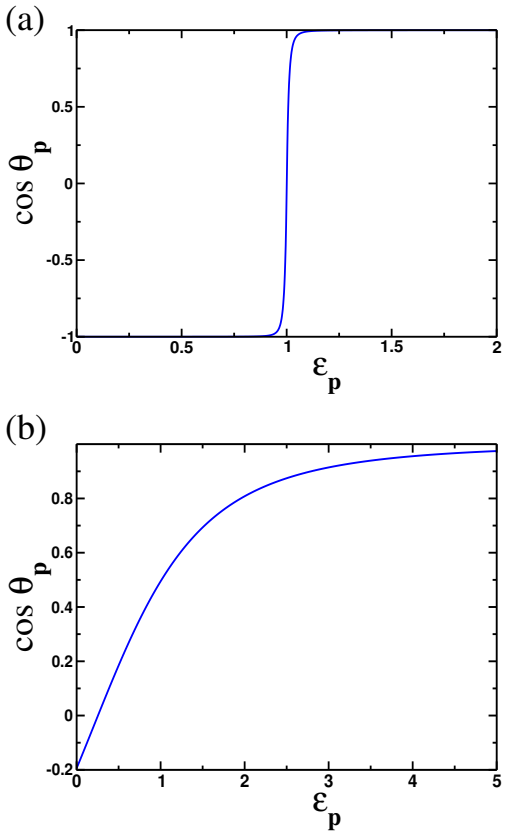


Figure 5.11: Spin distribution $\cos\theta_{\mathbf{p}}$ as a function of $\varepsilon_{\mathbf{p}}$ (in units of Fermi energy) at large times after the quench in 3d two channel model. In phases I and II, $-\cos\theta_{\mathbf{p}}/2$ is the projection of the spin $\vec{s}_{\mathbf{p}}$ onto its effective magnetic field (z-axis in phase I) around which it precesses. In equilibrium $\cos\theta_{\mathbf{p}} = \pm 1$ (1 in the ground state) for all momenta and in phase I $\cos\theta_{\mathbf{p}} = -1$ and 1 correspond to doubly occupied and unoccupied states, respectively. Quench parameters are $\gamma = 1$ and: (a) $\Delta_{0i} = 0.05\Delta_{\max}, \Delta_{0f} = 0.002\Delta_{\max}$ (BCS to deep BCS quench in phase I); (b) $\Delta_{0i} = 0.78\Delta_{\max}, \Delta_{0f} = 0.001\Delta_{\max}$ (BEC to deep BCS quench in phase I). In both cases $\mu_\infty \approx \varepsilon_F$. Note the Fermi-like shape of the distribution function in (a). Note that $\cos\theta_{\mathbf{p}} \to 1$ as $\varepsilon_{\mathbf{p}} \to \infty$, as it should, indicating that states at very high energies are empty.

Previous studies of the BCS dynamics[Volkov and Kogan(1973), Barankov et al.(2004), 19, Barankov and Levitov(2006), Yuzbashyan and Dzero(2006), Dzero et al.(2007)] were performed in the weak coupling regime when both Δ_{0i} and Δ_{0f} are much smaller than a characteristic high energy scale (Fermi energy for cold gases and Debye energy for conventional superconductors). This limit corresponds to an infinitesimal vicinity of the origin $\Delta_{0i} = \Delta_{0f} = 0$ in our quench phase diagrams in Figs. 5.2 - 5.5 . The weak coupling limit is universal in that it is independent of the resonance width and dimensionality and thus is the same in all diagrams. Critical lines separating regions I and II, and II and III are straight lines in this case coming out of the origin with slopes

$$\frac{\Delta_{0i}}{\Delta_{0f}} = e^{\pm\pi/2}. \tag{5.38}$$

Further, $h_1 = 0$ in Eq. (5.35) and Δ_∞, $\Delta_\pm$ take a simpler form given by Eqs. (5.150) – (5.152), and (5.154).

There are several qualitatively new effects beyond the weak coupling regime. At smaller resonance width $\gamma < \gamma_c = 16/\pi^2$, gapless region I terminates below $\Delta_{\max}$ at $\Delta_{0i} = \gamma\pi/4$ along the vertical axis in 2d. This means that as initial coupling gets stronger (Δ_{0i} increases), even quenches to arbitrarily weak final coupling (small Δ_{0f}) do not result in vanishing $\Delta(t)$ at large times in contrast to the weak coupling regime where quenches with sufficiently large Δ_{0f}/Δ_{0i}

always do. The I-II critical line also displays an interesting backwards bending behavior for $\gamma < \gamma_c = 16/\pi^2$, see the inset in Fig. 5.2(b) and Eqs. (5.161) and (5.157).

Region III of persistent oscillations terminates at a threshold value of $\Delta_{0f} < \Delta_{\max}$ in 3d, see Figs. 5.3 and 5.5. This means that even quenches from an infinitesimally weak initial coupling ($\lambda_i = 0+$ in the one channel model, which corresponds to a vicinity of the normal state) to final couplings stronger then a certain threshold value produce no oscillations and $|\Delta(t)|$ instead goes to a constant. At finite but small initial gap Δ_{0i} (e.g. along the dashed line in Fig. 5.3) there is a reentrant behavior in both 2d and 3d as the final coupling (Δ_{0f}) increases when first there are no oscillations, then they appear, and then disappear again. The threshold value of Δ_{0f} where the critical line separating regions II and III terminates is given by Eq. (5.170) (plotted as a function of the resonance width in Fig. 5.22) and Eq. (5.193) for one and two channel models, respectively. For more details about quench diagrams, such as the shape of the critical lines, various thresholds and termination points, values of parameters (e. g. $\Delta_\infty, \mu_\infty, \Delta_+$, and Δ_-) characterizing asymptotic $\Delta(t)$, see Sects. 5.3 and 5.4.

The large time asymptote of $\Delta(t)$ does not fully specify the steady state. One also needs to know the Bogoliubov amplitudes $u_{\mathbf{p}}(t \to \infty), v_{\mathbf{p}}(t \to \infty)$. We calculate them in Sect. 5.2.4 in all three steady states. In terms of spin vectors, this translates into steady state spin distribution. Even in regions I and II where $|\Delta(t)|$ goes to a constant, the steady state of the system is far from any equilibrium state. Time-independent $|\Delta(t)|$ means that in a frame that rotates around z-axis with frequency $2\mu_\infty$ the magnetic field $\vec{B}_{\mathbf{p}}$ that acts on spin $\vec{s}_{\mathbf{p}}$ in Eq. (5.7) is constant. In equilibrium $\vec{s}_{\mathbf{p}}$ aligns with $\vec{B}_{\mathbf{p}}$ or $-\vec{B}_{\mathbf{p}}$ (ground state). In steady states I and II it instead rotates around $\vec{B}_{\mathbf{p}}$ making a constant angle with it. Let $\theta_{\mathbf{p}}$ be the angle between $\vec{s}_{\mathbf{p}}$ and $-\vec{B}_{\mathbf{p}}$ (negative z-axis in steady state I), so that in the ground state $\theta_{\mathbf{p}} = 0$. Out of equilibrium $\theta_{\mathbf{p}}$ determines the steady state spin distribution function and is given by Eq. (5.134). This expression for $\cos\theta(\varepsilon_{\mathbf{p}})$ applies in all three steady states, but its interpretation in region III is slightly different and will be explained below. A plot of the distribution function $\cos\theta_{\mathbf{p}}$ is shown in Fig. 5.11. We explore the asymptotic states produced by detuning or interaction quenches in detail in Sect. 5.2.4. In Sect. 5.7 we provide further insight into their physical nature and discuss their experimental signatures.

We perform detailed analysis of linearized equations of motion that goes much beyond previous work even in the weak coupling regime and yields a range of new results. Small quenches of the detuning correspond to a small neighborhood of the diagonal in quench diagrams in Figs. 5.2 - 5.5, i.e. they fall within region II where $|\Delta(t)| \to \Delta_\infty$ and Eq. (5.34) applies. We show that within linear approximation $\Delta_\infty = \Delta_{0f}$ and $\mu_\infty = \mu_f$, i.e. there are no corrections to these equations linear in the change of detuning or, equivalently, in $\delta\Delta_0 = \Delta_{0f} - \Delta_{0i}$. This is in fact a general result that has been overlooked by previous work – to first order in deviations from the ground state $\Delta(t)$ always asymptotes to its ground state form for the Hamiltonian with which the system evolves at $t > 0$. Note however that when quadratic correction is taken into account one gets $\Delta_\infty < \Delta_{0f}$. For example, in the weak coupling regime we find

$$\Delta_\infty = \Delta_{0f} - \frac{(\delta\Delta_0)^2}{6\Delta_{0f}}. \tag{5.39}$$

We obtain an exact expression for $\Delta(t)$, Eqs. (5.231), (5.232), and (5.233), valid at all times and arbitrary coupling strength for both one and two channel models. In weak coupling regime this expression simplifies so that

$$|\Delta(t)| = \Delta_{0f} - 2\delta\Delta_0 \int_0^\infty \frac{dx}{\pi} \frac{\cos\left[2\Delta_0 t \cosh(\pi x/2)\right]}{1+x^2}, \tag{5.40}$$

From here short and long times asymptotes follow. At short times the order parameter amplitude rises or falls sharply as

$$|\Delta(t)| = \Delta_{0i} + \frac{\delta\Delta_0}{|\ln(\Delta_0 t)|}. \tag{5.41}$$

And the long time behavior in the weak coupling limit is

$$|\Delta(t)| = \Delta_{0f} - \frac{2\delta\Delta_0}{\pi^{3/2}} \frac{\cos(2\Delta_0 t + \pi/4)}{\sqrt{\Delta_0 t}}. \tag{5.42}$$

At stronger coupling in region II (but not II') the long time asymptote is still given by Eq. (5.42), only the coefficient in front of the second term on the right hand side is more involved.

Regions II and II' differ in the sign of the phase frequency μ_∞, $\mu_\infty > 0$ in II and $\mu_\infty < 0$ in II'. We will see below that frequency (Fourier) spectrum of quench dynamics in regions II and II' is $E_\infty(\varepsilon_{\mathbf{p}}) = \sqrt{(\varepsilon_{\mathbf{p}} - \mu_\infty)^2 + \Delta_\infty^2}$, so that the Fourier transform of a dynamical quantity reads $\int_0^\infty A(\varepsilon) e^{-2iE_\infty(\varepsilon)t} d\varepsilon$. For $\mu_\infty > 0$ the phase has a stationary point on the integration path at $\varepsilon = \mu_\infty$, while for $\mu_\infty < 0$ it is absent. As a result, the long time behavior in three dimensions in region II' changes

$$|\Delta(t)| = \Delta_{0f} \left(1 - c\frac{\delta\omega}{\gamma} \frac{\cos(2E_{\min} t + \pi/4)}{(2|\mu|t)^{3/2}}\right), \tag{5.43}$$

where $E_{\min} = \sqrt{\mu^2 + \Delta_0^2}$, c is of order one, and $\delta\omega = \omega_f - \omega_i$. The same expression holds for the one channel model after a replacement $\delta\omega/\gamma \to 1/\lambda_f - 1/\lambda_i$. Oscillation frequency $E_{\min}$ and $1/t^{3/2}$ decay are in agreement with Ref. [36] and reflect the fact that in the absence of a stationary point, the long time asymptote is dominated by the end point of integration at $\varepsilon = 0$, $E(0) = E_{\min}$, and the density of states in 3d vanishes as $\sqrt{\varepsilon}$ at small ε.

In two dimensions linear analysis yields a different approach to the asymptote in region II'

$$|\Delta(t)| = \Delta_{0f} \left(1 - \frac{\delta\omega}{\gamma} \frac{\sin(2E_{\min} t)}{|\mu| t \ln^2 t}\right), \tag{5.44}$$

because of a constant density of states and $\ln\varepsilon$ divergence of the Fourier amplitude of $|\Delta(t)|$ at small ε (see below). We also determine the time-dependent phase of the order parameter $\Phi(t)$ in all cases corresponding to Eqs. (5.40) – (5.44), asymptotes of individual spins $\vec{s}_{\mathbf{p}}(t)$ as $t \to \infty$, and many other new results for the linearized dynamics in Sect. 5.5.

Finally, we extend some of the above results for the long time behavior of $|\Delta(t)|$ to the nonlinear regime, though unlike the linear analysis these results are not rigorous. In region II

$$|\Delta(t)| = \Delta_\infty + c' \frac{\cos(2\Delta_\infty t + \pi/4)}{\sqrt{\Delta_\infty t}}, \tag{5.45}$$

where c' is a dimensionless coefficient. This answer holds for both one and two channel models in either dimension.

For region II' we argue that the answer depends on dimensionality similarly to the linear analysis and

$$|\Delta(t)| = \Delta_\infty \left(1 - c_1 \frac{\sin(2E_\infty^{\min} t)}{t \ln^2 t}\right) \quad \text{in 2d}, \tag{5.46}$$

$$|\Delta(t)| = \Delta_\infty \left(1 - c_2 \frac{\cos(2E_\infty^{\min} t + \pi/4)}{t^{3/2}}\right) \quad \text{in 3d}, \tag{5.47}$$

where $E_\infty^{\min} = \sqrt{\mu_\infty^2 + \Delta_\infty^2}$.

The approach to the gapless steady state (region I) is expected to be

$$|\Delta(t)| = \frac{c_4}{t \ln^r t} \quad \text{in 2d,} \tag{5.48}$$

where $r = 1$ or $r = 2$, and

$$|\Delta(t)| = \frac{c_3}{t^{3/2}} \quad \text{in 3d.} \tag{5.49}$$

We discuss these nonlinear large time asymptotes in more detail in Sect. 5.6.

5.2 Method

Here we describe a method that allows one to determine the asymptotic state of the system at long times. Both the quantum (5.5) and classical (5.9) two-channel models are integrable meaning that there are as many nontrivial conservation laws as there are degrees of freedom. There is an exact Bethe Ansatz type solution for the quantum spectrum [Gaudin(1983)]. In the classical case integrability implies a formal inexplicit solution of the equations of motion in terms of certain multivariable special (hyperelliptic) functions[Yuzbashyan et al.(2005c)] that can be helpful for understanding certain general features of the dynamics. Evaluating specific dynamical quantities of interest for realistic initial conditions with this solution is however roughly equivalent to just solving the equations of motion numerically. But the latter could be as well done directly without the formal exact solution. This is a typical situation in the standard theory of nonlinear integrable systems.

Fortunately, it was realized that at least for the BCS type models the large time dynamics dramatically simplifies in the thermodynamic limit, so that the number of evolving degrees of freedom effectively drops to just a few spins. Building on this insight, Yuzbashyan et. al. [19] were able to develop a method that goes beyond the standard theory and explicitly predicts the long time dynamics in the thermodynamic limit.

The main idea of this method is as follows. First, we construct a special class of *reduced* solutions of the classical equations of motion for the two-channel model such that the dynamics reduces to that of just few effective spins. Then, we choose a suitable reduced solution and fix its parameters so that its integrals of motion match those for a given quench in the thermodynamic limit. Reduced solutions have only few additional arbitrary constants and cannot generally satisfy all of the quench initial conditions (5.28). There are $2N + 2$ initial conditions (two angles per spin plus two initial conditions for the oscillator mode b) and only $N + 1$ correspond to the integrals of motion.

Next, exploiting the fact that for fixed $\Delta(t)$ BdG equations (5.31) are linear in the amplitudes $u_{\mathbf{p}}$ and $v_{\mathbf{p}}$, we derive the most general $t \to \infty$ asymptotic solution that has the same $\Delta(t)$ as the reduced one. It has the same integrals as the quench dynamics by construction and, in addition, $N + 1$ arbitrary independent constants to match the remaining initial conditions. We *conjecture* that so constructed asymptotic solution is the true large time asymptote of the actual quench dynamics. To verify this *few spin conjecture* it is sufficient to show that the large time asymptote of the actual $\Delta(t)$ matches that of the reduced (and therefore general asymptotic) solution. We do so numerically in the nonlinear case and analytically for infinitesimal quenches when the dynamics can be linearized.

We consider the two channel model in this and the following sections and then obtain similar results for the one channel (BCS) model in Sect. 5.4 by taking the broad resonance, $\gamma \to \infty$, limit.

5.2.1 Integrability and Lax vector construction

An object called Lax vector plays a key role in our approach. It encodes all the information about the integrals of motion and turns out to be especially useful in analyzing the quench

dynamics in the thermodynamic limit.

(how to guess about the Lax vector???)

The Lax vector is defined as

$$\vec{L}(u) = \sum_{\mathbf{p}} \frac{\vec{s}_{\mathbf{p}}}{u - \varepsilon_{\mathbf{p}}} - \frac{(\omega - 2\mu)}{g^2}\hat{\mathbf{z}} + \frac{2}{g^2}\left[(u-\mu)\hat{\mathbf{z}} - \vec{\Delta}\right], \tag{5.50}$$

where u is an auxiliary complex variable and $\vec{\Delta} \equiv \Delta_x \hat{\mathbf{x}} + \Delta_y \hat{\mathbf{y}}$. Poisson brackets of components of $\vec{L}(u)$ satisfy the following Gaudin algebra:

$$\left\{L^a(u), L^b(v)\right\} = \varepsilon_{abc}\frac{L^c(u) - L^c(v)}{u - v}. \tag{5.51}$$

(check. maybe it is not that hard?)

This implies an important equality

$$\left\{\vec{L}^2(u), \vec{L}^2(v)\right\} = 0. \tag{5.52}$$

Explicit evaluation of $\vec{L}^2(u)$ yields

$$\vec{L}^2(u) = \frac{(2u - \omega)}{g^4} + \frac{4\mathcal{H}_b}{\omega g^2} + \sum_{\mathbf{p}}\left(\frac{2\mathcal{H}_{\mathbf{p}}}{g^2(u - \varepsilon_{\mathbf{p}})} + \frac{s^2_{\mathbf{p}}}{(u - \varepsilon_{\mathbf{p}})^2}\right), \tag{5.53}$$

(check also) where

$$\begin{aligned} \mathcal{H}_{\mathbf{p}} &= g^2 \sum_{\mathbf{q}\neq\mathbf{p}} \frac{\vec{s}_{\mathbf{p}} \cdot \vec{s}_{\mathbf{q}}}{(\varepsilon_{\mathbf{p}} - \varepsilon_{\mathbf{q}})} + (2\epsilon_{\mathbf{p}} - \omega)s^z_{\mathbf{p}} + g\left(\bar{b}s^-_{\mathbf{p}} + bs^+_{\mathbf{p}}\right), \\ \mathcal{H}_b &= \bar{b}b + \sum_{\mathbf{p}} s^z_{\mathbf{p}}. \end{aligned} \tag{5.54}$$

It follows from Eq. (5.52) that these spin Hamiltonians mutually Poisson commute (anticommute?), i.e.

$$\{\mathcal{H}_{\mathbf{p}}, \mathcal{H}_{\mathbf{p}'}\} = \{\mathcal{H}_{\mathbf{p}}, \mathcal{H}_b\} = 0. \tag{5.55}$$

Moreover, the two-channel Hamiltonian (5.9) is

$$H_{2\mathrm{ch}} = \omega\mathcal{H}_b + \sum_{\mathbf{p}} \mathcal{H}_{\mathbf{p}}. \tag{5.56}$$

This implies that $\mathcal{H}_{\mathbf{p}}$ and $\mathcal{H}_b$ are conserved by $H_{2\mathrm{ch}}$ and establishes the integrability of the two-channel Hamiltonian. Note that $\vec{L}^2(u)$ is also conserved for any value of u and serves as a generator of the integrals of motion for the two-channel model. The same construction works in the quantum case as well; one only needs to promote classical dynamical variables to corresponding quantum operators and replace Poisson brackets with commutators.

Equations of motion can be conveniently and compactly written in terms of the Lax vector as

$$\dot{\vec{L}} = \left(-2\vec{\Delta} + 2u\hat{\mathbf{z}}\right) \times \vec{L}. \tag{5.57}$$

Comparing the residues at the poles at both sides of this equation, we see that it is equivalent the equations of motion for spins (5.8).

The square of the Lax vector is of the form

$$\vec{L}^2(u) = \frac{Q_{2N+2}(u)}{g^4 \prod_{\varepsilon_{\mathbf{p}}}(u - \varepsilon_{\mathbf{p}})^2}, \tag{5.58}$$

where N is the total number of distinct single particle energies $\varepsilon_{\mathbf{p}}$, the product is similarly over nondegenerate values of $\varepsilon_{\mathbf{p}}$, and $Q_{2N+2}(u)$ is a polynomial in u of degree $2N+2$. The roots of this *spectral* polynomial (or equivalently of $\vec{L}^2(u)$) play an important role in further analysis of the asymptotic behavior. Note that since $\vec{L}^2(u)$ is conserved, so are its roots. They thus constitute a set of integrals of motion alternative to Eq. (5.54). Since $\vec{L}^2(u) \geq 0$ for real u, its roots come in complex conjugate pairs.

5.2.2 Reduced solutions

Let us look for special solutions of equations of motion (5.57) such that the Lax vector factorizes into time-dependent and independent parts

$$\vec{L}^{\mathrm{red}}(u) = \sum_{\mathbf{p}} \frac{\vec{\sigma}_{\mathbf{p}}}{u-\varepsilon_{\mathbf{p}}} - \frac{(\omega-2\mu)}{g^2}\hat{\mathbf{z}} + \frac{2}{g^2}\left[(u-\mu)\hat{\mathbf{z}} - \vec{\Delta}\right] = \left(1 + \sum_{\mathbf{p}} \frac{d_{\mathbf{p}}}{u-\epsilon_{\mathbf{p}}}\right)\vec{L}_m(u), \quad (5.59)$$

where $\vec{\sigma}_{\mathbf{p}}$ (not to be confused with Pauli matrices) denote spins in this solution that can have arbitrary length to distinguish them from spins $\vec{s}_{\mathbf{p}}$ for the quench dynamics that have length $1/2$. Further, $d_{\mathbf{p}}$ are time-independent constants to be determined later and $\vec{L}_m(u)$ is the Lax vector for an effective m-spin system

$$\vec{L}_m(u) = \sum_{j=0}^{m-1} \frac{\vec{t}_j}{u-\eta_j} - \frac{(\omega'-2\mu)}{g^2}\hat{\mathbf{z}} + \frac{2}{g^2}\left[(u-\mu)\hat{\mathbf{z}} - \vec{\Delta}\right]. \quad (5.60)$$

Here $\vec{t}_j$ are new collective spin variables placed at new arbitrary "energy levels" η_j. Note that the bosonic field $\vec{b}$ and therefore $\vec{\Delta}$ are the same in the original and reduced models.

Substituting Eq. (5.59) into the equations of motion (5.57), we see that $\vec{L}_m(u)$ satisfies the same equation of motion. This means that variables $\vec{t}_j$ obey Bloch equations (5.8) with $\varepsilon_{\mathbf{p}} \to \eta_j$ and $\omega \to \omega'$, and are therefore governed by the same Hamiltonian

$$H^{\mathrm{red}}_{\mathrm{2ch}} = \sum_{j=0}^{m-1} 2\eta_j t^z_j + \omega'\bar{b}b + g\sum_{j=0}^{m-1}(\bar{b}t^-_j + bt^+_j). \quad (5.61)$$

We will need at most $m=1$ for analyzing the quench dynamics, so we will be able solve the equations of motions for $\vec{t}_j$ directly.

Matching the residues at $u=\varepsilon_{\mathbf{p}}$ on both sides of Eq. (5.59), we express original spins in terms of $\vec{t}_j$

$$\vec{\sigma}_{\mathbf{p}} = d_{\mathbf{p}}\vec{L}_m(\varepsilon_j), \quad (5.62)$$

Constants $d_{\mathbf{p}}$ are determined from the above equation using $\vec{\sigma}^{\,2}_{\mathbf{p}} = \sigma^2_{\mathbf{p}}$, where $|\sigma_{\mathbf{p}}|$ is the length of spin $\vec{\sigma}_{\mathbf{p}}$. Note that $\sigma_{\mathbf{p}}$ can be of either sign (for future convenience). We have

$$d_{\mathbf{p}} = -\frac{\sigma_{\mathbf{p}}}{\sqrt{\vec{L}^2_m(\varepsilon_{\mathbf{p}})}}. \quad (5.63)$$

It is important to note that $\sigma_{\mathbf{p}}$ are arbitrary constants at this point. We will determine them later so that the integrals of motion for the reduced solution match those for quench dynamics.

To satisfy Eq. (5.59), we also need to match the residues at $u=\eta_k$ and the $u\to\infty$ asymptotic. This leads to the following $m+1$ equations:

$$\begin{aligned} 1 + \sum_{\mathbf{p}} \frac{d_{\mathbf{p}}}{\eta_k - \varepsilon_{\mathbf{p}}} &= 0 \quad k = 0, \ldots, m-1 \\ \omega &= \omega' - 2\sum_{\mathbf{p}} d_{\mathbf{p}}. \end{aligned} \quad (5.64)$$

Equations (5.64) constrain the coefficients of the spectral polynomial

$$Q_{2m+2}(u) = g^4 \vec{L}_m^2(u) \prod_{k=0}^{m-1} (u - \eta_k)^2, \quad m \geq 0 \tag{5.65}$$

of the m-spin system. Indeed, using Eq. (5.63), we can cast these constraints into the following form:

$$\begin{aligned} \sum_{\mathbf{p}} \frac{\sigma_{\mathbf{p}} \varepsilon_{\mathbf{p}}^{r-1}}{\sqrt{Q_{2m+2}(\varepsilon_{\mathbf{p}})}} &= -\frac{\delta_{rm}}{g^2}, \quad r = 1, \ldots, m \\ \omega' = \omega + 2 \sum_{k=0}^{m-1} \eta_k &+ \sum_{\mathbf{p}} \frac{2\sigma_{\mathbf{p}} g^2 \varepsilon_{\mathbf{p}}^m}{\sqrt{Q_{2m+2}(\varepsilon_{\mathbf{p}})}}. \end{aligned} \tag{5.66}$$

Here $m \geq 0$. These equations can be viewed as equations for determining the lengths of the collective spins $\vec{t}_j$.

We thus constructed a class of solutions such that the dynamics reduces to that of a smaller number of spins. These *few spin solutions* however do not match the quench initial conditions, but, as we will see, the long time asymptote of $\Delta(t)$ after the quench coincides with $\Delta(t)$ of an appropriately chosen few spin solution. Specifically, $m = -1, 0$, and 1 are realized depending on the magnitude and the sign of the change in the detuning ω. Let us therefore consider these particular cases.

m=-1 spin solutions

$m = -1$ refers to the case when there are no collective spins and $b = 0$, i.e. the oscillator (which can be viewed as an infinite length limit of a spin) is effectively absent as well. In other words, $H_{\text{red}} = 0$ and $\vec{L}_m(u) = \frac{2u-\omega'}{g^2}\hat{\mathbf{z}}$. Eq. (5.62) then implies that all spins in the reduced solution are along the z-axis pointing in either positive or negative direction. It is convenient to redefine the sign of $\sigma_{\mathbf{p}}$ (only for $m = -1$) so that $\vec{\sigma}_{\mathbf{p}} = -\sigma_{\mathbf{p}}\hat{\mathbf{z}}$. We see directly from the equations of motion (5.8) that this configuration together with $b = 0$ is indeed a solution, a stationary one in the present case.

m=0 spin solutions

In this case the reduced problem consists of a free classical oscillator as there are no collective spins, i.e. $H_{\text{red}} = \omega' \bar{b} b$. Equations of motion reduce to $\dot{b} = -i\omega' b$. Therefore

$$\Delta(t) = -gb = ce^{-2i\mu t}, \tag{5.67}$$

where c is a complex constant and we defined $\mu = \omega'/2$.

Expressions for the original spins follow from the reduced Lax vector

$$\vec{L}_m(u) = -\frac{2}{g^2}\left(\vec{\Delta} - (u - \mu)\hat{z}\right), \tag{5.68}$$

Eqs. (5.62) and (5.63) imply

$$\vec{\sigma}_{\mathbf{p}} = \frac{\sigma_{\mathbf{p}}}{E(\varepsilon_{\mathbf{p}}; \Delta, \mu)}\left(\vec{\Delta} - (\varepsilon_{\mathbf{p}} - \mu)\hat{\mathbf{z}}\right), \tag{5.69}$$

where $E(\varepsilon_{\mathbf{p}}; \Delta, \mu) = \sqrt{(\varepsilon_{\mathbf{p}} - \mu)^2 + |\Delta|^2}$. We see that the ground state (5.15) is a one spin solution with $c = \Delta_0$ and $\sigma_{\mathbf{p}} = 1/2$ (to minimize the energy). Excited states are also one spin solutions with different parameters.

There is only one (last) constraint among Eqs. (5.66) for $m = 0$, which we recognize as a generalization of the gap equation (5.18).

m=1 spin solutions

This example is substantially more involved then the previous two. Now there is one collective spin $\vec{t}$ coupled to an oscillator,

$$H_{\rm red} = 2\eta t^z + \omega' \bar{b} b + g(\bar{b} t^- + b t^+), \tag{5.70}$$

making the dynamics rather nontrivial. Our main goal presently is to derive a differential equation for $|\Delta(t)| = g|b(t)|$ and to relate its coefficients to the spectral polynomial $Q_4(u)$ of the reduced $m = 1$ problem given in general by Eq. (5.65).

$H_{\rm red}$ conserves $\bar{b}b + t^z$. It follows that t^z can be expressed through $|b|^2$ as $t^z = c_1\Omega^2 + c_2$, where $c_{1,2}$ are constants and we introduced a notation

$$\Delta = \Omega e^{-i\Phi}. \tag{5.71}$$

Eq. (5.62) then implies that the z-component of the original spins in the reduced solution can be similarly expressed through $|\Delta|$ as

$$\sigma^z_{\mathbf{p}} = a_{\mathbf{p}}\Omega^2 + b_{\mathbf{p}}. \tag{5.72}$$

Note that constants $a_{\mathbf{p}}$ and $b_{\mathbf{p}}$ are inversely proportional to $\sqrt{\vec{L}^2_m(\varepsilon_{\mathbf{p}})}$ and therefore to $\sqrt{Q_4(\varepsilon_{\mathbf{p}})}$. It turns out that an efficient strategy to derive an equation for Ω and relate its coefficients to those of $Q_4(u)$ is somewhat indirect. First, we use equations of motion for $\vec{\sigma}_{\mathbf{p}}$ together with Eq. (6.3) to obtain an equation for Ω and expressions for $a_{\mathbf{p}}$ and $b_{\mathbf{p}}$. Identifying $\sqrt{Q_4(\varepsilon_{\mathbf{p}})}$ in the latter with the help of Eq. (5.63), we relate the coefficients.

Bloch equations (5.8) for spins in the reduced solution, $\vec{s}^{\,\rm red}_p \equiv \vec{\sigma}_{\mathbf{p}}$, can be written as

$$\dot{\sigma}^z_{\mathbf{p}} = -i(\sigma^-_{\mathbf{p}}\bar{\Delta} - \sigma^+_{\mathbf{p}}\Delta), \quad \dot{\sigma}^-_{\mathbf{p}} = -2i\sigma^z_{\mathbf{p}}\Delta - 2i\varepsilon_{\mathbf{p}}\sigma^-_{\mathbf{p}}. \tag{5.73}$$

Substituting $\sigma^z_{\mathbf{p}}$ from Eq. (6.3) into the first equation, we obtain

$$\sigma^-_{\mathbf{p}} e^{i\Phi} - \sigma^+_{\mathbf{p}} e^{-i\Phi} = 2i a_{\mathbf{p}}\dot{\Omega}. \tag{5.74}$$

Multiplying the second equation in (5.73) by $e^{i\Phi}$ and adding the resulting equation to its complex conjugate, we get

$$\frac{d}{dt}\left(\sigma^-_{\mathbf{p}} e^{i\Phi} + \sigma^+_{\mathbf{p}} e^{-i\Phi}\right) = 4a_{\mathbf{p}}\varepsilon_{\mathbf{p}}\dot{\Omega} - 2a_{\mathbf{p}}\dot{\Phi}\dot{\Omega}, \tag{5.75}$$

where we also used Eq. (5.74). Integrating this and adding the result to Eq. (5.74), we obtain

$$\sigma^-_{\mathbf{p}} e^{i\Phi} = 2a_{\mathbf{p}}\varepsilon_{\mathbf{p}}\Omega - a_{\mathbf{p}}A + i a_{\mathbf{p}}\dot{\Omega}, \tag{5.76}$$

where $A = \int dt \dot{\Phi}\dot{\Omega}$. Eq. (5.76) implies

$$|\sigma^-_{\mathbf{p}}|^2 = (2a_{\mathbf{p}}\varepsilon_{\mathbf{p}}\Omega - a_{\mathbf{p}}A)^2 + a^2_{\mathbf{p}}\dot{\Omega}^2. \tag{5.77}$$

Eqs. (5.77) and (6.3) combined with the conservation of the length of the spin, $(\sigma^z_{\mathbf{p}})^2 + |\sigma^-_{\mathbf{p}}|^2 = \sigma^2_{\mathbf{p}}$, yield a differential equation for Ω

$$(a_{\mathbf{p}}\Omega^2 + b_{\mathbf{p}})^2 + (2a_{\mathbf{p}}\varepsilon_{\mathbf{p}}\Omega - a_{\mathbf{p}}A + c_{\mathbf{p}})^2 + a^2_{\mathbf{p}}\dot{\Omega}^2 = \sigma^2_{\mathbf{p}} \tag{5.78}$$

Dividing the last equation by $a^2_{\mathbf{p}}$ and rearranging, we obtain

$$\begin{aligned}\dot{\Omega}^2 + \Omega^4 + \Omega^2\left(2\frac{b_{\mathbf{p}}}{a_{\mathbf{p}}} + 4\varepsilon^2_{\mathbf{p}}\right) - 4\varepsilon_{\mathbf{p}}A\Omega \\ + A^2 + \frac{b^2_{\mathbf{p}} - \sigma^2_{\mathbf{p}}}{a^2_{\mathbf{p}}} = 0\end{aligned} \tag{5.79}$$

It turns out that A is a certain function of Ω. To see this, let $x_{\mathbf{p}}$ be a set of numbers such that $\sum_{\mathbf{p}} x_{\mathbf{p}} = 0$, multiply Eq. (5.79) by $x_{\mathbf{p}}$ and sum over $\mathbf{p}$. This yields

$$A = 2\mu\Omega + \frac{\kappa}{\Omega}, \tag{5.80}$$

where μ and κ are arbitrary real constants. Substituting Eq. (5.80) into Eq. (5.79), we obtain

$$\begin{gathered}\dot{\Omega}^2 + \Omega^4 + 2\Omega^2\left[\frac{b_{\mathbf{p}}}{a_{\mathbf{p}}} + 2\xi_{\mathbf{p}}^2\right] + \\ \frac{\kappa^2}{\Omega^2} + \frac{b_{\mathbf{p}}^2 - \sigma_{\mathbf{p}}^2}{a_{\mathbf{p}}^2} - 4\kappa\xi_{\mathbf{p}} = 0,\end{gathered} \tag{5.81}$$

where $\xi_{\mathbf{p}} = \varepsilon_{\mathbf{p}} - \mu$. Note that the same equation obtains in the reduced problem with $a_{\mathbf{p}} \to c_1$, $b_{\mathbf{p}} \to c_2$ etc. It follows that coefficients must be $\mathbf{p}$-independent, i.e.

$$\frac{b_{\mathbf{p}}}{a_{\mathbf{p}}} + 2\xi_{\mathbf{p}}^2 = 2\rho, \quad \frac{b_{\mathbf{p}}^2 - \sigma_{\mathbf{p}}^2}{a_{\mathbf{p}}^2} - 4\kappa\xi_{\mathbf{p}} = 4\chi, \tag{5.82}$$

where ρ and χ are $\mathbf{p}$-independent constants. We find

$$\begin{aligned} b_{\mathbf{p}} &= -2(\xi_{\mathbf{p}}^2 - \rho)a_{\mathbf{p}}, \\ a_{\mathbf{p}} &= \frac{-\sigma_{\mathbf{p}}}{2\sqrt{(\xi_{\mathbf{p}}^2 - \rho)^2 - \kappa\xi_{\mathbf{p}} - \chi}}. \end{aligned} \tag{5.83}$$

As mentioned above $a_{\mathbf{p}}$ and $b_{\mathbf{p}}$ are inversely proportional to $\sqrt{Q_4(\varepsilon_{\mathbf{p}})}$. Eq. (5.83) therefore implies

$$Q_4(u) = [(u-\mu)^2 - \rho]^2 - \kappa(u-\mu) - \chi, \tag{5.84}$$

while the differential Eq. (5.81) for Ω reads

$$\dot{\Omega}^2 + \Omega^4 + 4\rho\Omega^2 + \frac{\kappa^2}{\Omega^2} + 4\chi = 0. \tag{5.85}$$

This equation can be solved in terms of elliptic function. Let $w = \Omega^2$. We have

$$\dot{w}^2 + 4w^3 + 16\rho w^2 + 16\chi w + 4\kappa^2 \equiv \dot{w}^2 + 4P_3(w) = 0. \tag{5.86}$$

Further, let $P_3(w) = (w-h_1)(w-h_2)(w-h_3)$, where $h_3 \geq h_2 \geq h_1$, and define

$$\omega = \Lambda^2 + h_1, \quad \Delta_+^2 = h_3 - h_1, \quad \Delta_-^2 = h_2 - h_1. \tag{5.87}$$

We get

$$\dot{\Lambda}^2 = (\Delta_+^2 - \Lambda^2)(\Lambda^2 - \Delta_-^2) \tag{5.88}$$

with the solution

$$\Lambda = \Delta_+ \mathrm{dn}\left[\Delta_+(t-t_0), k'\right], \quad k' = \frac{\Delta_-}{\Delta_+}, \tag{5.89}$$

where dn is the Jacobi elliptic function and t_0 is an arbitrary integration constant.

It also follows from Eq. (5.80) and the definition of A below Eq. (5.76) that the phase of the order parameter is determined as

$$\dot{\Phi} = \frac{dA}{d\Omega} = 2\mu - \frac{\kappa}{\Lambda^2 + h_1}, \quad \Delta = \sqrt{\Lambda^2 + h_1}e^{-i\Phi}. \tag{5.90}$$

5.2.3 Matching integrals of motion

Given the quench initial conditions, we can evaluate all integrals of motion. This is equivalent to evaluating $\vec{L}^2(u)$ in the initial state as it is conserved and contains all the integrals as residues at $u = \varepsilon_{\mathbf{p}}$. It turns out that in the thermodynamic limit it is possible to find a reduced (few spin) solution that has the same $\vec{L}^2(u)$, i.e. exactly the same integrals as the quench dynamics.

In the thermodynamic limit single-particle energies $\varepsilon_{\mathbf{p}}$ form a continuum on the positive real axis and $\vec{L}^2(u)$ therefore has a continuum of poles at $u > 0$. Additionally, $\vec{L}^2(u)$ also has a continuum of roots along the $u > 0$ half line as we show in Appendix 5.10. Thus $\sqrt{\vec{L}^2(u)}$ has a branch cut along $u > 0$ in the continuum limit. There can also be several *isolated* roots whose imaginary parts remain finite in this limit. Isolated roots play an important role in the dynamics; we will determine them below and see that there are at most four such roots (two pairs of complex conjugate roots) for our quench problem.

Eq. (5.59) implies

$$1 + \int d\varepsilon' \frac{d(\varepsilon')\nu(\varepsilon')}{u - \varepsilon'} = -z(u)\sqrt{\frac{\vec{L}^2(u)}{\vec{L}_m^2(u)}}, \quad z(u) = \pm 1, \tag{5.91}$$

where $\vec{L}^2(u)$ is evaluated for the quench initial conditions. Our task is to find the parameters for the reduced problem – $d(\varepsilon)$ and $\vec{L}_m^2(u)$ – so that this equation holds. Then the reduced problem has the same integrals of motion as the quench dynamics.

Both sides of Eq. (5.91) have a branch cut along the positive real axis and tend to 1 as $u \to \infty$ for an appropriate choice of the sign $z(\infty)$. Further, provided the isolated roots of $\vec{L}^2(u)$ coincide with the roots of $\vec{L}_m^2(u)$, there are no more branching points and both sides are analytic away from the shared branch cut at $u > 0$. If we further ensure that the left and the right hand sides of Eq. (5.91) have the same jump across the branch cut, then their difference is an entire function that vanishes at infinity. It is therefore identically zero by Liouville's theorem from complex analysis and Eq. (5.91) holds.

To equate jumps across the branch cut, we take $u \to \varepsilon \pm i0$, apply the well-known formula $1/(x \pm i0) = \mathcal{P}(1/x) \mp i\pi\delta(x)$, and subtract one result from another. This fixes $d(\varepsilon)$,

$$d(\varepsilon) = -\frac{z(\varepsilon)}{2i\pi\nu(\varepsilon)} \frac{\sqrt{\vec{L}^2(\varepsilon_-)} - \sqrt{\vec{L}^2(\varepsilon_+)}}{\sqrt{\vec{L}_m^2(\varepsilon)}}, \tag{5.92}$$

where $\varepsilon_\pm = \varepsilon \pm i0$. According to expression (5.63) for $d_{\mathbf{p}} \equiv d(\varepsilon_{\mathbf{p}})$ this is equivalent to fixing the lengths of the spins, $|\sigma_{\mathbf{p}}| \equiv |\sigma(\varepsilon_{\mathbf{p}})|$, in the few spin solution so that

$$\sigma(\varepsilon) = z(\varepsilon) \frac{\sqrt{\vec{L}^2(\varepsilon_-)} - \sqrt{\vec{L}^2(\varepsilon_+)}}{2i\pi\nu(\varepsilon)}. \tag{5.93}$$

Thus, the few spin solution with this $\sigma(\varepsilon)$ and $\vec{L}_m^2(u)$ whose roots are the same as the isolated roots of $\vec{L}^2(u)$ has the same integrals of motion as the quench problem.

5.2.4 Asymptotic solution for the quench dynamics

There are altogether $2(N + 1)$ initial conditions – two angles for each classical spin and two initial conditions for the oscillator. So far, we constructed a reduced m-spin solution that matches $N + 1$ integrals of motion. This satisfies $N + 1$ initial conditions. The dynamics of the

reduced m-spin Hamiltonian contains $2(m+1)$ constants, $m+1$ of which (integrals of motion for $H_{\rm red}$) are already fixed since we fixed $\vec{L}^2_m(u)$. The remaining $m+1$ constants are not sufficient to match the remaining $N \to \infty$ initial conditions for the quench dynamics at finite m. This is resolved as follows. We use the known m-spin solution to derive a general asymptotic (i.e. valid at $t \to \infty$) solution of the equations of motion for spins $\vec{s}_{\mathbf{p}}$ with the same $\Delta(t)$ and the same integrals of motion as the m-spin solution. Integrals of motion therefore are those for the quench dynamics. In addition, this general solution contains the correct number $N+1$ of independent constants. We therefore conjecture that this is the true solution for the quench dynamics at large times after the quench. By construction, to verify this *few spin conjecture*, it is sufficient to show that the true asymptote of $\Delta(t)$ coincides with $\Delta(t)$ in the m-spin solution because given $\Delta(t)$ we obtain the most general asymptotic solution of equations of motion.

As discussed above Eq. (5.33), each quench is characterized by three parameters – the resonance width γ and the final ω_f and initial ω_i values of the detuning. We determine in the next section that $\vec{L}^2(u)$ for the quench dynamics can have 0, 1, or 2 pairs of isolated complex roots for any γ depending on ω_i and ω_f. These by construction must also be all the roots of $\vec{L}^2_m(u)$, which has $m+1$ pairs of complex conjugate roots according to Eq. (5.65). Cases relevant for the quench phase diagram are therefore $m = -1, 0$, and 1.

It is worthwhile to consider the $m = -1$ case separately in some detail to illustrate this procedure. Suppose $\vec{L}^2(u)$ evaluated for the quench initial condition has no complex (isolated) roots away from the real axis. Then, there is an $m = -1$ spin solution constructed above that in the $N \to \infty$ limit has the same values of the integrals of motion as the spin dynamics. Spins in this solution are all along the z-axis, $\vec{\sigma}_{\mathbf{p}} = -\sigma_{\mathbf{p}}\hat{z}$, and $\Delta(t) = -gb(t) = 0$. It is a particular solution of the equations of motion (5.8) such that $b(t) = 0$.

The general solution of the *spin part* of the equations of motion in Eq. (5.8) with $b(t) = 0$ is: spins $\vec{s}_{\mathbf{p}}$ precess around the z-axis (or equivalently around the reduced spins $\sigma_{\mathbf{p}}$) with frequencies $2\varepsilon_{\mathbf{p}}$, i.e.

$$s^z_{\mathbf{p}} = \frac{\sigma^z_{\mathbf{p}}}{\sigma_{\mathbf{p}}}\frac{\cos\theta_{\mathbf{p}}}{2}, \quad s^-_{\mathbf{p}} = \frac{\sin\theta_{\mathbf{p}}}{2}e^{i\alpha_{\mathbf{p}}(t)}, \tag{5.94}$$

where $\theta_{\mathbf{p}}$ is the angle $\vec{s}_{\mathbf{p}}$ makes with $-\hat{\mathbf{z}}$ and $\alpha_{\mathbf{p}} = -2\varepsilon_{\mathbf{p}}t + \delta_{\mathbf{p}}$. Equivalently, this can be expressed as

$$\vec{s}_{\mathbf{p}} = \frac{\vec{\sigma}_{\mathbf{p}}}{\sigma_{\mathbf{p}}}\frac{\cos\theta_{\mathbf{p}}}{2} + \vec{s}^{\perp}_{\mathbf{p}}, \tag{5.95}$$

where $\vec{s}^{\perp}_{\mathbf{p}}$ is the component transverse to $\vec{\sigma}_{\mathbf{p}}$, which rotates around $\vec{\sigma}_{\mathbf{p}}$ with frequency $2\varepsilon_{\mathbf{p}}$. Note that the length of spin $\vec{s}_{\mathbf{p}}$ is $1/2$ as it should be for the quench initial conditions.

This spin configuration has N additional constants $\delta_{\mathbf{p}}$, but it does not satisfy the equation of motion for $b(t)$ in Eq. (5.8) because $b(t) = 0$, while $J_-(t) = \sum_{\mathbf{p}} s^-_{\mathbf{p}} = \sum_{\mathbf{p}} f_{\mathbf{p}} e^{-2\varepsilon_{\mathbf{p}}t} \neq 0$, where $2f_{\mathbf{p}} = \sin\theta_{\mathbf{p}} e^{i\delta_{\mathbf{p}}}$. However, in the thermodynamic limit $J_-(t) = \int f(\varepsilon)\nu(\varepsilon)e^{-2\varepsilon t} \to 0$ as $t \to \infty$ and this solution becomes self-consistent.

Next, we set $2\sigma_{\mathbf{p}} = \cos\theta_{\mathbf{p}}$ and substitute $\vec{s}_{\mathbf{p}} = \vec{\sigma}_{\mathbf{p}} + \vec{s}^{\perp}_{\mathbf{p}}$ into the Lax vector,

$$\vec{L}(u) = \vec{L}^{\rm red}(u) + \sum_{\mathbf{p}} \frac{\vec{s}^{\perp}_{\mathbf{p}}}{u - \varepsilon_{\mathbf{p}}}. \tag{5.96}$$

The second term vanishes by the Riemann-Lebesgue lemma (dephases) as $t \to \infty$ in the thermodynamic limit for u away from the real axis similarly to $J_-(t)$ and therefore $\vec{L}(u) \to \vec{L}^{\rm red}(u)$. Constants $\sigma_{\mathbf{p}}$ are given by Eq. (5.93) to match the integrals of motion. Then, the solution given by Eq. (5.94) with $2\sigma_{\mathbf{p}} = \cos\theta_{\mathbf{p}}$ has the same integrals of motion as the quench dynamics and the right number of additional constants to match the remaining initial conditions. As explained above, to verify that this is indeed the true asymptote of the quench dynamics, we

only need to show that asymptotic $\Delta(t)$ coincides with $\Delta(t)$ of the $m=-1$ spin solution, i.e. that $\Delta(t)\to 0$ at large times after the quench whenever $\vec{L}^2(u)$ has no isolated complex roots (region I in quench phase diagrams above). We confirm this numerically, see e.g. Figs. 5.5, 5.12, and Refs. [19, Yuzbashyan and Dzero(2006)]. There is also a justification of this statement based on the general theory of integrable Hamiltonian dynamics. It works for both $m=-1$ and $m=0$ and we present at the end of the $m=0$ case below Eq. (5.114).

To summarize: if $\vec{L}^2(u)$ has no isolated complex roots for given (quench) initial conditions, then $\Delta(t)\to 0$ at large times in the thermodynamic limit and the steady state spin configuration is

$$s^z_{\mathbf{p}}=-\frac{\cos\theta_{\mathbf{p}}}{2},\quad s^-_{\mathbf{p}}=\frac{\sin\theta_{\mathbf{p}}}{2}e^{-2i\varepsilon_{\mathbf{p}}t+i\delta_{\mathbf{p}}}, \tag{5.97}$$

where

$$\cos\theta(\varepsilon)=z(\varepsilon)\frac{\sqrt{\vec{L}^2(\varepsilon_-)}-\sqrt{\vec{L}^2(\varepsilon_+)}}{i\pi\nu(\varepsilon)}, \tag{5.98}$$

and $\theta_{\mathbf{p}}\equiv\theta(\varepsilon_{\mathbf{p}})$. This expression evaluates explicitly for quench initial conditions; the answer is given by Eq. (5.134). The sign $z(\varepsilon)=\pm 1$ is fixed by requiring that $\cos\theta(\varepsilon)$ be smooth and spins $\vec{s}_{\mathbf{p}}$ point in the negative z-direction at $\varepsilon_{\mathbf{p}}\to\infty$ (so that corresponding single particles states be empty).

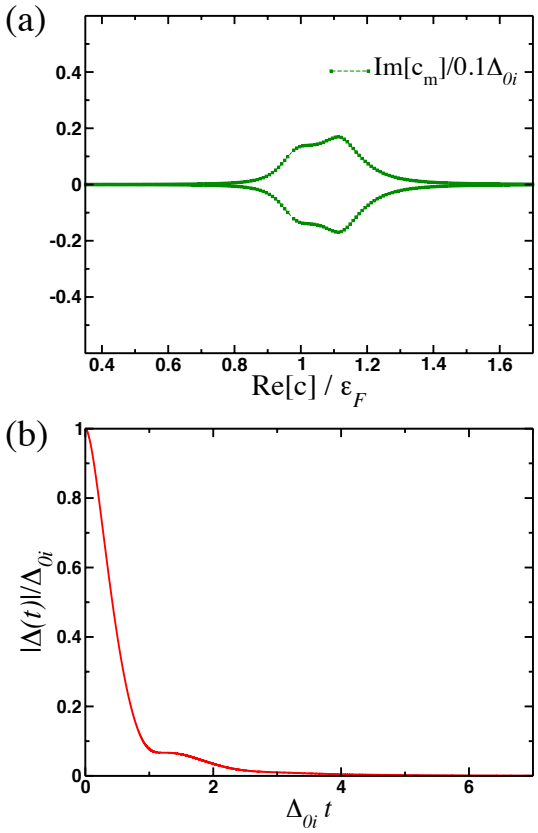


Figure 5.12: Order parameter $\Delta(t)$ vanishes whenever the square of the Lax vector $\vec{L}^2(u)$ has no isolated roots. Panel (a) shows real, Re$[c]$, and imaginary, Im$[c_m]$, parts of the roots c_m and panel (b) shows the corresponding $|\Delta(t)|$ for a detuning quench in a 3d 2-channel model with $\gamma=0.1$ and $N=1024$ spins. There are $N+1$ pairs of complex conjugate continual roots whose imaginary parts scale as $1/N$ so that in the $N\to\infty$ limit they form a continuum on the real axis. Here $\Delta_{0i}=0.34\Delta_{\max}$, $\Delta_{0f}=8.1\times 10^{-3}\Delta_{\max}$, $\mu_i=0.91\varepsilon_F$, and $\delta\omega=3.45\gamma$.

The logic for $m\geq 0$ is similar, but the calculation is a bit more involved. To derive the analog of Eq. (5.94), it is convenient to work with the Bogoliubov de Gennes equations (5.31).

In addition, there is an equation of motion for b in Eq. (5.8), which can be viewed as a self-consistency condition. In terms of $\Delta = -gb$ and Bogoliuobov amplitudes it reads

$$\dot{\Delta} = -i\omega\Delta + ig^2 \sum_{\mathbf{p}} 2 s_{\mathbf{p}} u_{\mathbf{p}} \bar{v}_{\mathbf{p}} \tag{5.99}$$

The reduced m-spin solution is a particular solution $(U_{\mathbf{p}}, V_{\mathbf{p}})$ of the BdG equations that also satisfies the above self-consistency condition (with $s_{\mathbf{p}} \to \sigma_{\mathbf{p}}$). It is straightforward to check that $(\bar{V}_{\mathbf{p}}, -U_{\mathbf{p}})$ is also a solution of the BdG equations with the same $\Delta(t)$. Since for any fixed $\Delta(t)$ these equations are linear in the amplitudes, their most general normalized solution with this $\Delta(t)$ is a linear combination of these two independent solutions

$$\begin{pmatrix} u_{\mathbf{p}} \\ \\ v_{\mathbf{p}} \end{pmatrix} = \cos\frac{\theta_{\mathbf{p}}}{2} \begin{pmatrix} U_{\mathbf{p}} \\ \\ V_{\mathbf{p}} \end{pmatrix} + \sin\frac{\theta_{\mathbf{p}}}{2} \begin{pmatrix} \bar{V}_{\mathbf{p}} \\ \\ -\bar{U}_{\mathbf{p}} \end{pmatrix}. \tag{5.100}$$

The coefficients are made real by dropping an unimportant overall time-independent phase and including the relative phase into the common phase of $U_{\mathbf{p}}$ and $V_{\mathbf{p}}$. At this point $\theta_{\mathbf{p}}$ is an arbitrary angle. This solution does not generally satisfy the self-consistency condition (5.99) at finite t, but, as we will see below, becomes self-consistent as $t \to \infty$.

Let us now determine the spins corresponding to this solution. Eq. (5.100) implies

$$\begin{aligned} |v_{\mathbf{p}}|^2 - |u_{\mathbf{p}}|^2 &= \left(|V_{\mathbf{p}}|^2 - |U_{\mathbf{p}}|^2\right)\cos\theta_{\mathbf{p}} - \\ &\quad \sin\theta_{\mathbf{p}}\left(\bar{U}_{\mathbf{p}}\bar{V}_{\mathbf{p}} + U_{\mathbf{p}}V_{\mathbf{p}}\right), \\ u_{\mathbf{p}}\bar{v}_{\mathbf{p}} &= U_{\mathbf{p}}\bar{V}_{\mathbf{p}}\cos\theta_{\mathbf{p}} + \frac{\sin\theta_{\mathbf{p}}}{2}\left(\bar{V}_{\mathbf{p}}^2 - U_{\mathbf{p}}^2\right). \end{aligned} \tag{5.101}$$

True spins $\vec{s}_{\mathbf{p}}$ are related to $u_{\mathbf{p}}$, $v_{\mathbf{p}}$ through Eq. (5.32) with $s_{\mathbf{p}} = 1/2$. Spins $\vec{\sigma}_{\mathbf{p}}$ are similarly related to $U_{\mathbf{p}}, V_{\mathbf{p}}$. Let

$$\begin{aligned} U_{\mathbf{p}} &= |U_{\mathbf{p}}| \exp\left[i\frac{\alpha_{\mathbf{p}} - \phi_{\mathbf{p}}}{2}\right], \\ V_{\mathbf{p}} &= |V_{\mathbf{p}}| \exp\left[i\frac{\alpha_{\mathbf{p}} + \phi_{\mathbf{p}}}{2}\right]. \end{aligned} \tag{5.102}$$

We can express the absolute values of the amplitudes and their relative phase through the spin components

$$|V_{\mathbf{p}}|^2 = \frac{1}{2} + \frac{\sigma_{\mathbf{p}}^z}{2\sigma_{\mathbf{p}}},\ |U_{\mathbf{p}}|^2 = \frac{1}{2} - \frac{\sigma_{\mathbf{p}}^z}{2\sigma_{\mathbf{p}}},\ e^{-i\phi_{\mathbf{p}}} = \frac{\sigma_{\mathbf{p}}^-}{|\sigma_{\mathbf{p}}^-|}, \tag{5.103}$$

while their common phase $\alpha_{\mathbf{p}}$ needs to be determined separately from the BdG equations.

We obtain in this notation

$$\begin{aligned} s_{\mathbf{p}}^z &= \frac{\sigma_{\mathbf{p}}^z}{\sigma_{\mathbf{p}}}\frac{\cos\theta_{\mathbf{p}}}{2} - \frac{|\sigma_{\mathbf{p}}^-|}{\sigma_{\mathbf{p}}}\frac{\sin\theta_{\mathbf{p}}}{2}\cos\alpha_{\mathbf{p}}, \\ s_{\mathbf{p}}^- &= \frac{\sigma_{\mathbf{p}}^-}{\sigma_{\mathbf{p}}}\frac{\cos\theta_{\mathbf{p}}}{2} + \frac{\sin\theta_{\mathbf{p}}}{2}e^{-i\phi_{\mathbf{p}}}\left(\frac{\sigma_{\mathbf{p}}^z}{\sigma_{\mathbf{p}}}\cos\alpha_{\mathbf{p}} - \right. \\ &\quad \left. i\sin\alpha_{\mathbf{p}}\right). \end{aligned} \tag{5.104}$$

Note that $\sigma_{\mathbf{p}}^z/\sigma_{\mathbf{p}}$ and $\sigma_{\mathbf{p}}^-/\sigma_{\mathbf{p}}$ are components of the unit vector along the spin in the reduced solution $\vec{\sigma}_{\mathbf{p}}$. Geometrically Eq. (5.104) says that $\vec{s}_{\mathbf{p}}$ makes a constant angle $\theta_{\mathbf{p}}$ (or $\pi - \theta_{\mathbf{p}}$ for negative $\sigma_{\mathbf{p}}$) with $\vec{\sigma}_{\mathbf{p}}$ and rotates around it with an angular velocity $\dot{\alpha}_{\mathbf{p}}$,

$$\vec{s}_{\mathbf{p}} = \frac{\vec{\sigma}_{\mathbf{p}}}{\sigma_{\mathbf{p}}}\frac{\cos\theta_{\mathbf{p}}}{2} + \vec{s}_{\mathbf{p}}^{\perp}. \tag{5.105}$$

To see this, consider a body set of axis for $\vec{\sigma}_{\mathbf{p}}$. Take z' along $\vec{\sigma}_{\mathbf{p}}$, x'-axis along the intersection of the zz' plane with the plane perpendicular to $\vec{\sigma}_{\mathbf{p}}$, and y' normal to $x'z'$ to form a right-handed coordinate system as usual. Then $\alpha_{\mathbf{p}}$ is the angle between $\vec{s}_{\mathbf{p}}^{\perp}$ and the x'-axis and Eq. (5.104) follows.

The contribution of the second terms on the right hand side of Eqs. (5.104) and (5.105) (terms containing $\alpha_{\mathbf{p}}$) to $\vec{L}(u)$ at u away from the real axis and to $J_{-}(t)$ vanishes (dephases) at large times at least for $m = 0$ and 1 in the thermodynamic limit same as in the $m = -1$ case considered above. For this to be true it is sufficient that $\alpha_{\mathbf{p}}$ contain a dispersing linear in t term, i.e.

$$\alpha_{\mathbf{p}} = -2e_{\mathbf{p}}t + F_{\mathbf{p}}(t), \tag{5.106}$$

where $e_{\mathbf{p}}$ is a continuous non-constant function of $\varepsilon_{\mathbf{p}}$ and $F_{\mathbf{p}}(t)$ is a bounded function of t. Note that for $m = -1$, $e_{\mathbf{p}} = \varepsilon_{\mathbf{p}}$ and $F_{\mathbf{p}}(t) = \delta_{\mathbf{p}} = \text{const}$.

To derive the asymptotic state, we follow the same procedure as for $m = -1$ above. We set $2\sigma_{\mathbf{p}} = \cos\theta_{\mathbf{p}}$, where $\cos\theta_{\mathbf{p}} \equiv \cos\theta(\varepsilon_{\mathbf{p}})$ is given by Eq. (5.98). Then, $\vec{L}(u) \to \vec{L}^{\text{red}}(u)$, $\Delta(t)$ is described by this m-spin solution at large times and satisfies the self-consistency condition (5.99), the asymptotic spin configuration (5.104) and the m-spin problem have the same integrals of motion as the quench dynamics. The remaining $N+1$ constants required to match the initial conditions are in $\alpha_{\mathbf{p}}$ (see below) and in the phase of $\Delta(t)$.

To determine $\alpha_{\mathbf{p}}$, rewrite the BdG eqs as

$$i\partial_t(\ln U_{\mathbf{p}}) = \varepsilon_{\mathbf{p}} + \Delta\frac{V_{\mathbf{p}}}{U_{\mathbf{p}}}, \quad i\partial_t(\ln V_{\mathbf{p}}) = -\varepsilon_{\mathbf{p}} + \bar{\Delta}\frac{U_{\mathbf{p}}}{V_{\mathbf{p}}}. \tag{5.107}$$

Adding these equations and using Eqs. (5.102) and (5.103), we get after some algebra

$$\dot{\alpha}_{\mathbf{p}} = -\frac{\sigma_{\mathbf{p}}(\bar{\Delta}\sigma_{\mathbf{p}}^{-} + \Delta\sigma_{\mathbf{p}}^{+})}{|\sigma_{\mathbf{p}}^{-}|^2}. \tag{5.108}$$

m=0

Suppose $\vec{L}^2(u)$ has a single pair of isolated complex roots at $u = \mu_\infty \pm i\Delta_\infty$. The 0-spin expression (5.67) for $\Delta(t)$ reads

$$\Delta(t) = \Delta_\infty e^{-2i\mu_\infty t - 2i\varphi}. \tag{5.109}$$

The notation Δ_∞ and μ_∞ anticipates that this is also the long time asymptote for the quench dynamics. Eq. (5.69) implies

$$\frac{\sigma_{\mathbf{p}}^{-}}{\sigma_{\mathbf{p}}} = \frac{\Delta(t)}{E_{\mathbf{p}}^{\infty}}, \quad \frac{\sigma_{\mathbf{p}}^{z}}{\sigma_{\mathbf{p}}} = -\frac{\xi_p}{E_{\mathbf{p}}^{\infty}}, \tag{5.110}$$

where $E_{\mathbf{p}}^{\infty} = E(\varepsilon_{\mathbf{p}}; \Delta_\infty, \mu_\infty) = \sqrt{(\varepsilon_{\mathbf{p}} - \mu_\infty)^2 + \Delta_\infty^2}$ and $\xi_{\mathbf{p}} = \varepsilon_{\mathbf{p}} - \mu_\infty$.

Eq. (5.108) obtains $\dot{\alpha}_{\mathbf{p}} = -2E_{\mathbf{p}}^{\infty}$. We see that $\alpha_{\mathbf{p}}$ is of the form (5.106) and therefore the large time asymptote of $\Delta(t)$ according to the few spin conjecture is given by Eq. (5.109). The asymptotic spin configuration is then Eq. (5.104) with $\cos\theta_{\mathbf{p}} \equiv \cos\theta(\varepsilon_{\mathbf{p}})$ given by Eq. (5.98). Explicitly, using Eq. (5.110) and $\alpha_{\mathbf{p}} = -2E_{\mathbf{p}}^{\infty}t - \delta_{\mathbf{p}}$, we obtain

$$\begin{aligned} s_{\mathbf{p}}^{z} &= -\frac{\xi_{\mathbf{p}}}{2E_{\mathbf{p}}^{\infty}}\cos\theta_{\mathbf{p}} - \frac{\Delta_\infty}{2E_{\mathbf{p}}^{\infty}}\sin\theta_{\mathbf{p}}\cos(2E_{\mathbf{p}}^{\infty}t + \delta_{\mathbf{p}}), \\ s_{\mathbf{p}}^{-}e^{2i\mu_\infty t + 2i\varphi} &= \frac{\Delta_\infty}{2E_{\mathbf{p}}^{\infty}}\cos\theta_{\mathbf{p}} - \frac{\sin\theta_{\mathbf{p}}}{2}e^{2iE_{\mathbf{p}}^{\infty}t + i\delta_{\mathbf{p}}} - \\ &\quad \left(\frac{\xi_p}{E_{\mathbf{p}}^{\infty}} - 1\right)\frac{\sin\theta_{\mathbf{p}}}{2}\cos(2E_{\mathbf{p}}^{\infty}t + \delta_{\mathbf{p}}). \end{aligned} \tag{5.111}$$

In a reference frame rotating with frequency $2\mu_\infty$ around z-axis, $\Delta(t) \to \Delta_\infty$ meaning that magnetic field acting on spin $\vec{s}_{\mathbf{p}}$ is time-independent. In this frame $\vec{s}_{\mathbf{p}}$ rotates around the field or, equivalently, around the reduced spin $\vec{\sigma}_{\mathbf{p}}$ with frequency $2E^\infty_{\mathbf{p}}$ as described by Eq. (5.111).

We can also determine the Bogoliubov amplitudes corresponding to the 0-spin solution from Eqs. (5.102) and (5.103)

$$\begin{aligned} U_{\mathbf{p}} &= \sqrt{\frac{1}{2} + \frac{\xi_{\mathbf{p}}}{2E^\infty_{\mathbf{p}}}} e^{-iE^\infty_{\mathbf{p}} t - i\mu_\infty t - i\varphi}, \\ V_{\mathbf{p}} &= \sqrt{\frac{1}{2} - \frac{\xi_{\mathbf{p}}}{2E^\infty_{\mathbf{p}}}} e^{-iE^\infty_{\mathbf{p}} t + i\mu_\infty t + i\varphi}. \end{aligned} \tag{5.112}$$

These in turn determine the "real" asymptotic amplitudes according to Eq. (5.100) and therefore the many-body wavefunction (5.29), which allows one to calculate various few-particle Green's functions.

As before, to verify the few spin conjecture in the present case it is enough to check that the large time asymptote of $\Delta(t)$ after the quench is given by Eq. (5.109) as long as $\vec{L}^2(u)$ has one pair of isolated complex conjugate roots (regions II and II' in quench phase diagrams above). We do so numerically, see e.g. Figs. 5.7, 5.13, and Refs. [19, Yuzbashyan and Dzero(2006)]. The large time asymptote of $|\Delta(t)|$ is in excellent agreement with Δ_∞ derived as the imaginary part of the isolated root, see e.g. Fig. 2 in Ref. [Yuzbashyan and Dzero(2006)]. This is however guaranteed by conservation laws without reliance on the few spin conjecture. Indeed, suppose we find $\Delta(t) \to \tilde{\Delta}_\infty e^{-2i\tilde{\mu}_\infty t - 2i\tilde{\varphi}}$. Starting with this, one can retrace the steps that lead to Eq. (5.111) backwards and show that $\vec{L}^2(u)$ has a single pair of isolated complex conjugate roots at $\tilde{\mu}_\infty \pm i\tilde{\Delta}_\infty$. In other words, $\tilde{\mu}_\infty = \mu_\infty, \tilde{\Delta}_\infty = \Delta_\infty$, and the constant φ is arbitrary in the 0-spin solution, so we can always set $\tilde{\varphi} = \varphi$. Let us prove this somewhat differently using Bloch rather than BdG equations.

Going to a reference frame rotating around z-axis with frequency $2\tilde{\mu}_\infty$ eliminates time dependence in the asymptotic $\Delta(t)$. In this frame, the effective magnetic field acting on each spin $\vec{s}_{\mathbf{p}}$ in Eq. (5.8) is $\vec{B}_{\mathbf{p}} = -2\tilde{\Delta}_\infty \hat{\mathbf{x}} + 2(\epsilon_{\mathbf{p}} - \tilde{\mu}_\infty)\hat{\mathbf{z}}$ and is time-independent. The spin therefore rotates around the field making a constant angle (call it $\pi - \theta_{\mathbf{p}}$) with it. It is straightforward to determine spin components in this situation. They are given by Eq. (5.111) with $\mu_\infty \to \tilde{\mu}_\infty$, $\Delta_\infty \to \tilde{\Delta}_\infty$, and absent $e^{2i\mu_\infty t + 2i\varphi}$ on the left hand side in the rotating frame.

Next, we evaluate Lax vector (5.50) for this spin configuration. For u away from the real axis, summations over $\mathbf{p}$ can be safely replaced with integrations in the continuum limit and contributions from oscillating terms on the right hand side of Eqs. (5.111) vanish at $t \to \infty$. The same cancelation occurs in the gap equation of motion (5.33), so that it becomes Eq. (5.200) that we will later also need in a different context. Using this gap equation to simplify the expression for $\vec{L}(u)$, we obtain

$$\vec{L}(u) = \left[\tilde{\Delta}_\infty \hat{\mathbf{x}} - (u - \tilde{\mu}_\infty)\hat{\mathbf{z}}\right] L_\infty(u), \tag{5.113}$$

where

$$L_\infty(u) = \frac{2}{g^2} - \sum_{\mathbf{p}} \frac{1}{2(u - \varepsilon_{\mathbf{p}})E^\infty_{\mathbf{p}}}. \tag{5.114}$$

We see that $\vec{L}^2(u) = [\tilde{\Delta}^2_\infty - (u - \tilde{\mu}_\infty)^2] L^2_\infty(u)$ has a pair of isolated roots at $u = \tilde{\mu}_\infty \pm i\tilde{\Delta}_\infty$, i.e. the parameters of the asymptotic $\Delta(t)$ must coincide with those of an isolated root.

Finally, there is a general argument explaining why the actual quench dynamics at $t \to \infty$ should be described by the above asymptotic solutions derived from -1 and 0 spin solutions at least when $\vec{L}^2(u)$ has none or only one isolated root pair ($m = -1$ and 0). The general

motion of a classical Hamiltonian integrable model with N degrees of freedom is quasi-periodic with N independent frequencies, $\vec{\omega} = (\omega_1, \ldots, \omega_N)$, that are determined solely by the values of its integrals of motion[Arnold(1978), Tabor(1989)]. There are two types of (quasi)periodic motion: libration and rotation[H. Goldstein(2002)]. Let us explain this terminology with a one-dimensional example. In libration, the coordinate returns to its initial value after each period, such as e.g. the coordinate of a harmonic oscillator. In rotation, it increases each time by a fixed amount, such as e.g. the angle of a rotating pendulum. Dynamical variables of libration type can be decomposed in a multi-dimensional Fourier series as follows,

$$Q(t) = \sum_{\vec{m}} c_{\vec{m}} e^{i\vec{\omega}\cdot\vec{m}t}, \tag{5.115}$$

where $\vec{m} = (m_1, \ldots, m_N)$ is a vector with integer components. Dynamical variables of rotation type contain an additional linear term, i.e.

$$Q(t) = c_0 t + \sum_{\vec{m}} c_{\vec{m}} e^{i\vec{\omega}\cdot\vec{m}t}, \tag{5.116}$$

see e.g. Ref. [H. Goldstein(2002)] for further details. In our case, the absolute value of the order parameter, $|\Delta(t)|$ is of libration type, while its phase is of rotation type.

The frequency spectra of asymptotic solutions constructed above are $\omega(\varepsilon_{\mathbf{p}}) = 2\varepsilon_{\mathbf{p}}$ for $m = -1$ and $\omega(\varepsilon_{\mathbf{p}}) = 2\sqrt{(\varepsilon_{\mathbf{p}} - \mu_\infty)^2 + \Delta_\infty^2}$ for $m = 0$. Important for us is that the spectra are continuous with no isolated frequencies in the thermodynamic limit. Since setting $2\sigma_{\mathbf{p}} = \cos\theta_{\mathbf{p}}$ ensures the quench dynamics has the same integrals as this solution (lives on the same invariant torus), it also must have an identical frequency spectrum. Assuming $|\Delta(t)|$ is continuously distributed over the spectrum as a collective variable, i.e. the discrete summation in Eq. (5.115) turns into a continuous Fourier transform, it must dephase at large times, $|\Delta(t)| \to$ const. Under the same assumption, the phase of the order parameter according to Eq. (5.116) must tend to a linear in time function as $t \to \infty$. Therefore, $\Delta(t)$ at large times is of the form $\Delta_\infty e^{-2i\mu_\infty t - 2i\varphi}$. Since finite Δ_∞ also implies an isolated root at $\mu_\infty \pm i\Delta_\infty$ while for $m = -1$ there are no isolated roots by definition, we must have $\Delta_\infty = 0$, i.e. $\Delta(t) \to 0$ in this case.

We also prove the few spin conjecture for infinitesimal quenches in Sect. 5.5.4 independently of above arguments and numerics.

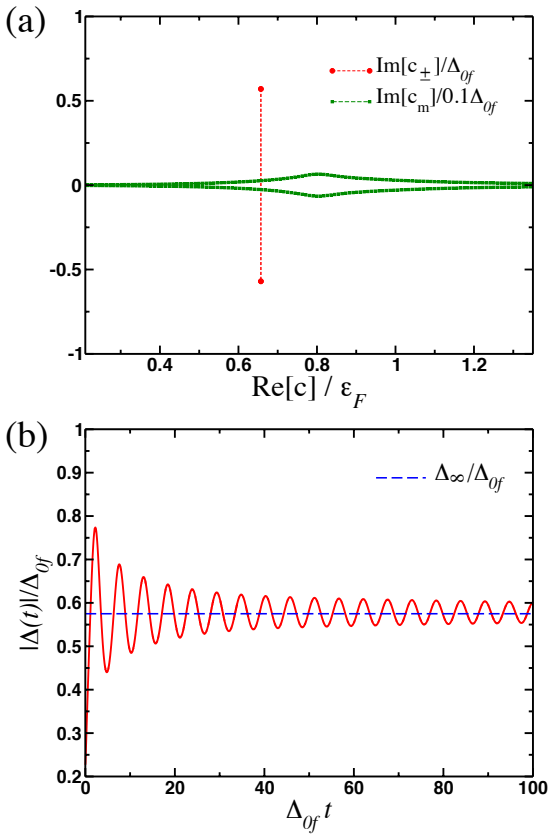


Figure 5.13: Roots of $\vec{L}^2(u)$ (top) and $|\Delta(t)|$ for a detuning quench in a 3d 2-channel model for $N = 1024$ spins, $\gamma = 1.0$. There is one pair of isolated roots $c_\pm = \mu_\infty \pm i\Delta_\infty$ whose imaginary part remains finite in the large N limit and $N-1$ continual roots c_m close to the real axis ($\mathrm{Im}[c_m]$ is zoomed in by 10). Observe $|\Delta(t)| \to \Delta_\infty$ in agreement with the few spin conjecture. Here $\Delta_{0i} = 0.18\Delta_{\max}, \Delta_{0f} = 0.78\Delta_{\max}$, and $\delta\omega = -2.26\gamma$.

m=1

Suppose we found that for some initial condition (quench parameters) $\vec{L}^2(u)$ has two pairs of isolated complex conjugate roots $c, \bar{c}, c', \bar{c}'$. Given c and c', the above method allows us to determine the long time asymptote of $\Delta(t)$, asymptotic spin configuration and time-dependent Bogoliubov amplitudes $u_{\mathbf{p}}(t), v_{\mathbf{p}}(t)$ for the dynamics of the two-channel model (5.9) starting from this initial condition at $t = 0$.

By construction c, c' are also the roots of $\vec{L}_m^2(u)$ furnishing the spectral polynomial for the reduced problem $Q_4(u) = (u-c)(u-\bar{c})(u-c')(u-\bar{c}')$ and therefore the parameters μ, ρ, κ, χ through Eq. (5.84). We further obtain from Eq. (5.90)

$$\Delta(t) = \sqrt{\Lambda^2 + h_1}\exp\left(-2i\mu t - i\int \frac{\kappa dt}{\Lambda^2 + h_1}\right), \tag{5.117}$$

where Λ is the Jacobi elliptic function dn,

$$\Lambda = \sqrt{h_3 - h_1}\,\mathrm{dn}\left[\sqrt{h_3 - h_1}(t - t_0), \sqrt{\frac{h_3 - h_2}{h_3 - h_1}}\right], \tag{5.118}$$

t_0 is a constant, and $h_3 \geq h_2 \geq h_1$ are the roots of the third order polynomial $P_3(w) = w^3 + 4\rho w^2 + 4\chi w + \kappa^2$. The amplitude $|\Delta(t)|$ oscillates between a minimum $\Delta_b = \sqrt{h_2}$ and a maximum $\Delta_a = \sqrt{h_1}$. Plots of Δ_a, Δ_b, and h_1 for various quenches are shown in Figs. 5.9 and

5.10. As we will now see, the parameter h_1 also quantifies the deviation from the weak coupling limit where $h_1 = 0$.

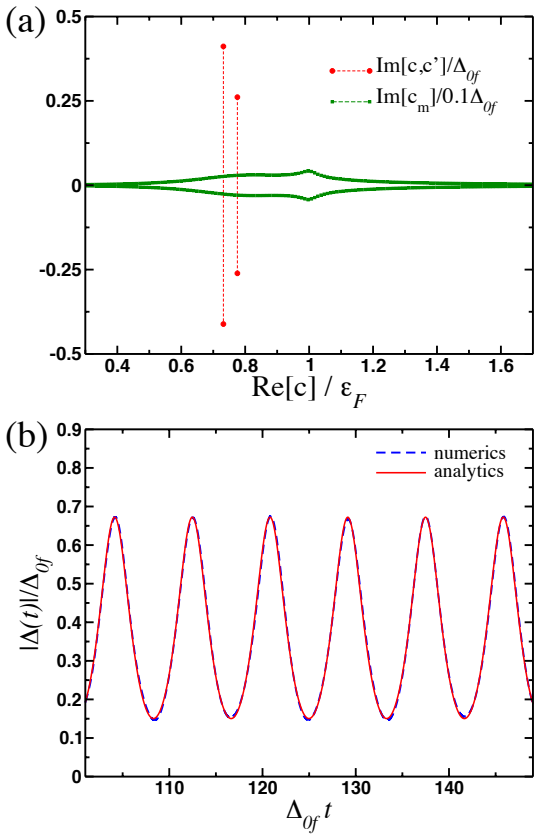


Figure 5.14: Roots of $\vec{L}^2(u)$ (top) and $|\Delta(t)|$ for a detuning quench in a 3d 2-channel model with $N = 1024$ spins and $\gamma = 1.0$. There are two pairs of isolated roots $(c, \bar{c})$ and $(c', \bar{c}')$ and $N - 2$ continual roots close to the real axis. The large time asymptote of $|\Delta(t)|$ is described by Eq. (5.117), where parameters h_i are extracted from the isolated roots in agreement with the few spin conjecture. The phase of $\Delta(t)$ is also in excellent agreement, see e.g. Figs. 5.8 and 5.15. Quench parameters are: $\Delta_{0i} = 2.68\Delta_{\max}, \Delta_{0f} = 0.76\Delta_{\max}$, and $\delta\omega = -4.13\gamma$.

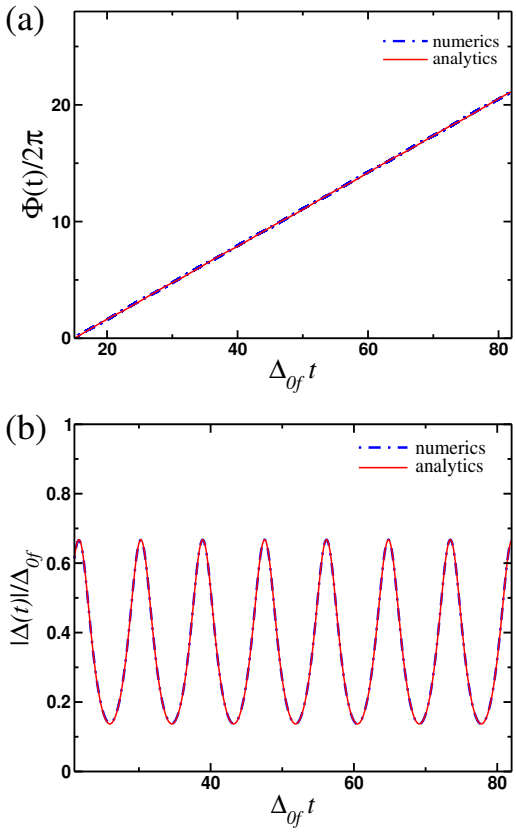


Figure 5.15: Magnitude and phase of $\Delta(t)$ in region III (two pairs of isolated roots) after detuning quench from deep BCS to BEC in 3d two-channel model for $\gamma = 1$. Numerical evolution with 5024 spins against Eq. (5.117). Parameters h_1, h_2, etc. are obtained from isolated roots of $\vec{L}^2(u)$ as described in the text. $\Delta_{0i} = 2.65 \times 10^{-2}\Delta_{\max}, \Delta_{0f} = 0.80\Delta_{\max}, \mu_i = 1.00\varepsilon_F, \delta\omega = -4.59\gamma$.

Of interest is the particular case when the parameter $\kappa = 0$. As we will see below, this is realized for quenches deep within the weak coupling BCS regime in the broad resonance limit when the two-channel model is equivalent to the BCS Hamiltonian (5.11). $\kappa = 0$ implies $h_1 = 0$, $4\chi = h_2 h_3$, $4\rho = -h_2 - h_3$, and $Q_4(u) = [(u-\mu)^2 - \rho]^2 - \chi$. Let $h_3 = \Delta_+^2, h_2 = \Delta_-^2$ in accordance with the notation of Eq. (5.87). The roots of $Q_4(u)$ in this case take a simple form with shared real part. Namely, they are

$$\mu \pm i\frac{\Delta_+ \pm \Delta_-}{2}, \tag{5.119}$$

and the expression (5.117) simplifies as well,

$$\Delta(t) = \Delta_+ \mathrm{dn}[\Delta_+(t-t_0)]e^{-2i\mu t - 2i\varphi}. \tag{5.120}$$

This expression for $\Delta(t)$ and the corresponding $m = 1$ spin solution were constructed in Ref. [Barankov et al.(2004)].

General expression for the reduced spins obtain from Eqs. (6.3), (5.76), and (5.83),

$$\begin{aligned} \frac{\sigma_{\mathbf{p}}^z}{\sigma_{\mathbf{p}}} &= -\frac{|\Delta|^2 - 2\xi_{\mathbf{p}}^2 + 2\rho}{2\sqrt{Q_4(\varepsilon_{\mathbf{p}})}}, \\ \frac{\sigma_{\mathbf{p}}^-}{\sigma_{\mathbf{p}}} &= -\frac{2\xi_{\mathbf{p}}\Delta - 2\mu\Delta + i\dot{\Delta}}{2\sqrt{Q_4(\varepsilon_{\mathbf{p}})}}, \end{aligned} \tag{5.121}$$

where $\xi_{\mathbf{p}} = \varepsilon_{\mathbf{p}} - \mu$ and Δ is given by Eq. (5.117). Bogoliubov amplitudes corresponding to the 1-spin solution can now be derived from Eq. (5.107). The imaginary and real parts of the right hand sides determine the absolute values of the amplitudes and their phases, respectively,

$$\begin{aligned} U_{\mathbf{p}} &= \frac{\sqrt{2c_{\mathbf{p}}^{+} - |\Delta|^2}}{2Q_4^{1/4}(\varepsilon_{\mathbf{p}})} e^{-i\mu t + i\xi_{\mathbf{p}} t} \exp\left[i \int \frac{\kappa - 4\xi_{\mathbf{p}} c_{\mathbf{p}}^{+}}{2c_{\mathbf{p}}^{+} - |\Delta|^2} dt \right], \\ V_{\mathbf{p}} &= \frac{\sqrt{2c_{\mathbf{p}}^{-} + |\Delta|^2}}{2Q_4^{1/4}(\varepsilon_{\mathbf{p}})} e^{i\mu t - i\xi_{\mathbf{p}} t} \exp\left[i \int \frac{\kappa + 4\xi_{\mathbf{p}} c_{\mathbf{p}}^{-}}{2c_{\mathbf{p}}^{-} + |\Delta|^2} dt \right], \end{aligned} \tag{5.122}$$

where $c_{\mathbf{p}}^{\pm} = \sqrt{Q_4(\varepsilon_p)} \pm (\xi_{\mathbf{p}}^2 - \rho)$.

The common phase of the amplitudes $\alpha_{\mathbf{p}}$ is the sum of their phases in the above equations, i.e.

$$\alpha_{\mathbf{p}} = \int \left[\frac{\kappa - 4\xi_{\mathbf{p}} c_{\mathbf{p}}^{+}}{2c_{\mathbf{p}}^{+} - |\Delta|^2} + \frac{\kappa + 4\xi_{\mathbf{p}} c_{\mathbf{p}}^{-}}{2c_{\mathbf{p}}^{-} + |\Delta|^2} \right] dt \tag{5.123}$$

The integrand is a periodic function of time. Therefore, $\alpha_{\mathbf{p}}$ is of the form (5.106), which is seen e.g. by expanding the expression under the integral in Fourier series. The linear part $e_{\mathbf{p}} t$ comes from the zeroth harmonics. We only need to show that $e_{\mathbf{p}}$ is a non-constant (dispersing) function of $\varepsilon_{\mathbf{p}}$. For this, we expand the integrand for large $\varepsilon_{\mathbf{p}}$, $e_{\mathbf{p}} = \varepsilon_{\mathbf{p}} + O(1)$. Therefore, $e_{\mathbf{p}}$ is indeed dispersing and the contribution of second terms on the right hand sides of Eq. (5.104) to $\vec{L}(u)$ and $J_{-}(t)$ dephases similarly to $m = -1, 0$ cases. By few spin conjecture the asymptotic behavior of $\Delta(t)$ is then given by Eqs. (5.117). The asymptotic spin configuration obtains by substituting Eqs. (5.123) and (5.121) into Eq. (5.104), where $\cos\theta_{\mathbf{p}} \equiv \cos(\varepsilon_{\mathbf{p}})$ is given by Eq. (5.98) and $e^{-i\phi_{\mathbf{p}}} = \sigma_{\mathbf{p}}^{-}/|\sigma_{\mathbf{p}}^{-}|$ straightforwardly derives from the second equation in (5.121).

As before, to verify the few spin conjecture it is sufficient to check that $\Delta(t)$ at large times after the quench is described by Eq. (5.117) whenever $\vec{L}^2(u)$ has two pairs of isolated roots. We do this numerically, see Figs. 5.14, 5.8, 5.15, and 5.16. In these plots we compare $\Delta(t)$ from direct numerical evolution of 5024 spins to Eq. (5.117), where parameters h_1, h_2, h_3, and μ obtain from the isolated roots of $\vec{L}^2(u)$. Note there are no fitting parameters apart from an overall shift t_0 along the time axis.

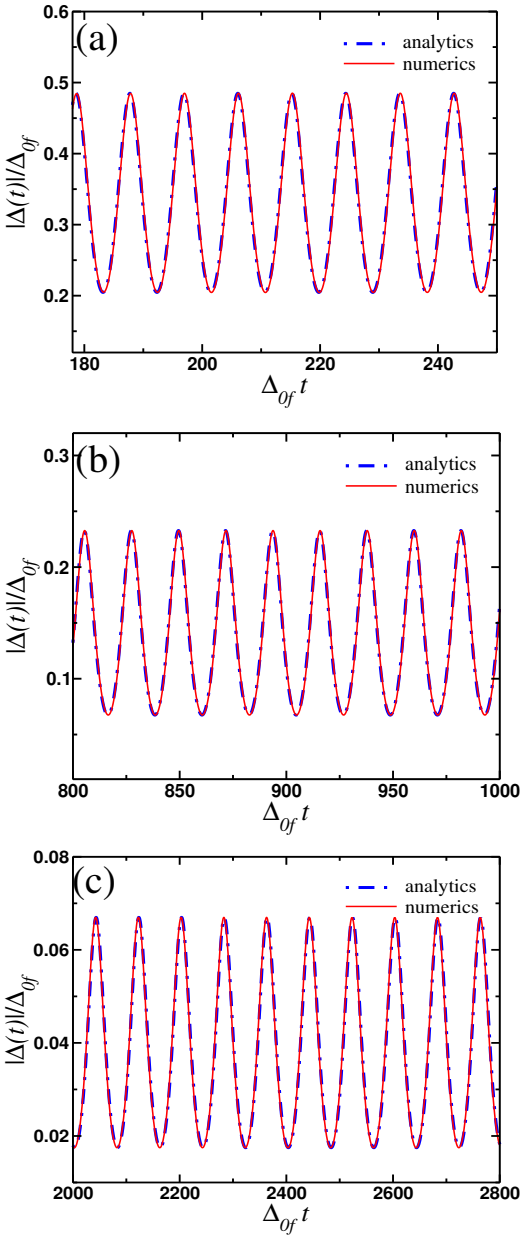


Figure 5.16: Post-quench $|\Delta(t)|$ for 3d 2-channel model in region III where $\vec{L}^2(u)$ has two pairs isolated roots. Numerical evolution with 5024 spins against Eq. (5.117). $\gamma = 0.1$, $\Delta_{0i} = 0.035\Delta_{\max}$ in all three panels. $\Delta_{0f}/\Delta_{\max} = 0.54, 0.67$, and 0.85 in (a), (b), and (c), respectively.

5.3 Quench phase diagram and asymptotic spin distribution for the 2-channel model

We established in the previous section that the long time dynamics of the system after a quench are determined by the isolated complex roots of $\vec{L}^2(u)$. We now proceed to evaluate the roots and thus construct the quench phase diagram – identify all possible steady states for quenches throughout the BCS-BEC crossover. We find that depending on the quench parameters $\vec{L}^2(u)$ has either zero, one, or two pairs of complex conjugate roots and the long time behavior is therefore that described in Sections 5.2.4, 5.2.4, or 5.2.4, respectively. Imaginary and real parts of the roots determine the parameters of the asymptotic behavior. For example, in the Volkov and Kogan regime (region II in our quench phase diagrams) where $\Delta(t \to \infty) \to \Delta_\infty e^{-2i\mu_\infty t - 2i\varphi}$, the roots are $\mu_\infty \pm i\Delta_\infty$. We first derive general equations for the roots, lines separating distinct regimes, and the asymptotic distribution function, and then consider various

cases, such as two and three dimensions, wide (one channel) and narrow resonance limits, and deep BCS and BEC regimes.

After the quench the system evolves with the Hamiltonian (5.9) where $\omega = \omega_f$ starting from the spin configuration (5.28) which is the ground state for $\omega = \omega_i$. Since $\vec{L}^2(u)$ is conserved, we can evaluate it at any t. It is convenient to do so at $t = 0$. The Lax vector at $t = 0$ obtains by plugging the initial condition into the definition (5.50)

$$\vec{L}(u)|_{t=0} = [\Delta_{0i}\hat{\mathbf{x}} - (u - \mu_i)\hat{\mathbf{z}}]\, L_0(u) - \frac{\delta\omega}{g^2}\hat{\mathbf{z}}, \tag{5.124}$$

where $\delta\omega = \omega_f - \omega_i$ and

$$L_0(u) = -\frac{2}{g^2} + \sum_{\mathbf{p}} \frac{1}{2(u - \varepsilon_{\mathbf{p}})E_i(\varepsilon_{\mathbf{p}})}, \tag{5.125}$$

$E_i(\varepsilon_{\mathbf{p}}) = E(\varepsilon_{\mathbf{p}}; \Delta_{0i}, \mu_i) = \sqrt{(\varepsilon_{\mathbf{p}} - \mu_i)^2 + \Delta_{0i}^2}$ and we also used the gap equation (5.18).

Taking the square of the above expression for $\vec{L}(u)$ and equating it to zero, we obtain an equation for the roots

$$(u - \mu_i \mp i\Delta_{0i})\left[\frac{2}{g^2} - \sum_{\mathbf{p}} \frac{1}{2(u - \varepsilon_{\mathbf{p}})E_i(\varepsilon_{\mathbf{p}})}\right] = \frac{\delta\omega}{g^2}. \tag{5.126}$$

Suppose first the single particle levels $\varepsilon_{\mathbf{p}}$ are discrete and there are $N \gg 1$ distinct $\varepsilon_{\mathbf{p}}$. Then, this is a polynomial equation with $N + 1$ pairs of complex conjugate roots. Most of the pairs are close to the real axis, at distances of the order of the spacing between $\varepsilon_{\mathbf{p}}$, which is inversely proportional to N (system volume) and goes to zero in the thermodynamic limit. In thermodynamic limit most of the roots of $\vec{L}^2(u)$ coalesce to the real axis merging with its poles to form a branch cut along the real axis. We fully verify this picture in this section and in Appendix 5.10. Here we consider the roots whose imaginary part remains finite as $N \to \infty$ and in Appendix 5.10 we evaluate the roots with vanishing imaginary parts to order $1/N$.

Consider first the ground state. This corresponds to $\delta\omega = 0$ in Eq. (5.126) and $\vec{L}^2(u) = [(u - \mu)^2 + \Delta_0^2]\, L_0^2(u)$. There is a pair of complex roots at $c_\pm = \mu \pm i\Delta_0$. The remaining $2N$ roots solve $L_0(u) = 0$ and are double degenerate and real, see Fig. 5.17. This is because $L_0(u)$ goes from $+\infty$ to $-\infty$ as u goes from the left vicinity of one pole at $u = \varepsilon_{\mathbf{p}}$ to the right vicinity of the next one along the real axis always crossing zero in between consecutive $\varepsilon_{\mathbf{p}}$. In the thermodynamic limit, spacings between $\varepsilon_{\mathbf{p}}$ vanish and real zeroes and poles merge into a continuos line. For $\delta\omega \neq 0$ the real roots acquire imaginary parts each degenerate root splitting into a complex conjugate pair as shown in Figs. 5.12, 5.13, and 5.14. The imaginary parts however scale as $1/N$.

We first take the continuum limit in Eq. (5.126) for u away from the real axis. Then, only isolated complex roots remain and we find that there are only zero, one or two pairs of such roots depending on $\delta\omega$. At $\delta\omega = 0$ there are two isolated complex conjugate roots at $u = \mu_i \pm i\Delta_{0i}$. One pair of roots persists for sufficiently small $|\delta\omega|$, but beyond a certain threshold the number of isolated roots changes as we now demonstrate. The continuum limit of Eq. (5.126) reads

$$\frac{2}{u - \mu_i \mp i\Delta_{0i}}\frac{\delta\omega}{\gamma} + \int_0^\infty \frac{f(\varepsilon)d\varepsilon}{(u - \varepsilon)E_i(\varepsilon)} = \frac{4}{\gamma}, \tag{5.127}$$

where as always we measure energies in units of ε_F and $f(\varepsilon)$ is the dimensionless density of states defined in Eq. (5.22).

As $\delta\omega$ is decreased or increased the single pair of roots can collapse to the real axis or a new pair of isolated roots can emerge from it. The threshold (critical) value of $\delta\omega$ when this occurs is determined by looking for roots of Eq. (5.127) with an infinitesimal imaginary part. Replace

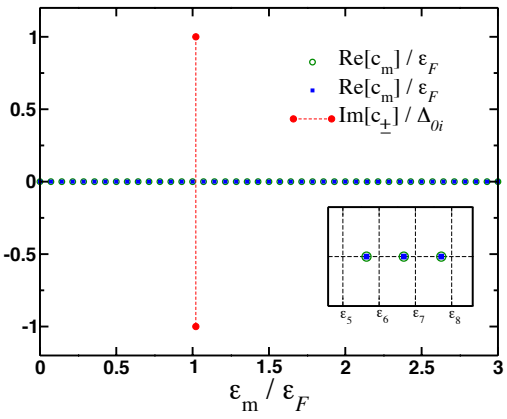


Figure 5.17: Roots of $\vec{L}^2(u)$ for the ground state of 3d 2-channel model for $N = 54$ spins and $\gamma = 1.0$. There are N doubly degenerate real roots c_m (shown as circles and squares), $N - 1$ of them located in between discretized energy levels $\varepsilon_{\mathbf{p}} \to \varepsilon_m$, and two isolated complex roots $c_\pm = \mu_i \pm \Delta_{0i}$. Here $\Delta_{0i} = 0.1\varepsilon_F$.

$u \to u \pm i\delta$ in Eq. (5.127) and use $(u - \varepsilon \pm i\delta)^{-1} = P(u - \varepsilon)^{-1} \mp i\pi\delta(u - \varepsilon)$ to separate its real and imaginary parts. The latter yields critical values of $\delta\omega$ when the number of roots changes

$$\frac{|\delta\omega|}{\gamma} = \frac{\pi f(u) E_i(u)}{2\Delta_{0i}}, \tag{5.128}$$

where u is real positive and obtains from the real part of Eq. (5.127)

$$\int_0^\infty \frac{f(\varepsilon)d\varepsilon}{(u - \varepsilon)E_i(\varepsilon)} + \mathrm{sgn}(\delta\omega)\frac{\pi(u - \mu_i)f(u)}{E_i(u)\Delta_{0i}} = \frac{4}{\gamma}. \tag{5.129}$$

Dashed integral indicates principal value.

Last two equations determine critical lines in quench phase diagrams shown in Figs. 5.2, 5.3, 5.20, and 5.21. We construct the diagrams in $(\Delta_{0f}, \Delta_{0i})$ plane – ground state gaps at final and initial detunings ω_i and ω_f. The resonance width (dimensionless interaction strength) γ is fixed throughout the diagram. Δ_{0i}, Δ_{0f}, and γ uniquely determine μ_i, ω_i, and ω_f through ground state Eqs. (5.25) and (5.26). Each point in this plane represents a particular quench of the detuning $\omega_i \to \omega_f$. We choose Δ_{0i} (or equivalently the ratio μ_i/Δ_{0i}) and the sign of $\delta\omega$ and solve Eq. (5.129) for real u. Eq. (5.128) then yields the final detuning ω_f and therefore Δ_{0f}. We thus obtain a critical line, Δ_{0f} as a function of Δ_{0i}, in the $(\Delta_{0f}, \Delta_{0i})$ plane. The number of isolated root pairs changes by one as one crosses this line.

It turns out there is one critical line for either sign of $\delta\omega$. There are therefore three nonequilibrium phases or regimes – qualitatively different long time behaviors, indicated as regions I, II (including subregion II'), and III in Figs. 5.2, 5.3, 5.20, and 5.21. Region II contains the $\Delta_{0f} = \Delta_{0i}$ or, equivalently, $\omega_f = \omega_i$ line which corresponds to no quench, i.e. to the system remaining in the ground state at all times. Therefore, in region II Eq. (5.127) yields a single pair of isolated complex roots $u = \mu_\infty \pm i\Delta_\infty$. This in turn implies that $\Delta(t) \to \Delta_\infty e^{-2i\mu_\infty t - 2i\varphi}$ as $t \to \infty$. For all quenches in region II the system thus goes into the asymptotic state described in Section 5.2.4.

Negative $\delta\omega$ corresponds to $\Delta_{0f} > \Delta_{0i}$. As we cross the critical line going from region II into region III the number of isolated root pairs changes by one. It can be shown both analytically and numerically by analyzing Eq. (5.127) that this number increases, i.e. there are two pairs of complex conjugate isolated roots in region III. For quenches in this part of the diagram the large time asymptote of $\Delta(t)$ is given by Eq. (5.117) and the large time state of the system is

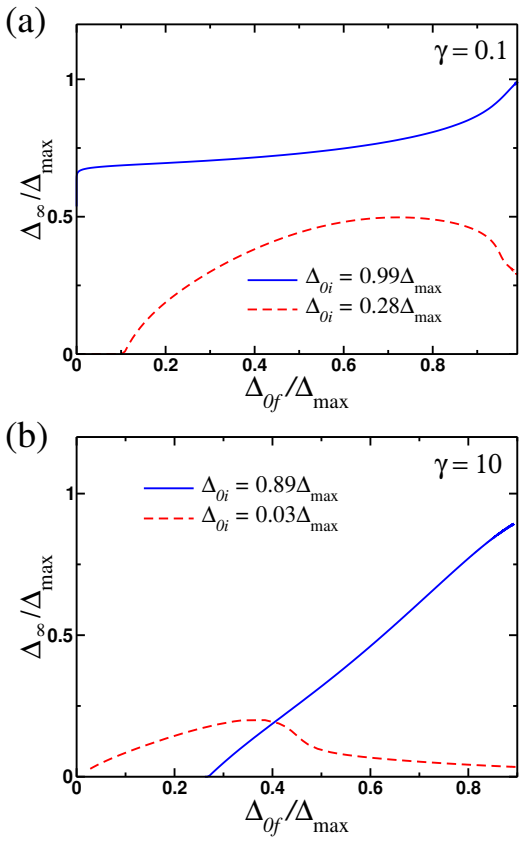


Figure 5.18: $\Delta(t) \to \Delta_\infty e^{-2i\mu_\infty t - 2i\varphi}$ as $t \to \infty$ after a detuning quench $\omega_i \to \omega_f$ in 3d 2-channel model in region II of the quench phase diagram in Fig. 5.3. Δ_∞ extracted from the single isolated root pair of the Lax vector norm is shown as a function of Δ_{0f} (ground state gap for ω_f) at two fixed values of Δ_{0i} (ground state gap for the initial detuning ω_i). Note that $\Delta_\infty > \Delta_{0f}$ for BEC to BCS quenches $\Delta_{0i} = 0.99\Delta_{\max}$ for $\gamma = 0.1$.

that obtained in Section 5.2.4. Plots of Δ_∞ and μ_∞ as functions of Δ_{0f} at two fixed values of Δ_{0i} are shown in Figs. 5.18 and 5.19.

Similarly, as we enter region I from region II, $\Delta_\infty \to 0$ and the single pair of isolated roots collapses to the real axis at the critical line. There are hence no isolated roots in region I and therefore $\Delta(t) \to 0$ for quenches in this regime and the system goes into the gapless steady state detailed at the beginning of Section 5.2.4.

Of interest is the line along which the real part of the root pair $\mu_\infty \pm i\Delta_\infty$ in region II vanishes, i.e. $\mu_\infty = 0$ (the line separating subregions II and II' in quench phase diagrams). This can be thought of as a nonequilibrium extension of the BCS-BEC crossover going from a positive to a negative chemical potential. Out of equilibrium, as we will see below, the change of sign of μ_∞ affects the approach of $\Delta(t)$ to its asymptote. For example, in 3d the approach changes from $1/t^{1/2}$ in II to $1/t^{3/2}$ in II'. Setting $u = \pm i\Delta_\infty$ in Eq. (5.127) and separating the real and imaginary parts, we obtain equations determining this line

$$\begin{aligned} \frac{\mu_i}{\Delta_{0i} - \Delta_\infty} \mathrm{Im}\,\mathcal{F} + \mathrm{Re}\,\mathcal{F} &= \frac{4}{\gamma} \\ \frac{\delta\omega}{\gamma} \frac{2(\Delta_\infty - \Delta_{0i})}{\mu_i^2 + (\Delta_\infty - \Delta_{0i})^2} &= \mathrm{Im}\,\mathcal{F}, \end{aligned} \tag{5.130}$$

where

$$\mathcal{F} = \int_0^\infty \frac{f(\varepsilon)d\varepsilon}{(i\Delta_\infty - \varepsilon)E_i(\varepsilon)}. \tag{5.131}$$

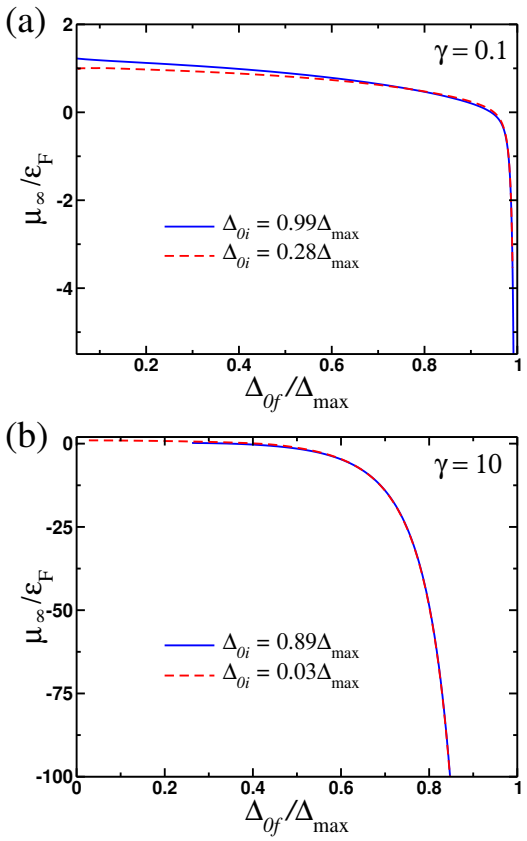


Figure 5.19: $\Delta(t) \to \Delta_\infty e^{-2i\mu_\infty t - 2i\varphi}$ as $t \to \infty$ after a detuning quench $\omega_i \to \omega_f$ in 3d 2-channel model in region II of the quench phase diagram in Fig. 5.3 where μ_∞ plays the role of the out of equilibrium analog of the chemical potential. Here μ_∞ is extracted from the single isolated root pair of the Lax vector norm and is shown as a function of Δ_{0f} (ground state gap for ω_f) at two fixed values of Δ_{0i} (ground state gap for the initial detuning ω_i). Note that μ_∞ behaves similarly to the ground state chemical potential in Fig. 5.1.

Eq. (5.130) determines the $\mu_\infty = 0$ line via a procedure similar to that for critical lines separating region I from II and II from III. For a given Δ_{0i}, the first equation yields Δ_∞. We then find $\delta\omega$ and consequently ω_f and Δ_{0f} from the second equation.

Note the intersection of the $\mu_\infty = 0$ line with the $\Delta_{0i} = \Delta_{0f}$ (no quench) line. Along the latter line we also have $\Delta_\infty = \Delta_{0i}$ and therefore at the intersection point $\mu_i = \mu_f = 0$ or the first term in the first equation in Eq. (5.130) would blow up. In equilibrium $\mu = 0$ corresponds to a certain ground state gap $\Delta_0 = \Delta_{0\times}$, which obtains from Eq. (5.25) and provides a characteristic energy scale for the crossover from the BCS to BEC regime. Vanishing of μ_i and μ_f at the intersection point implies that straight lines $\Delta_{0i} = \Delta_{0\times}$, $\Delta_{0f} = \Delta_{0\times}$, and $\Delta_{0i} = \Delta_{0f}$ and the $\mu_\infty = 0$ line must cross at the same point, which is indeed seen in all quench phase diagrams in Figs. 5.2, 5.3, 5.20, and 5.21.

Let us also obtain an explicit expression for the asymptotic spin distribution function Eq. (5.98) in all three regimes. Eq. (5.124) implies

$$\vec{L}^2(u) = \Delta_{0i}^2 L_0^2(u) + \left[(u-\mu_i)L_0(u) + \frac{\delta\omega}{g^2}\right]^2. \tag{5.132}$$

In the thermodynamic limit

$$L_0(u) = -\frac{2}{g^2} + \int_0^\infty \frac{f(\varepsilon)d\varepsilon}{2(u-\varepsilon)E_i(\varepsilon)}, \tag{5.133}$$

We evaluate $L_0(\varepsilon_\pm)$ using $(\varepsilon - \varepsilon' \pm i\delta)^{-1} = P(\varepsilon - \varepsilon')^{-1} \mp i\pi\delta(\varepsilon - \varepsilon')$. This results in

$$\begin{aligned}\cos\theta(\varepsilon) = &\frac{z(\varepsilon)}{i\pi f(\varepsilon)}\sqrt{A_-^2\Delta_{0i}^2 + \left[(\varepsilon-\mu_i)A_- + \frac{\delta\omega}{\gamma}\right]^2} \\ &-\frac{z(\varepsilon)}{i\pi f(\varepsilon)}\sqrt{A_+^2\Delta_{0i}^2 + \left[(\varepsilon-\mu_i)A_+ + \frac{\delta\omega}{\gamma}\right]^2},\end{aligned} \tag{5.134}$$

where

$$A_\mp = -\frac{2}{\gamma} \pm \frac{i\pi f(\varepsilon)}{2E_i(\varepsilon)} + \int_0^\infty \frac{f(\varepsilon')d\varepsilon'}{2(\varepsilon-\varepsilon')E_i(\varepsilon')}. \tag{5.135}$$

The integral here is the same as in Eq. (5.129). We evaluate it in elementary functions in 2d, in weak coupling BCS regime, and in BEC regime in Sects. 5.3.1 and 5.3.2 below, see also Eqs. (5.303) through (5.306) for explicit expressions. Note $\cos\theta(\varepsilon) = 1$ for $\delta\omega = 0$ (no quench) as it should. Representative plots of the spin distribution function for two quenches appear in Fig. 5.11. For future use we also write down the first two terms in large ε expansion of Eq. (5.134)

$$\cos\theta(\varepsilon) \approx 1 - \left(\frac{\delta\omega}{\gamma}\right)^2 \frac{2\Delta_{0i}^2}{E_i^2(\varepsilon)[H^2(\varepsilon) + \pi^2 f^2(\varepsilon)]}, \tag{5.136}$$

which are also independently the first two terms in its small $\delta\omega$ expansion. The function $H(\varepsilon)$ is defined in Eq. (5.307).

Next, we consider two and three dimensions separately as well as various special cases such as wide (single channel limit) and narrow resonance, deep BCS and BEC regimes.

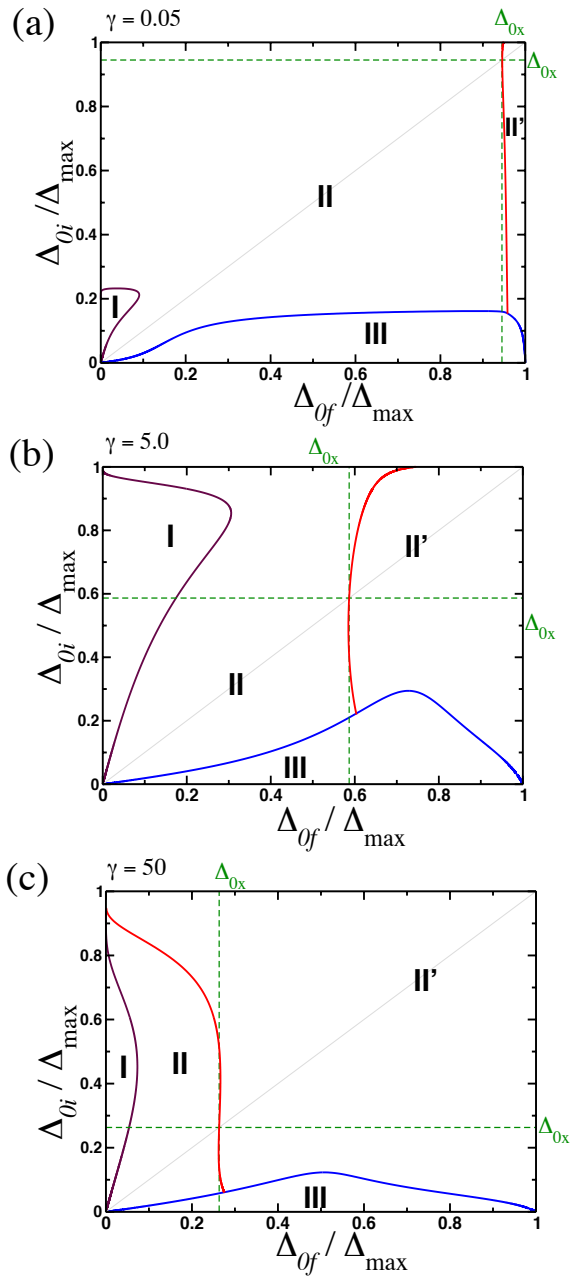


Figure 5.20: Detuning quench phase diagrams for 2-channel model in 2d for various resonance widths γ obtained from Eqs. (5.139) and (5.140). Each point represents a single quench labeled by Δ_{0i} and Δ_{0f} – pairing gaps the system would have in the ground state for initial and final detunings. At large times the system ends up in one of three steady states shown as regions I, II (including II'), and III. For quenches in region I the order parameter vanishes. In II $\Delta(t) \to \Delta_\infty e^{-2i\mu_\infty t - 2i\varphi}$ and in III $|\Delta(t)|$ oscillates persistently. Subregions II and II' differ in the sign of μ_∞ (out of equilibrium analog of the chemical potential): $\mu_\infty > 0$ in II and $\mu_\infty < 0$ in II'. The diagonal, $\Delta_{0i} = \Delta_{0f}$, is the no quench line. $\Delta_{0\times}$ is the ground state gap corresponding to zero chemical potential, i.e. $\Delta_{0\times}$ is given by Eq. (5.25) for $\mu = 0$.

5.3.1 2d

In 2d the dimensionless density of states $f(\varepsilon) = 1$ and all integrals above in this section can be evaluated in terms of elementary functions. It is convenient to introduce a notation

$$x = \frac{\mu_i}{\Delta_{0i}}, \quad v = \frac{u - \mu_i}{\Delta_{0i}}. \tag{5.137}$$

Eq. (5.127) reads

$$\ln\left[-\frac{(v+x)(v+\sqrt{1+v^2})}{\sqrt{1+x^2}\sqrt{1+v^2}-xv+1}\right] = -\frac{2\delta\omega(v\mp i)}{\gamma\sqrt{1+v^2}}+\frac{4\Delta_{0i}}{\gamma}\sqrt{1+v^2}. \tag{5.138}$$

The critical lines separating the three asymptotic regimes are determined by Eqs. (5.129) and (5.128), which become

$$\frac{|\delta\omega|}{\gamma} = \frac{\pi}{2}\sqrt{1+v^2}, \tag{5.139}$$

$$\ln\left[\frac{(v+x)(v+\sqrt{1+v^2})}{\sqrt{1+x^2}\sqrt{1+v^2}-xv+1}\right] = -\mathrm{sgn}(\delta\omega)\pi v+\frac{4\Delta_{0i}}{\gamma}\sqrt{1+v^2}, \tag{5.140}$$

where v is real and $v > -x$. It is straightforward to analyze Eq. (5.140) graphically and to find v and thus the critical lines numerically.

Positive $\delta\omega$ mean $\Delta_{0f} > \Delta_{0i}$ and the corresponding v determine the critical line separating regions I and II. In this case, for γ above a certain threshold γ_c to be determined below, there is a single root for any Δ_{0i}. This means that a horizontal $\Delta_{0i} = \text{const}$ line intersects the I-II line once for any value of the const and region I therefore extends all the way up to $\Delta_{0i} = \sqrt{\gamma} = \Delta_{\max}$ as seen in Figs. 5.2(c), 5.20(b) and 5.20(c). When $\gamma < \gamma_c$, the number of roots for positive $\delta\omega$ changes from one to two and then to zero as Δ_{0i} increases. The I-II line then displays peculiar reentrant behavior, see the inset in Fig. 5.2(b).

Negative $\delta\omega$ mean $\Delta_{0f} < \Delta_{0i}$. The roots v in this case yield the II-III critical line. There are two roots for Δ_{0i} below a certain threshold and no roots above it, implying that a horizontal $\Delta_{0i} = \text{const}$ line intersects the II-III critical line twice for a sufficiently small value of the const.

The shape of the critical lines as well as the complex roots of Eq. (5.138) can be determined analytically when the initial and/or final value of the detuning ω is deep in the BCS or BEC regime. The BCS limit corresponds to detuning $\omega \to +\infty$. For the ground state this implies $\mu \to \varepsilon_F = 1$, $\Delta_0 \to 0$. The gap equation (5.26) then yields

$$\ln\frac{4\varepsilon_\Lambda}{\Delta_0^2} = \frac{2\omega-4}{\gamma}. \tag{5.141}$$

Deep BEC regime obtains when $\omega \to -\infty$. In this case $\mu \to -\infty$ in the ground state. The gap and chemical potential equations switch roles in the sense that the former determines the chemical potential and the latter the ground state gap. Eq. (5.26) becomes

$$\ln\frac{\varepsilon_\Lambda}{|\mu|} = \frac{2\omega+4|\mu|}{\gamma} \tag{5.142}$$

and Eq. (5.25) reads in this limit

$$\Delta_0 = \left(\frac{1}{\gamma}+\frac{1}{4|\mu|}\right)^{-1/2}. \tag{5.143}$$

First, we consider quenches originating deep in the BCS regime, i.e. $\omega_i \to +\infty$ and therefore $\Delta_{0i} \to 0$, $\mu_i \to 1$. Such initial states correspond to $x \to +\infty$. Eq. (5.140) becomes

$$\ln\left[\frac{(v+x)(\sqrt{1+v^2}+v)}{x(\sqrt{1+v^2}-v)}\right] = -\mathrm{sgn}(\delta\omega)\pi v. \tag{5.144}$$

The roots are: $v \to 0$ for either sign of $\delta\omega$ and $v \to -x + 0$ for $\delta\omega < 0$. This translates into

$$u \approx \begin{cases} \mu_i, & \delta\omega > 0, \\ \mu_i \text{ or } +0, & \delta\omega < 0. \end{cases} \tag{5.145}$$

For $v \to 0$ Eq. (5.139) yields $\delta\omega/\gamma = \pm\pi/2$. Therefore, both Δ_{0f} and Δ_{0i} are deep in the BCS regime. The gap equation Eq. (5.141) implies $\Delta_0 \propto \exp(-\omega/\gamma)$ and hence

$$\frac{\Delta_{0i}}{\Delta_{0f}} = e^{\pm\pi/2}. \tag{5.146}$$

This result has been already obtained in Refs. [Barankov and Levitov(2006), Yuzbashyan and Dzero(2006)], which studied quenches within the single channel model in the weak coupling (BCS) limit. Weak coupling means small Δ_{0i} and Δ_{0f}, which corresponds to a vicinity of the origin, $\Delta_{0i} = \Delta_{0f} = 0$, in our phase diagrams. Eq. (5.146) is the slope of the I-II and II-III critical lines at the origin in Figs. 5.2, 5.3, 5.20, 5.21.

As we will see below, Eq. (5.146) also holds in 3d. This is expected on general grounds because in the BCS limit superconducting correlations come from a narrow energy window around the Fermi energy. Main contribution to integrals determining the roots comes from these energies. The density of states is then well approximated by a constant rendering the 2d and 3d cases equivalent.

The second root at $\delta\omega < 0$, $v \to -x + 0$, yields $\delta\omega/\gamma \approx -\pi x/2$. This means that the initial state is deep in the BCS regime, while $\omega_f \to -\infty$ and the ground state at ω_f is in the BEC limit. Further, $\mu_i \to \varepsilon_F = 1$, so $x \approx 1/\Delta_{0i}$. Subtracting Eq. (5.141) from Eq. (5.142), we obtain

$$\ln \frac{\Delta_{0i}^2}{4|\mu_f|} = -\frac{\pi}{\Delta_{0i}} + \frac{4|\mu_f|}{\gamma} + \frac{4}{\gamma}. \tag{5.147}$$

Here we assume γ is finite and treat the single channel limit $\gamma \to \infty$ separately below. Since $1/\Delta_{0i}$ term diverges much faster then the logarithm in the above equation, we get $4|\mu_f| \approx \pi\gamma/\Delta_{0i}$. Eq. (5.143) now obtains

$$\frac{\Delta_{0f}}{\Delta_{\max}} = 1 - \frac{\Delta_{0i}}{2\pi}, \tag{5.148}$$

This equation shows that the II-III critical line terminates at $(\Delta_{0f}, \Delta_{0i}) = (\Delta_{\max}, 0)$ linearly with a slope $\Delta_{0i}/(\Delta_{0f} - \Delta_{\max}) = -2\pi/\sqrt{\gamma}$.

Simpler expressions can also be derived for complex roots for quenches within the BCS regime, i.e. in the vicinity of the of the origin in the phase diagrams. By Eq. (5.145) the real parts of the roots in this regime $\mathrm{Re}[u] \approx \mu_i \approx \varepsilon_F$. Then, v is purely imaginary and also $|v| \ll x$ because $\mathrm{Im}[u]$ is related to the asymptotic value of order parameter amplitude, which is much smaller then ε_F. Eq. (5.138) becomes

$$\ln\left[\frac{v + \sqrt{1+v^2}}{v - \sqrt{1+v^2}}\right] = -\frac{v \mp i}{\sqrt{1+v^2}} \frac{2\delta\omega}{\gamma}. \tag{5.149}$$

This equation is symmetric with respect to complex conjugation and with respect to $v \to -v$. The latter symmetry reflects emergence of the particle-hole symmetry in the BCS limit. Note that when there is only one root, these two symmetries together require that it be purely imaginary.

Let $v = -i\cosh\phi$ in Eq. (5.149), where ϕ is either purely real or purely imaginary, so that v is purely imaginary. Eq. (5.149) yields depending on the sign choice on the right hand side

$$\phi = -\frac{\delta\omega}{\gamma}\coth(\phi/2), \tag{5.150}$$

$$\phi = -\frac{\delta\omega}{\gamma}\tanh(\phi/2). \tag{5.151}$$

Note that in this regime $\delta\omega/\gamma = \ln(\Delta_{0i}/\Delta_{0f})$. It is straightforward to analyze these equations graphically and to determine when they have solutions. We summarize the results.

Region I: $\Delta_{0i}/\Delta_{0f} > e^{\pi/2}$. There are no isolated roots and hence $\Delta(t) \to 0$ at large times.

Region II: $e^{-\pi/2} < \Delta_{0i}/\Delta_{0f} < e^{\pi/2}$. There is a single pair of isolated roots at $\mu_\infty \pm i\Delta_\infty$,

$$\mu_\infty = \varepsilon_F, \quad \Delta_\infty = \Delta_{0i}\cosh\phi, \tag{5.152}$$

where ϕ is real for $\delta\omega < 0$ and imaginary for $\delta\omega > 0$ and is the solution of Eq. (5.150). One can show $\Delta_\infty \leq \Delta_{0f}$ for any $\delta\omega$, where the equality is achieved only at $\delta\omega = 0$. The long-time dynamics is that described in Section 5.2.4.

It is instructive to evaluate Δ_∞, the asymptotic value of the magnitude of the gap, for infinitesimal quenches, when $|\Delta_{0f} - \Delta_{0i}| \ll \Delta_{0i}$. Expanding Eqs. (5.150) and (5.152) in small ϕ, we obtain after some calculation

$$\Delta_\infty = \Delta_{0f} - \frac{(\Delta_{0f} - \Delta_{0i})^2}{6\Delta_{0f}}. \tag{5.153}$$

Note that within linear analysis $\Delta_\infty = \Delta_{0f}$. As we show in Sect. 5.5, this is a general feature of linearized dynamics around the ground state regardless of coupling strength or initial conditions: $|\Delta(t)|$ tends to its ground state value corresponding to the Hamiltonian with which the system evolves at $t > 0$.

Region III: $\Delta_{0i}/\Delta_{0f} < e^{-\pi/2}$. There are two pairs of complex conjugate roots,

$$\varepsilon_F \pm i\Delta_{0i}\cosh\phi_1, \quad \varepsilon_F \pm i\Delta_{0i}\cosh\phi_2, \tag{5.154}$$

where ϕ_1 is the solution of Eq. (5.150) and ϕ_2 is the solution of Eq. (5.151); ϕ_2 is real when $\delta\omega/\gamma = \ln(\Delta_{0i}/\Delta_{0f}) \leq -2$ and imaginary otherwise. We see that the roots are indeed of the form Eq. (5.119). The asymptotic state is that of Section 5.2.4, while $\Delta(t)$ takes the simplified form Eq. (5.120).

Just as Eq. (5.146) the above results starting with Eq. (5.149) are universal in that they hold for quenches within the BCS regime independent of the dimensionality and also hold for the single channel model.

Next, consider quenches originating deep in the BEC, which corresponds to $\mu_i \to -\infty, \Delta_{0i} \to \sqrt{\gamma}$, and $x \to -\infty$. Since $v > -x$ in Eq. (5.140), we also have $v \to \infty$ provided a real root exists. Eq. (5.140) for $\delta\omega > 0$ simplifies to

$$\ln\left[\frac{v+x}{|x|}\right] = v\left(\frac{4\Delta_{0i}}{\gamma} - \pi\right) \tag{5.155}$$

For $4\Delta_{0i}/\gamma < \pi$, there is a single root at $v \to -x$, which corresponds to $u \approx 0$. Since $\Delta_{0i} \leq \sqrt{\gamma} = \Delta_{\max}$, the condition $\Delta_{0i} < \pi\gamma/4$ can be fulfilled only if $\gamma > \gamma_c$, where

$$\gamma_c = \frac{16}{\pi^2}. \tag{5.156}$$

For $\gamma \geq \gamma_c$ Eq. (5.140) at $\delta\omega > 0$ has a single root for any Δ_{0i} and, in particular, for $\Delta_{0i} \to \Delta_{\max}$. This means that the I-II critical line extends all the way up to $\Delta_{0i} = \Delta_{\max}$ terminating at $(\Delta_{0i}, \Delta_{0f}) = (\Delta_{\max}, 0)$.

It is interesting to work out the shape of the I-II critical line near its termination point. First, let $\gamma > \gamma_c$. Since $v \approx -x$, Eq. (5.139) implies $\delta\omega/\gamma \approx \pi|x|/2$. Using Eqs. (5.142) and (5.143) to determine Δ_{0i} and μ_i and Eq. (5.141) for Δ_{0f}, we get

$$\begin{aligned} \frac{\Delta_{0f}}{\Delta_{\max}} &= \frac{1}{\sqrt{2\varepsilon}}\exp\left(-\frac{\alpha}{2\varepsilon}\right), \\ \varepsilon = \frac{\Delta_{\max} - \Delta_{0i}}{\Delta_{\max}}, &\quad \alpha = \sqrt{\frac{\gamma}{\gamma_c}} - 1. \end{aligned} \tag{5.157}$$

This behavior is seen in Figs. 5.2(c), 5.20(b) and 5.20(c). Note the difference between $\gamma = 5$ and $\gamma = 50$ in Figs. 5.20(b) and 5.20(c) that correspond to $\alpha \approx 0.8$ and $\alpha \approx 4.6$, respectively.

Next, let $\gamma < \gamma_c$. In this case, the I-II critical line goes up, then bends backward reaching a maximum, goes down, and terminates on the Δ_{0i} axis below $\Delta_{\max}$, see e.g. the inset in Fig. 5.2(b). Near the termination point μ_i and ω_i are finite since $\Delta_{0i} < \Delta_{\max}$, while $\omega_f \to \infty$ since $\Delta_{0f} \to 0$. Eq. (5.139) implies $v \to \infty$ and $\delta\omega/\gamma \approx \pi v/2$. In this limit Eq. (5.140) becomes

$$\ln\left[\frac{2v}{\sqrt{1+x^2}-x}\right] = v\left(\frac{4\Delta_{0i}}{\gamma} - \pi\right). \tag{5.158}$$

We see that v diverges as $\Delta_{0i} \to \pi\gamma/4 = \pi\sqrt{\gamma}\Delta_{\max}/4 \equiv \Delta_{\rm th}$. Therefore, the I-II critical line terminates at $(\Delta_{0i}, \Delta_{0f}) = (\Delta_{\rm th}, 0)$. For Δ_{0i} above $\Delta_{\rm th}$ and below a certain upper value, which we do not determine explicitly, Eq. (5.140) has two roots. For Δ_{0i} below $\Delta_{\rm th}$ there is one root.

The shape of the I-II critical line as it approaches the termination point for $\gamma < \gamma_c$ obtains from Eq. (5.158). Let $\varepsilon = (\Delta_{0i} - \Delta_{\rm th})/\Delta_{\rm th} \ll 1$. Eq. (5.158) implies

$$v \approx \frac{1}{\pi\varepsilon}\ln\left[\frac{2(\sqrt{1+x^2}+x)}{\pi\varepsilon}\right]. \tag{5.159}$$

The gap equation (5.26) yields in 2d

$$\sqrt{1+x^2} + x = \frac{2(\gamma - \Delta_{0i}^2)}{\gamma\Delta_{0i}}. \tag{5.160}$$

Since $\omega_f \to \infty$ corresponds to the BCS limit, we have $\Delta_{0f} \propto e^{-\omega_f/\gamma} \propto e^{-\pi v/2}$. Combining this with the last two equations and using $\Delta_{0i} \approx \Delta_{\rm th} = \pi\gamma/4$, we get

$$\Delta_{0f} = C\exp\left(-\frac{1}{2\varepsilon}\ln\left[\frac{\gamma_c - \gamma}{\gamma\varepsilon}\right]\right), \tag{5.161}$$

where C is independent of ε.

The I-II critical line for $\gamma < \gamma_c$ is shown in Figs. 5.2(a), 5.2(b), and 5.20(a) that correspond to $\Delta_{\rm th}/\Delta_{\max} \approx 0.25, 0.78$, and 0.18, respectively. $\Delta_{\rm th}$ appears somewhat larger in these plots since exponentially small, but finite Δ_{0f} in Eq. (5.161) is not noticeable – the critical line effectively goes down along the Δ_{0i} axis. In the same way the I-II critical line appears to terminate below $\Delta_{\max}$ in Fig. 5.20 for $\gamma = 50$ due to exponential smallness of Δ_{0f} in Eq. (5.157).

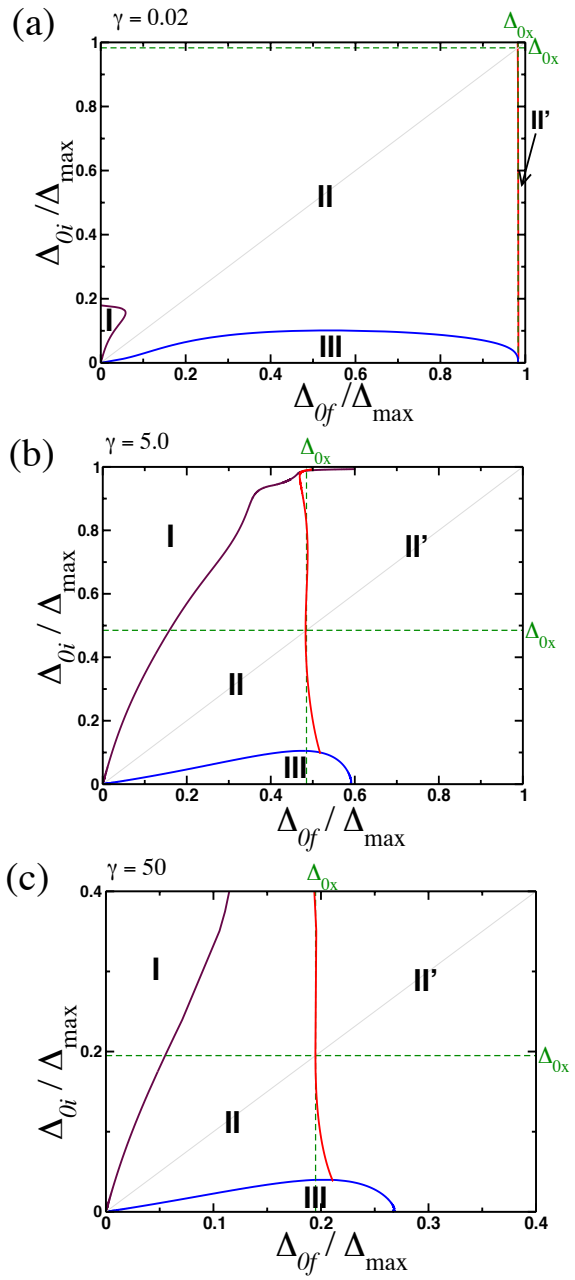


Figure 5.21: Detuning quench phase diagrams for 2-channel model in 3d for various resonance widths γ obtained from Eqs. (5.163) and (5.164). Otherwise same as Fig. 5.20.

5.3.2 3d

3d diagrams for various values of resonance width γ are shown in Figs. 5.3 and 5.21. Overall they are qualitatively similar to 2d diagrams. A notable difference is that in 3d region III of the oscillating order parameter $\Delta(t)$ for sufficiently large γ terminates at $\Delta_{0f} < \Delta_{\max} = \sqrt{2\gamma/3}$. This means that quenches from infinitesimally weak to sufficiently strong coupling produce no oscillations. Also, in contrast to the 2d case, the critical line separating the gapless region I in principle always extends all the way up to $\Delta_{0i} = \Delta_{\max}$ and terminates at $\Delta_{0f} = \Delta_{0f}^{\mathrm{I-II}} > 0$. This is however not noticeable at small γ because in this case the value of $\Delta_{0f}^{\mathrm{I-II}}$ is exponentially small.

In 3d the dimensionless density of states $f(\varepsilon) = \sqrt{\varepsilon}$ and Eq. (5.127) becomes

$$\int_{-x}^{\infty} \frac{dy\sqrt{\Delta_{0i}(x+y)}}{(v-y)\sqrt{y^2+1}} = -\frac{2\delta\omega}{\gamma(v \pm i)} + \frac{4\Delta_{0i}}{\gamma}, \tag{5.162}$$

where $y = \varepsilon/\Delta_{0i} - x$, and x and v are defined in Eq. (5.137). Similarly, Eqs. (5.129) and (5.128) determining critical lines read

$$\frac{|\delta\omega|}{\gamma} = \frac{\pi}{2}\sqrt{\Delta_{0i}(x+v)(v^2+1)}, \tag{5.163}$$

$$\int_{-x}^{\infty} \frac{dy\sqrt{\Delta_{0i}(x+y)}}{(v-y)\sqrt{y^2+1}} + \mathrm{sgn}(\delta\omega)\frac{\pi v\sqrt{\Delta_{0i}(x+v)}}{\sqrt{v^2+1}} = \frac{4\Delta_{0i}}{\gamma}, \tag{5.164}$$

The integral here is a complete elliptic integral. Substitution $y = 1/t - x$ reduces it to one of the Carlson elliptic integrals with known asymptotic behaviors in various regimes [Carlson and Gustafson(1994), DLMF()]. We however find it more convenient to evaluate the limiting behaviors by a direct analysis of the integral.

First, we consider initial states deep in the BCS regime, i.e. $\omega_i \to +\infty$, which implies $\Delta_{0i} \to 0$, $\mu_i \to 1$, and $x \to 1/\Delta_{0i} \to +\infty$. To evaluate the integral in Eqs. (5.162) and (5.164) in this regime, we split the integration range into three intervals: $(-x, -y_\Lambda), (-y_\Lambda, y_\Lambda), (y_\Lambda, \infty)$, where y_Λ is such that $1 \ll y_\Lambda \ll x$. Let the corresponding integrals be I_1, I_2 and I_3. To the leading order in $1/y_\Lambda$ and y_Λ/x we can replace $\sqrt{y^2+1} \to |y|$ in I_1, I_3 and $\sqrt{x+y} \to \sqrt{x}$ in I_2. The resulting integrals evaluate in terms of elementary functions

$$I_1 + I_3 = \frac{2\sqrt{x}}{v}\ln\frac{4x}{y_\Lambda} - \frac{\sqrt{x+v}}{v}\ln\frac{4x(\sqrt{x+v}+\sqrt{x})^2}{y_\Lambda^2 - 4x(\sqrt{x+v}-\sqrt{x})^2},$$

$$I_2 = \frac{\sqrt{x}}{\sqrt{1+v^2}}\ln\frac{(\sqrt{1+v^2}\sqrt{1+y_\Lambda^2}+vy_\Lambda)(v+y_\Lambda)}{(\sqrt{1+v^2}\sqrt{1+y_\Lambda^2}-vy_\Lambda)(v-y_\Lambda)},$$

where we used $1 \ll y_\Lambda \ll x$ to simplify expressions. The dependence on y_Λ should of course cancel from $I_1 + I_2 + I_3$ to the leading order in $1/y_\Lambda$ and y_Λ/x.

The gap equation (5.26) in the BCS regime is handled similarly by splitting the integral into three resulting in

$$\frac{\omega}{\gamma} - \frac{2}{\gamma} = \sqrt{\varepsilon_\Lambda} - 2 + \ln\frac{8}{\Delta_0}. \tag{5.165}$$

Suppose the final detuning is also in the BCS regime. The above equation then implies

$$\frac{\delta\omega}{\gamma} = \ln\frac{\Delta_{0i}}{\Delta_{0f}}, \tag{5.166}$$

same as in 2d. Because $\delta\omega/\gamma$ must remain of order one as $x \to +\infty$, it follows from Eq. (5.163) that v is also of order one for quenches within the BCS regime. Therefore $|v| \ll y_\Lambda$ in the above expressions for $I_1 + I_2$ and I_3. We obtain $|I_1 + I_2| \ll 1$ and

$$I_1 + I_2 + I_3 \approx I_3 \approx \frac{1}{1+v^2}\ln\left[\frac{v+\sqrt{1+v^2}}{v-\sqrt{1+v^2}}\right]. \tag{5.167}$$

Eq. (5.162) now turns into the 2d Eq. (5.149), Eq. (5.163) yields $|\delta\omega|/\gamma = \pi/2$ and therefore Eq. (5.146). Thus quenches within the BCS regime in 3d are identical to those in 2d and all results from Eq. (5.149) to Eq. (5.154) also hold in 3d. As we already commented above, this is expected since in the BCS regime superconductivity comes from the vicinity of the Fermi energy making the dependence of the density of states on the energy and thus the dimensionality inessential.

The horizontal $\Delta_{0i} = \text{const}$ line for infinitesimal values of the const intersects the II-III critical line twice, once near the origin, and the second time near the termination point of the II-III critical line. The former intersection corresponds to small v, as we saw above, and the latter to v of order x. To determine the termination point we therefore take $|v| \gg y_\Lambda$ in the above expressions for $I_1 + I_3$ and I_2. Eq. (5.162) becomes

$$\begin{gathered}\frac{\sqrt{x+v}}{\sqrt{x}} \ln \frac{(\sqrt{x+v}+\sqrt{x})^2}{-(\sqrt{x+v}-\sqrt{x})^2} = \\ -2\left[\frac{\delta\omega}{\gamma} + \ln\frac{8}{\Delta_{0i}} - \frac{2v\Delta_{0i}}{\gamma}\right] \pm \frac{2i\delta\omega}{v\gamma}.\end{gathered} \tag{5.168}$$

The real root of this equation is $v \approx -x \approx -1/\Delta_{0i}$ yielding

$$\frac{\delta\omega}{\gamma} = -\ln\frac{8}{\Delta_{0i}} - \frac{2}{\gamma}. \tag{5.169}$$

Combining this with Eq. (5.165), taking the limit $\Delta_{0i} \to 0$, and plugging into the gap equation (5.26), we obtain

$$4 + \frac{4\mu_f}{\gamma} = \int_0^\infty \left[\frac{1}{\varepsilon} - \frac{1}{\sqrt{(\varepsilon-\mu_f)^2 + \Delta_{0f}^2}}\right]\sqrt{\varepsilon}d\varepsilon, \tag{5.170}$$

where we sent the cutoff ε_Λ to infinity. Eq. (5.170) together with the chemical potential equation (5.25) determine the value of $\Delta_{0f}^{\text{II-III}}$ where the II-III critical line terminates on the Δ_{0f} axis. $\Delta_{0f}^{\text{II-III}}$ is a function of γ only, see Fig. 5.22.

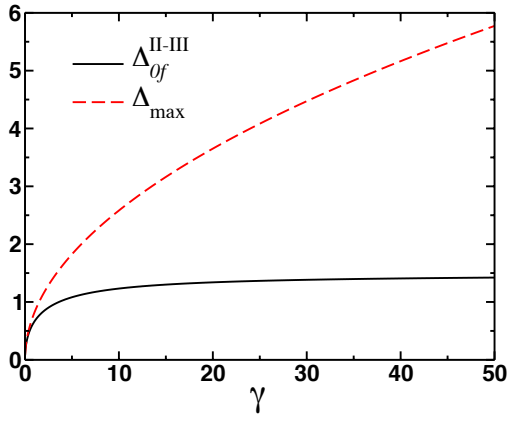


Figure 5.22: Termination point of the II-III critical line as a function of resonance width γ in units of Fermi energy for 3d 2-channel model. This line encloses region III of persistent oscillations in Figs. 5.3 and 5.21. It starts at the origin and ends at $\Delta_{0f}^{\text{II-III}}$ along the Δ_{0f} axis. This reflects an interesting phenomenon: there are no persistent oscillations for quenches to couplings stronger then a certain threshold (i.e. quenches to detunings ω_f such that the corresponding ground state gaps $\Delta_{0f} \geq \Delta_{0f}^{\text{II-III}}$) no matter how weak the initial coupling is (i.e. for any initial detuning). At $\gamma \to \infty$ (1-channel limit) $\Delta_{0f}^{\text{II-III}}$ saturates at $1.49\varepsilon_F$ in agreement with Eq. (5.194).

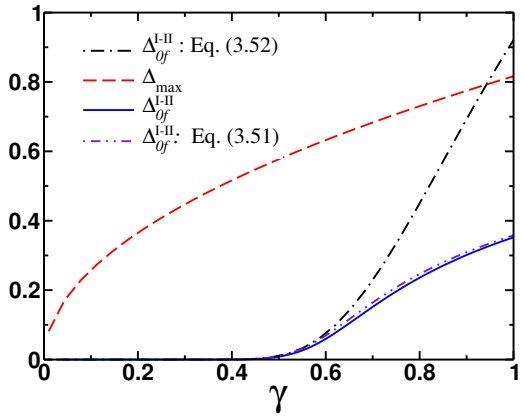


Figure 5.23: Unlike 2d, in 3d Δ_{0f} tends to a finite value $\Delta_{0f}^{\text{I–II}}$ along the I-II critical line as the initial detuning $\omega_i \to -\infty$ ($\Delta_{0i} \to \Delta_{\max}$) for quenched 2-channel model, see e.g. Fig. 5.21. The gapless regime thus persists even for quenches from arbitrarily large negative ω_i to finite ω_f. Here we compare $\Delta_{0f}^{\text{I–II}}$ (in units of the Fermi energy) as a function of the resonance width γ extrapolated from actual phase diagrams with that obtained from Eqs. (3.51) and (3.52). Note that $\Delta_{0f}^{\text{I–II}}$ is exponentially small at small γ, so that the I-II critical line *appears* to close earlier at zero Δ_{0f} in Fig. 5.21(a).

We also note that it follows from the above analysis that, just as in 2d, for initial states deep in the BCS regime there are three roots: $v \to 0$ for either sign of $\delta\omega$ and $v \to -x + 0$ for $\delta\omega < 0$. Therefore, Eq. (5.145) holds in 3d as well.

Second, consider quenches from deep BEC to larger detuning $\omega_f > \omega_i$, i.e. $\omega_i \to -\infty, \delta\omega > 0, \mu_i \to -\infty, x \to -\infty, \Delta_{0i} \to \Delta_{\max}$. Since $y \geq |x| \gg 1$ in Eq. (5.164), we can replace $\sqrt{y^2+1} \to y$. The principal value integral evaluates to $-\pi\sqrt{|x|}/v$ and Eq. (5.164) becomes

$$-\frac{\pi\sqrt{|x|}}{v} + \pi\sqrt{v-|x|} = \frac{4\sqrt{\Delta_{0i}}}{\gamma}, \tag{5.171}$$

where we also took into account that we need $v \geq |x|$ so that Eq. (5.163) yields real $\delta\omega$. The solution for large $|x|$ is

$$\sqrt{v-|x|} \approx \frac{4\sqrt{\Delta_{0i}}}{\pi\gamma} + \frac{1}{\sqrt{|x|}}. \tag{5.172}$$

Eq. (5.163) now yields

$$\frac{\delta\omega}{\gamma} \approx \frac{2|\mu_i|}{\gamma} + \frac{\pi}{2}\sqrt{|\mu_i|} + \frac{32\Delta_{\max}^2}{\pi^2\gamma^3}, \tag{5.173}$$

where we replaced $\Delta_{0i}^2 \to \Delta_{\max}^2 = 2\gamma/3$ up to terms of order $|\mu_i|^{-1/2}$. The overall correction to this expression is also proportional to $|\mu_i|^{-1/2}$ at large $|\mu_i|$.

Similar simplifications occur in the gap equation (5.26). We replace the square root with $\varepsilon - \mu_i$ to obtain

$$\frac{\omega_i}{\gamma} \approx \sqrt{\varepsilon_\Lambda} - \frac{2|\mu_i|}{\gamma} - \frac{\pi}{2}\sqrt{|\mu_i|}.$$

Last two equations determine ω_f and from the gap equation (5.26) for $\omega = \omega_f$ we obtain

$$\frac{128}{3\pi^2\gamma^2} - \frac{4\mu_f}{\gamma} = \int_0^\infty \left[\frac{\sqrt{\varepsilon}}{\sqrt{(\varepsilon-\mu_f)^2+\Delta_{0f}^2}} - \frac{1}{\sqrt{\varepsilon}}\right] d\varepsilon, \tag{5.174}$$

where we eliminated the cutoff similar to Eq. (5.170). This equation combined with Eq. (5.25) determines the termination point $(\Delta_{0i}, \Delta_{0f}) = (\Delta_{\max}, \Delta_{0f}^{\text{I–II}})$ of the I-II critical line. The plot of $\Delta_{0f}^{\text{I–II}}$ as a function of γ is shown in Fig. 5.23.

Note that, in contrast to the 2d case, this critical line formally always extends up to $\Delta_{0i} = \Delta_{\max}$ and $\Delta_{0f}^{\mathrm{I-II}}$ does not vanish as $\Delta_{0i} \to \Delta_{\max}$. This means that the gapless regime persists even for quenches to finite final detunings from initial states lying arbitrarily deep in the BEC regime. But for small γ the value of $\Delta_{0f}^{\mathrm{I-II}}$ is exponentially small and the critical line *appears* to have closed at smaller Δ_{0i}, see Figs. 5.3(a) and 5.21(a). Small γ implies large left hand side in Eq. (5.174) and therefore the final state deep in the BCS regime. In this regime $\mu_f \to 1$ and the integral in Eq. (5.174) is twice the right hand side of Eq. (5.165) without $\sqrt{\varepsilon_\Lambda}$ resulting in

$$\Delta_{0f}^{\mathrm{I-II}} = 8 \exp\left[-\frac{64}{3\pi^2\gamma^2} + \frac{2}{\gamma} - 2\right]. \tag{5.175}$$

We see from Fig. 5.23 that $\Delta_{0f}^{\mathrm{I-II}}$ becomes noticeable for $\gamma \gtrsim 0.45$. For smaller γ the gapless region I appears to close at smaller Δ_{0i} and zero Δ_{0f}. Fig. 5.23 also shows that Eq. (5.175) provides a reasonable estimate of $\Delta_{0f}^{\mathrm{I-II}}$ even for large γ, which will be useful in our analysis of the 1-channel model below.

5.4 One channel model

In this section we collect for reference purposes analogous results for the asymptotic steady state after a quench $\lambda_i \to \lambda_f$ in the one channel model given by Eqs. (5.3) and (5.5).

As explained in Sect. 5.1.1, the one channel model obtains in the broad resonance limit via replacements

$$\frac{\omega}{\gamma} = \frac{\omega}{g^2\nu_F} \to \frac{1}{\lambda}, \quad \gamma = g^2\nu_F \to \infty \tag{5.176}$$

(in units of ε_F). Our task is to go over equations of previous sections performing these replacements. All essential reasoning and methods are the same.

Chemical potential and gap Eqs. (5.25) and (5.26) now read

$$\frac{4}{d} = \int_0^\infty \left(1 - \frac{\varepsilon - \mu}{\sqrt{(\varepsilon-\mu)^2 + \Delta_0^2}}\right) f(\varepsilon) d\varepsilon, \tag{5.177}$$

and

$$\frac{2}{\lambda} = \int_0^{\varepsilon_\Lambda} \frac{f(\varepsilon)d\varepsilon}{\sqrt{(\varepsilon-\mu)^2 + \Delta_0^2}}, \tag{5.178}$$

respectively.

The Lax vector becomes

$$\vec{L}(u) = \sum_{\mathbf{p}} \frac{\vec{s}_{\mathbf{p}}}{u - \varepsilon_{\mathbf{p}}} - \frac{\hat{\mathbf{z}}}{\lambda\nu_F}. \tag{5.179}$$

Gaudin algebra, i.e. Eqs. (5.51) and (5.52), as well as the Lax equation of motion (5.57) are the same. The numerator of the conserved $\vec{L}^2(u)$ is now a polynomial of degree $2N$,

$$\vec{L}^2(u) = \frac{Q_{2N}(u)}{(\lambda\nu_F)^2 \prod_{\mathbf{p}} (u - \varepsilon_{\mathbf{p}})^2}, \tag{5.180}$$

where N is the number of nondegenerate $\varepsilon_{\mathbf{p}}$.

Reduced solutions are constructed in the same way with minor modifications. Specifically, the expressions for $\vec{L}^{\mathrm{red}}(u)$ in terms of $\vec{\sigma}_{\mathbf{p}}$ and $\vec{L}_m(u)$ in terms of $\vec{t}_j$ are replaced in Eqs. (5.59) and (5.60) with the corresponding 1-channel Lax vectors according to Eq. (5.179). The Hamiltonian governing the collective spin variables $\vec{t}_j$ is

$$H_{1\mathrm{ch}}^{\mathrm{red}} = \sum_{j=0}^{m-1} 2\eta_j t_j^z - \lambda\nu_F \sum_{j,k=0}^{m-1} t_j^- t_k^+. \tag{5.181}$$

Eqs. (5.62) and (5.63) as well as constraints (5.64) are the same, except that the last equation relating ω and ω' is absent. In terms of the m-spin spectral polynomial $Q_{2m}(u)$ the constraints become

$$\sum_{\mathbf{p}} \frac{\sigma_{\mathbf{p}} \varepsilon_{\mathbf{p}}^{r-1}}{\sqrt{Q_{2m}(\varepsilon_{\mathbf{p}})}} = -\frac{\delta_{rm}}{(\lambda \nu_F)^2}, \quad r = 1, \ldots, m. \tag{5.182}$$

Further, since the degree of the m-spin spectral polynomial is $2m$ rather then $2(m+1)$, an m-spin solution of the 2-channel model becomes an $(m+1)$-spin solution of the 1-channel model. This name change reflects the fact that the oscillator mode b in the 2-channel model is effectively an additional spin, which was not counted as such.

All remaining equations in Sect. 5.2, i.e. Eqs. (5.67) through (5.123), are identical for the one channel model, except Eq. (5.70) is replaced with Eq. (5.181) for $m = 2$ and the self-consistency condition (5.99) is now given by Eq. (5.13).

Equations determining isolated roots, critical lines, and $\mu_\infty = 0$ line for the 1-channel model are Eq. (5.127), Eqs. (5.129) and (5.128), and Eq. (5.130), respectively, with replacements

$$\frac{\delta\omega}{\gamma} \to \frac{1}{\lambda_f} - \frac{1}{\lambda_i} \equiv \beta, \quad \frac{1}{\gamma} \to 0. \tag{5.183}$$

Asymptotic spin distribution – the constant angle the spin $\vec{s}(\varepsilon)$ makes with the spin $\vec{\sigma}(\varepsilon)$ in the corresponding m-spin solution – is

$$\begin{aligned} \cos\theta(\varepsilon) = &\frac{z(\varepsilon)}{i\pi f(\varepsilon)} \sqrt{A_-^2 \Delta_{0i}^2 + \left[(\varepsilon - \mu_i) A_- + \delta\beta\right]^2} \\ &- \frac{z(\varepsilon)}{i\pi f(\varepsilon)} \sqrt{A_+^2 \Delta_{0i}^2 + \left[(\varepsilon - \mu_i) A_+ + \delta\beta\right]^2}, \end{aligned} \tag{5.184}$$

where

$$A_\pm = \pm \frac{i\pi f(\varepsilon)}{2E_i(\varepsilon)} + \int_0^\infty \frac{f(\varepsilon')d\varepsilon'}{2(\varepsilon - \varepsilon')E_i(\varepsilon')}. \tag{5.185}$$

Eq. (5.184) is in excellent agreement with the actual spin distribution obtained from direct simulation of spin dynamics[Yuzbashyan and Dzero(2006)], see Fig. 3 therein.

5.4.1 Quench phase diagram

Quench phase diagrams for 1-channel model in 2d and 3d are shown in Figs. 5.4 and 5.5. There is only one diagram in each case extending to positive infinity in both Δ_{0i} and Δ_{0f} directions because $\gamma \to \infty$ and therefore $\Delta_{\max} \to \infty$.

As we commented below Eqs. (5.146) and (5.154), the weak coupling part of the diagrams (the region of small Δ_{0i} and Δ_{0f} near the origin) is independent of the dimensionality and is exactly the same for 1-channel model. In other words, all results contained in Eqs. (5.149) through (5.154) and the surrounding text apply to the one channel model in both 2d and 3d; one only needs to replace $\delta\omega/\gamma \to \delta\beta$.

When either the initial or final coupling is outside the deep BCS regime, we need to treat 2d and 3d cases separately.

2d

It is straightforward to take the broad resonance limit in Eqs. (5.138) to (5.144). In particular, the critical lines are determined by taking this limit in Eqs. (5.139) and (5.140)

$$|\delta\beta| = \frac{\pi}{2}\sqrt{1+v^2}, \tag{5.186}$$

$$\ln\left[\frac{(v+x)(v+\sqrt{1+v^2})}{\sqrt{1+x^2}\sqrt{1+v^2}-xv+1}\right]=-\mathrm{sgn}(\delta\beta)\pi v. \tag{5.187}$$

Eq. (5.145) describing quenches originating in deep BCS remains as is, except the sign of $\delta\omega$ translates into the sign of $\delta\beta$. The two roots $u\approx\mu_i$ for either sign of $\delta\beta$ correspond to quenches also terminating in deep BCS, so they are in the universal regime given by Eqs. (5.149) through (5.154), which is shared by both models regardless of the dimensionality.

The analysis for the root $u\approx+0$ at $\delta\beta<0$ leading to Eq. (5.148) requires some modifications. $\gamma\to\infty$ limit in Eqs. (5.147) and (5.143) yields $4|\mu_f|=\Delta_{0i}^2e^{\pi/\Delta_{0i}}$, $\Delta_{0f}=\sqrt{4|\mu_f|}$ and finally

$$\Delta_{0f}=\Delta_{0i}e^{\pi/2\Delta_{0i}},\quad \Delta_{0i}\to 0. \tag{5.188}$$

This equation gives the asymptotic form of the II-III critical line in the $(\Delta_{0i},\Delta_{0f})$ plane in Fig. 5.4. We see that this line never terminates in the 2d 1-channel model.

Finally, let us work out the shape of the I-II critical line for large Δ_{0i}, i.e. for quenches originating deep in the BEC regime. Eq. (5.155) becomes

$$\ln\left[\frac{v+x}{|x|}\right]=-\pi v. \tag{5.189}$$

Now there is always a single root $v\to-x$ ($u\approx 0$). Eq. (5.186) implies

$$\delta\beta=\frac{1}{\lambda_f}-\frac{1}{\lambda_i}=\frac{\pi|x|}{2}=\frac{\pi|\mu_i|}{2\Delta_{0i}}. \tag{5.190}$$

We also need the gap equation in BCS and BEC limits and the chemical potential equation in the BEC limit. Sending γ to infinity in Eqs. (5.141), (5.142) and (5.143), we obtain

$$\ln\frac{4\varepsilon_\Lambda}{\Delta_{0i}^2}=\frac{2}{\lambda_i},\quad \ln\frac{\varepsilon_\Lambda}{|\mu_f|}=\frac{2}{\lambda_f},\quad \Delta_{0i}=\sqrt{4|\mu_i|}. \tag{5.191}$$

Combining these equations with Eq. (5.190), we get

$$\Delta_{0f}=\Delta_{0i}e^{-\pi\Delta_{0i}/8},\quad \Delta_{0i}\to\infty. \tag{5.192}$$

We see that Δ_{0f} exponentially vanishes along the I-II critical line (gapless regime closes) as Δ_{0i} increases. The vertical range of Fig. 5.4 is not enough to fully display this behavior, though we see that I-II line does incline towards the Δ_{0i} axis at large Δ_{0i}.

3d

In addition to quenches that fall within the universal weak coupling regime described in Eqs. (5.149) to (5.154) and the corresponding text, let us derive the termination point of the II-III critical line and analyze the I-II line at large Δ_{0i}.

First, we consider the II-III line. The termination point is given by Eq. (5.170). In the $\gamma\to\infty$ limit we have

$$4=\int_0^\infty\left[\frac{1}{\varepsilon}-\frac{1}{\sqrt{(\varepsilon-\mu_f)^2+\Delta_{0f}^2}}\right]\sqrt{\varepsilon}d\varepsilon. \tag{5.193}$$

Chemical potential equation (5.177) provides another relation between μ_f and Δ_{0f}. Numerical solution of these two equations is

$$\mu_f^{\mathrm{II-III}}\approx-1.4602\varepsilon_F,\quad \Delta_{0f}^{\mathrm{II-III}}\approx 1.4875\varepsilon_F. \tag{5.194}$$

This value of $\Delta_{0f}^{\text{II-III}}$ agrees with Fig. 5.22. Unlike 2d, in 3d region III encloses a finite area, resembling a dome in between the origin and the point $(\Delta_{0i}, \Delta_{0f}) = (0, \Delta_{0f}^{\text{II-III}})$.

Next, we turn to the critical line separating the gapless region I from region II. For finite γ we analyzed the termination point $(\Delta_{0i}, \Delta_{0f}) = (\Delta_{\max}, \Delta_{0f}^{\text{I-II}})$ of this line at the end of Sect. 5.3.2. In the single channel case, $\Delta_{\max} \to \infty$, so the I-II line does not close. As $\Delta_{0i} \to \infty$, the value of Δ_{0f} for a point on this line tends to $\Delta_{0f}^{\text{I-II}}$, which is determined by the $\gamma \to \infty$ limit of Eq. (5.174),

$$0 = \int_0^\infty \left[\frac{1}{\sqrt{(\varepsilon - \mu_f)^2 + \Delta_{0f}^2}} - \frac{1}{\varepsilon} \right] \sqrt{\varepsilon} d\varepsilon, \tag{5.195}$$

together with Eq. (5.177). The solution of these equations is

$$\mu_f \approx 0.5906 \varepsilon_F, \quad \Delta_{0f}^{\text{I-II}} \approx 0.6864 \varepsilon_F. \tag{5.196}$$

5.5 Transient Dynamics: Linear analysis

Here we solve the dynamics for small deviations from the ground state. Linear analysis for the one channel model in the weak coupling BCS regime was performed by Volkov and Kogan[Volkov and Kogan(1973)], see also Ref. [Yuzbashyan and Dzero(2006)]. Gurarie[36] extended this study to strongly coupled superconductors. Both these studies of the linearized dynamics conclude that

$$\Delta(t) \to \Delta_\infty e^{-2i\mu_\infty t - 2i\varphi} \tag{5.197}$$

as $t \to \infty$, but the approach to this asymptote is different. Our analysis adds several new results to this prior work. We demonstrate that within linear analysis the amplitude of the order parameter asymptotes to its ground state value for the Hamiltonian with which the system evolves after nonequilibrium conditions are created, i.e. $\Delta_\infty = \Delta_{0f}$, a point that seems to have been missed by the earlier work. Also, $\mu_\infty = \mu_f$ – the ground state chemical potential. In other words, $\Delta_\infty - \Delta_0$ and $\mu_\infty - \mu_f$ are second order in the deviation. This is a general result that holds for both one and two channel models and is independent of the type of perturbation that drives the system out of equillibrium.

Further, we solve linearized equations of motion using the machinery of the exact solution [Yuzbashyan et al.(2005c), Yuzbashyan et al.(2005a)], which provides much more detailed information. For example, we also determine the short time behavior, normal modes, full explicit long time form $\Delta(t)$ and individual spins with all prefactors and phases etc. unavailable to conventional linear analysis. Note that in quench phase diagrams constructed above small quenches correspond to the vicinity of the diagonal $\Delta_{0i} = \Delta_{0f}$, see e.g Figs. 5.20 and 5.21.

5.5.1 Asymptotic $\Delta(t)$ and spins

Consider an infinitesimal quench of the detuning $\delta\omega = \omega_f - \omega_i$. More generally, $\delta\omega$ can be any small parameter that measures the deviation from the ground state in the two or one channel model. We work to linear order in $\delta\omega$. Suppose $\Delta(t) \to \Delta_\infty e^{-2i\mu_\infty t - 2i\varphi}$. For the detuning or interaction quenches this follows from the few spin conjecture and quench phase diagrams derived above and we also verify it independently below. Let us go to a reference frame that rotates with frequency $2\mu_\infty$ around the z-axis. In this frame $\Delta(t) = \Delta_\infty$ and the magnetic field $\vec{B}_{\mathbf{p}} = (-2\Delta_\infty, 0, 2\varepsilon_{\mathbf{p}} - 2\mu_\infty)$ acting on spin $\vec{s}_{\mathbf{p}}$ in Eq. (5.8) is time-independent. Note that transformation to the rotating frame results in shifts to $\varepsilon_{\mathbf{p}}$ and ω_f. Then, the spin rotates around $\vec{B}_{\mathbf{p}}$ making a constant angle $\pi - \theta_{\mathbf{p}}$ with it. This is in fact the asymptotic

solution described in Sect. 5.2.4,

$$\vec{s}_{\mathbf{p}}(t) = \frac{\vec{n}_{\mathbf{p}}}{2}\cos\theta_{\mathbf{p}} + \vec{s}^{\perp}_{\mathbf{p}}(t), \tag{5.198}$$

where $\vec{n}_{\mathbf{p}}$ is a unit vector along $-\vec{B}_{\mathbf{p}}$,

$$n^x_p = \frac{\Delta_\infty}{E^\infty_{\mathbf{p}}}, \quad n^y_{\mathbf{p}} = 0, \quad n^z_{\mathbf{p}} = -\frac{\varepsilon_{\mathbf{p}} - \mu_\infty}{E^\infty_{\mathbf{p}}}. \tag{5.199}$$

Eq. (5.8) with $\dot{b} = 0$ further implies $\Delta_\infty = -gb = g^2 J_-/(\omega_f - 2\mu_\infty)$. The contribution of $\vec{s}^{\perp}_{\mathbf{p}}$ to J_- dephases as $t \to \infty$. The latter is therefore $\sum_{\mathbf{p}} n^x_p/2$ – the sum of components of $\vec{s}_{\mathbf{p}}$ along $\vec{B}_{\mathbf{p}}$ projected onto the xy-plane,

$$\Delta_\infty = \frac{g^2}{\omega_f - 2\mu_\infty}\sum_{\mathbf{p}} \frac{\Delta_\infty \cos\theta_{\mathbf{p}}}{2\sqrt{(\varepsilon_{\mathbf{p}} - \mu_\infty)^2 + \Delta^2_\infty}}. \tag{5.200}$$

In the ground state $\vec{s}_{\mathbf{p}}$ is aligned with $-\vec{B}_{\mathbf{p}}$, i.e. $\theta_{\mathbf{p}} = 0$. This implies that $\theta_{\mathbf{p}}$ must be proportional to $\delta\omega$ and therefore corrections to $\cos\theta_{\mathbf{p}} = 1$ are second order in $\delta\omega$. But for $\cos\theta_{\mathbf{p}} = 1$, Eq. (5.200) is the ground state gap equation (5.18) for $\omega = \omega_f$. Moreover, applying the same argument to J_z and Eq. (5.19), we find that Δ_∞ and μ_∞ also satisfy the ground state chemical potential equation (5.20). It follows that for small oscillations around the ground state one always has

$$\Delta_\infty = \Delta_{0f}, \quad \mu_\infty = \mu_f. \tag{5.201}$$

For the same reason the non-oscillatory part of $\vec{s}_{\mathbf{p}}$ (zeroth harmonic) in the steady state is the same as in the ground state at $\omega = \omega_f$, i.e. is given by Eq. (5.15) with $\Delta_0 \to \Delta_{0f}$ and $\mu \to \mu_f$.

The same is true for the one channel model. Note also that infinitesimal quenches in the BCS regime conform to this conclusion, see Eq. (5.153). Moreover, this result generalizes to finite spin dynamics, where, as we show below, zeroth harmonics of $\Delta(t)$ and $\vec{s}_{\mathbf{p}}$ to linear order in $\delta\omega$ coincide with the $\omega = \omega_f$ ground state values.

5.5.2 Normal modes and finite size dynamics

Now we turn to the linear analysis per se. At this point it is convenient to rewrite summations over $\mathbf{p}$ as summations over single particle energies. We adopt the following model of discrete spectrum. Let us discretize the magnitude of the momentum, $p \to p_k$. The corresponding energies are $\varepsilon_k = p_k^2/2m$ with degeneracy $N_k = N(\varepsilon_k)$ – the number of states in a momentum shell between p_k and p_{k+1}, which is a smooth function of ε_k. The level spacing $\delta_k = \varepsilon_{k+1} - \varepsilon_k$ is also assumed to depend on ε_k smoothly. We include this dependence in N_k, so without loss of generality we take it to be constant, $\delta_k = \delta$. Our final results depend only on the density of states $\nu(\varepsilon_k) = N_k/\delta$ – the number of states per unit energy. Equivalently, ε_i can represent levels of some other single particle potential, e.g. a 3d harmonic oscillator potential, see the discussion at the end of Sect. 5.1.1. All quantities and equations, including spins $\vec{s}_{\mathbf{p}}$, Hamiltonians, equations of motion and initial conditions, considered in this paper depend on $\mathbf{p}$ only through $\varepsilon_{\mathbf{p}}$. For any such quantity $A_{\mathbf{p}} = A(\varepsilon_{\mathbf{p}})$

$$\sum_{\mathbf{p}} A_{\mathbf{p}} = \sum_{k=1}^{N} N_k A_k \to \int \nu(\varepsilon) d\varepsilon, \tag{5.202}$$

where $A_k = A(\varepsilon_k)$. In particular, the Lax vector (5.50) reads

$$\vec{L}(u) = \sum_{k=1}^{N} \frac{N_k \vec{s}_k}{u-\varepsilon_k} - \frac{(\omega-2\mu)}{g^2}\hat{\mathbf{z}} + \frac{2}{g^2}\left[(u-\mu)\hat{\mathbf{z}} - \vec{\Delta}\right]. \tag{5.203}$$

A convenient tool for linear analysis of the dynamics are the separation variables introduced in Refs. [Yuzbashyan et al.(2005a)] and [Yuzbashyan et al.(2005c)] for the one and two channel models, respectively. As we will see, in linearized dynamics these variables are simply the normal modes. Separation variables u_j are defined as the solutions of $L_-(u_j) \equiv L_x(u_j) - iL_y(u_j) = 0$, i.e.

$$L_-(u) = \frac{2b}{g} + \sum_{k=1}^{N} \frac{N_k s_k^-}{u-\varepsilon_k} = 0. \tag{5.204}$$

Because $u = u_j$ are the zeroes of the rational function $L_-(u)$ and $u = \varepsilon_k$ are its poles, we can also write it as

$$L_-(u) = \frac{2b}{g}\frac{\prod_j (u-u_j)}{\prod_k (u-\varepsilon_k)}. \tag{5.205}$$

Matching the residues at $u = \varepsilon_k$ and $u = \infty$ in Eqs. (5.204) and (5.205), we express the spins in terms of u_j,

$$N_k s_k^- = \frac{2b}{g}\frac{\prod_j (\varepsilon_k - u_j)}{\prod_{m\neq k}(\varepsilon_k - \varepsilon_m)}, \tag{5.206}$$

$$J_- = \sum_k N_k s_k^- = \frac{2b}{g}\sum_k (\varepsilon_k - u_k). \tag{5.207}$$

Equations of motion in terms of new variables are

$$\dot{u}_k = -\frac{2i\sqrt{Q_{2N+2}(u_k)}}{\prod_{m\neq k}(u_k - u_m)}, \qquad \dot{b} = -2ib\left(\frac{\omega}{2} + \sum_k (\varepsilon_k - u_k)\right), \tag{5.208}$$

see Ref. [Yuzbashyan et al.(2005c)] for a detailed derivation. Here $Q_{2N+2}(u)$ is the spectral polynomial defined in Eq. (5.58).

Roots of $Q_{2N+2}(u)$ are the same as roots of $\vec{L}^2(u)$ determined by Eq. (5.126). In our new notation

$$(u - \mu \mp i\Delta_0)\left[\frac{2}{g^2} - \sum_k \frac{N_k}{2(u-\varepsilon_k)E(\varepsilon_k)}\right] = \frac{\delta\omega}{g^2}, \tag{5.209}$$

where $E(\varepsilon_k) = \sqrt{(\varepsilon_k - \mu)^2 + \Delta_0^2}$. Here and everywhere below in this subsection μ and Δ_0 without a subscript indicate ground state values μ_i and Δ_{0i} for the initial detuning $\omega = \omega_i$. In the ground state $\vec{L}^2(u) = [(u-\mu_i)^2 + \Delta_{0i}^2]\, L_0^2(u)$. There is a pair of complex roots $c_\pm = \mu_i \pm i\Delta_{0i}$ and $2N$ real double degenerate roots x_k that solve

$$L_0(x) = -\frac{2}{g^2} + \sum_k \frac{N_k}{2(x-\varepsilon_k)E(\varepsilon_k)} = 0, \tag{5.210}$$

A plot of $L_0(x)$ reveals that x_k are located between consecutive ε_k, i.e. $\varepsilon_k < x_k < \varepsilon_{k+1}$.

Since $\vec{L}^2(x_k) = L_x^2(x_k) + L_y^2(x_k) + L_z^2(x_k) = 0$ in the ground state and x_k is real, all components of $\vec{L}(x_k)$ must vanish, $L_x(x_k) = L_y(x_k) = L_z(x_k) = 0$. It follows that $L_-(x_k) = 0$ meaning that the separation variables are frozen in the real double roots, $u_k = x_k$. After a quench they start to move from these initial positions, $u_k(t) = x_k + \delta u_k$, where δu_k vanishes at $t = 0$ and is proportional to $\delta\omega$ for an infinitesimal quench. For $\delta\omega \neq 0$ real double roots of $Q_{2N+2}(u)$ split into pairs of complex conjugate roots $c_k = x_k + \delta c_k$ and $\bar{c}_k = x_k + \delta\bar{c}_k$. Therefore, the expression for $Q_{2N+2}(u_k)$,

$$\begin{aligned} Q_{2N+2}(u_k) = (u_k - c_k)(u_k - \bar{c}_k)\times \\ (u_k - c_+)(u_k - c_-)\prod_{m\neq k}(u_k - c_m)(u_k - \bar{c}_m), \end{aligned} \tag{5.211}$$

to lowest nonzero order in $\delta\omega$ becomes

$$\begin{aligned} Q_{2N+2}(u_k) = (\delta u_k - \delta c_k)(\delta u_k - \delta\bar{c}_k)\Omega_k^2\times \\ \prod_{m\neq k}(x_k - x_m)^2, \end{aligned} \tag{5.212}$$

$\Omega_k = \sqrt{(x_k - \mu)^2 + \Delta_0^2}$, not to be confused with function $\Omega(t)$ in Sect. 5.2.2. Similarly, the denominator of the equation of motion (5.208) for u_k to the lowest order $\prod_{m\neq k}(u_k - u_m) = \prod_{m\neq k}(x_k - x_m)$, so this equation reads

$$\delta\dot{u}_k = \pm 2i\Omega_k\sqrt{(\delta u_k - \delta c_k)(\delta u_k - \delta\bar{c}_k)}. \tag{5.213}$$

Corrections to the roots due to the quench obtain by setting $u = x_k + \delta c_k$ in Eq. (5.209) and linearizing in δc_k. Separating real and imaginary parts, $\delta c_k = a_k + ib_k$, we have

$$a_k = \frac{\delta\omega(x_k - \mu)}{g^2\Omega_k^2 F_k}, \quad b_k = \frac{\delta\omega\Delta_0}{g^2\Omega_k^2 F_k}, \tag{5.214}$$

where

$$F_k = \sum_m \frac{N_k}{2(x_k - \varepsilon_m)^2 E(\varepsilon_m)}. \tag{5.215}$$

Let us also evaluate the correction to the complex root pair $c_\pm = \mu_i \pm i\Delta_{0i}$. Writing the perturbed roots as $\mu' \pm i\Delta'$, we obtain from Eq. (5.209) to linear order in $\delta\omega$

$$\begin{aligned} \mu' - \mu_i &= \frac{\delta\omega}{g^2}\frac{\beta_k}{\alpha_k^2 + \beta_k^2}, \\ \Delta' - \Delta_{0i} &= -\frac{\delta\omega}{g^2}\frac{\alpha_k}{\alpha_k^2 + \beta_k^2}, \end{aligned} \tag{5.216}$$

where α_k and β_k are defined in Eq. (5.313). Comparing this with first order shifts in the ground state gap and chemical potentials that readily derive from Eqs. (5.315), we conclude that

$$\mu' = \mu_f, \quad \Delta' = \Delta_{0f}, \tag{5.217}$$

as it should be according to Sect. 5.2.4, see the text following Eq. (5.114) and also below.

Eq. (5.213) is a harmonic oscillator equation, which yields

$$\delta u_k(t) = a_k(1 - \cos 2\Omega_k t) + il_k \sin 2\Omega_k t, \tag{5.218}$$

where

$$l_k = \pm\sqrt{a_k^2 + b_k^2} = \frac{\delta\omega}{g^2\Omega_k F_k}. \tag{5.219}$$

In deriving Eq. (5.218) we took into account the initial condition $\delta u_k(0) = 0$ and used expressions (5.214). We set the sign in the last equation in Eq. (5.219) to be plus, which we will justify later in this subsection.

Eq. (5.218) shows that $u_k(t)$ are the normal modes of small oscillations around the ground state and that the normal frequencies are $2\Omega_k = 2\sqrt{(x_k-\mu)^2+\Delta_0^2}$, where x_k are the roots of Eq. (5.210). Eq. (5.218) also shows that in linear analysis separation variable $u_k(t)$ moves on an ellipse with semi-axes a_k and $\sqrt{a_k^2+b_k^2}$ around the roots $c_k, \bar{c}_k$. The latter are the focal points of the ellipse. The function $\sqrt{Q_{2N+2}(u)}$ entering equations of motion for separation variables has branch cuts connecting pairs of conjugate roots c_k and $\bar{c}_k$, so one can also say that separation variables move on ellipses around brunch cuts without crossing any of them, see Fig. 5.24.

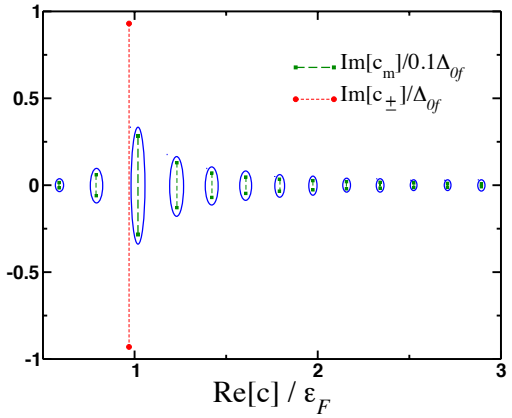


Figure 5.24: As a result of a quench doubly degenerate roots of $\vec{L}^2(u)$ in Fig. 5.17 split into pairs of complex conjugate roots c_m (not all $N = 54$ pairs of roots are shown). In linear analysis separation variables move periodically on ellipses around the brunch cuts of $(\vec{L}^2(u))^{-1/2}$ connecting complex conjugate c_m without crossing any of the brunch cuts. Each separation variable has its own distinct frequency and corresponds to a normal mode of small oscillations around the ground state. Here $\Delta_{0f} = 0.12\varepsilon_F$, $\delta\omega/\gamma = -0.1$, and other parameters are the same as in Fig. 5.17.

Next, we determine deviations of the spins $\delta\vec{s}_k(t)$ and the order parameter $\delta\Delta(t)$ from their initial ground state configuration (5.14) and (5.15). We go to a rotating reference frame,

$$s_k^- \to s_k^- e^{-2i\mu t}, \quad b \to be^{-2i\mu t}, \tag{5.220}$$

to get rid of the time dependence in the unperturbed dynamical variables. This shifts $\omega \to \omega - 2\mu$ in the equation of motion (5.208) and now $\dot{b} = 0$ in the ground state *before* the quench, i.e. for $\omega = \omega_i$. Linearizing Eq. (5.206), we obtain a decomposition of spin deviations in terms of the normal modes

$$\frac{\delta s_k^-(t)}{s_k^-(0)} = \frac{\delta\Delta(t)}{\Delta_0} - \sum_j \frac{\delta u_j}{\varepsilon_k - x_j}. \tag{5.221}$$

Similarly, the second equation in (5.208) linearized and integrated in the rotating frame *after* the quench, i.e. with $\omega = \omega_f$, yields

$$\begin{aligned} \frac{\Delta(t)}{\Delta_0} &= 1 - \sum_k l_k \frac{1-\cos 2\Omega_k t}{\Omega_k} - \\ & i\delta\omega t + 2it\sum_k a_k - i\sum_k \frac{a_k \sin 2\Omega_k t}{\Omega_k}, \end{aligned} \tag{5.222}$$

where we took into account $\Delta(t) = -gb(t)$, $\Delta(0) = \Delta_0$ and expressions (5.218). The $i\delta\omega t$ appears because for unperturbed u_k the bracketed term in the second equation in (5.208) vanishes for $\omega = \omega_i$, while after the quench $\omega = \omega_f$.

Linearizing spin equations of motion (5.8) directly and plugging expressions (5.221) and (5.222), one can verify that the correct sign in the last equation in Eq. (5.219) is indeed plus, even though there is probably a simpler way to show this.

The imaginary part in Eq. (5.222) comes from the phase of the order parameter, so we write

$$\begin{aligned}\Delta(t) = \left(\Delta_0 - \Delta_0 \sum_k l_k \frac{1-\cos 2\Omega_k t}{\Omega_k}\right) \times \\ \exp\left[-i\delta\omega t + 2it\sum_k a_k - i\sum_k \frac{a_k \sin 2\Omega_k t}{\Omega_k}\right].\end{aligned} \tag{5.223}$$

This coincides with Eq. (5.222) to first order in $\delta\omega$. Moreover, we know from Eq. (5.201) that the linear part of the phase (zeroth harmonic in the derivative of the phase) is $-2\mu_f t$ in the continuum limit, where μ_f is the ground state chemical potential at detuning ω_f. Similarly, the zeroth harmonic in the amplitude of $\Delta(t)$ is equal to Δ_{0f}. It turns out that this is true even in the discrete case, i.e.

$$\begin{aligned}\Delta_0 - \Delta_0 \sum_k \frac{l_k}{\Omega_k} = \Delta_{0f}, \\ 2\mu + \delta\omega - 2\sum_k a_k = 2\mu_f,\end{aligned} \tag{5.224}$$

where we restored the phase of $\Delta(t)$ to the original reference frame according to Eq. (5.220). Recall that in this subsection μ and Δ_0 without a subscript indicate ground state values μ_i and Δ_{0i} for the initial detuning $\omega = \omega_i$. With the help of Eqs. (5.214) and (5.219) these relations become

$$\begin{aligned}\sum_k \frac{x_k - \mu}{\Omega_k^2 F_k} = \frac{g^2}{2} - g^2 \frac{\delta\mu}{\delta\omega}, \\ \sum_k \frac{\Delta_0}{\Omega_k^2 F_k} = -g^2 \frac{\delta\Delta_0}{\delta\omega},\end{aligned} \tag{5.225}$$

where $\delta\mu = \mu_f - \mu$ and $\delta\Delta_0 = \Delta_{0f} - \Delta_0$. These are in fact identities, as we prove in Appendix 5.11. Thus,

$$\begin{aligned}\Delta(t) = \left(\Delta_{0f} + \Delta_0 \sum_k l_k \frac{\cos 2\Omega_k t}{\Omega_k}\right) \times \\ \exp\left[-2i\mu_f t - i\sum_k \frac{a_k \sin 2\Omega_k t}{\Omega_k}\right],\end{aligned} \tag{5.226}$$

in the original reference frame.

An expression for $s_k^-(t)$ obtains similarly from Eqs. (5.221) and (5.222) with the help of

identity (5.316),

$$s_k^-(t) = s_{kf}^- \Bigg(1 + \sum_j \frac{l_j \cos 2\Omega_j t}{\Omega_j} + \sum_j \frac{a_j \cos 2\Omega_j t}{\varepsilon_k - x_j} - i \sum_j \frac{l_j \sin 2\Omega_j t}{\varepsilon_k - x_j} \Bigg) \times \exp\left[-2i\mu_f t - i \sum_j \frac{a_j \sin 2\Omega_j t}{\Omega_j} \right], \tag{5.227}$$

where

$$s_{kf}^- \equiv s_f^-(\varepsilon_k) = \frac{\Delta_{0f}}{2\sqrt{(\varepsilon_k - \mu_f)^2 + \Delta_{0f}^2}}. \tag{5.228}$$

The last term in round brackets in Eq. (5.227) can be as well included into the phase – to linear order the two versions are equivalent. The present form is more convenient for the long time analysis below. We see that again non-oscillatory parts of the magnitude and phase of $s_k^-(t)$ and magnitude of s_k^z are the same as in the ground state for final detuning $\omega = \omega_f$.

Finally, the expression for $s_k^z(t)$ follows the conservation of $|\vec{s}_k| = 1/2$, $s_k^z = \pm\sqrt{1/4 - |s_k^-|^2}$ expanded to the linear order in $\delta\omega$,

$$s_k^z(t) = s_{kf}^z \Bigg(1 - \frac{\Delta_{0f}^2}{(\varepsilon_k - \mu_f)^2} \sum_j \frac{l_j \cos 2\Omega_j t}{\Omega_j} - \frac{\Delta_{0f}^2}{(\varepsilon_k - \mu_f)^2} \sum_j \frac{a_j \cos 2\Omega_j t}{\varepsilon_k - x_j} \Bigg), \tag{5.229}$$

where

$$s_{kf}^z \equiv s_f^z(\varepsilon_k) = -\frac{\varepsilon_k - \mu_f}{2\sqrt{(\varepsilon_k - \mu_f)^2 + \Delta_{0f}^2}}. \tag{5.230}$$

5.5.3 Continuum limit

In $N \to \infty$ limit, $x_k \to \varepsilon_k$ and summations in above expressions for $s_k^z(t), s_k^-(t)$, and $\Delta(t)$ turn into integrations. With the help of Eqs. (5.214), (5.219), (5.202), and (5.308), Eq. (5.226) obtains (as always in units of the Fermi energy ε_F)

$$\frac{\Delta(t)}{\Delta_{0f}} = \Big(1 + X_1(t)\Big) \exp\left[-2i\mu_f t - iX_2(t)\right], \tag{5.231}$$

where

$$X_1(t) = \frac{\delta\omega}{\gamma} \int_0^\infty \frac{2\cos\left[2E(\varepsilon)t\right] f(\varepsilon) d\varepsilon}{E(\varepsilon)\left[\pi^2 f^2(\varepsilon) + H^2(\varepsilon)\right]}, \tag{5.232}$$

$$X_2(t) = \frac{\delta\omega}{\gamma} \int_0^\infty \frac{2(\varepsilon - \mu)\sin[2E(\varepsilon)t] f(\varepsilon) d\varepsilon}{E^2(\varepsilon)[\pi^2 f^2(\varepsilon) + H^2(\varepsilon)]}, \tag{5.233}$$

$E(\varepsilon) = \sqrt{(\varepsilon - \mu)^2 + \Delta_0^2}$ and $H(\varepsilon)$ is defined in Eq. (5.307). In deriving this expression, we also used, $\Omega_k \to E(\varepsilon_k)$, $\nu(\varepsilon) = \nu_F f(\varepsilon)$, $g^2\nu_F = \gamma$, and $\delta = N_k/\nu(\varepsilon_k)$. Eq. (5.231) is in excellent agreement with numerical results, see e.g. Fig. 5.25.

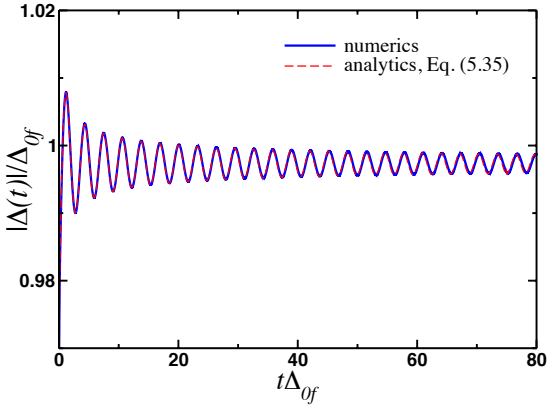


Figure 5.25: Comparison of Eq. (5.231) with $|\Delta(t)|$ computed by numerically evolving $N = 5024$ spins in a 3d 2-channel model after a detuning quench. Here $\gamma = 1.0, \Delta_{0i} = 0.122\Delta_{\max}, \Delta_{0f} = 0.126\Delta_{\max}$, and both Eq. (5.231) and the spin chain in the numerics are cutoff at $\varepsilon_\Lambda = 10\varepsilon_F$.

Expressions (5.229) and (5.227) for $s_k^-(t)$ and $s_k^z(t)$ contain two extra summations as compared to $\Delta(t)$. These are handled as in Appendix 5.11 by splitting each sum into two parts – over x_j inside and outside a small interval around ε_k. The same method works for summations over x_j because according to Eq. (5.307) $\varrho(\varepsilon)$ is a smooth function and therefore x_j are locally equally spaced with spacing δ just as ε_k. The second and the third sums in round brackets in Eq. (5.227) are

$$Y_1(\varepsilon,t) = \frac{\delta\omega}{\gamma}\int_0^\infty \frac{2(\varepsilon'-\mu)\cos[2E(\varepsilon')t]f(\varepsilon')d\varepsilon'}{(\varepsilon-\varepsilon')E(\varepsilon')[\pi^2 f^2(\varepsilon')+H^2(\varepsilon')]} - \frac{\delta\omega}{\gamma}\frac{2(\varepsilon-\mu)H(\varepsilon)\cos[2E(\varepsilon)t]}{E(\varepsilon)[\pi^2 f^2(\varepsilon)+H^2(\varepsilon)]}, \tag{5.234}$$

$$Y_2(\varepsilon,t) = \frac{\delta\omega}{\gamma}\int_0^\infty \frac{2\sin[2E(\varepsilon')t]f(\varepsilon')d\varepsilon'}{(\varepsilon-\varepsilon')[\pi^2 f^2(\varepsilon')+H^2(\varepsilon')]} - \frac{\delta\omega}{\gamma}\frac{2H(\varepsilon)\sin[2E(\varepsilon)t]}{\pi^2 f^2(\varepsilon)+H^2(\varepsilon)}, \tag{5.235}$$

respectively. Thus

$$\frac{s^-(\varepsilon,t)}{s_f^-(\varepsilon)} = \Big(1+X_1(t)+Y_1(\varepsilon,t)-iY_2(\varepsilon,t)\Big)\times \exp\left[-2i\mu_f t - iX_2(t)\right], \tag{5.236}$$

$$\frac{s^z(\varepsilon,t)}{s_f^z(\varepsilon)} = 1 - \frac{\Delta_{0f}^2}{(\varepsilon-\mu_f)^2}\Big(X_1(t)+Y_1(\varepsilon,t)\Big). \tag{5.237}$$

Functions X_1 and X_2 are related via differentiation. Define

$$\widetilde{X}_1(t) = \int_0^\infty K(\varepsilon)e^{2i\widetilde{E}(\varepsilon)t}d\varepsilon, \tag{5.238}$$

where $\widetilde{E}(\varepsilon) = \sqrt{(\varepsilon-\widetilde{\mu})^2+\Delta_0^2}$ and

$$K(\varepsilon) = \frac{\delta\omega}{\gamma}\frac{2f(\varepsilon)}{E(\varepsilon)\left[\pi^2 f^2(\varepsilon)+H^2(\varepsilon)\right]}. \tag{5.239}$$

Then,

$$X_1(t) = \mathrm{Re}\widetilde{X}_1(t)\Big|_{\widetilde{\mu}=\mu} \tag{5.240}$$

$$X_2(t) = \frac{1}{2t}\mathrm{Re}\frac{\partial \widetilde{X}_1(t)}{\partial \widetilde{\mu}}\Big|_{\widetilde{\mu}=\mu} \tag{5.241}$$

A similar relationship holds for Y_1 and Y_2.

5.5.4 Validity of the few spin conjecture

We are now in the position to prove the few spin conjecture for infinitesimal quenches independently of either numerics or arguments of Sect. 5.2. At $t \to \infty$ integrals in Eqs. (5.232) and (5.233) vanish by the Riemann-Lebesgue lemma. Therefore,

$$\Delta(t) \to \Delta_{0f} e^{-2i\mu_f t}. \tag{5.242}$$

According to the few spin conjecture this asymptotic behavior of $\Delta(t)$ occurs when there is a single isolated root pair at $\mu_f \pm i\Delta_{0f}$. Eq. (5.217) shows that our $\vec{L}^2(u)$ does have this pair of roots. Moreover, the remaining $2N$ roots are given by Eq. (5.214) and we explicitly see from Appendix 5.10 that their imaginary parts scale as $1/N$ at large N and that they merge into a continuum of roots on the real axis in $N \to \infty$ limit. Thus, there is indeed a single isolated root pair at $\mu_f \pm i\Delta_{0f}$ in the thermodynamic limit.

5.5.5 Weak coupling limit

Simpler expressions obtain in the weak coupling (BCS) limit when Δ_0 is much smaller then other energy scales (Fermi energy in gases and Debye energy in metals). This limit describes superconductivity in metals and applies to recent experiments on non-adiabatic BCS dynamics[Matsunaga et al.(2013), 98]. In our quench phase diagrams (Figs. 5.2 – 5.4 etc.) weak coupling regime corresponds to a small neighborhood of the origin.

At weak coupling $\mu \approx \varepsilon_F = 1$. Integrals (5.232) and (5.233) are dominated by energies close to the Fermi energy, $|\varepsilon - \mu| \sim \Delta_0$, where $f(\varepsilon) \approx 1$ independent of dimensionality. It is convenient to change the integration variable to $\xi = \varepsilon - \mu$ and extend the integration to the entire real axis. $X_2(t)$ vanishes by particle-hole symmetry (integrand is odd in ξ). The error due to these approximations is proportional to Δ_0/ε_F, which vanishes in weak coupling limit. Eq. (5.231) implies

$$|\Delta(t)| = \Delta_{0f} - 4\delta\Delta_0 \int_0^\infty \frac{\cos\left[2E(\xi)t\right] d\xi}{E(\xi)\left[\pi^2 + H^2(\xi)\right]}, \tag{5.243}$$

where $E(\xi) = \sqrt{\xi^2 + \Delta_0^2}$, $\delta\Delta_0 = \Delta_{0f} - \Delta_{0i}$, and

$$H(\varepsilon) = \ln\left[\frac{E(\xi) - \xi}{E(\xi) + \xi}\right]. \tag{5.244}$$

In deriving Eq. (5.243) we used the weak coupling gap formula $\Delta_0 \propto \exp(-\omega/\gamma)$ and Eqs. (5.305) and (5.307) [Note that at relevant energies $4E(\varepsilon)/\gamma \propto \Delta_0/\varepsilon_F \to 0$]. We also used the fact that the integrand is even in ξ to convert the integration range from $(-\infty, \infty)$ to $(0, \infty)$.

The phase of the order parameter defined through

$$\Delta(t) = |\Delta(t)| e^{-i\Phi(t)} \tag{5.245}$$

is simply $\Phi(t) = 2\varepsilon_F t$. Let us also note that in terms of $\xi = \Delta_0 \sinh(\pi x/2)$ Eq. (5.243) reads

$$|\Delta(t)| = \Delta_{0f} - 2\delta\Delta_0 \int_0^\infty \frac{dx}{\pi} \frac{\cos\left[2\tau \cosh(\pi x/2)\right]}{1+x^2}, \tag{5.246}$$

where $\tau = \Delta_0 t$.

5.5.6 Long time behavior of $\Delta(t)$: BCS side

Integrands in Eqs. (5.232) and (5.233) are highly oscillatory. The argument of the cosine is stationary at $\varepsilon = \mu$, $E'(\mu) = 0$. For $\mu > 0$ the stationary point is inside the integration range. For $\mu < 0$ there are no stationary points on the integration path. This leads to qualitatively different behavior of $\Delta(t)$ on the BCS ($\mu > 0$) and BEC ($\mu < 0$) sides.

Consider first the BCS regime. We evaluate $\widetilde{X}_1(t)$ in Eq. (5.238) in stationary phase approximation

$$\widetilde{X}_1(t) = K(\widetilde{\mu})\sqrt{\frac{\pi\Delta_0}{t}} e^{2i\Delta_0 t + i\pi/4} + O(1/t), \tag{5.247}$$

where we used $\widetilde{E}(\widetilde{\mu}) = \Delta_0$, $\widetilde{E}''(\widetilde{\mu}) = 1/\Delta_0$. With the help of Eq. (5.240) we obtain from Eq. (5.231) for the order parameter amplitude

$$|\Delta(t)| = \Delta_{0f} + \sqrt{\pi} K(\mu)\Delta_0^2 \frac{\cos(2\Delta_0 t + \pi/4)}{\sqrt{\Delta_0 t}}. \tag{5.248}$$

The phase of the order parameter obtains with the help of Eq. (5.241)

$$\Phi(t) = 2\mu_f t + \sqrt{\pi} K'(\mu)\Delta_0^2 \frac{\cos(2\Delta_0 t + \pi/4)}{2(\Delta_0 t)^{3/2}}. \tag{5.249}$$

Coefficients $K(\mu), K'(\mu)$ are given by Eqs. (5.239), (5.307), and (5.303). Simpler expressions for $G(\varepsilon)$ are available in 2d and in weak coupling (BCS) limit, see Eqs. (5.304) and (5.305). For example, in the BCS limit ($\Delta_0/\varepsilon_F \to 0$)

$$\Delta(t) = \left(\Delta_{0f} - \frac{2\delta\Delta_0}{\pi^{3/2}} \frac{\cos(2\Delta_0 t + \pi/4)}{\sqrt{\Delta_0 t}}\right) e^{-2i\mu_f t}, \tag{5.250}$$

where $\delta\Delta_0 = \Delta_{0f} - \Delta_{0i}$ and we additionally used $\Delta_0 \propto \exp(-\omega/\gamma)$. Note that the second term in Eq. (5.249) is proportional to Δ_0/ε_F. This expression for $\Delta(t)$ holds in the BCS limit for both one and two channel models in two and three dimensions. Eq. (5.250) for $\mu_f = 0$ appeared in Ref. [Yuzbashyan and Dzero(2006)] without derivation.

Let us also mention that long times for which asymptotes of the order parameter derived in this section apply in practice (e.g. in numerical simulations) mean t such that $1/\Delta_0 \ll t \ll 1/\delta$. At times of order of the inverse level spacing $1/\delta$ partial recurrences occur, see Fig. 5.26. Oscillations with frequency $2\Delta_0$ and $1/\sqrt{t}$ decay in the weak coupling limit of the one channel model were identified by Volkov and Kogan[Volkov and Kogan(1973)].

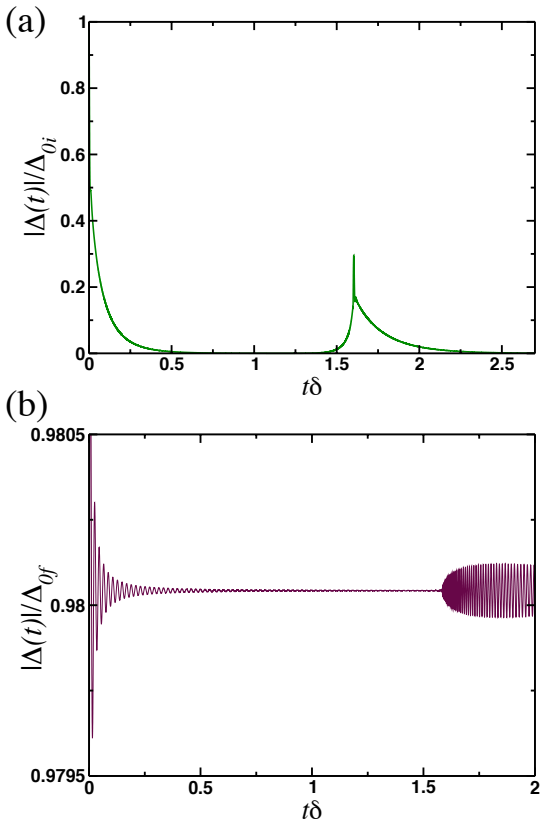


Figure 5.26: Finite size effects, such as partial recurrences in $|\Delta(t)|$, develop at times of order of the inverse level spacing $\delta \propto 1/N$ between discretized single-particle energy levels ε_k. Long time behaviors derived in our paper apply at times $t\delta \ll 1$. In other words, we take the thermodynamic limit first and large time limit second. Two detuning quenches in 3d 2-channel model are shown for $N = 5024$ and: (a) $\gamma = 0.5, \Delta_{0i} = 3.0 \times 10^{-2}\Delta_{\max}, \Delta_{0f} = 2.9 \times 10^{-4}\Delta_{\max}, \delta = 3.4 \times 10^{-3}\Delta_{\max}$, and (b) $\gamma = 0.1, \Delta_{0i} = 0.97\Delta_{\max}, \Delta_{0f} = 0.99\Delta_{\max}, \delta = 8.0 \times 10^{-3}\Delta_{\max}$.

5.5.7 Long time behavior of $\Delta(t)$: BEC side

In the absence of stationary points integrals of the type of Eq. (5.238) are dominated by the end point, $\varepsilon = 0$ here. Normally, they vanish as $1/t$ at large t, but in the present case $K(0) = 0$ in both 2d and 3d, so they vanish faster. Unlike the BCS side, the long time behavior on the BEC side is not universal in that it depends on the form of $K(\varepsilon)$ at small ε, i.e. on the density of states and on the asymptotic spin distribution. As a result, for example, it is different in two and three dimensions.

We first integrate by parts to obtain

$$\widetilde{X}_1(t) = -\frac{1}{2it}\int_0^\infty \left(\frac{K(\varepsilon)}{\widetilde{E}'(\varepsilon)}\right)' e^{2i\widetilde{E}(\varepsilon)t} d\varepsilon. \tag{5.251}$$

In 2d the dimensionless density of states $f(\varepsilon) = 1$ and it follows from Eqs. (5.239), (5.307), and (5.304) that $K(\varepsilon) \propto 1/\ln^2 \varepsilon$. We evaluate the large t asymptote of this integral by splitting the integration range into three: $(0, 1/\Lambda t), (1/\Lambda t, \Lambda/t)$, and $(\Lambda/t, \infty)$, where Λ is such that $1 \ll \ln\Lambda \ll \ln t$. In the first integral we expand the integrand in small ε, which leads to an integral $\int_0^{1/\Lambda t} d(\ln\varepsilon)/\ln^3\varepsilon$ and

$$\widetilde{X}_1(t) = \frac{\delta\omega}{\gamma}\frac{ie^{2i\widetilde{E}(0)t}}{\widetilde{E}'(0)E(0)}\frac{1}{t\ln^2 t}. \tag{5.252}$$

The other two integrals vanish as $1/t\ln^3 t$ and are therefore negligible. Eqs. (5.231), (5.240), (5.241) yield the amplitude and the phase of the order parameter

$$|\Delta(t)| = \Delta_{0f}\left(1 - \frac{\delta\omega}{\gamma}\frac{\sin(2E_{\min}t)}{|\mu|t\ln^2 t}\right), \tag{5.253}$$

$$\Phi(t) = 2\mu_f t - \frac{\delta\omega}{\gamma}\frac{\cos(2E_{\min}t)}{E_{\min}t\ln^2 t}, \tag{5.254}$$

where $E_{\min} = \sqrt{\mu^2 + \Delta_0^2}$.

In 3d $f(\varepsilon) = \sqrt{\varepsilon}$ and $K(\varepsilon) \propto \sqrt{\varepsilon}$ at small ε. This follows from Eqs. (5.239), (5.307), and (5.303) and is, for example, readily verified in the strong coupling limit with the help of the last expression in Eq. (5.306). We split the integration range in Eq. (5.251) into two: $(0, 1/\Lambda)$ and $(1/\Lambda, \infty)$, where $t \gg \Lambda \gg 1$. In the first integral we can expand in small t, which results in a Gaussian integral that behaves as $1/\sqrt{t}$ at large t. The second integral vanishes faster as $t \to \infty$. We thus determine the following (exact) large time asymptote:

$$\widetilde{X}_1(t) = -\frac{\pi^{1/2}}{(2t)^{3/2}}\frac{\delta\omega}{\gamma}\frac{e^{2i\widetilde{E}(0)t + i\pi/4}}{[-\widetilde{E}'(0)]^{3/2}E(0)H^2(0)}. \tag{5.255}$$

With the help of Eqs. (5.240) and (5.241) we finally derive

$$|\Delta(t)| = \Delta_{0f}\left(1 - c\frac{\delta\omega}{\gamma}\frac{\cos(2E_{\min}t + \pi/4)}{(2|\mu|t)^{3/2}}\right), \tag{5.256}$$

$$\Phi(t) = 2\mu_f t - c\frac{|\mu|}{E_{\min}}\frac{\delta\omega}{\gamma}\frac{\sin(2E_{\min}t + \pi/4)}{(2|\mu|t)^{3/2}}. \tag{5.257}$$

The coefficient c depends on μ, Δ_0, and γ. It is known exactly from Eq. (5.255), but involves $G(0)$ which in 3d is an elliptic integral according to Eq. (5.303). In the strong coupling BEC limit, $\mu \to -\infty$, $G(\varepsilon)$ is independent of ε and takes a simple form (5.306). In this case

$$c = \sqrt{\frac{\pi|\mu|}{\varepsilon_F}}\left(\frac{4|\mu|}{\gamma\varepsilon_F} + \pi\sqrt{\frac{|\mu|}{\Delta_0}}\right)^{-2}, \tag{5.258}$$

where we restored the original energy units.

5.5.8 Long time behavior of spins

Let us also work out the long time behavior of individual spins given by Eqs. (5.236) and (5.237) and compare it to the asymptotic spin distribution, Eqs. (5.111) and (5.134), obtained earlier. The latter result is based on the few spin conjecture, so the agreement with linear analysis provides yet another (though redundant because we already proved the few spin conjecture for infinitesimal quenches in Sect. 5.5.4) check.

Functions $X_{1,2}$ vanish as $t \to \infty$, while the large time limit of $Y_{1,2}$ derives from the following identity:

$$\lim_{t\to\infty}\int_0^\infty \frac{d\varepsilon' F(\varepsilon')e^{\pm 2iE(\varepsilon')t}}{\varepsilon' - \varepsilon} = \pm i\pi\alpha F(\varepsilon)e^{\pm 2iE(\varepsilon)t}, \tag{5.259}$$

where α is the sign of $tdE(\varepsilon')/d\varepsilon'$ at $\varepsilon' = \varepsilon$ and $F(\varepsilon')$ is an arbitrary bounded continuous function.

Applying this identity to Eqs. (5.234) and (5.235) and substituting resulting expressions into Eqs. (5.236) and (5.237), we obtain

$$\begin{aligned}\frac{s^-_\infty(\varepsilon,t)e^{2i\mu_f t}}{s^-_f(\varepsilon)} &= 1-\frac{2\delta\omega}{\gamma}\frac{\exp\left[-2iE(\varepsilon)t-i\phi\right]}{\sqrt{\pi^2 f^2(\varepsilon)+H^2(\varepsilon)}}\\ &-\frac{2\delta\omega}{\gamma}\left(\frac{\xi}{E(\varepsilon)}-1\right)\frac{\cos\left[2E(\varepsilon)t+\phi\right]}{\sqrt{\pi^2 f^2(\varepsilon)+H^2(\varepsilon)}},\end{aligned} \tag{5.260}$$

$$\frac{s^z_\infty(\varepsilon,t)}{s^z_f(\varepsilon)} = 1+\frac{2\delta\omega}{\gamma}\frac{\Delta^2_{0f}}{\xi E(\varepsilon)}\frac{\cos\left[2E(\varepsilon)t+\phi\right]}{\sqrt{\pi^2 f^2(\varepsilon)+H^2(\varepsilon)}}, \tag{5.261}$$

where $\xi=\varepsilon-\mu$ and ϕ is defined through

$$\begin{aligned}\cos\phi &= \frac{H(\varepsilon)}{\sqrt{\pi^2 f^2(\varepsilon)+H^2(\varepsilon)}},\\ \sin\phi &= \frac{\pi f(\varepsilon)\,\mathrm{sgn}(t\xi)}{\sqrt{\pi^2 f^2(\varepsilon)+H^2(\varepsilon)}}.\end{aligned} \tag{5.262}$$

In our case $t>0$, but we still kept it under the sign function to ensure proper behavior under time reversal, see Eq. (5.269). Eqs. (5.260) and (5.261) match Eq. (5.111) with

$$\theta(\varepsilon)\approx\sin\theta(\varepsilon)=\frac{2\delta\omega}{\gamma}\frac{\Delta_0}{E(\varepsilon)\sqrt{\pi^2 f^2(\varepsilon)+H^2(\varepsilon)}}. \tag{5.263}$$

(Not that in the present case $\Delta_\infty=\Delta_{0f}$ and $\mu_\infty=\mu_f$.) This indeed agrees with Eq. (5.136) obtained from the few spin conjecture.

5.5.9 Short time behavior

Here we analyze the short time behavior of $|\Delta(t)|$ for quenches within the universal weak coupling regime. For large quenches from weaker to stronger coupling, when $\Delta_{0f}/\Delta_{0i}\gg 1$, or from the normal state (zero initial coupling) in this regime $|\Delta(t)|$ grows as $e^{\Delta_{0f}t}$. This exponential growth reflects the instability of the normal state in the presence of superconducting interactions[Barankov et al.(2004), 19]. At the same time, even for small quenches $|\Delta(t)|$ rises or falls sharply at short times, see Figs. 5.7 and 5.25. Sharp growth is seen in experiment too, though most of it is probably due to a different mechanism[98].

A direct small t expansion of the cosine in Eq. (5.232) diverges at high energies. Cutting off the integral at ε_Λ (Debye energy in the case of metals), one obtains[Warner and Leggett(2005)] $\delta|\Delta(t)|\propto\delta\Delta_0(\varepsilon_\Lambda t)^2$. This is cutoff dependent and applies only to ultra-short times $t\ll 1/\varepsilon_\Lambda$ that vanish as the cutoff is sent to infinity. We are interested in times $1/\varepsilon_\Lambda\ll t\ll 1/\Delta_0$.

Consider Eq. (5.246). The argument of the cosine is small for $x\ll x_0$, where x_0 is determined by $e^{\frac{\pi x_0}{2}}=1/\tau$, i.e. $x_0=\frac{2}{\pi}\ln(1/\tau)$. Let us divide the domain of the integration into three intervals: $[0,x_0-a]$, $[x_0-a,x_0+a]$, and $[x_0+a,\infty)$ and let the corresponding integrals be I_1, I_2, and I_3, respectively. The auxiliary parameter a, $1\ll a\ll x_0$, is such that $1/a\to 0, a/x_0\to 0$ as $x_0\to\infty$. For example, one can take $a=\sqrt{x_0}$. Expanding the cosine in small τ in I_1 and integrating, we obtain

$$I_1=\frac{1}{2}-\frac{1}{\pi x_0}-\frac{a}{\pi x_0^2}+o(a/x_0^2). \tag{5.264}$$

In I_2 we replace $x^2+1\to x_0^2$ up to terms of order a/x_0. After this, a substitution $y=\exp\pi x/2$ transforms it into the cosine integral $\int dy\cos y/y$ with known behavior, leading to

$$I_2=\frac{a}{\pi x_0^2}+o(a/x_0^2). \tag{5.265}$$

And integrating by parts in I_3, we see that it is proportional to $e^{-\pi a/2}/x_0^2$, which is negligibly small. Thus,

$$I_1 + I_2 + I_3 = \frac{1}{2} - \frac{1}{2|\ln(\tau)|} + o\left(\frac{1}{|\ln(\tau)|}\right). \tag{5.266}$$

Note the cancelation of the auxiliary parameter a. Finally, plugging this into Eq. (5.246), we derive the short time behavior of the gap function amplitude

$$|\Delta(t)| = \Delta_{0i} + \frac{\Delta_{0f} - \Delta_{0i}}{|\ln(\Delta_0 t)|}. \tag{5.267}$$

5.6 Approach to the asymptote in the nonlinear case

Here we discuss the approach of $\Delta(t)$ to its large time asymptote in the nonlinear case. We will consider regimes I and II – the gapless phase and the phase where $\Delta(t) \to \Delta_\infty e^{-2i\mu_\infty t - 2i\varphi}$. Rather then rigorously deriving the $t \to \infty$ asymptote in its entirety as we did for the linearized dynamics, we present an argument based only on our knowledge of the frequency spectrum that works under certain general assumptions about relevant Fourier amplitudes.

As $t \to \infty$ spins tend to their steady state form, $\vec{s}(\varepsilon, t) \to \vec{s}_\infty(\varepsilon, t)$, where $\vec{s}_\infty(\varepsilon, t)$ is given by Eqs. (5.94) and (5.111) in regimes I and II, respectively. In phase II, in a reference frame rotating with frequency $2\mu_\infty$ around z-axis, $\vec{s}_\infty(\varepsilon)$ rotates with a constant frequency $2E_\infty(\varepsilon) = 2\sqrt{(\varepsilon - \mu_\infty)^2 + \Delta_\infty^2}$. As mentioned above, an integrable model with N degrees of freedom is characterized by N incommensurate frequencies [Arnold(1978)] that are determined by the integrals of motion and are fixed throughout its time evolution. The Fourier decomposition of any dynamical quantity can have only these basic frequencies in its spectrum. In particular,

$$|\Delta(t)| = \Delta_\infty + \int_0^\infty F(\varepsilon) \cos[2E_\infty(\varepsilon)t] f(\varepsilon) d\varepsilon \tag{5.268}$$

with some unknown function $F(\varepsilon)$.

Terms containing $\sin[2E_\infty(\varepsilon)t]$ are absent by time-reversal symmetry [cf. Eq. (5.231)] of the equations of motion (5.8) and (5.33) [see also Eq. (5.73)]

$$s^z(-t) = s^z(t),\ \ s^+(-t) = s^-(t),\ \ \bar{\Delta}(-t) = \Delta(t), \tag{5.269}$$

where we suppressed ε-dependence of spins for compactness. These relations hold at all times as long as the initial condition at $t = 0$ satisfies them, which our initial state (5.28) does.

A common practice in previous work is to attempt to determine the approach of $|\Delta(t)|$ to its asymptotic value Δ_∞ from the steady state spins $\vec{s}_\infty(\varepsilon, t)$. Consider the one channel case for simplicity. Continuum version of Eq. (5.13) at $t = \infty$ is

$$\Delta_\infty(t) = \lambda \int_0^\infty s_\infty^-(\varepsilon, t) f(\varepsilon) d\varepsilon. \tag{5.270}$$

The constant part of $s_\infty^-(\varepsilon, t)$ yields Δ_∞, while the contribution of the oscillating part integrated over ε vanishes (dephases) as $t \to \infty$. One can further determine the large time asymptote of Eq. (5.270) similarly to how we evaluated the large time behavior of Eq. (5.231). This is however *not* the correct asymptote of the actual $\Delta(t)$. Not only it does not yield the correct coefficient of the time-dependent part of $\Delta(t)$ [such as the coefficient c in Eq. (5.256)], but also the actual time dependence can be different.

At finite t there is a correction to the steady state value of the spin, $\vec{s}(\varepsilon,t) = \vec{s}_\infty(\varepsilon,t) + \delta\vec{s}(\varepsilon,t)$, so that the actual order parameter is

$$\Delta(t) = \lambda \int_0^\infty s_\infty^-(\varepsilon,t) f(\varepsilon) d\varepsilon + \lambda \int_0^\infty \delta s^-(\varepsilon,t) f(\varepsilon) d\varepsilon. \tag{5.271}$$

Even though $\delta s^-(\varepsilon,t)$ is small as compared to the oscillating part of $s_\infty^-(\varepsilon,t)$ at large times, this is no longer true after integrating these quantities over ε. Consider, for example, Eq. (5.236). We showed in Sect. 5.5.8 that $s_\infty^-(\varepsilon,t)$ comes from functions $Y_{1,2}(\varepsilon,t)$. But we see from Eq. (5.231) that the integral of these functions over ε vanishes and as a result they do not contribute to $\Delta(t)$ The correction $\delta s^-(\varepsilon,t)$ on the other hand comes from both $X_{1,2}(t)$ and $Y_{1,2}(\varepsilon,t)$. It is this contribution from $X_{1,2}(t)$ to $\delta s^-(\varepsilon,t)$ that actually determines $\Delta(t)$. Thus there is a partial cancelation between the two integrals in Eq. (5.271) and the true large time behavior of $\Delta(t)$ can only be determined by keeping both.

Nevertheless, $\Delta_\infty(t)$ being a legitimate dynamical quantity has the right frequency spectrum and also contains the dimensionless density of states $f(\varepsilon)$. So, it still produces a correct large time dependence when, for example, the latter is set by a stationary point as in Eq. (5.248) or by the behavior of $f(\varepsilon)$ at small ε as in Eq. (5.256). The situation on the BEC side in 2d is different. The $\ln^2 t$ dependence in the denominator of Eq. (5.253) comes from $K(\varepsilon) \propto 1/\ln^2 \varepsilon$ behavior of the Fourier amplitude at small ε, see Eq. (5.238) and the text below Eq. (5.251). This is in turn a consequence of $K(\varepsilon) \propto H^{-2}(\varepsilon)$ and $H(\varepsilon) \propto \ln \varepsilon$, which follow from Eqs. (5.239), (5.307), and (5.304). Were we to evaluate the large time asymptote of $|\Delta(t)|$ using Eq. (5.270), we would obtain $1/(t \ln t)$ instead of $1/(t \ln^2 t)$. To see this, note that Eq. (5.260) implies that the oscillating part of $s_\infty^-(\varepsilon,t)$ is proportional to $H^{-1}(\varepsilon)$, i.e. to $1/\ln\varepsilon$, at small ε and apply the same steps as in the text below Eq. (5.251). The $1/\ln\varepsilon$ dependence cancels in Eq. (5.271) due to the second term on the right hand side. We note also that Eqs. (5.111) and (5.134) imply $s_\infty^-(\varepsilon,t) \propto 1/\ln\varepsilon$ in all of region II in 2d, not just in the linear approximation.

Similar considerations apply in analyzing Eq. (5.268). Let us work out the large time behavior of $|\Delta(t)|$ in steady states I, II, and II' separately.

5.6.1 Regime II

In steady states II and II' $\Delta(t) \to \Delta_\infty e^{-2i\mu_\infty t - 2i\varphi}$. For quenches in region II $\mu_\infty > 0$, so it can be viewed as a nonequilibrium extension of the BCS regime. The frequency spectrum $2E_\infty(\varepsilon)$ has a stationary point at $\varepsilon = \mu_\infty$, $E'_\infty(\mu_\infty) = 0$, which in regime II lies within the integration range. The large time behavior of Eq. (5.268) obtains with the help of stationary point method [cf. Eq. (5.248)]

$$|\Delta(t)| = \Delta_\infty + \sqrt{\pi} F(\mu_\infty) \Delta_\infty^2 \frac{\cos(2\Delta_\infty t + \pi/4)}{\sqrt{\Delta_\infty t}}. \tag{5.272}$$

The only assumption about $F(\varepsilon)$ here is that it is smooth. This is an extension of Eq. (5.248) to nonlinear regime. In the weak coupling BCS limit this result was published in Ref. [19]. In this limit Δ_∞ is given by Eq. (5.152) and generally it obtains from Eqs. (5.138) and (5.162) in 2d and 3d, respectively, and Eq. (5.137) as the imaginary part of u. Here we see that expression (5.272) holds throughout the entire region II for both one and two channel models.

5.6.2 Regime II'

Regime II' has the same asymptotic $\Delta(t)$ as II by definition only with $\mu_\infty < 0$. There are now no stationary points on the integration path. The approach to the asymptote is therefore

determined by the behavior of $F(\varepsilon)f(\varepsilon)$ near the end points, $\varepsilon = 0$ in this case. We *assume* this behavior is the same as in linear analysis, since we expect the time dependence to have the same functional form throughout a given regime. According to Sect. 5.5.7, this means finite nonzero $F(0)$ in 3d and $F(\varepsilon) \propto 1/\ln^2 \varepsilon$ for $\varepsilon \ll 1$ in 2d.

Expanding Eq. (5.134) in small ε and using Eq. (5.111), we see that the spin components at $t \to \infty$ do behave the same as in linear analysis, though this in itself does not prove our assumption. Moreover, the asymptotic spin distribution (5.134) is continuous across critical lines separating various regimes, so the same small ε form holds in gapless region I as well.

As long as our assumptions about $F(\varepsilon)$ are correct, the analysis of the integral in Eq. (5.270) is the same as that in Sect. 5.5.7 resulting in

$$|\Delta(t)| = \Delta_\infty \left(1 - c_1 \frac{\sin(2E_\infty^{\min} t)}{t \ln^2 t}\right) \quad \text{in 2d}, \tag{5.273}$$

and

$$|\Delta(t)| = \Delta_\infty \left(1 - c_2 \frac{\cos(2E_\infty^{\min} t + \pi/4)}{t^{3/2}}\right) \quad \text{in 3d}, \tag{5.274}$$

at large times, where $E_\infty^{\min} = \sqrt{\mu_\infty^2 + \Delta_\infty^2}$ and c_1 and c_2 are real coefficients that depend on Δ_{0i}, Δ_{0f}, and γ.

5.6.3 Gapless regime

Finally, we turn to regime I. Now $\Delta(t) \to 0$ at $t \to \infty$. Spins $\vec{s}_\infty(\varepsilon)$ rotate with frequencies 2ε around z-axis, so that the Fourier transform of the order parameter magnitude is of the form

$$|\Delta(t)| = \int_0^\infty F(\varepsilon) \cos(2\varepsilon t) f(\varepsilon) d\varepsilon, \tag{5.275}$$

and $\sin(2\varepsilon t)$ term vanishes by time-reversal symmetry (5.269).

In 3d we similarly assume finite and nonzero $F(0)$. Steps outlined below Eq. (5.254) in Sect. 5.5.7 now lead to the following large time behavior:

$$|\Delta(t)| = \frac{c_3}{t^{3/2}}. \tag{5.276}$$

In 2d we speculate that $F(\varepsilon) \propto 1/\ln^r \varepsilon$ at small ε, where r is either 1 or 2. As discussed before in this Section, $s_\infty^-(\varepsilon, t) \propto 1/\ln \varepsilon$ in 2d, so that $\Delta_\infty(t) \propto 1/(t \ln t)$. The $1/\ln \varepsilon$ term however cancels from $F(\varepsilon)$ at least in linear analysis and it ends up being proportional to $1/\ln^2 \varepsilon$ instead. In the gapless case we allow for a possibility that such a cancelation does not occur. The analysis of the integral in Eq. (5.275), analogous to that leading to Eq. (5.256), then yields

$$|\Delta(t)| = \frac{c_4}{t \ln^r t}. \tag{5.277}$$

The gapless regime contains the $\Delta_{0i} = \Delta_{0f} = 0$ point, the origin of quench phase diagrams. It therefore includes the weak coupling limit $\Delta_{0i}/\varepsilon_F \to 0$ and $\Delta_{0f}/\varepsilon_F \to 0$. Eq. (5.275) becomes in this limit [see Sect. 5.5.5]

$$|\Delta(t)| = \int_{-\infty}^\infty F(\xi) \cos(2\xi t) d\xi, \tag{5.278}$$

where $F(\xi)$ is even in ξ. Now there can be no power law in t contribution at large t coming from integration limits. Instead, $|\Delta(t)|$ vanishes exponentially[Barankov and Levitov(2006),

Yuzbashyan and Dzero(2006)] as $A(t)e^{-2\alpha\Delta_{0i}t}$ independent of dimensionality, where $\alpha \sim 1$ and $A(t)$ is a decreasing power law, $A(t) \sim \Delta_{0i}$ at $t \sim 1/\Delta_{0i}$. Recall that throughout this paper we have been using units where $\varepsilon_F = 1$. To convert to arbitrary units in Eqs. (5.276) and (5.277), one needs to replace $t \to \varepsilon_F t$. Guided by linear analysis we further assume that coefficients c_4 and c_5 are of order Δ_{0f}, which we take to be comparable to Δ_{0i}. It is clear that at any finite $\Delta_{0i}/\varepsilon_F \ll 1$ power laws in Eqs. (5.276) and (5.277) coming from the lower integration limit will eventually win over the exponential decay. The comparison of $e^{-2\alpha\Delta_{0i}t}$ with $(\varepsilon_F t)^{-1}$ shows that the weak coupling result is valid at times such that $\ln(\varepsilon_F/\Delta_{0i}) \gg \Delta_{0i}t \gg 1$, while for $\Delta_{0i}t \gg \ln(\varepsilon_F/\Delta_{0i})$ it has to be replaced with Eqs. (5.276) and (5.277).

5.7 Experimental signatures

Far from equilibrium states of fermionic superfluids described in this paper can be observed in different systems with various experimental techniques.

Matsunaga et. al.[Matsunaga et al.(2013), 46] directly measured the time-dependent amplitude $|\Delta(t)|$ induced by an ultrafast electromagnetic perturbation in $Nb_{1\text{-}x}Ti_xN$ films using terahertz pump – terahertz probe spectroscopy. The underlying system is a BCS superconductor [weak coupling regime of one channel model (5.3)] and for perturbation strength below certain threshold its non-adiabatic dynamics falls within region II of our quench phase diagrams. Even though we considered BCS interaction quenches in one channel model in this paper, it is clear from our arguments that our results apply more generally to any kind of non-adiabatic global perturbation. Therefore, we expect $|\Delta(t)|$ to be described by Eq. (5.272) derived originally in nonlinear regime by Yuzbashyan et.al. [19]. These experiments indeed measure damped oscillations with frequency $2\Delta_\infty$, where Δ_∞ is the asymptotic value of $|\Delta(t)|$ even when the system is deep in the nonlinear regime and Δ_∞ is much different from the ground state gap. The power law approach however appears to be faster than $1/t^{1/2}$.

In this paper we primarily focused on detuning or interaction quenches in cold fermions. Experiments addressing superfluidity in these systems include measurements of the molecular condensate fraction[Regal et al.(2004), Zwierlein et al.(2004)], radio frequency absorption spectra[22], and observation of vortices[Zwierlein et al.(2005)]. Signatures of "far from equilibrium phases" I, II, and III – gapless, gapped (Volkov-Kogan), and oscillatory – in these experiments can be derived from the many-body wavefunction $\Psi(t)$ determined above.

The pseudospin (fermionic) part of $\Psi(t)$ is a direct product of spin-1/2 wavefunctions $\prod_{\mathbf{p}}(\bar{u}_{\mathbf{p}}|\downarrow\rangle + \bar{v}_{\mathbf{p}}|\uparrow\rangle)$ found in Sect. 5.2.4. In the gapless steady state

$$\begin{pmatrix} u_{\mathbf{p}} \\ \\ v_{\mathbf{p}} \end{pmatrix} = \cos\frac{\theta_{\mathbf{p}}}{2}\begin{pmatrix} 1 \\ 0 \end{pmatrix} e^{-i\varepsilon_{\mathbf{p}}t} + \sin\frac{\theta_{\mathbf{p}}}{2}\begin{pmatrix} 0 \\ 1 \end{pmatrix} e^{i\varepsilon_{\mathbf{p}}t - i\delta_{\mathbf{p}}}, \tag{5.279}$$

where $\cos\theta_{\mathbf{p}} \equiv \cos\theta(\varepsilon_{\mathbf{p}})$ is given by Eq. (5.134) in all three phases. The second term represents an occupied pair of states $\pm\mathbf{p}$ (pseudospin up), the first – empty (pseudospin down). $\Psi(t)$ in the gapless phase is a coherent superposition of eigenstates of a free Fermi gas with different energies reflecting the fact that $\Delta(t) \to 0$ implies vanishing of interactions between fermions on the mean-field level. Effectively the system is governed by a non-interacting Hamiltonian at $t \to \infty$. It nevertheless retains superconducting correlations. For example, in the weak coupling regime its superfluid density is half that in the ground state and in phase II[Yuzbashyan and Dzero(2006)]. Phase I is therefore a nonequilibrium gapless superfluid.

In the gapped steady state Eqs. (5.100) and (5.112) imply

$$\begin{pmatrix} u_{\mathbf{p}} e^{i\mu_\infty t} \\ v_{\mathbf{p}} e^{-i\mu_\infty t} \end{pmatrix} = \cos\frac{\theta_{\mathbf{p}}}{2} \overbrace{\begin{pmatrix} |U_{\mathbf{p}}| \\ |V_{\mathbf{p}}| \end{pmatrix} e^{-iE^\infty_{\mathbf{p}} t}}^{\text{ground state pair}} + \sin\frac{\theta_{\mathbf{p}}}{2} \overbrace{\begin{pmatrix} |V_{\mathbf{p}}| \\ -|U_{\mathbf{p}}| \end{pmatrix} e^{iE^\infty_{\mathbf{p}} t}}^{\text{excited pair}}, \tag{5.280}$$

where

$$|U_{\mathbf{p}}| = \sqrt{\frac{1}{2} + \frac{\xi_{\mathbf{p}}}{2E^\infty_{\mathbf{p}}}}, \quad |V_{\mathbf{p}}| = \sqrt{\frac{1}{2} - \frac{\xi_{\mathbf{p}}}{2E^\infty_{\mathbf{p}}}}, \tag{5.281}$$

$\xi_{\mathbf{p}} = \varepsilon_{\mathbf{p}} - \mu_\infty$, and we dropped the nonessential constant phase φ. Bogoliubov amplitudes $|U_{\mathbf{p}}|$ and $|V_{\mathbf{p}}|$ are the same as in the BCS ground state[Schrieffer(1989)] with gap Δ_∞ and chemical potential μ_∞. The two wavefunctions on the right hand side of Eq. (5.280) are the two orthonormal eigenstates of the BdG Hamiltonian

$$H_{\text{BdG}} = \begin{pmatrix} \xi_{\mathbf{p}} & \Delta_\infty \\ \Delta_\infty & -\xi_{\mathbf{p}} \end{pmatrix}. \tag{5.282}$$

The first one is a Cooper pair wavefunction in the BCS ground state and corresponds to an alignment of the pseudospin $\vec{s}_{\mathbf{p}}$ antiparallel to the effective magnetic field. The second one is an excited state of the Cooper pair ($\vec{s}_{\mathbf{p}}$ parallel to the effective magnetic field) termed an *excited pair* in the original BCS work[20]. It is interesting to note that these excitations of the condensate in superconducting metals carry no charge and spin, so non-adiabatic dynamics considered here provides a unique venue for creating and measuring them[Dzero et al.(2007)]. The steady state in phase II therefore is a coherent mixture of ground state and excited pairs – a superposition of eigenstates of the BCS Hamiltonian with gap Δ_∞ and chemical potential μ_∞.

A similar interpretation of the oscillatory state obtains by Fourier transforming the amplitudes (5.122)

$$\begin{pmatrix} u_{\mathbf{p}} e^{i\tilde{\mu} t} \\ v_{\mathbf{p}} e^{-i\tilde{\mu} t} \end{pmatrix} = \sum_{n=-\infty}^{\infty} \left\{ \cos\frac{\theta_{\mathbf{p}}}{2} \begin{pmatrix} a_{\mathbf{p}n} \\ b_{\mathbf{p}n} \end{pmatrix} e^{-i(e_{\mathbf{p}} - n\omega_\Delta)t} + \sin\frac{\theta_{\mathbf{p}}}{2} \begin{pmatrix} \bar{b}_{\mathbf{p}n} \\ -\bar{a}_{\mathbf{p}n} \end{pmatrix} e^{i(e_{\mathbf{p}} - n\omega_\Delta)t} \right\}, \tag{5.283}$$

where ω_Δ is the oscillation frequency of $|\Delta(t)|$, $\tilde{\mu}$ and $-2e_{\mathbf{p}}$ are the zeroth harmonics of the phase of $\Delta(t)$ and the common phase of the amplitudes, see Eqs. (5.102) and (5.106), and we again dropped the constant phase φ. This expression derives by first going to a frame rotating with frequency $2\tilde{\mu}$ to get rid of the linear term in the phase of $\Delta(t)$. This makes $e^{-i\phi_{\mathbf{p}}}$, the term involving the relative phase, periodic according to Eq. (5.103) and it does not contribute to the momentum dependent phases on the right hand side. Phase III therefore can be understood as a superposition of generalized excited and ground state pairs with dispersions $\pm e_{\mathbf{p}}$ and quanta of the amplitude (Higgs) mode $|\Delta(t)|$. As noted in Sect. 5.2.4, $e_{\mathbf{p}} \to \varepsilon_{\mathbf{p}}$ at large $\varepsilon_{\mathbf{p}}$.

The knowledge of the steady state allows us to compute far from equilibrium correlation and Green's functions in all three phases. For example[not(b)],

$$\begin{aligned} i\mathcal{G}_{\mathbf{p},>}(t,t') &= \langle \hat{a}_{\mathbf{p}\uparrow}(t)\, \hat{a}^\dagger_{\mathbf{p}\uparrow}(t')\rangle = \bar{u}_{\mathbf{p}}(t)u_{\mathbf{p}}(t'), \\ -i\mathcal{G}_{\mathbf{p},<}(t,t') &= \langle \hat{a}^\dagger_{\mathbf{p}\uparrow}(t')\, \hat{a}_{\mathbf{p}\uparrow}(t)\rangle = \bar{v}_{\mathbf{p}}(t')v_{\mathbf{p}}(t), \\ \mathcal{G}^+_{\mathbf{p}}(t,t') &= \langle \hat{a}^\dagger_{-\mathbf{p}\downarrow}(t)\, \hat{a}^\dagger_{\mathbf{p}\uparrow}(t')\rangle = v_{\mathbf{p}}(t)\bar{u}_{\mathbf{p}}(t'). \end{aligned} \tag{5.284}$$

With these we can evaluate various observables such as the superfluid density mentioned earlier in this section. Note also that the steady state momentum distribution $n_p^\infty(t)dp$ is simply related to the z-component of the pseudospin according to Eq. (5.6). Taking into account that $\mathbf{p}$ and $-\mathbf{p}$ are both included in $s^z_{\mathbf{p}}$ and integrating over the angles, we have

$$n_p^\infty(t) = 2p^2(2s^z_{\mathbf{p}} + 1). \tag{5.285}$$

Expressions for $s^z_{\mathbf{p}}$ in phases I, II, and II appear in Eq. (5.97), Eq. (5.111), and Eqs. (5.104) and (5.121), respectively.

Finally, let us discuss the signatures of nonequilibrium phases in radio frequency (RF) spectroscopy[Törmä and Zoller(2000), Regal and Jin(2003), et al.(2003), Kinnunen et al.(2004), Schunk et al.(2008), Basu and Mueller(2008), Schirotzek et al.(2008)]. Recall that in an atomic Fermi gas the pairing occurs between atoms in two different hyperfine states, $|\uparrow\rangle \equiv |1\rangle$ and $|\downarrow\rangle \equiv |2\rangle$. The RF photon transfers atoms from one of these states, say $|2\rangle$, to the third hyperfine state $|3\rangle$ that does not interact with $|1\rangle$ and $|2\rangle$. In an unpaired Fermi gas where atoms $|2\rangle$ are free, the RF absorption spectrum has a peak at the atomic transition energy $\omega = \mathcal{E}_{23}$. In the paired ground state, the peak shifts to $\omega > \mathcal{E}_{23}$ by an amount equal to the minimum binding energy of Cooper pairs[Törmä and Zoller(2000)].

The RF response of steady states I, II, and III was calculated in Ref. [Dzero et al.(2007)] for quenches within the BCS regime and in Ref. [Foster et al.(2013)] for quenched p-wave superfluids. The calculation in the present case is identical[not(c)], so we will not reproduce it here. The RF spectrum of phase I is similar to that of the normal state – a peak at $\omega = \mathcal{E}_{23}$. In phase II there are two peaks – at $\omega > \mathcal{E}_{23}$ and $\omega < \mathcal{E}_{23}$, which come from the ground state and excited pairs, respectively, see Eq. (5.280). The first peak corresponds to a process in which an RF photon breaks a ground state pair, the second – excited pair. The RF response of phase III similarly reflects the structure of the corresponding steady state wavefunction (5.283). There are two series of peaks spaced by ω_Δ, the frequency of oscillations of $|\Delta(t)|$, coming from processes where an RF photon breaks a ground state (excited) pair and absorbs or emits several quanta of the amplitude (Higgs) mode $|\Delta(t)|$.

5.8 Conclusion

In this paper we studied the coherent dynamics of an isolated BCS-BEC condensate in two and one channel (BCS) models in two and three spatial dimensions. Our main focus was on detuning quenches $\omega_i \to \omega_f$ (interaction quenches $\lambda_i \to \lambda_f$ in the one channel model). We constructed exact quench phase diagrams and predicted the order parameter dynamics $\Delta(t)$ and the full time-dependent wavefunction $\Psi(t)$ of the system at large times for any pair of values (ω_i, ω_f). In contrast to most previous work, we considered quenches beyond the weak coupling limit of BCS to BCS quenches. We add to this BCS to BEC and BEC to BCS quenches across the Feshbach resonance as well as quenches on the BEC side. We showed that the weak coupling limit is universal in that it is model and dimension independent. Outside of this limit, there are several qualitatively new features, the two channel model having richer quench phase diagram as it contains an extra parameter – dimensionless resonance width γ. All results for the one channel model obtain from the two channel ones by taking the broad resonance, $\gamma \to \infty$, limit.

We find the same three main nonequilibrium phases (asymptotic states) as in the weak coupling regime. Interestingly, this seems to be a universal, model independent feature of quench dynamics of fermionic condensates, at least when there is a global complex order parameter, so that the Cooper pairs interact only through this collective mode. The same three phases occur, for example, in p-wave superconductors[Foster et al.(2013), Foster et al.(2014)], spin-orbit coupled superfluids[Dong et al.(2014)], and s-wave superconductors with energy-dependent interaction[Barankov and Levitov(2007)]. One can speculate that similar universality according to the order parameter type exists among quench phase diagrams of multicomponent superfluids, such as three fermion species with pairing interactions or multi-band superconductors.

The above three main phases are: phase I where $\Delta(t)$ vanishes, phase II where $\Delta(t) \to \Delta_\infty e^{-2i\mu_\infty t}$ up to a constant phase factor, and phase III where $|\Delta(t)|$ oscillates persistently. It turns out μ_∞ plays the role of a nonequilibrium analog of the chemical potential. For quenches within the weak coupling regime $\mu_\infty \approx \varepsilon_F$, while for quenches to deep BEC $\mu_\infty \to -\infty$. Some of the new effects as one moves beyond the weak coupling regime are as follows. The oscillatory approach of $|\Delta(t)|$ to a constant (Volkov-Kogan behavior) changes from $1/\sqrt{t}$ for $\mu_\infty > 0$ to $1/t^{3/2}$ in three dimensions and $1/(t \ln^2 t)$ in two dimensions for $\mu_\infty < 0$, and the oscillation frequency changes from $2\Delta_\infty$ to $2\sqrt{\mu_\infty^2 + \Delta_\infty^2}$. For resonance width below a certain threshold, the asymptotic gap amplitude Δ_∞ can be much larger than Δ_{0f} – the ground state gap at final detuning ω_f. Similarly, exponential vanishing of $|\Delta(t)|$ in phase I gives way to a power law behavior. Persistent oscillations in phase III are first suppressed for stronger quenches and then disappear altogether. For example, in three dimensional one channel model there is a critical coupling λ_c, such that even quenches from an infinitesimally small λ_i to $\lambda_f > \lambda_c$ produce no such oscillations. As λ_f approaches λ_c from below, the oscillation amplitude first increases, then decreases and finally vanishes at $\lambda_f = \lambda_c$.

The post-quench asymptotic state of the condensate is a coherent superposition of ground state and excited pairs at each momentum (multiple bands of such pairs shifted by the oscillation frequency of $|\Delta(t)|$ in phase III). These are two orthogonal eigenstates of a Cooper pair in the self-consistent field, and, for instance, the BCS ground state is a direct product of ground state pair wavefunctions. Our steady state in phases I and II is a direct product of such time-dependent superpositions. In the Anderson pseudospin language, ground state (excited) pairs correspond to the alignment of pseudospin antiparallel (parallel) to the magnetic field. Even though we refer to these states as ground state or excited pairs, we should stress that they are not the same as similar states of Cooper pairs in the ground or excited states of the BCS Hamiltonian since the self-consistent field is different. Excited pairs are elusive excitations in superconductors – it is difficult to couple to them as they carry no charge or spin. Non-adiabatic dynamics of the BCS-BEC condensate provides an opportunity to access them, e.g. in the RF absorption spectrum.

Our treatment of the dynamics of the BCS-BEC condensate neglects the coupling to the non-condensed modes (mean field approximation) – molecules with nonzero momenta $\mathbf{q}$ in the two channel model. We check the validity of this approximation for the two channel model by estimating the rates of the decoherence processes due to these terms for post-quench steady states in phase II and comparing them to the typical timescale on which the quench dynamics occurs. Our preliminary results indicate that the mean field approach is justified for quenches sufficiently far from the $\mu_\infty = 0$ line in the quench phase diagrams, e.g. quenches within deep BEC, deep BCS, or across the resonance from deep BCS to deep BEC and vice versa. A more thorough study of these effects is necessary to fully clarify the situation.

In mean field various pairing Hamiltonians, e.g. one and two channel models considered here, chiral p-wave BCS, a certain class of d-wave BCS models[Richardson(2002)], are equivalent to integrable classical spin (or spin-oscillator) chains with long-range interactions. The most remarkable general feature of their dynamics is a reduction in the number of effective degrees of

freedom as $t \to \infty$. Consider e.g. the one channel model. As explained above, its dynamics in the thermodynamic limit at long times after the quench can be described in terms of just a few – zero (phase I), one (phase II), or two (phase III) – new collective classical spin variables. In other words, the number of spin at long times reduces from infinity to zero, one, or two. Moreover, the new spins time-evolve with the same Hamiltonian only with "renormalized" parameters. For example, in phase I the effective Hamiltonian at large times is simply $H = 0$, and in phase II it is $H = 2\mu_\infty S_z - gS_-S_+$, where $\vec{S}$ is the collective spin of length $|\vec{S}| = \Delta_\infty/g$, and g is the original BCS coupling constant. The order parameter $\Delta(t)$ coincides with that of the few spin problem, while the original spins relate to the collective ones in a more involved fashion.

It is this feature of the dynamics together with the integrability of the underlying model that allowed us to explicitly determine the exact post-quench asymptotic state of the system. In this paper we presented for the first time a comprehensive, consistent overview of a general method to explicitly evaluate the large time asymptotic solution in classical integrable systems that support this kind of reduction. We are not aware of any similar method for other integrable nonlinear models, the rather different soliton resolution conjecture[Duyckaerts et al.(2013)] being the closest analog we were able to identify.

An interesting open question is whether a similar reduction in the number of degrees of freedom in the course of time evolution occurs also in non-integrable pairing models. This can explain the aforementioned universality of the quench phase diagrams among systems characterized by a global complex order parameter. It seems non-accidental indeed that the non-integrable spin-orbit coupled superfluid[Dong et al.(2014)] has the same three main post-quench phases and that, moreover, $\Delta(t)$ in phase III is given by an elliptic function dn. Presumably a generalization of this method to non-integrable models would rely on more general considerations without recourse to integrability-specific techniques and thus would clarify the underlying physical mechanism. It would also make a number of interesting problems, such as e.g. the competition between chiral and anti-chiral components in p-wave superconductors upon switching on superconducting interactions and more generally the dynamical interplay among various components in a multicomponent superfluid, potentially amenable to in depth analysis.

5.9 Pair-breaking rates

In this appendix, we perform a preliminary analysis of the validity of neglecting $\mathbf{q} \neq 0$ terms far from equilibrium in the Hamiltonian (5.1). So far we have studied the quench dynamics of the condensate decoupled from these non-condensed modes. There are two kinds of relevant processes due to the $\mathbf{q} \neq 0$ terms: (i) excitation of molecules out of the condensate and (ii) excitation of fermionic quasiparticles through two-particle collisions. We estimate characteristic timescales of both processes in the post-quench steady state. We find that sufficiently far from the $\mu_\infty = 0$ line in our quench phase diagrams (see Figs. 5.3 and 5.21) these timescales are much larger than the characteristic time of the quench dynamics. This means that dropping $\mathbf{q} \neq 0$ terms is indeed justified at times it takes for the quench dynamics to develop and reach the steady state. At much later times, after the quench dynamics plays out, these terms set in, presumably leading to decoherence and eventual thermalization of our (isolated) system. We note also that the $\mu_\infty = 0$ line can be very roughly interpreted as a far from equilibrium generalization of the unitarity point. Quenches away from this line are from BCS or BEC initial detuning to far BCS and BEC side including quenches across the resonance.

In what follows we consider a three-dimensional condensate and, for simplicity, we content ourselves with steady states in phase II (including II') where pairing amplitude asymptotes to a constant, $|\Delta(t \to \infty)| = \Delta_\infty$.

5.9.1 Steady state molecular production

Here we compute the rate at which molecules with non-zero momentum are produced in steady state II where initially all molecules have zero momentum. To the lowest order in the interaction, the corresponding scattering amplitudes are[Phillips(2003)]

$$\mathcal{A}_b(\mathbf{p}_1,\mathbf{p}_2)\delta(E_{\rm fin}-E_{\rm in})=\int\limits_{-\infty}^{\infty}\langle\Psi_{\rm fin}|\hat{V}(t)|\Psi_{\rm in}\rangle dt, \tag{5.286}$$

where $|\Psi_{\rm in}\rangle$ and $E_{\rm in}$ are the steady state wavefunction and energy. $|\Psi_{\rm fin}\rangle$ obtains from $|\Psi_{\rm in}\rangle$ by destroying two pairs and creating a molecule with momentum $\mathbf{q}=\mathbf{p}_1+\mathbf{p}_2$ and two unpaired atoms with momenta $\mathbf{p}_1$ and $\mathbf{p}_2$. The energy of the final state is

$$E_{\rm fin}=E_{\rm in}+\zeta_{\mathbf{q}}\pm E^{\infty}_{\mathbf{p}_1}\pm E^{\infty}_{\mathbf{p}_2}, \tag{5.287}$$

where plus (minus) corresponds to a ground (excited) pair and

$$\zeta_{\mathbf{q}}=\frac{q^2}{4m}+\omega_f-2\mu_{\infty}, \tag{5.288}$$

is the energy of the molecule. The interaction $\hat{V}(t)$ is described by the last term in Eq. (5.1)

$$\begin{aligned}\hat{V}(t)=g\sum_{\mathbf{p}_1,\mathbf{p}_2}\Big[&\hat{b}^{\dagger}_{\mathbf{p}_1+\mathbf{p}_2}(t)\hat{a}_{\mathbf{p}_1\uparrow}(t)\hat{a}_{\mathbf{p}_2\downarrow}(t)+\\&\hat{b}_{\mathbf{p}_1+\mathbf{p}_2}(t)\hat{a}^{\dagger}_{\mathbf{p}_2\downarrow}(t)\hat{a}^{\dagger}_{\mathbf{p}_1\uparrow}(t)\Big].\end{aligned} \tag{5.289}$$

Since our initial state does not contain molecules with non-zero momentum, only the first term in Eq. (5.289) contributes to the matrix element (5.286). One also needs to keep in mind that our steady state contains superpositions of a ground state pair with energy $-E^{\infty}_{\mathbf{p}}$ and an excited pair with energy $+E^{\infty}_{\mathbf{p}}$ for each $\mathbf{p}$. Eqs. (5.280) and (5.286) then yield the following four scattering amplitudes[not(b)]:

$$\begin{aligned}\mathcal{A}_b^{(--)}(\mathbf{p}_1,\mathbf{p}_2)&=g\cos\frac{\theta_{\mathbf{p}_2}}{2}\cos\frac{\theta_{\mathbf{p}_1}}{2}|V_{\mathbf{p}_2}||V_{\mathbf{p}_1}|,\\ \mathcal{A}_b^{(+-)}(\mathbf{p}_1,\mathbf{p}_2)&=g\sin\frac{\theta_{\mathbf{p}_2}}{2}\cos\frac{\theta_{\mathbf{p}_1}}{2}|U_{\mathbf{p}_2}||V_{\mathbf{p}_1}|,\\ \mathcal{A}_b^{(++)}(\mathbf{p}_1,\mathbf{p}_2)&=g\sin\frac{\theta_{\mathbf{p}_2}}{2}\sin\frac{\theta_{\mathbf{p}_1}}{2}|U_{\mathbf{p}_2}||U_{\mathbf{p}_1}|,\end{aligned} \tag{5.290}$$

where - (+) describes breaking a ground state (excited) pair, and $\mathcal{A}_b^{(-+)}(\mathbf{p}_1,\mathbf{p}_2)=\mathcal{A}_b^{(+-)}(\mathbf{p}_2,\mathbf{p}_1)$.

Molecular production rate per atom at zero temperature obtains from these amplitudes and Fermi's Golden Rule[Phillips(2003)]

$$\begin{aligned}\tau^{-1}_{\rm mol}=\frac{2\pi}{N_f}\sum_{\mathbf{p}_1\mathbf{p}_2\alpha\beta}&|\mathcal{A}_b^{(\alpha\beta)}(\mathbf{p}_1,\mathbf{p}_2)|^2\times\\&\delta\left(\zeta_{\mathbf{p}_1+\mathbf{p}_2}-\alpha E^{\infty}_{\mathbf{p}_2}-\beta E^{\infty}_{\mathbf{p}_1}\right).\end{aligned} \tag{5.291}$$

In this expression N_f is the total number of fermions in the absence of molecules and we took into account that there are no molecules with non-zero momentum in our steady state.

Let us specialize to quenches into either deep BCS ($\omega_f\to+\infty$) or deep BEC ($\omega_f\to-\infty$). We expect a much higher rate in the latter case, because in the BCS regime $\zeta_{\mathbf{q}}\to+\infty$ requiring

excited pairs of extremely high energy to create a molecule. For quenches to far BEC side $\mu_\infty \to -\infty$, while Δ_∞ remains finite regardless of the initial detuning, see e.g. Figs. 5.18 and 5.19. It follows that $E^\infty_{\mathbf{p}} \approx \xi_{\mathbf{p}} = |\mu_\infty| + p^2/2m$ and Eq. (5.200) implies $\omega_f \approx 2\mu_\infty$. For $\alpha = \beta = -1$ the argument of the delta-function in Eq. (5.291) is always positive, i.e. energy conservation cannot be satisfied meaning that the ground state pairs do not contribute to the rate. Similarly, if $\alpha = \beta = 1$ (two excited pairs)

$$\begin{aligned} &\zeta_{\mathbf{p}_1+\mathbf{p}_2} - E^\infty_{\mathbf{p}_1} - E^\infty_{\mathbf{p}_2} \approx \frac{(\mathbf{p}_1+\mathbf{p}_2)^2}{4m} + \omega_f - \\ &\frac{p_1^2+p_2^2}{2m} = \omega_f - \frac{(\mathbf{p}_1-\mathbf{p}_2)^2}{4m} < 0. \end{aligned} \tag{5.292}$$

Therefore, only scattering processes involving one fermion from an excited and another from a ground state pair contribute. Expression (5.291) for the rate in this case is

$$\begin{aligned} \tau^{-1}_{\mathrm{mol}} \approx \frac{4\pi g^2}{N_f} \sum_{\mathbf{p}_1,\mathbf{p}_2} \sin^2\frac{\theta_{\mathbf{p}_2}}{2} \cos^2\frac{\theta_{\mathbf{p}_1}}{2} |U_{\mathbf{p}_2}|^2 |V_{\mathbf{p}_1}|^2 \times \\ \delta\left(\frac{3p_1^2 + 2\mathbf{p}_1\cdot\mathbf{p}_2 - p_2^2}{4m}\right), \end{aligned} \tag{5.293}$$

Next, we go from summations to integrations, integrate over the angle between $\mathbf{p}_1$ and $\mathbf{p}_2$, and change integration variables from momenta to energies, which results in

$$\begin{aligned} \tau^{-1}_{\mathrm{mol}} \approx \frac{3\gamma}{2\varepsilon_F} \int_0^\infty d\varepsilon_2 \sin^2\frac{\theta(\varepsilon_2)}{2} |U(\varepsilon_2)|^2 \times \\ \int_{\varepsilon_2/9}^{\varepsilon_2} d\varepsilon_1 \cos^2\frac{\theta(\varepsilon_1)}{2} |V(\varepsilon_1)|^2. \end{aligned} \tag{5.294}$$

We replace the cosine with one, use $|V(\varepsilon_1)|^2 \approx \Delta_\infty^2/4(\varepsilon_1+|\mu_\infty|)^2$, which follows from Eq. (5.281) together with $|U(\varepsilon_1)|^2 \approx 1$, and integrate over ε_1. According to Eq. (5.136), the probability of finding an excited pair

$$\sin^2\frac{\theta(\varepsilon_2)}{2} \to \frac{\Delta_{0i}^2(\delta\omega)^2}{16E_i^4(\varepsilon_2)} \quad \text{as } \varepsilon_2 \to \infty. \tag{5.295}$$

A larger rate obtains for finite ω_i than for ω_i close to ω_f. In this case $\delta\omega \approx 2\mu_\infty$ and $\sin^2[\theta(\varepsilon_2)/2]$ appreciably differs from zero at energies about $\sqrt{\Delta_{0i}|\mu_\infty|}$. We obtain

$$\tau^{-1}_{\mathrm{mol}} \sim \frac{\gamma\Delta_\infty^2\Delta_{0i}}{\varepsilon_F|\mu_\infty|} \to 0. \tag{5.296}$$

In deriving Eq. (5.295) we assumed finite resonance width γ. A separate estimate for the broad resonance limit for quenches to deep BEC finds a rate that also vanishes, but as $\gamma^{-1/3}|\mu_\infty|^{-1/2}$.

This result for the molecular production rate should be compared with the typical time scale τ_{dyn} of the quench dynamics for quenches to the far BEC side. Eqs. (5.256) and (5.274) imply

$$\tau^{-1}_{\mathrm{dyn}} \sim |\mu_\infty|. \tag{5.297}$$

We see that indeed $\tau_{\mathrm{dyn}} \ll \tau_{\mathrm{mol}}$.

5.9.2 Two-particle collisions

Next, we estimate the relaxation rate due to two-particle collisions. In contrast to the molecular production, we find that here the contribution coming from just the ground state pairs is of the same order of magnitude or larger than that from collisions that involve excited pairs. We therefore consider ground state pairs only and take the probability of finding such a pair at a given momentum $\mathbf{p}$ to be $\cos^2(\theta_{\mathbf{p}}/2) \approx 1$. Let us analyze quenches to the far BCS side of the Feshbach resonance from any initial detuning. In this case, $\omega_f \gg \mu_\infty \approx \epsilon_F$, see e.g. Fig 5.19. The total scattering amplitude for this case has been studied in Ref. [Galaiko(1972)] [see Eq. (71) therein], which also estimates the corresponding rate as

$$\tau_{\rm in}^{-1} \sim \left(\frac{g^2\nu_F}{\omega_f}\right)^2 \frac{\Delta_\infty^2}{\epsilon_F} = \gamma^2\epsilon_F \left(\frac{\Delta_\infty}{\omega_f}\right)^2. \tag{5.298}$$

In fact, this is the well-know Fermi liquid result for the quasiparticle lifetime. Indeed, $\lambda = g^2\nu_F/\omega_f$ is the strength of the effective interaction between fermions [see Eq. (5.4)] and Δ_∞ is the typical excitation energy – the energy scale at which spins deviate appreciably from their ground state positions.

Eq. (5.298) has to be compared with the characteristic timescale of the dynamics for quenches to the far BCS side. According to Eq. (5.272) this timescale is

$$\tau_{\rm dyn} \sim \frac{1}{\Delta_\infty}. \tag{5.299}$$

We see that $\tau_{\rm dyn} \ll \tau_{\rm in}$ for any finite resonance width γ since $\omega_f \to \infty$ in deep BCS. In the broad resonance limit too $\tau_{\rm dyn}/\tau_{\rm in} = \lambda^2\Delta_\infty/\varepsilon_F \ll 1$. This is because at large γ quenches to far BCS in phase II are only possible from initial detunings also on the far BCS side, see e.g. Figs. 5.3(c) and 5.5. It then follows from Eq. (5.152) that $\Delta_\infty \le \Delta_{0f} \ll \varepsilon_F$.

A preliminary analysis for quenches to the far BEC side shows that, at least for a finite resonance width γ and sufficiently large $|\omega_f|$, one still has $\tau_{\rm dyn} \ll \tau_{\rm in}$. Thus, neglecting two-particle collisions is justified at times it takes the quench dynamics to fully develop and reach its asymptote.

5.10 Finite size corrections to the roots

As mentioned in Sect. 5.3, in the thermodynamic limit $\vec{L}^2(u)$ for quench initial conditions has a continuum of roots along the positive real axis. Here we verify this and determine finite size corrections to these roots.

Roots of $\vec{L}^2(u)$ are determined by Eq. (5.126) or, equivalently, by Eq. (5.209) in notation explained in the beginning Sect. 5.5.2, which we employ here as well. The level spacing δ is of order $1/N$. Thermodynamic limit means $N \to \infty$, so ε_k become continuous with density $\nu(\varepsilon)$.

Let us look for a pair of complex conjugate roots close to ε_m writing it as $c_m = \varepsilon_m + \varsigma_m\delta$. We take $\varsigma_m \equiv \varsigma(\varepsilon_m)$ to be of order 1, to be confirmed below. Note that ς_m is generally complex. Our goal is to evaluate c_m to first order in $1/N$. We split the summation in Eq. (5.209) into two parts – over ε_k in a small interval $(\varepsilon_m - \Delta\varepsilon, \varepsilon_m + \Delta\varepsilon)$ and over remaining ε_k. The interval is however sufficiently large so that it contains many ε_k. Specifically, $\Delta\varepsilon \to 0$, but $\Delta\varepsilon/\delta \to \infty$ in thermodynamic limit. For example, $\Delta\varepsilon = \delta\sqrt{N}$ fulfills these conditions. The latter summation becomes a principal value integral in the $N \to \infty$ limit, while the former one to leading order

in $1/N$ reads

$$\frac{N(\varepsilon_m)}{2E(\varepsilon_m)\delta}\sum_{p=0}^{\infty}\left[\frac{1}{p+\varsigma_m}-\frac{1}{p+1-\varsigma_m}\right]= \frac{\pi\nu(\varepsilon_m)}{2E(\varepsilon_m)}\cot\pi\varsigma_m. \tag{5.300}$$

The first sum is from $\varepsilon_k < \varepsilon_m$, the second – from $\varepsilon_k > \varepsilon_m$. Here it is important that the degeneracy $N_k \equiv N(\varepsilon_k)$ and the spacing between ε_k vary smoothly with ε_k. As long as this is the case, we can include any variation of the spacing into N_k.

Thus, Eq. (5.209) to leading order in $1/N$ becomes

$$\frac{2}{g^2}-\int_0^{\infty}\frac{\nu(\varepsilon')d\varepsilon'}{2(\varepsilon_m-\varepsilon')E(\varepsilon')}-\frac{\nu(\varepsilon_m)}{2E(\varepsilon_m)}\cot\pi\varsigma_m = \frac{\delta\omega}{g^2}\frac{\varepsilon_m-\mu\pm i\Delta_0}{E^2(\varepsilon_m)}. \tag{5.301}$$

Recalling that $\nu(\varepsilon)=\nu_F f(\varepsilon)$ and $g^2\nu_F=\gamma$ in units of Fermi energy, we obtain

$$\pi\cot\pi\varsigma(\varepsilon)=\frac{4E(\varepsilon)}{\gamma f(\varepsilon)}-\frac{G(\varepsilon)}{f(\varepsilon)}-\frac{2\delta\omega}{\gamma}\frac{\varepsilon-\mu\pm i\Delta_0}{E(\varepsilon)f(\varepsilon)}, \tag{5.302}$$

where

$$G(\varepsilon)=E(\varepsilon)\int_0^{\infty}\frac{f(\varepsilon')d\varepsilon'}{(\varepsilon-\varepsilon')E(\varepsilon')}. \tag{5.303}$$

This principal value integral is the same as in Eq. (5.129). We evaluated it in elementary functions for various cases in Sects. 5.3.1 and 5.3.2. Specifically, in 2d

$$G_{2\mathrm{d}}(\varepsilon)=\ln\left[\frac{\varepsilon\left(\varepsilon-\mu+E(\varepsilon)\right)}{E(\varepsilon)\sqrt{\mu^2+\Delta_0^2}+\mu^2+\Delta_0^2-\mu\varepsilon}\right], \tag{5.304}$$

in weak coupling (BCS) limit, $\mu\approx\varepsilon_F\gg\Delta_0$, for energies not too far from the Fermi energy, in both 2d and 3d

$$G_{\mathrm{wc}}(\varepsilon)=\ln\left[\frac{E(\varepsilon)+\varepsilon-\mu}{E(\varepsilon)-\varepsilon+\mu}\right], \tag{5.305}$$

in strong coupling (BEC) limit in 2d and 3d,

$$G_{\mathrm{sc}}^{2\mathrm{d}}(\varepsilon)=\ln\frac{\varepsilon}{|\mu|},\quad G_{\mathrm{sc}}^{3\mathrm{d}}(\varepsilon)=-\pi\sqrt{\frac{|\mu|}{\Delta_0}}. \tag{5.306}$$

Ground state continual roots $x_k=\varepsilon_k+\varrho_k\delta$ obtain by setting $\delta\omega=0$ in Eq. (5.302), i.e.

$$\pi\cot\pi\varrho(\varepsilon)=\frac{4E(\varepsilon)}{\gamma f(\varepsilon)}-\frac{G(\varepsilon)}{f(\varepsilon)}\equiv\frac{H(\varepsilon)}{f(\varepsilon)}. \tag{5.307}$$

The quantity $F_k\equiv F(\varepsilon_k)$ defined in Eq. (5.215) evaluates similarly to Eq. (5.300),

$$F(\varepsilon)=-\frac{N(\varepsilon)}{2E(\varepsilon)\delta^2}\frac{\partial}{\partial\varrho}\sum_{p=0}^{\infty}\left[\frac{1}{p+1-\varrho}-\frac{1}{p+\varrho}\right]= \frac{\nu(\varepsilon)}{2E(\varepsilon)\delta}\frac{\pi^2f^2(\varepsilon)+H^2(\varepsilon)}{f^2(\varepsilon)}. \tag{5.308}$$

5.11 Identities

In this appendix we prove Eq. (5.225). To this end, consider a function

$$R(u) = L_0(u)\left[(u-\mu)^2 + \Delta_0^2\right], \tag{5.309}$$

where $L_0(u)$ is given by Eq. (5.210). Since zeroes of $L_0(u)$ are x_k and its poles are ε_k it alternatively can be written

$$R(u) = -\frac{2}{g^2}\frac{\prod_{k=1}^N (u-x_k)}{\prod_{k=1}^N (u-\varepsilon_k)}\left[(u-\mu)^2 + \Delta_0^2\right], \tag{5.310}$$

Eq. (5.225) follows by matching two leading terms in $1/u$ expansions of function $1/R(u)$ obtained with the help of these two alternative forms.

Because $1/R(u)$ is a rational function with poles at $u = x_k$ and $\mu \pm i\Delta_0$, we have

$$\begin{aligned}\frac{1}{R(u)} = \sum_k \frac{1}{(u-x_k)L_0'(x_k)\Omega_k^2} + \\ \frac{1}{2i\Delta_0(u-c_+)L_0(c_+)} - \frac{1}{2i\Delta_0(u-c_-)L_0(c_-)},\end{aligned} \tag{5.311}$$

where $c_\pm = \mu \pm i\Delta_0$ and we took into account that the square bracket in Eq. (5.309) evaluated at $u = x_k$ is equal to Ω_k^2. Note also that $L_0'(x_k) = -F_k$, see Eq. (5.215). Eq. (5.210) implies

$$L_0(c_\pm) = -\beta_k \mp i\alpha_k, \tag{5.312}$$

where

$$\begin{aligned}\alpha_k &= \sum_k \frac{N_k\Delta_0}{2\left[E(\varepsilon_k)\right]^{3/2}}, \\ \beta_k &= \frac{2}{g^2} + \sum_k \frac{N_k(\varepsilon_k-\mu)}{2\left[E(\varepsilon_k)\right]^{3/2}}.\end{aligned} \tag{5.313}$$

The leading term in $1/u$ expansion of $1/R(u)$ according to Eq. (5.310) is $-2/(g^2u^2)$. Therefore, the coefficient at $1/u$ in Eq. (5.311) vanishes and that at $1/u^2$ is $-2/g^2$. This yields

$$\begin{aligned}\sum_k \frac{\Delta_0}{F_k\Omega_k^2} &= \frac{\alpha_k}{\alpha_k^2+\beta_k^2}, \\ \sum_k \frac{x_k-\mu}{F_k\Omega_k^2} &= \frac{g^2}{2} - \frac{\beta_k}{\alpha_k^2+\beta_k^2}.\end{aligned} \tag{5.314}$$

Gap and chemical potential equations (5.18) and (5.20) in the notation of Sect. 5.5.2 read

$$\begin{aligned}\frac{\omega-2\mu}{g^2} &= \sum_k \frac{N_k}{2E(\varepsilon_k)}, \\ 2n &= \frac{2\Delta_0^2}{g^2} + \sum_k N_k\left(1 - \frac{\varepsilon_k-\mu}{E(\varepsilon_k)}\right).\end{aligned} \tag{5.315}$$

Differentiation of these equations with respect to ω obtains $\delta\mu/\delta\omega$ and $\delta\Delta_0/\delta\omega$ and comparison of the resulting quantities with the right hand side of Eq. (5.314) proves Eq. (5.225).

Another identity used in Sect. 5.5.2 derives by noting that according to Eq. (5.310) $1/R(\varepsilon_k) = 0$. Setting $u = \varepsilon_k$ in Eq. (5.311), we obtain after some algebra

$$\sum_j \frac{1}{(\varepsilon_k - x_m)F_m\Omega_m^2} = \frac{\alpha_k(\varepsilon_k-\mu) - \Delta_0\beta_k}{2\Delta_0(\alpha_k^2+\beta_k^2)\left[E(\varepsilon_k)\right]^2}. \tag{5.316}$$

6 Dynamical vanishing of the order parameter in a fermionic condensate by Yuzbashyan, Dzero

Abstract

We analyze the dynamics of a condensate of ultra-cold atomic fermions following an abrupt change of the pairing strength. At long times, the system goes to a non-stationary steady state, which we determine exactly. The superfluid order parameter asymptotes to a constant value. We show that the order parameter *vanishes* when the pairing strength is decreased below a certain critical value. In this case, the steady state of the system combines properties of normal and superfluid states – the gap and the condensate fraction vanish, while the superfluid density is nonzero.

Recently, several remarkable experiments have demonstrated Cooper pairing in cold atomic Fermi gases[[1]–[4]]. Key signatures of a paired state – condensation of Cooper pairs[1, 2] and the pairing gap[4] have been observed. In addition, trapped gases provide a unique tool to explore aspects of fermion pairing normally inaccessible in superconductors. One of the most exciting prospects is a study of far from equilibrium coherent dynamics of fermionic condensates[[15]–[9]], made possible due to the precise experimental control over interactions between atoms [10, 11]. The dynamics can be initiated by quickly changing the pairing strength with external magnetic field.

Here, we determine the time evolution of a fermionic condensate in response to a sudden change of interaction strength. Initially, the gas is in equilibrium at zero temperature on the BCS side of the Feshbach resonance ((???? what is it???)) with a coupling constant $g_i > 0$. At $t = 0$ the coupling is suddenly changed to a smaller value $g_f > 0$ on the same side of the resonance, $g_i \to g_f$, Fig. 6.1 (inset). Ground states of the system at the old, g_i, and new, g_f, values of the coupling are characterized by corresponding BCS gaps, Δ_i and Δ_f, respectively. We consider the case $\Delta_i \geq \Delta_f$. It has been shown previously that following the change of coupling, the time-dependent order parameter $\Delta(t)$ asymptotes to a constant value[9], $|\Delta(t)| \to \Delta_\infty$ on a timescale $\tau_\Delta = 1/\Delta_i$. Here we evaluate Δ_∞ in terms of Δ_i and Δ_f.

We show that when the coupling is decreased below a certain critical value, Δ_∞ *vanishes*, Fig. 6.1. On a τ_Δ timescale the system goes to a steady *non-stationary* state that combines properties of normal and superfluid states in a peculiar way. For example, the gap vanishes, while the superfluid density remains finite. Provided the system is continuously cooled, the BCS ground state with a gap Δ_f is reached on the energy relaxation timescale τ_ϵ, which is typically much larger than τ_Δ. Experimental signatures of the novel state include the absence of the gap in rf absorbtion spectrum and zero condensate fraction after a fast projection onto the Bose-Einstein Condensation (BEC) side (see below).

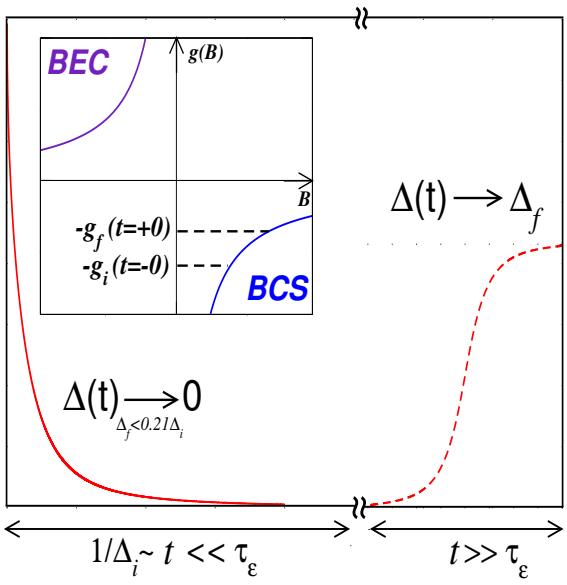


Figure 6.1: Time evolution of the BCS order parameter $\Delta(t)$ following an abrupt change of the coupling constant. The coupling is changed by varying the magnetic field on the BCS side of the Feshbach resonance (inset). The order parameter exponentially decays to zero (solid line) at times $t \sim 1/\Delta_i$ and the system goes into a *gapless* steady state. If the system is continuously cooled, the order parameter recovers to its equilibrium value Δ_f (dashed) at times longer than the quasiparticle relaxation time τ_ϵ.

At times $t \ll \tau_\epsilon$, dynamics of the condensate in the weak coupling regime can be described by the BCS model. Here we are interested in the thermodynamic limit, in which case one can use the BCS mean-field approach[23] ((??? what Anderson's work has to do with it???)). Using Anderson's pseudospin representation[23], one can describe the mean-field evolution by a *classical* spin Hamiltonian[23, 15, 6]

$$H = \sum_j 2\epsilon_j s_j^z - g \sum_{j,k} s_j^+ s_k^-, \tag{6.1}$$

where ϵ_j are single-particle energies relative to the Fermi level and $s_j^\pm = s_j^x \pm i s_j^y$. The summation in Eq. (6.1) is over $|\epsilon_j| < E_F$, where E_F is the Fermi energy. Dynamical variables $\mathbf{s}_j$ are vectors of fixed length, $|\mathbf{s}_j| = 1/2$. The BCS order parameter is $\Delta(t) = \Delta_x - i\Delta_y = g\sum_j s_j^-$. Equations of motion for classical spins $\mathbf{s}_j$ are

$$\dot{\mathbf{s}}_j = \mathbf{b}_j \times \mathbf{s}_j, \quad \mathbf{b}_j = (-2\Delta_x, -2\Delta_y, 2\epsilon_j)\,. \tag{6.2}$$

((??? so, to understand it, I need to understand Anderson's theory))
Components of spins are related to Bogoliubov amplitudes u_j and v_j

$$2s_j^z = |v_j|^2 - |u_j|^2, \;\; s_j^- = \bar{u}_j v_j, \tag{6.3}$$

At $t = 0$ the system is in the ground state with gap Δ_i. The ground state is obtained by aligning each spin $\mathbf{s}_j$ antiparallel to its "magnetic" field $\mathbf{b}_j$ [23] in order to minimize the total energy (6.1) for coupling constant $g = g_i$

$$s_j^x(0) = \frac{\Delta_i}{2\sqrt{\epsilon_j^2 + \Delta_i^2}}, \;\; s_j^z(0) = -\frac{\epsilon_j}{2\sqrt{\epsilon_j^2 + \Delta_i^2}}, \tag{6.4}$$

and $s_j^y(t=0)=0$.

At $t=0$ the coupling is changed, $g_i \to g_f$, and the initial spin configuration (6.4) is no longer an equilibrium for $t>0$. To determine the time evolution of the system, one has to solve Eqs. (8.3) with initial conditions (6.4).

We start with a linear analysis. Solving Eqs. (8.3) (with $g=g_f$) linearized around the spin configuration (6.4), we obtain up to terms of order $\delta\Delta/\Delta_f$

$$\Delta(t)=\Delta_f-8\delta\Delta\int_0^\infty d\epsilon\frac{\cos\omega(\epsilon)t}{\omega(\epsilon)\left[\pi^2+h^2(\epsilon)\right]}, \tag{6.5}$$

where $\delta\Delta=\Delta_f-\Delta_i$, $\omega(\epsilon)=2\sqrt{\epsilon^2+\Delta_f^2}$, and $h(\epsilon)=\sinh^{-1}(\epsilon/\Delta_f)$. In Eq. (6.5), besides the continuum limit, we took the weak coupling limit $E_F/\Delta_i\to\infty$.

The long time behavior of the order parameter in the linear approximation is obtained from Eq. (6.5) by stationary phase method (see also Ref. [24]),

$$\Delta(t)=\Delta_f-\frac{2\delta\Delta}{\pi^{3/2}\sqrt{\Delta_f t}}\cos\left(2\Delta_f t+\frac{\pi}{4}\right), \tag{6.6}$$

At times $t\gg\tau_\Delta$ the gap approaches a constant value $\Delta_\infty=\Delta_f$ to order $\delta\Delta/\Delta_f$.

Even though the gap is constant, the state of the system is non-stationary[17]. According to Eq. (8.3), at large times each spin $\mathbf{s}_j\equiv\mathbf{s}(\epsilon_j)$ precesses in its own constant field $\mathbf{b}_j=(-2\Delta_\infty,0,2\epsilon_j)$. For example, for the x-component of spins we derive from the linearized equations of motion,

$$\begin{aligned}s_x(\epsilon)=&\frac{\Delta_f}{2\sqrt{\epsilon^2+{\Delta_f}^2}}\\&-\frac{\delta\Delta\epsilon}{(\epsilon^2+\Delta_f^2)\sqrt{\pi^2+h^2(\epsilon)}}\cos\left[\omega(\epsilon)t+\phi(\epsilon)\right],\end{aligned} \tag{6.7}$$

However, the gap $\Delta(t)=g\sum_j s_j^x(t)$ contains oscillations with many different frequencies. At large times they go out of phase and cancel out in the continuum limit.

In the non-linear case it can be shown that the gap decays to a constant Δ_∞ by a similar mechanism[9]. To determine Δ_∞, we use the exact solution for the dynamics of the BCS model[6]. Consider the following vector function of an auxiliary parameter u: $\mathbf{L}(u)=-\hat{\mathbf{z}}/g+\sum_j\mathbf{s}_j/(u-\epsilon_j)$, where $\hat{\mathbf{z}}$ is a unit vector along the z-axis. Using Eq. (8.3), we obtain $d\mathbf{L}^2(u)/dt=0$, i.e. $\mathbf{L}^2(u)$ is conserved for any u.

To determine the steady state gap Δ_∞, we evaluate $\mathbf{L}^2(u)$ at $t=0$ for the initial spin configuration (6.4) and at $t\gg\tau_\Delta$, when each spin $\mathbf{s}(\epsilon)$ precesses in a constant field. Matching the two expressions, we derive for $\Delta_f\le\Delta_i$

$$\Delta_f=\Delta_i\exp(-\kappa\tan\kappa/2),\qquad \Delta_\infty=\Delta_i\cos\kappa, \tag{6.8}$$

where $0\le\kappa\le\pi/2$. This equation determines Δ_∞ in terms of Δ_i and Δ_f, see Fig. 6.2.

We make several observations. The steady state gap reaches its maximum $\Delta_\infty=\Delta_f$ at $\Delta_f/\Delta_i=1$. Otherwise, $\Delta_\infty<\Delta_f$. Expanding around the maximum, we find $\Delta_\infty=\Delta_f-(\delta\Delta)^2/6\Delta_f$ up to terms of higher order in $\delta\Delta/\Delta_f$. The linear term vanishes in agreement with Eq. (6.6).

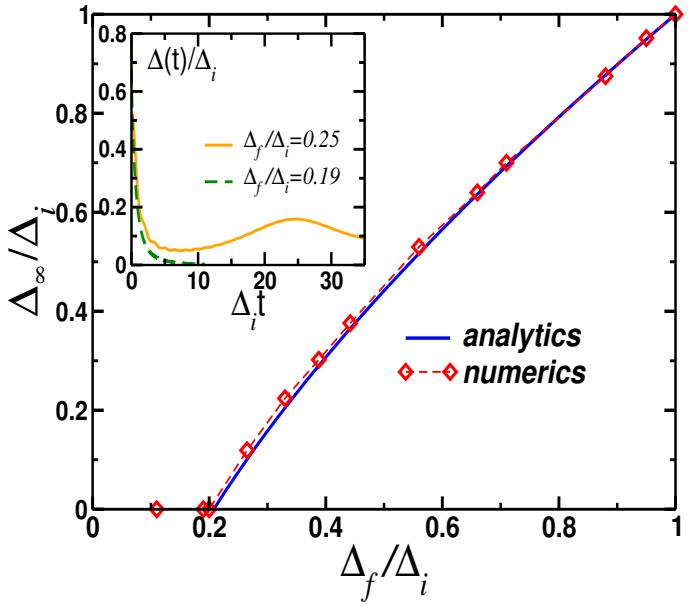


Figure 6.2: After a sudden change of the BCS coupling constant, the order parameter $\Delta(t)$ (inset) saturates to a constant value Δ_∞. The plot shows the steady state gap Δ_∞ in units of Δ_i as a function of the ratio Δ_f/Δ_i. The exact result given by Eq. (6.8) is compared to numerical solution of Eq. (8.3). Note that $\Delta_\infty = 0$ for $\Delta_f \leq 0.2\Delta_i$.

Most interestingly, we see from Eq. (6.8) that the order parameter vanishes in the steady state, $\Delta_\infty = 0$, when $\kappa = \pi/2$, i.e. for $(\Delta_f/\Delta_i)_c = e^{-\pi/2} \approx 0.21$. If Δ_f/Δ_i is below this critical ratio, Eq. (6.8) has no solutions – the system goes into a gapless steady state, $\Delta_\infty = 0$, for $\Delta_f \leq 0.21\Delta_i$. We also note from Eq. (6.8) and Fig. 6.2 that Δ_∞ has a cusp at $\Delta_f/\Delta_i = e^{-\pi/2}$, i.e. the transition to the gapless state is second order.

To gain further insight into properties of the gapless state, we need to know the spin configuration in this state. At large times spin $\mathbf{s}(\epsilon)$ rotates in a constant field $\mathbf{b}(\epsilon) = -2\Delta_\infty \hat{\mathbf{x}} + 2\epsilon\hat{\mathbf{z}}$, where $\hat{\mathbf{x}}$ and $\hat{\mathbf{z}}$ are unit vectors along the x and z axes, respectively. In the gapless case, $\mathbf{b}(\epsilon) = 2\epsilon\hat{\mathbf{z}}$. The spin configuration can be characterized by the angle $\theta(\epsilon)$ between $\mathbf{s}(\epsilon)$ and $-\mathbf{b}(\epsilon)$. This angle can be determined by matching the conserved quantity $\mathbf{L}^2(u)$ at $t = 0$ and $t \gg \tau_\Delta$,

$$\sin^2\theta(\epsilon) = \frac{G(\epsilon)}{2\pi^2} - \sqrt{\frac{G^2(\epsilon)}{4\pi^4} - \frac{4\beta^2\Delta_i^2}{\pi^2(\epsilon^2+\Delta_i^2)}}\ , \tag{6.9}$$

where $\beta = \ln(\Delta_i/\Delta_f)$ and

$$\begin{aligned} G(\epsilon) =& \pi^2 + 4\left[\sinh^{-1}(\epsilon/\Delta_i)\right]^2 \\ &+ \frac{8\beta\epsilon}{\sqrt{\epsilon^2+\Delta_i^2}}\sinh^{-1}(\epsilon/\Delta_i) + 4\beta^2 \end{aligned} \tag{6.10}$$

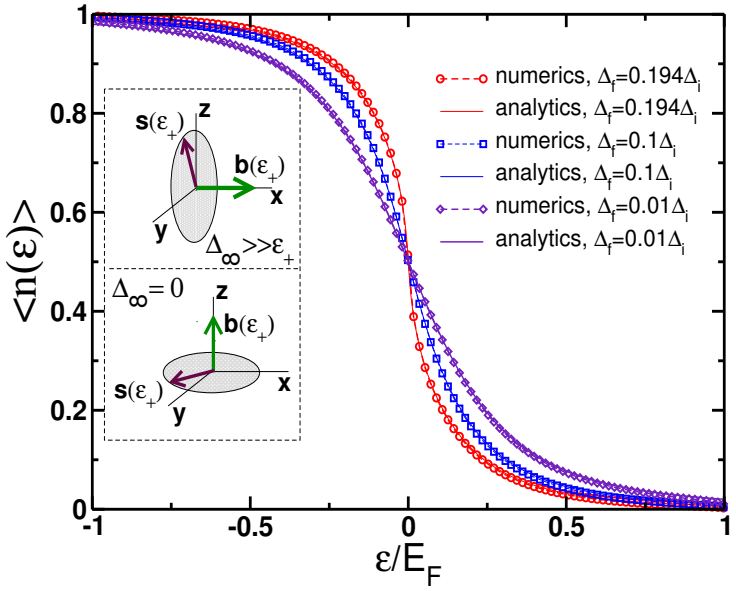


Figure 6.3: Plot of the average occupation number $\langle n(\epsilon)\rangle$ as a function of energy in the gapless state for various values of $\Delta_f/\Delta_i < e^{-\pi/2}$. The exact result given by Eq. (6.9) is compared to numerical solution of Eq. (8.3). Note that the distribution function around the Fermi level is smeared over a width $\delta\epsilon \propto \Delta_i$. The inset shows a spin $\mathbf{s}(\epsilon_+)$ at energy $0 < \epsilon_+ \ll \Delta_i$ just above and below the critical point.

Note from Eq. (8.3) that in the steady state the component of spin $\mathbf{s}(\epsilon)$ along the field, $s_\parallel(\epsilon) = -\cos\theta(\epsilon)/2$, is constant, while the one perpendicular to the field, $|\mathbf{s}_\perp| = \sin\theta(\epsilon)/2$ rotates with a frequency $\omega(\epsilon) = 2\sqrt{\epsilon^2+\Delta_\infty^2}$. The approach to the steady state can be studied by linearizing Eq. (8.3) around this state. In particular, we obtain the asymptotic behavior of $\Delta(t)$

$$\frac{\Delta(t)}{\Delta_\infty} = 1 + a\frac{\cos(2\Delta_\infty t + \pi/4)}{\sqrt{\Delta_\infty t}}, \quad \frac{\Delta_f}{\Delta_i} > e^{-\pi/2} \tag{6.11}$$

$$\frac{\Delta(t)}{\Delta_i} = A(t)e^{-2\alpha\Delta_i t} + B(t)e^{-2\Delta_i t}, \quad \frac{\Delta_f}{\Delta_i} < e^{-\pi/2} \tag{6.12}$$

Here $\alpha = -\cos p$ and $\pi/2 \le p \le \pi$ is the solution of $p = \ln(\Delta_i/\Delta_f)\cot(p/2)$. The parameter α has a property $\alpha \to 0$ when $\Delta_f/\Delta_i \to e^{-\pi/2}$ and $\alpha \to 1$ when $\Delta_f/\Delta_i \to 0$. The coefficient a in Eq. (8.1) is time-independent, $A(t)$ and $B(t)$ in Eq. (6.12) are decaying power laws, $A(t), B(t) \propto 1/t^\nu$ with $1/2 \le \nu \le 2$.

We conclude that the decay law of $\Delta(t)$ changes from power law to exponential as we cross the critical point. Above the critical point spins rotate with frequencies $\omega(\epsilon) = 2\sqrt{\epsilon^2+\Delta_\infty^2}$. The inverse square root decay and oscillations with frequency $2\Delta_\infty$ in Eq. (8.1) are due to the square root singularity in the spectral density $d\epsilon/d\omega \propto \omega/\sqrt{\omega^2-4\Delta_\infty^2}$, cf. Eqs. (6.5,6.6). Below the critical point Δ_∞ vanishes, $\omega(\epsilon) = 2\epsilon$, and the square root anomaly disappears.

What happens to the spin configuration as Δ_f/Δ_i is varied across the critical point? Consider a spin at energy $\epsilon_+ \ll \Delta_i$ just above the Fermi energy. Using Eq. (6.9), we obtain $\sin\theta(\epsilon_+) \approx \sin\theta(0) = 2\ln(\Delta_i/\Delta_f)/\pi$ for $\Delta_f > e^{-\pi/2}\Delta_i$ and $\sin\theta(0) = 1$ otherwise. The field $\mathbf{b}(\epsilon_+) = -2\Delta_\infty\hat{\mathbf{x}} + 2\epsilon_+\hat{\mathbf{z}}$ is along the x axis above the critical point ($\Delta_\infty \gg \epsilon_+$) and along the z axis below ($\Delta_\infty = 0$). At $\Delta_i = \Delta_f$ we have $\sin\theta(0) = 0$, i.e. the spin is parallel to the x axis. As Δ_f/Δ_i decreases, the x component of the spin also decreases until it vanishes at the critical point $\Delta_f = e^{-\pi/2}\Delta_i$. Just above it the spin lies in the yz plane and rotates around the x axis. Below the critical point it rotates in the xy plane around the z axis (Fig. 6.3).

In the gapless steady state each spin rotates around the z axis. Its z component is time-independent, $s_z(\epsilon) = -\cos\theta(\epsilon)/2$. It is related to the average occupation number per fermion species $\langle\hat{n}(\epsilon)\rangle$ at energy ϵ as $\langle\hat{n}(\epsilon)\rangle = s_z(\epsilon) + 1/2$ [23], i.e. $\langle\hat{n}(\epsilon)\rangle = (1 - \cos\theta(\epsilon))/2$. The distribution function $\langle\hat{n}(\epsilon)\rangle$ is smeared near the Fermi energy over a width $\delta\epsilon \propto \Delta_i$ (Fig. 6.3). Note that in this respect the gapless state is similar to the BCS ground state – the smearing over a width $\delta\epsilon \propto \Delta_i$ due to interactions is also present in the ground state distribution (6.4). In the normal state $s_z(\epsilon) = -\mathrm{sgn}\,\epsilon/2$ and $\langle\hat{n}(\epsilon)\rangle = \Theta(-\epsilon)$.

Given relation (6.3), one can reconstruct the time-dependent condensate wave function, and evaluate normal and anomalous correlation functions, e.g.

$$\langle\hat{c}_{\epsilon\sigma}(t)\hat{c}^\dagger_{\epsilon\sigma}(t')\rangle = e^{i\epsilon(t'-t)}\cos^2\tfrac{\theta(\epsilon)}{2} \tag{6.13}$$

$$\langle\hat{c}^\dagger_{\epsilon\uparrow}(t)\hat{c}^\dagger_{\epsilon\downarrow}(t')\rangle = e^{i\epsilon(t'+t)}\cos\tfrac{\theta(\epsilon)}{2}\sin\tfrac{\theta(\epsilon)}{2} \tag{6.14}$$

where $\hat{c}_{\epsilon\sigma}$ ($\hat{c}^\dagger_{\epsilon\sigma}$) annihilates (creates) a fermion of one of the two species $\sigma =\uparrow,\downarrow$ on energy level ϵ. Note that even though Δ_∞ vanishes, anomalous averages do not.

Next, we determine the superfluid density n_s in the gapless state. Consider a degenerate Fermi gas in an axially symmetric trap slowly rotating around the symmetry axis. The density n_s of the superfluid component can be defined as the rigidity of the superfluid with respect to an infinitesimal twist in the boundary conditions[14], $\hat{\psi}_\sigma(\mathbf{r}) \to e^{-i\alpha\phi}\hat{\psi}_\sigma(\mathbf{r})$, where ϕ is the azimuthal angle with respect to the symmetry axis, $\hat{\psi}_\sigma(\mathbf{r}) = \sum_j \hat{c}_{j\sigma}\varphi_j(\mathbf{r})$, and $\varphi_j(\mathbf{r})$ are the single particle wave functions. The twist generates a term $-\alpha\hat{J}$ in the Hamiltonian, where $\hat{J}$ is the current operator. The resulting supercurrent $J_s = n_s\alpha/m$ can be expressed in terms of correlation functions (6.13,6.14) using the standard linear response theory. We find $n_s = n/2$, where n is the particle density in the normal state. A similar calculation for nonzero Δ_∞ yields $n_s = n$ – the superfluid density in the gapped steady state is the same as in the BCS ground state. Since n_s is the second derivative of the free energy with respect to α, the jump from n to $n/2$ at the critical point agrees with the second order character of the transition. The reduction in n_s in the state with zero Δ_∞ is consistent with vanishing of the gap in this state[15].

We see that the superfluid density is finite in the gapless steady state. This reflects the existence of pair correlations (6.14) between fermions, a property that in equilibrium has been directly linked to nonzero n_s [16]. This situation is similar to the phenomenon of gapless superconductivity in metals[17], where the superconducting state is also characterized by non-vanishing anomalous Green's functions and zero spectral gap. A gapless state in superconductors is usually a consequence of strong perturbations - as the perturbation is increased, the superconducting metal first goes into a gapless state with finite n_s before it becomes normal.

A crude qualitative understanding of the dynamical transition to the gapless steady state can be derived from the following thermodynamic argument. After the change of coupling the initial state (6.4) has energy $\mathcal{E}(\Delta_f, \Delta_i) > 0$ relative to the ground state with gap Δ_f. In thermal equilibrium the system would have the same energy at a certain temperature $T_0(\Delta_f, \Delta_i)$. Let us keep Δ_i fixed and vary Δ_f. At $\Delta_f = \Delta_i$, $T_0 = 0$, while the critical temperature $T_c \approx 0.57\Delta_f > 0$. As Δ_f increases both T_0 and T_c grow, but T_c grows faster and T_0 never catches up with it. On the other hand, when Δ_f decreases, T_c also decreases, while T_0 grows. Evaluating $T_0(\Delta_f, \Delta_i)$, to the first order in the coupling constant we find that $T_0 \geq T_c$ for $\Delta_f/\Delta_i \leq 0.52 + 0.17\lambda$ and $T_0 < T_c$ otherwise. Here $\lambda = g/d$ is the dimensionless BCS coupling constant and $d = \langle\epsilon_{j+1} - \epsilon_j\rangle$ is the mean level spacing. We see that decreasing the coupling beyond a certain value provides enough energy for the transition to the normal state to occur in thermal equilibrium.

Let us discuss experimental manifestations of the dynamical transition to the gapless steady state. After the initial sweep ($g_i \to g_f$) on the BCS side of the resonance such that $\Delta_f/\Delta_i < e^{-\pi/2}$, the gapless state is reached on a timescale $\tau_\Delta = 1/\Delta_i$. The pairing gap measured in Ref. [4] is the energy cost ΔE of breaking a Cooper pair. This corresponds[23] to removing the

spin closest to the Fermi level in (6.1). The minimum energy cost is $\Delta E = \min|\mathbf{b}(\epsilon)\cdot\mathbf{s}(\epsilon)| = \Delta_\infty \cos\theta(0)$. Using Eq. (6.9), we obtain $\Delta E = \Delta_\infty\sqrt{1-4\ln^2(\Delta_i/\Delta_f)/\pi^2}$. In the steady state, $\Delta E = 0$, i.e. no gap in the rf absorbtion spectrum will be observed. Molecular condensate fraction [1, 2] *vanishes* in the gapless state, since $N_{k=0}/N \propto \Delta_\infty^2$ [18].

In conclusion, we determined the dynamics of the paired state of cold atomic fermions following an abrupt lowering of the pairing strength, $g_i \to g_f$. On a short $1/\Delta_i$ timescale, where Δ_i is the equilibrium gap for the initial coupling g_i, the system goes to a non-stationary steady state with a constant gap Δ_∞ and a distribution function given by Eqs. (6.8,6.9). When the coupling is reduced so that Δ_f/Δ_i is smaller than the critical value of $e^{-\pi/2}$, the steady state gap vanishes. The decay law of the time-dependent order parameter $\Delta(t)$ changes from power law to exponential as Δ_f/Δ_i goes through the critical point, Eqs. (8.1,6.12). The gapless state combines features of normal and superfluid states. In particular, the gap and the condensate fraction vanish, while the superfluid density is nonzero.

7 Onset of superconductivity in a voltage-biased NSN microbridge by Serbyn, Skvortsov

Abstract

We study the stability of the normal state in a mesoscopic NSN junction biased by a constant voltage V with respect to the formation of the superconducting order.

Using the linearized time-dependent Ginzburg-Landau equation, we obtain the temperature dependence of the instability line, $V_{\rm inst}(T)$, where nucleation of superconductivity takes place.

For sufficiently low biases, a stationary symmetric superconducting state emerges below the instability line.

For higher biases, the normal phase is destroyed by the formation of a non-stationary bimodal state with two superconducting nuclei localized near the opposite terminals.

(bimodal state ???)

The low-temperature and large-voltage behavior of the instability line is highly sensitive to the details of the inelastic relaxation mechanism in the wire.

Therefore, experimental studies of $V_{\rm inst}(T)$ in NSN junctions may be used as an effective tool to access parameters of the inelastic relaxation in the normal state.

Nonequilibrium superconductivity has being attracting significant experimental and theoretical attention over decades [Kopnin(2001), Gray(1981), Gulian and Zharkov(1999)], ranging from vortex dynamics [Langenberg and Larkin(1986)] to the physics of the resistive state in current-carrying superconductors [Vodolazov *et al.*(2003), Xiong *et al.*(1997), Rogachev *et al.*(2006), Li *et al.*(2011), Astafiev *et al.*(2012)].

It was recognized long ago [Ivlev and Kopnin(1984)] that a superconducting wire typically has a hysteretic current voltage characteristic specified by several "critical" currents.

(seems that I need to read their paper!)

In an up-sweep, a current exceeding the thermodynamic depairing current, $I_c(T)$, does not completely destroy superconductivity but drives the wire into a nonstationary resistive state [Meyer and Minnigerode(1972)], with the excess phase winding relaxing through the formation of phase slips [Langer and Ambegaokar(1967), McCumber and Halperin(1970)].

(todo: study ones phase slips..)

The resistive state continues until $I_2(T) > I_c(T)$, when the wire eventually becomes normal. In the down-sweep of the current voltage characteristic, the wire remains normal until $I_1(T) < I_2(T)$ when an emerging order parameter leads to the reduction of the wire resistance.

The theoretical description of a nonequilibrium superconducting state is a sophisticated problem, requiring a simultaneous account of the nonlinear order parameter dynamics and quasiparticle relaxation under nonstationary conditions. The resulting set of equations is extremely complicated [Langenberg and Larkin(1986), Kopnin(2001)] and can be treated only numerically [Keizer *et al.*(2006), Vercruyssen *et al.*(2012), Snyman and Nazarov(2009)] (even then the stationarity of the superconducting state is often assumed [Keizer *et al.*(2006), Vercruyssen *et al.*(2012)]).

(??????)

A more intuitive but somewhat oversimplified approach is based on the a time-dependent Ginzburg-Landau (TDGL) equation for the order parameter field $\Delta(\mathbf{r}, t)$.

The TDGL approach which is generally inapplicable in the gapped phase [Gorkov and Eliashberg(1968)], can be justified only in a very narrow vicinity of the critical temperature, T_c, provided that the electron-phonon (e-ph) interaction is sufficiently strong to thermalize quasiparticles [Kramer and Watts-Tobin(1978)].

(I'll read it later)

These generalized TDGL equations are analyzed numerically in Refs. [Vodolazov *et al.*(2003), Michotte *et al.*(2004), Vodolazov(2007), Elmurodov *et al.*(2008)].

(I'll read them later)

While the applicability of the TDGL equation in the superconducting region is a controversal issue, its linearized form can be safely employed to find the line $I_{\rm inst}(T)$ of the absolute instability of the normal state with respect to the appearance of an infinitesimally small order parameter $\Delta(\mathbf{r}, t)$ [Ivlev and Kopnin(1984), Rubinstein *et al.*(2007), Chtchelkatchev and Vinokur(2009)].

(I'll read them later)

If the transition to the superconducting state is second order, then $I_1(T)$ coincides with $I_{\rm inst}(T)$. Otherwise the actual instability takes place at a larger $I_1(T) > I_{\rm inst}(T)$. In both cases, $I_{\rm inst}(T)$ gives the lower bound for $I_1(T)$.

Previous results [Ivlev and Kopnin(1984), Rubinstein *et al.*(2007)] for the instability line of a superconducting wire connected to normal reservoirs (NSN microbridge) have been obtained in the limit of quasi-equilibrium, when strong e-ph relaxation renders the distribution function locally thermal.

This approximation breaks down for low-T_c superconducting wires shorter than the e-ph relaxation length, $l_{e\text{-ph}}(T_c)$ (e.g., for aluminium, $l_{e\text{-ph}}(T_c) \approx 40$ μm [Giazotto *et al.*(2006)]).

(???!!! why??? so length of a wire plays a role!??)

Such systems have recently been experimentally studied in Refs. [Vercruyssen *et al.*(2012)] (Al) and [Chen *et al.*(2009), Tian *et al.*(2005)] (Zn; reservoirs may be driven normal by a magnetic field).

It was found that for sufficiently large biases superconductivity arises near the terminals through a second-order phase transition, with $I_1(T) = I_{\rm inst}(T)$ [Vercruyssen *et al.*(2012)].

(todo: check it)

In this Letter we study the normal state instability line in an NSN microbridge biased by a DC voltage V, relaxing the assumption of strong thermalization. For small biases, $eV \ll T_c$, the instability line is universal and we reproduce the results of Refs. [Ivlev and Kopnin(1984), Rubinstein *et al.*(2007)].

(check, how exactly??)

The universality breaks down for larger biases, where we obtain $V_{\rm inst}(T)$ *as a functional of the normal state distribution function* and analyze it for various types of inelastic interactions.

We model the NSN microbridge as a diffusive wire of length L coupled at $x = \pm L/2$ to large normal reservoirs via transparent interfaces. The terminals are biased by a constant voltage V. The wire length, L, is assumed to be larger than the zero-temperature coherence length, $\xi_0 = \sqrt{\pi D/8T_{c0}}$, where D is diffusion coefficient, and T_{c0} is the critical temperature of the infinite wire.

(why??)

The equilibrium critical temperature, $T_c = T_{c0}(1 - \pi^2\xi_0^2/L^2)$, is smaller than T_{c0} due to the finite size effect [Boogaard *et al.*(2004)].

(this is interesting!!! I'll read about it, never have taken it into account)

In what follows we neglect superconducting fluctuations [Larkin and Varlamov(2002)].

General stability criterion.

—

An arbitrary nonequilibrium normal state becomes absolutely unstable with respect to superconducting fluctuations if an infinitesimally small order parameter, $\Delta(\mathbf{r}, t)$, does not decay with time but evolves to finite values.

(trivial statement?)

Evolution of $\Delta(\mathbf{r}, t)$ is described by the TDGL equation, and it suffices to keep only the linear term to judge its stability.

In dirty superconductors, the linearized TDGL equation can be readily derived from the Keldysh σ-model formalism [Levchenko and Kamenev(2007), Feigel'man *et al.*(2000), Kamenev(2011)] or dynamic Usadel equations [Langenberg and Larkin(1986)] by expanding in Δ.

(I have no idea, how to do it?)

It takes the form $(L_R)^{-1} * \Delta = 0$, where $(L^R)^{-1}$ is the inverse fluctuation propagator, and convolution in time and space indices is implied. In the frequency representation, $(L^R_\omega)^{-1}$ is an integral operator in real space specified by the kernel

$$(L^R_\omega)^{-1}_{\mathbf{r},\mathbf{r}'} = -\frac{\delta_{\mathbf{r},\mathbf{r}'}}{\lambda} + i\int_{-\omega_D}^{\omega_D} dE\, F(E,\mathbf{r})\, C_{\omega-2E}(\mathbf{r},\mathbf{r}'), \tag{7.1}$$

where λ is the dimensionless BCS interaction constant, ω_D is the Debye frequency, and C stands for the retarded Cooperon, $C_\varepsilon(\mathbf{r},\mathbf{r}') = \langle\mathbf{r}|(-D\nabla^2 - i\varepsilon)^{-1}|\mathbf{r}'\rangle$, vanishing at the boundary with the terminals.

(a complicated formula...)

The operator (7.1) is a functional of the normal-state nonequilibrium electron distribution function, $F(E,\mathbf{r})$, which contains information about the mechanism for inelastic relaxation in the wire.

(so, in which limit are we working, such that we have kinetics??? and we don't consider Cooper pairs separately at all, only allelectrons and phonons)

The distribution function should be determined from the kinetic equation

$$D\nabla^2 F(E,\mathbf{r}) + \mathcal{I}^{e\text{-}e}[F] + \mathcal{I}^{e\text{-ph}}[F] = 0, \tag{7.2}$$

with $\mathcal{I}^{e\text{-}e}[F]$ and $\mathcal{I}^{e\text{-ph}}[F]$ being the electron-electron (e-e) and e-ph collision integrals, respectively.

(and form of them is unknown...)

The corresponding energy relaxation lengths, $l_{e\text{-}e}(T) \propto T^{-1/4}$ and $l_{e\text{-ph}}(T) \propto T^{-3/2}$, behave as a negative power of the temperature T in quasi-equilibrium [Giazotto *et al.*(2006)].

(to understand it, read this article....)

In the absence of inelastic collisions, the kinetic equation (7.2) is solved by the "two-step" function [Nagaev(1995), Pothier *et al.*(1997)]:

$$F(E,x) = (1/2 - x/L)F_L(E) + (1/2 + x/L)F_R(E). \tag{7.3}$$

The distribution functions in the terminals, $F_{L,R}(E) = F_0(E \pm eV/2)$, are given by the equilibrium distribution function, $F_0(E) = \tanh(E/2T)$, shifted by $\pm eV/2$ ($e > 0$). In the opposite case of strong inelastic relaxation, the distribution function takes the form

$$F_{\text{in}}(E,x) = \tanh[(E - e\phi(x))/2T(x)], \tag{7.4}$$

where $\phi(x) = Vx/L$ is the potential in the normal state, and $T(x)$ is the effective temperature. For strong lattice thermalization ($l_{e\text{-ph}} \ll L \ll l_{e\text{-}e}$), $T(x) = T$. For the dominating e-e scattering ($l_{e\text{-}e} \ll L \ll l_{e\text{-ph}}$), $T^2(x) = T^2 + (3/4\pi^2)[1 - (2x/L)^2](eV)^2$ [Nagaev(1995)].

The order parameter evolution governed by the linearized TDGL operator (7.1) can be naturally described in terms of the eigenmodes $\Delta_k(\mathbf{r})e^{-i\omega_k t}$ annihilated by $(L^R_\omega)^{-1}$.

The normal state is stable provided $\operatorname{Im}\omega_k < 0$ for all eigenmodes. Below we analyze the spectrum of the operator (7.1) and determine the instability line in the coordinates T–V. In the general case, the spectrum can be obtained only numerically. Analytical considerations become possible when the operator (7.1) may be linearized in ω: $(L^R_\omega)^{-1} = i\tau\omega - \mathcal{H}$. The instability occurs when the real part of the lowest eigenvalue of the operator $\mathcal{H}$ turns to zero.

Weak-nonequilibrium regime.

—

In the limit of low biases, $eV \ll T_c$, the deviation from equilibrium is small everywhere in the wire and the distribution function acquires a universal form, $F(E,x) \approx F_0(E) - F_0'(E)\, e\phi(x)$, regardless of the relaxation mechanism. Then Eq. (7.1) takes the form

$$(L^R_\omega)^{-1} = i\pi\omega/8T - \ln(T/T_{c0}) - (\xi_0/L)^2\, \mathcal{H}_v,$$

with

$$\mathcal{H}_v = -\partial^2_{\tilde{x}} + 2iv\tilde{x}, \qquad \tilde{x} \in [-1/2, 1/2]. \tag{7.5}$$

The Hamiltonian $\mathcal{H}_v$ describes quantum-mechanical motion *in an imaginary electric field*, $v = eV/E_{\text{Th}}$, on the interval $\tilde{x} \equiv x/L \in [-1/2, 1/2]$, where $E_{\text{Th}} = D/L^2$ is the Thouless energy. Hard-wall boundary conditions, $\psi(\pm 1/2) = 0$, imposed on wave functions correspond to the complete suppression of superconductivity at the contacts with highly-conducting terminals due to the inverse proximity effect.

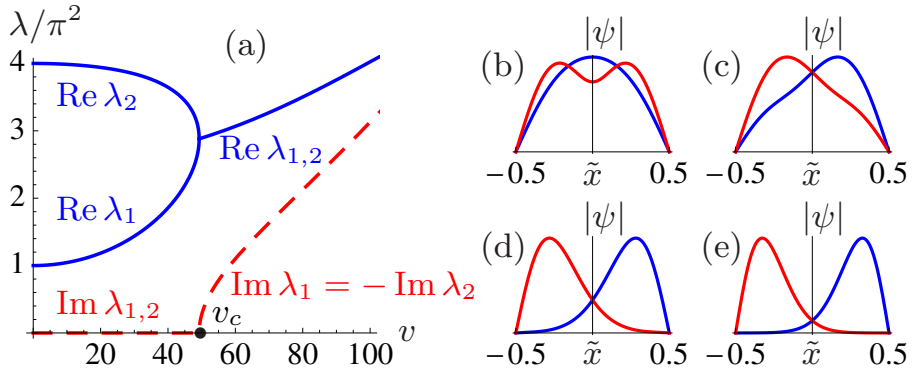


Figure 7.1: (Color online) (a) Real (solid blue line) and imaginary (dashed red line) parts of the lowest eigenvalues $\lambda_{1,2}(v)$ of the Hamiltonian (7.5). The spectrum is entirely real until $v = v_c \approx 49.25$. (b)–(e) Spatial dependence of the absolute values of the eigenfunctions, $|\psi_1(\tilde{x})|$ (blue) and $|\psi_2(\tilde{x})|$ (red), for $v = 0.8\,v_c$, $1.2\,v_c$, $5\,v_c$, and $10\,v_c$ respectively.

The Hamiltonian (7.5) has been recently analyzed in Ref. [Rubinstein *et al.*(2007)]. It belongs to a class of non-Hermitian Hamiltonians invariant under the combined action of the time-reversal, $\mathcal{T}$: $f(x) \mapsto f^*(x)$, and parity, $\mathcal{P}$: $f(x) \mapsto f(-x)$, transformations. The $\mathcal{PT}$-symmetry of the Hamiltonian (7.5) ensures that its eigenvalues $\lambda_n(v)$ are either real or form complex-conjugated pairs, providing a complex extension of the notion of Hermiticity [Bender and Boettcher(1998), Bender(2007)]. At $v = 0$, the spectrum is non-degenerate: $\lambda_n(0) = \pi^2 n^2$ ($n = 1, 2, \dots$). It evolves continuously with v and a nonzero $\mathrm{Im}\,\lambda(v)$ arises only when the two lowest eigenvalues, $\lambda_1(v)$ and $\lambda_2(v)$, coalesce [see Fig. 7.1 (a)]. This happens at $v = v_c \approx 49.25$ [Rubinstein *et al.*(2007)], indicating the transition to a complex-valued spectrum. For $v < v_c$, the ground state of (7.5) is $\mathcal{PT}$-symmetric, and hence $|\psi_1(\tilde{x})| = |\psi_1(-\tilde{x})|$. For $v > v_c$, the $\mathcal{PT}$-symmetry is spontaneously broken and there is a pair of states with the lowest $\mathrm{Re}\,\lambda(v)$: $\psi_L(\tilde{x}) = \psi_1(\tilde{x})$ and $\psi_R(\tilde{x}) = \psi_2(\tilde{x}) = \psi_1^*(-\tilde{x})$, shifted to the left (right) from the midpoint [see Fig. 7.1 (b)–(e)].

Spontaneous breaking of the $\mathcal{PT}$-symmetry associated with the spectral bifurcation at $v = v_c$ explains the appearance of asymmetric superconducting states observed in numerical simulations [Vodolazov and Peeters(2007)] and recent experiments [Vercruyssen *et al.*(2012)]. The normal-state instability line, $V_{\mathrm{inst}}(T)$, is specified implicitly by the relation

$$1 - T/T_{c0} = (\xi_0/L)^2\,\mathrm{Re}\,\lambda_1(eV_{\mathrm{inst}}(T)/E_{\mathrm{Th}}), \tag{7.6}$$

and exhibits a singular behavior at the critical bias V_* given by $eV_* = v_c E_{\mathrm{Th}} \approx 50 E_{\mathrm{Th}}$ (see inset in Fig. 7.2). The bifurcation of the instability line occurs at the temperature $T_* \approx T_{c0}(1 - 28.44\,\xi_0^2/L^2)$. For long wires ($L \gg \xi_0$), T_* is very close to T_c.

The time dependence of the emergent superconducting state is determined by $\mathrm{Im}\,\lambda_1(v)$. Below the bifurcation threshold, for $V_{\mathrm{inst}}(T) < V_*$, the system undergoes at $V = V_{\mathrm{inst}}(T)$ the transition to a *stationary* superconducting state, with the superconducting chemical potential being the half-sum of the chemical potentials in the terminals. This state is supercurrent-carrying, and can withstand a maximum phase winding of π achieved at the critical bias V_*. For larger voltages, $V_{\mathrm{inst}}(T) > V_*$, two modes, $\psi_L(x)$ and $\psi_R(x)$, nucleate simultaneously at $V_{\mathrm{inst}}(T)$. The resulting bimodal superconducting state is *non-stationary* since the left and right modes feel different electrochemical potentials and their phases rotate with opposite frequencies, $\Omega_{L,R}(V) = \mp E_{\mathrm{Th}}\,\mathrm{Im}\,\lambda_1(eV/T)$. This will result in the Josephson generation with the differential frequency $\Omega(V) = \Omega_R(V) - \Omega_L(V) \propto \sqrt{V - V_*}$ as $V_{\mathrm{inst}}(T) \to V_*$. Though these supercurrent oscillations are locked to the superconducting part they may excite oscillations of the normal current in the whole circuit. Thus the dc biased NSN microbridge may act as a voltage-tunable generator of an ac current, with the maximal amplitude of oscillations expected in the *coherent*

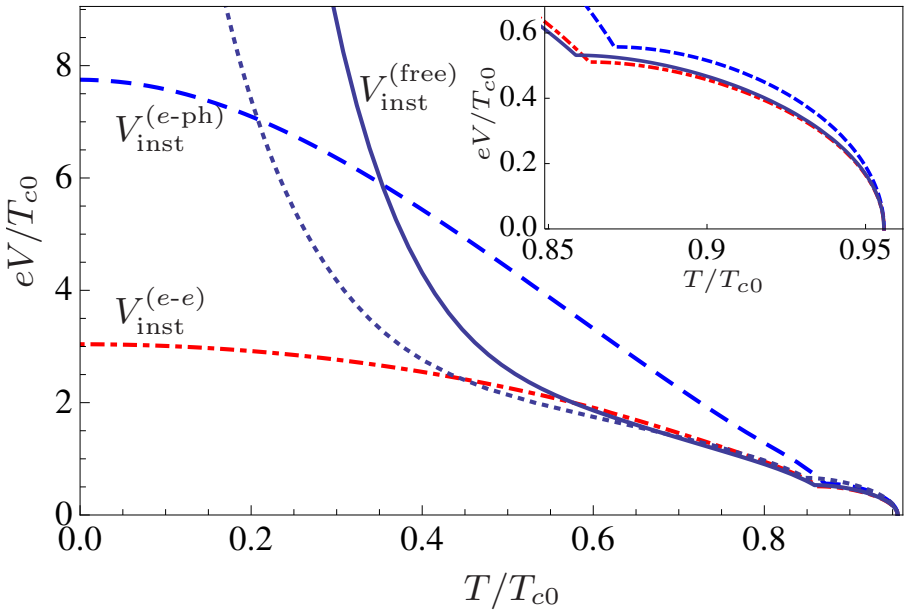


Figure 7.2: (Color online) Instability voltage as a function of temperature, $V_{\rm inst}(T)$, obtained numerically for a wire of length $L = 15\xi_0$ for three limiting types of the distribution function: without inelastic relaxation (solid blue line), and with dominant e-e (dot-dashed line) or e-ph (dashed line) relaxation. Dotted curve illustrates the suppression of $V_{\rm inst}^{(\rm free)}(T)$ by a finite terminal resistance, $\beta = 0.1$ (see text). Inset shows the behavior in the vicinity of the bifurcation point $eV_* \approx 50E_{\rm Th} \approx 0.57\,T_{c0}$.

regime, $V - V_* \sim V_*$. The possibility of experimental observation of such a generation remains an open problem.

Incoherent regime.

—

As the voltage is increased far above the bifurcation threshold, $V_{\rm inst}(T) \gg V_*$, the eigenmodes $\psi_{L,R}(x)$ gradually localize near the corresponding terminals, with their size, $a(V)$, becoming much smaller then the wire length [see Fig. 7.1 (b)–(e)]. This is the *incoherent* regime, where the overlap between $\psi_L(x)$ and $\psi_R(x)$ is exponentially small, supercurrent oscillations are suppressed, and nucleation of superconductivity near each terminal can be described independently [Vercruyssen *et al.*(2012)].

Using $a(V)/L$ as a small parameter and still working in the vicinity of T_c, we linearize $F(E,x)$ near the left terminal and reduce Eq. (7.1) to the form: $(L_\omega^R)^{-1} = i\pi(\omega + eV)/8T - \ln(T/T_{c0}) - \mathcal{H}_\alpha$, where the operator

$$\mathcal{H}_\alpha = -\xi_0^2\partial_{x_L}^2 + \alpha x_L, \qquad x_L \geq 0, \tag{7.7}$$

acts on the semiaxis $x_L \equiv x + L/2 \geq 0$ with the boundary condition $\psi(0) = 0$. The complex parameter α is a functional of the distribution function:

$$\alpha\Big(\frac{eV}{T}\Big) = -\int \frac{dE\,\partial_x F(E - eV/2, x)|_{x=-L/2+a(V)}}{2(E - i0)}. \tag{7.8}$$

The ground state of the Hamiltonian (7.7) has the energy $\gamma_0(\alpha\xi_0)^{2/3}$ and the wave function $\psi_0(x_L) = \mathrm{Ai}(x_L/a - \gamma_0)/\sqrt{a}\,\mathrm{Ai}'(-\gamma_0)$, where $-\gamma_0 \approx -2.34$ is the first zero of the Airy function,

and $a = (\xi_0^2/\alpha)^{1/3}$ is the nucleus size [Ivlev and Kopnin(1984)]. For the instability line we get:

$$1 - T/T_{c0} = \gamma_0 \xi_0^{2/3} \operatorname{Re} \alpha^{2/3}(eV_{\rm inst}(T)/T). \tag{7.9}$$

The left and right unstable states rotate with the frequencies $\Omega_{L,R}(V) = \mp[eV - \Omega_1(V)]$, where $\Omega_1(V) = (8T_{c0}/\pi)\gamma_0\xi_0^{2/3} \operatorname{Im} \alpha^{2/3}(eV/T)$ is a small correction to the Josephson frequency determined by the electrochemical potential of the corresponding terminal. At the instability line, $V = V_{\rm inst}(T)$, the size a of the unstable mode is of the order of the temperature-dependent superconducting coherence length $\xi(T) \sim (1 - T/T_{c0})^{-1/2}\xi_0$.

For long wires ($L \gg \xi_0$), the incoherent regime partly overlaps with the weak-nonequilibrium regime. Then for $eV_* \ll eV_{\rm inst}(T) \ll T_c$, Eq. (7.9) gives a universal answer

$$\frac{eV_{\rm inst}(T)}{T_{c0}} = \frac{2^{7/2}}{\pi}\frac{L}{\xi_0}\left(\frac{T_{c0} - T}{\gamma_0 T_{c0}}\right)^{3/2}, \tag{7.10}$$

which could have also been deduced from Eq. (7.6) using the quasiclassical approximation for $\lambda_1(v)$ at $v \gg 1$. Equation (7.9) exactly coincides with the result of Ref. [Ivlev and Kopnin(1984)], predicting that superconductivity nucleates near the terminals at a finite current $I_{\rm inst}(T) \approx 0.356\, I_c(T)$.

The position of the instability line in the incoherent regime at large biases, $eV_{\rm inst}(T) \gg T_c$, depends on the relation between the inelastic lengths $l_{e\text{-}e}$ and $l_{e\text{-ph}}$, the wire length L, *and* the nucleus size $a(V)$. The presence of the latter scale, which probes the distribution function near the boundaries of the wire, leads to a rich variety of regimes realized at different temperatures.

For the three limiting distributions [Eqs. (7.3) and (7.4)], the function $\alpha(u)$ can be found analytically: (i) $\alpha_{\rm free}(u) = [\psi(1/2+iu/2\pi)-\psi(1/2)]/L$ for the non-interacting case, $L \ll l_{e\text{-}e}, l_{e\text{-ph}}$, where $\psi(x)$ is the digamma function; (ii) $\alpha_{e\text{-ph}}(u) = i\pi u/4L$ for strong lattice thermalization, $l_{e\text{-ph}} \ll a(V) \ll L \ll l_{e\text{-}e}$; and (iii) $\alpha_{e\text{-}e}(u) = [i\pi u/4 + 3u^2/2\pi^2]/L$ for the dominant e-e interaction, $l_{e\text{-}e} \ll a(V) \ll L \ll l_{e\text{-ph}}$. In case (ii), the instability line $V_{\rm inst}^{e\text{-ph}}(T)$ is given by Eq. (7.10). In the vicinity of T_c, the instability lines in cases (i) and (iii) are given by:

$$\frac{eV_{\rm inst}^{(\rm free)}(T)}{T_{c0}} = 1.13 \exp\left\{\frac{L}{\xi_0}\left(\frac{T_{c0} - T}{\gamma_0 T_{c0}}\right)^{3/2}\right\}, \tag{7.11}$$

$$\frac{eV_{\rm inst}^{(e\text{-}e)}(T)}{T_{c0}} = \left(\frac{2\pi^2}{3}\frac{L}{\xi_0}\right)^{1/2}\left(\frac{T_{c0} - T}{\gamma_0 T_{c0}}\right)^{3/4}. \tag{7.12}$$

Counterintuitively, in cases (i) and (iii) the instability current $I_{\rm inst}(T) \propto V_{\rm inst}(T)/L$ has a nontrivial dependence on the system size, as opposed to Eq. (7.10). Such a behavior is a consequence of strong nonequilibrium in the wire. The limiting curves $V_{\rm inst}^{(\rm free)}(T)$, $V_{\rm inst}^{(e\text{-ph})}(T)$, and $V_{\rm inst}^{(e\text{-}e)}(T)$ for all temperatures obtained numerically from Eq. (7.1) for the wire with $L/\xi_0 = 15$ are shown in Fig. 7.2. The universal behavior at small biases can be easily seen (inset). Since the ratio L/ξ_0 is not very large, the instability line becomes strongly dependent on the distribution function already for $V \gtrsim V_*$.

The most exciting feature of our results is the exponential growth of $V_{\rm inst}(T)$ with decreasing temperature in the non-interacting case, Eq. (7.11). Hence, even a small deviation of the distribution function from the two-step form (7.3) will drastically modify $V_{\rm inst}(T)$. As an example, consider the effect of a finite resistance of the normal terminals. Then the function

$F_L(E)$ in Eq. (7.3) will be replaced by $F_L(E) = \beta F_0(E + eV/2) + (1-\beta)F_0(E - eV/2)$, where V is the voltage applied to the NSN microbridge, and $\beta = R_T/(R_N + 2R_T)$ [R_T and R_N are the resistances of the N and S part of the junction, respectively]. The resulting $V_{\rm inst}(T)$ for $\beta = 0.1$ is shown by the dotted blue line in Fig. 7.2. While $V_{\rm inst}(T)$ is unchanged for small biases, it is strongly suppressed compared to $V_{\rm inst}^{\rm (free)}(T)$ for large biases.

Low-temperature behavior.

—The exponential growth of $V_{\rm inst}^{\rm (free)}(T)$ in the non-interacting case formally implies that superconductivity at $T = 0$ might persist up to exponentially large voltages, $\ln(eV_{\rm inst}(0)/T_{c0}) \sim L/\xi_0 \gg 1$. This conclusion is wrong, since inelastic relaxation and heating become important with increasing V, even if they were negligible at $V = 0$. To study the low-T part of the instability line, we consider here a model of the e-ph interaction (e-e relaxation neglected) when the phonon temperature is assumed to coincide with the base temperature of the terminals and e-ph relaxation is weak at T_c: $l_{e\text{-ph}}(T_c) \gg L$ (as in the experiment [Vercruyssen *et al.*(2012)]).

With decreasing T below T_c, the instability line first follows Eq. (7.11). At the same time, $l_{e\text{-ph}}$ decreases and eventually the distribution function in the middle of the wire becomes nearly thermal with the effective temperature $T_{\rm eff}$. This happens when $T_{\rm eff}$ obtained from the heat balance equation [Giazotto *et al.*(2006)], $(eV/L)^2 \sim T_{\rm eff}^5/T_c^3 l_{e\text{-ph}}^2(T_c)$, becomes so large that $l_{e\text{-ph}}(T_{\rm eff}) \sim L$. The corresponding voltage, $V_{\rm ph}$, can be estimated as $eV_{\rm ph}/T_c \sim [l_{e\text{-ph}}(T_c)/L]^{2/3}$. Consequently, the exponential growth (7.11) persists for voltages $V_* \lesssim V \lesssim V_{\rm ph}$, corresponding to the temperature range $T_{\rm ph} \lesssim T \lesssim T_*$, where with logarithmic accuracy $1 - T_{\rm ph}/T_{c0} \sim (\xi_0/L)^{2/3}$.

For higher biases, $V > V_{\rm ph}$, electrons in the central part of the wire have the temperature $T_{\rm eff}$. However, the parameter α, Eq. (7.8), is determined by the distribution function in the vicinity of the terminals which is not thermal. Matching solution of the collisionless kinetic equation for $0 < x_L < l_{e\text{-ph}}(T_{\rm eff})$ at the effective right "boundary", $x_L = l_{e\text{-ph}}(T_{\rm eff})$, with the function (7.4) with $T(x) = T_{\rm eff}$, we obtain $\alpha \sim 1/l_{e\text{-ph}}(T_{\rm eff})$. Therefore, for $V \gtrsim V_{\rm ph}$ we get with logarithmic accuracy:

$$\frac{eV_{\rm inst}(T)}{T_{c0}} \sim \frac{L}{\xi_0}\left(\frac{l_{e\text{-ph}}(T_c)}{\xi_0}\right)^{2/3}\left(\frac{T_{c0}-T}{T_{c0}}\right)^{5/2}. \tag{7.13}$$

Equation (7.13) corresponding to the case $a(V) \ll l_{e\text{-ph}} \ll L$ is different from the expression (7.10) when phonons are important already at T_c, and $l_{e\text{-ph}} \ll a(V) \ll L$. The scaling dependence of Eq. (7.13) on L indicates that the stability of the normal state is controlled by the applied current, similar to Eq. (7.10). At zero temperature the instability current exceeds the thermodynamic depairing current by the factor of $(l_{e\text{-ph}}(T_c)/\xi_0)^{2/3} \gg 1$.

Discussion.

—Our general procedure locates the absolute instability line, $V_{\rm inst}(T)$, of the normal state for a voltage-biased NSN microbridge. Following experimental data [Vercruyssen *et al.*(2012)] we assumed that the onset of superconductivity is of the second order. While non-linear terms in the TDGL equation are required to determine the order of the phase transition [Serbyn and Skvortsov()], we note that were it of the first order, its position would be shifted to voltages higher than $V_{\rm inst}(T)$.

In the vicinity of T_c, the problem of finding $V_{\rm inst}(T)$ can be mapped onto a one-dimensional quantum mechanics in some potential $U(x)$. For small biases, $eV \ll T_{c0}$, the potential $U(x)$ does not depend on the distribution function details, explaining universality of the instability

line, including the bifurcation from the single-mode to the bimodal superconducting state at $eV \sim 50E_{\rm Th}$ [Rubinstein *et al.*(2007)] and nucleation of superconductivity in the vicinity of the terminals for larger biases [Ivlev and Kopnin(1984)].

For $eV \gtrsim T_{c0}$, the potential $U(x)$ becomes a functional of the normal-state distribution function, producing $V_{\rm inst}(T)$ that is strongly sensitive to inelastic relaxation mechanisms in the wire. For the dominant e-ph interaction, the instability is controlled by the electric field $\mathcal{E} = V/L$ [Eqs. (7.10) and (7.13)], while in the opposite case [Eqs. (7.11) and (7.12)], the instability cannot be solely interpreted as current or voltage-driven. At zero temperature, the (nonuniform) superconducting state can withstand a current which is parametrically larger than the thermodynamic depairing current.

High sensitivity of $V_{\rm inst}(T)$ to the details of the distribution function opens avenues for its use as a probe of inelastic relaxation in the normal state. The shape of $V_{\rm inst}(T)$ can be further used to determine the dominating relaxation mechanism and extract the corresponding inelastic scattering rate.

8 Relaxation and persistent oscillations of the order parameter in the non-stationary BCS theory by Yuzbashyan, Tsyplyatyev, Altshuler

(this is a little article that gives overview and then shows solutions in different regimes. I am not sure that relations of this approach to others are discussed)

Abstract

We determine the limiting dynamics of a fermionic condensate following a sudden perturbation for various initial conditions.

We demonstrate that possible initial states of the condensate fall into two classes.

In the first case, the order parameter asymptotes to a *constant* value. The approach to a constant is oscillatory with an inverse square root decay. This happens, e.g., when the strength of pairing is abruptly changed while the system is in the paired ground state and more generally for any *nonequilibrium* state that is in the same class as the ground state.

In the second case, the order parameter exhibits persistent oscillations with several frequencies. This is realized for nonequilibrium states that belong to the same class as excited stationary states.

(don't understand)

Our *classification* of initial states extends the concept of excitation spectrum to nonequilibrium regime and allows one to predict the evolution without solving equations of motion.

The response of a fermionic condensate to fast external perturbations presents a long-standing problem[[11]–[36]] (why is it not solved?).

The main difficulty is to describe the time evolution in the non-adiabatic (non-adiabatic??? never thought that it is important) regime when a nonequilibrium state of the condensate is created on a time scale shorter than the Cooper instability time $\tau_\Delta = 1/\Delta_0$, where Δ_0 is the equilibrium BCS gap. In this case the evolution of the system cannot be described in terms of a quasiparticle spectrum or a single time-dependent order parameter $\Delta(t)$ [1]. One has to account for the dynamics of individual Cooper pairs, making it a complex many-body problem.

The non-adiabatic regime can be accessed experimentally in ultra-cold Fermi gases, where the strength of pairing between fermions can be rapidly changed[13]. Non-adiabatic measurements can be also performed in quantum circuits utilizing superconducting qubits (nanoscale superconductors). Here nonequilibrium conditions can be generated by fast voltage pulses on a time scale comparable to τ_Δ[14].

Here we consider a BCS condensate that is out of equilibrium at $t = 0$ and study its time evolution for $t > 0$. Given the state of the system at $t = 0$, we predict the dynamics with no need for actually solving equations of motion. We show that physically meaningful initial states fall into two broad categories. In the first scenario, $|\Delta(t)|$ asymptotes to a constant value $\Delta_\infty < \Delta_0$. The approach to Δ_∞ is oscillatory with a $1/\sqrt{t}$ decay,

$$\frac{|\Delta(t)|}{\Delta_\infty} = 1 + a\frac{\cos(2\Delta_\infty t + \phi)}{\sqrt{\Delta_\infty t}}, \tag{8.1}$$

where the constants a and ϕ depend on details of the initial state. This scenario is realized, for example, when the pairing strength is abruptly changed, while the system is in the paired ground state. In the second scenario, $|\Delta(t)|$ oscillates persistently with several incommensurate frequencies. The number of frequencies as well as the limiting dynamics of individual pairs can be inferred directly from the initial state.

We propose a topological *classification* of initial states, which extends the concept of excitation spectrum to the nonequilibrium regime. If a state is in the same class as the paired ground state, Eq. (8.1) applies. Other states are topologically distinct, in which case persistent oscillations occur.

Our approach explains differences (which?) between previous studies of condensate dynamics.

A linear analysis around the BCS ground state yields[12] damped oscillations with a frequency $2\Delta_0$. Eq. (8.1) generalizes this result to the nonlinear case and a wide range of initial conditions (check that it is so. what about initial conditions???).

An oscillatory decay following a change in the coupling strength was observed numerically[19, 18] (what is going on in these papers? they confirmed the Volkov, Kogan results?).

We will see that this is due to the fact that initial states of Refs. [12, 19, 18] are in the same class (class???) as the BCS ground state.

Undamped periodic oscillations of $|\Delta(t)|$ have been found in Refs. [13, 14, 15]. They were also seen numerically for initial states close to a normal state[17]. (okay, but what is the difference with Volkov's statement of the problem?)

In contrast, Ref. [36] also starts from the normal state (meaning close to normal?), but obtains a saturation to $\Delta_\infty = \Delta_0/2$. It turns out[15] that this occurs if the initial state is a *paired* state with a small seed gap $\Delta_{in} \ll \Delta_0$ (this is very strange, why there is such dependence on the initial state??? is it an artificial state?). Quasiperiodic oscillations of the order parameter[8, 9] can also be realized (see below).

In the non-dissipative regime, one can use the BCS model to describe the dynamics of the condensate. Here we are interested in the thermodynamic limit. Then, the BCS mean-field is valid as long as the order parameter is nonzero (if the ord.par. is zero and we are close to the Tc, BCS model should also work, no? at high T, there maybe will be effects that are not described by BCS. Which by the way??).

There are several equivalent ways to derive mean-field evolution equations. Using Anderson's pseudospin representation[11], one can describe the mean-field evolution by a *classical*

spin Hamiltonian[8]

$$H_{BCS} = \sum_j 2\epsilon_j s_j^z - g \sum_{j,k} s_j^+ s_k^-, \tag{8.2}$$

(still, don't understand its meaning) where ϵ_j are the single-particle energies and $s_j^\pm = s_j^x \pm i s_j^y$. Dynamical variables $\mathbf{s}_j$ are vectors of fixed length, $|\mathbf{s}_j| = 1/2$. The BCS order parameter is $\Delta(t) = \Delta_x - i\Delta_y = g\sum_j s_j^-$ (why def with "-" sign? is it important?).

Mean-field equations of motion $\dot{\mathbf{s}}_j = \{H_{BCS}, \mathbf{s}_j\}$ follow from Hamiltonian (8.2) and the angular momentum Poisson brackets (why do we use Poisson br-s??? never thought about it), $\{s_j^x, s_k^y\} = -\delta_{jk} s_j^z$ etc.,

$$\dot{\mathbf{s}}_j = \mathbf{b}_j \times \mathbf{s}_j, \qquad \mathbf{b}_j = (-2\Delta_x, -2\Delta_y, 2\epsilon_j)\,. \tag{8.3}$$

The general non-stationary BCS problem can now be formulated as follows: given an initial distribution of spins, determine its evolution.

(there is the long standing question "why they use at all Anderson's formalism? I haven't learn it yet, I'll answer later")

Solution of Eq. (8.3) for each of the dynamical variables $\mathbf{s}_j(t)$ and $\Delta(t)$ is a superposition of harmonic oscillations with certain frequencies. (what is it and why??)

In the thermodynamic limit the frequency spectrum in general consists of continuum and discrete parts (and how is it in not thermodynamic limit?).

Consider, e.g., the absolute value of the order parameter $|\Delta(t)|$. Suppose the discrete part contains k incommensurate frequencies (contains what???).

Let their contribution to $|\Delta(t)|$ be $F_k(t)$,

$$|\Delta(t)| = F_k(t) + \int_{-D}^{D} d\omega A(\omega) \cos[\omega t + \phi(\omega)], \tag{8.4}$$

(why??)where D is the ultraviolet cutoff (Debye frequency in conventional BCS).

The integral in Eq. (8.4) vanishes as $t \to \infty$ for any well behaved $A(\omega)$. Hence, $|\Delta(t)| \to F_k(t)$ for $t \to \infty$, i.e. $|\Delta(t)|$ oscillates with k frequencies for $k \geq 1$ and $|\Delta(t)| \to \Delta_\infty$ if $k = 0$.

Given the initial state, the structure of the frequency spectrum can be determined using integrability of BCS dynamics[8, 9]. Frequencies of an integrable system depend only on its integrals of motion[28], which can be evaluated at $t = 0$. Frequencies can thus be determined without solving equations of motion.

Here we use the method of Ref. [9]. It is convenient to introduce the following vector function (Lax vector) of an auxiliary (spectral) parameter u:

$$\mathbf{L}(u) = -\frac{\hat{\mathbf{z}}}{g} + \sum_j \frac{\mathbf{s}_j}{u - \epsilon_j}, \tag{8.5}$$

where $\hat{\mathbf{z}}$ is a unit vector along the z-axis. (still haven't figure out what is the idea of Lax vector, but okay, it is a question for another article)

The square of the Lax vector is conserved by the evolution. The frequency spectrum is related to branch cuts of $w(u) = \sqrt{\mathbf{L}^2(u)}$. Note that the numerator of $\mathbf{L}^2(u)$ is a polynomial of degree $2n$, where n is the total number of levels ϵ_j. Since $\mathbf{L}^2(u) \geq 0$, all $2n$ roots come in complex conjugate pairs. For finite n, all roots are typically distinct leading to n isolated cuts connecting pairs of conjugate roots. This situation is described by the general solution[8] for finite n. One can also have a situation when $2(n-m)$ roots are real and therefore double degenerate. This

leaves m branch cuts corresponding to m pairs of complex conjugate roots. The dynamics can now be described in terms of only $m < n$ effective spins governed by Hamiltonian (8.2) with m spins and m new effective energy levels. These *m-spin* solutions contain only m incommensurate frequencies. One frequency corresponds to a uniform rotation of all spins around the z-axis. Thus, $|\Delta(t)|$ contains $m-1$ frequencies [9].

In the thermodynamic limit some roots of $\mathbf{L}^2(u)$ merge into continuous lines and give rise to the continuum part of the spectrum, while isolated pairs of roots correspond to the discrete part.

Thus, the number of discrete frequencies in $|\Delta(t)|$ is the number of isolated pairs of roots less one, $k = m-1$ (think about it, I don't understand the idea yet).

At large times $|\Delta(t)|$ exhibits persistent oscillations with k frequencies[17] and is described by an m-spin solution[16]. The number k is a topological property of the initial state. It is the number of handles on the Riemann surface of the function $\sqrt{\mathbf{L}^2(u)}$.

Discrete part of the frequency spectrum turns out to be related to discontinuities of the spin distribution $\mathbf{s}(\epsilon)$ as a function of ϵ. To see this, consider first stationary states. There are two types of such states. The BCS ground state and excited states with a constant $\Delta \neq 0$ are obtained by aligning each spin $\mathbf{s}_j$ self-consistently along its effective magnetic field $\mathbf{b}_j$. These states can be termed *anomalous* stationary states. Choosing the x-axis so that Δ is real, we obtain

$$2s_j^z = -\frac{e_j\epsilon_j}{\sqrt{\epsilon_j^2+\Delta^2}} \quad 2s_j^x = -\frac{e_j\Delta}{\sqrt{\epsilon_j^2+\Delta^2}}, \tag{8.6}$$

where $e_j = 1$ if the spin is antiparallel to the field and $e_j = -1$ otherwise. The self-consistency condition $\Delta = g\sum_j s_j^x$ yields the BCS gap equation. The state with all $e_j = 1$ is the BCS ground state. The state $e_k = -1$ and $e_{j\neq k} = 1$ is a state with a single excited pair[11] of energy $2\sqrt{\epsilon_k^2+\Delta_0^2}$. Using Eqs. (8.5, 8.6) and the gap equation, we derive

$$\mathbf{L}_s(u) = -(\Delta\hat{\mathbf{x}} + u\hat{\mathbf{z}})L_s(u), \tag{8.7}$$

$$L_s(u) = \sum_j \frac{e_j}{2(u-\epsilon_j)\sqrt{\epsilon_j^2+\Delta^2}} \tag{8.8}$$

We see that $\mathbf{L}_s^2(u) = (u^2+\Delta^2)L_s^2(u)$ has a pair of isolated roots at $u = \pm i\Delta$. All other roots are determined by the equation $L_s(u) = 0$ and are double degenerate.

First, consider the ground state, $e_j = 1$. Since $L_s(u) \to \pm\infty$ as $u \to \epsilon_j \pm 0$ for each j, all roots of $L_s(u)$ are real and located between consecutive ϵ_j. In the thermodynamic limit they merge into a line from $-D$ to D as shown in Fig. 8.1a. Note that the existence of a double real root between ϵ_j and ϵ_{j+1} relies on $e_j = e_{j+1}$. Further, Eq. (8.6) implies that when $e_j = e_{j+1}$, the components of spins $\mathbf{s}(\epsilon)$ are continuous at $\epsilon = \epsilon_j$. Now let $e_j = -e_{j+1}$. In this case the real root between ϵ_j and ϵ_{j+1} can disappear. Thus, discontinuities (jumps) in the spin distribution generate isolated complex roots (see Fig. 8.3a for an example). Since spins far from the Fermi level are not flipped, the total number of jumps is even. In general, for $2p$ jumps $L_s(u)$ can have up to p pairs of isolated roots.

One can study equations of motion (8.3) linearized around anomalous stationary states. Setting $\delta\mathbf{s}_j = \mathbf{A}_j e^{i\omega_k t}$, we solve for the normal modes. The eigenvalues turn out to be $\omega_j = 2\sqrt{u_j^2+\Delta^2}$, where u_j are the roots of $\mathbf{L}_s^2(u)$. For the ground state $x_j = \epsilon_j$ up to finite size corrections (cf. Ref. [11]).

Next, consider few examples of initial states far from equilibrium. Let the system be in an anomalous stationary state for $t < 0$. Suppose at $t = 0$ the coupling changes abruptly from g' to g. Using Eq. (8.5), one can show that the change in g results in a smooth deformation of

the root distribution. Lines of roots deform into lines. On the other hand, doubly degenerate roots become non-degenerate. A state that had p pairs of degenerate isolated roots in addition to a pair of roots $\pm i\Delta$ now has $m = 2p + 1$ pairs of non-degenerate roots, i.e. $2p + 1$ cuts of $\sqrt{\mathbf{L}^2(u)}$. As shown above, in this case $|\Delta(t)|$ exhibits persistent oscillations with $k = m-1 = 2p$ frequencies. This behavior is illustrated in Fig. 8.3c.

Let the initial state be the ground state with coupling g'. Then, the line of double real roots splits into two complex conjugate lines (Fig. 8.1b). There is only one pair of isolated roots as in the ground state. Therefore, $k = 0$ and $|\Delta(t)|$ *asymptotes to a constant* Δ_∞ at $t \gg \tau_\Delta$, as illustrated in Fig. 8.1c. According to Eq. (8.3), at large times spin $\mathbf{s}_j$ rotates in a constant magnetic field $\mathbf{b}_j = (2\Delta_\infty, 0, 2\epsilon_j)$ with a frequency $\omega(\epsilon_j) = 2\sqrt{\epsilon_j^2 + \Delta_\infty^2}$. Using this, one derives Eq. (8.1). The $1/\sqrt{t}$ decay law is set by the square root singularity in the spectral density[15]. Note that, even though $|\Delta(t)|$ asymptotes to a constant, the final state of the system is non-stationary. In the final state each spin precesses with its own frequency[36].

There is another type of stationary states – *normal* states. In these states each spin is aligned along the z-axis, $s_j^z = z_j/2 = \pm 1/2$. The Fermi state is $z_j = -\operatorname{sgn}\epsilon_j$ (levels below the Fermi energy are occupied, above – empty). States with other z_j correspond to particle-hole excitations of the Fermi gas. For example, a state $z_k = \operatorname{sgn}\epsilon_k < 0$ has a pair of fermions removed from the level ϵ_k. The Lax vector for normal states is $\mathbf{L}_n(u) = L_n(u)\hat{\mathbf{z}}$, where

$$L_n(u) = -\frac{1}{g} + \sum_j \frac{z_j}{2(u - \epsilon_j)} \tag{8.9}$$

All roots of $\mathbf{L}^2(u) = L_n^2(u)$ are thus doubly degenerate. Note the absence of a branch cut of $\sqrt{\mathbf{L}^2(u)}$ connecting the points $u = \pm i\Delta$. Further analysis is similar to that for anomalous states. The Fermi state has a single jump in the $s_z(\epsilon)$ at the Fermi level. This results in a pair of complex conjugate isolated roots (Fig. 8.2a), which can be determined from the equation $L_n(u) = 0$. In the thermodynamic limit, we obtain $u = \pm i\Delta_0/2$. The rest of the roots are real and form a line from $-D$ to D. For a general normal state with $2p+1$ jumps[18] in $s_z(\epsilon)$, one can have up to $p+1$ complex conjugate pairs of roots. Each root is doubly degenerate. Linearizing Eqs. (8.3) around a normal state, we obtain normal frequencies $\omega_j = 2u_j$, where $L_n(u_j) = 0$. In particular, the Fermi state has a single unstable mode that corresponds to $u_j = \pm i\Delta_0/2$. This mode grows as $e^{\Delta_0 t}$ indicating the pairing instability of the Fermi state[2, 3]. Remaining frequencies are real and correspond to the precession of spins at their natural frequencies, $\omega_k = 2\epsilon_k$ up to finite size corrections.

Let the system be in or close to a normal state at $t = 0$. First, we consider the Fermi state. Since, within mean-field, normal states are unstable equilibria, a small perturbation is needed to start off the dynamics. One can start e.g. from a non-stationary spin distribution close to the Fermi state[17]. A typical deviation splits all double degenerate roots as illustrated in Fig. 8.2b. Real roots split into two complex conjugate lines close to the real axis. Their contribution to $|\Delta(t)|$ is small in the deviation from the Fermi state and decaying. Degenerate complex roots at $u = \pm i\Delta_0/2$ split into $m = 2$ isolated cuts close to each other. Since $k = m-1 = 1$ in Eq. (8.4), $|\Delta(t)|$ will exhibit undamped periodic oscillations, as shown in Fig 8.2c. Its functional form is described by a 2-spin solution[16]. The roots close to the real axis indicate that the initial spin distribution does not match the 2-spin solution exactly (see the discussion of m-spin solutions above).

The dynamics in normal states can also be triggered by quantum fluctuations. In Ref. [36] this is modelled by adding a small *external* field $-2\Delta_{QF}\hat{\mathbf{x}}$ to Eq. (8.3). This violates conservation of $\mathbf{L}^2(u)$. We have $d\mathbf{L}^2(u)/dt = 2\Delta_{QF}L_y/g$. Being applied for a short time t^*, the external field drives the system out of the normal state. Treating the evolution of $\mathbf{L}^2(u)$ perturbatively, we find that the new positions of the roots are determined by the equation $L_n(u) = \pm 2i\Delta_{QF}t^*/g$. Degenerate complex roots split along the real axis into two cuts by $2\Delta_{QF}^2 t^* d/g$, where $d =$

$\langle \epsilon_{j+1} - \epsilon_j \rangle$ is the level spacing. The resulting root configuration shown in Fig. 8.2b contains two cuts. Thus, $k = 1$ and $|\Delta(t)|$ exhibits periodic oscillations, see Fig. 8.2c.

We see that for initial conditions close to the Fermi state a periodic solution is "dynamically selected"[17]. Other initial conditions "select" damped oscillations or multi-frequency undamped oscillations. In more conventional terms, this corresponds to a basic fact that the evolution of an integrable system depends on initial conditions. All diferent behaviors are captured by the general solution[8]. Here we systematically classified possible initial states and specialized the general solution to each type of initial conditions, i.e. we developed "selection rules" for the BCS dynamics. Which behavior is realized in a particular experimental setup depends on the initial state of the condensate. In this respect, the periodic solution is somewhat special: if we start from the ground state with a small $\Delta_{in} \ll \Delta_0$, the order parameter $|\Delta(t)|$ asymptotes to a constant value Δ_∞, see Eq. (8.1). In the thermodynamic limit, the damping disappears only when $\Delta_{in} = 0$[21].

Excited normal states have several jumps in the spin distribution and can therefore display oscillations with more than one frequency. Consider, e.g., a state where pairs in energy interval from $-\epsilon_a$ to $-\epsilon_b$ have been removed. The initial spin distribution is $s_z(\epsilon) = -\mathrm{sgn}[\epsilon(\epsilon+\epsilon_a)(\epsilon+\epsilon_b)]$. The $2p+1 = 3$ jumps[18] result in $p+1 = 2$ pairs of isolated double degenerate complex roots. As a small perturbation splits these roots into $m = 2p + 2 = 4$ cuts, $|\Delta(t)|$ oscillates with $k = m - 1 = 2p + 1 = 3$ incommensurate frequencies, see Fig. **??**.

In conclusion, we have shown how the non-stationary BCS dynamics can be predicted from the initial state of the condensate. We classified initial states by their integrals of motion – roots of $\mathbf{L}^2(u)$. For states with a root diagram as in the paired ground state, the order parameter $|\Delta(t)|$ displays damped oscillations described by Eq. (8.1). Other states are of the same type as excited stationary states of the BCS Hamiltonian. In these cases $|\Delta(t)|$ oscillates persistently with few incommensurate frequencies. The number of frequencies is related to the number of jumps in the pseudospin distribution of the corresponding stationary state. For the situation most relevant to the experiments on cold fermions – an abrupt change of the coupling – we predict damped oscillations with $1/\sqrt{t}$ decay.

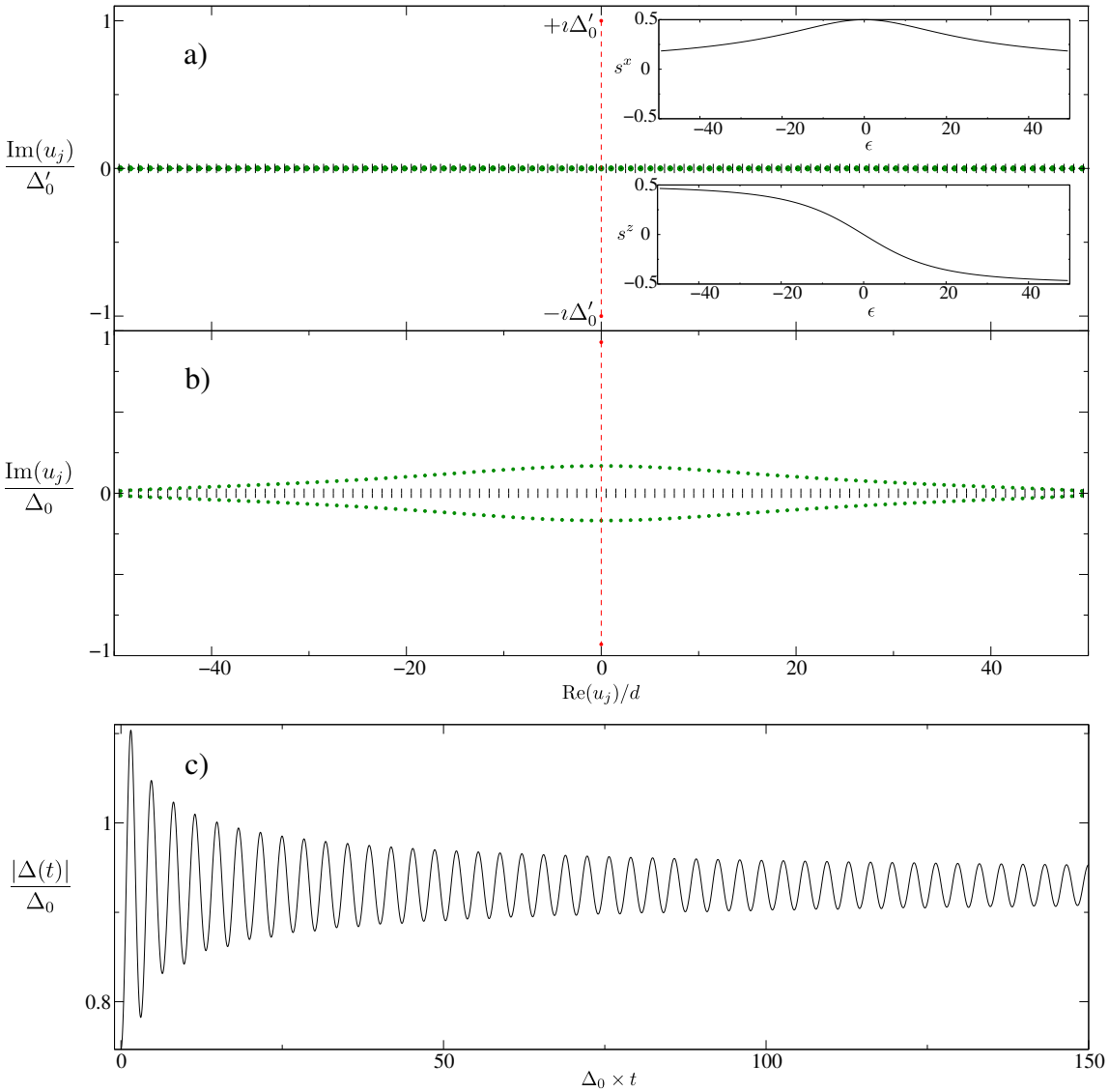


Figure 8.1: **a)** Roots u_j of $\mathbf{L}^2(u)$ for the BCS ground state of $n = 100$ spins with equilibrium gap Δ_0'. Axes: $\mathrm{Im}(u_j)/\Delta_0'$ and $\mathrm{Re}(u_j)/d$, where d is the level spacing. Insets: spin distribution $s^z(\epsilon)$ and $s^x(\epsilon)$ ($s^y(\epsilon) = 0$). The absence of discontinuities in the spin distribution ($2p = 0$) implies a single pair of isolated roots at $\pm i\Delta_0'$ (red circles connected by a dashed line). Remaining $2n - 2 = 198$ roots (solid green circles) are real, doubly degenerate, and located between consecutive energy levels ϵ_j (ticks on the real axis).

b) At $t = 0$ the coupling constant is abruptly increased so that the corresponding ground state gap is $\Delta_0 = 2.4\Delta_0'$, while the spin configuration remains the same as in part a). The line of double real roots deforms into two complex conjugate lines. The Riemann surface of $\sqrt{\mathbf{L}^2(u)}$ has $m = 2p + 1 = 1$ isolated cuts (red circles connected by a dashed line). This nonequilibrium state has the same number of isolated roots as the BCS ground state and, therefore, is in the same topological class. The frequency spectrum of $|\Delta(t)|$ is thus continuous: $k = m - 1 = 2p = 0$, i.e. no discrete frequencies in Eq. (8.4).

c) Time evolution of $|\Delta(t)|$ after the change $\Delta_0' \to \Delta_0$. In the absence of discrete frequencies, the order parameter $|\Delta(t)|$ asymptotes to a constant value Δ_∞ (see Eq. (8.1)).

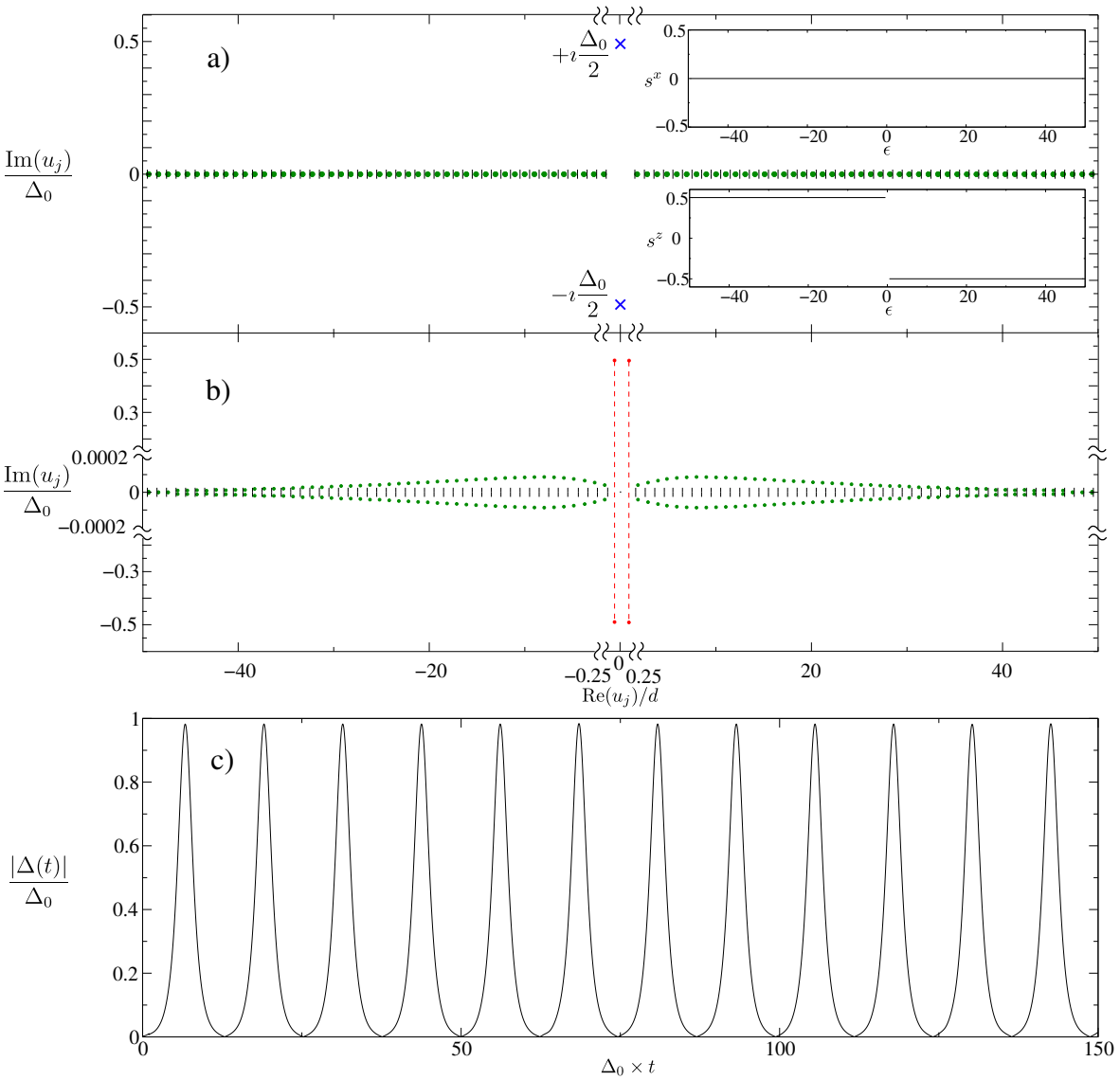


Figure 8.2: **a)** Roots u_j of $\mathbf{L}^2(u)$ for the Fermi state of $n = 100$ spins with ground state gap Δ_0. Axes: $\mathrm{Im}(u_j)/\Delta_0$ and $\mathrm{Re}(u_j)/d$, where d is the level spacing. Insets: spin distribution $s^z(\epsilon) = -\mathrm{sgn}\,\epsilon/2$ ($s^x(\epsilon) = s^y(\epsilon) = 0$). There is $2p+1 = 1$ discontinuity (a jump in $s^z(\epsilon)$ at the Fermi level) in the spin distribution resulting in $p+1 = 1$ pair of imaginary doubly degenerate roots $u_j = \pm i\Delta_0/2$ (blue crosses). Remaining $2n-4 = 196$ roots (solid green circles) are real, doubly degenerate and located between consecutive energy levels ϵ_j (ticks on the real axis). Since all spins are along the z-axis, this state is stationary (see Eq. (8.3)). The normal frequencies are $\omega_j = 2u_j$. The mode corresponding to $u_j = \pm i\Delta_0/2$ is unstable, it grows as $e^{\Delta_0 t}$.

b) Initially the system is in the Fermi state. A small "external magnetic field" $-2\Delta_{QF}\hat{\mathbf{x}} = -5.4 \times 10^{-2}\Delta_0\hat{\mathbf{x}}$ is added to Eq. (8.3) for a time $t^* = 1/\Delta_0$. The $p+1 = 1$ pair of double roots $u_j = \pm i\Delta_0/2$ splits into $m = 2p+2 = 2$ pairs of isolated roots (red circles connected by dashed lines); the line of real roots splits into two complex conjugate lines. This nonequilibrium state has the same number of isolated roots as the Fermi state and, therefore, belongs to the same topological class. The Riemann surface of $\sqrt{\mathbf{L}^2(u)}$ has $m = 2p+2 = 2$ isolated cuts. The frequency spectrum of $|\Delta(t)|$ has $k = m-1 = 2p+1 = 1$ discrete frequency in Eq. (8.4).

c) Time evolution of $|\Delta(t)|$ for the initial state described in part b). Since there is one discrete frequency, $|\Delta(t)|$ exhibits periodic oscillations. Its functional form is described by an $(m = 2)$–spin solution (see the text below Eq. (8.5)).

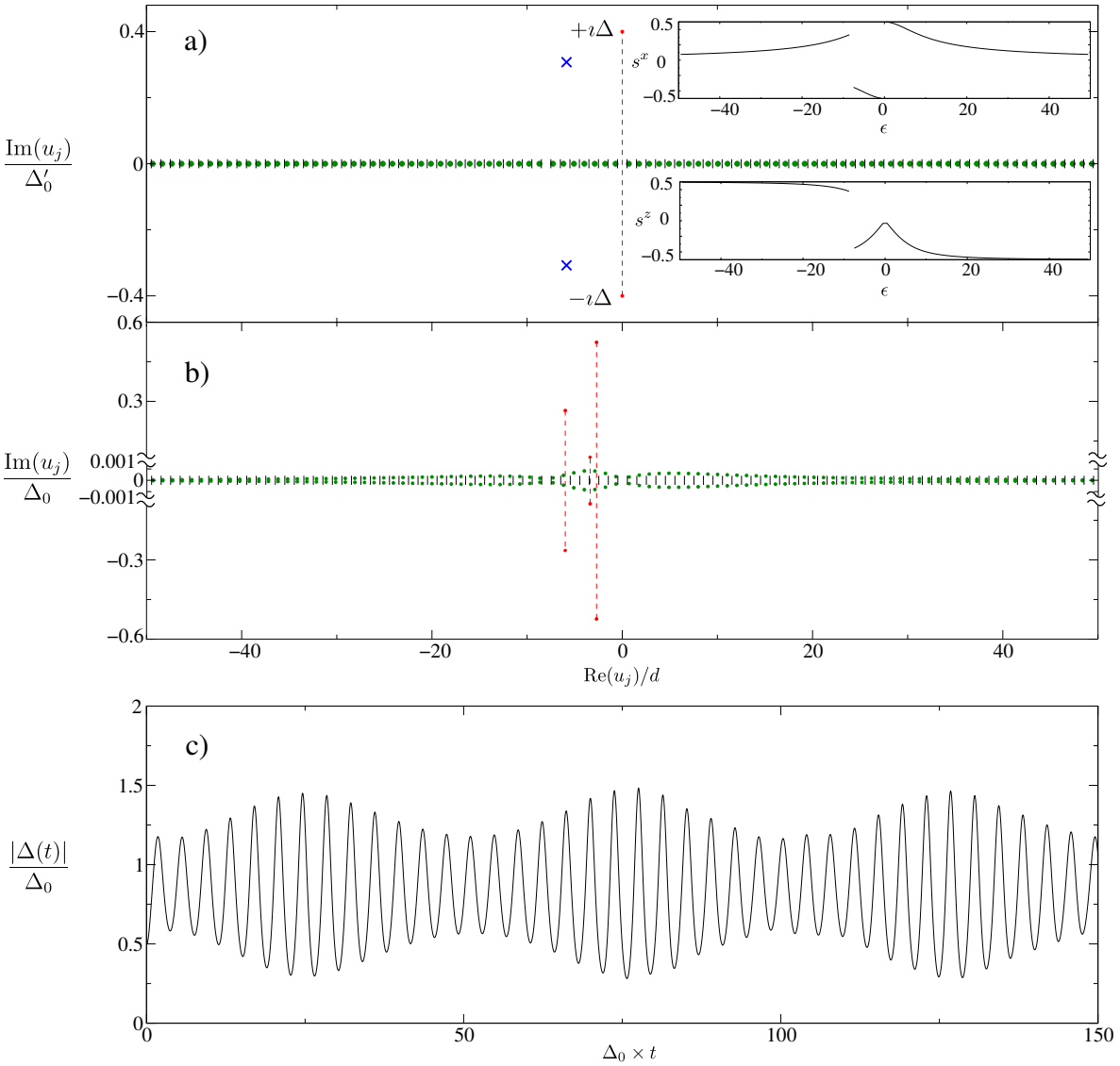


Figure 8.3: **a)** Roots u_j of $\mathbf{L}^2(u)$ of $n = 100$ spins in an excited stationary state. This *anomalous* state (see the text) has been obtained from the ground state with the gap Δ_0' by flipping spins in energy interval $(-0.37\Delta_0', 0)$. It has a gap $\Delta = 0.4\Delta_0'$. Axes: $\mathrm{Im}(u_j)/\Delta_0'$ and $\mathrm{Re}(u_j)/d$, where d is the level spacing. Insets: spin distribution $s^z(\epsilon)$ and $s^x(\epsilon)$ ($s^y(\epsilon) = 0$). Spin flips result in $2p = 2$ discontinuities in the spin distribution. Therefore, there is a $p = 1$ pair of isolated doubly degenerate roots (blue crosses) in addition to a pair of roots $u_j = \pm i\Delta$ (red circles connected by a dashed line). The remaining $2n - 6 = 194$ roots (solid green circles) are real, doubly degenerate, and located between consecutive energy levels ϵ_j (ticks on the real axis).

b) At $t = 0$ the coupling constant is abruptly increased so that the corresponding ground state gap is $\Delta_0 = 1.55\Delta_0'$, while the spin configuration remains the same as in part a). The $p = 1$ pair of isolated double roots splits into $2p = 2$ pairs of isolated roots. Together with a pair of roots coming from $u_j = \pm i\Delta$, there are $m = 2p + 1 = 3$ pairs of isolated roots (red circles connected by dashed lines). The line of double real roots deforms into two complex conjugate lines. The Riemann surface of $\sqrt{\mathbf{L}^2(u)}$ has $m = 2p + 1 = 3$ isolated cuts. This nonequilibrium state has the same number of isolated roots as the excited state in part a) and therefore is in the same topological class. The frequency spectrum of $|\Delta(t)|$ has $k = m-1 = 2p = 2$ discrete frequencies.

c) Time evolution of $|\Delta(t)|$ after the change $\Delta_0' \to \Delta_0$. Since there are $k = m - 1 = 2p = 2$ discrete frequencies in Eq. (8.4), the order parameter $|\Delta(t)|$ displays oscillations with two basic frequencies. Its functional form is described by an $(m = 3)$–spin solution (see the text below Eq. (8.5)).

b) Initially the system is in the stationary state described in part a). A small "external magnetic field" $-2\Delta_{QF}\hat{\mathbf{x}} = -5.4 \times 10^{-2}\Delta_0\hat{\mathbf{x}}$ is added to Eq. (8.3) for a time $t^* = 1/\Delta_0$. The $p+1 = 2$ pairs of degenerate roots $u_j = \mu_{1,2} \pm i\gamma_{1,2}$ split into $m = 2p+2 = 4$ pairs of isolated roots (red circles connected by a dashed line), while the line of real roots splits into two complex conjugate lines. This nonequilibrium state has the same number of isolated roots as the stationary state in part a) and, therefore, belongs to the same topological class. The Riemann surface of $\sqrt{\mathbf{L}^2(u)}$ has $m = 2p+2 = 4$ isolated cuts. Insets: Fourier spectra of $\mathrm{Re}\Delta(t)$ and $\mathrm{Im}\Delta(t)$ display $m = 2p+2 = 4$ basic frequencies. One frequency (ν_0) corresponds to a uniform rotation of all spins around the z-axis and cancels out in $|\Delta(t)|$. Thus, the frequency spectrum of $|\Delta(t)|$ has $k = m-1 = 2p+1 = 3$ discrete frequencies.

c) Time evolution of $|\Delta(t)|$ for the initial state described in part b). Since $k = m-1 = 2p+1 = 3$ in Eq. (8.4), $|\Delta(t)|$ exhibits quasiperiodic oscillations with three basic frequencies (see insets in Fig. **??**b). Its functional form is described by an ($m = 4$)–spin solution (see the text below Eq. (8.5)).

9 Solitons and Rabi Oscillations in a Time-Dependent BCS Pairing Problem by Barankov, Levitov, Spivak

(I don't understand anything here. I don't think that it is a good article, just abstract strange statements. but maybe at least formulas are clear in the model here??)

In summary, this work provides an exact solution for the BCS pairing formation problem. In the nonadiabatic regime (nearly nothing is explained here about nonadiabaticity), the dynamics is dissipationless and thus nonlinear. Soliton train solutions are obtained analytically and demonstrated to be generic and robust by a simulation.

9.1 Theory

Abstract

Motivated (what exactly motivates them???) by recent efforts to achieve cold fermions pairing near a Feshbach resonance, we consider the dynamics of formation of the Bardeen-Cooper-Schrieffer (BCS) state.

At times shorter than the quasiparticle energy relaxation time (still haven't figure out what do they mean about this relaxation??), after the interaction is turned on, the dynamics of the system is nondissipative (because it is a closed system, as it was before??? then it is always like this).

We show that this collective nonlinear evolution (collective nonlinear evolution?) of the BCS-Bogoliubov amplitudes u_p, v_p, along with the pairing function Δ, is an integrable (how is it??? BCS is integrable itself in mean field appr. right?) dynamical problem, and obtain a family of exact solutions in the form of single solitons and soliton trains (what is the formula for them?).

We interpret the collective oscillations as Bloch precession of Anderson pseudospins, where each soliton causes a pseudospin 2π Rabi rotation. (I don't understand this interpretation. what is the general idea here??)

Numerical simulations demonstrate robustness of the solitons with respect to noise and damping.

(what is Feshbach resonance????)
Dilute fermionic alkali gases cooled below degeneracy [1] are expected to host the paired BCS state [2, 3]. (why????)

One of the unique and attractive features of this system which makes it qualitatively different from superconducting metals is the possibility to control the strength of pairing interaction and change it by using the Feshbach resonances [4, 5, 6, 7, 8, 9]. (how exactly???? I'll write it in a note on clod gases)

Pairing enhancement near the resonances (Pairing enhancement????), as well as the high coherence of atomic systems (high coherence????), can allow to realize the strong coupling BCS regime (??? how the SC is different in it compared to a weak coupling??), as well as to explore the time dynamics of the paired state.

Since the characteristic energy scales in atomic vapors are relatively low, one can perform time-resolved measurements on the intrinsic microscopic time scales (how are they connected??), and explore a range of fundamentally new phenomena in the time dynamics of the paired state. These new prospects helped to revive interest in some of the basic issues of the BCS pairing problem [10, 11, 12, 13, 14, 15].
(which issues??)

In particular, one of the important questions has to do with the dynamics and characteristic times of formation of the BCS state in cold gases [16]. (maybe times are discussed in Houbiers99??? I'll check later)
The dynamics of the superconducting state in metals, described by BCS theory, has been a subject of active research for a long time [17]. (I am not sure that there is something about it in Tinkham, I'll check later. maybe, there are important explanations)

Generally, there are two important time scales to be considered: the quasiparticle energy relaxation time τ_ϵ, and the characteristic time of the order parameter change, τ_Δ, estimated as the inverse increment of Cooper instability [18, 19].
((???? I don't know why it is so??? didn't find answer in Schmid's article). nothing is about it in Volkov Kogan and Larkin's articles, I'll continue later this search)

For $\tau_\epsilon \ll \tau_\Delta$ (it is very not clear. do we mean that τ_ϵ is the time during which the dynamics occur, and τ_Δ is the time interval that is present in the system? what is τ_Δ???? a very not clear statement), quasiparticles quickly reach local equilibrium parameterized by a time-dependent order parameter $\Delta(t)$.
In this case the dynamics is described by the time-dependent Ginzburg-Landau (TDGL) equation for $\Delta(t)$, with the relaxation time scale *ca.* τ_Δ (what is the relaxation time scale?).
However, as noted by Gorkov and Eliashberg [20], this scenario applies only to relatively exotic situations. (??? I'll read it later, I have this article)
For example, it works for in a proximity of a transition point, $\Delta^2/T_c \ll \tau_\epsilon^{-1}$, or a fast pair breaking (e.g., due to paramagnetic impurities).
(work out this cases!!! paramagnetic impurities and proximity of a transition point)

In the opposite limit, which takes place at the temperatures not too close to critical,

$$\tau_\epsilon \gg \tau_\Delta \tag{9.1}$$

the system dynamics is usually described by Boltzmann kinetic equation for quasiparticles and a self-consistent equation for $\Delta(t)$ connecting it with the quasiparticle distribution function locally in time [21, 22].

(work out Aronov74 and LarkinOvchinikov!!! sounds like they are about something else)

The validity of this approach requires, in addition to (9.1), that the variation in time of both the quasiparticle distribution and the external parameters (e.g., magnetic field or voltage) is sufficiently slow on the τ_Δ time scale (what if it is not so?).

(in other words, gap changes fast, other parts of the system do not change, so seems that is is the same criterion! maybe it is a bad statement.)

The origin of this criterion is seen most easily if one notes that the order parameter can exhibit free oscillations with a frequency *ca.* τ_Δ^{-1} [23] (what did Anderson58 write about it?) (also, see below). (maybe I'll understand it from below)

Thus, at a slow parameter variation the order parameter $\Delta(t)$ (means "slow variation of order parameter", bad formulation) and the quasiparticle spectrum will adiabatically follow the changes of the quasiparticle distribution (quasiparticle spectrum is $\sqrt{\xi^2+\Delta^2}$, how can it follow the distribution??? it follows the change of the gap), without exciting the oscillations of Δ. (how could at all there be oscillations of Δ because of change of spectrum which is determined by the gap always??)

This approximation is relevant to the majority of situations in superconducting metals because of the relatively big value of Δ (what is meant by a big value of the gap?) and the difficulty of changing the external parameters and making measurements on the time scale of τ_Δ.

From this point of view, the cold fermionic gases present a completely new situation. The energy relaxation in these systems is quite slow (why???), while the external parameters, such as the detuning from Feshbach resonance, can change very quickly on the time scale of τ_Δ.

Thus the BCS correlations in this case build up in a coherent fashion while the system is out of thermal equilibrium. In such a situation, theory must account not only for the order parameter evolution, but also for the full dynamics of individual Cooper pairs and quasiparticles.

(not explained, why???)

It seems to be desirable to understand better this 'fast BCS buildup' regime, since the lifetime of the gas samples is finite (what is it??), while the time-resolved measurements can easily be performed with resolution better than τ_Δ.

In this article we consider the situation when the pairing interaction is switched on essentially instantly, on a time scale $\tau_0 \ll \tau_\Delta, \tau_\epsilon$. We shall discuss only the spatially uniform situation, relevant for samples of finite size, and explore the time evolution of the unpaired ideal Fermi gas, which is unstable with respect to Cooper pairing. At not too long times, $t \ll \tau_\epsilon$, the dynamics of the system is governed by nondissipative equations which conserve both the entropy and the total energy.

(which equations???)

A stationary superconducting state with the same energy as that of the initial state would have more quasiparticles, and thus would have entropy *higher* than the initial Fermi gas entropy.

(not clear, why entropy is here?)

This argument suggests that the system can reach a stationary (not necessarily equilibrium) state only at a very long time of the order τ_ϵ.

(not clear, why stationary is not equilibrium???)

On shorter times, which nevertheless can exceed τ_Δ), the system will exhibit a nonlinear time evolution. During this period of time *the concept of the quasiparticle spectrum is irrelevant*

and theory can rely neither on the kinetic equation, nor on TDGL equation.

(!!!!!!! WRIT THIS EXPLICITLY!!! FIND OUT, WHY IS IT SO??? a very big statement)

Below, we present an approach which describes the BCS state buildup and accounts for coherent dynamics of individual Cooper pairs. We shall focus on the zero temperature case, when $\tau_\Delta \simeq \Delta^{-1}$, and show that the result of Cooper instability is a periodic oscillation $\Delta(t)$ having the form of a soliton train.

(write, what is a train solution?)

This regime can be described by the BCS hamiltonian

$$\mathcal{H} = \sum_{\mathbf{p},\,\sigma} \epsilon_{\mathbf{p}} a^+_{\mathbf{p},\sigma} a_{\mathbf{p},\sigma} - \frac{\lambda(t)}{2} \sum_{\mathbf{p},\mathbf{q}} a^+_{\mathbf{p}\uparrow} a^+_{-\mathbf{p}\downarrow} a_{-\mathbf{q}\downarrow} a_{\mathbf{q}\uparrow}\,, \tag{9.2}$$

with the coupling turned on abruptly, $\lambda(t) = \lambda\theta(t - t_*)$.

(I thought that slow dynamics of the coupling constant is needed, but okay)

The main result of this work is that the time-dependent problem (9.2) is integrable. We generalize the BCS solution, which is exact for the separable pairing Hamiltonian (9.2), and demonstrate that at $t > t_*$ the many-body state evolves as

$$|\Psi(t)\rangle = \prod_{\mathbf{p}} \left(u_{\mathbf{p}}(t) + v_{\mathbf{p}}(t) a^+_{\mathbf{p},\uparrow} a^+_{-\mathbf{p},\downarrow}\right) |0\rangle \tag{9.3}$$

(which is obvious because it is the BCS wavefunction)

The Bogoliubov mean field treatment, which gives a state of the form (9.3), relies on the 'infinite range' (it is not true, we assume often that there is a Debye window) form of the pairing interaction in (9.2) (i.e., equal coupling strength of all $(\mathbf{p}, -\mathbf{p})$, $(\mathbf{q}, -\mathbf{q})$). Since the latter does not depend on the system being in equilibrium, one can introduce a time-dependent mean field pairing function

$$\Delta(t) = \lambda \sum_{\mathbf{p}} u_{\mathbf{p}}(t) v^*_{\mathbf{p}}(t) \tag{9.4}$$

(it is not clear, why this is still can be defined for nonequlibrium, but we can just take this equation from the equilibrium case and work with it)

The amplitudes $u_{\mathbf{p}}(t)$, $v_{\mathbf{p}}(t)$ can be obtained from the Bogoliubov-deGennes equation

$$i\partial_t \begin{pmatrix} u_{\mathbf{p}} \\ v_{\mathbf{p}} \end{pmatrix} = \begin{pmatrix} \epsilon_{\mathbf{p}} & \Delta \\ \Delta^* & -\epsilon_{\mathbf{p}} \end{pmatrix} \begin{pmatrix} u_{\mathbf{p}} \\ v_{\mathbf{p}} \end{pmatrix} \tag{9.5}$$

to be solved along with the self-consistency condition (9.4).

We recall that the unpaired state is a self-consistent, albeit unstable, solution of Eqs. (9.5),(9.4) with $\Delta = 0$, $T = 0$: $u^{(0)}_{\mathbf{p}}(t) = e^{-i\epsilon_{\mathbf{p}} t}\theta(\epsilon_{\mathbf{p}})$, $v^{(0)}_{\mathbf{p}}(t) = e^{i\epsilon_{\mathbf{p}} t}\theta(-\epsilon_{\mathbf{p}})$ (I didn't know formulas for u,v, derive it). The stability analysis [19] (read it later, interesting!!) shows that the deviation from the unpaired state grows as $\Delta(t) \propto e^{\gamma t} e^{-i\omega t}$,

$$\delta u_{\mathbf{p}}(t) = \frac{\Delta(t) v^{(0)}_{\mathbf{p}}(t)}{i\gamma - 2\epsilon_{\mathbf{p}} + \omega}, \quad \delta v_{\mathbf{p}}(t) = \frac{\Delta^*(t) u^{(0)}_{\mathbf{p}}(t)}{i\gamma + 2\epsilon_{\mathbf{p}} - \omega} \tag{9.6}$$

with the growth exponent γ and the constant ω given by

$$1 = \lambda \sum_{\mathbf{p}} \frac{\operatorname{sgn} \epsilon_{\mathbf{p}}}{2\epsilon_{\mathbf{p}} - \zeta}, \quad \zeta = \omega + i\gamma \tag{9.7}$$

The electron-hole symmetry near the Fermi level, $N(\epsilon_{\mathbf{p}}) = N(-\epsilon_{\mathbf{p}})$, makes the frequency shift ω vanish. ((???? why???))

Using the similarity between Eq. (9.7) and the BCS gap equation at $T = 0$, the exponent γ can be shown to be close to the BCS gap value Δ_0. (In fact, in the constant density of states approximation, the two quantities coincide: $\gamma = \Delta_0$. (maybe it is deriven in some papers before, currently I don't understand it)) Thus, we estimate the time $\tau_\Delta \simeq \Delta_0^{-1}$.

(this is maybe obvious from Abrahams66, but I have no idea how how it works???)

Our goal will be to provide insight in the evolution at later times, $t \geq \gamma^{-1}$ (it iwas just written that there will be just a stationary state, no evolution???). We rely on the nondissipative character of the Bogoliubov-deGennes dynamics (9.5),(9.4), manifest, for instance, in the energy $E = \langle\Psi(t)|\mathcal{H}|\Psi(t)\rangle$ conservation throughout the evolution. Since in the initial, unpaired state, E is larger than the BCS condensation energy, the system cannot relax to equilibrium. (it is written below that we consider fast times, that is why)

Eqs. (9.5),(9.4) hold at times shorter than quasiparticle thermalization time, $\tau_\epsilon^{-1} \propto \max[T^2, \epsilon^2]$ in Fermi liquid. For the temperatures away from the BCS transition, the time τ_ϵ is very long compared to the instability growth time

$$\tau_\epsilon \gg \gamma^{-1} \quad (\epsilon \simeq \Delta_0), \tag{9.8}$$

indicating (how does it indicate???) a long *nondissipative nonlinear phase* that follows the linear instability phase. Below we show that the evolution governed by Eqs. (9.5),(9.4) is described by soliton-like pulses in the $|\Delta|$. We obtain a family of exact solutions of the form of single solitons and soliton trains, and compare it with simulations.

We briefly note that the importance of coherent dynamics of individual Cooper pairs (9.3) in the time evolution of a paired state has been understood some time ago in the context of the discussion of the validity of the time-dependent Ginzburg-Landau equation approach [18, 19] (have no idea which role do individual Cooper pair play??).

It has been pointed out by Gorkov and Eliashberg [20, 17] that the time-dependent pairing function Δ is generally insufficient to describe the evolution. (why?? read their articles!!!)

For that to be possible, the pair breaking and energy relaxation must be fast compared to the time of change of Δ (why??). This can be realized only close to the BCS transition, or in special situations, such as superconductors with magnetic impurities [20]. (????)

Usually, however, the Cooper pairs *are not slaved* to the time-dependent $\Delta(t)$, and the dynamics of each pair has to be treated individually, via Eq. (9.5).

(have no idea, how??)

The interaction switching, while nonadiabatic, must also be gentle enough not to overheat the fermions above $T \simeq \Delta_0$. The effective temperature T_{eff} after switching can be estimated from the total energy increase, giving

$$aT_{\text{eff}}^2 = \sum_{\omega,\,1\ldots4} \hbar\omega n_1 n_2 (1-n_3)(1-n_4)|\lambda_\omega|^2 \delta(\hbar\omega - \delta E) \tag{9.9}$$

with $n_i = n(\epsilon_{\mathbf{p}_i})$, $\delta E = \epsilon_{\mathbf{p}_3} + \epsilon_{\mathbf{p}_4} - \epsilon_{\mathbf{p}_1} - \epsilon_{\mathbf{p}_2}$, $a = \frac{\pi^2}{6}\nu$.

(where does this formula come from????)

For the interaction switching from 0 to λ over a characteristic time τ_0, the RHS of (9.9) is of the order of $\lambda^2\tau_0^{-3}$. Thus the cold T_{eff} condition is $E_F\tau_0 \gg (\lambda n/\Delta_0)^{2/3}$, which is compatible with the nonadiabaticity requirement $\tau_0 \ll \tau_\Delta$.

(below, there is a solution, so in general I understand what is going on???)

At $T = 0$, a soliton solution of Eqs. (9.5),(9.4) can be constructed most naturally in terms of the variable (why??)

$$w_{\mathbf{p}} = \begin{cases} u_{\mathbf{p}}/v_{\mathbf{p}}, & \epsilon_{\mathbf{p}} > 0 \\ v_{\mathbf{p}}/u_{\mathbf{p}}, & \epsilon_{\mathbf{p}} < 0 \end{cases} \tag{9.10}$$

Consider first the case $\epsilon_{\mathbf{p}} > 0$. From Eq. (9.5) (do we typically solve BdG like this??? Never did like this yet) we obtain

$$i\partial_t w_{\mathbf{p}} = 2\epsilon_{\mathbf{p}} w_{\mathbf{p}} + \Delta(t) - \Delta^*(t) w_{\mathbf{p}}^2 \tag{9.11}$$

where $\Delta(t)$ is a function of time determined from (9.4).

(I'll redo these calculations later)

Motivated (don't understand this motivation, why???) by the stability analysis (9.6), (9.7), we try the ansatz $\Delta(t) = e^{-i\omega t}\alpha^{-1}(t)$ with $\alpha(t)$ real, and

$$w_{\mathbf{p}}(t) = 2\epsilon_{\mathbf{p}} f(t) - i\dot{f}(t), \quad f(t) \equiv \frac{1}{\Delta^*} = e^{-i\omega t}\alpha(t) \tag{9.12}$$

Substituting this in Eq.(9.11), we obtain an equation

$$i\xi_{\mathbf{p}}\dot{\alpha} + \ddot{\alpha} = \xi_{\mathbf{p}}(\xi_{\mathbf{p}}\alpha - i\dot{\alpha}) + \frac{1}{\alpha}\left(1 - (\xi_{\mathbf{p}}\alpha - i\dot{\alpha})^2\right) \tag{9.13}$$

with $\xi_{\mathbf{p}} = 2\epsilon_{\mathbf{p}} - \omega$. Remarkably, the terms with $\xi_{\mathbf{p}}$ cancel, and Eq. (9.13) takes the same form for all the states,

$$\alpha\ddot{\alpha} = \dot{\alpha}^2 + 1 \tag{9.14}$$

which justifies the ansatz (9.12). (check it, it should be easy)

By a variable substitution $\alpha = e^{\phi}$, Eq. (9.14) can be brought to the form $\ddot{\phi} = e^{-2\phi}$. Integrating the latter equation, obtain $\dot{\phi}^2 + e^{-2\phi} = \gamma^2$, with γ an integration constant. (trace better the origin of γ. is it an effective constant of the model?)

This yields $\dot{\alpha}^2 = \gamma^2\alpha^2 - 1$,

$$\alpha(t) = \frac{1}{\gamma}\cosh\gamma(t - t_0), \quad \Delta(t) = \frac{\gamma e^{-i\omega t}}{\cosh\gamma(t - t_0)} \tag{9.15}$$

(this is a great solution, check it later)

The modulus $|\Delta|$ time dependence (Fig.**??**, upper left), growing first, then decreasing and taking the system back to the unpaired state, reflects the absence of dissipation (because in BdG, there was no dissipation, right??? about time scales of validity of this solution - I don't understand it). The time t_0 at which $|\Delta|$ peaks is set by the initial condition at large negative times $t \sim t_*$.

For $\epsilon_{\mathbf{p}} < 0$, $w_{\mathbf{p}} = v_{\mathbf{p}}/u_{\mathbf{p}}$, the form of Eq. (9.11) remains the same up to a sign change $\epsilon_{\mathbf{p}} \to -\epsilon_{\mathbf{p}}$ and the permutation $\Delta \leftrightarrow \Delta^*$. Accordingly, the ansatz for $w_{\mathbf{p}}$ in this case is $w_{\epsilon_{\mathbf{p}}<0}(t) = 2|\epsilon_{\mathbf{p}}|f(t) - i\dot{f}(t)$, $f(t) \equiv \Delta^{-1} = e^{i\omega t}\alpha(t)$. The resulting equation for $\alpha(t)$ is identical to Eq. (9.14). (check later, it should be easy)

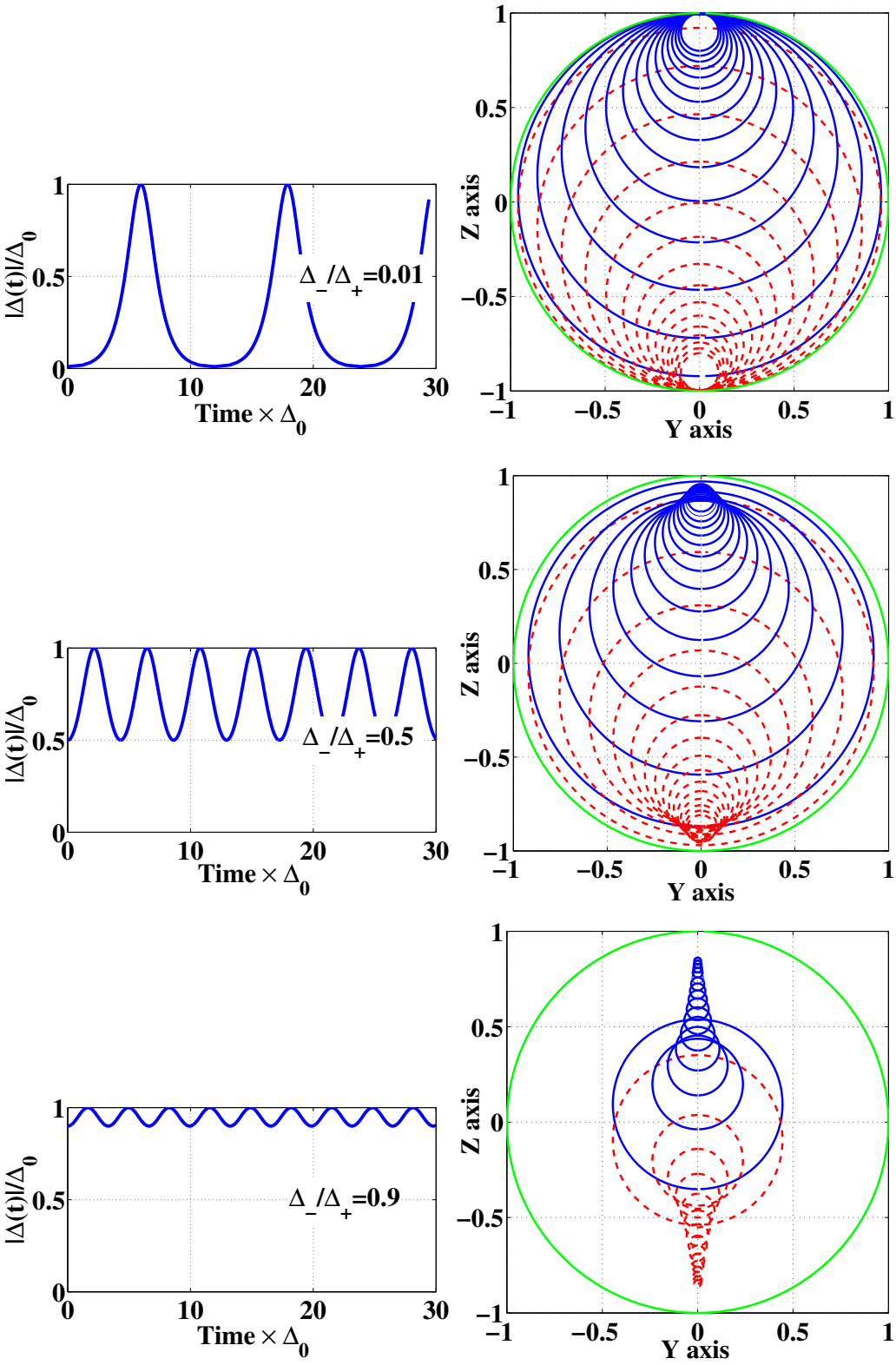
The last step is to analyze the requirements on this solution due to the self-consistency condition (so before, there are solutions that are not self consistent yet??? I don't see it yet) (9.4). For that, we rewrite Eq. (9.4) in terms of $w_{\mathbf{p}}(t)$ as

$$\Delta(t) = \lambda \sum_{\epsilon_{\mathbf{p}}>0} \frac{w_{\mathbf{p}}(t)}{1 + |w_{\mathbf{p}}(t)|^2} + \lambda \sum_{\epsilon_{\mathbf{p}}<0} \frac{w_{\mathbf{p}}^*(t)}{1 + |w_{\mathbf{p}}(t)|^2} \tag{9.16}$$

(check it, should be easy) and note that both the right and the left hand side have the same time dependence (why??), and are equal to each other provided that the quantity $\zeta = \omega + i\gamma$ satisfies Eq. (9.7). (I don't understand, why? this may be not that easy to see...)

This means (why??)that the gap modulus $|\Delta(t)|$ peak value is equal to the instability exponent γ defined by (9.7). (still I don't understand where γ comes into the game? is there an explicit formula for it??)

(to understand what is below, think about the Bloch sphere for SC!!)
(I don't understand, what is here Δ_-, Δ_+)



Coherent BCS dynamics on the Bloch sphere (9.17). Trajectories of individual Cooper pair states for the soliton train solutions (Eq. (9.27) and insets) oscillating in the limits $\Delta_- \leq \Delta(t) \leq \Delta_+$ are shown. Note that each state completes a full 2π Rabi cycle per soliton. The red and blue curves correspond to the energies $\epsilon_{\mathbf{p}}$ above and below the Fermi level.

At $T = 0$, in the case of a constant density of states (how is it?), γ is equal to the equilibrium BCS gap Δ_0, while ω vanishes due to particle-hole symmetry. Thus, remarkably, the modulus $|\Delta(t)|$ in this case peaks exactly at Δ_0. (check it later, I don't understand it, but maybe it follows from what is written before)

(write in the note on SC discussion of Bloch sphere, maybe it is not connected with Anderson's spins, since we don't use them at this stage at all) To illustrate the collective dynamics in the soliton solution, we plot the trajectories $u_{\mathbf{p}}(t)$, $v_{\mathbf{p}}(t)$ on the Bloch sphere $r_1^2 + r_2^2 + r_3^2 = 1$ using the parameterization

$$r_1 + ir_2 = 2u_{\mathbf{p}}v_{\mathbf{p}}^*; \quad r_3 = |u_{\mathbf{p}}|^2 - |v_{\mathbf{p}}|^2 \tag{9.17}$$

(Fig. **??**, left). Here, as well as in the soliton train solutions discussed below (Eq. (9.27)), each state $(u_{\mathbf{p}}, v_{\mathbf{p}})$ completes a full Rabi cycle per soliton. (completes a full Rabi cycle per soliton???)

The trajectories, which are small loops (don't understand the loops...) for the pairs with large energies $\epsilon_{\mathbf{p}}$, turn into a big circle as $\epsilon_{\mathbf{p}}$ tends to the Fermi level.

To gain further insight, we reformulate the Bogoliubov approach, following Anderson [23], in terms of pseudospins associated with individual Cooper pair states.

(still don't understand, why it is so useful??)

'Pauli spin' operators $\sigma_{\mathbf{p}}^{\pm} \equiv \frac{1}{2}(\sigma_{\mathbf{p}}^x \pm i\sigma_{\mathbf{p}}^y)$ can be assigned to each pair of fermions with opposite momenta as follows

$$\sigma_{\mathbf{p}}^+ = a_{\mathbf{p}\uparrow}^+ a_{-\mathbf{p}\downarrow}^+, \quad \sigma_{\mathbf{p}}^- = a_{-\mathbf{p}\downarrow} a_{\mathbf{p}\uparrow} \tag{9.18}$$

The identity $\sigma_{\mathbf{p}}^z \equiv [\sigma_{\mathbf{p}}^+, \sigma_{\mathbf{p}}^-] = a_{\mathbf{p}\uparrow}^+ a_{\mathbf{p}\uparrow} - a_{-\mathbf{p}\downarrow} a_{-\mathbf{p}\downarrow}^+$ allows to map the problem (9.2) onto an interacting spin problem

$$\mathcal{H} = \sum_{\mathbf{p}}{}' \epsilon_{\mathbf{p}} \sigma_{\mathbf{p}}^z - 2\lambda \sum_{\mathbf{p},\mathbf{q}}{}' \sigma_{\mathbf{p}}^+ \sigma_{\mathbf{q}}^- \tag{9.19}$$

where $\sum_{\mathbf{p}}'$ means a sum over the pairs of states $(\mathbf{p}, -\mathbf{p})$. (I hope that this is the typical Anderson's theory)

Since all the spins interact with each other equally, the mean field theory here is exact, just like for the BCS problem. The mean field hamiltonian for each spin is

$$\mathcal{H}_{\mathbf{p}} = \mathbf{b}_{\mathbf{p}} \cdot \sigma_{\mathbf{p}}, \quad \mathbf{b}_{\mathbf{p}} = (-\Delta', -\Delta'', \epsilon_{\mathbf{p}}) \tag{9.20}$$

(derive it! maybe it is not hard. work out Anderson's paper)

Here the z component of the effective field $\mathbf{b}_{\mathbf{p}}$, given by the single particle energy, is spin-specific (spin-specific?? there is no spin here), while the transverse components, the same for all of the spins, satisfy

$$\Delta \equiv \Delta' + i\Delta'' = \lambda \sum_{\mathbf{q}} \langle \sigma_{\mathbf{q}}^+ \rangle \tag{9.21}$$

which is analogous to the BCS gap relation. (isn't it the BCS gap relation but in terms of spins?)

In the ground state each spin is aligned with $\mathbf{b}_{\mathbf{p}}$, and the spins form a texture (which texture?) near the Fermi surface [23], with spin rotation described by the Bogoliubov angle.

Bloch representation

The dynamical problem of interest can be cast in the form of Bloch equations for the spins,

$$\dot{\sigma}_{\mathbf{p}} = i[\mathcal{H}_{\mathbf{p}}, \sigma_{\mathbf{p}}] = 2\mathbf{b}_{\mathbf{p}} \times \sigma_{\mathbf{p}} \tag{9.22}$$

with the field $\mathbf{b}_{\mathbf{p}}$ defined self-consistently by (9.20),(9.21). Anderson [23] used Eq. (9.22), linearized about the texture ground state, to study collective excitations of a superconductor (see also [24]). Linearized about the unpaired state, Eq. (9.22) yields an instability identical to (9.6), (9.7).

Simulations

(Have no idea what is meant here, I need to read it more)

The Bloch dynamics is suitable for simulation (Fig. 9.1), since Eq. (9.22) is linear in spin operators and can be replaced by an equation for the expectation values (9.17). Typical $\Delta(t)$, observed in the presence of thermal noise, is an orderly sequence of the cosh solitons (Fig. 9.1, top), indicating robustness of soliton solution (*cf.* Ref.[25]).

(one needs to read Galperin81 to understand it, maybe...)

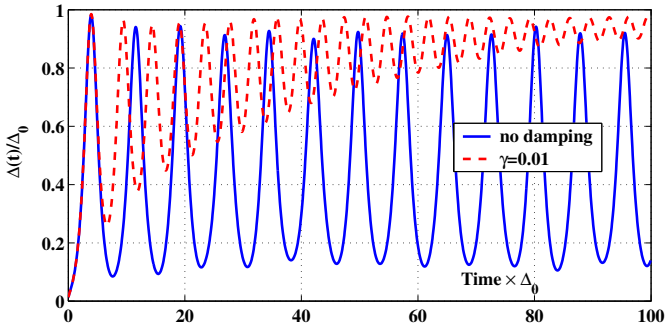


Figure 9.1: Bloch dynamics $\dot{\mathbf{r}}_{\mathbf{p}} = 2\mathbf{b}^{\text{eff}}_{\mathbf{p}} \times \mathbf{r}_{\mathbf{p}}$ for 10^3 spins with a constant density of states, with $\mathbf{b}^{\text{eff}}_{\mathbf{p}}$ defined by (9.20),(9.23). Initial conditions $r_{3,\mathbf{p}} = \tanh(\frac{1}{2}\beta\epsilon_{\mathbf{p}})$, $(r_1 + ir_2)_{\mathbf{p}} = e^{i\phi_{\mathbf{p}}}(1 - r_3^2)^{1/2}$, with $\beta^{-1} \equiv T = 0.1\Delta_0$ and random uncorrelated $0 < \phi_{\mathbf{p}} < 2\pi$ were used to simulate thermal noise.

The effect of damping can be studied by replacing

$$\mathbf{b}_{\mathbf{p}} \to \mathbf{b}^{\text{eff}}_{\mathbf{p}} = \mathbf{b}_{\mathbf{p}} - \gamma \mathbf{b}_{\mathbf{p}} \times \mathbf{r}_{\mathbf{p}} \tag{9.23}$$

with a dimensionless damping constant, $\gamma \sim 1/(\Delta_0 \tau_\epsilon)$. This destroys integrability and prompts relaxation to BCS equilibrium (Fig. 9.1, bottom).

Nonlinear Evolution

(what is different comparing to what was before?)

In our nonlinear dynamical problem, we have to solve the Bloch equations (9.22) together with the self-consistency relation (9.21). As above, we assume the pairing amplitude time dependence of the form $\Delta(t) = e^{-i\omega t}\Omega(t)$, where $\Omega(t)$ is real and ω is a constant frequency shift to be fixed by the relation (9.21). In the Larmor frame rotating with the frequency ω, Eq. (9.22), written for the spins average polarization $r_i = \langle \sigma^i_{\mathbf{p}} \rangle$ components, reads

$$\dot{r}_1 = -\xi_{\mathbf{p}} r_2, \quad \dot{r}_2 = \xi_{\mathbf{p}} r_1 + 2\Omega r_3, \quad \dot{r}_3 = -2\Omega r_2 \tag{9.24}$$

with $\xi_{\mathbf{p}} = 2\epsilon_{\mathbf{p}} - \omega$, as before. (check it, it can be not hard)

An exact solution can be obtained from the ansatz

$$r_1 = A\Omega, \quad r_2 = B\dot{\Omega}, \quad r_3 = C\Omega^2 - D \tag{9.25}$$

The first and the third equation (9.24) are satisfied by (9.25) provided $A = -\xi_{\mathbf{p}} B$ and $B = -C$, while the second equation (9.24) is consistent with the normalization condition $r_1^2 + r_2^2 + r_3^2 = 1$, and thus yields

$$C^2\xi_{\mathbf{p}}^2\Omega^2 + C^2\dot{\Omega}^2 + (C\Omega^2 - D)^2 = 1 \tag{9.26}$$

Eq. (9.26) will take the same form for all the spins,

$$\dot{\Omega}^2 + (\Omega^2 - \Delta_-^2)(\Omega^2 - \Delta_+^2) = 0, \quad \Delta_- \le \Delta_+ \tag{9.27}$$

provided that the constants D, C are chosen as

$$(D^2 - 1)/C^2 = \Delta_-^2\Delta_+^2, \quad 2D/C = \xi_{\mathbf{p}}^2 + \Delta_-^2 + \Delta_+^2 \tag{9.28}$$

with the sign factor $\operatorname{sgn}\epsilon_{\mathbf{p}}$. Eq. (9.27) defines an elliptic function $\Omega(t)$ oscillating periodically between Δ_- and Δ_+. At $\Delta_- \ll \Delta_+$, the solution is a train of weakly overlapping solitons (9.15) with $\Delta_+ = \gamma$ (Fig. **??**, left).

The real part of the self-consistency relation (9.21),

$$1 = \lambda \sum_{\mathbf{p}} \frac{\xi_{\mathbf{p}} \operatorname{sgn}\epsilon_{\mathbf{p}}}{\left((\xi_{\mathbf{p}}^2 + \Delta_-^2 + \Delta_+^2)^2 - 4\Delta_-^2\Delta_+^2\right)^{1/2}} \tag{9.29}$$

fixes one of the constants $\Delta_\pm$, the other one being a free parameter that controls the inter-soliton time separation. With the ratio Δ_-/Δ_+ varying from 0 to 1, the soliton frequency increases, and the weakly overlapping solitons (9.15) gradually become overlapping more strongly, turning into weak harmonic oscillations (Fig. **??**).

We note that the weak oscillation limit has been investigated by Volkov and Kogan [24] with the help of linearized Gorkov equation, and earlier by Anderson [23], who used pseudospin representation. The nonexponential decay of the lianearized oscillations [18, 24] was interpreted as collisionless damping, related to strong mixing of the oscillations of Δ with the states of two excited quasiparticles slightly above the superconducting gap.

The imaginary part of Eq. (9.21) fixes the value of the frequency shift ω (we recall that $\omega \neq 0$ in the presence of charge asymmetry). At $\Delta_- \ll \Delta_+$, Eq. (9.29) turns into Eq. (9.7) which, as we found above, defines the amplitude of a single soliton. In the opposite limit, $\Delta_- \to \Delta_+$, Eq. (9.29) coincides with the BCS gap equation.

There is an interesting relation between our problem and the self-induced transparency phenomenon [26] (self-induced transparency phenomenon??? I don't understand this paragraph, I'll read McCall67 maybe later and then think about it). In the latter, an optical pulse interacting with an ensemble of atoms can dissipate its energy by inducing resonant Rabi transitions in the atoms. However, when the pulse duration is tuned so that the atoms complete a full Rabi 2π cycle as the pulse goes by, the pulse sustains itself and propagates without dissipation. The Bloch equations describing this phenomenon bear striking similarity to our Eqs. (9.22), while the atoms' polarization is employed [26] to provide feedback on the pulse instead of our BCS self-consistency relation.

Before concluding, we note that the dynamics at finite temperature, in the regime described by Eq. (9.1), remains an open problem. In particular, we can not rule out the possibility of chaotic behavior. At $T = 0$ the problem has a relatively simple solution, periodic in time,

because in this case the quasiparticles with low energies are strongly coupled to the oscillations of Δ. In contrast, in the case $T\tau_\Delta \gg 1$ there are two groups of quasiparticles: those with energies $\epsilon_{\mathbf{p}} \sim \tau_\Delta^{-1}$, which fully participate in the oscillations, as above, and the quasiparticles with $\tau_\Delta^{-1} \ll \epsilon_{\mathbf{p}} \ll T$, coupled to $\Delta(t)$ much weaker and playing the role of a thermal bath, thereby providing dissipation.

9.2 My Notes about the article "Solitons, Rabi Oscillations in a TD BCS"

Summary of time scales

(write which are here and why???? it is not that clear in the article)

What does nonadiabaticity mean?

(really, I don't understand...)

10 Synchronization in the BCS Pairing Dynamics as a Critical Phenomenon by Barankov, Levitov

10.1 Theory

Abstract

Fermi gas with time-dependent pairing interaction hosts several different dynamical states. (which???)

Coupling between the collective BCS pairing mode and individual Cooper pair states can make the latter either synchronize or dephase. (why???)

We describe transition from phase-locked undamped (phase-locked undamped?) oscillations to Landau-damped (Landau-damped) dephased oscillations in the collisionless, dissipationless regime as a function of coupling strength.

In the dephased regime, we find a second transition at which the long-time asymptotic pairing amplitude vanishes.

Using a combination of numerical and analytical methods we establish a continuous (type II) character of both transitions.

(maybe in this article they show the proper way how to deal with Anderson's formalism? and these are the results if one decides to do it???)

Introduction

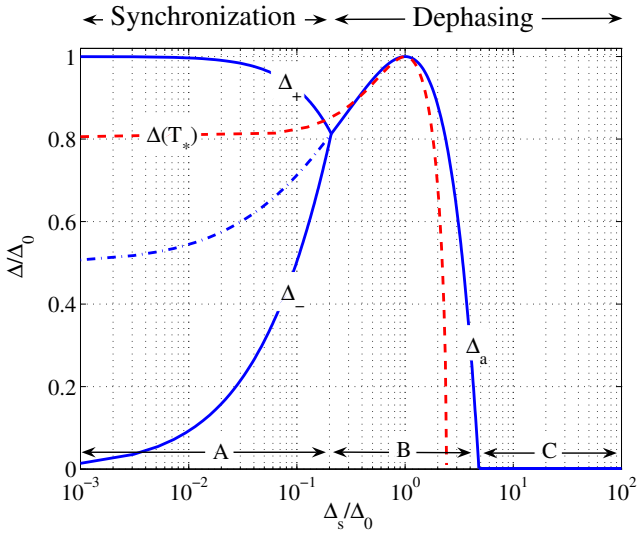


Figure 10.1: Three regimes of the pairing dynamics *vs.* the initial gap value Δ_s (why it is allowed that $\Delta_s = 100\Delta_0$???why B region is righter than the red curve???). In synchronized phase (A), $\Delta_s < \Delta_{AB}$, the pairing amplitude oscillates between Δ_- and Δ_+. In the dephased regime (B, C), the pairing amplitude saturates to a constant value, Δ_a, when $\Delta_{AB} \leq \Delta_s < \Delta_{BC}$, and decreases to zero at $\Delta_s \geq \Delta_{BC}$. Dashed line: The stationary gap value $\Delta(T_*)$ reached in a closed system after equilibration.

Recent discovery of BCS pairing in fermionic vapors [1, 2], made possible by control of interactions in trapped cold gases [3], has renewed interest in quantum collective phenomena [4].
(why????)
Advanced detection techniques and long coherence times in vapors enable time-resolved studies of new collective modes, such as spin waves [5] and the BCS pairing mode [6].
(another articles with a lot of theory about it...)
Interaction between a collective mode and constituting particles is key for our understanding of dynamics in various systems, from plasma to quantum gases.
(not explained, why???)
One of the most surprising of these phenomena is Landau damping which occurs in a collisionless regime via direct dissipationless energy transfer from the collective mode to single particles. Its nondissipative and thus reversible character [7] leads to a variety of regimes, notably to quenching of the damping, first explored in plasma physics [8].
(I need to read about it, never heard about it.)
Remarkably, a linearly damped mode can regrow and transform to a stationary oscillatory Bernstein-Greene-Kruskal mode. This fascinating prediction was confirmed experimentally only recently [9].
(????? never read about it before)

Naturally, the richness of these nonlinear phenomena makes it tempting to look for their analogs in cold gases. Collisionless damping in cold gases was considered, in the linear regime, for (why in all these models we can neglect collisions?) optical excitations [10], spin waves [11, 12], and excitations in optical lattices [13].
Motivated by the work on fermion superfluidity [1, 2, 6], here we focus on the pairing dynamics of fermions [14, 15, 16, 17] induced by a sudden change of interaction.

The collisionless regime becomes practical in this case due to long elastic collision times $\tau_{\rm el} \gg \tau_\Delta = \hbar/\Delta$ [14], where Δ is the BCS gap (is it explained there? I am not sure...).

The pairing mode of a small amplitude oscillates at a frequency $2\Delta/\hbar$ and exhibits collisionless dephasing [24]. (read Volkov's paper again!)

These conclusions were extended recently to the nonlinear regime [19] (where does this regime originate?).

This behavior changes drastically as the perturbation increases. The main result of this work, as summarized in Fig.10.1, is prediction of a dynamical transition resulting from competition between synchronization and collisionless dephasing, taking place as a function of the initial pairing gap, Δ_s.

We found three qualitatively different regimes (A, B, and C) with the critical points at $\Delta_{AB} = e^{-\pi/2}\Delta_0$ and $\Delta_{BC} = e^{\pi/2}\Delta_0$, where Δ_0 is the equilibrium pairing amplitude in the final BCS state. Below the A-B transition, $\Delta_s < \Delta_{AB}$, individual Cooper pair states synchronize and the pairing amplitude oscillates between Δ_+ and Δ_- without damping. In contrast, in the interval $\Delta_{AB} < \Delta_s < \Delta_{BC}$ the pairing amplitude is Landau-damped and exhibits decaying oscilation, saturating at an asymptotic value, Δ_a, with non-monotonic dependence on Δ_s. A second transition occurs at $\Delta_s \geq \Delta_{BC}$, where the dynamics becomes overdamped, and $\Delta(t)$ decreases to zero without oscillations. The oscillation amplitude and the asymptotic value Δ_a vanish continuously at the critical points A-B and B-C, as in a type II transition. We demonstrate that these results are consistent with the spectral analysis [20] based on the integrability of the problem.

We also address the behavior on a long time scale, $t \gtrsim \tau_{\rm el}$, after dissipation sets in. We find that energy relaxation in a closed system, such as an atom trap, makes it evolve to a new equilibrium state. Both the temperature T_* and the gap $\Delta(T_*)$ exhibit a nonmonotonic dependence on the initial conditions (Fig.1).

The Model

In our analysis of the BCS problem we employ the well known pseudospin formulation [23] in which spin 1/2 operators $s^\pm_{\mathbf{p}} = s^x_{\mathbf{p}} \pm i s^y_{\mathbf{p}}$ describe Cooper pairs $(\mathbf{p}, -\mathbf{p})$. The BCS Hamiltonian takes the form

$$\mathcal{H} = -\sum_{\mathbf{p}} 2\epsilon_{\mathbf{p}} s^z_{\mathbf{p}} - \lambda(t) \sum_{\mathbf{p},\mathbf{q}} s^-_{\mathbf{p}} s^+_{\mathbf{q}}, \tag{10.1}$$

where $\epsilon_{\mathbf{p}} = \mathbf{p}^2/2m - \mu$ is the free particle spectrum with μ the Fermi energy. Here we consider the time evolution induced by an instantaneous change of interaction from λ_s at $t < 0$ to λ at $t > 0$. In the spin formulation, Eq.(10.1), the dynamics is of a Bloch form

$$\frac{d\mathbf{r}_{\mathbf{p}}}{dt} = 2\mathbf{b}_{\mathbf{p}} \times \mathbf{r}_{\mathbf{p}}, \quad \mathbf{b}_{\mathbf{p}} = -(\Delta_x, \Delta_y, \epsilon_{\mathbf{p}}), \tag{10.2}$$

where $\mathbf{r}_{\mathbf{p}} = 2\langle \mathbf{s}_{\mathbf{p}} \rangle$ are classical vectors, and the effective magnetic field $\mathbf{b}_{\mathbf{p}}$ depends on the pairing amplitude Δ. The latter is defined self-consistently:

$$\Delta = \Delta_x + i\Delta_y = \frac{\lambda(t)}{2} \sum_{\mathbf{p}} r^+_{\mathbf{p}}, \quad r^+_{\mathbf{p}} = r^x_{\mathbf{p}} + i r^y_{\mathbf{p}}. \tag{10.3}$$

We first present numerical results for the dynamics (10.2), (10.3). The Runge-Kutta method of the 4th order was used with $N = 10^4, 10^5$ equally spaced discrete energy states within a band $W = 50\Delta_0$ with a constant density of states $\nu(E_F)$. As an initial state we take

$$r^+_{\mathbf{p}}(0) = \frac{\Delta_s}{\sqrt{\Delta_s^2 + \epsilon^2_{\mathbf{p}}}}, \quad r^z_{\mathbf{p}}(0) = \frac{\epsilon_{\mathbf{p}}}{\sqrt{\Delta_s^2 + \epsilon^2_{\mathbf{p}}}}. \tag{10.4}$$

which describes the $T = 0$ paired ground state [23].

Without loss of generality we set $\Delta(t) = \Delta_x$, since the phase of Δ is a constant of motion due to the particle-hole symmetry of the model. The interaction constants λ_s and λ define, via the self-consistency relation (10.3), the initial and final equilibrium BCS gap values, $\Delta_s = We^{-1/g_s}$, $g_s = \lambda_s \nu \ll 1$, $\Delta_0 = We^{-1/g}$, $g = \lambda\nu$, which we use to parameterize the system.

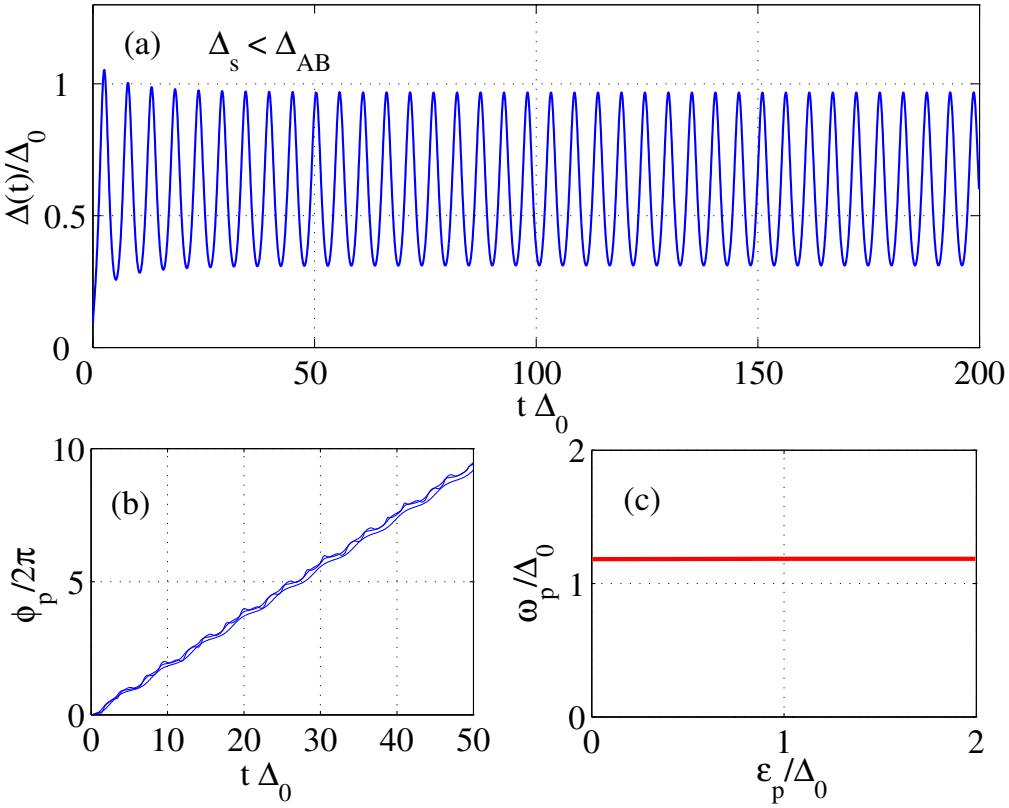


Figure 10.2: (a): The pairing amplitude $\Delta(t)$ for the initial state (10.4) with $\Delta_s = 0.05\Delta_0$ as recorded from the simulation, oscillating between $\Delta_+ = 0.97\Delta_0$ and $\Delta_- = 0.31\Delta_0$; Synchronization (b,c): the phase $\phi_{\mathbf{p}}$ time dependence, Eq.(10.6), for $\epsilon_{\mathbf{p}} = 0, \Delta_0, 2\Delta_0$, and frequency $\omega_{\mathbf{p}}$ *vs.* $\epsilon_{\mathbf{p}}$, Eq.(10.6).

We observe three qualitatively different dynamical regimes. The initial states with a relatively small gap give rise to undamped oscillations (Fig.10.3a). In this case $\Delta(t)$ oscillates non-harmonically between Δ_- and Δ_+ (the regime A in Fig.10.1). Synchronization of different Cooper pair states results from their interaction with the mode singled out by BCS instability of the initial state, similar to the evolution from the normal state [14].

Desynchronization takes place at $\Delta_s \geq \Delta_{AB} = 0.21\Delta_0$ giving rise to two different regimes exhibiting dephasing, underdamped and overdamped (B and C, Fig. 10.1). The former, illustrated in Fig.10.3a, is simplest to understand for a small initial deviation, $\Delta_s \simeq \Delta_0$ [24], by linearizing Bloch equations about the equilibrium state. The analysis predicts damped oscillations at long times:

$$\Delta(t) = \Delta_a + A(t)\sin(2\Delta_a t + \alpha), \quad A(t) \propto t^{-1/2}. \tag{10.5}$$

The power-law decay of $A(t)$ was explained in Ref. [24] by interaction of the collective mode with the continuous spectrum of excitations with energies above $2\Delta_a$ and linked to the linear Landau damping. In the spin formulation, the dephasing results from the Larmor frequency of spin precession $\mathbf{b}_{\mathbf{p}}$ being a continuous function of $\epsilon_{\mathbf{p}}$. An extension of this argument to the nonlinear regime was proposed recently in Ref. [19] which, however, did not clarify the range of its validity. The dephased time evolution similar to (10.5) was also reported in Refs. [16, 17, 22].

In the overdamped regime, $\Delta_s \geq \Delta_{BC} = 4.81\Delta_0$ (Fig.10.3b), $\Delta(t)$ decays to zero without oscillations. This behavior can be understood in the limit $\Delta_s/\Delta_0 \gg 1$, i.e. when the coupling in the initial paired state in (10.1) is suddenly completely turned off. For different spins precessing freely and independently one obtains

$$r_{\mathbf{p}}^{+}(t) = e^{-i2\epsilon_{\mathbf{p}}t} r_{\mathbf{p}}^{+}(0), \quad \Delta(t \gg \Delta_s^{-1}) \propto (\Delta_s t)^{-1/2} e^{-2\Delta_s t}.$$

The fast dephasing can also be understood by noting that the energy distribution in (10.4) corresponds to an effective temperature $T \sim \Delta_s$ which exceeds T_c for Δ_0 (see below).

To fully exhibit phase locking in the synchronized regime which abruptly disappears in the dephased regime, we now explore the phase dynamics. It is convenient to measure precession angles relative to time-independent $\tilde{\mathbf{b}}_{\mathbf{p}} = -(\Delta_a, 0, \epsilon_{\mathbf{p}})$, where Δ_a is the asymptote $\Delta(t \to \infty)$ in the regimes B, C, and the average value of oscillating $\Delta(t)$ in A (dash-dotted line in Fig. 10.1). The angle and frequency of precession are defined by

$$n_{\mathbf{p}}^{+} = n_{\mathbf{p}}^{x} + i n_{\mathbf{p}}^{y} \propto e^{-i\phi_{\mathbf{p}}(t)}, \quad \omega_{\mathbf{p}}(t) = d\phi_{\mathbf{p}}/dt, \tag{10.6}$$

where the vectors $n_{\mathbf{p}}$ are obtained from $r_{\mathbf{p}}$ by a rotation about the y axis which maps $\hat{z}$ onto $\tilde{\mathbf{b}}_{\mathbf{p}}$: $n_{\mathbf{p}}^{y} = r_{\mathbf{p}}^{y}$, $n_{\mathbf{p}}^{x} + i n_{\mathbf{p}}^{z} = e^{i\theta_{\mathbf{p}}}(r_{\mathbf{p}}^{x} + i r_{\mathbf{p}}^{z})$, with the rotation angle defined by $\tan\theta_{\mathbf{p}} = \Delta_a/|\epsilon_{\mathbf{p}}|$. The phase evolution, which becomes linear at long times $\tau \gg \Delta_0^{-1}$ (Figs.10.2,10.3), can be characterized by average frequency (phase slope) $\omega_{\mathbf{p}} = \langle d\phi_{\mathbf{p}}/dt \rangle = (\phi_{\mathbf{p}}(\tau) - \phi_{\mathbf{p}}(0))/\tau$. While in the regime A different $\mathbf{p}$ states phase lock (Fig.10.2b,c), in the regimes B, C the frequencies $\omega_{\mathbf{p}}$ have dispersion (Fig.10.3c,d). The latter reproduces quasiparticle spectrum, $\omega_{\mathbf{p}} = 2(\epsilon_{\mathbf{p}}^2 + \Delta_a^2)^{1/2}$ with the long-time asymptote Δ_a which vanishes in the overdamped regime C.

We observe a qualitative change in behavior, with $\omega_{\mathbf{p}}$ dispersing in the regions B, C and phase locking in the region A. However, the oscillation amplitude $\frac{1}{2}(\Delta_+ - \Delta_-)$ in A and the asymptotic amplitude Δ_a in B vanish continuously at the critical points $\Delta = \Delta_{AB}, \Delta_{BC}$ (Fig.10.1), indicating a type II transition.

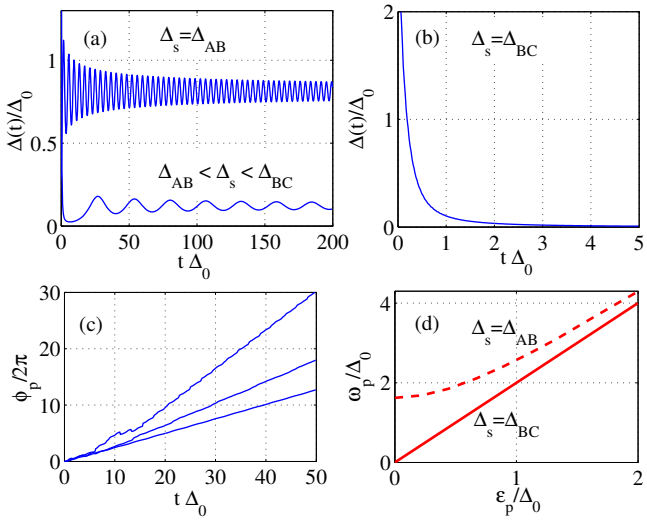


Figure 10.3: Dephased dynamics (a): Simulated $\Delta(t)$ for the initial states (10.4) with $\Delta_s = 0.21\Delta_0$, $4.5\Delta_0$ with the asymptotic values $\Delta_a = 0.81\Delta_0$, $0.12\Delta_0$; Overdamped dynamics (b): Same as in (a) with $\Delta_s = 4.81\Delta_0$ and $\Delta_a = 0$; (c): The phase $\phi_{\mathbf{p}}$ time dependence, Eq.(10.6), for energies $\epsilon_{\mathbf{p}} = 0, \Delta_0, 2\Delta_0$ (bottom to top) for $\Delta_s = 0.21\Delta_0$; (d): The frequency $\omega_{\mathbf{p}}$ *vs.* $\epsilon_{\mathbf{p}}$ for $\Delta_s = 0.21\Delta_0$ (dashed line) and $\Delta_s = 4.81\Delta_0$ (solid line).

Until now, we considered the dissipationless dynamics at times shorter than the quasiparticle relaxation time, $t \lesssim \tau_{\rm el}$. Using the energy balance argument, one can determine the system state at long times, $t \gg \tau_{\rm el}$. To account for system equilibration, one needs to consider the full

many-body Hamiltonian which enables elastic scattering of individual quasiparticles, omitted in Eq.(10.1). For a closed system, such as an atomic trap, the final temperature T_* and the gap Δ_* can be determined from the energy conservation condition $E_{t\gg\tau_{\rm el}}(T_*) = E_0$, where E_0 is the energy immediately after interaction switching,

$$E_0 = \sum_{\mathbf{p}} (\epsilon_{\mathbf{p}} - \tilde{\epsilon}_{\mathbf{p}}) + \frac{\Delta_s^2}{\lambda_s}\left(2 - \frac{\lambda}{\lambda_s}\right), \tag{10.7}$$

with the spectrum $\tilde{\epsilon}_{\mathbf{p}} = (\epsilon_{\mathbf{p}}^2 + \Delta_s^2)^{1/2}$, and $E_{t\gg\tau_{\rm el}}(T_*)$ is the energy of the final state:

$$E_{t\gg\tau_{\rm el}}(T_*) = \sum_{\mathbf{p}} \left[\epsilon_{\mathbf{p}} - (1-2n_{\mathbf{p}})\,\tilde{\epsilon}_{\mathbf{p}}(\Delta_*)\right] + \frac{\Delta_*^2}{\lambda}. \tag{10.8}$$

Here $n_{\mathbf{p}} = 1/\left(1 + e^{\tilde{\epsilon}_{\mathbf{p}}(\Delta_*)/T_*}\right)$ describes equilibrium with $T = T_*$, $\tilde{\epsilon}_{\mathbf{p}}(\Delta_*) = (\epsilon_{\mathbf{p}}^2 + \Delta_*^2)^{1/2}$. After integrating over $\epsilon_{\mathbf{p}}$, we arrive at the equation for T_*:

$$F\left(\frac{\Delta_*}{2T_*}\right) = 1 - \left(\frac{\Delta_s}{\Delta_*}\right)^2 + \alpha\left(\frac{\Delta_s}{\Delta_*}\right)^2 \ln\left(\frac{\Delta_s}{\Delta_0}\right)^2, \tag{10.9}$$

where $F(u) = 2\int_0^\infty dx \cosh 2x\,[1 - \tanh(u\cosh x)]$, and $\alpha = 1 - g\ln(\Delta_s/\Delta_0)$. From Eq.(10.9) we obtain T_* and the equilibrium gap $\Delta_* = \Delta(T_*)$. They are approximately constant, with $T_* \approx 0.72T_c$, $\Delta(T_*) \approx 0.81\Delta_0$ in the regime A, are described by a non-monotonic function in B, and vanish in C. The system turns normal in the final state for $\Delta_s \geq f(g)\Delta_0$, $f(g) = 2.2 + 0.86g + O(g^2)$. Numerical solution of Eq.(10.9) at $g = 0.26$ is displayed in Fig.10.1 (dashed line).

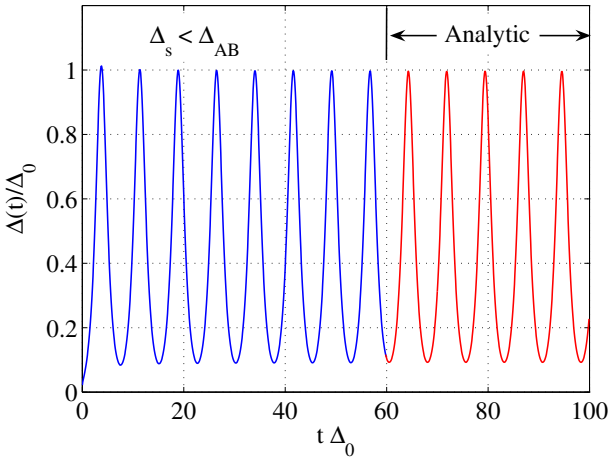


Figure 10.4: The pairing amplitude $\Delta(t)$ as a function of time for the initial state (10.4) with $\Delta_s = 0.01\Delta_0$ as recorded from numerical simulation. At long time, numerical $\Delta(t)$ matches the analytic form in Eq.(10.13), oscillating non-harmonically between $\Delta_+ = 0.997\Delta_0$ and $\Delta_- = 0.093\Delta_0$.

(so, what is the Lax vector after all??? see cited papers about it)

It is instructive to compare our results to the spectral analysis based on the integrability of the BCS Hamiltonian [23, 24, 20]. There is an infinite number of commuting integrals of motion, $R_{\mathbf{p}} = \mathbf{L}_{\mathbf{p}}\mathbf{s}_{\mathbf{p}}$, parameterized by $\mathbf{p}$, where following Ref. [20] we employ the Lax vector,

$$\mathbf{L}_{\mathbf{p}} = \hat{z} + \lambda \sum_{\mathbf{p}'\neq\mathbf{p}} \frac{\mathbf{s}_{\mathbf{p}'}}{\epsilon_{\mathbf{p}} - \epsilon_{\mathbf{p}'}}. \tag{10.10}$$

We will need $\mathbf{L}_\mathbf{p}^2 = 4(\mathbf{L}_\mathbf{p}\mathbf{s}_\mathbf{p})^2$ which is also conserved (due to the Pauli matrices algebra combined with Eq.(10.10)). The mean-field expressions are obtained by substituting the averages $\langle \mathbf{s}_\mathbf{p} \rangle$ instead of $\mathbf{s}_\mathbf{p}$.

The spectral polynomial defining the evolution of individual states is proportional to the square of the Lax vector [20], $Q(\epsilon) = \mathbf{L}^2(\epsilon) \prod_\mathbf{p} (\epsilon - \epsilon_\mathbf{p})^2$, where $\mathbf{L}(\epsilon_\mathbf{p}) = \mathbf{L}_\mathbf{p}$. The pairs of complex roots of the spectral equation $Q(\epsilon) = 0$ uniquely determine the long-time dynamics of the system [20]. Evaluation of $\mathbf{L}^2(y)$ for the initial state (10.4) is straightforward:

$$\mathbf{L}^2(y)/g^2 = \left(\ln \frac{\Delta_s}{\Delta_0} + yG(y) \right)^2 + G^2(y), \tag{10.11}$$

where $y = \epsilon/\Delta_s$ and

$$G(y) = \frac{1}{2} \int_{-\infty}^{\infty} \frac{dx}{y - \sinh x} = \frac{1}{2\sqrt{1+y^2}} \ln \frac{y + \sqrt{1+y^2}}{y - \sqrt{1+y^2}},$$

where y is complex. One can show that the roots of $\mathbf{L}^2(y)$ lie on the imaginary axis. Upon variation of Δ_s/Δ_0 they disappear at $y = 0$. Expanding about $y = 0$, we obtain

$$\mathbf{L}^2(y)/g^2 = \left(\ln \frac{\Delta_s}{\Delta_0} - \frac{\pi}{2} \right) \left(\ln \frac{\Delta_s}{\Delta_0} + \frac{\pi}{2} \right) + O(y), \tag{10.12}$$

Thus $\mathbf{L}^2(y)$ has no complex roots at $\Delta_s/\Delta_0 \geq e^{\pi/2}$, one pair of roots $y = \pm iu$ when $e^{-\pi/2} \leq \Delta_s/\Delta_0 \leq e^{\pi/2}$, with another pair appearing at $\Delta_s/\Delta_0 \leq e^{-\pi/2}$.

There is a direct correspondence between this behavior of the roots and the dynamical regimes A, B, and C observed numerically. The pairing amplitude is subject to fast dephasing and tends to zero when $\mathbf{L}^2(y)$ does not have complex roots. A pair of complex roots $y_a = \pm i\Delta_a/\Delta_s$ defines the long-time asymptote $\Delta(t) \approx \Delta_a$. Two pairs of roots, $y = \pm iu_1$ and $y = \pm iu_2$, correspond to the parameters $\Delta_\pm = (u_1 \pm u_2)\Delta_s$ of the elliptic function which defines the asymptotic behavior:

$$\Delta(t) = \Delta_+ \mathrm{dn}\left[\Delta_+(t - \tau_0), k\right], \quad k = 1 - \Delta_-^2/\Delta_+^2, \tag{10.13}$$

where the time lag τ_0 is a half of the period. As illustrated in Fig.10.4, Eq.(10.13) agrees well with $\Delta(t)$ found numerically. Thus the spectral analysis is in accord with the simulation of Bloch dynamics. It confirms the existence of the three regimes and also provides the exact values $\Delta_{AB} = e^{-\pi/2}\Delta_0$ and $\Delta_{BC} = e^{\pi/2}\Delta_0$.

Finally, we estimate the change of scattering length required to cross the A-B and B-C transitions. Using the BCS gap in a weakly interacting Fermi gas[25], $\Delta = 0.49 E_F e^{-1/g}$, $g = \frac{2}{\pi} k_F |a|$, we see that the conditions $\Delta_s/\Delta_0 = e^{\pm\pi/2}$, written as $1/g - 1/g_s = \pm\pi/2$, translate into $1/a - 1/a_s = \pm k_F$. At weak coupling this corresponds to a small change of scattering length, $\delta a/a \approx \pm k_F a$, easily achievable for magnetically tunable Feshbach resonance.

10.2 My Questions about Synchronization in the BCS Pairing Dynamics

Are these results confirmed experimentally?

(??? good question)

11 Nonequilibrium dynamics of weakly and strongly paired superconductors by Gurarie

(maybe the article reports a good analytical method of calculations of what is already known???)

Abstract

We study small oscillations of the order parameter in weakly and strongly paired superconductors driven slightly out of equilibrium, in the collisionless approximation.

While it was known for quite some time that the amplitude of the oscillations in a weakly paired superconductor decays as $t^{-1/2}$, we show that in a superconductor sufficiently strongly paired so that its fermions form bound states usually referred to as molecules, these oscillations decay as $t^{-3/2}$.

The transition between these two regimes happens when the chemical potential of the superconductor vanishes, thus the behavior of the oscillations can be used to distinguish weakly and strongly paired superconductors.

These results are obtained in the mean field approximation which may not be reliable in the crossover region between the strong and weak pairing, so we also obtain identical results within the two-channel model, which can be tuned to be reliable throughout the entire crossover, although it then describes a special type of interactions between the fermions which may be difficult to observe experimentally.
(so the author is not sure that his results are relevant??)

Finally, we interpret the result in the strongly paired superconductor as the probability of the molecular decay as a function of time.

The study of quantum quenches, or the evolution of a quantum system when its parameters suddenly change, acquired prominence due to recent studies in Refs. [Calabrese and Cardy(2006), Kollath et al.(2007)].

Yet a particular case of it, the study of small oscillations of the order parameter in a perturbed superconductor, started more than 30 years ago in Ref. [Volkov and Kogan(1973)].

This paper showed that if a small perturbation is applied to a superconductor leading to a deviation of its gap from its equilibrium value, then this perturbation will evolve as $\cos(2\Delta_0 t)/\sqrt{t}$, where Δ_0 is the equilibrium value of the gap.

This work was continued in Ref. [Barankov et al.(2004)]. These authors showed that large oscillations of the order parameter in a superconductor do not decay but in fact continue forever (as long as the collisionless approximation remains valid).

Subsequently with the help of the exact integrability of this problem [Dukelsky et al.(2004)] it was shown that the exist a critical strength of the perturbation such that if a perturbation beyond that strength is applied, it excites oscillations which continue forever while perturbations below that strength still decay, Ref. [Barankov and Levitov(2006), Yuzbashyan and Dzero(2006)].

At the same time, advances in atomic physics allow now to create superconductors out of ultracold fermionic atoms whose interactions can be externally controlled. If the interactions are weak, these artificial superconductors behave just like the usual superconductors of condensed matter physics (termed BCS superconductors).

But the interactions can also be adjusted to be strong, in which case these superconductors become more akin to a Bose condensate (BEC) of diatomic bosonic molecules. As the interactions are tuned, the superconductor is said to undergo a BCS-BEC crossover (which is accompanied by the chemical potential changing from positive to negative values). The possibility of this crossover was discussed in a number of papers throughout the last four decades (see Refs. [Eagles(1969), Leggett(1980), Nozières and Schmitt-Rink(1985)]), and it finally was observed a few years ago (see Refs. [Regal et al.(2004), Zwierlein et al.(2004)]).

The unprecedented control over the interactions that the ultracold gases provide allows to change them quickly thus easily creating an initial out-of-equilibrium perturbation by a sudden change of their strength.

A natural question which arises in this regard concerns the fate of the oscillations, decaying and persistent, as the superconductor undergoes the BCS-BEC crossover.

Refs. [Andreev et al.(2004), Barankov and Levitov(2004)] explored the large nondecaying oscillations of a tunable superconductor using the ansatz of Ref. [Barankov et al.(2004)].

However, this method was found to break down as the superconductor is tuned to the BEC regime, and it was not possible to tell whether this was an artifact of the technique or an indication that an oscillating solution is indeed not possible in a strongly paired superconductor (see, however, Ref. [Holland et al.(2001)]).

To remedy this situation, in this paper we consider small oscillations of the order parameter in a tunable superconductor. We show that as long as the oscillations remain small, they always decay regardless of the strength of interactions in the superconductor. However, while in the BCS superconductor the amplitude of these oscillations decay as $1/\sqrt{t}$, in the BEC regime they decay as $1/t^{3/2}$. The transition between the two regimes happens exactly where the chemical potential μ is equal to zero.

The theory we develop is based on the mean field (collisionless) approximation. Thus one can question its validity near the unitary point [Giorgini et al.(2008)] which lies between the BCS and BEC regimes of the superconductors (at positive chemical potential) and is known to go beyond the applicability of the mean field theory [Levinsen and Gurarie(2006)] (see also Ref. [Bulgac and Yoon(2009)] for recent studies of the dynamics near this point). Therefore, we repeat the calculation in the two channel model [Timmermans et al.(1999)] describing BCS-BEC crossover with narrow Feshbach resonance [Gurarie and Radzihovsky(2007)] where mean field theory is applicable throughout and recover the same result. This shows that an example of the BCS-BEC crossover exists whose order parameter oscillations unambiguously obey the scenario discussed here.

In the “deep BEC" side of the crossover, the superconductor becomes the Bose-Einstein condensate of the diatomic bosonic molecules. In this regime, the result $1/t^{3/2}$ has a very simple interpretation. Indeed, as we will see in this paper, the order parameter of such superconductor is proportional to the probability of finding two fermions of opposite spins at the same position in space. As the superconductor is perturbed, the wave function of a pair of fermions no longer coincides with their bound state, but rather consists of the linear combination of a bound and excited states. The part of the wave function in the excited states moves off to infinity so that the probability amplitude to find two particles in the same spot decreases as $1/t^{3/2}$ reaching a limiting finite value at large t which in turn follows from the behavior of a three dimensional propagator of a free particle. In fact, in this deep BEC regime this is true not only with a small but also with a relatively large initial perturbation (the precise criteria are developed below), in which case this picture makes it clear that the order parameter decays to a value smaller than the equilibrium value, just like in the BCS regime with certain perturbations [Yuzbashyan and

Dzero(2006)]. However, to fully analyze the case of large perturbations to the superconductor and to see whether nondecaying solutions are possible in the BEC regime, one needs to take advantage of the integrability of the equations of motion, something which was done successfully for the weakly paired superconductor and whose strongly paired superconductor applications are left for future work.

(what is the method which they use???)

In what follows, we describe the derivation of these results. Consider spin-1/2 fermions interacting via a short range attractive s-wave interaction of strength λ. Within the mean field approximation, these fermions can be studied on a strictly classical level. We accomplish this by introducing the Cooper pair number $n_p = \left\langle \hat{a}^\dagger_{\uparrow p} a_{\uparrow p} + \hat{a}^\dagger_{\downarrow p} a_{\downarrow p} \right\rangle /2$. The evolution of this number obeys the following classical Hamiltonian, a classical version of the Anderson-Richardson (or reduced BCS) Hamiltonian describing these kind of fermions,

$$H = 2\epsilon_p n_p - \frac{\lambda}{V} \sum_{p,q} \sqrt{n_p(1-n_p) n_q (1-n_q)} \cos(\phi_p - \phi_q), \tag{11.1}$$

where $\epsilon_p = p^2/(2m)$ is the free fermions dispersion, ϕ_p is the phase variable canonically conjugate to n_p, and V is the space volume. The equations of motion of this Hamiltonian have the following solution, corresponding to a stationary superconductor

$$\phi^0_p = -2\mu t, n^0_p = \frac{1}{2}\left(1 - \frac{\xi_p}{E_p}\right), \tag{11.2}$$

where as always μ is the chemical potential, t is time, $\xi_p = \epsilon_p - \mu$, $E_p = \sqrt{\xi_p^2 + \Delta_0^2}$, and finally Δ_0 is the equilibrium gap of the superconductor which can be found from the gap equation $1 = \frac{\lambda}{2V}\sum_p \frac{1}{E_p}$. Now consider the initial conditions for the motion described by Eq. (11.1) consisting of a small perturbation to the stationary solution Eq. (34.37). In fact, it is most physical to take as initial conditions Eq. (34.37) for a slightly different value of $\Delta = \Delta_0 + \delta\Delta_0$ as well as the slightly different value of μ (corresponding to a superconductor whose interactions were slightly perturbed in the initial moment of time). Then it is straightforward to see, with the help of the particle conservation condition $\sum_p \delta n_p = 0$, that the initial conditions read

$$n_p = n^0_p + \delta n^0_p,\ \delta n^0_p = \left(\xi_p - \frac{\tilde{f}_0}{f_0}\right) \frac{\Delta_0 \delta\Delta_0}{2E_p^3}, \tag{11.3}$$

where f_0 and $\tilde{f}_0$ are defined below in Eq. (11.8). We then expand the Hamiltonian Eq. (11.1) about the stationary solution to obtain the quadratic Hamiltonian for the deviations δn_p, $\delta\phi_p$. Subsequently we construct the solution to the equations of motion of this Hamiltonian by using the method of Green's functions. The expanded Hamiltonian takes the form

$$\delta H = \frac{1}{2}\sum_{p,q} \left[\delta\phi_p \Phi_{pq} \delta\phi_q + \delta n_p K_{pq} \delta n_q\right], \tag{11.4}$$

where

$$\Phi_{pq} = \frac{\Delta_0^2}{E_p}\delta_{pq} - \frac{\lambda}{2V}\frac{\Delta^2}{E_p E_q}, K_{pq} = \frac{4E_p^3}{\Delta_0^2}\delta_{pq} - \frac{2\lambda\xi_p\xi_q}{V\Delta_0^2}. \tag{11.5}$$

This represents a collection of harmonic oscillators, labelled by the index p. Now it is possible to construct a retarded Green's function corresponding to these oscillators, with the end result

$$\delta n_p(t) = i\sum_q \int_{-\infty+i0}^{\infty+i0} \frac{\Omega d\Omega}{2\pi} G_{pq}(\Omega)\, e^{-2i\Omega t}\, \delta n^0_q, \tag{11.6}$$

where

$$G_{pq}(\Omega)=\frac{\delta_{pq}}{\Omega^2-E_p^2}+\frac{\lambda}{2V}\frac{f\left(\Omega^2\xi_p\xi_q+E_q^2\left(\Omega^2-\Delta_0^2\right)\right)-\tilde{f}\left(\xi_pE_q^2+\xi_q\Omega^2\right)}{\Omega^2E_p\left(\Omega^2-E_p^2\right)\left(\Omega^2-E_q^2\right)\left[\tilde{f}^2+f^2\left(\Delta_0^2-\Omega^2\right)\right]}.$$

Here we introduced the functions

$$f=\frac{\lambda}{2V}\sum_p\frac{1}{E_p\left(\Omega^2-E_p^2\right)},\ \tilde{f}=\frac{\lambda}{2V}\sum_p\frac{\xi_p}{E_p\left(\Omega^2-E_p^2\right)}. \tag{11.7}$$

In what follows we will also need these same functions evaluated at $\Omega=0$, or

$$f_0=-\frac{\lambda}{2V}\sum_p\frac{1}{E_p^3},\ \tilde{f}_0=-\frac{\lambda}{2V}\sum_p\frac{\xi_p}{E_p^3}. \tag{11.8}$$

The derivation of Eq. (11.7) is technical and not particularly instructive, so it will be published elsewhere.

Armed by the explicit expression for the fluctuations $\delta n_p(t)$ we can now discuss how to calculate the time dependent gap function. It is easiest to study the square of its absolute value,

$$|\Delta(t)|^2=\frac{\lambda^2}{V^2}\sum_{p,q}\sqrt{n_p(1-n_p)n_q(1-n_q)}\cos(\phi_p-\phi_q). \tag{11.9}$$

In turn, this quantity can be decomposed into the sum of Δ_0^2, the square of the unperturbed gap, and the perturbation $\delta\left|\Delta\right|^2$, given by

$$\delta\left|\Delta(t)\right|^2=\frac{2\lambda}{V}\sum_p\xi_p\,\delta n_p(t). \tag{11.10}$$

We combine this with the initial conditions Eq. (11.3) as well as with Eqs. (11.6) and (11.7) to find that

$$\delta\left|\Delta(t)\right|^2=\frac{i\Delta_0\delta\Delta_0}{\pi}\int_{-\infty+i0}^{\infty+i0}\Omega d\Omega\,e^{-2i\Omega t}\frac{\tilde{f}^2+f^2\left(\Delta_0^2-\Omega^2\right)-ff_0\Delta_0^2-f\tilde{f}_0^2/f_0}{\Omega^2\left[\tilde{f}^2+f^2\left(\Delta_0^2-\Omega^2\right)\right]}.$$

This equation represents the main result of this paper.

It reduces to the main result of Ref. [Volkov and Kogan(1973)] at weak pairing.
(produce it!!!!!!! read the Kogan1973)
So, it represents the generalization of their result to a superconductor of an arbitrary pairing strength.

The integration here goes over the straight line slightly above the real axis, as shown on Fig. 11.1 with a dashed line. We expect the functions f and $\tilde{f}$ to have singularities on the real axis where $|\Omega|$ hits the minimum of E_p and cuts at larger $|\Omega|$. It may seem that there is also a singularity at $\Omega=0$, but it is actually fictitious as the numerator of Eq. (11.11) vanishes at $\Omega\to 0$. At $t<0$ the contour can be closed in the upper half plane resulting in zero for the integral as expected. At positive time $t>0$ we can deform the contour as shown on Fig 11.1 by a solid line with arrows. Then at large positive times, the main contribution to the integral comes from the vicinity of the singular points, or the turning points of the new contour.

To evaluate f and $\tilde{f}$, we replace summation over p in Eq. (11.7) by the integration over $Vd^3p/(2\pi)^3$. In the BCS regime, it is standard to pass to the integration over the variable

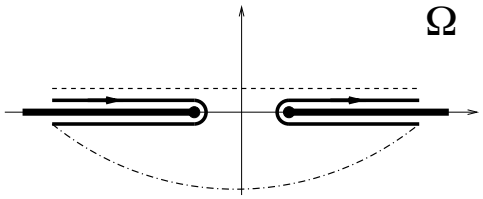


Figure 11.1: The contour of integration in Eq. (11.11) in the complex plane of Ω. Dashed line shows the initial contour, while solid black line, together with a dashed-dotted semicircle, is the deformed contour. The dashed-dotted part of the new contour can be deformed away to infinity and does not contribute.

$\xi = \epsilon_p - \mu$ so that $d^3p/(2\pi)^3 \approx \nu d\xi$, where $\nu = \sqrt{m^3\mu}/(\pi^2\sqrt{2})$ is the density of states, and then extend the integration over ξ all the way to the entire real axis. Then $\tilde{f} = 0$ as its integral is antisymmetric in ξ. At the same time, f is given by

$$f = i\frac{\nu\lambda}{\Omega\sqrt{\Delta_0^2 - \Omega^2}} \ln\left[\sqrt{1 - \frac{\Omega^2}{\Delta_0^2}} + i\frac{\Omega}{\Delta_0}\right]. \tag{11.11}$$

It is then easy to see that the integrand in Eq. (11.11) has a singularity as Ω approaches Δ_0 which goes as $1/\sqrt{\Omega - \Delta_0}$ in agreement with the discussion above (Δ_0 coincides with the minimum of E_p). Introducing the variable $s = \Omega - \Delta_0$ and taking into account that at $t \gg 1/\Delta_0$ only small s contributes to the integral, we find after adding both left and right contours (which are complex conjugate of each other)

$$\delta\,|\Delta(t)|^2 \sim \mathrm{Re}\; e^{-2i\Delta_0 t}\int_0^\infty \frac{ds e^{-ist}}{\sqrt{s}} \sim \frac{\cos(2\Delta_0 t)}{\sqrt{t}}. \tag{11.12}$$

Alternatively, in the BEC regime where $\mu < 0$, the integration measure in Eq. (11.7) must be kept as $Vd^3p/(2\pi)^3$ and both functions f and $\tilde{f}$ are not zero. The minimum of E_p is equal to $E_{\min} = \sqrt{\mu^2 + \Delta_0^2}$. The functions f and $\tilde{f}$ are now finite when $|\Omega|$ reaches $E_{\min}$, but they are not regular at that point. Generally they behave as $f \sim \mathrm{const} + i\sqrt{\Omega - E_{\min}}$. The origin of such a drastically different behavior lies in the fact that the minimum of E_p is reached when $p = 0$. Then, the potential divergence in the integral at $\Omega = E_{\min}$ is removed by the p^2 coming from the measure of integration p^2dp. All this can be checked explicitly in the deep BEC regime where $|\mu| \gg \Delta_0$ and the analytic expressions behaving precisely in this way can be obtained by direct integration.

Now if we substitute this into Eq. (11.11) we find that the constant piece is single valued as Ω goes from the upper to lower branch of the contour on Fig. 11.1 and therefore its contribution from each of the contours cancels. So it is the square root part which contributes. This gives at large times $t \gg 1/E_{\min}$

$$\delta\,|\Delta|^2 \sim \mathrm{Re}\; e^{-2itE_{\min}}\int ds\, e^{-ist}\sqrt{s} \sim \frac{\cos(2tE_{\min})}{t^{\frac{3}{2}}}. \tag{11.13}$$

As we see, the transition from the behavior Eq. (34.13) to Eq. (11.13) occurs exactly at $\mu = 0$ as this is the point where the minimum of the spectrum E_p shifts to $p = 0$.

One can worry if this derivation really works for a superconductor in the vicinity of the unitary point where the mean field theory breaks down. To have a controllable theory, we repeated this calculation for the two channel model, based on the equations of motion introduced in Ref. [Andreev et al.(2004)]. That model has an additional coupling g such that if $g^2m^2/n^{1/3} \gg 1$ (here n is the density), then the two channel model is equivalent to Eq. (11.1)

considered earlier in this paper. In the opposite limit, the two channel model still undergoes a crossover but with the mean field theory applicable throughout. The answer for the two channel model can be worked out using the same methods as the ones described here. It looks almost identical to Eq. (11.11), except in all occurences of $\tilde{f}$ and $\tilde{f}_0$ one needs to substitute $\tilde{f} \to \tilde{f} - 2\lambda/g^2$, $\tilde{f}_0 \to \tilde{f}_0 - 2\lambda/g^2$. This replacement does not change any of the arguments presented here for the one channel model, thus all the conclusions remain valid.

Finally, we observe that in the deep BEC regime all $n_p^0 \ll 1$. Then the Hamiltonian Eq. (11.1) can be significantly simplified, reducing in this limit to the Schrödinger equation of one pair of fermions in a delta-function potential, as discussed at length in Ref. [Nozières and Schmitt-Rink(1985)]. Replacing $1 - n_p \approx 1$, and introducing the pair wave function $\psi_p = \sqrt{n_p}\, e^{i\phi_p}$, we find $H = 2\epsilon_p |\psi_p|^2 - \frac{\lambda}{V}\left|\sum_p \psi_p\right|^2$ leading to

$$i\partial_t \psi = 2\epsilon_p \psi_p - \frac{\lambda}{V}\sum_q \psi_q. \tag{11.14}$$

The "gap function" in this language is $\Delta = \lambda \sum_p \psi_p / V$ which has an obvious meaning of the probability of finding two opposite-spin fermions at the same point in space. We can solve the linear equation (11.14) with arbitrary initial conditions directly. The solution for the gap function reads

$$\begin{aligned} \Delta(t) &= \frac{\lambda}{V}\sum_p \int_{-\infty+i0}^{\infty+i0} d\Omega\, e^{-i\Omega t} \frac{1}{1+\Pi}\frac{\psi_p^0}{\Omega - 2\epsilon_p}, \\ \Pi &= \frac{\lambda}{V}\sum_p \frac{1}{\Omega - 2\epsilon_p} = \text{const} + \frac{\lambda m^{\frac{3}{2}}\sqrt{-\Omega}}{4\pi} \end{aligned} \tag{11.15}$$

with ψ_p^0 being the initial value of ψ_p. To compute the integral over Ω, we deform the contour of integration in a way similar to that shown on Fig. 11.1. Unlike Eq. (11.11), the integrand here has a simple pole at a negative value of $\Omega = \Omega_b$ where $\Pi(\Omega_b) = -1$, but similarly to Eq. (11.11) in the BEC regime, it has cut at $\Omega > 0$ where it behaves as const $+ i\sqrt{\Omega}$.

The pole corresponds to the bound state and results in a contribution to $\Delta(t)$ corresponding to the bound molecule (that is, the equilibrium solution). The cut produces the decaying behavior going precisely as $1/t^{3/2}$, thus overall $|\Delta(t)|^2 \approx \text{const} + \cos(\Omega_b t)/t^{3/2}$ (for comparison with Eq. (11.13) observe that $\Omega_b = 2\mu$ in this regime). However now we see that this decay is correct for arbitrary initial conditions, as long as the applicability conditions $|\psi_p^0| \ll 1$ are satisfied. The value $|\Delta(t)|^2$ decays to is smaller than the equilibrium value of the gap function, since it is reduced by the overlap, smaller than 1, of the initial state and the bound state. The only initial distributions out of reach of this method are the ones where $|\psi_p^0|$ are no longer much smaller than 1.

In conclusion, we showed that the amplitude of the small oscillations of the order parameter in a superconductor decays as $1/t^{1/2}$ in the BCS ($\mu > 0$) and as $1/t^{3/2}$ in the BEC ($\mu < 0$) regimes. Applicability of this result to the Fermi gas close to the unitary point remains an open question. It would also be very interesting to see if, with modern experimental techniques, these oscillations can be detected in real superconductors and whether this theory can be generalized to superconductors with the d-wave symmetry of the gap.

12 Theory of Anderson pseudospin resonance with Higgs mode in superconductors by Tsuji, Aoki

(here, there is a specific effect and example how to work with Anderson spins)

Abstract

A superconductor illuminated by an ac electric field with frequency Ω is theoretically found to generate a collective precession of Anderson's pseudospins, and hence a coherent amplitude oscillation of the order parameter, with a doubled frequency 2Ω through a nonlinear light-matter coupling.

We provide a fundamental theory, based on the mean-field formalism, to show that the induced pseudospin precession resonates with the Higgs amplitude mode of the superconductor at $2\Omega = 2\Delta$ with 2Δ being the superconducting gap.

The resonant precession is accompanied by a divergent enhancement of the third-harmonic generation (THG). By decomposing the THG susceptibility into the bare one and vertex correction, we find that the enhancement of the THG cannot be explained by individual quasiparticle excitations (pair breaking), so that the THG serves as a smoking gun for an identification of the collective Higgs mode.

We further explore the effect of electron-electron scattering on the pseudospin resonance by applying the nonequilibrium dynamical mean-field theory to the attractive Hubbard model driven by ac electric fields.

The result indicates that the pseudospin resonance is robust against electron correlations, although the resonance width is broadened due to electron scattering, which determines the lifetime of the Higgs mode.

12.1 Introduction

Dynamical control of quantum many-body states of matter without destroying quantum coherence is becoming a central challenge in condensed matter physics. While recent developments in ultrafast laser experiments have enabled one to study relaxation dynamics of quantum systems after pulse excitation, an alternative direction we can pursue is to look at far-from-equilibrium quantum states that are realized *during photoirradiation*.

From this viewpoint, superconductivity is an intriguing ground to look for a novel optical control. A superconducting state can be described in terms of pseudospins introduced by Anderson in 1958.[Anderson(1958)] Indeed, a collective precession of the pseudospins represents a Higgs amplitude mode [Anderson(1958), Volkov,Kogan (1973), Littlewood (1981), 27, Pekker and Varma(2015)], i.e., a coherent amplitude oscillation of the superconducting order parameter with a frequency 2Δ (the superconducting gap), which is a condensed matter analog of the Higgs boson in elementary particle physics,[Eng(), 1, 13] and the σ meson in nuclear physics.[Nam(a)] This naturally emerges as a massive mode along the radial direction in the Mexican-hat potential profile when a spontaneous symmetry breaking occurs in systems coupled to gauge fields [9, Eng(), 1, 13]. The Higgs mode in superconductors has been experimentally observed by Raman [Sooryakumar and Klein(1980), 28] and THz pump-probe[4] spectroscopies. A natural question then is whether one can manipulate the dynamics of the pseudospins like one does for real spins by applying a magnetic field. Usually, however, it has been supposed to be difficult to photo-control the pseudospins, since the pseudospins do not directly couple to electromagnetic fields (in the linear-response regime).

In this paper, we theoretically show that, if we go over to a *nonlinear* regime, an ac electric field with frequency Ω does indeed generate a collective precession of Anderson's pseudospins with frequency 2Ω through the nonlinear light-matter coupling, which results in a 2Ω amplitude oscillation of the superconducting order parameter. We further find that a *resonance* between the induced pseudospin precession and the Higgs mode emerges when $2\Omega = 2\Delta$. This is remarkable, since this occurs *not* at $\Omega = 2\Delta$ but at Ω well below 2Δ (subgap regime), where

quasiparticle excitations are suppressed. We may call the phenomenon "Anderson pseudospin resonance" (APR). APR may seem analogous to the nuclear magnetic resonance (NMR) or electron spin resonance (ESR), but APR is distinct in that the effect is essentially a *collective phenomenon as a resonance with the Higgs amplitude mode.* We show that APR should appear as a divergent enhancement of the third-order nonlinear optical response [third harmonic generation (THG)]. We further find that the enhancement of THG cannot be explained by quasiparticle excitations, which hence distinguishes the collective Higgs mode from individual pair breaking processes, both of which lie at the same energy scale. APR has been experimentally observed very recently by a THz laser experiment [46].

12.2 Phenomenological time-dependent Ginzburg-Landau theory

To understand how the order parameter and the Higgs amplitude mode dynamically respond to electromagnetic fields, it is instructive to first overview the time-dependent Ginzburg-Landau (GL) theory. This gives a simple macroscopic (and phenomenological) description of the superconducting order parameter as a low-energy effective field theory, although we have to mention that the time-dependent GL theory has a serious problem in describing the Higgs mode and its resonance in superconductors as we shall stress toward the end of this section, which makes us opt for a microscopic theory in later sections.

Let us consider the GL "Lagrangian density" as a functional of the complex order parameter $\Psi(\boldsymbol{r},t)$ in a general form of

$$\mathcal{L} = -\left[a|\Psi|^2 + \frac{b}{2}|\Psi|^4 + \frac{1}{2m^*}|(-i\nabla - e^*\boldsymbol{A})\Psi|^2\right] + c|(i\partial_t - e^*\phi)\Psi|^2 + d\Psi^\dagger(i\partial_t - e^*\phi)\Psi \quad (12.1)$$

where a, b, c and d are coefficients, ϕ and $\boldsymbol{A}$ are the scalar and vector potentials, and e^* and m^* are the effective electric charge and effective mass, respectively. The Lagrangian density (12.1) is invariant under the gauge transformation $\Psi(\boldsymbol{r},t) \to e^{ie^*\chi(\boldsymbol{r},t)}\Psi(\boldsymbol{r},t)$, $\phi(\boldsymbol{r},t) \to \phi(\boldsymbol{r},t) - \partial_t\chi(\boldsymbol{r},t)$, $\boldsymbol{A}(\boldsymbol{r},t) \to \boldsymbol{A}(\boldsymbol{r},t) + \nabla\chi(\boldsymbol{r},t)$. At temperatures $T < T_c$, $a = a_0(T - T_c)$ becomes negative, and the global $U(1)$ symmetry [$\Psi(\boldsymbol{r},t) \to e^{ie^*\chi}\Psi(\boldsymbol{r},t)$ with a constant χ] is spontaneously broken. The other coefficients are taken to be positive. To describe the dynamics of the order parameter, we have included the kinetic terms, one with a coefficient c that represents the kinetic term of Klein-Gordon-type equations, and another with d that represents the kinetic term of Gross-Pitaevskii-type equations.

Now, we expand $\mathcal{L}$ (12.1) around the ground state $\Psi_0 = \sqrt{-a/b}$ (the phase is chosen as such without loss of generality). There are two kinds of elementary excitations from the ground state: the variation along the radial direction and another along the circumferential direction on the complex plane of the order parameter. We write them as $\Psi(\boldsymbol{r},t) = [\Psi_0 + H(\boldsymbol{r},t)]e^{i\theta(\boldsymbol{r},t)}$, where H and θ denote the Higgs and Nambu-Goldstone (NG) fields, respectively. The expansion gives us

$$\begin{aligned}\mathcal{L} = {} & c(\partial_t H)^2 + ce^{*2}\left(\phi + \frac{1}{e^*}\partial_t\theta\right)^2(\Psi_0 + H)^2 \\ & - de^*\left(\phi + \frac{1}{e^*}\partial_t\theta\right)(\Psi_0 + H)^2 + 2aH^2 - \frac{1}{2m^*}(\nabla H)^2 \\ & - \frac{e^{*2}}{2m^*}\left(\boldsymbol{A} - \frac{1}{e^*}\nabla\theta\right)^2(\Psi_0 + H)^2 + \cdots \end{aligned} \quad (12.2)$$

in which we have dropped total-derivative terms as well as higher-order interactions.

The terms proportional to $\phi\partial_t\theta$ and $\boldsymbol{A}\cdot\nabla\theta$ in Eq. (12.2) indicate that the NG phase mode turns into a longitudinal component of the gauge field. As a result of the Anderson-Higgs

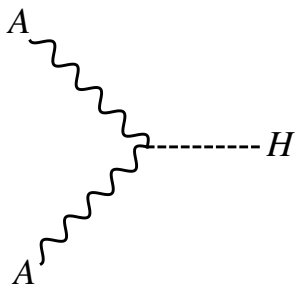


Figure 12.1: The Feynman diagram for the interaction vertex that connects the Higgs field H (dashed line) and electromagnetic field $\boldsymbol{A}$ (wavy lines).

mechanism,[9, Eng(), 1, 13] the NG mode is absorbed to the gauge field, and is pushed to very high energy scale of the plasma frequency ω_p. We can thus regard θ in Eq. (12.2) to be an unphysical degree of freedom, which one can eliminate by taking the unitary gauge,

$$\begin{aligned}\mathcal{L} = c(\partial_t H)^2 + (ce^{*2}\phi^2 - de^*\phi)(\Psi_0^2 + 2\Psi_0 H) + 2aH^2 \\ - \frac{1}{2m^*}(\nabla H)^2 - \frac{e^{*2}\Psi_0^2}{2m^*}\boldsymbol{A}^2 + \frac{e^{*2}\Psi_0}{m^*}\boldsymbol{A}^2 H + \cdots .\end{aligned} \tag{12.3}$$

One can see that the terms $ce^{*2}\phi^2$ and $\frac{e^{*2}\Psi_0^2}{2m^*}\boldsymbol{A}^2$ represent the mass of the gauge field generated via the Anderson-Higgs mechanism.

In the case of electrically neutral superfluids ($e^* = 0$), the Anderson-Higgs mechanism does not occur, so that the Higgs field mixes with the NG field via the term proportional to $d(\partial_t\theta)H$ in Eq. (12.2), and the Higgs mode is no longer considered to be an isolated excitation. Furthermore, there are interactions between H and θ via the terms proportional to $c(\partial_t\theta)^2 H$ and $(\nabla\theta)^2 H$ in Eq. (12.2), which causes the relaxation of the Higgs into lower energy NG bosons, which makes the Higgs mode unstable. At this point, it has been often emphasized that the particle-hole symmetry is important in forcing $d \sim 0$ to suppress such a mixing between the Higgs and NG modes.[27, Pekker and Varma(2015)] In other words, the Higgs mode is to be protected by the particle-hole symmetry. However, this argument for the stability of the Higgs mode is not needed in the case of charged superconductors (although the particle-hole symmetry is a good symmetry near the Fermi surface in superconductors), since *the NG field decouples from the Higgs field [in Eq. (12.3)] due to the Anderson-Higgs mechanism* as stated above.

Equation (12.3) suggests that the interaction between the Higgs and gauge fields is given by ϕH, $\phi^2 H$ and $\boldsymbol{A}^2 H$. The linear coupling ϕH is suppressed in superconductors due to the inherent particle-hole symmetry ($d \sim 0$). The leading interaction is the second-order process $\phi^2 H$ and $\boldsymbol{A}^2 H$, the latter of which, e.g., is represented by a Feynman diagram shown in Fig. 12.1. The nonlinear Higgs-gauge coupling implies that H describes a scalar boson having no electric charge. These nonlinear couplings ($\phi^2 H$ and $\boldsymbol{A}^2 H$) have indeed been used in the discovery of the Higgs particle at the LHC experiment[23, 24] (where $\boldsymbol{A}$ corresponds to the vector bosons W or Z).

From Eq. (12.3) (with $d = 0$), we can derive the equation of motion for the Higgs field,

$$\left(c\partial_t^2 - \frac{1}{2m^*}\nabla^2\right) H = 2aH + e^{*2}\Psi_0\left(c\phi^2 - \frac{1}{2m^*}\boldsymbol{A}^2\right), \tag{12.4}$$

which is "relativistic" (with an emergent Lorentz symmetry),[Pekker and Varma(2015)] meaning that the first time-derivative is absent even though we started from the non-relativistic GL Lagrangian (12.1). Let us first look at the case of $\phi = \boldsymbol{A} = 0$. By putting $H(\boldsymbol{r}, t) \sim e^{i\boldsymbol{q}\cdot\boldsymbol{r} - i\omega t}$,

we obtain the dispersion relation for the Higgs mode,

$$\omega(\boldsymbol{q})^2 = -\frac{2a}{c} + \frac{q^2}{2m^*c} = \omega_H^2 + \frac{q^2}{2m^*c}, \tag{12.5}$$

where the mode is a gapped (massive) excitation with a characteristic frequency (mass)

$$\omega_H = \sqrt{-\frac{2a}{c}}. \tag{12.6}$$

From this, one can see that $\omega_H \propto (T_c - T)^{1/2} \propto \Delta$. In fact, the microscopic calculation[Anderson(1958), Littlewood (1981)] shows that $\omega_H = 2\Delta$, which exactly coincides with the lowest energy necessary to create a pair of Bogoliubov quasiparticles. Using the microscopic result[Gor()] of $b(\Psi_0/\Delta)^2 = 3/(4\epsilon_F)$ (with ϵ_F the Fermi energy), we have $c = -2a/(2\Delta)^2 = 2b\Psi_0^2/(2\Delta)^2 = 3/(8\epsilon_F)$. With this and $m^* = 2m$, we reproduce the well-known relation,[Littlewood (1981)]

$$\omega(\boldsymbol{q})^2 = (2\Delta)^2 + \frac{1}{3}v_F^2 q^2, \tag{12.7}$$

where $v_F = \sqrt{2\epsilon_F/m}$ is the Fermi velocity. From Eq. (12.2), it is obvious that the dispersion for the NG mode (or Bogoliubov mode) shares the same form $\omega(\boldsymbol{q})^2 = q^2/(2m^*c) = v_F^2 q^2/3$ with the Higgs mode besides the mass term. This agrees with the previously known result.[Bogoliubov et al.(1958)]

Next, we turn to a situation where the system is driven by a continuous and homogeneous ac electric field $\boldsymbol{A}(t) = \boldsymbol{A}e^{-i\Omega t}$. The problem becomes equivalent to a forced oscillation of a harmonic oscillator, and the solution for Eq. (12.4) is given by

$$H(t) = \frac{1}{(2\Omega)^2 - \omega_H^2}\frac{e^{*2}\Psi_0 A^2}{2m^*c}e^{-2i\Omega t}. \tag{12.8}$$

This captures the fundamental aspect of the resonance phenomenon discussed in the paper. Due to the nonlinear coupling to the electric field, the elementary frequency of the oscillation of the Higgs field is 2Ω (rather than Ω). When 2Ω matches with the eigenfrequency of the Higgs field ω_H, the resonance occurs and the oscillation amplitude diverges as $(2\Omega - \omega_H)^{-1}$. From a microscopic point of view, this phenomenon can be understood as a resonant precession of Anderson pseudospins as we shall discuss in Sec. 12.3.

The current $\boldsymbol{j} = \partial\mathcal{L}/\partial\boldsymbol{A}$ is expressed as

$$\boldsymbol{j} = -\frac{ie^*}{2m^*}[\Psi^\dagger\nabla\Psi - (\nabla\Psi^\dagger)\Psi] - \frac{e^{*2}}{m^*}\boldsymbol{A}\Psi^\dagger\Psi.$$

Expanding Ψ around Ψ_0, we obtain the leading nonlinear current response against $\boldsymbol{A}$,

$$\boldsymbol{j}_{\rm NL}(t) = -\frac{2e^{*2}\Psi_0}{m^*}\boldsymbol{A}(t)H(t).$$

This takes the form of a London equation, where the current is proportional to $\boldsymbol{A}(t)$. Remarkably, the nonlinear current is also *proportional to the Higgs field* $H(t)$, so that the current can, and does indeed, sensitively reflect the temporal change of the Higgs field. Since $\boldsymbol{A}(t)$ oscillates with frequency Ω, while $H(t)$ oscillates with 2Ω, the current $[\propto \boldsymbol{A}(t)H(t)]$ ends up with oscillating with frequency 3Ω. This implies that a *giant third harmonic generation* (THG) is induced near the resonance ($2\Omega \sim \omega_H$) with the Higgs mode.

So far, we have discussed the Higgs mode and its resonance with electromagnetic waves based on the time-dependent GL theory (12.1). Apart from the fact that the characteristic

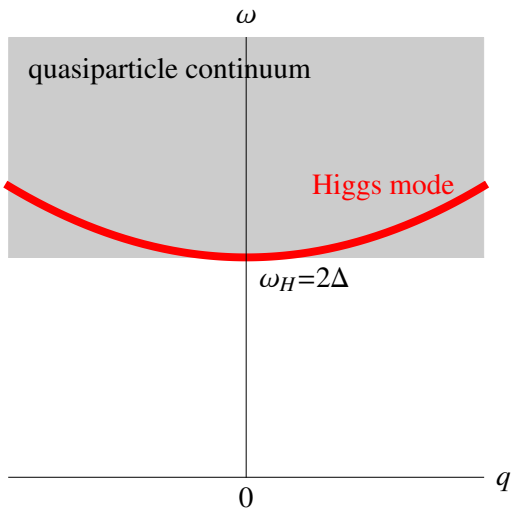


Figure 12.2: (Color online) Schematic excitation spectrum of s-wave superconductors. The red curve is the collective Higgs mode, while the shaded region represents the quasiparticle excitation continuum.

frequency ω_H of the Higgs mode cannot be determined within GL theory, the problem of GL theory is that it does not take account of relaxations of the Higgs mode into quasiparticles. As shown in Fig. 12.2, the Higgs mode is degenerate with the lower bound of the quasiparticle excitation continuum ($\omega_H = 2\Delta$). The coincidence of the two energies is known as the Nambu relation.[21, Vol(b)] Since the Higgs mode lies at the same energy scale as the quasiparticle excitations, it can easily decay into individual quasiparticles. Furthermore, at low temperatures the relaxation time of quasiparticles becomes much longer than the time scale of the order-parameter variation in clean superconductors. As a result, one cannot neglect quasiparticle excitations, and the dynamics of the order parameter is necessarily entangled with those of quasiparticles. The low-energy effective theory of the Higgs mode may not be expressed only in terms of Ψ, but may involve fermionic degrees of freedom. The crucial questions that arise are (i) whether the Higgs resonance discussed here would survive or not after we take account of the relaxation to quasiparticles (pair-breaking process), and (ii) if it would survive, then how one can distinguish the collective Higgs mode from individual quasiparticle excitations, both of which are energetically degenerate. These motivate us to move on to the underlying microscopic theory in the subsequent sections.

12.3 Microscopic theory for Anderson pseudospin resonance

Having identified the necessity of going beyond GL theory, we start from the pairing Hamiltonian for an s-wave superconductor coupled to a dynamical electric field,

$$H_{\rm pair} = \sum_{\boldsymbol{k},\sigma} \epsilon_{\boldsymbol{k}-e\boldsymbol{A}(t)} c^\dagger_{\boldsymbol{k}\sigma} c_{\boldsymbol{k}\sigma} - U \sum_{\boldsymbol{k},\boldsymbol{p}} c^\dagger_{\boldsymbol{k}\uparrow} c^\dagger_{-\boldsymbol{k}\downarrow} c_{-\boldsymbol{p}\downarrow} c_{\boldsymbol{p}\uparrow}, \tag{12.9}$$

where $\epsilon_{\boldsymbol{k}}$ is the band dispersion measured from Fermi energy ϵ_F, e the elementary charge, $\boldsymbol{A}(t) = \boldsymbol{A}\sin\Omega t$ the vector potential for the ac electric field $\boldsymbol{E}(t)$ introduced by Peierls substitution (in the temporal gauge), $c^\dagger_{\boldsymbol{k}\sigma}$ the creation operator for electrons, and $-U(<0)$ is the attractive pairing interaction. We consider a superconducting thin film, into which the electric field can penetrate. For $H_{\rm pair}$ (12.9), the BCS mean-field description becomes exact. We define the

superconducting gap function,

$$\Delta = \Delta' + i\Delta'' = U \sum_{\boldsymbol{k}} \langle c^\dagger_{\boldsymbol{k}\uparrow} c^\dagger_{-\boldsymbol{k}\downarrow} \rangle, \tag{12.10}$$

that serves as the order parameter in the BCS theory. We can replace the momentum sum with an integral $D(\epsilon_F) \int_{-\omega_D}^{\omega_D} d\epsilon$ with $D(\epsilon_F)$ the density of states at the Fermi energy and ω_D the energy cut off (e.g., the Debye frequency of the bosonic pairing glue such as phonons). The interaction strength is characterized by a dimensionless $\lambda = UD(\epsilon_F)$. In the following we set $\hbar = 1$, and use ω_D as the unit of energy.

Anderson's pseudospin [Anderson(1958)] is defined by

$$\boldsymbol{\sigma}_{\boldsymbol{k}} = \frac{1}{2} \Psi^\dagger_{\boldsymbol{k}} \cdot \boldsymbol{\tau} \cdot \Psi_{\boldsymbol{k}}, \tag{12.11}$$

where $\Psi_{\boldsymbol{k}} = (c_{\boldsymbol{k}\uparrow}, c^\dagger_{-\boldsymbol{k}\downarrow})^t$ is the Nambu spinor, and $\boldsymbol{\tau} = (\tau^x, \tau^y, \tau^z)$ are the Pauli matrices. The pseudospin satisfies the usual commutation relations for angular momentum, $[\sigma^j_{\boldsymbol{k}}, \sigma^k_{\boldsymbol{k}}] = i\varepsilon_{jkl}\sigma^l_{\boldsymbol{k}}$. With this, the pairing Hamiltonian (12.9) is recast in a form,

$$H_{\rm pair} = 2 \sum_{\boldsymbol{k}} \boldsymbol{b}_{\boldsymbol{k}} \cdot \boldsymbol{\sigma}_{\boldsymbol{k}}, \tag{12.12}$$

which can be regarded as a spin system in an effective magnetic field,

$$\boldsymbol{b}_{\boldsymbol{k}} = \left(-\Delta', -\Delta'', \frac{\epsilon_{\boldsymbol{k}-e\boldsymbol{A}(t)} + \epsilon_{\boldsymbol{k}+e\boldsymbol{A}(t)}}{2} \right). \tag{12.13}$$

The z component of $\boldsymbol{b}_{\boldsymbol{k}}$ represents the light-matter coupling involving contributions from both the particle and hole sectors. Since $\boldsymbol{b}_{\boldsymbol{k}}$ is a function even in $\boldsymbol{A}(t)$ if the system is parity symmetric ($\epsilon_{-\boldsymbol{k}} = \epsilon_{\boldsymbol{k}}$), we can readily recognize that the linear coupling vanishes, so that the leading effect of the electric field starts from $O(\boldsymbol{A}(t)^2)$. The self-consistency condition (12.10) reads

$$\Delta = U \sum_{\boldsymbol{k}} (\sigma^x_{\boldsymbol{k}} + i\sigma^y_{\boldsymbol{k}}) \tag{12.14}$$

in the pseudospin notation. While the dynamics cannot be described by the conventional GL equation, which would be valid only when the time scale of the order-parameter motion is much longer than that of quasiparticle relaxations, in the present formalism the time evolution is determined by a Bloch equation for the pseudospins, [Volkov,Kogan (1973), Barankov et al.(2004), 32]

$$\partial_t \boldsymbol{\sigma}_{\boldsymbol{k}} = i[H_{\rm pair}, \boldsymbol{\sigma}_{\boldsymbol{k}}] = 2\boldsymbol{b}_{\boldsymbol{k}} \times \boldsymbol{\sigma}_{\boldsymbol{k}}. \tag{12.15}$$

Anderson pseudospins have been recently used to analyze the dynamics of charge fluctuations in a time-resolved Raman experiment for high-T_c cuprates. [102, Lor()]

We can analytically solve Eq. (12.15) up to the leading (second) order in $\boldsymbol{A}(t)$. This is achieved by linearizing Eq. (12.15) with the time-independent and time-dependent parts separated as $\boldsymbol{\sigma}_{\boldsymbol{k}}(t) = \boldsymbol{\sigma}_{\boldsymbol{k}}(0) + \delta\boldsymbol{\sigma}_{\boldsymbol{k}}(t)$ and $\Delta(t) = \Delta + \delta\Delta(t)$. We assume that the initial state is superconducting at zero temperature. The initial Δ may be taken to be real positive without loss of generality. Thus the initial condition reads $\sigma^x_{\boldsymbol{k}}(0) = \Delta/\omega_{\boldsymbol{k}}$ and $\sigma^z_{\boldsymbol{k}}(0) = -\epsilon_{\boldsymbol{k}}/\omega_{\boldsymbol{k}}$ with $\omega_{\boldsymbol{k}} = 2(\epsilon^2_{\boldsymbol{k}} + \Delta^2)^{1/2}$. The linearized equations of motion are

$$\partial_t \delta\sigma^x_{\boldsymbol{k}}(t) = -2\epsilon_{\boldsymbol{k}} \delta\sigma^y_{\boldsymbol{k}}(t), \tag{12.16}$$

$$\partial_t \delta\sigma^y_{\boldsymbol{k}}(t) = 2\epsilon_{\boldsymbol{k}}\, \delta\sigma^x_{\boldsymbol{k}}(t) + 2\Delta\, \delta\sigma^z_{\boldsymbol{k}}(t) + \frac{1}{\omega_{\boldsymbol{k}}} \left[e^2\Delta \sum_{ij} \partial_{k_i}\partial_{k_j}\epsilon_{\boldsymbol{k}} A_i(t) A_j(t) - 2\epsilon_{\boldsymbol{k}}\delta\Delta(t) \right], \tag{12.17}$$

$$\partial_t \delta\sigma^z_{\boldsymbol{k}}(t) = -2\Delta\, \delta\sigma^y_{\boldsymbol{k}}(t). \tag{12.18}$$

Note that $\partial_t(\Delta\delta\sigma^x_{\boldsymbol{k}} - \epsilon_{\boldsymbol{k}}\delta\sigma^z_{\boldsymbol{k}}) = 0$. From this, along with the initial condition $\delta\boldsymbol{\sigma}_{\boldsymbol{k}}(0) = 0$, it turns out that the relation $\Delta\delta\sigma^x_{\boldsymbol{k}} = \epsilon_{\boldsymbol{k}}\delta\sigma^z_{\boldsymbol{k}}$ holds all the time, which helps us to reduce the number of the equations.

We solve the equations by a Laplace transformation, $\mathcal{L}[\delta\Delta(t)](s) =: \delta\Delta(s)$, etc. Let us call the direction of the electric field x. Then we have $\sum_{ij}\partial_{k_i}\partial_{k_j}\epsilon_{\boldsymbol{k}}A_i(t)A_j(t) = \partial^2_{k_x}\epsilon_{\boldsymbol{k}}|\boldsymbol{A}(t)|^2$. When the crystallographic directions are equivalent, we have $\partial^2_{k_x}\epsilon_{\boldsymbol{k}} \to d^{-1}\nabla^2_{\boldsymbol{k}}\epsilon_{\boldsymbol{k}}$ with d the spatial dimension. If the band dispersion is isotropic with $\epsilon_{\boldsymbol{k}} = \epsilon(|\boldsymbol{k}|)$, we expand $\epsilon_{\boldsymbol{k}}$ around the Fermi wave number k_F as $\epsilon_{\boldsymbol{k}} = \sum_{n=1}^{\infty} c_n(|\boldsymbol{k}| - k_F)^n$. With this, we can define a series expansion,

$$d^{-1}\nabla^2_{\boldsymbol{k}}\epsilon_{\boldsymbol{k}} = \alpha_0 + \alpha_1\epsilon_{\boldsymbol{k}} + \alpha_2\epsilon^2_{\boldsymbol{k}} + \cdots, \tag{12.19}$$

where $\alpha_0 = 2c_2d^{-1} + c_1(1-d^{-1})k_F^{-1}$, $\alpha_1 = c_1^{-1}[6c_3d^{-1} + (1-d^{-1})(2c_2k_F^{-1} - c_1k_F^{-2})]$, etc., with each coefficient $\alpha_n \sim O(\epsilon_F^{1-n})$. Since the α_0 term just gives a trivial phase $\exp(i\alpha_0e^2\int_0^t dt'\,A(t')^2)$ to $\Delta(t)$, which can be gauged out, the α_1 term provides the leading contribution around the Fermi surface (with $\omega_D \ll \epsilon_F$). For anisotropic band structures, the same expansion is still sometimes possible. For instance, the d-dimensional cubic lattice (with cosine bands $\epsilon_{\boldsymbol{k}} = -2\sum_i \cos k_i - \epsilon_F$) has $d^{-1}\nabla^2_{\boldsymbol{k}}\epsilon_{\boldsymbol{k}} = \alpha_0 + \alpha_1\epsilon_{\boldsymbol{k}}$ with $\alpha_0 = -\epsilon_Fd^{-1}$ and $\alpha_1 = -d^{-1}$.

Thus, in most cases of our interest, we arrive at

$$\frac{\delta\Delta(s)}{\alpha_1e^2A^2\Delta} = \frac{\Omega^2}{s(s^2+4\Omega^2)}\left[1 - \frac{1}{\lambda(s^2+4\Delta^2)F(s)}\right], \tag{12.20}$$

where $A = |\boldsymbol{A}|$ and

$$\begin{aligned} F(s) &= \int_{-\infty}^{\infty} d\epsilon\,\frac{1}{2\sqrt{\epsilon^2+\Delta^2}(s^2+4\epsilon^2+4\Delta^2)} \\ &= \frac{1}{s\sqrt{s^2+4\Delta^2}}\sinh^{-1}\left(\frac{s}{2\Delta}\right). \end{aligned} \tag{12.21}$$

In the above, we have replaced the range of integration from $\int_{-\omega_D}^{\omega_D}$ to $\int_{-\infty}^{\infty}$, which is allowed in the BCS regime ($\omega_D \gg \Delta$). $F(s)$ can be analytically continued on the complex plane, where branch cuts $\mathcal{B}_\pm(\delta) = \{\pm 2i\Delta \pm ire^{\pm i\delta} | r \in [0,\infty)\}$ with δ small but nonzero are introduced (Fig. 12.3).

To obtain $\delta\Delta(t)$ with an inverse Laplace transformation, we need to evaluate a Bromwich integral,

$$I(t) = \frac{1}{2\pi i}\int_{\gamma-i\infty}^{\gamma+i\infty} ds\,e^{st}\frac{\Omega^2}{s(s^2+4\Omega^2)(s^2+4\Delta^2)F(s)}, \tag{12.22}$$

where $\gamma \in \mathbb{R}$ is taken to be larger than any of the real parts of the poles in the integrand. There are three first-order poles at $s = 0, \pm 2i\Omega$ and two branching points at $s = \pm 2i\Delta$ (Fig. 12.3) in the integrand, where $s = \pm 2i\Delta$ corresponds to the Higgs amplitude mode, while $s = \pm 2i\Omega$ to the forced precession of the Anderson pseudospins driven by the electric field. As one changes Ω, the poles merge with the branching points at $2\Omega = 2\Delta$, which causes a *resonance* between the forced pseudospin precession and the Higgs mode.

To make it more explicit, we evaluate the integral (12.22) by taking the contour as depicted in Fig. 12.3, which surrounds the three poles but avoids the branch cuts. This kind of contour is often used to calculate similar integrals (see, e.g., Ref. [Volkov,Kogan (1973)]). We take $\delta > 0$ so that the contours along the branch cuts $\mathcal{B}_\pm(\delta)$ do not touch the poles $s = \pm 2i\Omega$ when $\Omega > \Delta$. Since the contributions from infinity vanish, we are left with the residues of the poles and the line integrals ($\mathcal{C}_\pm$ in Fig. 12.3 and their Hermitian conjugates) along the branch

cuts. The asymptotic behavior of the integrals $\mathcal{C}_\pm$ for $t \to \infty$ is evaluated by the saddle-point method. Finally we end up with long-time asymptotic forms of the order parameter,

$$\frac{\delta\Delta(t)}{\alpha_1 e^2 A^2 \Delta} \sim \frac{1}{4\lambda}\left[\frac{2}{\pi^{3/2}}\frac{\Omega^2}{\Omega^2-\Delta^2}\frac{1}{\sqrt{\Delta t}}\cos\left(2\Delta t+\frac{\pi}{4}\right)-1\right]+\frac{1-\cos 2\Omega t}{4} \tag{12.23}$$

$$+\frac{1}{4\lambda}\times\begin{cases}\dfrac{\Omega}{\sqrt{\Delta^2-\Omega^2}}\dfrac{\cos 2\Omega t}{\sin^{-1}\left(\frac{\Omega}{\Delta}\right)} & \Omega<\Delta \\ \dfrac{\Omega}{\sqrt{\Omega^2-\Delta^2}}\dfrac{\cos(2\Omega t-\varphi)}{\sqrt{[\cosh^{-1}\left(\frac{\Omega}{\Delta}\right)]^2+\left(\frac{\pi}{2}\right)^2}} & \Omega>\Delta\end{cases}, \tag{12.24}$$

where φ is the phase shift given by

$$\varphi=\tan^{-1}\left(\frac{\pi/2}{\cosh^{-1}\left(\frac{\Omega}{\Delta}\right)}\right). \tag{12.25}$$

The first term in Eq. (12.24) can be interpreted as the Higgs amplitude mode induced by an effective change of the interaction parameter due to the ac field, $U \to U_{\rm eff} = (1-\frac{1}{2}\alpha_1 e^2 A^2)U$. [Tsuji et al.(2009)] Indeed, it approaches the result for the interaction-quench problem [Barankov and Levitov(2006), Yuzbashyan and Dzero(2006)] in the limit of $\Omega \to \infty$. The Higgs mode is amplified by the ac electric field around $2\Omega = 2\Delta$. The term decays algebraically as $t^{-1/2}$,[Volkov,Kogan (1973)] which suggests that the Higgs mode effectively has an infinite lifetime within the BCS approximation.

In the long-time limit, the constant term and the term oscillating with frequency 2Ω survive. The constant term in $\delta\Delta(t)$ is proportional to $\alpha_1(1-\lambda^{-1})$, which implies, intriguingly, that we can attain an *amplification* of superconductivity on time average when this term is positive. The 2Ω oscillation term represents the APR. If we write the last term in Eq. (12.24) as $\frac{1}{4\lambda}\mathscr{A}\cos(2\Omega t-\varphi)$, the amplitude $\mathscr{A}$ and the phase shift φ are universal functions that depend only on the ratio $2\Omega/2\Delta$ (Fig. 12.4). The amplitude $\mathscr{A}$ diverges as $|2\Omega-2\Delta|^{-1/2}$ at $2\Omega = 2\Delta$ (resonance condition). It clearly differs from the result of the time-dependent GL (12.8), $|2\Omega-2\Delta|^{-1}$. The reduction of the power from 1 to 1/2 signifies that the Higgs mode is a bit less stable, where each pseudospin precession gradually dephases. Physically we can interpret this as coming from Landau damping; that is, the collective mode decays into individual quasiparticle excitations even in the collision-less equation (12.15). An anomaly is also found in the phase shift φ: for $2\Omega < 2\Delta$, φ is locked to zero, i.e., the 2Ω oscillation of the order parameter is in-phase with $\boldsymbol{E}(t)^2$. As soon as 2Ω exceeds 2Δ, the φ discontinuously jumps to $\pi/2$ and starts to drift (Fig. 12.4). Along with the order-parameter oscillation, the pseudospin itself continues to precess around the axis parallel to $\boldsymbol{\sigma}_{\boldsymbol{k}}(0)$, with two modes of frequencies $\omega_{\boldsymbol{k}}$ and 2Ω surviving in $t \to \infty$ (the former of which dephases). By numerically simulating Eq. (12.15), we also confirmed that APR generally occurs for finite-temperature initial states and for pulsed electric fields that contain large enough number of oscillation cycles.

APR appears in various physical quantities. What is readily accessible experimentally is the electric current,

$$\boldsymbol{j} = e\sum_{\boldsymbol{k},\sigma} \boldsymbol{v}_{\boldsymbol{k}-e\boldsymbol{A}(t)} c^\dagger_{\boldsymbol{k}\sigma} c_{\boldsymbol{k}\sigma} \tag{12.26}$$

($\boldsymbol{v}_{\boldsymbol{k}} = \nabla_{\boldsymbol{k}}\epsilon_{\boldsymbol{k}}$ is the group velocity). The current is expressed in the pseudospin notation as $\boldsymbol{j} = e\sum_{\boldsymbol{k}}[\boldsymbol{v}_{\boldsymbol{k}-e\boldsymbol{A}(t)} - \boldsymbol{v}_{\boldsymbol{k}+e\boldsymbol{A}(t)}]\sigma^z_{\boldsymbol{k}} + \frac{e}{2}\sum_{\boldsymbol{k}\sigma}[\boldsymbol{v}_{\boldsymbol{k}-e\boldsymbol{A}(t)} + \boldsymbol{v}_{\boldsymbol{k}+e\boldsymbol{A}(t)}]c^\dagger_{\boldsymbol{k}\sigma}c_{\boldsymbol{k}\sigma}$. If we expand it in $\boldsymbol{A}(t)$, the linear response is given by $\boldsymbol{j}^{(1)} = -2\alpha_1 e^2 \boldsymbol{A}(t)\sum_{\boldsymbol{k}}\epsilon_{\boldsymbol{k}}\sigma^z_{\boldsymbol{k}}(0) + e\sum_{\boldsymbol{k}\sigma} v_{\boldsymbol{k}} c^\dagger_{\boldsymbol{k}\sigma}c_{\boldsymbol{k}\sigma}$, which is irrelevant to APR. In fact, the linear-response optical conductivity does not show any divergence for

$\Omega \neq 0$. [108] The leading term that reflects the change of the order parameter is the third-harmonic generation (THG),

$$\boldsymbol{j}^{(3)}(t) = -2\alpha_1 e^2 \Delta U^{-1} \delta\Delta(t) \boldsymbol{A}(t), \tag{12.27}$$

where we have used $\epsilon_{\boldsymbol{k}} \delta\sigma^z_{\boldsymbol{k}} = \Delta \delta\sigma^x_{\boldsymbol{k}}$. The consequence is remarkable: although the frequency Ω is below the energy gap, we do obtain the colossal nonlinear response due to divergence of $\delta\Delta(t)$. It may be used as an efficient THz harmonic emitter.

12.4 Response function for Anderson pseudospin resonance

To reinforce our picture for APR phenomenon, we can approach it from an alternative, diagrammatic point of view. This allows one to decompose the THG susceptibility into the bare and vertex-correction diagrams, each of which contains individual and collective excitations, respectively. Thus we can unambiguously distinguish the Higgs mode from quasiparticle excitations that are degenerate at the superconducting gap energy. To this end, we take the Nambu-Gor'kov Green's function defined by

$$\hat{G}_{\boldsymbol{k}}(t,t') = \begin{pmatrix} -i\langle \mathcal{T} c_{\boldsymbol{k}\uparrow}(t) c^\dagger_{\boldsymbol{k}\uparrow}(t')\rangle & -i\langle \mathcal{T} c_{\boldsymbol{k}\uparrow}(t) c_{-\boldsymbol{k}\downarrow}(t')\rangle \\ -i\langle \mathcal{T} c^\dagger_{-\boldsymbol{k}\downarrow}(t) c^\dagger_{\boldsymbol{k}\uparrow}(t')\rangle & -i\langle \mathcal{T} c^\dagger_{-\boldsymbol{k}\downarrow}(t) c_{-\boldsymbol{k}\downarrow}(t')\rangle \end{pmatrix},$$

where $\mathcal{T}$ represents the time ordering. With this, the gap function is expressed as

$$\Delta(t) = -\frac{i}{2} U \sum_{\boldsymbol{k}} \mathrm{Tr}\left[\tau_1 \hat{G}^<_{\boldsymbol{k}}(t,t)\right], \tag{12.28}$$

where $\hat{G}^<_{\boldsymbol{k}}$ is the lesser Green's function, and $\Delta(t)$ is assumed to be real.

Now we take variations of both sides of Eq. (12.28) with respect to the external field $\boldsymbol{A}(t)$. In this section, we consider the monochromatic wave $\boldsymbol{A}(t) = \boldsymbol{A} e^{-i\Omega t}$. Since the leading change of the order parameter $\delta\Delta(t) = \delta\Delta e^{-2i\Omega t}$ is the second order in $\boldsymbol{A}(t)$, we have

$$\delta\Delta = \delta^2_A \Delta = -\frac{i}{2} U \sum_{\boldsymbol{k}} \mathrm{Tr}\left[\tau_1 \delta^2_A \hat{G}^<_{\boldsymbol{k}}\right], \tag{12.29}$$

where δ_A represents the functional derivative with respect to $\boldsymbol{A}$. In the BCS theory, the Nambu-Gor'kov Green's function is given by the Dyson equation $\hat{G}_{\boldsymbol{k}} = (i\partial_t - \hat{\xi}_{\boldsymbol{k}} + \Delta\tau_1)^{-1}$ with $\hat{\xi}_{\boldsymbol{k}} \equiv \xi_{\boldsymbol{k}-e\boldsymbol{A}\tau_3}\tau_3$. Hence the variation of the order parameter reads

$$\begin{aligned} \delta^2_A \Delta = &-iU \sum_{\boldsymbol{k}} \mathrm{Tr}\left[\tau_1 \hat{G}_{\boldsymbol{k}} (\delta_A \hat{\xi}_{\boldsymbol{k}}) \hat{G}_{\boldsymbol{k}} (\delta_A \hat{\xi}_{\boldsymbol{k}}) \hat{G}_{\boldsymbol{k}}\right]^< \\ &- \frac{i}{2} U \sum_{\boldsymbol{k}} \mathrm{Tr}\left[\tau_1 \hat{G}_{\boldsymbol{k}} (\delta^2_A \hat{\xi}_{\boldsymbol{k}} - \delta^2_A \Delta\tau_1) \hat{G}_{\boldsymbol{k}}\right]^<. \end{aligned} \tag{12.30}$$

Here the lesser component of the products of the Green's functions should be understood by Langreth's rule [e.g., $(GG)^< = G^R G^< + G^< G^A$]. Equation (12.30) determines $\delta\Delta = \delta^2_A\Delta$ self-consistently. This is diagrammatically represented in the first line of Fig. 12.5. One can show that the first term on the right hand side of Eq. (12.30) vanishes in the BCS theory. By solving Eq. (12.30) in the frequency domain, we end up with

$$\delta\Delta = \frac{\frac{i}{2}\alpha_1 U \sum_{\boldsymbol{k},\omega} \xi_{\boldsymbol{k}} \mathrm{Tr}\left[\tau_1 \hat{G}_{\boldsymbol{k}}(\omega + 2\Omega)\tau_3 \hat{G}_{\boldsymbol{k}}(\omega)\right]^<}{1 - \frac{i}{2} U \sum_{\boldsymbol{k},\omega} \mathrm{Tr}\left[\tau_1 \hat{G}_{\boldsymbol{k}}(\omega + 2\Omega)\tau_1 \hat{G}_{\boldsymbol{k}}(\omega)\right]^<}. \tag{12.31}$$

Note that $\langle \tau_1 \hat{G} \tau_1 \hat{G} \rangle$ appearing in the denominator is the dynamical pair-pair correlation function.

The amplitude of the 2Ω oscillation of $\delta\Delta$ diverges (i.e., APR occurs) when the denominator of Eq. (12.31) vanishes due to fluctuations in the τ_1 channel. Thus the resonance sensitively reflects the structure of the pair-pair correlation function. We should emphasize that the τ_1 fluctuation appears without considering self-energy corrections beyond the mean-field BCS formalism. Namely, the τ_1 fluctuation is already present in the response to electromagnetic fields in the BCS regime before we further include fluctuations by, e.g., the random phase approximation.

As indicated in the second line of Fig. 12.5, $\delta\Delta$ can also be expressed in terms of the τ_1 vertex. Formally, the Higgs mode is defined as a pole of the τ_1 vertex. Therefore, the divergence of $\delta\Delta$ can indeed be rephrased as a resonance with the Higgs mode.

The explicit calculation for the correlation functions within the BCS theory enables one to write down $\delta\Delta$ (12.31) analytically as

$$\delta\Delta = \frac{1}{2}\alpha_1 e^2 A^2 \Delta \left[\frac{1}{\lambda\, R(\Omega, T)} - 1 \right], \tag{12.32}$$

where the resonance function $R(\Omega, T)$ is given by

$$\begin{aligned} R(\Omega, T) = \mathcal{P} \int_{\Delta}^{\infty} d\omega \frac{\Omega^2 - \Delta^2}{(\Omega^2 - \omega^2)\sqrt{\omega^2 - \Delta^2}} \tanh\left(\frac{\omega}{2T}\right) \\ - \frac{i\pi}{2}\theta(\Omega - \Delta) \frac{\sqrt{\Omega^2 - \Delta^2}}{\Omega} \tanh\left(\frac{\Omega}{2T}\right) \end{aligned} \tag{12.33}$$

with $\mathcal{P}$ denoting the principal value of the integral.

In the limit of $2\Omega \to 2\Delta$ (i.e., $\Omega \to \Delta$), $R(\Omega, T)$ has an asymptotic form of

$$R(\Omega, T) \sim \begin{cases} \dfrac{\pi}{2} \dfrac{\sqrt{\Delta^2 - \Omega^2}}{\Delta} \tanh\left(\dfrac{\Delta}{2T}\right) & \Omega \to \Delta - 0 \\ -\dfrac{i\pi}{2} \dfrac{\sqrt{\Omega^2 - \Delta^2}}{\Delta} \tanh\left(\dfrac{\Delta}{2T}\right) & \Omega \to \Delta + 0. \end{cases} \tag{12.34}$$

Hence $|\delta\Delta|$ diverges in this limit as

$$|\delta\Delta| \sim \frac{\alpha_1 e^2 A^2 \Delta^2}{\pi\lambda \tanh\left(\frac{\Delta}{2T}\right)} \frac{1}{|\Omega^2 - \Delta^2|^{1/2}}. \tag{12.35}$$

Remarkably, the divergence persists at arbitrary temperatures $T < T_c$ with the fixed critical exponent $\frac{1}{2}$, which indicates that the APR is robust against thermal fluctuations.

In the zero-temperature limit, $R(\Omega, T)$ is reduced to

$$R(\Omega, T) \overset{T \to +0}{\sim} \begin{cases} \dfrac{\sqrt{\Delta^2 - \Omega^2}}{\Omega} \sin^{-1}\left(\dfrac{\Omega}{\Delta}\right) & \Omega < \Delta \\ \dfrac{\sqrt{\Omega^2 - \Delta^2}}{\Omega} \left[\cosh^{-1}\left(\dfrac{\Omega}{\Delta}\right) - i\dfrac{\pi}{2} \right] & \Omega > \Delta. \end{cases} \tag{12.36}$$

Plugging this into Eq. (12.32), one can see that it precisely reproduces the result (12.24) derived in the previous section [note that the seeming difference of the factor $\frac{1}{2}$ is due to the assumption of $\boldsymbol{A}(t) = \boldsymbol{A} e^{-i\Omega t}$ in the present section and $\boldsymbol{A}(t) = \boldsymbol{A} \sin \Omega t$ in the previous section].

In the language of the Green's function, the current is given by

$$j(t) = ie \sum_{\boldsymbol{k}} \mathrm{Tr}\left[\hat{v}_{\boldsymbol{k}} \hat{G}^{<}_{\boldsymbol{k}}(t,t)\right], \tag{12.37}$$

where $\hat{v}_{\boldsymbol{k}} \equiv v_{\boldsymbol{k}-e\boldsymbol{A}(t)\tau_3}$. If we focus on the THG response that is relevant to APR, we can take the third derivative with respect to $\boldsymbol{A}(t)$ to obtain

$$\begin{aligned} j^{(3)} = ie \sum_{\boldsymbol{k}} \mathrm{Tr}\left[(\delta_A^3 \hat{v}_{\boldsymbol{k}}) \hat{G}^{<}_{\boldsymbol{k}}\right] \\ + ie \sum_{\boldsymbol{k}} \mathrm{Tr}\left[(\delta_A \hat{v}_{\boldsymbol{k}}) \hat{G}_{\boldsymbol{k}} (\delta_A^2 \hat{\xi}_{\boldsymbol{k}} - \delta_A^2 \Delta\tau_1) \hat{G}_{\boldsymbol{k}}\right]. \end{aligned} \tag{12.38}$$

Here we have used the fact that odd-order derivatives of $\hat{G}^{<}_{\boldsymbol{k}}(t,t)$ vanish as indicated by the pseudospin analysis [see Eqs. (12.16)-(12.18)].

The first term in Eq. (1) is of higher order in (ω_D/ϵ_F) than the other terms, so that it is negligible. Then the leading contributions to $j^{(3)}$ are the second and third terms, which we write as

$$j^{(3)} = \chi^{(3)}_{\mathrm{tot}} A^3 = (\chi^{(3)}_0 + \chi^{(3)}_{\mathrm{vc}}) A^3. \tag{12.39}$$

$\chi^{(3)}_{\mathrm{tot}}$ is the total THG susceptibility, which comprises the bare susceptibility $\chi^{(3)}_0$ and vertex correction $\chi^{(3)}_{\mathrm{vc}}$. The Feynman diagram for these is depicted in Fig. 12.6. Here one can single out the contribution of the 2Ω collective oscillation of the order parameter to the THG signal, which is $\chi^{(3)}_{\mathrm{vc}}$. In other words, we can distinguish the effect of quasiparticle excitations from the contribution of the Higgs mode.

We can evaluate the components of the susceptibility explicitly in the BCS theory with the function $R(\Omega, T)$ (12.33) as

$$\chi^{(3)}_0 = \alpha_1^2 e^4 \frac{\Delta^2}{U} \left[\lambda\, R(\Omega,T) - 1\right], \tag{12.40}$$

$$\chi^{(3)}_{\mathrm{vc}} = -\alpha_1^2 e^4 \frac{\Delta^2}{U} \frac{\left[\lambda\, R(\Omega,T) - 1\right]^2}{\lambda\, R(\Omega,T)}. \tag{12.41}$$

Taking the sum of the two susceptibilities, we obtain the total contribution,

$$\chi^{(3)}_{\mathrm{tot}} = \chi^{(3)}_0 + \chi^{(3)}_{\mathrm{vc}} = -\alpha_1^2 e^4 \frac{\Delta^2}{U} \left[\frac{1}{\lambda\, R(\Omega,T)} - 1\right]. \tag{12.42}$$

With Eqs. (12.32) and (12.42), we reproduce the previous relation (12.27). Note that the term $\lambda\, R(\Omega,T)$ appears in the denominator for $\chi^{(3)}_{\mathrm{tot}}$ and in the numerator for $\chi^{(3)}_0$ in the opposite ways.

In Fig. 12.7, we plot $\chi^{(3)}_{\mathrm{tot}}$ along with $\chi^{(3)}_0$ for several values of λ at $T = 0$. When we change λ, we evaluate the gap by $\Delta = \omega_D/\sinh(1/\lambda)$. We can see that $\chi^{(3)}_{\mathrm{tot}}$ diverges in a similar manner as $\delta\Delta$ (Fig. 12.4) at $2\Omega = 2\Delta$, while $\chi^{(3)}_0$ only shows kink structures. This endorses that the resonance peak is indeed a manifestation of the effect of the Higgs mode, and cannot be explained by quasiparticle excitations or pair breaking contained in $\chi^{(3)}_0$. As one increases λ, the amplitude of the divergence becomes larger. For $\lambda > 1$, $\chi^{(3)}_{\mathrm{tot}}$ and $\chi^{(3)}_0$ vanish at the value of $2\Omega/2\Delta$ at which $\lambda\, R(\Omega,T) = 1$ is satisfied. Consequently, the susceptibility spectrum shows a sharp dip structure. This can be exploited to experimentally discern whether $\lambda > 1$ or not. We also notice that the shape of the resonance peak is significantly asymmetric about $2\Omega = 2\Delta$, which becomes more prominent for larger λ. The asymmetry originates from the mixing of the

collective mode (discrete level) with quasiparticle excitations (continuous levels). While this is reminiscent of the Fano resonance, the form of the resonance function is not identical with the Fano form.

If we look at the real and imaginary parts of the THG susceptibility in Fig. 12.8, the spectral features are again very different between $\chi^{(3)}_{\rm tot}$ and $\chi^{(3)}_0$. $\mathrm{Re}\,\chi^{(3)}_{\rm tot}$ and $\mathrm{Im}\,\chi^{(3)}_{\rm tot}$ diverge as $\Omega \to \Delta - 0$ and $\Omega \to \Delta + 0$, respectively, whereas $\mathrm{Re}\,\chi^{(3)}_0$ remains finite and $\mathrm{Im}\,\chi^{(3)}_0$ vanishes in these limits. Both $\chi^{(3)}_{\rm tot}$ and $\chi^{(3)}_0$ have zero imaginary parts at $\Omega < \Delta$. This simply reflects that photoabsorption is not allowed with frequencies below the energy gap even in the nonlinear-response regime.

If we turn to the temperature dependence of the THG susceptibility in Fig. 12.9, $\chi^{(3)}_{\rm tot}$ diverges for temperatures $T < T_c$, similarly to the behavior of $\delta\Delta$ (12.35). The shape of the resonance peak does not change significantly against temperature. The insensitivity of the THG signal against temperature should facilitate experiments where a scan of the pump frequency Ω is difficult: one can instead scan temperature to change Δ for a fixed Ω. In Ref. [46], the THG resonance peak was in fact mapped out in this way.

12.5 Effect of electron-electron scattering

So far, the argument has been based on the pairing Hamiltonian (12.9), which has the long-range interaction in real space. For more realistic models of superconductivity with short-range interactions, the analysis above is considered to be a static mean-field approximation, whose validity is restricted to the weak-coupling regime. Furthermore, the equation of motion (12.15) does not involve thermalization processes, which correspond to changes in the pseudospin length $|\sigma_{\boldsymbol{k}}|$ due to correlation effects. Thus let us go beyond the static mean field by considering the attractive Hubbard model with a driving ac field,

$$H_{\rm Hubbard} = \sum_{\boldsymbol{k}\sigma} \epsilon_{\boldsymbol{k}-e\boldsymbol{A}(t)} c^\dagger_{\boldsymbol{k}\sigma} c_{\boldsymbol{k}\sigma} - U \sum_i c^\dagger_{i\uparrow} c_{i\uparrow} c^\dagger_{i\downarrow} c_{i\downarrow}, \tag{12.43}$$

where i labels the lattice sites and U is an attractive Hubbard interaction. We take, as an example, a one-dimensional dispersion $\epsilon_k = -2\cos k$ with the bandwidth $W = 4$ and $\alpha_1 = -1$ (later in this section we also consider an infinite-dimensional lattice). We calculate the time evolution by means of the nonequilibrium dynamical mean-field theory (DMFT) [Freericks et al.(2006), Aoki et al.(2014), not()], which is extended here to the Nambu formalism for treating superconductors. For an impurity solver for DMFT, we employ the third-order perturbation theory [Tsuji and Werner(2013)], which is supposed to be reliable in the region $U < W$. The system is set at half filling with $U = 3.5$, which belongs to a strong-coupling regime ($2\Delta_{T=0}/T_c \approx 5.0$ well above the BCS value).

The time evolution of the local superconducting order parameter, $\Phi(t) = \langle c^\dagger_\uparrow c^\dagger_\downarrow \rangle$, for various initial temperatures (β^{-1}) is shown in Fig. 12.10. With increased total energy due to the continuous excitation, the overall value of the order parameter gradually decreases. On top of that, the coherent oscillation of the order parameter with frequency 2Ω emerges [with the same oscillation period of $\boldsymbol{E}(t)^2$ shown in Fig. 12.10]. The oscillation is particularly enhanced around $\beta = 6.5$, and becomes invisible for $\beta = 9.0$. The phase-shift anomaly is not clearly observed in this interaction regime. We evaluate the energy gap 2Δ in equilibrium from the single-particle spectral function $A(\omega)$, which is calculated by Fourier transformation of the real-time simulation. If we measure the amplitude of the 2Ω oscillation of the order parameter, $\delta\Phi$, at the third cycle, we can clearly see in the inset of Fig. 12.11 that a resonance peak indeed emerges at $2\Omega = 2\Delta$ (the error bars represent inaccuracy in measuring Δ). The peak position corresponds to $\beta \approx 6.4$. The result indicates that APR indeed exists beyond the static mean-field level.

However, we do notice a deviation from the BCS result; i.e., the resonance has a finite width (the inset of Fig. 12.11). There are several factors that determine the resonance width. Besides extrinsic experimental factors such as the limited measurement time scale or energy dissipation to external environment (which is absent in our calculations), one intrinsic factor is the finite lifetime τ of the Higgs amplitude mode, which can decay into individual excitations [note that Higgs does not decay into the Nambu-Goldstone (NG) mode in charged superconductors, since the energy of the NG mode is lifted to the plasma frequency, at least away from the critical regime near $T = T_c$]. If the Higgs mode decays exponentially, the poles $s = \pm 2i\Delta$ acquire a real part on the complex plane (Fig. 12.3), and are thus prevented from meeting the branching points $\pm 2i\Omega$, resulting in broadening of the resonance peak. We can numerically evaluate the decay rate by generating the Higgs mode at $\beta = 6.4$ with a small perturbation (here we use an interaction quench [Tsuji et al.(2013)]), where $\Phi(t)$ is fitted with $\Phi_0 e^{-t/\tau}\cos(2\Delta t + \theta)$ on top of a linear drift (Fig. 12.11). A rapid oscillation in Fig. 12.11 comes from the divergence of the 1D density of states at band edges, and is irrelevant to the Higgs mode. From the derived τ, we estimate the resonance width as indicated by the bar in the inset of Fig. 12.11, which roughly coincides with the peak width of APR with the background subtracted (Fig. 12.11).

While we have applied the nonequilibrium DMFT to a system with 1D density of states for simplicity, we can actually confirm that the result does not change qualitatively for the infinite-dimensional hypercubic lattice with the Gaussian density of states $D(\epsilon) = e^{-\epsilon^2}/\sqrt{\pi}$, where the DMFT formalism is no longer an approximation but becomes exact. Let us consider the hypercubic lattice with the electric field applied along the diagonal direction, $\boldsymbol{A}(t) = A(t)(1, 1, 1, \dots)$. The energy dispersion reads[Turkowski and Freericks(2005), Aoki et al.(2014)]

$$\epsilon_{\boldsymbol{k}-\boldsymbol{A}(t)} = \epsilon_{\boldsymbol{k}}\cos A(t) + \bar{\epsilon}_{\boldsymbol{k}}\sin A(t), \tag{12.44}$$

where $\epsilon_{\boldsymbol{k}} = -1/\sqrt{d}\sum_{i=1}^{d}\cos k_i$ and $\bar{\epsilon}_{\boldsymbol{k}} = -1/\sqrt{d}\sum_{i=1}^{d}\sin k_i$. This makes the momentum summation of the lattice Green's function in the nonequilibrium DMFT a double integral with respect to ϵ and $\bar{\epsilon}$. The double integral becomes computationally very heavy, especially in the present case where we have to keep track of the system evolving over a long enough interval to capture the slow order-parameter dynamics. To overcome the difficulty here we make use of the following formula,

$$\begin{aligned}
&\sum_{\boldsymbol{k}} G_{\boldsymbol{k}}(t,t') \\
&= \int d\epsilon d\bar{\epsilon} D(\epsilon)D(\bar{\epsilon})(i\partial_t + \mu - \epsilon\cos A - \bar{\epsilon}\sin A - \Sigma)^{-1} \\
&= \frac{1}{2}\Bigg[\int d\epsilon D(\epsilon)\left(i\partial_t + \mu - \epsilon\cos A - \frac{1}{\sqrt{2}}\sin A - \Sigma\right)^{-1} \\
&\quad + \int d\epsilon D(\epsilon)\left(i\partial_t + \mu - \epsilon\cos A + \frac{1}{\sqrt{2}}\sin A - \Sigma\right)^{-1}\Bigg] \\
&\quad + O(A^3),
\end{aligned} \tag{12.45}$$

to reduce the double integral to a single one, where μ is the chemical potential, Σ is the self-energy, and we have used $\int d\bar{\epsilon}D(\bar{\epsilon})\bar{\epsilon}^2 = 1/2$. The formula is valid up to the second order in A, which is sufficient for the present purpose, since our interest is in the order-parameter oscillation arising from the second-order nonlinear effect. An advantage of the above formula is that the first and second terms are in the form of the Green's function with $\bar{\epsilon}$ replaced by $\pm 1/\sqrt{2}$, so that the implementation is straightforward. We also remark that keeping the form of the Green's function is vital for maintaining the numerical stability. As an impurity solver for the nonequilibrium DMFT for the hypercubic lattice, here we employ the second-order iterative

perturbation theory[Tsuji and Werner(2013)] to further reduce the computational cost. If we look at the time evolution of the order parameter in the infinite-dimensional hypercubic lattice in Fig. 12.12, the 2Ω oscillation of the order parameter is prominent around $\beta = 14.0$ and 16.0, which is close to the resonance condition $2\Omega(= 4\pi/37.5 = 0.335) = 2\Delta(\approx 0.32$, evaluated from the nonequilibrium DMFT calculation for the spectral function). Away from this, the oscillation tends to be suppressed and the oscillation becomes incoherent. This shows that APR also occurs in the nonequilibrium DMFT calculation for the infinite-dimensional lattice where DMFT becomes exact. Thus the essential features of APR do not depend on a particular form of the density of states.

12.6 Summary

To summarize, we theoretically propose a phenomenon that may be called Anderson pseudospin resonance (APR) for a superconductor driven by an ac electric field, which is confirmed by solving the equation of motion analytically within the BCS approximation, and by solving the attractive Hubbard model via the nonequilibrium DMFT. APR can be distinguished from quasiparticle excitations or pair breaking processes near the superconducting gap energy by looking at the divergent enhancement of third harmonic generation. APR provides not only a new pathway of controlling superconductors, but also provides an avenue offering information about dynamical aspects of the order parameter and the Higgs mode in superconductors. Important future problems include whether APR occurs for other pairing symmetries such as the anisotropic d-wave pairing.

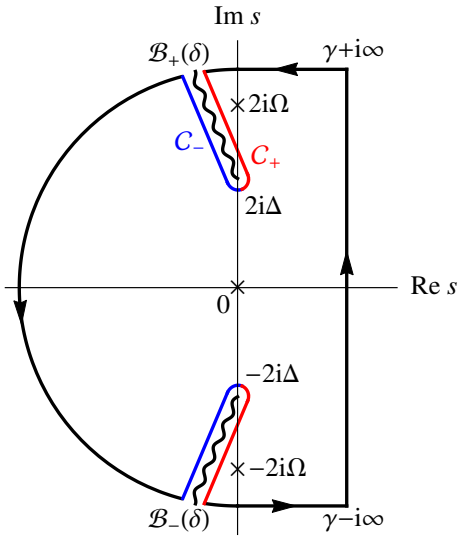


Figure 12.3: (Color online) The integral contour (solid closed curve) that we take on the complex plane to evaluate the integral (12.22). Crosses and wavy lines represent poles and branch cuts, respectively.

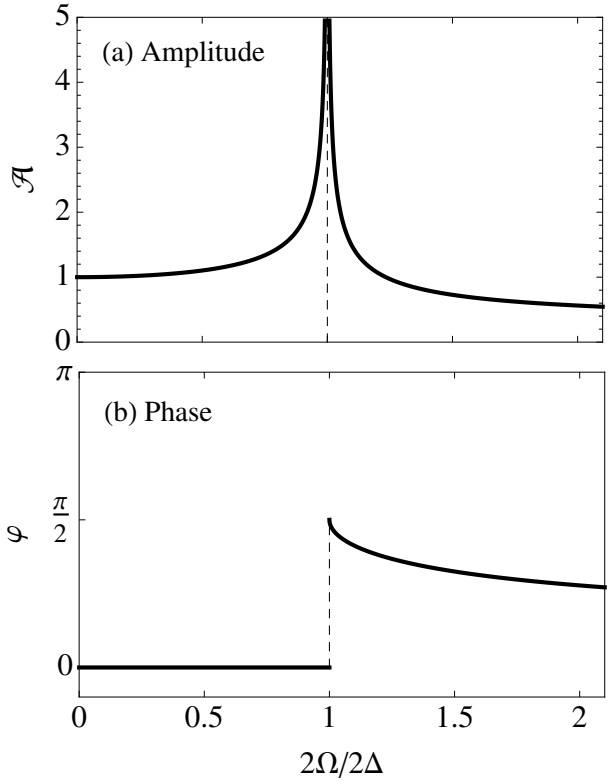


Figure 12.4: (a) The amplitude $\mathscr{A}$ and (b) phase shift φ of the 2Ω oscillation of the superconducting order parameter $\delta\Delta(t)$ [Eq. (12.24)] against $2\Omega/2\Delta$.

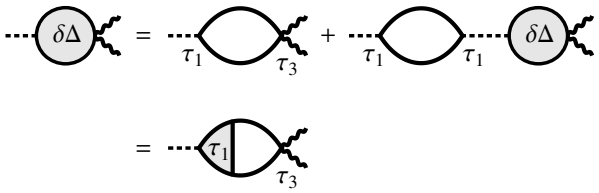


Figure 12.5: The diagrammatic representation of the self-consistent Eq. (12.30) for $\delta\Delta$ and its relation to the τ_1 vertex. The wavy and dashed lines represent the gauge field $\boldsymbol{A}$ and the interaction vertices, respectively.

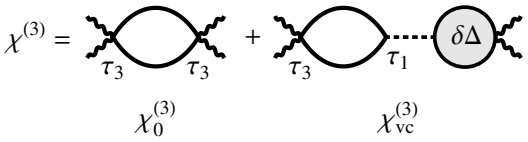


Figure 12.6: Feynman diagram for the THG susceptibility of superconductors. The first and second terms on the right-hand side correspond to $\chi_0^{(3)}$ and $\chi_{\rm vc}^{(3)}$, respectively.

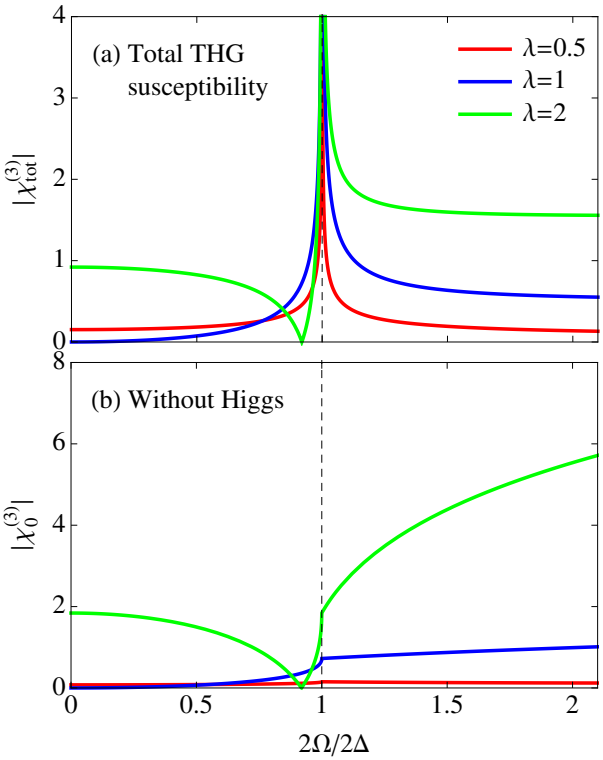


Figure 12.7: (Color online) The amplitude of (a) the full and (b) bare THG susceptibilities for superconductors at $T = 0$ with $\lambda = 0.5, 1, 2$ in units of $\alpha_1^2 e^4 \omega_D^2 D(\epsilon_F)$.

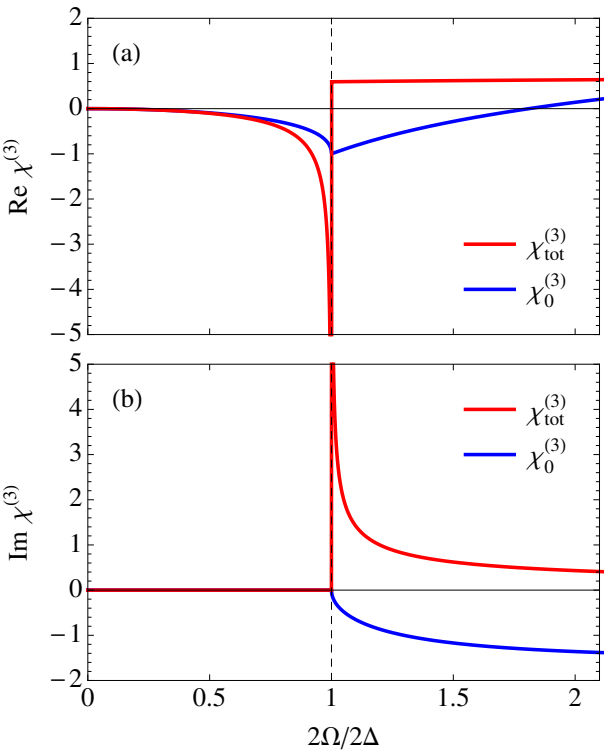


Figure 12.8: (Color online) (a) The real and (b) imaginary parts of the THG susceptibility for superconductors at $T = 0$ with $\lambda = 1$ in units of $\alpha_1^2 e^4 \omega_D^2 D(\epsilon_F)$.

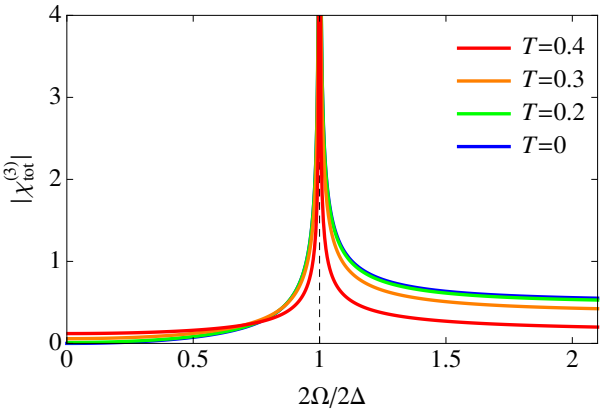


Figure 12.9: (Color online) The temperature dependence of the THG susceptibility for superconductors with $\lambda = 1$ in units of $\alpha_1^2 e^4 \omega_D^2 D(\epsilon_F)$. Here, $T_c = 0.446$.

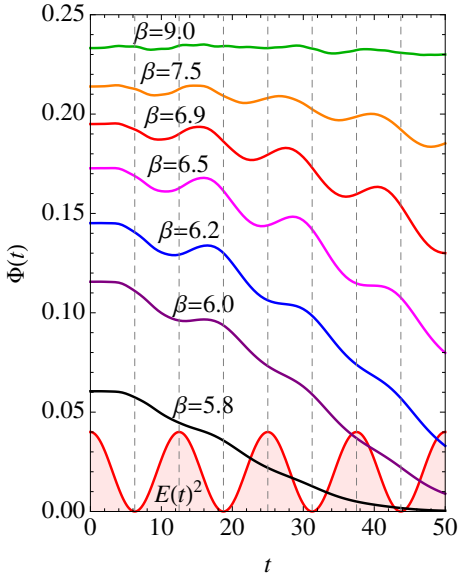


Figure 12.10: (Color online) Temporal evolution of the superconducting order parameter $\Phi(t)$ calculated with the nonequilibrium DMFT for the attractive Hubbard model with the 1D density of states at half filling driven by an ac field with $U = 3.5$, $A = 0.15$, and $\Omega = 2\pi/25$ for several temperatures (β^{-1}) for the initial states. The sinusoidal curve represents $\boldsymbol{E}(t)^2 \propto \cos^2 \Omega t$. Dashed lines are a guide to the eye.

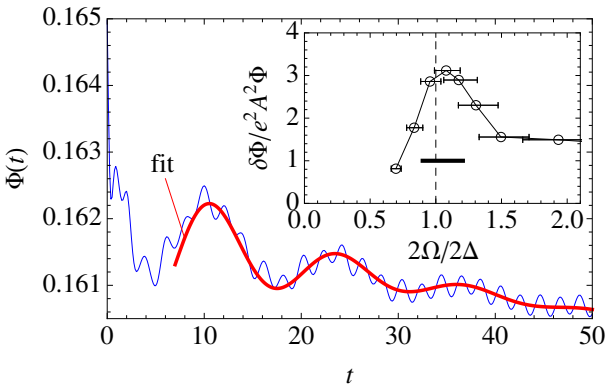


Figure 12.11: (Color online) Temporal evolution of the order parameter $\Phi(t)$ after a quench $U \to U - \delta U$ at $t = 0$ with $U = 3.5$ and $\delta U = 0.01$ in the attractive Hubbard model at $\beta = 6.4$. The rapid oscillation comes from a band-edge effect, while the slower one corresponds to the Higgs mode. Thick (red) curve is a fit (see text). Inset: The amplitude of the 2Ω oscillating component of the order parameter $\delta\Phi$ for the attractive Hubbard model driven by an ac field with $U = 3.5$, $\Omega = 2\pi/25$, and various Δ. The bar shows the width estimated from the lifetime of the Higgs mode.

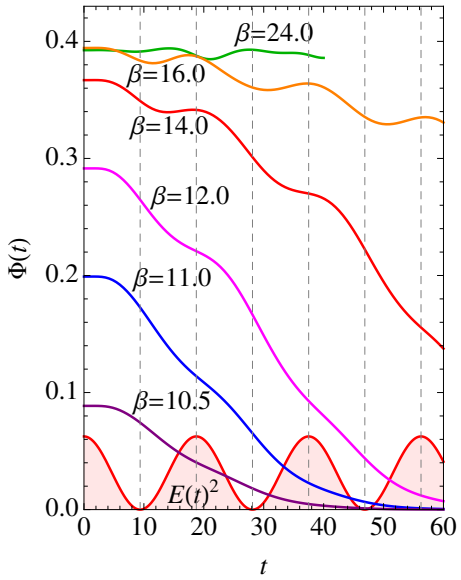


Figure 12.12: (Color online) Temporal evolution of the superconducting order parameter $\Phi(t)$ calculated with the nonequilibrium DMFT for the attractive Hubbard model with the infinite-dimensional (Gaussian) density of states at half filling driven by the ac field with $U = 2.25$, $A = 0.2$, and $\Omega = 2\pi/37.5$, for several temperatures (β^{-1}) for the initial states. The sinusoidal curve represents $\boldsymbol{E}(t)^2 \propto \cos^2 \Omega t$. Dashed lines are a guide to the eye.

13 Higgs Mode in Superconductors by Shimano, Tsuji

Abstract

When a continuous symmetry of a physical system is spontaneously broken, two types of collective modes typically emerge: the amplitude and phase modes of the order-parameter fluctuation. For superconductors, the amplitude mode is recently referred to as the "Higgs mode" as it is a condensed-matter analogue of a Higgs boson in particle physics. Higgs mode is a scalar excitation of the order parameter, distinct from charge or spin fluctuations, and thus does not couple to electromagnetic fields linearly. This is why the Higgs mode in superconductors has evaded experimental observations over a half century after the initial theoretical prediction, except for a charge-density-wave coexisting system. With the advance of nonlinear and time-resolved terahertz spectroscopy techniques, however, it has become possible to study the Higgs mode through the nonlinear light-Higgs coupling. In this review, we overview recent progresses on the study of the Higgs mode in superconductors.

13.1 Introduction and a Brief Historical Overview

Spontaneous breaking of a continuous symmetry is a fundamental concept of phase transition phenomena in various physical systems ranging from condensed matter to high-energy physics [1]. For instance, a ferromagnetic transition is characterized by the spontaneous breaking of spin rotational symmetry. Likewise, superconductivity is characterized by the spontaneous breaking of U(1) rotational symmetry with respect to the phase of a macroscopic wavefunction [2].

When a continuous symmetry is spontaneously broken, there emerge two types of collective modes in general: fluctuations of the phase and amplitude of the order parameter as schematically shown in **Figure** 13.1***a***. The phase mode (also termed Nambu-Goldstone (NG) mode) is primarily a gapless (massless) mode [3, 4, 5, 6, 7, 8] as required by the symmetry. An acoustic phonon is such an example that is associated with spontaneous breaking of translational symmetry in a crystal lattice. The amplitude mode, on the other hand, is generally a gapped (massive) mode since its excitation costs an energy due to the curvature of the potential (**Figure** 13.1***a***). The amplitude mode (especially for superconductors) is often called the Higgs mode according to the close analogy with the Higgs boson in particle physics. It may sound strange that one talks about the Higgs particle in condensed matter systems, but in fact the origin of the idea of Higgs physics can be found in the course of the study of superconductivity [3, 4, 5, 6, 7, 8, 9]. Namely, the standard model in particle physics can in some sense be viewed as a relativistic version of the Ginzburg-Landau theory [2], i.e., a low-energy effective theory of superconductors. The emergence of the Higgs mode is a universal and fundamental phenomenon in systems with spontaneous symmetry breaking.

In the case of superconductors where the order parameter couples to gauge fields, the Higgs mode occupies a special status since it is the lowest collective excitation mode (**Figure** 13.1***b***). The massless phase mode is absorbed into the longitudinal component of electromagnetic fields, and is lifted up to high energy in the scale of the plasma frequency due to the Anderson-Higgs mechanism [4, 5, 6, 9, 10, 11, 12, 13]. As a result, the amplitude mode becomes stable against the decay to the phase mode in superconductors. The existence of the amplitude mode in superconductors was suggested by Anderson [5, 14] soon after the development of a microscopic theory of superconductivity by Bardeen, Cooper, and Schrieffer (BCS) [15]. In an s-wave (BCS-type) superconductor, the Higgs-mode gap energy $\omega_{\rm H}$ coincides with the superconducting gap energy 2Δ [5, 16, 17, 2, 12] (see also [20, 21]). This is eventually consistent with Nambu's conjectural sum rule [21, 22]: $\omega_{\rm H}^2 + \omega_{\rm NG}^2 = 4\Delta^2$ with the NG mode gap energy $\omega_{\rm NG} = 0$. Since the Higgs mode lies at the lower bound of the quasiparticle continuum near zero momentum,

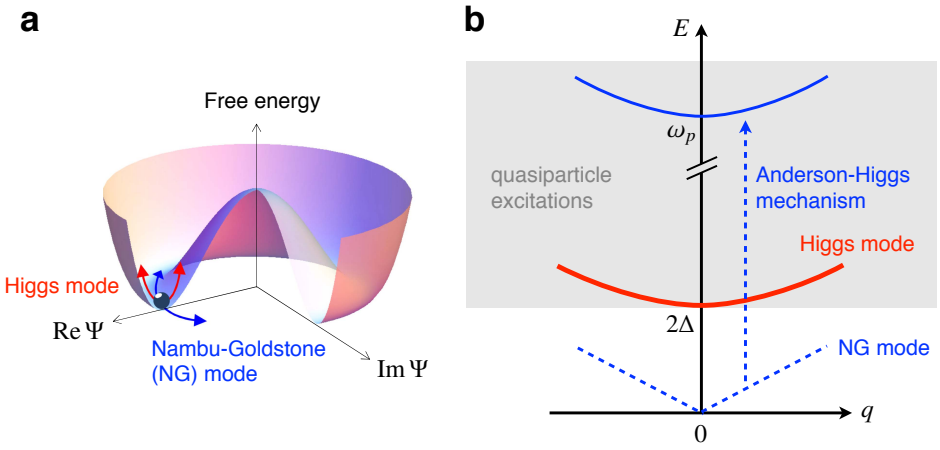


Figure 13.1: (*a*) A schematic picture of the Higgs (red) and Nambu-Goldstone (blue) modes represented on the Mexican-hat free-energy potential as a function of the complex order parameter Ψ. (*b*) A schematic excitation spectrum of an *s*-wave superconductor. Due to the Anderson-Higgs mechanism, the Nambu-Goldstone mode acquires an energy gap in the order of the plasma frequency ω_p, while the Higgs mode remains in low energy with an energy gap 2Δ, above which the quasiparticle excitation continuum overlaps.

the decay of the Higgs mode to single-particle excitations is suppressed and becomes a much slower power law [16]. For nonzero momentum, the Higgs mode can decay by transferring its energy to quasiparticle excitations. The energy dispersion and the damping rate of the Higgs mode has been derived within the random phase approximation [2, 12].

Provided that the theory of the Higgs particle originates from that of superconductivity and that the Higgs particle has been discovered in LHC experiments in 2012 [23, 24], it would be rather surprising that an experimental observation of the Higgs mode in superconductors, a home ground of Higgs physics, has been elusive for a long time. There are, however, good reasons for that: The Higgs mode does not have any electric charge, electric dipole, magnetic moment, and other quantum numbers. In other words, the Higgs mode is a scalar excitation (which is distinct from, e.g., charge fluctuations). Therefore it does not couple to external probes such as electromagnetic fields in the linear-response regime. Another reason is that the energy scale of the Higgs mode lies in that of the superconducting gap, which is in the order of millielectron volts in typical metallic superconductors. To excite the Higgs mode, one needs an intense terahertz (THz) light source (1 THz $\sim$ 4 meV $\sim$ 300 μm), which has become available only in the last decade.

One exception (and the first case) for the observation of the Higgs mode in superconductors in the early stage was the Raman scattering experiment for a superconductor 2H-$NbSe_2$ [3, 26]. It is exceptional in the sense that superconductivity and charge density wave (CDW) coexist in a single material. The Raman peak observed near the superconducting gap energy 2Δ in 2H-$NbSe_2$ was first interpreted as a single-particle excitation across the gap [3, 26]. Soon later, Littlewood and Varma have theoretically elucidated that the peak corresponds to the scalar excitation of the amplitude mode (i.e., the Higgs mode) [2, 12] (see also Reference [27]). A renewed interest in the Raman signal has recently revealed the importance of the coexisting CDW order for the Higgs mode to be visible in the Raman response [28, 29, 30]. Indeed, the Raman peak of the Higgs mode has been shown to be absent in a superconducting NbS_2, which is a material similar to $NbSe_2$ but has no CDW order [28].

It has been a long-standing issue as to whether the Higgs mode can be observed in superconductors without CDW order. On the theoretical side, there have been various pro-

posals for the excitation of the Higgs mode, including a quench dynamics [16, Barankov and Levitov(2004), 32, Barankov and Levitov(2006), 34, 35, 36, 37] as well as a laser excitation [38, 39, 40, 41, 42, 43, 44]. It is only after the development of ultrafast pump-probe spectroscopy techniques in the low-energy terahertz-frequency region that a clear observation of the Higgs-mode oscillation has been reported in a *pure* s-wave superconductor NbN [4] (with 'pure' meaning no other long-range order such as CDW). Subsequently, it has been experimentally demonstrated through the THz pump-probe and third harmonic generation (THG) measurements [46] that the Higgs mode can couple to electromagnetic fields in a *nonlinear* way. In the THG experiment, a resonant enhancement of THG was discovered [46] at the condition $2\omega = 2\Delta$ with ω the frequency of the incident THz light, indicating the nonlinear light-Higgs coupling in a two-photon process [42].

Meanwhile, it has been theoretically pointed out that not only the Higgs mode but also charge density fluctuation (CDF) can contribute to the THG signal [47]. It was shown that the CDF gives a much larger contribution than the Higgs mode in a clean-limit superconductor within the BCS mean-field approximation. While the relative magnitude of the Higgs-mode and CDF contributions to the THG has been under debate [47, 48, 49, 50], theoretical progresses have recently been made on the theory of the light-Higgs coupling, showing that both the effects of phonon retardation [48] and nonmagnetic impurity scattering [51, 52, 53, 54] drastically enhance the Higgs-mode contribution to nonlinear optical responses, far exceeding the CDF contribution.

The experiments have been extended to high-T_c cuprate superconductors, showing the presence of the Higgs-mode contribution to the pump-probe signal in d-wave superconductors [55]. Recently the THG has also been identified in various high-T_c cuprates [56]. The Higgs mode can be made visible in a linear optical response if dc supercurrent is flowing in a superconductor [57]. The infrared activated Higgs mode in the presence of supercurrents has recently been observed in a superconductor NbN [58].

In this review article, we overview these recent progresses in the study of the Higgs mode in superconductors (where the Anderson-Higgs mechanism is taking place), with an emphasis on the experimental aspects. In a broader context, collective amplitude modes are not limited to superconductors but are ubiquitous in condensed matter systems that may not be coupled to gauge fields (hence without the Anderson-Higgs mechanism). Those include squashing modes in superfluid ^{3}He [59], amplitude modes in bosonic and fermionic condensates of ultracold-atom systems [16, 61], amplitude modes in quantum antiferromagnets [13], and so on. A comprehensive review including these topics can be found in Reference [6].

13.2 Nonlinear Light-Higgs Coupling

In this section, we review from a theoretical point of view how the Higgs mode in superconductors couples to electromagnetic fields in a *nonlinear* way. It is important to understand the mechanism of the nonlinear light-Higgs coupling for observing the Higgs mode in experiments. In fact, the Higgs mode does not have a linear response against electromagnetic fields in usual situations, which has been an obstacle for experiments to detect the Higgs mode in superconductors for a long time.

13.2.1 A phenomenological view

Let us first take a phenomenological point of view based on the Ginzburg-Landau (GL) theory [2], which provides us with a quick look at the nonlinear light-Higgs coupling. For early developments based on the time-dependent GL theory, we refer to References [64, 65, 66, 67, 68]. In the GL theory, the free energy density f is assumed to be a function of a complex order-

parameter field $\psi(\boldsymbol{r})$,

$$f[\psi] \quad = f_0 + a|\psi(\boldsymbol{r})|^2 + \frac{b}{2}|\psi(\boldsymbol{r})|^4 + \frac{1}{2m^*}|(-i\nabla - e^*\boldsymbol{A})\psi(\boldsymbol{r})|^2, \tag{13.1}$$

where $a = a_0(T - T_c)$, a_0 and b are some constants, m^* and e^* are the effective mass and the effective charge of the Cooper pair condensate, and $\boldsymbol{A}$ is the vector potential that represents the external light field ($\boldsymbol{E}(t) = -\partial\boldsymbol{A}(t)/\partial t$). The amplitude of the order parameter corresponds to the superfluid density (i.e., $|\psi|^2 = n_s$), while the phase corresponds to that of the condensate.

The free energy density (13.1) is invariant under the global U(1) phase rotation $\psi(\boldsymbol{r}) \to e^{i\varphi}\psi(\boldsymbol{r})$ and more generally under the gauge transformation $\psi(\boldsymbol{r}) \to e^{ie^*\chi(\boldsymbol{r})}\psi(\boldsymbol{r})$, $\boldsymbol{A}(\boldsymbol{r}) \to \boldsymbol{A}(\boldsymbol{r}) + \nabla\chi(\boldsymbol{r})$ for an arbitrary scalar field $\chi(\boldsymbol{r})$. In addition, the GL free energy density (13.1) is invariant against the particle-hole transformation $\psi(\boldsymbol{r}) \to \psi^\dagger(\boldsymbol{r})$. The presence of the particle-hole symmetry (including the time derivative terms in the action) is crucial [27, 6, 69] in decoupling the Higgs amplitude mode from the phase mode (Nambu-Goldstone mode) in electrically neutral systems such as superfluid ultracold atoms. Without the particle-hole symmetry, the Higgs mode quickly decays into the phase mode and becomes short-lived. In superconductors (which consist of electrically charged electrons), on the other hand, the phase mode acquires an energy gap in the order of the plasma frequency due to the Anderson-Higgs mechanism. This prevents the Higgs mode from decaying into the phase mode. The particle-hole symmetry itself is realized as an approximate symmetry in the Bogoliubov-de Gennes Hamiltonian, which describes microscopic low-energy physics of superconductors around the Fermi energy at the mean-field level.

When the temperature goes below the critical temperature (i.e., $a < 0$), the global U(1) symmetry is spontaneously broken, and the system turns into a superconducting state. The order-parameter fluctuation from the ground state ($\psi(\boldsymbol{r}) = \psi_0$) can be decomposed into amplitude $H(\boldsymbol{r})$ and phase $\theta(\boldsymbol{r})$ components,

$$\psi(\boldsymbol{r}) \quad = [\psi_0 + H(\boldsymbol{r})]e^{i\theta(\boldsymbol{r})}. \tag{13.2}$$

Then, the GL potential can be expressed up to the second order of the fluctuation as

$$f \quad = -2aH^2 + \frac{1}{2m^*}(\nabla H)^2 + \frac{e^{*2}}{2m^*}\left(\boldsymbol{A} - \frac{1}{e^*}\nabla\theta\right)^2(\psi_0 + H)^2 + \cdots. \tag{13.3}$$

The first term on the right hand side of Equation 13.3 indicates that the Higgs mode has an energy gap (**Figure** 13.1***b***) proportional to $(-a)^{1/2} \propto (T_c - T)^{1/2}$. The microscopic BCS mean-field theory predicts that the Higgs gap is actually identical to the superconducting gap 2Δ [5, 16, 17, 2, 12]. The phase field $\theta(\boldsymbol{r})$ does not have such a mass term, so that at first sight one would expect to have a massless Nambu-Goldstone mode. However, $\theta(\boldsymbol{r})$ always appears in the form of $(\boldsymbol{A} - \nabla\theta/e^*)$ in Equation 13.3, which allows one to eliminate $\theta(\boldsymbol{r})$ from the GL potential by taking a unitary gauge $\boldsymbol{A}' = \boldsymbol{A} - \nabla\theta/e^*$. As a result, we obtain (denoting $\boldsymbol{A}'$ as $\boldsymbol{A}$)

$$f \quad = -2aH^2 + \frac{1}{2m^*}(\nabla H)^2 + \frac{e^{*2}\psi_0^2}{2m^*}\boldsymbol{A}^2 + \frac{e^{*2}\psi_0}{m^*}\boldsymbol{A}^2H + \cdots. \tag{13.4}$$

One can see that the phase mode is absorbed into the longitudinal component of the electromagnetic field. At the same time, there appears a mass term for photons (the third term on the right hand side of Equation 13.4) with the mass proportional to $\sqrt{e^{*2}\psi_0^2/m^*}$ (Anderson-Higgs mechanism). Due to this, electromagnetic waves cannot propagate freely inside superconductors but decay exponentially with a finite penetration length (Meissner effect).

From Equation 13.4, one immediately sees that there is no linear coupling between the Higgs and electromagnetic field. This is consistent with the fact that the Higgs mode does

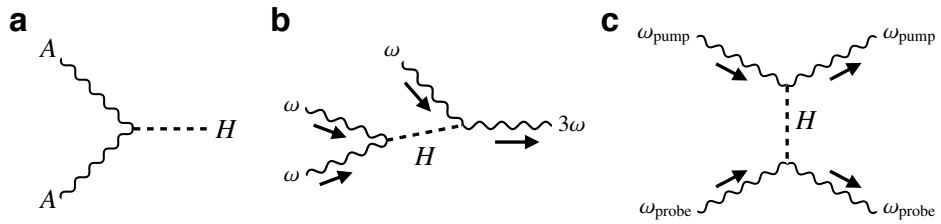


Figure 13.2: (*a*) Diagrammatic representation of the nonlinear light-Higgs coupling $\boldsymbol{A}^2 H$ in Equation 13.4. (*b*) Third harmonic generation mediated by the Higgs mode. (*c*) Pump-probe spectroscopy mediated by the Higgs mode.

not have an electric charge, magnetic moment, and other quantum numbers, which has been a main obstacle in observing the Higgs mode by an external probe for a long time. On the other hand, there is a nonlinear coupling term $\boldsymbol{A}^2 H$ in Equation 13.4, which is responsible for the Higgs mode to contribute in various nonlinear processes. In **Figure** 13.2***a***, we illustrate the diagrammatic representation of the nonlinear light-Higgs coupling, where two photons are coming in with frequencies ω_1 and ω_2 and one Higgs is emitted with frequency $\omega_1 + \omega_2$. This is analogous to the elementary process of the Higgs particle decaying into W bosons that had played a role in the discovery of the Higgs particle in LHC experiments [23, 24].

Due to the nonlinear interaction between the Higgs mode and electromagnetic fields, one can induce a nonlinear current given by

$$\boldsymbol{j} = -\frac{\partial F}{\partial \boldsymbol{A}} = -\frac{ie^*}{2m^*}[\psi^\dagger \nabla\psi - (\nabla\psi^\dagger)\psi] - \frac{e^{*2}}{m^*}\boldsymbol{A}\psi^\dagger\psi. \tag{13.5}$$

Again, we expand ψ around the ground state ψ_0 in Equation 13.5 and collect leading terms in H, which results in

$$\boldsymbol{j} = -\frac{2e^{*2}\psi_0}{m^*}\boldsymbol{A}H. \tag{13.6}$$

This is nothing but the leading part of the London equation $\boldsymbol{j} = -(e^{*2}n_s/m^*)\boldsymbol{A}$ (let us recall that the amplitude of the order parameter corresponds to the superfluid density, $|\psi|^2 = n_s$).

When a monochromatic laser with frequency ω drives a superconductor, the amplitude of the order parameter oscillates with frequency 2ω due the nonlinear coupling $\boldsymbol{A}^2 H$ (**Figure** 13.2***a***). Together with the oscillation of $\boldsymbol{A}$ with frequency ω in Equation 13.6, the induced nonlinear current shows an oscillation with frequency 3ω. As a result, one obtains the third harmonic generation mediated by the Higgs mode (**Figure** 13.2***b***). Since the Higgs mode has an energy 2Δ at low momentum, one can resonantly excite the Higgs mode by a THz laser with a resonance condition $2\omega = 2\Delta$. Given that the nonlinear current is proportional to the Higgs-mode amplitude (Equation 13.6), the third harmonic generation can be resonantly enhanced through the excitation of the Higgs mode. The Higgs-mode resonance in third harmonic generation has been experimentally observed for a conventional superconductor [46].

Another example of nonlinear processes to which the Higgs mode can contribute is a pump-probe spectroscopy where pump and probe light is simultaneously applied (**Figure** 13.2***c***). In this case, photons with different frequencies $\omega_{\rm pump}$ and $\omega_{\rm probe}$ are injected, and those with the same respective frequencies are emitted. There are three possibilities of the frequency carried by the Higgs mode: $\omega_{\rm pump} \pm \omega_{\rm probe}$ and $\omega_{\rm pump} - \omega_{\rm pump} = \omega_{\rm probe} - \omega_{\rm probe} = 0$. If one uses a THz pump and optical probe, i.e., $\omega_{\rm pump} \lesssim 2\Delta$ and $\omega_{\rm probe} \gg 2\Delta$, the first two channels do not contribute since the excitation of the Higgs mode is far off-resonant. The remaining zero-frequency excitation channel contributes to the pump-probe spectroscopy. This process has been elaborated in the experimental study of the Higgs mode in *d*-wave superconductors [55].

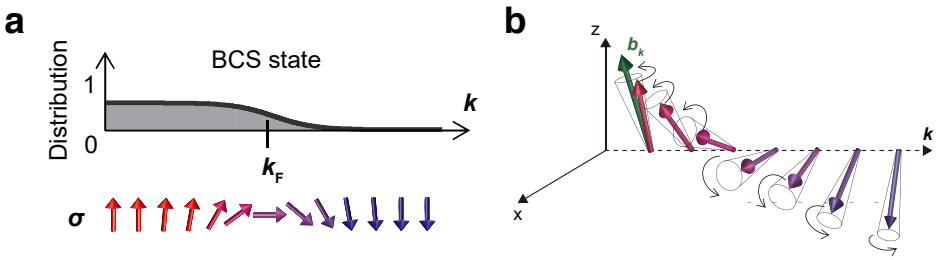


Figure 13.3: (*a*) Momentum distribution of a superconducting state (above) and its pseudospin representation due to Anderson (below). (*b*) Pseudospin precession induced by a laser field. Figures are taken from Reference [46].

13.2.2 A microscopic view

In the previous subsection, we reviewed the phenomenology for the nonlinear light-Higgs coupling using the Ginzburg-Landau theory. However, strictly speaking, the application of the Ginzburg-Landau theory to nonequilibrium problems is not microscopically justified in the case of gapped superconductors [70, 71, 72]. The reason is that in a usual situation one cannot neglect the effect of quasiparticle excitations whose relaxation time is longer than the time scale of the order-parameter variation. Moreover, the Higgs mode and quasiparticle excitations are energetically degenerate at low momentum (**Figure** 13.1***b***), so that it is inevitable to excite quasiparticles at the same time when one excites the Higgs mode. This motivates us to take a microscopic approach for further understanding.

Let us adopt the time-dependent BCS or Bogoliubov-de Gennes equation, which is efficiently represented by the Anderson pseudospin $\boldsymbol{\sigma}_{\boldsymbol{k}} = \frac{1}{2}\langle \Psi^\dagger_{\boldsymbol{k}} \boldsymbol{\tau} \Psi_{\boldsymbol{k}} \rangle$ [5]. Here $\Psi^\dagger_{\boldsymbol{k}} = (c^\dagger_{\boldsymbol{k}\uparrow}, c_{-\boldsymbol{k}\downarrow})$ is the Nambu spinor, $\boldsymbol{\tau} = (\tau_x, \tau_y, \tau_z)$ are Pauli matrices, $c^\dagger_{\boldsymbol{k}\sigma}$ ($c_{\boldsymbol{k}\sigma}$) is the creation (annihilation) operator of electrons with momentum $\boldsymbol{k}$ and spin σ, and $\langle \cdots \rangle$ denotes the statistical average. Physically, the x and y components of the Anderson pseudospin correspond to the real and imaginary parts of the Cooper pair density, respectively, and the z component corresponds to the momentum occupation distribution of electrons (**Figure** 13.3***a***). With this notation, the BCS mean-field Hamiltonian is written as

$$H_{\mathrm{BCS}} = 2\sum_{\boldsymbol{k}} \boldsymbol{b}_{\boldsymbol{k}}(t) \cdot \boldsymbol{\sigma}_{\boldsymbol{k}}, \tag{13.7}$$

$$\boldsymbol{b}_{\boldsymbol{k}}(t) = \left(-\Delta'(t), -\Delta''(t), \frac{1}{2}(\epsilon_{\boldsymbol{k}+\boldsymbol{A}(t)} + \epsilon_{\boldsymbol{k}-\boldsymbol{A}(t)}) \right). \tag{13.8}$$

Here $\boldsymbol{b}_{\boldsymbol{k}}(t)$ is a pseudomagnetic field acting on pseudospins, Δ' and Δ'' are the real and imaginary parts of the superconducting gap function, respectively, and $\epsilon_{\boldsymbol{k}}$ is the band dispersion of the system. The equation of motion for the pseudospins is given by the Bloch-type equation,

$$\frac{\partial}{\partial t}\boldsymbol{\sigma}_{\boldsymbol{k}}(t) = 2\boldsymbol{b}_{\boldsymbol{k}}(t) \times \boldsymbol{\sigma}_{\boldsymbol{k}}(t), \tag{13.9}$$

supplemented by the mean-field condition $\Delta'(t) + i\Delta''(t) = \frac{V}{N}\sum_{\boldsymbol{k}}[\sigma^x_{\boldsymbol{k}}(t) + i\sigma^y_{\boldsymbol{k}}(t)]$ with V the attractive interaction and N the number of k points. The time evolution of the superconducting state is thus translated into the precession dynamics of Anderson pseudospins (**Figure** 13.3***b***).

The coupling to the electromagnetic field appears in the z component of the pseudomagnetic field, $b^z_{\boldsymbol{k}} = \frac{1}{2}(\epsilon_{\boldsymbol{k}+\boldsymbol{A}(t)} + \epsilon_{\boldsymbol{k}-\boldsymbol{A}(t)})$. If we expand $b^z_{\boldsymbol{k}}$ in terms of $\boldsymbol{A}(t)$, we obtain $b^z_{\boldsymbol{k}} = \epsilon_{\boldsymbol{k}} + \frac{1}{2}\sum_{ij}\frac{\partial^2 \epsilon_{\boldsymbol{k}}}{\partial k_i \partial k_j} A_i A_j + O(A^4)$. The linear coupling term vanishes, which is consistent with the phenomenology that we have reviewed in the previous subsection. The leading nonlinear

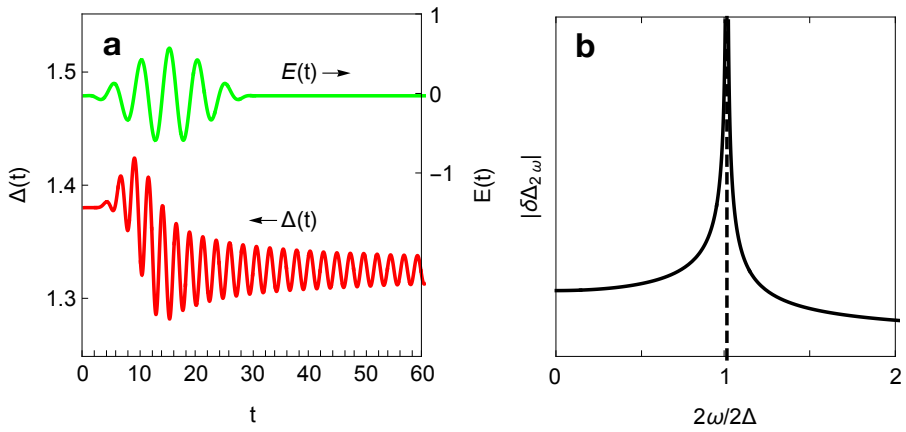


Figure 13.4: (a) A numerical result for the time evolution of the superconducting gap $\Delta(t)$ driven by an electric field pulse $E(t)$ with the frequency $\omega = 2\pi/5 \sim 1.26$. Here we take a two dimensional square lattice with a bandwidth 8 at half filling. The interaction is $V = 4$, and the initial temperature is $T = 0.02$. The polarization of the electric field is parallel to x axis. The left (right) vertical axis represents the value of $\Delta(t)$ ($E(t)$) as indicated by the arrows. (b) The amplitude of the 2ω oscillation of the superconducting gap as a function of $2\omega/2\Delta$. (b) is reproduced from Reference [42].

coupling term is quadratic in $\boldsymbol{A}(t)$. In **Figure** 13.4***a***, we show a numerical result for the time evolution of the gap function $\Delta(t)$ when the system is driven by a multi-cycle electric-field pulse. One can see that the 2ω oscillation of the gap is generated during the pulse irradiation, after which a free gap oscillation continues with the frequency 2Δ and the amplitude slowly damping as $t^{-1/2}$ [16].

For a monochromatic wave $\boldsymbol{A}(t) = \boldsymbol{A}_0 \sin \omega t$, one can solve the equation of motion semi-analytically by linearizing with respect to the quadratic coupling $A_i(t)A_j(t)$ around the equilibrium solution. The result shows that the amplitude of the gap function varies as [42]

$$\delta\Delta(t) \propto |2\omega - 2\Delta|^{-\frac{1}{2}} \cos(2\omega - \phi) \tag{13.10}$$

for $\omega \sim \Delta$, where ϕ is a phase shift. The induced oscillation frequency is 2ω, reflecting the nonlinear coupling between the Higgs mode and electromagnetic fields, $\boldsymbol{A}^2 H$. The oscillation amplitude diverges when the condition $2\omega = 2\Delta$ is fulfilled (**Figure** 13.4***b***). This is much the same as the spin resonance phenomenon: The forced collective precession of the pseudospins with frequency 2ω due to the nonlinear coupling resonates with the Higgs mode whose energy coincides with 2Δ. The power of the divergence $\frac{1}{2}$ in Equation 13.10 is smaller than that of a resonance with an infinitely long-lived mode ($\sim |2\omega - \omega_*|^{-1}$). The reason is that the precession gradually dephases due to the momentum-dependent frequency $\omega_{\boldsymbol{k}} = 2\sqrt{\epsilon_{\boldsymbol{k}}^2 + \Delta^2}$ for each pseudospin so that the average of the pseudospins $\delta\Delta(t) = \frac{V}{N}\sum_{\boldsymbol{k}} \delta\sigma_{\boldsymbol{k}}^x(t)$ shows a power-law damping of oscillations. The phase shift ϕ exhibits a $\frac{\pi}{2}$ jump as one goes across the resonance by changing the drive frequency ω.

In the case of the square lattice and the polarization of the electric field parallel to the diagonal direction in the xy plane, for example, the current is given by $\boldsymbol{j}(t) \propto \boldsymbol{A}(t)\delta\Delta(t)$ [42, 46], which corresponds to the phenomenological relation $\boldsymbol{j}(t) \propto \boldsymbol{A}(t)H(t)$ (Equation 13.6). As expected, the Higgs mode induces a resonant enhancement of the third harmonic generation. Later, it has been pointed out [47] that the current relation is valid only in rather special situations such as the square lattice and the polarization parallel to the diagonal direction. In general, the BCS mean-field treatment (in the clean limit) suggests that the Higgs-mode contribution to the third harmonic generation is subdominant as compared to that of individual

quasiparticle excitations. Since the energy scales of the Higgs mode and the quasiparticle pair excitations are in the same order ($\sim 2\Delta$, see **Figure** 13.1***b***), the competition between the two contributions always matters. This point will be further examined in the next subsection.

13.2.3 Impurity and phonon assisting

As we have seen in the previous subsection, the Higgs-mode contribution to the third harmonic generation is generally subdominant in the BCS clean limit. However, there is a growing understanding from recent studies [48, 49, 51, 52, 53, 54] that if one takes into account effects beyond the BCS mean-field theory in the clean limit (such as impurity scattering and phonon retardation) the light-Higgs coupling strength drastically changes.

To understand the impact of these effects, let us consider the linear optical response. The current induced by a laser field is decomposed into the paramagnetic and diamagnetic components $\boldsymbol{j} = \boldsymbol{j}_{\rm para} + \boldsymbol{j}_{\rm dia}$ with [73]

$$\boldsymbol{j}_{\rm para} = \sum_{\boldsymbol{k}\sigma} \frac{\partial \epsilon_{\boldsymbol{k}}}{\partial \boldsymbol{k}} \langle c^\dagger_{\boldsymbol{k}\sigma} c_{\boldsymbol{k}\sigma} \rangle, \tag{13.11}$$

$$\boldsymbol{j}_{\rm dia} = -\sum_{\boldsymbol{k}\sigma i} \frac{\partial^2 \epsilon_{\boldsymbol{k}}}{\partial \boldsymbol{k} \partial k_i} A_i \langle c^\dagger_{\boldsymbol{k}\sigma} c_{\boldsymbol{k}\sigma} \rangle. \tag{13.12}$$

As we have seen in the pseudospin picture in the previous subsection, only the diamagnetic coupling contributes to the optical response in the mean-field level with no disorder, resulting in $\mathrm{Re}\,\sigma(\omega) \propto \delta(\omega)$ and $\mathrm{Im}\,\sigma(\omega) \propto 1/\omega$ for the superconducting state. For finite frequency ($\omega \neq 0$), the real part of the optical conductivity vanishes in the BCS clean limit. This does not necessarily mean that the real part of the optical conductivity is suppressed in real experimental situations. For example, in superconductors with a disorder the real part of the optical conductivity is nonzero and not even small for $\omega \neq 0$. In fact, a superconductor NbN used in the experiment of the third harmonic generation turns out to be close to the dirty regime ($\gamma \gg 2\Delta$, where γ is the impurity scattering rate) as confirmed from the measurement of the optical conductivity [4].

Table 1: Relative order of magnitudes of the third-order current $\boldsymbol{j}^{(3)}$ in general situations [53].

mode	channel	clean $\to$ dirty
Higgs	dia ($\boldsymbol{A}^2$)	$(\Delta/\epsilon_F)^2$
	para ($\boldsymbol{p}\cdot\boldsymbol{A}$)	$(\epsilon_F\gamma/\Delta^2)^2 \to (\epsilon_F/\gamma)^2$
Quasiparticles	dia ($\boldsymbol{A}^2$)	1
	para ($\boldsymbol{p}\cdot\boldsymbol{A}$)	$(\epsilon_F\gamma/\Delta^2)^2 \to (\epsilon_F/\gamma)^2$

In much the same way as the optical conductivity, the nonlinear response intensity is strongly affected by the impurity effect. The γ dependence of the relative order of magnitudes of the third-order current is summarized in Table 1, where ϵ_F is the Fermi energy and the unit of $\boldsymbol{j}^{(3)}$ is taken such that the diamagnetic-coupling contribution of the quasiparticles is set to be of order 1 (which does not significantly depend on γ). In the BCS clean limit ($\gamma \to 0$), we have only the diamagnetic coupling, for which the Higgs-mode contribution is subleading in the order of $(\Delta/\epsilon_F)^2$ compared to the quasiparticles. However, in the presence of impurities ($\gamma \neq 0$) the paramagnetic coupling generally emerges to contribute to the third harmonic generation. Its relative order of magnitude changes as $(\epsilon_F\gamma/\Delta^2)^2 \to (\epsilon_F/\gamma)^2$ from the clean to dirty limit. The maximum strength of the paramagnetic coupling is achieved around $\gamma \sim \Delta$, where the

relative order reaches $(\epsilon_F/\Delta)^2$ for both the Higgs mode and quasiparticles. Thus, the impurity scattering drastically enhances the light-Higgs coupling: in the clean limit the Higgs-mode contribution is subleading to quasiparticles, whereas in the dirty regime it becomes comparable to or even larger than the quasiparticle contribution. The precise ratio between the Higgs and quasiparticle contributions may depend on details of the system. Recent studies [52, 53, 54] suggest that in the dirty regime the Higgs-mode contribution to THG is an order of magnitude larger than the quasiparticle contribution. An enhancement of the paramagnetic coupling also occurs for strongly coupled superconductors due to the phonon retardation effect [48].

13.2.4 Further developments

So far, we have reviewed the phenomenological and mean-field treatments of the nonlinear light-Higgs coupling for conventional s-wave superconductors with or without disorder. For strongly coupled superconductors with an electron-phonon coupling constant $\lambda \gtrsim 1$ (which is the case for NbN superconductors [74, 75, 76]), one has to take account of strong correlation effects. One useful approach for this is the nonequilibrium dynamical mean-field theory [77], which takes into account local dynamical correlations by mapping a lattice model into a local impurity model embedded in an effective mean field. With this, the Higgs mode in strongly coupled superconductors modeled by the Holstein model has been analyzed [42, 48, 78, 79]. A closely related nonequilibrium Keldysh method has been employed to study the Higgs mode in a time-resolved photoemission spectroscopy [43, 80] and time-resolved optical conductivity [81]. Another approach is to use the gauge-invariant kinetic equation [82, 83, 84, 85], where the shift of the center-of-mass momentum of Cooper pairs ("drive effect") caused by a laser pulse has been emphasized.

For multi-band superconductors with multiple gaps such as MgB_2, there are not only Higgs modes corresponding to amplitude oscillations of multiple order parameters but also the so-called Leggett mode [86], which corresponds to a collective oscillation of the relative phase between different order parameters. Based on the mean-field theory, possible laser excitations of the Higgs and Leggett modes in multiband superconductors have been studied [53, 87, 88, 89, 90].

For non-s-wave superconductors, one can expect even richer dynamics of the order parameters. For example, d-wave superconductors allow for various different symmetries of amplitude modes [9]. The quench dynamics of the d-wave [92] and $p + ip$-wave [93] Higgs modes have been explored. For recent experimental progresses on pump-probe spectroscopies and third harmonic generation in d-wave superconductors, we refer to Section 13.3.3. It has also been proposed [94] that by measuring Higgs modes for various quench symmetries one can obtain information on the symmetry of the gap function ("Higgs spectroscopy").

13.3 Experiments

In this section, we overview recent progresses on experimental observations of the Higgs mode in superconductors. Those include Raman experiments in CDW-coexisting superconductors 2H-$NbSe_2$ and TaS_2 (Section 13.3.1), THz spectroscopies and third harmonic generation in a pure s-wave superconductor NbN (Section 13.3.2) and in high-T_c cuprates (Section 13.3.3), and THz transmittance experiments in NbN under supercurrent injection (Section 13.3.4).

13.3.1 Higgs mode in a superconductor with CDW

The pioneering work on the observation of the Higgs mode in superconductors dates back to 1980 when a Raman experiment was performed in 2H-$NbSe_2$, a transition metal dichalcogenide

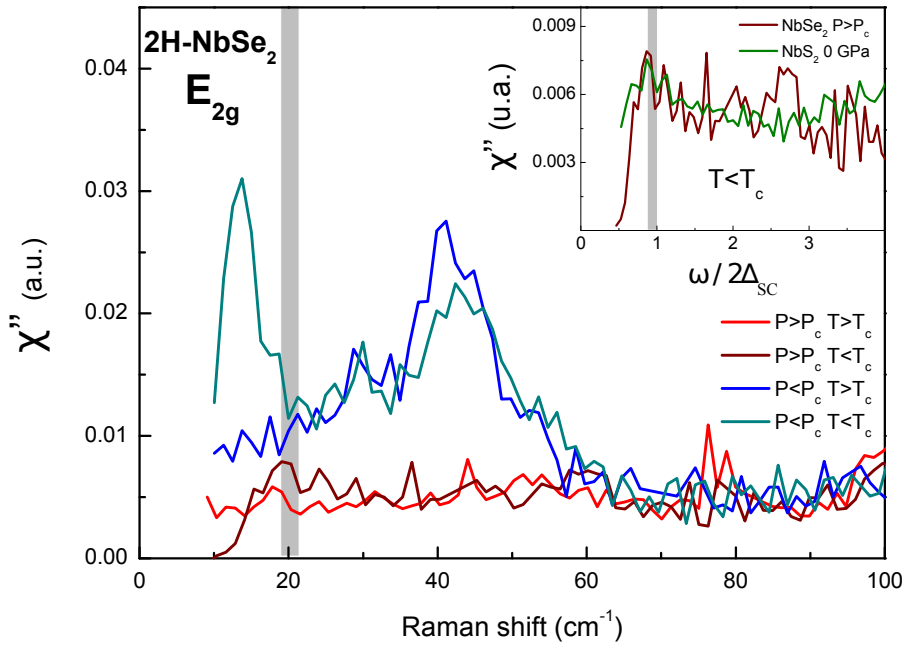


Figure 13.5: Raman spectra in E_{2g} symmetry of 2H-$NbSe_2$ measured at various temperatures and pressures. Under the ambient pressure ($P < P_c$) and in the superconducting phase ($T < T_c$) (green), a sharp peak identified as the Higgs mode appears below the superconducting gap $2\Delta \sim 20$ cm^{-1} marked by the gray vertical line. In the CDW phase ($T > T_c$) (blue), only the CDW amplitude mode is observed around 40 cm^{-1}. Under the pressure ($P > P_c$) where CDW collapses, only a pair breaking peak is discerned at $T < T_c$ (brown), and no peak is identified at $T > T_c$ (red). Inset: Raman spectra in the superconducting state without CDW in 2H-$NbSe_2$ (above 4 GPa) and non-CDW-coexisting NbS_2 (0 GPa), both of which show only the pair breaking peak. Frequency is normalized by 2Δ. Figure is taken from Reference [30].

in which superconductivity coexists with CDW [3, 26]. A new peak was observed below T_c, distinct from the amplitude mode associated with the CDW order. Although it was initially recognized as a pair breaking peak, soon after it was identified as the collective amplitude mode of the superconducting order (i.e., the Higgs mode) [2, 12] (see also [27, 6]).

A renewed Raman experiment has been conducted recently, revealing the transfer of the oscillator strength from the amplitude mode of CDW (amplitudon) to the Higgs mode [28]. Subsequently the Raman experiment under hydrostatic pressure has been performed in 2H-$NbSe_2$ [30] (**Figure** 13.5). With applying the hydrostatic pressure the CDW order is suppressed and concomitantly the Raman peak identified as the Higgs mode was shown to disappear with leaving only the Cooper pair breaking peak. A more clear separation between the in-gap Higgs mode and the pair breaking peak was recently reported in a similar CDW-coexisting superconductor, TaS_2 [95]. These results indicate that the existence of CDW plays an important role on the visibility of the Higgs mode in the Raman spectrum. A theoretical study has demonstrated that, due to the coupling of the superconducting order to the coexisting CDW order, the Higgs mode energy is pushed down below the superconducting gap 2Δ [29]. Accordingly, the Higgs mode becomes stable due to the disappearance of the decay channel into the quasiparticle continuum.

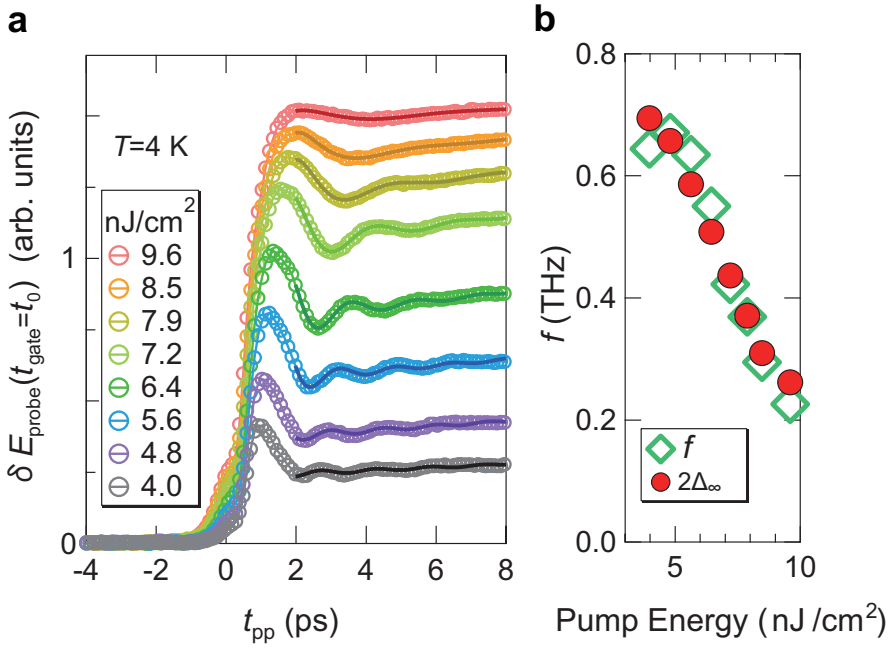


Figure 13.6: Higgs-mode oscillation after the nonadiabatic excitation of quasiparticles in NbN induced by a monocycle THz pump. (a) The temporal evolution of the change of the probe electric field, $\delta E_{\rm probe}$, as a function of the pump-probe delay time $t_{\rm pp}$ at various pump intensities. The solid curves represent the results fitted by a damped oscillation with a power-law decay. (b) The oscillation frequency f obtained from the fits and the asymptotic gap energy $2\Delta_\infty$ as a function of the pump intensity. Figures are taken from Reference [4].

13.3.2 Higgs mode in a pure s-wave superconductor

Nonadiabatic quench with a single-cycle THz pump pulse

One way to excite the Higgs mode is a nonadiabatic quench of the superconducting state, which can be induced by, for example, a sudden change of the pairing interaction that generates the order-parameter dynamics,

$$\frac{|\Delta(t)|}{\Delta_\infty} \simeq 1 + a\frac{\cos(2\Delta_\infty t + \phi)}{\sqrt{\Delta_\infty t}}, \tag{13.13}$$

at long time. Here $2\Delta_\infty$ is the long-time asymptotic superconducting gap, a is some constant, and ϕ is a phase shift. The behavior (Equation 13.13) has been theoretically derived on the basis of the time-dependent BCS mean-field theory [16, Barankov and Levitov(2006), 34, 35]. A similar dynamics has also been investigated after a laser-pulse excitation [38, 39, 40, 41, 43, 44].

Despite intensive theoretical studies on the Higgs mode in superconductors, the observation of the Higgs mode has long been elusive except for the case of 2H-$NbSe_2$, until when the ultrafast THz-pump and THz-probe spectroscopy was performed in a conventional s-wave superconductor $Nb_{1-x}Ti_xN$ [4]. In this experiment, quasiparticles are instantaneously injected at the superconducting-gap edge to quench the superconducting order parameter nonadiabatically. A strong single-cycle THz pump pulse with the center frequency around 1 THz ($\sim$ 4 meV) was generated from a $LiNbO_3$ crystal by using the tilted-pulse-front method [96, 97, 98], in order to excite high density quasiparticles just above the gap of $Nb_{1-x}Ti_xN$ thin films with 2Δ = 0.72-1.3 THz ($\sim$ 3.0-5.4 meV) at 4 K. The details of the THz pump-THz probe scheme were given in Ref. [99]. The subsequent dynamics of the superconducting order parameter was probed by a weaker probe THz pulse in transmission geometry. **Figure** 13.6 shows pump-probe

delay dependence of the transmitted probe THz electric field at a fixed point of the probe pulse waveform which reflects the order parameter dynamics. A clear oscillation is identified after the pump with the oscillation frequency given by the asymptotic value of the superconducting gap $2\Delta_\infty$ caused by the quasiparticle injection. The decay of the oscillation is well fitted by a power-law decay predicted for the Higgs-mode oscillation. With increasing the pump intensity, the oscillation period shows a softening, as the asymptotic value of $2\Delta_\infty$ becomes smaller with higher quasiparticle densities. By recording the probe THz waveform at each pump-probe delay, one can extract the dynamics of the complex optical conductivity $\sigma(\omega) = \sigma_1(\omega) + i\sigma_2(\omega)$ (not shown). The spectral-weight oscillation with frequency $2\Delta_\infty$ was clearly identified both in the real and imaginary parts [100], the latter of which reflects the oscillation of the superfluid density (i.e., the amplitude of the superconducting order parameter).

The intense single-cycle THz pump pulse was crucial to excite the quasiparticles instantaneously at the gap edge which acts as a nonadiabatic quench of the order parameter, thereby inducing a free oscillation of the Higgs mode. On the contrary, when a near-infrared optical pulse was used as a pump, a relatively slow rise time ($\sim$ 20 ps) was observed for the suppression of the order parameter, though dependent on the excitation fluence [99, 101]. In this case, the photoexcited hot electrons (holes) emit a large amount of high frequency phonons ($\omega > 2\Delta$) (HFP) which subsequently induces the Cooper pair-breaking until quasiparticles and HFP reach the quasiequilibrium. This process was well described by the Rothwarf-Taylor phonon-bottleneck model [101], and usually takes a time longer than $(2\Delta)^{-1}$, which breaks the nonadiabatic excitation condition needed for the quench experiment. It should be noted here that even if one uses the near-infrared or visible optical excitation, the instantaneous quasiparticle excitation can occur if the stimulated Raman process is efficient [102].

The decay of the Higgs mode is also an important issue. Since the Higgs-mode energy 2Δ coincides with the onset of quasiparticle continuum, the Higgs mode inevitably decays into the quasiparticle continuum even without any collisions [16, 17]. However, this does not mean that the Higgs mode is an overdamped mode. In fact, the decay due to the collisionless energy transfer is expected to be proportional to $t^{-1/2}$ in the BCS superconductor, ensuring a much longer lifetime compared with the oscillation period. The energy dispersion of the Higgs mode for finite wavenumber q has been calculated as

$$\omega_H \simeq 2\Delta + \frac{v_F^2}{12\Delta}q^2 - i\frac{\pi^2 v_F}{24}q \tag{13.14}$$

where v_F is the Fermi velocity [12]. From Equation 13.14 one can estimate that as the wavenumber q increases and the mode energy enters into the quasiparticle continuum, the lifetime of Higgs mode is shortened and turns into an overdamped mode. For the case of NbN, $\Delta \sim 0.6$ THz and $v_F \sim 2 \times 10^6$ m/s [76] and the imaginary part exceeds the real part in Equation 13.14 at $q > \Delta/v_F \sim 0.3$ $(\mu\text{m})^{-1}$. In the single-cycle THz-pump experiment in a thin film of NbN [4], the value of in-plane wavenumber q estimated from the spot size of the pump ($\sim$ 1 mm) is at most ~ 1 $(\text{mm})^{-1}$, which is far smaller than Δ/v_F. In such a small q limit, the Higgs mode is considered as a well-defined collective mode [12].

Multicycle THz driving with subgap frequency and third harmonic generation

To excite the Higgs mode in an on-resonance condition, one can use a narrowband multicycle THz pump pulse with the photon energy tuned below the superconducting gap 2Δ. With this, the amplitude of the superconducting order parameter was shown to oscillate with twice the frequency of the incident pump-pulse frequency ω during the pulse irradiation (**Figure** 13.7***a*-*d***) [46]. The observed 2ω modulation of the order parameter was attributed to the forced oscillation of the Higgs mode caused by electromagnetic fields. In fact, the time-dependent Ginzburg-Landau theory shows that there is a coupling term between the Higgs (H) and field ($\boldsymbol{A}$) as

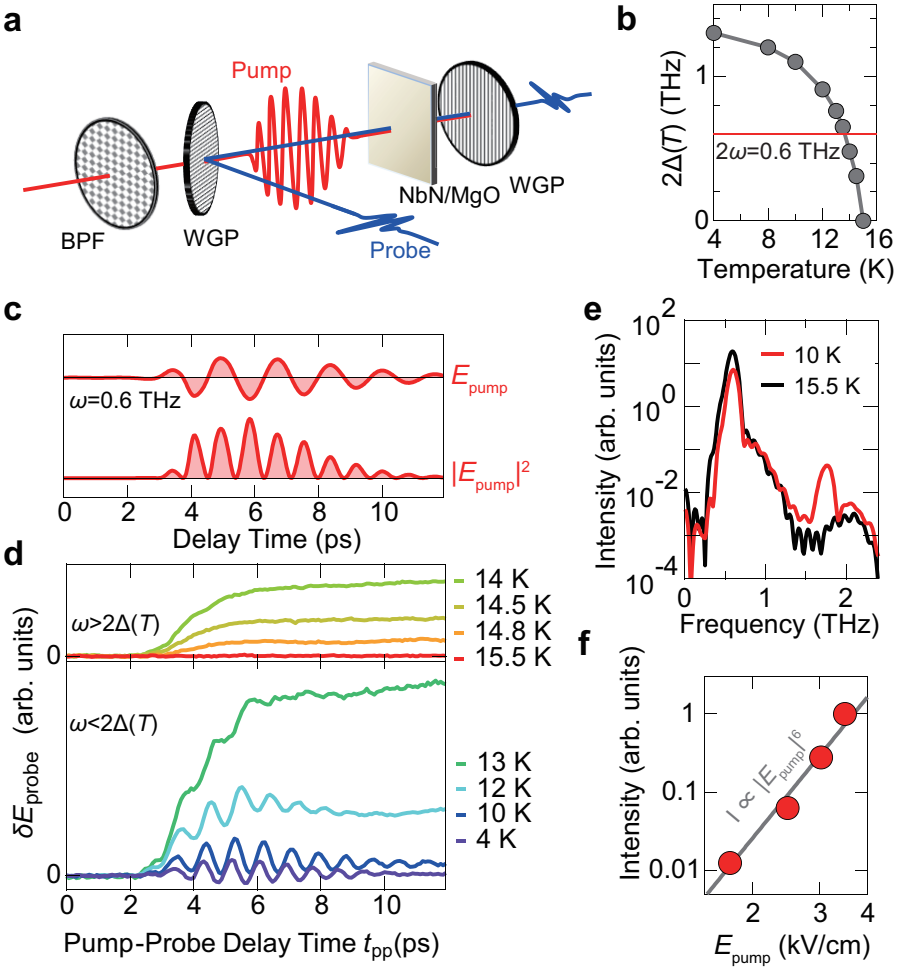


Figure 13.7: Forced Higgs oscillation and third harmonic generation from a superconducting NbN film under the multicycle THz pump. (a) Schematic setup for the multicycle THz pump and THz probe spectroscopy. BPF: a bandpass filter, WGP: a wire grid polarizer. (b) Temperature dependence of the superconducting gap energy. Horizontal line indicates the center frequency of the pump pulse, $\omega = 0.6$ THz. (c) Waveform of the pump THz electric field $E_{\rm pump}$ and the squared one, $|E_{\rm pump}|^2$. (d) The change in the transmitted probe THz electric field $\delta E_{\rm probe}$ as a function of the pump-probe delay time t_{pp} at the tempareture range $\omega > 2\Delta(T)$ (top panel) and $\omega < 2\Delta(T)$ (bottom panel). Increase of $\delta E_{\rm probe}$ corresponds to the reduction of the order parameter. (e) Power spectra of the transmitted pump THz pulse above and below $T_c = 15$ K. (f) THG intensity as a function of the pump THz field strength. Figures are taken from Reference [46].

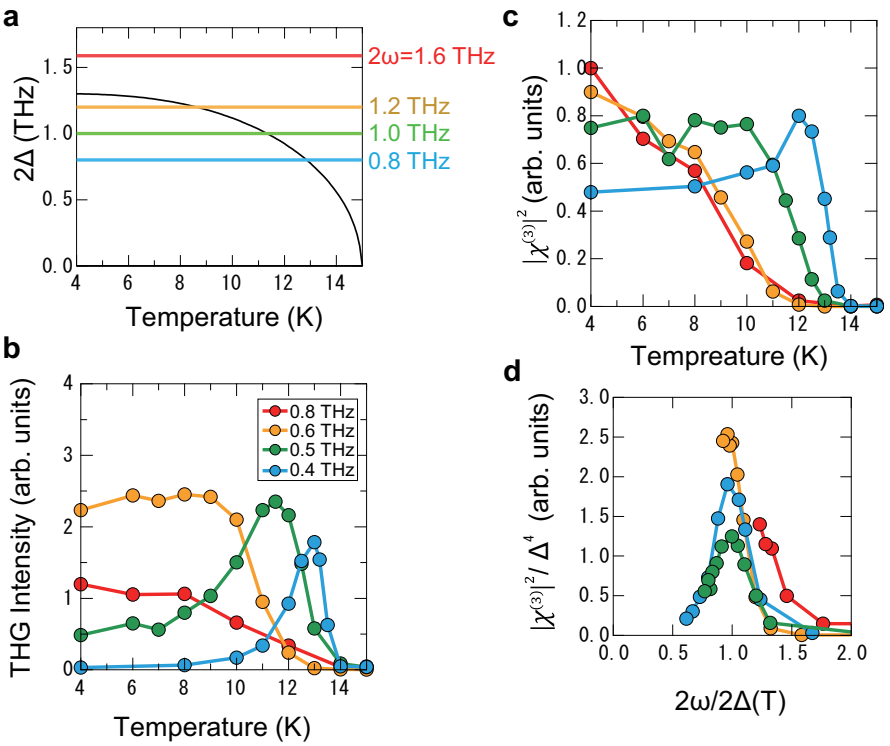


Figure 13.8: Temperature dependence of THG signal from NbN. (a) Temperature dependence of the supercondcuting gap $2\Delta(T)$. Twice the THz pump frequencies 2ω are shown by horizontal lines. (b) Measured THG intensities at each frequencies as a function of temperature. (c) THG intensities normalized by the temperature dependent internal field inside the superconducting film and the transmittance of the THG signal, which corresponds to the susceptibility of THG, $|\chi^{(3)}|^2$. (d) Further normalized value of $|\chi^{(3)}|^2$ by the temperature dependent gap $\Delta(T)^4$ as a function of normalized frequency $2\omega/2\Delta(T)$. Relative intensities between different frequencies are arbitrary. Data are taken from Reference [100].

expressed by $\boldsymbol{A}^2 H$ (Section 13.2.1), which results in the 2ω-order parameter modulation. The nonlinear electromagnetic response of superconductors has been studied in the frequency range far below 2Δ and near T_c where the Ginzburg-Landau theory is applicable [64, 70, 103, 104, 105]. In the theory developed by Gor'kov and Eliashberg (GE), a closed set of equations for the order parameter Δ and the field $\boldsymbol{A}$ was derived, which predicts the 2ω modulation of Δ and the THG from the induced supercurrent $\boldsymbol{j} \propto \boldsymbol{A}^2\Delta$ [70]. The GE theory was experimentally demonstrated through the observation of THG of a microwave field in a paramagnetically doped superconductor [104].

The THz pump experiments have shed a new light on the investigation of the nonlinear electromagnetic response of superconductors at the gap frequency region. Subsequent to the observation of the 2ω modulation of the order parameter, namely the forced oscillation of the Higgs modes, the THG was observed under the irradiation of a subgap multicycle THz pump pulse in NbN thin films as shown in **Figure** 13.7$\boldsymbol{e}$, $\boldsymbol{f}$. Importantly, the THG was shown to be resonantly enhanced when a condition $2\omega = 2\Delta$ is satisfied [46]. The temperature dependence of THG intensity for various frequencies in a NbN film is shown in **Figure** 13.8: the temperature dependence of the gap 2Δ and the incident frequencies (**Figure** 13.8$\boldsymbol{a}$), the raw data of THG intensities (**Figure** 13.8$\boldsymbol{b}$), those normalized by the internal field inside the superconducting film which is proportional to the third-order susceptibility $|\chi^{(3)}|^2$ (**Figure** 13.8$\boldsymbol{c}$), and the THG intensity further normalized by the proportional factor of the THG intensity $\Delta(T)^4$ versus the frequency normalized to the gap, $2\omega/2\Delta(T)$ (**Figure** 13.8$\boldsymbol{d}$). These results clearly show the

two-photon resonances of the Higgs mode with the field.

As previously described in Section 13.2.3, however, it was theoretically pointed out that there is a contribution also from the quasiparticle excitation (or called charge density fluctuations) in THG, which also exhibits the $2\omega = 2\Delta$ resonance [47]. Within the BCS mean-field approximation in the clean limit, the quasiparticle term was shown to exceed the Higgs mode contribution in THG. At the same time, it was predicted that the THG from the quasiparticle term should exhibit polarization dependence with respect to the crystal axis while the Higgs term is totally isotropic in a square lattice [47]. In the experiments in NbN, the THG intensity was shown to be independent from the incident polarization angle with respect to the crystal orientation and notably the emitted THG does not have orthogonal components with respect to the incident polarization of the fundamental (ω) wave [49]. Such a totally isotropic nature of THG cannot be well accounted for by the CDF term even if one considers the crystal symmetry of NbN [50] and indicates the Higgs mode as the origin of THG. Recently, the importance of $\boldsymbol{p} \cdot \boldsymbol{A}$ term on the coupling between the Higgs mode and the gauge field was elucidated. In particular, the $\boldsymbol{p} \cdot \boldsymbol{A}$ term contribution is largely enhanced when one consider the phonon retardation effect beyond the BCS approximation [48] and more prominently when one considers the nonmagnetic impurity scattering effect [52, 53, 54], dominating the quasiparticle term by an order of magnitude as described in Section 13.2.3. This paramagnetic term was also shown to dominate the diamagnetic term, although its ratio depends on the ratio between the coherence length and the mean free path. The NbN superconductor is in the dirty regime as manifested by a clear superconducting gap structure observed in the conductivity spectrum, and the paramagnetic term should significantly contribute to THG.

13.3.3 Higgs mode in high-T_c cuprates

Higgs modes can exist not only in s-wave superconductors but also in unconventional superconductors. For example, in d-wave superconductors such as high-T_c cuprates one can expect various types of collective modes, including not only the totally isotropic oscillation of the gap function in relative momentum space (A_{1g} mode) but also those that oscillate anisotropically (e.g., A_{2g}, B_{1g}, B_{2g} modes) [9]. These are reminiscent of Bardasis-Schrieffer mode for the case of s-wave superconductors [106]. Possible collective modes have been classified based on the point group symmetry of the lattice [9], and the relaxation behavior of the A_{1g} mode induced by a quench has been discussed [92]. A theoretical proposal has been made to observe the Higgs mode in a d-wave superconductor through a time- and angle-resolved photoemission spectroscopy [80].

The observation of the Higgs mode in d-wave superconductors was recently made in THz-pump and optical-probe experiments in high-T_c cuprates, $Bi_2Sr_2CaCu_2O_{8+x}$ (Bi2212) [55]. An oscillatory signal of the optical reflectivity that follows the squared THz electric field was observed, which is markedly enhanced below T_c as shown in **Figure** 13.9. This signal was interpreted as the THz-pump induced optical Kerr effect, namely the third-order nonlinear effect induced by the intense THz pump pulse. In the Bi2212 system, both A_{1g} and B_{1g} symmetry components with respect to the polarization-angle dependence (which should be distinguished from the relative-momentum symmetry classification mentioned above) were observed in the THz-Kerr signal. The doping dependence shows that the A_{1g} component is dominant in all the measured samples from under to near-optimal region. From the comparison with the BCS calculation of the nonlinear susceptibility, the A_{1g} component was assigned to be the d-wave Higgs-mode contribution.

The observed oscillatory signal corresponds to the 2ω modulation of the order parameter as observed in an s-wave NbN superconductor under the subgap multicycle THz pump irradiation. Accordingly, like in the case of s-wave systems, one can expect the THG signal

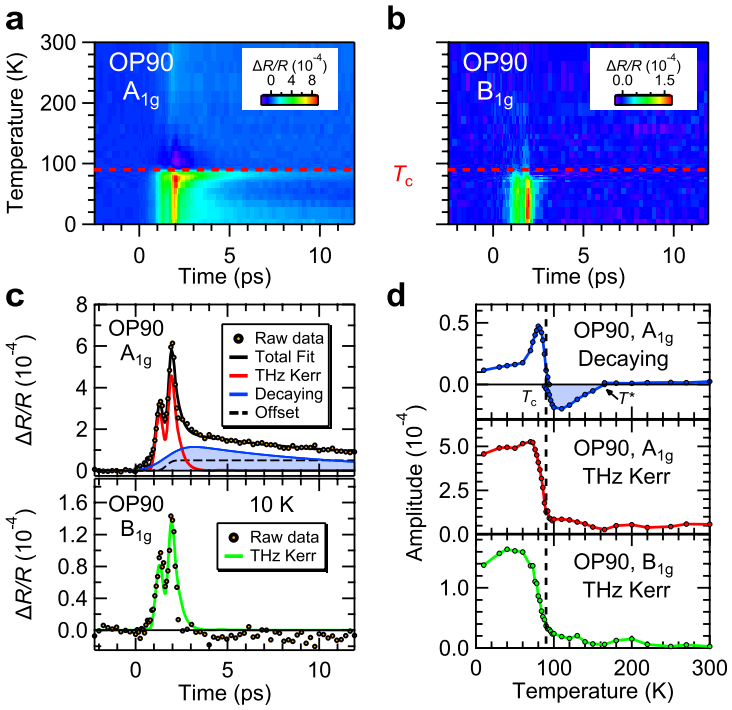


Figure 13.9: Forced oscillation of Higgs mode in an optimally doped (OP90) $Bi_2Sr_2CaCu_2O_{8+x}$ measured by THz pump and optical reflection probe experiment. Temperature dependences of reflectivity change $\Delta R/R$ as a function of pump-probe delay time in (a) A_{1g} and (b) B_{1g} components. Red dashed lines indicate T_c. (c) The A_{1g} and B_{1g} components against the pump-probe delay time at 10 K. Fitting curves are also shown by solid lines. (d) Temperature dependences of the A_{1g} decaying component (blue) (incoherent quasiparticle excitation), the A_{1g} oscillatory component (red) (forced Higgs oscillation), and the B_{1g} oscillatory component (green) (likely the charge density fluctuation). Figures are taken from Reference [55].

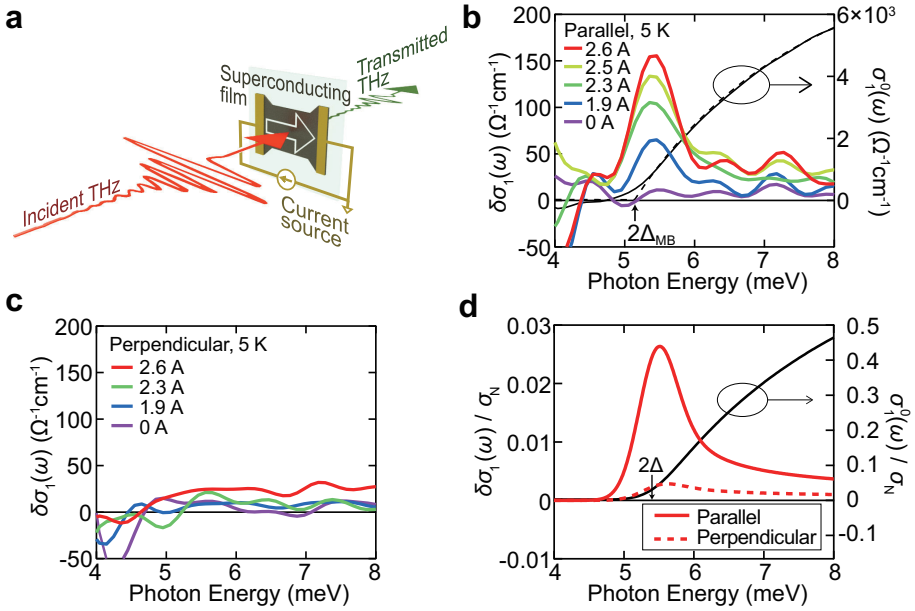


Figure 13.10: (*a*) Schematic view of the terahertz transmittance experiments under supercurrent injection. The change of the optical conductivity induced by supercurrent injection taken with the THz probe electric field (*b*) parallel or (*c*) perpendicular to the current direction. The optical conductivity spectra measured without the current is also plotted in (*b*). The dashed line represents a fit by the Mattis-Bardeen model [107, 108], and the superconducting gap estimated from the fit is indicated by the vertical arrow. (*d*) Theoretically expected changes of optical conductivity induced by the supercurrent injection with respect to the normal state conductivity σ_N. Figures are taken from Reference [58].

from high-T_c cuprates. Recently, THG was indeed observed ubiquitously in $La_{1.84}Sr_{0.16}CuO_4$, $DyBa_2Cu_3O_{7-x}$, $YBa_2Cu_3O_{7-x}$, and overdoped $Bi_2Sr_2CaCu_2O_{8+x}$ [56] by using 0.7 THz coherent and intense light source at the TELBE beamline at HZDR.

13.3.4 Higgs mode in the presence of supercurrents

So far, we have seen the Higgs mode excitation by the nonadiabatic quench with instantaneous quasiparticle injection or through the quadratic coupling with the electromagnetic wave. Recently, it has been theoretically shown that when there is a condensate flow (i.e., supercurrent), the Higgs mode linearly interacts with electromagnetic waves with the electric field polarized along the direction of the supercurrent flow [57]. Namely, the Higgs mode should be observed in the optical conductivity spectrum at the superconducting gap $\omega = 2\Delta$ under the supercurrent injection. This effect is explained by the momentum term in the action, $S \propto \int \boldsymbol{Q}^2(t)|\Delta(t)|^2 dtdr$, where $\boldsymbol{Q}(t) = \boldsymbol{Q}_0 + \boldsymbol{Q}_\Omega(t)$ is the gauge-invariant momentum of the condensate, $\boldsymbol{Q}_0$ is the dc supercurrent part, and $\boldsymbol{Q}_\Omega(t) = \mathrm{Re}[\boldsymbol{Q}_\Omega \exp(i\Omega t)]$ is the time-dependent part driven by the ac probe field, respectively. $\Delta(t) = \Delta_0 + \delta\Delta(t)$ is the time-dependent superconducting order parameter. The action S includes the integral of $\delta\Delta_{2\Omega}\boldsymbol{Q}^2_{-\Omega}$ and $\delta\Delta_\Omega \boldsymbol{Q}_0 \boldsymbol{Q}_{-\Omega}$ where $\delta\Delta_{\Omega(2\Omega)}$ is the Fourier component of the oscillating order parameter. The first term corresponds to the quadratic coupling of the Higgs mode to the gauge field as described Section 13.2. The second term indicates that the Higgs mode linearly couples with the gauge field under the supercurrent with the condensate momentum $\boldsymbol{Q}_0$ parallel to the probe electric field.

Recently, in accordance with the theoretical prediction, the Higgs mode was observed in the optical conductivity in an *s*-wave superconductor NbN thin film under the supercurrent

injection by using THz time-domain spectroscopy [58]. **Figure** 13.10***a*** shows the schematic experimental setup. **Figures** 13.10***b*** and ***c*** show the change of the real part of the optical conductivity induced by the supercurrent injection with the probe polarization (***b***) parallel and (***c***) orthogonal to the current direction. A clear peak is observed at the gap edge $\omega = 2\Delta$ in the parallel geometry, showing a good agreement with the spectra calculated on the basis of the theory developed by Moor et al. [57] as represented in **Figure** 13.10***d***. This result indicates that, without resorting to the sophisticated nonlinear THz spectroscopy, the Higgs mode can be observed in the linear response function when the condensate has a finite momentum, expanding the feasibility for the detection of the Higgs mode in a wider range of materials.

The visibility of the Higgs mode in the optical conductivity has also been addressed in a two-dimensional system near a quantum critical point [7, 110] (see also [111, 112]). Experimentally, an extra spectral weight in the optical conductivity below the superconducting gap was observed in a strongly disordered superconducting film of NbN, which was interpreted in terms of the Higgs mode with its mass pushed below the pair breaking gap due to the strong disorder [5]. However, the assignment of the extra spectral weight below the gap remains under debates. It can also be described by the Nambu-Goldstone mode which acquires the electric dipole in strongly disordered superconductors [114, 115, 116, 117]. The extra optical conductivity was also accounted for by the disorder induced broadening of the quasiparticle density of states below the gap [118].

13.4 Future Perspective

Having seen the Higgs mode in s-wave and d-wave superconductors, it is fascinating to extend the observation of the Higgs mode to a variety of conventional/unconventional superconductors.

The study of the Higgs mode in multiband superconductors would be important, as it would give deeper insights into the interband couplings. For instance, the application of the nonlinear THz spectroscopy to iron-based superconductors is highly intriguing, as it may provide information on the interband interactions and pairing symmetry [87, 119, 120]. The Leggett mode, namely the collective mode associated with the relative phase of two condensates [86] is also expected to be present in multiband superconductors. The Leggett mode has been observed in a multiband superconductor MgB_2 by Raman spectroscopy [121]. The nonlinear coupling between the Leggett mode and THz light has also been discussed [53, 87, 88, 89, 90]. Recently, a THz-pump THz probe study in MgB_2 has been reported, and the results were interpreted in terms of the Leggett mode [122]. However, the dominant contribution of the Higgs mode over the Leggett mode in the nonlinear THz responses was theoretically pointed out in the case of dirty-limit superconductors [53]. Therefore, further experimental verification of the Higgs and Leggett modes is left as a future problem.

The ultimate fate of the behavior of the Higgs mode in a strongly correlated regime and, what is more, in a BCS-BEC crossover regime is an intriguing problem. In particular, the decay profile of the Higgs mode has been predicted to change from the BCS to BEC regime [36, 37, 8, 124, 125]. Experimentally, such a study has been realized in a cold-atom system, showing a broadening of the Higgs mode in the BEC regime [61]. Further investigation on the Higgs mode in the BCS-BEC crossover regime will be a future challenge in solid-state systems.

The Higgs mode in spin-triplet p-wave superconductors (whose candidate materials include Sr_2RuO_4) is another issue to be explored in the future. Like in the case of superfluid ^{3}He [22, 59, 126], multiple Higgs modes are expected to appear due to the spontaneous symmetry breaking in the spin channel, and its comparison with high-energy physics would be interesting.

As yet another new paradigm, the observation of the Higgs mode would pave a new pathway for the study of nonequilibrium phenomena, in particular for the photoinduced superconduc-

tivity [127, 128, 129, 130]. Being a fingerprint of the order parameter with a picosecond time resolution, the observation of the Higgs mode in photoinduced states should offer a direct evidence for nonequilibrium superconductivity. In strongly correlated electron systems exemplified by the unconventional superconductors, elucidation of the interplay between competing and/or coexisting orders with superconductivity is an important issue to understand the emergent phases. The time-domain study of collective modes associated with those orders is expected to provide new insights for their interplay.

Part V
Old, Fundamental Theories

14 Experiments on charge imbalance in superconductors by Clarke

14.1 1. Introduction

When a disequilibrium is created between the electron-like and hole-like excitations in a superconductor, a charge imbalance, Q^*, is created. Charge imbalance is of practical interest, first, because it can be used to explain a wide variety of nonequilibrium processes that occur in superconductors, and, second, because it provides a valuable tool for measuring various electronrelaxation rates, most notably the electron–phonon scattering rate. The importance of the disequilibrium of the electron- and hole-like branches was first realized by Pippard et al. (1971) in their explanation of the excess resistance associated with the normal metal-superconductor (NS) boundary. However, the first quantitative understanding of charge imbalance was put forward by Tinkham and Clarke (1972) to explain the results of experiments in which electrons were injected via a tunnel junction into superconducting tin films (Clarke 1972). Among other results, these authors showed that the charge imbalance relaxation rate, $\tau_{Q^*}^{-1}$, due to inelastic scattering was of order $\tau_{\mathrm{E}}^{-1}\,[\Lambda(T)/k_{\mathrm{B}}T]$ near T_{c}, where τ_{E}^{-1} is the electron-phonon scattering rate at T_{c} and at the Fermi energy, and $\Delta(T)$ is the energy gap.

The first detailed paper on the theory of charge imbalance was that of Tinkham (1972): this article laid the groundwork for a great deal of the subsequent theoretical development. The next major theoretical article was that of Schmid and Schön (1975) who used a Green's function approach to distinguish two different nonequilibrium modes: a transverse mode, in which the quasiparticle populations on the two branches differ (charge imbalance). and a longitudinal mode, in which the quasiparticle population on the two branches is equal but out of equilibrium, thereby modifying the energy gap, $\Delta(T)$. Subsequently, Pethick and Smith (1979a) introduced a two-fluid approach to relaxation and collective motion in superconductors. This approach is conceptually simple, and produces the same results as the Schmid Schön theory in the limit $\Delta(T)/k_{\mathrm{B}}T \ll 1$ in which both theories are valid.

The purpose of the present chapter is to describe experiments in which charge imbalance plays a central role for our understanding of the physical mechanisms that are involved. It is, of course, necessary to present a theoretical framework, which appears in section 2. However, I have given a minimum of theoretical discussion throughout the paper, but instead have quoted results
and listed appropriate references. Section 3 describes the early work on Sn from which it was possible to extract an accurate value for τ_{E}^{-1}. Section 4 outlines work on Al in which both elastic scattering in the presence of gap anisotropy and electron electron scattering may also relax charge imbalance. Section 5 is concerned with charge relaxation via elastic scattering in the presence of magnetic impurities or of a supercurrent. This section concludes the discussion of charge imbalance that has been generated by tunnel injection. Section 6 deals with the resistance of the NS interface in terms of charge imbalance, while section 7 describes phase-slip centers. Section 8 is concerned with charge imbalance in the presence of a temperature gradient in three different types of experiment: the voltage induced across a NS interface, the spatially decaying charge imbalance induced near the end of a superconducting film, and the charge imbalance induced by a uniform supercurrent. While all of the topics above are concerned with steady state charge imbalance, it is also possible to consider dynamic effects, such as the

response to an impulse or fluctuations. Section 9 briefly describes such effects. Finally, section 10 contains some concluding remarks.

I should emphasize that this chapter is not an exhaustive account of charge imbalance phenomena, nor is the list of references by any means complete. However, I have attempted to list enough references to enable interested readers to find their way into the literature. Parts of this work have been published in an earlier review (Clarke 1981).

14.2 2. Theory of charge imbalance

In this section we outline the concepts of quasiparticle charge and charge imbalance, the generation and detection of charge imbalance by tunneling, and the relaxation of charge imbalance via electron-phonon scattering. The discussion follows the work of Tinkham and Clarke (1972). Tinkham (1972), Waldram (1975), Pethick and Smith (1979a), and Kadin et al. (1980).

14.2.1 2.1. Quasiparticle charge and charge imbalance

We begin by considering the total electronic charge, $Q_{\rm tot}$, in a superconductor, the overall charge at frequencies far below the plasma frequency being maintained at zero by the equal and opposite charge of the ion cores. From the BCS theory (Bardeen et al. 1957) we have

$$Q_{\rm tot} = \frac{2}{\Omega}\sum_k \left[u_k^2 f_k + v_k^2\,(1 - f_{-k})\right], \tag{2.1}$$

where the sum is over k states above and below k_F, and the factor of 2 arises from the sum over spin. In eq. (2.1), Ω is the volume of the superconductor,
and f_k is the occupancy of the state k, which, in thermal equilibrium, is the Fermi function. The u_k and v_k are the usual BCS factors given by

$$u_k^2 = \frac{1}{2}\,(1 + \xi_k/E_k) \tag{2.2}$$

and

$$v_k^2 = \frac{1}{2}\,(1 - \xi_k/E_k)\,, \tag{2.3}$$

where

$$\xi_h = \frac{\hbar^2 k^2}{2m} - \mu_s \tag{2.4}$$

is the kinetic energy of the electron of mass m in the state k referred to the chemical potential of the superfluid, μ_s, and

$$E_k = \left(\Delta^2 + \xi_k^2\right)^{1/2} \tag{2.5}$$

is the quasiparticle excitation energy. The energy E_k is positive for all values of k, while ξ_k is positive for $k > k_{\rm F}$ and negative for $k < k_{\rm F}$. The quantity v_k^2 is the probability that the state k is occupied by a Cooper pair, while $u_h^2 = 1 - v_h^2$ is the probability that the state k is unoccupied by a Cooper pair.

We can regard eq. (2.1) as the sum of a superfluid contribution

$$Q_{\rm s} = \frac{2}{\Omega}\sum_k v_k^2 \tag{2.6}$$

and a quasiparticle contribution

$$Q^* = \frac{2}{\Omega}\sum_k \left(u_k^2 - v_k^2\right) f_k = \frac{2}{\Omega}\sum_k q_k f_k, \tag{2.7}$$

where we have set $f_{-k} = f_k$. In eq. (2.7) we have introduced the very important concept of the effective quasiparticle charge

$$q_k = u_k^2 - v_k^2 = \xi_k / E_k, \tag{2.8}$$

and defined the charge imbalance per unit volume, Q^*, which is the central subject of this chapter. We note that $q_k \to +1$ for $\xi_k \gg A\,(k > k_{\rm F})$, and $q_k \to -1$ for $\xi_k \ll -\Delta\,(k < k_{\rm F})$. It is evident in Eq. (2.7) that if $f_k\,(\xi_k)$ is the Fermi function, which is even in ξ_k about μ_k, the quasiparticle charge, Q^*, is zero since q_k is odd in $\check{\zeta}_h$. Thus, the total electronic charge is $(2/\Omega)\sum_h^2$ at all temperatures, as we expect.

We now turn to a nonequilibrium situation in which f_k is no longer the Fermi function. In this case, Q^* may be nonzero and $\mu_{\rm s}$ shifted from its equilibrium value, the Fermi energy, by an amount $\delta\mu_{\rm s}$. As we shall see, Q^* and $\delta\mu_s$ are intimately related. As an example, suppose that we add excitations to the $k > k_{\rm F}$ quasiparticle branch in a particular region of the superconductor. Overall charge neutrality will ensure that pairs with an equivalent charge are
removed from the region. Thus, the chemical potential of the pairs must decrease by an amount $\delta\mu_{\rm s}$, as indicated in fig. 1a. At the same time, the excitation spectrum shifts because its minimum still occurs at the pair chemical potential, as shown in fig. 1b. The effective quasiparticle charge is still $q_k = \xi_k/E_k$, but ξ_k is now referred to the shifted chemical potential, $\mu_s - \delta\mu_s$. Thus, the addition of a single electron-like excitation induces some quasiparticles near the bottom of the excitation spectrum to cross branches, producing a small increase in the charge of all the electron-like quasiparticles, and a small decrease in the charge of all the hole-like quasiparticles.

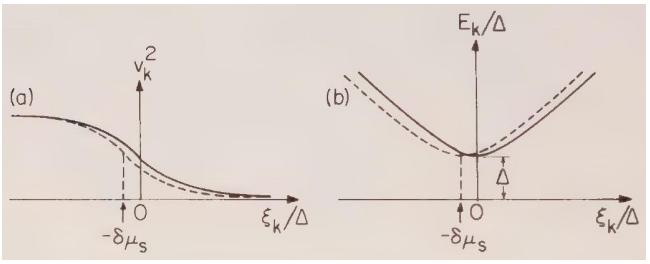


Fig. 1. The effect on (a) condensate density, and (b) quasiparticle excitation spectrum, when electron-like excitations are added to the superconductor. The solid and dashed lines represent equilibrium and displacement from equilibrium, respectively.

The quantities Q^* and $\delta\mu_{\rm s}$ are related as follows. By charge neutrality

$$Q^* + Q_{\rm s}|_{\delta\mu_{\rm s}\neq 0} = \frac{2}{\Omega}\sum_k v_k^2\Big|_{\delta\mu_{\rm s}=0}, \tag{2.9}$$

$$Q^* = \frac{2}{\Omega}\sum_k \left(v_k^2|_{\delta\mu_{\rm s}=0} - v_k^2|_{\delta\mu_{\rm s}\neq 0}\right). \tag{2.10}$$

Now the reduction in the number of pairs represented by the right-hand side of eq. (2.10) is just $2N(0)\delta\mu_{\rm c}$, where $N(0)$ is the single-spin density of states per unit volume at the Fermi energy. Thus

$$Q^* = -2N(0)\delta\mu_{\rm s} \tag{2.11}$$

We see that eq. (2.1) is really a self-consistent equation for $\mu_{\rm s}$: given any distribution, f_k, the constancy of $Q_{\rm tot}$ determines μ_s.

In the steady state with Q^* continuously injected at a rate $\dot{Q}_i^*$, the excess distribution relaxes at a rate $\tau_{Q^*}^{-1}$ to produce a steady state charge imbalance Q^*. Thus

$$\tau_{Q^*}^{-1} = \dot{Q}_{\rm i}^*/Q^*. \tag{2.12}$$

The relaxation of Q^* may occur through both inelastic and elastic processes, as we will discuss in sections 2.3 and 4 .

14.2.2 2.2. Tunneling generation and detection of charge imbalance

We follow closely the approach developed by Tink ham (1972) and Pethick and Smith (1979a) to calculate the charge imbalance generated in a superconductor (S) by quasiparticle tunnel injection from a normal metal (N), and the voltage induced by this charge imbalance across a second NIS tunnel junction at zero bias current.

When a NIS junction is biased at a voltage V, the rate at which quasiparticles are injected into the state k of the superconductor is

$$\begin{aligned}\dot{f}_k\Big|_i =& \frac{2\pi}{\hbar}|T|^2\mathcal{N}_{\rm n}(0)\left[u_k^2 f^0\left(E_k - eV\right) + v_k^2 f^0\left(E_k + eV\right) - f_k\right] \\ =& \frac{2\pi}{\hbar}|T|^2\mathcal{N}_{\rm n}(0)\left\{\frac{1}{2}\left[f^0\left(E_k + eV\right) + f^0\left(E_k - eV\right)\right] - f_k \right. \\ & \left. + \frac{1}{2}q_k\left[f^0\left(E_k - eV\right) - f^0\left(E_k + eV\right)\right]\right\}.\end{aligned} \tag{2.13}$$

Here, $|T|^2$ is the square of the tunneling matrix element, assumed to be independent of energy, and $\mathcal{N}_n(0)$ is the single-spin density of states in the volume of the metal. The Fermi functions $f^0\left(E_k \pm eV\right)$ refer to the normal metal, while f_k is the actual distribution in the superconductor, which is not, in general, the Fermi distribution.

We convert eq. (2.13) into an expression for the rate of quasiparticle charge injection by multiplying by q_k and summing over k. Noting that only even terms contribute, we find

$$\dot{Q}_{\rm i}^* = \frac{2\pi}{\hbar\Omega}|T|^2\mathcal{N}_{\rm n}(0)\sum_k q_k^2\left[f^0\left(E_k - eV\right) - f^0\left(E_k + eV\right)\right]. \tag{2.14}$$

We have neglected the small contribution of the even part of $q_h f_h$ since the voltages generated by the nonequilibrium distribution are very small compared with the injection voltage. It is convenient to write eq. (2.14) in the integral form:

$$\begin{aligned}\dot{Q}_{\rm i}^* &= \frac{4\pi}{\hbar\Omega}|T|^2\mathcal{N}_{\rm n}(0)\mathcal{N}(0)\int_0^5 \frac{\xi^2}{E^2}\left[f^0(E - eV) - f^0(E + eV)\right]{\rm d}\zeta \\ &= \frac{G_{\rm NN}}{e^2\Omega}\int_\Delta^\infty \rho^{-1}(E)\left[f^0(E - eV) - f^0(E + eV)\right]{\rm d}E\end{aligned} \tag{2.15}$$

where we have used ${\rm d}\xi = (E/\xi){\rm d}E$. In eq. (2.15), $\mathcal{N}'(0)$ is the single-spin density of states in the volume of the superconductor when it is in the normal state,

$$\rho(E) = E/\left(E^2 - \Delta^2\right)^{1/2} = E/|\xi| = \left|{\rm q}_k^{-1}\right| (E > \Delta)$$

is the normalized BCS density of states in the superconductor, and $G_{\rm NN} = 4\pi e^2|T|^2 \times \mathcal{N}_{\rm n}(0)\mathcal{N}(0)/\hbar$ is the conductance of the tunnel junction when the superconductor is in the normal state.

From eq. (2.13), we can obtain an expression for the net current injected into a superconductor from a normal metal. Summing over k and simplifying, we find

$$I = \frac{2\pi e}{\hbar}|T|^2\mathcal{N}_{\rm n}(0)\sum_k \left[f^0\left(E_k - eV\right) - f^0\left(E_k + eV\right) - 2q_k\delta f_k\right] \tag{2.16}$$

where $\delta f_k = f_k - f^0$. We note that the E_k in f^0 are referred to the modified chemical potential. [Pethick and Smith (1979a) denote this f^0 by $f^{0(1.e.)}$, where "l.e." means local equilibrium; our δf_k is precisely the same as their $\delta f_k^{1.e}$.] For any injection voltage of practical interest the last term in eq. (2.16) is negligible, and we can write I in the integral form:

$$\begin{aligned} I &= \frac{4\pi e}{\hbar}|T|^2\mathcal{N}_{\rm n}(0)\mathcal{N}(0)\int_0^\infty \left[f^0(E - eV) - f^0(E + eV)\right]\mathrm{d}\xi \\ &= \frac{\mathrm{G_{NN}}}{e}\int_\Lambda^\infty \rho(E)\left[f^0(E - eV) - f^0(E + eV)\right]\mathrm{d}E \end{aligned} \tag{2.17}$$

We will find it useful to obtain an expression for eq. (2.17) in the limit $eV \ll k_{\rm B}T$ in which we can expand the Fermi functions to give $f^0(E \pm eV) = f^0(E) \pm [\partial f^0(E)/\partial E]\,\mathrm{eV}$. This approximation leads to

$$I = G_{\rm NN}\int_\Delta^\infty 2\rho(E)\left(-\frac{\partial f^0(E)}{\partial E}\right)V\ \mathrm{d}E, \quad (eV \ll k_{\rm B}T) \tag{2.18}$$

Since the conductance, $G_{\rm NS}$, is just I/V, we obtain the reduced tunneling conductance for $eV/k_{\rm B}T \to 0, g_{\rm NS}(0) = G_{\rm NS}(0)/G_{\rm NN}$:

$$g_{\rm NS}(0) \equiv \mathrm{Y}(T) = 2\int_\Delta^\infty \rho(E)\left(-\frac{\partial f^0(E)}{\partial E}\right)\mathrm{d}E \tag{2.19}$$

where $\mathrm{Y}(T)$ is the Yoshida function.

We are now in a position to calculate the voltage generated by the steady state charge imbalance as measured by a second tunneling contact to a normal metal. This voltage, $V_{\rm d}$, referred to the equilibrium chemical potential of the superconductor far away from the injected region is measured with zero current flowing through the detector junction. Since eq. (2.16) is equally true for the injection and detection junctions, we can set $I = 0$, and use the low voltage expansion of the Fermi functions to obtain

$$V_{\rm d} = \frac{2\sum q_k f_k}{2e\sum\left[-\partial f^0(E)/\partial E\right]} = \frac{Q^*}{2N(0)e g_{\rm NS}(0)} \tag{2.20}$$

We have thus found a simple relation between Q^* or, equivalently, $-2N(0)\delta\mu_{\rm s}$, and the voltage measured by the detector junction. If the detector junction does not show the ideal BCS behavior, one should use the measured normalized conductance in eq. (2.20), rather than the BCS value.

To complete our description of tunneling generation and detection of charge imbalance we combine eqs. (2.12), (2.15), (2.17), and (2.20) so that we can deduce $\tau_{Q^*}^{-1}$ in terms of measurable or precisely calculable quantities. To do this, it is convenient to introduce the parameter F^* that enables us to express $\dot{Q}_{\rm i}^*$ in terms of the injection current $I_{\rm i}$:

$$F^* = e\Omega\frac{\dot{Q}_i^*}{I_i} = \frac{\int_\Delta^\infty \rho^{-1}(E)\left[f^0\left(E - eV_{\rm i}\right) - f^0\left(E + eV_{\rm i}\right)\right]\mathrm{d}E}{\int_\Delta^\infty \rho(E)\left[f^0\left(E - eV_{\rm i}\right) - f^0\left(E + eV_{\rm i}\right)\right]\mathrm{d}E} \tag{2.21}$$

We have used V_i to denote the injection voltage. From eqs. (2.12), (2.20), and (2.21) we find

$$\tau_{Q^*}^{-1} = \frac{\dot{Q}_\mathrm{i}^*}{Q^*} = \frac{F^* I_\mathrm{i}}{2N(0)e^2\Omega g_\mathrm{NS}(0)V_\mathrm{d}} \tag{2.22}$$

The quantity F^* is readily calculable, while the quantities $I_\mathrm{i}, \Omega, g_\mathrm{NS}(0)$, and V_d are those measured in the experiment.

In the limit of low injection voltages, $eV_\mathrm{i} \ll k_\mathrm{B}T$, the Fermi functions in eq. (2.21) may be expanded to yield

$$F^* = Z(T)/\mathrm{Y}(T), \quad (eV_\mathrm{i} \ll k_\mathrm{B}T)\,, \tag{2.23}$$

where

$$Z(T) \equiv 2\int_\Delta^\infty \rho^{-1}(E)\left(-\frac{\partial f^0(E)}{\partial E}\right)\mathrm{d}E \tag{2.24}$$

However, this limit is not very useful for most practical experiments with tunneling injection, where the voltage is large compared with both $\Delta(T)/e$ and $k_\mathrm{B}T/e$. In these limits, one obtains

$$F^* = 1 - \pi\Delta/2\,|eV_i|\,, \quad [eV_i \gg k_BT, \quad eV_i > \Delta(T)]\,. \tag{2.25}$$

For a typical injection voltage, $eV_\mathrm{i}/\Delta = 30$, we find $F^* = 0.95$.

14.2.3 2.3. Charge imbalance relaxation via electron-phonon scattering

When an electron-like excitation (for example) is injected into a superconductor, in general it not only creates a charge imbalance but also increases the energy of the quasiparticle distribution above the equilibrium value. Thus, the processes that restore thermal equilibrium involve both cooling and charge relaxation, but these are not necessarily distinct processes. For example, if the quasiparticle is injected at any energy well above both $k_\mathrm{B}T$ and $A(T)$, it may scatter with the emission of a phonon to a lower energy on the same quasiparticle branch. In this process, the quasiparticle has not only cooled, but also given up some of its charge because q_k has been reduced from its initial value near unity to a lower value. This kind of inelastic process is governed by the coherence factor (Tinkham 1975)

$$(uu' - vv')^2 = \frac{1}{2}\left(1 + \frac{\xi\xi' - \Delta^2}{EE'}\right) \tag{2.26}$$

A second means of phonon-mediated charge relaxation is by recombination, a process that is governed by the coherence factor (Tinkham 1975)

$$(vu' + uv')^2 = \frac{1}{2}\left(1 + \frac{\Delta^2 - \xi\xi'}{EE'}\right) \tag{2.27}$$

In addition to inelastic processes, elastic scattering from non-magnetic or magnetic impurities can also relax Q^*, provided the quasiparticle changes branches. For the case of non-magnetic impurities in an isotropic superconductor, this process is strictly forbidden by the coherence factor in eq. (2.26), as can be seen immediately by realizing that if E and E' refer to different branches, $u' = v$ and $v' = u$. On the other hand, the coherence factor does not vanish for scattering from non-magnetic impurities in the case of anisotropic superconductors, or from magnetic impurities even in the isotropic case. We defer a discussion of elastic processes until sections 4 and 5.

It is evident that the calculation of the charge imbalance relaxation rate is, in general, a very complicated undertaking. In the limit $\Delta(T) \ll k_{\mathrm{B}}T$, and in the absence of elastic processes, the situation simplifies, and one finds (Tinkham 1972, Schmid and Schön 1975, Pethick and Smith 1979a)

$$\left(F^{*}\tau_{Q^{*}}\right)^{-1} = \left(\pi\Delta/4k_{\mathrm{B}}T\right)\tau_{E}^{-1}, \quad \left[\Delta(T) \ll k_{\mathrm{B}}T\right]. \tag{2.28}$$

In eq. (2.28), ${\tau_E}^1$ is the inelastic scattering rate at T_c for a quasiparticle at the Fermi energy; the rate actually increases with the energy of the quasiparticle, but we shall neglect this dependence. For the more general case when $\Delta(T)$ is not small, one must resort to numerical calculations. Chi and Clarke (1979, 1980) solved the Boltzmann equation on a computer to find both the steady state quasiparticle distribution and the charge imbalance relaxation rate for a wide range of temperatures and several values of the injection voltage. We
briefly summarize the results of these calculations, referring to Chi and Clarke's results by "CC".

The Boltzmann equation can be written in the form

$$\dot{f}_{\xi} = G_{\tilde{\zeta}} - G_{\mathrm{in}\tilde{\zeta}} - G_{\mathrm{el}\xi}. \tag{2.29}$$

The first term G_ξ is the rate of injection into $\check{\zeta}_h$. while $G_{\mathrm{in}\,;}$ and $G_{\mathrm{el}\,;}$ are the inelastic and elastic rates at which quasiparticles scatter out of ξ_h; for the moment we set $G_{\mathrm{el}:} = 0$. In a steady state situation $\dot{f}_\xi = 0$. For tunneling from a normal metal into a superconductor the injection rate is given by the first line of eq. (2.13) with the terms labeled with ξ rather than k :

$$\begin{aligned} G_{\xi} = &\left[G_{\mathrm{NN}}/2N(0)e^{2}\Omega\right]\left\{\frac{1}{2}(1+\xi/E)\left[f^{0}\left(E-eV_{i}\right)-f^{0}(E)\right]\right. \\ &\left.-\frac{1}{2}(1-\xi/E)\left[f^{0}(E)-f^{0}\left(E+eV_{\mathrm{i}}\right)\right]\right\}. \end{aligned} \tag{2.30}$$

We have used the Fermi distribution for the distribution functions, thereby assuming that departure from equilibrium is small. The inelastic scattering rate is proportional to $x^2F(\Omega)$, the average of the product of the square of the matrix elements for the electron phonon interaction and the phonon density of states. We assume that $F(\Omega)$ is quadratic in Ω, and can be written in the form $F\left(k_{\mathrm{B}}T_{c}\hbar\right)\left(\Omega k_{\mathrm{B}}T_{\mathrm{c}}\right)^{2}$. With this assumption, $G_{\mathrm{in}\tilde{n}}$ can be written down using the Golden Rule (Kaplan et al. 1976, Chang and Scalapino 1977, Chang 1979, CC):

$$\begin{aligned} G_{\mathrm{in}\varsigma} = &\frac{2\pi}{\hbar}\alpha^{2}F\left(k_{\mathrm{B}}T_{\mathrm{c}}/\hbar\right) \\ &\times\left\{\left[1+n^{0}\left(E+E'\right)\right]f_{\xi}f_{\xi'}-n^{0}\left(E+E'\right)\left(1-f_{\xi}\right)\left(1-f_{\xi'}\right)\right\} \\ &+\frac{1}{2}\left(1+\frac{\xi\xi'}{EE'}-\frac{\Delta^{2}}{EE'}\right)\left(E-E'\right)^{2}\theta\left(E-E'\right) \\ &\times\left\{\left[1+n^{0}\left(E-E'\right)\right]f_{\xi}\left(1-f_{\xi'}\right)-n^{0}\left(E-E'\right)f_{\xi'}\left(1-f_{\xi}\right)\right\} \\ &+\frac{1}{EE'}\left(1+\frac{\xi\xi'}{EE'}-\frac{\Delta^{2}}{EE'}\right)\left(E-E'\right)^{2}\theta\left(E'-E\right) \\ &\times\left\{n^{0}\left(E'-E\right)f_{\xi}\left(1-f_{\xi'}\right)-\left[1+n^{0}\left(E'-E\right)\right]f_{\xi'}\left(1-f_{\xi}\right)\right\}\Big]. \end{aligned} \tag{2.31}$$

In eq. (2.31), $Z_1(0)$ is the electron- phonon renormalization factor, typically about 2 for most metals. () is the Heaviside function, which is zero for negative arguments and unity for positive arguments, and $n^0(\Omega)$ is the Bose Einstein distribution function for the phonons.

In solving the Boltzmann equation. it is convenient to write $f = f^0 + \delta f$, where f^0 is the Fermi function at energy $(\xi^2 + d^2)^{12}$ and ξ is referred to the
shifted chemical potential. We rewrite the equation in terms of even and odd components of $\delta f_\xi, (\delta f_\xi + \delta f_{-\xi})/2$ and $(\delta f_\xi - \delta f_{-\xi})/2$, make initial guesses for these components and iterate the Boltzmann equation until the solution is selfconsistent. We calculate Q^* from $2N(0)\sum q_\xi (\delta f_\xi - \delta f_{-\xi})$ and $\tau_{Q^*}^{-1}$ from $\dot{Q}_i^*/Q^*$, using eq. (2.15).

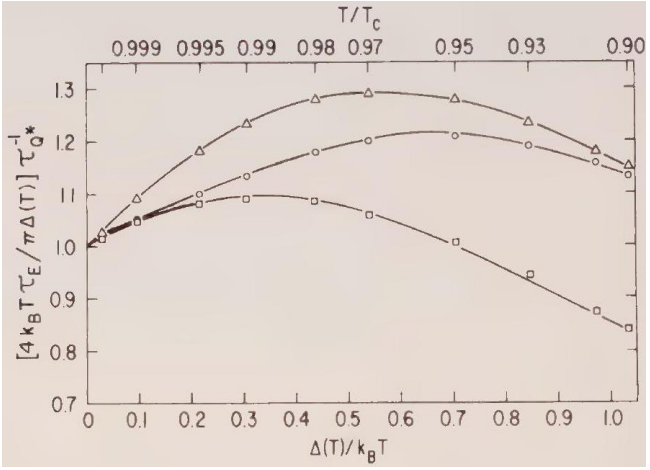


Fig. 2. $\left(4 k_{\mathrm{B} } T \tau_{\mathrm{E}} / \pi \Delta(T)\right) \tau_{Q^{*}}^{-1}$ versus $\Delta(T)/k_{\mathrm{B}}T$ and T/T_{c} : computed values for $eV_{\mathrm{i}} := (\square)0.01\Delta(T)$; (O) $10\Delta(T)$; $(\triangle)10k_{\mathrm{B}}T_{\mathrm{c}}$. (Chi and Clarke 1980.)}

Figure 2 shows the computed value of $\left[4k_{\mathrm{B}}T\tau_{\mathrm{E}}/\pi\Delta(T)\right]\tau_{Q^*}^{-1}$ versus $A(T)k_{\mathrm{B}}T$ for three injection voltages. At T_c, the computed value is precisely unity, but as the temperature is lowered, the function first increases and then decreases. At all temperatures below T_c, $\tau_{Q^-}{}^{-1}$ increases with injection voltage, reflecting the increase in the inelastic scattering rate with increasing energy. Figure 3 shows the computed temperature dependence of $\tau_{Q^*}^{-1}$ down to $0.3T_{\mathrm{c}}$ for two values of injection voltage. The relaxation rate goes through a peak and then decreases steadily as the temperature is lowered. It should be emphasized first, that the time τ_E is itself strongly temperature dependent, and second, that in real superconductors elastic scattering in the presence of gap anisotropy is likely to increase the value of $\tau_{Q^2}{}^1$ substantially at low temperatures. Finally, we note that according to eq. (2.22) the measured voltage V_{d} is proportional to $F^*\tau_{Q^*}I_{\mathrm{i}}$. In fig. 4 we plot both $\tau_{Q^*}{}^1$ and $(F^*\tau_{Q^*})^{-1}$ versus $eV_{\mathrm{i}}/\Delta(T)$. For $eV_{\mathrm{i}} \gtrsim 64(T)$, we observe that $F^*\tau_{Q^*}$ becomes independent of V_{i}, and that V_{d} becomes linear in I_{i}.

This concludes our theoretical survey. We now move on to discuss experimental results.

14.3 3. Experiments on tin

Historically, the first measurements of charge imbalance using tunneling injection were on Sn films, and it is convenient to begin with a discussion of these results because it is possible to obtain a temperature range in which the charge relaxation due to elastic scattering is negligible compared with that due to inelastic scattering (Clarke 1972, Clarke and Paterson 1974, Moody and Paterson 1979).

The configuration used in all tunneling injection experiments is shown in fig. 5. After oxidizing the Al base electrode (XX′), typically 150 nm thick, one deposits a Sn electrode (YY′), 200 to 400 nm thick. An insulating layer of varnish or (in the later experiments) SiO is used to mask off a window near the center of the injector junction. The Sn film is oxidized

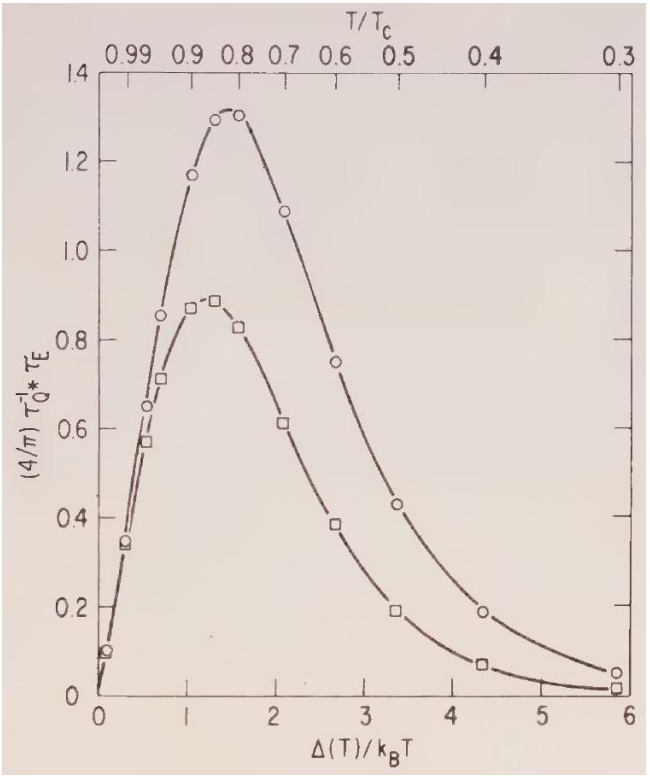


Fig. 3. Computed values for $(4 / \pi) \tau_{Q^{*}}^{-1}$ versus $\Delta(T)/k_{\mathrm{B}}T$ and T/T_{c} for (□)$eV_{\mathrm{i}} = 0.01\Delta(T)$, and (O)$eV_{\mathrm{i}} = 10\Delta(T)$. (Chi and Clarke 1980.)

slightly, and a diagonal strip (ZZ′) of CuAl(3wt%Al) about 2μ m thick is evaporated to form the detector junction. To reduce the series resistance of the CuAl strip, it is covered with a Pb film; the Cu film is made sufficiently thick and dirty to eliminate Josephson tunneling between the Al and Pb films.

Typically, four samples were fabricated simultaneously on a single substrate, and the detector junctions were connected in series. The voltage across the junctions was measured with a null-balancing SQUID voltmeter (see, for example, Clarke 1976) that ensured that the detector voltage was measured at zero current. Each junction could be investigated independently by applying a current to the appropriate injector junction. The samples and the SQUID were

immersed in liquid helium, and carefully shielded against external magnetic field fluctuations. The current voltage characteristics of both the injector and detector junctions were determined: typically, the injector junctions had a resistance of about $1\Omega\,(V_{\mathrm{i}} > 2\Delta/e)$, while the detector junctions were about $10^{-5}\Omega$. The conductance of the detector junctions was often in excess of the BCS prediction, but it was found that if one used the measured values of $g_{\mathrm{NS}}(0)$ in eq. (2.22), different samples produced values of $\tau_{Q^*}^{-1}$ in good agreement with each other.

In fig. 6 we have plotted

$$g_{\mathrm{NS}}(0)\Omega V_{\mathrm{d}}/I_{\mathrm{i}} = F^{*}\tau_{Q^{*}}/2N(0)e^2 \text{ versus } T/T_{\mathrm{c}}$$

for three Sn samples of different thicknesses, and one sample in which the Sn has been alloyed with 3wt% In (Clarke and Paterson 1974). The mean free path in the pure Sn samples was boundary limited, while that in the alloy was estimated to be 42 nm . The fact that the data for the pure Sn samples lie on a smooth curve demonstrates' that $F^{*}\tau_{Q^{*}}$ scales with Ω. Near $T_{\mathrm{c}}, V_{\mathrm{d}}/I_{\mathrm{i}}$, which is proportional to $F^{*}\tau_{Q^{*}}$ increases rapidly with increasing temperature. The solid line in fig. 6 is a fit of the curve $g_{\mathrm{NS}}(0)\Omega V_{\mathrm{d}}/I_{\mathrm{i}} = 4.0 \times 10^{-14} k_{\mathrm{B}}T_{\mathrm{c}}/\Delta(T)\Omega\mathrm{cm}^3$ to the

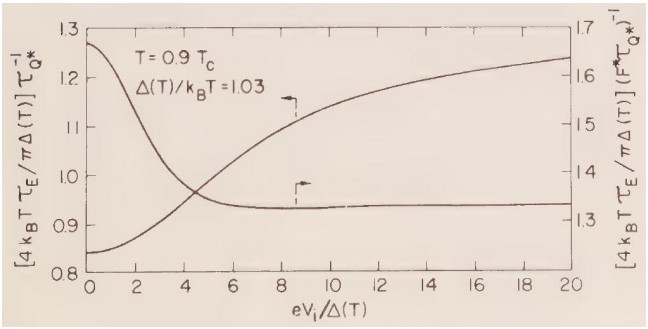


Fig. 4. $\left[4 k_{\mathrm{B} } T \tau_{\mathrm{E}} / \pi \Delta(T)\right] \tau_{Q^{*}}^{-1}$ and $\left[4 k_{\mathrm{B}} T \tau_{\mathrm{E}} / \pi \Delta(T)\right]\left(F^{*} \tau_{Q^{*}}\right)^{-1}$ versus $e V_{\mathrm{i}} / \Delta(T)$ for $T=0.9 T_{\mathrm{c}}$. (Chi and Clarke 1980.)

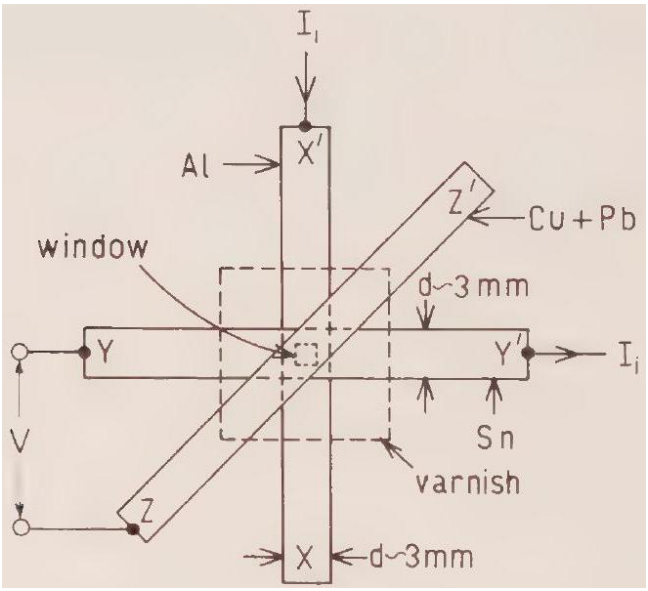


Fig. 5. Configuration of tunneling experiment to generate and detect charge imbalance in a Sn film. A SQUID voltmeter is used to measure the voltage between the Sn and Cu films generated by the current passed between the Al and Sn films. (Clarke 1972.)

data at high temperatures. Using the value $N(0)=1.39 \times 10^{22} \mathrm{eV}^{-1} \mathrm{~cm}^{-3}$ [computed from $N(0)=3 \gamma / 2 \pi^{2} k_{\mathrm{B}}^{2}$, where γ is the coefficient of the electronic heat capacity taken from Kittel (1976)] in eq. (2.22) we find $\left(F^{*} \tau_{Q^{*}}\right)^{-1}=5.6 \times 10^{9}\left(\Delta / k_{\mathrm{B}} T_{\mathrm{c}}\right) \mathrm{s}^{-1}$. Equating this value with the prediction of eq. (2.28), we find $\tau_{\mathrm{E}}=1.4 \times 10^{-10}$ s.

Below $T / T_{\mathrm{c}}=0.95, F^{*} \tau_{Q^{*}}$ is larger for the SnIn sample than for the Sn samples. This difference arises from the contribution of elastic charge relaxation in the clean samples, a topic that we consider in the following section.

14.4 4. Experiments on aluminum

14.4.1 4.1. Charge relaxation via elastic scattering from non-magnetic impurities

The coherence factor $(u u^{\prime}-v v^{\prime})^{2}$ forbids charge relaxation via elastic scattering when the energy gap is isotropic. However, in the presence of gap anisotropy a quasiparticle may be

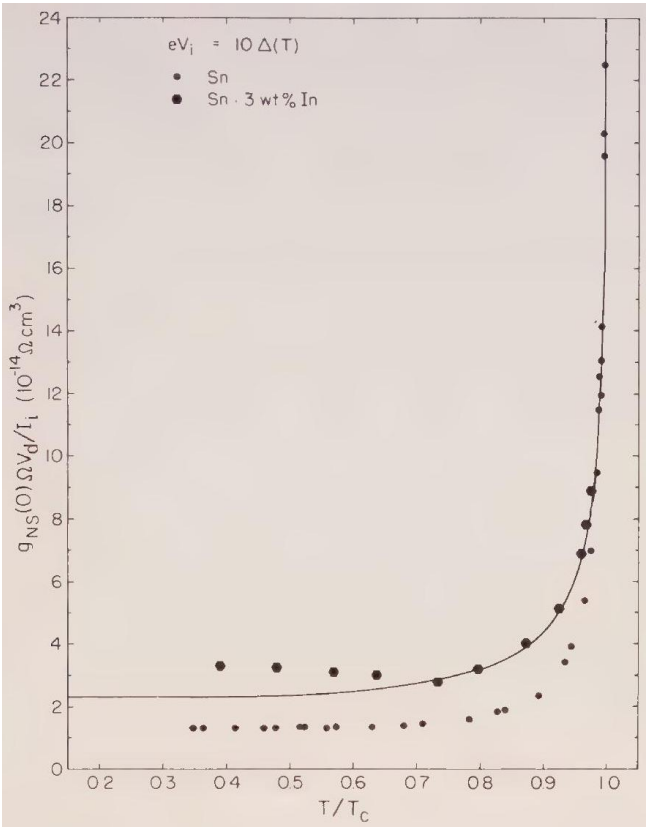


Fig. 6. $g_{\mathrm{NS}}(0) \Omega V_{\mathrm{d}} / I_{\mathrm{i}}$ versus T/T_{c} for pure Sn and SnIn . The solid line is a fit of $k_{\mathrm{B}}T_{\mathrm{c}}/\Delta(T)$ to the data for SnIn for $T/T_{\mathrm{c}} \gtrsim 0.7$. (Clarke and Paterson 1974.)}

scattered between two regions of the Fermi surface at which the energy gap is different, so that the coherence factor is no longer zero. This situation was first discussed by Tinkham (1972), and subsequently by Chi and Clarke (1979) using a computer solution of the Boltzmann equation. We briefly outline the latter treatment.

The elastic scattering rate G_{els} that appears in the Boltzmann equation [eq. (2.29)] is given by

$$G_{\mathrm{el}\xi} = \frac{\tau_1^{-1}}{2} \left\langle \rho_{\Delta'}(E) \left[1 - \frac{\Delta\Delta'}{E^2} - \left(1 - \frac{\Delta^2}{E^2}\right)^{1/2} \left(1 - \frac{\Delta'^2}{E^2}\right)^{1/2} \right] \right\rangle_{\Delta,\Delta'} \times \left[f_\xi \left(1 - f_{\xi'}\right) - f_{\xi'} \left(1 - f_\xi\right) \right]. \tag{4.1}$$

Here, τ_1^{-1} is the elastic scattering rate of an electron when the metal is in the normal state, $\rho_{1'}(E)$ is the final density of states, one-half times the terms in the first pair of square brackets is the coherence factor, and the two terms in the second pair of square brackets are the occupation factors for elastic scattering from ξ to ξ' and the reverse process, respectively. The symbol $\rangle_{A,1'}$ indicates an angular average over the gap-anisotropy distribution. To first order, we can replace $\rho_{A'}(E)$ with $\rho_{\bar{A}}(E)$, where $\bar{A}$ is the average energy gap. To average the coherence factor we express it in terms of the mean square gap anisotropy $\langle\delta^2\rangle = \left\langle(\Delta - \bar{\Delta})^2\right\rangle$. Neglecting terms of order $\langle\delta^2\rangle^{1/2}/\bar{\Delta}$, one can write $\left\langle(uu' - vv')^2\right\rangle = \langle\delta^2\rangle/2\left(E^2 - \bar{\Delta}^2\right)$ for $E\rangle\,\bar{\Delta}$; for $E \leqslant \bar{\Delta}$, one takes the value at $\boldsymbol{E} = \bar{\Delta} + \langle\delta^2\rangle^{1/2}/2$.

For clean superconductors the normalized mean square gap anisotropy (Markowitz and

Kadanoff 1963) $\langle a^2 \rangle = \langle \delta^2 \rangle / \bar{\Delta}^2$ is constant, independent of temperature. However, for dirty superconductors (Anderson 1959) $\langle a^2 \rangle$ is reduced from its clean limit value $\langle a^2 \rangle_0$ to a value given approximately by $\langle a^2 \rangle = \langle a^2 \rangle_0 / \left[1 + \left(\hbar/2\tau_1\bar{\Delta}\right)^2\right]$. Combining these expressions, we find

$$G_{\mathrm{el}\xi} = \tau_1^{-1} \frac{\langle a^2 \rangle_0}{1 + \left(\hbar/2\tau_1\bar{\Delta}\right)^2} \frac{\bar{\Delta}^2 E}{2\left(E^2 - \bar{\Delta}^2\right)^{3/2}} \left(f_\xi - f_{-\xi}\right) \tag{4.2}$$

$$\left(E \geqslant \bar{\Delta} + \langle \delta^2 \rangle^{1/2}/2\right)$$

where we have set $\xi' = -\xi$; this is an excellent approximation for the values of anisotropy encountered in real metals.

We can use eq. (4.2) to interpret the results obtained for Sn and SnIn in fig. 6. For the clean films we expect the mean free path, l, to be typically 300 nm , while for the SnIn film it was estimated to be 42 nm . Using $v_{\mathrm{F}} = 0.65\times\ 10^6$ ms^{-1} [calculated from $v_{\mathrm{F}} = (\pi^2 k_{\mathrm{B}}^2/e^2\gamma)\,\sigma/l$ (Pippard 1965), where σ is the conductivity, and $\sigma/l = 9.5 \times 10^{10}\Omega^{-1}$ cm^1 (Chambers 1952)], we estimate τ_1 to be 2.2 ps and 15.5 ps for the clean Sn and SnIn films, respectively. Thus, the factor $1/\tau_1 \left[1 + \left(\hbar/2\tau_1\bar{\Delta}\right)^2\right]$ is about 0.85 for the Sn films and 0.19 for the SnIn film. Now below about $0.8T_{\mathrm{c}}$, the total measured rate (including both elastic and inelastic processes) is roughly two times higher in Sn than in SnIn , leading us to conclude that the elastic contribution is small for SnIn , but comparable with the inelastic rate in Sn . As we increase the temperature towards T_c, $\hbar/2\tau_1\bar{\Delta}$ becomes large compared with unity, and $G_{\mathrm{el}\xi}$ scales roughly as $\bar{\Delta}^4$. Thus, in the limit $T \to T_{\mathrm{c}}$, the elastic contribution becomes negligible compared with the inelastic process, and the data for the Sn and SnIn samples become indistinguishable.

Chi and Clarke (1979) measured ${\tau_{Q^*}}^1$ in Al films in which the mean free path was reduced by evaporating them in an oxygen atmosphere. The experimental configuration was similar to that shown in fig. 5, except that it was not necessary to deposit a Pb film over the Cu film. They compared their results with computer solutions of the Boltzmann equation in which eq. (4.2) was included in the limit $\left(\hbar, 2\bar{A}\tau_1\right) \gg 1$ appropriate to the experiments. Figure 7 shows $\left(F^*\tau_{Q^*}\right)^{-1}$ versus $\Delta(T)/k_{\mathrm{B}}T_{\mathrm{c}}$ for five representative samples with parameters listed in table 1. The values $v_{\mathrm{F}} = 1.36 \times 10^6$ ms^{-1} [calculated from the free electron value divided by the thermal effective electron mass (Kittel 1976)], $\rho l = 9 \times 10^{16}\Omega$ m^2 (Fickett 1971), and $N(0) = 1.74 \times 10^{28}$eV^{-1} m^{-3} (Gschneidner 1964) were used. The solid lines are the best fit to the theory using τ_{E}^{-1} and the characteristic elastic charge relaxation rate

$$\tau_{Q^*\,\mathrm{el1}}^{-1}(0) = 2\tau_1 \left(k_{\mathrm{B}}T_{\mathrm{c}}\right)^2 \left\langle a^2 \right\rangle_0 / \hbar^2$$

Table 1
Measured and calculated quantities for five Al samples

Sample	T_c(K)	1(nm)	$^{\tau}$E (ns)	$\tau_0^{-1} = e_{el}^{-1}(0)t_E$	$\langle a^2 \rangle_0$
8	1.267	78	13	0.62	0.022
11	1.306	23	8	0.(19)3	0.01^-
12	1.411	12.5	5.8	0.062	0.025
13	1.573	6.0	1.5	0.031	0.00^-e
15	2.113	1.0	1.0	(a)	(a)

[0] "The upward curvature was too small to enable an estimate of $\tau_{Q^*\,\mathrm{el}}^{-1}(0)$ to be made.

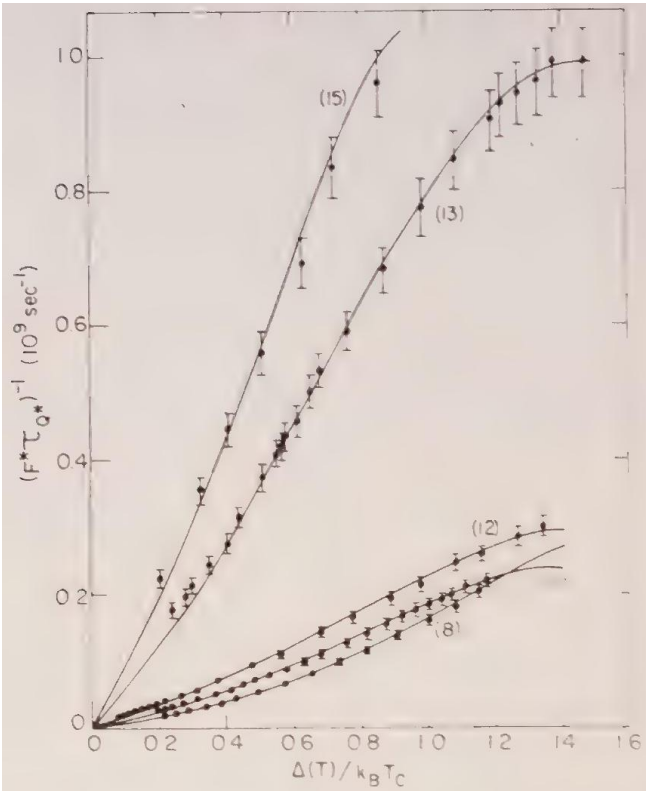


Fig. 7. Measured values of $\left(F\^{}{* \tau_{Q^{\{*\}}\right)}{-1}$ versus Ik_BT_s for 5 samples listed in table 1 (sample numbers shown in parentheses). The solid lines are best fits to the solution of the Boltzmann equation. (Chi and Clarke 19-9.)}

as fotume parameters. For each sample. the value of $\tau_f{}^1$ was obtained from the data in the limm A(T) k_1 I. $\rightarrow$ (). Whice ? (f)) was determined from the upward curvature required to fit the data at lower temperatures. It should be realized that the actual gap anisotropy in these folms is very small. Thus. for the clearest film listed in the table: $a^2, = 2, 10)^4 \, /a^2/0$ at $0.9I_6$. The high seristantly of τ_y : {o :ers small gap ansortropes reflects the relatively slow melasic scallering rate in Al. For the cleanest films studied (not listed in table 1) the average value of τ_{f} was about 12 ns .

14.4.2 4.2. Inelastic scattering in aluminum

(his and Clarke also extracted values of τ_{ff} from their data over a wide range of mean free paths. rangeng from about $4(x)$nm to 1 nm . The transition termperatures of these films increased from about 1.2 K for the cleanest films to about 2.1 K for the dirocest film. They found that the apparent value of τ_f decreased much more rapidly than I. "which would be expected from an electron phonon meteractoron). from about 12 ns for T $\approx$ 1.2 K to about 1 ns for $I \approx 2.1$ K. This rapid increase in the inelastic scattering rate with I_c remained a puzzle for several sears. but recent usork on the enhancement of electron electron scaltering due to localizatonn effects provides a rather convincing explanatuon (cordon et al. 1983, Santhanam and Prober 1984). We briefly describe this work.

The theory of Abrahams et al. (1981) predicts that for dirty ($l < hv_{\mathrm{F}}/k_{\mathrm{B}}T$), iw ()-dimensional lin; $13k_k, T - d^2$ isamples the electron electron scattering rate is given by

$$\mathrm{re}^{-1} = \frac{e^2 R}{2\pi\hbar^2} k_{\mathrm{B}} T \ln\left(T_1/T\right), \tag{4.3}$$

where d is the film thickness. R is the resistance of a square film and T_1 is roughly 103^2 K. Cjordon et al. and Santhanam and Prober extracted values of -: from measurements of the magnetoconductance of dirty Al films. and found good agreement with eq. (4.3). Near T. Entin-Wohlman and Orbach (19'x l) showed that the charge relaxation rate due to electron electron scattering is given by

$$\left(F^* \tau_{Q^*}\right)_{ee}^{-1} = \left(\pi\Delta/4k_B T\right) \tau_{et}^{-1}, \tag{4.4}$$

so that one can immediately apply eq. (4.3) to the inelastic scattering rates measured near T, by (C. Setting $T = 1$ K in the logarithmic term in eq. (4.3) fand neglecting the temperature dependence of this term) we find $z_{:,}{}' \approx 1.5$, $10^8 R - T_{\mathrm{c}} \mathrm{s}^{-1}$. For the dirtiest samples studied by CC ($T_{\mathrm{c}} \approx 2$ K.$R_- \approx 6\Omega$), one predicts : ≈ 10.5 ns from eq. 14.31 . a value within a factor of 2 of the cepperimental results. Both Gordon et al. and Santhanam and Prober show that the CC data for dirty Al are quite well fitted by eq. (4.3).

For the cleanest samples studied by CC, the electron-electron scattering rate should be negligible compared with the electron-phonon scattering rate. The measured value of τ_{E}, about 12 ns , is a factor of 3 or more below the value of about 40 ns calculated by Kaplan et al. (1976) and Lawrence and Meador (1978). The magnetoconductance data of Gordon et al., however, lead to $\tau_{\mathrm{E}} \approx 12$ ns in the clean limit, a value that is very compatible with the CC value. This discrepancy between measured and theoretical values of τ_E in Al thus appears to be well substantiated, and is worthy of further study.

We note in passing that the values of $\langle a^2 \rangle_0$ obtained by CC assume, of course, that the inelastic scattering consists of electron-phonon processes only. If, as now seems highly probable. electron-electron scattering was significant or even dominant in the dirtier samples. since the distribution in the presence of electron electron scattering differs from that in the presence of electron phonon scattering, the values of $\langle a^2 \rangle_0$ quoted for these samples will be somewhat in error.

It is also possible to determine the inelastic and elastic scattering rates as a function of energy by measuring the nonequilibrium distribution injected via a tunnel junction by means of a second tunnel junction (Kaplan et al. 1977. Chang 1977. Kirtley et al. 1978. Gray 1981). In measurements on clean Al films, Gray found $\tau_{\mathrm{f}} \approx 12$ ns, in excellent agreement with the CC result, while Kirtley et al. found $\tau_1 \approx 0.25$ ns in Al films with $T_2 \approx 2.4$ K. More surprisingly, an analysis of both experiments produced an elastic scattering time that was essentially independent of the quasiparticle energy. This result is clearly in disagreement with the prediction of eq. (4.2), and not understond in the present theoretical framework.

14.5 5. Charge relaxation in the presence of magnetic impurities or a supercurrent

14.5.1 5.1. Elastic scattering from magnetic impurities

The addition of magnetic impurities to a superconductor destroys the degeneracy between time-reversed electron states through the exchange interaction between the conduction electrons and the impurities, giving the Cooper pairs a finite lifetime. The inverse of this lifetime, the pair breaking rate, is the elastic spin-flip scattering rate for electrons in the normal metal. τ_s^{-1} (Abrikosov and Gorkov 1960). The presence of impurities can have a dramatic effect on the charge relaxation rate as was first pointed out by Schmid and Schön (SS. 1975) and later studied by Pethick and Smith (1981a,b), Entin-Wohlman and Orbach (1979), and Lemberger

and Clarke (LC, 1981a). This effect occurs because the coherence factor for elastic spin-flip scattering from one quasiparticle branch to the other in an isotropic
superconductor is not zero, but of the form

$$(uu' + vv')^2 = 4u^2v^2 = \Delta^2/E^2. \tag{5.1}$$

Since this factor approaches unity as $E \to A$, we expect the spin-flip scattering to have an appreciable effect on $\tau_{Q^*}^{-1}$ when $\tau_{\rm S}^{-1} \gtrsim \tau_{\rm E}^{-1}$.

Schmid and Schön found

$$(F^*\tau_{Q^*})^{-1} = \frac{\pi\Delta}{4k_{\rm B}T_{\rm c}\tau_{\rm E}}\left(1 + \frac{2\tau_{\rm E}}{\tau_{\rm S}}\right)^{1/2}, \quad \left(\tau_{Q^*}^{-1} \ll \tau_{\rm E}^{-1}\right) \tag{5.2}$$

A factor $(1 + \hbar^2\Gamma/\Delta^2\tau_{\rm E})^{1/2}$ has been omitted in eq. (5.2), where $\Gamma = (2\tau_{\rm E})^{-1} + \tau_{\rm S}^{-1}$, since it is very close to unity for all values of $\tau_{\rm E}, \tau_{\rm S}$, and Δ used in the experiments to be described later.

LC included a term

$$G_{{\rm sf}\xi} = \frac{1}{\tau_{\rm S}}\frac{\Delta^2}{E^2}\frac{E}{|\xi|}(f_\xi - f_{-\xi}) \tag{5.3}$$

in the Boltzmann equation to account for spin-flip scattering, and computed solutions with $G_{{\rm cl}j} = 0$ (since this term is negligible compared with G_{sf} for concentrations of magnetic impurities of experimental interest). Figure 8 shows $(F^*\tau_{Q^*})^{-1}$, normalized to the SS factor $(\pi/4\tau_{\rm E})(1 + 2\tau_{\rm E}/\tau_{\rm S})^{1/2}$ versus $\Delta/k_{\rm B}T_{\rm c}$ for several values of $\tau_{\rm E}/\tau_{\rm S}$. For values of $\Delta/k_{\rm B}T_{\rm c} < 1$, the computed values of $(F^*\tau_{Q^*})^{-1}$ lie above the SS result, and, furthermore, increase monotonically compared with the SS prediction as $\tau_{\rm E}/\tau_{\rm S}$ increases.

Using a configuration similar to that in fig. 5, Lemberger and Clarke measured ${\tau_{Q^*}}^1$ in Al films doped with Er. Figure 9 shows $(F^*\tau_{Q^*})^{-1}$ versus $A/\ k_{\rm B}T_{\rm c}$ for 3 samples with the parameters listed in table 2 ; the values of $N(0)$ and ρl were the same as those used by CC. It was assumed that $\tau_{\rm f} = 12\,(1.2/T_{\rm c})^3$ ns; the estimated spin-flip time was taken from Craven et al. (1971), $\tau_{\rm S}^{-1} = 1.9\times10^{13} n_{\rm Er}{\rm S}^1$, where $n_{\rm Ir}$ is the concentration of Fratoms. The rate $(F^*\tau_{Q^*})^{-1}$ is linear in $\Lambda, k_{\rm B}T_{\rm c}$ for $\Lambda/k_{\rm B}T_{\rm c} \lesssim 0.8$, which is consistent with the SS result (eq. 5.2) provided that one assumes that this expression can be extrapolated to much higher values of A/k_BT_c than one can justify theoretically. The data in this range were used to calculate the values of τ, (meas.) listed in table 2. The slope S of the linear region for all the samples studied is plotted versus the SS expression $(\pi/4\tau_{\rm E})(1 + 2\tau_{\rm r}/\tau_{\rm S})^{1\,2}$ in fig. 10. One sees that the data generally fall on a straight line through the origin, indicating that eq. (5.2) predicts the data remarkably well for $\Delta/k_{\rm B}T_{\rm c} \lesssim 0.8$.

Figure 9 also shows curves computed from the Boltzmann equation. It is immediately apparent that the fit to the data is much worse than that of the SS prediction. The discrepency between the computed and experimental curves is further emphasized in fig. 11, where $(SF^*\tau_{Q^*})^1$ is plotted versus $\Lambda/k_{13}T_{\rm c}$ for one sample of each Er concentration. It is apparent that the data, normalized in this way, lie on a universal curve, in complete contrast to the computed

curves shown in fig. 8, in which the same quantity increases markedly with $\tau_{\rm E}/\tau_{\rm S}$ at a given temperature.

More recently, Beyer Nielsen et al. (1982) have examined this problem using a quasiclassical Green's function approach, taking into account the broadening of the states due to the presence of the magnetic impurities. Their results lie very much closer to Lemberger and Clarke's solutions to the Boltzmann equation than to the SS results.

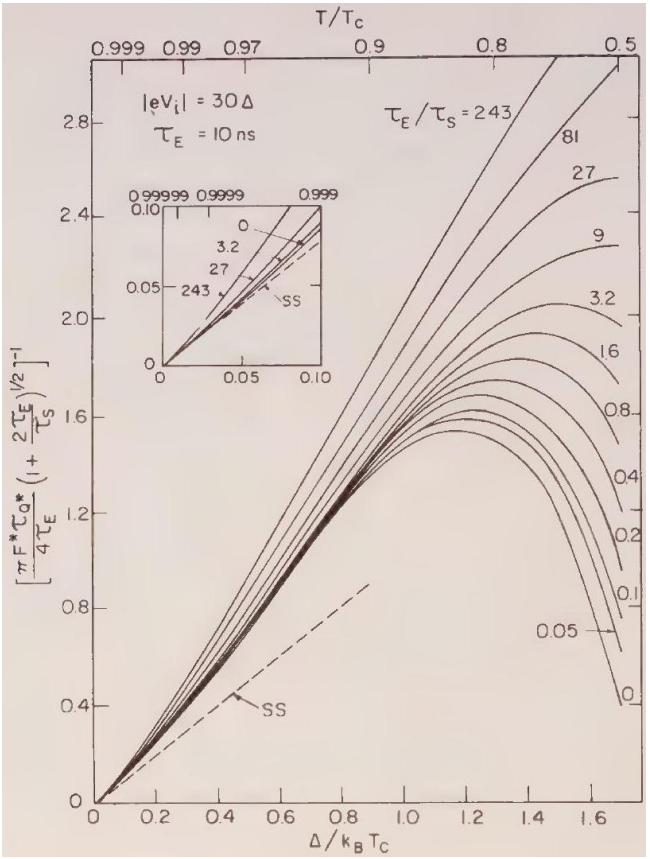


Fig. 8. $\left(F^{*}\tau_{Q^{*}}\right)^{-1}$ normalized to $(\pi/4\tau_{\mathrm{E}})\,(1+2\tau_{\mathrm{E}}/\tau_{\mathrm{S}})^{1/2}$ versus $\Delta/k_{\mathrm{B}}T_{\mathrm{c}}$. The curves approach the origin with unity slope. The dashed line is an extrapolation of the SS theory to low temperatures. The inset shows the region near the origin. (Lemberger and Clarke 1981a.)

This marked discrepancy between the data and the solutions to the kinetic equation is extremely puzzling. It cannot be explained by invoking an additional charge relaxation mechanism in the experiments because the experimental rate $(F^{*}\tau_{Q^{*}})^{1}$ lies substantially below, rather than above, the computed rate. One can rule out the possibility of impurity-impurity

Table 2
Measured and calculated parameters for AlEr films.

Sample	Er-conc (ppm)	T_{c} (K)	l (nm)	$^{\tau}$ E (ns)	τ_{S} (est.) (ps)	τ_{S} (meas.) (ps)
1	21	1.338	38	8.6	2500	1100
6	81	1.350	32	8.3	650	860
7	220	1.410	22	7.4	240	210

interactions, and of Kondo anomalies. However, it is noteworthy that the mean free path of most of the samples was sufficiently short that electron electron scattering played at least some role in the charge relaxation. Thus, it is just possible that the discrepancy arises from the different quasiparticle

distributions that occur in the presence of electron-phonon and electronelectron scattering. Since electron-electron scattering does not reduce the energy of the quasiparticles, there will be a smaller quasiparticle population at low energies compared with that in the presence of an equal electron-phonon

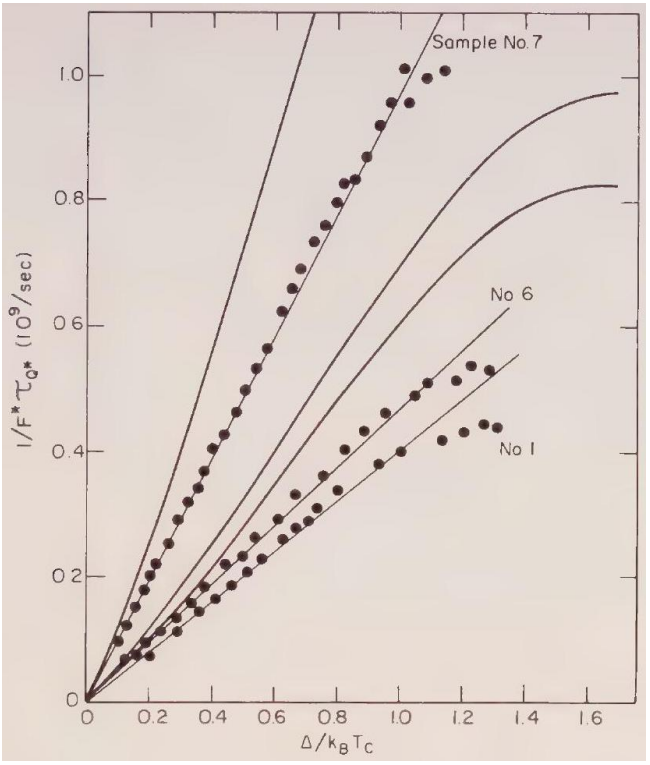


Fig. 9. Experimental values of $\left(F^{*}\tau_{Q^{*}}\right)^{-1}$ versus $\Delta/k_{\mathrm{B}}T_{\mathrm{c}}$ for samples with Er concentrations of 21 (no. 1), 81 (no. 6), and 220 (no. 7) at.ppm, with straight lines drawn through the data by eye. The other curves, which represent computer solutions to the Boltzmann equation, have the same slope as the data in the limit $\Delta/k_{\mathrm{B}}T_{\mathrm{c}} \to 0$. (Lemberger and Clarke 1981a.)}

scattering rate. As a result, the charge relaxation rate due to magnetic impurity scattering will be reduced, since $G_{\mathrm{sf}\xi}$ is proportional to Δ^2/E^2 (eq. 5.3). Thus, the presence of electron-electron scattering is expected to lower the overall charge relaxation rate compared with the value one would compute assuming that the measured inelastic relaxation rate was due solely to electron-phonon processes. Obviously, only a solution of the Boltzmann equation with the inclusion of an appropriate electron-electron relaxation term (Entin-Wohlman and Orbach 1981) will resolve this issue.

14.5.2 5.2. Elastic scattering in the presence of a supercurrent

In the presence of a supercurrent, the quasiparticle energies are raised by an amount $p_k \cdot v_s$, where p_h is the momentum of a quasiparticle in state k, and v_s is the superfluid velocity (Aronov 1974, Gal'perin et al. 1974). Thus, quasiparticles at the Fermi energy where v_s and p_k are in the same direction are raised by $p_{\mathrm{F}}v_{\mathrm{s}}$, while those where v_{s} and p_k are in opposite directions are lowered by $p_{\mathrm{F}}v_{\mathrm{s}}$. This current-induced anisotropy allows elastic scattering to relax charge imbalance in much the same way as gap anisotropy. Maki (1969) has shown that an appropriate electron relaxation rate for thin films $\left[d \ll (l\xi_0)^{1/2}\right]$ in the dirty limit ($l \ll \xi_0$) is

$$\frac{1}{\tau_{\mathrm{S}}} = \frac{lv_{\mathrm{F}}}{6}\left(\frac{p_{\mathrm{S}}}{\hbar}\right)^2, \tag{5.4}$$

where $\xi_0 = \hbar v_{\mathrm{F}}/\pi\Delta(0)$, and p_{S} is the momentum of a Cooper pair. We can use eq. (5.4) in eq. (5.2) or (5.3) to predict the charge relaxation rate as a function of p_{s}. For the case of magnetic impurities LC found that at a given temperature $\left(F^{*}\tau_{Q^{*}}\right)^{-1}$ was proportional to

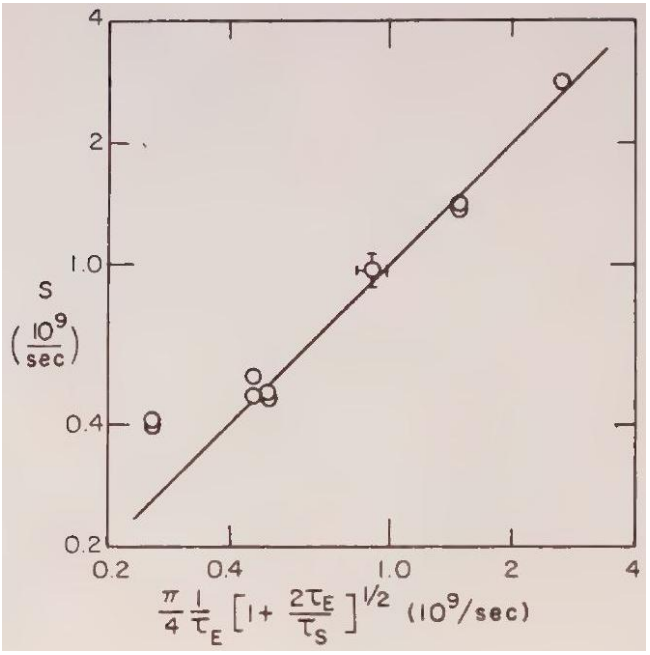


Fig. 10. S, the slope of $\left(F\hat{}\{*\tau_\{Q^{\{*\}}\right)\{-1\}$ versus $\Delta/k_{\mathrm{B}}T_{\mathrm{c}}$ for small $\Delta/k_{\mathrm{B}}T_{\mathrm{c}}$, versus $(\pi/4\tau_{\mathrm{E}})\left(1+2\tau_{\mathrm{E}}/\tau_{\mathrm{S}}\right)^{1/2}$ for all samples. The solid line through the origin has unity slope. (Lemberger and Clarke 1981a.)}

$\left(1+2\tau_{\mathrm{E}}/\tau_{\mathrm{S}}\right)^{1/2}$, as predicted by SS. Thus, we can immediately write down an expression for the detector voltage at a given temperature and injection current in the presence of a supercurrent, I_{S} :

$$V_{\mathrm{d}}\left(I_{\mathrm{S}}\right)=\frac{V_{\mathrm{d}}(0)}{\left(1+2\tau_{\mathrm{E}}/\tau_{\mathrm{S}}\right)^{1/2}}=\frac{V_{\mathrm{d}}(0)}{\left(1+b^{\mathrm{SS}}I_{\mathrm{S}}^{2}\right)^{1/2}},\tag{5.5}$$

where from eq. (5.4)

$$b^{\mathrm{SS}}=2\tau_{\mathrm{E}}/\tau_{\mathrm{S}}I_{\mathrm{S}}^{2}=\tau_{\mathrm{E}}lv_{\mathrm{F}}p_{\mathrm{S}}^{2}/3\hbar^{2}I_{\mathrm{S}}^{2}\tag{5.6}$$

For uniform currents much less than the critical current we can use the relations (Tinkham 1975) $p_{\mathrm{S}}=2mv_{\mathrm{S}}, j_{\mathrm{S}}=n_{\mathrm{S}}ev_{\mathrm{S}}, n_{\mathrm{S}}=mc^{2}/4\pi e^{2}\lambda^{2}$ and, in the dirty limit, $\lambda(0)\approx\lambda_{L}(0)\left(\xi_{0}/l\right)^{1/2}$ to find

$$b^{\mathrm{SS}}=\left(\frac{8\pi e}{\hbar c^{2}}\right)^{2}\frac{\tau_{\mathrm{E}}v_{\mathrm{F}}\xi_{0}^{2}\lambda_{\mathrm{L}}^{4}(0)}{3ld^{2}w^{2}}\frac{\lambda^{4}\left(T/T_{\mathrm{c}}\right)}{\lambda^{4}(0)}.\tag{5.7}$$

Here, w is the film width, $\lambda_{\mathrm{L}}(0)$ is the London penetration depth, and $\lambda\left(T/T_{\mathrm{c}}\right)/\lambda(0)$ is a well-known function (Tinkham 1975).

Lemberger and Clarke (1981b) solved the Boltzmann equation in the presence of a supercurrent by replacing $1/\tau_{\mathrm{s}}$ in eq. (5.3) with eq. (5.4) to obtain

$$G_{\mathrm{S}\xi}=\frac{l\mathrm{v}_{\mathrm{F}}}{6}\left(\frac{p_{\mathrm{S}}}{\hbar}\right)^{2}\frac{\Delta^{2}}{E|\xi|}\left(f_{\xi}-f_{-\xi}\right)\tag{5.8}$$

With this substitution, the results computed in section 5.1 can be carried over to the present case. Thus, for fixed temperature and injection voltage,

$$V_{\mathrm{d}}\left(I_{\mathrm{S}}\right)=\frac{V_{\mathrm{d}}(0)}{\left(1+b^{\mathrm{num}}\,I_{\mathrm{S}}^{2}\right)^{1/2}}\tag{5.9}$$

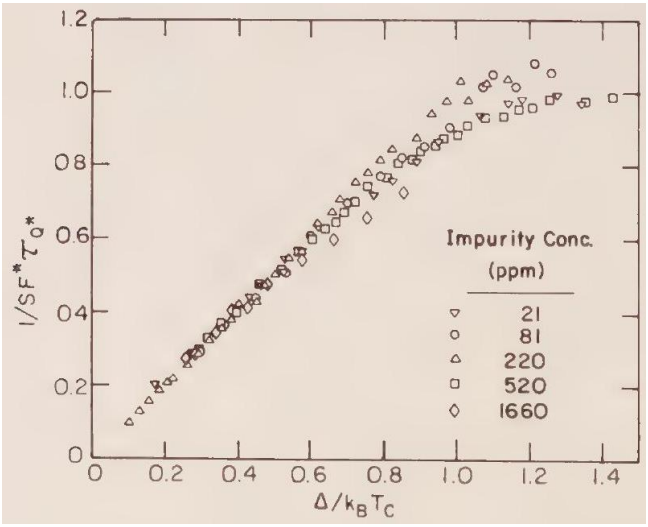


Fig. 11. $\left(S F^{*} \tau_{Q^{*}}\right)^{-1}$ versus $A/k_{\mathrm{B}}T_{\mathrm{c}}$ for one representative sample of each impurity concentration. (Lemberger and Clarke 1981a.)

where $b^{\mathrm{num}}(T)$ is the numerical value produced by the computer. In general, $b^{\mathrm{num}}(T)$ will differ from $b^{\mathrm{SS}}(T)$, as is evident in section 5.1 , and we can compare both values with the measured value, $b^{\mathrm{meas}}(T)$.

Lemberger and Clarke (1981b) performed experiments using the usual geometry with a supercurrent introduced along the Al film in which the charge

imbalance is generated. To increase the uniformity of the current distribution, a Nb groundplane was sputtered onto the substrate and covered with an insulating layer before the sample was deposited. A representative plot of $V_{\mathrm{d}}(I_{\mathrm{S}})$ versus I_{S} is shown in fig. 12. As predicted by eqs. (5.5) and (5.9), the value of $|V_{\mathrm{d}}|$ decreased quadratically with increasing $|I_{\mathrm{S}}|$ at low supercurrents, becoming linear in I_{S} at higher supercurrents. The slight asymmetry in the curves about $I_{\mathrm{S}} = 0$ was due to the non-negligible value of I_{i}. After shifting the origin appropriately, curves of the form $(1 + hI_5^2)^{12}$ were fitted; the quality of the fit is excellent. Experimentally determined values of h are shown in fig. 13 for two samples, together with the fitted curves h^{SS} and h^{num} . The temperature dependence of b^{SS} is in excellent agreement with the data, while b^{num} is in substantial disagreement. Furthermore, the ratio $\left\langle b^{\mathrm{SS}}(T), b^{\mathrm{meal}}(T)\right\rangle$ varies between 1/3 and 1/2, an agreement which, given the uncertainties in the values of $v_{\mathrm{F}}, l, \lambda_{\mathrm{L}}(0)$, and τ_{E}, is considered quite acceptable.

We therefore draw the same conclusions as for the case of magnetic impurities: The Schmid-Schön theory fits the measured data very accurately, even at values of $\Delta/k_{\mathrm{B}}T_{\mathrm{c}}$ much larger than one could reasonably expect, while the computed solution to the Boltzmann equation does not fit the data. However, it is again just possible that this discrepancy could be resolved by the inclusion of electron electron scattering in the Boltzmann equation.

14.6 6. Resistance of the normal metal-superconductor interface

We now begin a discussion of a series of situations other than tunnel injection in which charge imbalance plays a role. The first of these concerns the electrical resistance of the normal metal-superconductor (NS) interface, a subject about which there exists a substantial literature. The first important experimental work was that of Pippard et al. (1971) who measured the electrical resistance of superconductor-normal-metal-superconductor (SNS) sandwiches in which the normal metal was too thick and/or too dirty to sustain a Josephson supercurrent.

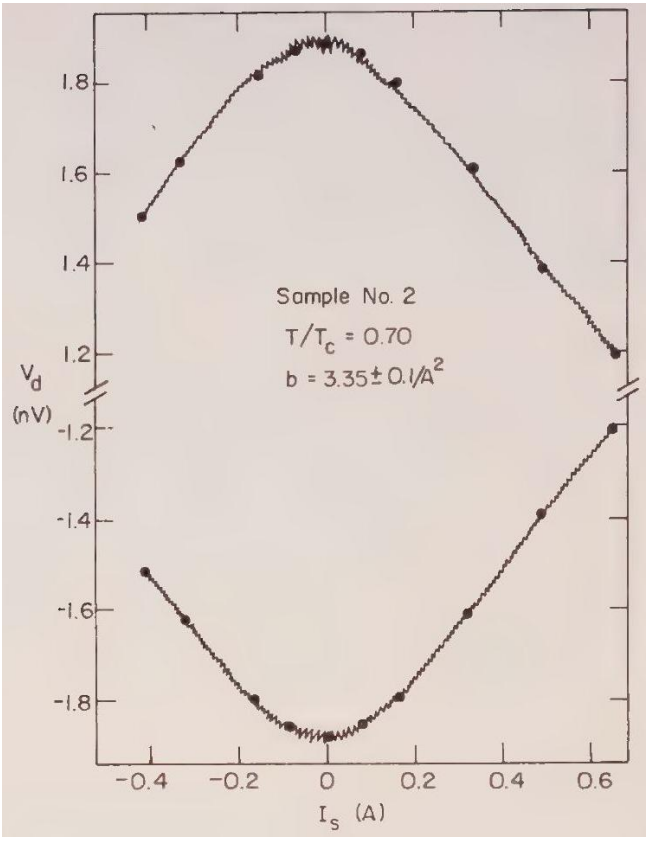


Fig. 12. Typical experimental plot of V_{d} versus I_{s} for fixed I_{i}. The points are a fit to a function of the form $V_{\mathrm{d}}(I_{\mathrm{s}}) = V_{\mathrm{d}}(0)/\left(1 + bI_{\mathrm{s}}^2\right)^{1/2}$, with b as the fitting parameter. (Lemberger and Clarke 1981b.)

They observed that, near the transition temperature of the superconductor, T_c, the resistance increased rapidly with increasing temperature. Yu and Mercereau (1972) showed that the excess resistance was associated with a potential that decayed exponentially into the superconductor. Subsequently, Harding et al. (1974) studied the resistance of SNS sandwiches in which the mean free path of the superconductor was shortened by alloying, and found an additional boundary resistance at low temperatures as well as a greatly enhanced rise in resistance near T_c. More recently, Hsiang and Clarke (1980) made measurements on a series of samples in the clean limit, and used their results to obtain values of τ_E in Pb, Sn, and In.

The theory of the NS interface resistance has been widely investigated. The work of Rieger et al. (1971), who used a time-dependent Ginzburg-Landau theory, contained some essentially correct ideas, but did not produce the correct quasiparticle propagation length in the superconductor. Pippard et al. (1971) and Harding et al. (1974) used a Boltzmann equation approach that was later extended by Waldram (1975), and reviewed by Pippard (1981). The microscopic theory was developed by Schmid and Schön (1975), and has been extended by Ovchinnikov (1977, 1978), Artemenko and co-workers (Artemenko and Volkov 1977, Artemenko et al. 1978) and Krhenbhl and Watts-Tobin (1978, 1979). Hsiang and Clarke (1980) gave a simple description valid in the limit $\Delta/k_{\mathrm{B}}T \ll 1$ by adapting the tunnel injection theory that accounted quantitatively for their experimental data, and that was verified by Pethick and Smith (1981a) using their two-fluid model. Most recently, Blonder et al. (1982) have used the Bogoliubov equations to treat the transmission and reflection of particles at the NS interface that includes a barrier of arbitrary strength.

In the clean limit $l \gg \xi(T)$ the essential picture that emerges from this work is as follows.

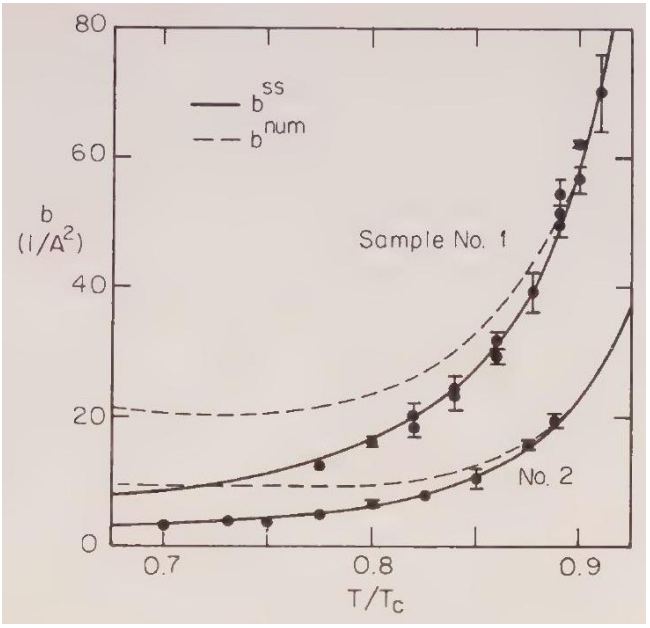


Fig. 13. Data points are measured values of b, solid and dashed lines are fits of b^{ss} and b^{num} to the data. The values of T_{c}, l, and τ_{E} are 1.370 K, 25 nm and 5.3 ns for sample 1 and 1.514 K, 11 nm, and 2.7 ns for sample 2 . The average values of $b^{\mathrm{SS}}/b^{\mathrm{meas}}$ over the temperature range studied are 0.36 and 0.51 for samples 1 and 2 ; the value $i_L(0) = 160$ nm (Meservey and Schwartz 1969) was used. (Lemberger and Clarke 1981b.)}

When a charge imbalance is created in one region of a superconductor, it relaxes over a length

$$\lambda_{Q^*} = (l v_{\mathrm{F}} \tau_{Q^*}/3)^{1/2} = (D\tau_{Q^*})\,,^{1/2}, \tag{6.1}$$

where we assume $l \ll v_{\mathrm{F}}\tau_{Q^*}$. Very close to T_{c} almost all of the excitations incident from N propagate into S , so that, in the presence of an external
current, a quasiparticle current flows in the superconductor. In the usual situation where the transverse dimensions of the interface are much larger than the London penetration depth, there is no net current in the interior of the superconductor. The internal quasiparticle current is cancelled by a pair current, with a corresponding flow of supercurrent on the surface. The electric field is continuous at the interface, and the electric field, the electric potential, Q^*, and the quasiparticle current all decay exponentially into S with a characteristic length i_{Q^*} (see fig. 14). When the temperature is lowered somewhat, a substantial fraction of quasiparticles have energies $\lesssim \Delta_\infty(T)$, and are Andreev reflected (Andreev 1964) at or near the NS interface. In this process, a $k_>$ ($k_<$)quasiparticle incident from N is scattered onto the $k_<$ ($k_>$) branch, and the current carried by these two excitations continues in the superconductor as a supercurrent. Thus, there is no boundary resistance associated with these quasiparticles, and there is a discontinuity in the electric field at the interface (fig. 14). The potential is continuous at the interface, but its spatial derivative is not. In the presence of a current, the boundary scattering processes introduce disequilibrium in the quasiparticle distributions within an inelastic scattering length on either side of the interface.

As the temperature is lowered still further ($\Delta_x \gg k_{\mathrm{B}}T$), essentially all of the quasiparticles are Andreev reflected at the interface, and there is no quasiparticle current in S. Correspondingly, the electric field and potential are zero in S (fig. 14) and there is no boundary resistance. (In fact, the Andreev scattering process occurs over a distance $\sim \xi_0$, so that the discontinuities in the electric field and the derivative of the potential extend over this region. Furthermore, there will be a small boundary resistance of order $\zeta\rho_s/A$ that is negligible in most practical

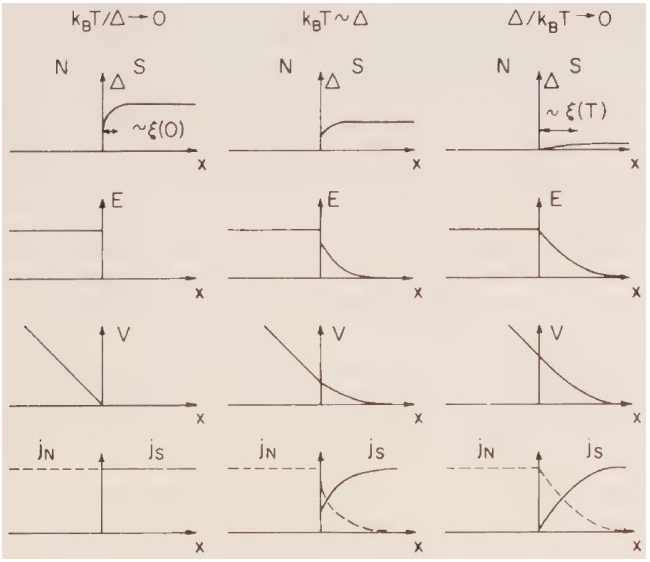


Fig. 14. Variation of energy gap, $\triangle$, electric field, E, electric potential, V, normal current, \$j_{\mathrm{N }}\$, and supercurrent, j_{S}, across an NS interface for $k_{\mathrm{B}}T/\Delta \to 0, k_{\mathrm{B}}T \sim \Delta$, and $\Delta/k_{\mathrm{B}}T \to 0$. The gap is taken to be zero in N, and the normal-state properties are assumed to be the same in the two metals.
(Hsiang and Clarke 1980.)}

situations.)

We now outline the simple model of Hsiang and Clarke (HC) that is valid in the limit $A_\infty(T)/k_{\mathrm{B}}T \ll 1$. We assume that the transition temperature of the normal metal is much less than T, so that we can set $A = 0$ for $x < 0$ (fig. 14). In the superconductor, Δ rises from its value at the boundary, $\Delta_0(T)$, to its full value, $A_y(T)$, over a distance of roughly the Ginzburg-Landau (1950) coherence length, $\zeta(T)$, that is always much less than i_{0^*} in the temperature range investigated experimentally. However, we note that quasiparticles with energies greater than $\Delta_\gamma(T)$ may undergo some charge relaxation in the region where Δ varies spatially. At least in the limit $\Delta \ll k_{\mathrm{B}}T$, this contribution to the overall relaxation rate is likely to be small, and we shall neglect it. We assume that the current densities are sufficiently low that they do not perturb Δ. We further assume that quasiparticles with energies greater than $\Delta_x(T)$ are transmitted into S with probability unity; this is the most serious approximation because some of the quasiparticles in this energy range will undergo Andreev reflection. Quasiparticles with energies $\langle A_x(T)$ are Andreev reflected at a plane taken as $x = 0$ [since $\xi(T) < i_{Q^*}$]. Finally, we assume that the quasiparticles are close to thermal equilibrium even in the vicinity of the interface; we emphasize that this is a reasonable approximation only for A, $\ll k_{\mathrm{B}}T$.

The charge imbalance generated by the uniform injection of a current I_{i} into volume Ω of a superconductor in the limit $e_{\mathrm{i}} \ll k_{\mathrm{B}}T$ is given from eqs. (2.21) to (2.23) by

$$Q^* = \frac{Z(T)}{Y(T)} \frac{I_{\mathrm{i}} \tau_{Q^*}}{e\Omega}, \quad (eV_{\mathrm{i}} \ll k_{\mathrm{B}}T)\,. \tag{6.2}$$

In the case of the NS interface, I_{i} is just the quasiparticle current injected into S , and is related to the total current, I, by

$$\mathrm{Y}(T) = I_{\mathrm{i}}/I. \tag{6.3}$$

Equation (6.3) follows from the realization that in a SIN tunnel junction at low voltages a fraction $[1 - \mathrm{Y}(T)]$ of the current that flows at T_c cannot flow at a temperature $T < T_c$

because there are no states available in S at energies $< .1(T)$, whereas at the NS interface, in our approximation, this same fraction $[1 - \mathrm{Y}(T)]$ of the total current is transmitted into S as a pair current.

Combining eqs. (6.1) to (6.3), and replacing the exponentially decaying Q^* with a value that is constant at the value $Q^*(0)$ for $x \leqslant \lambda_{Q^*}$ and 0 for $x > \lambda_{Q^*}$, we find

$$Q^*(0) = \frac{Z(T) I \tau_{Q^*}}{eA\lambda_{Q^*}} \tag{6.4}$$

The excess voltage, V_b, at each interface of the SNS sandwich adds to the voltage developed across the normal metal, and the total potential across the sandwich is measured with superconducting leads making metallic contact with the superconducting films. This is in contrast to the usual tunneling measurement of Q^*, where the potential is measured by a tunneling contact to a normal metal. Thus, we set $g_\mathrm{NS}(0) = 1$ in eq. (2.20), and combine the result with eq. (6.4) to obtain the boundary resistance

$$R_\mathrm{b} = \frac{V_\mathrm{b}}{I} = \frac{Z(T)\dot{\lambda}_{Q^*}\rho}{A}, \quad (\Delta \ll k_\mathrm{B}T)\,. \tag{6.5}$$

In eq. (6.5) we have set $\tau_{Q^*} = 3i_{Q^*}^2/l_\mathrm{F}$ and used the free electron model (Kittel 1976) to calculate $\rho_\mathrm{s} = 3/2e^2N(0)lv_\mathrm{F}$. As $T \to T_\mathrm{c}, Z(T) \to 1$, and the boundary resistance is just the resistance of a length $\hat{\lambda}_{Q^*}$ of the superconductor in the normal state. As the temperature is lowered, $Z(T)$ decreases, reflecting the fact that fewer quasiparticles are able to propagate into the superconductor. At low temperatures (Clarke et al. 1979a) $Z(T) \approx (k_BT/\Delta)^{12} \exp(-\Delta/k_\mathrm{B}T)$, so that R_b vanishes exponentially as $T \to 0$, as we expect. However, we repeat our warning that the model is not expected to be quantitatively correct at intermediate temperatures.

If one measures R_b near T_c one can deduce values of τ_{Q^*}. As was discussed in sections 2.3 and 4, in general, both inelastic and elastic scattering contribute to $\tau_{Q^*}^{-1}$. We can make a crude estimate of the elastic relaxation rate in the presence of gap anisotropy for the materials used in the experiments to be described by assuming $E \sim k_\mathrm{B}T_\mathrm{c}$ in eq. (4.2). This leads us to the conclusion that electron phonon scattering should dominate at temperatures above $0.9T_\mathrm{c}$. Since $\Delta, k_\mathrm{B}T \approx 1$ at $T; T_\mathrm{c} = 0.9$, it appears that in the range of validity of eq. (6.5), $\Delta, k_\mathrm{B}T \ll 1$, the charge relaxation should be dominated by inelastic scattering, and we assume that $\tau_{Q^*} = 4k_\mathrm{B}T\tau_\mathrm{E}/\pi\Delta_\sigma(T)$.

HC measured the resistances of the SNS junctions listed in table 3. The PbBi − CuAl samples were made by evaporating the materials onto glass substrates; the CuAl was $\sim 2\mu$ m thick, while the PbBi was $\sim 20\mu$ m thick, considerably greater than i_{Q^*} over the experimental temperature range. In the remaining samples, the superconductor (up to 80μ m thick) was evaporated onto the two sides of Ir foils about 70μ m thick. The foils were cleaned by sputter etching in argon, the argon was pumped out of the system, and the superconducting material was evaporated onto each side of the foil. Two or three samples were connected in series and their resistances measured with a

[a] Values of τ_E are averaged over 2 or 3 samples of each type.

[b] Kaplan et al. (1976).

SQUID voltmeter. The variation of resistance with temperature is shown in fig. 15 for one representative sample of each type. Near T_c, the resistance rises rapidly with increasing temperature, while at low temperatures the resistance is nearly independent of temperature. To within the experimental accuracy, the low temperature resistance was equal to the estimated resistance of the normal metal.

To compare the data with eq. (6.5), in fig. 16 we plot the measured resistance versus $Z(T)\,(k_\mathrm{B}T/\Delta)^{1/2}$. The solid lines are a least squares fit to the data for $T > 0.9T_\mathrm{c}$ ($0.96T_\mathrm{c}$ for Sn). The fit is good-in fact, for (a), (c) and (d) it is surprising that such good agreement

Table 3
Properties of SNS junctions. ${

^{a}$}

Superconductor/ normal metal	Type	Measured τ_E (10^{-10} s)	Calculated [b]τ_E (10^{-10} s)
$Pb_{0.99}Bi_{0.01} - Cu_{0.97}Al_{0.03}$	film	0.25	0.23(Pb)
$Sn - Ir$	foil	2.6	2.7
$Sn_{0.99}In_{0.01}{}^{-}Ir$	foil	1.1	2.7(Sn)
In-Ir	foil	1.1	1.0

extends down to temperatures as low as $0.9T_c$ where $\Delta \sim k_B T$. The slope of the lines in fig. 16 is $4\,(l v_F \tau_E/3\pi)^{1/2}\,\rho_s/A$, and yields the average values of τ_E listed in table 3 . The values of τ_E calculated by Kaplan et al. (1976) from $\alpha^2 F$ are also listed for comparison. The agreement is generally quite good. Using the fitted values of τ_E, we have plotted the resistance predicted by eq. (6.5) in fig. 15. Except for Sn , the extrapolated lowtemperature resistance is in good agreement with the measured resistance, thus providing a good check on the consistency of our results. Particularly in the cases of PbBi and In , the fit is remarkably good even at intermediate temperatures, a result that is probably coincidental, particularly since the expression used for τ_{Q^*} is quite inappropriate in this range. However, it may be that the increase in the elastic charge relaxation rate as the temperature is lowered tends to compensate for the decrease in the inelastic rate, thus keeping τ_{Q^*} roughly constant at temperatures below about $0.9T_c$.

As pointed out in the description of the tunneling model, the effect of Andreev reflection on the quasiparticle distribution is neglected. The detailed theory of Waldram (1975) takes into account the nonequilibrium quasiparticle distribution, but the fact that one would have to use several parameters to fit the experimental data makes a meaningful test of the theory somewhat difficult. More recently, Blonder et al. (1982) have developed a theory in which they interpose a tunneling barrier of arbitrary strength between the normal metal and the superconductor, and calculate the probabilities of reflection and

transmission as a function of this strength. They have used this model to account for the current-voltage characteristics of $Cu - Nb$ point contacts that could be varied from tunneling to metallic contacts (Blonder and Tinkham 1983) and for the subharmonic gap structure observed in various types of weak links (Klapwijk et al. 1982, Octavio et al. 1983). The model is strictly

applicable only to the case of a hole with a radius much less than l in an insulating screen between two metals, so that the resistance is due to the constriction impeding the ballistic propagation of electrons. This leads to the assumption that the incoming electrons from the S side are described by a Fermi function, $f^0(E)$, while those coming in from the N side are described by $f^0(E - eV)$. Within this approximation, Blonder et al. compute the Andreev reflection of quasiparticles at the interface for varying strengths of the
tunneling barrier. For the case of a clean metallic contact, their result agrees with eq. (6.5) at T_c but has a somewhat different temperature dependence at lower temperatures, the exact form depending on the degree of disorder at the interface and the ratio of the Fermi velocities in the two metals. However, this picture of a small-area constriction impeding the ballistic propagation of electrons, while highly appropriate for point contacts or microbridges, is unlikely to be an appropriate description of the large area SNS sandwiches studied here.

To conclude this section on the NS interface, we note briefly that Hsiang (1980) studied the effect of a magnetic field applied parallel to the plane of SNS sandwiches in which the superconductor was $Pb_{0.98}Bi_{0.02}$, and the normal metal was Cd . The PbBi films are bulk, type-II superconductors in which the spin relaxation rate is given by (Maki 1969, de Gennes 1966, Tinkham 1975)

$$\frac{1}{\tau_s} = \frac{l v_F e H}{3c}. \tag{6.6}$$

Hsiang measured the boundary resistance as a function of applied magnetic field and temperature, and extracted values of $\tau_{Q^*}^{-1}(T,H)$. Using eq. (6.6) in eq. (5.2) he was able to estimate τ_s^{-1} as a function of H. Although there was a good deal of spread in the results, he was able to establish reasonable agreement between the measured value of τ_s^{-1} and the value predicted by eq. (6.6).

14.7 7. Phase-slip centers

A subject of major importance that has received widespread attention is the phase-slip center (PSC) in one-dimensional superconducting filaments or films. Reviews of this subject have been written by Tinkham (1979) and Skocpol (1981). Webb and Warburton (1968) first reported the appearance of discrete voltage steps in the current-voltage characteristics of Sn whiskers very close to T_c. Similar effects were observed by Meyer and von Minnigerode (1972) and Meyer (1973). However, the first understanding of the origin of the effect was put forward in the classic paper by Skocpol, Beasley and Tinkham (SBT) (1974), and we will begin with a brief outline of this work.

Figure 17 shows a typical IV characteristic obtained by SBT for the whole length of a Sn strip, 140μ m long, 4μ m wide, and 0.1μ m thick, shown inset. As the current is increased from zero, there is an initial zero-voltage region followed by a series of voltage steps to resistive regions, the dynamic resistance of which increases by approximately equal increments. As the current is reduced, there is a corresponding series of voltage steps to lower voltages, but with considerable hysteresis. The SBT explanation of these phenomena is as follows (see fig. 18).

As the current, I, is increased, eventually it exceeds the critical current, I_c, at the weakest point in the microbridge. The order parameter in this region collapses to zero and the current is forced to flow as a normal current, thereby allowing the superfluid to build up again and to resume carrying the current. This cycle repeats at a frequency 2eV/h, where V is the average voltage across the region. Each time the order parameter falls to zero, the phase difference between the two ends of the bridge slips by 2π : hence the name "phase-slip center". The width of the region over which the superfluid oscillates is roughly $2\xi(T)$. Now since the superfluid current oscillates between zero and its critical value, on the average approximatley one-half of the current in this region flows as a supercurrent, and the other half as a normal current. Since the temperature is very close to T_c, virtually all of the normal current will propagate into the superconducting regions on either side of the phase-slip region, where it will be converted into a supercurrent over a characteristic length i_{Q^*}. The time average of the pair electrochemical potential, $\bar{\mu}_s$, is constant on either side of the phase-slip region, with a difference eV between the two sides. The time averaged quasiparticle potential, μ_{qp}, changes
smoothly with distance as indicated in fig. 18. Thus, the voltage across the PSC (at distances large compared with λ_{Q^*}) is given by

$$V = 2\,(I - \beta I_c)\,\rho_s \lambda_{Q^*}/A, \tag{7.1}$$

where $\beta \approx 1/2$, and we have used eq. (6.5) with $Z(T) = 1$. The dynamic resistance is

$$\partial V/\partial I = 2\rho_s \lambda_{Q^*}/A. \tag{7.2}$$

This picture explains the essential features of fig. 17. Each step in voltage corresponds to the creation of a PSC, each of which contributes $2\rho_s\lambda_{Q^*}/A$ to the dynamic resistance. SBT were able to set outer limits on the location of each PSC by measuring the voltages across different probes on their bridge (inset, fig. 17). In the example shown in fig. 17, they found

that the first four steps were produced by one PSC forming successively in each of the regions II, I, IV and III, while the fifth step was produced by a second PSC appearing in region IV. However, one very puzzling feature was the fact that the measured characteristic length for the charge imbalance relaxation was essentially independent of temperature, with a magnitude of approximately $(lv_{\rm F}\tau_{\rm E}/3)^{1/2}$. This fact prevented the SBT explanation from being a completely satisfying picture of the PSC. However, Dolan and Jackel (1977) resolved this difficulty in an elegant experiment in which they prepared a microbridge with a series of superconducting voltage leads along one side of the bridge and a series of normal voltage leads along the other. The probes were typically 2μ m apart, and formed tunnel junctions with the microbridge. In this way, they were able to measure the average superfluid and normal potentials, $V_{\rm S} = \mu_{\rm s}/e$ and $V_{\rm N} = \mu_{\rm qp}/e$, across a PSC, the position of which was defined by a small notch in the microbridge. Figure 19 shows their measured values of $V_{\rm S}$ and $V_{\rm N}$. As expected, V_S changes abruptly, since $\xi(T)$ is less than the probe spacing, while V_N changes over a much greater length. Values of τ_{Q^*} deduced from the spatial variation of $V_{\rm N}$ showed the predicted $(T_{\rm c} - T)^{-1/4}$ temperature dependence, and produced the value ${\tau_{Q^*}}^{-1} = 6.3 \times 10^9\,(\Delta/k_{\rm B}T_{\rm c})\,{\rm s}^1$, in excellent agreement with the results of Clarke and Paterson (1974) discussed in section 3. Since this work on PSC was performed at $T \geqslant 0.98T_{\rm c}$, inelastic scattering should completely dominate the charge relaxation.

It was subsequently shown (Kadin et al. 1978) that heating effects can modify the $I - V$ characteristics so as to mask the temperature dependence of i_{Q^*}. Very near T_c, the step becomes rounded, and, as the current is increased, the step due to the entry of the next PSC may appear before the asymptotic value of the dynamic resistance is reached. Further below T_c, local heating distorts the IV characteristic by adding curvature and creating hysteresis. Kadin et al. were able to show that when heating effects were taken into account, the temperature dependence of λ_{Q^*} was as expected. Recently, Stuivinga et al. (1983b) have presented a detailed model of heating effects in PSCs.

Kadin et al. (1978) also studied the effect of a magnetic field, H, applied parallel to the plane of tin PSCs, and found that the inferred value of τ_{Q^*} was reduced by the field. The magnetic field dependence of $\tau_{Q^*}^{-1}$ was consistent with the prediction of Schmid and Schön (eq. 5.2), with (Maki 1969, De Gennes 1966, Tinkham 1975)

$$\tau_{\rm s}^{-1} = \frac{\Delta(0,0)H^2}{hH_{\rm c}^2(0)}. \tag{7.3}$$

Here, $A(0,0)$ is the energy gap at zero temperature in zero magnetic field, and $H_c(0)$ is the parallel critical field at zero temperature. This work was the first experimental demonstration of the essential correctness of the SS theory of charge imbalance relaxation in a magnetic field.

More recently, Aponte and Tinkham (1983) made careful measurements on Sn microbridges with a series of probes, and found values of i_{Q^*} with the expected temperature dependence. Their plot of λ_{Q^*} versus $1 - T/T_{\rm c}$ is reproduced in fig. 20, and we see that the best fit to the slope is -0.28 . However, given the size of th error bars, this slope is not significantly different from $-\frac{1}{4}$. From the measured values of λ_{Q^*} they deduce

$$\tau_{Q^*} = (1.0 \pm 0.2) \times 10^{-10}\Delta(0)/\Delta(T){\rm s}.$$

$\left[\tau_{Q^*}^{-1} = (5.7 \pm 1.1) \times 10^9 A(T)/k_{\rm B}T_{\rm c}{\rm s}^1\right.$, in excellent agreement with the results of Clarke and Paterson (1974) and Dolan and Jackel (1977).]

Klapwijk and Mooij (1976) studied PSCs in Al films, and also found that the characteristic length obtained from IV characteristics was independent of

temperature. However, recently Stuivinga et al. (1981, 1983a) measured the charge relaxation length directly using a series of probes, and found that λ_{Q^*} scaled rather accurately as $(1 - T/T_{\rm c})^{-1/4}$. They deduced a value for $\tau_{\rm E}$ of 4 ns (using $\rho l = 4 \times 10^{-16}\Omega$ m^2). This value

is about a factor of 3 smaller than that obtained by Chi and Clarke (section 4). Stuivinga et al. point out that the low value of τ_E rules out the possibility that elastic scattering in the presence of the supercurrent could have enhanced $\tau_{Q^*}^{-1}$ significantly, as they had suggested earlier (Stuivinga et al. 1982). Furthermore, their films were clean enough (the maximum value of $R_\square$ was about 0.4Ω) that electron-electron collisions should not have contributed in a major way to the measured inelastic relaxation rate. Thus, the very low measured value of τ_E remains a puzzle, although, as we shall see in section 8.2, other measurements of λ_{Q^*} in Al produce comparable values.

Very little experimental work has been carried out on the region of the core, for the obvious reason that its dimensions are so small. However, Skocpol and Jackel (1981) were able to make probes sufficiently small to measure the variation of Δ across a PSC in Sn and found that Δ was greatly suppressed in the core, as one would expect.

The interaction between neighboring PSCs or, in general, any type of weak link, is a complicated subject. Lindelof and Bindslev Hansen (1981) have given an extensive review. The effect of one PSC on the critical current of another arises from a spatially decaying charge imbalance. Such effects were first observed by Jillie et al. (1977), but the only quantitative results appear to be those of Aponte and Tinkham (1983), whose work we now briefly describe. Two neighboring PSCs were fabricated on the same strip of Sn, each PSC being nucleated at a narrowed portion of the strip so that its position was accurately known. The $I-V$ characteristics of the PSC between probes C and L
(inset, fig. 21) were measured as a function of the current flowing through the PSC between probes L and D . For values of I(LD) less than the critical current of the PSC in segment LD, there is no effect on the PSC in segment CL . For larger values of I(LD), there is a change in the apparent critical current of CL, which is increased (decreased) when the applied currents in the two segments are flowing in the same (opposite) direction. However, the magnitude of the change in I_c(CL) is not the same for the two directions of current in LD: the decrease when the currents are opposed is larger than the increase when the currents are in the same direction. This asymmetry reflects the two contributions to the interaction: a heating term, which depresses I_c(CL) irrespective of the direction of I(LD), and a term due to the diffusion of a quasiparticle current from the source PSC to the detector PSC. The diffusive quasiparticle current produced by LD will be in the same direction as the applied current I (LD), so that in the regions outside the probes L and D , there will be an exponentially decaying supercurrent in the opposite direction to I (LD) that cancels the quasiparticle current at each point. When the applied currents are in the same direction, the supercurrent induced in the detector CL by the source LD will be in the opposite direction to I(CL), thus reducing the supercurrent that flows (below the critical current of CL) and enhancing the critical current. On the other hand, when the applied currents are opposed, the critical current of CL will be depressed. By decomposing the change in I_c(CL) into symmetric and antisymmetric components, Aponte and Tinkham were able to separate out the heating and quasiparticle contributions. The normal

current in the center ($x = 0$) of the PSC, $I_N(0) = I - \beta I_c$, was obtained by dividing eq. (7.1) by eq. (7.2); β was found to be 0.6 . The quasiparticle current in a uniform strip would be $I_N(0)\exp(-x/i_{Q^*})$; however, it was necessary to correct for the diffusion of the quasiparticles into the probes. With this correction, the value of $\hat{\lambda}_{Q^*}$ yielded $\tau_{Q^*} = (1.2 \pm 0.4) \times 10^{-10}\Delta(0)/\Delta(T)$S, in excellent agreement with the value obtained from the direct measurement of i_{Q^*} described earlier. Given the fact that the heating effects were also in accord with a simple model, this picture of the effect of one PSC on the critical current of another appears to describe the experimental facts very well.

The interaction of two PSCs when both are at nonzero voltage is more complicated. Under appropriate conditions, the voltages and hence the frequencies of two nearby PSCs can become locked together (Palmer and Mercereau 1977, Jillie et al. 1977, 1980, Lindelof and Bindslev

Hansen 1977, 1981). It appears most likely that the interaction arises from charge imbalance waves, a subject that we will discuss briefly in section 9 .

In concluding this section, we remark that it is rather satisfying that the simple model for the PSC proposed by Skocpol, Beasley and Tinkham gives such a good account of most of the experimental observations. One needs only to consider the time-averaged electrochemical potentials, without delving into the details of the time dependent processes, to explain all the observed phenomena with the exception of the voltage locking effect.

14.8 8. Charge imbalance induced by a temperature gradient

Although the usual thermoelectric effects observed in normal metals, namely the Seebeck and Peltier effects and the Thompson heat, vanish in superconductors, there are observable effects due to temperature gradients in superconductors. Schön (1981a) and Van Harlingen (1982) have recently reviewed the various effects that can occur. In the present section we describe three experiments in which a temperature gradient induces a charge imbalance.

14.8.1 8.1. Thermoelectric generation of charge imbalance at a NS interface

Artemenko and Volkov (1976) were the first to point out that charge imbalance could be induced by a temperature gradient across an NS interface. The quasiparticle current in a superconductor, j_{N}, contains a contribution $(\ \sigma/e\ )\ (\ eE - \nabla\mu_0\ )$, where σ is the electrical conductivity of the quasiparticles, E is the electric field, and μ_0 is the quasiparticle chemical potential (which depends only on the number of electrons and the temperature). Now since the pairs in a superconductor do not accelerate in the steady state, we have $e\boldsymbol{E} - \nabla\mu_{\mathrm{c}} = 0$, so that the transport equation can be written in the form

$$\begin{aligned} j_{\mathrm{N}} &= (\sigma/e)\nabla\left(\mu_{\mathrm{s}} - \mu_0\right) L_{\mathrm{T}}(-\nabla T) \\ &= \left[\sigma/2N(0)e^2\right](-\nabla Q^*) + L_{\mathrm{T}}(-\nabla T), \end{aligned} \tag{8.1}$$

where $L_{\mathrm{T}}(T)$ is the thermoelectric coefficient, and we have made use of eq. (2.11). In the relaxation time approximation, the steady state charge imbalance is determined from the Boltzmann equation (Pethick and Smith 1979a):

$$\frac{\mathrm{d}Q^*}{\mathrm{d}t} = -\nabla\cdot j_{\mathrm{N}} - Q^*/\tau_{Q^*} = 0. \tag{8.2}$$

We now consider the one-dimensional case of a NS interface, where the normal metal occupies the region $x < 0$ and the superconductor occupies the region $x \geqslant 0$, in the presence of a temperature gradient $\mathrm{d}T/\mathrm{d}x$. In addition to the constraint $j_{\mathrm{S}}(x) + j_{\mathrm{N}}(x) = 0$ that holds throughout the superconductor, the requirement that each current be continuous across the boundary $x = 0$ imposes the condition $j_{\mathrm{S}}(0) = j_{\mathrm{N}}(0) = 0$. As a result, $\nabla\cdot j_{\mathrm{N}} \neq 0$ near the interface, and there will be a corresponding charge imbalance. Combining eqs. (8.1) and (8.2), in one dimension we find

$$j_{\mathrm{N}} - \lambda_{Q^*}^2 \frac{\mathrm{d}^2 j_{\mathrm{N}}}{\mathrm{d}x^2} = L_{\mathrm{T}}\left(-\frac{\mathrm{d}T}{\mathrm{d}x}\right) \tag{8.3}$$

and

$$Q^* - \lambda_{Q^*}^2 \frac{\mathrm{d}^2 Q^*}{\mathrm{d}x^2} = \tau_{Q^*} L_{\mathrm{T}} \frac{\mathrm{d}^2 T}{\mathrm{d}x^2} \tag{8.4}$$

For the case $\mathrm{d}^2T/\mathrm{d}x^2 = 0$, using the constraint $j_{\mathrm{N}}(0) = 0$ we can solve eqs. (8.3) and (8.4) to find

$$Q^*(x) = 2N(0)e^2\lambda_{Q^*}S\left(\frac{\mathrm{d}T}{\mathrm{d}x}\right)\exp\left(-\frac{x}{\lambda_{Q^*}}\right) \tag{8.5}$$

and

$$j_{\mathrm{N}}(x) = L_{\mathrm{T}}\left(\frac{-\mathrm{d}T}{\mathrm{d}x}\right)\left[1-\exp\left(\frac{-x}{\lambda_{Q^*}}\right)\right] \tag{8.6}$$

where $S \equiv L_{\mathrm{T}}/\sigma$ is the thermopower in the superconducting state. Figure 22 sketches j_N, j_S and Q^* versus x. From eq. (8.5), we see that the voltage at the NS interface due to charge imbalance is

$$\frac{Q^*(0)}{2N(0)e^2} = \frac{\lambda_{Q^*}S\ \mathrm{d}T}{\mathrm{d}x}$$

These effects may be investigated experimentally by measuring the potential difference across a SNS' sandwich in the presence of a heat current (we assume

that the normal layer is thick enough to exclude Josephson tunneling). The excess voltages due to the charge imbalance at the NS interface are $-i_{Q^*}SP/\ A\kappa$ and $-\lambda'_{Q^*}S'P/A\kappa'$, where $P = A\kappa(-\mathrm{d}T/\mathrm{d}x) = A\kappa'(-\mathrm{d}T/\mathrm{d}x)'$ is the heat current, κ and κ' are the thermal conductivities of S and S', and A is the cross sectional area. Thus, the total voltage drop across a SNS' sandwich is

$$V = -\left(\frac{d_{\mathrm{N}}S_{\mathrm{N}}}{A\kappa_{\mathrm{N}}} + \frac{\lambda_{Q^*}S}{A\kappa} + \frac{\lambda'_{Q^*}S'}{A\kappa'}\right)P \tag{8.7}$$

where the first term is just the contribution of the normal layer of thickness d_N and thermal conductivity κ_{N}.

Van Harlingen (1981) measured these effects in $\mathrm{Pb}-\mathrm{Cu}-\mathrm{PbBi}$ and $\mathrm{In}-\mathrm{Al}-\mathrm{Sn}$ sandwiches. The sample was mounted in a vacuum can and the voltage generated across the two superconductors (at regions far from the interfaces) in the presence of a known heat current was measured with a null-balancing SQUID voltmeter. Figure 23a shows V/P versus T for a $\mathrm{Pb}-\mathrm{Cu}-\mathrm{PbBi}$ sample. Near the transition temperature, T_c, of the Pb there is a divergence in V/P that arises from the rapid increase in λ_{Q^*} in $\mathrm{Pb}: \lambda_{Q^*}(T) = \lambda_{Q^*}(0)(1-t)^{-1/4}$. The transition temperature of the PbBi was considerably higher than that of the Pb , so that the voltage produced by the charge imbalance in the PbBi varied relatively slowly with temperature below 7.2 K . The dip in fig. 23a is characteristic of the thermopower of Cu , and arises from the Kondo effect in the presence of magnetic impurities. The solid line is a fit to the data well below T_{c}, extrapolated to T_{c}. The difference between this line and the data near T_{c} represents the voltage, V_{s}, due to the charge imbalance in the Pb , and is plotted versus $(1-t)^{-1/4}$ in fig. 23b. We see that near $T_{\mathrm{c}}V_{\mathrm{c}}/P$ is proportional to $(1-t)^{-1/4}$, as expected. Van Harlingen estimated S from the slope of this line, $-\lambda_{Q^*}(0)S/A\kappa$, using a value for κ obtained from the measured electrical conductivity and the Wiedemann-Franz law, and the value $\lambda_{Q^*}(0) = 2.7\mu$ m

obtained from the measured electrical resistance of the SNS' junction. His value of $S = -7.8\times10^{-7}\mathrm{VK}^{-1}$ near T_{c} compares with the value of $-2.2\times\ 10^{-7}\mathrm{VK}^{-1}$ obtained by Christian et al. (1958) on Pb in the normal state. Given the strong dependence of S on the impurity content of the material, this discrepancy is by no means unreasonable; unfortunately, it was not possible to measure S independently in the material used in the experiment.

Van Harlingen found comparable results on $\mathrm{In}-\mathrm{Al}-\mathrm{Sn}$ sandwiches near the In transition temperature. Subsequently, Battersby and Waldram (1984) studied similar effects in $\mathrm{Pb}-\mathrm{Cu}-$

Pb and Pb − Cu − PbBi sandwiches, and obtained excellent agreement between the value of the thermopower in Pb and that measured directly on a bulk sample prepared in a similar way.

14.8.2 8.2. Spatial dependence of charge imbalance induced by a temperature gradient near a superconducting boundary

Mamin et al. (1983, 1984) performed experiments designed to measure the spatial decay of the charge imbalance [eq. (8.5)] near the end of an Al film in the presence of a temperature gradient. Their sample configuration is shown in fig. 24. The Al film, deposited on a glass substrate, was 500μ m wide and typically 300 nm thick. A series of probes was fabricated on top of the Al film with a photolithographic lift-off procedure. Each probe consisted of 800 nm of Cu(3wt%Al) followed by about 5 nm of Fe and 200 nm of Pb(5wt%In). The Fe layer prevented Josephson tunneling between the Al and the PbIn. Near the end of the Al film, the probes were 2μ m wide with a 6μ m separation between centers. The voltage developed across each junction was measured with a null-balancing SQUID voltmeter relative to a wide probe far from the end of the film; the voltmeter was connected to each probe in turn by means of a mechanical superconducting switch operated from outside the cryostat. The normal state thermopower was measured in another part of the Al film, again by means of the SQUID voltmeter. The substrate was mounted in a vacuum can, and a heater and thermometers were attached to allow a known temperature gradient to be established.

The value of $\lambda_{Q^*}(T)$ was determined by injecting current through one probe

and measuring the voltage at nearby probes. In all cases, the observed voltage was accurately exponential over as much as five decades: a representative example is shown in fig. 25. The measured value of $\lambda_{Q^*}(T)$ is plotted versus $(1 - T/T_c)$ in fig. 26: The slope is -0.22 ± 0.03. The value of $\tau_{Q^*} = 2N(0)\ e^2\lambda^2_{Q^*}/\sigma$ estimated from the measured values of λ_{Q^*} and σ and with $N(0) = 1.74 \times 10^{28}\mathrm{cV}^{-1}\ \mathrm{m}^{-1}$ (Gschneidner 1964) yields $\tau_E = 1.6 \pm 0.2$ ns, assuming that only electron- phonon scattering contributes to the charge relaxation near T_c as is implied by the fact that $\lambda_{Q^*} \propto (1 - T/T_c)^{-14}$. Two other samples yielded $\tau_E = 2.7 \pm 0.5$ ns and 2.3 ± 0.4 ns. The average value of τ_E, about 2 ns , is about a factor of 6 smaller than that obtained by Chi and Clarke (section 4). All three samples were sufficiently clean that charge relaxation due to electron-electron scattering should have been quite negligible. To eliminate the possibility that the Al films in the decay measurements differed in some way from those used in the CC experiments. Mamin et al. fabricated two samples in which the Al was deposited simultaneously, one in the configuration of fig. 24 and one in the configuration of fig. 5. The inferred values of τ_E were about 2 and 11 ns , respectively, in agreement with previous results. We note that the value of τ_E

obtained from the decay measurements is only about a factor of two smaller than that obtained by Stuivinga et al. (1981, 1983*a*) from measurements on phase-slip centers in Al (section 7). At the time of writing, there is no explanation for the discrepancy in the values of τ_E observed in the tunnel injection and spatial decay measurements. However, we emphasize that this discrepancy concerning τ_E does not enter into the discussion of thermoelectric effects, for which only the measured value of $\lambda_{Q^*}(T)$ is required.

We now turn to a discussion of the charge imbalance generated by a temperature gradient. Figure 27 shows $V(x)$ versus distance for a sample at four different temperatures. In contrast to the behavior observed for the current injection experiments, the data show significant downward curvature near the end of the Al film. A straight-line fit to the data points farthest from the end of the Al film yields a decay length of $24 \pm 4\mu$ m that is independent of temperature, and always longer than the temperature-dependent length measured in the current injection case. Thus, one concludes that the charge imbalance decay length measured in the thermoelectric experiment is not equal to λ_{Q^*}, presumably because the temperature gradient is non-uniform

over a region near the end of the Al film where the heat flow enters the film from the substrate. In a quasi-one-dimensional model, it is easy to show that the gradient is given by

$$\frac{\mathrm{d}T}{\mathrm{d}x} = \left.\frac{\mathrm{d}T}{\mathrm{d}x}\right|_{\infty} \left[1 - \exp\left(-\frac{x}{\lambda_{\mathrm{T}}}\right)\right], \tag{8.8}$$

where $\mathrm{d}T/\,\mathrm{d}x|_{\infty}$ is the gradient far from the end of the film and $\lambda_{\mathrm{T}} = (yd/y_{\mathrm{K}})^{1/2}$. Here, g and d are the thermal conductivity and thickness of the Al film, and y_k is the Kapitza resistance of a unit area between the film and substrate. If we assume $d = 300$ nm, $g = 6\mathrm{Wm}^{-1}\ \mathrm{K}^{-1}$, and $y_{\mathrm{K}} = 5 \times 10^{3}\mathrm{Wm}^{-2}\ \mathrm{K}^{-1}$ at T_{c} (Kaplan 1979), we find $\lambda_{\mathrm{T}} \approx 20\mu$ m. When eq. (8.8) is inserted in eqs. (8.3) and

(8.4), one finds

$$V(x) = \frac{i_{Q^*}^2}{i_{Q^*}^2 - i_T^2} \left(i_{Q^*} \mathrm{e}^{-x/i_{Q^*} - i_T \mathrm{e}^{-x/i_T}}\right) S \left.\frac{\mathrm{d}T}{\mathrm{d}x}\right|_x. \tag{8.9}$$

Figure 27 shows the fit of the data to eq. (8.9) using values of $i_{2,2}(T)$ from the current injection experiments, and regarding S and i_1 as adjustable parameters. The fits are generally satisfactory. The inferred value of S near T_c was $(-2.7 \pm ().6)/10$ " VK ^{1}, compared with a value measured in the normal state of $1-1.(15-10.(16), 10^{3}$ VK ^{1}. Two other samples yielded values of $(-1.4 \pm 0.3) \times 10^{-8}\mathrm{VK}^{-1}$ and $(-1.0 \pm 0.3) \times 10^{-8}\mathrm{VK}^{-1}$ compared with normal state values of $(-().94 \pm (0.(0), 10, 1)^{-8}$ VK ^{1} and $(-1.12 \pm 0.(06),$ 10 "VK 1: respectively. ()verall, the experiments provide a strong experimental verification of the theory of thermoelectric effects in superconductors. and. In particular, demonstrate that there is no discontinuity in the value of L_{T} at T_{c}.

14.8.3 8.3. Supercurrent-induced charge imbalance in the presence of a temperature gradient

A quite different kind of effect due to a temperature gradient was first pointed out by Pethick and Smith (1979b) who predicted that a charge imbalance proportionai to $\boldsymbol{I} \cdot \nabla T$ should exist in the presence of a supercurrent $\boldsymbol{I}$. Clarke ct al. (1979b) observed this effect in Sn films, and established that the measured voltage was proportional to $\boldsymbol{I} \cdot \nabla T$, as predicted. but was two to three orders of magnitude smaller than the predicted value. This discrepancy arose because the theory assumed that the elastic scattering rate was negligible compared with the inclastic rate, whereas the reverse was true in the experiment. Three further theories then appeared (Schmid and Schön 1979. Clarke and Tinkham 198(), Beyer Nielsen et al. 198() in attempts to account quantitatively for the temperature dependence and magnitude of the data. More recently. Heidel and Garland (1981) soberved similar effects in Al films, while Fjordboge et al. (1981) have given a more detailed account of their work on Sn .

The experimental configuration used by Fjordhoge et al. is shown in fig. 28. The Sn for $\mathrm{Sn} - 3\mathrm{ut}''$, InI film was typically $3(x)$nm thick and 0.1 mm wide in the narrow region. After the Sn was oxidized. three Cu $\left(+3'''^{,\mathrm{Al}}\right)$ disks $\sim 1\mu$ m thick were deposited. followed by three Ph strips. In a given experiment. one of the three $\mathrm{Sn}\,\mathrm{Sn}()x$ (u tunnel junctions was used to measure the quasiparticle potential relative to the pair potential with a SQUID voltmeter. The substrate was mounted in a vacuum can. with a heater at each end. and thermometers were attached to the reverse side. In figs. 29 and 3() we plot measured values of V versus I for five values of ∇T. and V versus ∇T for 10 values of I for a representative sample. The voltage is clearly proportional to $I \cdot \nabla T$. Figure 31 shows $Vy.$, (f) $I\nabla T$ versus t for the same sample: to within the experimental

resolution, all 8 samples showed the same behavior. In fig. 32, we plot $Vg_{\mathrm{NS}}\,(0)\ T/I\nabla T$ versus $(\ 1-t\ )$ for the same sample; the divergence at temperatures above about $0.8T_{\mathrm{c}}$ is close

to $(1-t)^{-1}$. It was found that the magnitude of the quantity $Vg_{\rm NS}(0)T(1-t)A/I\nabla T$, where A is the cross-sectional area of the films,

was very nearly the same for relatively clean Sn films in which the mean free path was limited by boundary scattering, and for SnIn films in which the mean free path was limited by impurity scattering to about 60 nm .

Figure 33 indicates the physical origin of the effect. In fig. 33a there is a thermal gradient, but no applied supercurrent. Quasiparticles moving from the left are at an effective temperature $T-\delta T$, while those moving from the right are at $T+\delta T$, where T is the local temperature. Thus, there is an imbalance in the populations of the $k > k_{\rm F}$ and $k < k_{\rm F}$ branches on the right-hand side of the Fermi surface, but an equal and opposite imbalance on the left-hand side: as a result, $Q^* = 0$. If we now impose a superfluid velocity v_S (fig. 33b) the excitation energies are raised and lowered on opposite sides of the Fermi surface by an amount $p_k \cdot v_s$ (see section 5.2). The induced asymmetry ensures that the population imbalances on opposite sides of the Fermi surface no longer cancel, and the resulting charge imbalance is the origin of the observed voltage. We now briefly review the theoretical situation.

The result of Schmid and Schön (1979) can be written in the form

$$V = \frac{p_{\rm F} l}{6 e g_{\rm NS}(0)} \frac{v_{\rm s} \cdot \nabla T}{T} \frac{\Delta}{k_{\rm B} T (1-Z) \cosh^2 (\Delta / 2 k_{\rm B} T)} \ln (8 \Delta \tau_{\rm E} / \hbar) \,. \tag{8.10}$$

Here, $p_{\rm F}$ is the Fermi momentum, and Z is given by eq. (2.24). Clarke and Tinkham (1980) used a simple kinetic approach to obtain

$$V = \frac{p_{\rm F} l}{6 e g_{\rm NS}(0)} \frac{v_{\rm s} \cdot \nabla T}{T} \frac{\Delta}{k_{\rm B} T (1-Z) \cosh^2 (\Delta / 2 k_{\rm B} T)} . \tag{8.11}$$

Equation (8.10) exceeds eq. (8.11) by a factor of $\ln (8 \Delta \tau_E / \hbar)$, which varies relatively slowly with temperature over the experimental range studied, with an average value of about 6. Apart from this factor, the Schmid-Schön and Clarke-Tinkham approaches yield the same result. One can convert $v_{\rm s}$ into a current density by writing

$$v_{\rm s} = j_{\rm s} / n_{\rm s} e = \mu_0 j_{\rm s} \lambda^2 (T) e / m$$

and using the result $i^2(T) = i_L^2(0) \left(1 + \check{\zeta}_0, l\right) (1-t^4)^{-1}$ (Tinkham 1975) to find

$$c_{\rm s} = \frac{\mu_0 j_{\rm c} e i_1^2(0) \left(1 + \check{\zeta}_0 / l\right)}{m (1-t^4)} . \tag{8.12}$$

Near $T_{\rm c}, 1 - Z \to \pi \Delta k_{\rm B} T, \cosh^2 (\Delta, 2 k_{\rm B} T) \to 1.$ and $1 - t^4 \to 4(1-t)$, so that the

temperature dependence of the voltage at fixed current is dominated by the temperature dependence of $v_s, (1-t)^{-1}$, in good agreement with the experimental results. The curves calculated for the two theories with $v_{\rm F} = 6.5 \times 10^5$ ms^{-1}, $\lambda_{\rm L}(0) = 5 \times 10^{-8}$ m, and $\xi_0 = 2.3 \times 10^{-7}$ m are plotted in fig. 32. The curves were fitted at $T/T_{\rm c} = 0.99$ by multiplying eq. (8.11) by 2.4 , and eq. (8.10) by 0.4 . A detailed critique of these two theories can be found in the paper by Pethick and Smith (1981b).

Beyer Nielsen et al. (1980) and, subsequently, Pethick and Smith (1981a, b) have solved the Boltzmann equation in the clean limit for the case where $\tau_{\rm E}^{-1} \to 0$ and for an isotropic energy gap to obtain

$$V = \frac{p_{\rm F} l}{e g_{\rm NS}(0)} \frac{v_{\rm s} \cdot \nabla T}{T} \left[\frac{1.93 \Delta / k_{\rm B} T}{\cosh^2 (\Delta / 2 k_{\rm B} T)} + \frac{8/15}{\exp (\Delta / k_{\rm B} T) + 1} \right] . \tag{8.13}$$

Equation (8.13) is also plotted in fig. 32, and evidently has a different temperature dependence than the experimental data. In eq. (8.13), the first term in square brackets dominates

the second for $T/T_c \leqslant 0.998$, that is, throughout the experimentally realizable range. The first term arises from quasiparticles in the energy range $\Delta - p_F v_s$ to $\Delta + p_F v_s$, in which the available phase space for charge relaxation via elastic scattering is reduced. This effect is particularly pronounced for quasiparticles with energies near $\Delta - p_F v_s$. As a result, the charge imbalance in this "pocket" takes a relatively long time to relax compared with that at energies above $A + p_F v_s$, which is accounted for by
the second term in square brackets in eq. (8.13). However, it appears that, in practice, the energy levels in the pocket are sufficiently smeared out that the calculated enhancement of the relaxation time is not very significant. There are at least three mechanisms by which this smearing may occur: inelastic scattering, gap anisotropy, and impurity scattering (Schön 1981a, 1981b, Beyer Nielsen et al. 1982). When the contribution of the pocket is eliminated, the second term in square brackets becomes dominant but, unfortunately, is valid only very close to T_c. Beyer Nielsen et al. (1982) have used a Green's function approach to calculate the voltage in the dirty limit in the presence of electronphonon scattering, and find

$$V = \frac{2p_F l}{3e g_{NS}(0)} \frac{v_s \cdot \nabla T}{T} \frac{F(\Delta/k_B T)}{1+\lambda}, \tag{8.14}$$

where λ is the electron-phonon interaction parameter, and F is a specified dimensionless function. Near T_c, eq. (8.14) agrees with the Schmid-Schön result, eq. (8.10). Figure 34 shows eq. (8.14) plotted versus T/T_c together with the data obtained by Fjordbge et al. (1981) for their dirtiest sample. The theoretical curve has been fitted at one temperature by scaling with a factor of 0.43 . Given that effects of anisotropy are not included in the theory, the fit is satisfactory.

As noted above, Heidel and Garland (1981) measured similar effects in Al.

The spread in their values of $V g_{NS} T/I \cdot \nabla T$ from sample to sample was an order of magnitude, substantially greater than for the work on Sn . This variation perhaps reflects variations in the homogeneity of the Al films. The temperature dependence of the data fitted the SS and CT theories (eqs. 8.10 and 8.11), but not the prediction of eq. (8.13), which, of course, is valid only in the clean limit, while the samples were definitely in the dirty limit. Heidel and Garland also examined two samples with 520 and 1660 ppm Er, respectively, and found no significant difference in the magnitude of the effect compared with the samples with no magnetic impurities. This result is consistent with the idea (Clarke and Tinkham 1980) that the charge imbalance generation is a volume process in which the generation and relaxation processes cannot be independently varied. Thus, the value of Q^* is imposed by the temperature gradient, the magnitude depending only on the transport mean free path which limits the distance over which the gradient is effective in producing a nonequilibrium population. Thus, times such as τ_E and τ_{Q^*} play very little role in determining the magnitude of Q^*. This situation is in complete contrast to the other charge imbalance experiments described earlier, such as tunnel injection, the NS interface, phase-slip centers or generation by a temperature gradient in the absence of an applied supercurrent, where the generation occurs at a welldefined spatial homogeneity, and the generation and relaxation of Q^* are quite distinct processes. Thus, as we have seen in section 5.1, the effect of a small amount of Er in Al dramatically lowers Q^* in tunnel injection experiments.

14.9 9. Dynamical charge imbalance

All of the experiments and the associated theories described above are concerned with a steady state situation, in which the charge imbalance is maintained at a constant value by a suitable generation process. However, it is appropriate to remark briefly on dynamical charge imbalance effects where, for example, one considers the time decay of a pulse of charge

imbalance. Under such circumstances, Kadin et al. (1980) show that the appropriate decay rate is τ_{E}^{-1}, rather than $\tau_{Q^*}^{-1}$. The physical reason for the difference is as follows. In a steady state measurement, the charge imbalance relaxes by means of changes in the distribution function alone, the charge, q_k, associated with a given k value remaining fixed. This leads to the well-established result $\tau_{Q^*}^{-1} = (\pi\Delta/4k_{\mathrm{B}}T)\,\tau_{\mathrm{E}}^{-1}$. On the other hand, when a pulse of charge imbalance decays with time, in addition to the relaxation of the distribution there is an accompanying change in q_h as the nonequilibrium value of μ_s decays towards its equilibrium value. Kadin et al. show that in the limit $\Delta(T)/k_{\mathrm{B}}T \ll 1$, this additional process modifies the charge imbalance relaxation rate to τ_{E}^{-1}.

Kadin et al. show that, in general, Q^* should obey a charge imbalance relaxation equation

$$D\tau_{Q^*}\nabla^2 Q^* = \tau_0\tau_E\ddot{Q}^* + (\tau_0 + \tau_E)\,\dot{Q}^* + Q^* \tag{9.1}$$

where $\tau_0 = \tau_1(n, n_1)$ is the response time of the supercurrent to a change in the total current (n and n, are the densities of electrons and superfluid electrons in the normal and superconducting states). In the low frequency limit, eq. (9.1) immediately yields the static decay length ($D\tau_{Q^*})^{1/2}$ (eq. 6.1). However, in general, eq. (9.1) describes damped, dispersive charge imbalance waves with the dispersion relation

$$-\Lambda^2 k^2 = (1 + i\omega\tau_0)\,(1 + i\omega\tau_E)\,, \tag{9.2}$$

where A is a characteristic length, for waves of the form exp[i($\omega t - k \cdot r$)].
One might expect charge imbalance waves to be generated by PSCs, so that the Josephson oscillations of two neighboring PSCs could be locked together by this mechanism, resulting in voltage locking. As mentioned in section 7, such effects have been observed, and although the evidence is perhaps not overwhelming, it seems very plausible that charge imbalance waves are responsible for this interaction.

The concept of dynamical charge imbalance also occurs in a quite different situation, namely charge imbalance fluctuations (Lemberger 1981). Whenever a charge imbalance is generated, there is an associated electrical resistance: it is, of course, this resistance that is measured directly in the measurements on the NS interface described in section 6. Lemberger (1981) has pointed out that in thermal equilibrium there must be fluctuations in Q^* related to this resistance via Nyquist's theorem (Nyquist 1928). We briefly describe this analysis.

Lemberger calculates the mean square fluctuation $\left\langle(\delta\mu_\varsigma)^2\right\rangle$ in the limit $A(T)/k_{\mathrm{B}}T \ll 1$, neglecting gradients in $\delta\mu_\varsigma$. Thus, the result can be applied only to situations in which $\delta\mu_s$ is spatially uniform, for example, charge imbalance injected into a superconducting film of thickness $^{\ll i}{}_{,Q^*}$ via a tunnel barrier of area $\geqslant i_{2^*}^2$. By combining the theory of charge imbalance with equilibrium thermodynamics, he obtains the result that in thermal equilibrium (no applied current)

$$\left\langle(\delta\mu_{\mathrm{s}})^2\right\rangle = 2\,(k_{\mathrm{B}}T)^2\,/\pi N(0)\Omega\Delta(T), \quad [\Delta(T) \ll k_{\mathrm{B}}T]\,. \tag{9.3}$$

For tunneling injection into a superconductor, the resistance $R_{Q^*} = V_{\mathrm{d}}I_{\mathrm{i}}$ in the limit $\Delta(T), k_{\mathrm{B}}T \ll 1$ is easily obtained from eq. (2.22) with $F^* = 1, y_{\mathrm{ss}}(0) = 1$ and $\tau_{Q^*} = 4k_{\mathrm{B}}T\tau_{\mathrm{E}}/\pi\Delta(T)$:

$$R_{Q^*} = 4k_{\mathrm{B}}T\tau_{\mathrm{E}}/2\pi N(0)e^2\Omega\Delta(T) \tag{9.4}$$

This resistance is in series with the tunneling resistance of the barrier. It was observed by Clarke and Paterson (1974) and Lemberger and Clarke (1981a) as a dip in the conductance of the detector junctions near T_{c}, and measured in detail by Lemberger (1981).

To apply the Niquist result, one assumes that the RC time constant of the injection junction is much less than E_t, that the resistance of the injection junction is large compared with $R_{e'*}$. and that σ_0 is small compared with τ_E. Under these conditions, the Nyquist theorem yields

$$\left\langle (\delta\mu_{\mathrm{s}} e)^2 \right\rangle = 4k_{\mathrm{B}} T R_{Q^*} B. \tag{9.5}$$

where B is the bandwidth for the fluctuations. Substituting cys. (9.3) and (9. 4) in eq. (9.5), one tinds $B = 1 + \tau_2$. Thus, the relaxation time for eharge imbalance fluetuations. as for other dynamical charge imbalance relaxation processes is τ_{E}

Apart from the witage locking of neighboring PSCs, there appears to be no experimental work on dynamical charge imbalance processes. This is obviously an area in which more research is needed.

14.10 10. Concluding summary

In this chapter. We have resiewed the essential deas of charge imbalance in superconductors, and discussed the various physical situations in which charge imbalance plays a role. We first considered the situation in which charge imbalance is injected via a tunnel junction at a rate $Y^* = F^* l$, x^2 and then relaxes in one or more of seleral possible ways to produce a steady state voltage $I = ()^*2$ Ville'ks. (t) that is measured by a tunneling contact to a normal metal. Such measurements yeld the charge imbalance relatation rate. ... In the absence of gap anisotropt or magnetic scattering and the the limit $11T \wedge_B T \to 0$, the charge relatation is due solely to electron-phonon processes and occurs at a rate $|F^* - |^*| = 1 - 1|T|$ the V^* : meglecting electron electron scattering for the moment).

Under appropriate conditions. elastic scattering also relates charge imbalance. In the presence of nomero sap ansofropy the coherence factor mu-a be for branch crossing is no longer zero and clastic scattering produces charge relaxation at a rate that scales approximately as $A^+(T)$ near $T_{\cdot}$ This effect has been observed m both Sn and Al . The mean free path in the Al films us as reduced by sugen depenge a provess that also enhanced $l_{\cdot\cdot}$in some cases substantally. The films with significantly enhanced transition temperatures exhboted much faster inclaster relaxation rates than could be explaned me merms of electron phonon scatterng: tecent work has explained these rates rather satustactorily an terms of electron electron scattering. The presence of magnetic mpurtase can greatly enhance - : hecause the coherence factor for branch crossing late + :!^{2} approaches units at low energies. Expermental data abtamed on Al. doped what Fr. are meacellent agreement with the Schmid Schön prediction $(F^* \tau_{e'*}^{-1}) = [\pi \Delta(T)/4k_{\mathrm{B}} T_c \tau_{\mathrm{i}}][(1 + 2\tau_{\mathrm{i}}/\tau_{\mathrm{s}})^{1/2}$ over a wherenge of balues of $a_i a_i$ for $1h_k I_i \leqslant$ 0.8. Charge relaxation can
also be induced by a supercurrent: the current induces an asymmetry across the Fermi surface that allows branch relaxation via elastic scattering. The results from experiments on dirty Al are again in excellent agreement with the Schmid-Schön result. However, computer solutions of the Boltzmann equation in the last two cases produced results that were strikingly different from the experimental data. It now seems probable that electron-electron scattering was non-negligible in all of these samples, and it is possible that the inclusion of this process in the Boltzmann equation would remove the discrepancy.

The next three sections were concerned with various experiments in which charge imbalance plays a central role. The resistance of the NS interface near T_{c} can be explained in terms of charge imbalance injected into the superconductor where it decays with a characteristic length λ_{Q^*}. A simple modification of the tunneling theory for the injection of Q^* yields a result that is in excellent agreement with experiments on Pb, Sn, and In , and that produces very reasonable values of τ_{E}. The voltage steps and dynamic resistance of the $I-V$ characteristics of microstrips containing phase slip centers is nicely explained in terms of the charge imbalance injected from

the normal core of each PSC into the neighboring superconducting regions. The interaction of nearby PSCs at zero voltage can also be explained in terms of this static model, but the frequency locking that occurs at nonzero voltages probably involves an interaction via charge imbalance waves.

Three experiments were described in which a temperature gradient was involved. The first involved the measurement of the charge imbalance induced in a superconductor near a normal contact in the presence of a temperature gradient across the NS interface. The second was concerned with measurements of the spatial decay of the charge imbalance near the end of an Al film along which a temperature gradient was maintained. Both of these experiments involve the thermopower S of the superconductor. In each case, the agreement of theory and experiment was very satisfactory, and the measured values of S were in reasonable accord with measured normal state values. The third experiment involved the charge imbalance generated by a temperature gradient in the presence of an applied supercurrent. The agreement between the results and theoretical predictions is now in a very satisfactory state.

The last section briefly described dynamical charge imbalance effects, in particular charge imbalance waves and charge imbalance fluctuations. This is an area where there seems to be considerable scope for further experimental work.

Values of the electron-phonon scattering rate, τ_{E}^{-1}, have been extracted from experiments on tunnel injection, the NS interface, and PSCs, in which one measures the steady state value of Q^* induced by a known injection rate into a known volume, and also from measurements of i_{Q^*} in which one
measures the spatial decay of Q^* along a superconducting strip. The values of τ_E obtained for each of the metals Pb.Sn, and In are generally consistent and in good agreement with predictions based on x^2F. with an overall spread of perhaps a factor of two in each case. On the other hand, the values of τ_{F} obtained for relatively clean Al films are very puzzling. Measurements from tunneling injection and detection yield about 12ns, a value that is in good agreement with values obtained from magnetoconductance data. This value is 3 or 4 times lower than the calculated value. Furthermore, estimates of τ_F obtained from i_{Q^*} measured near PSCs or near a tunnel injection junction yield values of τ_{F} of 4 and 2 ns. respectively. Although it is now clear that electron-electron scattering can play an important or even dominant role in relatively dirty Al , it is most improbable that it plays a significant role in clean films. Thus, at present, there seems to be no explanation of these very large discrepancies in the values of τ_E.

It is noteworthy that Al was the material used in the measurements of ${\tau_{\ell^*}}^1$ in the presence of magnetic impurities or of a supercurrent. Which are in disagreement with the predictions of the Boltzmann equation. In this case it is possible, but by no means certain. that electron electron scattering may explain the discrepancy. Thus, although Al has been a widely used material in experiments on charge imbalance it is clearly a "bad actor", at least partly because the electron phonon scattering tate is so slow that other charge relaxation mechanisms are of much greater relative importance than they are in Pb, Sn, and In. Obviously, much remains to be done to resolve these issues.

Despite the problems associated with Al. however. experiments on charge imbalance are generally in remarkably good agreement with theoretical predictions, illustrating in a rather strihong way some of the fundamental subtleties of superconductivity, such as quasiparticle charge coherence factors, and a variety of pair breaking mechanisms.

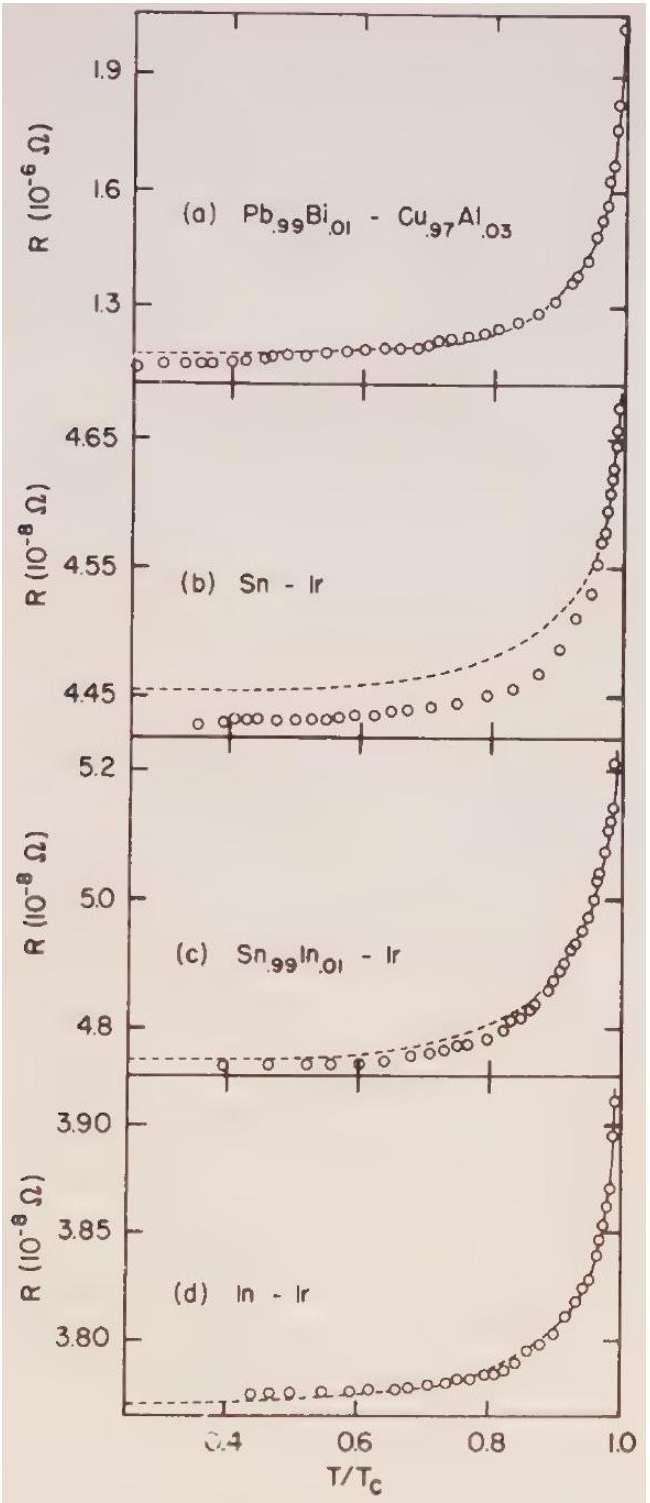


Fig. 15. Circles are the measured total resistance versus $T / T_{\mathrm{c }}$ for the SNS junctions listed in table 3. The solid lines above $0.9T_{\mathrm{c}}$ [$0.96T_{\mathrm{c}}$ in (b)] are the fit to eq. (6.5), while the dashed lines show the extrapolation of the theory to lower temperatures. (Hsiang and Clarke 1980.)}

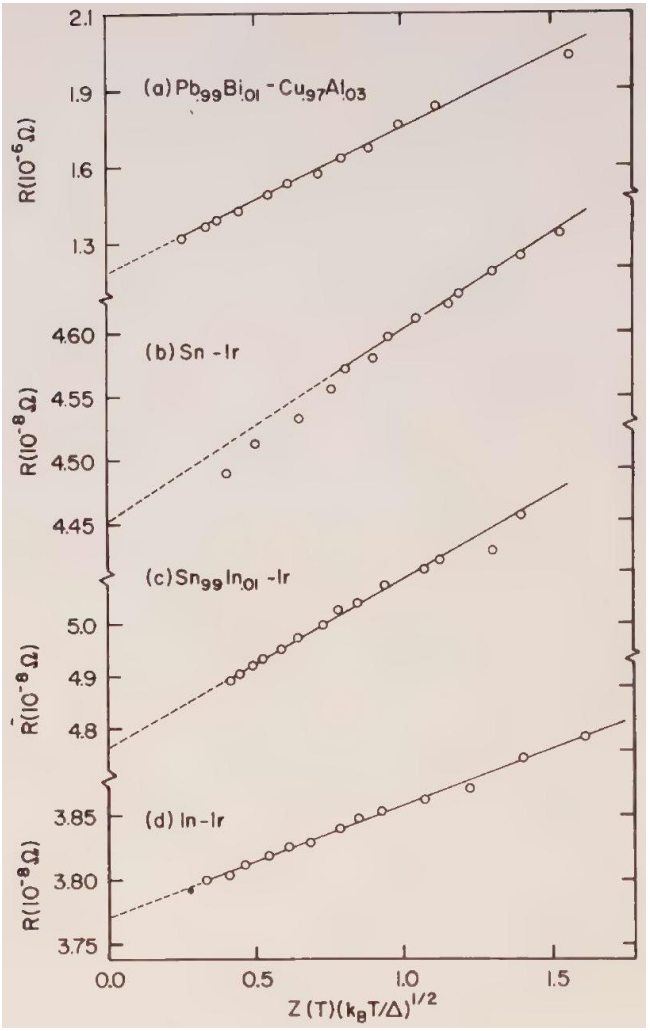


Fig. 16. Total measured resistance versus \$Z(T)\left(k_{\mathrm{B } } T / \Delta\right)^{1 / 2}\$ for the samples shown in fig. 15. The solid lines are a least-squares fit to the data for $T > 0.9T_{\mathrm{c}}$ [$0.96T_{\mathrm{c}}$ for (b)]. (Hsiang and Clarke 1980.)}

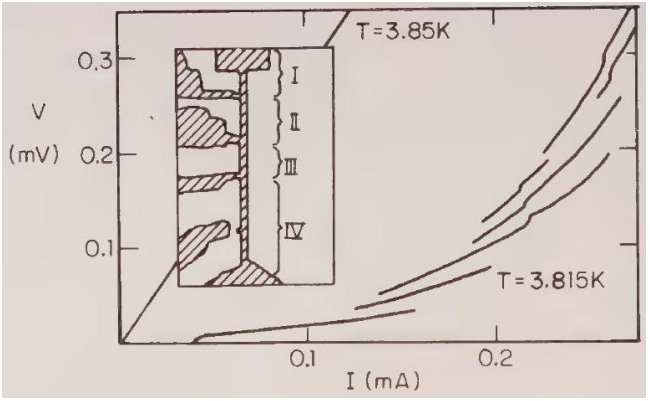


Fig. 17. I versus V for the whole length of the Sn bridge, \$140 \mu \mathrm{~m \$ long, 4μ m wide, and 0.1μ m thick, shown inset. (Skocpol et al. 1974.)}

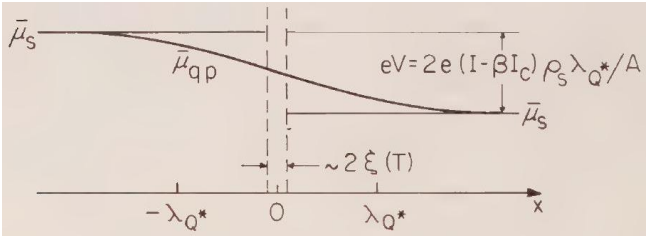


Fig. 18. Schematic representation of phase-slip center.

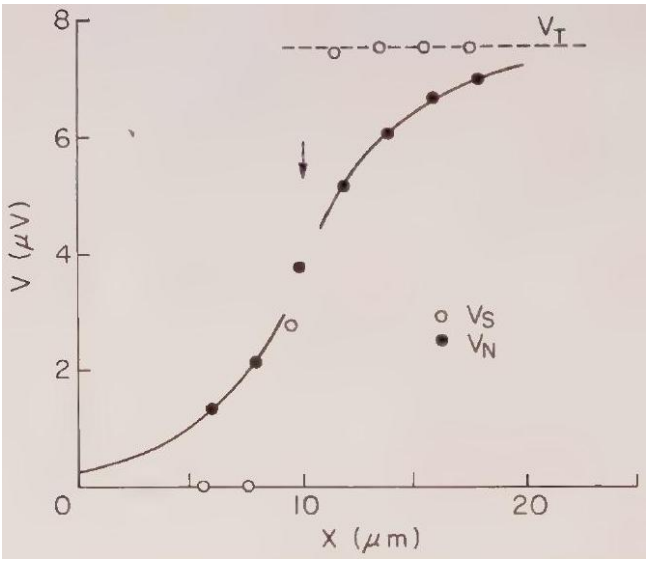


Fig. 19. Spatial variation of $V_{S
$ and V_N across a PSC in a SN microbridge at the position marked with an arrow. (Dolan and Jackel 1977.)}

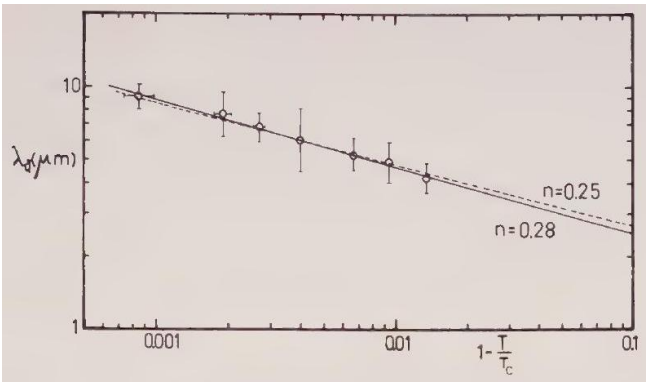


Fig. 20. Temperature dependence of the quasiparticle diffusion length in Sn PSC. The best fit (solid line) for $n = 0.28$ is compared to the expected $\left(1-T / T_{c
\right)^{-1 / 4}$ divergence (dashed line). (Aponte and Tinkham 1983.)}

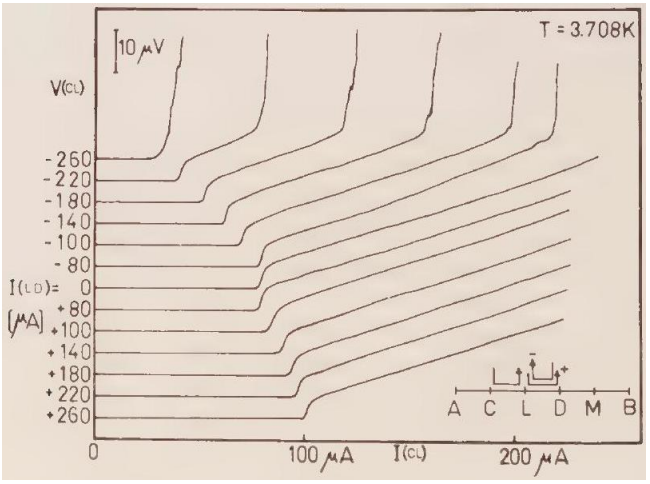


Fig. 21. I V characteristics of segment CL taken for different fixed values of the current through the segment LD. Plus and minus signs correspond to the cases when the currents in the two segments flow in the same or opposite directions, respectively. (Aponte and Tinkham 1983.)

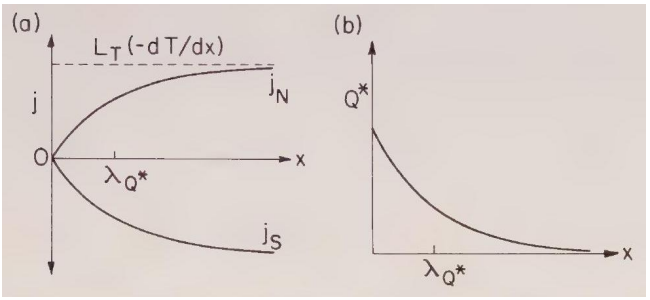


Fig. 22. (a) Normal current ($j_{N $) and supercurrent (j_S), and (b) Q^* versus distance x near the end of a superconductor in the presence of a temperature gradient $\mathrm{d}T/\mathrm{d}x$. (Mamin et al. 1984.)}

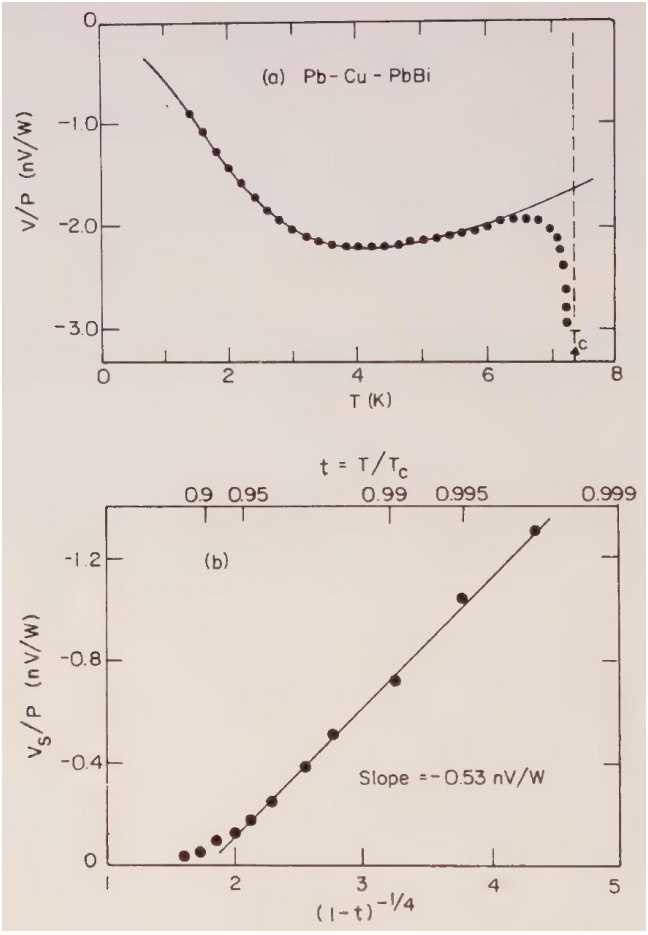


Fig. 23. (a) Plot of the measured thermoelectric voltage per unit power V/P versus T for a $\mathrm{Pb
-$ Cu − PbBi sample. The solid curve is characteristic of the normal thermopower of Cu . (b) Fit of the charge imbalance contribution V_s/P to the temperature dependence of $i_{Q^*}, (1-t)^{-1/4}$. (Van Harlingen 1981.)}

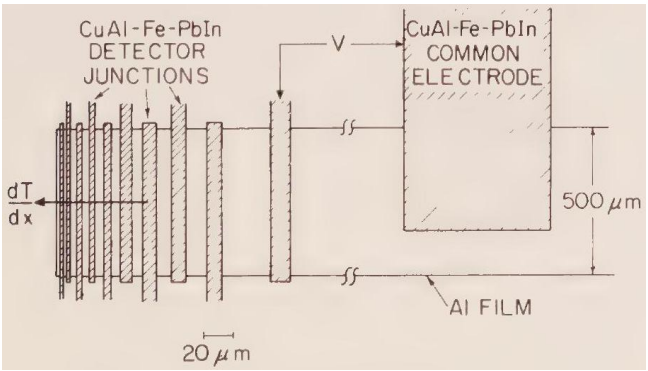


Fig. 24. Sample configuration for measurement of $Q^{*
$ induced by temperature gradient. Note different length scales. (Mamin et al. 1984.)}

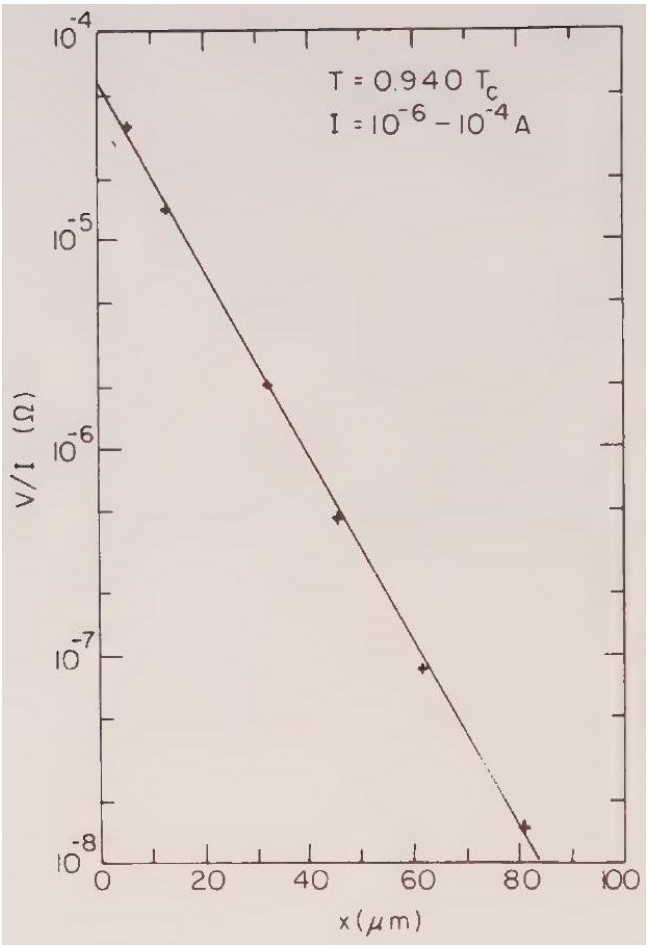


Fig. 25. Measuring $\lambda_{Q^{*
}$ from current injection: voltage, V, normalized to injected current, I, for a series of probes. (Mamin et al. 1984.)}

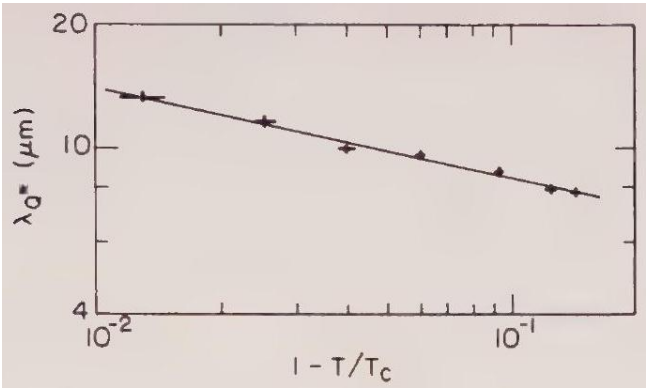
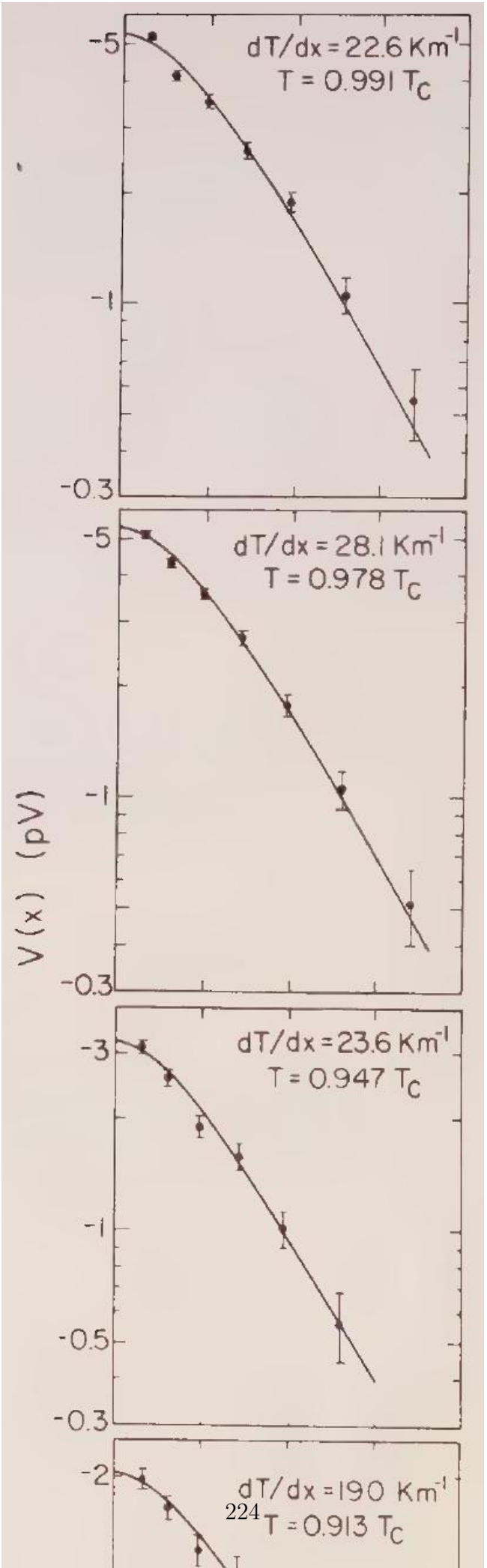


Fig. 26. Temperature dependence of $\lambda_{Q^{*
}$ from current injection: λ_{Q^*} versus $(1 - T/T_c)$. (Mamin et al. 1984.)}


dT/dx = 22.6 Km⁻¹
T = 0.991 Tc
dT/dx = 28.1 Km⁻¹
T = 0.978 Tc
dT/dx = 23.6 Km⁻¹
T = 0.947 Tc
dT/dx = 190 Km⁻¹
T = 0.913 Tc
V(x) (pV)
-5
-1
-0.3
-3
-0.5
-2

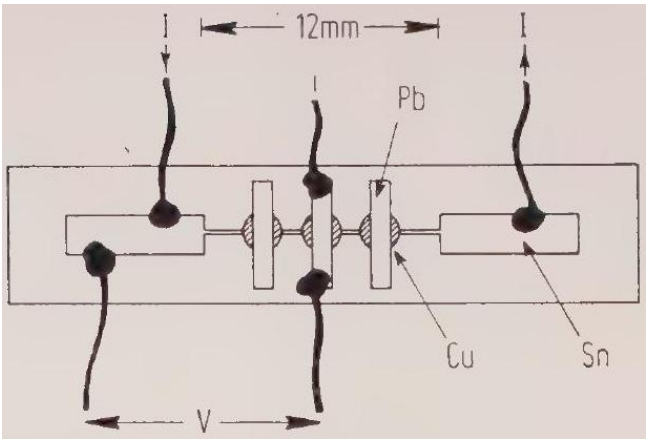


Fig. 28. Sample configuration for $\boldsymbol{I \cdot \nabla T$ experiment. (Fjordbge et al. 1981.)}

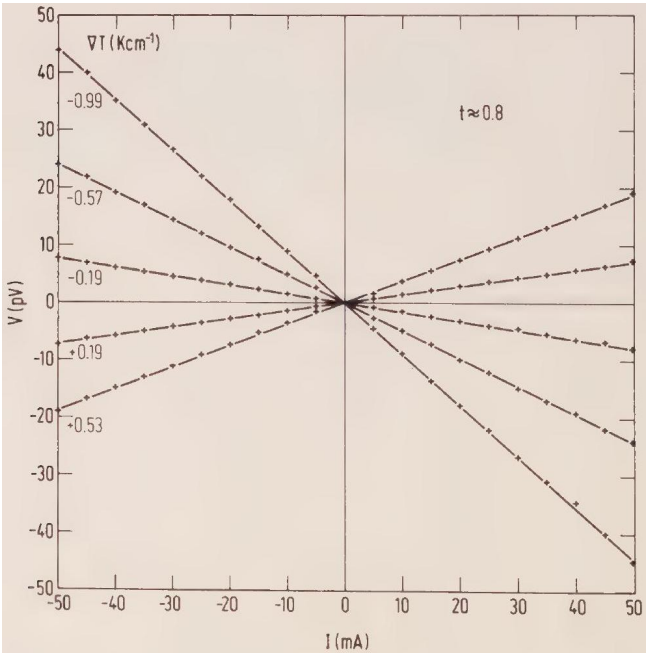


Fig. 29. V versus I for five values of ∇T. (Fjordbge et al. 1981.)

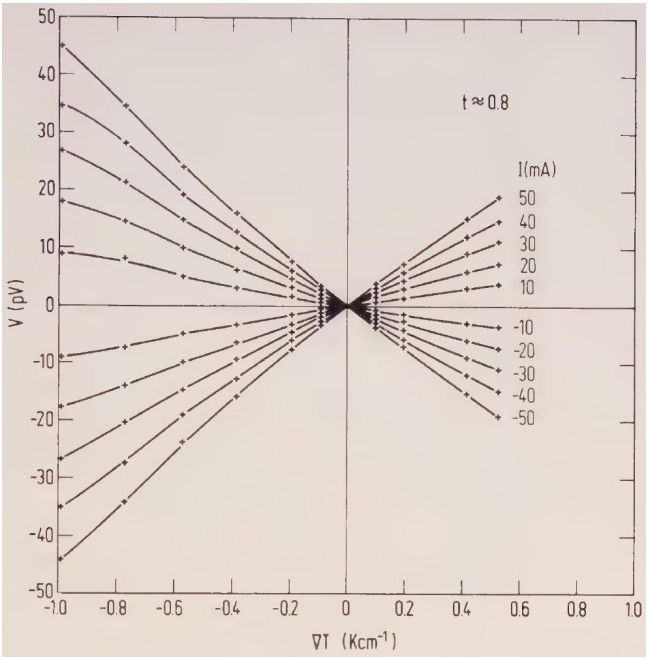


Fig. 30. V versus ∇T for ten values of I. At each value of ∇T, the voltage is defined to be zero at $I = 0$. (Fjordbge et al. 1981.)

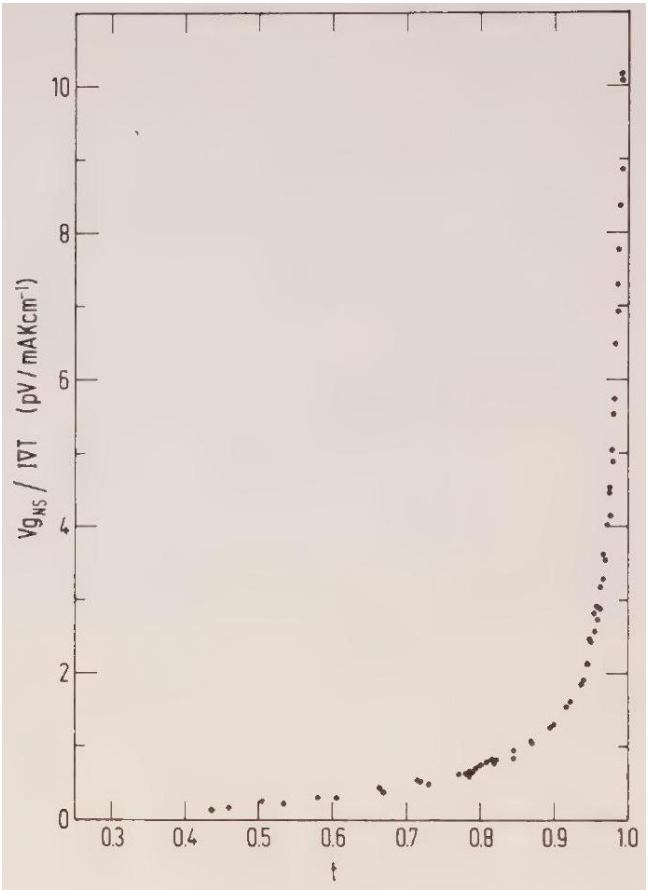


Fig. 31. $V g_{\text {NS
}(0) / I \nabla T$ versus reduced temperature, t. (Fjordbge et al. 1981.)}

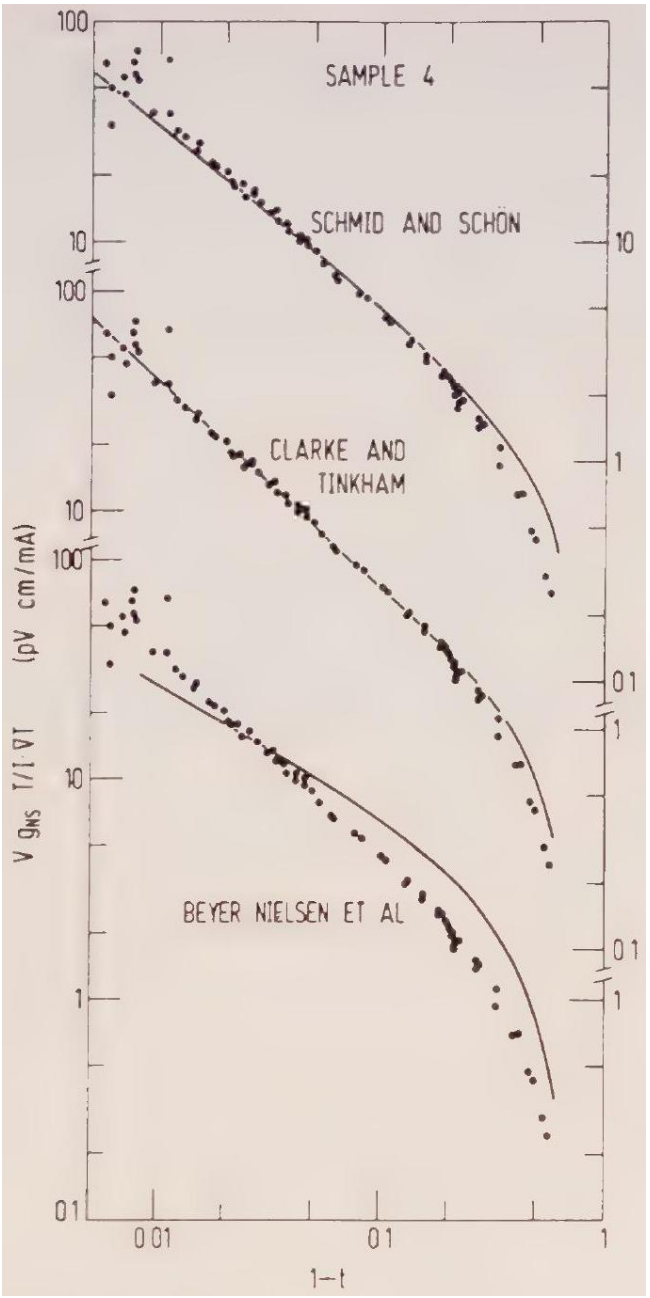


Fig. 32. $V g_{\mathrm{NS }}(0) / I \nabla T$ versus $(1-t)$. The three theoretical formulas have been fitted to the experimental data by scaling them appropriately. (Fjordboge et al. 1981.)

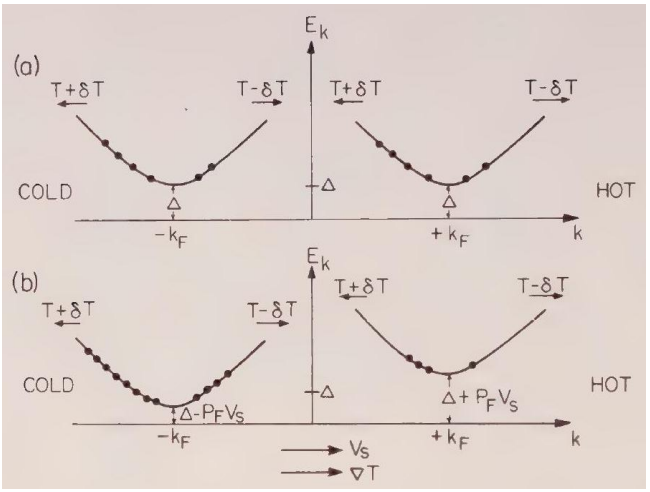


Fig. 33. Schematic representation of quasiparticle excitations in presence of (a) temperature gradient and (b) temperature gradient and applied supercurrent.

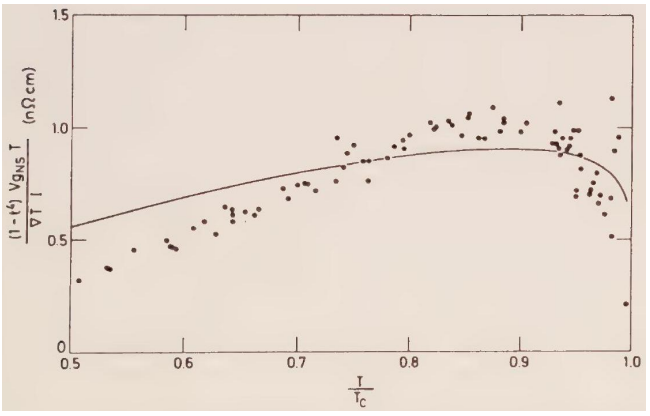


Fig. 34. Comparison of theory of Beyer Nielsen et al. (1982) with data from dirty tin sample of Fjordbge et al. (1981). (Beyer Nielsen et al. 1982.)

15 Nonequilibrium Phenomena in Superconducting Weak Links by Aslamazov, Volkov

15.1 1. Introduction

Soon after the pioneering work of Josephson was published (1962), a microscopic theory for the Josephson phenomenon was constructed for tunneling junctions; the stationary case was considered by Ambegaokar and Baratoff (1963), while a nonstationary theory was developed by Werthamer (1966), and by Larkin and Ovchinnikov (1966) with the help of the Gorkov microscopic equations. Besides in tunnel structures, the Josephson phenomenon was discovered and investigated in a number of other superconducting weakly connected systems (see Likharev's review, 1979, and Barone and Paterno 1981), including the so-called S-c-S junctions with a direct Ohmic contact between two superconductors. The weak link in such systems is due to the geometrical constriction (c) at the point of contact. When a constriction of that kind (a weak link) connects the superconducting films, the so-called bridges are produced (fig. 1a), while in the case of bulk superconductors, one obtains point superconducting contacts (fig. 1b). The $S-c-S$ systems possess a number of practical advantages.

A microscopic theory of the S-c-S systems was long to come into being; some progress was achieved only recently, owing to the development of a general theory of nonequilibrium processes in superconductors (Eliashberg 1971, Gor'kov and Eliashberg 1968, Larkin and Ovchinnikov 1975, 1977,

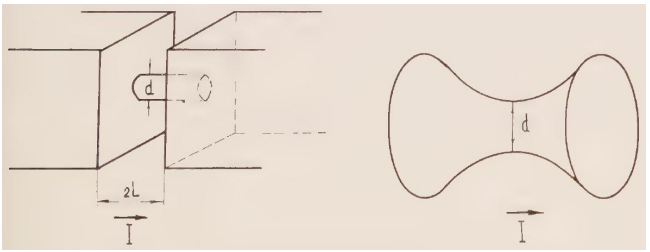


Fig. 1. Schematic picture of (a) a variable-thickness bridge and (b) a point of contact.

Schmid and Schön 1975). This is due to the fact that nonequilibrium effects are not essential in tunnel junctions. The voltage V shifts the Fermi levels in the electrodes with respect to each other by the value eV, while the transitions of electrons through the isolating layer may be described by the tunnel Hamiltonian in the first approximation with regard to transparency. The distribution functions of electrons remain the equilibrium ones (of the Fermi type).

The situation differs in bridges and contacts. When a current in the bridge (or at the contact) exceeds the critical value, then the energy gap (more precisely, the order parameter) oscillates in time with Josephson frequency $\omega_j = 2eV/\hbar$; an electric field is created in the bridge and, as a result, the distribution function of quasiparticles may considerably differ from the equilibrium one. The nonequilibrium processes which arise result in substantial differences in the behaviour of bridges and contacts as compared to tunnel junctions.

In this chapter the nonequilibrium phenomena in S-c-S systems will be considered and the behaviour of these systems, governed by the above mentioned phenomena, will be analysed.

15.1.1 1.1. Josephson effect in systems with direct Ohmic contact

Let us start with a simple theory, developed by Aslamazov and Larkin (1969) on the basis of the Ginzburg-Landau equations. The theory does not take into account nonequilibrium

phenomena, but it enables us to visualize the Josephson effect in systems with a direct contact. In the case when the characteristic dimension of the constriction L is small [as compared to the size of the Cooper pair $\xi(T) = \xi(0)\left(1 - T/T_c\right)^{-1/2}$], the order parameter $\hat{\Delta}$ changes rapidly in space and in the Ginzburg-Landau equation the gradient term is of first-rate importance,

$$\nabla^2 \hat{A} = 0. \tag{1.1}$$

The boundary condition for this equation is $\hat{C}\hat{A}/\hat{C}n = 0$ (on the superconductor surface). Far away from the constriction (when the distance is large as compared to $\breve{\zeta}$) the current density is assumed to be small with regard to the critical one, and therefore the value of $\hat{\Delta}$ is equal to its value in the bulk superconductor.

We shall search for the solution of eq. (1.1) in the form

$$\Delta(r) = \Delta_0 \left\{ f(r) \mathrm{e}^{1x_1} + [1 - f(r)] \mathrm{e}^{1x_2} \right\}, \tag{1.2}$$

where the function $f(r)$ tends to 1 when going from the point of contact towards one of the superconductors and tends to zero when directed towards the other one. It is clear that in this case A_0 is the absolute value of the order parameter far away from the contact, while χ_1 and χ_2 stand for the values of its phase on both sides of the contact.

Substituting the expression (1.2) into eq. (1.1), we see that the function $f(r)$ also satisfies the Laplace equation which may be solved when the geometry of the contact is known; thus the dependence of the order parameter on the coordinates can be found. In particular, for a narrow (one-dimensional) contact of length $2L$ we obtain:

$$\begin{aligned} \hat{\Delta}(x) &= \Delta_0 \left(\cos\chi_0 + \mathrm{i}\frac{x}{L}\sin\chi_0 \right) \\ |\hat{A}(x)| = \Delta(x) &= \Delta_0 \left(\cos^2\chi_0 + \frac{x^2}{L^2}\sin^2\chi_0 \right)^{1/2} \end{aligned} \tag{1.3}$$

where the phase difference $\chi_2 - \chi_1 = 2\chi_0$.

In order to describe the electrodynamical properties of the system, let us write the equation for the current. Assuming the mean free path l of electrons in the contact to be much less than dimensions of the contact, we obtain the expression

$$j = -\sigma\nabla\varphi - \frac{\pi e v D}{4T_c}\mathrm{i}\left(\hat{\Delta}\nabla\hat{\Delta}^* - \hat{\Delta}^*\nabla\hat{\Delta} \right), \tag{1.4}$$

where σ is the conductivity of the metal in the normal state, φ is the scalar potential, v is the density of states and $D = V_\mathrm{F}1/3$ is the diffusion coefficient. The second term corresponds to the Ginzburg-Landau equation for the density of superconducting current, written for simplicity in the "dirty" limit, $1 \ll \xi(0)$.

The potential φ, as well as the order parameter $\hat{A}$, can be found from the Laplace equation and, therefore, may be expressed in terms of the function $f(r)$. Thus, substituting the expression (1.2) into eq. (1.4), we get

$$j = -\nabla f(r)\left[\sigma V - \frac{\pi e v D \Delta_0^2}{2T_c}\sin 2\chi_0 \right] \tag{1.5}$$

where $V = \varphi_2 - \varphi_1$ is the contact voltage. Integrating the expression over the contact cross-section, we obtain the total current,

$$I = \frac{V}{R} + I_\mathrm{c}\sin\left(\frac{2e}{\hbar}\int^\mathrm{t} V\ \mathrm{d}t' \right), \quad I_\mathrm{c} = \frac{\pi A_0^2}{4eRT} \tag{1.6}$$

where R is the resistance of the contact in the normal state, while the phase difference of the order parameter is expressed via the voltage with the use of the Josephson relationship

$$h\frac{\partial\chi_0}{\partial t} \equiv h\dot{\chi}_0 = eV. \tag{1.7}$$

When the total current through the contact does not exceed I_c, then, as seen from eq. (1.6), it has the solution $V = 0$. This corresponds to a constant superconducting current passing through the contact (a stationary Josephson
effect). The value I_c as determined by eq. (1.6) is the critical current of a contact. The same expression for the critical current was obtained, on the basis of the microscopic equations of Eilenberger (1968), by Kulik and Omelyanchuk (1975), and Kulik et al. (1977), who also considered the nonlocal case $l \gg L$ and the case of arbitrary temperatures.

For $I > I_c$ an alternating voltage appears at the contact (the nonstationary Josephson effect). This voltage can be found by solving eq. (1.6):

$$V(t) = \frac{R\,(I^2 - I_c^2)}{I - I_c + 2I_c \sin^2\left(eR\sqrt{I^2 - I_c^2}t\right)} \tag{1.8}$$

By averaging the expression (1.8) over time, one obtains for the currentvoltage characteristic (CVC) curve of the contact

$$\bar{V} = R\sqrt{I^2 - I_c^2} \tag{1.9}$$

which is a hyperbola. The mean voltage, as should be expected, is related to the frequency of electromagnetic oscillations by the Josephson relation: $\hbar\omega_J = 2e\bar{V}$.

Let us now study how the CVC is affected by the external microwave field (AC-field). In this case the total current through the contact oscillates with the frequency ω of the external field:

$$I(t) = I_0 + I_1 \sin(\omega t + \delta) \tag{1.10}$$

where I_1 is proportional to the amplitude of the external field and is usually small compared to I_0. From eq. (1.6) one can obtain an expression of the first order with respect to I_1 relating the mean current I_0 and the mean voltage $\bar{V}$ on the contact

$$RI_0 = \sqrt{\bar{V}^2 + V_c^2} - \frac{I_1 R V_c}{2\sqrt{\bar{V}^2 + V_c^2}} \sin\left(\omega t - \frac{2e\bar{V}t}{\hbar} - \delta\right) \tag{1.11}$$

where $V_c = RI_c$, while the bar denotes averaging in time. As seen from eq. (1.11), at resonance voltage, $\bar{V} = \hbar\omega/2e$, a "step" appears in the CVC of the contact; the mean current at a fixed voltage varies continuously depending on the phase shift δ between the oscillations of the external field and the Josephson-type oscillations in the contact. It should be noted that perturbation theory can no longer be used for finding the shape of the CVC near the "step".

The theory developed in this section clarifies the main properties of $S - c - S$ systems and corresponds to the experimental data at small voltages (compared to the absolute value of the order parameter) and temperatures close enough to T_c. However, the theory in question is incapable of explaining such important features as the shoulder on the CVC for contacts with decreasing temperature, the stimulation of the contact's superconductivity by an external

SHF field, and a certain excess current (a permanent addition to the normal current) at high voltages. This is due to the fact that the theory does not take into account the nonequilibrium distribution of electrons on the energy levels. In the theory, the energy relaxation time was assumed to be small as compared to the other characteristic parameters of the system.

Some progress in solving the problem has been achieved by means of the time-dependent Ginzburg-Landau equation derived by Gorkov and Eliashberg (1968) for superconductors with paramagnetic impurities. Thus, Likharev and Yakobson (1975) used this equation to obtain the expression for the excess current, while Jensen and Lindelof (1976) explained the appearance of the shoulder on the CVC curve. However, the time-dependent Ginzburg Landau equation is (strictly speaking) applicable only to gapless superconductors. A consistent theory of these phenomena, taking into account the nonequilibrium electron distribution on the energy levels in the contact, is developed in sections 2 and 3.

15.1.2 1.2. Methods for studying nonequilibrium phenomena in weak links

The microscopic equations for the Green functions $\widehat{G}$ are taken as the basis for analysing the nonequilibrium phenomena (see ch. 4). In the general case, these complicated equations can not be solved. However, one can obtain approximate solutions in two limiting cases (depending on the relative value of the contact length $2L$ as compared to the characteristic parameter η). When the bridge length $2L$ satisfies the inequality

$$2L \gg \sqrt{D/\Delta} \equiv \eta(T) \sim \xi(T)\,(1 - T/T_{\mathrm{c}})^{1/4} \tag{1.12}$$

then the gradient terms in the equations for $\hat{G}$ turn out to be small and the so called local approximation may be used. This means that the quasiparticles' spectrum $\varepsilon = V\overline{\zeta^2 + \Delta^2}$ (here $\check{\zeta} = (p - p_F)\,V_F$) and the density of states are of the same form as they are in a homogeneous superconductor, except that the gap Δ depends on coordinates and time: $\Delta = \Delta(x,t)$. The density of states $N(\varepsilon)$ given below differs from zero for $\varepsilon > \Delta(x,t)$ and equals

$$N(\varepsilon) = \frac{\varepsilon}{\sqrt{\varepsilon^2 - \Delta^2(x,t)}}, \quad \varepsilon > \Delta(x,t). \tag{1.13}$$

In this case, one can introduce the energy distribution function of the quasiparticles $F(\varepsilon)$ for which a simple kinetic equation is available. The order parameter can be found from the Ginzburg Landau equation, in which the nonequilibrium phenomena may be described by means of an additional term. It then turns out that $\mathrm{S}-\mathrm{c}-\mathrm{S}$ systems have a specific electron energy diffusion mechanism which is stronger than the direct acceleration of electrons by the field, as first considered by Eliashberg (1970) for uniform systems. In the center of the bridge, the absolute value of the order parameter decreases as compared
to its value A_0 in the banks (due to the high density of the superconducting current). Therefore, the electrons with energies $\varepsilon < \Delta_0$ are confined in the potential well formed by Δ and they carry on a bounded motion. In the case of alternating current (for example, in an external AC field or under Josephson oscillations), oscillations of the order parameter in the contact appear, whereas its value in the banks is not changed (the current density in the banks is small). As a result, the electrons reflect from the walls of the "shaking" potential well and their energy increases. However, for energy values $\varepsilon > A_0$ the electrons can freely diffuse from the contact to the banks in which equilibrium is maintained. Thus, the mechanism described results in a decrease of the quasiparticles' number in the contact; this corresponds to effective cooling and stimulation of superconductivity in the contact.

In the other limiting case,

$$2L \ll \eta(T), \tag{1.14}$$

the gradient terms in the equations of microscopic theory play the dominant role. Therefore, the excitation spectrum and the density of states $N(\varepsilon)$ are considerably changed. Thus, in the

energy interval

$$\tilde{\Delta} \equiv \Delta_0 \left|\cos \chi_0\right| < \varepsilon < \Delta_0 \tag{1.15}$$

the density of states $N(\varepsilon)$ equals (see Appendix A2.1)

$$N(\varepsilon) = \frac{\varepsilon}{\sqrt{\varepsilon^2 - \tilde{\Delta}^2}} \cosh\left(a\frac{x}{L}\right) \cos\left(\frac{\pi}{2}\frac{x}{L}\right) \tag{1.16}$$

Here

$$a = \ln\left|\frac{\Delta_0 \sin\chi_0 + \sqrt{\varepsilon^2 - \tilde{\Delta}^2}}{\sqrt{\Delta_0^2 - \varepsilon^2}}\right|$$

When comparing eqs. (1.3) and (1.16), one can see that the function $N(\varepsilon)$ also differs from zero in the "forbidden" region when $\varepsilon < A(x,t)$. It becomes zero only when the energy ε becomes less than the order parameter in the center of the bridge $\tilde{A}$. Thus, the energy gap in the bridge coincides with the value of the order parameter in the center of the bridge $\tilde{A}(t)$. The physical interpretation of the processes occurring in the short bridge becomes less illustrative. However, this shortcoming is compensated by the fact that the complicated equations for the Green functions are considerably simplified and admit an exact solution over a wide range of currents and voltages. This case will be considered in section 3.

To simulate a bridge or contact take as a model a bridge with variable thickness; this model was widely used (see Likharev's review, 1979). According to the model (see fig. 1a) a bridge is a filament of length $2L$ and diameter d (where $d \ll L$), connecting two bulk superconductors (superconducting banks). The smallness of the filament diameter as compared to its length $2L$ allows us
to assume that all the functions in the bridge depend on one coordinate x along the filament. As we shall see, the final results do not depend on the geometrical characteristics of the model and are determined only by the normal resistance of the bridge R. One can show that the same results will be valid for bridges of differing shapes (for example for contacts in the shape of a hyperboloid of revolution, etc., fig. 1b). It should also be noted that everywhere in this chapter, except in section 3.5, we shall consider the "dirty" case, i.e. we shall assume the free path $l = V_F \tau_{ir}$ to be less than the correlation length $\xi(0)$ and the dimensions of the bridges: $l \ll \{\xi(0), d, L\}$.

15.2 2. Stimulation of superconductivity in bridges of length $2L > \eta(T)$

One of the most striking manifestations of the nonequilibrium electron energy distribution in bridges is the increase of the critical current in the presence of an external microwave field. This phenomenon may be observed both in long superconducting bridges whose properties resemble those of uniform film structures and in short bridges and point superconducting contacts (see ch. 3).

A theory explaining the stimulation of superconductivity in films in the presence of AC fields was constructed by Eliashberg (1970) and Ivlev and Eliashberg (1971) and is described in chapter 6. In the present chapter we deal with nonuniform systems, for which the dependence of the superconducting order parameter on the coordinates is essential. We investigate the case of bridges which are not too short: with the length of the bridge $2L$ larger than the characteristic parameter $\eta(T)$, since for $2L < \eta$ the critical current decreases in the presence of an AC field (section 3.1).

One more manifestation of the superconductivity stimulation with a nonequilibrium electron distribution is the bending of the bridge's CVC for decreasing temperature. The reason for the nonequilibrium state in this case is not the external AC field, but the intrinsic voltage of the system which appears on the contact for currents exceeding the critical value. This phenomenon, as well as stimulation by microwave fields, takes place when the bridge length satisfies the inequality $2L > \eta(T)$.

The results described in this section were obtained by Aslamazov and Larkin (1976, 1978).

15.2.1 2.1. General expressions for the order parameter and electron distribution function in contacts

The stimulation of superconductivity manifests itself in the most pronounced manner near the critical temperature T_c of a superconductor. Therefore, to describe the phenomenon, we shall use the Ginzburg Landau equation, in
which the nonequilibrium of the electron energy distribution is taken into account. With sufficiently smooth and slow changes of the order parameter,

$$\hbar\omega < \hbar D/L^2 < \Delta \tag{2.1}$$

this equation may be written as

$$\frac{\pi D}{8T}\frac{\partial^2\Delta}{\partial r^2} - \frac{TI_s^2}{2\pi e^2 v^2 D S^2 \Delta^3} + \frac{T_c - T}{T_c}\Delta - \frac{7\zeta(3)\Delta^3}{8\pi^2 T^2} + \Phi(\Delta) = 0 \tag{2.2}$$

$$\Phi(\Delta) = \Delta\int_\Delta^\infty \left[F(\varepsilon) - \tanh\frac{\varepsilon}{2T}\right]\left(\varepsilon^2 - \Delta^2\right)^{-1/2}\,\mathrm{d}\varepsilon \tag{2.3}$$

The electron energy distribution function $n(\varepsilon)$ is expressed in terms of $F(\varepsilon)$ using

$$n(\varepsilon) = \frac{1}{2}[1 - F(\varepsilon)] \tag{2.4}$$

and is assumed to be weakly dependent on time and coordinates (the energy relaxation time of electrons in superconductors, τ, is large as compared to both the period of electromagnetic field, $\sim \omega^{-1}$, and the time $\sim L^2 D$ of the spatial electron diffusion along the contact). The second term in eq. (2.2) describes the variations of the order parameter's phase %, connected with the value of the superconducting current I_s by the formula

$$I_s = \pi e v D S A^2 \nabla\chi/2T \tag{2.5}$$

where S is the cross-sectional area of the contact. The use of the equilibrium expression (2.5) for the superconducting current is justified in the case when the function F differs slightly from the equilibrium function $\tanh(\varepsilon 2T)$ (see Appendix of ch. 13. For higher microwave radiation power or a higher voltage on the contact, the deviation $F(\varepsilon) - \tanh(\varepsilon/2T)$ may be on the order of the equilibrium value $\tanh(\varepsilon/2T)$. In this case the nonequilibrium expression for the superconducting current should be used, as derived in the Appendix of ch. 13. This, however, affects only the numerical coefficients in the final results.

Before averaging the function $F(\varepsilon, r, t)$ over time and coordinates let us write out, in the case $2L > \eta$, the kinetic equation obtained by Larkin and Ovchinnikov (1977):

$$D\frac{\partial^2 F}{\partial \boldsymbol{r}^2} - \frac{\partial F}{\partial t}\frac{\partial}{\partial\varepsilon}\left(\varepsilon^2 - \Delta^2\right)^{1/2} + \frac{\partial F}{\partial\varepsilon}\frac{\partial}{\partial t}\left(\varepsilon^2 - \Delta^2\right)^{1/2} = I_{\mathrm{ph}}(F), \tag{2.6}$$

where in the right-hand side a collision integral is written. The direct effect of the electromagnetic field on the distribution function is not taken into account in this equation, since it is

small for contacts which are not too long. Using this equation one can obtain the averaged-out equation (over time and
coordinates) for the function $F(\varepsilon)$:

$$\frac{1}{\tau_\varepsilon}\left[F(\varepsilon)-\tanh\frac{\varepsilon}{2T}\right]\left\langle\overline{\varepsilon\left(\varepsilon^2-A^2\right)^{-1/2}}\right\rangle=\frac{\partial}{\partial\varepsilon}\left(D_\varepsilon\frac{\partial F}{\partial\varepsilon}\right) \tag{2.7}$$

$$D=-\left\langle\begin{matrix}\hat{c}\theta\\ it\end{matrix}\left(D\frac{\partial^2}{\hat{c}r^2}\right)^{-1}\frac{\partial(l}{it}\right\rangle\cdot\theta=\left(\varepsilon^2-A^2\right)^{12}-\left\langle\left(\varepsilon^2-A^2\right)^{12}\right., \tag{2.8}$$

where the left-hand side of eq. (2.7) describes the relaxation of the quasiparticles while the right one gives the energy diffusion; D, is the energy diffusion coefficient, the brackets $/\cdots$, denote averaging over the area of the contact where : $-A$, and the bar denotes averaging over time. The boundary condition for finding the inverse operator in eq. (2.8) requires the derivative normal to the surface $\varepsilon = A(r)$ to be equal to zero. Equations (2.7) and (2.8) are valid when condition (2.1) is fulfilled. These equations are derived in Appendix 1.

15.2.2 2.2. Stimulation of the critical current of the bridge for low-power microwave radiation

In order to find the maximum value of a superconducting current passing through the contact in the presence of an AC field by means of eq. (2.5). one must know the nonequilibrium distribution function and the order parameter in the contact, which may be obtained from eqs. (2.2) and (2.7). For low-power radiation, the nonequilibrium term $\Phi(\Delta)$ in eq. (2.2) is small and therefore, when calculating the energy diffusion coefficient D_ε, one may use the dependence of the order parameter $A(r.t)$ determined from the equilibrium Ginzburg Landau equation. Then, by solving the kinetic equation (2.7) one can find the nonequilibrium distribution function and, using eq. (2.3), find the nonequilibrium term $\Phi(\Delta)$ and the correction to the critical current.

The time dependence of the order parameter is determined by the alternating voltage induced on the contact by the AC field: the phase difference of the order parameter in the banks is related to the voltage V' by the Josephson relation (1.7). Therefore both superconducting and normal currents pass through the contact. However. unless the value of the superconducting current exceeds the critical value, the DC component of the normal current and hence the mean voltage on the contact equals zero. The given parameter is the radiation power. which is proportional to the mean square of the voltage on the contact, and may be measured in dimensionless units:

$$P=\frac{e^2}{h}\frac{\tau_{\frac{l}{V^2}}}{T} \tag{2.9}$$

First, let us consider the most interesting case of a long ($L \gg \xi$) and narrow contact (fig. 2) when the order parameter $.A = A(x)$. over almost the entire area

inside the contact, is close to its value for an infinitely long contact and only near the edges in the domain $L - x \lesssim \xi$ a "linking" takes place with the equilibrium value Δ_0 at the banks (the current density at the banks is small). If, in addition, the superconducting current I_s is close to its critical value for an infinite contact,

$$I_c^0=9.1e\hbar^{-1/2}\nu SD^{1/2}\left(T_c-T\right)^{3/2}$$

then the order parameter is close to the value $\Delta_\infty=\left(\frac{2}{3}\right)^{1/2}\Delta_0$. The spatial variations of the order parameter, $\Delta^2(x)-\Delta^2(0)$ practically over the entire contact area, as seen from eq. (2.2) are of the order

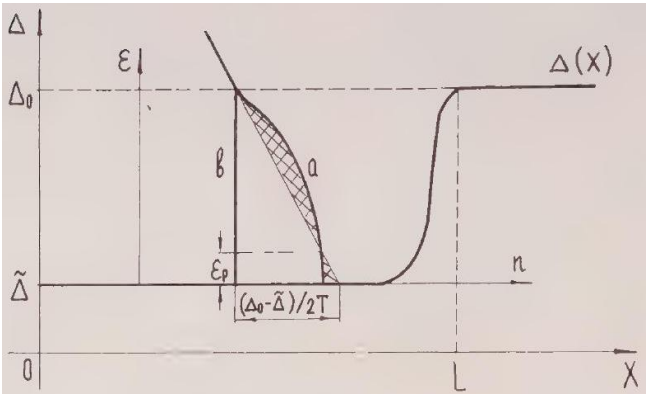


Fig. 2. The order parameter $\Delta(x)$ and distribution function of quasiparticles $n(\varepsilon)$ in the bridge. Curve (a) corresponds to low radiation power; hatching shows the regions of rarefication and condensation (double hatching) of quasiparticles as compared to the equilibrium distribution (the sloping straight line). The vertical straight line "b" relates to high radiation power, when equal energy distribution is established for the quasiparticles confined inside the bridge.

$$\Delta_\alpha^2 - \Delta^2(0) \sim \Delta_\infty^2 \left(\xi^2/L^2\right)$$

and therefore are relatively small. The scale of these variations can be characterized by means of the parameter $\delta = A_\infty - \Delta(0)$.

Thus the electrons with energies $\xi < \Delta_0$ prove to be confined in the contact and exercise a finite motion reflecting from the walls of the potential well at the points where $A = \varepsilon$. In an external AC field, the order parameter in the contact depends on time, $\Delta = \Delta(x,t)$, and electrons reflect from the walls of the "shaking" potential well. As a result, electron energy diffusion occurs as described by eq. (2.8). When the electron energy is not too close to the value of the order parameter in the contact center, $\varepsilon - \Delta_\infty \gg \delta$, then the bottom of the well may be considered flat; for the energy diffusion coefficient D, we then obtain from eq. (2.8):

$$D_1 = \frac{1}{4D}\frac{1}{\varepsilon^2 - A^2}\left\langle\left[\int_0^1\left(\left\langle\frac{\hat{i}A^2}{\hat{i}t}\right\rangle - \frac{\hat{i}A^2}{\hat{i}t}\right)\mathrm{d}x\right]^2\right\rangle. \tag{2.10}$$

As seen from this formula, the energy diffusion is due to the fact that the amplitude of oscillations Δ depends on the coordinates (because, if not, then $\langle\partial\Delta^2/\partial t\rangle = \partial\Delta^2/\partial t$) and the bottom of the well does not oscillate as a whole. In order to find the time dependence of the order parameter, let us note that

$$\frac{\partial\Delta^2}{\partial t} = \frac{\partial\Delta^2}{\partial\chi_0}\dot{\chi}_0 = \frac{eV}{\hbar}\frac{\partial\Delta^2}{\partial\chi_0}. \tag{2.11}$$

To calculate the derivative $\partial\Delta^2/\partial\chi_0$, we shall use the system obtained from eqs. (2.2) and (2.5) by substituting the equilibrium function $F(\varepsilon) = \tanh(\varepsilon/2T)$ into it:

$$\frac{\pi D}{8T}\frac{\partial^2\Delta}{\partial x^2} - \frac{TI_\mathrm{s}^2}{2\pi e^2 v^2 D S^2 A^3} + \frac{T_\mathrm{c} - T}{T_\mathrm{c}}\Delta - \frac{7\zeta(3)}{8\pi^2}\frac{\Delta^3}{T^2} = 0, \tag{2.12}$$

$$\chi_0 = \frac{2TI_\mathrm{s}}{\pi evSD}\int_0^L \Delta^{-2}(x)\mathrm{d}x, \quad \Delta(\pm L) = \Delta_0. \tag{2.13}$$

The value of the current I_s in the system will be considered constant and equal to the critical current of the contact without irradiation (the superconducting current oscillates near to the maximum and therefore the amplitude is small).

The set of equations (2.12) and (2.13) can be easily solved; using the derivative $\hat{c}A^2/\hat{c}t$ obtained by means of eqs. (2.11) and (2.8) we can find the energy diffusion coefficient

$$D_\varepsilon = 0.44e^2v^2S^2D\frac{\dot{\chi}_0^2\Delta_\infty^8}{T^2I_s^2}\frac{1}{\varepsilon^2-\Delta_\infty^2} = 0.23P\frac{T^2\Delta_0^2}{\tau_\varepsilon\left(\varepsilon^2-\Delta_\gamma^2\right)}, \quad \varepsilon-\Delta_\infty \gg \delta. \tag{2.14}$$

As seen from eq. (2.14), the energy diffusion is most intensive near the bottom of the well, and sharply decreases with increasing ε.

In the other limiting case, $\varepsilon-\Delta_\alpha \ll \delta$, for finding D_ε the region close to the center of the contact is essential; there the order parameter changes according to the parabolic law; thus the general equation (2.8) shows that the coefficient D_b ceases to depend on energy and, up to a numerical coefficient, is determined by eq. (2.14) at $\varepsilon-\Delta_\infty \sim \delta$.

The expression obtained for the energy diffusion coefficient shows how to solve the kinetic equation (2.7) and find the nonequilibrium distribution function. Hence we shall use the results obtained for the uniform case (Ch. 6). Although the cause of energy diffusion in the uniform case is the direct acceleration of electrons by the electric field, the dependence of $D.$ on energy has the same form as that in eq. (2.14). Therefore, at energies close to the value of the gap A, an intensive energy diffusion, as shown in chapter 4, leads to
a diminishing number of quasi-particles, as in the uniform case

$$F(\varepsilon)-\tanh(\varepsilon/2T) = 0,1\tau^{1/10}P^{2/5}, \quad \varepsilon-\Delta_\infty \ll \varepsilon_\mathrm{p}, \tag{2.15}$$

$$\tau = (T_\mathrm{c}-T)/T_\mathrm{c}, \quad \varepsilon_\mathrm{p} = T\tau^{1/10}P^{2/5}. \tag{2.16}$$

At higher energies, the correction may be found by substituting the equilibrium function $F(\varepsilon)=\tanh(\varepsilon/2T)$ into the right-hand side of the kinetic equation (2.7):

$$F(\varepsilon)-\tanh\frac{\varepsilon}{2T} = -0.23P\frac{\mathrm{T}\Delta_0^2}{\left(\varepsilon^2-A_x^2\right)^{3\,2}}, \quad \varepsilon-\Delta_\infty \gg \varepsilon_\mathrm{p} \tag{2.17}$$

The negative sign in the right-hand side of eq. (2.17) indicates an excess of quasiparticles in a given energy interval, as compared to the equilibrium distribution [the distribution function $n(\varepsilon)$ is related to $F(\varepsilon)$ by eq. (2.4)]. Thus (Tinkham. 1979) the quasiparticles are rarefied at energies close to the gap. whereas, on the contrary, they condense in the region of higher energies (fig. 2).

Equations (2.15) and (2.17) describe the nonequilibrium distribution function for a long bridge at energies not too close to the value of the order parameter in the contact: $\varepsilon-d, \gg \delta$. since the bottom of the potential well was assumed flat. Hence, for sufficiently long contacts, the inequality $\varepsilon_\mathrm{p} \gg \delta$ is fulfilled, starting from very small radiation powers, so that for all significant energy values the nonequilibrium distribution function is given by eus. (2.15) and (2.17).

Let us also note that for energies $\varepsilon > \Delta_0$ we must take into account the spatial diffusion of electrons from the contact to the banks. Let us assume that the diffusion is intensive enough and that the distribution function of electrons with energies $\varepsilon > \Delta_0$ in the contact is the same as in the banks (i.e the equilibrium one). Deviations from equilibrium in bridges of constant thickness when the spatial diffusion is hampered, will be discussed in section 2.3 .

The next step is to find the nonequilibrium term $\Phi(1)$ in the GinzburgLandau equation, using the known distribution function. As seen from eq. (2.3), the sign of $\Phi(\Delta)$ and hence the sign of the effect [stimulation or suppression of superconductivity-see eq. (2.2)] is determined by the rival contributions of energies close to the gap, where there is a lack of quasiparticles [$F(\varepsilon)-\tanh(\varepsilon/2T) > 0$, effective cooling], and high energies with excess quasiparticles [$F(\varepsilon)-\tanh(\varepsilon : 2T) < 0$, overheating]. Hence the above contributions almost entirely compensate

each other; however, the residue (where the radiation power is not too small) is positive and linearly increases with increasing radiation power (stimulation!).

In order to verify this, let us write out the nonequilibrium term $\Phi(\Delta)$ as follows

$$\Phi\left(\Delta_\infty\right) = \int_{\Delta_\infty}^{\Delta_0} \frac{\Delta_\infty}{\left(\varepsilon^2 - \Delta_\infty^2\right)^{1/2}} \left[F(\varepsilon) - \tanh\frac{\varepsilon}{2T}\right] \mathrm{d}\varepsilon$$

$$= \int_{\Delta_\infty}^{\Delta_0} \left\langle \frac{\varepsilon}{\left(\varepsilon^2 - \Delta^2\right)^{1/2}} \right\rangle \left[F(\varepsilon) - \tanh\frac{\varepsilon}{2T}\right] \mathrm{d}\varepsilon + \Phi^{\mathrm{res}}\left(\Delta_\infty\right) \tag{2.18}$$

$$\Phi^{\mathrm{res}}\left(\Delta_,\right) = \int_{\Delta^1}^{\Delta_0} \left[\frac{\Delta_x}{\left(\varepsilon^2 - \Delta_\infty^2\right)^{1/2}} - \left\langle \frac{\varepsilon}{\left(\varepsilon^2 - \Delta^2\right)^{1,2}} \right\rangle\right] \left[F(\varepsilon) - \tanh\frac{\varepsilon}{2T}\right] \mathrm{d}\varepsilon \tag{2.19}$$

It follows from the kinetic equation (2.7) that the integrand in the first term of eq. (2.18) is the total derivative of the quasi-particles' flux $D_\varepsilon \partial F/\partial\varepsilon$. The integral is small, since for $\varepsilon = \Delta_\infty$ the derivative $\hat{\partial} F/\hat{C}\varepsilon$ vanishes (the flux is zero at the bottom of the well), while for $\varepsilon = \Delta_0$ the value of D_ε is already small (eq. 2.14). This corresponds to the above-mentioned almost complete cancellation of the contributions from the energy regions with rarefication and condensation of quasiparticles. In order to calculate the residue $\Phi^{\mathrm{res}}\ \left(\Delta_\gamma\right)$, we shall use eq. (2.19). In this integral it is reasonable to divide the interval of integration with respect to energy into two regions: $\Delta_\infty < \varepsilon < \Delta_\infty + \varepsilon_{\mathrm{p}}$ and $\Delta_\infty + \varepsilon_{\mathrm{p}} < \varepsilon < \Delta_0$, in which the integrals may be computed with logarithmic precision [the value of ε_{p} is determined by expression (2.16)]. For energies $\Delta_\infty + \varepsilon_{\mathrm{p}} < \varepsilon < \Delta_0$ we shall use eq. (2.16) for $F(\varepsilon)$ and consider that

$$\left\langle \left(\varepsilon^2 - \Delta^2\right)^{-1/2} \right\rangle = \left(\varepsilon^2 - \Delta_\infty^2\right)^{-1/2}$$

(assuming that $\varepsilon_{\mathrm{p}} \gg \delta$). As a result, we obtain:

$$\Phi_1^{\mathrm{res}}\left(\Delta_x\right) = \int_{\Delta_y + \varepsilon_p}^{\Delta_0} \frac{\Delta_\infty - \varepsilon}{\left(\varepsilon^2 - \Delta_\infty^2\right)^{1/2}} \left[F(\varepsilon) - \tanh\frac{\varepsilon}{2T}\right] \mathrm{d}\varepsilon$$
$$= 0.1 PT \ln\left(\Delta_0/\varepsilon_p\right) \tag{2.20}$$

The positive sign of the nonequilibrium corresponds to stimulation of superconductivity in the contact. The contribution to the nonequilibrium term $\Phi_2^{\mathrm{res}}\ \left(\Delta_\infty\right)$ from the low energy region $\Delta_\infty < \varepsilon < \Delta_\infty + \varepsilon_{\mathrm{p}}$ is due to the difference between $\left\langle \left(\varepsilon^2 - \Delta^2\right)^{-1/2} \right\rangle$ and $\left(\varepsilon^2 - \Delta_\infty^2\right)^{-1/2}$, and this is small for sufficiently long contacts. When calculating $\Phi_2^{\mathrm{rec}}\ (\Lambda)$ with logarithmic accuracy, one can take the lower limit of integration equal to $\Delta_\infty + \delta$, using eq. (2.15) for the distribution function. The dependence $\Delta(x)$ is found from eq. (2.12) and permits the calculation of $\left\langle \left(\varepsilon^2 - \Delta^2\right)^{-1/2} \right\rangle$. As a result, we obtain

$$\Phi_2^{\mathrm{res}}\left(\Delta_\infty\right) = 0,1 \tau^{1/10} P^{2/5} \Delta_\infty \int_{\Delta_x + \delta}^{\Delta_x + \varepsilon_{\mathrm{p}}} \left[\left(\varepsilon^2 - \Delta_\infty^2\right)^{-1/2} - \left\langle \left(\varepsilon^2 - \Delta^2\right)^{-1/2} \right\rangle\right] \mathrm{d}\varepsilon$$
$$= -0.08 \frac{\left(D\Delta_0\right)^{1/2}}{L} \tau^{-3/20} P^{2/5} \ln\frac{\varepsilon_{\mathrm{p}}}{\delta} \tag{2.21}$$

This contribution to the nonequilibrium term shows suppression of superconductivity, but its value decreases with increasing length L of the contact. Let us note the surprising fact that after the cancellation of the main

contributions from the low- and high-energy regions (the first integral in 2.18), the positive term Φ_1^{res} in the residue $\Phi^{\text{res}} = \Phi_1^{\text{res}} + \Phi_2^{\text{res}}$ comes precisely from the high-energy region where the quasiparticles are dense.

After the nonequilibrium term $\Phi(\Delta)$ is determined, we shall find the critical current in the AC field using the Ginzburg-Landau equation. In the case of a long contact, one can neglect the first (gradient) term and, as a result, for the superconductivity current will be obtained

$$I_{\text{s}}^2 = 2\pi e^2 v^2 D S^2 \left(\Delta^3/T\right) \left[\tau\Delta - \frac{7\zeta(3)}{8\pi^2}\frac{\Delta^3}{T^2} + \Phi(\Delta)\right] \tag{2.22}$$

The critical current I_c is found by maximizing the expression. At low irradiation powers $\Phi(\Delta)$ is small. Therefore, to find the correction to the critical current, the value of $\Delta = \Delta_\propto$ may be substituted into the expression; this value corresponds to the critical current of the contact without irradiation; for $\Phi\left(\Delta_\propto\right) = \Phi_1^{\text{res}}\left(\Delta_\propto\right) + \Phi_2^{\text{res}}\left(\Delta_\infty\right)$ one can use eqs. (2.20) and (2.21). As a result, we obtain

$$\frac{I_{\text{c}} - I_{cx}^0}{I_{cx}^0} = 0.06\tau^{-3/2} P \ln\left(\frac{\Delta_0}{\varepsilon_{\text{p}}}\right) - 0,14\frac{\eta}{L}\tau^{-23/20} P^{2/5} \ln\left(\frac{\varepsilon_{\text{p}}}{\delta}\right) \tag{2.23}$$

This expression has a minimum for powers $P_1 \sim (\eta/L)^{5/3}\tau^{7/12}$. Therefore, at very low irradiation power (the lesser it is, the higher is L, and the closer is T to a T_c) a decrease of the critical contact current should result. However, starting from powers of the order of P_1, the critical current linearly increases with increasing irradiation power. A linear stimulation of the critical current was observed in many experiments, and in several cases one managed to reveal a minimum of the critical current at a low irradiation power. The experimental situation is discussed in detail in ch. 1.

Expression (2.23) obtained for the dependence of the critical current of the contact on the irradiation power relates to the case of a long contact, $2L > \xi$. For short contacts, $\eta < 2L < \xi$ [the first condition implies the validity of the original expressions (2.2), (2.4) and (2.7)] the situation is somewhat different. The power interval in which the critical current decreases increases in this case. However, starting from the power $P_2 \sim \tau^{3/2}$, the nonequilibrium term in the Ginzburg-Landau equation (2.2) again becomes greater than the first term describing the spatial changes of Δ. As a result, the order parameter ceases to depend on coordinates as it does in the case of a long contact, and stimulation of the critical current occurs. This case is considered in the next section.

We shall also give here a comparison of the values of the critical current stimulation phenomena when stimulated by an AC field with a direct acceleration by an electric field (Eliashberg mechanism) and for the stimulation due to the "shaking" of the potential well. Using the results of the uniform case (ch. 6), we conclude that the stimulation due to low-power
electric fields is also linear, the corresponding coefficient in $(\Delta/T)(\eta/L)^2$, however, being less than that in eq. (2.23). Thus in the region where the results obtained are valid, $\eta < 2L < (D/\omega)^{1/2}$, the stimulation in the bridge is mainly due to the "shaking" of the potential well. The right-hand inequality has a simple physical meaning: during a period of the electromagnetic oscillation $\sim \omega^{-1}$ an electron diffusing along the contact experiences many reflections from the "shaking" walls of the well (the diffusion time is L^2/D). This condition is violated by increasing the contact length L, and then the relative contribution of "shaking" decreases (to find it, one must take into account the frequency dependence D_ε). Then, the direct acceleration of electrons by the field may become more important.

15.2.3 2.3. Superconductivity stimulation at high irradiation powers

With increasing irradiation power the nonequilibrium term in the GinzburgLandau equation (2.2) increases as well. For its estimation, we shall use eq. (2.20), obtained by means of perturbation theory which implies that the term in question becomes predominant in eq. (2.2) for $P > \tau^{3/2}$. Hence, for both long and short contacts, the order parameter for nearly all the contact, except the edges, only slightly depends on coordinates, while its value in the contact $\tilde{\Delta}$ is related to the superconductivity current I_s by eq. (2.22), in the right-hand side of which only the summand containing the nonequilibrium ferm $\Phi(\Lambda)$ is essential. Thereby, the deviation of the distribution function from that of equilibrium may be still small when the power $P < \tau^{1/2}$. Thus, in the power interval $\tau^{3/2} < P < \tau^{1/2}$ the nonequilibrium term in the Ginzburg-Landau equation is already large, while the distribution function is still close to the equilibrium one. In this case the critical current I may be found accordingly (in a self-consistent way). Assuming the current to be a given parameter we shall find D_i using eq. (2.14). Then by solving the kinetic equation (2.7) in the framework of perturbation theory (by substituting into the right-hand side of $F(\varepsilon) = \tanh(\varepsilon/2T)$), we shall find the correction to the equilibrium distribution function and, using it (and eq. 2.20) find the nonequilibrium term $\Phi_1(\tilde{A})$ (the contribution Φ_2 is small for sufficiently long contacts as it is for low irradiation power). As a result, we obtain

$$\Phi_1(\tilde{\Delta}) = 0.03\mathrm{e}^2 v^2 S^2 D P \frac{\tilde{\Delta}^6}{T^2 I_s^2} \ln \frac{\Delta_0 - \tilde{\Delta}}{\tilde{\varepsilon}_p} \tag{2.24}$$

By substituting this expression into eq. (2.22) (in which only the nonequilibrium term should be taken into account) we obtain a self-consistent equation for finding the current I_s. The critical current may be found by maximizing I_s, which is realized at a $\tilde{A}$ close to A_0 and where I_s is equal to

$$I_c = 0.53 I_{c\infty}^0 \tau^{-3/8} P^{1/4} \ln^{1/4}\left(\tau^{1/2} P\right). \tag{2.25}$$

Thus, in an intermediate power region the critical current depends nonlinearly on the irradiation power ($\tau^{3/2} < P < \tau^{1/2}$).

In the high-power region, $P > \tau^{1/2}$, the critical current reaches saturation. Thereby, the distribution function has a limit shape (fig. 2) and ceases to depend on the irradiation power: for all the electrons located inside the contact, a homogeneous equipartition energy distribution is set up, whereas the distribution function of electrons capable of diffusing into the banks remains equilibrium:

$$F(\varepsilon) - \tanh\frac{\varepsilon}{2T} = \begin{cases} \frac{\Delta_0 - \varepsilon}{2T}, & \varepsilon < \Delta_0 \\ 0, & \varepsilon > \Delta_0 \end{cases} \tag{2.26}$$

Equation (2.26) is formally obtained from the kinetic equation (2.7), in which the left-hand term (the relaxation term) for high irradiation power may be put equal to zero. Then, for the quasiparticles' flow we get $D_\varepsilon(\partial F/\partial\varepsilon) = \text{const.}$; since this equals zero at the bottom of the potential well, then for all energies $(\partial F/\partial\varepsilon) = 0$, i.e. $F(\varepsilon) = \text{const}$. This constant may be found using the "linking" condition with the equilibrium distribution function at $\varepsilon = A_0$. The result obtained may be easily understood from the physical viewpoint in the case when we are coming from a low-power region: the region of rarefication near the bottom of the well increases with increasing power and finally it stabilizes for all the electrons "located" in the well.

For a known distribution function one can find the nonequilibrium term using eq. (2.3):

$$\Phi(\Delta) = \frac{\Delta\Delta_0}{2T}\left[\ln\frac{1 + (1 - \Delta^2/\Delta_0^2)^{1/2}}{\Delta/\Delta_0} - \left(1 - \frac{\Delta^2}{\Delta_0^2}\right)^{1/2}\right]. \tag{2.27}$$

By substituting this expression into the expression (2.27) for a superconducting current (in which again the nonequilibrium term is essential), we see that the maximum current corresponds to $\tilde{\Delta} = 0,7\Delta_0$ and is equal to

$$I_c^* = 0,43evSD^{1/2}\Delta_0^{5/2}/\hbar^{3/2}T. \tag{2.28}$$

This is the maximum critical current of the contact in the microwave field. Note that eq. (2.28) is, in fact, found with accuracy up to a numeric coefficient, since in our derivation of eq. (2.22) the equilibrium expression was used for a superconducting current (see section 2.1).

Let us now compare the expression (2.28) for the maximum critical current with that of a critical current without irradiation, I_c^0. The current I_c^* does not depend on the bridge length and decreases when the temperature approaches T_c according to the law τ^{54}. The value of I_c^0 also decreases when nearing T_c, however, the law by which it decreases depends on the bridge dimension. For a short bridge ($2L < \xi$) the critical current is $I_c^0 \sim \tau$, while for a long one ($2L > \breve{\zeta}$)
the critical current will be $I_c^0, \sim \tau^{32}$. Therefore, the relative correction to the critical current far from T_c (when $2L > \xi$) increases with increasing temperature according to the law $\tau^{-1/4}$, then reaches its maximum, $\sim [L/\xi(0)]^{1/2}$, at the temperature when $2L \sim \xi$, and in the interval $\xi > 2L > \eta$ decreases according to the law $\tau^{1/4}$. For $2L < \eta$ the relative correction to the critical current is already small. The temperature dependence of the stimulation effect of the critical current is shown in fig. 3. Thus, the effect of superconductivity stimulation is most pronounced in the temperature interval when $2L \sim \check{\xi}$. The picture described here is in a good agreement with experimental data for contacts which are not too long (see ch. 5).

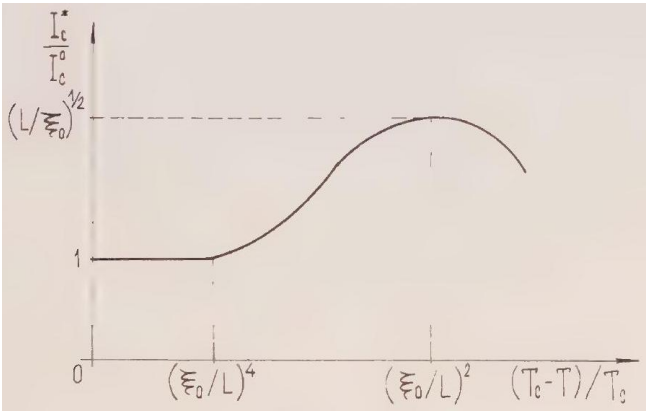


Fig. 3. Temperature dependence of the ratio of the maximum critical bridge current I_{c}^{*} in an AC field to that in the absence of radiation (I_c^0) ($2L$ is the length of the bridge; $\xi_0 = \zeta(0)$ is the coherence length at zero temperature).}

When the maximum superconductivity current was found, the direct suppression of superconductivity by the AC field was not taken into account. This is valid until the power of the AC field is not too high, and the AC component of the superconducting current is snall as compared to the value of the maximum current (I_s is generally speaking less than I_c^* since the oscillations of the superconducting current occur near the maximum). The amplitude of the alternating current I may be estimated using eq. (2.5):

$$\tilde{I}_C(t) \sim \mathrm{evSD}\left(\Delta^2 T\right)\omega^{-1}\hat{i}(\nabla\%)\hat{i}t.$$

where $\nabla\chi \sim \chi_0/L$ and the value of $\dot{\chi}_0$ is related to the voltage on the contact V in accordance to eq. (2.9). Comparing the values $I_s(t)$ and I_s^* we see that suppression leads to a considerable

decrease of the superconductivity current at the voltages $eV \sim \hbar\omega(L/\eta)$. The corresponding dimensionless power
$P \sim (\hbar\omega^2\tau_\varepsilon/T)\,(L/\eta)^2$ proves to be proportional to the large value of the energy relaxation time τ_ε and therefore is high as compared to the power $P \sim \tau^{1/2}$ at which the critical current reaches saturation.

Let us also discuss the questions relating to the spatial diffusion of electrons from the contacts to the banks. This diffusion was assumed to lead to an equilibrium for electrons with energies $\varepsilon > A_0$. This condition is fulfilled in variable-thickness bridges, when the thickness of the film is larger in the banks, while the character of electron diffusion is spatial. However, in bridges of constant thickness, because of the two-dimensional character of the diffusion, the distribution function slowly (according to a logarithmic law) approaches equilibrium when going from the contact to the banks. In this case the contact is a source of nonequilibrium quasiparticles which propagate far towards the banks (to the distance $\sim \sqrt{D\tau_\varepsilon}$).

The "shaking" of the order parameter in such contact results in an insufficiency of quasiparticles with energies $\varepsilon > \Delta_0$ in the region of thickness $\sim \omega$ near the value Δ_0. Therefore, in constant-thickness bridges stronger stimulation may be observed than in those with a variable thickness. This phenomenon was experimentally observed by Latyshev and Nad' (1979) (see ch. 1).

15.2.4 2.4. Superconductivity stimulation in bridges by direct current

When the current through a contact exceeds the critical value, the mean voltage $\bar{V}$ appears on the contact, and the superconducting current has an alternating component with the frequency $\omega = 2e\bar{V}, \hbar$ (the nonstationary Josephson effect). In this case the electron energy distribution function differs from the equilibrium one; the cause of the nonequilibrium is both direct acceleration of electrons by the electric field and oscillation of the order parameter in the contact, produced by the alternating constituent of the superconducting current.

In this section we shall again consider contacts of length $2L$ satisfying condition (2.1). In this case the energy diffusion of electrons is mainly due to the oscillations of the order parameter in the contact, as it was in the case of superconductivity stimulation by an external AC field. However, the amplitude of the oscillations of the order parameter's modulus in the contact in this case can no longer be considered small (see section 1.1).

The condition (2.1) for the contact length provides for sufficiently smooth and slow variations of the order parameter, so that in order to describe the nonequilibrium phenomena one can again use the set of equations (2.2), (2.5) and (2.7). As a result, the energy electron diffusion caused by the oscillations of the order parameter in the contact for a current $I > I_c$ leads to a decreasing number of quasiparticles (with the energies $\varepsilon < \Delta_0$) trapped in the contact. This corresponds to effective cooling of the contact, and the superconducting
current through the contact strongly increases even for low voltage values on the contact.

In order to verify this, we shall first calculate the value of the nonequilibrium term $\Phi(\Lambda)$ for Δ close to Λ_0 and show that $\Phi(\Delta) > 0$. To do this, it suffices to find the deviation of the distribution function from equilibrium, $F(\varepsilon) - \tanh(\varepsilon/2T)$ for ε close to Δ_0. Beginning from low voltages, the distribution function assumes the limiting nonequilibrium form: for $\varepsilon < \Delta_0$ the distribution is homogeneous with respect to energies and $F(\varepsilon)$ weakly depends on energy; at the same time for $\varepsilon > \Delta_0$ the function $F(\varepsilon)$ is close to the equilibrium one, since the electrons with such energies easily diffuse from the contact and mix with the equilibrium electrons in the banks (the current density there is small).

Thus, the calculation may be performed in a self-consistent manner. Using the limiting expression (2.26) for $F(\varepsilon)$ when ε is close to Δ_0 we shall find the value of the nonequilibrium

term by the expression (2.3) for Δ close to Δ_0; then solving the Ginzburg Landau equation with the known term $\Phi(\Delta)$, we determine the dependence of the order parameter on time and coordinates. Next, we use eq. (2.8) to calculate the energy diffusion coefficient D_2. With its help we can solve the kinetic equation (2.7) and confirm the validity of the assumption on the form of the distribution function.

By substituting the limiting expression (2.26) for $F(8)$ into eq. (2.3) we obtain for the nonequilibrium term, when Δ is close to Δ_0

$$\Phi(\Delta) = \frac{\sqrt{2}}{3}\frac{\Delta_0^2}{T}\left(1 - \frac{\Delta}{\Delta_0}\right)^{3/2} \tag{2.29}$$

Comparison of the orders of magnitude of the terms in the Ginzburg Landau equation (2.2). where $\Phi(\Delta)$ is given by eq. (2.29), shows that considerable variations of the order parameter (by the value of $\tilde{A} - \Lambda_0$) occur only near the edges of the contact at a distance $\Delta x \sim \eta\left(1 - \tilde{\Delta}/\Delta_0\right)^{-1/4}$, while the value of the order parameter in the contact $\bar{A}$ is determined by the value of the superconducting current,

$$\hbar T I_s^2/2\pi e^2 v^2 S^2 \Delta_0 = \tilde{\Delta}^2 \Phi(\tilde{\Delta}) \tag{2.30}$$

The oscillations of $\tilde{A}$ are caused by those of the superconducting current. which, in turn, are due to the oscillations of the phase difference 2% of the order parameter in the banks. The derivative %, is related to the alternating voltage V by the Josephson relation. Therefore using eqs. (2.30), (2.5) and (1.7) we can find the derivative

$$\partial\tilde{\Delta}/\partial t = -2.3eV\frac{\eta}{L}\Delta_0\left(1 - \frac{\tilde{\Delta}}{\Delta_0}\right)^{1/4} \tag{2.31}$$

so that for $\tilde{\Delta}$ close to Δ_0, the voltage $V = RI$. since mainly normal current flows through the contact (I is a given value of the total current through the contact).

To find D_ε one should also know the dependence of the order parameter on coordinates. Let us assume that near the edges the value Δ^2 linearly depends on coordinates, while it is constant elsewhere. Then, using eq. (2.8) and taking into account eq. (2.31) we get

$$D_\varepsilon = 0.1\frac{\eta}{L}e^2 IR\bar{V}\Delta_0\left(1 - \frac{\varepsilon}{\Delta_0}\right)^{-1/4}. \tag{2.32}$$

We see that for ε close to Δ_0 the energy diffusion coefficient strongly increases and this causes the stabilization of equally populated levels (2.26) in some region of energies close to Δ_0 even at low voltages $\bar{V}$.

The limiting nonequilibrium distribution function can be found from the kinetic equation (2.7) by setting its left-hand side (relaxation term) equal to zero:

$$F(\varepsilon) = C\int_0^\varepsilon D_\varepsilon^{-1}\,\mathrm{d}\varepsilon \tag{2.33}$$

where the constant C is found from the linkage condition at $\varepsilon = \Delta_0$ with the equilibrium value ($\Delta_0/2T$). By substituting expression (2.32) for $D_;$ into this formula, we have

$$F(\varepsilon) = \frac{\Delta_0}{2T}\left[1 - \left(1 - \frac{\varepsilon}{\Delta_0}\right)^{5/4}\right] \tag{2.34}$$

where the second summand is written with accuracy up to a numerical coefficient, since for a precise determination using eq. (2.33) one must know D_z at all the energy values.

The expression (2.34) for $F(\varepsilon)$ thus derived shows that deviations of the distribution function from the constant value $(\Delta_0/2T)$ are, for ε close to A_0, smaller than $(\Delta_0 - \varepsilon)$. Therefore, we can state that the nonequilibrium additional term $F(\varepsilon) - \tanh(\varepsilon/2T) \approx (\Delta_0 - \varepsilon)/2T$ is positive, this corresponding to an insufficiency of quasiparticles and superconductivity stimulation in the contact. The nonequilibrium term in the Ginzburg-Landau equation is then also positive and is given by (2.29).

Let us now estimate the voltages at which eq. (2.29) gives the correct value of the nonequilibrium term for values of Δ not close to Δ_0 as well. For this it is necessary for the limiting expression (2.26) for $F(\varepsilon)$ to be also applicable in the region $\varepsilon \lesssim \Delta_0$. Let us find, with the help of perturbation theory, the correction F^1 to the limiting distribution function. By substituting the limiting expression (2.26) into the left-hand side of the kinetic equation (2.7) and using the expression (2.32) for $D(\varepsilon)$ we obtain up to a numerical coefficient

$$F^1 = -\frac{\hbar L}{e^2\eta}\frac{1}{\tau_\varepsilon \bar{V}}\frac{\Delta_0^2}{TIR}\left(1 - \frac{\varepsilon}{\Delta_0}\right)^{5/4}. \tag{2.35}$$

For ε close to Δ_0 this correction is always small. However, for it to be small as compared to the limiting value $\Delta_0/2T$ at $\varepsilon \lesssim A_0$ the voltage $\bar{V}$ must satisfy the condition

$$\bar{V} > \left(\hbar/e^2\tau_\varepsilon\right)(L/\eta)\left(\Delta_0/IR\right). \tag{2.36}$$

When this condition is fulfilled, formula (2.29) gives the correct order of magnitude for the nonequilibrium term for values of Δ not close to Δ_0 as well.

Let us discuss the shape of the CVC of the contact. It considerably differs from hyperbolic for $2L > \eta$ when the nonequilibrium effects are taken into account. In fact, the nonequilibrium effects lead to a considerable increase of the maximum superconducting current I_s^* which can flow through the contact. The current is determined by maximizing the right-hand side of eq. (2.30), the maximum being necessarily reached at some value $\tilde{\Delta} < \Delta_0$ (the right-hand side vanishes for $\tilde{\Delta} = 0$ and $\tilde{\Delta} = \Delta_0$, while in the intermediate region it is positive). Using eq. (2.29) for I_s^* we obtain (up to a numerical coefficient):

$$I_s^* = 0.4evSD^{1/2}{A_0}^{5/2}/\hbar^{3/2}T. \tag{2.37}$$

This value for $2L > \eta$ is always higher than the critical current of the contact I_c (it is L/η times higher for short contacts, $\eta < 2L < \xi$, and $\tau^{-1/4}$ times more for long ones, $2L > \xi$).

Thus already at low voltages, determined by expression (2.36), the current through the contact considerably increases and becomes close to I_s^*. When the voltage is increased further, the current grows slowly, since its change is caused only by the increase of the normal component. A plateau and a typical shoulder* (fig. 4) appear on the CVC. The voltage corresponding to the

inflexion point can be obtained by substituting the current value (2.37) into expression (2.36). For short contacts, $\eta < 2L < \xi$, this value does not depend on the contact's characteristics:

$$V^* \sim \hbar T/e\tau_\varepsilon\Delta_0$$

The dynamic picture of the Josephson effects in the plateau region is the following. During the greater part of the period the superconducting current close to I_s^* flows through the contact accompanied by a relatively weak normal current. The value of the superconducting current is determined by the phase difference of the order parameter within the banks. Near the maximum value the superconducting current I_s quadratically depends on the phase difference, and for the total current I through the contact one has the equation

[0]*The term "a shoulder" is used for describing the shape of the $I(V)$ characteristic and the term "a foot" is used in the case of a $V(I)$ characteristic. Here we use the term "a shoulder".

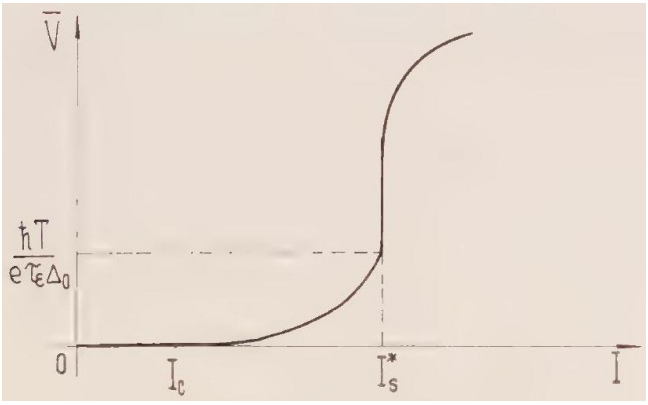


Fig. 4. The current-voltage characteristic of the bridge with length $2L > \eta(T)$ (nonequilibrium effects are taken into account).

$$I = \frac{\hbar}{eR}\dot{\chi}_0 + I_s^* - I_s^* \frac{4\eta^2}{L^2}\left(\chi_0 - \chi_0^{\max}\right)^2 \tag{2.38}$$

where $\chi_0^{\max}$ is the value of the phase difference corresponding to the maximum superconductivity current. The first term corresponds to the normal current through the contact, determined by Ohm's law, the derivative $\hat{c}^2 I_s/\partial\chi_0^2$ in the last summand is found with accuracy up to a numerical coefficient [using eqs. (2.5) and (2.30)].

The solution of equation (2.38) is of the form

$$\chi_0 - \chi_0^{\max} = \frac{L}{2\eta}\left(\frac{I - I_s^*}{I_s^*}\right)^{1/2} \tan\left(\frac{2eR}{\hbar}\frac{\eta}{L}\left[I_s^*\left(I - I_s^*\right)\right]^{1,2} t\right) \tag{2.39}$$

As seen from eq. (2.39), for I close to I_s^* the phase χ in fact hardly changes for the greater part of the period and it is mainly the superconducting current which passes through the contact; this justifies the use of eq. (2.38) in the expansion of the superconducting current in terms of the phase difference values.

The rare pulses of normal current result in the appearance of a voltage on the contact. However, the shape of the pulses can not be obtained from eq. (2.38) [one needs to know the precise form of the dependence $I_s(\chi_0)$], while the mean voltage is expressed in terms of the oscillation frequency by means of the Josephson relation:

$$\bar{V} = \hbar\omega/2e = (\eta/L)R\sqrt{I_s^*\left(I - I_s^*\right)} \tag{2.40}$$

Thus, in the high-voltage range a new term is added to the current I_s^*; it depends quadratically on the voltage.

The law describing how the current reaches the plateau from the low voltage range may be obtained using eq. (2.35) which gives a correction to the limiting distribution function. After using this and eq. (2.3) to calculate the correction of the non-equilibrium term $\Phi(\Delta)$ and then using formula (2.30), we obtain the
correction to the maximum current

$$I - I_s^* \approx -\left(\Delta_0 L/e^2\eta R\right)\left(\hbar/\tau_\varepsilon \bar{V}\right). \tag{2.41}$$

This implies that with increasing voltage the current approaches the value of I_s^* according to a hyperbolic law.

The current-voltage characteristic of the bridge at $2L > \eta$ is shown in fig. 4. The temperature dependence of the inflexion point and the shape of the CVC in the plateau region are in

good agreement with the experimental data of Octavio et al. (1978) Gubankov et al. (1977) and Divin and Nad' (1978) (see ch. 1).

15.3 3. Short bridges, $2L < \eta(T)$

In this case we shall use the microscopic equations for the 4×4 matrix Green function (see ch. 4)*. The components of the matrix $\hat{G}$ are 2×2 matrices of the retarded, G^{R} (advanced, G^{A}) Green functions determining the system's spectrum, as well as the matrix $\hat{G}$ determining the kinetic properties of the system. The matrix $\hat{G}$ may be expressed in terms of the quasiparticles' distribution functions $F^{(L)}$ and $F^{(T)}$ as follows (Larkin and Ovchinnikov 1975, 1977)

$$\hat{G} = \hat{G}^{\mathrm{R}}\hat{F} - \hat{F}\hat{G}^{\mathrm{A}}, \quad \hat{F} = F^{(\mathrm{L})}\hat{1} + F^{(\mathrm{T})}\hat{\sigma}_2. \tag{3.1}$$

Here $\hat{\sigma}_z$ is the Pauli matrix. The function $F^{(L)}$ characterizes the symmetrical part of the populations of the excitation spectrum branches. It determines the gap in the spectrum and in the equilibrium case is equal to $F_{\mathrm{eq}}^{(\mathrm{L})} = \tanh(\varepsilon, 2T)$. The function $F^{(T)}$ describes the energy distribution of the population imbalance of the electron-like and hole-like branches of the quasiparticles' spectrum. It determines the electric potential φ [in the general case the gauge invariant potential $\phi = e\varphi + (\hbar/2)(\hat{C}\chi/\hat{C}t)$] and equals zero in the equilibrium case.**

For the functions $F^{L/I'}$ the corresponding kinetic equations may be obtained (see ch. 4). However, in the present case of short bridges it is easier to use directly the original equations, rather than to apply the presentation of $\hat{G}$ in the form (3.1). Then, providing the condition (1.14) is fulfilled, in the equation for the anisotropic part of $\hat{G}$ determining the current, one can neglect all the terms except the gradient. Then we obtain:

$$\frac{\partial \hat{G}_1^{\mathrm{R(\ A)}}}{\partial x} = 0, \quad \frac{\partial \hat{G}_1}{\partial x} = 0. \tag{3.2}$$

The terms neglected are small with respect to the parameters L^2A/D and $L^2/D\tau_\varepsilon$, where τ_ε is the energy relaxation time. This implies that the anisotropic components $\hat{G}_1^{\mathrm{R(A)}}$ and $\hat{G}_1$ do not depend on x :

$$\hat{G}_1^{\mathrm{R(\ A)}} = \hat{C}^{\mathrm{R(\ A)}}, \quad \hat{G}_1 = \hat{C} \tag{3.3}$$

In order to determine the dependence on time of the matrices $\hat{C}^{\mathrm{R(A)}}$ and $\hat{C}$, we shall use the exact normalization relation (see Appendix 2.1), which should be written at the points $x = \pm L$ where all the functions except $\hat{C}^{\mathrm{R(A)}}$ and $\hat{C}$ are known. Thus we shall express the matrix $\hat{C}$ in terms of the functions in the banks. Similarly, the current I is determined by the values of the order parameter in the banks.

The normalization relation describes, in particular, the energy relaxation which will prove to be significant for quasiparticles with energies (1.15). The total current I is expressed through the matrix $\hat{C}$ by means of the formula

$$I(t) = -\frac{1}{LR}\int_0^\infty \mathrm{d}\varepsilon\, \mathrm{Tr}\left(\hat{\sigma}_z\hat{C}\right) \equiv -\frac{1}{LR}\int_0^\infty \mathrm{d}\varepsilon C_z(\varepsilon, t) \tag{3.4}$$

One cannot find the matrix $\hat{C}$ for arbitrary voltages V (and hence, for the frequencies ω), since to do this one has to solve a complicated integral equation. It is, however, possible in the limiting cases when V is small as compared to Δ_0 and for high voltages V. For small V one can use the equilibrium expansion in V/Δ_0 i.e. one can consider the function G to be slightly

[0]*This section is based on the results of Artemenko, Volkov and Zaitsev (1979).

**For more detail see the reviews by Artemenko and Volkov (1979), Pethik and Smith (1979), and Schmid (1981).

changed for the period of time of the order of Δ_0^{-1}. At higher voltages $V \gg A_0$ one can carry out the expansion of all the functions in a power series in Δ_0/V and then find the sum of the principal terms of the series.

15.3.1 3.1. Small voltages, $V \ll \Delta_0$; temperatures close to T_c

Now let us consider the case of small voltages V [respectively, the case of the frequencies $\omega = (2e/\hbar)V], V \ll \Delta_0$. We shall restrict the temperatures to those close to the critical one T_c since only then the characteristic frequency of the Josephson oscillations $\omega_c = (2e/\hbar)V_c$ (where $V_c = I_c R = \pi\Delta_0^2/4T$) will be less than Δ_0. For a given current $I \gtrsim I_c$ the harmonics in the spectrum of the Josephson oscillations have approximately the same value. However, to realize bias voltage conditions is very difficult since the resistance of the bridge is rather low. At the same time, the temperature T should not be too close to T_c since we shall assume the smearing of the density of states due to the inelastic processes to be small. This implies the restriction $\Delta_0\tau_\varepsilon \gg 1$.

The Green function determining the current, $\hat{G}_1$, is represented as a sum of two parts: the regular, $\hat{C}^{(r)}$, and anomalous, $\hat{C}^{(a)}$, parts. The first of them differs from zero for currents $I < I_c$ (i.e. in the equilibrium case) as well. When
substituting $C_=^{(r)}$ into eq. (3.4) we obtain the ordinary Josephson current* (see eq. 1.6).

The form of the anomalous function $C_z^{(a)}$ essentially depends on energy. When the quasiparticles' energy exceeds the energy gap in the banks ($\varepsilon > A_0$), then the form of $C_=^{(a)}$ at $\varepsilon \sim T$ is the same as that in the normal state at a given current. Integrating $C_=^{(4)}$ over the energy region $\varepsilon \sim T$ gives the ordinary Ohmic current V/R.

When the quasiparticles' energy is within the range determined by (1.15), the form of the function $C_=^{(a)}$ depends on the energy relaxation time, while its value is anomalously large. The high value of $C_z^{(a)}$ is caused by the slow relaxation of the quasiparticles confined inside the region $|x| < L$ (rather than inside the region determined by the inequality $\varepsilon \geqslant \Delta(x,t)$ in the previous section, since in this case the quasiparticles could move in the "forbidden" region $\tilde{\Delta} < \varepsilon < \Delta(x,t)$ as well!). Hence, the relaxation of these quasiparticles occurs either because of inelastic processes, or due to their expulsion into the energy region $\varepsilon > \Delta_0$. The current. Integrating $C_:^{(a)}$ over the energy region $\varepsilon \sim T$ gives the ordinary Ohmic "anomalous") is equal to

$$I^{(a)} = I_c P\{\chi_0\}, P\{\chi_0\} = \frac{\sin(2\chi_0)}{2}\int_0^1 \frac{k^3\,\mathrm{d}k}{\sqrt{1-k^2}\sqrt{1-k^2\sin^2\chi_0(t)}} \times \int_{-\infty} \mathrm{d}\theta \frac{\mathrm{d}\%_0(\theta)}{\mathrm{d}\theta}\frac{\sin(2\%_0(\theta)}{\sqrt{1-k^2\sin^2\chi_0(\theta)}}\exp\left(\frac{\theta-t}{\tau_c}\right) \tag{3.5}$$

The total current through the bridge equals

$$I = I_c\sin(2\chi_0) + \frac{V}{R} + I_c P\{\chi_0\} \equiv I_c\widetilde{P}\{\chi_0\} + \frac{\hbar}{eR}\frac{\partial\chi_0}{\partial t}. \tag{3.6}$$

The anomalous current $I_c P\{\chi_0\}$ in eq. (3.6) gives the deviation from a simple resistive model (see formula eq. 1.6). This deviation does not depend on the bridge length L [certainly, provided the condition (1.14) is fulfilled] and is determined by the ratio between the inverse time of the energy relaxation $\nu_i \equiv \tau_\varepsilon^{-1}$ and the characteristic frequency of the phase difference's variation $2\%_0(t)$. Let us consider the limiting cases
(a) $\lambda \equiv V_c\tau_\varepsilon = (\pi\Delta_0^2\tau_\varepsilon/4T) \ll 1$.

This means, that at $V \lesssim V_c$ the oscillations in the bridge proceed slowly in the time scale τ_ε. At voltages satisfying the condition $V \ll v' = V_c$ i. the functions depending on $\%(\theta)$ in (3.5) can be taken out from under the integral sign [by

substituting $\chi_0(\theta)$ for $\chi_0(t)$] and after integration over k one obtains

$$P\{\chi_0\} = \frac{\partial\chi_0}{\partial t}\tau_\varepsilon \cot\chi_0 \left(2[\chi_0] - \sin(2\chi_0)\right)$$
$$= \frac{\partial\chi_0}{\partial t}\tau_\varepsilon \sum_{n=0}^{\infty} b_n \cos(2n\chi_0) \tag{3.7}$$

Here $[\chi_0]$ is a function with period π, which is equal to χ_0 at $|\chi_0| < \pi/2$, $b = 21\mathrm{n}2 - 1 \simeq 0.39$, and $b_1 = 41\mathrm{n}2 - 3 \simeq -0.23$.
The first term of the series in eq. (3.7) determines the changes of the contact resistivity, the rest gives a contribution to the interference current.

The form of the CVC is found using the formula

$$V = \pi \left[\int_{-\pi/2}^{\pi/2} \mathrm{d}\chi_0 \left(\frac{\partial\chi_0}{\partial t}\right)^{-1}\right]^{-1}. \tag{3.8}$$

The integral can be calculated by substituting $\partial\chi_0/\partial\mathrm{t}$ from (3.6) and (3.7) into (3.8) and integrating over the complex plane. Then we obtain:

$$V = R\left(I^2 - I_c^2\right)^{1/2}\left[1 + \lambda u\left(I/I_c\right)\right]^{-1}, \tag{3.9}$$

where

$$u(a) = \frac{\sqrt{a^2-1}}{a}\ln\frac{2\left(a+\sqrt{a^2-1}\right)}{a} + \frac{1}{a}\operatorname{arctg}\frac{1}{\sqrt{a^2-1}} - 1$$

The difference between the CVC and the resistive model, determined by the factors in the brackets, is small because i is small. For $I \gg I_c$ the asymptotic resistance of the bridge, $R_{as} = R\{1 + \lambda(21\mathrm{n}2 - 1)\}^{-1}$ decreases slightly due to the contribution of the quasiparticles with energies (1.15).

At voltages $V \gg \nu_r$, the functions in eq. (3.5) containing $\chi_0(\theta)$ oscillate rapidly in time. Therefore, one can integrate eq. (3.5) over time θ considering the exponent as constant and subtracting from the expression obtained its timeaveraged value*. Then for $P\{\chi_0\}$ we obtain:

$$P\{\chi_0\} = \sin(2\chi_0)\left\{\int_0^1 \mathrm{d}k \frac{k}{\sqrt{1-k^2}} \frac{\left\langle\sqrt{1-k^2\sin^2\chi_0}\right\rangle_t}{\sqrt{1-k^2\sin^2\chi_0}} - 1\right\}. \tag{3.10}$$

The averaging over time is carried out using the function ($\hat{c}\chi_0/\hat{c}t$), which can be expressed from eq. (3.6):

$$\left\langle\sqrt{1-k^2\sin^2\chi_0}\right\rangle_t = \frac{V}{\pi}\int_{-\pi/2}^{\pi/2} \frac{\left(1-k^2\sin^2\chi_0\right)^{1/2}\,\mathrm{d}\chi_0}{\mathrm{d}\chi_0/\mathrm{d}t}$$
$$= \frac{V}{\pi R}\int_{-\pi/2}^{\pi/2} \frac{\left(1-k^2\sin^2\chi_0\right)^{1/2}\,\mathrm{d}\chi_0}{\mathrm{I} - I_c\tilde{P}\{\chi_0\}}. \tag{3.11}$$

[0]*The derivation of the equations required can be found in the article by Artemenko et al. (1979a) and in Appendix 2.

[0]*The last circumstance was not taken into account by Schmid et al. (1980), which resulted in their conclusion concerning rather strong stimulation of superconductivity in short bridges.

In the limiting case $\lambda \ll 1$ considered, the inequality $V \gg \nu_\varepsilon$ means that $I \gg I_c$. Then, neglecting the term $I_c \widetilde{P}\{\chi_0\}$ in eq. (3.11), we obtain

$$\left\langle \sqrt{1 - k^2 \sin^2 \chi_0} \right\rangle_t = \frac{2}{\pi} E(k),$$

where $E(k)$ is the complete elliptic integral. By substituting this expression into eq. (3.10), we find for the current

$$I = \frac{\hbar}{eR} \frac{\partial \chi_0}{\partial t} + I_c \frac{2}{\pi} \sin(2\chi_0) \int_0^1 \mathrm{d}k \frac{kE(k)}{\sqrt{1-k^2}\sqrt{1-k^2\sin^2\chi_0}} \tag{3.12}$$

Thus, at high oscillating frequencies, the anomalous current $I^{(a)}$ becomes nondissipative and does not depend on τ_ε. Here, the dependence $\widetilde{P}\{\chi_0\}$ differs from sinusoidal (see fig. 5). This implies that upon irradiation of the bridge

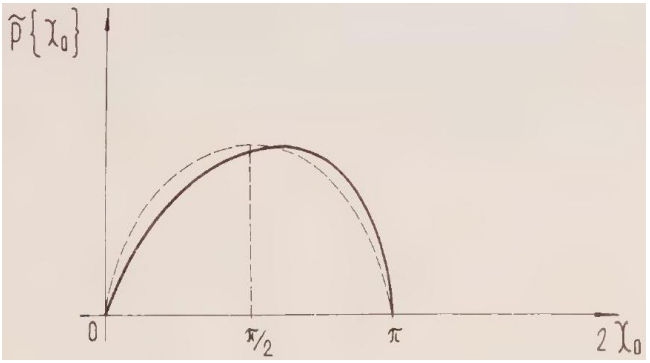


Fig. 5. The curve $P\left(\chi_{0}\right)$ obtained by numerical calculation of the integral in (3.12). The dots denote the function $\sin(2\chi_0)$.}

with frequency ω subharmonic current steps appear on the CVC of the bridge at voltages $2eV = (n/m)\hbar\omega$ (n and m are integers).

(b) $\lambda = \tau_\varepsilon V_c \gg 1$.

This means that during τ_ε a lot of oscillations occur in the bridge. Then practically for all V the form of the function $P\{\chi_0\}$ is determined by (3.10). By substituting (3.11) into (3.10), we obtain for $\widetilde{P}\{\chi_0\}$ the integral equation

$$\tilde{P}\{\chi_0\} = \int_{-\pi/2}^{\pi/2} \mathrm{d}\chi_1 \frac{Q(\chi_0, \chi_1)}{I - I_c \tilde{P}\{\chi_1\}} \tag{3.13}$$

where

$$Q(\chi_0, \chi_1) = \frac{V}{2\pi R} \sin(2\chi_0) \int_0^1 dk \frac{k}{\sqrt{1-k^2}} \left[\frac{1-k^2\sin^2\chi_1}{1-k^2\sin^2\chi_0}\right]^{1/2}$$

and the voltage V is determined by eq. (3.8). Thus, for $\lambda \gg 1$ the very form of $\tilde{P}\{\chi_0\}$ depends on the current value I.

When $I \gtrsim I_c$, then the function $\tilde{P}\{\chi_0\}$ can apparently be found only numerically. However, we can make some conclusions about the form of the CVC. Let the voltage V range within the interval $v_r \ll V \ll V_c$. Then the main contribution to the integral (3.8) is determined by a region near the maximum of the function $\widetilde{P}\{\chi_0\}$, which can be expanded in this region as follows:

$$\tilde{P}(\chi_0) = \tilde{P}\{\chi_m\} - \frac{1}{2}\left|\tilde{P}_{//}\right|(\chi_0 - \chi_m)^2 .$$

Then, from (3.13) we can find

$$\widetilde{P}\{\chi_0\} = \sin(2\chi_m)\int_0^1 \frac{k\ \mathrm{d}k}{\sqrt{1-k^2}}\left[\frac{1-k^2\sin^2\chi_m}{1-k^2\sin^2\chi_0}\right]^{1/2} \tag{3.14}$$

The angle χ_m is determined from the equation $\partial\tilde{P}\{\chi_0\}, \hat{c}\chi_0 = 0$. Using eq. (3.14), we can find $2\chi_m = 1.92$. From eq. (3.8), we obtain the formula for the CVC

$$V = R\left[2\left|\widetilde{P}_{\chi\chi}\right|(I - 0.94I_c)\right]^{1/2} \tag{3.15}$$

Hence, at small voltages the current I is below the critical one, i.e there is a hysteresis on the CVC.

Let us also study the effect of a weak AC signal with frequency $\omega \gg v_\varepsilon$ on the critical current I_c. In this case $\chi_0(t) = \chi_c + \chi_-(t)$, where χ_c is a constant part and $\chi_\sim = \chi_1\sin(\omega t)$ is a small variable part. The current is found from the expressions (3.6) and (3.10):

$$\begin{aligned} I =& \frac{\hbar}{eR}\frac{\partial\chi_-}{\partial t} + I_c\sin(2\chi_0(t)) \\ &+ I_c\sin(2\chi_0)\int_0^1 \mathrm{d}y\frac{\overline{q(\chi_0,y)} - q(\chi_0,y)}{q(\chi_0,y)} \end{aligned} \tag{3.16}$$

where

$$q(\chi_0,y) = \left[\left(1+y^2\right) + \left(1-y^2\right)\cos(2\chi_0)\right]^{1/2}$$

while the averaging is performed over the period $2\pi,\omega$. Let us expand this expression in powers of χ_1 up to second order, average it over time and put $\chi_0 = \pi/2$. Then we obtain

$$I_{max} = I_c\left(1 - \frac{1}{4}\pi\chi_1^2\right)$$

Hence, in this case, a weak AC signal leads to the suppression of I_c, as was the case for the resistive model. It is of interest to note, however, that the anomalous current $I^{(a)}$ under the influence of radiation leads to the stimulation of the superconducting current:

$$I_c\overline{P\{\chi_0\}} = I_c\left(2 - \frac{1}{4}\pi\right)\chi_1^2.$$

However, the "Josephson" suppression $I_c\overline{\sin(2\chi_0)} = I_c(1-2\chi_1^2)$ proves to be stronger. In longer bridges ($2L > \eta$), the stimulation of I_c proves to be proportional to the parameter $I_c(2L/\eta)$ and is large as compared to I_c. Here we can neglect the suppression of the maximum current by the superconducting current for the radiation powers considered.

The question concerning the effect of strong radiation on the current I of a short bridge was not considered.

15.3.2 3.2. The form of the distribution functions

Let us discuss the form of the distribution functions $F^{(L)}$ and $F^{(T)}$ (see eq. 3.1); this will enable us to clarify the physical background of the processes taking place*. For energies $\varepsilon > A_0$, the function $F^{(T)}$ describing the distribution of the potential Φ is determined (see Appendix 2.2) by the formula:

$$F^{(\mathrm{T})} = \frac{\partial\chi_0}{\partial t}\frac{\sqrt{\varepsilon^2-\widetilde{\Delta}^2}}{2T\Delta_0\sin\chi_0}\tanh\left[\frac{x}{L}\operatorname{arcsinh}\frac{\Delta_0\sin\chi_0}{\sqrt{\varepsilon^2-\Delta_0^2}}\right]\cosh^{-2}(\varepsilon/2T).$$

At higher energies ($\varepsilon \gg \Delta_0$) the function $F^{(T)}$ has the same form as in the normal state,

$$F^{(T)} \simeq \frac{\partial\chi_0}{\partial t}\left(\frac{x}{2L}\right)\cosh^{-2}(\varepsilon/2T);$$

the Ohmic current V/R is proportional to the integral over energies of the gradient of this function $\hat{\partial}F^{(\mathrm{T})}/\hat{\partial}x$. The function $F^{(\mathrm{L})}$ determining the order parameter Δ at $\varepsilon > \Delta_0$ approximately coincides with that in the equilibrium state: $F^{(\mathrm{L})} \simeq \tanh(\varepsilon/2T)$.

For energies in the interval determined by (1.15), the function $F^{(L)}$ in the bridge does not depend on x and equals

$$\begin{aligned}F^{(L)} - \tanh(\varepsilon/2T) =& \frac{(\Delta_0^2-\varepsilon^2)}{4T\left|\sin\chi_0\right|}\int_{-\infty}^{t}\mathrm{d}t_1\frac{\partial\chi_0\left(t_1\right)}{\partial t_1}\\ &\times\frac{\sin\left[2\chi_0\left(t_1\right)\right]\exp\left[\left(t_1-t\right)/\tau_\varepsilon\right]\operatorname{sgn}\varepsilon}{\left[\Delta_0^2\sin^2\chi_0(t)-(\Delta_0^2-\varepsilon^2)\sin^2\chi_0\left(t_1\right)\right]^{1/2}}\end{aligned} \tag{3.17}$$

It follows from (3.17) that the deviation of the distribution function $F^{(L)}$ from the equilibrium $\tanh(\varepsilon/2T)$ tends to zero at $\varepsilon \to \Delta_0$, i.e. the function $F^{(L)}$ is continuous at $\varepsilon = \Delta_0$. Let us determine the explicit form of the function $F^{(\mathrm{L})}$ at $V\tau_\varepsilon \ll 1$. By performing the integration in (3.17) in the same way as it was done in section (3.1) we find

$$\begin{aligned}F^{(\mathrm{L})} - \tanh\left(\frac{\varepsilon}{2T}\right) &= \tau_\varepsilon\frac{\partial\chi_0}{\partial t}\frac{\Delta_0^2-\varepsilon^2}{2T\varepsilon}\cot\chi_0\\ &= \frac{\Delta_0^2-\varepsilon^2}{T\varepsilon} - \frac{\tilde{\Delta}^2\left(\tau_\varepsilon \mathrm{V_c}\right)}{\Delta_0^2\sin\left(2\chi_0\right)}\left[\frac{I}{I_\mathrm{c}}-\sin\left(2\chi_0\right)\right].\end{aligned} \tag{3.18}$$

We have substituted here the expression for $\partial\chi_0/\partial t$ from eqs. (3.6) and (3.7) and neglected the small summand containing λ. Since

$$F^{(\mathrm{L})} - \tanh\frac{\varepsilon}{2T} = -2\delta n$$

where δn is the variation of the quasiparticles' population number, equation (3.18) implies that a decrease of the energy gap in the center of the bridge $\tilde{\Delta}$ leads to the rarefication of the quasiparticle gas ($\delta n < 0$), while an increase of the gap $\tilde{\Delta}$ leads to the compression of the quasiparticle gas ($\delta n > 0$). Indeed, when $I > 0$, the phase χ_0 increases with time, $\chi_0 \sim It$, while the gap in the center of the bridge $\tilde{\Delta} = \Delta_0\left|\cos\chi_0\right|$ decreases for $0 < \chi_0 < \pi/2$ [then $\sin\left(2\chi_0\right) > 0$] and increases for $-\frac{1}{2}\pi < \chi_0 < 0$ [then $\sin\left(2\chi_0\right) < 0$]. Thus, there is much in common in the processes occurring in short bridges ($2L < \eta$) and in longer ones ($2L > \eta$). The difference is that the distribution function in short bridges ceases to depend on τ_ε at

[0]*It should be noted, that the function $F^{(L)}$ coincides with the function $F(\varepsilon)$ of section 2.

voltages which are high as compared to V_c, and the anomalous current becomes of the order of magnitude of the Josephson current. In bridges with length $2L > \eta$, the distribution function reaches the limiting form (it does not depend on τ_ε) at voltages higher than (T/Δ) v_ε, while the superconducting current increases as much as (L/η) times.

15.3.3 3.3. High voltages, $V > \Delta_0$; arbitrary temperatures

As we mentioned in the Introduction, at $V \gg \Delta_0$ the function G_1 can be found by taking the sum of a power series in Δ_0/V. The formulas for current in this case resemble the corresponding expressions in the case of tunneling junctions (Larkin and Ovchinnikov 1966, Werthamer 1966).

The oscillating components of the current has the form

$$I_{\rm osc} = I_1 \sin(2Vt) + I_2(V) \cos(2Vt), \tag{3.19}$$

where

$$I_1 \sim (\Delta_0/V)\,, \quad I_2 \sim (\Delta_0/V) \ln (V/\Delta_0) \qquad \text{at} \qquad \Delta \sim T.$$

Thus, the amplitudes of the Josephson current components in the bridge decrease with an increase of the voltage V.

As for the direct current $I_{\rm DC}$ through the bridge (contact), here differences appear with respect to the tunneling junctions. The expression for I_{DC} can be obtained by summing the series in formula (A.2.4). Also using the formula (3.4) after a number of rather tedious calculations we obtain:

$$\begin{aligned} I_{\rm DC} =& \frac{1}{2R} \int \mathrm{d}\varepsilon N_{\rm s}(\varepsilon + v) N_{\rm s}(\varepsilon - v) \\ & \times \left[D(\varepsilon + v) + D(\varepsilon - v) - 1 \right] \left\{ \tanh\left(\frac{\varepsilon + v}{2T} \right) - \tanh\left(\frac{\varepsilon - v}{2T} \right) \right\} \end{aligned} \tag{3.20}$$

Where $v = V/2$, and

$$\begin{aligned} D(\varepsilon) &= \left[\operatorname{arcsinh} f^{\rm R}(\varepsilon) - \operatorname{arcsinh} f^{\rm A}(\varepsilon) \right] \left[f^{\rm R}(\varepsilon) - f^{\rm A}(\varepsilon) \right]^{-1}, \\ N_{\rm s}(\varepsilon) &= \varepsilon \left(\varepsilon^2 - \Delta^2 \right)^{-1/2} = \frac{1}{2} \left[g^{\rm R}(\varepsilon) - g^{\rm A}(\varepsilon) \right]. \end{aligned}$$

The expression (3.20) resembles that for the quasiparticle current through the tunnel junction. The integrand is the product of the density of states in the banks $N_{\rm s}$, shifted with respect to each other along the energy scale by the value V, and the difference of the distribution functions, shifted by V as well. The difference from the tunneling junction consists in the appearance of the factor in the square brackets, which can be given the name of the "tunneling probability" $P(\varepsilon)$. The coefficient $P(\varepsilon)$ has a singularity at $|\varepsilon \pm v| < \Delta$, since here $f^{\rm R} = f^{\rm A}$, while the numerator in D differs from zero when tracing the points of branching from above (in $f^{\rm R}$) and from below (in $f^{\rm A}$). The product $N_{\rm s}(\varepsilon + v) N_{\rm s}(\varepsilon - v) P(\varepsilon)$ differs from zero at all energies, i.e. all the states contribute to the current, including those under the gap. This is clear from the physical point of view, since in the presence of a channel with direct conductivity, quasiparticles with energy $\varepsilon < A$ also contribute to the current. Such quasiparticles, moving in the bridge, transform themselves in the banks into Cooper pairs [in the pure case this process corresponds to the Andreev reflection (Andreev 1964)].

The contribution to conductivity of the states with the energy $|\varepsilon \pm v| \lesssim \Delta$ results in an excess current. Let us calculate the integral in (3.30), taking into account the fact that

$$\left(f^{\mathrm{R}}-f^{\mathrm{A}}\right)D(\varepsilon)=\ln\left(\frac{\varepsilon+\Delta}{\varepsilon-\Delta}\right)\theta(|\varepsilon|-\Delta)+\ln\left(\frac{\Delta+\varepsilon}{\Delta-\varepsilon}\right)\theta(\Delta-|\varepsilon|),$$

$$\left(g^{\mathrm{R}}-g^{\mathrm{A}}\right)\left(f^{\mathrm{R}}-f^{\mathrm{A}}\right)^{1}=\frac{\varepsilon}{\Delta}\theta(|\varepsilon|-\Delta)+\frac{\Delta}{\varepsilon}\theta(\Delta-|\varepsilon|).$$

$$\theta(x)=1,\quad x>0\quad\text{and}\quad\theta(x)=0,\quad x<0.$$

We obtain:

$$I_{\mathrm{DC}}=\frac{V}{R}+I_{\mathrm{exc}}\tanh\left(\frac{eV}{2T}\right),\quad I_{\mathrm{exc}}=\frac{\Delta_0}{eR}\left(\frac{1}{4}\pi^2-1\right)\tag{3.21}$$

The second term in (3.20) describes the excess current, which does not depend on voltage at $V>(\Delta_0,T)$. The value of I_{exc} is considerably higher than I_{c} near T_{c}, and $I_{\mathrm{exc}}\sim I_{\mathrm{c}}$ at $T\ll T_{\mathrm{c}}$. The formula (3.21) correlates well with experimental data (see ch. 1).

The excess current appears also in the contact $\mathrm{S}-\mathrm{c}-\mathrm{N}$ (c is the constriction) where its value is two times smaller (Artemenko et al. 1979b). In the case of a $\mathrm{S}_1-\mathrm{c}-\mathrm{S}_2$ contact the gap Δ_0 in (3.21) should be replaced by $(\Delta_1+\Delta_2)/2$ (Artemenko et al. 1981).

The expression (3.21) and the analysis carried out in the previous subsection, makes it possible to represent the form of the CVC of the short bridge or that of the contact at $V<A_0$ and $V>A_0$. Fig 6 shows the form of the CVC of the short bridge at $\Delta/T\ll 1$ and $\tau_\varepsilon V_{\mathrm{c}}\ll 1$. In this case, according to (3.9) at low voltages ($V<\Delta_0$) the CVC practically does not differ from the hyperbola obtained for the resistive model. At voltages $V>A_0$, the excess current appears and the form of the CVC is determined by (3.21).

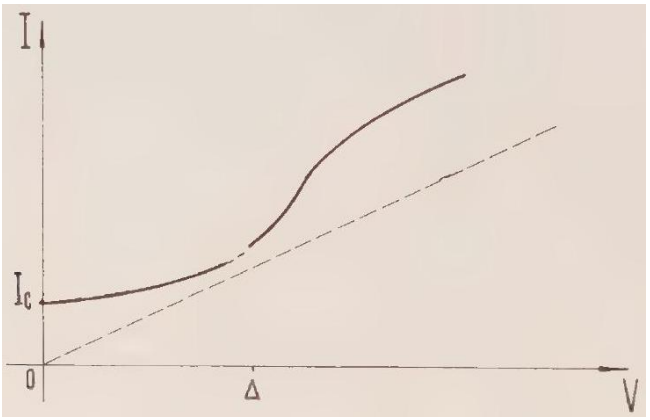


Fig. 6. Form of the current-voltage characteristic of a bridge of length $2L<\eta(T)$ in the high- and low-voltage regions; $\left(e \tau_{\varepsilon V_{\mathrm{c}}} \hbar^{-1}\right)<1,\left(\Delta_{0} / T\right)<1$). The dots show the CVC corresponding to the resistive model. The straight line shows Ohm's law.}

15.3.4 3.4. Bridges with low impurity content (pure case)

A stationary Josephson phenomenon in pure contacts was considered by Kulik and Omelyanchuk (1977). They have assumed the following model of the contact: in a thin, impenetrable screen there exists an orifice with diameter d much smaller than the correlation length $\check{\zeta}(0)$ and the mean free path l. A theory of the nonstationary Josephson effect within the framework of this model was constructed by Zaitsev (1980)*. The conclusions of the theory in the pure case qualitatively agree with those obtained for "dirty" contacts; in

particular, at $V \ll \Delta$ and $\Delta \ll T$ the current is determined by eq. (3.6), in which the functional $P\{\chi_0\}$ has the form

$$P\{\chi_0\} = \frac{\sin(2\chi_0)}{2|\cos\chi_0|}\int_{-\infty}^{t} d\theta \frac{\hat{\tau}\chi_0}{\partial\theta}\frac{\sin[2\chi_0(\theta)]}{|\cos\chi_0(\theta)|}\exp\left(\frac{\theta - t}{\tau_i}\right)$$

When $\lambda = \tau_\varepsilon V_c \ll 1$, then the current equals

$$I = \frac{1}{R}\frac{\partial\chi_0}{\partial t}[1 + \lambda - \lambda\cos(2\chi_0)] + I_c\sin(2\chi_0).$$

If $\lambda \gg 1$, then at $V \gg \nu_\varepsilon$

$$I = \frac{\hbar}{eR}\frac{\partial\chi_0}{\partial t} + I_c b\frac{\sin(2\chi_0)}{|\cos\chi_0|}$$

where the coefficient b is connected with the current I and voltage V by the following parametric relation

$$I = 2I_c s b(s), \quad V = 2V_c\sqrt{s^2-1}\,b(s), \tag{3.22}$$
$$b(s) = \frac{\sqrt{s^2-1}}{\pi}\ln\frac{s+1}{s-1}.$$

The formula (3.22) determines the CVC of the pure contact. Its form is shown in fig. 7. The hysteresis in the CVC of a pure contact for $\lambda \gg 1$ is more pronounced than it is in a "dirty" contact.

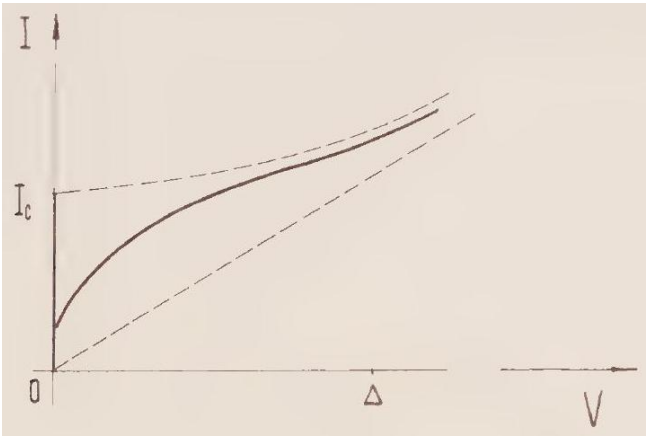


Fig. 7. The shape of the CVC of a short bridge in the low-voltage range in the case of $e \tau_{\varepsilon} V_{c} \hbar^{-1}>1$. The curve corresponds to numerical calculation using eq. (3.22) for the pure case; the straight dashed line shows Ohm's law.}

At higher voltages ($V \gg \Delta$) there is an excess current on the CVC and its value equals $I_{\text{exc}} = \frac{8}{3}A/eR$.

Thus, in a pure contact the value of I_{exc} exceeds that in a "dirty" one.

[0]*In this work a theory of the pure S − c − N contact is also given. An excess current in a pure S -c-N contact was also calculated by Dorozhkin (1980) and Klapwijk et al. (1982) with the use of simple physical ideas.

15.4 4. Discussion

The analysis carried out has shown that in S-c-S systems, in contrast to tunneling junctions, nonequilibrium processes are of importance. This is mainly due to the contribution to conductivity of quasiparticles confined in the bridge or contact, i.e. those quasiparticles whose energy ranges within the interval $\tilde{A} < \varepsilon < A_0$. Such quasiparticles exercise a bounded motion in the contact, in contrast to the electrons with energies $\varepsilon > \Delta_0$, which diffuse into the banks, where equilibrium is maintained. Therefore, under nonequilibrium conditions the distribution function of the confined electrons relaxes slowly due to inelastic electron-phonon collisions only. Hence, the contribution to the current by such nonequilibrium particles is large and depends on the energy relaxation time τ_ε. Phenomena which are the result of nonequilibrium processes qualitatively differ from each other, depending upon the relative magnitudes of the bridge length $2L$ and the characteristic parameter $\eta(T)$.

For short bridges ($2L < \eta$), the confined particles contribute to the current I which is described, at small voltages ($eV < A_0$), by the functional $P\{\chi_0\}$ [see eqs. (3.5) and (3.6)]. If the characteristic frequency of the Josephson oscillations $2eV_c/\hbar = 2eRI_c/\hbar$ is low as compared to the inverse energy relaxation time $\tau_r{}^1$, then the additional current $I^{(a)}$ caused by the confined quasiparticles is dissipative. Despite the fact that the current $I^{(a)}$ is proportional to τ_e, it only results in a small increase of the bridge conductivity in this case.

When the characteristic frequency of the Josephson oscillations $2eV_c/\hbar$ is high as compared to τ_ε^{-1}, then the anomalous current $I^{(a)}$ becomes nondissipative; it does not depend on the energy relaxation time and its value is of the order of the critical current I_c. Here the dependence of the nondissipative current I_5 on the phase difference $2\%_0$ differs from the sinusoidal one (it is sinusoidal in the stationary case). A small hysteresis appears on the CVC at small voltages.

The results mentioned above were obtained by Artemenko et al. (1979a). Schmid et al. (1980) made the same qualitative conclusions about the nature of the current $I^{(a)}$: dissipative for small V_c and nondissipative for higher V_c. However, the expression they obtained for the distribution function of the confined quasiparticles at higher V_c (as compared to $h/2e\tau_n$), differs from the one given in section 3.2, and this resulted in their conclusion about stimulation and appearance of a shoulder in the CVC in short bridges of length $2L < \eta$.

An analysis of the shape of the CVC for small voltages ($V \ll \tau_\varepsilon$) was performed by Golub (1976), who also obtained a weak increase of conductivity. However, in this work he assumed the gradient terms to be small, so that the additional contribution to the bridge's conductivity contained a small parameter $[L/\xi(T)]^2$. His assumption can be justified only for longer bridges $2L > \eta(T)$. Besides, Golub did not take into account the anomalous current component $I^{(\mathrm{a})}$ which even for $2L \approx \eta(T)$ gives a greater contribution than the one he obtained.

The expression for the current I in short bridges ($2L < \eta$) at higher voltages ($eV > A_0$) resembles that for the current in tunneling junctions. The current components I_osc which oscillate in time decrease with an increase of V : $I_\mathrm{osc} \sim (\Lambda_0/V)$ as in the case of tunneling junctions; but the situation for DC current differs from the case of tunneling junctions. Besides the Ohmic component V, R, the current I_DC in a short bridge contains the so-called excess current I_exc tanh(eV/2 T), where I_exc does not depend on V. Both the excess current and the anomalous current at small voltages are determined by the contribution of quasiparticles with energy $\varepsilon \lesssim \Delta_0$. In contrast to tunneling junctions, where the states under the gap $\varepsilon \leqslant \Delta_0$ do not contribute to the current $\mathrm{I_{DC}}$, in the case of a bridge, all the states contribute to the current I_DC. This is due to the fact that, for a bridge, all the quasiparticles move under the action of the electric field, including those with energy $\varepsilon \leqslant \Delta_0$. The charge in the banks is transferred by Cooper pairs, while the quasiparticle current is converted into the pair current by the mechanism of Andreev reflection of quasiparticles (strictly speaking this is true only in the pure limit). In tunneling junctions, such a process is of the second order with respect to

transparency (the electron must go through the barrier and return back in the form of a hole); therefore the current I_{exc} will appear in tunneling junctions in higher order approximations with respect to transparency. In the bridge the number of states with energy $\varepsilon \lesssim \Delta_0$ is proportional to Δ_0, so the excess current I_{exc} here is proportional to the order parameter value. This agrees with the experimental data (see ch. 1).

When the length of the bridge $2L$ exceeds the characteristic parameter $\eta(T)$. the nonequilibrium effects may lead to stimulation of superconductivity in the contact. The stimulation occurs in an external AC field or when the value of the current in the contact exceeds some critical value (stimulation by DC current). The cause of stimulation is strong energy diffusion due to the oscillations of the order parameter (gap) in the contact, which lead to a decrease of the number of the quasiparticles in the contact and respectively to the effective decrease of temperature. As a result, a specific shoulder appears on the current voltage characteristics of the contact, while the critical current in the AC field considerably increases.

We emphasize once more that the stimulation phenomenon occur only when the length of the bridge is sufficiently large ($2L > \eta(T)$). When the critical temperature T_{c} is approached, the parameter $\eta = (D, 1_0)^{1\,2}$ increases and this
condition is necessarily violated. Near T_{c} for $2L < \eta$ the CVC is close to a hyperbola (except for the high-voltage range, where excess current is present), while the critical current in the presence of an AC field decreases (see section 3.1). This agrees with the experimental data described in ch. 1 : the shoulder on the CVC and the stimulation of the critical current are observed only at a sufficient distance from T_{c} when $2L > \eta(T)$, and, as shown by Gubankov et al. (1977) and Latyshev and Nad' (1979), the two phenomena are correlated and manifest themselves simultaneously.

Let us also discuss some of the problems which, to our mind, are of interest for further study. The question of the agreement between the experimental and theoretical data, relating to the initial part of the bridge's CVC (when $2L > \eta$) is not quite clear. In order to find the current-voltage characteristic of the bridge in the low-voltage region, one can no longer use the limiting expression (2.26) for the distribution function. Here the voltage range where perturbation theory is valid is very small; in order to find the initial part of the CVC, one has to solve the set of equations (2.2), (2.5) and (2.7) simultaneously, which can not be done analytically.

The development of the theory for the high-frequency case ($\omega > D/L^2$) is also of interest; then a transition to the uniform nonequilibrium situation, considered by Eliashberg (1970) and Ivlev (1971) should occur.

The theory developed does not take into account the suppression of superconductivity by the AC current. This suppression is not significant in the range of AC radiation powers where the nonequilibrium phenomena are manifested to their full extent (due to a great energy relaxation time), but this may lead to current oscillation on further increase of the radiation power.

As for short bridges of length $2L < \eta$, the voltage region $eV = A_0, 2A_0$ etc. remains unstudied; here singularities may appear on the CVC. Besides, the effect of a high amplitude alternating signal on the bridge (e.g. its effect on the critical current) has not been studied.

The authors are grateful to A.I. Larkin, S.N. Artemenko and A.V. Zaitsev for valuable discussions.

15.5 Appendix 1

The complete distribution function may be written as follows:

$$F = F_{00} + F_{01} + F_{10} + F_{11}, \tag{A1.1}$$

where

$$F_{00} = F(\varepsilon) = \langle \bar{F} \rangle, \quad F_{01} = \overline{F - \langle F \rangle},$$
$$F_{10} = \langle F - \bar{F} \rangle, \qquad F_{11} = F - \bar{F} - \langle F \rangle + \langle \bar{F} \rangle,$$

and the brackets $\langle \cdots \rangle$ mean averaging over the contact area in which $\Delta < \varepsilon$, while the overbar stands for averaging in time.

By analogy, one can write

$$\left(\varepsilon^2 - \Delta^2\right)^{1/2} = \left(\varepsilon^2 - \Delta^2\right)_{00}^{1/2} + \left(\varepsilon^2 - \Delta^2\right)_{10}^{1/2}$$
$$+ \left(\varepsilon^2 - \Delta^2\right)_{01}^{1/2} + \left(\varepsilon^2 - \Delta^2\right)_{11}^{1/2} \tag{A1.2}$$

where the indices mean the appropriate averaging.
By substituting the expressions (A1.1) and (A1.2) into equation (2.6) and using the momentum presentation, we obtain:

$$- Dk^2 \left(F_{01} + F_{11}\right) + \left(\frac{\partial}{\partial t} F_{10} + \frac{\partial}{\partial t} F_{11}\right) \frac{\partial}{\partial \varepsilon} \left(\varepsilon^2 - \Delta^2\right)^{1/2}$$
$$- \frac{\partial F}{\partial \varepsilon} \left[\frac{\partial}{\partial t} \left(\varepsilon^2 - \Delta^2\right)_{10}^{1/2} + \frac{\partial}{\partial t} \left(\varepsilon^2 - \Delta^2\right)_{11}^{1/2}\right] = -I_{\text{ph}}. \tag{A1.3}$$

By averaging this equation in time, we obtain

$$-Dk^2 F_{01} + \overline{\left(\frac{\partial}{\partial t} F_{10} + \frac{\partial}{\partial t} F_{11}\right) \left[\frac{\partial}{\partial \varepsilon} \left(\varepsilon^2 - \Delta^2\right)_{10}^{1/2} + \frac{\partial}{\partial \varepsilon} \left(\varepsilon^2 - \Delta^2\right)_{11}^{1/2}\right]}$$
$$- \overline{\left(\frac{\partial}{\partial \varepsilon} F_{10} + \frac{\partial}{\partial \varepsilon} F_{11}\right) \left[\frac{\partial}{\partial t} \left(\varepsilon^2 - \Delta^2\right)_{10}^{1/2} + \frac{\partial}{\partial t} \left(\varepsilon^2 - \Delta^2\right)_{11}^{1/2}\right]} = -I_{\text{ph}}. \tag{A1.4}$$

In deriving eq. (A1.4) we used the condition $\bar{F}_{11} = 0$, and also

$$\overline{\left(\frac{\partial}{\partial t} F_{10} + \frac{\partial}{\partial t} F_{11}\right) \frac{\partial}{\partial \hat{\varepsilon}} \left[\left(\varepsilon^2 - \Delta^2\right)_{00}^{1/2} + \left(\varepsilon^2 - \Delta^2\right)_{01}^{1/2}\right]} = 0,$$
$$\overline{\frac{\partial}{\partial t} \left[\left(\varepsilon^2 - \Delta^2\right)_{10}^{1/2} + \left(\varepsilon^2 - \Delta^2\right)_{11}^{1/2}\right] \frac{\partial}{\partial \varepsilon} \left(F_{00} + F_{01}\right)} = 0, \tag{A1.5}$$

the means of the total derivatives with respect to time.
By averaging eq. (A1.4) over coordinates and using the condition $\langle F_{11} \rangle = 0$. we obtain

$$\frac{\partial}{\partial t} F_{10} \frac{\partial}{\partial \varepsilon} \left(\varepsilon^2 - \Delta^2\right)_{10}^{1/2} - \frac{\partial}{\partial \varepsilon} F_{10} \frac{\partial}{\partial t} \left(\varepsilon^2 - \Delta^2\right)_{10}^{1/2}$$
$$+ \left\langle \frac{\partial}{\partial t} F_{11} \frac{\partial}{\partial \varepsilon} \left(\varepsilon^2 - \Delta^2\right)_{11}^{1/2} \right\rangle - \left\langle \frac{\partial}{\partial \varepsilon} F_{11} \frac{\partial}{\partial t} \left(\varepsilon^2 - \Delta^2\right)_{11}^{1/2} \right\rangle = -I_{\text{ph}}. \tag{A1.6}$$

Using integration by parts, eq. (A1.6) may be written in the form

$$\frac{\partial}{\partial \varepsilon} \left[\frac{\partial}{\partial t} F_{10} \left(\varepsilon^2 - \Delta^2\right)_{10}^{1/2}\right] - \frac{\partial}{\partial \varepsilon} \left\langle F_{11} \frac{\partial}{\partial t} \left(\varepsilon^2 - \Delta^2\right)_{11}^{1/2} \right\rangle = -I_{\text{ph}}. \tag{A1.7}$$

Let us show now that the first term in eq. (A1.7) equals zero (we find $\hat{\partial} F_{10} / \partial t$), and also find the expression for F_{11}. To effect this we have to subtract from (A1.3) the expression (A1.4) averaged in time and use the fact that the variable part of Δ is small. Then we obtain

$$- Dk^2 F_{11} + \left(\frac{\partial}{\partial t} F_{10} + \frac{\partial}{\partial t} F_{11} \right) \frac{\partial}{\partial \varepsilon} \left(\varepsilon^2 - \Delta^2 \right)_{00}^{1/2} - \frac{\partial}{\partial \varepsilon} F_{00} \left[\frac{\partial}{\partial t} \left(\varepsilon^2 - \Delta^2 \right)_{10}^{1/2} + \frac{\partial}{\partial t} \left(\varepsilon^2 - \Delta^2 \right)_{11}^{1/2} \right] = 0 \tag{A1.8}$$

By averaging eq. (A1.8) over the coordinates, we obtain for $\partial F_{10}/\partial t$:

$$\frac{\partial}{\partial t} F_{10} = \frac{\partial}{\partial \varepsilon} F_{00} \left[\frac{\partial}{\partial t} \left(\varepsilon^2 - \Delta^2 \right)_{10}^{1/2} \right] \left[\frac{\partial}{\partial \varepsilon} \left(\varepsilon^2 - \Delta^2 \right)_{00}^{1/2} \right]^{-1}. \tag{A1.9}$$

Using expression (A1.9), one can transform the first term of eq. (A1.7.) as follows:

$$\frac{\partial}{\partial \varepsilon} \left[\overline{\frac{\partial}{\partial t} F_{10} \left(\varepsilon^2 - \Delta^2 \right)_{10}^{1/2}} \right] = \frac{\partial}{\partial \varepsilon} \left\{ \frac{1}{2} \frac{\partial}{\partial \varepsilon} F_{00} \left[\frac{\partial}{\partial \varepsilon} \left(\varepsilon^2 - \Delta^2 \right)_{00}^{1/2} \right]^{-1} \frac{\partial}{\partial t} \overline{\left[\left(\varepsilon^2 - \Delta^2 \right)_{10}^{1/2} \right]^2} \right\} \tag{A1.10}$$

The last expression equals zero, being the mean value of the derivative.
To find F_{11}, we subtract the same equation, averaged over coordinates, from (A1.8):

$$-Dk^2 F_{11} + \frac{\partial}{\partial t} F_{11} \frac{\partial}{\partial \varepsilon} \left(\varepsilon^2 - \Delta^2 \right)_{00}^{1/2} - \frac{\partial}{\partial \varepsilon} F_{00} \frac{\partial}{\partial t} \left(\varepsilon^2 - \Delta^2 \right)_{11}^{1/2} = 0 \tag{A1.11}$$

The second term in eq. (A 1.11) for the case of low frequencies $\omega \ll Dk^2$ is small compared to the first one. Therefore, we obtain:

$$F_{11} = - \left(Dk^2 \right)^{-1} \frac{\partial}{\partial \varepsilon} F_{00} \frac{\partial}{\partial t} \left(\varepsilon^2 - \Delta^2 \right)_{11}^{1/2} \tag{A1.12}$$

By substituting eq. (A1.12) into eq. (A1.7), we obtain for the averaged function F_{00} :

$$- \frac{\partial}{\partial \varepsilon} \left\langle \frac{\partial}{\partial t} \left(\varepsilon^2 - A^2 \right)_{11}^{1/2} \left(Dk^2 \right)^{-1} \frac{\partial}{\partial t} \left(\varepsilon^2 - A^2 \right)_{11}^{1/2} \right\rangle \frac{\partial}{i\varepsilon} F_{00} = I_{\text{ph}} \tag{A1.13}$$

Near T_c at $\Delta < T$ the collision integral I_{ph} may be written in the form

$$I_{\text{ph}}(F) = \tau_\varepsilon^{-1} \left[F(\varepsilon) - \tanh \frac{\varepsilon}{2T} \right] \overline{\left\langle \varepsilon \left(\varepsilon^2 - \Delta^2 \right)^{-1/2} \right\rangle} \tag{A1.14}$$

Finally, to find the dependence of the averaged distribution function $F(\varepsilon) = F_{00}$, we obtain eq. (2.7), where the energy diffusion coefficient D_i, is given by eq. (2.8).

15.6 Appendix 2

15.7 A2.1. Retarded (advanced) Green functions

As mentioned before, in short contacts ($2L < \eta$) the anisotropic parts of the Green functions $\hat{C}^{\text{R}(A)}$ do not depend on x [see eqs. (3.2) and (3.3)]. They are related to the isotropic parts $\hat{G}^{\text{R(A)}}$ as follows (see ch. 4)

$$\hat{C} = -l\hat{G} \frac{\hat{c}\hat{G}}{\partial x}. \tag{A2.1}$$

To shorten the expression, the indices $R(A)$ are omitted here. The solution of eq. (A2.1) has the form

$$\hat{G}(x) = \hat{G}(0) \exp\left(-\hat{C}\frac{x}{l}\right). \tag{A2.2}$$

The relations of normalization (see ch. 4) imply, that the matrices $\hat{G}(0)$ and $\hat{C}$ anticommutate, while $(\hat{G}(0))^2 = \hat{1}$. Let us put in (A2.2) $x = \pm L$, then add and substract the results obtained. This will give:

$$\hat{G}_+ = \hat{G}(0)\cosh(\hat{C}L/l), \hat{G}_- = -\hat{G}(0)\sinh(\hat{C}L/l). \tag{A2.3}$$

Here $\hat{G}_\pm = \frac{1}{2}[\hat{G}(L) \pm \hat{G}(-L)]$. Let us multiply the matrices $\hat{G}_\pm$. Taking into account the anticommutation of the matrices $\hat{G}(0)$ and $\hat{C}$, we find

$$\hat{C} = -\frac{1}{2L}\operatorname{arcsinh}\left(2\hat{G}_+\hat{G}_-\right) = -\frac{1}{2L}\sum_{k=0}^{\infty}\alpha_{2k+1}\left(2\hat{G}_+\hat{G}_-\right)^{2k+1}. \tag{A2.4}$$

The matrices $\widehat{G}_\pm$may be easily calculated, if one notes that

$$\hat{G}(\pm L) = \hat{S}(\pm L)\hat{g}\hat{S}^+(\pm L), \tag{A2.5}$$

where, for example,

$$\hat{g}^R = g^R\dot{\sigma}_z + f^R\dot{\hat{\sigma}}_i, \quad g^R = \frac{\varepsilon}{\Delta_0}f^R = \varepsilon, \zeta^R, \quad \zeta^R = \sqrt{(\varepsilon + \mathrm{i}0)^2 - A_0^2}.$$

i.e. $\hat{g}^{\mathrm{R}}$ is the equilibrium retarded Green function with the real order parameter. The matrix $\hat{S}$ makes it possible to take into account the phase difference in the bridge

$$\hat{S}(\pm L) = \cos(\chi_0/2) \pm \mathrm{i}\hat{\sigma}_z \sin(\chi_0/2). \tag{A2.6}$$

Considering the phase $\%_0$ as slowly changing with time and using eq. (A2.6), we find

$$\hat{G}_+ = g\hat{\sigma}_z + \mathrm{i}\hat{\sigma}_y f\cos\chi_0, \quad \hat{G}_- = \mathrm{i}\hat{\sigma}_x f\sin\chi_0 \tag{A2.7}$$

where $\hat{\sigma}_{x,y}$ are the Pauli matrices. Using the condition that $\left(\hat{G}_+\hat{G}_-\right)^2$ is a unit matrix, one can easily calculate the sum in eq. (A2.4), obtaining

$$\hat{C}^{\mathrm{R(A)}} = C_z^{\mathrm{R(A)}}\hat{\sigma}_z + C_y^{\mathrm{R(A)}}\hat{\sigma}_y, \quad C_z = -\mathrm{i}\frac{l}{L}\frac{\Delta_0\cos\chi_0}{\tilde{\zeta}}A = -\frac{\mathrm{i}\Delta_0\cos\chi_0}{\varepsilon}C_y \tag{A2.8}$$

where

$$A = \frac{1}{2}\operatorname{arcsinh}\left(\frac{\xi}{\zeta}f\sin\chi_0\right) = \operatorname{arcsinh}(f\sin\chi_0)$$
$$\tilde{\zeta}^{\mathrm{R}} = \sqrt{(\varepsilon + \mathrm{i}0)^2 - \tilde{\Delta}^2}; \quad \tilde{\Delta} = \Delta_0|\cos\chi_0|$$

The formula for $\hat{C}^{\mathrm{R(A)}}$ was first obtained by Kulik and Omelyanchuk (1975), Mitsay (1976) and also, using another method (presented here) by Artemenko et al. (1979a).

Let us now determine the isotropic parts of $\hat{G}^{\mathrm{R(A)}}(x)$, through which the reduced density of states $N(\varepsilon)$ is expressed. Let us represent the exponent in eq. (A2.2) in the form of a series. Working in the same way as we did in finding' $\hat{C}^{\mathrm{R(A)}}$, we obtain

$$\hat{G}(x) = \hat{G}(0)\left[\cosh\left(A - \frac{x}{L}\right) + \frac{-\varepsilon\hat{\sigma}_y + i\hat{\sigma}_z\Delta\cos\chi_0}{\tilde{\zeta}}\sinh\left(A\frac{x}{L}\right)\right]. \tag{A2.9}$$

The matrix $G(0)$ [as it follows from (A2.9)] is related to $G_+$by

$$\hat{G}(0) = \hat{G}_+\cosh A = \frac{\zeta}{\tilde{\zeta}}\hat{G}_+ \tag{A2.10}$$

Using eqs. (A2.9) and (A2.10), we determine the density of states

$$N(\varepsilon) = \frac{1}{2}\operatorname{Tr}\hat{\sigma}_z\left(\hat{G}^{\mathrm{R}} - \hat{G}^{\mathrm{A}}\right) = \frac{\varepsilon}{2\zeta^{\mathrm{R}}}\cosh\left(A^{\mathrm{R}}\frac{x}{L}\right) - \frac{\varepsilon}{2\zeta^{\tilde{\mathrm{A}}}}\cosh\left(A^{\mathrm{A}}\frac{x}{L}\right) \tag{A2.11}$$

We are interested in energies $|\varepsilon| > \tilde{\Delta}$ (since at $|\varepsilon| < \tilde{\Delta}, N(\varepsilon) = 0$); then

$$\tilde{\zeta}^{\mathrm{R}} = -\tilde{\zeta}^{\mathrm{A}} = \sqrt{\varepsilon^2 - \tilde{\Delta}^2}\operatorname{sgn}\varepsilon.$$

If the energy exceeds the gap in the banks $|\varepsilon| > \Delta_0$, then $A^{\mathrm{R}} = -A^{\mathrm{A}} \equiv a\operatorname{sgn}\varepsilon$, where a is determined in (1.16). Therefore, we have

$$N(\varepsilon) = \frac{|\varepsilon|}{\sqrt{\varepsilon^2 - \tilde{\Delta}^2}}\cosh\left(a\frac{x}{L}\right) \tag{A2.12}$$

When energy ranges within the interval (1.15), then for finding A the branching points should be followed in A^{R} from above, while in A^{A} they should be
followed from below. Then we obtain

$$A^{\mathrm{R}} = -\left(A^{\mathrm{A}}\right)^* = a - \mathrm{i}\frac{\pi}{2}\operatorname{sgn}\left(\sin\chi_0\right).$$

This taken into account, we find from eq. (A2.11) the expression (1.16) for $N(\varepsilon)$.

15.8 A2.2. The Green function $\hat{G}_1$. Distribution functions

For finding the $\hat{G}_1 = \hat{C}$ matrix independent of x (see eq. 3.3), we use the normalization relationship

$$\hat{G}^{\mathrm{R}}\hat{C} + \hat{C}\hat{G}^{\mathrm{A}} = -\left(\hat{C}^{\mathrm{R}}\hat{G} + \hat{G}\hat{C}^{\mathrm{A}}\right) \tag{A2.13}$$

Expression (A2.13) should be written down at the points $x = \pm L$, where all the functions, except $\hat{C}$, are known. There are several ways of determining $\hat{C}$. It is convenient to present C in the form

$$\hat{C} = \hat{C}^{\mathrm{R}}\hat{F} - \hat{F}\hat{C}^{\mathrm{A}}, \tag{A2.14}$$

where matrix $\hat{F}$ also does not depend on x and has the form $\hat{F} = F_x\hat{\sigma}_x + F_1\hat{1}$. Let us substitute eq. (A2.14) into eq. (A2.13) and take into account the anticommutation of G^{R} and C^{R}. Then we obtain:

$$\hat{C}^{\mathrm{R}}(\hat{B} - \hat{G}) + (\hat{B} - \hat{G})\hat{C}^{\mathrm{A}} = 0, \tag{A2.15}$$

where $\hat{B} = \hat{G}^{\mathrm{R}}\hat{F} - \hat{F}\hat{G}^{\mathrm{A}}$. The determinant of eq. (A2.15) composed of the elements of the matrix $\hat{C}^{R(A)}$ is not equal to zero. This implies that

$$\hat{G}^{\mathrm{R}}\hat{F} - \hat{F}\hat{G}^{\mathrm{A}} = \hat{G} = \hat{G}^{\mathrm{R}}\hat{F}_0 - \hat{F}_0\hat{G}^{\mathrm{A}}. \tag{A2.16}$$

Here we introduced the matrix $\hat{F}_0$, which is connected at $x = \pm L$ with the equilibrium distribution function in the banks, $\hat{F}_0 = \hat{S}(t)F_{\rm eq}\ (t-t')\,S^+\,(t')$. The Fourier image $F_{\rm eq}\ (t-t')$ equals $F_{\rm eq}\,(\varepsilon) = \tanh(\varepsilon/2T)$.

Let us add and substract the equations (A2.16) at the points $x = \pm L$. Then we obtain:

$$\hat{G}^{\rm R}_{\pm}\hat{F}^{\rm (a)} - \hat{F}^{\rm (a)}G^{\rm A}_{\pm} = \hat{G}^{\rm R}_{\pm}\hat{F}_{-} - \hat{F}_{-}\hat{G}^{\rm A}_{\mp}, \tag{A2.17}$$

where

$$\hat{F}^{(a)} = \hat{F} - \hat{F}^{(r)}, \quad \hat{F}^{(r)} = \hat{F}_{+}, \quad \hat{F}_{+} = \frac{1}{2}\left[\hat{F}_0(L) \pm \hat{F}_0(-L)\right].$$

The regular function $\hat{F}^{(r)}$ determines the superconducting current, while the anomalous one $\hat{F}^{(a)}$ stands for the quasiparticle current. The functions $\hat{F}_{\pm}$are easily found at $V \ll \Delta_0$ with the use of (A2.6).

$$\hat{F}_{+} = \hat{1}\tanh(\varepsilon/2T), \quad \hat{F}_{-} = {\rm i}\hat{\sigma}_2\frac{1}{4T}\frac{\partial\chi_0}{\partial t}\cosh^{-2}\left(\frac{\varepsilon}{2T}\right). \tag{A2.18}$$

Let $|\varepsilon| > \Delta_0$. Consider the version of equation (A2.17) with the minus signs in the left-hand side. Calculating the trace we find:

$$F^{\rm (a)}_x = -\frac{i\varepsilon}{4T\Delta_0\sin\chi_0}\frac{\partial\chi_0}{\partial t}\cosh^{-2}\left(\frac{\varepsilon}{2T}\right) \tag{A2.19}$$

Multiplicating eq. (A2.17) by σ_γ and calculating the trace gives $F^{(a)}_1 = 0$. For the function $C^{(a)}_z$ determining the current (3.4), we obtain from (A2.14) and (A2.8): $C^{\rm (a)}_z = -{\rm i}\left(C^{\rm R}_v + C^{\rm A}_v\right)F^{\rm (a)}_x$.

Integrating in (3.4) over the region $|\varepsilon| > \Delta$ we obtain the Ohmic current $V'R$.

Let energy range within the interval (1.15). We consider the version of eq. (A2.17) with the plus signs in the left-hand side. Multiplying this equation by $\hat{\sigma}_z$ and calculating the trace, then multiplying by $\hat{\sigma}_1$ and calculating the trace once more, we see that the left-hand side contains the coefficients of $F^{(a)}_1$ and $F^{\rm (a)}$ which are factors of the type ($f^{\rm R} - f^{\rm A}$), which equal zero within the energy interval considered, when no energy relaxation is taken into account. To obtain the final value of $F^{(a)}_1$ and $F^{(a)}_x$, we take into account the damping in the spectrum: then $f^{\rm R} - f^{\rm A} = iv_\varepsilon(\hat{\partial}f, \hat{\partial}\varepsilon)$. Besides, one should perform the quasiclassical expansion in the left-hand side. For example:

$$\hat{G}^{\rm R}_{-}\hat{F}^{\rm (a)} = \hat{G}^{\rm R}_{-}(\varepsilon)\hat{F}^{\rm (a)}(\varepsilon) + \frac{1}{2{\rm i}}\left\{\frac{\partial\hat{G}^{\rm R}}{\partial t}\frac{\partial\hat{F}^{\rm (a)}}{\partial\varepsilon} - \frac{\partial\hat{G}^{\rm R}}{\partial\varepsilon}\frac{\partial\hat{F}^{\rm (a)}}{\partial t}\right\}$$

Then, after simple transformations, we obtain the equation for the function $\widetilde{F}^{(a)}_1 = F^{(a)}_1\exp(v_t t)$:

$$\begin{aligned}\frac{\partial\tilde{F}^{\rm (a)}_1}{\partial t} + \frac{\partial\left(\ln\sin\chi_0\right)}{\partial t}\left[\frac{\partial\ln\sqrt{\Delta_0^2-\varepsilon^2}}{\partial\varepsilon}\right]^{-1}\frac{\partial\tilde{F}^{\rm (a)}_1}{\partial\varepsilon} \\ = -\frac{1}{2T}\frac{\partial\chi_0}{\partial t}\frac{\cot\chi_0}{\cosh^2(\varepsilon/2T)}\cdot\left[\frac{\partial\ln\sqrt{\Delta_0^2-\varepsilon^2}}{\partial\varepsilon}\right]^{-1}\end{aligned} \tag{A2.20}$$

From (A2.20) we find the expression for $\tilde{F}^{(a)}_1$ and hence also for $F^{(a)}_1$:

$$F^{(a)}_1 = \frac{\Delta_0}{4T}\cosh -2\left(\frac{\varepsilon}{2T}\right)\int_{-\infty}^{t}{\rm d}\theta\frac{\partial\chi_0(\theta)}{\partial\theta}\frac{\sin\left[2\chi_0(\theta)\right]\exp[\theta-t)\tau]}{|\kappa|\sqrt{\kappa^2-\sin^2\chi_0(\theta)}} \tag{2}$$

where $\kappa = [\Delta_0 \sin \chi_0(t)] / \sqrt{\Delta_0^2 - \varepsilon^2}$. The function $F_x^{(a)}$ is small as compared with $F_1^{(a)}$ with regard to the parameter $\max((1,1,1)1_0$. Using the expressions (A2.21). (A2.14) and (A2.8) we find from eq. (3.4) the anomalous current $I^{(1)}$ (see eq. 3.5).

To determine the distribution functions we consider eq. (A2.16) and present the matrix. $\hat{F}$ in the form of eq. (3.1). Let us substitute the expression for $\hat{G}^{R(A)}(x)$ from (A2.9) into (A2.16) and equalize the coefficients of the matrices
$\dot{\sigma}_1(k = 1, x, y, z)$. Then we obtain:
(a) $|\varepsilon| > \Lambda_0$. Then

$$F^{(T)} = \frac{1}{4T} \frac{i\%}{\hat{C}t} \frac{\sqrt{\varepsilon^2 - \Delta_0^2}}{\Delta_0 \sin \%} \sqrt{\frac{\varepsilon^2 - \tilde{\Delta}^2}{\varepsilon^2 - \Delta_0^2}} \frac{\tanh(a(x/L))}{\cosh^2(\varepsilon/2T)}.$$

The function $F^{(L)} = \tanh(\varepsilon/2T)$, i.e. it remains the equilibrium one.
(b) $\tilde{A} < |\varepsilon| < A_0$. Then

$$F^{(L)} - \tanh(\varepsilon/2T) = F_1^{(a)}.$$

ard F; is determuned by expression (A2.21). The function F at the energers under consideration is small.

16 Time-Dependent Superconductivity in SNS Bridges: An Example of TDGL Theory by De Lozanne, Beasley

16.1 1. Introduction

Superconducting microbridges have played a major role in the recent advances toward a fundamental understanding of time-dependent, nonequilibrium superconductivity. The complex temporal and spatial variations of the superconducting wavefunction that are associated with the phase slippage process in such bridges have provided important and challenging theoretical problems. Phase slippage necessarily must arise when a finite DC voltage difference exists across a superconductor; consequently the current voltage characteristics of the various microbridge structures have been the focus of much interest. Historically interest in these questions arose out of the failure of the traditional time-dependent Ginzburg Landau (TDGL) theory to account for the I-V curves of filamentary superconductors and constriction-type superconducting microbridges. A comprehensive review of these developments along with others can be found in the chapter by Kadin and Goldman (1985) in the present volume.

There is, however, a class of superconducting microbridges for which the traditional TDGL theory appears to work. These are so-called planar superconductor normal-superconductor (SNS) bridges. An understanding of these bridges is thus of interest as a contrast to the more conventional constriction bridges and as a testing ground for the applications of TDGL theory. They also appear to have considerable technological promise as a practical alternative to tunneling Josephson junctions in many applications. In this chapter we review the current understanding of the dynamical behavior of such bridges and discuss the theoretical implications in the broader framework of time-dependent, nonequilibrium superconductivity.

We begin in the next section with a description of these bridges and the physical basis upon which they have been modeled. In section 3 the TDGL equations are discussed along with the limits of their validity. The equations are cast into a simple form for the case of a narrow, gapless microbridge. Some numerical results illustrating the predictions of this theory are also

given in this section. Comparisons with the experimental results available to date are presented in section 4.

16.2 2. SNS Microbridges

16.2.1 2.1. Bridge structure

Figure 1 illustrates various types of SNS Josephson junction structures. Most of the quantitative experimental work on SNS microbridges has been done using bridges with a planar (fig. 1a, 1c) or step-edge (fig. 1b, 1d) geometry. SNS junctions with a sandwich geometry (fig. 1e) were studied earlier but are less satisfactory because of the inherently small resistances and voltages involved. Also they are generally wide compared to the Josephson penetration depth λ_J, and therefore the phase slippage process is accomplished by the more complicated phenomenon of vortex flow. Bridges on the other hand have much larger resistances, hence higher voltages, and can be narrow enough to be onedimensional, which provides considerable theoretical simplification. The fabrication and general properties of these bridges have been described elsewhere (Komarovskikh et al. 1975, Warlaumont et al., 1979, van Dover et al. 1980, 1981, de Lozanne et al. 1983, Dilorio et al. 1983, Liengme et al. 1983). Similar structures have also been made with semimetal (Gudkov et al. 1979. Ivanov et al. 1981) and degenerate semiconductor (Ruby and van Duzer 1981, Alfeev et al. 1979) weak links. These structures can be thought of as SNS devices with a lower electron density in N. Thus given the appropriate parameters they presumably can also be modeled by the TDGL theory.

A common denominator of all SNS bridges that have actually been fabricated is that the banks are SN bilayers themselves (1a-1d). This is in contrast to the more idealized structure usually assumed theoretically in which the banks are homogeneous superconductors (fig. 1f). The fact that the normal metal extends into the banks turns out to have some advantage in the practical performance of the devices, reduced heating, for example. Moreover, it ensures continuity of the order parameter across the actual bridge/bank interface since it is all one material.

16.2.2 2.2. Model

One may view the Josephson coupling in planar SNS microbridges as arising in two essentially independent steps (see fig. 2) (van Dover et al. 1981). First, superconductivity is induced into N in the SN bilayer banks by virtue of the proximity effect (fig. 2a). This first step can be treated theoretically (at least near T_c) by simply solving the Ginzburg-Landau equations in S and N with SN boundary conditions similar to those of de Gennes. Second, once the order parameter in N is known, in establishing the Josephson coupling one may essentially forget about the presence of the superconductor and treat the structure as a homogeneous bridge with rigid boundary conditions, i.e., with the order parameter constant in the banks independent of what happens in the bridge. These rigid boundary conditions are enforced by the presence of the S layer, and in most practical cases by the variable thickness geometry of the bridge itself*. With this picture it follows as mentioned above that there is no discontinuity of the order parameter at the bank bridge boundary because the same material (N) is on both sides of this boundary (fig. 2b). For purposes of comparison, the behavior generally assumed in a sandwich SNS junction and an ideal planar SNS bridge are shown in fig. 3. Finally, given rigid boundary conditions and the value of the order parameter in N . in principle the behavior of the bridge can be calculated using the appropriate equations (G − L or

[0]*For a complete review of variable thickness bridges and their relation to rigid boundary conditions, see the article by Likharev (1979).

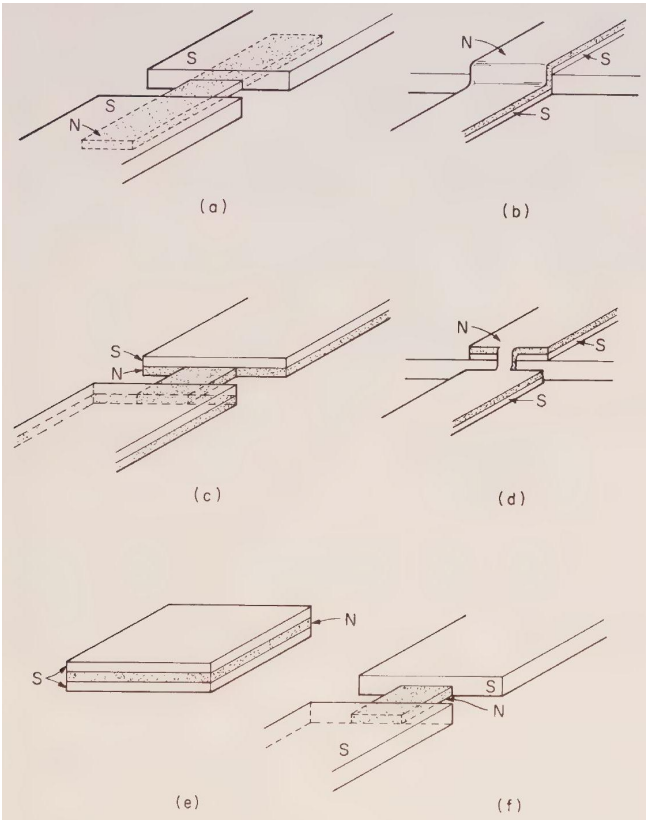


Fig. 1. Schematic representation of the various types of SNS structures: (a) planar microbridge, no constriction in N (Warlaumont et al. 1979, Liengme et al. 1983); (b) step-edge microbridge, no constriction in N (de Lozanne et al. 1983); (c) planar microbridge, with constriction in N (van Dover et al. 1980, Komarovskikh et al. 1975); (d) step-edge microbridge, with constriction in N (Dilorio et al. 1983); (e) planar SNS sandwich; (f) structure commonly assumed in theoretical models.

Usadel equations for the static case, the TDGL cquations for the dynamic case).

Strong support for this model in the case of the static properties of planar SNS bridges has been given by the semi-quantitative agreement of its predictions with the measurements of the temperature dependence of the I_cR_N product for Nb/Au and Pb/Cu planar microbridges (van Dover et al. 1980, 1981, Liengme et al. 1983). On the basis of this success the same ideas have been extended to dynamic situations using the traditional TDGL equations. and again satisfactory agreement is found with the experimental results, at least at the present stage of development. These results are the topic of the remainder of this review.

16.3 3. TDGL theory and results

16.3.1 3.1. The TDGL equations ,

Originally, the TDGL equations were shown by Gor'kov and Eliashberg (1968) to be rigorously valid at all temperatures in a superconductor rendered gapless by paramagnetic impurities. Kramer and Watts-Tobin (1978) obtained a more general version that is valid for a dirty superconductor near T_c, taking into account inelastic electron-phonon scattering. Their result reduces to that of Gor'kov and Eliashberg in the limit of zero gap. Finally, Schön and Ambegaokar (1979) derived a TDGL equation which includes various pairbreaking mechanisms on equal footing: namely electron-phonon scattering, paramagnetic impurities, supercurrent

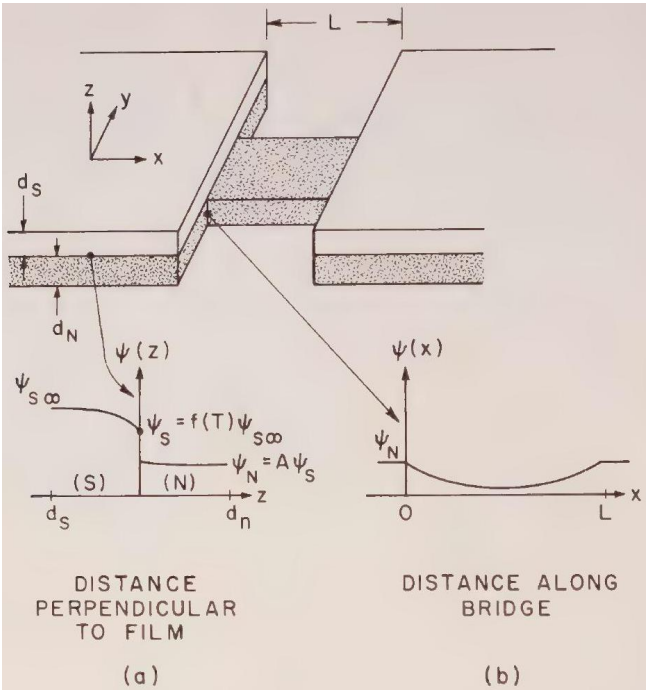


Fig. 2. Model used to analyze the behavior of planar constriction SNS microbridges (fig. 1c). (a) Behavior of the order parameter as one moves down from the superconductor into the normal metal. The sharp change of the order parameter at the SN interface is due to the different material parameters in each metal. (b) Behavior of the order parameter as a function of distance along the bridge. Note that there is no discontinuity of the order parameter at $X = 0$ and $X = L$ because there is no change of material parameters at those points. (From van Dover et al. 1980, 1981.)

depairing, magnetic fields and spatial variation of the order parameter. Again, this latest result reduces to the previous two in the appropriate limits. The generalized pair-breaking parameter of Schön and Ambegaokar has the following form:

$$\Gamma = \frac{1}{2\tau_{\mathrm{E}}} + \frac{1}{\tau_{\mathrm{S}}} + \frac{D}{2}Q^2 - \frac{D}{2}\frac{\nabla^2\Delta_0}{\Delta_0}, \tag{1}$$

where τ_{E} is the inelastic electron-phonon scattering time, τ_{S} is the magnetic spin flip time, D is the diffusion coefficient ($D = v_{\mathrm{f}}^2\tau_{\mathrm{imp}}/3$), Δ_0 is the temperature-dependent equilibrium pair potential and

$$Q = \nabla\theta + 2eA$$

is proportional to the superfluid momentum.
The general TDGL equation (Schön and Ambegaokar 1979) is given by*

$$\frac{\pi}{8kT}\left[\frac{\eta}{2|\Delta|\tau_{\mathrm{E}}}\left(\frac{\partial}{\partial t} + 2\mathrm{i}e\Phi\right) + \left(2|\Delta|\tau_{\mathrm{E}}\zeta - \frac{\eta}{2|\Delta|\tau_{\mathrm{E}}}\right)\frac{|\dot{\Delta}|}{|\Delta|}\right]\Delta$$
$$= \left[\alpha - \beta|\Delta|^2 + \xi^2(0)(\nabla - 2\mathrm{i}eA)^2\right]\Delta \tag{2}$$

where

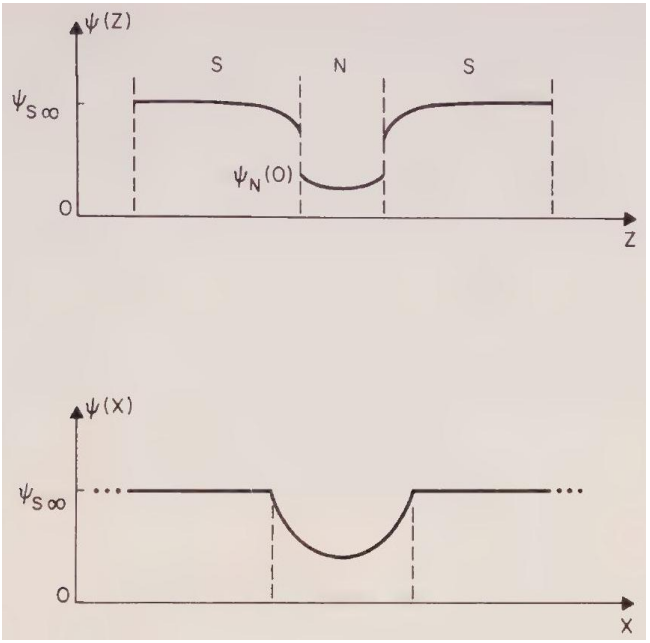


Fig. 3. Comparison of the spatial dependence of the order parameter along the direction of current flow for the SNS structures shown in figs. 1e and 1f. (a) Sandwich structure. Current flow is in the vertical direction. The order parameter in S is pulled down near the boundaries due to the large area of contact with N ; the discontinuity at the interfaces is due to the different material parameters in S and N. (b) Commonly assumed theoretical structure (Likharev 1979, Likharev and Yakobson 1975), see fig. 1f. Here the current flow is in the horizontal direction. The normal state material parameters are assumed to be the same in S and N , hence there is no discontinuity at the $\mathrm{S / \mathrm{N}$ interfaces. Furthermore, the small area of contact between S and N (due to the variable thickness geometry) produces negligible depression of the order parameter in S near the interfaces.}

$$
\begin{aligned}
&\eta = (2\gamma\tau)^{1/2}\left(1+\gamma/2\Delta_0^2\tau\right)^{-1/2}, && \alpha = (T_\mathrm{c}-T)/T_\mathrm{c},\\
&\zeta = \left[1+(\gamma/\Delta_0)^2\right]^{1/2} - \gamma/\Delta_0 + 1/2\Delta_0\tau, && \beta = 7\zeta(3), 8\pi^2k^2T_\mathrm{c}^2,\\
&\gamma = -\mathrm{i}\omega/2 + \Gamma, && \xi^2(0) = \tfrac{\pi\hbar}{8kT_\mathrm{c}}D,\\
&1/\tau = -\mathrm{i}\omega + 1/\tau_\mathrm{E},
\end{aligned}
\tag{3}
$$

and the current is determined by

$$
j = \frac{\pi\sigma_0}{4ekT}\,\mathrm{Im}\left\{\Delta^*(\nabla - 2\mathrm{i}e\boldsymbol{A})\Delta\right\} - \sigma_0(\nabla\Phi - \dot{A}), \tag{4}
$$

where Im stands for the imaginary part. It is assumed in the derivation of this TDGL equation that the quasiparticle relaxation processes are fast enough to justify neglecting the effects of diffusion. This is another way of saying that the equations are local. This is valid as long as

$$
|\Delta|^2/k_\mathrm{B}T < 1/\tau_\mathrm{E}. \tag{5}
$$

0

- Minor typographical errors in the original publication (Schön and Ambegaokar 1979) are corrected here.

Furthermore, it is assumed that the problem is linear (small departures from equilibrium) and that the frequency is low:

$$\omega \ll 1/\tau_{\mathrm{E}}. \tag{6}$$

This general TDGL equation reduces to the result of Kramer and WattsTobin (1978) when electron-phonon interactions are the only scattering mechanism, so that $\gamma = 1/2\tau_{\mathrm{E}}$. The equation reduces further to the original TDGL equation,

$$\frac{\pi}{8kT}\left[\frac{\partial}{\partial t} + 2\mathrm{i}e\Phi\right]\Delta = \left[\alpha - \beta|\Delta|^2 + \xi^2(0)(\nabla - 2\mathrm{i}eA)^2\right]\Delta \tag{7}$$

obtained by Gor'kov and Eliashberg (1968), in the limit of zero gap. In fact, in this limit, all of these three equations agree even in the numerical coefficients, which have customarily been thought to be different for Gor'kov and Eliashberg's equation. This can be seen easily when the latter equation is written in the notation of Hu and Thompson (1972). The confusion has stemmed from the use of different normalization factors as explained in greater detail below.

For the case of narrow microbridges (width $< \lambda_{\mathrm{J}}, \xi$) magnetic self-field effects are negligible ($A =$ constant $\equiv 0$) so that the current distribution and the order parameter are constant over the cross-section of the bridge; consequently the TDGL equations become one-dimensional. To normalize these equations it is customary to measure lengths in terms of $\xi(T)$ and Δ in terms of $\Delta_0 = \sqrt{|\alpha|/\beta}$. (Note that this definition applies both below and above T_c. Below T_{c}, Δ_0 is the equilibrium order parameter. Above T_{c}, it is simply a measure of the magnitude of Δ at which the nonlinear term becomes important.) Then, given the normal state conductivity σ_0, currents, voltages and times are measured in terms of

$$J_0 = \frac{\pi\sigma_0\Delta_0^2}{4ekT\xi} \tag{8}$$

$$V_0 = \frac{\xi J_0}{\sigma_0} \tag{9}$$

and

$$\tau_j = \frac{\hbar}{2eV_0} \tag{10}$$

With these normalizations the ordinary TDGL equations become

$$u(\dot{\psi} + \mathrm{i}\mu\psi) = -\left(1 + |\psi|^2\right)\psi + \psi'' \tag{11}$$

$$j = \mathrm{Im}\left(\psi^*\psi'\right) - \mu' \tag{12}$$

Here the prime and the dot represent partial derivatives with respect to normalized length and time respectively. Following the usual custom we have introduced the parameter

$$u = \frac{\tau_A}{\tau_j} = \frac{\pi^2}{16}\frac{\Delta_0^2}{kT}\frac{1}{\alpha} \tag{13}$$

which is the relaxation time of the order parameter in normalized units. Note also that τ_{J} can be physically interpreted as the relaxation time governing current transfer between the normal and superconducting channels. Finally, note that u depends on the value of Δ_0, which is not the same under all conditions. For an ordinary superconductor near $T_{\mathrm{c}}, \Delta_0(T) = \Delta_{\mathrm{g}}(T)$ where Δ_{g} is the energy gap. In this case $u = 5.79$. When paramagnetic impurities are present, Δ_0 is different (Kulik and Yanson 1972) and one gets $u = 12$, reflecting the different normalization.

16.3.2 3.2. Applicability of the TDGL equations to planar SNS bridges

There are two issues to be considered in assessing the applicability of the above TDGL equations to planar SNS microbridges. The first is whether the equations themselves apply in a normal metal and the second deals with the boundary conditions at the ends of the bridge.

As regards the first, one would argue that the equations should apply in the normal metal because they have been shown to be valid when a wide variety of pair-breaking mechanisms are present and the material is dirty (Schön and Ambegaokar 1979). One may therefore conclude that they should be valid in a dirty normal metal, which is by nature gapless. Note, for example, that the Aslamazov Larkin (1968) result for the fluctuation conductivity above T_c can be derived from TDGL theory (Tinkham 1980). On the other hand, the usual G − L requirement that $T \approx T_c$ is certainly not valid for a normal bridge with $T_{cN} = 0$. In the derivation of the GL equation from the microscopic theory this requirement is used to ensure that the order parameter and its spatial variations are small. The former is certainly true far above T_{cN}. Thus it seems that these equations should be at least qualitatively correct for a dirty normal metal into which superconductivity has been induced by the proximity effect. but where now the material parameters should be treated phenomenologically. In particular, u is no longer known and must be treated as an adjustable parameter. The length $\check{\xi}$ (and hence the parameter α) can presumably be
estimated reliably from the familiar expressions for in the theory of the proximity effect (van Dover et al. 1980, 1981).

Linfortunately there is an additional complication in comparing the results attained from SNS microbridges with the existing theoretical calculations based on egs. (11) and (12). Although some calculations have been carried out treating u as an adjustable parameter in all cases known to us it has been assumed that $|\psi| = 1$ (i.e.. $\psi = e^{15\cdot\omega}$) at the end of the bridge. This is true only for an SSS variable thickness bridge. where in fact the theory is not adequate over any accessible temperature region for other reasons. For an S.NS bridge A. (I) $\neq A_{,}$, but rather is given by the proximity coupling in the S.S. bilayer (fig. 2). If the basic TDGL equations are normalized with respect to A (()) rather than Δ_0, only the first TDGL equation is changed and becomes

$$u(\psi + i\mu\psi) = \left(1 + \eta|\psi|^2\right)\psi + \psi'' \tag{14}$$

where $\eta = \left\{A(())A_{(i)}\right)^2$ gauges the strength of the nonlinear term. Now. also. $J_{(j)}$. $V_{(0.)} =$, and u are still determined by eqs. (8). (9). (10) and (13), respectively. but where $A_{.}(f)$ is substituted for A_f. Hence in comparing experimental results with these calculations. there is an implicit assumption that $\eta = 1$, whereas for $T \gg T_{cN}$ one might expect $\eta \gg 1$. The really quite good agreement between theory and experiment found empirically despite this problem may reflect the fact that for rigid boundary conditions as $l \to ()$ the nonlinear term becomes negligible compared to the gradient term in any event (Aslamazov and Larkin 1968).

16.3.3 3.3. Results of TDGL

As discussed above most of the work with the TDGL equations has typically used the form given by eqs. (11) and (12) with the boundary conditions $\omega(x = 1), t) = 1$ and $\psi(x - L, t) = e^{\omega}$. These equations are usually solved numerically by standard methods. both with analog computers (Fjordboge and Lindelof 1978) and with digital computers (van Dover et al. 198(). 1981. Likharev and Yakobson 1975. Kramer and Baratoff 1977). In this section we present numerical solutions of eqs. (11) and (12) that give some insight into the behavior of the equations and their dependence on the relevant parameters ide Lozanne 1982).

Two important parameters determine the solution of eqs. (11) and (12), namely the normalized relaxation time. u, and the normalized length of the bridge. $l \equiv L \div (T)$. As the relaxation time of the order parameter $(u)g(v)es$ to tero one would expect the results to approach those of the Resistively Shunted Junction (RSJ) model for a microbridge (i.e.. with no capacitance). in which the only relaxation mechanism is the L − R time constant of the Josephson circuit which is given by τ_j in our notation. A number of numerical "experiments" demonstrate this. The simplest one is to consider a junction biased with $I_h < I_.$.

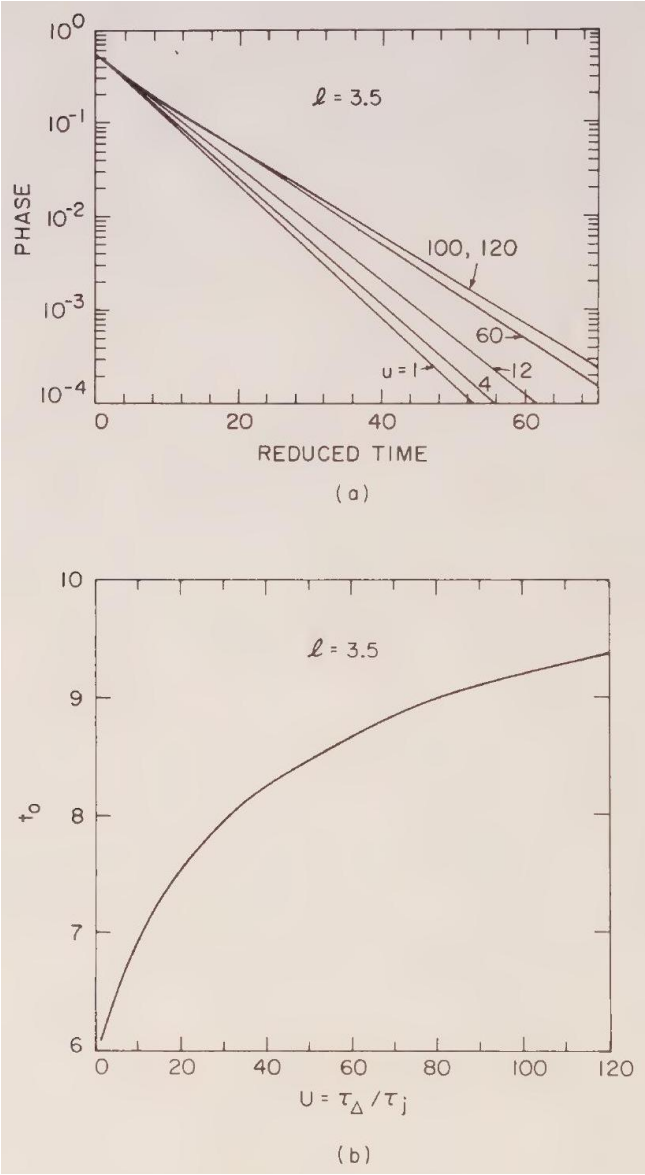


Fig. 4. (a) Relaxation of the phase as a function of reduced time showing an exponential dependence $\phi=\phi_{0
\mathrm{e}^{-t / t_{0}}}$. (b) Dependence of t_0 on the relaxation time of the order parameter τ_Δ (in reduced units of τ_j).}

letting the equations achieve their time-independent solution. Then the current is suddenly turned off and the phase of the order parameter measured as a function of time. The result, shown in fig. 4a, indicates that the phase has an exponential time dependence, $\phi = \phi_0 \mathrm{e}^{-t/t_0}$, where t_0 is a constant which increases with increasing relaxation time (u). This "experiment" can be easily visualized with the pendulum analogy of a Josephson junction. At $t = 0$ the pendulum is dropped from an initial angle ϕ_0 with the vertical and it moves down through a

fluid whose "viscosity" is determined in part by . As gets smaller the pendulum relaxes faster. As $u \to 0$ there is still some viscosity left, because the junction is now modeled by the RSJ equations with zero capacitance, i.e., the overdamped case. Figure 4 b shows the behavior of t_0 as a function of u. As $u \to 0$ we see that $t_0 \to 6\tau_j$. [In the RSJ model $t_0 \to 1\tau_j$; the different numerical factor is due to the difference in $I_c R : (I_c R)_{RSJ} = 6\,(I_c R)_{TDGL}$].

Figure 5 shows the time averaged voltage as a function of bias current for a number of values of u (van Dover et al. 1981). The results of the RSJ model are shown for comparison. At these low voltages the TDGL $I - V$'s are similar in shape to those of the RSJ model. In fact, over this voltage range the TDGL $I \cdot V$ can be fitted to the RSJ form by introducing an effective resistance R_{eff} ,

$$V^2 = R_{\text{eff}}^2 \left(I^2 - I_c^2\right). \tag{15}$$

At higher voltages the $I - V$'s are fundamentally different from the RSJ model,

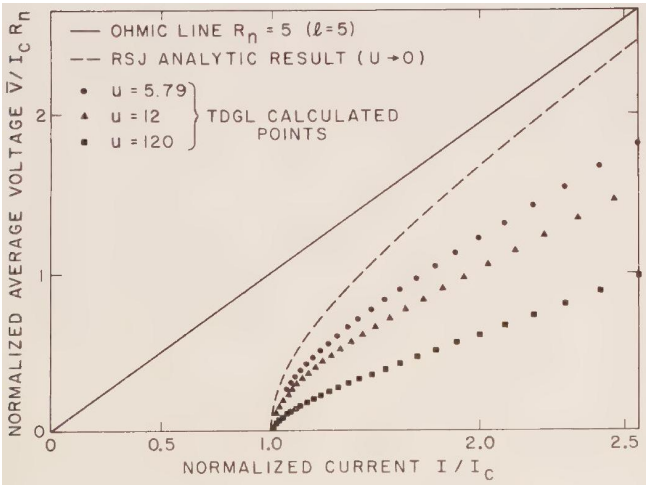


Fig. 5. Effect of the relaxation time of the order parameter on the $I - V$ near I_{c}. As the relaxation time is decreased the TDGL curves approach the RSJ result (dashed curve).

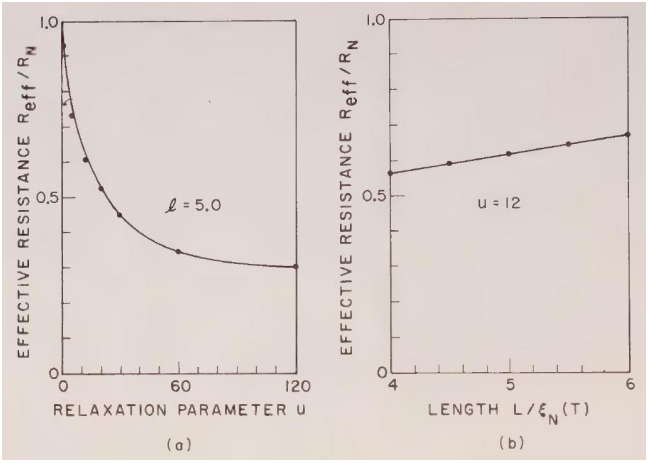


Fig. 6. Behavior of the low voltage effective resistance R_{err} as a function of the relaxation time (a) of the order parameter and (b) of the reduced length.

as shown below and originally noted by Likharev and Yakobson (1975). The behavior of $R_{\rm eff}$ as a function of u is shown in fig. 6a. Again, we see that as $u \to 0$ the effective resistance approaches that of the RSJ model ($R_{\rm eff} \to R_{\rm N}$, the device resistance). The dependence of $R_{\rm eff}$ on the length of the bridge is comparatively weaker, as shown in fig. 6b. Analytic expressions have also been obtained by Likharev and Yakobson (1975).

16.4 4. Comparison with experiments

The measured $I-V$ curves of several planar SNS microbridges (those in fig. 1c) follow the predictions of the TDGL equations with $u = 12$ as is illustrated in fig. 7. This value of u should be regarded as a best fit, although it was originally thought to be the theoretically predicted value. Here the current and voltage axes of the TDGL results have been normalized to match the measured critical current and normal resistance, respectively [this effectively determines the normalizations given in eqs. (8.9)]. SNS bridges with other geometries (figs. 1a,b,d) show similar features (de Lozanne et al. 1983, Komarovskikh et al. 1975. Liengme et al. 1983, de Lozanne 1982), although direct comparison between theory and experiment has not been made.

A further test of the theory, and probably a much more demanding one, is to compare it with experiments in which the current bias has a high frequency

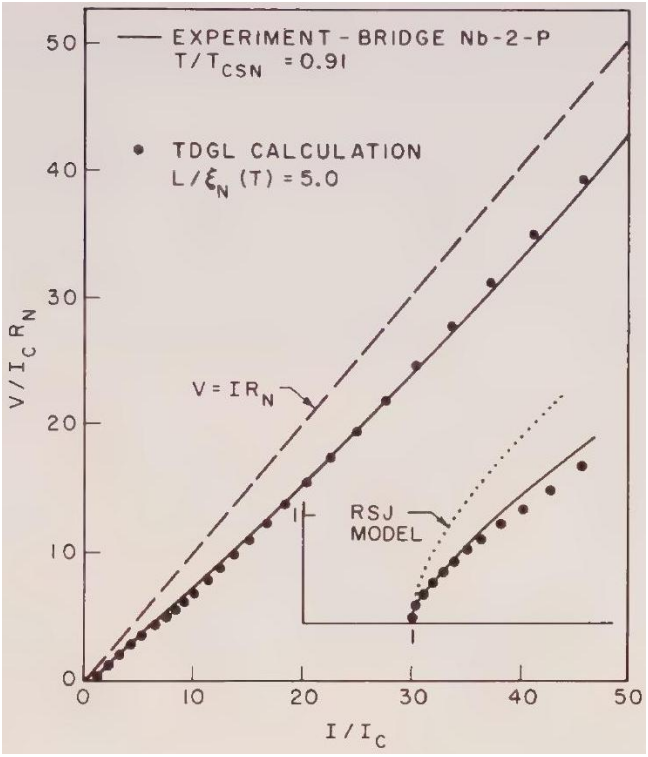


Fig. 7. Comparison of the experimental $I-V$ curves of a planar SNS microbridge (van Dover et al. 1980, 1981) near its critical temperature ($T_{\rm cSN}$) with the results of the TDGL model.}

AC component, as is the case for a microbridge irradiated with microwaves. Here the microwave frequency should be on the order of the characteristic Josephson frequency ($2el_cR/\hbar$) or higher, in order to probe the dynamics of the order parameter when it is out of equilibrium. Such a test has been carried out using a well-characterized planar SNS microbridge, whose $I \cdot V$'s have been reported earlier (van Dover et al. 1981). The reduced length of this bridge ($l = 3.5$) has been determined from SEM pictures together with the measured resistivity of the normal metal (which determines its coherence length). and independently from measurements

of $I_cR(T)$ (van Dover et al. 1981). Thus the parameters of the TDGL theory are previously determined to be $l = 3.5, u = 12$. The comparison with the experimental $I - V$ is shown in fig. 8a; the current axis is scaled to match the measured critical current, and the voltage axis is scaled so that it matches the measured voltage at a bias of 0.7 mA . The agreement is quite good. Also shown is the RSJ $\boldsymbol{I - V}$, scaled in a similar way, which gives a much poorer fit. When microwaves are applied to this microbridge sharp constant-voltage steps appear (van Dover et al. 1981). The only modification needed in the theoretical models is to add an AC term to the DC current bias. The amplitude of the AC bias is adjusted so that the theoretical critical current

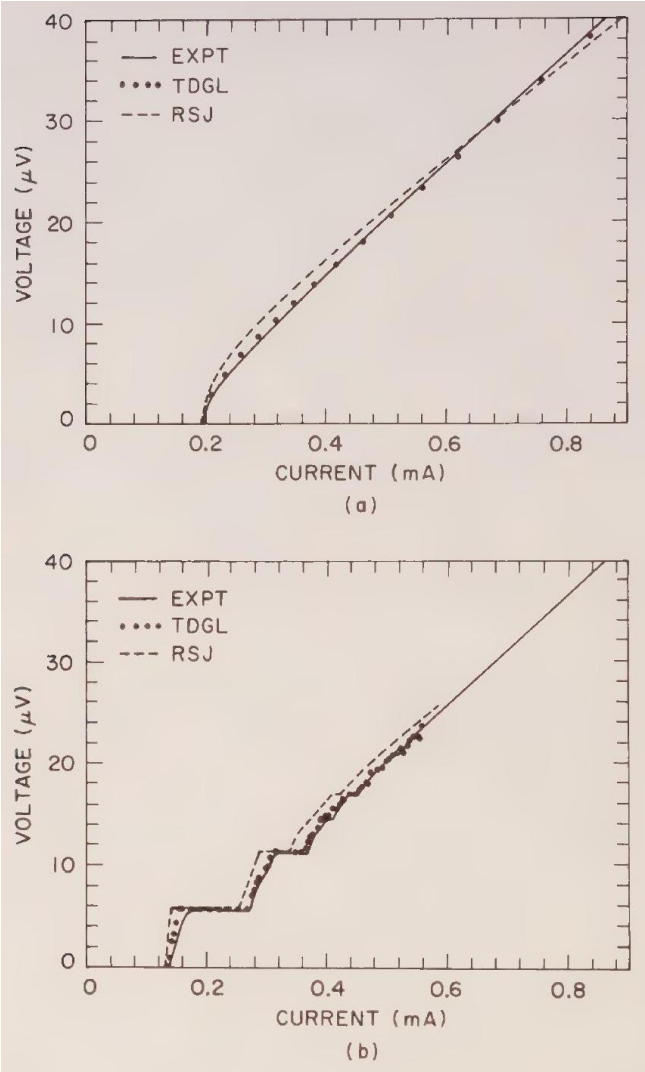


Fig. 8. Comparison of the experimental $I - V$ curves of a planar SNS microbridge (van Dover et al. 1980, 1981) with the results of the TDGL and RSJ models in the case of (a) DC bias and (b) $\mathrm{DC +\mathrm{AC}}$ bias. The data were taken at $T = 8.05$ K, while $T_{\mathrm{cSN}} = 8.85$ K.}

matches the experimental one with microwaves. The current and voltage axes cannot be scaled because they were already defined by the $I - V$ without microwaves. Figure 8 b shows that the TDGL equations give a very good fit to most of the IV, much better than that of the RSJ model (Russer 1972).

Warlaumont et al. (1979) have shown that the hysteresis observed in the low voltage part of the $I - V$ curve of SNS microbridges can be related to the relaxation time

of the order parameter in the context of the TDGL theory. They found experimentally that as the temperature is lowered hysteresis sets in when $\Gamma = ul^2 \geqslant 2$, where $l \equiv L/\xi_N(T_{cs})$. Thermal effects were ruled out as a possibility for this hysteresis. Numerical simulations by Kramer and Baratoff (1977) give hysteresis for $\Gamma \geqslant 38$ when $l = 1$. The same result has been obtained by Fjordbge and Lindelof (1978) using analog simulations. This discrepancy between the experimental and numerical values of Γ could be due to the fact that $l > 1$ in the experiments. Yet another possibility is that the formulas that determine Γ are strictly valid near T_c, which in this case is zero, so that the experiment is far above T_c.

16.5 5. Conclusions

From a semi-phenomenological standpoint the use of the TDGL equations to explain the behavior of SNS microbridges has been rather successful. Both the $I - V$ curve and, more importantly, the $I - V$ with microwave steps show close agreement between experiment and theory. A fully rigorous comparison, i.e., one without any adjustable parameters, is hindered by the fact that the bridge material (N) is far above its T_c and therefore outside of the GL region. This results in phenomenological parameters which show up in the normalization factors.

To make the theory apply far above T_c might require a full microscopic treatment. Work along these lines has been carried out by Golub (1980), yet the Green's function formalism used in that paper is not yet amenable to modeling of actual devices. In fact, the only result that could be compared with experiments is the effective resistance, R_{eff} . So far the formalism has proved too complex to yield $I - V$ curves or to reduce to a TDGL-like equation. More work is needed in this area to obtain results that can be meaningfully compared with experiments.

The fact that SNS microbridges seems to be modeled well by the TDGL equations and the technological promise that they hold will hopefully provide interest for more fundamental theoretical work in this field.

17 Pair Breaking in Nonequilibrium Superconductors by Beyer, Pethick, Rammer, Smith

17.1 1. Introduction

Nonequilibrium properties of superconductors may be described within two rather different theoretical frameworks. The first one, which characterizes the nonequilibrium state in terms of quasiparticles, is the more intuitive, but it is limited to situations where the variations are small on time scales of order $\hbar/\Delta$ and length scales $\hbar v_F/\Delta$, and where the width of the quasiparticle states may be neglected. Here Δ is the temperature-dependent gap and v_F the Fermi velocity. The second one is more general as it is based on the quasiclassical Green function. It can be applied to situations involving rapid spatial and temporal variations, as well as situations when the width of the quasiparticle states is significant, causing the quasiparticle picture to lose its meaning.

The quasiparticle approach to nonequilibrium problems was first used by Bardeen, Rickayzen and Tewordt (1959) in the context of thermal conductivity, and later elaborated by Betbeder Matibet and Nozires (1969), Aronov (1974), Aronov and Gurevich (1974), Pethick and Smith (1978, 1979a), Aronov et al. (1981), and many others. The Green function approach is due to Eilenberger (1968), Eliashberg (1971), Larkin and Ovchinnikov (1968, 1977), and Schmid and Schön (1975).

In the quasiparticle approach the kinetic equation resembles closely the Boltzmann equation used for normal metals, with the superfluid corrections modifying only the dispersion relation

and the transition probabilities. The kinetic equation in the Green function approach may be derived using the Keldysh (1964) method. The distribution functions that have been introduced (e.g. Schmid and Schön 1975) differ in some respects from the quasiparticle distribution function, as do the forms of the kinetic equations within the two approaches. This makes a comparison of the two methods less immediate, in particular as regards the important role of pair breaking. Recently, Shelankov (1980) has shown how to define distribution functions in the quasiclassical Green function approach in a way that makes the comparison of the Green function and quasiparticle approaches more direct, but until now most of the calculations within the quasi-classical approach have not employed Shelankov's definitions.

Our purpose in this chapter is to review calculations of the effects of pair breaking in a number of nonequilibrium situations. We shall first discuss the
basic formalism, and compare the Green function and quasiparticle approaches. Then we shall describe calculations carried out with the quasiclassical Green function approach. Until recently, most calculations within this approach had been carried out for temperatures close to T_c, and for weak coupling superconductors. What we wish to show is that the quasiclassical Green function approach can be employed for carrying out realistic calculations of pair-breaking effects away from T_c, and for strong coupling superconductors, and that such calculations are not significantly more complicated than those based on the quasiparticle picture. Consequently, a meaningful comparison of theory and experiment is now possible.

Although the kinetic equations for the quasiclassical Green function are more general and contain the quasiparticle Boltzmann equation as a limit, the concept of quasiparticles is so useful that one would like to put precise limits on its applicability. Furthermore, since a number of numerical calculations have been based on the quasiparticle approach, it is desirable to assess their range of validity. A detailed investigation of the relationship between the two approaches, based in part on numerical calculations of charge imbalance, was performed recently by Beyer Nielsen et al. (1982) and here we shall review and extend some of their results and also discuss the case of thermal conductivity, which was treated recently by Beyer Nielsen and Smith (1982). When dealing with pair-breaking phenomena we treat simultaneously the effects of strong electron phonon coupling, magnetic impurities and supercurrents, and indicate the differences and similarities between these various pair-breaking mechanisms.

The plan of the chapter is as follows. In section 2 we discuss the expressions for the electric and thermal currents, and for the charge imbalance, and compare the results obtained within the two frameworks. Section 3 reviews the effects of pair breaking on charge imbalance, thermal conductivity, and frequency-dependent conductivity, and includes a discussion of strongcoupling effects. Finally, section 4 illustrates the quasiparticle and Green function approaches to the calculation of thermal conductivity and charge imbalance. The physical situation is one in which the relaxation is dominated by impurity scattering in the presence of a superflow. In this last section, we go into more detail in our discussion in order to illustrate some of the concepts introduced in the previous sections of this chapter.

17.2 2. Densities and currents

The relation between the quasiparticle and Green function approaches may be elucidated by comparing the form of the expressions for the densities and currents.

17.2.1 2.1. The quasiparticle method

In the quasiparticle formalism the state of the superconductor is described by a quasiparticle distribution function $f_{p\sigma}$, which gives the local density of quasiparticles of momentum p and spin σ, supplemented by quantities describing the condensate, such as its velocity, v_s, and the

superconducting gap. The character of the quasiparticle is specified by the dispersion relation relating its energy E_p to the momentum, which in the absence of a supercurrent is

$$E_p = \sqrt{\xi_p^2 + \Delta^2} \tag{2.1}$$

where $\xi_p = \varepsilon_p - \mu, \varepsilon_p$ being the normal state energy and μ the chemical potential. The effective charge carried by a quasiparticle is $q = \breve{\zeta}/E$ (in units of the electronic charge), and the associated current of charge is vq, where $v = \hat{c}E\hat{c}p$ is the group velocity (Pethick and Smith 1979a). This current of (normal) charge differs, however, from the usual normal current, as we shall see below.

The total density of particles in the quasiparticle approach is given by

$$n = \sum_{p\sigma} u_p^2 f_p + v_p^2 \left(1 - f_{-p}\right), \tag{2.2}$$

where f_p is the distribution function for BCS-Bogoliubov quasiparticles, and u_p and v_p are the usual BCS coherence factors

$$u_p^2 = \frac{1}{2}\left(1 + \frac{\xi_p}{E_p}\right) \tag{2.3}$$

and

$$v_p^2 = \frac{1}{2}\left(1 - \frac{\xi_p}{E_p}\right) \tag{2.4}$$

with $\dot{\varsigma}_p = \varepsilon_p - \mu$ as above. In the general case the chemical potential, μ, which may vary in space, is the energy required to add an electron to the superconductor at the point r, without altering the quasiparticle distribution.

The total density n may be separated into two contributions as follows:

$$n = \sum_{p\sigma} v_p^2 + \sum_{p\sigma} \left(u_p^2 - v_p^2\right) f_p. \tag{2.5}$$

The first term is simply the density of electrons at zero temperature, corresponding to a chemical potential μ, provided particle hole symmetry applies. The second term in eq. (2.5) is in accordance with common usage denoted by Q^*. We see that in a certain sense Q^* is the charge associated with the quasiparticles, since each excitation may be regarded as carrying a charge $q_p = u_p^2 - \iota_p^2 = \dot{\zeta}_p, E_p$. It is important to note, however, that q_p depends on the local chemical potential, and therefore when the system is perturbed from
equilibrium, the second term in eq. (2.5) will change because of changes in the coherence factors as well as in the quasiparticle distribution. Note also that when particle-hole symmetry applies f_p in eq. (2.5) may be replaced by the deviation from local equilibrium $\delta f^{le} = f_p - f_p^{le}$. In the absence of a supercurrent, f_p^{le} is the equilibrium (Fermi) distribution function $f^0(E) = [\exp(E/T) + 1]^{-1}$ evaluated using the actual quasiparticle energy in the nonequilibrium state. In the presence of a supercurrent it is given by eq. (2.9). For the second term in eq. (2.5) we therefore have

$$Q^* = \sum_{p\sigma} q_p \delta f_p^{\ell \mathrm{e}} = \sum_{p\sigma} q_p \left(f_p - f_p^{\ell \mathrm{e}}\right) \tag{2.6}$$

The quantity Q^*, commonly referred to as the charge imbalance, is therefore a measure of the amount by which the quasiparticle distribution is asymmetric about the actual Fermi surface, not the Fermi surface in equilibrium. Physically, it is precisely the quantity measured

in tunnel injection experiments of the type pioneered by Clarke (1972) and analysed in detail by Tinkham and Clarke (1972) and by Tinkham (1972).

The charge imbalance Q^* is the quantity of importance in many timeindependent situations. However, another way of writing the expression for the charge density which is particularly useful in time-dependent situations is to express changes in the total charge density as a sum of one contribution coming from changes in the quasiparticle distribution, and another coming from changes in the coherence factors. The two contributions are referred to as the charge of the normal component, and the charge of the superconducting component, respectively, and form the basis for the development of a two-fluid model for the charge density, as described in detail by Pethick and Smith (1978, 1979a).

The total particle number current density j may be written as

$$j = nv_{\mathrm{s}} + \sum_{p\sigma}^{p} f_p \tag{2.7}$$

since the total current carried by a quasiparticle is p/m. The superfluid velocity is denoted by v. When eq. (2.7) is written in terms of δf^{te}, the deviation from local equilibrium, one finds, to first order in v_{s},

$$j = n_{\mathrm{s}}v_{\mathrm{s}} + \sum_{p\sigma}^{p} \delta f_p^{\ell \mathrm{e}} \tag{2.8}$$

since $f_p = f_p^{le} + \delta f_p^{le}$, where

$$f_p^{\ell \mathrm{e}} = f^0\left(E_p + p \cdot v_s\right) \tag{2.9}$$

is the distribution function for quasiparticles in equilibrium with the lattice in the presence of superfluid flow. (In this discussion we neglect Fermi liquid effects, which would result in E_p being a function of v_s.) The superfluid density
n_8 is given in terms of the Yoshida function Y_0 by the usual clean-limit result,

$$\frac{n_{\mathrm{s}}}{n} = 1 - \int_{-\infty}^{\infty} \mathrm{d}\xi \left(-\frac{\partial f^0(E)}{\partial E}\right) = 1 - Y_0 \tag{2.10}$$

The second term in eq. (2.8) is commonly referred to as the normal current j_n, while $j_{\mathrm{s}} = n_{\mathrm{s}}v_{\mathrm{s}}$ is the supercurrent.

The thermal current associated with the quasiparticle excitations is

$$j_{\mathrm{th}} = \sum_{p\sigma} E_p v_p \delta f_p^{le} \tag{2.11}$$

since E_p is the quasiparticle energy measured with respect to the chemical potential. Unlike the normal current j_n the thermal current involves the group velocity v_p of the excitations.

17.2.2 2.2. The Green function method

The basic ingredient of the microscopic approach is the Nambu Green function, which contains information about the nature of the excitation spectrum, the distribution function for excitations and also the properties of the condensate. The Green function is a function of two sets of coordinates, but for many purposes it is convenient to transform to center-of-mass and relative coordinates, and then perform a Fourier transformation, so that the Green function depends on the center-of-mass coordinates and the relative momentum and frequency variables. The Green functions in this mixed representation correspond closely to the Wigner distribution

function. The equations for the Green functions are more complicated than those for the distribution function in the quasiparticle approach, because the Green function depends on both momentum and frequency, whereas the quasiparticle distribution function depends only on the momentum. However, in many cases of physical interest sufficient information is contained in the quasiclassical Green function, g, which is obtained by integrating the Green function over the magnitude of the momentum variable and therefore depends on only the frequency and the direction of the momentum, as well, of course, as on the center-of-mass coordinates. For superconducting systems it is convenient to work with a 2×2 matrix representation for Green functions in particle-hole space. The nonequilibrium properties are conveniently described using the formalism developed by Keldysh (1964), who introduced a further 2×2 matrix representation to distinguish the various orderings of these arguments on the chosen integration contour. In the simplest 2×2 matrix representation the Green functions and the self energies are arranged in the form of matrices,

$$G = \begin{pmatrix} G^{\mathrm{R}} & G^{\mathrm{K}} \\ 0 & G^{\mathrm{A}} \end{pmatrix}, \quad \Sigma = \begin{pmatrix} \Sigma^{\mathrm{R}} & \Sigma^{\mathrm{K}} \\ 0 & \Sigma^{\mathrm{A}} \end{pmatrix} \tag{2.12}$$

where

$$\begin{aligned} G^{\mathrm{R}} &= G^{\mathrm{R}}(1,2) = \left\{G^{>}(1,2) - G^{<}(1,2)\right\} \theta\left(t_1 - t_2\right), \\ G^{\mathrm{A}} &= -\left\{G^{>}(1,2) - G^{<}(1,2)\right\} \theta\left(t_2 - t_1\right), \\ G^{\mathrm{K}} &= G^{>}(1,2) + G^{<}(1,2). \end{aligned} \tag{2.13}$$

Here $G^{>}$and $G^{<}$are 2×2 matrices in Nambu space and are given by

$$G^{>}(1,2) = -i \left\langle \begin{pmatrix} \psi_{\uparrow}(1)\psi_{\uparrow}^{\dagger}(2) & \psi_{\uparrow}(1)\psi_{*}(2) \\ -\psi_{\downarrow}^{\dagger}(1)\psi_{\uparrow}^{\dagger}(2) & -\psi_{\downarrow}^{\dagger}(1)\psi_{\downarrow}(2) \end{pmatrix} \right\rangle \tag{2.14}$$

and

$$G^{<}(1,2) = \mathrm{i} \left\langle \begin{pmatrix} \psi_{\uparrow}^{\dagger}(2)\psi_{\uparrow}(1) & \psi_{v}(2)\psi_{\uparrow}(1) \\ -\psi_{\uparrow}^{\dagger}(2)\psi_{*}^{\dagger}(1) & -\psi_{*}(2)\psi_{*}^{\dagger}(1) \end{pmatrix} \right\rangle. \tag{2.15}$$

In eqs. (2.14) and (2.15) $\psi(1)$ and $\psi^{\dagger}(1)$ denote the electron field operators $\psi\left(r_1, t_1\right)$ and $\psi^{+}\left(r_1, t_1\right)$.

To illustrate the significance of the Keldysh function, G^{K}, we may evaluate eqs. (2.14) and (2.15) for a normal translationally invariant, non-interacting Fermi system with a particle distribution function $f_{p\sigma}$, where p is the particle momentum and E_p the particle energy (measured from the chemical potential). One then gets for the 11 -components of $G^{>}$and $G^{<}$

$$G^{>}(1,2)_{11} = -\mathrm{i} \sum_{p} \left(1 - f_{p\sigma}\right) \exp\left[\mathrm{i}p \cdot \left(r_1 - r_2\right) - \mathrm{i}E_p\left(t_1 - t_2\right)\right] \tag{2.16}$$

and

$$G^{<}(1,2)_{11} = \mathrm{i} \sum_{p} f_{p\sigma} \exp\left[\mathrm{i}p \cdot \left(r_1 - r_2\right) - \mathrm{i}E_p\left(t_1 - t_2\right)\right]. \tag{2.17}$$

From these expressions one sees, by subtraction, that the retarded and advanced functions do not contain the distribution function, but the Keldysh function does, since the sum of (2.16) and (2.17) is given by

$$G^{\mathrm{K}}(1,2)_{11} = -\mathrm{i}\sum_{p}(1-2f_{p\sigma})\exp\left[\mathrm{i}p\cdot(r_1-r_2)_{\mathrm{e}} - \mathrm{i}E_p(t_1-t_2)\right]. \tag{2.18}$$

As discussed above, the Green functions may be integrated over the magnitude of the momentum, corresponding to the variable $\xi = p^2/2m - \mu$, with μ the chemical potential. With the center-of-mass coordinates given by $r = \frac{1}{2}(r_1 + r_2)$ and $t = \frac{1}{2}(t_1 + t_2)$ the ξ-integrated Green function g is

$$g(\hat{\boldsymbol{p}}, E; rt) = \frac{\mathrm{i}}{\pi}\int_{-\infty}^{\infty}\mathrm{d}\xi G(\boldsymbol{p}, E, rt), \tag{2.19}$$

where p is the momentum variable and E the frequency variable associated with Fourier transforming with respect to the coordinates $r_1 - r_2$ and $t_1 - t_2$, respectively.

The matrix Green function satisfies the Dyson equation

$$\left(G_0^{-1} - \Sigma\right)\otimes G = \delta(1-2), \tag{2.20}$$

where $\otimes$ implies integration over internal variables, $(A\otimes B)(1,2) = \int \mathrm{d}3A(1,3)B(3,2)$. The operator G_0^{-1} is the inverse of the non-interacting Green function. A more convenient equation for G, more closely related to the Boltzmann equation, may be derived by subtracting the conjugate of eq. (2.20) from it:

$$\left[G_0^{-1} - \Sigma\otimes G\right] = 0. \tag{2.21}$$

A kinetic equation may then be derived from the off-diagonal (in Keldysh space) component of (2.21). We shall not describe this procedure in any detail, but refer the reader to the excellent review by Schmid (1981). In the applications discussed in the present chapter the Dyson equation (2.21) simplifies to an ordinary commutator involving the ξ-integrated Green function g instead of G :

$$\left[g_0^{-1} - \Sigma, g\right] = 0. \tag{2.22}$$

This equation must be supplemented by the normalization condition

$$gg = 1, \tag{2.23}$$

obtained by Eilenberger (1968) and Larkin and Ovchinnikov (1968). The diagonal part of equation (2.22) determines the retarded and advanced functions while the off-diagonal part becomes an equation for the distribution function which is associated with g^K. The particular choice of distribution functions made by Schmid and Schön (1975) corresponds to writing first

$$g^{\mathrm{K}} = g^{\mathrm{R}}h - hg^{\mathrm{A}}, \tag{2.24}$$

where g^K, g^R and g^A are 2×2 matrices in Nambu space. A diagonal distribution matrix h is then used to introduce the scalar distribution functions f^L and f^{T},

$$h = \left(1 - 2f^{\mathrm{L}}\right) - 2f^{\mathrm{T}}\tau_3. \tag{2.25}$$

As we mentioned above, the Keldysh component of the Green function contains effects both from changes in the spectral density of excitations, and from changes in their distribution function. In using eq. (2.24) one is attempting to separate out the two contributions to the Keldysh component. However, as we shall show below [see particularly the discussion after eq. (2.30)], eqs. (2.24) and (2.25) do not succeed completely in separating the two contributions to the Keldysh function. An elegant alternative way of making the separation has been described by

Shelankov (1980); in the limit when the
quasiparticle picture is valid the distribution function he introduces reduces to the usual quasiparticle distribution function, without any accompanying spectral density factors. In local equilibrium $1 - 2f^{\mathrm{L}} = \tanh(E/2T)$ and $f^{\mathrm{T}} = 0$. In the cases discussed below we may without loss of generality represent g^{R} and g^{A} in the simple form

$$g^{\mathrm{R}} = \alpha\tau_3 + \beta\tau_1, \quad g^{\mathrm{A}} = -\alpha^*\tau_3 + \beta^*\tau_1 \tag{2.26}$$

where $\tau_i (i = 1, 2, 3)$ are the usual Pauli matrices.
The functions α and β depend on the frequency variable E and the direction in momentum space $\hat{\boldsymbol{p}}$. They are written in terms of the real functions N_i, R_i $(i = 1, 2)$ as

$$\alpha = N_1 + \mathrm{i}R_1, \quad \beta = N_2 + \mathrm{i}R_2. \tag{2.27}$$

In the microscopic approach the charge imbalance Q^* introduced in eq. (2.6) takes the form

$$Q^* = -N(0)\frac{1}{4}\int_{-\infty}^{\infty} \mathrm{d}E \left\langle \mathrm{Tr}\, g^K \right\rangle \tag{2.28}$$

where $\langle \ldots \rangle$ denotes the average

$$\langle \ldots \rangle = \int \frac{\mathrm{d}\Omega_{\hat{p}}}{4\pi} \ldots \tag{2.29}$$

and $N(0)$ is the density of states per spin at the Fermi energy in the normal state of the metal.

When (2.24) is inserted into (2.28) one finds

$$Q^* = 2N(0)\int_{-\infty}^{\infty} \mathrm{d}E \left\langle N_1 f^{\mathrm{T}} \right\rangle \tag{2.30}$$

which should be compared with (2.6). In the quasiparticle limit the two distribution functions are thus seen to be related by $N_1 f^{\top} = \delta f^{le}$, since $\xi \mathrm{d}\xi = E\ \mathrm{d}E$, when $E = \sqrt{\xi^2 + \Delta^2}$.

The particle current j is given by

$$j = -\frac{N(0)}{4m}\int_{-\infty}^{\infty} \mathrm{d}E \left\langle p\, \mathrm{Tr}\left(\tau_3 g^{\mathrm{K}}\right) \right\rangle \tag{2.31}$$

and the heat current, j_{th} , by (Beyer Nielsen and Smith 1983)

$$j_{\mathrm{th}} = -\frac{N(0)}{4m}\int_{-\infty}^{\infty} \mathrm{d}E \left\langle Ep\, \mathrm{Tr}\, g^{\mathrm{K}} \right\rangle \tag{2.32}$$

In the static case these may be rewritten as

$$j = \frac{2N(0)p_{\mathrm{F}}}{m}\int_{-,}^{,} dE \left\langle N_1 \hat{p} \left(f^{\mathrm{L}} - \frac{1}{2} \right) \right\rangle \tag{2.33}$$

$$j_{\mathrm{th}} = \frac{2N(0)p_{\mathrm{F}}}{m}\int_{-\infty}^{\infty} \mathrm{d}E \left\langle E\hat{\boldsymbol{p}} N_1 f^{\mathrm{T}} \right\rangle \tag{2.34}$$

where p_{F} denotes the Fermi momentum.
Equations (2.30)-(2.32) are a natural starting point for developing a twofluid model. One writes densities and currents as the sum of two types of contribution-those coming from changes in the distribution function of excitations, which one associates with the normal component, and those coming from changes in spectral densities, which one associates with the superfluid component. Since the quantities $N_1 f^{\mathrm{T}}$ and $(f^{\mathrm{L}} - \frac{1}{2})$ correspond to the distribution function, eqs. (2.30)

and (2.34) show that the charge imbalance and the thermal current are naturally related to the normal component, while eq. (2.33) shows that the total current has both normal and superfluid components.

An important point to notice is that deviations in f^{L} and $N_1 f^{\mathrm{T}}$ are naturally related to the quantity δf_p^{le}, the difference between the quasiparticle distribution function, f_p, and an equilibrium distribution evaluated using the actual quasiparticle energy in the nonequilibrium state, $f^0(E_p)$. In the Green function approach the effects of quasiparticle energy shifts are taken into account implicitly, since the basic variable is the energy, not the momentum. The quasiparticle approach focuses attention on the distribution function for quasiparticles of a given momentum while the Green function approach focuses attention on excitations of a given energy. One consequence of this is that in the limit when the quasiparticle picture is valid, the distribution functions f^{L} and $N_1 f^{\mathrm{T}}$ for fixed E refer to states whose momenta depend on nonequilibrium contributions to the quasiparticle dispersion relation.

It is instructive to compare the expressions (2.30) and (2.33) for the density and current for a clean superconductor in the presence of a superflow characterized by velocity v_{s}. As we shall see in more detail in section 4 , the density-of-states function N_1 is given in the clean limit by

$$N_1 = \frac{|E - p_{\mathrm{F}} v_{\mathrm{s}} \cos\theta|}{\sqrt{(E - p_{\mathrm{F}} v_{\mathrm{s}} \cos\theta)^2 - \Delta^2}} \Theta\left(|E - p_{\mathrm{F}} v_{\mathrm{s}} \cos\theta| - \Delta\right), \tag{2.35}$$

where θ is the angle between p and the direction of superflow v_{c}. When one inserts eq. (2.35) into eq. (2.33), makes use of the expansion

$$N_1 \simeq N_1^0 - \frac{\partial N_1^0}{\partial E} p_{\mathrm{F}} v_{\mathrm{s}} \cos\theta \tag{2.36}$$

where N_1^0 is given by (2.35) with $\iota_{\mathrm{s}} = 0$, writes $f^{\mathrm{L}} = f^0(E) + \delta f^{\mathrm{L}}$, and integrates by parts, one finds

$$j = n_{\mathrm{s}} v_{\mathrm{s}} + \frac{2N(0)p_{\mathrm{F}}}{m} \int_{-\infty}^{\infty} \mathrm{d}E \left\langle N_1 \delta f^{\mathrm{L}} \hat{\boldsymbol{p}} \right\rangle \tag{2.37}$$

The term $n_s v_s$ in (2.37) originates in the term ($f^0 - \frac{1}{2}$), while the second term in (2.37) comes from the contribution δf^{L}, and corresponds to the normal part of the current j in eq. (2.8).* On the basis of the comparison of (2.37) and (2.8) we conclude that δf^{L}, which may depend on both the direction of momentum and energy, corresponds to δf_p^{le}. Finally let us compare the thermal currents (2.11) and (2.34). It is apparent that we must identify $N_1 f^{\mathrm{T}}$ in the BCS-limit with δf_p. as in the case of charge imbalance. In section 4 we study these distribution functions in more detail in a current-carrying superconductor with impurity scattering as the dominant relaxation mechanism, and solve the Dyson equation for the retarded and advanced Green functions as well as the kinetic equation for f^{T}. In the following section we discuss some examples of pair breaking effects on the calculated currents and densities in both the quasiparticle and Green function frameworks.

17.3 3. Pair-breaking effects

In order to determine the charge imbalance or the currents in a situation of physical interest one must in general solve a kinetic equation for the distribution function as in any other nonequilibrium problem. The kinetic equation depends on the physical quantity of interest as well as on whether one works with BCS-Bogoliubov quasiparticles or with the fully microscopic Green function picture. Naturally these two approaches must in some limit be equivalent. The subject of this section is to indicate when this is so, and to show in some detail how the results

obtained within the two approaches differ when pair breaking effects become significant. In the case of charge relaxation such a detailed, quantitative investigation was performed recently by Bever Nielsen et al. (1982), and we shall refer to many of their results in the following. Similar effects in the thermal conductivity were examined recently by Beyer Nielsen and Smith (1982), for situations where electron-phonon scattering and magnetic impurity scattering are the sources of pair breaking. In this section we provide the reader with an overview of what has been achieved as regards the quantitative understanding of the effects of pair breaking on charge relaxation and thermal conduction. We shall not, however, attempt to summarize the work that has gone into solving kinetic equations under a variety of other circumstances such as those related to radiation

surrulated superconductivity or gap relaxation, which are discussed elecwhere in the present volume.

Wher considering par-breaking effects on nonequilibrium properties it is iriportant or smphasive that in the quasiparticle approach such effects are included. to lowest order in the appropriate scattering rates. sia the cordlision mitegral in the Boltaman equation. The advantage of the Green function approach is that it allows one to include pair breaking to ail orders by taking mes accosunt the effects of pass breaking on the retarded and advanced Green functuors. We shall see how this works in two important cases of pair hreaking: (a) magnetic impunts and electron phomon scattenng and (b) scattering by ordinary impurities in the presence of a supercurrent.

17.3.1 3.1. Scattering by magnetic impurities and phonons

It is well known that ordinary impurt? scattering has no pair breaking effects. In accordance zith Anderson's theorem. By contrast. scattering by magnetic mpurmes. characteryed by the scattering rate I. mas be expected to influence the density of states significantly when I, becomes comparable with the energy gap 1. Withm the BCS theor; the densit; of states V_{is} ; is gien b; $|u^2 - t^2|^{-1}$, where u and v are the coherence factors given by eqs. (2.3) and 124). When ardten in terms of the quasiparticle energ: Ethe BCS density of states is

$$N_1(E) = \frac{E}{\sqrt{E^2 - 1^2}}\theta(|E| - \Delta) \tag{3.1}$$

since in this limit the real part of x, eq. (2.27), is the usual BCS density of states.

Pair breaking due to scattering by magnetic impurities and that due to electron phonon scatterng both remove the smgularity in eq. 13.11 at the gap codge through in rather different manners. When magnetic impunty scatterng acts on its own, one finds that $N_1(E = \Delta) \sim (\Delta\Gamma_0)^{13}$ for $\Gamma_0 \ll \Delta$, while when electron-phonon scattering acts alone, one has $N_1(E = \Delta) \sim (\Delta\Gamma_p)^{12}$ for $I. = 1.$ where I_s is the rate of scattering of ejectrons by phonom. A further difference between the two pair breaking mechamsms is that in the magnetic impurity case $N_1(E)$ vanishes for $|E| < 1 - \frac{1}{2}(I^{-2} \cdot 1)^{1/3}$ if pair breaking is weak. If " 1 1. while on the case of electron phonon scatterng \, $|E|$, 1 , finte for all value of E. ... ath $\Lambda_1(0) \sim I_2$ dif $I_2 = 1$. The density of state function I_1 (E). which mas be obtaned from the s-integrated retarded (sreen function q^2 ich

0

- Note that in situations where a perturbation is applied to a current-carrying superconductor the second term in (2.33) may contain terms proportional to v_s. The question of whether such terms are regarded as a contribution to the normal current or the supercurrent depends on ones viewpoint. On the one hand there is dissipation associated with the current, and so it may be considered to be a normal component, but, on the other hand, these currents do enter the expression for the penetration depth, and it may therefore be argued that they should be considered as contributions to the supercurrent.

eqs. 2.26, 2.27), is found in general by solving a quartic equation, which is derlied irom the equation of motoon for a^2 and the normallaturs conduon or a. eq. (2.23). The equation of motom for y^2 is the diagonal part of eq. 12.221. the difference between the Dyson equation and its conjugate. In term: of the
complex renormalization function $Z(E)$ and the gap function $\phi(E)$ of the Eliashberg (1971) theory the equation of motion is

$$ZE\beta - \mathrm{i}\phi\alpha + \mathrm{i}\Gamma_s\alpha\beta = 0 \tag{3.2}$$

and the normalization condition obtained from (2.23) is

$$\alpha^2 + \beta^2 = 1. \tag{3.3}$$

The generalized density of states functions N_1 and $R_i(i = 1, 2)$ are defined by the real and imaginary parts of α and β, according to eq. (2.27). In the BCS limit, where $A = \Phi/Z$ may be chosen to be real, one sees that N_1 is given by eq. (3.1),

$$R_1(E) = -\frac{E}{\sqrt{\Delta^2 - E^2}}\Theta(\Delta - |E|) \tag{3.4}$$

and

$$N_2 = -\Delta R_1/E, \tag{3.5}$$
$$R_2 = \Delta N_1/E. \tag{3.6}$$

When the pair breaking effects of phonons and magnetic impurities are included in eq. (3.2) the density of states functions become finite for all E. In a realistic case the evaluation of N_i and $R_i(i = 1, 2)$ may be quite laborious, since Z and Φ must in general be determined as functions of E by solving the Eliashberg equations. For a strong-coupling material like Pb the resulting density of states has structure at energies around 50 K which may be observed directly in tunneling experiments. The functions N_1 and R_1 serve as input to the kinetic equations appropriate to the physical situation under consideration. In figs. 1 and 2 we plot N_1 and N_2 for two different cases: (1) a weak-coupling superconductor with magnetic impurities, and (2) a model for Pb . The calculation for the latter case was carried out by Beyer Nielsen and Smith (1982). For the phonon spectra they used Scalapino's (1969) model for the phonon spectrum of Pb , supplemented by a Debye tail at low energies. The densities of states appear remarkably similar to those for the weak-coupling case in the absence of pair breaking, except for some broadening due to the finite quasiparticle lifetime. The most important difference is that the energy is measured in terms of the actual energy gap at the gap edge calculated including strong-coupling effects, not the BCS value of the gap: for the case considered $\Delta(E = \Delta) \simeq 1.21\Delta_{\mathrm{BCS}}$.

The kinetic equation is derived within the Green function approach from the off-diagonal component of eq. (2.22). We shall not go into the details of deriving the collision integral, since rather complete discussions have been given by Schmid (1981) and by Beyer Nielsen et al. (1982). The latter authors showed in detail how strong-coupling effects are included in the formulation,

but did not perform specific calculations for this case. Calculations of thermal conductivity and charge relaxation for the strong-coupling superconductor Pb were performed recently by Beyer Nielsen and Smith (1982). Below we specify the collision integral appropriate to charge relaxation and thermal conduction in terms of the distribution function $f^{\top}$, which determines the charge imbalance and heat current according to eqs. (2.30) and (2.34). For convenience we omit the effect of ordinary impurity scattering on the thermal conductivity, but this may be included easily. The general form of the kinetic equation is

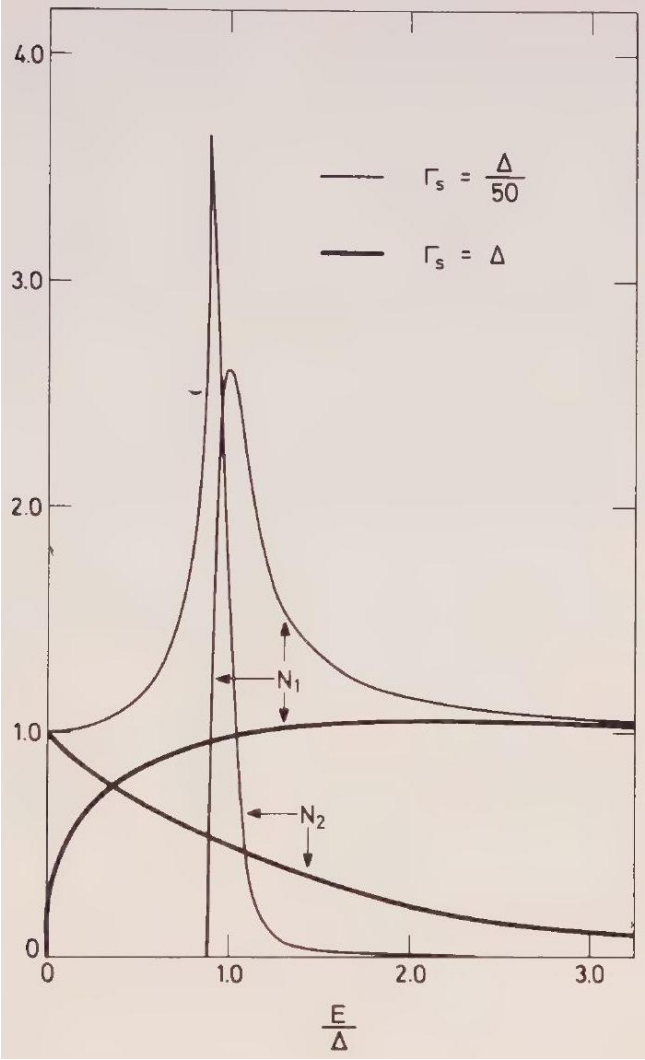


Fig. 1. The generalized density of states functions $N_{1} $ and N_2 for the case of magnetic scattering alone, for scattering rates $\Gamma_s = 0.02\Delta$ (thin lines), and $\Gamma_s = \Delta$ (thick lines). For $\Gamma_s = \Delta, N_1$ and N_2 are singular at $E = 0$, but for higher scattering rates N_1 and N_2 both remain finite at $E = 0$.}

$$X = I\left(f^{\mathrm{T}}\right) \tag{3.7}$$

where the driving term, X, may be due to tunnel injection or to the combined influence of a supercurrent and a temperature gradient, as discussed further below. The collision integral $I\left(f^1\right)$ for the case of charge relaxation (Schmid 1981, Beyer Nielsen et al. 1982) is

$$\begin{aligned} I\left(f^{\mathrm{T}}\right) = & -2\left(N_1 \operatorname{Im} ZE + N_2 \operatorname{Re} \Phi\right) f^{\mathrm{T}}(E) \\ & + \int_{-\infty}^{\infty} \mathrm{d}E' B\left(E, E'\right)\left(N_1(E) N_1\left(E'\right) + N_2(E) N_2\left(E'\right)\right) f^{\mathrm{T}}\left(E'\right) \end{aligned} \tag{3.8}$$

where

$$B\left(E, E'\right) = \pi \alpha^2 F\left(\left|E - E'\right|\right) \frac{\cosh\left(E'/2T\right)}{\sinh\left(\left|E - E'\right|/2T\right) \cosh(E/2T)}. \tag{3.9}$$

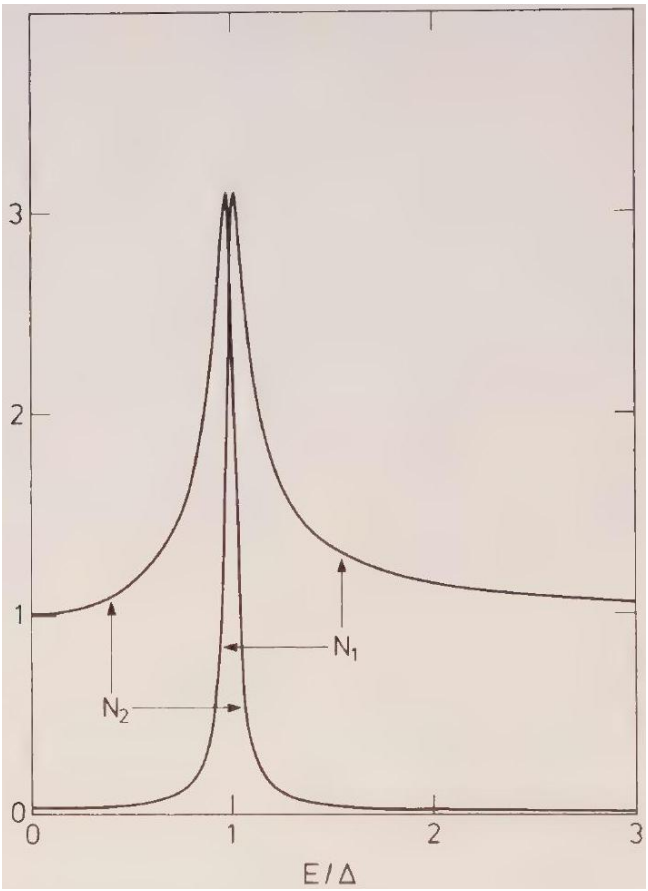


Fig. 2. The generalized density of states functions $N_{1} $ and N_2 for the strong-coupling superconductor Pb for the case of scattering by phonons alone at a temperature $T = 0.964T_c$. The phonon spectrum used is described in the text, and the gap Δ, which was obtained by solving the Eliashberg equations, is 0.436 meV . For this model $\mathrm{Re}\, Z(0)/\tau_{\mathrm{in}} \simeq 0.146 k_{\mathrm{B}} T_{\mathrm{c}}$, and the electronphonon scattering rate at the gap edge, $2\,(\mathrm{Im}\, ZE - (R_2/N_1)\,\mathrm{Im}\,\phi)_{|E=\Delta}$, equals 0.218Δ at $T = 0.964T_{\mathrm{c}}$.}

The function $\alpha^2F(E)$ entering eq. (3.9) is the effective phonon density of states, equal to bE^2 in a Debye model, where b is a constant. The collision integral for thermal conduction, calculated by Beyer Nielsen and Smith (1982), is the same as that for charge relaxation, except that α^2F in eq. (3.9) must be replaced by α_1^2F, an effective density of states for transport which is evaluated in the same way as α^2F, but with the inclusion of an additional factor $\hat{p} \cdot \hat{p}$ in the sum over phonon states. Here $\hat{\boldsymbol{p}}$ and $\hat{\boldsymbol{p}}$ are the directions of the initial and final electrons in the process in which an electron is scattered by a phonon. As a convenient measure of the strength of the electron-phonon interaction one may introduce the normal state relaxation time τ_{in} at T_{c} and at the Fermi energy,

$$\frac{1}{\tau_{\mathrm{in}}} = \frac{4\pi}{\mathrm{Re}\, Z(0)} \int_0^\infty \mathrm{d}E \frac{\alpha^2 F(E)}{\sinh\,(E/T_{\mathrm{c}})} \tag{3.10}$$

Next we specify the driving term X_{inj} appropriate to tunnel injection of charge. This is

$$X_{\mathrm{inj}} \;=\; \text{const.}\; N_1(E)\left(f^0(E - eV) - f^0(E + eV)\right), \tag{3.11}$$

where V is the injection voltage. In the case of thermal conductivity the driving term is

$$X_{\mathrm{th}} = \;\text{const.}\; EN_1(E)\left(\partial f^0/\partial E\right), \tag{3.12}$$

as shown in detail in the following section.
Before we discuss the results of solving the kinetic equation (3.7) let us show how to recover the ordinary quasiparticle Boltzmann equation. In this limit one must consistently treat the pair breaking parameters as small. This means that, since N_2 appears explicitly in the collision integral in the combination $2\,\mathrm{Re}\,\Phi N_2$, one needs to include in N_2 terms linear in Γ_s and Γ_p. One finds (Beyer Nielsen et al. 1982)

$$2\,\mathrm{Re}\,\Phi N_2 = \frac{2|E|}{\sqrt{E^2-\Delta^2}}\left(\frac{E^2}{E^2-\Delta^2}\Gamma_\mathrm{p} - \mathrm{Im}\,ZE\right) + \frac{2\Delta^2E^2}{\left(E^2-\Delta^2\right)^2}\Gamma_\mathrm{s}. \tag{3.13}$$

Combining this term with the remainder of the collision integral (3.8) and introducing the function $N_1 f^\top$, which in the limit of weak pair breaking goes over to the distribution function $\delta f'^c$ of the quasiparticle approach. one finds after dividing by $N_1^2 = q^{-2}$ the Boltzmann equation

$$\begin{aligned}&\text{const.}\ \left(f^0(E-eV)-f^0(E+eV)\right)q\\ &\quad = -2\left(\Gamma_\mathrm{p}+\frac{\Delta^2}{E^2}\frac{E}{|\xi|}\Gamma_\mathrm{s}\right)\delta f^{\ell\mathrm{e}} + q\int_{-\infty}^{\infty}\mathrm{d}\xi' B\left(E,E'\right)q'\delta f^{\ell\mathrm{e}}\left(\xi'\right)\end{aligned} \tag{3.14}$$

Beyer Nielsen et al. (1982) solved the kinetic equation obtained by equating (3.8) and (3.11) for a weak-coupling Debye model and varying amounts of magnetic impurity scattering; the results were compared with

solutions of the Boltzmann equation (3.14). The calculations were performed at arbitrary temperatures, and hence are not restricted by the condition $\Delta \ll T$. The results Beyer Nielsen et al. obtained by solving the Boltzmann equation are consistent with those obtained earlier by Lemberger and Clarke (1981), who also based their analysis on the quasiparticle Boltzmann equation (3.14).

The results of calculations based on the fully microscopic theory and on the Boltzmann equation are compared in fig. 3. Note how close the two sets of results are despite the fact that the pair-breaking parameter $1/\tau_\mathrm{s} = \Gamma_\mathrm{s}/\,\mathrm{Re}\,Z(0)$ is
comparable to Δ over much of the temperature range: in the example chosen $1/\tau_\mathrm{s} = 0.77T_\mathrm{c}$.

Also shown in the figure is a result due to Schmid and Schön (1975) for the charge relaxation rate ${\tau_{Q^*}}^{-1}$ near T_c. To lowest order in Δ/T, they found the charge relaxation time τ_{Q^*} to be given to a good approximation by

$$\frac{1}{\tau_{Q^*}} = \frac{\pi}{4}\frac{\Delta}{T_\mathrm{c}}\sqrt{\frac{1}{\tau_\mathrm{in}}\left(\frac{1}{\tau_\mathrm{in}}+\frac{2}{\tau_\mathrm{s}}\right)} \tag{3.15}$$

As one can see from fig. 3, this result is a good approximation only for $\Delta/T \lesssim 0.1$. For energy gaps in the range $0.2 < \Delta/T < 0.8$ the charge relaxation rate is proportional to Δ to a good approximation, but the coefficient differs from that in eq. (3.15). This behaviour is consistent with the experimental data of Lemberger and Clarke (1981). For more discussion of the data and their comparison with theory see Beyer Nielsen et al. (1982).

Turning to the case of thermal conductivity we again consider the effects of pair breaking due to electron-phonon scattering. In pure weak-coupling superconductors, the thermal conductivity should increase with decreasing temperature below T_c, according to weak-coupling calculations. However, the fact that in the strong-coupling superconductor Pb the thermal conductivity is found to fall rapidly just below T_c (Watson and Graham 1963) clearly demonstrates the inadequacy of weak-coupling equations for dealing with strong-coupling materials. A kinetic equation for strong-coupling superconductors was derived from the Kubo formula by Ambegaokar and Tewordt (1964), and the thermal conductivity for Pb near T_c was calculated in the relaxation time approximation by Ambegaokar and Woo (1965). The latter authors found

$\kappa_{\rm s}(T)/\kappa_{\rm n}(T) \simeq 1 - 11\,(1 - T/T_{\rm c})$, where $\kappa_{\rm n}$ and $\kappa_{\rm s}$ are the thermal conductivities in the normal and superconducting states, respectively, whereas experimentally the coefficient in this relation was found to be about -9 , compared with a typical value of -1.6 for weak-coupling superconductors (Gunault 1961). Subsequently calculations for Pb and Hg have been performed by Vashishta and Carbotte (1972), who used essentially the same formalism and approximations. These results show that strong-coupling effects are able to account for κ,κ_n in Pb behaving very differently from the way it does in weak-coupling superconductors.

Recently Beyer Nielsen and Smith (1982) have derived a kinetic equation for thermal conduction in strong-coupling superconductors on the basis of the quasiclassical Green function approach. Their equations appear to be rather different from those of Ambegaokar and Tewordt (1964), but in fact the two sets of equations may be shown to be equivalent, apart from some terms which are unimportant numerically. Beyer Nielsen and Smith (1982) then solved their kinetic equation for the case of Pb , using functions N_i and R_i calculated from gaps and renormalization factors obtained from solutions of the Eliashberg
equations for a strong-coupling superconductor. The calculations were made at arbitrary temperatures and did not employ the relaxation time approximation. The kinetic equation and the Eliashberg equations were both solved for the same phonon spectrum. which was taken to be that given by a model due to Scalapino (1469), supplemented by a Debye tail at low energics. Close to T_c the theoretical thermal conductivity is given by

$$\kappa_{\rm s}(T)\kappa_{\rm n}(T) \simeq 1 - 7\left(1 - \frac{T}{T_{\rm c}}\right).$$

and $\kappa_s(T)$ displays a maximum well below T_s in agreement with experiment (Mezahov-Deglin 1979).

Strong-coupling effects enter the calculations of transport coefticients in a number of different ways: they change the gap from the BCS value. they give quasiparticle states a finite width, and they modify the collision term, as a consequence of departures of the phonon spectrum from the Debye form. In the calculations for Pb . broadening of the quasiparticle states is unimportant. and the behaviour of the thermal conductivity is well accounted for by the quasiparticle Boltzmann equation neglecting broddening provided the collision term contains the correct phonon density of states and provided the strong-coupling result for the gap is used (Beyer Nielsen and Smith 14Si). In weah-coupling calculations the phonon spectrum is approximated by a Debye model, but in the calculations of Beter Vielsen and Smith the Debre tail of the phonon spectrum dominates only for $T \leqslant 0.4T_0$ and the structure in the temperature dependence of h, is due mainly to a laree peak in the transorre phonon density of states at an energy of about 50 K .

Calculations of the charge relaxation time for strong-compline superconductors have been carried out by Beyer Vielsen and Smith (19S21. For the case of electron phonon scattering they find that if broddening of the quasiparticle states can be neglected. the charge relaxation rate is given by

$$\tau_{Q^*}^{-1} = (\pi 4)(1T)\tau_{\rm in}^{-1} \quad \text{close to } T_{\rm c}$$

provided I is interpreted as the value of $\operatorname{Rec}\Phi/$ / 1 at the sap edge. * Line the phonon spectrum described abowe they hate carried out calculations for Pb . and find that $e^{-}F^{-}$in is about 1.5 times the weak-coupling value at I $T = 1.2$. times it at $dT = 2,4$ times it at $dT = 3$, and 5 times it at $dT = 5$. As a function of TT_c, the difference between the weak- and strong-coupling calculations is even more pronounced, because of the more rapid rise in . I with decreasing temperature in the strong-coupling calculation.

[0]*In agreement with Beyer Nielsen et al. (1982) we use here a definition of τ_Q that includes the renormal-

As a last example of the effects of pair breaking we mention the frequency- sepandent conducuraty of a ding cupercond cator anken may be roce ared by whermptime a mall P} curress on a large Jor coment, as in the angmal experiment by Peters and Meanner (1971). Recently Pitger and Meanner 119401 roprasad and exagudest thus experiment They analy, eas there ereamental data in terms of the theory due to Schmid (1968, 1969) who derived an interpolation formula for the frequency-dependent conductivity in the presence of electron powon restionerg Pitger and Meanon found that is 2 an necessary to introduce an excess conductivity to account for their experimental results near T_c at relatively high frequencies. This excess conductivity may be explained by the effects of pair breaking, as shown by Beyer Nielsen et al. (1984).

The interpotaton formala dae to S.armed 1964. 19631 applien to tex reagen near T_c, where $t \ll T_c$ and is in addition restricted in validity to the frequency region $\omega \ll \Delta$. It was shown by Ovchinnikov et al. (1981) that at very low remperatures the frequence: cependence of the conductury a deamermed by the relaxation time at the gap edge. In their recent calculation Beyer Nielsen et al rigit exterded and apposimate reatmente to arbarrary ; above of or. and t T, subject only to the condition $\omega \ll t$. From numerical solutions to the kinetic equations these authors investigated the validity of the relaxation time spporamator. and anted that ∴ aork quite well sase: the rans 'Ion temperature, where the frequency-dependent conductivity involves two characteristic times, z_{is} and the gap-relaxation time. :- - (r. - (1) 1) 1T. To illustrate the result we consider the case when T is close to T_c. In the relaxation time approximation Beyer Vieken et al. (1984) find

$$= \frac{\mathrm{i}\sigma_s \pi}{2} \frac{\Delta^2}{T} \int_1 1 - \frac{\Gamma}{3\Gamma_s} \left(1 + \frac{(2 - \mathrm{i}\omega_{sin})^2}{2\,(1 - \mathrm{i}\omega_s)\,(1 - \mathrm{i}\omega_{si})} \right)' \Bigg\}' \tag{13.161}$$

provided $t/T \ll 1$ and $\omega T \ll t/T$, where $\Gamma = 2D p_F^2$, σ_n is the normal state DC conductivity, $p_F = m_e v_F$ is the momentum of an electron in the condensate, $D = \frac{1}{3} t_2^2 \tau_{\mathrm{imp}}$ is the diffusion coefficient in the normal state. and

$$\Gamma_c = \frac{T' = (3)}{6\pi^3} \frac{\Delta^2}{T} = \frac{4}{3\pi} (T_c - T)\,.$$

Schmid's interpolation formula is

$$== \frac{\mathrm{i}\pi\sigma_s}{2 \cos \frac{\Delta^2}{T} \int_1 1 - \frac{\Gamma}{3\Gamma_2} \left(1 - \frac{2}{1 - \mathrm{i}\omega_s} \right)' \Bigg\}} \tag{3.17}$$

which agrees with (3.16) in the limit when $t/T \ll 1$. At slightly lower temperatures, down to $0.95\,T_c$, both (3.16) and (3.17) fit the numerical solution quite well, the former yielding a more accurate description of the collisionless limit $\omega\tau_{\mathrm{in}} \gg 1$. As we mentioned above, calculations of the conductivity have been carried out for a wide range of conditions, but because the results cannot be expressed in particularly simple form we shall not display them here.

Pair breaking effects due to phonons are of importance also to the thermoelectric effect which one observes when a supercurrent passes through a superconductor in the presence of a temperature gradient. This will be treated in the next section.

---

ization factor ReZ(0). Note that Beyer Nielsen and Smith (1982) used a definition of τ_{Q^*} without Re$Z(0)$.

17.4 4. Impurity scattering in the presence of a supercurrent. Effects of a temperature gradient

In this section we illustrate a number of the points made in the previous sections by discussing in detail the derivation of a kinetic equation appropriate to impurity scattering in the presence of a supercurrent and a temperature gradient. Electron-phonon scattering is neglected in this section in order to keep the discussion simple. Within this model we show how the charge imbalance and the thermal conductivity are calculated from the same kinetic equation. A great virtue of this problem is that the majority of the results can be obtained analytically. In addition, the problem is an important one since impurity scattering is the dominant scattering mechanism in many experiments. Most of the calculations for the charge imbalance have been described by Beyer Nielsen et al. (1982), but here we show in addition how to obtain simple analytic results not only in the clean and dirty limits, but also in between. The results for the dependence of the thermal conductivity on the superfluid velocity have not been published before. The generation of charge imbalance by the simultaneous application of a temperature gradient and a supercurrent was first proposed by Pethick and Smith (1979b) and subsequently observed by Clarke et al. (1979) and Fjordboge et al. (1981). The relaxation by impurities has been considered by Schmid and Schön (1979), Clarke and Tinkham (1980) and Beyer Nielsen et al. (1980).

In the clean limit, a quasiparticle with energy $E > A + p_{\mathrm{F}} l_{\mathrm{s}}$ can scatter into any direction, but for $\Delta - p_{\mathrm{F}} v_{\mathrm{s}} < E < \Delta + p_{\mathrm{F}} v_{\mathrm{s}}$, the momenta of possible states are limited to a cone whose vertex is directed antiparallel to the superfluid velocity. As a consequence, the scattering rates for states in the pocket with energy in the range $\Delta - p_{\mathrm{F}} v_{\mathrm{s}} < E < \Delta + p_{\mathrm{F}} v_{\mathrm{s}}$ are very different from those for states with $E > A + p_{\mathrm{F}} l_{\mathrm{s}}$. The calculations we describe will show how, as the impurity scattering rate is increased, the pocket of states gets smoothed out by depairing due to the finite supercurrent, as was pointed out first by Schön (1981a).

The fundamental equation of motion (2.22) involves the inverse of the noninteracting Green function $\hat{g}_0{}^{-1}$. The matrix $\hat{g}_0{}^{-1}$ is proportional to a unit
matrix in Keldysh space, $\hat{g}_0^{-1} = \hat{1} g_0^{-1}$. In the stationary case, where we consider only impurity scattering in the presence of a supercurrent, g_0^{-1} is a 2×2 matrix in Nambu space,

$$g_0^{-1} = \tau_3 \left(E - p \cdot v_s\right) + \mathrm{i} \frac{p \cdot \nabla}{m} - e\phi \tag{4.1}$$

Here E is the energy (frequency) variable, $p = p_{\mathrm{F}} \hat{p}$ is the momentum, and ϕ the electrostatic potential. The self energy $\hat{\Sigma}^{\mathrm{R}}$ consists of the usual pairing contribution and a part $\hat{\Sigma}_{\mathrm{imp}}$ due to impurity scattering,

$$\hat{\Sigma}^{\mathrm{R}} = -\mathrm{i}\Delta\tau_1 + \hat{\Sigma}_{\mathrm{imp}}. \tag{4.2}$$

We neglect for simplicity the effects of phonon renormalization, although they may readily be kept (Beyer Nielsen et al. 1982). The impurity part of the self energy is calculated with a self-consistent Born approximation. With the further assumption that the scattering in the normal state is pure s-wave, the impurity contribution to the self energy may be written as

$$\hat{\Sigma}_{\mathrm{imp}} = -\frac{\mathrm{i}}{2\tau_{\mathrm{imp}}} \langle \hat{g}(\hat{p}, E, r) \rangle \tag{4.3}$$

where $\langle \ldots \rangle$ denotes the angular average (2.29), and τ_{imp} is the normal state impurity scattering time. The equation of motion (2.22) is solved by the ansatz (2.24-2.26). With this ansatz the normalization condition is simply

$$\alpha^2 + \beta^2 = 1. \tag{4.4}$$

The kinetic equation for $f^{\top}$ is obtained from the component of (2.22) which is off-diagonal in Keldysh space, and proportional to τ_3 in Nambu space:

$$\mathrm{Tr}\left\{\tau_3\left(\left(\,\mathrm{g}_0^{-1}-\Sigma^{\mathrm{R}}\right)g^{\mathrm{K}}-\Sigma^{\mathrm{K}}g^{\mathrm{A}}-g^{\mathrm{K}}\left(g_0^{-1}-\Sigma^{\mathrm{A}}\right)+g^{\mathrm{R}}\Sigma^{\mathrm{K}}\right)\right\}=0 \tag{4.5}$$

When g_0^{-1} and Σ are inserted from eqs. (4.1)-(4.5) together with the expressions (2.24) and (2.25) for g^{K} the following kinetic equation results:

$$\begin{aligned}N_1\frac{p}{m}\cdot\nabla f^{\mathrm{L}}=-\frac{1}{\tau_{\mathrm{imp}}}\{&\left\{\left(N_1\left\langle N_1\right\rangle+N_2\left\langle N_2\right\rangle\right)f^{\mathrm{T}}\right.\\&\left.-N_1\left\langle N_1f^{\mathrm{T}}\right\rangle-N_2\left\langle N_2f^{\mathrm{T}}\right\rangle\right\}-2AN_2f^{\mathrm{T}}\end{aligned} \tag{4.6}$$

The integral equation (4.6) is separable and may readily be solved, once $f^{\mathrm{L}}\simeq f^0(E)$ is inserted on the left-hand side. When v_{s} is parallel to ∇T, equation (4.6) may be written as

$$\begin{aligned}c(E)N_1x=&\left(N_1\left\langle N_1\right\rangle+N_2\left\langle N_2\right\rangle\right)f^{\mathrm{T}}\\&-N_1\left\langle N_1f^{\mathrm{T}}\right\rangle-N_2\left\langle N_2f^{\mathrm{T}}\right\rangle+\gamma^{-1}N_2f^{\mathrm{T}},\end{aligned} \tag{4.7}$$

with $\gamma=\frac{1}{2\tau_{\mathrm{imp}}\,\Delta}$ and $c(E)=v_{\mathrm{F}}\tau_{\mathrm{imp}}\left|\nabla T\right|(E/T)\left(\partial f^0/\partial E\right)$. We can now find the desired averages $\left\langle N_1f^{\top}\right\rangle$ and $\left\langle N_1f^{\top}x\right\rangle$,

$$\left\langle N_1f^{\mathrm{T}}\right\rangle=c\frac{\left\langle N_1^{-1}\tau x\right\rangle+\gamma\left\langle N_1x\right\rangle\left\langle N_1^{-2}N_2\tau\right\rangle}{1-\left\langle N_1^{-1}\tau\right\rangle} \tag{4.8}$$

and

$$\begin{aligned}\left\langle N_1f^{\mathrm{T}}\mathrm{x}\right\rangle=&c\left(\left\langle N_1^{-1}\tau x^2\right\rangle+\gamma\left\langle N_1x\right\rangle\left\langle N_2N_1^{-2}\tau x\right\rangle\right)\\&+\left\langle N_1f^{\mathrm{T}}\right\rangle\left\langle N_1^{-1}\tau x\right\rangle,\end{aligned} \tag{4.9}$$

where the quantity τ is defined by

$$\frac{1}{\tau}=N_1^{-3}\left(N_1\left\langle N_1\right\rangle+N_2\left\langle N_2\right\rangle+\gamma^{-1}N_2\right). \tag{4.10}$$

The results (4.8)-(4.10) are obtained most easily by eliminating $\left\langle N_2f^{\mathrm{T}}\right\rangle$ by averaging eq. (4.7) over angle. From (4.8) and (4.9) the charge imbalance Q^* and heat current j_{th} are obtained as

$$Q^*=2N(0)\int_{-\infty}^{\infty}\mathrm{d}E\left\langle N_1f^{\mathrm{T}}\right\rangle \tag{4.11}$$

and

$$j_{\mathrm{th}}=2N(0)v_{\mathrm{F}}\int_{-\infty}^{\infty}\mathrm{d}EE\left\langle N_1f^{\mathrm{T}}x\right\rangle \tag{4.12}$$

Although formally the problem is solved by these results one must know N_1 and N_2 as functions of energy and angle in order to carry out the integrals over these two variables. Let us first discuss some simple limits, when the selfconsistency equations may be solved analytically. The component of (2.22) diagonal in Keldysh space yields one equation which α and β must satisfy,

$$\left(E-p_{\mathrm{F}}v_{\mathrm{s}}\cos\theta\right)\beta-\mathrm{i}\Delta\alpha+\frac{\mathrm{i}}{2\tau_{\mathrm{imp}}}(\langle\alpha\rangle\beta-\langle\beta\rangle\alpha)=0. \tag{4.13}$$

This must be solved together with the normalization condition (4.4).

17.4.1 4.1. Dirty limit

The effect of strong impurity scattering is to wash out most of the anisotropy associated with the supercurrent. The self-consistency equations may be solved by an ansatz which retains only s and p waves:

$$\begin{aligned} \alpha &= \alpha_0 + \alpha_1 x, \\ \beta &= \beta_0 + \beta_1 x, \end{aligned} \tag{4.14}$$

where $x = \cos\theta$. One finds readily that, provided $1/\tau_{\text{imp}} \gg \sqrt{E^2 - \overline{A^2}}$, α_0 and β_0 satisfy the equations

$$\alpha_0^2 + \beta_0^2 = 1 \tag{4.15}$$

$$E\beta_0 - \mathrm{i}\Delta\alpha_0 + \mathrm{i}\Delta\frac{\delta^2}{3\gamma}\alpha_0\beta_0 = 0 \tag{4.16}$$

where $\delta = p_{\mathrm{F}} v_{\mathrm{s}}/\Delta$. The equations (4.15) and (4.16) are identical with those for magnetic impurity scattering if one replaces $\Delta\delta^2/3\gamma$ in eq. (4.16) by the rate Γ_{s} for scattering by magnetic impurities. The quantities β_1 and α_1 are obtained by combining the p -wave component of the normalization condition,

$$\alpha_0\alpha_1 + \beta_0\beta_1 = 0, \tag{4.17}$$

with the p-wave component of (4.13). The result is

$$\beta_1 \simeq \frac{1}{\mathrm{i}}\frac{\delta}{\gamma}\alpha_0\beta_0 \tag{4.18}$$

and

$$\alpha_1 \simeq \mathrm{i}\frac{\delta}{\gamma_{\prime}}\beta_0^2. \tag{4.19}$$

One therefore obtains the important relations

$$N_1 = N_1^0 - x\frac{2\delta}{\gamma}N_2^0 R_2^0, \tag{4.20}$$

$$N_2 = N_2^0 + x\frac{\delta}{\gamma}\left(N_1^0 R_2^0 + N_2^0 R_1^0\right) \tag{4.21}$$

which express N_i in terms of the isotropic parts of the density of states functions which are obtained from eqs. (4.15) and (4.16) and the relationships $\alpha_0 = N_1^0 + \mathrm{i}R_1^0$ and $\beta_0 = N_2^0 + \mathrm{i}R_2^0$.

Instead of working directly with the formal solution it is easier to expand $N_1 f^{\mathrm{T}}$. Writing

$$N_1 f^{\mathrm{T}} = f_0 + f_1 x \tag{4.22}$$

one finds from insertion into eq. (4.7)

$$\frac{f_0}{c} = \frac{N_1^0}{N_2^0}\gamma\left\langle N_1 x\right\rangle = -\frac{2}{3}\delta N_1^0 R_2^0 c \tag{4.23}$$

and

$$\frac{f_1}{c} = \frac{1 + 2(\Gamma/\Delta) N_2^0 \left(R_2^0\right)^2 \left(1 + \left(N_2^0/N_1^0\right)^2\right)}{1 + \left(N_2^0/N_1^0\right)^2 + \gamma^{-1} N_2^0 / \left(N_1^0\right)^2}, \tag{4.24}$$

where $\Gamma = \frac{1}{3}\delta^2\Delta/\gamma = 2Dp_s^2$ is the characteristic rate for pair breaking by the superflow. In the limit $v_s \to 0, N_2^0$ tends to zero for $E > \Delta$, and therefore f_1/c, given by eq. (4.24), tends to unity. The difference between the right-hand side and unity is therefore a measure of how much the heat current is affected by the superflow. We plot $-f_0/c$ and f_1/c for $\Gamma = 10^{-2}\Delta$ in figs. 4 and 5 as functions of E, taking $\gamma = 1$ in (4.24). To find the thermal conductivity, κ, one needs to perform the energy integral in the heat current

$$j_{\rm th} = \frac{2}{3} N(0) v_F \int_{-\infty}^{\infty} {\rm d}E E f_1(E) \tag{4.25}$$

The trace in Nambu space of the Keldysh component of the kinetic equation is

$$N_1 \frac{\boldsymbol{p}\cdot\boldsymbol{\nabla}}{m} f^{\rm T} = -\frac{1}{\tau_{\rm imp}} \left[\left(N_1 \langle N_1 \rangle - R_2 \langle R_2 \rangle \right) f^{\rm L} - N_1 \left\langle N_1 f^{\rm L} \right\rangle + N_2 \left\langle N_2 f^{\rm L} \right\rangle \right]. \tag{4.26}$$

If, in the spirit of the standard Chapman-Enskog development, one inserts a local equilibrium distribution function ($f^{\rm T} = 0$) on the left-hand side, the driving term vanishes and $f^{\rm L}$ is then given by a local equilibrium distribution function $f^L = \left(e^{E/T(r)} + 1\right)^{-1}$. Only if one works to higher order in λ/L, where λ is a typical mean free path and L is a typical length scale for spatial variations, does $f^{\rm L}$ deviate from equilibrium.

17.4.2 4.2. Intermediate case

The transition from the clean limit to the dirty limit has been discussed extensively by Schön (1981a,b) and by Beyer Nielsen et al. (1981, 1982). The effect of impurities is found to depend strongly on energy. For the case of weak impurity scattering one finds that the charge relaxation rate for states in the pocket with energy $\Delta - p_F v_s \leqslant E \leqslant \Delta + p_F v_s$ is of order $(1/\tau_{\rm imp})\,(p_F v_s/\Delta)^{1/2}$. Pair breaking in the pocket region can not be treated as small when the charge relaxation rate is comparable to a typical quasiparticle energy, measured with respect to the gap Δ. Thus for energies near Δ the transition between clean and dirty behaviour occurs when

$$\frac{1}{\tau_{\rm imp}} \left(\frac{p_F v_s}{\Delta}\right)^{1/2} \sim p_F v_s, \quad \text{or} \quad \frac{1}{\tau_{\rm imp}\,\Delta} \sim \left(\frac{p_F v_s}{\Delta}\right)^{1/2}. \tag{4.27}$$

For high energies ($|E - A| \gg \Delta$), the transition between clean and dirty behaviour occurs when

$$\frac{1}{\tau_{\rm imp}} \simeq E. \tag{4.28}$$

For $|E| - \Lambda - p_F v_s \gg p_F v_s$, Beyer Nielsen et al. (1982) find for the quantity of importance in the expression for the charge imbalance, eq. (4.11),

$$\left\langle N_1 f^{\rm T} \right\rangle = -\tau_{\rm imp} v_s \cdot \nabla T \frac{E}{T} \frac{\partial f^0}{\partial E} v_F p_F \frac{\frac{4}{15}\left(E^2 - A^2\right)^2 + 2\left(E^2 - \Delta^2\right)\Gamma_{\rm imp}^2 + \frac{2}{3}\Gamma_{\rm imp}^4}{\left(E^2 - \Delta^2 + \Gamma_{\rm imp}^2\right)^2 \left(E^2 - \Delta^2\right)}, \tag{4.29}$$

where $\Gamma_{\rm imp} = 1/(2\tau_{\rm imp})$. This result shows that the transition between the clean and dirty limit occurs when $\sqrt{E^2 - A^2} \simeq 1/(2\tau_{\rm imp})$, which reduces to (4.28) when $|E - \Delta| \gg \Delta$. Close to $T_{\rm c}$ the region when $|E| - \Delta - p_{\rm F} v_{\rm s} \leqslant p_{\rm F} v_{\rm s}$ contributes little

to the charge imbalance, and to leading order in Δ the charge imbalance (4.11) may be obtained by integrating over E the high energy expression (4.29) with Δ put equal to zero. One finds

$$Q^* = \frac{4}{15} N(0) p_{\rm F} v_{\rm F} \tau_{\rm imp} v_{\rm s} \cdot \frac{\nabla T}{T} I\left(\Gamma_{\rm imp}/T\right), \tag{4.30}$$

where

$$\begin{aligned} I\left(\Gamma_{\rm imp}/T\right) &= \int_{-x}^{\infty} {\rm d}E \left(\frac{-\partial f^0}{\partial E}\right) \left(2 + \frac{11\left(\Gamma_{\rm imp}\right)^2}{E^2 + \Gamma_{\rm imp}^2} - \frac{8\Gamma_{\rm imp}^4}{\left(E^2 + \Gamma_{\rm imp}^2\right)^2}\right) \\ &= 2 + 7y\psi'\left(\frac{1}{2} + y\right) + 4y^2\psi''\left(\frac{1}{2} + y\right) \end{aligned} \tag{4.31}$$

where $y = \Gamma_{\rm imp}/(2\pi T)$, and ψ' and ψ'' are the tri-gamma function and its derivative. In the clean limit ($\Gamma_{\rm imp}/T \to 0$), I is 2 and

$$Q^* = \frac{8}{15} N(0) v_{\rm F} \tau_{\rm imp} v_{\rm s} \frac{\nabla T}{T}$$

while in the dirty limit I is 5 and

$$Q^* = \frac{4}{3} N(0) v_{\rm F} \tau_{\rm imp} v_{\rm s} \frac{\nabla T}{T}$$

The transition between these two limiting behaviours is shown in fig. 6, in which eq. (4.31) is plotted as a function of $\Gamma_{\rm imp}/T$.

Finally we discuss the lowest energy, E_g, at which there is a finite density of states. This is the lowest energy for which β_0, the angular average of β, has a finite imaginary part. From eq. (4.13) and the normalization condition (4.4) one finds the following quintic equation for β_0 :

$$\frac{2}{3}\gamma\delta^2\beta_0^5 + \left(\delta^2 + 2\delta x_0\gamma^2\right)\beta_0^4 + 4\delta\gamma x_0\beta_0^3 + \left(\gamma^2 + 2\delta x_0\right)\beta_0^2 + 2\gamma\beta_0 + 1 = 0, \tag{4.32}$$

where $\gamma = \Gamma_{\rm imp}/\Delta, \delta = p_{\rm F} v_{\rm s}/\Delta$, and $x_0 = (E - \Delta)/p_{\rm F} v_{\rm s}$. In the clean limit one finds

$$E_{\rm g} \simeq \Delta - p_{\rm F} v_{\rm s} \left(1 - \frac{2}{3}\frac{\gamma}{\sqrt{\delta}}\right), \quad \gamma \ll \sqrt{\delta}, \tag{4.33}$$

while in the dirty limit

$$E_{\rm g} \simeq \Delta - p_{\rm F} v_{\rm s} \frac{\sqrt{3}}{2} \left(\frac{\sqrt{\delta}}{\gamma}\right)^{2/3}, \quad \gamma \gg \sqrt{\delta}. \tag{4.34}$$

Note that the transition from the clean to the dirty limit occurs when $\gamma \sim \sqrt{\delta}$, or $1/2\tau_{\rm imp} \simeq \sqrt{p_{\rm F} v_{\rm s} \Delta}$, in agreement with eq. (4.27). A graph of $E_{\rm g}$ versus $\gamma\sqrt{\delta}$ in the intermediate regime is shown in fig. 7.

17.4.3 4.3. Clean limit

In the clean limit quasiparticles with $E > A + p_{\rm F}v_{\rm s}$ can scatter in all directions, but for $E < A + p_{\rm F}v_{\rm s}$ the solid angle into which quasiparticles can scatter is restricted because the minimum energy of a quasiparticle is $A + p_{\rm F}v_{\rm s}x$, where

$x = \hat{p}\cdot\hat{v}_{\rm s}$. This leads to rather different behaviours of the quasiparticle distribution function depending on whether E is greater or less than $\Delta + p_F v_s$. The charge imbalance for this case was first calculated by Beyer Nielsen et al. (1980), and the result for the thermal conductivity is new. One finds

$$Q^* = 2N(0)v_{\rm F}\tau_{\rm imp}\frac{\hat{v}_{\rm s}\cdot\nabla T}{T}\int_{1-p_{\rm F},}^{\infty}{\rm d}E\left(\frac{\partial f^0}{\hat{c}E}\right)E\frac{\langle q\tau x\rangle}{1-\langle q\tau\rangle} \tag{4.35}$$

and

$$\kappa = 4N(0)v_{\rm F}^2\tau_{\rm imp}\frac{1}{T}\int_{1-p_{\rm F}}^{\infty}{\rm d}E\left(\frac{-\partial f^0}{\partial E}\right)E^2\left\{\left\langle q\tau x^2\right\rangle + \frac{\langle q\tau x\rangle^2}{1-\langle q\tau\rangle}\right\}. \tag{4.36}$$

where $q = N_1^{-1}$ and τ is the $\gamma = 0$ limit of eq. (4.10). We now consider the contributions to the integrands for $E > A + p_{\rm F}v_{\rm S}$ and $E < \Delta + p_{\rm F}v_{\rm S}$.
(a) $E > \Delta + p_{\rm F}v_{\rm s}$. For $E - \Delta > p_{\rm F}v_{\rm s}$ one may expand quantities in powers of $v_{\rm s}$, and one finds

$$\begin{aligned}
\langle q\tau\rangle &= 1 - \frac{1}{3}\frac{\delta^2}{(e^2-1)^2} + \cdots \\
\langle q\tau x\rangle &= -\frac{4}{45}\frac{\delta^3 e}{(e^2-1)^3} + \cdots \\
\left\langle q\tau x^2\right\rangle &\simeq \frac{1}{3} - \frac{7}{45}\frac{\delta^2}{(e^2-1)^2} + \cdots
\end{aligned} \tag{4.37}$$

(b) $\Delta - p_{\rm F}v_{\rm s} < E < \Delta + p_{\rm F}v_{\rm s}$. In the pocket one finds

$$q\tau = \begin{matrix} 2\sqrt{\varepsilon - (1+x)} \\ \sqrt{\varepsilon}\dfrac{4}{3}\varepsilon - (1+x)\end{matrix}, \tag{4.38}$$

where $\varepsilon = 1 + (E-1)p_{\rm F}l'$ s is a dimensionless energy parameter which varies from 0 to 2 . For the angular averages one finds

$$\begin{aligned}
\langle q\tau\rangle &= 2\left(1 - \frac{\pi}{3\sqrt{3}}\right) \simeq 0.7908. \\
\langle q\tau x\rangle &= -2\left(1 - \frac{\pi}{3\sqrt{3}}\right) + 2\varepsilon\left(1 - \frac{4\pi}{9\sqrt{3}}\right), \\
\left\langle q\tau x^2\right\rangle &= 2\left(1 - \frac{\pi}{3\sqrt{3}}\right) - 4\varepsilon\left(1 - \frac{4\pi}{9\sqrt{3}}\right) + \varepsilon^2\left(\frac{12}{5} - \frac{32\pi}{27\sqrt{3}}\right).
\end{aligned} \tag{4.39}$$

In fig. 8 we plot the function $-\langle q\tau x\rangle(1 - \langle q\tau\rangle)$, which determines the charge
imbalance according to (4.35), as a function of ε. The corresponding plot for the function $\langle q\tau x^2\rangle + \langle q\tau x\rangle^2/(1 - \langle q\tau\rangle)$ in eq. (4.36) is shown in fig. 9.

In order to calculate the physically observable quantities, Q^* and κ, as functions of the temperature, the energy integrals (4.35) and (4.36) must be performed. For the case of charge

imbalance, this was done by Beyer Nielsen et al. (198()). In the case of thermal conductivity one finds in this clean limit a

change linear in v_s from the usual $v_s = 0$ result for the impurity-limited thermal conductivity. Because of the above mentioned smearing effects on the pocket caused by the impurities, such an effect is probably not experimentally observable.

17.5 5. Conclusion

We have reviewed the quasiclassical approach to non-equilibrium phenomena in superconductors and discussed solutions to kinetic equations that are appropriate to a variety of physical circumstances when pair breaking effects are significant. The results are compared with those based on solving a conventional kinetic equation for Bogoliubov quasiparticles. In many situations the latter approach yields surprisingly accurate answers, but there are cases, such as the thermoelectric effect associated with a supercurrent and a temperature gradient, when pair breaking effects under normal experimental conditions require use of the quasiclassical approach. From the point of view of getting reliable numerical solutions to the kinetic equations and obtaining the associated relaxation rates the quasiclassical approach is not significantly more difficult than the conventional Boltzmann equation method, although the latter is conceptually simpler. The theoretical results reviewed in this chapter have been derived without making any assumptions on the magnitude of the energy gap relative to the temperature. They are therefore applicable at all temperatures and make possible a detailed comparison of experiment with theory.

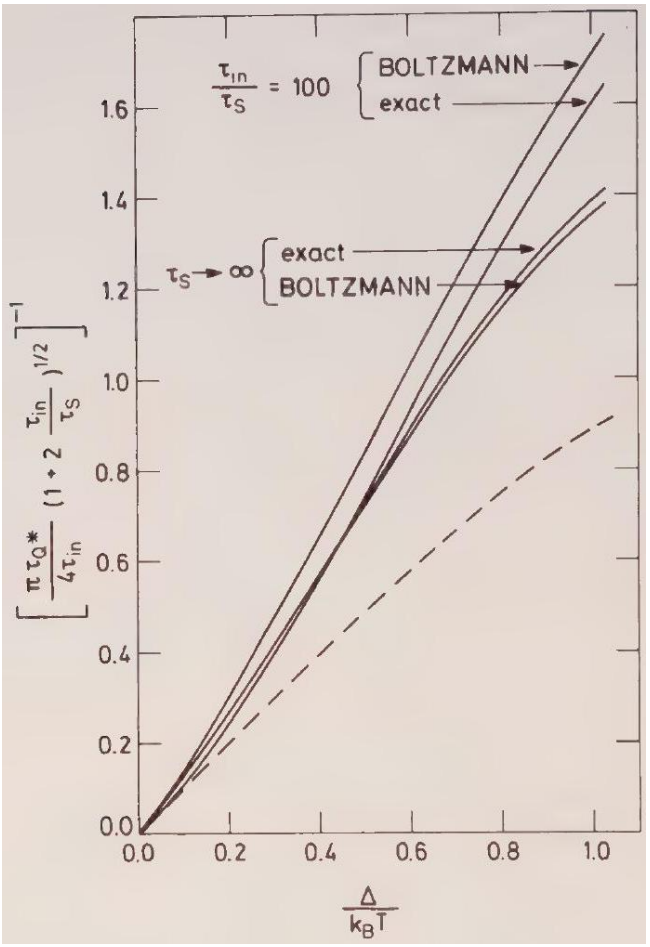


Fig. 3. Plot of the quantity $\left[\left(\pi \tau_{Q^{*
} / 4 \tau_{\mathrm{in}}\right)\left(1+2 \tau_{\mathrm{in}} /
\tau_{\mathrm{s}}\right)^{1 / 2}\right]^{-1}$ as a function of Δ/T. The dashed line is the Schmid and Schön expression Δ/T_c for this quantity. (See eq. 3.15.) The full curves show results calculated from the Boltzmann equation, and from the equations with broadening included ("exact"), as described in the text. The curves are for $\tau_{\mathrm{in}}/\operatorname{Re} Z(0) = 130/T_{\mathrm{c}}$, appropriate for Sn , and for (i) the case of no magnetic scattering ($\tau_s \to \infty$) and (ii) a case with magnetic scattering strong compared with phonon scattering ($\tau_{\mathrm{in}}/\tau_{\mathrm{s}} = 100$). For intermediate values of the magnetic scattering rate the curves vary smoothly between the two cases exhibited. The injection voltage is given by $eV = 30\Delta$.}

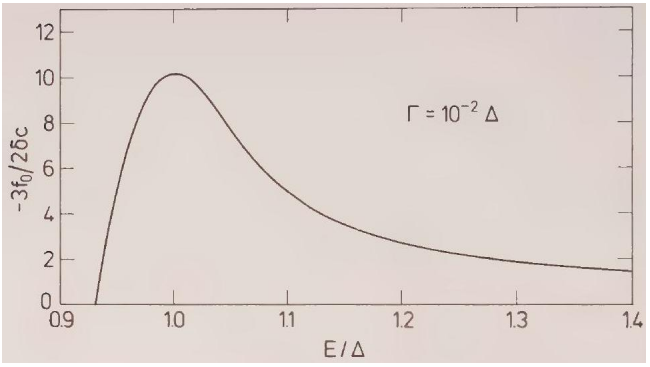


Fig. 4. The function $-f_{0
} / c$, divided by $2\delta/3$, (eq. 4.23), as a function of E/Δ for $\Gamma = 10^{-2}\Delta$. The quantity f_0 is proportional to the charge imbalance on a shell of energy **E**.}

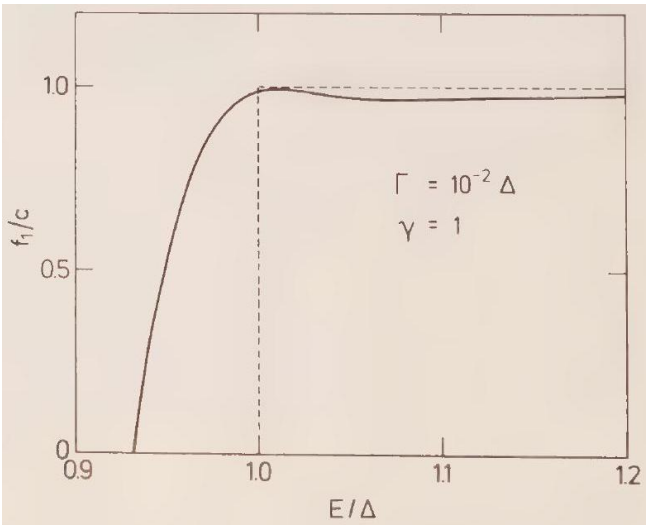


Fig. 5. The function f_{1 / c (eq. 4.24) as a function of E/Δ for $\Gamma = 10^{-2}\Delta$ and $\gamma = 1$. The quantity f_1 is proportional to the heat current on a shell of energy E. (See eq. 4.25 .)}

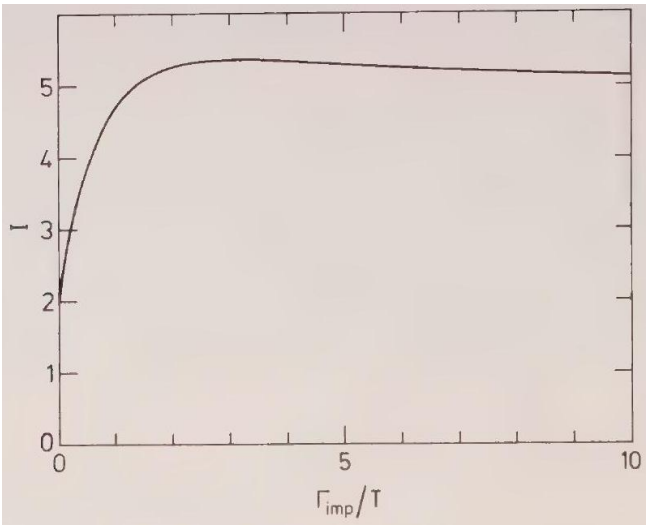


Fig. 6. The quantity I (eq. 4.31) as a function of $\Gamma_{1 m n T$.}

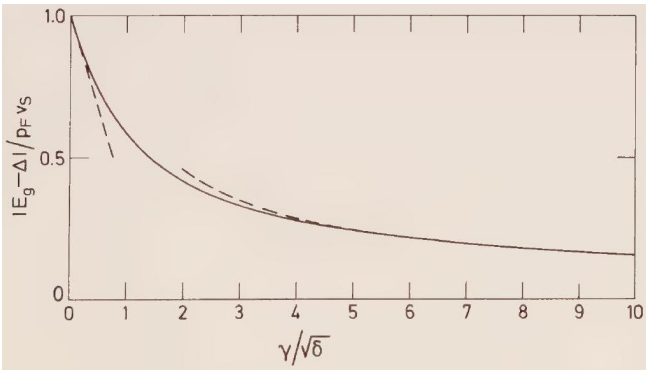


Fig. 7. The minimum energy $E_{\mathrm{g
}}$ at which the density of states is finite, as a function of $\gamma/\sqrt{\delta}$ (full line). The dashed lines show the asymptotic expressions (4.33) and (4.34) for low and high values of $\gamma/\sqrt{\delta}$, respectively.}

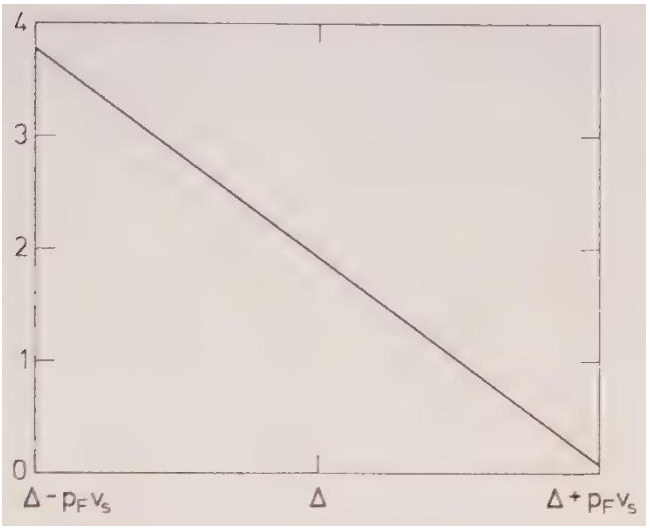


Fig. 8. The angle-averaged deviation function $-\langle q\tau x\rangle/(1-\langle q\tau\rangle)$, produced by a supercurrent and a temperature gradient, in the pocket region $E-p_{F
v_{s} \leqslant E \leqslant \Delta+p_{F} v_{b}$ for a clean superconductor. This quantity is proportional to the charge imbalance on a shell of energy E. (See eq. 4.35.)}

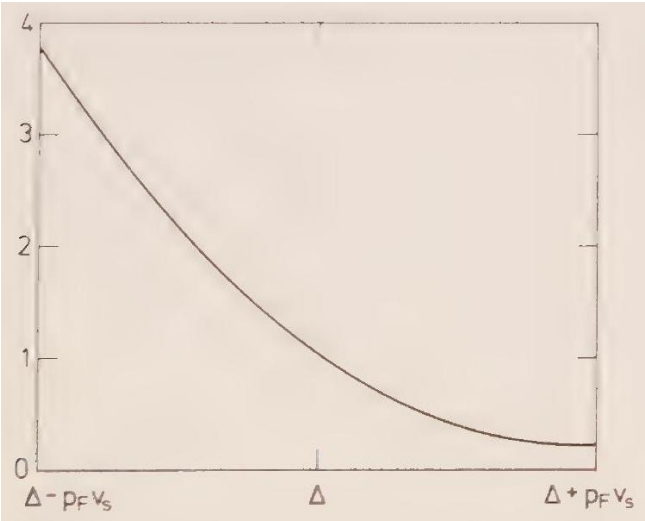


Fig. 9. The first moment of the distribution function, $\left\langle q \tau x^{2} \right\rangle+\langle q \tau x\rangle^{2} /(1-\langle q \tau\rangle)$, produced by a supercurrent and a temperature gradient, in the pocket region, $\Delta - p_F v_s \leqslant E\Delta + p_F v_s$, for a clean superconductor. This quantity is related to the heat current on a shell of energy E. (See eq. 4.36.)}

18 Experimental Study of Enhanced Superconductivity by Dmitriev, Gubankov and Nad

18.1 1. Introduction

Not very long ago it was generally believed that an electromagnetic field, when applied to a superconductor, should reduce its superconducting parameters: the critical current I_c, the critical magnetic field H_c and the critical temperature T_c, that is, cause superconductivity suppression. This standpoint was based on consideration of the physical mechanisms of the interaction between an electromagnetic field and a superconductor: absorption by Cooper pairs of electromagnetic field quanta $\hbar\omega$ with energies higher than the Cooper-pair coupling energy, acceleration of superconducting electrons to supercritical velocities at which their kinetic energy is larger than the coupling energy, and electromagnetic energy absorption by normal electrons and resulting heating of the superconductor.

However, experiments in 1966-1970 revealed that an electromagnetic field with frequency about 10 GHz acting on a superconductor causes I_c, H_c and T_c to increase, that is, it enhances superconductivity (Wyatt et al. 1966a,b, Dayem and Wiegand 1967, Dmitriev et al. 1970).

A theoretical explanation of such unusual and unexpected behaviour of a superconductor in an electromagnetic field was proposed by Eliashberg (1970) who took into account the interaction of the field with quasi-particle excitations which so modifies the quasi-particle energy distribution that the superconducting pairing is enhanced.

Eliashberg's theory did not win general acceptance very easily. The reason was that it applied to a uniform superconductor, while the early experimental observations used films (bridges) and point contacts (Dmitriev et al. 1973). And only after Eliashberg and his coworkers (see the chapter by Eliashberg and Ivlev in this volume) had further developed their theory and some experiments corroborated the theoretical results the essence of the effect was understood; its principle is that under an electromagnetic field a superconductor goes to a new nonequilibrium steady state characterized by stronger superconducting properties due to quasi-particle transition from the lowenergy region near the edge of the energy gap to the higher-energy region, with the total number of quasi-particles preserved.

The papers mentioned above thus pioneered in a new branch of research: nonequilibrium superconductivity in alternating fields. It was realized that if
an electromagnetic field drives the superconductor to a new nonequilibrium state, then, the theory of the nonstationary Josephson effect should take into account the effects of nonequilibrium quasi-particles arising from the Josephson self-radiation in weakly coupled superconductors. This provided an explanation for the initial parts of the current-voltage characteristics of Josephson weak links and the peculiarities of superconductivity enhancement in superconducting contacts, which had not been physically explained by that time (Aslamazov and Larkin 1976, 1978). The concept of nonequilibrium superconductivity also became the base of work on superconductivity enhancement by sound and tunnel current. The possible superconductivity enhancement by a direct current in tunnel junctions had been suggested by Parmenter (1961). However, that paper referred to quasi-particle injection (extraction) into one of the contact films, which is radically different from enhancement by the electromagnetic field, with a constant total number of quasi-particles.

The understanding of the enhancement mechanisms has been contributed to by scientists of many nations and investigations through wide ranges of temperature and frequency on samples of various superconducting materials and various geometries: film bridges, homogeneous strips, proximity-effect bridges and varying-thickness bridges, point contacts and tunnel junctions. These investigations permitted, on one hand, to ascertain the generality of superconductivity enhancement and, on the other hand, to find the features peculiar to uniform and constricted

superconductors. There appeared a rapidly developing branch of physics dealing with nonequilibrium superconductivity, which is important both for the solution of the fundamental problems of nonequilibrium superconductivity and for its practical application. In recent years, the concept of nonequilibrium superconductivity has essentially evolved, extensively and intensively, from the initial state-of-the-art.

In this chapter, the term "nonequilibrium" will be applied to a superconductor in which the quasi-particle distribution function is different from that in thermodynamic equilibrium. The nonequilibrium state in a superconductor can be induced by:
(1) irradiating the superconductor with an electromagnetic or sound field;
(2) passing a direct current higher than the critical current, through a uniform superconductor or a superconductor containing a weak link with metallic conductivity;
(3) passing a direct tunnel current through a superconductor containing a tunnel barrier;
(4) tunnel injection (extraction) of normal excitations into the superconductor.

Each process involves complex and peculiar effects, providing both the deviation from equilibrium and the tendency to equilibrium. Such processes in
the superconductor generate a range of wonderful phenomena: enhancement and suppression of superconductivity, development of a state with a spatially inhomogeneous order parameter $\hat{\Delta}$, excess currents, collective oscillations, reduction of ultrasound absorption, to mention only some of them.

In this paper we shall only deal with nonequilibrium phenomena resulting in superconductivity enhancement and also touch upon the problem of the spatially inhomogeneous state and excess current.

18.2 2. Discovery of microwave-enhanced superconductivity

After the nonstationary Josephson effect had been predicted theoretically and observed experimentally, active search and investigation of new types of weakly coupled superconductors commenced. In particular, the IV characteristics of thin film bridges (Dayem bridges) with the radius of constriction less than 1μ m displayed current steps induced by a microwave field (Anderson and Dayem 1964).

An experimental investigation of the influence of a 10 GHz electromagnetic field on the $I-V$ curve of tin thin film bridges with the radius of constriction larger than 1μ m (the characteristic dimensions of such bridges are: length and width about 2μ m, thickness about 2000Å.$R_{4.2} \approx 0.3\Omega$) did not find the nonstationary Josephson effect, i.e. under irradiation, the $I-V$ characteristic did not develop steps. Another effect was however revealed: a radiationinduced increase in the bridge critical current (Wyatt et al. 1966a,b, Dayem and Wiegand 1967, Dmitriev et al. 1970), see fig. 1. The effect reduced as temperature went down. Investigation of the transition temperature of the bridges from the normal to the superconducting state showed that in an electromagnetic field a sample becomes superconductive at higher temperatures than in the absence of the field (fig. 2). Thus, in addition to I_c, the bridge critical temperature T_c becomes higher under the effect of an electromagnetic field.

Figure 3a represents the dependence of the bridge critical current on the radiating power for a range of values of a d.c. magnetic field perpendicular to the plane of the bridge (Dmitriev et al. 1970). One can see that this dependence is similar to $I_c(P)$ for various temperatures shown in fig. 1 . The lower curve of fig. 3a suggests that a sample in the resistive state under the influence of a magnetic field $H \gtrsim H_c$ may be converted to superconductive by applying microwave irradiation. Thus, the irradiation also causes the critical magnetic field H_c to increase, fig. 3b.

So, those early experiments ascertained that an electromagnetic field might enhance superconductivity, that is, cause an increase in the superconducting parameters of the sample: I_c, T_c

and H_c.

The above experimental results were obtained from samples of various

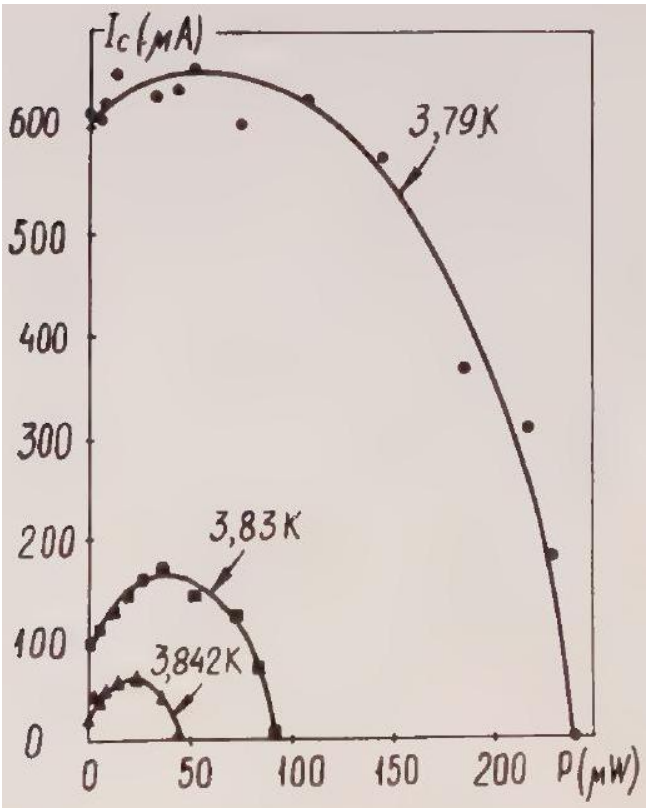


Fig. 1. Experimental dependence of critical current through Sn constriction as a function of microwave power at different temperatures. Incident power frequency is ~ 10 GHz. $T_c = 3.845$ K.

superconductors: Sn , In and Al , which evidenced the general nature of the phenomenon. The bridges were however of different dimensions, including very small Josephson junctions. This created some difficulties for the physical interpretation of the quantitative results.

In order to account for the experimental data collected by that time, a phenomenological approach to the superconductivity enhancement effect was developed. It was widely discussed if the enhancement could be explained by the influence of the irradiation on fluctuations in the bridge. In the experimental temperature dependence of the bridge resistance $R(T)$ there are two steps

(Wyatt et al. 1966b), representing the transition to the superconducting state of the bridge banks at T_c^B and the bridge itself at T_c^b, such that usually $T_c^B > T_c^b$. One of the reasons could be an essentially larger influence of fluctuations on T_c^b than on T_c^B. Later, Ovchinnikov (1973) proposed a microscopic theory for this idea. The experimentally observed fact that $\delta T_c = T_c^H - T_c^b$ and the increase in T_c^b of the bridge under the effect of an electromagnetic field by δT_c suggested the idea that the field affects the bridge fluctuations, namely suppresses them and leads to a certain "order" (Hunt and Mercereau 1967, Hunt 1969).

The fluctuation model can include the additional Cooper-pair coupling energy due to fluctuation energy reduction caused by the said "order" (Dmitriev et al. 1973). Inclusion of such a contribution of the field to the energy balance equation for a bridge with a current results in a current density expression from which the superconductivity enhancement effect follows. This model was a qualitatively adequate description of the superconductivity enhancement near T_c and was based on the assumption that an electromagnetic field modulates the bridge order

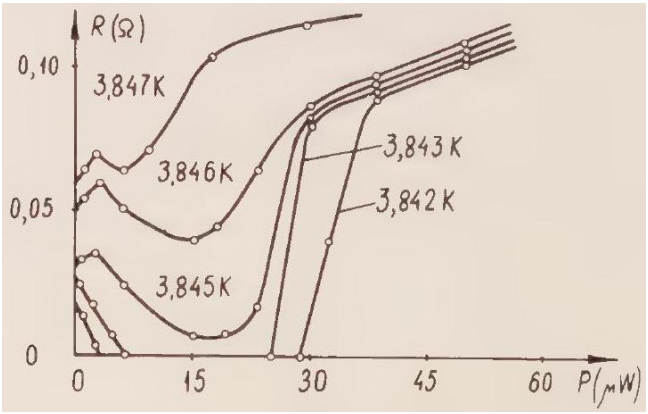


Fig. 2. Experimental dependence of Sn bridge resistance as a function of microwave power at different temperatures. Incident power frequency is $\sim 10 \mathrm{GHz
. T_{\mathrm{c}}=3.84 \mathrm{˚K}$.}

parameter in such a manner that its time average increases with the field. In this model the dependence of the weak-link coupling energy on the phase difference φ (Anderson 1967) had the form

$$E = E_0(1 - \cos\varphi), \quad \partial\varphi/\partial t = (2e/\hbar)V\cos\omega t$$

where V is the microwave voltage. However this model did not provide a detailed physical picture of the electromagnetic field effect on quasi-particles and therefore did not contain some experimental features of the dependences on frequency, field intensity and also temperature of the superconductivity enhancement measured later. Besides, being based on the fluctuation influence principle, the model was unable to describe the enhancement effect at temperatures sufficiently below T_{c} where fluctuations play but an insignificant role. So, there was still a need for further theoretical development.

The next step in the development of phenomenological theories was a model based on certain features of nonequilibrium superconductivity (Lindelof 1976). It is in short as follows: since $T_c^b < T_c^B$ then at a given temperature in the middle of the bridge the relative number of normal electrons is higher than that of superconducting electrons, that is, the order parameter has a minimum at the bridge centre. The electromagnetic field injects the normal electrons into the bridge banks, where they become excited and require some time to relax to equilibrium with the condensate. The law of conservation of charge requires that at the bridge centre the normal-electron deficiency should be covered by an inflow of superconducting electrons from the banks. In the average, under the electromagnetic field, the relative number of superconducting electrons in the bridge increases, whence there may be a high superconducting current. However, this model, which described the superconductivity enhancement as such, was also unable to account for its particulars at various frequencies, field intensities and temperatures.

Thus, the phenomenological models, which allowed for the presence of weak links in the superconductor (spatial inhomogeneity of the order parameter), were not able to explain the experiment in detail. Meanwhile, the microscopic theory developed for uniform superconductors (Eliashberg 1970) still wanted thorough experimental check, because most experiments by that time had been run on superconductors with the order parameter spatially inhomogeneous along the distance $\sim \xi(T)$.

A demand then arose for new advances in the investigation of superconductivity enhancement by an electromagnetic field. By experiments, uniform samples were to be studied, the similarity of the new results with those available for bridges was to be shown and the experi-

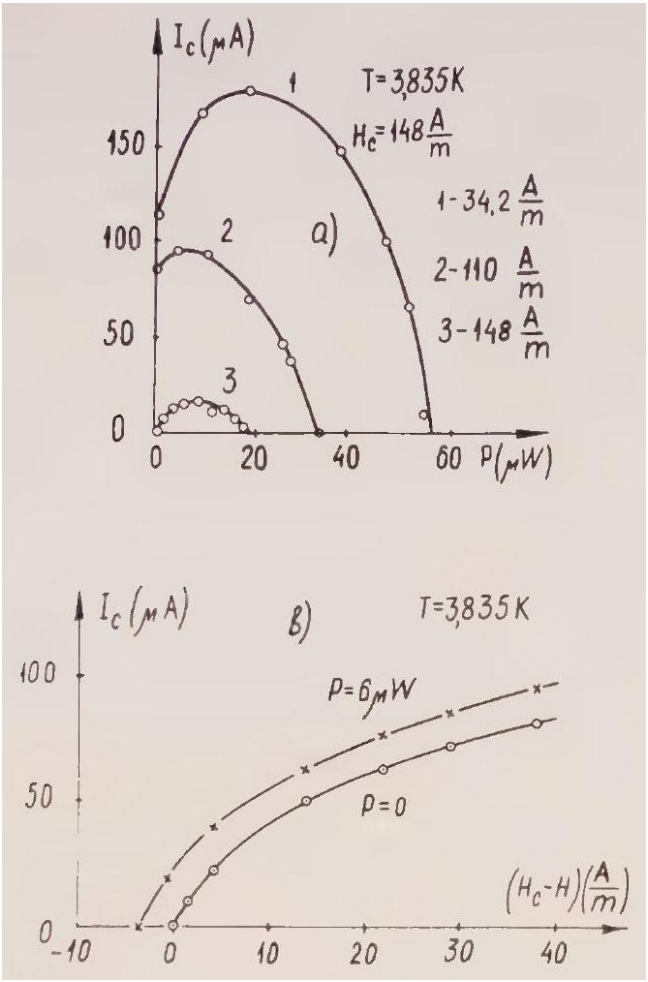


Fig. 3. Experimental dependence of the critical current of a tin bridge (a) on incident power for a range of intensities of a d.c. magnetic field perpendicular to the bridge plane and fixed temperature, (b) on d.c. magnetic field, for fixed incident power and temperature. $T_{\mathrm{c}}=3.85 \mathrm{~K}$.

mental results were to be compared to the conclusions of Eliashberg's microscopic theory. In the theory, the objective was not only to get a more profound insight into the mechanism of superconductivity enhancement in the uniform superconductor, but also to
develop a microscopic picture of the effect allowing for the features of the inhomogeneous superconductor associated with the spatial dependence of the order parameter. The theoretical developments should then, in turn, be checked by experiments on samples adequate to the theory.

18.3 3. Microwave-enhanced superconductivity in uniform superconductors

As was mentioned above, the phenomenological explanations of superconductivity enhancement (Hunt and Mercereau 1967, Hunt 1969, Christiansen et al. 1971, Dmitriev et al. 1973) were unsuccessful. Some of the early results could not be explained, quantitative comparison of experimental data with the mostly qualitative theories was impossible and the physical nature of this strange phenomenon was still unknown.

As an alternative to the phenomenological approach, Eliashberg and colleagues (1970-1973) developed a microscopic theory of nonequilibrium states of a superconductor in an electromag-

netic field. In a series of papers they derived a superconductor dynamic theory which made allowance explicitly for inelastic processes and revealed the physics of such nonequilibrium phenomena. It was shown that because of the long energy relaxation time of excitations even in fields low compared to the critical field, essential redistribution of excitations in energy may occur with the spectrum density unchanged. For the external field frequency $\omega < 2\Delta/\hbar$, some excitations with energies $\varepsilon \sim \Delta$ move to $\varepsilon \sim \Delta + \hbar\omega$, while preserving their total number. A decrease in the occupancy of states with $\varepsilon \sim \Delta$, which play the predominant role in quasiparticle pairing and determine the gap, should lead to enlargement of the gap (see eq. (1) of the chapter by Eliashberg and Ivlev). Besides, as was shown by Chang and Scalapino (1977, 1978), since the recombination of particles with the high energy $\varepsilon \sim \Delta + \hbar\omega$ is fast, an increase of the number of high-energy particles as a result of redistribution may cause the total number of quasi-particles to decrease and thereby cause the gap to enlarge as well.

In the case of thin uniform films, one may neglect the position dependence of A. Moreover, in the neighbourhood of T_c the order parameter relaxation time τ_Δ is long (Gor'kov and Eliashberg 1969), and for the frequencies with $\omega\tau_1 \gg 1$ involved here one may neglect time oscillations of Δ as well. Thus, in theory, in a thin superconducting film under the influence of an electromagnetic field there should arise a homogeneous, stationary, nonequilibrium state with an enlarged gap. In this section we shall present results of various experimental investigations of superconductivity enhancement by an electromagnetic field, analyze them and compare with theory. These results became the experimental basis of the enhancement mechanism proposed by Eliashberg and coauthors and contributed to the complete understanding of the physical nature of the phenomenon.

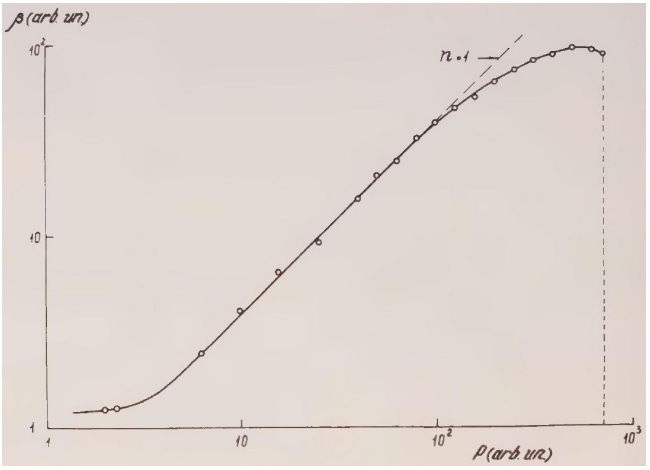


Fig. 4. Dependence of critical current $\beta=I_{c
(P) / I_{c}(0)$ in a Sn bridge of length 42μ m and width 1μ m on the 9.4 GHz incident power at $T_c - T = 3$mK.}

For the realization of the spatially homogeneous nonequilibrium state of a superconductor in an electromagnetic field, the energy gap should be constant and the current distribution uniform through the sample. These requirements are met by long ($L > \xi(T)$) thin ($d < \xi(T)$) narrow ($w < \lambda^2/d$) film bridges on substrates with good thermal conductivity at cryogenic temperatures. Such bridges, $\sim 100\mu$ m long, $\sim 1\mu$ m wide, were prepared by evaporation of a thin (1000Å) superconductive film through a mask represented by a thicker (about 1μ m) film (of metal or collodion) with a narrow slit (Andratskii et al. 1973, Latyshev and Nad 1975, 1976). The slit was made with a special device which provided plane-parallel cutting motion and allowed to control the cutting tool pressure and cutting angle. After evaporation the masking film was removed. Bridges produced in such a way had sharp edges and a narrow

superconducting transition (appr. 0.01 K) due to a certain inhomogeneity of T_c along the polycrystalline film of the bridge (Skocpol et al. 1974). The width uniformity was controlled by an electronic microanalyzer with accuracy to $\sim 0.1\mu$ m. Samples with large inhomogeneities were rejected. The $I-V$ characteristics were recorded by an XY-recorder with an error of $0.3^{(1)}{}_0$. The temperature maintenance and measurement accuracy was not worse than 1μ m.

The experiments (Shepard 1971, Latyshev and Nad' 1975, 1976, Klapwijk and Mooij 1976, Dmitriev and Khristenko 1978) showed that for all long
narrow bridges, with lengths from 1 to $10^3\mu$ m, irradiated by an electromagnetic field, there was a growth of the critical current I_c, and I_c as a function of the radiating power P was qualitatively similar to the dependences in fig. 4. There is a region of linear growth of I_c with P, a region of saturation, and finally a region of steeply falling I_c in a narrow power range (~ 0.1 dB). The increase of the clearly observable critical current near T_c may be even by a factor up to 50 . The saturation and fall regions are characterized by a hysteresis developing in the bridge $I-V$ characteristics (Latyshev and Nad' 1976). Figure 5 represents dependences of the critical current density j_c on the radiating power for a 1.2 mm long tin bridge at various temperatures (Latyshev and Nad' 1976). It is easily seen that in the range $T \gtrsim T_c$, i.e. from the resistance state, there occurs "induction" of the critical current (curve 1), and at $T < T_c$ it grows, reaches a maximum and there is a rapid transition to the normal state. The data presented in figs. 4 and 5 were obtained for the irradiation frequency $\omega/2\pi \sim 10$GHz. At such frequencies, though the relative growth of the critical current $\beta = I_c(P)/I_c(0)$, as is seen in fig. 5, becomes lower with temperature decrease, enhancement, i.e. $\beta > 1$, is still observed through a wide temperature range $T_c - T = 0.4$ K; for $\omega/2\pi \geqslant 30$GHz, there is enhance-

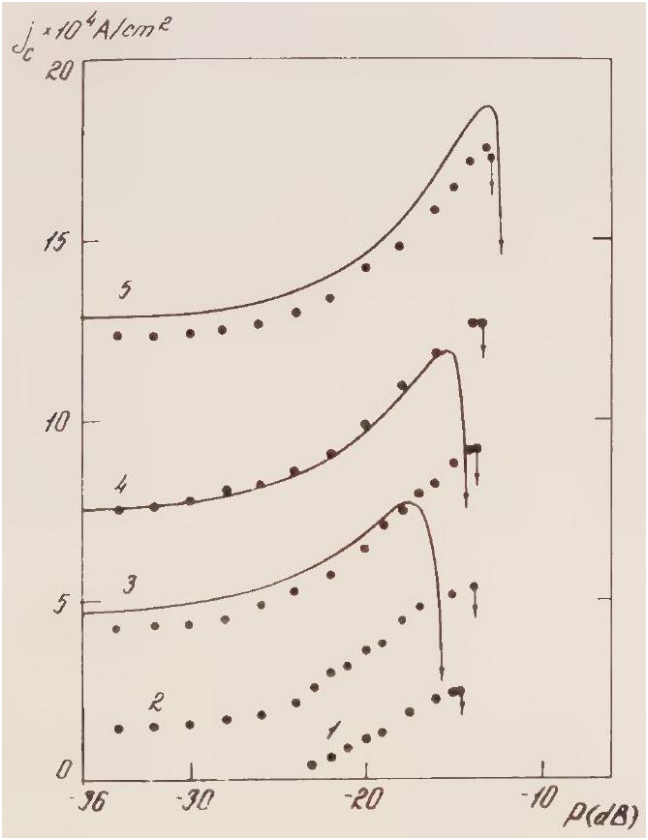


Fig. 5. Dependence of critical current density of a bridge of length 1.2 mm and width \$2.4 \mu \mathrm{˜m
\$ on incident power at different temperatures: (1) 3.796 K ; (2) 3.778 K ; (3) 3.759 K ; (4) 3.747 K ; (5) 3.728 K . Solid curves represent calculation by eq. (1).}

ment even to the lowest temperatures studied, $T_c - T \approx 1.0$ K (Latyshev and Nad' 1974). On Al bridges, the enhancement was observed to 0.04 K (Pals and Dobben 1979). However the maximum critical current $I_c(P)$ at $T \neq 0$ never exceeded the equilibrium values of the critical current at 0 K .

From these data it is evident that in an electromagnetic field there is enhancement of the critical current not only in short but also in long uniform bridges, and not only in close proximity to T_c but far away from it as well. Two facts were inconsistent with the phenomenological explanation of superconductivity enhancement. In particular, if one explains the enhancement by fluctuation suppression in the bridge by the irradiation (Hunt 1969), then in order to account for the observed increase in I_c by 30% as we move away from T_c by 1 K , the effective temperature introduced by Hunt (1969) must exceed 2000 K , which is hardly reasonable. On the other hand, both results are consistent with the mechanism proposed by Eliashberg (1970). It also agrees with the linear rise of I_c at the initial part of $I_c(P)$, fig. 4.

However, if the effects observed are indeed superconductivity enhancement effects, not simply fluctuation suppression, then the magnitude of the bridge critical current in an electromagnetic field should exceed, apart from the experimental I_c without the field, also the theoretical maximum critical current I_c^{GL} of Ginzburg-Landau theory. For the case of uniform distribution over the bridge cross-section, I_c^{GL} was calculated with the use of the generally known formulae, which include the dependences of the penetration depth $\lambda(T)$ and the coherence length $\xi(T)$ on the electron mean free path l, i.e. the purity of the superconductive film (Latyshev and Nad 1976). These dependences for nonmagnetic impurities are specified by Gorkov's (1959) equation $\chi = \chi(\xi_0/l)$. Adding the formula for the film thickness, $d = L\rho_{300}W/(R_{300} - R_{4.2})$ we arrive at the following relation, which does not contain the film width:

$$I_c^{GL} = \frac{c\Phi_0}{12\sqrt{3}\pi^2} \frac{\rho_{300}}{R_{300} - R_{4.2}} \frac{L\chi^{1/2}}{\lambda_p^2 - \xi_p^2}, \tag{1}$$

where Φ_0 is the flux quantum, ρ_{300} the resistivity of bulk tin samples at 300 K . R_{300} and $R_{4.2}$ the film resistances at 300 and 4.2 K respectively, and

$$\xi_p = 0.74\xi_0 (1 - T/T_c)^{-1/2}, \quad \lambda_p = \lambda_L(0)/\sqrt{2}\,(1 - T/T_c)^{1/2}$$

with $\lambda_L(0) = 355$Å and $\xi_0 = 2300$Å for Sn . The value for χ was taken from Gor'kov's (1959) paper.

In fig. 6, for a 42μ m long and 1μ m wide bridge, the dependence calculated by eq. (1) is represented by a solid curve. The error due to inaccurate measurements of all the quantities entering eq. (1) was not larger than $7°_0$. The solid circles show the experimental points for $I_c(P)$ (the experimental error is within the circle diameter). It is seen from fig. 6 that for a narrow long uniform bridge with a uniform current distribution at $T \sim T_c$, the experimental $I_c(P)$ values are in good agreement with $I_c^{Gl.}(T)$ from theory. This means that in

such bridges, at $P = 0$, the maximum possible depairing current for the equilibrium is realized [similar results were obtained for similar bridges by Andratskii et al. (1973)]. As is seen from fig. 6, the critical current under irradiation (open circles) is much higher than the thermodynamically equilibrium critical current values and is not zero at temperatures above the equilibrium critical temperature.

Figure 6 also suggests that an increase of I_c under microwave irradiation is attended by a shift of the superconducting transition curve, $R(T)$, towards higher temperatures, which proves that the bridge critical temperature increases. Similar dependences were observed on the other bridges made of Sn and Al (Klapwijk and Mooij 1976, Latyshev and Nad' 1977, 1978, Dmitriev and Khristenko 1978, Mooij et al. 1980). When a bridge which is not irradiated ($P = 0$) is cooled, the dependence $R(T)$ first develops a small step representing the superconducting

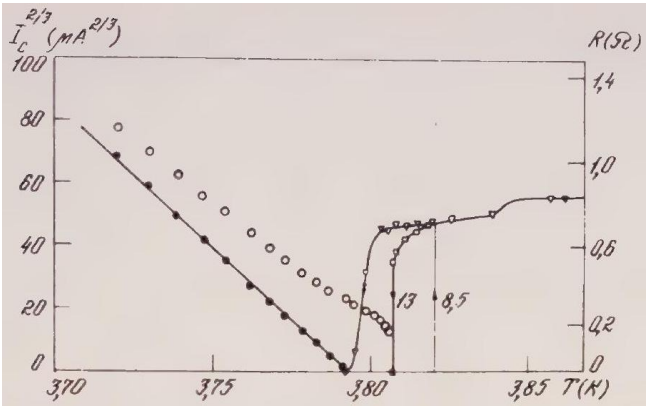


Fig. 6. Temperature dependence of (·) the critical current of an irradiated Sn bridge of length $42 \mu \mathrm{~m
$ and width 1μ m$I_c(0)$, (o) the critical current at the optimum power $I_c\,(P_{\rm opt}\,)$, and the bridge resistance $R(T)$ for $P = 0$ and two incident powers corresponding to attenuation 13 dB and 8.5 dB . Points ∇ and $\square$ are obtained from the slope of the bridge $I - V$ curve.}

transition of the hridge banks at $T = T_c^{\rm B}$. Then, at $T_c^{\rm B} > T > T_c^{\rm b}$, there is a plateau with a minor resistance reduction, and finally, at $T = T_c^{\rm b}$, the superconducting transition (N $\rightarrow$ S) of the bridge proper occurs. Its width (at levels $0.1 - 0.9$ of $R_{\rm N}$) is usually $\leqslant$ 10mK.

If the irradiation power is relatively small, the transition, as has been mentioned, is shifted to higher temperatures and becomes essentially narrower (fig. 7 , curve for 47 dB). According to the theory (Ivlev et al. 1973) and the experimental dependences $I_c(P)$ (Latyshev and Nad' 1976), wherever in the bridge $T_{\rm c}$'s are lower, the action of the irradiation leads to larger critical parameter increases than where T_c is higher. Hence, while the critical parameter grows in all parts of the bridge, it levels out over the area of the bridge.

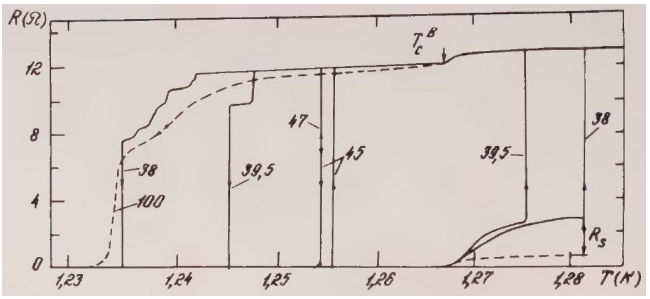


Fig. 7. Temperature dependence of the resistance of an Al bridge of length $50 \mu \mathrm{~m
$ and width 1μ m for various incident powers (the figures show the attenuation in dB). $R_{\rm s}$ is the excess resistance of the S $-$ N boundary.}

These processes are reflected by the observed shift to higher temperatures and narrowing of the superconducting transition (Latyshev and Nad' 1977). A theoretical treatment was provided by Aslamazov (1978).

As the power increases further, the transition from the superconducting state (S) to normal (N)(S $\rightarrow$ N) takes place at higher temperatures than the N $\rightarrow$ S transition, i.e. temperature hysteresis appears in the $R(T)$ dependence (Klapwijk and Mooij 1976, Latyshev and Nad' 1977) and becomes larger with P. The S $\rightarrow$ N transition is jumplike in this case. Above a certain power, the N $\rightarrow$ S and S $\rightarrow$ N transitions cease to shift to higher temperatures and

start to move back to lower temperatures. The S → N transition displacement is several times larger than the width. All other conditions being equal, the magnitude of the displacement essentially depends on heat transfer: δT_c for samples in liquid helium is approximately twice that for samples in helium gas (Latyshev and Nad' 1977). A correlation is also seen between the dependences of I_c and T_c on the radiating power: after the maximum is attained, they both drop sharply. The maximum displacement for Sn bridges was 30 mK , though it never exceeded the difference $T_c^B - T_c^b$, i.e. in Sn bridges, T_c^b was never increased by irradiation to above T_c^B. In the fluctuation model of superconductivity enhancement the fact that T_c could not increase above T_c^B was thought to be essential. On the contrary, in the microscopic theory T_c^b could be increased to above the equilibrium value of T_c^B. To clear up this question, Latyshev and Nad' (1978) performed experiments on aluminium bridges with long energy relaxation times and better heat transfer (superfluid He and better matching of the acoustic impedances of the aluminium and the quartz substrate). As is seen from fig. 7, the bridge critical temperature under the irradiation may markedly (by 13 mK) exceed T_c^B which is free from irradiation effects, because of the low density and inhomogeneous induced microwave currents. This means that in
long bridges the banks do not essentially influence superconductivity enhancement. It is not true that irradiation merely makes T_c^b closer to T_c^B; it causes changes in the bridge properties, and first of all (according to Eliashberg) it causes redistribution of quasi-particle energies, with the immediately resulting growth of T_c and I_c. The maximum T_c growth observed was in this case 73 mK (5.2% of T_c). Pals and Dobben (1979) observed T_c rise by 100 mK .

On the basis of the obtained data and the theory of Eliashberg and coauthors, the N → S and S → N transitions of a bridge in an electromagnetic field may be represented as follows. According to the theory, in an electromagnetic field, the dependence of Δ on T is not unambiguous (see the chapter by Eliashberg and Ivlev, fig. 3). By lowering the irradiated bridge temperature, one can hardly obtain the transition to the S -state at $\left((T - T_c)/T_c\right)_{max}$, because for formation of the superconducting state with a gap it is necessary that first a gap should arise (at least by fluctuations), which subsequently is enlarged by the irradiation. According to the theory, the enhancement by irradiation is realized through transfer of some of the excitations from a region with a singularity in the density of states to a higher energy region. In other words, this effect can only take place if there is a singularity in the density of states. This standpoint is supported by experimental data (figs. 6 and 7), which show that a bridge may be switched from N- to S -state by irradiation at T only slightly higher than T_c, where there is a possibility of fluctuational generation of S-state "germs". After such transition the bridge gets to a state with a nonequilibrium gap. If T is increased now, the bridge passes T_c of the N → S transition and, on reaching the maximum of $A(T, P)$ at a higher T, jumps back to the normal state. This transition is a firstorder transition. Experiment reveals indeed such a hysteresis and a steplike S → N transition.

It is seen from the temperature dependence of the critical current of an irradiated bridge as measured by the conventional method (fig. 6) that $I_c^{max}(T)$ drops down to zero at a certain temperature higher than T_{c0}, without irradiation (see also Klapwijk et al. 1977, Dmitriev and Khristenko 1978). By applying a special pulsed technique, allowing to avoid heating of the sample in the resistive state by microwave irradiation and providing measurement of $I_c^{max}(T)$ by heating of the bridge from the S-state, Pals and Dobben (1978, 1979) showed that in this environment $I_c^{max}(T)$ smoothly decreases to zero. A possible explanation is the following. In a bridge which is not irradiated, at $T \to T_c$, both I_c and Δ smoothly tend to zero. In an irradiated bridge, at $T \to T_{cm} > T_{c0}$, Δ smoothly reduces to a finite value, Δ_m, and I_c^{max} smoothly tends to zero (Dmitriev and Khristenko 1979). At $T_{cm} > T > T_{co}$, the superconducting state is metastable and as we approach T_{cm}, the magnitude of the free energy relative minimum diminishes (Schmid 1977), and the steplike transition to normal state from the state with a

finite gap may be triggered by any arbitrarily small current.

Direct observations of the energy gap enhancement in a superconductor in an electromagnetic field were very important. Kommers and Clarke (1977) irradiated ($\omega/2\pi = 10$GHz) at $T \lesssim T_c$ an $Al - Al_2O_3 - Al$ tunnel junction with electrodes ranging in thickness from 800 to 3000Å and width 300μ m, on BaF_2 substrate. Figure 8 represents the dependence of the junction differential resistance dV/dI on the voltage for a variety of incident powers. The electrode films had slightly different gaps Δ_1 and Δ_2 and at $P = 0$, in the dependence of $dV/\mathrm{d}I$ on V, the minimum **a** corresponds to $(A_1 + A_2)/e$ and the minimum **b** to $(A_1 - A_2)/e$. As is seen from fig. 8, incident power growth is attended by an appreciable displacement of the minimum a corresponding to a 80% increase in ($\Delta_1 + \Delta_2$), while the minimum **b** is displaced by no more than 3μ V. The minima **c**, **d** and **e** represent various singularities of the $I - V$ curve due to tunnelling accompanied by photon absorption or emission (Dayem and Martin 1962). There is also a hysteresis in the dependence of ($\Delta_1 + \Delta_2$) on T and a jumplike S → N transition, if temperature rises at a fixed incident power.

Hall et al. (1980) measured I_c, T_c and Δ enhancement in a narrow Al film with four cross-shaped $Al - Al_2O_3 - Al$ tunnel junctions formed along it. Radiation of frequences 0.1 to 12 GHz was applied to the Al film through a strip line between the film and a ground plane. In the frequence range 2 to 4 GHz there was a 100% enhancement of the energy gap ($T \lesssim T_c$), increase of the critical temperature by 16 mK above the equilibrium T_{c0} and an associated increase in I_c. Thus, these direct measurements, agreeing with the above data, are unambiguous evidence that in an electromagnetic field the superconductor energy gap becomes larger.

The dependence of superconductivity enhancement on the radiation frequency was noticed in one of the first works to deal with this effect (Dayem and Wiegand 1967). It was found that at a temperature close to T_c the growing I_c of Sn bridges is only observed at frequencies above about 1 GHz . Detailed investigations of the frequency dependence of the effect were carried out by Latyshev and Nad' (1974, 1975, 1976) (see also Dmitriev and Khristenko 1978). I_c of long Sn bridges was measured as a function of the incident power for fixed frequencies at some temperature points in the range $T_c - T \lesssim 1$ K. The measurement cycles used different frequencies from 8 to 78 GHz . The maximum increase in I_c for a certain optimum power P_{opt} is convenient to characterize as

$$\beta_m = I_c(P_{opt})/I_c(0);$$

then the enhancement condition is $\beta_m > 1$. The dependences $\beta_m - 1$ thus obtained for various frequencies typical for all samples of length $L \gg 1\mu$ m are represented in fig. 9 (Latyshev and Nad' 1974). For frequencies below 25 GHz , the I_c enhancement is maximum near T_c (where "induction" of I_c is also observed at $T > T_c$). As the temperature is lowered, the enhancement decreases and at a certain temperature disappears (within the experimental error). At above 25GHz, I_c enhancement near T_c is absent; it starts at some temperature dependent on frequency, then attains a maximum and decreases, however without vanishing even down to the lowest temperatures measured. The boundary points of the enhancement effect region of existence are given by points of intersection of the $\beta_m - 1$ curves with the $T_c - T$ axis (fig. 9). By plotting these boundary points of onset and vanishing of the I_c enhancement in a plot with the x-coordinate $(T_c - T)/T_c$ and y-coordinate $\omega/2\pi$ (fig. 10; Latyshev and Nad' 1974, 1976), one obtains two curves bounding the region of the enhancement effect: it is observed inside this enclosure and is not outside. Some of the points of fig. 10 were obtained from data of Dayem and Wiegand (1967), and Dmitriev and Khristenko (1978). They are in fairly good agreement with the results of Latyshev and Nad'.

Eliashberg's theory is that irradiation causes enlargement of the energy gap only at frequencies $\omega > \omega_c$, where the temperature-dependent critical frequency

ω_c, for $\omega < \Delta/\hbar$, is specified by

$$\omega_c^2 \ln \frac{8\Delta}{\hbar\omega_c} = 2\pi\tau_\varepsilon^{-1}\Delta/\hbar \tag{2}$$

where τ_ε is the excitation relaxation time. The dependence $\omega_c(T)/2\pi$ obtained by eq. (2) is represented by the broken curve in fig. 10 for $\tau_\varepsilon = 1.4 \times 10^{-10}$ s. The agreement of the experimental data and the theoretical curve is good enough. Note that the measurements described provide an experimental method to determine the quasi-particle relaxation time for superconductors. The value for τ_ε obtained by this method agrees fairly well with those by other methods (Clarke and Paterson 1974).

At frequencies above ω_c, as the frequency rises, the enhancement goes through a maximum and vanishes at frequencies corresponding to the upper boundary (fig. 10; Latyshev and Nad' 1974, 1976). In the vicinity of T_c the upper frequency boundary lies somewhat higher than $2A(T)$, owing to gradual rise of the competitive mechanism of pair breaking at $\omega > 2A/\hbar$. One of the results of the increasing quasi-particle number is also increasing radiation absorption leading to a higher "effective temperature" of the film (to be more accurate, it leads to larger deviation of the phonon distribution from equilibrium), and eventually to a smaller energy gap. This phenomenology is corroborated by a calculation based on the microscopic theory with allowance made for the changes in the phonon distribution function (Chang and Scalapino 1977, 1978). These authors showed that the gap growth is much smaller at frequency $\omega \gtrsim 2A/\hbar$ and the upper boundary should be a little above the dependence $2\Delta(T)$, in agreement with the experiment (fig. 10). The absence of the enhancement in Sn bridges at above 70 GHz seems to be due to the fact that at these frequencies, $\hbar\omega$ is within the order of magnitude of kT. As was shown by estimations based on a theoretical paper by Ivlev et al. (1973), the enhancement should vanish at $h\omega > kT$. Besides, the upper boundary position in this frequency range may be affected by thermal effects as well. The dependence of the enhancement on the radiation frequency was observed also by direct investigations of superconductor gap enhancement. Thus, e.g.. for an Al film, the growth of Δ was zero at frequencies $\omega/2\pi < 1$GHz, was maximum at about 4 GHz and was appreciably reduced at $\omega/2\pi > 10$GHz (Hall et al. 1980).

The theory of Eliashberg and co-workers predicted that as the power increased, the film critical temperature would approximately double and accordingly the critical current would grow too, with saturation at high powers, $\sim (T_c/\omega)^4$. However, in an experiment (see figs. 4 and 5), at much lower powers (for a Sn bridge it was three orders of magnitude lower than predicted), the dependences $I_c(P)$ and $T_c(P)$ reach a maximum and then abruptly fall off. The maximum increment of T_c was no more than 30 mK for a Sn bridge (Latyshev and Nad' 1977) and 100 mK for an Al bridge (Pals and Dobben 1979).

To explain the disagreement between theory and experiment, it is appropriate to realize two experimental findings. First, irradiation increases the hysteresis in the $I-V$ curve, due to heat generation in the bridge; the minimum critical current I_c', realized at decreasing current, does not grow; instead it tends to zero and at $I_c' = 0$ there is a sharp decreases in I_c (Latyshev and Nad' 1976, Pals and Dobben 1979). Secondly, the I_c and T_c growth amounts, all other things being equal, depend on the heat transfer from the films: δI_c and δT_c are higher for direct contact of the bridge with liquid helium (and still higher in case of superfluid helium), than with gaseous helium (Latyshev and Nad' 1977, Klapwijk et al. 1978, Pals and Dobben 1979). These two facts evidence an essential influence of heat generation and transfer on superconductivity enhancement in bridges (see also Dmitriev et al. 1970). In the development of the microscopic theory it was supposed that heat transfer was so efficient (i.e. practically infinite), that irradiation did not drive phonons out of equilibrium. In real experimental conditions, heat transfer is certainly finite and is not likely to be high. In this case the energy given by excited quasiparticles to phonons has not enough time to flow to the thermostat, and the phonon distribution function may change markedly. This alteration may be treated very approximately

as a film "effective temperature" increase. For quantitative comparison with experiment, the microwave impedance of a long bridge with $R > 10\Omega$ was measured, so that the current induced in the bridge could be determined. Figure 5 presents dependences for three helium bath temperatures (solid curves). In the calculation the only fitting parameter was the quasi-particle energy relaxation time τ_ε. The curves in fig. 5 were obtained for $\tau_\varepsilon = 1.4 \times 10^{-10}$ s, in good agreement with the value obtained from measurements of the frequency boundaries. The result of the calculation, as is seen in fig. 2, has new qualitative singularities: a maximum and a sharp decrease in the $I_c(P)$ dependence, in general agreement with experiment.

This "effective temperature" concept is of course a very rough approximation. In reality the nonequilibrium phonon distribution function may differ very essentially from the thermal one with the effective temperature. If the heat transfer is finite and there is electron phonon interaction, the phonon distribution function self-consistently tunes itself to the nonequilibrium electron distribution function. Proceeding from Eliashberg's theory and the heat transfer restriction, Chang and Scalapino (1977, 1978) calculated the nonequilibrium electron and phonon distribution functions for an irradiated superconducting film and the gap value as a function of the incident power. The resulting dependence $\Delta(P)$ has a maximum like the calculations of Latyshev and Nad' (1976) who found a maximum in $I_c(P)$. These data taken together suggest that one of the most important restrictions to the growth of the critical film parameters is due to "effective" heating, or the departure of the phonon distribution from equilibrium in a microwave field, to be more accurate.

However, even in the absence of heating there may be agents to restrict the

enhancement. One of them is superconductivity suppression because of growing microwave current amplitude under large incident power, which was theoretically considered by Aslamazov and Gavrilov (1980). Another is the possible creation of inhomogeneous states in a superconductor by irradiation ($\omega < 24/\hbar$), see Ivlev (1977) and Eckern et al. (1979). Let us consider this point in some detail. At an incident power P smaller than the power P_{opt} corresponding to the maximum enhancement of the critical current I_c and critical temperature T_c, there is a possibility of development of a spatially inhomogeneous state in long bridges. This is reflected by steps in $R(T)$ curves measured at small currents (fig. 11, Latyshev and Nad' 1977) and steps in the $I - V$ curves at $I > I_c$ (fig. 12, Dmitriev and Khristenko 1979). As P approaches

P_{opt} , I_c and T_c grow as usual. At $P \sim P_{\text{opt}}$, spatial inhomogeneities are levelled out, as is suggested by the narrowing of the superconducting transition curve (fig. 11, curves for attenuation 20 and 15 dB ; interpretation to be found above) and by vanishing of the steps in the $I - V$ curve (fig. 12, curves for attenuation 22 and 19.35 dB). When P_{opt} is exceeded, I_c and T_c start to decrease rapidly (I_c falls off to zero in a narrow power range), and the $R(T)$ and $I - V$ curves break up into a number of steps, representing the bridge transition to the resistive state. The film state is stable at horizontal sections of $R(T)$ (fig. 11). In this case, some parts of the bridge are in normal, others in superconducting states (the characteristic size of these parts is about 10μ m). If the temperature is increased from this resistive state, then for each step there are local hysteretic effects.

During further power increase at a fixed temperature (fig. 12), the bridge resistance rises by jumps of almost equal size, till the entire bridge becomes normal.

It will be noted that the steps observed at $P > P_{\text{opt}}$ are associated with individual features of the bridges (viz., their inhomogeneity). For some thicker (about 3000Å) bridges, which seem more homogeneous, there were no steps in $R(T)$ curves. If steps in $R(T)$ were observed on bridges of similar dimensions, which had equal widths, thicknesses and approximately equal lengths (varying by $1 - 2\mu$ m), then they were quantitatively different, i.e. were unequal in number and size. Besides, if a short narrowing ($\sim 1\mu$ m) is made in the bridge, then the number of steps increases by 1 , with all the rest, if any, unchanged. This seems to suggest that the microwave irradiation-induced steps are somehow associated with sample inhomogeneity.

A spatially inhomogeneous state may arise from instability of the homogeneous nonequilibrium superconducting state in a microwave field (Ivlev 1977, Eckern et al. 1979) with the inhomogeneities fixed at the bridge defects. This state appears and developes at powers $P > P_{\rm opt}$, where $I_{\rm c}$ and $T_{\rm c}$ start to decrease; therefore it may prove to be among the sources of restriction to superconductivity enhancement by a microwave field.

The superconductivity enhancement effects described in this section essentially depend on the amount of inhomogeneity in the bridge. The characteristic length of the irradiation-induced inhomogeneity in Sn bridges is roughly 10μ m. It was mentioned above that superconductivity enhancement in bridges longer than $\xi(T)$ is qualitatively identical. There are differences only for bridges with $L < \xi(T)$ (in Sn bridges, $L < 1\mu$ m), whose properties largely depend on spatial gradients of the energy gap (see below). Thus, the above described experimental results corroborate and also develop Eliashberg's physical interpretation of superconductivity enhancement in uniform strips by an electromagnetic field, which is based on formation of nonequilibrium stationary states as a result of quasi-particle redistribution in energies.

18.4 4. Superconductivity enhancement by phonons and tunnel effect

As was mentioned earlier, one of the possible means to produce a nonequilibrium situation in a superconductor, apart from an electromagnetic field, is to expose it to phonon radiation (sound field). This is how an experiment was devised involving observation of superconductivity enhancement by a field of sound waves of frequency about 10 GHz (Tredwell and Jakobson 1975). The critical current was investigated as a function of the sound field intensity both for Al-Sn Josephson point contacts $[L < \xi(T),\ I_{\rm c} \sim (1 - T/T_{\rm c})]$ and Sn bridges, and for long bridges $\left[L > \xi(T),\ I_{\rm c} \sim (1 - T/T_{\rm c})^{3/2}\right]$. In both cases there was an enhancement of the critical current caused by nonthermal phonons. In short samples there was a temperature threshold of the enhancement (for $T/T_{\rm c} > 0.996$, the critical current was suppressed), similar to the case of the electromagnetic field (see below). Calculations made by Tredwell and Jakobson based on Eliashberg's idea of a change in shape of the energy distribution function of quasi-particles under the action of a field were in fair agreement with experiment for both Josephson junctions (fig. 13a) and long bridges (fig. 13b). These results suggest that in the case of an external field the sample geometry is of minor importance, influencing only some details of the enhancement effect (see below). The main contribution comes from nonequilibrium excitations due to

changes in the interaction of superconductor quasi-particle subsystems in an external electromagnetic or sound field.

Experiments in sound waves were not restricted to small samples. Experimental investigations of sound propagation characteristics in pure single-crystalline bulk samples of gallium (Fil' et al. 1975, 1976, 1980) showed that the superconductor electron subsystem is essentially nonlinear for propagation of finite-amplitude sound oscillations. Figure 14 presents the central experimental result of the investigation; in a superconductor, the impact of powerful sound pumping on the absorption of a weak acoustic measuring signal differing in frequency from the pumping signal. One can see that in a wide temperature range the attenuation of the measuring signal, with simultaneous sound pumping of the sample, essentially decreases. This fact is not related to the amplitude-dependent internal friction; it is due to direct perturbation of the superconductor electron subsystem (Fil' et al. 1976). By varying the mutual orientation of wave vectors of two signals, it was revealed that the perturbation embraces only a comparatively narrow region of the phase space near $q \cdot v_{\rm F} = 0$ (q is the wave vector of the pumping signal and $v_{\rm F}$ the Fermi velocity of excitations).

Formally the nonlinear sound attenuation curves in this case (fig. 14) may be described by the BCS expression for the attenuation coefficients α_S and α_N :

$$\alpha_{\rm S}/\alpha_{\rm N} = 2(\exp \Delta(T)/kT + 1)^{-1}$$

with Δ substituted by the nonequilibrium value of $\Delta_n(T)$. Results of such a calculation are presented in the inset of fig. 14. The value of $\Delta_n(T)$ so calculated proves to have a temperature dependence

$$\Delta_{\rm n}(T)/\Delta_{\rm n}(0) = [\Delta(T)/\Delta(0)]_{\rm BCS},$$

coinciding with the BCS one to within the measurement error, but the parameter $\Delta_n(0)$ is appreciably higher than its equilibrium value.

These experimental results have not yet found an unambiguous theoretical description. An analysis of the influence of a nonequilibrium quasi-particle distribution function in a sound pumping field on the character of sound propagation in superconductors (Bulyzhenkov and Ivlev 1976) shows that this influence is only essential in the temperature range $\Delta T/T_{\rm c} \sim \omega/T_{\rm c}$, and is satisfactorily consistent with experimental data for superconducting junctions, fig. 13. For a sound frequency about 150 MHz , as used in the experiments studying sound absorption in bulk superconductors, $\omega/T_{\rm c} \lesssim 10^{-12}$, much below the temperature range in which the said effect is seen (fig. 14). Therefore this area of theoretical studies is still open to application of further efforts. Some recent papers describe the direct enhancing effect of sound on Cooper pairing (Bar'yakhtar and Seminozhenko 1976, 1977. Seminozhenko and Yatsenko 1980), and take into account the particular character of the nonequilibrium quasi-particle distribution in the superconductor irradiated by sound waves (Galaiko et al. 1981). However, at present neither of the mechanisms discussed in these papers has unambiguous correspondence with the experimental results. Therefore further theoretical and experimental studies are desirable, in particular direct measurements of the energy gap of a superconductor in a sound wave field.

As mentioned above, the nonequilibrium state leading to superconductivity enhancement may be set up by quasi-particle tunnelling in a superconductor tunnel junction system,

$$\mathrm{S_B - I - S_A - I - S_B}$$

(Parmenter 1961) ($\mathrm{S_B}$ and $\mathrm{S_A}$ are superconducting films, I insulators, $2A_{\rm B}$ and $2A_{\rm A}$ the energy gaps of $\mathrm{S_B}$ and $\mathrm{S_A}$ respectively, so that $\Delta_{\rm B} \gg \Delta_{\rm A}$) (fig. 15). At a temperature $T \lesssim T_{\rm cA}$, in the superconductor $\mathrm{S_A}$ the number of normal excitations is sufficient, while in superconductors $\mathrm{S_{B3}}$ it is negligibly small. By applying a voltage $V = 2\,(A_B - A_A)\,/e$ between two S_B contacts, one can reduce the number of normal excitations of both signs in the superconductor $\mathrm{S_A}$ through their tunnelling to the superconductors $\mathrm{S_B}$. According to BCS theory. such decrease in the quasi-particle excitation number should lead to higher A and $T_{\rm c}$ of S_A. As was found later (Kirichenko et al. 1979), quasi-particles may be extracted even in a simpler structure, $\mathrm{S_B - I - S_A}$. Moreover, quasi-particle extraction (injection) from a superconductor is not vital to superconductivity enhancement. It is sufficient to pass a direct tunnel current through a symmetric S-I-S junction. If the junction voltage is $V < 2\Delta/e$ then the tunnel

current flow results in energy redistribution of quasi-particle excitations to higher energies in each of the superconducting electrodes, with the total number of excitations remaining unchanged, and a superconductivity enhancement situation is realized which is similar to that considered by Eliashberg in an electromagnetic field (Peskovatskii and Seminozhenko 1976).

In the experimental environment, superconductivity enhancement resulting from tunnel current flow was observed on a symmetric $\mathrm{Al_1Al_2O_3Al}$ junction in the structure $\mathrm{AlAl_2O_3 - Al - Al_2O_3 - Al}$ (Gray 1978). The first tunnel junction (generator) had low resistance, and its electrodes were in nonequilibrium. The second junction (detector) had much higher resistance and was used to measure the IV characteristics from which the change of the gap of the Al medium film was determined. The difference between the nonequilibrium and equilibrium

gaps, $\delta\Delta/\Delta_0$, was up to 0.5% at $T \approx 1.2$ K (fig. 16). A similar experiment on a symmetric $Sn - SnO, -Sn - SnO, -Sn$ junction yielded a maximum value of $\delta\Delta/A_0$ about $4^0{}_0$, the δA_m value increasing with temperature in a linear fashion (Mitsen et al. 1980), see fig. 17.

The superconductivity enhancement resulting from quasi-particle extraction from the superconductor, was experimentally studied on the structure $Al_B - Al_2O_3 - Al_A - Al_2O_3 - Al$ (Chi and Clarke 1979). Quasi-particles were extracted from the Al_A film through the first tunnel junction to the Al_B film with a larger gap. The nonequilibrium energy gap in the Al_A film was measured by the second tunnel junction characteristics. The measured maximum excess of the nonequilibrium gap over equilibrium was up to 40%.

A comparison of experimental results with corollaries of theoretical works found qualitative agreement between them. However our knowledge of this

type of nonequilibrium superconductivity is still insufficient, and detailed comparison is hardly possible before new efforts bring new results.

18.5 5. Superconductivity enhancement and nonequilibrium phenomena in weakly coupled superconductors

The term "weakly coupled superconductors" is the common name of superconductive structures with local suppression of the order parameter $\hat{A}$. This suppression is usually produced by placing a thin nonsuperconducting layer (an insulator or a normal metal) between two superconductors, or by making a short narrow neck between bulk superconducting electrodes (point contact or thin film bridge). If the lower order parameter area is sufficiently small, not larger than $\breve{\zeta}$, then the principal parameters of the superconductor undergo changes substantial for this scale, and therefore their spatial gradients are very high.

In this section, we shall deal with weakly coupled superconductors with metallic conductivity of superconductor-constriction-superconductor type. In such structures stationary and nonstationary Josephson effects are observed. In the case of the nonstationary Josephson effect ($\boldsymbol{V} \neq 0$), as was theoretically shown by Aslamazov and Larkin (1969), the gap in the weak link region oscillates with the Josephson frequency, $\omega = 2eV/\hbar$, thus causing also oscillations of the same frequency of the superconducting and normal components of the junction current and the Josephson self-radiation [the high-frequency Josephson radiation of point contacts was first observed by Dayem and Grimes (1966), and that of thin film bridges by Gubankov et al. (1975)]. The $I - V$ curve of a junction of dimensions $L \gg l, w, L \ll \xi(T)$ (l being the electron mean free path) at $T \approx T_c$ is, according to Aslamazov and Larkin's (1969) theory, hyperbolic,

$$V = R\sqrt{I^2 - I_c^2}$$

with the critical current $I_c = cA_0^2/\sigma_N R$, where σ_N is the specific conductivity, A_0 the order parameter of bulk electrodes away from the constriction, and the constant (c was introduced by Gorkov (1959); the current across the junction is the sum of the normal (V/R) and superconducting ($I_c \sin\varphi$) currents, $\varphi = (2e/\hbar)\int V\, dt$ being the difference of the wave function phases of the superconducting electrodes. This description of weakly coupled superconductors corresponds to the so-called resistive model (McCumber 1968, Stewart 1968), which offers a satisfactory explanation to the main experimental dependences in such structures and serves as the basis for the calculation of characteristics for various Josephson devices (Likharev and Ulrich 1978. Volkov et al. 1978). However, recent theoretical and experimental
studies have shown that in point contacts and small film bridges an important role is played by nonequilibrium effects. As a result, the $I - V$ curves and microwave properties of real point contacts and bridges may appreciably differ from those in the resistive model. The theoretical aspects of nonequilibrium effects in weakly coupled superconductors are treated by Aslamazov and Volkov (1985) in the present volume. Here we shall present the main experimental

results for the most interesting nonequilibrium effects in weakly coupled superconductors: the superconductivity enhancement in short junctions and the excess current effect.

For the manifestation of the Josephson effect proper, the characteristic dimensions of bridge-type or point contact-type weakly coupled superconductors (L, w) should not exceed 2 or $3\xi(T)$ (Gubankov et al. 1976); otherwise, nonstationary effects are most likely to be due to motion of magnetic flux quanta (Gubankov et al. 1973). Most of the results to be presented in this section were obtained in studies of tin bridges of variable thickness, with the following characteristic parameters.

bridge film: length $L = 0.4 - 0.6\mu$ m, width $w = 0.5 - 2\mu$ m, thickness $d = 300 - 1000$Å;

bank film: thickness $d^{\mathrm{B}} = (2-5) \times 10^3$Å;
$\xi(0) = 800 - 1000$Å, a normal-state resistance $R_{\mathrm{N}} = 0.05 - 0.5\Omega$. Variable-thickness bridges are better than point contacts for nonequilibrium effect studies, because they allow to control precisely the geometrical and other characteristic parameters of the weak coupling region.

In the discussion of characteristic parameters of these structures, it should be mentioned that the critical temperature of the bank film, $T_{\mathrm{c}}^{\mathrm{B}}$, is as a rule a few hundredths of a degree higher than the critical temperature of the bridge proper, T_c^b. This experimental fact was noted by more than one group of investigators (see above) and was ascribed to various effects: fluctuations, differences between properties of the bank and the bridge, etc. $T_{\mathrm{c}}^{\mathrm{B}}$ is usually determined by appearance of nonlinearity in the $I-V$ curve and from the dependence $R(T)$ measured at small current ($I \leqslant 1\mu$ A). In the temperature range $T_{\mathrm{c}}^{\mathrm{b}} < T < T_{\mathrm{c}}^{\mathrm{B}}$ where the structure superconductor normal-metalsuperconductor is realized, the critical current is nonzero because of the small size of the normal-metal region: its characteristic length is comparable with the coherence length of the bridge material. The temperature dependence of the critical current at $T_{\mathrm{c}}^{\mathrm{b}} < T < T_{\mathrm{c}}^{\mathrm{B}}$ is nonlinear and looks like that predicted by the theory (Aslamazov et al. 1968) for short S-N-S bridges. In case of further moderate temperature decrease ($T \lesssim T_{\mathrm{c}}^{\mathrm{b}}$), the $I_{\mathrm{c}}(T)$ dependence becomes usually linear, in agreement with the calculation of Aslamazov and Larkin (1969), and Kulik and Omelyanchuk (1978). The value of $T_{\mathrm{c}}^{\mathrm{b}}$ is found from $R(T)$ or by extrapolation of the linear part of $I_c(T)$ to the intersection with the T-axis.

The temperature evolution of the $I-V$ characteristics of one small variablethickness tin bridge is shown in fig. 18. It is representative of such structures and has been observed by several groups of authors (Octavio et al. 1978, Gubankov et al. 1977, Latyshev and Nad' 1979). It is characterized by the following features. At $T \lesssim T_{\mathrm{c}}^{\mathrm{B}}$, the bridge $I-V$ curve becomes nonlinear, there appears a superconducting part with $V = 0$. At $T \lesssim T_{\mathrm{c}}^{\mathrm{b}}$ and moderately high voltages, the $I-V$ shape becomes almost hyperbolic; as the voltage grows, there is an excess-current effect (Pankove 1966). As we move down from T_c, the situation changes: in the beginning of the IV resistive part, there appears a linear section with the differential resistance $R_{\mathrm{d}} < R$, which in the higher current region transits into a section of rapidly increasing $R_{\mathrm{d}} > R$. Near this transition one can distinguish the bump point I_{s}^0 (see the insert in fig. 18). As the temperature is lowered further [$T_{\mathrm{c}} - T > 0.5$ K], in the low V region, one can see hysteresis-shaped voltage jumps. Such temperature evolution of the $I-V$ characteristics of small bridges in the region of moderately high voltages is in agreement with Aslamazov and Larkin's (1976) calculation with allowance for

the effect of nonequilibrium electrons. The dynamic processes are in this case described by an equation similar to eq. (2.7) in the chapter by Aslamazov and Volkov.

The physical picture of the appearance of singularities in the $I-V$ curve of short bridges at sufficiently small voltages and temperatures slightly lower than T_c is as follows. As I_c is exceeded, the nonstationary Josephson effect starts in the bridge, with the gap in the constriction oscillating with Josephson frequency $\omega = 2\mathrm{e}V h$ which increases with the voltage (Aslamazov

and Larkin 1969). The quasi-particles in the constriction with energy $:< \Delta_H$ receive some surplus chergy from collisions against the oscillating walls of the potential well $A(x)$, and as a result, their distribution function $f(x)$ changes. The change of $f(x)$ may be such that the time-averaged energy magnitude of the gap increases, causing growth of the bridge current, i.e. resulting in superconductivity enhancement. This mechanism is similar (with the exception of the "pumping" source) to the superconductivity enhancement in uniform bridges treated by Eliashberg (197()). At voltages $V > \tau_i^{-1}$, i.e. where the Josephson oscillation period is smaller than the energy relaxation time. there appears a linear section in the $I-V$ curve, with $R_{\mathrm{d}} < R$. When the current reaches the characteristic value I', there occurs a sharp increase in the time-averaged voltage. caused by the growing normal component of the current. There is only superconductivity enhancement if the constriction size is smaller than but larger than a certain characteristic length $\eta = \xi(T)\,(\delta T/T_{\mathrm{c}})^{1/4}$ (Aslamazov and Larkin 1976, Artemenko et al. 1979a) for which electrons with energies smaller than A_{B} can diffuse from the constriction. Since the value of η depends on temperature. the inequality $L > \eta$ becomes true some distance below T_c; that is, superconductivity enhancement by the "direct current" in three-dimensional contacts has a temperature threshold, which is observed experimentally (Octavio et al. 1978, Gubankov et al. 1977, Latyshev and Nad' 1979). Indeed, as is seen in fig. 18, the characteristic features of the $I-V$ curve (low R_{d} section in the beginning of the resistive region, "bump" region with $R_{\mathrm{d}} > R$ near I_{c}^0) appear at $\delta T = T_{\mathrm{c}} - T \simeq 0.02 - 0.04$ K, where L grows above η. In accordance with theoretical predictions the shape of the $I-V$ curve is near-parabolic above the bump point I'. while below. down to the linear region with low R_{d}. it is near-hyperbolic (Octavio 1978); for some samples the temperature dependence of $(I_{\mathrm{s}}^0/I_{\mathrm{c}})^4$ in the range $\delta T \simeq 0.08 - 0.2$ K is linear (Gubankov et al. 1977). The deviation of $(I_{\mathrm{c}}^0/I_{\mathrm{c}})^4$ from linear at small δT may be associated with the increasing error in I'. determination. and that at large δT with the appearance of heat-induced voltage jumps in the I l curve. As was found by experiments, the differential resistance of the linear $I-V$ section at $I \gtrsim I_c$ decreases with temperature in inverse proportion to $T_{\mathrm{c}} - T$ (Gubankov et al. 1977, Octavio et al. 1978). Figure 19 represents $R_d(T)$ in a wide temperature range for Sn bridges of different lengths from 0.5 to 0.9μ m. The dashed straight line is $A = T_{\mathrm{c}}\,(T_{\mathrm{c}} - T)^{-1}$ for $A = 0.01$. One can see that the experimen-

tal dependence $R_{\mathrm{d}}(T)$ goes as $(T_{\mathrm{c}} - T)^{-1}$. The theoretical linear part was obtained by Aslamazov and Larkin (1976) for bridges of length $\eta(T) \ll L < \xi(T)$ only for voltages $\tau_\varepsilon^{-1} < V < \tau_\varepsilon^{-1} T/\Delta$. According to this theory, $R_{\mathrm{d}} \sim (T_{\mathrm{c}} - T)^{-5/2}$. For tin bridges, L becomes larger than $\eta(T)$ at $kT/\Delta \leqslant 3$, and therefore, the range of applicability of the theoretical calculation is rather narrow, making it difficult to compare theory and experiment quantitatively.

Figure 20 presents the temperature dependence of the characteristic voltage V^0 corresponding to zero second derivative (the bump point of I^0) of the $I-V$ characteristics for some of the studied samples (Gubankov et al. 1980). It is seen that V^0, depends but slightly on the tin bridge parameters and changes with temperature as $(T_{\mathrm{c}} - T)^{1/2}$. These experimental data, combined with the theory of Aslamazov and Larkin (1976), allow to estimate the energy relaxation time τ_1 for quasi-particles. For tin it is $\tau_0^{\mathrm{Sn}} = (2-6) \times 10^{-10}$ s. This range is in agreement with the value of Latyshev and Nad (1976), and Octavio et al. (1978): $\tau_\varepsilon^{\mathrm{Sn}} = (25) \times 10^{10}$ s. In a similar way, by using the $V_{\mathrm{s}}^0(T)$ dependences obtained by Hansen et al. (1978), we have the following for aluminium and lead bridges: $\tau_\varepsilon^{\mathrm{Al}} = 2 \times 10^{-9}$ s and $\tau_\varepsilon^{\mathrm{Pb}} = 10^{-11}$ s. All these τ_ε values are several times smaller than the theoretical electron-phonon scattering time τ_0 in a normal metal at $T = T_c$. [see data presented in the paper by Gorkov and Eliashberg (1969)].

It should be noted that changes in bridge dimensions result in appreciable alteration of the $I-V$ characteristics. In very short bridges (for Sn, $L < 0.5\mu$ m), in a sufficiently wide temperature range near T_{c} (about 40 mK), the $I-V$ curve was close to hyperbolic, without distinct nonequilibrium singularities at $I > I_c$, which in general agrees with the theory (Aslamazov and

Larkin 1976, Artemenko et al. 1979a) which says that the energy diffusion of quasi-particles is hindered, for $L < \eta(T)$, and though the processes preserve their nonequilibrium character, the linear part at $I \gtrsim I_c$ and the IV kink point should vanish (for details see the chapter in the present volume by Aslamazov and Volkov). As L grows towards $L \sim \xi(T)$, the $I \cdot V$ part with small differential resistance was less pronounced and was seen in a narrower temperature range located closer to T_c. In long bridges ($L \gg \xi(T)$) the low differential resistance part is not observed at all (Latyshev and Nad' 1979); the transition to the resistive state occurs by a jump from $V = 0$ to a certain finite voltage at $I = \text{const.}$; there is no superconductivity enhancement by "direct current". At lower temperature, the superconductivity enhancement in bridges should vanish if $L \gg \xi(T)$ (Aslamazov and Larkin 1976). This conclusion, generally speaking, conforms to experimental data, although the theory does not allow for thermal effects. In real experiments, heating of the weakly coupled area by current is usually most pronounced at low T, where L is larger than $\check{\zeta}(T)$ and
can have a certain effect upon superconductivity enhancement, suppressing the above considered singularities of the $I - V$ curve due to enhancement. An analysis of thermal effects in weakly coupled superconductors was carried out by Nad' and Polyanskii (1973) and also by Skocpol et al. (1974). They showed in particular that the hysteretic effects and voltage jumps occurring when the critical current is exceeded at relatively low temperatures, as well as the local hysteresis in the $I - V$ curve in places with gap singularities, are due to heating of the bridge film by the current.

It might be well to mention that some $I - V$ singularities similar to fig. 18 and those discussed above were observed on superconducting point contacts too (Divin and Nad' 1978). However, detailed study of these features of point contacts is rather difficult because of the impossibility of correct determination of geometric and other characteristic parameters of the weakly coupled area.

Let us now consider superconductivity enhancement in weakly coupled superconductors in an external electromagnetic field (Dmitriev et al. 1973, 1976, Dmitriev and Khristenko 1979, Gregers-Hansen and Levinsen 1971, Levinsen 1974, Klapwijk and Mooij 1976, Dayem and Wiegand 1967. Latyshev and Nad' 1974, Peskovatskii and Strizhko 1979, Octavio et al. 1978. Gubankov et al. 1977, Hansen et al. 1978, Bevza et al. 1976).

The physical causes of the superconductivity enhancement in short bridges and point contacts subjected to microwave irradiation were analyzed theoretically by Aslamazov and Larkin (1978). In contrast to long homogeneous films in which, according to Eliashberg's (1970) theory, nonequilibrium and enhancement (see the preceding section) result from direct influence of the electromagnetic field on quasi-particles, in short, spatially inhomogeneous bridges or contacts (with the characteristic dimension $\tilde{} \check{\zeta}(T)$) these effects are associated with gap oscillations in the weakly coupled area. When there is no microwave irradiation and the bias current is higher than the critical value, these oscillations have the frequency of the Josephson selfgeneration and give rise to IV singularities similar to those considered above. Under external irradiation, when the bias current is lower than the critical value and Josephson generation does not arise, the "vibration" of the potential well forming in the constriction has the frequency of the applied irradiation and also can cause energy diffusion of electrons, shift of their distribution function, effective enhancement of the gap and superconductivity enhancement, i.e. critical current growth.

Thus, the theory (Aslamazov and Larkin 1976, 1978) maintains that the superconductivity enhancement effects in weakly coupled superconductors depending on the bias current $I > I_c$ (i.e. the influence of the Josephson selfoscillations) and conditioned by an external electromagnetic irradiation have common nature. Experimental data corroborate this conclusion.

Experimental investigation of superconductivity enhancement by microwave irradiation in short bridges and contacts involved a wide frequency range:

from 0.1 GHz to 150 GHz (Dayem and Wiegand 1967, Dmitriev et al. 1973, Latyshev and Nad' 1974, 1976, 1979, Dmitriev and Khristenko 1976, 1979. Klapwijk et al. 1977, Octavio et al. 1978, Gubankov et al. 1978). The magnitude of the effect may be characterized by the relative increase of the critical current under irradiation to the maximum value $\beta_{\rm m} = (I_{\rm c}^{\rm max} - I_{\rm c})/I_{\rm c}$.

Figure 21 represents typical temperature dependences of β for various radiation frequencies and the temperature dependence of $(I_{\rm s}^0 - I_{\rm c})/I_{\rm c}$ (Gubankov et al. 1980). Superconductivity enhancement by irradiation is much lower at frequencies $\omega/2\pi \lesssim 10$GHz; in the range $\omega/2\pi \lesssim 1\text{GHz} \simeq \tau_\varepsilon^{-1}$, the effect was not seen at all. This suggests that superconductivity enhancement by irradiation is due to nonequilibrium phenomena. However, unlike the experimental results for long thin films (Latyshev and Nad' 1975, 1976, Klapwijk and Mooij 1976) and the theoretical predictions for spatially homogeneous superconductors (Eliashberg 1970), small point contacts and bridges of variable thickness did not display an increase of the critical temperature, at least at frequencies 1 to 150 GHz . Moreover, microwaveinduced superconductivity enhancement in short bridges has a temperature threshold (Jillie et al. 1975, Dmitriev et al. 1976, Dmitriev and Khristenko 1978, Gubankov et al. 1977). For example, in the bridge whose $\beta(T)$ and $(I_{\rm s}^0 - I_{\rm c})/I_{\rm c}$ are represented in fig. 21 , at a frequency of $\omega/2\pi \approx 10$GHz, this effect appeared and rose as the temperature was reduced, only if δT was higher than a certain threshold value: $\delta T > \delta T_{\rm th} \approx 0.02$ K.

It is obvious also from $\beta(T)$ that the maximum critical current value in a microwave field is never in excess of $I_{\rm s}^0$ and is realized at temperatures such that $L \leqslant \xi(T)$. For Sn bridges, as the radiation frequency rises, $\delta T_{\rm th}$ goes through a minimum, usually at $\omega/2\pi \simeq 10$GHz, and β has its maximum magnitude at $\omega/2\pi \simeq 40 - 50$GHz. The temperature range of superconductivity enhancement also changes in a nonmonotonic fashion: at growing frequency it widens and shifts to higher temperatures ($\delta T_{\rm th}$ decreases) and then becomes narrower, shifting downwards from $T_{\rm c}$ ($\delta T_{\rm th}$ increases).

The study of the frequency dependence of superconductivity enhancement in short bridges leads to the conclusion that in this case, as for long homogeneous films, there are lower and upper frequency boundaries for occurrence of the effect. The lower boundary is determined by the Eliashberg (1970) condition (see the preceding section). The existence of the upper frequency boundary was revealed experimentally by Latyshev and Nad' (1974). At temperatures close to $T_{\rm c}$ the upper frequency boundary is determined by the energy gap magnitude A. The most probable cause may be the fact that at $\hbar\omega > 2\Delta$ the predominant process is Cooper depairing due to irradiation

absorption, which leads to the usual gap diminution. However, when $\omega/2\pi \sim 100$GHz, the upper frequency boundary lies below that determined by the condition $\omega = 24/\hbar$, probably for the same reasons as in the case of long bridges.

There is a correlation between rising critical current and growing voltage V_A corresponding to the gap singularity, evidencing gap enhancement as well. Figure 22 supplies an example of the changing position of the characteristic gap singularity in $\mathrm{d}V/\mathrm{d}I$ versus $\vec{V}$ for a short bridge under the action of irradiation (Gubankov et al. 1978). One can see that V_Δ enhancement is about 2%. The small increase of V_Δ under microwave irradiation seems to be due to the fact that superconductivity enhancement by "direct current" may essentially affect the gap magnitude in short bridges even in the absence of microwave field.

As the incident power P grows, the amount $I_c(P)$ changes as follows (Dmitriev et al. 1976, Dmitriev and Khristenko 1978, Latyshev and Nad' 1979, Peskovatskii and Strizhko 1979, Gubankov et al. 1980). When the power is small, the critical current grows slowly, sometimes remains practically constant or even slightly (by some 2%) falls off. Then follows a relatively sharp increase of $I_{\rm c}$, up to the maximum value (fig. 23). After that the critical current decreases, oscillating, approximately as $\sqrt{P}$, that is, in the same way as does the critical current of the usual Josephson junction. Thus, at a certain power, where the critical current ceases to

grow, the superconductivity enhancement effect is suppressed by the nonstationary Josephson effect. This seems to be the reason that $[I_c(P)]^{max}$ does not increase to I_s^0, as was predicted by Aslamazov and Larkin (1978).

We have considered superconductivity enhancement in short bridges for the case of $\eta < L < \xi$. The change of the $I-V$ characteristics is qualitatively different in bridges of significantly larger size (for Sn bridges, $L > 1\mu m$). In this case irradiation leads to origination of superconducting current at $T > T_c$, and to its considerable increase (tens of times) at $T \lesssim T_c$ (Dmitriev et al. 1973, Latyshev and Nad' 1974). The I-V curve of such bridges in the absence of irradiation has neither a resistive region with small R_d for $I > I_c$, nor Josephson steps; the transition to the resistive state, both in and out of microwave field, occurs jumpwise even at comparatively high temperatures where the $I-V$ curve in the absence of irradiation has no hysteresis. Some representative dependences of I_c^{max}/I_c for bridges with various values of L are shown in fig. 24 (Latyshev and Nad' 1979). We see that with increase of the bridge length, the boundary of the enhancement shifts. Simultaneously with the shift to T_c there is growth of β, and finally at $L > L_{th} = (D/\omega)^{1/2} \approx 1\mu$ m (where $D = \frac{1}{3}c_1/l$ is the diffusion coefficient) the character of the temperature dependence of the enhancement alters: the β value is maximum at $T \gtrsim T_c$ and gently falls off as the temperature drops.

Thus, it is rather obvious that it is spatial inhomogeneity that distinguishes

Aslamazov and Larkin's mechanism of enhancement from that of Eliashberg. Indeed, it is only in a spatially inhomogeneous environment that Josephson generation can occur, and consequently superconductivity can be enhanced if a direct transport current is passed. The shift from Aslamazov and Larkin's (1976, 1978) enhancement mechanism to that of Eliashberg (1970) may be made by changing the bridge geometry, e.g., through increasing its length. As the boundary of the transition in this case, one may regard the quantity L_{th} (Latyshev and Nad' 1979): the Aslamazov-Larkin mechanism, dominates below $L = L_{th}$, the Eliashberg mechanism dominates above.

It is worth emphasizing in conclusion that for all the differences in superconductivity enhancement between spatially homogeneous and inhomogeneous systems, the fundamental source of the effect is the same: a nonequilibrium of the quasi-particle distribution function induced by external microwave radiation or by Josephson self-radiation. This should always be borne in mind when analyzing the superconductivity enhancement in various experimental environments.

18.6 6. The excess current effect

The current-voltage characteristics of short superconductive bridges and contacts have, in addition to the above peculiarities due to nonequilibrium processes, one more essential distinctive feature as opposed to the resistive model. At high voltages, the dependence $I(V)$ does not obey Ohm's law $I = V/R$; instead, it assumes an asymptotic shape shifted upwards by a certain amount I_{ex}, independent of V in a wide voltage range. This excess current was first observed experimentally by Pankove in 1966, and its presence in the $I-V$ curve is an unambiguous indication of weak coupling with metallic conductivity. Until recently however its physical nature was unclear. The range of proposed current mechanisms either based on pure phenomenology (Deaver and Pierce 1972), or applicable only to gapless superconductors (Likharev and Yakobson 1975) were not able to account for all the experimentally observed features of the effect.

One very important experimental result which contributed essentially to understanding of the excess current physics was the observation that the
excess current is directly proportional to the magnitude of the energy gap in short bridges and superconducting contacts (Divin and Nad' 1978, 1979, Zhilinski et al. 1980). It was so

important in particular because the theoretical papers of Rieger et al. (1972), and Likharev and Yakobson (1975) suggested that $I_{\rm ex}$ should be directly proportional to the weak coupling critical current $I_{\rm c}$, rather than to Δ.

Figure 25 shows the temperature dependences of the excess and critical currents of a contact with normal resistance $R_{\rm N} = 8.4\Omega$ (Divin and Nad' 1978). The measurements used stable superconducting Nb – Nb point contacts with the principal Josephson properties depending on microshorts. I_{cx} of the contacts was measured at $V \approx 5$mV, where throughout the temperature range, $V > 2\Delta/e$. The same figure shows experimental points representing the temperature dependence of the voltage $1,2V_{2,1}$ corresponding to the gapinduced singularity of the point-contact $I - V$ curve at $V = 2\Delta/e$. As is seen, the
dependences $I_{\rm c}(T)$ and $I_{\rm ex}\,(T)$ are markedly different. $I_{\rm c}(T)$ is linear near $T_{\rm c}$ and somewhat off-linear at $T/T_{\rm c} < 0.6$, agreeing in general with the theoretical $I_{\rm c}(T)$ for microshorts (solid curve; Kulik and Omelyanchuk 1978). The dependence $I_{\rm ex}\,(T)$ coincides well with $\frac{1}{2}V_{21}$, and these both are in agreement with the BCS $\Delta(T)$ (broken curve). In the neighbourhood of $T_{\rm c}, I_{\rm ex} \gg I_{\rm c}$ and at $T < T_{\rm c}, I_{\rm ex} \sim I$. Weitz et al. (1978) noted that the excess current was observed in all superconducting point contacts irrespective of whether the IV curve of the irradiation contacts at $V > A/e$ had current steps, which are a characteristic indication of the nonstationary Josephson effect. In other words, the nonstationary Josephson effect cannot be the ultimate cause of the excess current.

Artemenko et al. (1978, 1979*b*) considered the excess current effect on the rigorous basis of the microscopic theory and showed that in a superconducting point contact or a short bridge of length

$$L < \xi(T)\,(1 - T/T_{\rm c})^{1/4} = \eta(T)$$

at $eV > A$ and any temperature, the current is determined by the following expression:

$$I = V/R + (\Delta/R)\left(\frac{1}{4}\pi^2 - 1\right)\tanh(eV/2kT) \tag{3}$$

In the voltage region $eV \geqslant \lambda$, the current across the contact is equal to the sum of the Ohmic current V/R and the excess current

$$I_{\rm ex} = (\Delta/R)\left(\frac{1}{4}\pi^2 - 1\right)\tanh(\mathrm{eV}/2kT).$$

Thus, theory as well as experiment suggested that $I_{\rm ex} \sim \Delta$ at high V. Note that the experimental $I_{\rm ex}$ values represented in fig. 25 were measured at $V \approx 5\mathrm{mV} \gtrsim 5kT$, where the value of $\tanh(eV/2kT)$ differs from 1 by less than 2%. Quantitative comparison of experimental and theoretical $I_{\rm ex}$ values showed that for point contacts, the theory gives $I_{\rm cx}$ higher by a factor of 1.5 , possibly owing to particulars of the conduction mechanism of the real point contacts (Divin and Nad' 1978, 1979). Measurements on short ($L \leq 0.5\mu$ m) bridges of variable thickness (which are physically more definite) conducted by Zhilinski et al. (1980) yielded results similar to those for the contacts; however in this case there was quantitative agreement between experimental and theoretical $I_{\rm ex}$ values.

The theory of Artemenko et al. (1978) was the first where the excess current was obtained as a function of voltage:

$$I_{\rm ex} \sim \tanh(eV/2kT).$$

The experimental measurement of $I_{\rm ex}\,(V)$ was carried out by Divin and Nad (1979). The $I_{\rm ex}\,(V)$ values were determined by the difference between two experimental $I - V$ curves of

the contact for $T \lesssim T_c$ ($I = V/R + I_{ex}$) and $T > T_c$ ($I = V/R$). Figure 26 shows $I_{ex}(V)$ for a contact with $R = 5.9\Omega$ at two fixed

temperatures, starting with $V \gtrsim \Delta/e$ and up to high voltages $eV > 5kT$ where $I_{ex}(V)$ is practically constant. All the I_{ex} values were normalized to the excess magnitude at $eV \gtrsim 5kT$. The solid curve represents the theoretical dependence $\tanh(eV/2kT)$. It is seen from fig. 26 that the experimental and theoretical dependences agree well. The slight difference, a little larger at lower temperatures, may be due to the increasing contribution of the Josephson current component which falls off as $1/V$ at $eV > \Delta$ (Artemenko et al. 1979b). The $I_{ex}(V)$ results for variable thickness bridges (Zhilinski et al. 1980) at temperatures not very close to T_c are similar to those for contacts (fig. 26). However, near T_c the difference between the theoretical and experimental $I_{ex}(V)$ is more pronounced for the bridge, resulting probably from the effect of self-heating on the bridge which is larger than on the contact.

The microscopic theory of Artemenko et al. (1979b) is rigorously applicable only to the weak coupling with length $L < \eta(T)$. This holds for Nb − Nb point contacts with $R \sim 10\Omega$ in the range $T_c - T \leqslant 1$ K (Divin and Nad' 1979) and for Sn bridges of length $L \leq 0.5\mu$ m in the range $T_c - T \leq 100$mK (Zhilinski et al. 1980). As the temperature drops out of these ranges. η becomes smaller than L and accordingly, as we have mentioned, in the near-hyperbolic $I - V$ curves at $T \lesssim T_c$ there appears a linear part and a typical bump (fig. 18). However, as is shown by $I_{ex}(T)$ experiments, in bridges with $L \leqslant 0.5\mu$ m, a temperature drop reflecting an increase in L/η to 2.5 does not lead to appreciable disturbance of the proportionality between I_{ex} and A (Zhilinski et al. 1980). A decrease of I_{ex} and a pronounced departure from $I_{ex} \sim \Delta$ are found for bridges with $L \gtrsim 1\mu$ m, in qualitative agreement with excess current calculation for long bridges (Zaitsev 1980).

The excess current was also observed in the $I - V$ curves of superconductornormal metal (S-N) point contacts (Pankove 1966, Chien and Farrell 1975, Bevza et al. 1977, Gubankov and Margolin 1979, Dorozhkin 1980). As in the case of S S contacts, the main scale for the effect in S-N contacts is the energy gap magnitude Λ. For all S N contacts I_{ex} is proportional to the value of the energy gap (Gubankov and Margolin 1979, Dorozhkin 1980). The $I - V$ curve of high-resistance contacts ($R \gtrsim 10\Omega$) which seem to have a small constriction diameter and much impurity and many defects ("dirty" contacts) displays a gap-induced singularity at $V \simeq A/e$ and the contact resistance at $V \to 0$ changes nonmonotonically with temperature: $R = R_N$ at $T \simeq T_c$ and $T \to 0$; at $T \simeq 0.8T_c$ the minimum is attained, $R = 0.87R_N$ (Gubankov and Margolin 1979). In lowresistance contacts ($R < 1\Omega$) and those prepared by electrical break-down of an insulating film ("pure" contacts), resistance decreases monotonically with temperature (Chien and Farrell 1975, Dorozhkin 1980). These experimental results are in qualitative agreement with microscopic theories for "dirty" ($l \ll \max(d, \pounds)$; Artemenko et al. 1979b) and for "pure" ($l \gg \max(d, L)$; Zaitsev 1980b) contacts.

Artemenko et al. (1979b), by a microscopic approach, and Dorozhkin (1980), by common sense reasoning, interpreted the excess current as due to quasi-particles with energyes $\varepsilon < \Delta$. In short S − S and S − N contacts, quasiparticles with energy $\varepsilon > \Delta$ carry current in the same way as in normal $N - N$ contacts with Ohmic $I - V$ curve $I = V/R$. However, unlike $N - N$ contacts, those with one or two superconducting electrodes have one more conduction channel for quasiparticles with $\varepsilon < \Delta$. The transfer of quasi-particles from one electrode into the other, to the energy range $\varepsilon < \Delta$ under the gap, takes place, with a finite probability, by processes similar to the Andreev reflection (Andreev 1964). This surplus conduction with the energy scale Δ is responsible for the excess current in the IV characteristics of short $S - S$ and $S - N$ contacts.

18.7 7. Conclusion

The earliest experiments investigating superconductivity enhancement were one of the starting points of nonequilibrium superconductivity studies. They were followed by a series of fundamental theoretical and experimental works dealing with nonequilibrium processes and superconductivity enhancement. At present, although studies in this area are still under way, we can think of the general concept of nonequilibrium phenomena in superconductors exposed to electric and electromagnetic fields and also to sound waves.

It was found that in addition to the "depairing" studied before, these fields can also cause growth of superconductor critical parameters, i.e. enhance superconductivity. The ultimate cause of such effects lies in the changing state of the assembly of unpaired electrons (quasiparticles), leading to changes of
properties of paired (superconducting) electrons. When, e.g., an electromagnetic field or high-frequency sound act on homogeneous superconductors, quasi-particles with energy $\varepsilon \gtrsim \Delta$ near the edge of the gap absorb quanta of the irradiation and shift to a higher energy region, thus reducing the occupancy of states near the gap edge which are predominant in pairing processes. This is equivalent to superconductor cooling and gap enhancement.

In weakly coupled superconductors with metallic conductivity, not exposed to an external high-frequency field, with a current greater than critical, quasiparticles are pumped by Josephson self-oscillations which bring a similar result: enhancement of the gap in the weak-coupling region and rise of the superconducting current ($I-V$ bump). With a current smaller than critical, applied electromagnetic irradiation causes "forced" oscillations of the gap in the bridge constriction and superconductivity enhancement. We will emphasize again that the enhancement effects in such different systems with different "pumping sources" have essentially an identical nature; that is, changing quasi-particle distribution function and the resulting enhancement of the superconductor energy gap. In very short bridges and contacts with $L < \eta(T)$, nonequilibrium processes do not seem to induce any appreciable gap enhancement, though they give rise to anomalous currents, responsible for the $I-V$ singularities and for the excess current in such systems.

However there are some problems associated with nonequilibrium processes and superconductivity enhancement which have not yet been understood exhaustively. Among these, it is appropriate to refer first to the problem of the origin of spatially inhomogeneous states in long uniform conducting channels, carrying a direct current $I > I_c$, both with and without external high-frequency fields (phase slip centres). In the case of weakly coupled superconductive systems, too little attention has yet been given to the $I-V$ singularities in the low-voltage region (linear part) and in the voltage region corresponding to the energy gap value (gap-induced singularities). The properties of very short bridges with $L < \eta(0)$ have also been studied insufficiently. Our hope is that further experimental and theoretical efforts will bring answers to these questions as well.

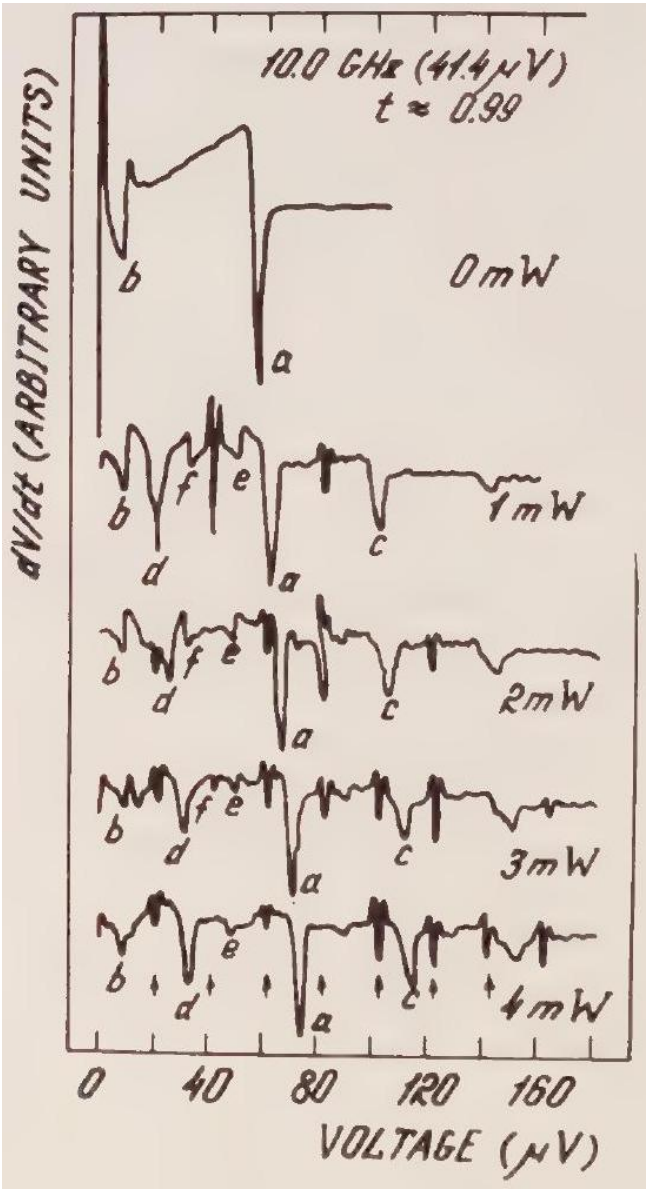


Fig. 8. Differential resistance $\mathrm{d V / \mathrm{d} I$ of an $Al - Al_2O_3 - Al$ tunnel junction as a function of voltage for various incident powers indicated near each curve. The irradiation frequency is 10 GHz . $T/T_c \approx 0.99$.}

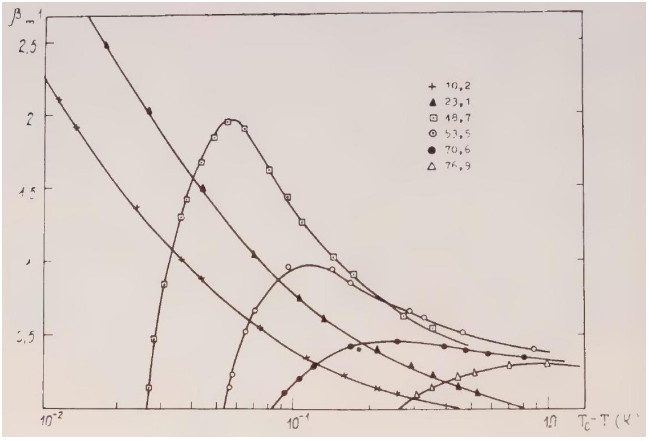


Fig. 9. Temperature dependence of the maximum enhancement of the critical current $\beta_{\mathrm{m}}=I_{\mathrm{c}}^{max}(P) / I_{\mathrm{c}}(0)$ for a variety of irradiation frequencies (in GHz).}

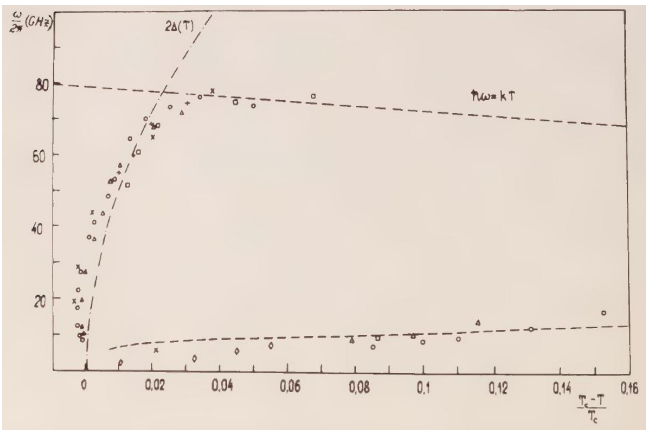


Fig. 10. Frequency boundaries of the region of existence of critical current enhancement. The points represent Sn bridges of various lengths from 2 to $700 \mu \mathrm{˜m $ (Latyshev and Nad' 1976, Dmitriev and Khristenko 1978); ⋄ are data of Dayem and Wiegand (1967).}

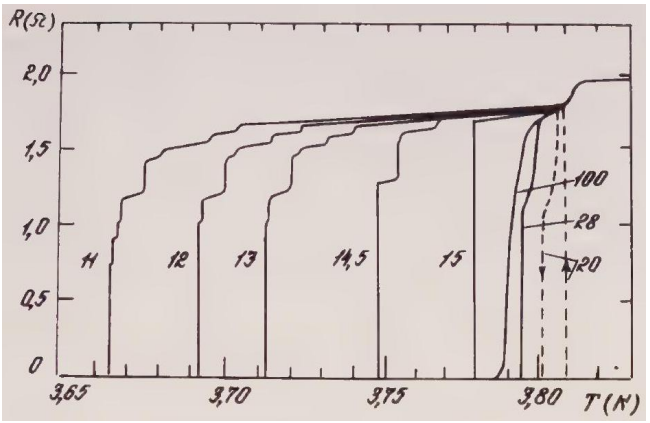


Fig. 11. Temperature dependence of the resistance of a Sn bridge, measuring $0.15 \times 1.5 \times 47 \mu \mathrm{˜m ^{3}$, for various incident powers (the figures indicate the attenuation in dB).}

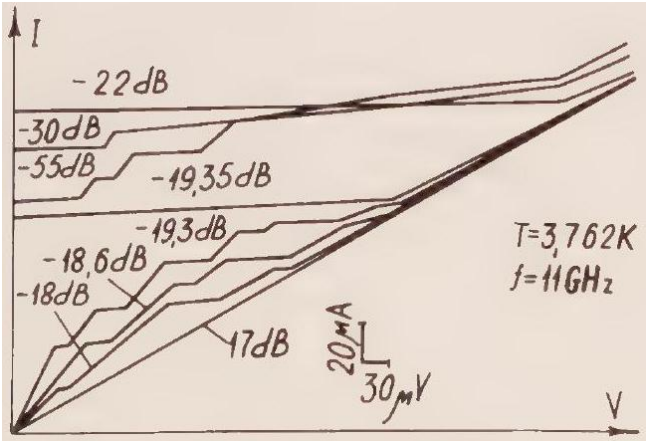


Fig. 12. The steplike structure of the $I-V$ curve of a narrow, long tin film ($T_{\mathrm{c}}=3.814 \mathrm{~K}$) for various electromagnetic irradiation levels (the figures show the attenuation in dB).}

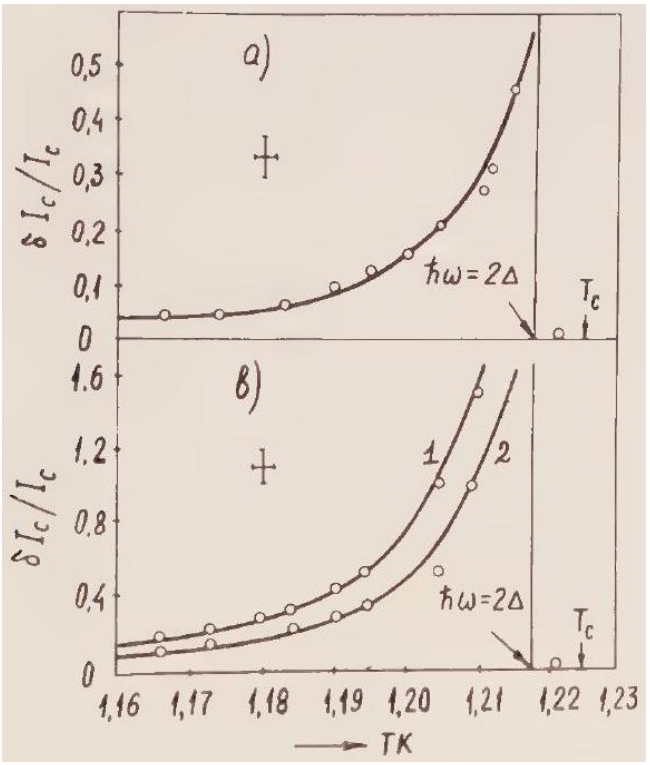


Fig. 13. (a) Relative increase in the critical current as a function of temperature for a short microbridge with $I_{\mathrm{c}} \sim\left(1-T / T_{\mathrm{c}}\right)$. Solid line shows prediction of Eliashberg's theory modified for phonon excitation. (b) Same as (a), for a long microbridge with $I_{\mathrm{c}} \sim(1-T/T_{\mathrm{c}})^{3/2}$ and two phonon power levels: (1) 0 dB , (2) -3 dB .}

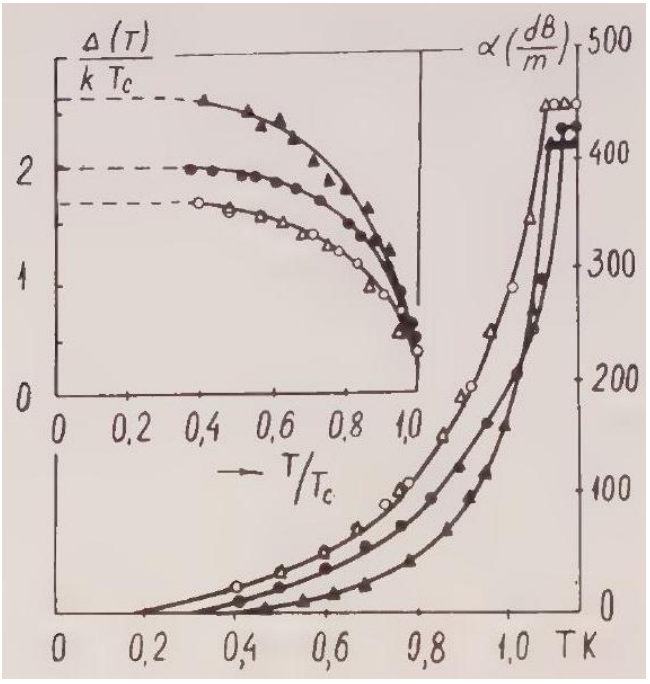


Fig. 14. Experimental temperature dependence of the attenuation of the longitudinal sound in superconducting gallium. $\mathrm{O

, \triangle$ in the absence of a sound pumping field; pumping level μ_1; pumping level $\mu_2 > \mu_1$. Signal and pumping frequencies are 54.2 MHz and 150 MHz respectively. The inset shows the temperature dependence of the nonequilibrium gap as calculated from attenuation curves by the BCS formula for the sound attenuation coefficient.}

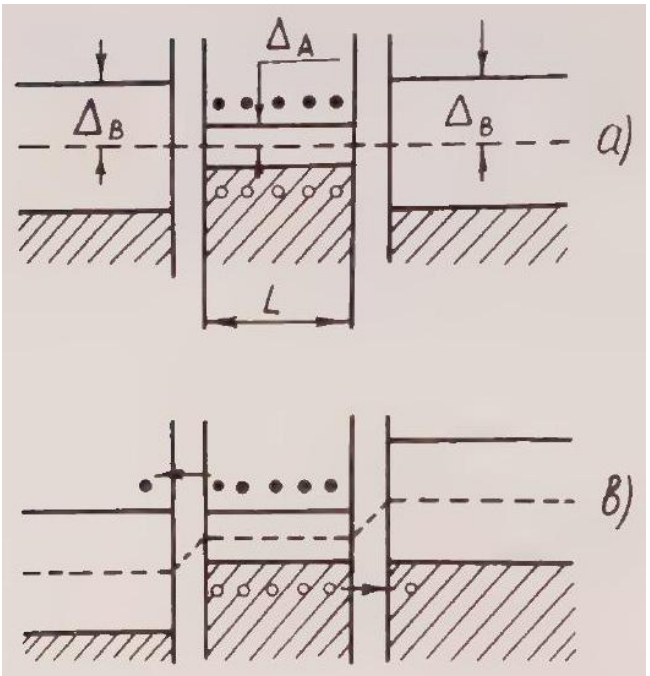


Fig. 15. Energy level diagrams for a system of a superconducting film of thickness L and energy gap $2 \Delta_{\mathrm{A

}$ separated by insulating layers from superconducting contacts with energy gap 21_{B} : (a) zero bias; (b) $= 2\left(\Delta_{\mathrm{B}} - \Delta_{\mathrm{A}}\right)/e$.}

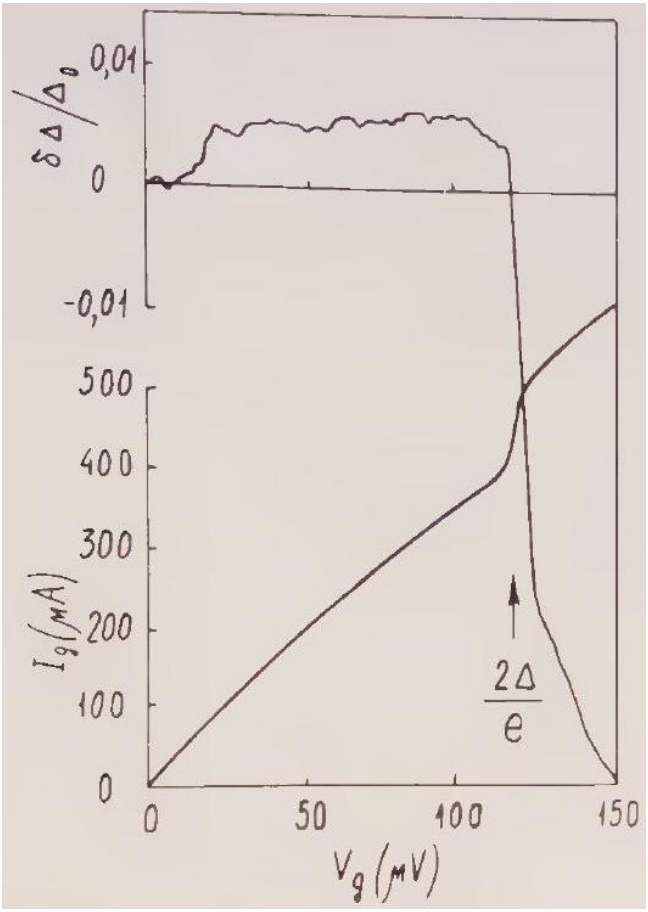


Fig. 16. The normalized change in gap in the detector junction as a function of generator voltage. The current in the generator is also plotted to show the pair breaking structure at $V_{\mathrm{g}}=2 \Delta / e$.

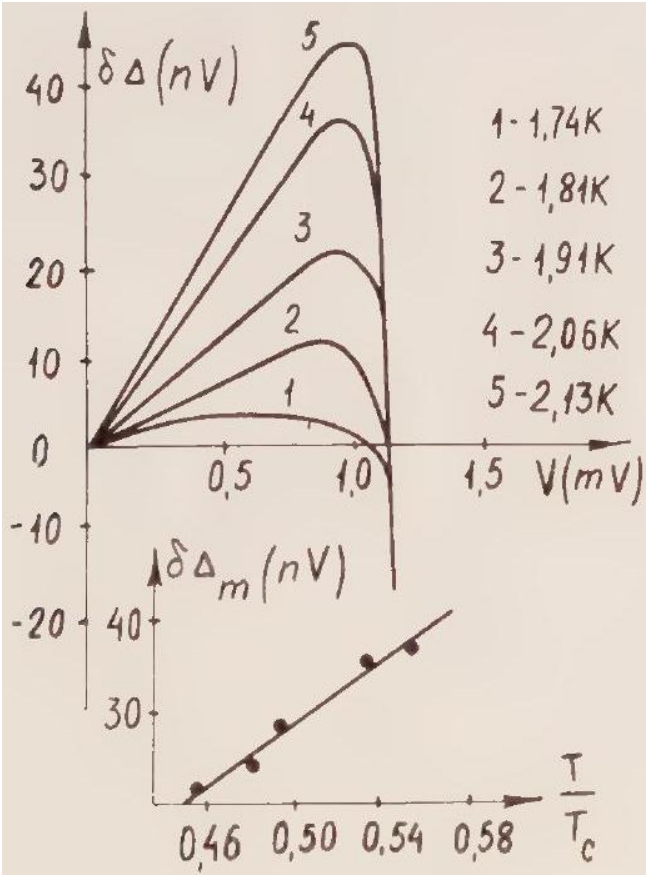


Fig. 17. (a) Experimental dependence of the gap change on the voltage across the generator contact for several temperatures. (b) The maximum gap change as a function of temperature.

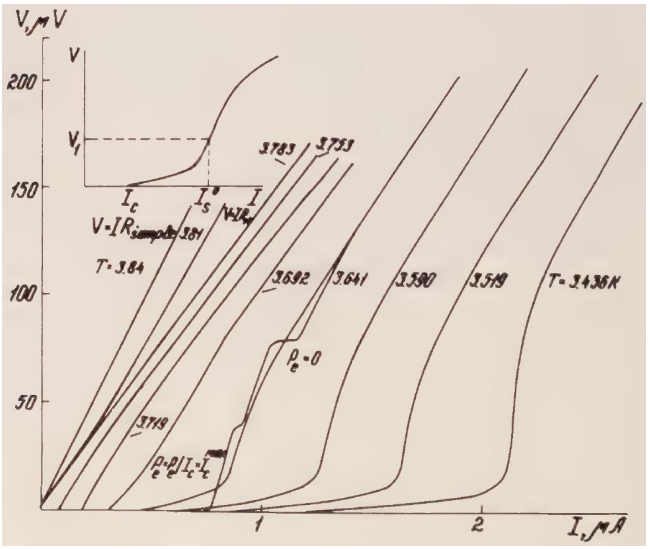


Fig. 18. Alteration of the $I - V$ curve of a short bridge induced by temperature variation; for $T=3.641 \mathrm{˜K
$, the $I - V$ curve for the bridge under a small microwave irradiation with $\omega/2\pi = 38.2$GHz is also shown. The insert shows the $I - V$ curve for the short bridge as calculated with allowance for nonequilibrium effects (Aslamazov and Larkin 1976).}

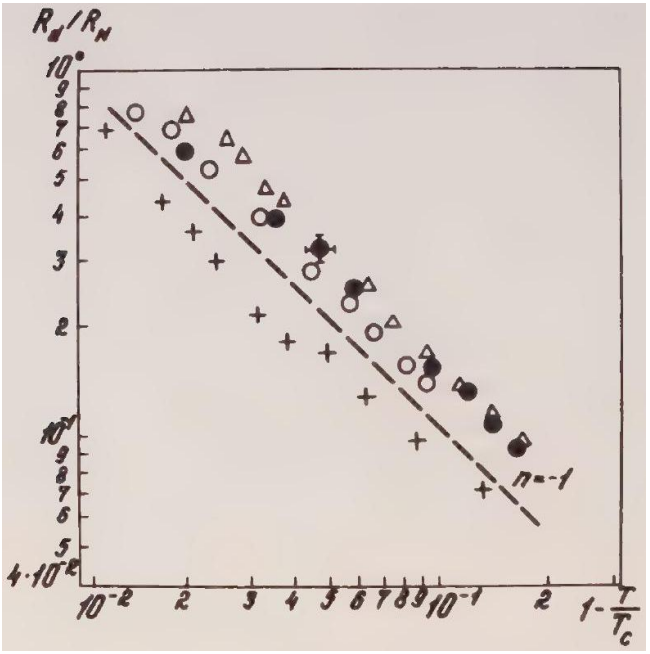


Fig. 19. Temperature dependence of ratio $R_{\mathrm{d
} } / R_{\mathrm{N}}$ for bridges of various lengths: (•)0.5μ m; (O) 0.6μ m; (+) 0.65μ m.}

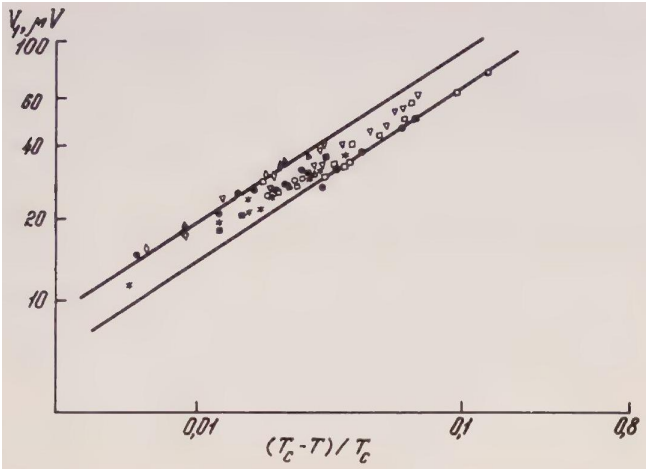


Fig. 20. Temperature dependence of the characteristic voltage $V_{1
$ for a number of short bridges of lengths 0.5 to 1μ m, corresponding to current I_s^0. The solid curves show theoretical dependences $V_1(T)$ calculated for $\tau_\varepsilon = 2 \times 10^{-10}$ s and $\tau_\varepsilon = 6 \times 10^{-10}$ s (Gubankov et al. 1980).}

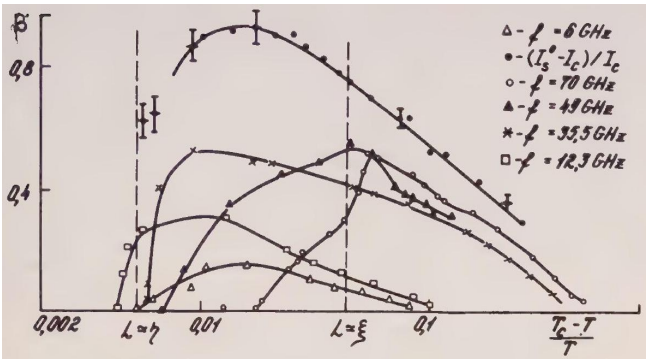


Fig. 21. Temperature dependences of β values (for various microwave field frequencies) the ratio \$\left(I_{\mathrm{s
}^{0}-I_{\mathrm{c}}\right) / I_{\mathrm{c}}\$ of a short bridge (0.5μ m). The temperatures for which ξ and η are comparable with L are marked with broken lines.}

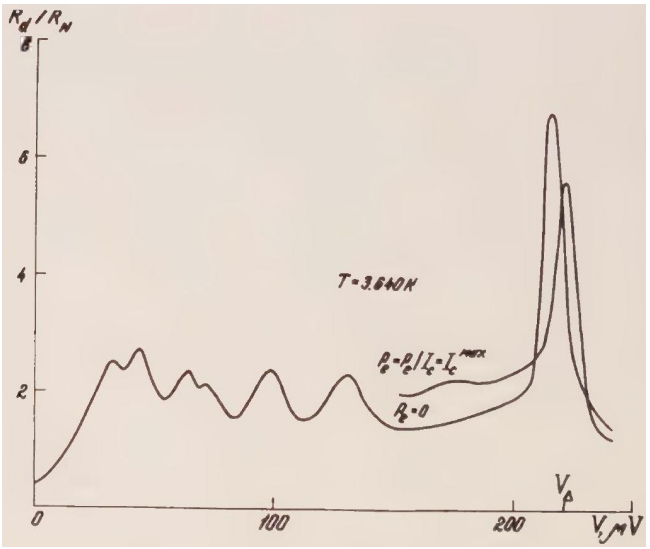


Fig. 22. Differential resistance as a function of the bias voltage for a short bridge (\$0.5 \mu \mathrm{˜m
\$) in the absence of irradiation ($P = 0$) and under microwave irradiation ($\omega/2\pi = 9.8$GHz) corresponding to the maximum critical current enhancement.}

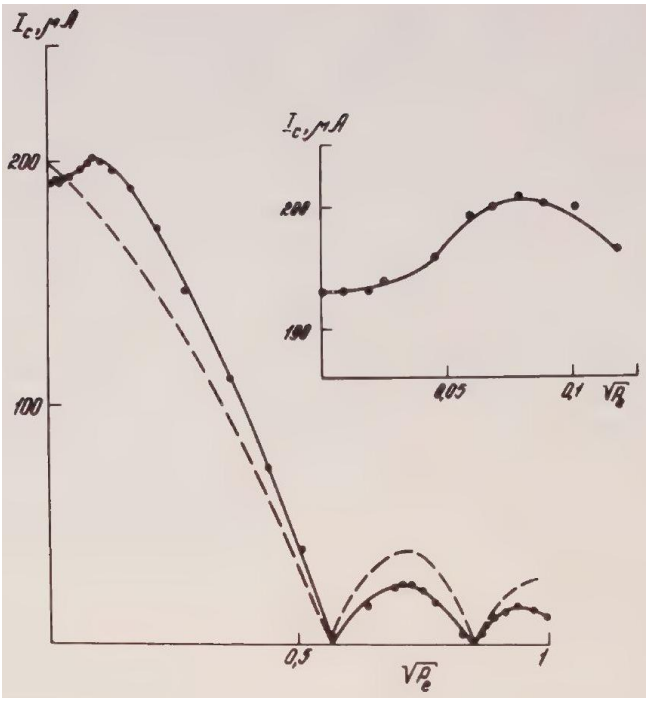


Fig. 23. Critical current of a short bridge (\$0.5 \mu \mathrm{˜m \$) as a function of the microwave power P ($\omega/2\pi = 9.8$GHz). The insert shows the initial part of $I_c(P)$ upscaled.}

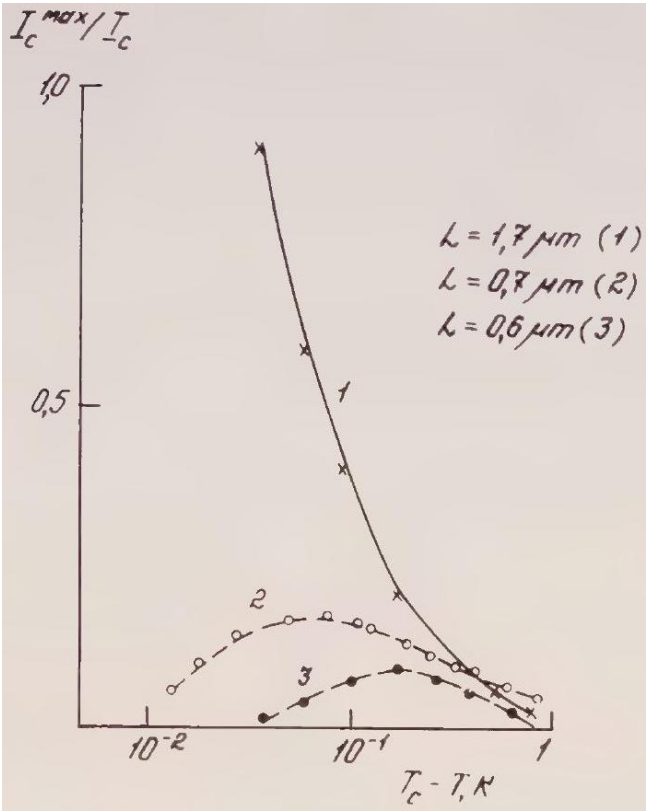


Fig. 24. Temperature dependences of \$I_{\mathrm{c }\^{}{\max } / I_{\mathrm{c}}}\$ for bridges of various lengths L indicated in the plot.}

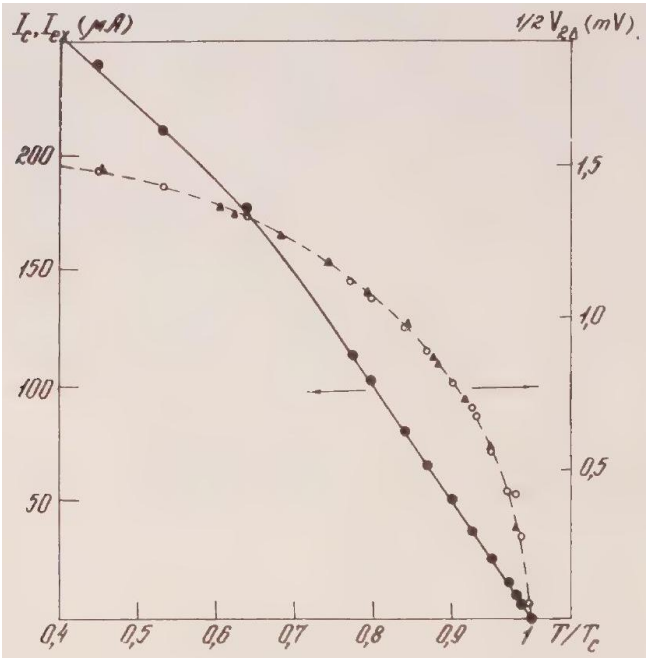


Fig. 25. Temperature dependences of (•) critical current $I_{\mathrm{c}},(\bigcirc)$ excess current I_{ex} and voltage corresponding to the gap-induced singularity $\frac{1}{2}V_{24}$ of the superconducting point contact with $R_{\mathrm{N}} = 8.4\Omega$. The solid curve shows the theoretical $I_{\mathrm{c}}(T)$ for superconducting microshorts (Kulik and Omelyanchuk 1978). The broken line is $\Delta(T)$, according to BCS theory.}

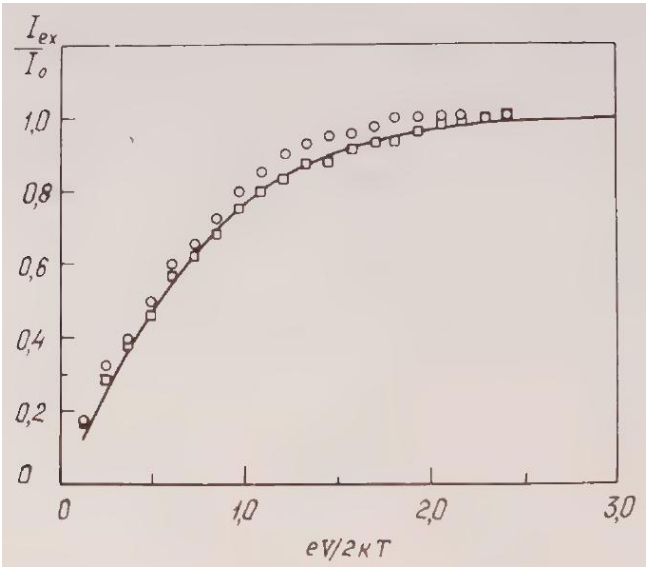


Fig. 26. Voltage dependence of the excess current I_{ex} of a superconducting point contact with $R_{\mathrm{N}} = 5.9\Omega$ for () $T = 9.57$ K and () $T = 9.61$ K.I_{ex} is normalized to its value I_0 at $eV \gtrsim 5\mathrm{kT}$. The solid curve is $\tanh(eV/2kT)$.}

19 Theory of Superconductivity Stimulation by Eliashberg, Ivlev

19.1 J. Introduction

Among many nonequilibrium phenomena in superconductors the stimulation of superconductivity is one of the most interesting effects. On the one hand, typical kinetic properties of superconductors become apparent here, on the other hand, this effect can be checked experimentally.

By superconductivity stimulation effect we understand the improvement of superconducting properties, i.e., the order parameter, critical current and field enhancement, due to some external influences changing the electron distribution function. These are microwave or acoustic radiation, or tunneling injection of electrons. The order parameter is known to obey the BCS equation

$$\frac{1}{g} = \int_{\Delta}^{\omega_{\mathrm{D}}} \mathrm{d}\varepsilon \frac{1-2n_{\varepsilon}}{\sqrt{\varepsilon^2-\Delta^2}} \tag{1}$$

where g is the electron phonon interaction constant, n_z is the electron distribution function. Due to root singularity in the density of states one may expect the order parameter to be sensitive to details of the distribution function. Parmenter (1961) had already supposed that the distribution function is affected by quasiparticle injection.

Eliashberg (1970) suggested that an electromagnetic field gives rise to superconductivity enhancement. This idea was then developed by Ivlev and Eliashberg (1971) and Ivlev et al. (1970). Being absorbed by quasiparticles, the electromagnetic field changes their distribution function in such a way that at smaller energies there is a deficit of electrons and at larger energies there is an excess of electrons. As is seen from eq. (1) such nonequilibrium state yields an increase in the order parameter. The kinetic theory of nonequilibrium states under microwave radiation has been developed by Eliashberg (1971).

Nonequilibrium stationary states form a large and important class of kinetic phenomena in superconductors. Stability of such states is maintained by an external source functioning continuously. Because of energy exchange with a thermostat, a dynamical equilibrium is established in a sample. To estimate approximately the degree of efficiency of radiation influence on a superconductor we assume that due to an electric field with frequency ω the temperature of the metal changes because of heating. Then the relative temperature change

$$\frac{\partial T}{T} \approx \frac{1}{C}\frac{\tau_{\varepsilon}}{T}\frac{\partial q}{\partial t},$$

where $C \approx mnp_0$ is the heat capacity of electrons, $\partial q/\partial t = \sigma E^2$ is the energy pumping rate, τ_{ε} is the characteristic energy relaxation time. Hence

$$\frac{\delta T}{T} \approx D\left(\frac{e}{c}A\right)^2 \tau_{\varepsilon}\frac{\omega^2}{T^2}$$

where D is the diffusion coefficient; the parameter $\delta T/T$ can play the role of the shift from equilibrium state. It can be rather big due to a long energy relaxation time. Actually, the reverse time of this relaxation is

$$\gamma' = \frac{1}{\tau_{\varepsilon}} \approx \mathrm{g}\frac{T^3}{\omega_D^2}$$

in the case of electron-phonon interaction. Close to the transition temperature of real superconductors the parameter $\gamma \times 10^{-7} - 10^{9}$ s^{-1}, which is much less than the typical scales of the energy gap and transition temperature. That is why this action of the electromagnetic field is more efficient than the usual suppression of the order parameter by the vector potential of the field. If the impurity concentration is large enough, then momentum relaxation associated with elastic scattering on impurities will be more effective than energy relaxation. This means that the nonequilibrium distribution function will be basically isotropic in the momentum space. A non-stationary part of distribution function will be small in the limit $\omega \gg\propto \gamma/\tau_{\varepsilon}$.

Afterwards the theory of stimulated superconductivity has been essentially developed. Aronov and Gurevich (1972) considered stimulation by tunneling injection. Tredwell and Jacobsen (1975) calculated the acoustic pumping effect. Chang and Scalapino (1977) showed that a contribution to stimulation was made by decreasing the total number of quasiparticles. Aslamasov and Larkin (1978) studied the influence of the gap oscillation effect in a bridge on the stimulation under microwave radiation. Peskovatski and Seminozhenko (1976) calculated the stimulation of superconductivity by tunneling injection. The theory of injection effect on superconductivity was developed by Chang (1978) and by Chi and Clarke (1979).

A detailed survey on experimental achievements in the field of stimulated superconductivity is given in the present volume by Dmitriev, Gubankov, and Nad' (1985). We shall, therefore, not consider these in detail. Since the first experiments by Wyatt et al. (1966) and Dayem and Wiegand (1967) on enhancement of superconductivity in bridges by radiation the mechanism of observed effects has been unclear for a long time.

Due to experimental research of Latyshev and Nad' (1974), Tredwell and Jacobsen (1975), Klapwijk and Mooij (1976), Kommers and Clarke (1977) and
other experimentalists it was possible to establish the adequacy of the experiments and the Eliashberg (1970) theory.

The direct observation of the gap enhancement by Tredwell and Jacobsen (1975) and by Kommers and Clarke (1977) proves most convincingly the validity of this theory. A similar gap enhancement at tunneling injection was observed by Gray (1978). Superconductivity stimulation by electromagnetic field, acoustic wave and tunneling injection can be included in the same group of phenomena.

This paper is made up as follows. In section 2 the equations required are derived. In section 3 the theory of superconductivity stimulated by microwave radiation is given, and the order parameter, critical temperature and current enhancement are considered. The frequency range of existence of the effect and limits of radiation power are considered. In section 4 acoustic pumping is studied. In section 5 the specificity of superconductivity stimulation by tunneling injection is singled out, since electron-hole imbalance may be of great importance. In section 6 the stability of spatially homogeneous nonequilibrium states is discussed.

19.2 2. Derivation of equations

The behaviour of superconductors in electromagnetic and acoustic fields as well as under the effect of tunneling injection is now examined. As well as mentioned above, the difference of electron and hole branches population must be taken into account. Moreover, as often occurs in experiment, the impurity concentration is not small and consequently, the value $\xi_p = v\,(p - p_0)$ is a bad quantum number. Hence we proceed from the Green functions depending on an energy variable ε, and integrated on ξ_p. The kinetic equation for the electron distribution function under pumping conditions was obtained by Eliashberg (1971) with the method of analytical continuation. We will then summarize these equations, branch imbalance taken into account. We use the Keldysh technique (1964) to write equations rather compactly.

We write a Green function before integration as

$$-G^{+} = \frac{n_\varepsilon}{2}\left[\left(\frac{\varepsilon}{\xi_\varepsilon^{\mathrm{R}}}+1\right)\frac{1}{\xi-\xi_\varepsilon^{\mathrm{R}}-\mathrm{i}/2\tau}+\left(\frac{\varepsilon}{\xi_\varepsilon^{\mathrm{A}}}-1\right)\frac{1}{\xi+\xi_\varepsilon^{\mathrm{A}}+\mathrm{i}/2\tau}\right] + \frac{1-n_{-\varepsilon}}{2}\left[\left(\frac{\varepsilon}{\xi_\varepsilon^{\mathrm{R}}}-1\right)\frac{1}{\xi+\xi_\varepsilon^{\mathrm{R}}+\mathrm{i}/2\tau}+\left(\frac{\varepsilon}{\xi_\varepsilon^{\mathrm{A}}}+1\right)\frac{1}{\xi-\xi_\varepsilon^{\mathrm{A}}-\mathrm{i}/2\tau}\right] \tag{2}$$

Here the following designations are introduced:

$$\xi_\varepsilon^{\mathrm{R}} = -\left(\xi_\varepsilon^{\mathrm{A}}\right)^{*} = \begin{cases}\sqrt{\varepsilon^2-\Delta^2}\,\mathrm{sign}\,\varepsilon & \Delta^2<\varepsilon^2\\ \mathrm{i}\sqrt{\Delta^2-\varepsilon^2} & \varepsilon^2<\Delta^2\end{cases}$$

τ is the impurities scattering time. A label on the left marks the function according to Gor'kov, and on the right according to Keldysh.

After integration with respect to ξ the Keldysh equations for superconductor functions in matrix form are:

$$\begin{aligned}
(\omega-vk)^{-}g_{\varepsilon\varepsilon-\omega} &= \frac{e}{c}v\left({}^{-}gA-A^{-}g\right)+\mathrm{i}\left\{\sigma_z{}^{-}\Sigma^{-}g-\sigma_z{}^{-}\Delta^{+}f\right\}+I_{\mathrm{imp}}\\
(2\varepsilon-\omega+vk)^{+}f_{\varepsilon\varepsilon-\omega} &= -\frac{e}{c}v\left({}^{+}fA+A^{+}f\right)+\mathrm{i}\left\{\sigma_z{}^{+}\Sigma^{+}f-\sigma_z{}^{+}A^{-}g\right\}+{}^{+}K_{\mathrm{imp}}\\
(\omega+vk)^{+}\mathrm{g}_{\varepsilon\varepsilon-\omega} &= \frac{e}{c}v\left({}^{+}gA-A^{+}g\right)+\mathrm{i}\left\{\sigma_z{}^{+}\Sigma^{+}g-\sigma_z+\Delta^{-}f\right\}+{}^{+}I_{\mathrm{imp}}\\
(2\varepsilon-\omega-vk)^{-}f_{\varepsilon\varepsilon-\omega} &= -\frac{e}{c}v\left({}^{-}fA+A^{-}f\right)+\mathrm{i}\left\{\sigma_z{}^{-}\Sigma^{-}f-\sigma_z{}^{-}A^{+}g\right\}+{}^{-}K_{\mathrm{imp}}
\end{aligned} \tag{3}$$

Associated with elastic scattering on impurities the last terms in the equations of system (3) determine the angular parts of Green functions and reduce to zero when averaged over momentum directions. As an example, we will write out two of them:

$$\begin{aligned}
{}^{-}T_{\mathrm{imp}} &= \frac{1}{2\pi\tau}\left\{\left\langle{}^{-}g\right\rangle\sigma_z{}^{-}g-{}^{-}g\sigma_z\left\langle{}^{-}g\right\rangle+{}^{-}f\sigma_z\left\langle{}^{+}f\right\rangle-\left\langle{}^{-}f\right\rangle\sigma_z{}^{+}f\right\},\\
{}^{+}K_{\mathrm{imp}} &= \frac{1}{2\pi\tau}\left\{\left\langle{}^{+}g\right\rangle\sigma_z{}^{+}f-{}^{+}g\sigma_z\left\langle{}^{+}f\right\rangle+{}^{+}f\sigma_z\left\langle{}^{-}g\right\rangle-\left\langle{}^{+}f\right\rangle\sigma_z{}^{-}g\right\}.
\end{aligned} \tag{4}$$

Angle brackets mean averaging over momentum directions.
The second terms in the right-hand sides of equations (3) describe interaction of electrons with phonons as well as inelastic scattering on them, and processes producing Cooper coupling. In expressions (3) and (4) Keldysh matrices are taken for the Green functions and self-energy parts,

$$g = \begin{pmatrix} g^{\mathrm{c}} & g^{-}\\ g^{+} & \tilde{g}^{\mathrm{c}}\end{pmatrix} \tag{5}$$

of which the elements both for Green functions and self-energy parts are connected by Keldysh identities (1964).

In the approximation, corresponding to the kinetic equation when

$${}^{+}g_{ij}\left(n_\varepsilon\right) = {}^{-}g_{ij}\left(1-n_{-\varepsilon}\right), \quad {}^{+}f_{ij} = -{}^{-}_{f ij}$$

Green functions diagonal with respect to energy and satisfying equations (3) are

$$\begin{aligned}
{}^{-}g^{+} &= -\mathrm{i}\pi\left[u_\varepsilon\left(1+\beta_\varepsilon\right)+\alpha_\varepsilon\right], & {}^{-}g^{\mathrm{c}} &= {}^{-}g^{+}+\mathrm{i}\pi u_\varepsilon\\
{}^{-}g^{-} &= -\mathrm{i}\pi\left\{u_\varepsilon\left(\beta_\varepsilon-1\right)+\alpha_\varepsilon\right\}, & {}^{-}\tilde{g}^{\mathrm{c}} &= {}^{-}g^{-}-i\pi u_\varepsilon\\
f^{+} &= -\mathrm{i}\pi\mathrm{v}_\varepsilon\left(\beta_\varepsilon+1\right). & f^{\mathrm{c}} &= f^{+}+\mathrm{i}\pi v_\varepsilon
\end{aligned} \tag{6}$$

Here and below we will use the notations

$$u_\varepsilon = \frac{\varepsilon}{\Delta} v_\varepsilon = \frac{|\varepsilon|}{\sqrt{\varepsilon^2 - \Delta^2}} \theta\left(\varepsilon^2 - \Delta^2\right)$$
$$\alpha_\varepsilon = n_\varepsilon + n_{-\varepsilon} - 1, \quad \beta_\varepsilon = n_\varepsilon - n_{-\varepsilon} \tag{7}$$

For self-energy parts associated with electron-phonon interaction we have

$$\sum_{ij} = g \int \frac{\mathrm{d}\varepsilon'}{2\pi} \int \frac{\mathrm{d}O_\mathrm{p}}{4\pi} \gamma^k_{i_1 j_1} g_{i_1 j_1} \Gamma^{k_1}_{j_1 j} D_{k_1 k} \tag{8}$$

A phonon propagator is

$$\mathrm{D}^\pm = 2\pi \mathrm{i}\omega_n \left[N\omega_k f\left(\omega \mp \omega_k\right) + \left(1 + N\omega_k\right) f\left(\omega \pm \omega_k\right)\right]$$
$$D_{\mathrm{c}(\hat{\mathrm{c}})} = D^\pm \pm \frac{\omega_k}{2} \left[\frac{1}{\omega - \omega_k + \mathrm{if}} - \frac{1}{\omega + \omega_k + \mathrm{if}}\right] \tag{9}$$

Performing in eq. (8) integration over momentum directions and using the relation

$$\int \frac{\mathrm{d}O_\mathrm{p}}{4\pi} = \int \frac{\omega_k \, \mathrm{d}\omega_k}{2\left(sp_0\right)^2}$$

we write out an expression for ${}^-\Sigma^+$

$$-\Sigma^+ = -\frac{\pi g}{2\left(sp_0\right)^2} \int d\varepsilon' \left(\varepsilon' - \varepsilon\right)^2 \left[u_{\varepsilon_1}\left(\beta_{\varepsilon_1} + 1\right) + \alpha_{\varepsilon_1}\right]$$
$$\times \left[\left(1 + N_{\varepsilon_1 - \varepsilon}\right) \theta\left(\varepsilon_1 - \varepsilon\right) + N_{\varepsilon - \varepsilon_1} \theta\left(\varepsilon - \varepsilon_1\right)\right] \tag{10}$$

Similarly one can see that

$$\Delta = \frac{1}{2}\mathrm{i}\left(\tilde{\Delta}^\mathrm{c} - \Delta^\mathrm{c}\right) \tag{11}$$

Due to gauge invariance we assume Δ to be a real value.
It is better to write out equations arising from system (3) for the Green functions diagonal on energy $g_\varepsilon = g^+ + g^-$and $f_\varepsilon = f^+ + f^-$

$${}^\mp g = 2\mathrm{i}\pi\left(u_\varepsilon \beta_\varepsilon \pm \alpha_\varepsilon\right), \quad {}^\pm f = 2\mathrm{i}\pi v_\varepsilon \beta_\varepsilon \tag{12}$$

Such a definition of the distribution function somewhat differs from that in the paper of Larkin and Ovchinnikov (1977). Averaging over momentum directions gives

$$\left\langle(\omega - vk)^- g\right\rangle = \left\langle \frac{e}{c} v \left({}^- g A - A^- g\right)\right\rangle$$
$$+ 2\mathrm{i}\left\{{}^-\Sigma^- g^+ - {}^- g^- {}^-\Sigma^+ - {}^- f^- \Delta^+ - {}^-\mathrm{D}^- f^+\right\}$$
$$+ \left\langle \Delta\left({}^+ f - {}^- f\right)\right\rangle + I^\mathrm{T} \tag{13}$$
$$\left\langle 2\varepsilon\left({}^+ f - {}^- f\right)\right\rangle = 2\mathrm{i}\left\{{}^+ f\left({}^+\Sigma^- - {}^-\Sigma^-\right) + \left({}^+ g^+ - {}^- g^+\right)\Delta^-\right.$$
$$\left. - {}^- f\left({}^+\Sigma^+ - {}^-\Sigma^+\right) - \left({}^+ g - {}^- g^-\right) A^+\right\} - \langle vk(+f + f)\rangle$$
$$- \left\langle {}^e_c v A\left({}^+ f - {}^- f\right) + \left({}^+ f - {}^- f\right) \frac{e}{c} v A\right\rangle + K^\mathrm{T} \tag{14}$$

where I^{T} and K^{T} are associated with tunneling.
In the absence of order parameter phase and in equilibrium $\langle {}^{+}f_{\varepsilon} - f_{\varepsilon}\rangle = 0$. Deviation of this value from zero is due to the intrusion of an additional part even in energy to the distribution function. The procedure of obtaining the kinetic equation is to find the function difference from eq. (14) and insert it into eq. (13). In the right-hand side of eq. (13) an effective phonon collision integral is obtained. In addition, such a substitution cancels the London current in a term $v\ \mathrm{kg}_{\varepsilon}$ corresponding to divergency of the total current. Only its diffusive part is conserved as Gor'kov and Eliashberg (1968) showed by their diagram method.

To proceed solving the system of equations (13), (14) one should find A_{ω} depending parts of Green functions non-diagonal on energy. This can be done by solving system (3) before averaging over momentum, when impurity collision integrals are given by equations (4). However, to avoid this cumbersome procedure, by analogy with the technique of Gorkov and Eliashberg (1968) we take into account the fact that in the linear field approximation the off-diagonal Green functions are in the form

$$
\begin{aligned}
{}^{-}G_{\varepsilon\varepsilon-\omega} &= \frac{e}{c} v A\omega \left(-G_{\varepsilon} - G^{\mathrm{A}}_{\varepsilon-\omega} + {}^{-}F_{\varepsilon} + F^{\mathrm{A}}_{\varepsilon-\omega} - {}^{-}G^{\mathrm{R}}_{\varepsilon} - G_{\varepsilon-\omega} + {}^{-}F^{\mathrm{R}}_{\varepsilon} + F_{\varepsilon-\omega}\right), \\
+F_{t,-\omega} &= -\frac{e}{c} v A\omega \left({}^{+}F_{\varepsilon} - G^{\mathrm{A}}_{\varepsilon-\omega} - {}^{+}\mathrm{G}_{\varepsilon} + {}^{+}\mathrm{F}^{\mathrm{A}}_{\varepsilon-\omega} + {}^{+}F^{\mathrm{R}}_{\varepsilon} - G_{\varepsilon-\omega} - {}^{+}\mathrm{G}^{\mathrm{R}}_{\varepsilon} + F_{\varepsilon-\omega}\right),
\end{aligned}
\tag{15}
$$

where

$$
\begin{aligned}
G_i =& \frac{1-2n_{\varepsilon}}{2}\left[\left(\frac{\varepsilon}{\xi^{\mathrm{R}}_i}+1\right)\frac{1}{\xi-\xi^{\mathrm{R}}_i-\mathrm{i}/2\tau} + \left(\frac{\varepsilon}{\xi^{\mathrm{A}}_i}-1\right)\frac{1}{\xi+\xi^{\mathrm{A}}_{\varepsilon}+\mathrm{i}/2\tau}\right] \\
&+ \frac{1-2n_{-\varepsilon}}{2}\left[\left(\frac{\varepsilon}{\xi^{\mathrm{R}}_{\varepsilon}}-1\right)\frac{1}{\xi+\xi^{\mathrm{R}}_{\varepsilon}+\mathrm{i}/2\tau} + \left(\frac{\varepsilon}{\xi^{\mathrm{A}}_{\varepsilon}}+1\right)\frac{1}{\xi-\xi^{\mathrm{A}}_{\varepsilon}-\mathrm{i}/2\tau}\right] \\
+F_{\varepsilon} =& \frac{2n_{\varepsilon}-1}{2}\left[\frac{\Delta}{\xi^{\mathrm{R}}_{\varepsilon}}\frac{1}{\xi+\xi^{\mathrm{R}}_{\varepsilon}+\mathrm{i}/2\tau} + \frac{\Delta}{\xi^{\mathrm{A}}_{\varepsilon}}\frac{1}{\xi-\xi^{\mathrm{A}}_{\varepsilon}-\mathrm{i}/2\tau}\right] \\
&+ \frac{2n_{-\varepsilon}-1}{2}\left[\frac{\Delta}{\xi^{\mathrm{R}}_{\varepsilon}}\frac{1}{\xi-\xi^{\mathrm{R}}_{\varepsilon}-\mathrm{i}/2\tau} + \frac{\Delta}{\xi^{\mathrm{A}}_{\varepsilon}}\frac{1}{\xi+\xi^{\mathrm{A}}_{\varepsilon}+\mathrm{i}/2\tau}\right].
\end{aligned}
\tag{16}
$$

At this stage of calculations one should make concrete suppositions on the length of the mean free path of electrons. We will then study superconductors in the dirty limit. In this limiting case we integrate on ξ off-diagonal Green functions (15) and find

$$
\begin{aligned}
&- g_{\varepsilon\varepsilon-\omega} = -\pi\tau\frac{e}{c} v A_{\omega} \\
&\times\left\{(1-2n_{\varepsilon})\left[\frac{\varepsilon(\varepsilon-\omega)+\Delta^2}{\varepsilon\xi_{\varepsilon-\omega}}u_{\varepsilon} + \frac{\varepsilon-\omega}{\xi_{\varepsilon-\omega}}\right] - (1-2n_{\varepsilon})\left[\frac{\varepsilon(\varepsilon-\omega)+\Delta^2}{\varepsilon\xi_{\varepsilon-\omega}}u_{\varepsilon} - \frac{\varepsilon-\omega}{\xi_{\varepsilon-\omega}}\right]\right. \\
&\left.+(1-2n_{\varepsilon-,})\left[\frac{\varepsilon(\varepsilon-\omega)+\Delta^2}{(\varepsilon-\omega)\xi^{R}_{\varepsilon}}u_{\varepsilon-(\omega)} + \frac{\varepsilon}{\xi^{R}_{\varepsilon}}\right] - \left(1-2n_{(\cdot)-\varepsilon}\right)\left[\frac{\varepsilon(\varepsilon-\omega)+\Delta^2}{(\varepsilon-\omega)\xi^{R}_{\varepsilon}}u_{\varepsilon-(1)} - \frac{\varepsilon}{\xi^{R}_{f}}\right]\right\} \\
&\left({}^{+}f - {}^{-}f\right)_{\varepsilon\varepsilon-\omega} = 4\pi\tau\Delta\frac{e}{c} v A\omega\left(\frac{\alpha_{\varepsilon-\omega}}{\xi^{R}_{\varepsilon}} - \frac{\alpha_{\varepsilon}}{\xi^{A}_{\varepsilon-\omega}}\right).
\end{aligned}
\tag{17}
$$

Inserting expression (17) into (13) and (14) the equation for the Green function $g_{\varepsilon} = {}^{+}g_{\varepsilon} + {}^{-}g_{\varepsilon}$ can be written. Note that, according to eq. (12),

$$
u_{\varepsilon}\frac{\partial n_{\varepsilon}}{\partial t} = \frac{\partial}{\partial t}\left[g_{\varepsilon} - g_{-\varepsilon} + u_{\varepsilon}\left(g_{\varepsilon} + g_{-\varepsilon}\right)\right]\frac{1}{8\mathrm{i}\pi}.
\tag{18}
$$

The kinetic equation is given by (Bulyzhenkov and Ivlev 1978)

$$u_\varepsilon \frac{\partial n_\varepsilon}{\partial t} - D\nabla^2 n_\varepsilon + 2D\left(\frac{e}{c}A\right)^2 \frac{A^2}{\varepsilon^2 - \Delta^2}\left(n_\varepsilon + n_\varepsilon - 1\right) + I_\varepsilon = a_\varepsilon + t_\varepsilon. \tag{19}$$

Here, the vector potential in the left-hand side corresponds to the constant London current, a_ε in the right-hand side is the microwave pumping:

$$\begin{aligned} a_\varepsilon =& D\left(\frac{e}{c}\right)^2 A\omega A_{-\omega} \\ &\times \left\{ u_\varepsilon u_{\varepsilon-\omega}\left[1 + \frac{\Delta^2}{\varepsilon(\varepsilon-\omega)}\right](\beta_{\varepsilon-\omega} - \beta_\varepsilon) + u_\varepsilon u_{\varepsilon+\omega}\left[1 + \frac{\Delta^2}{\varepsilon(\varepsilon+\omega)}\right](\beta_{\varepsilon-\omega} - \beta_\varepsilon) + \alpha_{\varepsilon-\omega} \right. \\ &\left. + \alpha_{\varepsilon+\omega} - u_\varepsilon u_{\varepsilon-\omega}\left[1 + \frac{\Delta^2}{\varepsilon(\varepsilon-\omega)}\right]\alpha_\varepsilon - u_\varepsilon u_{\varepsilon+\omega}\left[1 + \frac{\Delta^2}{\varepsilon(\varepsilon+\omega)}\right]\alpha_\varepsilon \right\} \end{aligned} \tag{20}$$

t_ε is the tunnel source of quasiparticles, its expression will be written below. As seen from eq. (19) current is an additional source of branch imbalance
relaxation in a superconductor. This effect was discovered by Gor'kov and Kopnin (1973). If the microwave field is strong enough, it can be the main reason for relaxation and can determine the type of distribution function.

The phonon collision integral is obtained from equations (13), (14) and (18) taking into account eqs. (6)-(9), as shown by Bulyzhenkov and Ivlev (1978):

$$\begin{aligned} I_\varepsilon =& \frac{g}{\omega_{\mathrm{D}}^2}\left\{ \int_\varepsilon^\infty \mathrm{d}\varepsilon_1 \left(\varepsilon_1 - \varepsilon\right)^2 \left(u_\varepsilon u_{\varepsilon_1} - v_\varepsilon v_{\varepsilon_1} + 1\right)\left[n_\varepsilon\left(1 - n_{\varepsilon_1}\right) N_{\varepsilon_1 - \pi^-} - n_{\iota_1}\left(1 - n_\varepsilon\right)\left(1 + N_{\varepsilon_1 \iota}\right)\right] \right. \\ &+ \int_{-\infty}^{\varepsilon} \mathrm{d}\varepsilon_1 \left(\varepsilon - \varepsilon_1\right)^2 \left(u_\varepsilon u_{\varepsilon_1} - v_\varepsilon v_{\varepsilon_1} + 1\right)\left[n_\varepsilon\left(1 - n_{\varepsilon_1}\right)\left(1 + N_{\varepsilon_1}\right) - n_{\varepsilon_1}\left(1 - n_\varepsilon\right) N_{l-\varepsilon_1}\right] \\ &+ \int_{-\infty}^{-\varepsilon} \mathrm{d}\varepsilon_1 \left(\varepsilon + \varepsilon_1\right)^2 \left(u_\varepsilon u_{\varepsilon_1} + v_\varepsilon v_{\varepsilon_1} - 1\right)\left[n_\varepsilon n_{\varepsilon_1} N_{\varepsilon+\varepsilon_1} - \left(1 - n_\varepsilon\right)\left(1 - n_{\varepsilon_1}\right)\left(1 + N_{\varepsilon+\varepsilon_1}\right)\right] \\ &\left. + \int_\varepsilon^\infty \mathrm{d}\varepsilon_1 \left(\varepsilon + \varepsilon_1\right)^2 \left(u_\varepsilon u_{\varepsilon_1} + v_\varepsilon v_{\varepsilon_1} - 1\right)\left[n_\varepsilon n_{\iota_1}\left(1 + N_{\varepsilon+\varepsilon_1}\right) - \left(1 - n_\varepsilon\right)\left(1 - n_{\varepsilon_1}\right) N_{\varepsilon+\varepsilon_1}\right] \right\} \end{aligned} \tag{21}$$

This is a collision integral of the same type as that in the quasiparticle description with the variable ξ. Hence eqs. (19)-(21) coincide with the Eliashberg (1971) equations, if $\alpha_\varepsilon = 0$. The collision integral (21) can also be derived from the results in works by Larkin and Ovchinnikov (1977).

The first two terms in (21) conserve the total number of electron excitations like in a normal metal, the last two terms describe non-conservation of the total number of particles. Just these lead to the relaxation of branch imbalance, as has been investigated in detail by Tinkham and Clarke (1972).

Processes corresponding to the first two terms (21) conserve the total number of electronic excitations. The last two terms describe the transition of a pair of excitations into a condensate. This decreases the number of electrons near the Fermi surface. A source producing changes in the chemical potential must be added to the right-hand side of the kinetic equation (19). Tunneling of electrons from another sample into a superconductor is considered as such a source. Note, when obtaining the expression from a tunnel source, the corresponding term in the right-hand side of eq. (19) is formally equivalent to an impurity collision integral of type (4), in which instead of functions averaged over directions there are those pertaining to another metal. The superconductor in question is believed to be at zero voltage, the other metal at

voltage V. This metal may be either superconducting or normal. In this metal due to the time dependence of the phases of Green functions,

$$^{\mp}g_{\mathrm{v}}\left(t-t'\right)=\,^{\mp}g\left(t-t'\right)\exp\left[\mp\mathrm{i}V\left(t-t'\right)\right],$$

their Fourier-components are

$$^{\mp}g=\,^{\mp}g(\varepsilon\mp V).$$

Introducing the value w proportional to the probability of tunneling, in accordance with symmetrization (18), the expression for a tunneling source in the kinetic equation (19) is derived from eqs. (13) and (14) (Bulyzhenkov and Ivlev 1978):

$$\begin{aligned}t_{\varepsilon}=w[&u_{\varepsilon-V}\left(\beta_{\varepsilon-V}-\beta_{\varepsilon}\right)+u_{\varepsilon+1}\left(\beta_{\varepsilon}-\beta_{\varepsilon+V}\right)+\alpha_{\varepsilon-V}-\alpha_{\varepsilon+V}\\&-u_{\varepsilon}\left(u_{\varepsilon-V}+u_{\varepsilon+V}\right)\alpha_{\varepsilon}+u_{\varepsilon}u_{\varepsilon-V}\left(\beta_{\varepsilon-V}-\beta_{\varepsilon}\right)\\&+u_{\varepsilon}u_{\varepsilon+V}\left(\beta_{\varepsilon+V}-\beta_{\varepsilon}\right)+\mathrm{u}_{\varepsilon}\left(\alpha_{\varepsilon-V}-\alpha_{\varepsilon+V}\right)+\left(\mathrm{u}_{\varepsilon+V}-\mathrm{u}_{\varepsilon-V}\right)\alpha_{\varepsilon}].\end{aligned}\tag{22}$$

In linear approximation, when $\alpha_{\varepsilon}=0$ and $\beta_{\varepsilon}=-\tanh(\varepsilon/2\tau)$, a tunneling source for the NS contact was obtained by Volkov and Zaitzev (1975). The source (22) in the kinetic equation (19) describes tunneling injection only of normal excitations, whereas the processes of direct particle transition into supercurrent contribute in total tunnel current.

To obtain the tunneling current, one should calculate the right-hand side of the continuity equation by integration of equation (13) with respect to energy. In the right-hand side after integration a non-zero contribution is made only by the tunneling source

$$\begin{aligned}&\frac{mp_0e}{\pi^2}\left\{\frac{\pi e}{c}D\nabla(\Delta\beta\Delta A)-D\nabla\int_{\Delta}^{x}\mathrm{d}\varepsilon u_{\varepsilon}\nabla\alpha_{\varepsilon}\right\}\\&=2w\int_{\Delta}^{\infty}\mathrm{d}\varepsilon\left[u_{\varepsilon}u_{\varepsilon-V}\left(\beta_{\varepsilon-V}-\beta_{\varepsilon}\right)+u_{\varepsilon}u_{\varepsilon+V}\left(\beta_{\varepsilon}-\beta_{\varepsilon+V}\right)\right.\\&\quad\left.-\left(\mathrm{u}_{\varepsilon-V}+\mathrm{u}_{\varepsilon+V}\right)\alpha_{\varepsilon}+\mathrm{u}_{\varepsilon}\left(\alpha_{\varepsilon-V}+\alpha_{\varepsilon+V}\right)\right]\frac{mp_0e}{\pi^2}\end{aligned}\tag{23}$$

For the equilibrium distribution function, $\alpha_{\varepsilon=0}$ and $\beta_{\varepsilon}=-\tanh(\varepsilon/2T)$, this expression given the Giaever current [see review by Douglass and Falicov (1964)].

The first term in the left-hand side of eq. (23) is the divergence of the London current, the second term is that of the normal current. As far as the stationary situation is examined, the time derivative of the charge density is absent. The value in the right-hand side of eq. (23) is the total tunnel current. Note that the functions without an argument shift of value V are relevant to the superconductor of interest.

Thus, the kinetic equation (19) with the phonon collision integral (21) and the tunneling source (22) along with the continuity equation (23) allow, in principle, to solve kinetic problems in the situation with shift of a chemical potential. Electroneutrality is performed automatically due to the shift of the initial energy. Responsible for this is an electrostatic potential which in the static case provides a small contribution of the order ϕ/ε_r to all the values except for charge density.

19.3 3. Superconductivity stimulation by electromagnetic field

In this section we observe the effect of superconductivity stimulation by microwaves. As indicated in the Introduction, this effect is due to transfer of quasiparticles by the electromagnetic field into the region of large energies. Consequently, effective cooling occurs in the region of energies with a singularity in the density of states.

We will first assume a superconductor film to be thin enough that phonons interact mainly with the walls of the sample but not with electrons. In this case the phonon system serves as a thermostat for electrons. Therefore, the phonon distribution function may be in equilibrium.

The equations derived in the previous section describe the situation without branch imbalance. If taking $n_\varepsilon = 1 - n_{-\varepsilon}$ and $t_\varepsilon = 0$ in eqs. (19)-(21), we get at $\varepsilon > 0$

$$\begin{aligned} I_\varepsilon = 2\alpha u_\varepsilon \Bigg\{ & \left[1 + \frac{\Delta^2}{\varepsilon(\varepsilon-\omega)}\right] u_{\varepsilon-\omega} \left(n_{\varepsilon-\omega} - n_\varepsilon\right) \\ & - \left[1 + \frac{\Delta^2}{\varepsilon(\varepsilon+\omega)}\right] u_{\varepsilon+\omega} \left(n_\varepsilon - n_{\varepsilon+\omega}\right) \\ & - \left[1 - \frac{\Delta^2}{\varepsilon(\omega-\varepsilon)}\right] u_{\omega-\varepsilon} \left(n_\delta + n_{\omega-\varepsilon} - 1\right) \theta(\omega - \Delta - \varepsilon) \Bigg\} \\ \alpha = D \left(\frac{e}{c}\right)^2 & A_\omega A_{-\omega} \end{aligned} \tag{24}$$

In the situation with symmetry between electrons and holes the collision integral is

$$\begin{aligned} I_\varepsilon = \frac{2g}{\omega_{\mathrm{D}}^2} \Bigg\{ & \int_1^\varepsilon \mathrm{d}\varepsilon_1 \left(\varepsilon - \varepsilon_1\right)^2 u_\varepsilon u_{\varepsilon_1} \left(1 - \frac{\Delta^2}{\varepsilon\varepsilon_1}\right) \\ & \times \left[n_\varepsilon \left(1 - n_{\varepsilon_1}\right) \left(1 + N_{\varepsilon-\varepsilon_1}\right) - n_{\varepsilon_1} \left(1 - n_\varepsilon\right) N_{\varepsilon-\varepsilon_1}\right] \\ & + \int_\varepsilon^\infty \mathrm{d}\varepsilon_1 \left(\varepsilon_1 - \varepsilon\right)^2 u_\varepsilon u_{\varepsilon_1} \left(1 - \frac{\Delta^2}{\varepsilon\varepsilon_1}\right) \\ & \times \left[n_\varepsilon \left(1 - n_{\varepsilon_1}\right) \mathrm{N}_{\varepsilon_1-\varepsilon} - n_{\varepsilon_1} \left(1 - n_\varepsilon\right) \left(1 + N_{\varepsilon_1-\varepsilon}\right)\right] \\ & + \int_A^\infty \mathrm{d}\varepsilon_1 \left(\varepsilon_1 + \varepsilon\right)^2 u_\varepsilon u_{\varepsilon_1} \left(1 + \frac{\Delta^2}{\varepsilon\varepsilon_1}\right) \\ & \times \left[n_\varepsilon n_{\varepsilon_1} \left(1 + N_{\varepsilon+\varepsilon_1}\right) - \left(1 - n_\varepsilon\right) \left(1 - n_{\varepsilon_1}\right) N_{\varepsilon+\varepsilon_1}\right]\Bigg\} \end{aligned} \tag{25}$$

Close to the transition temperature when $\Delta \ll T$, if the field frequency is not large, $\omega \ll T$, then the typical scale of correction to the equilibrium part of distribution function is small compared to temperature. In this case, non-local terms will be small and the collision integral (25) can be written in τ approximation, as shown by Eliashberg (1971):

$$I_\varepsilon = 2\gamma u_\varepsilon \left(n - n_{\mathrm{F}}\right)_\varepsilon, \quad \gamma = 7\zeta(3) \frac{gT^3}{\omega_{\mathrm{D}}^2}. \tag{26}$$

The BCS equation for the order parameter is to be added to the equations derived. Close to the critical temperature it differs from the usual GinzburgLandau equation only by a nonequilibrium term

$$\begin{aligned} & \frac{T_{\mathrm{c}} - T}{T} - \frac{7\zeta(3)}{8\pi^2} \frac{\Delta^2}{T^2} - \frac{\pi}{T}\alpha \left(1 + b\frac{\omega^2}{\gamma T}\right) + F = 0 \\ & F = -2 \int_\Delta^\infty \frac{\mathrm{d}\varepsilon}{\sqrt{\varepsilon^2 - \Delta^2}} \left(n - n_{\mathrm{F}}\right)_\varepsilon \end{aligned} \tag{27}$$

Here, the

$$-\frac{\pi}{T}\alpha\frac{b\omega^2}{\gamma T} (b \approx 1)$$

term is added to the Ginzburg-Landau equation (22). It cannot be calculated by using τ-approximation for a collision integral since the relevant part of distribution function is localized on energies of the order of the temperature (Ivlev et al. 1973). The value b can be obtained only from a numerical solution of the kinetic equation, in which ail the terms are taken into account in the collision integral.

At high field frequencies the order parameter oscillates weakly and depends on the square of the field averaged in time:

$$\overline{A^2(t)} = 2A_{t,}A$$

We also need the relation between the vector potential and the current density. Later we consider a one-dimensional sample, such as a long superconductor with small cross dimensions compared to the coherence length and I.ondon penetration depth. Due to electroneutrality the current density will be constant along such a sample. Close to the transition temperature the current density has the form

$$j_\omega = \sigma\frac{\mathrm{i}\omega}{c}A_\omega - \frac{\pi\Delta^2}{2Tc}\sigma A_\omega. \tag{28}$$

In the temperature range

$$\omega \gg \Delta^2/T \tag{29}$$

to be examined later one may neglect the London current. In this situation if either current or voltage is given or not, the vector potential does not depend on the order parameter, $j_\omega = \sigma(i\omega/c)A_\omega$. Nonlinear corrections to this ratio are insignificant in comparison to effects of non-linearity in eq. (27).

Thus, the system of equations (24), (26), (27) enables one to calculate nonequilibrium stationary states of a superconductor under electromagnetic radiation.

We first consider the energy dependence of the distribution function in linear approximation on microwave power. It follows from eqs. (24) and (26) with the notation $n'_\varepsilon = n_\mathrm{e} - n_\mathrm{F}$ that

$$n'_\varepsilon = \frac{\alpha}{\gamma}\frac{\omega}{4T}\Bigg[\frac{\varepsilon(\varepsilon-\omega)+\Delta^2}{\varepsilon\sqrt{(\varepsilon-\omega)^2-\Delta^2}}\theta(\varepsilon-\Delta-\omega) - \frac{\varepsilon(\varepsilon+\omega)+\Delta^2}{\varepsilon\sqrt{(\varepsilon+\omega)^2-\Delta^2}}\theta(\varepsilon-\Delta) + \frac{\varepsilon(\omega-\varepsilon)-\Delta^2}{\varepsilon\sqrt{(\omega-\varepsilon)^2-\Delta^2}}\theta(\varepsilon-\Delta)\theta(\omega-\Delta-\varepsilon)\Bigg]. \tag{30}$$

Hence it is clear that at $\varepsilon = \Delta + \omega$ the distribution function tends to infinity. If one is to find the form of n_ε, then the next higher orders of expansion in α/γ must be taken into account. This peculiarity is not essential for calculation of the additional term F to the Ginzburg Landau equation (27), however, one should study the details of the distribution function. We consider now the spatially homogeneous problem and point out some properties of the solution of eq. (24):

(1) At $\omega < 24$ there is conservation of number of quasiparticles over the threshold since new particles are not produced by the field:

$$\int_\Delta^\infty \mathrm{d}\varepsilon\frac{\varepsilon}{\sqrt{\varepsilon^2-\Delta^2}}n'_\varepsilon = 0 \tag{31}$$

(2) As the exact distribution function has no singularities, the singularity at $\varepsilon = \Delta + \omega$ in the right-hand side of equation (24) must be compensated. Consequently

$$n(\Delta) = n(\Delta+\omega) \tag{32}$$

(3) In τ-approximation (26) at $\omega < 24$ this property results in

$$n'(\Delta) = 0 \tag{33}$$

The function $n'(\varepsilon)$ is schematically plotted in fig. 1. The dashed line shows the dependence corresponding to (30). Singularities at $\varepsilon = \Delta + n\omega (n = 0, 1, 2, \dots)$ are localized on intervals of energy

$$\varepsilon_1 \approx \Delta(\alpha/\gamma)^2 \tag{34}$$

Naturally, solution (30) is valid almost everywhere if the singularity region (34)

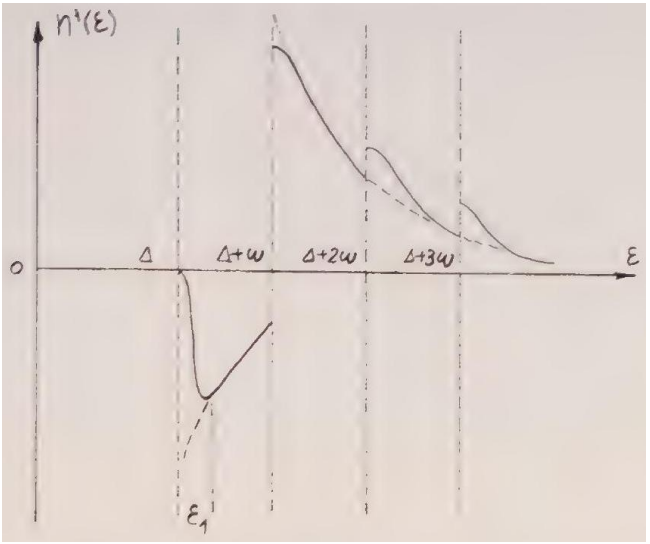


Fig. 1. Energy dependence of the nonequilibrium correction to the distribution function under microwave radiation.

is much smaller than r. Hence we obtain a limit for the field intensity for validity of the linear approximation (30) to calculate the term F in the Ginzburg-Landau equation:

$$\frac{x}{\gamma}\sqrt{\frac{\Delta}{\omega}} \ll 1. \tag{35}$$

Function F has the form

$$\begin{aligned} F =& \frac{\omega^2}{2T}\frac{\alpha}{\gamma}\int_\Delta^x \mathrm{d}\varepsilon \frac{\varepsilon(\varepsilon+\omega)+\Delta^2}{\varepsilon(\varepsilon+\omega)\sqrt{\varepsilon^2-\Delta^2}\sqrt{(\varepsilon+\omega)^2-\Delta^2}} \\ &+ \frac{\alpha\omega}{2T_\gamma}\int_\Delta^{\omega-\Delta} \mathrm{d}\varepsilon \frac{\varepsilon(\varepsilon-\omega)+\Delta^2}{\varepsilon\sqrt{\varepsilon^2-\Delta^2}\sqrt{(\varepsilon-\omega)^2-\Delta^2}}\theta(\omega-2\Delta). \end{aligned} \tag{36}$$

The last term corresponds to production of new quasiparticles by the field. when the frequency is beyond the threshold. Introducing a new function $\phi(p)$: one can rewrite expression (36) as

$$F = \frac{\omega}{2T}\frac{\alpha}{\gamma}\phi\left(\frac{\omega}{\Delta}\right) \quad \phi(p) = \begin{cases} p\ln\frac{8}{ep} & p \ll 1, \\ \pi & 1 \leqslant p. \end{cases} \tag{37}$$

Equation (27) determines the temperature dependence of the order parameter at given frequency and intensity of field. The latter is taken to obey the relation

$$\gamma \ll \omega \ll T. \tag{38}$$

The dependence $F(\Delta)$ is shown in fig. 2. At $\Delta = \frac{1}{2}\omega$ the slope is undefined. The temperature dependence is given in fig. 3, where the dashed line shows the

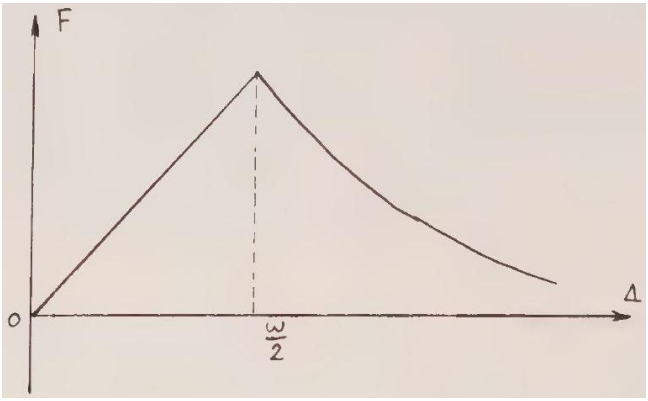


Fig. 2. The dependence of the nonequilibrium term in the Ginzburg-Landau equation on the gap.

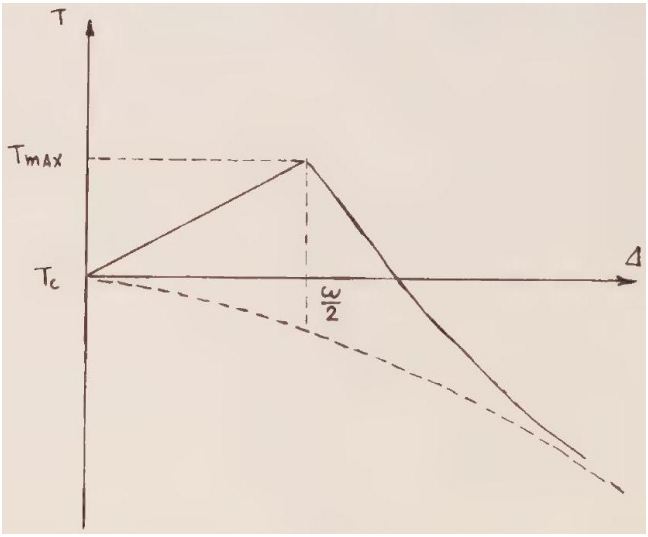


Fig. 3. Temperature dependence of the gap under weak microwave radiation. Dashed line shows equilibrium dependence.

equilibrium function. If the radiation intensity is not too low,

$$\frac{c}{T} \ll \frac{x}{r}, \tag{39}$$

the temperature dependence of the order parameter is determined mainly by the term f and it concides with the equilibrium one only at large A.

The temperature dependence of A obtained has a hysteretic feature. This means, that the jump from one regme to another under changing of temperature has another callse. Now, we will examine the "ideal" picture of superconductivity stimulation. that is, instabilities are supposed not to develop. and the regime remains spatially homogeneous.

From the formula obtained, the distortion of the electron distribution function by radiation yields an increase in the order parameter istimulated superconductivity effect), if the frequency is larger than some critical value (:):

$$\omega_{\mathrm{c}}^2 \ln {}^{xA}_{e(1)_{\mathrm{c}}} = 2\pi; \Delta. \tag{0}$$

Hence. as the temperature is increased. T, may be exceeded but the order parameter dres not ger to zero. The maximum temperature in the limit $\omega/T \ll \%/y \ll 1$ is determined by

$$\frac{I(\%) - T}{T_c} = \frac{\omega}{2T}\frac{x}{\gamma}\varphi(2) = \frac{\pi}{2\sqrt{3}}\frac{\omega}{T}\frac{x}{\gamma}. \tag{41}$$

At this temperature 1 - fro. As the temperature is further increased. the order parameter tends to zero.

At high intensities mequalit; (39) does not hold and the perturbation theors on 2 fails. Here radiaton strongly affects the distribution function by spreading it over the range of energes exceeding (%) It is sery important that due to root sirgularity in the density of states there is alady a part of the nonequilibrium distribution function changing at energles which are much smaller than temperature. For this reason the nonequilibrium part of the distribution function can be represented as the sum of two parts,

$$n_2' = n - n_F = n_1(\varepsilon) + n_2(\varepsilon), \tag{42}$$

where the scale of changes in $n_2(2)$ is 7 . but $n_3(2)$ changes at much smaller energies. The collision integral is

$$I \cap n = 2; \frac{\varepsilon}{\sqrt{\varepsilon^2 - \Delta^2}} n_1(\varepsilon) + I\left\{n_2\right\}. \tag{43}$$

Only the linearized part of the collision integral plays a rote. Such an approximation is valid of $n'' = 1$. This holds for our case too. From eq. 1251 we
have

$$\begin{aligned}
I\left\{n_2\right\} &= \frac{2g}{\omega_D^2} \\
&\times \left\{ \int_1^{\varepsilon} \mathrm{d}\varepsilon_1 \left(\varepsilon - \varepsilon_1\right)^2 u_\varepsilon u_{\varepsilon_1} \left(1 - \frac{\Delta^2}{\varepsilon\varepsilon_1}\right) \left[n_2(\varepsilon)\left(1 + N_{\varepsilon-\varepsilon_1} - n_{\varepsilon_1}^{\mathrm{F}}\right) - n_2\left(\varepsilon_1\right)\left(N_{\varepsilon-\varepsilon_1} + n_\varepsilon^{\mathrm{F}}\right)\right] \right. \\
&+ \int_{\varepsilon}^{\infty} \mathrm{d}\varepsilon_1 \left(\varepsilon_1 - \varepsilon\right)^2 u_\varepsilon u_{\varepsilon_1} \left(1 - \frac{\Delta^2}{\varepsilon\varepsilon_1}\right) \left[n_2(\varepsilon)\left(N_{\varepsilon_1-\varepsilon} + n_{\varepsilon_1}^{\mathrm{F}}\right) - n_2\left(\varepsilon_1\right)\left(1 - n_\varepsilon^{\mathrm{F}} + N_{\varepsilon_1} - \varepsilon\right)\right] \\
&\left. + \int_{\Delta}^{\infty} \mathrm{d}\varepsilon_1 \left(\varepsilon_1 + \varepsilon\right)^2 u_\varepsilon u_{\varepsilon_1} \left(1 + \frac{\Delta^2}{\varepsilon\varepsilon_1}\right) \left[n_2(\varepsilon)\left(n_{\varepsilon_1}^{\mathrm{F}} + N_{\varepsilon_1-\varepsilon}\right) + n_2\left(\varepsilon_1\right)\left(n_\varepsilon^{\mathrm{F}} + N_{\varepsilon_1+\varepsilon}\right)\right] \right\}
\end{aligned} \tag{44}$$

Integration of eq. (24) from Δ to ε in the spatially homogeneous case (we assume $\omega < 24$) yields

$$\begin{aligned}
&2\gamma \int_{\Delta}^{\varepsilon} \mathrm{d}\varepsilon_1 u_{\varepsilon_1} n_1\left(\varepsilon_1\right) + \int_{\Delta}^{\varepsilon} I\left\{n_2\right\} \mathrm{d}\varepsilon_1 \\
&\quad = 2\alpha \int_{\varepsilon-\omega}^{\varepsilon} \mathrm{d}\varepsilon_1 u_{\varepsilon_1} u_{\varepsilon_1+\omega} \left(1 + \frac{\Delta^2}{\varepsilon_1\left(\varepsilon_1 + \omega\right)}\right) \left(n_{\varepsilon_1+\omega} - n_{\varepsilon_1}\right)
\end{aligned}$$

We will consider further the region of energies $\varepsilon \gg \omega$. Since corrections for the distribution function change slowly over the range ω, expansion to first order can be performed in the integral

$$2\gamma\int_{\Delta}^{\varepsilon}\mathrm{d}\varepsilon_1 u_{\varepsilon_1}n_1+\int_{\Delta}^{\varepsilon}T\left\{n_2\right\}\mathrm{d}\varepsilon_1 =2\alpha\omega^2\frac{\varepsilon^2+\Delta^2}{\varepsilon^2-\Delta^2}\left(\frac{\partial n_1}{\partial\varepsilon}+\frac{\partial n_2}{\partial\varepsilon}\right) + 4\alpha\omega^2\frac{\partial n^{\mathrm{F}}}{\partial\varepsilon}\frac{\Delta^2}{\varepsilon^2-\Delta^2}+2\alpha\omega^2\frac{\partial n_{\mathrm{F}}}{\partial\varepsilon}. \tag{45}$$

Solution (45) must obey the integral relation

$$2\gamma\int_{\Delta}^{\infty}\mathrm{d}\varepsilon u_{\varepsilon}n_1+\int_{\Delta}^{\infty}\mathrm{d}\varepsilon_1 I\left\{n_2\right\}=0 \tag{46}$$

Equation (45) is divided into two parts: one changing considerably and the other changing slowly at energies of the order of temperature. Each is considered separately

$$2\gamma\int_{A}^{\varepsilon}\mathrm{d}\varepsilon_1 u_{\varepsilon_1}n_1=2\alpha\omega^2\frac{\varepsilon^2+\Delta^2}{\varepsilon^2-\Delta^2}\frac{\partial n_1}{\partial\varepsilon}+4\alpha\omega^2\frac{\partial n_{\mathrm{F}}}{\partial\varepsilon}\frac{\Delta^2}{\varepsilon^2-\Delta^2}$$
$$\int_{\Delta}^{\infty}\mathrm{d}\varepsilon u_{\varepsilon}n_1=0 \tag{47}$$

The slowly changing part of the distribution function $n_2(\varepsilon)$ is small on parameter Δ/T compared to n_1. Its contribution to the total number of quasiparticles over the threshold is not small, but it is small in units of F, hence $n_2(\varepsilon)$ is not considered.

By introducing a new variable $y=(1/\Delta)\sqrt{\varepsilon^2-\Delta^2}$, and a new function

$$N(y)=\frac{2T}{\Delta}\int_0^y n_1\left(y_1\right)\mathrm{d}y_1, \tag{48}$$

we obtain from (47) the equation

$$N''-\frac{y^3}{\left(y^2+2\right)\sqrt{y^2+1}}\beta N=\frac{y}{\left(y^2+2\right)\sqrt{y^2+1}},\quad \beta=\frac{\gamma\Delta^2}{\alpha\omega^2} \tag{49}$$

to be solved with boundary conditions $N(0)=0$ and $N(\infty)=0$; the second condition is the result of conservation of the total number of excitations with energies comparable to temperature.

Basically, this method of solving the initial difference equation (24) consists of making it differential since at large intensity values the characteristic scale of changes in the distribution function is much larger than ω.

Solution (49) can be expressed in the form

$$N(y)=-N_0(y)\int_0^y \mathrm{d}y_1 N_0^{-2}\left(y_1\right)\int_{y_1}^{\infty}\frac{y_2}{\left(y_2^2+2\right)\sqrt{y_2^2+1}}N_0\left(y_2\right)\mathrm{d}y_2, \tag{50}$$

where $N_0(y)$ is the solution of the corresponding homogeneous equation decreasing at infinity. It is best of all to find the form of $N_0(y)$ in the limiting cases of low and high intensities.

First of all we consider low intensities $\beta\gg 1$, i.e., $\alpha/\gamma\ll\Delta^2/\omega^2$. Then in equation (49) small y are of importance:

$$N''-\frac{1}{2}y^3\beta N=\frac{1}{2}y. \tag{51}$$

The solution of the homogeneous equation is

$$N_0(y)=f\left(\frac{1}{5}\sqrt{2}y^{5/2}\beta^{1/2}\right), \tag{52}$$

where

$$f(\xi) = \int_1^\infty \frac{\mathrm{e}^{-\xi t}}{\left(t^2-1\right)^{7/10}}\,\mathrm{d}t$$

Then one can readily find N along with the distribution function at small and large values of the variable compared to $\beta^{-15}, y^{\cdot \ll \beta^{-15}}$ corresponds to small ξ :

$$N(y) = -N_0(0)\int_0^y \mathrm{d}y_1 N_0^{-2}\left(y_1\right)\int_0^\infty \frac{1}{2}y_2 N_0\left(y_2\right)\mathrm{d}y_2;$$

at $y \gg \beta^{-1/5}\xi$ is large and

$$f(\xi) = \xi^{-3/10}\frac{\mathrm{e}^{-\xi}}{2^{7/10}}\int_0^\infty \frac{\mathrm{e}^{-x}}{x^{7/10}}\,\mathrm{d}x$$

Thus, for the distribution function we have

$$n_1(g) = \begin{cases} -\frac{\Delta}{T}\beta^{-2/5}\frac{\pi}{2(40)^{1/5}}\left[\Gamma\left(\frac{1}{5}\right)\sin\frac{2}{5}\pi\right]^{-1} & y \ll \beta^{-1/5}, \\ \frac{\Delta}{\beta T}y^{-3} & \beta^{-1/5} \ll y, \end{cases} \tag{53}$$

The value F can be obtained with logarithmic accuracy when the principal change of the distribution function is localized in the region $y \ll 1$:

$$\begin{aligned} F &= -2\int_0^\infty \frac{\mathrm{d}y}{\sqrt{y^2+1}}n_1(y) \\ &= 2\int_0^\infty \mathrm{d}y\left(1-\frac{1}{\sqrt{y^2+1}}\right)n_1(y) = \int_0^\infty y^2 n_1(y)\mathrm{d}y = \frac{\Delta}{5\beta\ \mathrm{T}}\ln\beta. \end{aligned} \tag{54}$$

We have taken into account that the integral in semi-infinite limits from the distribution function equals zero due to conservation of the total number of quasiparticles.

As was reported, formula (54) is valid for $\beta \gg 1$. Moreover, the given approach holds if the spreading of the distribution function over energy exceeds ω. The last condition is equivalent to

$$\frac{\alpha}{\gamma}\sqrt{\frac{\Delta}{\omega}} > 1,$$

in other words $v^{\omega/A} \ll \beta^{-1/5}$. This is contrary to condition (35) for applicability of perturbation theory. Thus, the condition of validity for eq. (54) is

$$\sqrt{\frac{\omega}{\Delta}} \ll \frac{\alpha}{\gamma} \ll \frac{A^2}{\omega^2}. \tag{55}$$

Note, that at $\alpha_1\hat{\gamma} \sim_V \overline{(1)/\Lambda}$ on the verge of applicability of perturbation theory formula (54) matches expression (37) with logarithmic accuracy, if $\omega \ll A$.

In the opposite limiting case with sufficiently high intensities, $\beta \ll 1(\alpha/\gamma \gg \Delta^2/\left(\omega^2\right)$, the solution has the following structure. The principal change of nonequilibrium addition to the distribution function occurs on the scale $y \approx 1$, and there is a part with small amplitude but attenuating weakly (over distances $y \approx \beta^{-1/2}$). This is of no importance for calculating F. The solution
of the homogeneous equation $N_0(y)$ is changed just over such long distances. Hence to calculate a localized part of n_1 one takes $N_{0'}$ constant. In this case formula (50) gives

$$n_1(y) = -\frac{\Delta}{2T}\left(\frac{\pi}{2} - \tan^{-1}\sqrt{y^2+1}\right) + n_1' \tag{56}$$

The slowly changing part n_1' has the form

$$n_1' = C\frac{A}{T} f\left(y\beta^{1/2}\right), \tag{57}$$

with f a function of the order of unity. The contribution of function $n_1(y)$ to the total number of quasiparticles is

$$\begin{aligned}\int_\Delta^\infty \mathrm{d}\varepsilon u_\varepsilon n_1 &\approx -C_1\frac{\Delta}{T}\ln\beta + \int_0^\infty n_1'(y)\mathrm{d}y \\ &\approx -C_1\frac{\Delta}{T}\ln\beta + C\frac{\Delta}{T}\beta^{-1/2}\int_0^\infty f(z)\mathrm{d}z = 0 \quad C_1 \approx 1\end{aligned}$$

Now we have an estimation $C \approx \beta^{1/2}\ln\beta \ll 1$, which confirms the abovementioned:
Calculating the value of F by eq. (56), we have

$$F = \frac{\pi}{4}\ln(3+2\sqrt{2})\frac{\Delta}{T} \approx 1.38\frac{\Delta}{T}. \tag{58}$$

Thus, formulae (54) and (58) yield values of F in the limiting cases $\Delta^2/\omega^2 \gg \alpha/\gamma$ and $\Delta^2/\omega^2 \ll \alpha/\gamma$, correspondingly.

To find the temperature dependence of the order parameter one has to use equation (27). It is of importance which is the given value, the amplitude of the current density or that of the electric field. This circumstance depends on experimental conditions. We first consider the situation with the electric field given, i.e., α is constant. The dependence of Δ/T on temperature is shown in fig. 4.

Similarly to the low-power case, the transition from the super conducting to the normal state will occur by a jump with a finite value of the order parameter

$$\Delta \approx \omega(\alpha/\gamma)^{1/2}. \tag{59}$$

At $\Delta \lesssim \omega$ the theory fails. The value of the order parameter (39) corresponds to the highest possible temperature which we also call critical, $T_c(\alpha)$:

$$\frac{T_\mathrm{c}(\alpha) - T_\mathrm{c}}{T_\mathrm{c}} = C\sqrt{p} - \pi p\left(b + \frac{\gamma T}{\omega^2}\right) \quad p = \frac{\alpha}{\gamma}\frac{\omega^2}{T^2}. \tag{60}$$

$C\sqrt{p}(C \approx 1)$ is the maximum value of F. Our theory holds up to $A/T \ll 1$.
From (59) it follows that it is valid at $p \ll 1$ or

$$\alpha/\gamma \ll T^2/\omega^2. \tag{61}$$

Let us consider two frequency limits
(1) $\omega \ll \sqrt{\gamma T_\mathrm{c}}$.
In this case expression (60) has its maximum at $p = p_\mathrm{c}$:

$$\left[\frac{T_c(\alpha) - T_c}{T_c}\right]_{\max} = \frac{c^2}{4\pi}\frac{\omega^2}{\gamma T_c}, \quad p_c = \frac{\alpha_c}{\gamma'}\frac{\omega^2}{T^2} = \left(\frac{c}{2\pi}\frac{\omega^2}{\gamma T}\right)^2 \ll 1.$$

The dependence of the critical temperature on radiation power is shown in fig. 5 as a curve with a maximum. Thus, we have an optimum magnitude of microwave power giving the maximum stimulation of superconductivity.

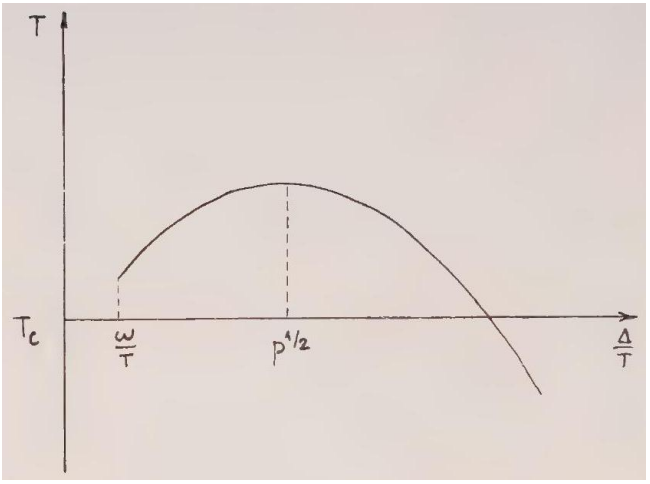


Fig. 4. Temperature dependence of the gap under strong microwave radiation.

$$\sqrt{\gamma} T_c \ll \omega \ll T_c. \tag{2}$$

In this case formula (60) also gives formally a curve with a maximum, however. its position is defined by values $p \approx 1$ lying on the edge of applicability of the theory. Apparently, in this case there is a similar picture (fig. 5). Hence the value

$$\left[\frac{T_c(\alpha) - T_c}{T_c}\right]_{\max} \approx 1 \tag{28}$$

We now take a situation with the current density given. Here from eq.

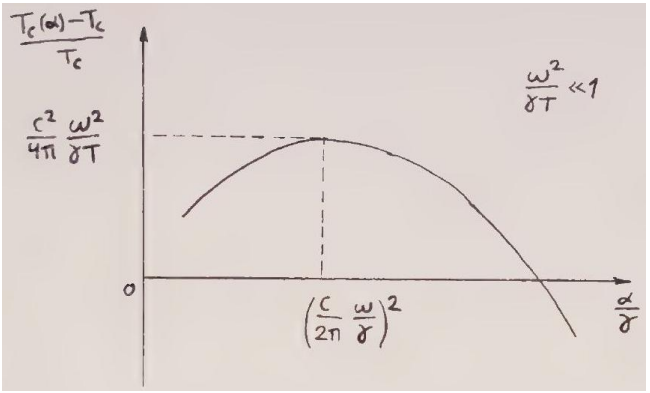


Fig. 5. The dependence of the relative increase of critical temperature on radiation power.

follows

$$\alpha = D\left(\frac{e}{c}\right)^2 \boldsymbol{A}_\omega A_{-\omega} = \frac{\pi^2}{m p_0 \omega^2 \sigma} \frac{j_\omega j_{-\omega}}{1 + \left(\frac{\pi\Delta^2}{2T\omega}\right)^2}. \tag{62}$$

If $\alpha/\gamma \ll T/\omega$, the London current can be neglected. The results coincide with previous ones. At $\alpha/\gamma \geqslant 7/\omega$ according to eq. (62) a formal change in $\alpha \to (2\ \mathrm{T}\omega/\pi\Delta^2)^2\,\alpha$ can be performed. We consider case (2), i.e., frequencies $\omega \gg \sqrt{\gamma T_c}$. Then the value of the order parameter determining the transition into the normal state is

$$\frac{\Delta}{T} \approx \left(\frac{\alpha}{\gamma}\right)^{1/6} \left(\frac{\omega}{T}\right)^{2/3}. \tag{63}$$

The dependence of the transition temperature on power has the form

$$\frac{T_{\rm c}(\alpha) - T_{\rm c}}{T_{\rm c}} \approx \left(\frac{\alpha}{\gamma}\right)^{1/6} \left(\frac{\omega}{T}\right)^{2/3}. \tag{64}$$

The maximum increase in transition temperature on the edge of applicability of the theory is

$$\left[\frac{T_c(x) - T_c}{T_c}\right]_{\max} \approx 1,$$

as in the previous case. Aslamazov and Gavrilov (1980), considering superconductivity stimulation, paid attention to the significance of the depairing term in the Ginzburg-Landau equation.

The dependence of transition temperature on power, when current density is given and the frequency satisfies $\omega \gg \sqrt{\gamma T_{\rm c}}$, is shown in fig. 6.

To obtain the temperature dependence of the critical current under conditions of superconductivity stimulation, note that near the transition temperature there is a typical value $eA_0/c \ll \Delta$, where the static vector potential A_0 is associated with the direct current:

$$j = -\frac{\pi\sigma}{2T_c}\frac{\Delta^2}{T}A_0 \tag{65}$$

With the Ginzburg-Landau equation (27) the dependence of the current squared the on order parameter can be obtained

$$j^2 = \frac{mp_0}{2}\sigma T_{\rm c}^3 \frac{\Delta^4}{T^4}\left[\frac{T_{\rm c} - T}{T} - \frac{7\xi(3)}{8\pi^2}\frac{\Delta^2}{T^2} + F\right]. \tag{66}$$

The maximum current is reached at $\Delta = \frac{1}{2}\omega$ if $\omega/T \ll \alpha/\gamma \ll 1$:

$$j_{\max} = \frac{21\sqrt{3}\breve{\zeta}(3)}{64\pi^2} j_0 \left(\frac{\omega}{T}\right)^2 \left(\frac{T_{\max} - T}{T_{\rm e}}\right)^{1/2} \approx 0.06 j_0 \left(\frac{\omega}{T}\right)^2 \left(\frac{T_{\max} - T}{T_{\rm c}}\right)^{1/2}. \tag{67}$$

The current j_0 is determined in such a way that in the absence of radiation $j_{\rm c} = j_0\left[(T_{\rm c} - T)/T_{\rm c}\right]^{3/2}$. Spreading of root singularity in the density of states associated with constant current, occurs at energies

$$(\varepsilon - \Delta) \approx \Delta^{1/3}\left[D\left(\frac{e}{c}A_0\right)^2\right]^{2/3}.$$

If this region is smaller than ω, then the right-hand side of formula (66) does not depend on A_0, and the maximum current is defined by (67). Since

$$D\left(\frac{e}{c} - A_0\right)^2 \approx (T_{\max} - T),$$

formula (67) is valid not too far from $T_{\max}$ $(T_{\max} - T) \ll \omega$.

Hitherto, we have considered the case of relatively low frequencies, $\omega \ll T$. This corresponds to the microwave range. In the literature the frequency limits of stimulated superconductivity have been discussed by Latyshev and Nad' (1974) and Dmitriev and Khristenko (1978). A lower frequency limit is found from formula (40). We will show that in "the ideal model" neglecting

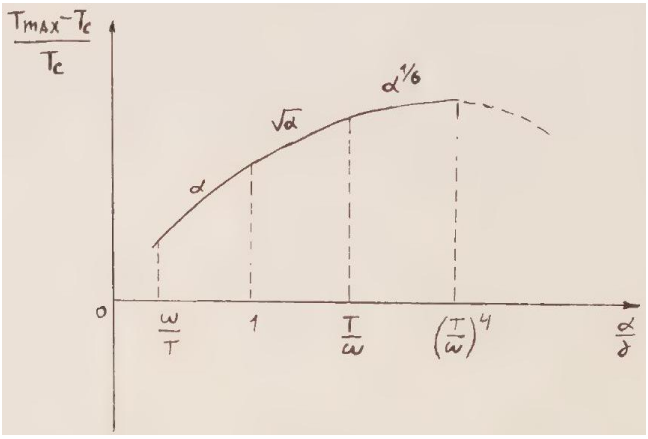


Fig. 6. The dependence of the relative increase of the critical temperature on power in conditions of fixed high-frequency current density.

the nonequilibrium of the phonon system, the formation of instabilities and heterogeneity of a sample, the upper frequency limit of the effect is $\omega_{\max} \approx T$.

We consider here the case with frequencies $\omega \gg T$. Close to the transition temperature $\Delta \ll T$, and in order to calculate the distribution function localized at energies of the order of the temperature one can put $\Delta = 0$ in the kinetic equation (24). In linear approximation on intensity, as shown by Vardanyan and Ivlev (1973), this gives

$$
\begin{aligned}
n'_\varepsilon \Bigg(& \frac{\varepsilon^3}{3T^3} + 2\int_0^\infty \frac{x^2\,\mathrm{d}x}{\mathrm{e}^x-1} + 2\int_{\varepsilon/T}^\infty \frac{x^2\,\mathrm{d}x}{\mathrm{e}^x+1} + \frac{4\varepsilon}{T}\int_0^{\varepsilon/T} \frac{x\,\mathrm{d}x}{\mathrm{e}^x+1} + \frac{2\varepsilon^2}{T^2}\int_{\varepsilon/T}^\infty \frac{\mathrm{d}x}{\mathrm{e}^x+1} \\
& + \frac{2}{\mathrm{e}^{\varepsilon/T}+1}\int_{\varepsilon/T}^\infty x^2 n'_x \mathrm{d}x + \frac{4\varepsilon/T}{\mathrm{e}^{\varepsilon/T}+1}\int_0^{\varepsilon/T} x n'_x \mathrm{d}x + \frac{2\varepsilon^2/T^2}{\mathrm{e}^{\varepsilon/T}+1}\int_{\varepsilon/T}^\infty n'_x \mathrm{d}x \\
& + \int_{\varepsilon/T}^\infty \frac{x^2\,\mathrm{d}x}{\mathrm{e}^x-1} n'\left(x-\frac{\varepsilon}{T}\right) - \int_0^\infty \frac{x^2\mathrm{e}^x}{\mathrm{e}^x-1}\,\mathrm{d}x n'\left(x+\frac{\varepsilon}{T}\right) - \int_0^{\varepsilon/T} \frac{x^2\,\mathrm{d}x}{\mathrm{e}^x-1} n'\left(\frac{\varepsilon}{T}-x\right) \\
& = 7\xi(3)^\alpha \begin{cases} \tanh\frac{\varepsilon}{2T} - \left[\exp\left(\frac{\omega-\varepsilon}{T}\right)+1\right]^{-1} & \varepsilon < \omega \\ \left[\exp\left(\frac{\varepsilon-\omega}{T}\right)+1\right]^{-1} & \omega < \varepsilon \end{cases}
\end{aligned}
\tag{68}
$$

The value of γ is determined by formula (26). The function n'_t must obey the normalization condition obtained by integration of the kinetic equation (24). This condition has the meaning of a balance of the total number of quasiparticles

$$
\begin{aligned}
\int_0^x n'_r \frac{\mathrm{d}\varepsilon}{T} \Bigg(& 2\int_0^r \frac{x^2\,\mathrm{d}x}{\mathrm{e}^x+1} + \int_T^r \frac{x^2\,\mathrm{d}x}{\mathrm{e}^x-1} \\
& + \frac{4\varepsilon}{T}\int_0^\infty \frac{x\,\mathrm{d}x}{\mathrm{e}^x+1} + \frac{2\varepsilon^2}{T^2}\int_0^\infty \frac{\mathrm{d}x}{\mathrm{e}^x+1}\Bigg) = 7\zeta(3)\frac{\alpha\omega}{\gamma}.
\end{aligned}
\tag{69}
$$

The basic part of the distribution function, localized at $\varepsilon \approx T$ must be found from the solution of the homogeneous equation (68). The source in the righthand side is necessary only for normalization. Neglecting the right-hand side of eq. (68) at $\varepsilon \ll \omega$, we obtain n'_ε at $T \ll \varepsilon$ from the equation

$$
\frac{\varepsilon^3}{3T^3} n'_\varepsilon - \int_0^\infty x^2 n'\left(x+\frac{\varepsilon}{T}\right)\mathrm{d}x = 0 \tag{70}
$$

Hence the solution is

$$n'_\varepsilon \approx \varepsilon^{-4} \tag{71}$$

At $\varepsilon \ll T$ equation (68) becomes

$$n'_\varepsilon \int_0^\infty \frac{x^2\,\mathrm{d}x}{\mathrm{e}^x+1} = \frac{\varepsilon}{4T}\int_0^\infty x^2 n'_x \mathrm{d}x + \frac{\varepsilon}{2T}\int_0^\infty \frac{x^2}{\tanh\frac{1}{2}x}\frac{\partial n'}{\partial x}\,\mathrm{d}x \tag{72}$$

giving $n'_c \propto \varepsilon$. With the normalization condition (69) taken into account, the distribution function may finally be represented in the form

$$n'_t = \frac{\alpha}{\gamma}\frac{\omega}{T} f\left(\frac{\varepsilon}{T}\right) \quad f(x) \approx \begin{cases} x & x \ll 1, \\ x^{-4} & 1 \ll x. \end{cases} \tag{73}$$

Calculating value F by means of eq. (27),

$$F = -\frac{2\alpha}{\gamma}\frac{\omega}{T}\int_0^\infty \frac{\mathrm{d}x}{x} f(x) \tag{74}$$

we have $F < 0$. No superconductivity stimulation by radiation with frequency $\omega \gg T$ takes place since under these conditions the basic mechanism is the increase of total number of quasiparticles. Thus one can conclude that the maximum frequency of radiation stimulating superconductivity is $\omega_{\max} \approx T$, if nonequilibrium of the phonon system is neglected.

In real conditions the acoustic contact of a superconducting film with the substrate can be imperfect. It means that before leaving a sample phonons have interacted with electrons. So the distribution function of phonons will differ from the nonequilibrium one. Chang and Scalapino (1971) have calculated just this situation. They proceeded from the kinetic equation (24) with an electron collision integral (25) and a phonon collision integral of the type

$$\begin{aligned}
&\left[N_\omega - N_\omega(T)\right]/\tau_{\mathrm{es}} = \\
&\lambda\left\{2\int_{\Delta t\omega}^\infty \mathrm{d}\varepsilon \frac{\varepsilon(\varepsilon-\omega)-\Delta^2}{\sqrt{\varepsilon^2-\Delta^2}\sqrt{(\varepsilon-\omega)^2-\Delta^2}}\left[n_\varepsilon\left(1-n_{\varepsilon-\omega}\right)\left(1+N_\omega\right)-\left(1-n_\varepsilon\right)n_{\varepsilon-\omega}N_\omega\right]\right. \\
&\quad\left.+\int_1^{\omega-\Delta}\mathrm{d}\varepsilon\frac{\varepsilon(\omega-\varepsilon)+\Delta^2}{\sqrt{\varepsilon^2-\Delta^2}\sqrt{(\omega-\varepsilon)^2-\Delta^2}}\left[n_\varepsilon n_{\omega-\varepsilon}\left(1+N_\omega\right)-\left(1-n_\varepsilon\right)\left(1-n_{\omega-\varepsilon}\right)N_\omega\right]\right\}
\end{aligned} \tag{75}$$

The value λ here is proportional to the constant of electron phonon interaction, τ_{es} is the characteristic time of electron interaction with the substrate, and $N_\omega(T)$ is the equilibrium distribution function of substrate phonons with temperature T. At given substrate temperature $T = 0.9T_{\mathrm{c}}$, various frequencies and τ_{es}, in particular, the dependence of the order parameter on radiation power was calculated. Similarly to the case of equilibrium phonons the gap reaches its maximum value at some radiation power. The upper frequency limit of the effect is here less than $\frac{3}{2}\boldsymbol{A}$. Moreover, it was found that the effect reduces when τ_{es} is increased. Due to the τ-approximation for the collision integral to be valid near the transition temperature, the total number of quasiparticles is constant if $\omega < 24$. On deviation from T_{c} down the nonlocal part of the collision integral becomes significant. The total number of quasiparticles may decrease. As shown by Chang and Scalapino (1977), at $T = 0.9T_{\mathrm{c}}$ and a good contact with a thermostat there is an additional mechanism of superconductivity stimulation owing to a decrease of the total number of quasiparticles. This mechanism becomes important not very close to T_{c}. At $T = 0.9T_{\mathrm{c}}$ it is already important. Thus, as seen from these calculations, the stimulation of superconductivity by microwaves is more effective if there is a good acoustic connection between

a sample and a thermostat. The influence of sample heating on the jump to the normal state by increasing the power was theoretically calculated by Latyshev and Nad' (1976).

Kozub and Spivak (1981) have studied the influence of electromagnetic radiation on a bulk superconductor placed in a magnetic field parallel to its surface. The value of the energy gap on the surface is less than that in the volume, therefore, a fraction of the surface quasiparticles appeared to be blocked in this region. The influence of radiation on these particles is much stronger since unblocked particles can readily diffuse into the bulk. Influencing the caught particles, radiation leads to superconductivity stimulation as well. The critical magnetic field is then increased.

19.4 4. Superconductivity stimulation by acoustic waves

As mentioned in the Introduction, acoustic waves of sufficiently large amplitude can serve as a source for pumping energy into the electronic system. The frequency of these waves must be in the range of the typical energy parameters of the superconductor, in particular the gap. The mechanism of acoustic wave attenuation in metal has electron character. Hence the disturbance of the electron system will be considerable.

If the superconducting sample is a thin film on substrate, in which an acoustic wave propagates, then this situation is similar to that with electromagnetic radiation. Analogous effects will also take place in a bulk superconductor through which sound is propagating. If the temperature is close to
the critical one, then $\Delta \ll T$. The basic change of the distribution function will localize at energies of order A. Most of the thermal quasiparticles play the role of a thermostat.

In experiments by Tredwell and Jacobsen (1975) the nonequilibrium state was created in a thin superconducting film by longitudinal waves. They gave. together with interesting experimental data, the kinetic equation for the case of acoustic pumping. This equation is analogous to eq. (24), except for the coherence factor corresponding to the scale potential $\varepsilon(\varepsilon-\omega)-d^2$ and the value α being defined differently. Close to the transition temperature the correction to the distribution function is

$$n'_\varepsilon = \frac{\alpha_1}{\gamma}\frac{\omega}{4T}\Big[\frac{\varepsilon(\varepsilon-\omega)-\Delta^2}{\varepsilon\sqrt{(\varepsilon-\omega)^2-\Delta^2}}\theta(\varepsilon-\Delta-\omega) - \frac{\varepsilon(\varepsilon+\omega)-\Delta^2}{\varepsilon\sqrt{(\varepsilon+\omega)^2-\Delta^2}}\theta(\varepsilon-\Delta) + \frac{\varepsilon(\omega-\varepsilon)+\Delta^2}{\varepsilon\sqrt{(\omega-\varepsilon)^2-\Delta^2}}\theta(\varepsilon-\Delta)\theta(\omega-\Delta-\varepsilon)\Big]. \tag{76}$$

The value x_1 is proportional to the absorbed power of an acoustic wave, and it depends on the dirtiness of a sample. The interaction of a longitudinal sound wave with metal is described by a deformation potential (see, e.g.. Kittel 1963). In the system of coordinates moving in each point along with lattice displacement, the addition to the Hamiltonian, associated with the acoustic wave, is in the form:

$$H' = (\operatorname{div} u)(p\cdot n)(v\cdot n) - \phi$$

where u is the lattice displacement vector, n is the unit vector directed along the wave vector of the sound. ϕ is determined from the condition of electroneutrality, equivalent with good accuracy to the requirement $\overline{H'}=0$ (the overbar means averaging over angles). Hence

$$\phi = \frac{pv}{3}\operatorname{div} u.$$

As is known, attenuation is determined by the Landau mechanism at $k\cdot l \gg 1$, by the diffusion mechanism at $kl \ll 1$. In the first case $\alpha_1 \approx \varepsilon_{\mathrm{F}}^2(ku)^2/kv$, in the second case $x_1 \approx$

$\tau\varepsilon_1^2\,(h(t)^2$ in agreement with the Pippard formula for attenuation of longitudinal sound. We express the energy flux of the acoustic wave $W \approx \rho s(\hat{\partial}u/\hat{\partial}t)^2$ through the α_1/γ value in the dirty case. It is more valid for films

$$W \approx g\left(\frac{T^4}{\varepsilon_{\rm F}^3\omega_{\rm D}}\right)\frac{1}{T\tau}\frac{x_1}{\gamma}\rho v s^2\cdot 10^{-7}\ \mathrm{W/cm^2}, \tag{77}$$

where g is the electron phonon constant, and s the velocity of sound. Substituting typical values of metal parameters $r_{\rm F}\approx 10^8$ cms.$s\approx 10^6$ cm s,
$\omega_{\rm D}\approx 10^2$ K, $\varepsilon_{\rm F}\approx 10^4$ K, $T\approx 1$ K, we get if $T\tau\approx 1$

$$W \approx \frac{\alpha_1}{\gamma}10^{-1}\ \mathrm{W/cm^2} \tag{78}$$

The nonequilibrium state is established when $x_1,\gamma\sim 1$. Hence the desired power level will be 10^{-1} W/cm^2. Experimentally it is very likely to be achieved.

With the function (76), the nonequilibrium term in the Ginzburg Landau equation acquires the form

$$\begin{aligned} F =& \frac{\omega^2}{2T}\frac{\alpha_1}{\gamma}\int_\Delta^\infty \mathrm{d}\varepsilon\frac{\varepsilon(\varepsilon+\omega)-\Delta^2}{\varepsilon(\varepsilon+\omega)\sqrt{\varepsilon^2-\Delta^2}\sqrt{(\varepsilon+\omega)^2-\Delta^2}} \\ & -\alpha_1\omega \\ & \gamma 2T\int_\Delta^{\omega-\Delta}\mathrm{d}\varepsilon\frac{\varepsilon(\omega-\varepsilon)+\Delta^2}{\varepsilon\sqrt{\varepsilon^2-\Delta^2}\sqrt{(\omega-\varepsilon)^2-\Delta^2}}\theta(\omega-2\Delta) \end{aligned} \tag{79}$$

Expression (36) is similar to this. In the limiting cases it gives

$$F=\begin{cases} \frac{\omega^2}{2\Delta T}\frac{\alpha_1}{\gamma} & \omega\ll\Delta, \\ \pi\Delta\alpha_1\left[\left(1-\frac{1}{\sqrt{3}}\right)-\theta(\omega-2\Delta)\right] & \mid(\omega-2\Delta\mid<\Delta, \\ T\gamma\gamma\begin{bmatrix}\pi\Delta & \alpha_1\\ -\frac{\pi}{2T} & \Delta\ll\omega.\end{bmatrix} \end{cases} \tag{80}$$

The Ginzburg Landau equation for the situation with longitudinal sound differs from eq. (27) by the absence of a depairing term depending on a vector potential:

$$\frac{T_c-T}{T}-\frac{7\zeta(3)}{8\pi^2}\Delta^2T^2+F=0 \tag{81}$$

The temperature dependence of the order parameter following from this is shown in fig. 7. We see that only at $A>\frac{1}{2}()$. gap enhancement occurs. If the acoustic intensity is not too low,

$$\frac{\alpha_1}{i}>\frac{\omega}{T}\frac{7\zeta(3)}{16\pi^3}\frac{\sqrt{3}}{\sqrt{3}-1}, \tag{82}$$

then there is superconductivity at temperatures above critical. Tredwell and Jacobsen (1975) used tunnel technique to measure the gap in the presence of pumping by longitudinal sound. The results were compared with given calculations on the basis of formulae of type (79) and (81). Good agreement between theory and experiment was found.

Superconductivity stimulation can be performed by transverse sound as
well. In this case the addition associated with sound to the Hamiltonian is

$$H'=-\frac{\partial u_x}{\partial z}p_xv_z+\frac{e}{c}v_xA_x, \tag{83}$$

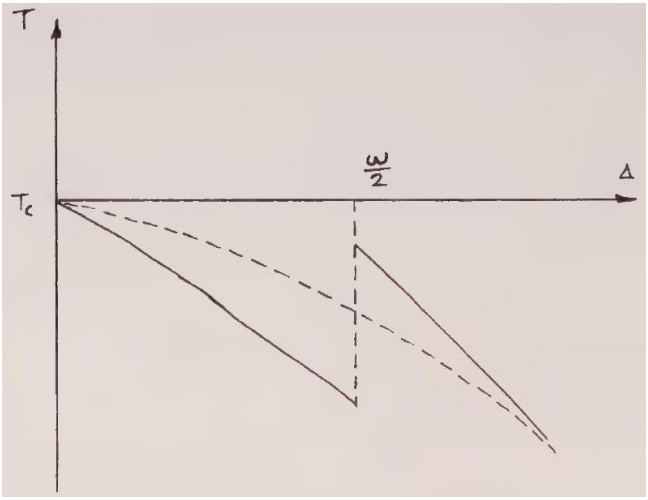


Fig. 7. The temperature dependence of the gap at acoustic pumping. Dashed line shows equilibrium dependence.

where u_v is the lattice displacement, and sound propagates along the =-axis. The first term is the deformation potential. The vector potential arises from the condition that the Maxwell equations be obeyed. In sufficiently pure superconductors close to the transition temperature attenuation will have electromagnetic character, fitting the last term in (83). On the contrary, in a dirty superconductor attenuation is defined by the deformation mechanism fitting the first term in (83). Consequently, at low impurity concentrations the kinetic equation will be of type (24), at high concentrations it will be of type (76) with a scalar coherence factor. Transverse sound will also lead to superconductivity stimulation. Note that besides this effect, strong nonlinear effects can also occur in the absorption and the velocity of sound, induced by changes in the distribution function homogeneous and isotropic with respect to momentum (30), as shown by Bulyzhenkov and Ivlev (1976a, b).

19.5 5. Superconductivity stimulation by tunnel injection

In the situations we have considered above, the redistribution of quasiparticles leading to superconductivity enhancement was provided by absorption of high-frequency electromagnetic and acoustic field quanta. There is also a way,
first proposed by Parmenter (1961), to influence superconductivity by tunnel injection of quasiparticles. In this situation the stationary state appears, as usual, due to energy exchange with a thermostat.

Processes occurring at tunneling can be depicted very roughly as in fig. 8a, where arrows show electron transfer through a tunnel barrier. Electron transfer through a barrier takes place due to the differences in density of states and distribution function at the same energy value.

It should be noted that tunneling can result in a more varied picture of the nonequilibrium state than can radiation by a monochromatic field, since in this case the magnitudes of the energy gaps do not obligatory coincide, and one can vary the voltage V at will, in analogy with the field frequency.

Tunnel experiments are of interest because details of the current voltage characteristics of contacts can give information on the shape of the distribution function instead of integral characteristics as obtained if only the order parameter is known, as shown by Kaplan et al. (1977). The position of the centre of the energy gap in a superconductor is conventionally called the chemical potential of Cooper pairs,

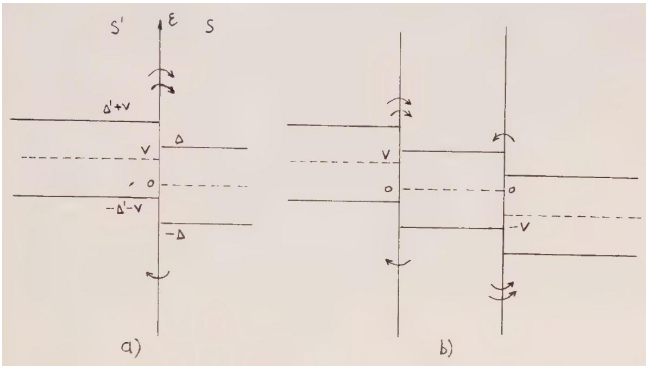


Fig. 8. Representation of the tunneling processes: (a) asymmetrical scheme; (b) symmetrical scheme.

$$\mu_{\rm p} = -\frac{1}{2e}\frac{\partial\chi}{\partial t},$$

where χ is the phase of the order parameter $\Delta = |\Delta|e^{i}$. The correction to the chemical potential of normal electrons is given by

$$\mu_{\rm n} = \int_{-\infty}^{\infty} (n_\varepsilon - n_{\rm F})\,{\rm d}\varepsilon \tag{84}$$

The integration in this formula can be extended to $-\infty$, since the function $(n_\varepsilon - n_F)$ in the real situation is well localized near the Fermi surface. An electrostatic potential ϕ fixing the shift of the zero position of electron energy is found from the conditions of electroneutrality

$$\delta\rho = \frac{3ne^2}{m{\rm p}_0}\,(\mu_{\rm n} - \phi) \tag{85}$$

The value

$$\Phi = \mu_{\rm n} - \mu_{\rm p} = \phi - \frac{1}{2e}\frac{\partial\chi}{\partial t} \tag{86}$$

is a gauge-invariant scalar potential determining the difference between the chemical potentials of normal electrons and Cooper pairs. To be more exact, Φ is the electron-hole imbalance. The theory of such phenomena has been developed in detail by Tinkham and Clarke (1972).

A tunnel contact is a convenient object to create and observe branch imbalance. Although it is not the subject of our review, electron-hole imbalance should be taken into account in the consideration of superconductivity stimulation in tunnel contacts. The only exception is the case of a completely symmetric system of tunneling contacts (fig. 8b). Clearly, in the central sample the electron and hole branches will be equally populated, and $\Phi = 0$. This case is closer to the situation with monochromatic radiation, when Φ is negligible in comparison with the parameter $\omega/\varepsilon_{\rm F}$.

Figure 9 shows a typical scheme to observe nonequilibrium effects on tunneling. A nonequilibrium is created in a superconductor S by injection through a low-resistance contact G (generator) from a superconductor S′ or normal metal N . If the length L of the contact surpasses the diffusion length L_1 then the distribution function will be homogeneous in the mid region far from the ends. In this region it is necessary to place a high-resistance contact with a detecting superconductor S_D or normal metal N_D not influencing the state of superconductor S . The gap and the magnitude of electron-hole imbalance can be measured using the current voltage characteristics of the detector.

In the superconductors S and S′ throughout all the stationary state the chemical potential of Cooper pairs remains constant in space. If the parameter ($L_1 - L$) exceeds the imbalance relaxation length, then at $x = L_1$ normal electrons and Cooper pairs will have the same potentials. The injection voltage V in this case has an ordinary meaning for the superconductors S and S′. They differ only by the equilibrium electron distributions being shifted an amount V.

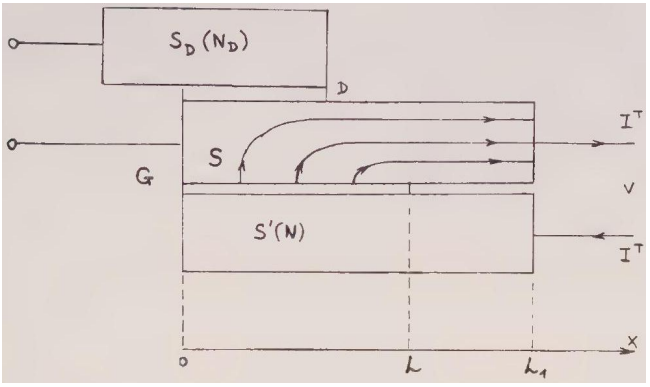


Fig. 9. Scheme of the experiment on the creation of nonequilibrium states by tunneling.

Note that if ($L_1 - L$) is smaller than the imbalance relaxation length the determination of the voltage V will not be trivial.

As follows from formula (23), the density of tunneling current through a contact is

$$j_{\mathrm{T}} = \frac{2mp_0e}{\pi^2} w \, \mathrm{d} \int_{\Delta}^{\infty} \mathrm{d}\varepsilon \left[u_\varepsilon u'_{\varepsilon-\mathrm{V}} \left(\beta'_{\varepsilon-\mathrm{V}} - \beta_\varepsilon \right) \right.$$
$$\left. + u_\varepsilon u'_{\varepsilon+\mathrm{V}} \left(\beta_\varepsilon - \beta'_{\varepsilon+\mathrm{V}} \right) - \left(u'_{\varepsilon-\mathrm{V}} + u'_{\varepsilon+\mathrm{V}} \right) \alpha_\varepsilon + u_\varepsilon \left(\alpha'_{\varepsilon-\mathrm{V}} + \alpha'_{\varepsilon+\mathrm{V}} \right) \right], \tag{87}$$

where d is the thickness of the superconductor S . The quantities with subscript ε refer to the superconductor S ; and those with shifted arguments $\varepsilon \pm V$ refer to the superconductor S'. The values β_1, α_2 and u_1 are defined by relation (7), in which only for S' the substitution $\Delta \to \Delta'$ should be made. Evidently, $\alpha_a \propto \Phi$.

Passing uniformly through the contact G into the superconductor S , as seen from fig. 9, the tunneling current then flows along the thin film S . This results in a non-zero current divergence in S ($\operatorname{div} j = j_{\mathrm{T}}/d$). The current consists of London and normal current; according to (27). Even if the distribution function is homogeneous along the film S , the vector potential changes with coordinate:

$$D \frac{mp_0e^2}{2\pi c} \frac{\Delta^2}{T} A = -\frac{j_{\mathrm{T}}}{d} x. \tag{88}$$

The maximum value, at $x = L$, is of the order of magnitude

$$\left[\frac{D}{\gamma} \left(\frac{e}{c} A \right)^2 \right]^{1/2} \propto \frac{j_{\mathrm{T}}}{dmp_0e} \frac{T}{\Delta^2 \gamma} \frac{L}{l_{\mathrm{D}}}. \tag{89}$$

The diffusion length $l_{\mathrm{D}} \propto \sqrt{D/\gamma}$ used in this theory is introduced here. The part of equation (19) even in ε describes the attenuation of the imbalance α_{e} in space. As shown by Schmid and Schön (1975), Artemenko et al. (1978) and Bulyzhenkov and Ivlev (1979), if $(D/\gamma)(eA/c) \geqslant 1$ then this value starts to affect greatly the imbalance relaxation rate. Consequently, the problem can be thought to be spatially homogeneous only in films short enough that $(D/\gamma)(eA/\mathcal{C})^2 \ll 1$. With relation (89) taken into account, we get the limitation on tunnel current density at given length L of the contact and thickness d of the film:

$$\frac{j_{\mathrm{T}}}{dmp_0e}\frac{T}{\Delta^2\gamma}\frac{L}{l_{\mathrm{D}}}\ll 1. \tag{90}$$

As stated above, the problem on nonequilibrium states at injection can be thought to be spatially homogeneous only under special limitations on contact linear parameters and tunnel current. This long preface for the problem of injection-stimulated superconductivity is due to the complexity of these phenomena compared to pumping by a monochromatic field.

A detailed calculation of tunnel-injection-stimulated superconductivity for the symmetrical situation of the type fig. 8 b has been made by Aronov and Gurevich (1972). For exactly the same case Peskovatski and Seminozhenko (1976) derived the kinetic equation and calculated the change in the order parameter.

The kinetic equation (19), in which no derivatives with respect to time and coordinate are considered and $A_{10}=0$, is divided into two parts, one even and one odd in the energy:

$$\frac{1}{2}\left(I_\varepsilon+I_{-\varepsilon}\right)=R_\varepsilon,\quad \frac{1}{2}\left(T_\varepsilon-T_{-\varepsilon}\right)=L_\varepsilon \tag{91}$$

R_i and L_i are obtained by the corresponding symmetrizations of the source (22):

$$\begin{aligned}R_\varepsilon &= w[u'_{\varepsilon-V}\left(\beta'_{\varepsilon-V}-\beta_\varepsilon\right)+u'_{\varepsilon+V}\left(\beta_\varepsilon-\beta'_{\varepsilon-V}\right)\\ &\quad +\alpha'_{\varepsilon-V}+\alpha'_{\varepsilon+V}-u_\varepsilon\left(u'_{\varepsilon-V}+u'_{\varepsilon+V}\right)\alpha_\varepsilon]\\ L_\varepsilon &= w[u_\varepsilon u'_{\varepsilon-V}\left(\beta'_{\varepsilon-V}-\beta_\varepsilon\right)+u_\varepsilon u'_{\varepsilon+V}\left(\beta'_{\varepsilon+V}-\beta_\varepsilon\right)\\ &\quad +u_\varepsilon\left(\alpha'_{\varepsilon-V}-\alpha'_{\varepsilon+V}\right)+\left(\mathrm{u}'_{\varepsilon+V}-\mathrm{u}'_{\varepsilon-V}\right)\alpha_\varepsilon]\,.\end{aligned} \tag{92}$$

The distribution function is determined by the sum of the even and odd parts,

$$n_\varepsilon=\frac{1}{2}\left(1+\alpha_\varepsilon+\beta_\varepsilon\right), \tag{93}$$

where the even part α_1 defines the chemical potential shift and the odd part β_c is responsible for the change in the order parameter. The anomalous term F in
the Ginzburg-Landau equation (27) becomes

$$F=-\int_0^\infty\frac{\mathrm{d}\varepsilon}{\varepsilon}u_\varepsilon\beta'_\varepsilon, \tag{94}$$

where $\beta'_\varepsilon=\beta_\varepsilon+\tanh(\varepsilon/2T)$, then in equilibrium $\beta_\varepsilon=-\tanh(\varepsilon/2T)$.
As shown by Artemenko and Volkov (1975), close to the transition temperature

$$\alpha_\varepsilon=\frac{1}{u_\varepsilon}\frac{\Phi}{2T}\frac{1}{\cosh(2\varepsilon/2T)}. \tag{95}$$

Hence from eqs. (91) and (92), supposing S' to be in equilibrium, we have

$$\Phi=V\frac{w}{\gamma}\left(\frac{w}{\gamma}+\frac{\pi\Delta}{8T}\right)^{-1}. \tag{96}$$

In the limit of strong injection $w/\gamma\gg A/T$, this yields $\Phi=V$. In the odd part of the collision integral one should keep the part linear in β'_ε and quadratic in α_ε :

$$\frac{1}{2}\left(I_\varepsilon-I_{-\varepsilon}\right)=\frac{1}{2}\left(I_\varepsilon-I_{-\varepsilon}\right)_{\mathrm{lin}}+A_\varepsilon, \tag{97}$$

in which the following notation is introduced:

$$\frac{1}{2}\left(I_\varepsilon - I\right)_{\rm lin} = \frac{g}{\omega_D^2}$$
$$\times\left\{\int_\varepsilon^\infty \mathrm{d}\varepsilon_1 \left(\varepsilon_1-\varepsilon\right)^2 \left(u_\varepsilon u_{\varepsilon_1} - v_\varepsilon v_{\varepsilon_1}\right)\left[\beta'_\varepsilon\left(n^{\rm F}_{\varepsilon_1}+N_{\varepsilon_1}-\varepsilon\right) - \beta'_{\varepsilon_1}\left(1-n^{\rm F}_\varepsilon+N_{\varepsilon_1-\varepsilon}\right)\right]\right.$$
$$+\int_\Delta^\varepsilon \mathrm{d}\varepsilon_1 \left(\varepsilon-\varepsilon_1\right)^2 \left(u_\varepsilon u_{\varepsilon_1} - v_\varepsilon v_{\varepsilon_1}\right)\left[\beta'_\varepsilon\left(1-n^{\rm F}_{\varepsilon_1}+N_{\varepsilon-\varepsilon_1}\right) - \beta'_{\varepsilon_1}\left(n^{\rm F}_\varepsilon+N_{\varepsilon-\varepsilon_1}\right)\right]$$
$$\left.+\int_\Delta^\infty \mathrm{d}\varepsilon_1 \left(\varepsilon+\varepsilon_1\right)^2 \left(u_\varepsilon u_{\varepsilon_1} + v_\varepsilon v_{\varepsilon_1}\right)\left[\beta'_\varepsilon\left(n^{\rm F}_{\varepsilon_1}+N_{\varepsilon+\varepsilon_1}\right) + \beta'_{\varepsilon_1}\left(n^{\rm F}_\varepsilon+N_{\varepsilon+\varepsilon_1}\right)\right]\right\}$$
$$A_\varepsilon = -\frac{g}{\omega_{\rm D}^2}\alpha_\varepsilon\left[\int_\Delta^\varepsilon \mathrm{d}\varepsilon_1\left(\varepsilon^2+\varepsilon_1^2\right)\alpha_{\varepsilon_1} + 2\varepsilon\int_\varepsilon^\infty \mathrm{d}\varepsilon_1\varepsilon_1\alpha_{\varepsilon_1}\right]. \tag{98}$$

Substituting this into eq. (91), we obtain

$$\frac{1}{2}\left(I_\varepsilon - I_{-\varepsilon}\right)_{\rm lin} = L_\varepsilon + A_\varepsilon. \tag{99}$$

The solution corresponding to L_i is localized at energies $\varepsilon\times\Lambda \ll T$. So to find the solution near the critical temperature the collision integral can be represented in τ-approximation. The solution corresponding to A_ε at energies of the order of the temperature is

$$\beta'^{(A)}_\varepsilon = \frac{\Phi^2}{4T^2}\tanh\frac{\varepsilon}{2T}\left(\cosh\frac{\varepsilon}{2T}\right)^{-2} \quad (\varepsilon\gg\Lambda). \tag{100}$$

As a result, as shown by Ivlev (1978), the potential Φ affects the odd part of the distribution function in the following way:

$$\beta'_\varepsilon = \beta'^{(A)}_\varepsilon + \frac{\omega}{\gamma T}\left(V-\frac{\Phi}{u_\varepsilon^2}\right)\left(u'_{\varepsilon+V}-u'_{\varepsilon-V}\right) \tag{101}$$

with Φ given by expression (96). Here corrections to the β_c are neglected, as it took place in the case of electromagnetic radiation because there is more essential nonlinearity in the value of Φ.

With (101) the anomalous term F (99) becomes

$$F = -\frac{7\zeta(3)}{4\pi^2}\frac{\Phi^2}{T^2} + \frac{w}{\gamma T}\int_0^\infty \frac{\mathrm{d}\varepsilon}{\varepsilon}u_\varepsilon\left(V-\frac{\Phi}{u_\varepsilon^2}\right)\left(u'_{\varepsilon-V}-u'_{\varepsilon+V}\right) \tag{102}$$

Galaiko (1974) has indicated the presence of the term Φ^2, T^2 in the equation for the order parameter.

As follows from eq. (87), the tunnel current is

$$j_{\rm T} = \frac{4mp_0 l}{\pi^2}wd(V-\Phi) = \frac{4mp_0 e}{\pi^2}wVd\frac{\pi\Delta/8T}{w/\gamma+\pi\Delta/8T} \tag{103}$$

Consequently, inequality (90) takes the form

$$\frac{\Phi}{\Delta} \ll \frac{l_{\rm D}}{L}, \tag{104}$$

with Φ defined by formula (96). Since $l_{\rm D} \ll L, \Phi$ is much less than Δ.

The general conclusion can be drawn that the spatially uniform tunneling contact in conditions of branch imbalance is to be considered with care. First of all this refers to the interpretation of experimental data on the basis of homogeneous consideration. The dependence of the order parameter in conditions of imbalance (fig. 8a) is determined by the Ginzburg-Landau equation

$$\frac{T_c - T}{T} - \frac{7\zeta(3)}{8\pi^2}\frac{\Delta^2}{T^2} + F = 0, \tag{105}$$

with the anomalous term (102). Condition (104) should be obeyed.
The picture looks much simpler if a symmetrical scheme is used (fig. 8b), where there is no branch imbalance, though the use of such schemes is less convenient experimentally. As shown by Peskovatski and Seminozhenko (1976) in this case the situation is analogous to pumping by an electromagnetic field, except for a coherence factor. From eqs. (19) and (22) at $\alpha_\varepsilon = 0$ we find the kinetic equation

$$I_\varepsilon = 2wu_\varepsilon \left[u'_{\varepsilon-V}\left(n'_{\varepsilon-V} - n_\varepsilon\right) + u'_{\varepsilon+V}\left(n'_{\varepsilon+V} - n_\varepsilon\right)\right].$$

The phonon collision integral is given by formula (25). Near the transition temperature it has the form (26). Due to this the anomalous term in equation
(105) is given, at small w/γ, as

$$F = \frac{wV}{\gamma T}\int_\Delta^\infty \frac{\mathrm{d}\varepsilon}{\sqrt{\varepsilon^2 - \Delta^2}}\left[\frac{\varepsilon + V}{\sqrt{(\varepsilon+V)^2 - \Delta_1^2}}\theta\left((\varepsilon+V)^2 - \Delta_1^2\right)\right.$$
$$\left. - \frac{|\varepsilon - V|}{\sqrt{(\varepsilon - V)^2 - \Delta_1^2}}\theta\left((\varepsilon - V)^2 - \Delta_1^2\right)\right]. \tag{106}$$

In the limit of small $w/\gamma \ll \Delta/T$ the same formula holds in the asymmetric scheme (fig. 8a) as far as imbalance can be neglected.

From eq. (102) it follows that the relative change of the order parameter is

$$\frac{\delta\Delta}{\Delta} \approx \frac{T^2}{\Delta^2}\frac{4\pi^2}{7\zeta(3)}F. \tag{107}$$

Formulas (106) and (107) permit to calculate the voltage dependence of the change in the order parameter at tunneling. In order to do so we take $\Delta_1 > \Delta$. Then at low voltage $V \ll (\Delta_1 - \Delta)$

$$\frac{\delta\Delta}{\Delta} = \frac{8\pi^2}{7\zeta(3)}\frac{T^2}{\Delta^2}\frac{wV^2}{\gamma T\Delta_1}\int_1^\infty \frac{x^2\,\mathrm{d}x}{\sqrt{x^2-1}\left(x^2 - \Delta^2/\Delta_1^2\right)^{3/2}} \tag{108}$$

At voltages $|V - \Delta_1 + \Delta| \ll \Delta$, with logarithmic accuracy we have

$$\frac{\delta\Delta}{\Delta} = \frac{2\pi^2}{7\zeta(3)}\frac{T^2}{\Delta^2}\frac{w}{\gamma T}(\Delta_1 - \Delta)\sqrt{\frac{\Delta_1}{\Delta}}\ln\frac{\Delta}{|V - \Delta_1 + \Delta|} \tag{109}$$

At voltages $|V - \Delta_1 - \Delta| \ll \Delta$

$$\frac{\delta\Delta}{\Delta} = \frac{2\pi^3}{7\zeta(3)}\frac{w}{\gamma T}(\Delta_1 + \Delta)\sqrt{\frac{\Delta_1}{\Delta}}\frac{T^2}{\Delta^2}\theta(\Delta_1 + \Delta - V) \tag{110}$$

It is seen that for voltages surpassing the value $A_1 + A$ stimulation is absent.
It should be noted that formulae (106)-(110) are valid if

$$\Delta, \Delta_1, V \ll T.$$

Gray (1978) was the first to observe experimentally the tunnel-injectionstimulated superconductivity effect. Superconductivity enhancement was observed up to voltages equal to the sum of the gaps according to formula (110). At high voltages superconductivity suppression

occurred, apparently, due to the phonon system deviating from equilibrium. Chang (1978) calculated injection stimulation with phonon nonequilibrium as well as with electromagnetic radiation.

Detailed experimental and theoretical researches into tunnel injectionstimulated superconductivity were carried out by Chi and Clarke (1979) for aluminium contacts. The theoretical and experimental results agreed well up to voltages $\Delta_1 - \Delta$ in agreement with formula (109). At high voltages the agreement was worse because of phonon non-equilibrium.

19.6 6. Investigation of stability of nonequilibrium states created by microwave radiation $\omega < 24$ near T_c.

Stability of nonequilibrium states occurs owing to the balance of pumping and energy exchange with a thermostat. The local stability of such states means that infinitesimal initial fluctuations attenuate in time. These fluctuations can not be obligatory homogeneous in this case. A superconductor in a nonequilibrium state can, in principle, show instability with respect both to infinitesimal and to finite fluctuations.

In this connection the paper of Eckern et al. (1979) on stability at microwave pumping near the transition temperature should be mentioned. Eckern et al. studied, in particular, the stability with regard to large fluctuations. Using the method of Langevin forces they showed that between T_c and $T_{c\,\max}$ as determined from eq. (41) a temperature T_k exists, at which a jump-like transition to the normal state occurs. At temperatures in the range $T_k < T < T_{c\,\max}$ the superconducting state is overheated.

A superconductor is an example of a system where the pumping source and the diffusion coefficient depend on the order parameter determined from the BCS condition as well. All this makes the analysis of stability of superconductor nonequilibrium states a non-trivial problem. It is not the aim of the present chapter to give a detailed survey on the analysis of stability at different ways of pumping. Only microwave radiation with frequency $\omega < 2\Delta$ and temperatures near the critical are studied. Spatially heterogeneous fluctuations are taken to be one-dimensional.

The kinetic equation and the Ginzburg-Landau equation summarized for the non-equilibrium case have the form

$$-\frac{D}{2\gamma}\frac{\partial 2n}{\partial x^2}\frac{\sqrt{\varepsilon^2-\Delta^2}}{\varepsilon}+(n-n_F)=\frac{\alpha}{\gamma}\left[\frac{\varepsilon(\varepsilon-\omega)+\Delta^2}{\varepsilon\sqrt{(\varepsilon-\omega)^2-\Delta^2}}\,(n_{\varepsilon-\omega}-n_\varepsilon)\,\theta(\varepsilon-\Delta-\omega)\right.$$
$$\left.-\frac{\varepsilon(\varepsilon+\omega)+\Delta^2}{\varepsilon_V}\,(n_\varepsilon-n_{\varepsilon+\omega})\,\theta(\varepsilon-\Delta)\right] \tag{111}$$

$$\Delta\left[\frac{T_c-T}{T}-\frac{7\zeta(3)}{8\pi^2}\frac{\Delta^2}{T^2}+F\right]+\frac{\pi D}{8T}\frac{\partial^2\Delta}{\partial x^2}=0 \tag{112}$$

F is defined by the ratio (27).

To analyse the local stability of the system (111), (112), time derivatives should be taken into account. We restrict ourselves to investigation of the boundary of the stability region. For this purpose it is sufficient to use static equations. System (111), (112) is linearized with respect to small deviations $\Delta \to \Delta + \Delta_1$ and $n \to n + n_1$, where small values $\Delta_1 \propto n_1 \propto e^{ikx}$. Frequencies $\omega \ll \Delta$, and consequently large values of k, are considered to have a rather large first term in the left-hand side of eq. (111). Then the value F is to be varied only on
Δ, provided n is constant. It gives for $(\varepsilon - \Delta) \ll \Delta$.

After integration by parts we obtain

$$\delta F = -\Delta_1 \sqrt{\frac{2}{\Delta}} \int_{\Delta}^{\infty} \frac{\mathrm{d}\varepsilon}{\sqrt{\varepsilon - \Delta}} \frac{\partial n'_{\varepsilon}}{\partial \varepsilon} \tag{113}$$

The correction to distribution the function at $\omega \ll \Delta$ and $\Delta < \varepsilon < \Delta + \omega$ is

$$n'_e = -\frac{\alpha}{\gamma} \frac{\omega}{4\ \mathrm{T}} \sqrt{\frac{2A}{\varepsilon + \omega - A}} \cdot \frac{\sqrt{\varepsilon - A}}{\sqrt{\varepsilon - A} + \alpha\sqrt{2A}} \tag{114}$$

This formula takes into account the singularity near threshold shown in fig. 1. Formulas (113) and (114) were derived by Ginzburg and Spivak (1981). In their paper. from formulas analogous to (113), (114) the conclusion about local instability was drawn as well. By substituting eq. (114) into eq. (113) and varying equation (122). the dispersion law of low fluctuations is obtained

$$\sqrt{\frac{2\omega}{\Delta}} \ln\left(\frac{Dk^2}{\gamma}\sqrt{\frac{\omega}{\Delta}}\right) - \frac{\pi D k^2}{8\Delta} = \frac{7\zeta(3)}{\pi^2}\frac{\Delta}{T} \quad \frac{Dk^2}{\gamma}\sqrt{\frac{\omega}{\Delta}} \geqslant 1. \tag{115}$$

Omitting logarithmical dependences, the position of the stability boundary is determined by the relation

$$\frac{A}{T}\sqrt{\frac{A}{(1)}} \propto 1 \tag{116}$$

At these values of the order parameter. as follows from formula (37). the . 1 enhancement is not yet considerable. and temperature does not exceed $T_{\cdot}$ On raising the temperature when A is getting smaller than the value determined by formula (116), instability development will result either in inhomogeneous structure of the superconductor or in the normal state. This question needs further study.

Note, that in calculations of superconductivity stimulation the singularity of the distribution function near the point $\delta = A$ is insignificant. but it is very important in stability analysis. Veglecting this singularity one could draw the wrong conclusion that on microwave radiation the nonequilibrium state of a superconductor is always locally stable up to the maximum temperature.

The validity of formula (115) is basicaliy associated with the presence of root singularity in density of states. Singularity spreading must be small:

$$\varepsilon_0 \ll \Delta \left(\frac{\alpha}{\gamma}\right)^2. \tag{117}$$

Note that formula (115) is valid if the condition $A(\alpha/\gamma)^2 \ll \omega$ is obeyed. The instability considered does not occur in superconductors where the singularity is spread by phonons and inhomogeneities of the sample. Moreover, it is not realized, apparently, at high intensities $(\alpha/\gamma)\sqrt{\Delta/\omega} \gg 1$, when the distribution function is spread strongly.

Hence the conclusion is that in superconductors with a sharp peak in the density of states the experimental observation of superconductivity stimulation becomes complicated due to possible instability. The theory of stimulation of superconductivity reported in previous sections refers to the case of slightly spread singularity in the density of states on the interval of energies not higher than ω.

20 Dynamical Effects in Nonequilibrium Superconductors: Some Experimental Perspectives by Kadin, Goldman

20.1 1. Introduction

Dynamical processes on a microscopic level play an essential part in all major phenomena in condensed matter physics. What is more remarkable in the case of superconductivity is that these microscopic processes are strongly coupled to the macroscopic order parameter. It is the interaction between dynamics on these two levels that gives rise to the great richness of phenomena in nonequilibrium superconductivity.

In order to obtain a clear picture of the nature of the nonequilibrium state, it is important to consider the equilibrium state and how it is maintained. For many purposes, a superconductor can be considered a coupled system of three components: the condensate, the quasiparticles, and the phonons (see fig. 1). The ground state condensate of the Cooper pairs carries all of the "super" properties of superconductivity, and is characterized by a complex order parameter, or equivalently as will be shown below, by the magnitude of the energy gap A and the condensate chemical potential $\varepsilon_{..}$At a temperature of absolute zero, the condensate constitutes the entire system, but for higher T, excitations above the condensate appear as quasiparticles. Since the quasiparticles are charged (either electron-like or hole-like), charge as well as energy can be transferred between the condensate and the quasiparticles. The quasiparticle system is characterized by a distribution function $f(6)$. which plays a central role in nonequilibrium superconductivity. Finally, the quasiparticles are coupled to the phonons, and these two systems can exchange energy, but not, of course. charge. We recognize that the existence of the Cooper pairs

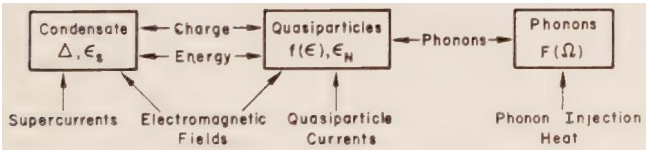


Fig. 1. Schematic picture of a superconductor. comprised of the condensate the quasiparticles and the phonons. Different types of probes and perturbations couple directly to the different subsystems of the superconductor.

requires the exchange of virtual phonons, but for our purposes, the condensate and the phonons can be considered as not directly interacting.

Thermal equilibrium is maintained by allowing the phonons in the superconductor to exchange energy with a thermal bath at temperature T (in practice, usually via phonon coupling to some other system or material). The phonons in turn interact with the quasiparticles via inelastic electron-phonon scattering, maintaining a thermal distribution of quasiparticles. The superconducting condensate carries no entropy, and thus is effectively at $T = 0$. However, it is coupled to the quasiparticles by the BCS gap equation and by overall charge neutrality, so that in equilibrium a thermal value $\Delta(T)$ results.

Although we will identify a generalized two-fluid picture from the above separation of condensate and quasiparticles, we point out that this is distinctly different from the old two-fluid picture where some of the electrons were effectively superconducting and the rest were normal (Gorter and Casimir 1934). Here, in thermal equilibrium, all of the electronic charge is contained in the condensate, and the net charge in the quasiparticles is zero, there being equal numbers on the electron-like and the hole-like branches of the quasiparticle spectrum. This requirement need not hold in the nonequilibrium state, leading to the concept of quasiparticle

charge imbalance [discussed in the review in this volume by Clarke (1985)], which has considerable bearing on several aspects of nonequilibrium superconductivity to be discussed in the present chapter.

Generally speaking, any mechanism that couples to a system so as to probe its state can also be used to perturb it from its equilibrium condition. Often, the same device is used both as a perturbation and as a probe, or in other language as both the injector and the detector. In our schematic picture of superconductivity in fig. 1, we have listed some of the major types of probes and the subsystems with which they directly interact. Supercurrents and pairtunneling couple to the condensate, while quasiparticle currents and tunneling affect the quasiparticle distribution. Electromagnetic fields couple to both electronic components, while phonon injection and external heating enter the superconductor via the phonon system.

The various types of external perturbations can also be classified in another way, according to whether their primary effect is to transfer charge or energy to the superconductor. Energy-mode perturbations (or "condensation processes") ultimately affect the magnitude of the energy gap Δ, and are similar in some respects to heating and cooling. Phonons and light are of this class, and quasiparticle tunneling has a strong energy-mode component. Charge-mode perturbations ("conversion processes") couple to electrochemical potentials, currents, and the phase of the superconducting order parameter, and produce the charge imbalance mentioned above. Examples are external currents and tunneling injection. Another equivalent set of terminology for these two modes is longitudinal and transverse (Schmid and Schön 1975a), according to
whether the induced change in the complex order parameter represented in the complex plane is parallel to (a change in the magnitude) or perpendicular to (a change in the phase) the equilibrium order parameter.

Most external perturbations can be applied in either a steady-state (DC) mode, a modulated (AC) mode, or a transient (pulsed) mode. In all of these cases, what is generally inferred is a relaxation time of the quantity being measured, usually a macroscopic variable. This is typically related to the characteristic time of the underlying microscopic process, but the macroscopic and microscopic times need not be the same. Furthermore, the DC relaxation time may even be different from the transient response time for the same physical quantity, for example the energy gap A. In addition, if spatially resolved measurements yield input on characteristic lengths as well, a more complete dynamical equation can be inferred.

One can also apply a high frequency AC field to a superconductor in order to couple to an AC collective mode or another nonequilibrium wave phenomenon. In fact, if one makes use of the AC Josephson effect, one can obtain this sort of AC coupling by applying a DC field. One can therefore use a Josephson junction (or other weak link) both to induce and to detect an AC nonequilibrium perturbation, via an analysis of the DC response. This is the basis for the measurements of the "pair-field susceptibility" (Ferrell 1969, Scalapino 1970), where a DC electromagnetic field gives rise to an effective pair field that is modulated in time and space. The resulting modulated nonequilibrium perturbation is measured using a DC supercurrent.

One of these collective modes, associated with a charge-mode perturbation (Schmid and Schön 1975b, Artemenko and Volkov 1975), has been referred to as a "charge imbalance wave". One can make use of a quantitative analogy between these waves in a generalized two-fluid picture of superconductivity, and electromagnetic waves propagating down a transmission line (Kadin et al. 1980), to provide insight into a range of phenomena in nonequilibrium superconductivity. One particularly interesting application is to the phase-slip center (Rieger et al. 1972 and Skocpol et al. 1974a), involving the currentinduced breakdown of superconductivity in a quasi one-dimensional filament.

Another superconducting system which is rich in dynamical nonequilibrium phenomena is the microbridge, a short superconducting bridge coupling two superconducting banks essentially

in equilibrium. The very large local current densities in the bridge region drive the superconducting order parameter into oscillations at the Josephson frequency, leading to a series of effects, many of which are evident in the DC $I-V$ characteristics. Because of these driven oscillations, closely-spaced microbridges or phase-slip centers also interact in a way that can lead these oscillations to become synchronized.

A set of recent reviews of the field of nonequilibrium superconductivity, in addition to those in the present volume, may be found in the proceedings of the 1980 Maratea summer school, edited by Gray (1981a). Other reviews that
complement or overlap the present treatment are those by Pals et al. (1982), Lindelof (1981), Pethick and Smith (1979, 1980), Artemenko and Volkov (1979), Tinkham (1979), Likharev (1979), Aronov and Spivak (1978), Chang and Scalapino (1978), Dmitriev and Khristenko (1978), Kaplan et al. (1976); Entin-Wohlman and Orbach (1978, 1979), and Langenberg (1974).

We continue the chapter in section 2 with a review of the theoretical framework within which we will work, with an emphasis on the quasiparticle distribution function and dynamical equations of the order parameter, working up to a discussion of charge imbalance waves. In section 3, we show how the $I-V$ characteristics of a Josephson tunnel junction can be used to determine the order parameter dynamics, and the significance of the propagating collective mode thus inferred. We follow this in section 4 with the development of a simple dynamical model for the phase-slip center, and analyze the characteristics of microbridges, both single and in combination, with an emphasis on those features that can be explained via simple semiphenomenological pictures. Finally, the chapter closes in section 5 with a brief summary and a discussion of the potential impact of nonequilibrium superconductivity on related work in the future, both basic and applied.

20.2 2. Basic theory of nonequilibrium superconductors

20.2.1 2.1. Quasiparticle distributions and self-consistency equations

For a simple BCS-superconductor with a gap A, the condensate consists of an assemblage of momentum-paired electron states ($k, -k$), with an occupation fraction v_k^2 of electron k-states (see fig. 2a) given by

$$v_k^2 = (1 - \xi_k/\varepsilon_k)/2, \tag{2.1}$$

where $\xi_k = \varepsilon_k - \varepsilon_s$ is the (normal) electronic kinetic energy referred to the condensate chemical potential ε_s, and $E_k = [\xi_k^2 + A^2]^{1/2}$ is the quasiparticle excitation energy (fig. 2b). In equilibrium, ε_s coincides with the normal electronic Fermi energy ε_{F}, but this need not always be so. It is important to realize that the energy smearing in eq. (2.1) (i.e. the existence of empty states below ε_{s} and filled states above, even at $T = 0$) is an essential feature of the BCS ground state, in that it allows Cooper pairs near ε_s to scatter coherently around the Fermi sphere via exchange of virtual phonons, thus lowering their energies.

A quasiparticle excitation consists of a pairing state ($k, -k$) with one and only one of the two states occupied, thereby making it unavailable for pairing. Whether this quasiparticle represents an electron or a hole (or something in between) depends on the likelihood that this paired state would otherwise have been occupied in the condensate. For $\xi_k \ll 0$, both states would have been

occupied, making the quasiparticle a hole, for $\xi_h \gg 0$ the quasiparticle is likewise clearly an electron. For $\left|\check{\zeta}_k\right| < \Delta$, the paired state may or may not be in the condensate, giving the quasiparticle a mixed character with effective charge

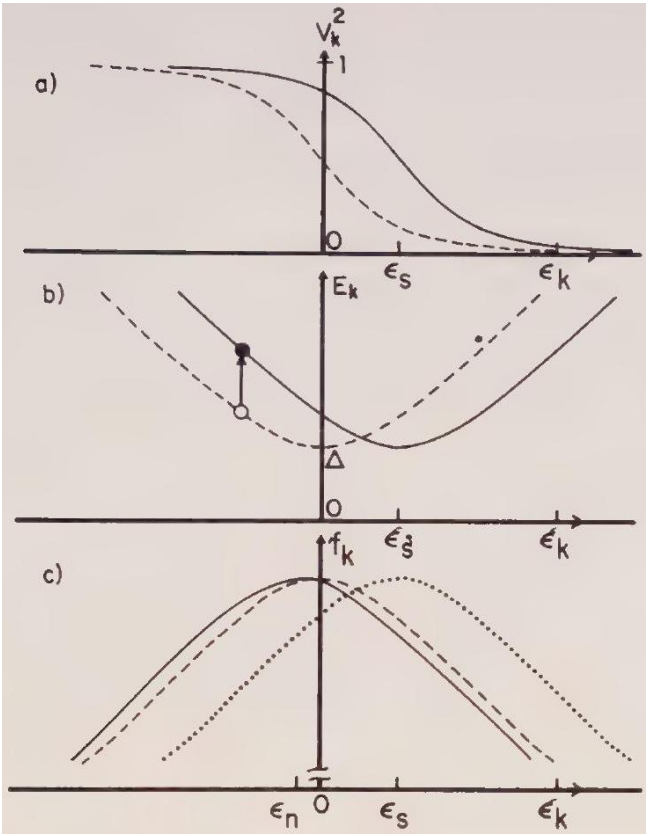


Fig. 2. The effects of a shift in the condensate chemical potential ε_{s} on the condensate and on the quasiparticles. The dashed lines indicate equilibrium, the solid lines disequilibrium, and the dotted line in (c) local equilibrium. (a) v_k^2 gives the occupation of electrons in the condensate. (b) A shift in ε_{s} shifts the excitation spectrum, but in the absence of inelastic collisions, a given quasiparticle remains at the same value of ε_k but changes its excitation energy E_k and its effective charge q_k. (c) If the nonequilibrium quasiparticles can be characterized by a quasi-equilibrium distribution $f_0\left(\varepsilon_k-\varepsilon_n\right)$ around a "normal" chemical potential ε_n, this is actually closer to the global equilibrium distribution $f_0\left(\varepsilon_k\right)$ than to the local equilibrium distribution $f_0\left(\varepsilon_k-\varepsilon_s\right)$. The extent of the disequilibrium in the figures here is exaggerated for clarity. (From Kadin et al. 1980.)}

$$q_k = e\left[v_k^2 - \left(1 - v_k^2\right)\right] = e\xi_k/\varepsilon_k. \tag{2.2}$$

The occupation of quasiparticle states is given by the distribution function $f\left(\varepsilon_k\right)$, which in thermal equilibrium is given by the Fermi function

$$f_0\left(\varepsilon_k\right) = \left[1 + \exp\left(E_k/k_{\mathrm{B}}T\right)\right]^{-1}. \tag{2.3}$$

Note that the form of this equilibrium distribution depends implicitly through E_k on the condensate parameters Λ and ε_s. These are determined from $f\left(\varepsilon_k\right)$ using two self-consistency equations, the first of which (the BCS gap equation) follows from energy considerations, and the second (the condensate potential equation) from charge conservation.

The BCS gap equation is usually presented in the form

$$1/V = \sum_k \left(1 - 2f_k\right)/2E_k = N(0)\int_0^{\hbar\omega_c} \mathrm{d}\varepsilon(1 - 2f(\varepsilon))/E \tag{2.4}$$

where Δ is contained implicitly in E_k. The upper limit $\hbar\omega_c$ is a necessary cut-off to prevent the integral from diverging, where ω_c is of the order of the phonon Debye frequency. Here $N(0)$ is the normal electronic density of states at the Fermi level for one spin, and we have assumed that $f(\varepsilon_k)$ is isotropic in momentum space. The gap equation can be written in a more tractable form if we note that

$$\int_0^{\hbar\omega_c} \frac{d\varepsilon}{E} \simeq \ln(2\hbar\omega_c) - \ln\Delta, \tag{2.5}$$

for $\Delta \ll \hbar\omega_c$. Since $f(\varepsilon) = 0$ for the case of $\Delta(T = 0)$, we obtain

$$-\ln[A/\Delta(0)] = \int_{-\alpha}^{\alpha} d\varepsilon f(\varepsilon) / \left[(\varepsilon - \varepsilon_s)^2 + \Delta^2\right]^{1/2}, \tag{2.6}$$

where now the integral is convergent, so that the cut-off is unnecessary.
For the condensate potential equation, we first define the total charge density in the quasiparticles as the charge imbalance (also sometimes referred to as "branch imbalance") (Tinkham and Clarke 1972)

$$Q^* = 2N(0) \int d\varepsilon q(\varepsilon) f(\varepsilon) \tag{2.7}$$

In equilibrium, $Q^* = 0$, since there are equal numbers of excitations on the electron-like and the hole-like branches of the quasiparticle spectrum. This need not be true for a nonequilibrium state, but the total electronic charge must still be essentially zero. This is true because charge neutrality is a metallic property that holds over far shorter times ($\varepsilon_0/\sigma \sim 10^{-19}$ s) and far shorter distances (the Thomas-Fermi screening length $\sim 1\mathring{A}$) than those relevant for superconductivity. The remaining charge must lie in the condensate, which can only occur if the condensate chemical potential ε_s has been shifted from its equilibrium value (Waldram 1975, Volkov and Zaitsev 1975):

$$Q^* = 2N(0)e \int \left(v^2\big|_{\varepsilon_s=0} - v^2\big|_{\varepsilon_s=0} \right) d\varepsilon = -2N(0)e\varepsilon_s. \tag{2.8}$$

Then

$$-\varepsilon_s = \int_{-\infty}^{\infty} d\varepsilon f(\varepsilon) (\varepsilon - \varepsilon_s) / \left[(\varepsilon - \varepsilon_s)^2 + \Lambda^2\right]^{1/2} \tag{2.9}$$

eq. (2.9) is the condensate potential equation. Note the similar self-consistent natures of eqs. (2.6) and (2.9). Thus, the condensate is sensitive to what are in effect two moments of the quasiparticle distribution $f(\varepsilon)$. At least for small deviations from equilibrium, the gap Δ depends on the even part of $f(\varepsilon)$ about ε_s, and the potential ε_s depends on the odd part.

The key to understanding nonequilibrium superconductors lies in the realization that while the consistency equations (2.6) and (2.9) should be valid down to times of order $h/\Delta \sim 10^{11} - 10^{-12}$ s (to establish the superconducting pairing), the quasiparticle distribution $f(\varepsilon)$ can change only on the much slower time scale of the inelastic electron-phonon collision time $\tau_E \sim 10^{-7} - 10^{-10}$ s (depending on the material). Therefore, although in principle Δ and ε_s can change very quickly, in practice they are locked into instantaneous quasiparticle distributions which are changing more slowly. A similar relation also holds in the spatial domain. It is important to note, however, that this entire approach breaks down in the case of a gapless superconductor (Gor'kov and Eliashberg 1968) (for $T > T_c$, or for a high concentration of magnetic impurities), where the condensate becomes largely decoupled from $f(\varepsilon)$, and the order parameter relaxation becomes governed by intrinsic condensate times (e.g. τ_{GL}, the Ginzburg-Landau relaxation time near T_c)

In principle, the distribution $f(\varepsilon)$ has as many degrees of freedom as there are quasiparticles. In practice, a small number of simple approximate forms appear to be relevant in many cases. For example, an energy-mode perturbation can simply heat up the quasiparticles, suggesting a distribution characterized by an effective electronic temperature $T^* > T$ (Parker 1975). This does not require that the phonons also be at T^*, since it is a nonequilibrium state. This distribution has been found to apply in a number of experimental situations. An alternative distribution has been proposed for an increased number of quasiparticles, which is characterized by the equilibrium T but a systematic shift in the excitation energy E by μ^* (Owen and Scalapino 1972), but a distribution purely of this type has not been seen experimentally.

For the charge-mode distribution, the simplest nonequilibrium distribution (Pethick and Smith 1979) is one given by

$$f_0\left(\varepsilon-\varepsilon_{\mathrm{n}}\right)=\left\{1+\exp\left(\left[\left(\varepsilon-\varepsilon_{\mathrm{n}}\right)^2+\Delta^2\right]^{1/2}/k_{\mathrm{B}}T\right)\right\}^{-1} \tag{2.10}$$

This is a thermal distribution, but one which as a function of electron kinetic energy ε has its maximum at a value ε_n, the effective normal chemical potential, different from both the "global equilibrium" value $\varepsilon_{\mathrm{r}}=0$, and the "local equilibrium" (with the nonequilibrium condensate) ε_s (see fig. 2c). One can
estimate the relative sizes of ε_{n} and ε_{s} (which must have opposite signs from charge conservation) by evaluating the charge imbalance Q^* in a Taylor series expansion in $(\varepsilon_s-\varepsilon_n)$, and retaining only the lowest order term. For T close to T_{c}, one has

$$Q^*=2N(0)\int \mathrm{d}\varepsilon q\left(\varepsilon-\varepsilon_{\mathrm{s}}\right) f_0\left(\varepsilon-\varepsilon_{\mathrm{n}}\right)\approx\left(\varepsilon_{\mathrm{s}}-\varepsilon_{\mathrm{n}}\right)2N(0)e\left(1-\pi\Delta/4k_{\mathrm{B}}T\right) \tag{2.11}$$

Comparing this to eq. (2.8), from electroneutrality we have, to lowest order in $\Lambda/k_{\mathrm{B}}T$, that

$$\varepsilon_{\mathrm{n}}\approx-\varepsilon_{\mathrm{s}}\left(\pi\Delta/4k_{\mathrm{B}}T\right). \tag{2.12}$$

Therefore, near T_c, when Δ is very small and there are many quasiparticles, a small shift in ε_{n} will require a very much larger shift in ε_{s} in the other direction in order to maintain electroneutrality.

There are a number of ways experimentally to induce a nonequilibrium value of $f(\varepsilon)$ rather directly. If a voltage is applied across a tunnel barrier between a superconductor and a normal metal, quasiparticles of one sign will tunnel into the superconductor, and quasiparticles of the other sign will be extracted. This will clearly induce a charge imbalance in the superconductor, but in addition a careful examination would show that more quasiparticles (with higher energy) are added than extracted. In general this latter effect will cause the gap to decrease (Chi and Clarke 1979, Gray 1978a). The counterelectrode of the tunnel junction can also be a superconductor, in which case it is possible to extract more quasiparticles than are injected, and to actually increase the gap in the superconductor with the smaller value of Δ, as shown experimentally by Chi and Clarke (1979).

Microwaves also act to change $f(\varepsilon)$ (Eliashberg 1970). If the energy of the microwave photon $\hbar\omega$ is less than the energy 2Δ required to break a pair, the photons cannot directly produce additional quasiparticles, but they can redistribute the quasiparticles already present, by increasing their energies. There may be, however, a decrease in the number of quasiparticles near the gap edge, which leads from the gap equation to an increase in the magnitude of the gap. This paradoxical effect, predicted by Eliashberg (1970), gives superconductive "cooling" as a consequence of microwave heating. Gap enhancement has been observed experimentally (Kommers and Clarke 1977, Pals and Dobben 1979, 1980, Hall et al. 1980), together with a relatively larger enhancement of the critical current J_c (Klapwijk and Mooij 1976a, Latyshev and Nad' 1976). Furthermore, a slight enhancement of T_{c} itself has also been observed for Al

films in the presence of microwaves (Klapwijk et al. 1977, Pals and Dobben 1979, Mooij et al. 1980). Note however, from the gap equation (2.6), that the enhanced gap can never be more than $A(0)$, and is usually much less because of heating effects. There is now general agreement that superconductivity is enhanced by microwaves although some anomalies remain. Dahlberg et al.
(1979) observed that critical current enhancement was not always accompanied by gap enhancement. Also Van Attekum and Ramekers (1982) and Van Attekum et al. (1983) found order parameter enhancement half that expected from critical current enhancement.

Similar critical current and gap enhancement effects has also been observed with injected monochromatic phonons rather than microwave photons (Tredwell and Jacobsen 1975, 1976, Seligson and Clarke 1983). A more complete discussion of stimulated superconductivity is carried out in the chapters of the present volume by Dmitriev et al. (1985) and Eliashberg and Ivlev (1985), and in the review by Dmitriev and Khristenko (1978).

Another type of nonequilibrium energy-mode state is one which develops a spatially inhomogeneous value of the gap, while the energy is being pumped into the system uniformly (Chang and Scalapino 1974, Baru and Sukhanov 1975, Elesin 1974, 1976, 1977a,b, Smith 1977, Eckern et al. 1979). This gap instability has been predicted for a sufficiently large input of energy from optical illumination, microwaves, and high energy tunnel injection. There has been some experimental verification of these effects (Iguchi 1978a,b, Iguchi and Langenberg 1980, Smith 1980), although it has proven difficult to unambiguously distinguish the real effect from that due to possible inhomogeneities in the sample and/or energy input (Dynes et al. 1977, Iguchi and Langenberg 1980, Gray and Willemsen 1978).

Quasiparticle tunneling is one of the standard methods for detecting a nonequilibrium distribution $f(\varepsilon)$ (Gray 1981b). Often a double tunnel junction configuration is used, where the center film is common to both junctions, and one junction (usually low resistance) is used for quasiparticle injection while the other (usually relatively high resistance) is used for detection. Since the tunnel conductance $\mathrm{d}I/\mathrm{d}V$ for voltages less than A is actually a measure of the quasiparticle density of states convoluted with a function representing thermal smearing, it is possible to determine $f(\varepsilon)$ rather directly (Smith 1980). In addition, the value of Δ is made evident by the increased current at $eV = \Delta$, enabling a check on the validity of the BCS gap equation (Gray 1981b).

Furthermore, tunnel junction probes can also be used to measure the nonequilibrium potential difference $\varepsilon_\mathrm{s} - \varepsilon_\mathrm{n}$ (Clarke 1972). Quasiparticle currents J_n are driven by a difference in the quasiparticle electrochemical potential $\mu_\mathrm{n} = \varepsilon_\mathrm{n} + e\phi$ (where ϕ is the usual electric potential), and supercurrents J_s are accelerated by a gradient in $\mu_s = \varepsilon_s + e\phi$. A normal counterelectrode will exchange charge with the quasiparticles, but not with the condensate (at least near T_c), and therefore in a potentiometric situation this normal probe will measure μ_n. On the other hand, a superconducting counterelectrode allows current flow via both the condensate and quasiparticle channels. In a stationary situation, μ_s must be constant in space, so that the superconducting probe will measure μ_s. Since μ_n will then not be constant across this junction, quasiparticle current will flow across the probe. However, this is canceled by

the counterflow of J_s, which does not need a potential gradient to drive it. The voltage measured potentiometrically between the two probes (fig. 3a) will thus be

$$\Phi = \left(\mu_\mathrm{n} - \mu_\mathrm{s}\right)/e = \left(\varepsilon_\mathrm{n} - \varepsilon_\mathrm{s}\right)/e. \tag{2.13}$$

Furthermore, the superconducting probe can even be an extension of the superconducting film, and the normal probe can also be a normal contact via a clean normal-superconducting boundary (see fig. 3b) (Yu and Mercereau 1972, 1975).

There is also a spatial aspect to problems in nonequilibrium superconductivity. For example, for current flow at a normal-superconducting boundary (Pippard et al. 1971), the current

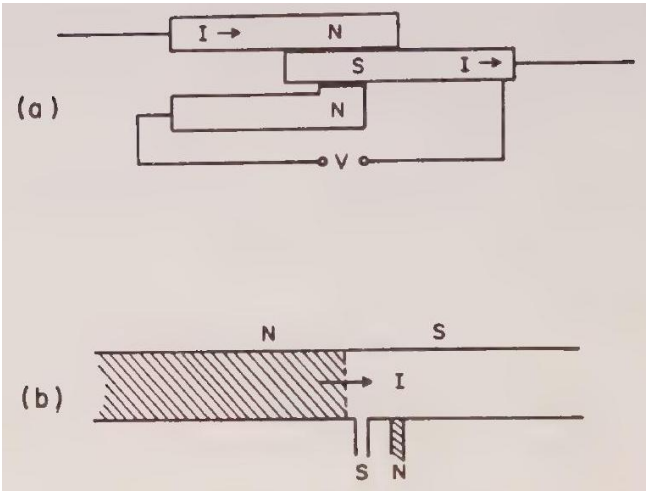


Fig. 3. Experimental configurations which yield a nonequilibrium quasiparticle potential difference. (a) Double tunnel-junction experiment of Clarke (1972). (b) Normal and superconducting microprobes near a current-carrying N/S boundary, as in the experiment of Yu and Mercereau (1972, 1975).

in the normal metal couples directly (at least close to T_c) to quasiparticle current in the superconductor. Since farther into the superconductor, this same current is carried by the condensate, there will be an excess boundary resistance (Pippard et al. 1971. Hsiang and Clarke 1980) accompanied by a local build-up near the boundary of quasiparticles of one sign, i.e. a charge imbalance. More generally, quasiparticle relaxation with a time τ_{R} leads to a characteristic quasiparticle diffusion length $\Lambda = (D\tau_{\mathrm{R}})^{1/2}$ over which the disequilibrium relaxes in space for a steady-state process, where D is the quasiparticle diffusion length. For high frequencies, a propagating wave solution is possible. In both cases, some of the same types of probes (tunneling, etc.) can be used to measure this spatial variation, provided they can be made small enough - typically several μm or less. For example, small

superconducting and normal tunnel junction probes of a superconducting strip placed near a phase-slip center have been used to measure the spatial variation of the electrochemical potential μ_{s} and μ_{n} of the condensate and the quasiparticles (see fig. 4) (Dolan and Jackel 1977, Stuivinga et al. 1982, 1983).

20.2.2 2.2. Dynamical equations and relaxation times

The simplest approach to superconducting dynamics, certainly on the phenomenological level, lies with the time-dependent Ginzburg-Landau (TDGL) equation, which extends the static GL equation to handle time-dependent phenomena (Cyrot 1973). The GL free energy density functional can be written in the form

$$f_{\mathrm{GL}} = f_{\mathrm{N}} + \alpha|\psi|^2 + (\beta/2)|\psi|^4 - \hbar^2/2m(\nabla - 2\mathrm{i}eA/\hbar)^2\psi, \tag{2.14}$$

where $\psi \sim \Delta\exp(\mathrm{i}\theta)$ is the complex superconducting order parameter. The simplest response of the condensate to changes is a diffusive one on the time scale (near T_{c}) of the GL relaxation

$$\tau_{\mathrm{GL}} = \pi\hbar/8k_{\mathrm{B}} \mid T - T_{\mathrm{c}}\mathrm{l}, \tag{2.15}$$

leading to a dynamical equation

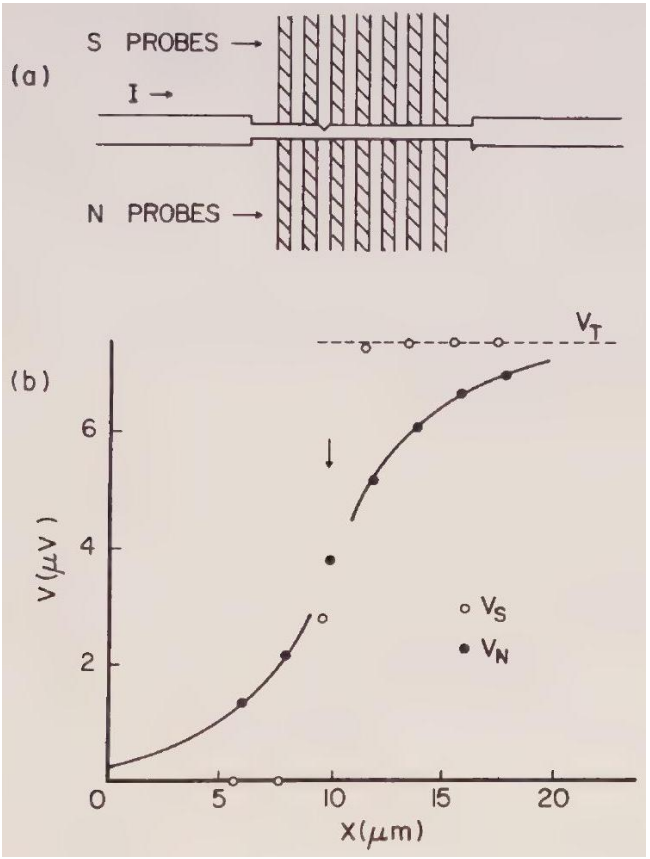


Fig. 4. Potentials near a PSC: the experiment of Dolan and Jackel (1977). (a) Experimental configuration, with arrays of superconducting and normal tunnel-junction microprobes. (b) Spatial dependence of the measured potentials. (From Dolan and Jackel 1977.)

$$\tau_{\rm GL}\partial\psi/\partial t = \pm\psi - (\beta/|\alpha|)|\psi|^2\psi + \xi^2\nabla^2\psi, \tag{2.16}$$

where $-\psi$ applies for $T > T_{\rm c}$. It can be shown that the GL coherence length ξ is actually the diffusion length for $\tau_{\rm GL}$ [i.e. $\xi = (D\tau_{\rm GL})^{1/2}$], emphasizing the diffusive nature of the equation.

Unfortunately, the validity of eq. (2.16) is far less universal than its static equivalent, essentially because it only takes into account the condensate and does not even consider the corresponding changes in the quasiparticles. For $T > T_{\rm c}$, the quasiparticle spectrum is normal, so that the quasiparticles are essentially decoupled from the condensate and can be largely ignored. The same is effectively true for any other "gapless" superconductor. In both cases, the simple TDGL equation is expected to hold. For the other limit, for a superconductor with a gap in the excitation spectrum, the order parameter is strongly coupled to the quasiparticle distribution function. Since quasiparticle relaxation is usually slower (except extremely close to T_c) than the corresponding intrinsic condensate relaxation times (e.g. $\tau_{\rm GL}$), the former provides a bottleneck in the relaxation process and must be examined in more detail.

Quasiparticle relaxation can involve either a recombination process that decreases the number of quasiparticles by two, or a scattering process that merely changes the excitation energy, but both are inelastic processes that in general require a phonon. This means that although the various relaxation processes are not all the same, most of them scale with the characteristic electron-phonon scattering time $\tau_{\rm E}$. This is the same time that enters into the electronic thermal conductivity in normal metals (although not the one associated with the electrical conductivity). The time τ_E is strongly temperature dependent, going as $1/T^3$ for $T \ll \theta_{\rm D}$ (Debye temperature). In fact, it is just as strongly energy-dependent as well, going as $1/E^3$ of the

phonon energy (hence the subscript **E** in τ_{E}). Nevertheless, at least for small deviations from equilibrium, τ_{E} can often be considered as essentially a constant characteristic of a particular material. Most of the experimental work on nonequilibrium superconductors has been done using simple elemental materials, namely Al, Sn, In or Pb . In general, the longer τ_E the more significant the nonequilibrium effects, making A1 with $\tau_{\mathrm{E}}(T_{\mathrm{c}}) \sim 10^{-8}$ often the material of choice. The others (Sn, In, and Pb , resp.) have values $3, 1.5$, and 0.5×10^{-10} s (Kaplan et al. 1976).

Another aspect of the relaxation problem is that it has been typically approached from the two opposite ends of the temperature range, which exhibit distinctly different properties. For $T \ll T_{\mathrm{c}}$, one has $k_{\mathrm{B}}T \ll \Delta$, and for a
state not too far from equilibrium the superconducting order parameter is unlikely to be perturbed substantially from equilibrium. However, any excess quasiparticles are likely to stay around for a long time, since recombination is a two-body process, and there are few equilibrium quasiparticles with which to recombine. In particular, the recombination time τ_R is given theoretically by

$$\tau_{\mathrm{R}} \sim \tau_E \exp\left(2\Delta/k_{\mathrm{B}}T\right). \tag{2.17}$$

This exponential form has been confirmed in several experiments from steadystate measurements (Langenberg 1974).

One persistent problem with these measurements, which exists as well for higher temperatures, has been referred to in the literature as "phonon trapping". Because of finite sample size and phonon mismatch at the boundaries between the superconducting film and the insulating substrate, the nonequilibrium recombination phonon with energy 24 may "decay" into a pair of quasiparticles in the superconductor (by breaking a Cooper pair) rather than simply leaving the film. This recycling of phonons may occur, on the average, a number of times before it finally leaves the film. This problem can be somewhat minimized by using a very thin film well-bonded to a crystalline substrate with similar acoustic properties (Kaplan 1979). An alternative analysis of the same problem can be made on the macroscopic level (a "simple heating" model) by considering the relative quality of thermal links between the quasiparticle system, the phonons in the film, and the external world in equilibrium at temperature T.

For the regime with $T \sim T_{\mathrm{c}}, \Delta \ll k_{\mathrm{B}}T$, the approach is somewhat different. Here, there are plenty of equilibrium quasiparticles so that quasiparticle recombination is not a bottleneck, and scattering and recombination occur at essentially the same rate $1/\tau_E$. In this regime, the order parameter is strongly perturbed by small changes in $f(\varepsilon)$, and great attention is paid to the relaxation times associated with macroscopic variations of the order parameter, namely those of the gap Δ and the potential ε_{s}.

Because of the strong coupling of the condensate and the quasiparticles in this regime close to T_c, the time measured in an experiment depends on the nature of the experiment, even for the same physical quantity. Taking the variation of the gap as an example, as the gap changes, the states, whether occupied or not, simply ride up or down, each individual state is conserved and remains at the same value of kinetic energy ε, provided no inelastic collisions occur (Schmid and Schön 1975a).

However, the equilibrium distribution is a function of the quasiparticle excitation energy E and hence of Δ, so that the instantaneous state of "local equilibrium" changes with Δ. Since one expects that collisions with phonons will relax the distribution toward this state of local equilibrium, rather than (directly) towards global equilibrium (with the equilibrium value of Δ), this coupled aspect of the collective relaxation requires careful consideration.

We consider first the relaxation of a longitudinal (energy) mode perturbation, in the regime close to T_c. In this case, every scattering event acts to change the energy of a quasiparticle by $\sim k_{\mathrm{B}}T$, which is more than sufficient to relax the disequilibrium. Then, the nonequilibrium

distribution will relax with a time τ_{E} towards the thermal distribution corresponding to the nonequilibrium value of the gap:

$$\partial f/\partial t = \left[f_0(\varepsilon, \Delta, T) - f\right]/\tau_{\mathrm{E}} + (\dot{f})_{\mathrm{inj}}. \tag{2.18}$$

Here, f is the actual instantaneous nonequilibrium distribution, which corresponds to the gap Δ from the BCS gap equation. For example, one might have $f \approx f_0\left(\varepsilon, A, T^* > T\right)$ where $A = A_{\mathrm{eq}}\left(T^*\right)$. It is important to recognize that f is relaxing toward a non-physical distribution that it can never actually achieve, the only physical equilibrium distribution being $f_0\left(\varepsilon, A_{\mathrm{eq}}\left(T\right), T\right)$. The nonphysical distribution corresponds to "local equilibrium" with the phonons at temperature T but not equilibrium with the condensate, whereas the "global equilibrium" distribution involves equilibrium with both. For that matter, the actual distribution f is effectively in quasi-equilibrium with the condensate, although not with the thermal phonons.

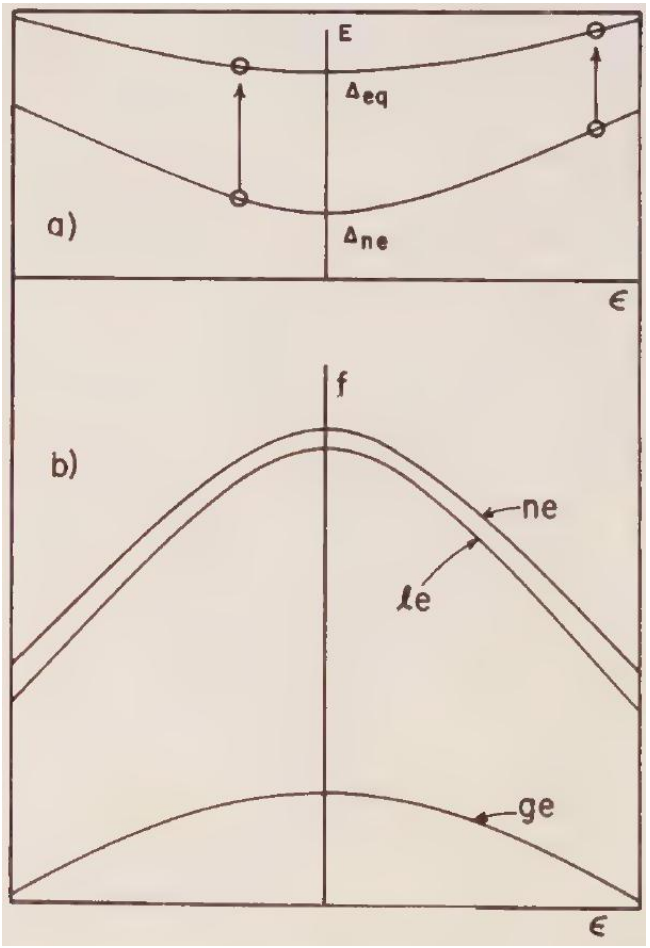


Fig. 5. Quasiparticle excitations energies (a) and distributions (b) for an energy-mode disequilibrium. The "hot" nonequilibrium (ne) distribution, the local equilibrium (ℓ e) distribution \$f_{0
\left(\varepsilon, \Delta_{ne}, T\right)\$, and the global equilibrium (ge) distribution $f_0\left(\varepsilon, \Delta_{\mathrm{eq}}, T\right)$ are indicated.}

Figure 5 illustrates the three relevant distributions for an initial "hot" nonequilibrium distribution f. As f relaxes toward the local equilibrium distribution $f_0(\varepsilon, \Delta, T), \Delta$ increases, causing the latter distribution to decrease and move away from f. Thus, f is relaxing toward a distribution which is continually moving away from it, so that the overall real-time relaxation time will clearly be greater than τ_{E}. Quantitatively, in evaluating the time-derivative of the

gap equation (2.6), one must take into account not only the direct change in f, but also the implicit change in E :

$$-\dot{\Delta}/\Delta = \int \mathrm{d}\varepsilon \left[\dot{f}/E - \left(f/E^2\right)(\mathrm{d}E/\mathrm{d}\Lambda)\dot{\Delta}\right]. \tag{2.19}$$

Grouping terms and evaluating integrals, all to lowest order in $\Delta/\Delta_{\mathrm{eq}}$ and $\Delta/k_{\mathrm{B}}T$, one obtains an overall relaxation time

$$\tau_{\Delta} = 3.7\tau_{\mathrm{E}}\left(k_{\mathrm{B}}T/\Delta\right). \tag{2.20}$$

This is the same time that has also been obtained by other methods, and has been referred to as $\tau_{\mathrm{R}}^{(\mathrm{L})}$ (for longitudinal) (Schmid and Schön 1975a). This divergence in the transient response time near T_{c} has in fact been directly observed, by examining in real-time the characteristics of a tunnel junction irradiated by a fast laser pulse (Schuller and Gray 1976, 1977). Other investigations of superconducting relaxation using laser probes have been carried out by Chi et al. (1981) and by Gorlach and Huebner (1983). We emphasize, however, that the effective relaxation time in steady state should remain as simply τ_E, since in steady state the excitation energy E remains fixed. This is reasonable, since this should go over continuously to a simple thermal healing length for $T > T_{\mathrm{c}}$.

For the relaxation of a transverse nonequilibrium distribution (a charge imbalance), the analysis is similar, although a bit more complicated. First, the appropriate microscopic relaxation time is not simply τ_{E}, as it was for the longitudinal case. In fact, charge imbalance relaxation cannot occur at all in the normal (non-superconducting) state, when a quasiparticle is difinitely either an electron or a hole. It can occur only via scattering events that change the effective charge of quasiparticle, namely those which involve states near the gap edge with mixed electron- hole character. Therefore, for $\Delta \ll k_{\mathrm{B}}T$ (i.e. T close to T_{c}), the average inelastic scattering event can relax a charge imbalance only to the order of $\Delta/k_{\mathrm{B}}T$. More detailed calculations have shown that the effective average microscopic relaxation time for charge imbalance τ_{Q*} is

$$\tau_{\mathrm{Q}*} = \left(4k_{\mathrm{B}}T/\pi\Delta\right)\tau_{\mathrm{E}} \tag{2.21}$$

in this regime close to T_c (Tinkham 1972, Schmid and Schön 1975a). This result has been well documented experimentally in steady-state measurements on the nonequilibrium potential ε_{s} in double-tunnel junction measurements of Clarke and co-workers (Clarke 1972, Clarke and Paterson 1974, Paterson
1978). Further confirmation has been found in steady-state measurements of the quasiparticle diffusion length near normal-superconducting boundaries and phase-slip centers (Dolan and Jackel 1977, Hsiang and Clarke 1980).

Given the above quantity $\tau_{\mathrm{Q}*}$ as the effective microscopic relaxation time for charge imbalance, one can proceed to obtain the corresponding transient relaxation time (analogously to that derived earlier for longitudinal relaxation), by writing first

$$\dot{f} = -\left[f - f_0\left(\varepsilon - \varepsilon_{\mathrm{s}}\right)\right]/\tau_{Q*}. \tag{2.22}$$

Note that $f_0\left(\varepsilon - \varepsilon_s\right)$ represents the local equilibrium distribution toward which f is relaxing, but which again is unphysical, since such an actual distribution would violate charge conservation. (Also see fig. 2c.) If the actual nonequilibrium distribution f is close to $f_0\left(\varepsilon - \varepsilon_{\mathrm{n}}\right)$, then near to T_{c}, as shown in eq. (2.12), ε_{n} is far closer to $\varepsilon_{\mathrm{F}} = 0$ than it is to ε_{s}, and for a transient process, this will enhance the relaxation towards global equilibrium. In fact, a detailed calculation shows that the transient relaxation time $\tau_{\mathrm{R}} = \tau_{\mathrm{E}}$ (Schmid and Schön 1975a, Kadin

et al. 1978). This particular result has not been directly confirmed experimentally, although some consequences of it have seen.

In certain circumstances, non-phonon forms of inelastic relaxation may become relevant. For example, when the electron-phonon time is very long (e.g. in Al), the direct electron-electron scattering may become significant. Furthermore, in sufficiently disordered materials, the electron electron rate may be enhanced substantially. Another scattering time that is relevant to many of the relaxation processes in superconductors is the elastic spin-flip scattering time τ_{s} from magnetic impurities. Since these events induce pairbreaking, even a small concentration can have a large effect on gap relaxation in both the longitudinal and the transverse modes (Schmid and Schön 1975a, Lemberger and Clarke 1981a, Aspen and Goldman 1979, 1981a). Other pairbreaking interactions, including an external magnetic field and a large supercurrent, have a comparable large effect on the relaxation times (Kadin et al. 1978, Lemberger and Clarke 1981b).

Another characteristic time of the condensate (which does not involve the electron-phonon time τ_E) is the supercurrent response τ_j. Consider a superconductor, in the two-fluid sense, as a parallel combination of an inductive channel with kinetic inductance $L_h = 4\pi i^2, c^2$ (i is the magnetic penetration depth), and a quasiparticle channel with normal resistance ρ near T_c. Then, a sudden change in the current (less than the critical current I_c) will initially be carried by the (noninductive) normal channel, until the supercurrent can respond in a time

$$\tau_{\mathrm{J}} = L_{\mathrm{k}}/\rho = \tau\,(n/n_{\mathrm{s}}) = \begin{cases} \tau/2\,(1 - T/T_{\mathrm{c}}) & (\text{ clean }), \\ 2k_{\mathrm{B}}T\hbar/\pi\Delta^2 & (\text{ dirty }), \end{cases} \tag{2.23}$$

evaluated for the clean and dirty limits near T_{c}. Typically, $\tau_{\mathrm{J}} \sim 10^{-11}$ s, smaller than τ_{E}, and a factor of 5.79 smaller than τ_{GL}. The relaxation and response times of the superconductor under various conditions are summarized in table 1.

Given the varied hierarchy of relaxation times and quasiparticle distributions, the previous discussion clearly suggests that no simple universal TDGL equation is likely to be appropriate for all situations. Nevertheless, a number of attempts have been made, with varying degrees of generality (Schmid 1981). One of these (Tinkham 1981, Schmid 1978) includes the nonequilibrium part of the distribution explicitly in the form

$$\left[\alpha + \delta\alpha^* + \left(\beta/T_{\mathrm{c}}^2\right)\Delta^2 - \xi^2(0)\nabla^2\right]\Delta = 0 \tag{2.25}$$

where the quantity

$$\delta\alpha^* = \delta T^*/T_{\mathrm{c}} = \int_{-\infty}^{\infty} \delta f(\varepsilon)/E \;\mathrm{d}\varepsilon \tag{2.26}$$

is known as the control function, and can also be expressed in terms of an effective temperature change $\delta \mathrm{T}^* = \delta\alpha^*\ \mathrm{T_c}$, although the distribution does not have to be strictly thermal. The time dependence of this equation comes in given the fact that δf, the deviation of the distribution from local equilibrium, decays with a characteristic time τ_{E}, leading to an equation

$$\left[1 - \psi^2 + \xi^2(T)\nabla^2\right]\psi = 2\tau_\Delta/\tau_{\mathrm{E}} \int^t \mathrm{d}t' \partial\psi/\partial t' \exp\left(t' - t\right)/\tau_{\mathrm{E}} \approx 2\tau_\Delta \psi \partial\psi/\partial t \tag{2.27}$$

where the latter form is appropriate when f changes slowly on the scale of τ_{E}. Both forms implictly assume that $\tau_{\mathrm{E}} \gg \tau_{\mathrm{GL}}$, and that f is changing slowly on the scale of τ_{GL}.

Another generalized TDGL equation, which attempts to interpolate from a regime dominated by τ_{GL} to one determined by τ_{E}, is that of Kramer and Watts-Tobin (1978), which can be written in the form

Table 1
Scattering and relaxation times in superconductors near $T_{c

$.}

General class	Characteristic time	Order of
Quasiparticle scattering times	Impurity elastic scattering τ	13-15
	Inelastic electron-phonon scattering τ_E	7-10
	Spin-flip scattering $\tau_{\rm s}$	$\lesssim 12$
Condensate relaxation times	Ginzburg Landau time $\tau_{\rm GL} \sim 0.4\hbar/k_{\rm B}T_{\rm c}\left(1-T/T_{\rm c}\right)$	10-11
Coupled system relaxation	Energy-mode transient relaxation $\tau_\Delta \sim 1.2\tau_{\rm E}\left(1-T/T_{\rm c}\right)^{-1/2}$	6-9
	Energy-mode steady-state relaxation	7-10
	$\sim \tau_{\rm E}$ Charge-mode transient relaxation	7-10
	$\sim \tau_{\rm E}$ Charge-mode steady-state relaxation $\tau_{Q^*} \sim 0.4\tau_{\rm E}\left(1-T/T_{\rm c}\right)^{-1/2}$	6-9

$$\left[1-|\psi|^2+\xi^2(T)\nabla^2\right]\psi=\left[\frac{\partial}{\partial t}+\frac{2ie\phi}{h}+\frac{1}{2}\gamma^2\frac{\partial f^2}{\partial t}\right]\psi\left[\frac{u}{\left[1+\gamma^2 f^2\right]^{1/2}}\right] \tag{2.28}$$

where $\gamma = 2\tau_E\Delta/h, u = 5.79$ from TDGL theory, and $f = |\psi/\psi_{\rm eq}\left(T\right)|$. It appears, however, to be somewhat more restricted in its applicability than eq. (2.27) above. A further point about these two sets of equations is that both were derived primarily to deal with energy-mode nonequilibrium states. Neither contains the terms which would describe the propagating charge imbalance waves that we will discuss in section 3.

An experiment by Pals and Wolter (1979) (also Wolter et al. 1981a,b) brings out some of the issues that we have been discussing in relation to relaxation times and dynamical equations. They applied a sharp current step with $I > I_{\rm c}$ to a narrow superconducting Al microstrip, and measured the delay time between the application of the current step and the development of a voltage across the strip. This delay time was of order τ_1, but dependent on the current and the temperature; the larger the current the faster the development of a voltage. A simple qualitative explanation was proposed by Tinkham (1981) and subsequently made more rigorous by Geier and Schön (1982), given the condition, generally valid for Al , that $\tau_{\rm J} \ll \tau_{\rm E}$. Over a time $\sim \tau_{\rm J}$, the entire current step changes from normal current $J_{\rm n}$ to supercurrent $J_{\rm s}$. This would clearly be expected to give a narrow voltage pulse, but it would be too fast to be resolved. In the presence of the supercurrent, the magnitude of the superconducting order parameter is depressed, but not totally to zero, since the quasiparticle distribution is one that is appropriate for a larger gap. As the distribution f decays, Δ decreases along with it, until the condition is reached that the supercurrent can no longer carry the entire current. Then a voltage begins to appear, and the order parameter suddenly (i.e. over a time $\sim \tau_{\rm J}$) collapses. The more complete calculation has been made from eq. (2.27), taking the supercurrent density $j = f^2 g$, and using the full integro differential form, and it confirms the basic picture we have been discussing (Geier and Schön 1982). Subsequent experimental investigations have tended to confirm this approach in more detail (Frank et al. 1983, Frank and Tinkham 1983, Pals et al. 1982).

20.2.3 2.3. Charge imbalance dynamics and the transmission-line picture

It was believed for quite some time that the propagating mode of the superconducting order parameter, because of the electric charge, was at the
plasma frequency (Anderson 1958). A mode with an acoustic dispersion relation was, in fact, observed by Carlson and Goldman (1975, 1976), from measurements of the pair-field susceptibility (to be discussed in the next section). Subsequent analysis showed that this could occur via a counterflow of supercurrent J_s and "normal" quasiparticle current J_n (Schmid and Schön 1975b, Artemenko and Volkov 1975). What was not appreciated at the time any of this work was done was that Thouless and Tilley (1961) had much earlier discussed phonon-like modes in charged superconductors from a rather different point of view. We will examine this phenomenon from the point of view of charge imbalance, which provides a clear and consistent picture of these waves. In essence, a net inflow of J_n will produce a charge imbalance, which by electroneutrality must be accompanied by a net outflow of J_s and a shift in ε_s. This in turn acts as a restoring force to produce currents in the opposite direction. These oscillations do in fact propagate, and can be viewed as waves of charge imbalance. The waves are, however, relatively heavily damped because of charge imbalance decay (by dissipative electron-phonon collisions), damping out over a distance of order of the transverse mode quasiparticle diffusion length $\Lambda_{Q}* = (D\tau_{Q}*)^{1/2} = 1 - 10\mu$ m.

In the regime close to T_c, a simple analog model for these charge imbalance waves has been developed, using signal propagation down a transmission line to represent charge imbalance waves propagating down a nonequilibrium superconductor (Kadin et al. 1980). In the relevant regime, the equations governing the transmission line are isomorphous to those in the generalized two-fluid model of the nonequilibrium superconductor (Pethick and Smith 1979). This heuristic framework will be presented below, and it will be used again in a later section for a model for the phase-slip center.

In order to deal with spatially inhomogeneous disequilibria, we use the electrochemical potentials μ_c for the superfluid condensate and μ_n for the quasiparticles, as defined earlier. Close to T_c, since ε_n is small, $\mu_n \approx e\phi$. We then use the standard GL expressions $\mu_s = -(h/2)\mathrm{d}\theta/\mathrm{d}t$ and

$$\boldsymbol{J}_s = n_s e v_s = (n_s e/2m)\left(\hbar\nabla\theta - 2e\boldsymbol{A}\right) \tag{2.29}$$

to obtain the following equation for the time evolution of $\boldsymbol{J}_s$:

$$\tau_J \dot{\boldsymbol{J}}_s = -\sigma\nabla\mu_s/e - \sigma\dot{A} = \sigma\boldsymbol{E} + D\nabla Q^*, \tag{2.30}$$

where $E = -\nabla\varphi - \mathrm{d}A/\mathrm{d}t$ is the electric field, and $\sigma = \mathrm{n}e^2\tau/m = 2N(0)e^2D$ is the normal electronic conductivity. For the normal current density J_n, we use the usual relation

$$J_n = \sigma E = -\sigma\nabla\mu_n/e - \sigma\dot{A} \tag{2.31}$$

but with the understanding that this is a good approximation only near T_c, where most of the quasiparticles have a well defined charge $\pm e$. Pethick and Smith (1979) have compared the true normal current (defined by $\boldsymbol{J}_n = \boldsymbol{J} - \boldsymbol{J}_-$) with the current carried by the flow of quasiparticles (which they call $\boldsymbol{J}_n^0$), and
have demonstrated that the distinction between these two goes to zero as $\Delta/k_B T$, as do the corrections to eq. (2.31) above.

The presence of $\boldsymbol{J_n}$ means that charge can leave the quasiparticle system in a given region of space not only through inelastic scattering, but also through the net inflow or outflow of quasiparticle current as determined by the term $\boldsymbol{\nabla}\cdot\boldsymbol{J}_n$. Because this acts to produce a direct

change in the distribution function, it is subject to the same enhancement factor due to the condensate response as that due to charge imbalance decay or quasiparticle injection. Thus we have

$$\dot{Q}^* = (4k_{\rm B}T/\pi\Delta)\left[\left(-\dot{Q}^*/\tau_{Q*}\right) - \nabla\cdot J_{\rm n}\right]. \tag{2.32}$$

If we take the $\boldsymbol{\nabla}\cdot\left(\tau_{\rm J}\dot{\boldsymbol{J}}_{\rm s} - \boldsymbol{J}_{\rm n}\right)$ from eqs. (2.30) and (2.31), and τ_J times the time derivative of eq. (2.32), and assume $\boldsymbol{\nabla}\cdot\boldsymbol{J}_{\rm tot} = 0$ from electro-neutrality, we obtain the following partial differential equation involving only the charge imbalance Q^* :

$$D\tau_{Q*}\nabla^2 Q^* = \tau_{\rm J}\tau_{\rm E}\ddot{Q}^* + (\tau_{\rm J}+\tau_{\rm E})\,\dot{Q}^* + Q^* \tag{2.33}$$

This is the charge imbalance wave equation we have been seeking. In the low frequency limit $\omega \ll \tau_{\rm J}^{-1}, \tau_{\rm E}^{-1}$, it describes charge imbalance decay with a characteristic decay length $\Lambda_{Q*} = (\mathrm{D}\tau_{Q*})^{1/2}$ (henceforth simply Λ will be used). This length, as pointed out earlier, has been used to characterize the penetration of an electric field into a superconductor-normal metal interface. In the high frequency limit ($\omega \gg \tau_{\rm E}^{-1}, \tau_{\rm F}^{-1}$), eq. (2.33) describes waves of charge imbalance, propagating with velocity $v = \Lambda/\left(\tau_{\rm J}\tau_{\rm E}\right)^{1/2}$. Substituting the clean and dirty limit formulas for $\tau_{\rm J}$, we have

$$v = \begin{cases} 0.53 v_{\rm F}(1-t)^{1/4} & (\text{ clean }), \\ 0.61 v_{\rm F}\,(l/\xi_0)\,(1-t)^{1/4} & (\text{ dirty }), \end{cases} \tag{2.34}$$

where $v_{\rm F}$ is the Fermi velocity, $l = v_{\rm F}\tau$ is the mean free path, and $\xi_0 = \hbar v_{\rm F}/\pi\Delta(0)$ is the BCS coherence length. These expressions are identical to those initially derived for this propagating mode within other theoretical frameworks (Schmid and Schön 1975b, Artemenko and Volkov 1975).

For the more general case where neither frequency limit is appropriate, eq. (2.33) describes damped dispersive waves of charge imbalance with the dispersion relation

$$-\Lambda^2 K^2 = (1+i\omega\tau_{\rm J})\,(1+i\omega\tau_{\rm E}) \tag{2.35}$$

Thus, the two phenomena of DC electric field penetration into a superconductor and the high-frequency collective mode are both special cases of the more general phenomenon of charge imbalance dynamics in a superconductor.

These relationships can be represented in an appealing picture by reference to fig. 6. If we define the gauge-invariant nonequilibrium potential Φ

$$\Phi = \phi + \hbar\dot{\theta}/2e = -\varepsilon_{\rm s}/e = Q^*/2N(0)e^2 \tag{2.36}$$

we can rewrite eqs. (2.32) and (2.33) in the form (for a one-dimensional wire with cross-sectional area A)

$$\frac{\partial I_{\rm n}}{\partial x} + G\Phi + C\dot{\Phi} = 0, \tag{2.37}$$

$$\frac{\partial \Phi}{\partial x} + RI_{\rm n} - L\dot{I}_{\rm s} = 0, \tag{2.38}$$

where the parameters (each per unit length) are:

$$R = 1/\sigma A, \quad G = \sigma A/\Lambda^2, \quad L = \tau_{\rm J}/\sigma A, \quad C = 2N(0)e^2 A\,(\pi\Delta/4k_{\rm B}T)\,, \tag{2.39}$$

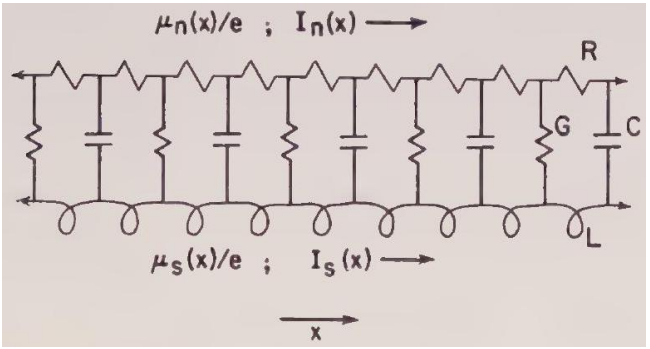


Fig. 6. Transmission-line equivalent of the charge imbalance wave equation. (From Kadin et al. 1980.)

This system of equations is isomorphic to the (standard) equations governing current flow on the transmission line of fig. 6. The resistive line represents the channel for the normal current $I_{\rm n}$ and its voltage $\mu_{\rm n}/e$, and the inductive line represents the condensate channel with I_s and μ_s/e (ignoring the magnetic vector potential A). The voltage between the lines is the nonequilibrium potential $\Phi = (\mu_{\rm n} - \mu_{\rm c})/e$. Equations (2.37) and (2.38) then follow directly from Kirchhoff's laws.

The circuit parameters R, L, C, and G have a simple and appealing physical interpretation. The relaxation of Φ is governed by the time constant $\tau_{\rm E} = C/G$, while the ratio L/R is the response time $\tau_{\rm f}$ for the supercurrent when $\Phi = 0$. The resistance per unit length R is just that, while the inductance per unit length L is the usual London theory kinetic inductance of the supercurrent.

To assist in the interpretation of C and G, we introduce the quantity

$$Q_{\rm n} = (\pi\Delta/4k_{\rm B}T)\, Q^*, \tag{2.40}$$

which is a measure of the departure of the distribution function from global equilibrium, as distinguished from Q^*, which measures the departure from local equilibrium (Pethick and Smith 1979). Neglecting conversion processes.
$\mathrm{d}Q_{\rm n}/\mathrm{d}t = -\nabla \cdot \boldsymbol{J}_{\rm n}$. Thus, $Q_{\rm n}$ is the quantity which is analogous to the "free charge density" in the transmission line. The capacitance per unit length C is then equal to $Q_{\rm n}A\Phi$, which differs from Q^*A/Φ by the factor $\pi\Delta/4k_{\rm B}T$. This factor can be interpreted as an effective dielectric constant, representing the response of the condensate in enhancing this "free charge" in the quasiparticles. The conductance per unit length G gives the proportionality between the rate at which $Q_{\rm n}A$ changes by conversion processes ($Q^*A/\tau_{Q*} = -Q_{\rm n}A/\tau_E$) and the nonequilibrium potential Φ. Other standard parameters governing the transmission line also have direct physical significance in terms of the charge imbalance dynamics. For example, the propagation constant of the line is

$$K \equiv [(R + \mathrm{i}\omega L)(G + \mathrm{i}\omega C)]^{1/2} \tag{2.41}$$

This relates to the wave vector of the charge imbalance waves eq. (2.35) by $K = \mathrm{i}k(\omega)$, giving the low-frequency decay length $\Lambda = (RG)^{-1,2}$ and the highfrequency wave velocity $v = (LC)^{-1/2}$. The characteristic impedance of the line is

$$Z(\omega) = [(R + \mathrm{i}\omega L)/(G + \mathrm{i}\omega C)]^{1/2}, \tag{2.42}$$

which, for low frequencies, gives $Z(0) = RA$, the resistance of the line corresponding to the characteristic decay length. For many purposes, a semiinfinite length of the transmission line

can be represented by this single lumped impedance $Z(\omega)$ connected between the two channels. Standard formulas for finite lengths of transmission line are also available.

The heuristic utility of this transmission line picture is illustrated for two types of measurements in fig. 7. For the spatially uniform quasiparticle injection experiment of Clarke (1972), in fig. 7a, a constant current I tunnels from a normal film through a resistive oxide barrier into a superconducting film below. This current creates the "free charge" in the normal channel at a rate $(\mathrm{d}Q_\mathrm{n}/\mathrm{d}t)_\mathrm{inj} = I/LA$, charging up the capacitors. They discharge at the same rate through the leakage conductance G. so that the current I leaves the nonequilibrium region as a pure supercurrent in the condensate channel. The induced nonequilibrium potential is therefore

$$\Phi = I/(GL) = \mathrm{I}\tau_{Q*}/\left(2N(0)e^2LA\right), \tag{2.43}$$

where L is the length of the nonequilibrium region, much larger than Λ to minimize edge effects. This result is essentially the same as that originally derived by Tinkham and Clarke (1972), for the measurement of the nonequilibrium potential measured using superconducting and normal probes in the nonequilibrium region. We re-emphasize here that if the current is suddenly turned off, the potential Φ will decay exponentially with a time $\tau_\mathrm{E} = C_/G$ and not τ_{Q*}. Furthermore, the additional junction resistance (per unit area)

$$\mathrm{R}_{Q*} = 1/G = \tau_{Q*}/2N(0)e^2, \tag{2.44}$$

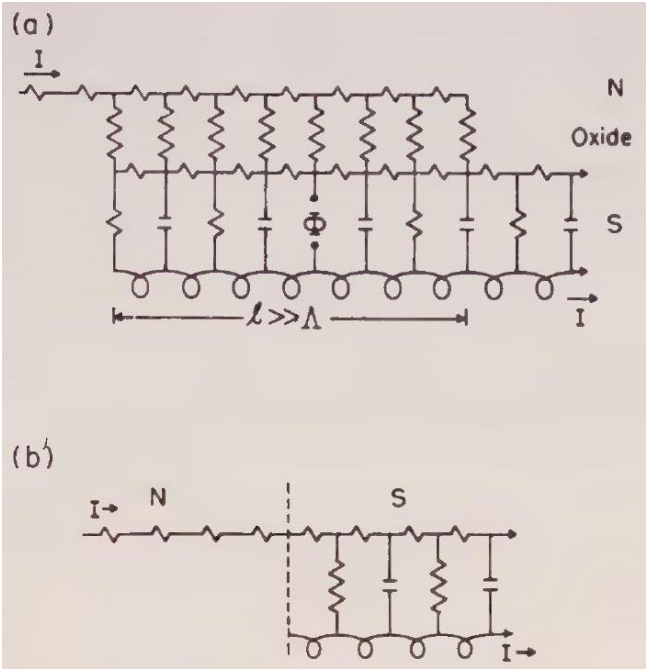


Fig. 7. Use of the transmission-line equivalent to model (a) uniform quasiparticle injection, and (b) current flow through a normal-superconducting boundary. (From Kadin et al. 1980.)

evident in fig. 7a, has been directly measured experimentally (Lemberger 1981a,b).
Another important phenomenon in which charge imbalance plays a crucial role is the excess resistance on the superconducting side of a current-carrying superconducting-normal interface (Pippard et al. 1971, Hsiang and Clarke 1980). We can represent this (again, for T near T_c) by the equivalent circuit of fig. 7b, in which the normal current connects up to the "normal" channel on the superconducting side. Over a length equal to Λ, the current leaks over to the condensate line by charge imbalance decay, and the excess resistance is $Z(0) = R\Lambda$. Furthermore, the equivalent circuit gives rather directly the exponentially decaying nonequilibrium

potential near the boundary, observed by Yu and Mercereau (1972, 1975) using small normal and superconducting probes.

We reiterate that these pictures are only strictly valid very close to T_c. For lower temperatures, the fact that quasiparticles near the gap edge have both electron-like and hole-like characteristics becomes important. A fraction of the injected current of order A/k_BT enters the condensate line directly in fig. 7a, reducing the contribution to the charge imbalance. Similarly, electrons with energy $E < 1$ approaching the N − S boundary from the normal side in fig. 7 b are reflected as holes via Andreev (1964) reflection, with superconducting pairs to carry the current in the superconductor. A microscopic analysis which calculates the fraction of current Andreev-reflected at the boundary has been used successfully to explain the observed boundary resistance over a wide range of temperatures (Hsiang and Clarke 1980). With these and other extensions, this transmission line picture should continue to provide a heuristic guide to the understanding of superconducting dynamics involving transverse disequilibria.

20.3 3. Pair-field susceptibility and Josephson tunneling

20.3.1 3.1. Introduction and experimental configuration

We have described how the use of quasiparticle tunneling provides in-sight into the relaxation processes in nonequilibrium superconductors. In this section we will review how another aspect of Josephson tunneling can be used to measure the superconducting pair-field susceptibility, which in turn allows a direct determination of the dynamical equations governing the evolution of the order parameter. Although it has been studied theoretically (Ferrell 1969, Scalapino 1970, Kadin and Goldman 1982) and experimentally (Anderson and Goldman 1970, Yoshihiro and Kajimura 1970) for more than a decade, the physical basis of the measurement of the pair-field susceptibility and its connection with more familiar aspects of the Josephson effect and superconducting order parameter dynamics have not been widely appreciated.

In magnetic systems, the most direct methods for the determination of the dynamics of the magnetization M involve the measurement of the magnetic susceptibility χ_M, and its dependence on the wave-vector k and frequency ω. Alternatively, the structure function $S(k\omega)$ is inferred, which is related to the susceptibility by the fluctuation- dissipation theorem. A superconducting system does not have a thermodynamic conjugate field which induces superconductivity in the same way that a laboratory magnetic field H produces a finite magnetization in a paramagnet. However, in both the superconducting and the magnetic case, within the spirit of mean field theory, one can treat the internal interaction as an effective field acting on a given region of the material. In a superconductor, this internal interaction is long range (on the order of the coherence length $\xi \sim 1000$Å) and gives rise to the well-known proximity effect in a clean contact between a superconductor and a normal metal. It has perhaps not been generally appreciated, however, that the same type of physical effect (albeit weaker) occurs across a tunneling barrier, and it is precisely this type of coupling that gives rise to the usual Josephson effects between two superconducting electrodes. Thus, even in a tunnel junction between a superconductor and a normal metal, there is a small induced order parameter on the normal side (see fig. 8). Furthermore, there is as a consequence a small "excess" supercurrent across the junction, for finite nonzero voltages as it will turn out, which is a measure of the generalized superconducting susceptibility $\chi(k,\omega)$ or pair-field susceptibility (PFS). Similar considerations are relevant when both electrodes are superconducting, and the excess pair current for $V = 0$ is also related to the susceptibility.

The geometry of the effect consists of a high-conductance tunnel junction between a strong superconductor (critical temperature T_c') and a weak superconductor ($T_c < T_c'$), where the measurements are made at a temperature T above, near, or slightly less than T_c, in order to

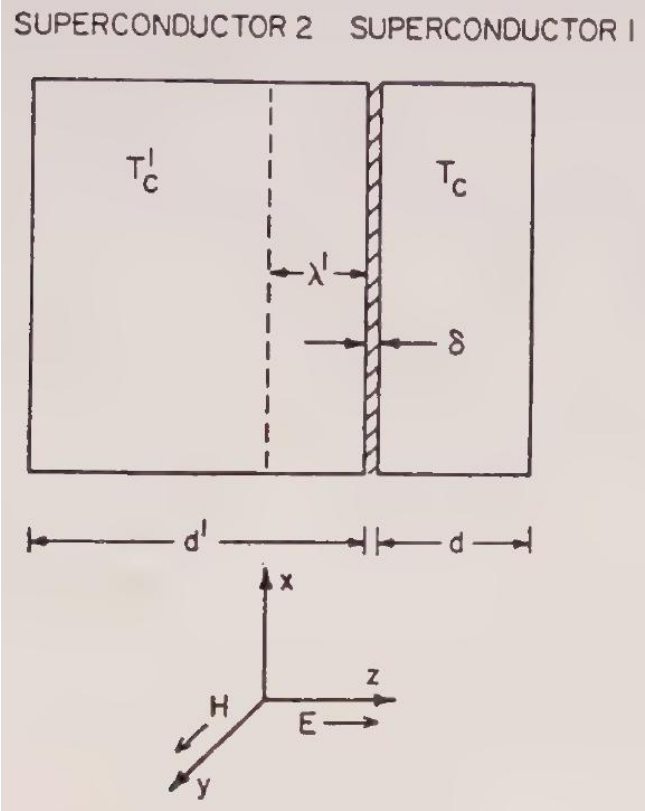


Fig. 8. Schematic of tunnel junction for measurement of the pair-field susceptibility for $T \sim T_{\mathrm{c}} \ll T_{\mathrm{c}}^{\prime}$. The magnetic field is in the y direction and the electric field and current flows are in the z direction. (From Carlson and Goldman 1976.)

probe the properties of the weak superconductor. In typical experiments the strong superconductor is Pb , with $T_{\mathrm{c}}^{\prime} = 7.2$ K. The weak superconductor has been Sn (Anderson and Goldman 1970) ($T_{\mathrm{C}} = 3.8$ K), Al in the dirty limit ($T_{\mathrm{c}} \geqslant 1.2$ K), (Anderson et al. 1972), Al with paramagnetic Er impurities (Aspen and Goldman 1981a) (T_c from 1 to 2 K , with differing concentrations), and Ag/Pb proximity sandwiches in the Cooper limit (Aspen and Goldman 1981b). A review of the experimental results has been given by Goldman (1981).

The tunnel junctions have been of the cross-film type, with a junction area of order 0.1 mm^2 defined by means of a window in an insulating (e.g. Bi_2O_3) layer. The oxide barriers have been native oxides of either Al or Pb .

For an ideal tunnel junction with $T \ll T_{\mathrm{c}}$, the quasiparticle current should be exponentially small for low voltages $V \ll \Delta$:

$$I_{\mathrm{qp}}(V) \sim \left(V / R_{\mathrm{NN}}\right) \exp\left[-\left(\Delta^{\prime} - eV\right) / k_{\mathrm{B}} T\right] \ll V / R_{\mathrm{NN}}. \tag{3.1}$$

This exponential smallness is important, because it acts as a background for a small excess current at low, but nonzero voltages. This excess current turns
out, as we will show, to be a form of the Josephson effect which is second order in the tunnel conductance (as opposed to first order for the usual zero-voltage Josephson supercurrent). Thus, the excess current associated with the PFS cannot be detected at all in the usual high-resistance junctions, and can only be seen in low resistance junctions when the quasiparticle background is significantly reduced. In practice, the effect has been seen in junctions with normal state resistance $R < 1\Omega$, but without any pinhole shorts. The excess supercurrent can be identified as a Josephson current by its extreme sensitivity to a small magnetic field in the

plane of the junction (fig. 8), one far too small to affect the electrodes themselves. Finally, the apparent violation of the AC Josephson effect (a DC supercurrent at a finite voltage) can also be understood, and does not present a problem (Kadin and Goldman 1982).

One of the basic features of the Josephson interaction, following from its dependence on the phase of the order parameter, is that it is gauge-invariant with respect to electromagnetic fields. This means, as we will show below, that a DC voltage across a Josephson junction gives rise to a temporal modulation of the interaction at the Josephson frequency $\omega_0 = 2\mathrm{eV}/\hbar$, and that similarly, a constant magnetic field in the plane of the junction leads to a spatial modulation interaction with wave vector $q_0 \sim H$. In this way, the action of a constant electromagnetic field is to produce a purely harmonic modulation of the effective pair field by which the strong superconductor affects the weak superconductor (the perturbation in the other direction is negligible). This induces a harmonic response in the weak superconductor, which then in turn leads via the Josephson effect back to a DC excess supercurrent. The final result is that

$$I_{\mathrm{ex}} \sim \left(1/R_{\mathrm{NN}}\right)^2 \chi''\left(q_0\omega_0\right), \tag{3.2}$$

where $\chi''\left(q_0\omega_0\right)$ is the imaginary part of the pair-field susceptibility. Thus the dynamics of the order parameter in the weak superconductor can be fully mapped out by examining I_{ex} as a function of V and H. Our derivation of this effect, which emphasizes phenomenological pictures rather than the most general theoretical framework (for the latter, see the review by Schön (1985) in this volume), was taken in large part from Kadin and Goldman (1982), and represents a generalization of the initial treatment of the problem by Ferrell (1969).

As we mentioned above, the weak superconducting film will be affected by the presence of a strong superconductor across the barrier. This interaction can be represented by the Josephson free energy $F_{\mathrm{J}} = -\left(\hbar I_0/2e\right)\cos\gamma$, which gives rise in the usual way to the supercurrent in the junction $I_{\mathrm{s}} = I_0 \sin\gamma$. Here γ is the gauge-invariant phase difference across the barrier, and I_0 is the critical current, which is inversely proportional to the normal-state junction resistance R_{n} and goes as $|\psi|$. If we assume that the thickness $d \ll \xi \sim 1000\mathrm{\AA}$, the interaction is uniform through the thickness and we can express it in terms of a
free energy density

$$f_J = -\left(\hbar j_0/2ed\right)\cos\gamma = -(\hbar\bar{C}/2ed)|\psi|\cos\gamma, \tag{3.3}$$

where $j_0 = \bar{C}|\psi|$ is the maximum critical current density. In the regime of interest where $|\psi|$ is small and $T \sim T_{\mathrm{c}} \ll \mathrm{T}'_{\mathrm{c}}$, j_0 is given by

$$j_0 = \left(G_{\mathrm{N}}\Delta_{\mathrm{in}}/4e\right)\ln\left(T'_{\mathrm{c}}/T\right), \tag{3.4}$$

where G_{N} is the normal conductance per unit area of the junction, and Δ_{in} is the induced BCS gap parameter related to $|\psi|$ (in the dirty limit) by

$$\Delta_{\mathrm{in}} = |\psi|\left(4k_{\mathrm{B}}Th/\pi n\tau\right)^{1/2}. \tag{3.5}$$

Consider the case where there is a constant voltage V_0 across the junction and an external magnetic field H_0 in the plane of the junction (fig. 8). Then γ can be written

$$\gamma = \theta - 2eV_0t/\hbar - \left(2e/\hbar\int A\cdot\ \mathrm{d}z = \theta - \omega_0t - q_0x \tag{3.6}$$

where

$$q_0 = \left(2e/\hbar\right)\left(\lambda' + d/2 + \delta\right)H_0 \tag{3.7}$$

Here the penetration depth i' of the strong superconductor is less than its thickness (which is normally the case), while $d \ll \lambda$ for the weak superconductor, and δ is the barrier thickness, usually negligible. Then

$$f_J = -\left[\psi\zeta^*(x,t) + \psi^*\zeta(x,t)\right] \tag{3.8}$$

where

$$\zeta = (\hbar\bar{C}/4ed)\exp\left[i\left(q_0x + \omega_0t\right)\right] \tag{3.9}$$

The quantity ζ can be viewed as an effective pair field, conjugate to the order parameter ψ, which is modulated in space and time for constant values of V and H. This will cause an induced order parameter for $T > T_c$, or an induced part of the order parameter for $T < T_c$. These two cases will be discussed separately below.

20.3.2 3.2. Pair-field susceptibility for $T > T_c$

For $T > T_c$, the simple TDGL equation is valid, but with the addition of the Josephson interaction term (eq. 3.8) to the free energy in eq. (2.14). Taking the variational derivative $\delta f/\delta\psi^*$ leads directly to

$$\tau_{GL}\frac{\partial\psi}{\partial t} + \psi - \xi^2\nabla^2\psi = C_1\exp\left[\mathrm{i}\left(q_0x + \omega_0\mathrm{t}\right)\right] \tag{3.10}$$

where $C_1 = \hbar C/(4ed|\alpha|)$, and we have taken the other film to be at voltage V_0,
and also neglect the vector potential A in $\nabla - 2ieA/h$, since for small fields its effect can be largely accounted for as a shift in T_c. The quantity on the left of eq. (3.10) above is the usual TDGL equation for $T > T_c$. If the right-hand side were equal to zero, then in steady-state one would have $\psi = 0$. If the quantity on the right included thermal fluctuations, we would still have the time average of the order parameter $\langle\psi\rangle = 0$, although $\langle|\psi|^2\rangle$ would be nonzero, giving rise to excess electrical conductance of the film in the normal state above T_c (Skocpol and Tinkham 1975). In the present case, the quantity on the right is the effective pair-field which excites a particular mode of oscillation with wave vector q_0 and frequency ω_0 determined by the external electromagnetic field. The induced order parameter which results takes the form

$$\psi_{\mathrm{in}}\left(x,t\right) = C_1\exp\left[\mathrm{i}\left(q_0x + \omega_0t\right)\right] / \left[\mathrm{i}\omega_0\tau_{GL} + \left(1 + \xi^2q_0^2\right)\right]. \tag{3.11}$$

This can also be expressed in the language of linear response theory, where one can define the order parameter response function $\chi\left(x - x', t - t'\right)$ such that

$$\psi(x,t) = \int \mathrm{d}x' \int \mathrm{d}t'\zeta\left(x',t'\right)\chi\left(x - x', t - t'\right) \tag{3.12}$$

or in terms of Fourier transforms,

$$\psi_{\mathrm{in}}(k,\omega) = \zeta(k,\omega)\chi(k,\omega), \tag{3.13}$$

where in the present case

$$\zeta(k,\omega) = \alpha C_1\delta\left(k - q_0\right)\delta\left(\omega - \omega_0\right) \tag{3.14}$$

$$\chi(k,\omega) = \left\{\alpha\left[i\omega\tau_{GL} + \left(1 + k^2\xi^2\right)\right]\right\}^{-1} \tag{3.15}$$

so that

$$\psi_{in}(x,t) = \zeta(x,t)\chi\left(q_0,\omega_0\right). \tag{3.16}$$

In other works, χ may be defined to correspond to Δ_{in} rather than to ψ_{in}, leading to the replacement of α in eq. (3.15) by $N(0)\left(T-T_c\right)T_c$. In addition, the definition of the susceptibility χ in terms of linear response theory is equivalent to the quantum-mechanical definition in terms of the commutator of operators

$$\chi\left(r-r',t-t'\right) = \begin{cases} -(i/h)\left\langle\left[\hat{\Psi}(r,t),\hat{\Psi}^{-}\left(r',t'\right)\right]\right\rangle & \mathrm{t} > t' \\ 0, & \mathrm{t} < t' \end{cases} \tag{3.17}$$

where ψ is the order parameter operator, [ ] represents the commutator, and $\rangle$ is the expectation value at finite temperature.

One can now obtain the "excess" supercurrent from the usual expression

$$I_{ex} = \int_0^{\mathrm{w}}\int_0^{L} \mathrm{d}x\ \mathrm{d}y j_J = (4edA/h)\,\mathrm{Im}\left(\psi_{in}\zeta^*\right) = 4edA/\hbar|\zeta|^2\chi''\left(q_0\omega_0\right). \tag{3.18}$$

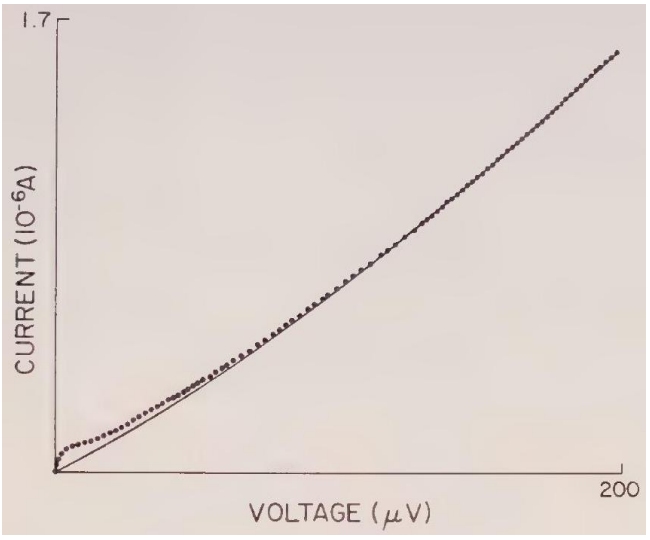


Fig. 9. Total I-V characteristic (points) for an $\mathrm{Al -\mathrm{Al}\{2\}\ \mathrm{O}\{3\}-\mathrm{Pb}$ junction at 1.96778 K . The solid line is the quasiparticle background determined from, and a least squares fit to, the data over the range $V = 150 - 200\mu$ V. The excess current is the portion of the curve above the solid lines. (From Carlson and Goldman 1976.)}

This general relationship between I_{ex} and χ is also valid below T_c, as will be shown below. For the case of $T > T_c$ here, the detailed dependences on V and H, in accordance with the simple TDGL equation,

$$I_{ex} = \left(\hbar C^2 WL/4ed\alpha\right)\omega_0\tau_{GL}/\left[\left(\omega_0\tau_{GL}\right)^2 + \left(1+{q_0}^2\xi^2\right)^2\right], \tag{3.19}$$

have been confirmed experimentally (Anderson and Goldman 1970, Anderson et al. 1972). Figure 9 shows a I V characteristic for an $Al_1 - Al_2O_3 - Pb$ junction, and fig. 10 presents the excess current I_{ex} obtained by subtracting off the quasiparticle background current and a small leakage current. Figure 11 shows the peak voltage V_p of the excess current voltage characteristic where in zero magnetic field $V_p = (2e/\hbar)\,(1/\tau_{GL})$.

Note that the I_{ex} is antisymmetric for the two polarities of voltage, and in fact is zero for zero voltage. This is unusual for a supercurrent, but is easily explained via a simple picture (fig. 12). Because of the $\cos\gamma$ term in the interaction energy, the ψ_{in} "wants" to point in the same direction in the complex plane as ψ' of the strong superconductor. This orientation will also yield the maximum value of the magnitude of ψ_{in} , but since the supercurrent goes as $\sin\gamma$, this corresponds to $I_{ex} = 0$. This is the case for $V = 0$. For $V > 0$, on the other hand, ψ' is rotating in the complex plane at an angular frequency $\omega_0 = 2eV/\hbar$. The induced order parameter "tries" to follow, but it has a characteristic response time τ_{GL}, so that as the frequency increases it begins to

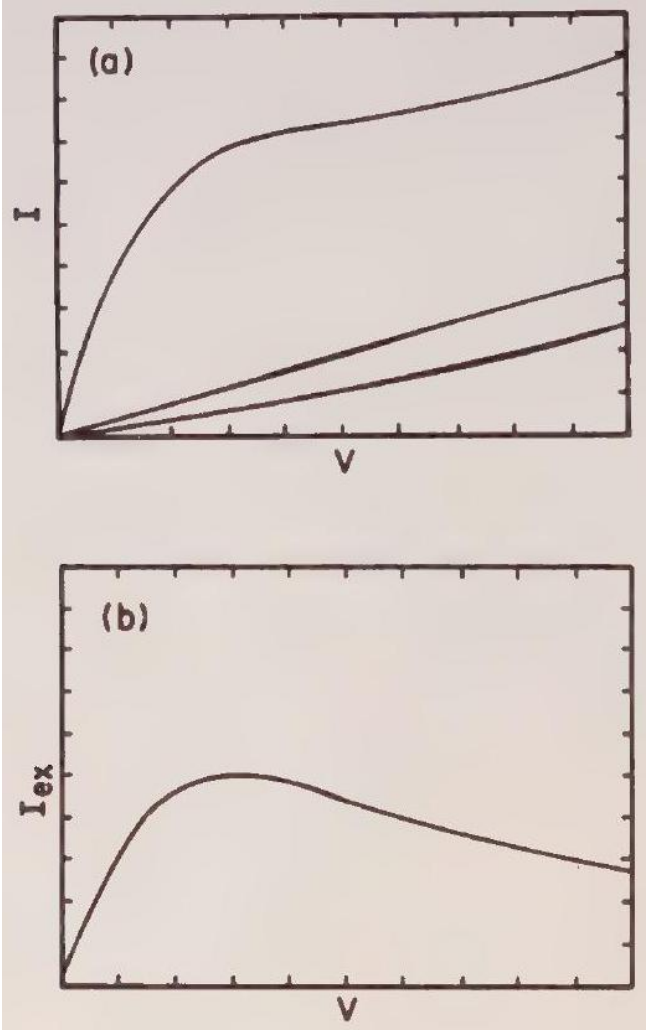


Fig. 10. (a) Typical total current, leakage current, and quasiparticle current versus voltage, from top to bottom, respectively. (b) Excess current obtained by subtracting the leakage and quasiparticle currents from the total current in (a). In both parts the units are arbitrary.

lag behind. This gives a nonzero value of I_{ex} of the right sign. As this phase lag increases, however, the interaction energy decreases, so that the length of the vector representing ψ_{in} also decreases. Thus, as suggested in fig. 11, the projection of ψ_{in} perpendicular to ψ', which gives the magnitude of I_{ex}, will increase to a maximum and then return to zero for high voltage.

The physical picture in fig. 12 indicates clearly that $I_{ex} = I_0 \sin\gamma$ is timeindependent for non-zero voltages, and is not the time-average of some oscillating current. This is true even though the coupling across the junction is time dependent. These facts would seem to contradict the AC Josephson relation, but this apparent paradox can be resolved using the concept of

charge imbalance. As we pointed out earlier, the usual charge imbalance experiments involved, in effect, a tunnel injection of normal current I_n from a normal metal into a superconductor, which ultimately left the film as supercurrent I_s. This caused a build-up of "normal" charge density Q^* in the superconductor

$$Q^* = I_n \tau_{Q*} / \Omega \tag{3.20}$$

where Ω is the nonequilibrium volume. For the present case we are focussing

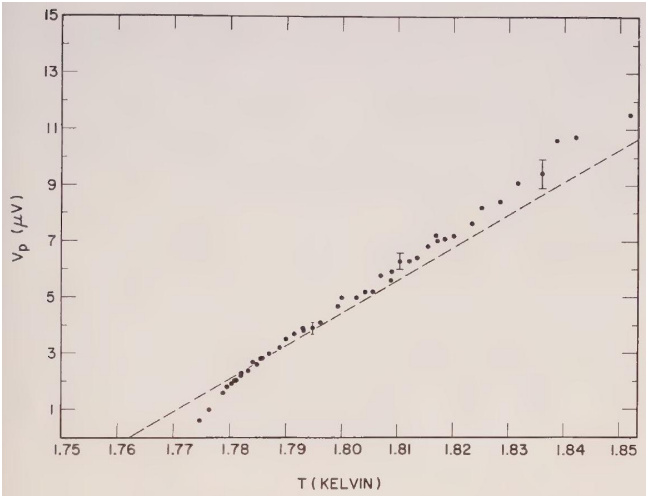


Fig. 11. Peak voltage $V_{\mathrm{p}}=\hbar / 2 e \tau_{\mathrm{GL}}$ versus T for an $\mathrm{Al}-\mathrm{Al_2O_3}-\mathrm{Pb}$ junction. (From Goldman, 1981.)

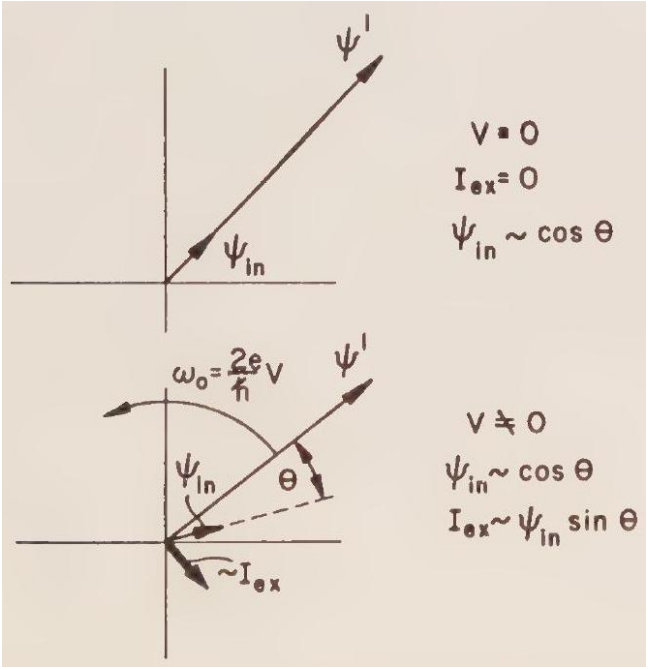


Fig. 12. Physical picture of a pair-field susceptibility measurement for $T > T_c$.

on the normal film. In the absence of superconducting order, there can be no charge imbalance since relaxation cannot occur. However, because of the interaction with the strongly superconducting electrode, the normal film has become effectively a weak "gapless" superconductor, even above T_c. In terms of the transmission-line picture in fig. 6, it has a superconducting

channel. In effect, the excess pair current I_{ex} is a supercurrent injected into the normal film, which presumably leaves the film at the boundaries as normal current I_n. Therefore, this will produce a charge imbalance

$$Q^* = -I_{ex}\tau_R/\Omega \tag{3.21}$$

for some effective relaxation time τ_R. The negative sign is taken because the process is essentially the opposite to that described by eq. (3.20). Also, as it is a true supercurrent across the junction it should flow with no resistance, i.e. no voltage difference between the condensate electrochemical potential μ_s on the two sides. This is consistent only if the voltage V_0 in the quasiparticle channel across the junction is equal to the internal voltage drop Φ between the normal and superconducting channels of the weak superconductor (we are neglecting the small chemical potential shift on the strongly superconducting side). This requirement implies that the relaxation time τ_R must satisfy the relation

$$\tau_R = 2N(0)e^2V_0Lwd/I_{ex}. \tag{3.22}$$

Substituting the expression for I_{ex} in the low voltage, $q_0 = 0$, limit, one obtains

$$\tau_R = mN(0)D/\left|\psi_{in}\right|^2 = 2k_BTh/\pi\Delta_{in}^2, \tag{3.23}$$

using the theory of dirty superconductors. In fact, this relaxation time is identical to that derived by more standard methods for charge imbalance relaxation in a gapless superconductor below its T_c (Schmid and Schön, 1975a). Thus, the measurement of the pair-field susceptibility in this regime can be alternately viewed as a measurement of the steady-state charge imbalance relaxation time in a weak induced superconductor.

We emphasize that, although the results of measurements of the pair-field susceptibility must be identical to the spectrum of spontaneous thermal fluctuations (both deriving from the dynamical equations of the order parameter), the excess current I_{ex} is not a direct consequence of these fluctuations as it is determined in linear response. This may not have been widely appreciated, as the early work was developed at the same time as the effects of thermal fluctuations were being analyzed (Skocpol and Tinkham 1975). Since I_{cx} is a Josephson current, it depends on the existence of a stable phase correlation across the barrier. Such a correlation cannot result from spontaneous thermal fluctuations, which therefore do not contribute to the excess current. In fact, thermal fluctuations will act against well-defined features in the excess current, producing some broadening in the structure (Kadin and

Goldman 1982). On the other hand, in a measurement of excess electrical conductivity of a film above T_c only correlations within the film are important, and thermal fluctuations do contribute to these.

20.3.3 3.3. Pair-field susceptibility for $T < T_c$

The determination of the pair-field susceptibility follows the same principles as for $T > T_c$, but it is somewhat more complicated for several reasons, both experimental and theoretical. First, there is the usual DC Josephson current for zero voltage, associated with the equilibrium value of the order parameter, which must be suppressed using a voltage and a magnetic field in order to see the (much smaller) desired effect. Shorts in the tunnel barrier are even more deleterious here, since they can give rise to time-averaged supercurrents even for nonzero voltages. On the theoretical side, the simple TDGL equation is no longer valid except in special cases, and a sufficiently generalized dynamical equation is likely to be much more complicated. The situation is further confused by the fact that, as discussed earlier, longitudinal mode and transverse mode disequilibria tend to obey different dynamical equations, but the resulting I_{ex}

yields a single susceptibility, which is a linear combination of the two modes, and makes them difficult to separate.

The most remarkable result in the experiments measuring I_{ex} below T_c was the observation of a second peak for an Al film (Carlson and Goldman 1973, 1975), which suggested the (then surprising) existence of a propagating collective mode in the superconductor, one which was later identified with the transverse collective mode (charge-imbalance waves) (Schmid and Schön 1975b, Artemenko and Volkov 1975). This peak is illustrated in fig. 13, which shows $I_{ex}/V \sim S(q,\omega)$ for a range of temperatures above and below T_c. Presented in this way, the earlier peak associated with the time lag in the order parameter response is shifted to $V = 0$. The width of this peak is still a measure of this time lag, however, and the decreased width for $T < T_c$ is consistent with what we would expect for an increased time (e.g. τ_1). Furthermore, the position of the displaced peak ω_p is approximately proportional to q (fig. 14), in a way one would expect for resonant behavior associated with a wave of velocity $v = \omega/q$. The fact that the peak is broad, and eventually damps out entirely at low temperatures, is not surprising either, since charge imbalance waves are highly damped.

In explaining the theoretical behavior for $T < T_c$, we begin with the simple TDGL equation, even though it is valid in this regime only for gapless superconductors. In the same way as that obtained earlier, the TDGL equation including the interaction term is

$$\tau_{GL}\frac{\partial\psi}{\partial t} - \left(1 - |\psi|^2/\psi_{eq}^2\right)\psi - \xi^2\nabla^2\psi = C_1 \exp\left[\mathrm{i}\left(q_0 x + \omega_0 t\right)\right] \tag{3.24}$$

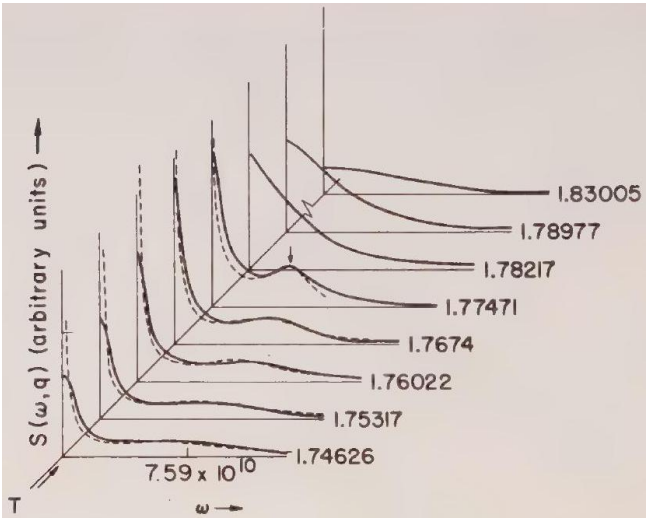


Fig. 13. Structure factor $I_{\mathrm{ex}} / V \sim S(q, \omega)$ in arbitrary units versus T and ω. The magnetic field is 125 Oe. Curves are shown only for the $\omega > 0$ portion and are symmetric about $\omega = 0$. $T_c(H) = 1.780$ K. Dashed lines are from Schmid and Schön (1975b). (From Carlson and Goldman 1976.)}

where the differences in sign relative to eq. (3.10) follow from the sign change of α. Since we are looking at small variations in ψ about its equilibrium value ψ_{eq} , we define

$$\psi = \psi_{eq} + \delta\psi^{L} + \mathrm{i}\delta\psi^{T} \tag{3.25}$$

where $\delta\psi^{L}$ and $\delta\psi^{T}$ are real functions that are small compared to ψ_{eq} . Substituting in and separating into real and imaginary parts, one obtains two equations

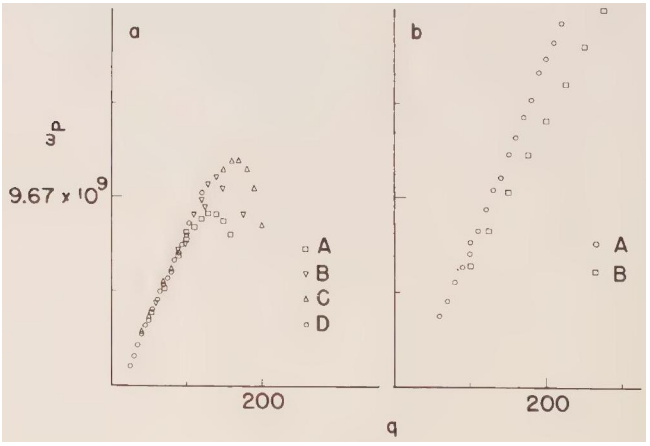


Fig. 14. (a) Position of peak in the structure factor $S(q,\omega)$ of Al plotted versus q in units of magnetic field at several temperatures. The points A-D correspond to $T = 1.771, 1.767, 1.764$ and 1.753 K , respectively. (b) Frequencies of peaks in $S(q,\omega)$ at fixed $\omega=6.32 \times 10^{-3}$. (From Carlson and Goldman 1976.)

$$\left(\tau_{\mathrm{GL}}\frac{\partial}{\partial t} + 2 - \xi^2\nabla^2\right)\delta\psi^{\mathrm{L}} = C_1\cos\left(q_0 x + \omega_0 t\right), \tag{3.26}$$

$$\left(\tau_{\mathrm{GL}}\frac{\partial}{\partial t} - \xi^2\nabla^2\right)\delta\psi^{\mathrm{T}} = C_1\sin\left(q_0 x + \omega_0 t\right). \tag{3.27}$$

Clearly, the longitudinal variation $\delta\psi^L = g\psi_{\mathrm{eq}}$ exhibits somewhat different behavior than the transverse variation $\delta\psi^\top = i\theta\psi_{\mathrm{cq}}$, even without a more complicated dynamical equation. Equations (3.26) and (3.27) can be solved to yield

$$\delta\psi^L = \zeta(x,t)\chi^L\left(q_0,\omega_0\right) + \text{ c.c. }, \tag{3.28}$$

$$\delta\psi^T = \zeta(x,t)\chi^T\left(q_0,\omega_0\right) + \text{ c.c.}, \tag{3.29}$$

where

$$\chi^{\mathrm{L}}(k,\omega) = \left[2|\alpha|\left(\mathrm{i}\omega\tau_{\mathrm{GL}} + \xi^2k^2\right)\right]^{-1} \tag{3.30}$$

and

$$\chi^{\mathrm{T}}(k,\omega) = \left[2|\alpha|\left(i\omega\tau_{\mathrm{GL}} + \xi^2k^2\right)\right]^{-1}. \tag{3.31}$$

The pair field ζ is the same as in eq. (3.13) and c.c. represents the complex conjugate. Note that this is no longer simply a linear response, since there is also a "conjugate-linear" response proportional to the complex conjugate of ζ. However, as the conjugate term gives a contribution at frequency $2\omega_0$, it is only the linear response term that contributes to the time-averaged DC excess current

$$I_{\mathrm{ex}} = \frac{\hbar\bar{C}^2wL}{4ed}\,\mathrm{Im}\left[\chi^{\mathrm{L}}\left(q_0,\omega_0\right) + \chi^{\mathrm{T}}\left(q_0,\omega_0\right)\right]. \tag{3.32}$$

This current is in addition to the usual Josephson supercurrent for $V = 0$, $H \simeq 0$, and $I_{\mathrm{s}} = CwL\psi_{\mathrm{eq}}\,\sin\gamma$. Note that the excess supercurrent is of higher order in the small coupling

constant $\bar{C}$, and can only be seen when the usual supercurrent is not present or is greatly reduced in magnitude.

In eqs. (3.26) and (3.27), both $\delta\psi^{\mathrm{T}}$ and $\delta\psi^{\mathrm{L}}$ obey diffusive equations, i.e. with only a first derivative in time. This will clearly not produce the "displaced peak" seen in fig. 13, that we have associated with propagating waves, and which requires a second derivative in time. As an example of how the present approach would deal with a generalized TDGL equation which contains the propagating mode, consider eq. (2.28) (Kramer and Watts-Tobin 1978), as modified by Skocpol (1981) (also Octavio and Skocpol 1981) to account for charge imbalance waves:

$$\frac{\tau_{\mathrm{GL}}}{(1+\gamma^2 f^2)^{1/2}}\left(\frac{\partial}{\partial t}+\frac{2\mathrm{i}e\phi}{\hbar}+\frac{2\mathrm{i}\tau_{\mathrm{E}}}{\hbar}\dot{\phi}+\frac{\gamma^2}{2}\frac{\partial f^2}{\partial t}\right)\psi=\left(1-f^2\right)\psi+\xi^2\left(\nabla-\frac{2\mathrm{i}eA}{\hbar}\right)^2\psi. \quad (3.33)$$

We will work in the experimentally accessible regime where $\gamma = 2\tau_{\mathrm{E}}\Delta(\mathrm{T})/\hbar \gg 1$. Adding in the pair field ξ and proceeding as before, one obtains the pair of equations

$$\left(\tau_A\frac{\partial}{\partial t}+2-\xi^2\right)\delta\psi^L = C_1\cos\left(q_0x+\omega_0t\right) \quad (3.34)$$

$$\left(2\tau_{\mathrm{GL}}/\hbar\right)\left(\dot{\Phi}+\tau_{\mathrm{E}}\ddot{\Phi}\right)-\xi^2\nabla\cdot q = \left(C_1/\psi_{\mathrm{eq}}\right)\sin\left(q_0x+\omega_0t\right) \quad (3.35)$$

where here $q = \nabla\theta - 2ieA/\hbar$ is the gauge-invariant phase gradient. From the first equation one obtains, as expected

$$\chi^{\mathrm{L}}(k,\omega) = \left[2|\alpha|\left(i\omega\tau_A+2+\xi^2k^2\right)\right]^{-1} \quad (3.36)$$

i.e. the same as eq. (3.30) but with $\tau_\Delta = \tau_{\mathrm{GL}}\gamma$ substituted for τ_{GL}. One can solve the transverse equation using $J_{\mathrm{s}} = \psi^2$ ehq,m and applying the condition of electroneutrality in a two-fluid picture as done before eq. (2.33) to derived charge imbalance waves. The following equation in the nonequilibrium potential ϕ results:

$$\left[\tau_{\mathrm{J}}\tau_{\mathrm{E}}+\tau_{\mathrm{E}}\frac{\partial^2}{\partial t^2}+\left(\tau_{\mathrm{J}}+\tau_{\mathrm{E}}\right)\frac{\partial}{\partial t}+1-\Lambda^2\nabla^2\right]\Phi$$
$$=\frac{\hbar\gamma}{2\tau_{\mathrm{GL}}}\frac{\hbar\mathrm{C}}{4ed|\alpha|\psi_{\mathrm{eq}}(T)}\left[\omega_0\tau_j\cos\left(q_0x+\tau_0t\right)+\sin\left(q_0x+\tau_0t\right)\right] \quad (3.37)$$

From this, one obtains the transverse susceptibility

$$\chi^{\mathrm{T}}(k,\omega) = \Gamma\left(1+\mathrm{i}\omega\tau_J\right)/2\mathrm{i}\omega\tau_{\mathrm{GL}}\left[\left(1+\mathrm{i}\omega\tau_{\mathrm{J}}\right)\left(1+\mathrm{i}\omega\tau_{\mathrm{E}}\right)+\Lambda^2k^2\right]. \quad (3.38)$$

For high frequencies $\omega \gg \tau_{\mathrm{J}}^{-1}, \tau_{\mathrm{E}}^{-1}$, this clearly exhibits a resonance at a frequency

$$\omega = \mathrm{k}\Lambda/\left(\tau_{\mathrm{J}}\tau_{\mathrm{E}}\right)^{1/2} \quad (3.39)$$

corresponding to a wave with velocity

$$v = \left(A\tau_1\tau_1\right)^{12} = [2D, \|(T), h]^{12} \quad (3.40)$$

as expected for charge imbalance waves, and found experimentally by Carlson and Goldman (1973) in the excess current $I_{\mathrm{ex}} \sim \chi''(k,\omega)$.

Experiments have also been carried out for $T < T_c$ on weakly superconducting Al films doped with paramagnetic Er ions, for varying concentrations of Er designed to give different degrees

of pair-breaking via spin-flip scattering (Aspen and Goldman 1981a). These measurements of the pair-field susceptibility confirmed the theoretical expectations that a sufficient amount of pairbreaking would eliminate the propagating mode.

Another feature of the data below T_c is the appearance of a resonant peak at the gap voltage, largely independent of the wave vector q, which can be identified with a high-frequency resonance in the longitudinal mode contribution to $\chi''(k,\omega)$. This resonance is included in several theoretical analyses (Dinter 1977, 1978, Entin-Wohlman and Orbach, 1978, Schön and Ambegaokar 1979), and may be analogous to the "Riedel singularity" (Riedel 1964) in the Josephson response of an ideal superconducting weak link. On the other hand, an alternative interpretation based on two-particle tunneling and pair-breaking by the AC Josephson effect (Simanek and Hayward 1974) cannot be ruled out by the data alone.

Finally, an alternative way of looking at the presence of I_{ex} for $T < T_c$ is by noting that the AC pair field ζ acts analogously to an external AC voltage of frequency $\omega = 2eV/\hbar$ across the Josephson junction. In the latter situation the external signal at ω mixes with the internal Josephson oscillator at ω to give a DC constant voltage step, together with an oscillatory current at 2ω. The position along the constant voltage step is related to the phase difference between the external and internal oscillators. In the present case, this phase difference is fixed by the interaction that gives rise to $d\psi_{in}$, so that this additional degree of freedom is absent.

20.4 4. Phase-slip centers and microbridges

20.4.1 4.1. Phase-slip centers

It is often so that a simple geometry greatly facilitates the study of physical phenomena. A superconducting filament is one such system, which is geometrically simple, but makes for a surprisingly rich and complex system. If the cross-sectional dimensions are small compared with the coherence length $\xi(T)$ (which in practice, close to T_c, may be about a μm), the filament can be treated as effectively one-dimensional. A real version of such an idealized sample can be a thin-film microstrip or a whisker crystal, with length of order 100μ m. The current-induced breakdown of superconductivity in such a sample is still not understood in its full complexity. We will deal with the problem in terms of approximations which are amenable to physical interpretation, while including references to some of the more rigorous treatments. (See the review by Galaiko and Kopnin (1985) in the present volume.)

The resistive transition of such a sample near T_c, as seen in the DC $I-V$ curve, is characterized by the appearance of a series of voltage steps, each followed by a sloping plateau of approximately constant differential resistance, as shown in fig. 15. Each increment of differential resistance is about the same from one plateau to the next, at least for the first few steps. This basic picture has been observed in microstrips of Sn (Skocpol et al. 1974a), Al (Klapwijk and Mooij 1976b), In (Jillie 1976), and other elements and alloys (Boone et al. 1977, Mller and Baumann 1978), and in whisker crystals of Sn and Sn alloys (Meyer and von Minnigerode 1972, Meyer and Tidecks 1976, Tidecks and Meyer 1979). These constant increments of differential resistance suggests that the phenomena consists of the successive onset of a series of similar dissipative units arrayed along the filament. This was confirmed by Skocpol (Skocpol et al. 1974a), who fabricated a microstrip with a series of side-tabs located at intervals along the length of the strip, which acted as voltage probes. The
dissipative units were found to enter singly, and tended to space themselves relatively far apart. It makes sense, therefore, to speak in terms of discrete spatially localized units, although as will be discussed later, their interaction is also of interest.

Skocpol, Beasley, and Tinkham (SBT) (Skocpol et al. 1974a,b) proposed a model in which each of these units is identified as a phase-slip center (PSC). Each PSC first appears at its own

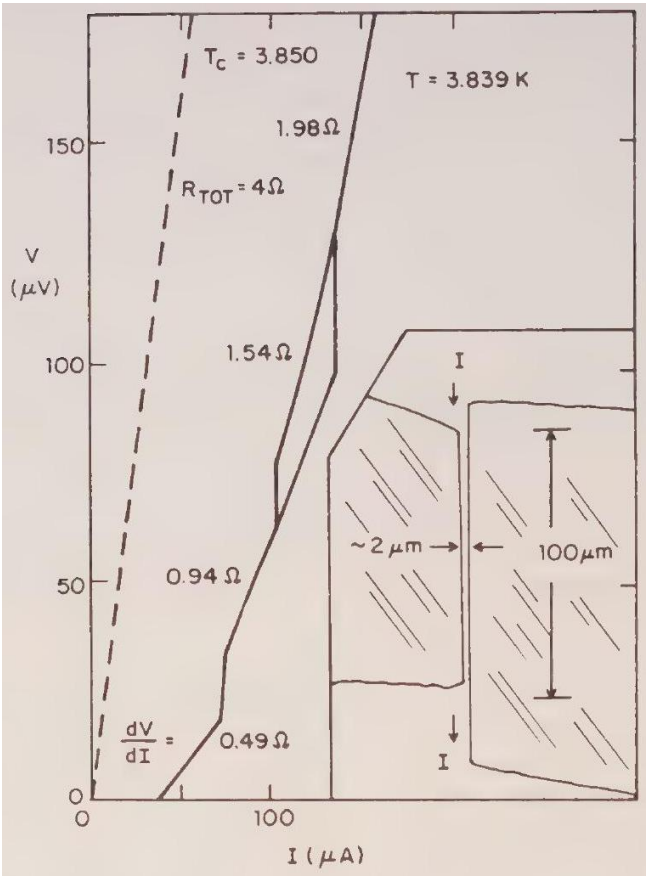


Fig. 15. Current-voltage curve for a Sn microstrip. Note the step structure with the incremental increase in the differential resistance. The inset shows the geometry of the sample.

local value of the critical current, as determined by the local critical temperature and cross-sectional area, and by the presence of other PSCs nearby. The differential resistance of each PSC is approximately equal to the normal-state resistance of a length $2A$, where the precise identity of Λ was unclear originally, but has since been shown to be the diffusion length for the charge imbalance relaxation time τ_{Q^*}. In the Sn sample of fig. 15, Λ was about 6μ m and the corresponding relaxation time $\sim 10^{-9}$ s.

The nonequilibrium region is not fully normal, however, since extrapolating the straight-line slope down to the current axis gives a positive value. This implies that only a portion of the current, associated with the excited quasiparticles, contributes resistance, and the remainder, a (fairly) constant fraction of the critical current, is carried as dissipationless supercurrent. This suggests that we can deal with the problem in terms of the generalized twofluid model discussed earlier, which we illustrated using the transmission-line picture.

In equilibrium, within the SBT model of the PSC, the electrochemical potentials μ_n and μ_s are equal far from the center of the dissipative region, but show fundamentally different behavior in the nonequilibrium region near a PSC. As indicated in fig. 16, a voltage drop across a PSC must appear as a change in both of these potentials, but the change occurs over two different length scales. A gradient in μ, produces an acceleration of the supercurrent I_s and leads to a relaxation oscillation (or phase-slip cycle) of the order parameter within a region of order of the GL coherence length $\xi(T)$. The timeaveraged potential μ, changes abruptly within this region and is constant outside. The phase-slip process causes the time-averaged supercurrent I at the core region to be depressed below the value it has far away, so that if the total current is to remain constant, the dissipative normal current I_n, which is driven by gradients in μ_{11}, must make up the difference. This interconversion between normal and supercurrent must take

place over the scale of Λ (typically larger than ξ), the length required for the nonequilibrium quasiparticles carrying $I_{\rm n}$ to come back into equilibrium with the pair condensate.

This picture of the DC effects near a PSC was confirmed quite directly in the experiment of Dolan and Jackel (1977), where a closely spaced array of superconducting and normal probes measured the spatial behavior of these time-averaged potentials. As predicted, the value of μ_n jumped abruptly at the center of the PSC, while $\mu_{\rm n}$ relaxed exponentially back to the equilibrium value on each side of the center with a decay length which fit the form $A = (D\tau_{Q^*})^{1/2}$.

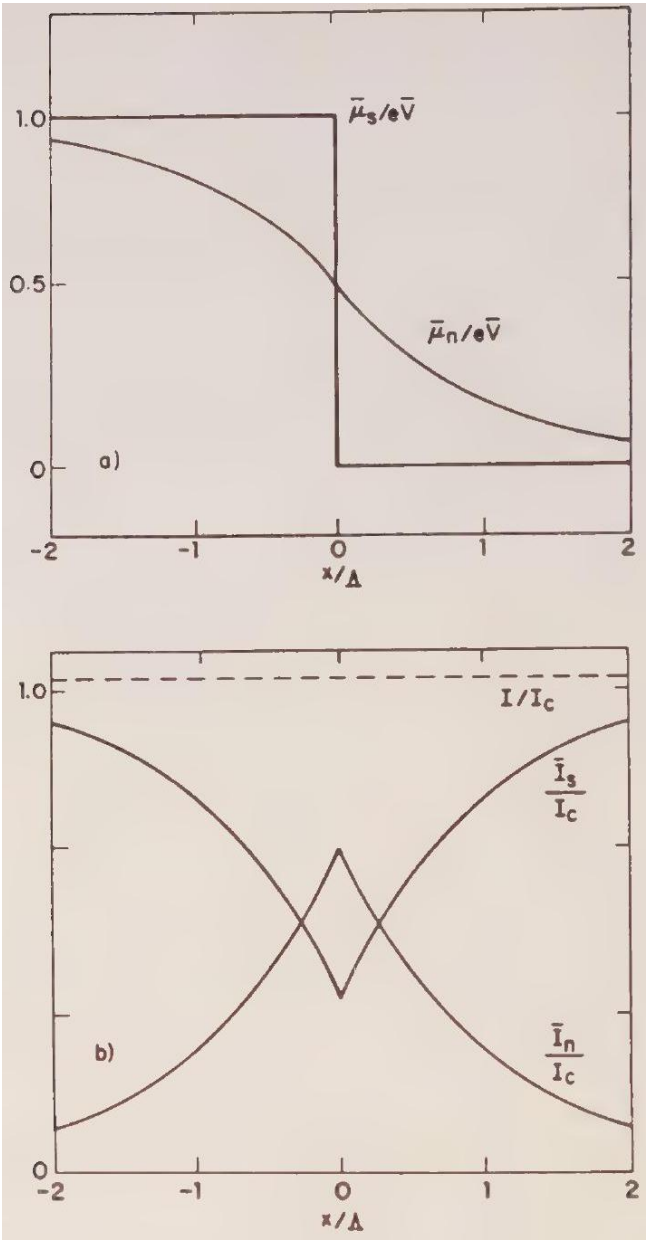


Fig. 16. (a) Time-averaged potentials and (b) currents in the SBT model of the phase-slip center. (From Kadin et al. 1980.)

The weak divergence in $\Lambda \sim (T_{\rm c} - T)^{-1/4}$ was not apparent in many of the earlier measurements on $I - V$ curves of PSCs, in part because of slight variations in $T_{\rm c}$ and the difficulty of clearly separating one PSC from the next very close to the transition. Furthermore, heating-related effects farther from $T_{\rm c}$ have often produced distortions of the $I - V$ curves which can mask the slight divergence. Nevertheless, within the limited temperature range over which

changes in differential resistance of a PSC accurately reflected changes in the decay length, Dolan and Jackel (1977) did find that this resistance corresponded to the normal resistance of a length Λ_{Q^*} and further careful work has confirmed this (Kadin et al. 1978, Stuivinga et al. 1982, 1983, Aponte and Tinkham 1983).

In the limit where $\Lambda \gg \xi$, that is being considered in fig. 16 (even if it is sometimes of marginal validity), the details of the superconducting dynamics in the core region, which produce the actual phase-slip process itself, are not crucial to the model. However, the fact that there are high-frequency Josephson oscillations in the core is important in determining the timedependent behavior of the currents and potentials in the larger region outside the core.

A simple model which incorporates the DC results of SBT, but explicitly includes AC effects, is that of Kadin et al. (1980) (KSS), which represents the problem in terms of a Josephson oscillator coupled to the transmission-line picture of propagating charge imbalance waves (fig. 17a). The oscillations in

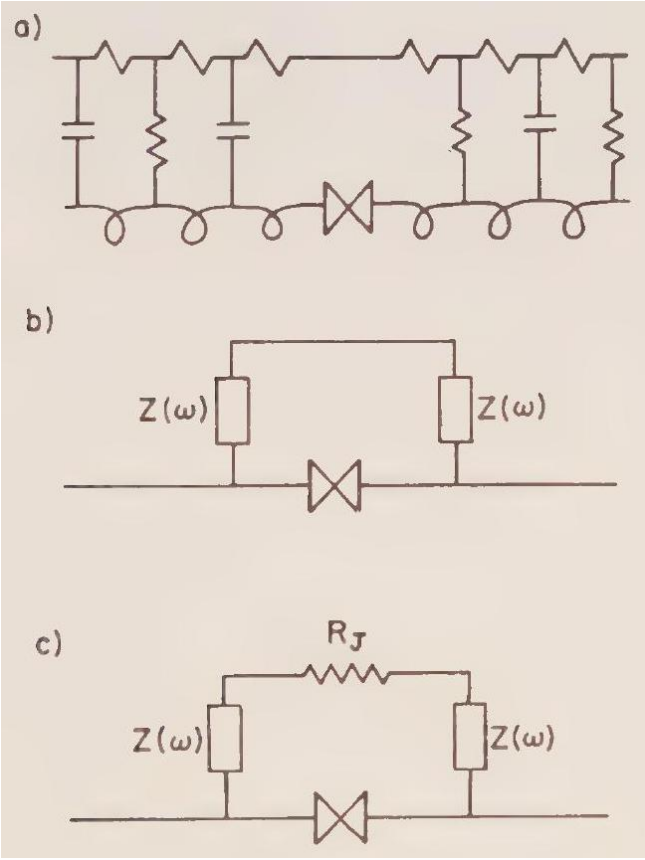


Fig. 17. Equivalent circuits for a phase-slip center. (a) The ideal Josephson element is located on the inductive (condensate) line of the transmission line. (b) The equivalent of (a) as far as the currents and potentials at the center are concerned, where $Z(\omega)$ is the complex frequencydependent characteristic impedance of the transmission line. (c) A generalization of (b) to allow for cases where the intrinsic resistance $R_{3

$ of the Josephson element is not small compared to $Z(\omega)$. (From Kadin et al. 1980.)}

the magnitude of the gap, which constitute the phase-slip process, are assumed to be restricted to a core region with size ξ that is small compared to the length scale A characterizing variations in the charge imbalance, and that this core region may be modeled by a discrete Josephson oscillator of zero length and zero resistance, with a current-phase relation of the form

$$I_{\mathrm{s}}(x=0,t)=I_{\mathrm{c}}f(\Delta\theta(t)), \tag{4.1}$$

where $\Delta\theta$ is the phase difference across the core, f is some function with period 2π and amplitude unity, and I_c is the critical current of the core. The form of this function must be given ad hoc, although one would not necessarily expect the purely sinusoidal dependence appropriate for weak links small compared to ξ.I_{c} is taken to be equal to or slightly smaller than the critical current of the adjacent regions of the filament. The Josephson oscillator lies in the condensate line because it is driven by the difference in μ_s :

$$V(t)=\left[\mu_{\mathrm{s}}\left(x=0^{-},t\right)-\mu_{\mathrm{s}}\left(x=0^{+},t\right)\right]/e=\Phi\left(0^{+}\right)-\Phi\left(0^{-}\right) \tag{4.2}$$

where the condition that μ_n is continuous through the origin follows from the assumption of negligible junction resistance.

As we commented earlier, the effect of the semi-infinite line on either side of the Josephson oscillator can also be obtained by replacing the line with its characteristic impedance $Z(\omega)$, as in fig. 17b. The voltage across the junction can then be expressed as

$$V(t)=2\int \mathrm{d}\omega \mathrm{e}^{\mathrm{i}\omega t}Z(\omega)\bar{I}_{\mathrm{n}}(0,\omega) \tag{4.3}$$

This relation assumes, of course, that there is not another PSC or a reflective discontinuity in the transmission line nearby, on the scale of Λ. In the more general case of a total current with an AC component, the AC current far from the Josephson element would be split between I_{s} and I_{n} in accordance with the ratio between R and $i\omega L$, so that a modified fig. 17b would include connections to both sides of $Z(\omega)$. One can also consider cases where the junction resistance itself is not negligible compared to $Z(\omega)$, e.g. for a small in-line tunnel junction, as in the schematic in fig. 17c.

The high-voltage DC behavior of the PSC takes a particularly simple form. At the center of the PSC most of the current $I \geqslant I_{\mathrm{c}}$ must be normal current I_{n}, which in terms of fig. 17c flows through the shunt impedance. The oscillations in I, of order I_{c} are then relatively small, so that the Josephson element is subject to an almost constant voltage bias. Therefore, the phase difference $\Delta\theta$ across the element increases nearly linearly with time, and one can express the $I-V$ relation in the form

$$\bar{V}=2Z(0)\left(I-I_{\mathrm{s}}(\overline{0,t})\right)=2R\Lambda\left(I-I_{\mathrm{c}}\langle f\rangle\right) \tag{4.4}$$

where

$$\langle f\rangle=\int_{0}^{2\pi}f(\Delta\theta)\mathrm{d}(\Delta\theta)/2\pi \tag{4.5}$$

is the average value of the periodic function f and the horizontal bars represent averages over time. In the high-voltage regime, the model predicts a constant differential resistance

$$\mathrm{d}\bar{V}/\mathrm{d}I=2Z(0)=2R\Lambda\equiv R_{\mathrm{eff}} \tag{4.6}$$

and an extrapolated excess current $I_{\mathrm{ex}}=\langle f\rangle I_{\mathrm{c}}$, in agreement with the SBT model. This is equivalent to a simple resistively shunted junction (RSJ) model with shunt resistance R_{eff} . Note, however, that R_{eff} is not the intrinsic junction resistance, which we have assumed to be negligible, but the resistance of the nonequilibrium region which extends to a distance Λ on either side of the core.

This leads to a characteristic voltage in the problem, $V_{\mathrm{c}}=I_{\mathrm{c}}R_{\mathrm{eff}}$, at which the fundamental Josephson frequency is

$$\omega_c \equiv 2eI_cR_{\rm eff}/\hbar = 4eI_cR\Lambda/\hbar \tag{4.7}$$

For much lower voltages, the Josephson oscillations become more pulse-like and are dominated by higher harmonics of $2eV/\hbar$ up to of order ω_c. For larger voltages, on the other hand, the oscillations become small perturbations on the DC average. One can further compare ω_c^{-1} to the characteristic times τ_J and τ_E. For a typical real material in a reasonable temperature range, one has $\omega_c\tau_E \gg 1$ and $\omega_c\tau_J > 1$. In the "high frequency" regime where both are very large, a particularly simple approximation becomes valid. In this case, the effective AC impedance shunting the junction in fig. 17b becomes a simple resistance

$$R_{\rm ac} = R_{\rm eff}\sqrt{\tau_J/\tau_E} \tag{4.8}$$

The $I-V$ curves for this situation can be expressed in terms of the solution of the resistively shunted junction (RSJ) model (see e.g. Solymar 1972) for the resistance $R_{\rm ac}$, in the form

$$I = I_{\rm RSJ}\left(\bar{V}, R_{\rm ac}\right) + \bar{V}\left(1/R_{\rm eff} - 1/R_{\rm ac}\right) \tag{4.9}$$

that is, with a correction that accounts for the different de resistance. In fig. 16 we have plotted the $I-V$ relation of eq. (4.9) for various values of τ_E/τ_J, using the linear current-phase relation.

The most striking feature about the curves of fig. 18 is the existence of nonzero voltage solutions for currents less than the critical current I_c. so that V is a hysteretic function of I (the more customary control variable in experiments). For the special case $\tau_E = \tau_J$, eq. (4.9) gives exactly the RS.J curve, while if $\tau_E < \tau_J$, the curve lies to the right of the RSJ curve [i.e. it has a larger $I(V)$]. In the more usual case $\tau_F > \tau_j$ and this hysteresis occurs. This is true

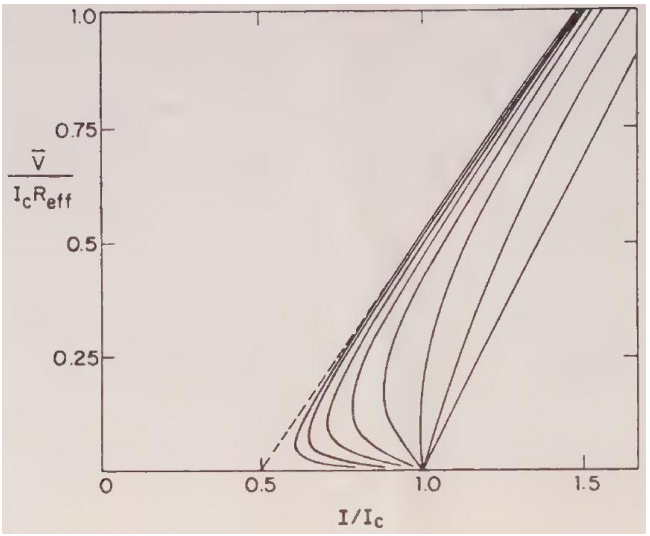


Fig. 18. $I-\bar{V}$ characteristics in the high-frequency limit for the linear $f(\Delta\theta)$ and various values of τ_E/τ_J. The curves are scaled so that all have the same critical current and high-voltage differential resistance. The values of τ_E/τ_J corresponding to the curves from left to right are $1024, 256, 64, 16, 4, 1, \frac{1}{4}$, and $\frac{1}{16}$. The dashed line is the high-voltage asymptote. (From Kadin et al. 1980.)

for any current–phase relation, and since the RSJ curve always rises vertically at $I = I_C, \tau_E > \tau_J$ provides the condition for hysteresis. This condition can be understood by noting that $R_{\rm ac} \ll R_{\rm eff}$, so that the voltage driving the Josephson oscillation is closer to being a

constant voltage bias. The resulting $I - V$ curve then lies closer to the voltage-biased line which forms the high-voltage asymptote, and as is evident from fig. 16, it approaches this line at lower and lower voltages as τ_E/τ_J is increased.

In an actual experiment, one typically measures voltage versus current at a series of temperatures near T_c. In fig. 19, we plot theoretical curves from the KSS model in an analogous way, showing the onset and development of hysteresis. They correspond to the linear current phase relation in the highfrequency limit, and were obtained from curves as shown in fig. 16 using the temperature scaling relations ($t \equiv T/T_c$)

$$\tau_E/\tau_J \sim (1-t); \quad I_c R_{eff} \sim (1-t)^{5/4} I_c \sim (1-t)^{3/2}. \tag{4.10}$$

Within the given approximations, these curves are independent of material. The onset of hysteresis at $\tau_{F/\tau_1} = 1$ would correspond to $T_c - T = 4$mK for Sn , and 0.05 mK for Al (Kaplan et al. 1976, Chi and Clarke 1979, and Clarke and Paterson, 1974).

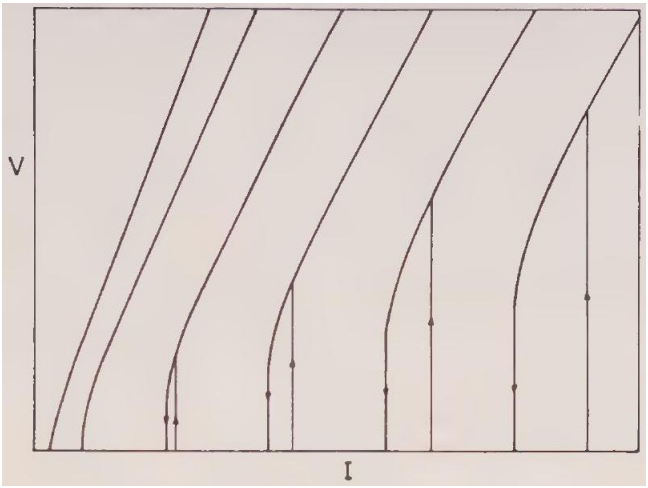


Fig. 19. I-V curves for the linear current-phase relation in the high-frequency limit for various values of τ_E/τ_J, with the temperature dependence reintroduced in accordance with $\tau_E/\tau_J \sim (1 - T/T_c)$, $I_c \sim (1 - T/T_c)^{3/2}$ and $I_c R_{eff} \sim (1 - T/T_c)^{5/4}$. The arrows pointing upward represent hysteretic switching at the critical current I_c into the dissipative state, and the down-ward-pointing arrows represent switching back into the zero-voltage state at the current I_m. The values of τ_E/τ_J corresponding to the curves from left to right are $\frac{1}{2}, 1, 2, 3, 4$, and 5 . (From Kadin et al. 1980.)}

The development of hysteresis in fig. 19 is qualitatively very similar to that seen in many experiments on both microstrips and whiskers. Quantitative comparisons, however, are complicated by a number of factors that are difficult to fold into such a model, such as noise-induced smearing of IV curves close to T_c and heating effects farther from T_c. In particular, heating has been shown to account reasonably well for hysteresis in some cases (Skocpol et al. 1974b, Kadin et al. 1978, Likharev 1979). The intrinsic hysteresis in the KSS model is a supplementary mechanism which should become important near T_c, where heating-induced hysteresis disappears more rapidly. The onset of hysteresis close to T_c does seem to be consistent with the picture, although some rather large sample-to-sample variations remain to be explained. Furthermore, in clean tin whisker crystals, where heating effects are somewhat less severe, Meyer and Tidecks (1976) have noted a saturation effect in the hysteresis similar to that predicted by the KSS model.

Since the model consists of a driven Josephson oscillator coupled to a transmission line, it can also be used to exhibit AC effects, in particular the propagation of charge imbalance waves away from the center. Looking first at oscillations in time at the center, fig. 20 shows I_{n} and Φ for parameters appropriate to Sn at $T/T_{\mathrm{c}} = 0.99, V = I_{\mathrm{c}}R_{\mathrm{eff}}$, and $I_{\mathrm{c}} = I_{\mathrm{c}}$ (strip), using the linear current-phase relation. The oscillations repeat with the Josephson period, and

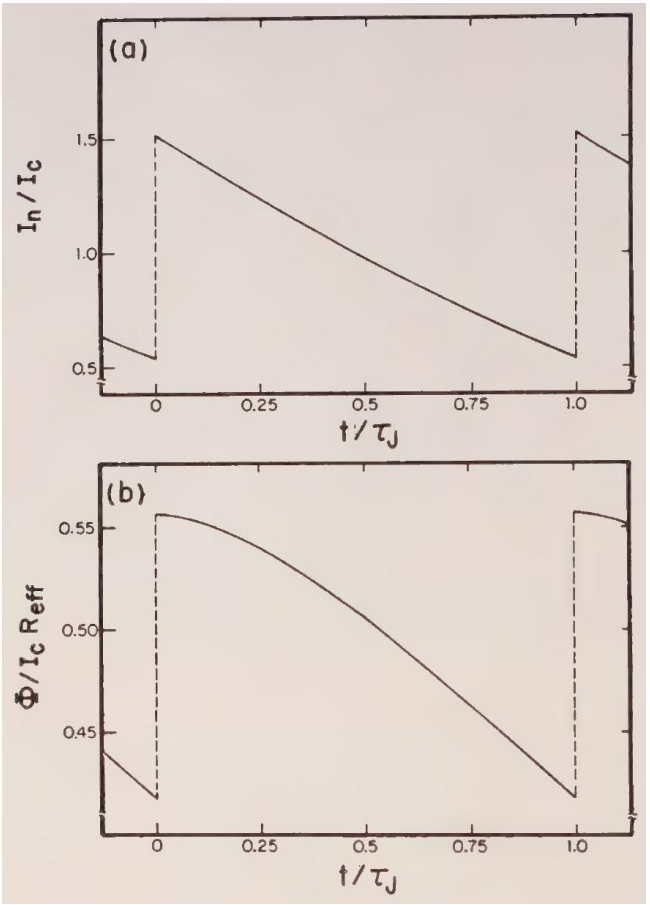


Fig. 20. Time dependence within a single Josephson period of the oscillations in the center for (a) $I_{\mathrm{n}}(0, t) / I_{\mathrm{c}}$ and (b) $\Phi(0,t)/I_{\mathrm{c}}R_{\mathrm{eff}}$ using the linear $f(\Delta\theta)$ and parameters $\tau_{\mathrm{E}}/\tau_{\mathrm{J}} = 11, \omega_{\mathrm{c}}\tau_J = 2.2$, $V = I_{\mathrm{c}}R_{\mathrm{eff}}$, and $I = 1.5I_{\mathrm{c}}$, appropriate for Sn at $T/T_{\mathrm{c}} = 0.99$. Both I_{n} and Φ are discontinuous at the beginning and end of each cycle for the linear $f(\Delta\theta)$. (From Kadin et al. 1980.)}

the abrupt jumps at the end of each cycle represent the discontinuous phaseslip process built into the piecewise-linear $f(\Delta\theta)$. These act as the source for the driven waves shown in fig. 21 as a function of position at a fixed time. The discontinuous nature of these jumps is again an artifact of the linear currentphase relation, but here they make the progression of the waves easily visible. Their wavelength λ is given in the high-frequency approximation as

$$\lambda = (\Lambda/\sqrt{\tau_{\mathrm{J}}\tau_{\mathrm{E}}})\,(h/2e\bar{V}), \tag{4.11}$$

which works out to 0.85Λ for the case of fig. 21 . The corresponding spatial behavior of μ_{n} and μ_{s} is shown in fig. 22, and clearly conforms in its time average to the earlier picture of SBT. It is also evident that the waves are decaying as they move away from the center. For the high-frequency limit in the condition $\tau_{\mathrm{E}} \gg \tau_{\mathrm{J}}$ the AC decay length Λ_{AC} is smaller than the DC decay length Λ by a factor $\sim (\tau_{\mathrm{J}}/\tau_{\mathrm{E}})^{1/2}$, which for figs. 18-20 is about 0.6 A . The difference

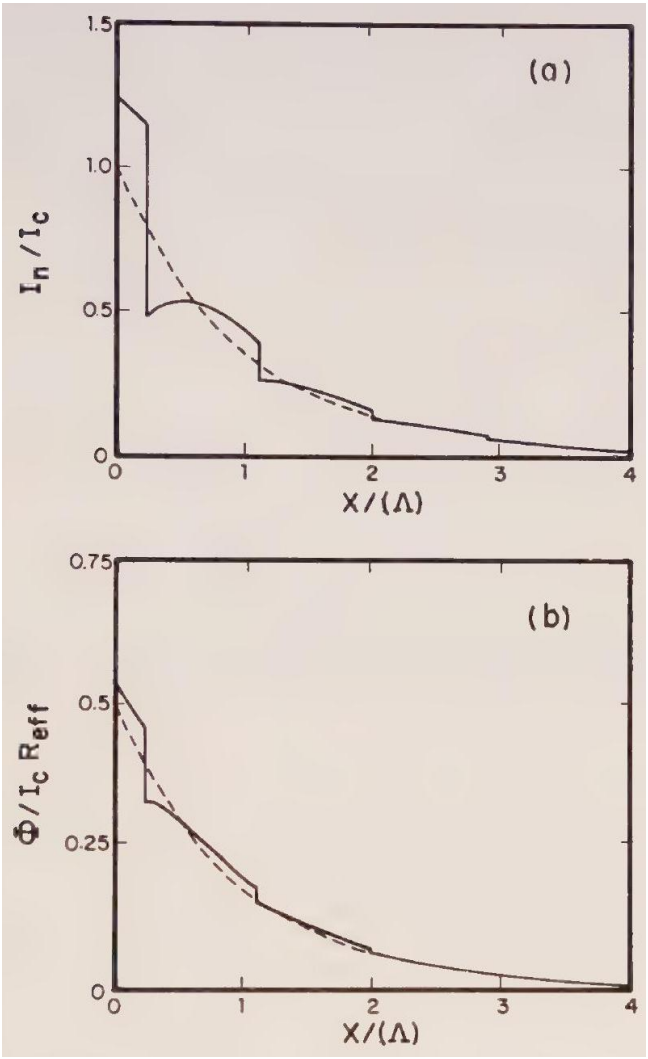


Fig. 21. Spatial dependence (for $x > 0$) of (a) $I_{\mathrm{n}} / I_{\mathrm{c}}$ and (b) $\Phi / I_c R_{\mathrm{eff}}$ for the same parameters as in fig. 20. The dashed curves are the DC averages. (From Kadin et al. 1980.)

between the two lengths is more dramatic for Al , for which τ_{E} is about 80 times larger than it is for Sn . This is demonstrated in fig. 23, where I_{n}

is plotted for Al with $T/T_{\mathrm{c}} = 0.99$ and $V = I_{\mathrm{c}} R_{\mathrm{eff}} /2$. In this case one has $\Lambda_{\mathrm{AC}} = \Lambda/8$, although in fact Λ_{AC} has in fact not decreased relative to Sn ; rather it is Λ proportional to $\tau_{\mathrm{E}}^{1,2}$ that has increased. In real terms, Λ remains on the order of a few μm, and in a later section we will consider the interaction of multiple PSCs spaced on this scale, via these driven oscillations of nonequilibrium charge imbalance.

There is also an AC voltage V_∞ across the PSC, even far away from the center, so that a PSC can act as a (weak) source of external microwaves, and conversely will show a Josephson step upon radiation with microwaves. However, this AC voltage is actually much smaller in amplitude than the value $I_c R_{\mathrm{eff}}$ that one might initially infer. In fact, it follows from the KSS model that in the regime we have been dealing with,

$$V_\infty \approx I_{\mathrm{c}} R_{\mathrm{eff}} /2\omega \left(\tau_{\mathrm{J}} \tau_{\mathrm{E}}\right)^{1/2} , \tag{4.12}$$

which is not only smaller than one might expect, but in addition it has a faster roll-off with voltage (Kadin et al. 1980). This behavior is qualitatively consistent with the observation of a rather small AC Josephson step for a PSC in

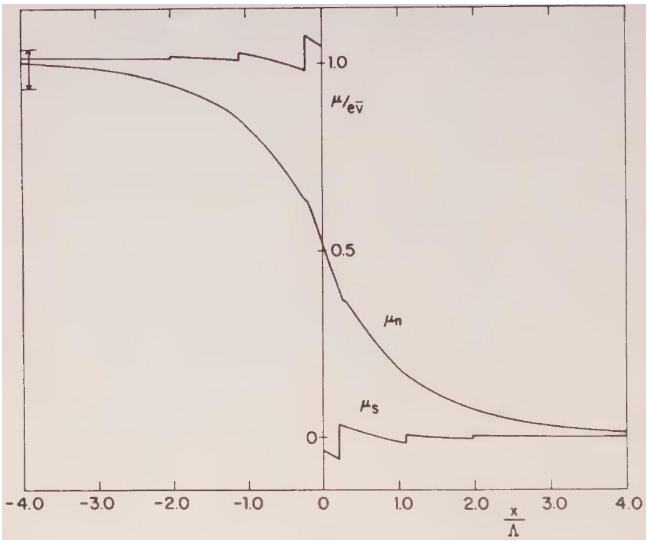


Fig. 22. Spatial dependence of the potentials $\mu_{\mathrm{n} } / e \bar{V}$ and $\mu_s/e\bar{V}$ for the same set of parameters as in fig. 21. The behavior for $x < 0$ is included to make clear the symmetry of the solutions. The range of variation of $\mu(-\infty)/e\bar{V}$ is indicated by arrows on the left. (From Kadin et al. 1980.)}

Sn (Skocpol et al. 1974a) and the absence of such an effect for a PSC in Al (Klapwijk and Mooij 1976a,b).

Finally, we reiterate that the KSS picture does not represent a complete selfconsistent model of a PSC, in that the treatment of the phase-slip process in the core is not really treated as a true nonequilibrium process. In particular, Baratoff (1982a,b) has pointed out, on the basis of numerical analysis of the complete set of nonlinear equations, that the oscillations in the core may be expected to be largely decoupled from the charge imbalance waves out in the "wings". Nevertheless, the qualitative pictures in the KSS model are likely to retain some validity. For completeness, we also mention several other theoretical approaches to the self-consistent treatment of PSC: Kulik (1980), Ivlev and Kopnin (1980, 1981, 1982), and Watts-Tobin et al. (1981). The subject is by no means closed.

20.4.2 4.2. Superconducting microbridges

The Josephson effect was originally derived for and seen in tunnel junctions, but quite early on, similar phenomena were seen in a wide assortment of other weak links. In particular, the two basic types that have been studied in detail are the thin film microbridge (basically a microscopic constriction in a
superconducting film) and the point contact (a sharpened superconducting wire contacting a plate). We will concentrate on the microbridge, although in fact microbridges have evolved to become more and more like point contacts in an attempt to imitate the three-dimensional geometry of the latter. Since various extensive reviews of microbridge behavior (Lindelof, 1981, Bindslev Hansen and Lindelof 1981, Likharev 1979) have already appeared recently, the current treatment will attempt to identify several aspects of microbridge behavior that illustrate the points that we have been making in earlier sections, namely that dynamic non-equilibrium phenomena at the Josephson frequency can be reflected in the DC $I - V$ characteristics. See also the reviews by Aslamazov and Volkov (1985) and by de Lozanne and Beasley (1985) in the present volume.

In a typical tunnel junction, the connection between the two superconductors is an interven-

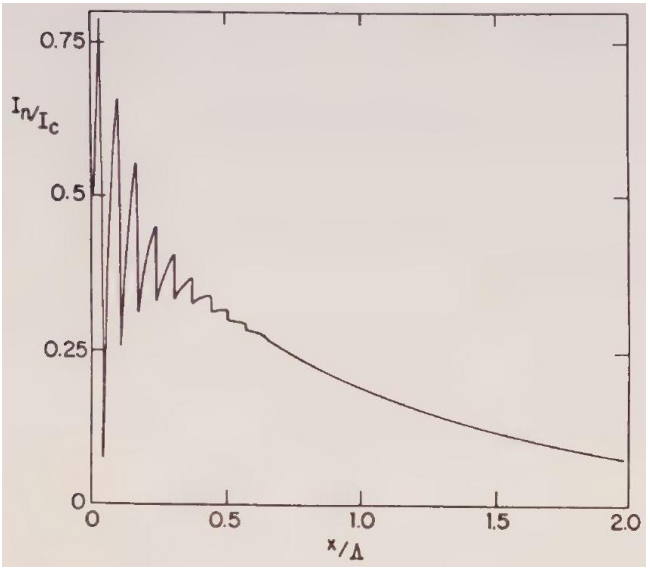


Fig. 23. Spatial dependence of $I_{\mathrm{n} } / I_{\mathrm{c}}$ for the linear $f(\Delta\theta)$ and parameters $\tau_{\mathrm{E}} = 280\tau_{\mathrm{J}}, \omega_{\mathrm{c}}\tau_{\mathrm{J}} = 11$, $\bar{V} = 0.5 I_{\mathrm{c}} R_{\mathrm{eff}}$, and $I = 1.0 I_{\mathrm{c}}$, appropriate to Al at $T/T_{\mathrm{c}} = 0.99$. Note that the horizontal scale is expanded by a factor of two compared with fig. 21. (From Kadin et al. 1980.)}

ing layer of insulator, and the interaction is due to the overlap of the weak evanescent tails of the wave functions on the two sides. The current densities in the superconductor itself are rather small, and nonequilibrium effects are kept to a minimum, and are relatively easily understood. In the microbridge, on the other hand, the bridge typically consists of the same superconducting material as the banks, so that the weak interaction must be produced geometrically. In fact, in order to produce an ideal Josephson effect, all the dimensions of the bridge region must be less than the GL coherence length $\breve{\zeta}(T)$, typically less than a micron (Likharev 1979). In the voltage state, AC Josephson effects are produced by periodically driving the gap to zero by the application of a large current density. Even in the banks, the nonequilibrium effects can often not be neglected, and in the bridge region itself, these effects must necessarily be in the highly nonlinear regime. For examples of different microbridge geometries, see fig. 24.

One of the simplest of these nonequilibrium effects near the bridge, yet one of the most crucial, is Joule heating. The effective dimensionality of the bridge is of great importance here. For a one-dimensional bridge (i.e. a PSC), the hot electrons will diffuse out over quite a substantial distance (typically several microns) before the heat is finally transferred to the substrate. For two and three dimensions, on the other hand, there is a dilution process that acts to lower the temperature even without transfer of heat out of the film. Even then, a simple, general argument shows that for an ideal three-dimensional contact, the temperature T_{m} in the middle of the bridge will be enhanced above T_0 of the bath according to

$$T_{\mathrm{m}} = \left[T_0^2 + (3.2\ \mathrm{V})^2\right]^{1/2} \tag{4.13}$$

where the voltage V is given in mV and the temperatures are in K (Tinkham et al. 1977). For high-voltage (and thus high-frequency) operation, this emphasizes the necessity of trying to achieve a three-dimensional geometry, within a thin film. This has been achieved experimentally with a so-called variable-

thickness bridge (VTB) (Klapwijk and Mooij 1975, Gubankov et al. 1977, Octavio et al. 1977), where the thickness of the bridge region is much less than that of the banks. It has been in these types of microbridges that the best and most consistent Josephson performance has

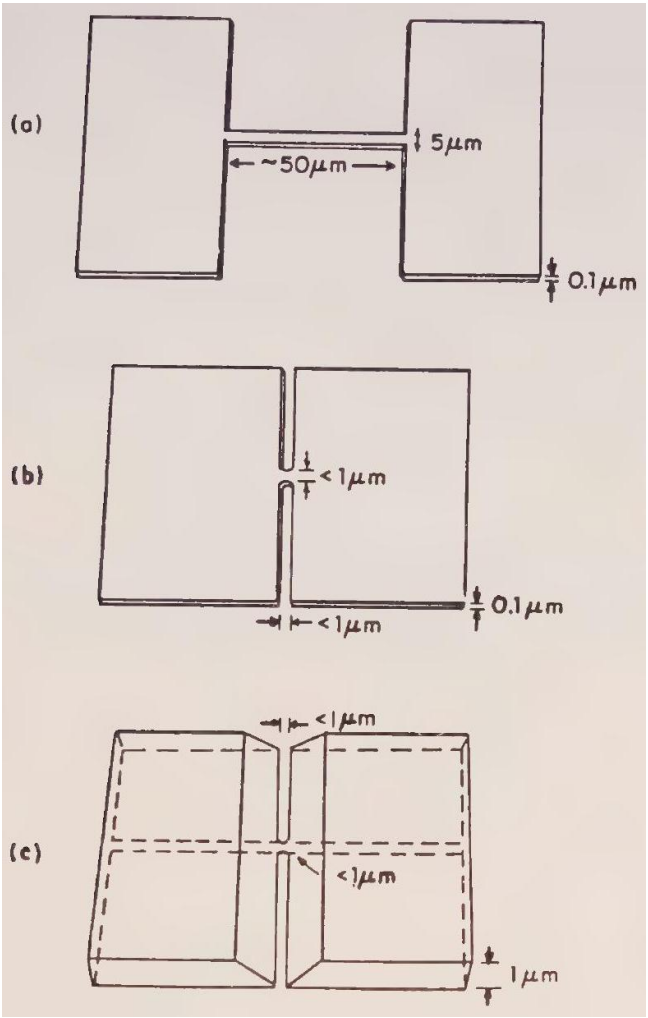


Fig. 24. (a) Long microbridge; (b) two-dimensional uniform thickness microbridge; (c) variablethickness bridge. (From Octavio et al. 1977.)

been found. This is fortunate, because the theoretical analyses have, for reasons of simplifying the calculations, been going in the same direction, with the "one-dimensional superconductor with ends in equilibrium" (ODSEE) (Likharev, 1979). We will discuss some of the features seen in these kinds of bridges, together with simple physical explanations of their origins.

Given the fact that these small VTBs have an almost ideal sinusoidal supercurrent-phase relation, and that the capacitance across the bridge is generally negligible, one might initially expect that the simple resistivelyshunted junction (RSJ) model might provide an acceptable first estimate of the $I - V$ characteristics of such a junction. In fact, there are several very striking deviations from this simple behavior, as suggested in fig. 25. As the current is increased above the critical current I_c, there is first the low-voltage "foot" (Octavio et al. 1978, Gubankov et al. 1977, 1980), followed by a fairly sharp rise in voltage at an "enhanced critical current", and several noticeable wiggles at subharmonics of the energy gap 24 . Finally, at high voltages there is a quasi-ohmic region, which however extrapolates to the current axis with a positive current.

The current understanding of the low-voltage foot is that it is a manifestation of nonequilibrium "dynamic cooling" in a short microbridge. The following physical explanation, due to Tinkham (1979, 1981), was further refined by Schmid et al. (1980) and is closely related to other calculations of Golub (1976) and Aslamazov and Larkin (1976). In this picture (see fig. 26), the bridge is so short that the quasiparticles in the bridge region are in equilibrium with the

banks, provided that their energies are at least as great as the energy gap Δ_0 of the banks. In the presence of current, the gap is decreased in the bridge, and the quasiparticles with energies $E < \Delta_0$ are essentially trapped. They can bounce back and forth within the bridge (via Andreev reflection) (Andreev 1964), but cannot leave the bridge except by an inelastic scattering event, set by the electron-phonon time τ_E. A current greater than the critical current I_{c_0} will cause the gap in the bridge to oscillate cyclically at

the Josephson frequency between Δ_0 and 0 (in the center). Now, at low frequencies $\omega\tau_E \ll 1$, this does not present a problem; the low-energy quasiparticles have time to remain at equilibrium. In the other limit $\omega\tau_E \gg 1$, however, the low-energy quasiparticles are permanently under-represented. Their occupancies are more appropriate for higher-energy quasiparticles. Given this, and the fact that the low-energy quasiparticles are actually most important in determining the gap, the value of the gap and of the effective critical current I_{c_1} (here signifying the amplitude of the Josephson oscillations) will be enhanced above the equilibrium value I_{c_0}. For intermediate frequencies $\omega\tau_E$ on the order of unity, there will be an intermediate degree of critical current enhancement. This enhancement will saturate at a Josephson frequency of several times $1/\tau_E$, above which the $I \cdot V$ curve takes a form similar to a RSJ with a larger value of I_c. The theory (Schmid et al. 1980) predicts that $I_{c_1}/I_{c_0} = 1.33$, which agrees very well with experiments (Octavio et al. 1978) after corrections for finite length have been put in.

The "excess current" suggests the presence of a time-averaged supercurrent in parallel with the normal dissipative current, although other interpretations are also possible. This excess current, which also appears in PSCs, typically has a value of $0.6 - 0.8$ of the enhanced value of I_c (Octavio et al. 1978, Gubankov et al. 1977, 1980). Deviations from a purely sinusoidal currentphase relation might be able to explain some of this, although this does not appear to be the case for these small bridges. It has also been suggested, on the basis of TDGL theory, that the excess current is really an "insufficient voltage" due to the finite response time of the gap, taken together with the rigid boundary conditions (Likharev and Yacobson 1975). Finally, a recent analysis has suggested that the main contribution to this excess current may not be due to dynamic processes at all, but rather to a static process involving transport of current across the bridge region with the help of Andreev reflection at the boundaries with the banks (Artemenko et al. 1979). This excess current will occur even in a normal superconducting contact, where clearly Josephson dynamics are not relevant. The theory predicts a value

$$I_{ex} = 4\Delta/3eR_N, \tag{4.14}$$

in the limit of small contacts of zero length, where the latter form has assumed an ideal junction I_cR product. This picture has also been extended within a unified theory to allow for a transition between a "clean" bridge contact (which shows the effect) and a "dirty" tunnel contact (which does not) in terms of the scattering at the interface (Blonder et al. 1982). Reasonable agreement with this theory has been achieved with point contacts (Divin and Nad' 1979, Blonder and Tinkham 1983).

The subharmonic gap structure is another example where the effect may or may not be related to dynamic effects at the Josephson frequency. These features, which show up most clearly in the conductance $\sigma = dI/dV$, are shown

for one Sn microbridge in fig. 27. They appear approximately at voltages $V = 2\Delta(T)/ne$, where $n = 1, 2, 3, \ldots$, up to as many as 12 , and with peak heights that typically tend to decrease monotonically with n. If one assumes that this relation should actually be exact, and that deviations from it are due to local heating in the bridge, then these features can be used as a thermometer for the bridge temperature, as has been done by Octavio (Octavio et al. 1977), giving good agreement with the heating model of Tinkham et al. (1977).

The origin of the subharmonic gap structure remains a subject of debate. Earlier models involved multiparticle tunneling (Schrieffer and Wilkins 1963) or self-coupling of the Josephson

radiation to the microbridge (Werthamer 1966). However, the former does not explain subharmonics of index greater than two whereas the latter can account directly only for the even subharmonics (n even). Combining the latter with single particle tunneling can give the odd subharmonics, but a quantitative fit given the similar magnitudes of both harmonics has been lacking. Lindelof (1981) has recently suggested
that rather than the usual Josephson radiation, quantized charge imbalance waves created by the microbridge could produce these features. Finally, the recent picture that used Andreev (1964) reflection to explain the excess current (Klapwijk et al. 1982, Octavio et al. 1983) has also been applied to explain subharmonic gap structure via multiple Andreev reflection of trapped quasiparticles inside the bridge. Again, this does not involve dynamics at the Josephson frequency. This picture has no difficulty with the odd and even harmonics, and furthermore can explain the features in point contacts between unlike superconductors with different values of Δ in a way that the selfcoupling models cannot. A complete quantitative test of the various models, however, requires a refinement of both the theories and the experiments on real bridges.

20.4.3 4.3. Interactions between microbridges or phase-slip centers

In attempting to understand the superconducting dynamics in a microbridge or phase-slip center, one of the more important techniques is to use a Josephson device to probe the dynamics produced by the first Josephson device (i.e. the microbridge or PSC). In fact, many of the effects discussed in previous chapters have in effect used just this technique, except that the detector was the same device as the "injector" of the nonequilibrium dynamics. There are some cases where the configuration of a strong injector and a weak probe is most illustrative. There are others in which a more symmetric configuration involving Josephson oscillators mutually influencing each other has been involved, and still others where a single junction has been used in a resonant mode as a self-detector.

Consider first the experiment of Skocpol and Jackel (1981), illustrated schematically in fig. 28a, where a superconducting tin microstrip contained a localized weak spot, and nearby, on the scale of the AC decay length for charge imbalance (about 2μ m), was located an array of small Josephson tunnel junctions, with lead counter-electrodes. For currents exceeding the critical current, a PSC was nucleated at the weak spot, and would be expected to generate charge imbalance waves which extend out to the tunnel junction probes. In particular, the condensate electrochemical potential μ_s should oscillate with frequency $2eV\hbar$, where V is the total voltage across the PSC. This in turn should modulate the phase difference across the junction, and should give a small constant-voltage AC Josephson step at probe voltages $V' = n\hbar\omega/2e = nV$, for integers $n = \pm 1, \ldots$, in exactly the same way as would an external microwave current. An effect of the type desired was in fact seen in the IV characteristics of the closest probe junction, although it was smaller than expected. This may have been due in part to the depressed value of the gap in the center of the PSC, also measured using the tunnel junction probes. It was not possible, however, in these measurements to obtain information on the wave nature of the inferred oscillating potentials.

The experimental configuration that we have been discussing, indicated in fig. 28b, is topologically equivalent to that in fig. 28c, used to investigate the interaction between two microbridges spaced several microns apart. These experiments, and others on arrays of microbridges, have shown that under certain circumstances the voltages across the individual bridges tend to lock together, and their Josephson oscillations to synchronize. The former effect can be seen simply by examining the DC $I - V$ characteristics, while the latter has been seen most directly by measuring coherence in the microwave radiation emitted by the bridges. This subject of the short-range interaction between two or more weak links has been reviewed by Lindelof and Bindslev Hansen (1981).

The voltage locking is illustrated by an example from Jillie et al. (1977, 1980), using In microbridges spaced less than 2μ m apart (fig. 29). Typically, the current through one of the microbridges was held fixed, while that through the other was varied. Some results of these experiments are shown in fig. 30, and compared with a numerical simulation (Jillie et al. 1980). In addition to the static effects, which can be simply modeled in terms of the steady-state diffusion of excited quasiparticles from one bridge to the other, there are some

striking dynamic effects involving voltage locking or frequency pulling. The voltage locking, which occurs for a fairly narrow range of currents, is always accompanied by a sharp change in the differential resistance $\mathrm{d}V/\mathrm{d}I$ of the junctions. This phenomenon of voltage locking is not fundamentally different from that of a constant-voltage Josephson step under the influence of a highfrequency signal. However, since the two junctions are comparable in their oscillator strengths, they exert a similar frequency-pulling effect on eath other when their frequencies are close. As nonlinear oscillators, they also exhibit a similar (but weaker) effect when their frequencies are small integral multiples of each other (note the small "dimples" in fig. 30 b, c).

The strength of the voltage locking was characterized by the total change in the differential resistance from both bridges, and is shown for two temperatures near T_c in fig. 31 as a function of locking voltage. The remarkable feature of this is that the interaction strength oscillates with voltage (frequency), in a way that suggests rather strongly the presence of driven waves.

The simple model to explain the effects involved assuming that a fraction (of order $20^\circ_\circ$) of the quasiparticle current from each bridge also flows through the other one. This is equivalent to the schematic diagram in fig. 32. With an optimum value for this effective shunt resistance R_s that couples the two resistively-shunted oscillators, a reasonable fit to many of the features of the voltage locking could be obtained. However, this cannot account for the very striking modulation in the strength of the voltage locking interaction.

One simple modification is to introduce the idea of a delay time for the excited quasiparticles to get from one bridge to the other. If one assumes a fixed delay time, independent of frequency, together with an oscillatory excitation process, one is led directly to the phenomenon of waves in the superconductor, and back to a consideration of charge imbalance waves as a possible cause of voltage locking in the closely-spaced bridges.

This delay time can be analyzed by replacing the simple resistor coupling of fig. 32a with a delay line, which is another word for a finite length of transmission line, as used by KSS (Kadin et al. 1980) to model charge imbalance dynamics near a PSC. This is essentially equivalent to considering the region between the two bridges as a resonant cavity for the charge imbalance waves (Lindelof and Bindslev Hansen 1977).

A numerical simulation of the equations has been carried out (Blackburn 1983), but one can also make use of lumped element equivalents of the transmission line. One can then transform the problem of charge imbalance wave coupling to one with a single complex impedance shunting the two bridges. The general expression will depend on the detailed geometry and be rather complicated, but for the case where the bridges are not too close together, this shunting impedance takes the form

$$Z_\mathrm{s} = 3Z_0 \exp(i2kl), \tag{4.15}$$

where Z_0 again is the characteristic impedance of the line (eq. 2.42), k is its (complex) propagation vector (eq. 2.41), and $2l$ is the distance between the bridges. This form immediately gives the roll-off of the interaction with distance, and furthermore shows that the complex phase of the coupling impedance rotates both with distance and with voltage (through the frequency dependence of k). One can show that the optimum coupling is one that is inductive (i.e. pure imaginary), and that for identical bridges, the pure resistive coupling will actually yield a vanishingly small range of voltage locking. Therefore, the effective coupling strength should oscillate as a function of voltage before dying out, as in fact was observed in the experiments.

Given these conditions, one can estimate the apparent wave velocity from the experiments, and it is roughly in accord with what is expected theoretically. However, although a detailed fit has not been carried out, there are some serious detailed differences, in particular the temperature dependence of the inferred wave velocity. The theory suggests a velocity that goes as $(1 - T/T_c)^{1/4}$, whereas the data gives an exponent of order $\frac{1}{2}$. The situation is complicated by a number of factors, and remains unresolved. There have also been several other proposals to explain this voltage-locking behavior, including one (Lindelof and Bindslev Hansen 1981) that depends on DC quasiparticle injection and does not require the Josephson effect at all.

One recent experiment (Kadin et al. 1981) attempted to study the role played by charge imbalance waves near a PSC by providing a boundary to reflect the waves produced by the PSC back to the center, thereby using it as its own detector. This was done using a narrow channel of length $2L$ much less than the AC decay length, which broadened suddenly to wide banks. Assuming that a PSC was localized in the center of this channel and sending out waves in both directions, then the waves should be expected to reflect at
the ends with inversion, returning to the center with a phase lag

$$\Delta\theta = \pi + 4\pi L/\lambda. \tag{4.16}$$

This is equivalent within the transmission-line model to "shorting out" the ends at distance L from the center. One can used the lumped element equivalent of the finite length of the transmission line (fig. 32b,c) to obtain a shunting impedance

$$Z = 2Z_0 \tanh(KL), \tag{4.17}$$

which has resonances that occur when the condition $\Delta\theta = 0$ is satisfied, i.e.

$$2L = \lambda/2, 3\lambda/2, \ldots, \text{ etc. }, \tag{4.18}$$

and these would also be expected to show up as features in the differential resistance of the bridge, since varying the voltage will vary the wavelength of the charge imbalance waves. These ideas were tested on a set of narrow. In channels about 0.3μ m wide, and from 0.5μ m to 4μ m in length. These samples did indeed exhibit a set of bumps in $\mathrm{d}V/\mathrm{d}I$ in approximately the voltage range expected. Some of these features were associated with resonances in the charge imbalance waves driven by the PSC, and the velocity and temperature dependence of the waves thus inferred were in rough accord with the theoretical predictions. No other obvious sources (such as microwave resonances or subharmonic gap structure) could account for these features. On the other hand, detailed agreement with theory was lacking, suggesting at least that the model and/or the treatment of the boundary conditions were oversimplified.

There have also been attempts, both experimentally and theoretically, to examine large arrays of closely-spaced microbridges for coherent interactions. In one such experiment, a linear array of up to 2000Nb/Ta proximity-effect microbridges were fabricated with spacings that went down to less than 2μ m (Palmer and Mercereau 1974, 1977). For the smallest separations, these were found to exhibit coherent behavior of their Josephson oscillations at low frequencies. Although coupling via magnetic flux modulation in these very wide bridges (100μ m) has been proposed as a possibility, coupling via charge imbalance waves has also been considered. Within the KSS model, the finite length of transmission line of distance $2L$ between each adjacent pair of Josephson oscillators can be represented by its "tee" equivalent, as represented in fig. 32a, where $Z_1 = Z_0 \tanh(KL, 2)$ and $Z_2 = Z_0, \sinh(KL)$. For an array of such identical PSC's, driven by an external DC current, symmetry requires that the nonequilibrium potential $\Phi = 0$ halfway between the junctions. Then, no current goes through the transverse impedances Z_2, and the problem reduced essentially to the single PSC in a resonant cavity treated above, so that the array should show the same resonant features in its $I - V$ characteristics. This picture

also accounts for the DC interaction between the PSCs, in that the differential resistance of such an array of identical equally spaced PSCs in
a filament of length S takes the form

$$\mathrm{d}V/\mathrm{d}I = 2\Lambda n R \tanh(S/2n\Lambda). \tag{4.19}$$

This properly interpolates between the value of $2nAR$ for non-interacting junctions and SR for a larger number of closely spaced bridges.

Artemenko, Volkov, and Zaitsev (1978a,b) have treated the similar problem of a large array of proximity-effect bridges, using a more elaborate theoretical framework, which however is approximated by a set of equations that are virtually identical to the picture of fig. 32 before calculations are actually carried through. They have pointed out that, among other consequences, the periodic array of Josephson oscillators in the superconducting filament alters the propagation characteristics of the charge imbalance waves, leading to the development of a band structure, including forbidden gaps, in much the same way as a band structure develops for electron propagation in a periodic lattice. This also follows from fig. 32, if one replaces each Josephson oscillator by its characteristic Josephson inductance $L_j = h/2eI_c$ appropriate for small amplitudes, and then uses Kirchhoff's current and voltage laws between each of the nodes.

It is important to note that the schematic circuit of fig. 30 is essentially equivalent to the actual circuit of devices that have been artificially fabricated to permit coherent coupling of two or more Josephson oscillators, which need not be spaced very closely together, each of which can be represented as a simple RSJ. In these arrays of junctions, an external shunt (which need not be purely resistive) permits some microwave current to recirculate through the series array, and provides a phase reference onto which the individual oscillators can lock, in the same way as to an external microwave signal. Not surprisingly, since one-dimensional long-range order tends to be unstable, the long-range interaction provided by the single loop around the entire array has been found to be more effective in producing long-range phase coherence than local interaction between adjacent bridges. These are of technological as well as fundamental interest, since the total microwave power coupled from an array of n such coherently synchronized oscillators can approach n^2 times the power of an individual oscillator, with a radiation linewidth that is narrowed by a factor of n. One of the more successful configurations for obtaining this coherence involved a parallel configuration for DC biasing, but a series arrangement at microwave frequencies (Sandell et al. 1979). This ensured that the junctions were automatically locked to the same frequency, and the shunt impedance had merely to synchronize the phases of the individual oscillations. One such array of about 100 In microbridges, fabricated by electron-beam lithography, did in fact produce a measured 10,000 times the microwave power from a single junction, in agreement with the predicted scaling (Jain et al. 1981). Arrays of other kinds of junctions, including tunnel junctions, have also been examined, using various types of coupling, including coupling via a
resonant cavity or a resonance in the array itself (e.g., Davidson 1981, Bindslev Hansen et al. 1981, Bindslev Hansen 1982, Likharev et al. 1981). Finally, there has also been considerable work recently on large two-dimensional arrays of junctions (e.g., Resnick et al. 1981, Voss and Webb 1982, Abraham et al. 1982). The ultimate significance of all this work, and its possible relation to nonequilibrium superconductivity, remain to be seen.

20.5 5. Discussion and conclusions

In this chapter we have treated a number of experimental configurations which are illustrative of the richness and complexity of the phenomena in the field known as nonequilibrium

superconductivity. We have reviewed the theory emphasizing physical models rather than formal mathematical development. The latter can be found in a number of the other chapters of this volume. In our view the use of simple physical models is essential to process by which experiments to probe these phenomena are designed in a creative way. Detailed theory is of course needed for the quantitative analysis of experimental results. The chapter has been focussed strongly on the use of the AC Josephson effect to produce and to probe the dynamics of the order parameter. This approach allows for the study of high-frequency dynamics through measurement of DC current-voltage characteristics. Thus rather complicated nonequilibrium phenomena can be studied using remarkably simple tools, ammeters and voltmeters. Within this framework our detailed discussion has focussed on investigations of the pair-field susceptibility, studied using tunneling junctions, and experiments with phase-slip centers, and microbridges. Central to the discussion is the transmission-line model of dynamical charge imbalance effects, which is developed to facilitate understanding charge imbalance waves. Special attention has been paid to physical explanations of the measurement of the pair-field susceptibility which have not been widely appreciated. A number of other fundamental experiments relating to nonequilibrium superconductivity, but not necessarily involving the AC Josephson effect, are treated in the section in which the basic theory is developed.

Superconductors out of equilibrium have been excellent model systems for the study of nonequilibrium statistical mechanics, in part because the equilibrium superconducting state is so well understood. In a few instances there are remarkable parallels between measurements in the superconducting state and similar studies of other physical systems out of equilibrium. The most striking example of this is the study of the pair-field susceptibility which yields results which are similar to those obtained in neutron scattering experiments on magnetic systems used to probe the dynamics of the magnetic order parameter. Propagating charge imbalance waves in superconductors were originally discovered in a pair-field susceptibility experiment. In the absence of any
detailed theory they were identified as a propagating collective mode of the superconducting order parameter by exploiting the analogy with magnetic systems.

Recently the inelastic and elastic electron scattering times that parametrize the theory of nonequilibrium superconductivity have become further accessible to experimental study in the context of the investigation of electronic localization in thin wires (Chaudhari et al. 1980) and thin films (Gordon et al. 1983, Santhanam and Prober 1984). In the study of weak localization in thin films the internal consistency of the data and the agreement of the temperature-dependent resistance and magnetoresistance with theory is extremely quantitative. Turning the problem around, the determination of relaxation times from the analysis of localization data may stimulate detailed, first-principles microscopic calculations.

Despite the breadth of the work in nonequilibrium superconductivity, most of the quantitative experimental studies have been carried out at temperatures very close to T_c where the coupled equations for the order parameter and quasiparticle distribution function have particularly simple analytic forms and are actually differential equations. Extensions to low temperatures will probably require more extensive numerical analysis of the theory than has been previously used, as analytical results may not be obtainable. On the experimental side, future work at low temperatures will have to overcome the problem of heating. Studies of transient response over short time scales, which are possible using superconducting sampling devices e.g., Faris (1980), may be an important tool in finessing this heating problem.

It should also be noted that most experiments in the area of nonequilibrium superconductivity have been carried out in regimes rather close to equilibrium and under nearly linear conditions. Nonlinear effects, which have been hardly touched experimentally, may be a fruitful field of study when long-wavelength-high-intensity electromagnetic sources such as the Free Electron Laser become available.

Finally, the issues which are raised in nonequilibrium superconductivity are very important for the understanding of superconducting devices and possible hybrid systems containing both superconducting and semiconducting devices. Quasiparticle injection by tunneling is central to the operation of both the superconducting transistor (Gray 1978b), the quiteron (Faris et al. 1983) and three-terminal edge junctions (Hunt and Buhrman 1983). These are threeterminal superconducting devices of a type which may be very useful in the practical application of superconducting digital electronics, i.c. for the superconducting computer. Optimization of their performance will require detailed knowledge of nonequilibrium superconductivity. In a superconducting computer, or a hybrid computer containing semiconducting active devices and narrow superconducting interconnects, there will probably be quasiparticle injection into the interconnects and current flow across superconducting
semiconducting or superconducting-normal boundaries. As the scale of integration of such systems becomes larger and the device spacing gets smaller one can expect the lengths of the superconducting interconnects to become shorter than the nonequilibrium lengths associated with the processes that we have discussed in this chapter. The consequences of this for the technology have not really been explored.

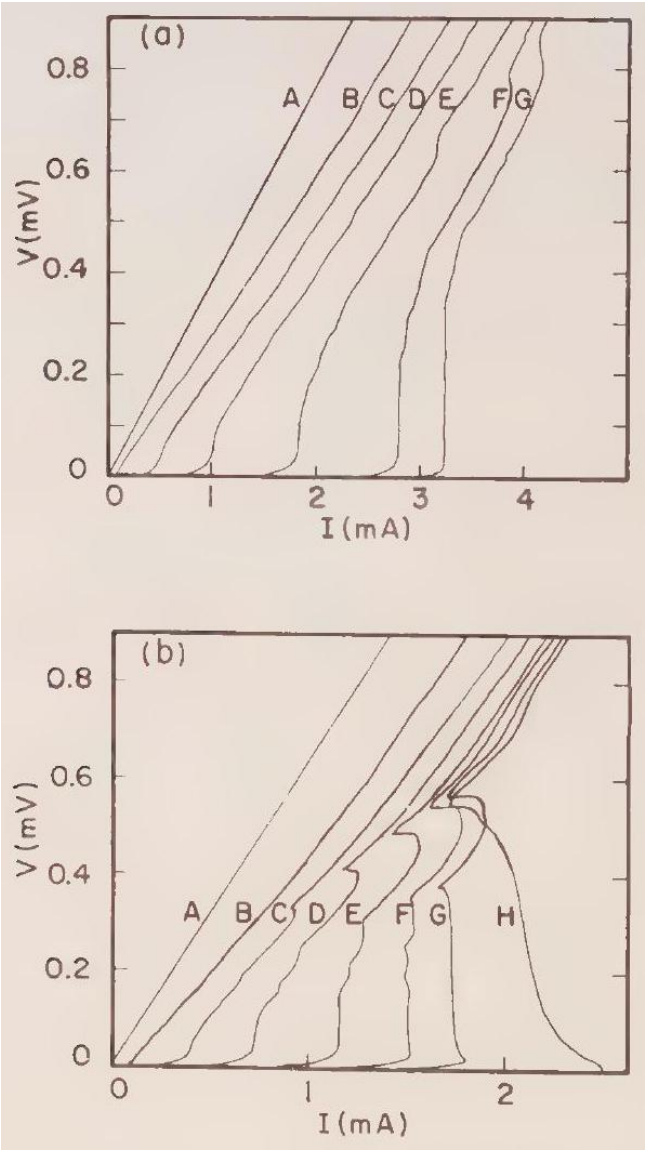


Fig. 25. (a) I I'characteristics of well-cooled microbridge. A through G correspond to temperatures of $4.20, 3.68, 3.56, 3.38, 3.05, 2.52$, and 2.10 K , respectively. (b) $I - V$ characteristics of a very well-cooled microbridge. A through H correspond to $4.2, 3.73, 3.62, 3.49, 3.28, 3.18, 2.97$, and 2.10 K , respectively. (From Octavio et al. 1977.)

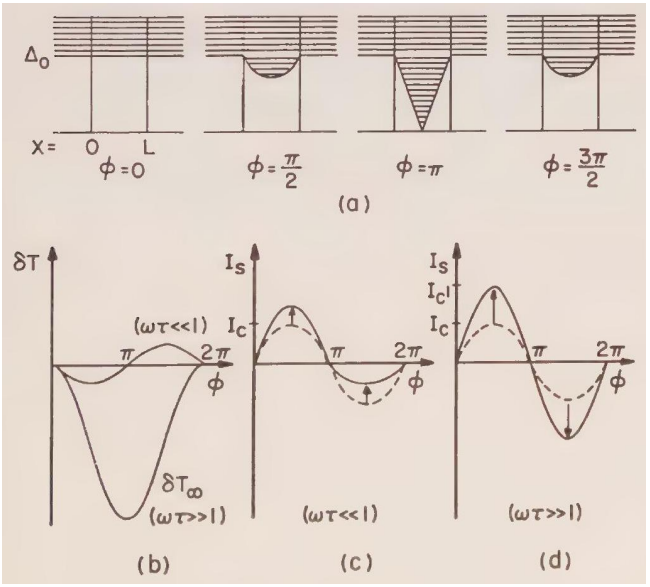


Fig. 26. (a) Cyclic depression of the gap. Quasiparticle levels above $\Delta_{0 $ remain in thermal equilibrium by rapid diffusive contact with the banks. Those in levels below Δ_0 (heavy shading) can be out of equilibrium. (b) Effective temperature shifts for rapid and slow modulation of Δ. (c) $I_s(\phi)$ for $\omega\tau_E \ll 1$, showing increase in forward current. (d) $I_s(U)$ for $\omega\tau_E \gg 1$, showing increase of effective I_c to $I_{cl} > I_c$. In (c) and (d), equilibrium supercurrents are shown in dashed curves for comparison. (From Tinkham 1981.)}

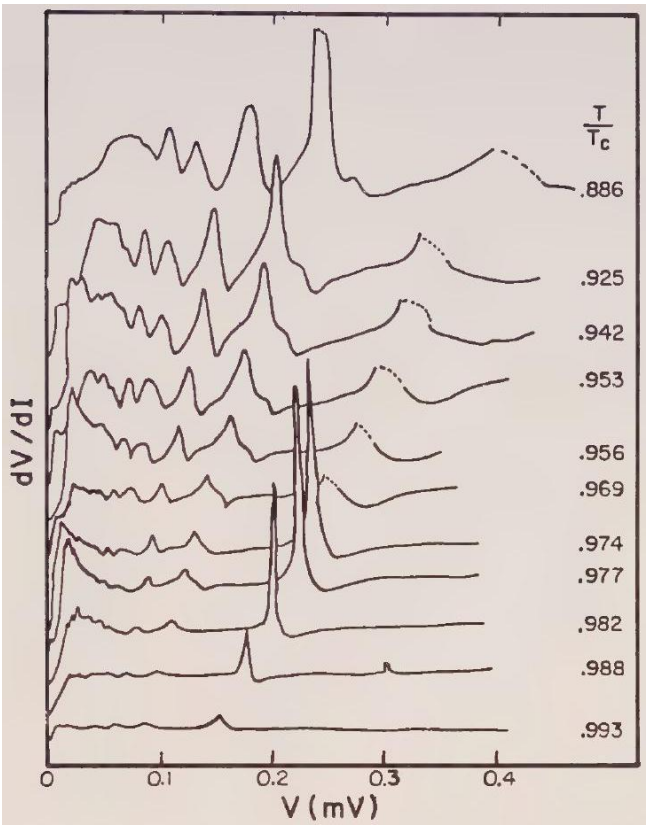


Fig. 27. Derivative curves showing the variation of the subharmonic gap structure with temperature. (From Octavio et al. 1977.)

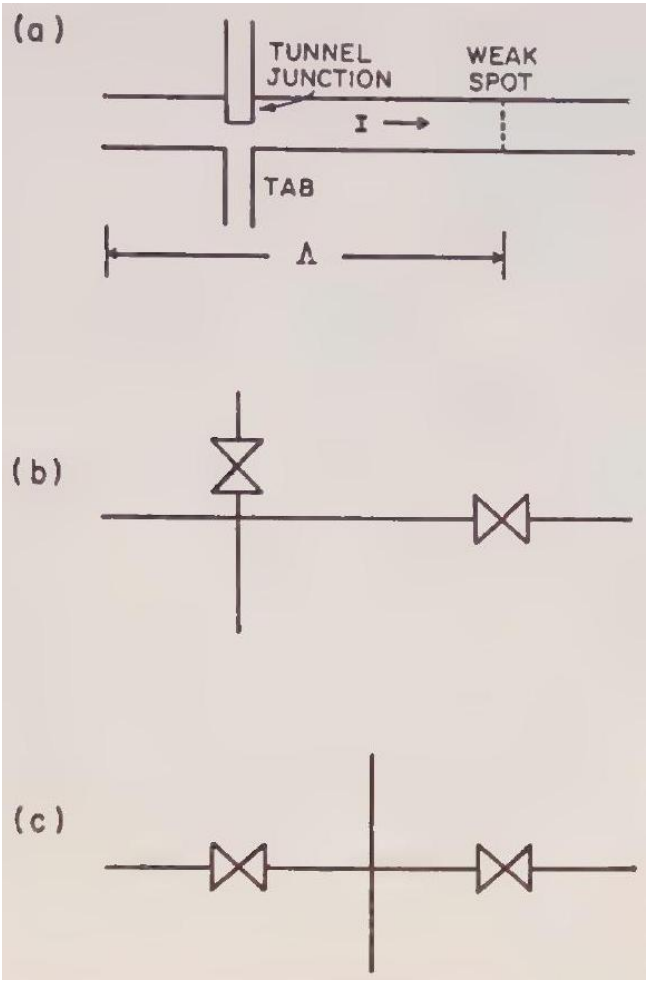


Fig. 28. Detection scheme for charge imbalance waves near a PSC: (a) physical picture; (b) schematic; (c) equivalent of (b), emphasizing the similarity with the configuration for investigating coupled microbridges.

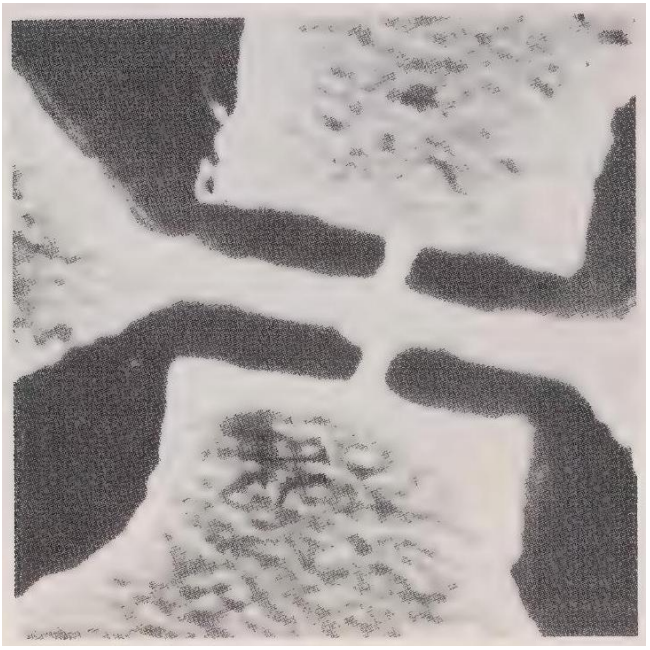


Fig. 29. SEM micrograph of one of the samples used by Jillie (1976). The light areas are a 100 nm thick In film.

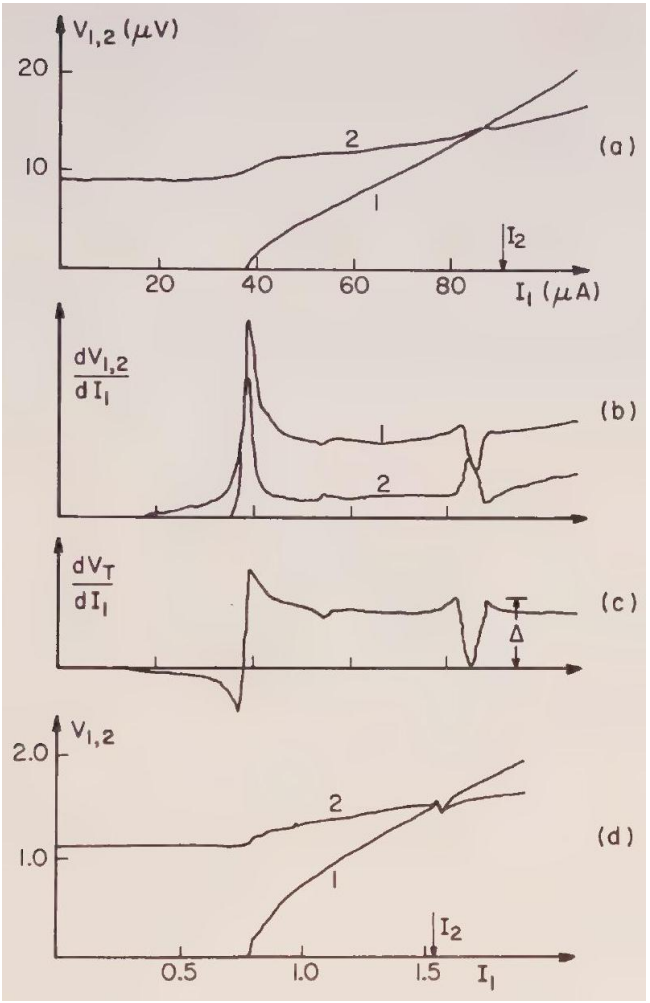


Fig. 30. Experimental results (a), (b), (c) and a numerical simulation (d) for a series opposed biased pair of indium microbridges \$2 \mu \mathrm{˜m
\$ apart showing voltage locking: (a) $I - V$ curves with I_2 held constant (91μ A) and I_1 swept; (b) the differential resistance of the two curves shown in (a); (c) the total differential resistance $\mathrm{d}V_\mathrm{T}/\mathrm{d}I_1 = 0$. In the locking region A ($\mathrm{d}V_\mathrm{T}/\mathrm{d}I_1$) is a measure of the strength of the interaction. (d) Numerical simulation using the correct parameters for the coupled bridges ($\alpha_1 - \alpha_2 = 0.21$). (From Jillie et al. 1980.)}

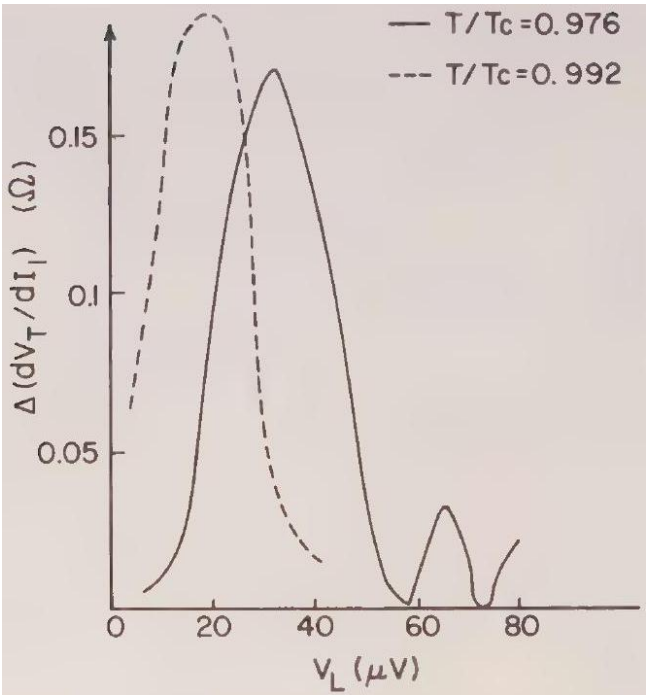


Fig. 31. Voltage and temperature dependence of voltage locking interaction strength, Δ, for the series opposed case. (Jillie et al. 1977.)

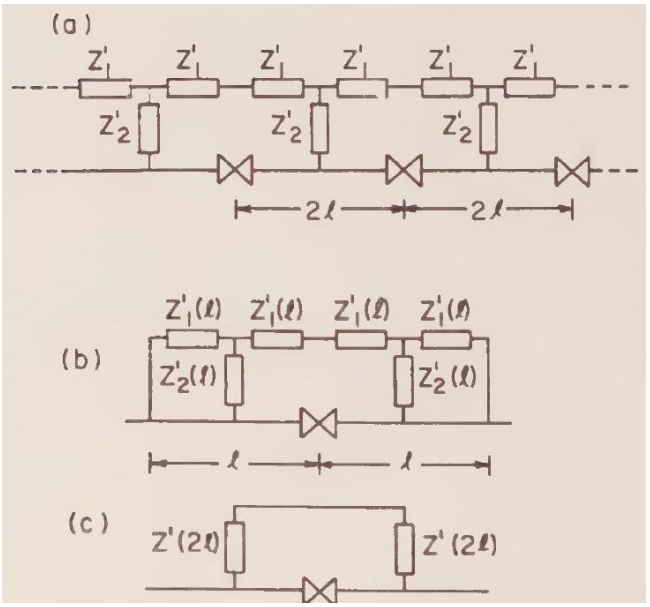


Fig. 32. Lumped-element equivalents for (a) a long series of closely-spaced PSCs, and (b) a single PSC in a short filament (length $2l$), using the tee section. (c) The equivalent of (b), using $Z_{1
^{\prime}(2 l)=Z_{0} \tanh (K l)$.}

21 Nonequilibrium Properties of Superconductors (Transport Equation Approach) by Aronov, Galperin, Gurevich, Kozub

21.1 1. Introduction

The purpose of this review article is to formulate a relatively simple quasiclassical approach to the description of nonequilibrium properties of superconductors. We want to present a method which is as close to the Boltzmannequation description for normal metals as possible. The advantage of this approach is that it ensures not only quantitative but also qualitative insight into the physical picture.

The electron system of a superconductor has two-component character: it consists of the Cooper pair condensate and normal excitations - quasielectrons and quasiholes. It is the close resemblance in the behaviour of the quasiparticles in superconductors and of the electrons in normal metals that makes one hope that the transport equation can be applicable also for superconductors.

Geilikman (1958) and Kresin (1959) were the first to employ these ideas. These authors investigated the electron contribution to the thermal conductivity of a superconductor. The same approach was used by Privorotskii (1962), who studied ultrasonic absorption. Afterwards in such a way the solutions of several problems were obtained.

However, the important problem remained to generalize such an approach for the case of large perturbations, when the response is non-linear. Furthermore, it was important to consider the problems connected with moving condensate.

The last but not the least problem was to derive the transport equation from first principles. In the course of such a derivation which will also be presented in this chapter we shall discuss the limits of applicability of the Boltzmann equation.

We should like to stress an essential point of difference between normal metals and superconductors. Quantum effects in superconductors are much more pronounced. The characteristic quantum length for superconductors (the so-called coherence length $\check{\zeta}_0 = \hbar v_F/\Delta$) is much larger than the de Broglic length $\hbar_i p_{\mathrm{F}}$ in normal metals [here $2\pi h$ is the Planck constant, $l_{\mathrm{F}}\,(p_1)$ is the Fermi velocity (momentum) while A is the modulus of the order parameter of a superconductor]. Furthermore, the characteristic energy scale in superconductors is of the order of Δ, which is much smaller than the Fermi energy μ, i.e. the characteristic energy for normal metals.

To understand the role of quantum effects it is natural to start from most general equations, which was done by several authors. A set of equations for the Green functions (with regard to condensate motion) which could be used to analyse transport phenomena was derived by Stephen (1965). This was an essential achievement. However it was difficult to use these equations for explicit calculations of transport phenomena.

Galaiko (1973, 1974, 1975) proposed a transport equation for the electron density matrix. Rather general problems could be treated with the help of this equation. Still it was much more sophisticated than the usual Boltzmann equation.

A very powerful treatment of transport phenomena was developed on the basis of the set of equations for the Green function integrated over the variable $\check{\zeta}_p = p^2/2m - \mu$ (i.e. over the modulus of the electron momentum p). For small deviations from equilibrium this method was proposed by Eilenberger (1968) [see also the paper by Prange and Kadanoff (1964), who developed the same method for normal metals]. Eliashberg (1971) generalized this method for large deviations from equilibrium, where the corresponding equations are nonlinear. This approach was extended by Larkin and Ovchinnikov (1973, 1977) and by Schmid and Schön

(1975a).

Recently Shelankov (1980) proposed a concise form of generalized nonlinear transport equation that transforms directly into the usual Boltzmann equation (discussed in this article) for the case of rare collisions.

Numerous examples of applications of some of those methods can be found in other chapters in this book (Larkin and Ovchinnikov 1985, Galaiko and Kopnin 1985, Eliashberg and Ivlev 1985, Galitskii et al. 1985).

The advantage of these methods is that they remain valid even if the concept of the excitation spectrum is lost, e.g. if the order parameter A varies rapidly as a function of space coordinates r (or time t) or if the momentum is not a good quantum number (e.g. because of frequent collisions with impurities) as in the case of the so-called dirty superconductors. However, such widening of the range of applicability of the theory results inevitably in some loss of clarity of the physical picture.

Having all this in mind we have made an attempt to derive a quasi-classical transport equation similar to the Boltzmann equation for the normal state (Gal'perin et al. 1973a. Aronov and Gurevich 1974). This equation is not so general as those mentioned above. However, it describes many problems of interest.

In what follows we shall describe such an approach and some of its applications.

In section 2 the full set of equations describing transport in the electron system of a superconductor is formulated. It consists of the transport equation for the quasiparticles, and the self-consistency equation for the modulus of the order parameter and the equations for electromagnetic potentials; the specific feature of a superconductor is the fact that such a set also includes the continuity equation as an independent one. In that section the conditions of applicability of the approach are also discussed.

In section 3 the classification of perturbations representing different kinds of nonequilibrium phenomena, depending on the features of quasiparticle relaxation, is given.

In section 4 the proposed approach is used for discussion of stationary nonequilibrium phenomena in superconductors in the presence of laser pumping.

In section 5 the main thermodynamic equations-the energy conservation law and the H-theorem-are derived with the help of the transport equation approach. In this way the approach is proved to be consistent with the main thermodynamic principles.

The hydrodynamical approach applicable to the case of strong impurity scattering is presented in section 6. The full system of macroscopic equations is derived and some transport phenomena are discussed. Special attention is given to specific phenomena connected with imbalance of the population of the electron-like and the hole-like branches of the quasiparticle spectrum.

The specific features of the thermoelectric effect in superconductors are discussed in section 7; a critical review of some papers concerning the supercurrent-induced thermoelectric effect is also given there.

In section 8 the acoustical phenomena in superconductors are treated; these are both inhomogeneous and time-dependent; the Boltzmann equation approach is a valuable tool to study the response of a superconductor to perturbations of this kind. It is important that this approach makes it possible in a relatively simple way to study corresponding nonlinear problems, such as nonlinear ultrasonic damping and the acousto-electric effect, which are rather difficult to be studied by other methods.

A microscopic derivation of the basic equations with the help of the Keldysh diagram technique is presented in section 9.

21.2 2. The full set of equations describing transport

At finite temperatures the electron system of a superconductor is twocomponent: it consists of a condensate of Cooper pairs and of normal excitations. The unique electromagnetic behavior of a superconductor is due to the condensate. This is a quantum coherent state described by the order parameter, i.e. by the wave function $\Delta e^{1/}$. Its modulus is equal to half of the energy gap in the excitation spectrum.

The kinetic properties (such as thermal conductivity, ultrasonic attenuation ctc.) of superconductors are determined mainly by the normal excitations.

We shall begin with a description of the quasiparticle spectrum in the quasiclassical approximation.

Let us suppose that the following conditions of applicability of the quasiclassical approach hold:

$$\hbar\omega \ll \Delta, \tag{1}$$

$$qd \ll 1. \tag{2}$$

Here ω is the angular frequency of the external perturbation, q is its wave vector, while d is the characteristic quantum length. For the majority of problems d is of the order of the coherence length ξ_0. However, in general, as we shall see below, it may differ for different problems.

One can obtain the quasiparticle spectrum in this approximation from the Bogoliubov-De Gennes equations (see e.g. De Gennes 1968):

$$\begin{array}{ll} \tilde{\varepsilon}_p = \varepsilon_p + p_s v, & \varepsilon_p = \sqrt{\xi_p^2 + \Delta^2}, \\ \tilde{\xi}_p = \xi_p + \phi + \frac{p_s^2}{2m}, & \xi_p = E_p - \mu = \frac{p^2}{2m} - \mu. \end{array} \tag{3}$$

Here E_p is the spectrum of electrons in the normal state.* Two gauge-covariant quantities, p_s and ϕ, enter eq. (6). The condensate momentum p_s is given by

$$p_\mathrm{s} = \frac{\hbar}{2}\left(\nabla\chi - \frac{2e}{\hbar c}A\right) \tag{4}$$

while the covariant potential ϕ is

$$\phi = \frac{\hbar}{2}\frac{\partial\chi}{\partial t} + e\varphi \tag{5}$$

where e is the electron charge, c is the light velocity and A and φ are the vector and scalar potentials, correspondingly.

Our purpose is to formulate the transport equation for the distribution function n_p of quasiparticles, i.e. of the normal excitations in a superconductor. This equation has the form

$$\frac{\partial n_p}{\partial t} + \frac{\partial\tilde{\varepsilon}_p}{\partial p}\frac{\partial n_p}{\partial r} - \frac{\partial\tilde{\varepsilon}_p}{\partial r}\frac{\partial n_p}{\partial p} + I\{n_p\} = 0. \tag{6}$$

Here

$$I = I_\mathrm{im} + I_\mathrm{ph} + I_\mathrm{ee} \tag{7}$$

is the collision operator describing collisions of the quasiparticles with impurities [the first term in eq. (7)], with phonons (second term) and with each other (third term).

[0]*For simplicity, in most of this chapter we consider the case of an isotropic quadratic spectrum: $E(\boldsymbol{p}) = p^2/2m$. The generalization to the anisotropic case is straightforward.

The first term has the form

$$I_{\mathrm{im}} = \frac{\pi N_{\mathrm{i}}(2\pi)^4}{m^2} \int (\,\mathrm{d}\rho)_{p'} \left|f_{p,p'}\right|^2 \left(u_p u_{p'} - v_p v_{p'}\right)^2 \left(n_p - n_{p'}\right) \times \delta\left(\tilde{\varepsilon}_p - \tilde{\varepsilon}_{p'}\right)$$
$$(\mathrm{d}p)_{p'} = \frac{2\ \mathrm{d}^3 p'}{(2\pi\hbar)^3} \tag{8}$$

Here N_{i} is the impurity concentration, $f_{p,p'}$ is the amplitude of scattering of a normal electron from the state p to the state p', u_p and v_p are the well-known Bogoliubov-Valatin amplitudes, given by

$$u_p^2 = \frac{1}{2}\left(1 + \tilde{\zeta}_p/\varepsilon_p\right), \quad v_p^2 = \frac{1}{2}\left(1 - \tilde{\zeta}_{p/\varepsilon_p}\right) \tag{9}$$

Note that it is the quantity ε_p rather than $\tilde{\varepsilon}_p$ that enters these expressions.
The term in the integrand which is proportional to n_p is the so-called "outterm", which describes the collisional events where an excitation with momentum p makes a transition into a state with momentum p'. Another term in eq. (8) proportional to n_p is the so-called "in-term" which describes the reversed transitions.

The collision term I_{ph} has the form

$$I_{\mathrm{ph}} = I^{(\mathrm{s})}\left\{n_p\right\} + I^{(\mathrm{r})}\left\{n_p\right\}$$

where

$$\begin{aligned} I^{(s)}\left\{n_p\right\} = -\frac{2\pi}{\hbar} \int \frac{\mathrm{d}^3 q}{(2\pi)^3} \left|c_q\right|^2 \left(u_p u_{p-\hbar q} - v_p v_{p-\hbar q}\right)^2 \\ \times \left\{n_{p-\hbar q}\left(1-n_p\right)\left[\left(1+N_{-q}\right)\delta\left(\tilde{\varepsilon}_p - \tilde{\varepsilon}_{p-\hbar q} + \hbar\omega q\right) + N_q \delta\left(\tilde{\varepsilon}_p - \tilde{\varepsilon}_{p-\hbar q} - \hbar\omega_q\right)\right]\right. \\ - n_p\left(1-n_{phq}\right)\left[N_q \delta\left(\tilde{\varepsilon}_p - \tilde{\varepsilon}_{p-hq} + \hbar\omega_q\right)\right. \\ \left.\left. + \left(1+N_q\right)\delta\left(\tilde{\varepsilon}_p - \tilde{\varepsilon}_{p-\hbar q} - \hbar\omega_q\right)\right]\right\} \end{aligned} \tag{10}$$

$$\begin{aligned} I^{(\tau)}\left\{n_p\right\} = -\frac{2\pi}{\hbar} \int \frac{\mathrm{d}^3 q}{(2\pi)^3} \left|c_{\mathrm{q}}\right|^2 \left(u_p v_{p-\hbar q} + u_{p-\hbar q} v_p\right)^2 \delta\left(\tilde{\varepsilon}_p + \varepsilon_{-p+\hbar q} - \hbar\omega_q\right) \\ \times \left[\left(1-n_p\right)\left(1-n_{-p+\hbar q}\right) N_q - n_p n_{-p+\hbar q}\left(1+N_q\right)\right] \end{aligned} \tag{11}$$

Here c_q is the matrix element of the electron phonon interaction, ($_q$ is the phonon frequency, and N_q is the phonon distribution function for the phonon wave vector q. This function in general should be determined from the phonon Boltzmann equation

$$\frac{\partial N_q}{\partial t} + \frac{\partial \omega_q}{\partial q}\frac{\partial N_q}{\partial r} + I_{\mathrm{ph-ph}}\left\{N_q\right\} + I_{\mathrm{phe}}\left\{n_p, N_q\right\} = 0 \tag{12}$$

The collision operator $I_{\mathrm{phph}}\left\{N_q\right\}$ describes scattering of phonons by other phonons and lattice defects. The phonon-electron collision operator, $I_{\text{ph-e}}\ \left\{n_p, N_q\right\}$ can be divided into two parts: $I_{\mathrm{phe}} \equiv I^{(s)}_{\mathrm{phc}} + I^{(r)}_{\mathrm{ph-c}}$
where

$$\begin{aligned} I^{(s)}_{\mathrm{phc}} = & \frac{2\pi}{\hbar} \int (\,\mathrm{d}p)_p \left|c_q\right|^2 \left(u_p u_{p+\hbar q} - v_p v_{p+\hbar q}\right)^2 \\ & \times \left[n_p\left(1+n_{p+\hbar q}\right) N_q - n_{p+\hbar q}\left(1-n_p\right)\left(N_q+1\right)\right] \delta\left(\tilde{\varepsilon}_p - \tilde{\varepsilon}_{p+\hbar q} + \hbar\omega_q\right), \end{aligned} \tag{13}$$

$$\begin{aligned} I^{(r)}_{\mathrm{ph-c}} = & \frac{2\pi}{\hbar} \int (\,\mathrm{d}p)_p \left|c_q\right|^2 \left(u_p v_{p-\hbar q} + u_{p-\hbar q} v_p\right)^2 \\ & \times \left[N_q\left(1-n_p\right) n_{\hbar q - p} - n_p n_{\hbar q - p}\left(1+N_q\right)\right] \delta\left(\tilde{\varepsilon}_p + \varepsilon_{\hbar q - p} - \hbar\omega_q\right). \end{aligned} \tag{14}$$

The term $I_{\rm ph}^{(s)}$ e describes scattering of phonons by quasiparticles while the term $I_{\rm ph}^{(r)}$ is due to creation-annihilation processes in the course of electron phonon collisions.

We shall not write the electron-electron collision term explicitly.* Let us mention, however, that it describes processes of two types, i.e. processes of the type $2 \to 2$, conserving the number of the quasiparticles (two quasiparticles collide and as a result come into two other quantum states) and processes of the type $3 \leftrightarrows 1$ (as a result of such a collision two quasiparticles are either generated or absorbed).

Containing only the gauge-covariant quantities $p_{\rm s}$ and ϕ, eq. (6) is gaugecovariant itself. The solution of a transport problem in superconductors is in general selfconsistent: the nonequilibrium distribution should be sought simultaneously with the excitation spectrum which, in its turn, depends on the excitation distribution, as well as on external fields. Thus, another important equation in our case is the equation for the energy gap in the nonequilibrium state. As we shall see (section 9), in the quasiclassical approximation this equation has the same form as in the equilibrium case:

$$1 = -\frac{\lambda_{\rm e}}{2} \int (\ {\rm d}p)_p \frac{1 - 2n_p}{\varepsilon_p}, \tag{15}$$

where λ_e is the effective constant of electron-electron coupling. In the vicinity of the transition point to the normal state eq. (15) reduces to the well-known Ginzburg Landau equation, where the term with the space derivatives (of the

order of $q\check{\zeta}_0 \ll 1$) is discarded while some additional term due to the nonequilibrium part of the distribution function is present. The latter is sometimes called "the anomalous term" (see Gor'kov and Eliashberg 1968).

Now let us discuss the limits of applicability of the equations formulated above in more detail. For this purpose, let us evaluate the characteristic length d entering the criterion (2). Let us turn to the pair of the Bogoliubov-De Gennes equations

$$\begin{aligned} &\left[\frac{1}{2m}\left(-{\rm i}\hbar\frac{\partial}{\partial r} - \frac{e}{c}\boldsymbol{A}\right)^2 + e\varphi - \mu\right] u + \Delta {\rm e}^{{\rm i}\chi} v = \tilde{\varepsilon} u, \\ &-\left[\frac{1}{2m}\left(-{\rm i}\hbar\frac{\partial}{\partial r} + \frac{e}{c}\boldsymbol{A}\right)^2 + e\varphi - \mu\right] v + \Delta {\rm e}^{-{\rm i}\chi} u = \tilde{\varepsilon} v \end{aligned} \tag{16}$$

in the WKB-approximation. In this case one may seek the solution of eq. (16) in the form

$$\begin{pmatrix} u(r) \\ v(r) \end{pmatrix} = \begin{pmatrix} u_p \\ v_p \end{pmatrix} \exp\left(\frac{\rm i}{\hbar}\int p\ {\rm d}r\right) \tag{17}$$

where the variation of the amplitudes u_p and v_p [given by eq. (9)] with the space coordinate r is supposed to be slow.

The general solution of the eq. (16) for a given energy $\tilde{\varepsilon}$ is a superposition of two terms of the type (17), which can be discriminated by the sign of $\tilde{\xi}_p$ (the two branches of the excitation spectrum). The two corresponding absolute values of the momentum, $p^{\pm}$, can be found from

$$\tilde{\varepsilon} = \sqrt{\xi_{\rm p}^2 + \Delta^2} + p_{\rm s} v \tag{18}$$

In the first approximation in the small parameter $\left|\vec{\xi}_p\right| / \mu$ the solutions are*

[0]*The explicit expression for this term was derived by Eliashberg (1971) (for the ξ_p-even part of the distribution function).

$$p_{\pm} = \left[2m\left(\mu \pm \sqrt{\left(\tilde{\bar{\varepsilon}} - \boldsymbol{P}_{\mathrm{s}} v_{\mathrm{F}}\right)^2 - \Delta^2}\right)\right]^{1/2} \tag{19}$$

One can see that there are two quantum scales that appear in the theory. The first one, $\hbar/p_{\mathrm{F}}$, is the same as in the normal state. The second one,

$$\frac{\hbar}{|p_+ - p_-|} \simeq \frac{\hbar v_{\mathrm{F}}}{\xi_p} \tag{20}$$

describes the large-scale quantum oscillations of the quasiparticle wave lunction. This scale has been introduced by Azbel (1970) as a characteristic length determining the validity of the quasiclassical approach.

An additional limitation is due to electron scattering and has the form

$$1 \gg d \tag{21}$$

l being the characteristic electron mean free path. One should keep in mind that the characteristic value of ξ_p [entering eq. (20)] depends on the problem under consideration. Consequently, one should check the validity of these criteria in every case.

If we are interested in the contribution of all quasiparticles and the temperature T is of the order of T_{c}, then d is of the order of $\xi_0(0)$ (the coherence length at $T = 0$). If, on the contrary, the quasiparticles with small $\widetilde{\zeta}_p$ are important the situation is more complicated and additional analysis is usually required.

As is the case with condition (2), condition (1) imposed on the perturbation frequency is not always sufficient. At low temperatures a more restrictive criterion exists:

$$\hbar\omega \ll \bar{\xi}_p \tag{22}$$

where $\bar{\xi}_p$ is the characteristic value of $\bar{\xi}_p$.

Another restriction on the perturbation frequency may appear as a result of analysis of the equation for the gap if the latter is changed by nonequilibrium processes. If the deviation from equilibrium is small such a criterion, as we shall see, has the form

$$\hbar\omega \ll \Delta^2/T.$$

This criterium was first formulated by Gor'kov and Eliashberg (1968, 1969). In the vicinity of the transition temperature it is much more restrictive than the condition $\hbar\omega \ll \Delta$.

Now let us discuss properties of the collision operators entering the transport equations for quasiparticles (eq. 6) and phonons (eq. 12). We shall begin with discussion of the impurity collision operator, I_{im} (eq. 8). This operator vanishes when acting upon an arbitrary function of the total excitation energy, $\tilde{\delta}_p$. At the same time, the electron-phonon collision operator I_{ph} [eqs. (10) and (11)] vanishes when acting upon the equilibrium Fermi function $n^{(0)}$,

$$n^{(0)}(\tilde{\varepsilon}) = [\exp(\tilde{\varepsilon}/T) + 1]^{-1} \tag{23}$$

if the phonon distribution is the equilibrium one. It is necessary to emphasize that if $p_s \neq 0$ this function has a current-carrying part which reflects the existence of persistent current in superconductors in the equilibrium state.

The impurity collision operator can be rewritten in the form

$$I_{\mathrm{im}}\{n_p\} = \int (\mathrm{d}p)_{p'} W_{pp'} (n_{p'} - n_p) \left(1 + \frac{\widetilde{\xi}_p \widetilde{\xi}_{p'} - \Delta^2}{\varepsilon_p \varepsilon_{p'}}\right) \delta(\tilde{\varepsilon}_p - \tilde{\varepsilon}_{p'}) \tag{24}$$

[0]*For most purposes this approximation is adequate. However, as we shall see later, in the theory of v_s-dependent thermoelectric current this approximation is not sufficient.

One can draw an important conclusion from this expression: if $p_s = 0$ the operator $I_{\rm im}$ vanishes when acting upon an arbitrary function of ξ_p. In other words, the impurity scattering smears the quasiparticles over a surface of constant $\widetilde{\xi}_p$ in the momentum space. This smearing results in relaxation of the part of the distribution function which is asymmetric in p. Note that in a situation where $p_{\rm s} = 0$ the operator $I_{\rm im}$ satisfies the relation

$$I_{\rm im} n_p = \left(|\xi_p| / \varepsilon_p\right) I_{\rm im}^{\rm n} n_p, \tag{24a}$$

where $I_{\rm im}^{\rm n}$ is the impurity-scattering operator for the normal metal.
Let us give as an example an expression for the "out" part of the impurity collision operator in the case $p_{\rm s} = 0$:

$$I_{\rm im}^{\rm out}\, n_p \equiv n_p/\tau^{\rm out} \;= \left(\left|\widetilde{\zeta}_p\right| / \varepsilon_p\right) n_p/\tau_{\rm im}, \tag{25}$$

where $\tau_{\rm im}$ is the lifetime of the electron with momentum p due to the impurity collisions in the normal state. Thus, if $p_{\rm s} = 0$, the impurity collisions conserve the $\check{\zeta}_p$-parity of the distribution function. This means that the total numbers of quasielectrons ($\tilde{\xi} > 0$) and quasiholes ($\tilde{\xi} < 0$) are conserved separately, and therefore the impurity scattering does not result in relaxation of the inbalance between the two branches, provided $\boldsymbol{p}_{\rm s} = 0$.

One can offer a rather transparent physical interpretation of this fact. Indeed, the coherence factor describing interbranch transitions is proportional to the matrix element squared $\left|\left\langle \psi_p^{\rm el} \mid \psi_{p'}^{\rm hole} \right\rangle\right|^2$, where $\left|\psi_p^{\rm el}\right\rangle$ and $\left|\psi_p^{\rm hole}\right\rangle$ are the quasi-electron and quasihole states, correspondingly. If $p = p'$, this amplitude vanishes because $\left|\psi_p^{\rm el}\right\rangle$ and $\left|\psi_p^{\rm hole}\right\rangle$ are the orthogonal solutions of the Bogoliubov-De Gennes equations. If the quasiparticle spectrum is isotropic this property exists for arbitrary directions of p and p' because $\left|\tilde{\zeta}_p\right| = \left|\tilde{\zeta}_{p'}\right|$ for elastic scattering provided $p_{\rm s} = 0$. This is why such an imbalance can relax, e.g., due to electron-phonon collisions (Tinkham 1972).

To make an estimate of characteristic electron -phonon times of relaxation one should know whether the phonon distribution is the equilibrium one or not. For many important cases the non-equilibrium part of the phonon distribution function is small and can be discarded in the course of estimation of the electron-phonon scattering rate. Thus, in this section we shall assume the phonon distribution to be the equilibrium one. If this is the case the electron-phonon imbalance relaxation time $\tau_{\rm Q}$ can be estimated as $\tau_{\rm ph}$ (provided $T_{\rm c} - T$ is of the order of $T_{\rm c}$) or as $\tau_{\rm ph}(T/\Delta)$ (provided $T_{\rm c} - T \ll T_{\rm c}$) (Tink ham 1972, Clarke and Tink ham 1972). Here $\tau_{\rm ph}$ is of the order of $h\left(\omega_1^2\right), T^3$, i.e. of the order of the electron-phonon relaxation time in normal metals ((ω_D) is the Debye phonon frequency).

If $p, \neq 0$ or $\Lambda(p)$ is anisotropic the imbalance can relax through the impurity collisions as well. This can be seen straight forwardly from eq. (24) because ε_p and $\varepsilon_{p'}$ rather than $\tilde{\varepsilon}_p$ and $\tilde{\varepsilon}_{p'}$ enter the expression for the coherence factor $\left(u_p u_{p'} - v_p v_{p'}\right)^2$. The relaxation rate is of second order in the quantity ($p_s v, \varepsilon_c$),
$\varepsilon_{\rm c}$ being the characteristic quasiparticle energy. The corresponding relaxation time $\tau_{\rm Q}$ can be estimated as

$$1/\tau_{\rm Q} \simeq \left(1/\tau_{\rm im}\right)\left(p_{\rm F} v_{\rm s}/T_{\rm c}\right)^2, \tag{26}$$

if $T_{\rm c} - T \ll T_{\rm c}$ (see Galako and Shumeko 1976, and Shelankov 1977). The same physical considerations are valid if the gap parameter $A(p)$ is anisotropic. If the anisotropy is small so that

$$\frac{\Delta(p) - \langle\Delta\rangle}{\langle\Delta\rangle} \ll 1,$$

where the angular brackets denote the average over the Fermi surface, we have the following estimate

$$1/\tau_{\mathrm{Q}} \simeq (1/\tau_{\mathrm{im}})\,\frac{\langle(\Delta - \langle\Delta\rangle)^2\rangle}{\langle\Delta\rangle^2}. \tag{27}$$

This type of relaxation was also studied by Galako and Shumeko (1976). The imbalance relaxation can be produced also by other mechanisms, such as paramagnetic impurity scattering (Schmid and Schön 1975a). We shall consider here only the nonmagnetic impurity scattering.

Thus, one can discriminate between 3 types of relaxation:
(1) Relaxation of the part of the distribution function asymmetrical in p ("smearing" over a surface of constant $\widetilde{\zeta}_p$). These processes are usually the most rapid. This type of relaxation can be due to impurity collisions, the characteristic time being of the order of τ_{im}. So to describe such a relaxation one can for many cases discard the phonon part in the collision term of the Boltzmann equation for the quasiparticles.
(2) So-called imbalance relaxation, of the part of the distribution function symmetric in p and odd in $\widetilde{\widetilde{\xi}}_p$. It may be due to electron - phonon collisions, or (in the presence of p) to impurity collisions, or to other mechanisms discussed above.
(3) Energy relaxation, i.e relaxation of the part of the distribution function depending on the total energy $\tilde{\varepsilon}$. This type of relaxation is due to electronphonon and electron-electron collisions. If $T \simeq T_{\mathrm{c}}$, the characteristic relaxation time due to electron-phonon collisions is of the order of $\tau_{\mathrm{ph}}(T_{\mathrm{c}})$. However, at $T \ll T_{\mathrm{c}}$ one should discriminate between the contributions of the two types of inelastic electron-phonon processes mentioned above. The contribution of scattering processes conserving the total number of quasiparticles to the scattering rate is of the order of $\tau_{\mathrm{ph}}^{-1}(T)(T,\Delta)^{12}$, whereas the contribution of creation-annihilation processes is of the order of

$$\tau_{\mathrm{ph}}^{-1}(\Delta)x. \tag{28}$$

Here x is the so-called dimensionless concentration of the quasiparticles,
defined as

$$x = \frac{\pi^2\hbar^3}{2mp_{\mathrm{F}}\Delta}\int(\,\mathrm{d}p)_p n_p. \tag{29}$$

The corresponding equilibrium quantity equals (Schrieffer and Ginsberg 1962)

$$x_0 = (\pi T/2\Delta)^{1/2}\exp(-\Delta/T) \tag{30}$$

The rate of electron-electron collisions at $T \simeq T_{\mathrm{c}}$ is of the same order as for normal metals:

$$\tau_{\mathrm{ee}}^{-1} \simeq T_{\mathrm{c}}^2/\hbar\mu, \tag{31}$$

whereas at $T \ll T_{\mathrm{c}}$ two different characteristic electron-electron times exist. The characteristic rate of processes of the type $2 \to 2$ is proportional to the concentration of the quasiparticles and is given by

$$\tau_{\mathrm{ee}}^{-1} \simeq \frac{\Delta^2}{\hbar\mu}x, \tag{32}$$

while for 31 processes (such as recombination or shock ionization) we have

$$\tau_{\mathrm{ee}}^{(\mathrm{r})-1} \simeq \frac{\Delta^2}{\hbar\mu}x^2. \tag{33}$$

Thus, the characteristic time $\tau_{\rm ee}^{(\rm r)}$ is proportional to x^{-2}.
Before formulating the full set of equations describing transport in superconductors let us note some useful sum rules for the collision operators of the electron and phonon Boltzmann equation (we shall use these rules in section 4). These relations can be obtained from the explicit expressions for the collision operators, eqs. (10), (11), (13) and (14), and have the form

$$\int (\mathrm{d}p)_p I_{\rm ph}^{(\rm s)} \{n_p, N_q\} = 0 \tag{34}$$

$$\int \frac{\mathrm{d}^3 q}{(2\pi)^3} I_{\rm ph-c}^{(\rm s)} \{n_p, N_q\} = -\frac{1}{2} \int (\,\mathrm{d}p)_p I_{\rm ph}^{(\rm r)} \{n_p, N_q\} \tag{35}$$

$$\int (\mathrm{d}p)_p \tilde{\varepsilon}_p \left\{ I_{\rm ph}^{(\rm s)} + I_{\rm ph}^{(\rm r)} \right\} = -\int \frac{\mathrm{d}^3 q}{(2\pi)^3} \hbar\omega_{\rm q} \left(I_{\rm ph-c}^{(\rm r)} + I_{\rm ph-c}^{(\rm s)} \right) \tag{36}$$

The first relation is due to the fact that scattering processes conserve the total number of the quasiparticles (as we have mentioned above). The second one describes the conservation of the total number of quasiparticles and high-
frequency phonons in the course of creation-recombination events. The last relation represents the energy conservation law in the electron-phonon collisions.

Now we can proceed to the main purpose of the present section, i.e. formulating the full set of equations describing kinetics in superconductors.

The Boltzmann equation and the equation for the modulus of the order parameter include such quantities as the external fields (or, more definitely, potentials A and φ), as well as the phase χ of the order parameter. The fields can be determined from the Maxwell equations

$$\operatorname{curl} \boldsymbol{E} = -\frac{1}{c}\frac{\partial H}{\partial t}, \quad \operatorname{curl} \boldsymbol{H} = \frac{4\pi}{c}\boldsymbol{j} \tag{37}$$

where j is the total current density.
In normal metals one would need one equation to complete the set. This is the neutrality condition $N = \text{const.}$, where N is the electron concentration. In a superconductor one needs one more equation, which reflects the existence of an extra variable, i.e. the phase χ. For this purpose the continuity equation

$$e\frac{\partial N}{\partial t} + \operatorname{div} j = 0 \tag{38}$$

may be used. It can be obtained by averaging the corresponding operator identity*. The averaging procedure gives the following explicit expressions for N and j (see, e.g. Gal'perin et al. 1973a):

$$N = \int (\mathrm{d}p)_p \left[u_p^2 n_p + v_p^2 (1 - n_{-p}) \right] \tag{39}$$

$$j = e \int (\,\mathrm{d}p)_p v n_p + eN v_{\rm s} \tag{40}$$

where $v = \partial E_p / \partial p$.
Equation (38) in normal conductors can be obtained straightforwardly by integration of the Boltzmann equation over $(\mathrm{d}p)_p$ and, thus, is a direct sequence of electron number conservation. In a superconductor the number of excitations is not conserved so the Boltzmann equation itself bears no explicit relation to the particle number conservation. Thus, equation (38) for a superconductor is a subsidiary equation. Combining it with the neutrality condition we obtain the two equations that complete our set

$$N = \text{ const.}, \tag{41}$$

$$\operatorname{div} j = 0. \tag{42}$$

for most cases it is natural to seek the distribution function n_p as a sum of the Jocal-equilibrium part (eq. 23) and the nonequilibrium term $n_p'' : n_p = n''' \left(\hat{i}_p\right) - n_p''$. Substituting this sum into eq. (4()) and retaining the linear terms in v one gets

$$\begin{aligned} j &= e \left|(dp)_p v n_p'^1 - e\right|^{\hat{i}(dp)_p v(p\cdot v)\ {}_{ii;}^{in'()}} + eNv \\ &= eNv_s + e \int (dp)_p v n_p^{(1)} \end{aligned} \tag{43}$$

The first term in eq. (43) represents the s()-called supercurrent or persistent current the coefficient I. being the so-called superconducting electron density

$$N_{\mathrm{s}} = N_0 \left(1 + 2 \int_0^\infty \mathrm{d}\xi \frac{\hat{O} n^{(0)}}{\hat{C}\varepsilon}\right) \tag{44}$$

The second term is the normal current. Such a classification is adequate only for approximation linear in τ. Note that it is the "bare" electron velocity t rather than the excitation group velocity ri ; p that enters the expression for the normal current.

Differentiating eq. (4) with respect to time and using eq. (5) we get the following identity for p_s :

$$\frac{\mathrm{d}p_{\mathrm{s}}}{\mathrm{d}t} = \nabla\phi + e\boldsymbol{E} \tag{45}$$

which clarifies the physical meaning of the potential to. In some papers isee for example. Stephen 1965. Kemoklidze and Pitaevskii 1967. Betbeder Matibet and Nozires 1969, Galako 1973, 1975) it is represented in another form

$$\frac{\hat{c}p_{\mathrm{s}}}{\hat{c}t} + \frac{1}{m}\left(p_{\mathrm{s}}\nabla\right)p_{\mathrm{s}} = \nabla\left(\phi + p_{\mathrm{s}}^2/2m\right) + eE + \frac{e}{mc}\left[p_{\mathrm{s}} \times H\right], \tag{46}$$

which reflects the idea that the electron chemical potential in a superconductor acquires an additional term

$$\dot{r}\mu = -\left(\phi + \frac{p_{\mathrm{s}}^2}{2m}\right) \tag{47}$$

$\delta\mu$ depends. in particular. on the rate of space and time ariation of the phase of the order parameter %. We shall sometimes refer. for the sake of brevity. to "the transport equation approach" when we mean the approach based on the complete set of equations written in this section.

[0]*Note that the continuity equation can also be obtained as the imaginary part of the equation for the anomalous Green function.

21.3 3. Different kinds of perturbation and different nonequilibrium phenomena

In considering various nonequilibrium and transport phenomena in superconductors it is useful to discriminate between different kinds of perturbations. We shall base such a classification on the parity of the non-equilibrium distribution in p and $\widetilde{\zeta}_p$. For most of the problems in question this classification is natural.

Thus, we shall consider four kinds of perturbations which create nonequilibrium distributions*

(a) even in ξ_p, odd in p,
(b) odd in $\widetilde{\xi}_p$, even in p,
(c) even in $\widetilde{\xi}_p$, even in p,
(d) odd in $\widetilde{\xi}_p$, odd in p.

(a) Perturbations creating distributions even in $\tilde{\zeta}_p$ and odd in p generate electric current (the typical example is the perturbation proportional to $p_s v$). Such distributions relax through impurity collisions, the response being proportional to τ_{im}.

(b) Perturbations creating distributions even in p and odd in $\widetilde{\zeta}_p$ produce imbalance between the quasielectron and quasihole branches of the excitation spectrum. The imbalance can manifest itself by the potential ϕ. Indeed, making use of the neutrality condition (eq. 41) one obtains

$$\frac{\partial N}{\partial \mu}\phi = -\int (\mathrm{d}p)_p \frac{\tilde{\xi}_p}{\varepsilon_p}\left[n^{(0)}\left(\tilde{\varepsilon}_p\right) - n_p\right] \tag{48}$$

The distribution shifted from equilibrium can relax in this case through phonons, paramagnetic impurities or (in the presence of supercurrent or anisotropy of the gap) through nonmagnetic impurities. The corresponding relaxation time is τ_{Q} introduced in section 2 .

The potential produced by the imbalance is a measurable quantity. For instance, it can be measured in tunnel experiments. The first such experiment was made by Clarke and Tinkham (1972).

Imbalance perturbations are typical for cases where the normal current is inhomogeneous (for instance, if current flows through a N − S boundary). The existence of such phenomena was indicated by Rieger et al. (1971). Afterwards, they were studied theoretically in more detail by Volkov (1974) and by Artemenko and Volkov (1976, 1979).

Note that perturbations of the types (a) and (b) do not lead to changes of the gap, at least in lowest order in T/μ.

(c) Perturbations creating distributions even both in p and in $\tilde{\zeta}_p$ produce no current. Typical examples of such perturbations are "heating" of the excitations by an external microwave field or by an intensive sound wave. The deviations of the distribution function from equilibrium can relax only through inelastic processes (for instance, through scattering by phonons). It is the only type of perturbations that influences the energy gap Δ.

The phenomena of superconductivity stimulation, first considered by Eliashberg (1970) and widely discussed thereafter, are due to perturbations of this kind. Various phenomena of excitation pumping into a superconductor are also described by contributions of this kind to the nonequilibrium distribution function. Some of these phenomena are described in the next section.

(d) Perturbations creating distributions odd both in p and ξ_p are the kind of perturbation that gives rise to thermoelectric effects (see sections 6 and 7).

[0]*Note that the classification based on $\widetilde{\xi}_p$-parity is effective only if one is interested in the contribution of the lowest nonvanishing order in T/μ (cf. section 7).

21.4 4. Stationary nonequilibrium distribution under pumping

The purpose of the present section is to illustrate the role of two different kinds of collisional events described by the collision operator of the Boltzmann equation, i.e. scattering processes and creation- annihilation processes. To this end we shall consider as an example the formation of a nonequilibrium distribution function under pumping of excitations.

There are several different methods to create a nonequilibrium distribution function by pumping, such as (1) laser pumping, (2) tunnel injection, or (3) microwave pumping. Only the case of laser pumping will be considered here. Discussions of other cases and of related phenomena can be found in the review papers by Aronov and Spivak (1978), by Eliashberg and Ivlev (1985) and by Galitskii et al. (1985).

Under laser pumping quasiparticles are created in a wide range of energies $\varepsilon \gg A$. Thereafter they relax down emitting phonons of all frequencies. If the phonon spectrum is linear and $|c_q|^2$, q the steady-state distribution function at high energies goes as some power of the energy. In thin films, according to Vardanyan and Ivlev (1973),

$$n(\varepsilon) \propto (\Delta/\varepsilon)^4. \tag{49}$$

In thick films, because of reabsorption of high frequency phonons (see Aronov et al. 1976)

$$n(\varepsilon) \propto (\Delta/\varepsilon)^5 \tag{50}$$

The distribution function near the gap is practically independent of its form at high energies and has the quasiequilibrium form with nonvanishing chemical potential. The temperature and chemical potential of the quasiparticles are determined by energy and quasiparticle number conservation.

If the film thickness a is smaller than the diffusion length $L = \sqrt{D\tau_\varepsilon}$, D being the quasiparticle diffusion coefficient while τ_ε is the time of energy relaxation, the spatial distribution of the quasiparticles is homogeneous.

Averaging the Boltzmann equation over the cross-section of the sample, integrating over $(\mathrm{d}p)_p$ and making use of eq. (34) we obtain the condition of quasiparticle number conservation in the following form

$$\int (\mathrm{d}p)_p I^{(r)}\{n_p, N_q\} = \int (\mathrm{d}p)_p \langle Q_p \rangle_{\mathrm{s}}. \tag{51}$$

Here $\langle Q_p \rangle_{\mathrm{s}}$ is the capacity of the source of the quasiparticles at some given energy averaged over the cross-section of the sample.

The high-frequency phonons with $\hbar\omega_{\mathbf{q}} > 2\Delta$ play an especially important role in this effect because the total variation of the number of the quasiparticles is due to the variation of the number of these phonons. Indeed, the disappearance of such a high-frequency phonon is equivalent to the generation of two quasiparticles, as stated by eq. (35).

Let us now integrate the phonon Boltzmann equation (12) over the sample and make use of eq. (35). As a result we obtain the conservation law for the number of quasiparticles in the form

$$\int (\mathrm{d}q) \left(\frac{\partial \omega_q}{\partial q} n\right) N_q \Big|_{\mathrm{s}} = \frac{1}{2} a \int (\,\mathrm{d}p)_p \langle Q_p \rangle_{\mathrm{s}} - a \int_{\hbar\omega_q > 2\Delta}, \quad (\,\mathrm{d}q) I^{(\mathrm{s})}_{\mathrm{ph-c}}(\mathrm{d}q) \equiv \frac{\mathrm{d}^3 q}{(2\pi)^3}. \tag{52}$$

Here n is the normal to the surface of the sample. The lhs of this equation describes the exchange by high-frequency phonons between the film and the thermal bath; the first term in the rhs represents creation of quasiparticles by laser pumping while the second term

describes absorption of phonons by quasiparticles and multiple generation of quasiparticles due to absorption and re-emission of high-frequency phonons.

The energy conservation law can be written in the form

$$R = \int (\mathrm{d}q) \left(\frac{\partial \omega_q}{\partial q} n \right) \hbar \omega_q N_q \Big|_{\mathrm{s}} = a \int (\ \mathrm{d}p)_p \varepsilon_p \left\langle Q_p \right\rangle_{\mathrm{s}} . \tag{53}$$

R is the energy flux density which is absorbed by the superconductor.
The mean free path $l_>$of high-frequency phonons in a superconductor is determined by generation and recombination processes and is of the order of the corresponding mean free path in a normal metal. The mean free path $l_<$of lowfrequency phonons ($\hbar\omega_{\mathrm{q}} < 2\Lambda$) is determined by scattering events and is of the order of

$$l_< \simeq \frac{l_>}{x}, \quad x \ll 1. \tag{54}$$

Here x is the dimensionless concentration of quasiparticles introduced in section 2.

One can discriminate between the following two cases of importance.
(1) A thin film. In this case the mean free paths of all phonons are larger than the effective thickness of the film $\tilde{a} = a, t, t$ being the transparency coefficient of the film boundaries with respect to phonons. All phonons are in equilibrium, the quasiparticles are scattered by the equilibrium phonons, and the quasiparticle lifetime in the sample is determined by recombination. If the scattering time is smaller than the recombination time [according to eq. (28) this means that $x \leqslant (T_0 A)^{1\,2}$] the quasiparticles have a quasiequilibrium distribution function (Owen and Scalapino 1972):

$$n(\varepsilon) = \exp\left(\frac{v - \varepsilon}{T_0} \right) \tag{55}$$

The chemical potential v is determined by the conservation law for the quasiparticle number and is given by

$$v = A + \frac{T_0}{2} \ln \left[\frac{2\Delta}{\pi T_0} \left(x_0^2 + \frac{\hbar\Omega}{2\Delta} \Gamma \right) \right] . \tag{56}$$

Here

$$I = \frac{8\pi e^2 R_{()}}{c(\hbar\Omega)^2} \tau_A \frac{x}{a} D$$

% is the skin depth. R_r, is the radiation intensity. Ω is the frequency of radiation, τ_1 is the electron phonon scattering time in the normal metal provided the electron energy is equal to $2A$.

As long as the quasiparticle concentration is small the variation of the energy gap relates to the concentration x as

$$\frac{A_0 - \Delta}{A_0} \simeq 2x \ll 1. \tag{57}$$

Here A_0 is the energy gap at $T = 0$ in equilibrium.
(2) A thick film, $l_> < \tilde{a} \ll l_<$, or $x \ll l_> \mid \tilde{a}$. In this case the conditions are essentially different for high-frequency (hw) ${}_4 - 21$) and low-frequency (hry ${}_4 - 21$) phonons. The film is transparent for low-frequency phonons. which is not the case for high-frequency phonons because the latter take part in the processes of creation and annihilation of the quasiparticles (Rothwarf and Taylor 1967). In the stationary state these processes establish partial equilibrium among the

highfrequency phonons and the quasiparticles. Their distribution functions are given by

$$n(\varepsilon) = \exp[(v-\varepsilon)/T],$$
$$N(\omega) = \begin{cases} \exp[(2v-\varepsilon)/T], & \hbar\omega > 2\Delta, \\ \left[\exp\left(\hbar\omega/T_0\right) - 1\right]^{-1}, & \hbar\omega < 2\Delta. \end{cases} \tag{58}$$

Substituting eq. (58) in eq. (52) we obtain the equation for the quasiparticle concentration:

$$\frac{3\Delta^3 x^2}{\pi^3\hbar^3 w^2}\left(t + \frac{2\sqrt{2}a}{\pi l_>}\right) = c\frac{R}{2\Delta}, \quad w \equiv \partial\omega_q/\partial q, \tag{59}$$

where $c \lesssim 1$. The coefficient c measures the fraction of the energy that is transformed into low-frequency phonons and thus does not take part in generation of quasiparticles.

The first term in the lhs describes the escape of high-frequency phonons through the film boundary, the second term in the lhs reflects the variation of the quasiparticle concentration due to absorption of high-frequency phonons and subsequent emission of low-frequency phonons. Therefore the total lifetime of the quasiparticles in the film is given by

$$1/\tau_{\rm e} = (1/\tau_{\rm r})\left(\frac{l_>}{\tilde{a}} + \frac{2\sqrt{2}}{\pi}x\right). \tag{60}$$

To determine the temperature let us introduce the characteristic energy of the quasiparticles at which the rate of quasiparticle scattering by low-frequency phonons is equal to the rate of recombination (Aronov and Spivak 1977, 1978). According to eq. (28) this energy is equal to $\varepsilon_1 - \Delta \simeq \Delta x^{2/7}$. Let us suppose that $\varepsilon_1 - \Delta > T$. The last inequality may be fulfilled in a nonequilibrium state only if $x \gg (T/A)^{7,2}$. Let us call the energy interval $A < \varepsilon < \varepsilon_1$ the active region. In the active region fast generation-recombination processes lead to quasi-equilibrium distribution functions with the form (58). These processes redistribute the excess energy (as compared to T) among all the quasiparticles. Quasiparticles reach the active region emitting phonons. The quasiparticle active region is of the order of the width of the active region, $\bar{\varepsilon} - \Lambda \simeq \beta A x^{27}$, where β is of the order of unity. These considerations are sufficient to determine the temperature T. Let us multiply eq. (52) by 2Δ and subtract it from eq. (55). Then we obtain

$$\int (\mathrm{d}q)(nw)\left(\hbar\omega_q - 2\Delta\right) N_q\Big|_{\rm s} - a\int_{\hbar\omega_q > 2A}(\,\mathrm{d}q) 2\Delta I^{(s)}_{\rm ph-c}$$
$$- a\int_{\hbar\omega q < 2A}(\,\mathrm{d}q)\hbar\omega_q I^{(s)}_{\rm ph-c} = a\int(\,\mathrm{d}q)_p\left(\varepsilon_p - \Delta\right)\langle Q_p\rangle_s. \tag{61}$$

Substituting eq. (58) in eq. (61) we obtain the equation for the temperature in the following form

$$\frac{\tau_{\rm e}}{\tau_{\rm s}\left(\tau_0\right)} F\left(T/T_0\right) = \beta\frac{\Delta}{T}x^{2/7}. \tag{62}$$

Here we suppose that the characteristic energy of the quasiparticles which they bring in the active region is $\beta\Delta x^{2/7}$. The function $F\left(T/T_0\right)$ has the form

$$F(t) = t^{7/2}\int_0^\infty \mathrm{d}y y^3 \frac{\mathrm{e}^{-y}-\mathrm{e}^{-ty}}{1-\mathrm{e}^{-ty}}\int_0^\infty \mathrm{d}x \mathrm{e}^{-\mathrm{x}}\frac{2x+y}{\sqrt{x(x+y)}} \tag{63}$$

$$T = T_0, \quad \text{at} \quad \frac{\tau_\mathrm{s}}{\tau_\mathrm{e}}\frac{\Delta}{T}x^{2,7} \ll 1$$

$$T = \Delta x^{2,7}\left(\frac{\beta l_>}{\tilde{a}}\right)^{2/9}, \quad \text{at} \quad \frac{\tau_\mathrm{s}}{\tau_\mathrm{e}}\frac{\Delta}{T}x^{2/7} \gg 1$$

and the width of the active region is much greater than the temperature because of the inequality $(\tilde{a}/l_>)^{2/9} \geqslant 1$.

At larger pumping rates ($1 \geqslant x \geqslant 1 > /\tilde{a}$) the film becomes opaque for low-frequency phonons as well. Their temperature because of quasiparticle phonon scattering becomes equal to the temperature of the quasiparticles. However, the chemical potential of the quasiparticles is by no means equal to zero. Their concentration is determined by eq. (59), where one must retain only the second term in the lhs.

21.5 5. Energy conservation and entropy production

Let us demonstrate that the transport equation approach in the presence of external fields is compatible with the energy conservation law. For simplicity, we shall consider only the elastic scattering of quasiparticles.

For our purpose it is convenient to multiply eq. (6) by the quasiparticle energy $\tilde{\varepsilon}_p$ and integrate it over $(\mathrm{d}p)_p$. The integral of the elastic collision operator vanishes and one can obtain

$$\frac{\partial}{\partial t}\int(\,\mathrm{d}p)\tilde{\varepsilon}_p n_p + \frac{\partial}{\partial x_i}\int(\,\mathrm{d}p)\tilde{\varepsilon}_p\frac{\partial\tilde{\varepsilon}_p}{\partial p_i}n_p = \int(\mathrm{d}p)n_p\frac{\partial\tilde{\varepsilon}_p}{\partial t}, \tag{64}$$

$$\frac{\partial\tilde{\varepsilon}_p}{\partial t} = \frac{\tilde{\xi}_p}{\varepsilon_p}\frac{\partial\tilde{\xi}_p}{\partial t} + v\frac{\partial p_s}{\partial t} + \frac{\Delta}{\varepsilon_p}\frac{\partial\Delta}{\partial t}, \quad \frac{\partial\tilde{\xi}_p}{\partial\tilde{t}} = \frac{\partial}{\partial t}\left(\phi + \frac{p_\mathrm{s}^2}{2m}\right). \tag{65}$$

Here we have taken into account that the integral

$$\int(\mathrm{d}p)\frac{\partial}{\partial p_i}\left(A_p\frac{\partial\tilde{\varepsilon}_p}{\partial x_i}\right) \tag{66}$$

where A_p is an arbitrary function of quasimomentum p, vanishes as a consequence of the periodicity of the integrand in p-space, its period being the reciprocal lattice vector.

To get the energy conservation law one should transform the rhs of eq. (64) in the following way

$$\frac{\partial}{\partial t}\left(\phi + \frac{p_\mathrm{s}^2}{2m}\right)\int(\mathrm{d}p)\frac{\widetilde{\xi}_p}{\varepsilon_p}n_p + \frac{\partial p_\mathrm{s}}{\partial t}\int(\,\mathrm{d}p)vn_p + \frac{1}{2}\frac{\partial\Delta^2}{\partial t}\int(\,\mathrm{d}p)\frac{n_p}{\varepsilon_p}. \tag{67}$$

Using eqs. (3) and (4) we get

$$\int(\mathrm{d}p)n_p\frac{\partial\tilde{\varepsilon}_p}{\partial t} = N\frac{\partial\phi}{\partial t} - \frac{j}{e}\frac{\partial p_\mathrm{s}}{\partial t} - \int(\mathrm{d}p)v_p^2\frac{\partial}{\partial t}\left(\phi + \frac{p_\mathrm{s}^2}{2m}\right) + \frac{1}{2}\frac{\partial\Delta^2}{\partial t}\int(\,\mathrm{d}p)\frac{n_p}{\varepsilon_p}. \tag{68}$$

To transform the third and fourth terms in the rhs of eq. (5) let us note that

$$\frac{\partial}{\partial t}\int(\,\mathrm{d}p)\tilde{\varepsilon}_p v_p^2 = -\int(\mathrm{d}p)v_p^2\frac{\partial}{\partial t}\left(\phi + \frac{p_\mathrm{s}^2}{2m}\right) + \frac{1}{2m}\frac{\partial\Delta^2}{4\partial t}\int(\,\mathrm{d}p)\varepsilon_p{}^1. \tag{69}$$

Taking this expression into account and combining it with the self-consistency equation (15), we obtain

$$\int (\mathrm{d}p) n_p \frac{\partial \tilde{\varepsilon}_p}{\partial t} = N \frac{\partial \phi}{\partial t} + \frac{1}{e} j \frac{\partial p_\mathrm{s}}{\partial t} + \frac{\partial}{\partial t} \left(\int (\,\mathrm{d}p) \tilde{\varepsilon}_p v_p^2 + \frac{\Delta^2}{2\lambda_\mathrm{e}} \right). \tag{70}$$

Inserting eq. (70) into eq. (64) we obtain

$$\frac{\partial}{\partial t}(\mathscr{E} - N\phi) + \operatorname{div} \left(\boldsymbol{W} - \frac{1}{e}\phi j \right) = j\boldsymbol{E}. \tag{71}$$

Here the quantity

$$\boldsymbol{W} = \int (\mathrm{d}p)_p \tilde{\varepsilon}_p \frac{c\tilde{\varepsilon}_p}{\partial p} n_p \tag{72}$$

is the electron part of the energy density flux, while

$$\mathscr{E} = \int (\mathrm{d}p)_p \tilde{\varepsilon}_p \left(n_p - v_p^2 \right) - \frac{\Lambda^2}{2\lambda_\mathrm{e}} \tag{73}$$

is the electron contribution to the energy density. One can show that this quantity is equal to the average of the BCS Hamiltonian in the presence of external fields.

With the help of the Maxwell equation curl $\boldsymbol{H} = (4\pi/c)j$ one can rewrite eq. (71) in a manner which explicitly represents the conservation law for the total
(quasiparticle and field) energy

$$\frac{\partial U}{\partial t} + \operatorname{div} u = 0. \tag{74}$$

Here

$$U = \mathscr{E} - N\phi + \boldsymbol{H}^2/8\pi \tag{75}$$

is the total energy density while

$$u = W - (\phi/e)j + (c/4\pi)[E \times H] \tag{76}$$

is the total energy flux density.

To take inelastic collisions with phonons into account one should include, into the full set of equations, also the Boltzmann equation for the phonon distribution function (eq. 12). As a result the explicit expressions for the energy density and the energy flux density should be modified to include the phonon terms.

Now let us obtain the expression for the entropy production rate with the help of the transport equation approach. We shall start with the usual combinatorial expression for the entropy density S of the quasiparticles obeying Fermi statistics:

$$\begin{aligned} S &= \int (\mathrm{d}p)_p \sigma_p \left(n_p \right) \\ \sigma_p &= -\left[n_p \ln n_p + (1 - n_p) \ln \left(1 - n_p \right) \right] \end{aligned} \tag{77}$$

Differentiating this quantity with respect to time we have

$$\frac{\partial S}{\partial t} = \int (\mathrm{d}p)_p \frac{\partial \sigma_p}{\partial p} \frac{\partial n_p}{\partial t}.$$

Inserting $\partial n_p/\partial t$ from the transport equation (6) we get

$$\frac{\partial S}{\partial t} + \operatorname{div} s = -\int (\mathrm{d}p)_p \frac{\partial \sigma_p}{\partial n_p} I\{n_p\}, \tag{78}$$

Here

$$s = \int (\mathrm{d}p)_p \frac{\partial \tilde{\varepsilon}_p}{\partial p} \sigma_p \tag{79}$$

is the entropy flux density. The flux is determined in terms of the group velocity $\partial\tilde{\varepsilon}_p/\partial p$, in contrast to the normal current density which is expressed through $v = \partial E_p/\partial p$ (see eq. 40). In the derivation of eq. (78) we have taken into account that integrals of the type (66) with $A_p \equiv \sigma_p$ vanish.

We wish to emphasize that if n_p is an arbitrary function of the total energy $\hat{\varepsilon}_p$ it follows from the explicit expression (79) that the entropy flux density (and therefore the heat flux density) vanishes. In particular, this is the case for the equilibrium state with a finite persistent current.

Indeed, in such a case a_p depends only on the total energy and the integrand in eq. (79) can be written as the full derivative

$$\int (\mathrm{d}p) \frac{\partial \tilde{\varepsilon}_p}{\partial \boldsymbol{p}} \sigma_p = \int (\mathrm{d}p) \frac{\partial \boldsymbol{F}}{\partial \boldsymbol{p}} = 0; \quad F = \int^{\hat{\varepsilon}_p} \sigma_p(\varepsilon)\mathrm{d}\varepsilon$$

To obtain this result one employs no special properties of the quantity σ_p, only its dependence on the $\hat{\varepsilon}_p$. In a similar way one can verify that the quasiparticle velocity averaged over a surface of constant energy $\tilde{\varepsilon}_p = \varepsilon = \text{const.}$, vanishes (for the proof one may consider $\delta(\varepsilon - \tilde{\varepsilon}_{p'})$ instead of $\sigma(\tilde{\varepsilon}_p)$ in the integrand). The absence of the entropy flux in the equilibrium is closely related with this mathematical fact.

Now let us demonstrate the H-theorem for superconductors, i.e. the nonnegative sign of the entropy production rate $(\partial S/\partial t)_{\text{coll}}$, which enters the rhs of eq. (78). For the case of elastic impurity scattering we insert the expression for I_{im} (eq. 8) into eq. (78). Then we interchange the integration variables p and p' and take the half-sum of the expressions in the integrand. Employing the relation $|f_{pp'}|^2 = |f_{p'p}|^2$, which is valid for centro-symmetric crystals, we get

$$\begin{aligned}\left(\frac{\partial S}{\partial t}\right)_{\text{coll}} =& \pi N_{\text{i}} \frac{(2\pi)^4}{m^2} \int (\,\mathrm{d}p)_p \int (\,\mathrm{d}p)_{p'} |f_{pp'}|^2 (n_p - n_{p'}) \\ &\times \ln \frac{(1-n_{p'})\, n_p}{n_{p'}\,(1-n_p)} (u_p u_{p'} - v_p v_{p'})^2\, \delta(\tilde{\varepsilon}_p - \tilde{\varepsilon}_{p'})\end{aligned} \tag{80}$$

One can see that the integrand is always non-negative. Thus, $(\hat{C}S/\hat{C}t)_{\text{coll}}$ is also non-negative. This statement is the well-known Boltzmann H-theorem for superconductors.

If phonon scattering is taken into account the whole procedure is more cumbersome. In this case one should consider the Boltzmann equations both for normal excitations and for phonons in the superconductor. As a result, one gets the following expression for the total entropy density production of the electron-phonon system:

$$\begin{aligned}\left(\frac{\partial S}{\partial t}\right)_{\text{coll}} =& \pi \int (\mathrm{d}p)_p \int (\,\mathrm{d}p)_{p'} |c_{p-p'}|^2 \\ &\times \Big\{ (u_p u_{p'} - v_p v_{p'})^2 \ln \frac{n_p (1-n_{p'})\, N_{p-p'}}{(1-n_p)\, n_{p'}\, (1+N_{p-p'})} \\ &\times \delta(\tilde{\varepsilon}_p - \tilde{\varepsilon}_{p'} + \hbar\omega_{p-p'}) \left[n_p (1-n_{p'})\, N_{p-p'} - n_{p'} (1-n_p)(1+N_{p-p'}) \right]\end{aligned}$$

$$+ (u_p v_{p'} + u_{p'} v_p)^2 \ln \frac{n_p n_{-p'} (1 + N_{p+p'})}{(1 - n_p)(1 - n_{-p'}) N_{p+p'}} \delta (\tilde{\varepsilon}_p + \tilde{\varepsilon}_{-p'} - \hbar\omega_{p+p'})$$
$$\times [n_p n_{-p'} (1 + N_{p+p'}) - (1 - n_p)(1 - n_{-p'}) N_{p+p'}]\} \tag{81}$$

One can see that there are two types of irreversible processes that contribute to the entropy generation. The first type is simple scattering of quasiparticles by phonons. These processes are represented by the first term in the braces in eq. (81); this term differs from the similar term in the normal state only by the coherence factor $(u_p u_{p'} - l_p v_{p'})^2$ and by the form of energy spectrum $\tilde{\varepsilon}_p$. The second contribution is due to the creation-annihilation processes we have discussed above.

21.6 6. Hydrodynamical approach

In this section we shall obtain a closed set of equations for macroscopic variables describing nonequilibrium behavior of a superconductor in nonuniform external fields. Thereafter these will be referred to as hydrodynamical equations. They are the equations for the full set of macroscopic variables (such as potential ϕ, normal current, temperature gradient, etc.) describing the nonequilibrium state of a superconductor.

One may hope to justify such an approach if inelastic scattering of excitations is relatively rare, i.e. if they are scattered much more often by impurities than by phonons. The second restriction is connected with the characteristic scales of time and space variation of external fields; one should assume these scales to be much larger than the corresponding characteristic electron quantities, $\tau_{\rm im}$ and $l_{\rm im}$, with $l_{\rm im}$ the excitation mean free path due to the impurity collisions.

The procedure of derivation of macroscopic equations is analogous to the well-known Chapman Enskog method (see also Gantsevich et al. 1974, where this method is applied to derive macroscopic equations describing the nonequilibrium behavior of a normal conductor). Let us confine ourselves to the case where the equations are linear in the variable $v_{\rm s}$.

Assume the quantities $\omega\tau_{\rm im}$ as well as $ql_{\rm im}$ to be small. Then one can iterate the linearized transport equation, as well as the neutrality condition, in powers of these quantities. The linearized transport equation can be written in the form

$$\frac{\partial n_p^{(1)}}{\partial t} + \left(\begin{matrix} \xi \\ \varepsilon \end{matrix} \dot{\phi} + \dot{p}_{\rm s} v \right) \frac{\partial n^{(0)}}{\partial \varepsilon} + \frac{\xi}{\varepsilon} v \frac{\partial n_p^{(1)}}{\partial r} - \frac{\xi}{T} (v \nabla T) \frac{\partial n^{(0)}}{\partial \varepsilon} + I_{\rm im} n_p^{(1)} + I_{\rm ph} n_p^{(1)} = 0. \tag{82}$$

Let us average eq. (82) over all directions in momentum space. We get

$$\overline{\frac{\partial n_p^{(1)}}{\partial t}} + \frac{\xi}{\varepsilon} \phi \frac{\partial n^{(0)}}{\partial \varepsilon} + \overline{\frac{\xi}{\varepsilon} v \frac{\partial n_p^{(1)}}{\partial r}} + I_{\rm ph} n_p^{(1)} = 0 \tag{83}$$

where the bar denotes the averaged quantity. The averaged impurity collision operator, naturally, vanishes.

Subtracting eq. (83) from eq. (82) and applying an iteration procedure in the small parameters $\omega\tau_{\rm im}$ and $ql_{\rm im}$ to the difference equation one gets

$$n_p^{(1)} = \overline{n_p^{(1)}} - \frac{\xi}{\varepsilon} I_{\rm im}^{-1} v_k \overline{\frac{\partial n_p^{(1)}}{\partial x_k}} - I_{\rm im}^{-1} \left(v_k p_{\rm sk} - v_k \frac{\partial T}{\partial x_k} \frac{\xi}{T} \right) \frac{\partial n^{(0)}}{\partial \varepsilon} \tag{84}$$

One can get the equation for $\overline{n_p^{(1)}}$ by substituting eq. (84) in eq. (83):

$$\frac{\partial \overline{n_p^{(1)}}}{\partial t} + \frac{\xi}{\varepsilon}\phi\frac{\partial n^{(0)}}{\partial \varepsilon} + I_{\rm ph}\overline{n_p^{(1)}} - \frac{\xi}{\varepsilon}v_{\rm i}I_{\rm im}^{-1}v_{\rm k}\frac{\partial^2 \overline{n_p^{(1)}}}{\partial x_i \partial x_k} - \\ - \overline{v_i I_{\rm im}^{-1} v_k}\frac{\xi}{\varepsilon}\frac{\partial}{\partial x_i}\left(p_{\rm sk} - \frac{\partial T}{\partial x_{\rm k}}\frac{\xi}{T}\right)\frac{\partial n^{(0)}}{\partial \varepsilon} = 0 \tag{85}$$

Now let us turn to the calculation of the current density. Inserting eq. (84) into expression (40) for the current we get

$$j_i = eN_{\rm s}v_{{\rm s}i} - \eta_{ik}\frac{\partial T}{\partial x_k} + \frac{1}{e}\sigma_{ik}^{(\rm s)}\dot{\rm p}_{{\rm s}k} - eD_{ik}\frac{\partial v_{\rm s}}{\partial x_{\rm k}} \tag{86}$$

Here the first term is the supercurrent while the second term is the normal thermoelectric current which we shall consider in more detail in section 7 ; the thermoelectric transport coefficient η_{ik} is given by

$$\eta_{ik} = -\frac{e}{T}\int (\,{\rm d}p)_p v_i I^{-1} v_k \xi_p \frac{\partial n^{(0)}}{\partial \varepsilon_p} \tag{87}$$

The third term is the normal Ohmic current proportional to the (non-steady) electric field $\boldsymbol{E} = e^{-1}\dot{\boldsymbol{p}}_{\rm s}$. The transport coefficient $\sigma_{ik}^{(s)}$ is given by

$$\sigma_{ik}^{(\rm s)} = -e^2\int (\,{\rm d}p)_p v_i(-{\rm i}\omega + I)^{-1}v_k\frac{\partial n^{(0)}}{\partial \varepsilon_p} \tag{88}$$

This quantity may be called the conductivity of the normal component in the superconducting state.

If only impurity scattering is present then in the immediate vicinity of the critical temperature $T_{\rm c}$ the ratio $\sigma^{(s)}/\sigma^{(n)}$ (where $\sigma^{(n)}$ is the conductivity in the normal state) calculated on the basis of eq. (88) is given by

$$\sigma^{(\rm s)}/\sigma^{(\rm n)} = 1 + (\Delta/2T)\ln\omega\tau_{\rm im}$$

However, this result appears to be incorrect in the general case, for it can be seen that the characteristic energies in the integrand determining the logarithmic term are small. At such small energies one should be cautious and check the applicability of the Boltzmann equation. It follows from eq. (88) that the logarithmic term is determined by the energy ξ_p of the order of $\omega\tau_{\rm im}\Delta$. However, this conclusion in also appears to be incorrect in the general case. It can be seen from the quantum-mechanical approach (see Ovchinnikov 1977 and Artemenko and Volkov 1979) that the characteristic value of ξ_p turns out to be of the order of $(\hbar\omega\Delta)^{1/2}$. If this quantity is much larger than $\omega\tau_{\rm im}\,\Delta$ it cuts off the integral. So in the general case the expression for the ratio $\sigma^{(s)}/\sigma^{(n)}$ has the form

$$\sigma^{(\rm s)}/\sigma^{(\rm n)} = 1 + (\Delta/T)\ln\Lambda; \quad \Lambda = \max\left[\omega\tau_{\rm im}, (\hbar\omega/\Delta)^{1/2}\right]. \tag{89}$$

Such a divergence of the conductivity at very small frequencies could be removed by taking into account other mechanism of momentum relaxation which do not contain the factor ξ_p/ε_p in the expression for the inverse relaxation time, such as electron-phonon scattering, paramagnetic impurities, etc., which can be done on the basis of the Boltzmann equation.

The fourth term in eq. (86) introduces a new macroscopic quantity into the theory, i.e.

$$v_{\rm s} = \int ({\rm d}p)_p\,{\rm sign}\,\xi_p n_p(1) \tag{90}$$

It has the meaning of the population difference between the two branches with $\xi_p > 0$ and $\tilde{\zeta}_p < 0$ and may be considered as the measure of imbalance between the quasi-electron and quasihole branches (briefly discussed in section 5). The corresponding transport coefficient,

$$D_{ik} = \int (\mathrm{d}p)_p \frac{|\xi_p|}{\varepsilon_p} v_i I^{-1} v_k \frac{\partial n^{(0)}}{\partial \varepsilon_p} \tag{91}$$

which in the isotropic case simply equals $\frac{1}{3} v_{\mathrm{F}}^2 \tau_{\mathrm{tr}} \delta_{ik} 2n^{(0)}(\Lambda)$, has the meaning of a diffusion coefficient.

The closed set of hydrodynamical equations can be obtained only in the vicinity of T_{c}, i.e. if $T_{\mathrm{c}} - T \ll T_{\mathrm{c}}$. Taking this restriction into account, multiplying eq. (85) by sign ξ_p and integrating it over p, one obtains

$$\begin{aligned} &\frac{\pi\Delta}{4T}\frac{\partial\phi}{\partial t} + \frac{\phi}{\tau_{\mathrm{Q}}}\frac{\partial N}{\partial\mu} - \frac{\partial N}{\partial\mu} D_{ik} \frac{\partial^2\phi}{\partial x_i \partial x_k} \\ &\quad = -\frac{\partial}{\partial x_i}\left(\frac{1}{e^2}\sigma_{ik}^{(\mathrm{n})}\dot{p}_{\mathrm{s}k} - \frac{1}{e}\eta_{ik}\frac{\partial T}{\partial x_k}\right) \end{aligned} \tag{92}$$

Here we have employed the relation $v_s = \phi\hat{c}N/\hat{c}\mu$, which is a consequence of the neutrality condition. The branch-imbalance relaxation time τ_{Q} introduced in section 2 can be defined here quantitatively by the relation

$$\phi\frac{\partial N}{\partial\mu}\frac{1}{\tau_{\mathrm{Q}}} = \int (\mathrm{d}p)_p \frac{\xi_p}{\varepsilon_p} I n_p^{(1)} \tag{93}$$

One can see from eq. (92) that in homogeneous situation the potential ϕ relaxes in a period of the order of $\tau_{\mathrm{Q}}\pi\Delta/4T$. As for the inhomogeneous case, the diffusion should also be taken into account. One can see from eq. (92) that the characteristic length of the spatial variation of the potential ϕ is the diffusion length

$$L_{\mathrm{b}} = \sqrt{D\tau_{\mathrm{Q}}} \propto \Delta^{-1/2}.$$

It increases near T_{c} and diverges at $T = T_{\mathrm{c}}$. Note that eq. (92) has the form of the continuity equation for the quantity v_{s} (or $\phi\partial N/\partial\mu$), the rhs of eq. (92) being the source of an imbalance.

Let us now discuss what becomes of equations (86) and (92) of the hydrodynamical approach in the normal state. In this limit $\Delta \to 0$, and the Einstein relation between D_{ih} and σ_{th} holds. As a result, it can be shown, using eq. (86) and the relation $v_{\mathrm{s}} = \phi\partial N/\partial\mu$, that eq. (92) becomes a trivial consequence of the continuity equation $\operatorname{div} j = 0$.

To solve eq. (92), appropriate boundary conditions should be formulated. Discussions of the boundary conditions may be found in papers by Artemenko and Volkov (1975a, 1976a) and Aronov (1976). For example, for the simplest case of a superconductor-insulator boundary, where no specific boundary mechanism of imbalance relaxation exists, these conditions require the normal current density (and therefore the supercurrent density as well) to vanish on the boundary surface. Artemenko and Volkov (1975a, 1976a) were the first to show that in the presence of a temperature gradient the electric field $E = -e^{-1}\nabla\phi$ appears in a superconductor near an S−N boundary. This thermoelectric field decreases as a function of the distance from the boundary, the characteristic decrease length being L_{b}. It is necessary to note that other types of perturbations can also produce imbalance in superconductors. For instance, electromagnetic or sound waves can produce photoelectric or acoustoelectric fields of this nature (Aronov 1976). The latter will be discussed in more detail in section 8.

Investigating excess current in Josephson junctions Carlson and Goldman (1975) have discovered a collective mode in superconductors near the transition temperature T_c. Schmid and

Schön (1975a,b) and Artemenko and Volkov (1975b) later showed theoretically that a sound-like collective mode can exist in a superconductor near T_c. In such a wave the oscillating quantities are the branch imbalance v_1 (or potential ϕ) and v_1, no spatial charge appearing. The normal current and the supercurrent flow in the opposite directions, the total current being zero. It is the absence of a net current and consequently the
absence of any magnetic field that provides the possibility for these waves to exist in the bulk of a superconductor.

To find the dispersion law for such a collective mode one should apply Fourier transformation to eqs. (86) and (92). Making use of the continuity equation $\operatorname{div} j = 0$ we get (Artemenko and Volkov 1975b)

$$\begin{aligned}\omega^2 =& 4T\bar{\Delta}\frac{N_s}{m}\frac{\partial\mu}{\partial N}\left(q^2 + L_{\mathrm{b}}^{-2}\right) + \mathrm{i}\omega\left(\frac{e^2 N_s}{m\sigma^{(\mathrm{n})}} + \frac{1}{\tau_{\mathrm{ph}}}\right) \\ &+ \mathrm{i}\omega D q^2 \frac{4T}{\pi\Delta}\frac{\sigma^{(\mathrm{s})} - \sigma^{(\mathrm{n})}}{\sigma^{(\mathrm{n})}}\end{aligned} \tag{94}$$

It can be readily seen from this equation that if

$$\frac{1}{\tau_{\mathrm{ph}}}, \quad \frac{1}{\tau_{\mathrm{im}}}\frac{N_{\mathrm{s}}}{N} \ll \omega \ll \frac{1}{\tau_{\mathrm{im}}}\frac{N_{\mathrm{s}}}{N}\frac{\sigma^{(\mathrm{n})}}{\sigma^{(\mathrm{s})} - \sigma^{(\mathrm{n})}}, \tag{95}$$

such a collective mode exists, its damping being small. The dispersion law of this mode is given by (Artemenko and Volkov 1975b)

$$\omega^2 = \frac{4T}{\pi\Delta}\frac{N_{\mathrm{s}}}{m}\frac{\partial\mu}{\partial N}q^2, \tag{96}$$

i.e. this mode is of the acoustic type. Near the transition point $N_{\mathrm{s}} \propto \Delta^2 \propto (T_{\mathrm{c}} - T)$, consequently the wave velocity is proportional to $\Delta^{1/2} \propto (T_{\mathrm{c}} - T)^{1/4}$.

To analyse the conditions (95) of small damping one should know the ratio $\left(\sigma^{(s)} - \sigma^{(n)}\right)/\sigma^{(n)}$. As we have seen one cannot determine this quantity correctly using the transport equation approach.

As a conclusion to this section we shall formulate the Onsager relations for the transport coefficient. For this purpose let us calculate the thermal flux density Q. Linearizing eq. (77) for σ_p in $n_p^{(1)}$ and inserting it in eq. (79) we get

$$\mathrm{Q}_i = Ts_i = \int (\mathrm{d}p)_p \xi_p v_i n_p^{(1)} \tag{97}$$

Inserting eq. (84) for $n_p^{(1)}$ we have in linear approximation in the gradients

$$Q_{\mathrm{i}} = \xi_{ik}E_k - \kappa_{ik}\partial T/\partial x_k, \tag{98}$$

where

$$\begin{aligned}\xi_{\mathrm{ik}} &= -e\int (\ \mathrm{d}p)_p \xi_p v_i I^{-1} v_k \partial n^{(0)}/\partial\varepsilon \\ \kappa_{ik} &= -\int (\mathrm{d}p)_p \xi_p v_i I^{-1} v_k \partial n^{(0)}/\partial\varepsilon\end{aligned} \tag{99}$$

One can verify that the matrix elements of the linearized collision operator $l_{pp'}$
obey the relations

$$I_{pp'}\frac{\partial n^{(0)}}{\partial \varepsilon} = I_{-p',-p}\frac{\partial n^{(0)}}{\partial \varepsilon}. \tag{100}$$

These relations are a consequence of the time reversal asymmetry of the mechanical equations. We conclude from eq. (100) that

$$\left(\frac{\partial n^{(0)}}{\partial \varepsilon}\right)^{-1}\left(I^{-1}\right)_{pp'} = \left(\frac{\partial n^{(0)}}{\partial \varepsilon}\right)^{-1}\left(I^{-1}_{-p',-p}\right).$$

Using eqs. (87), (88) and (99) we easily obtain the following relations

$$\sigma^{(\mathrm{s})}_{ik} = \sigma^{(\mathrm{s})}_{ki}, \quad T\eta_{ik} = \zeta_{ki}, \quad \kappa_{ik} = \kappa_{ki}. \tag{101}$$

These are the Onsager relations for a superconductor. They were first established by Luttinger (1964).

21.7 7. Thermoelectric phenomena

Here we shall discuss briefly thermoelectric effects in superconductors. The physical picture of these phenomena is appropriate to point out some specific features of transport in the superconducting state and to illustrate the approach presented above.

It was shown in section 6 that in the presence of a temperature gradient in a superconductor a thermoelectric current of normal excitations proportional to ∇T appears, its nature being similar to the thermoelectric current in the normal state. The corresponding thermoelectric coefficient η in the case of impurity scattering is given by [cf. eq. (87); see Gal'perin et al. 1973, 1974)]

$$\eta = \frac{2\pi^2}{9}\frac{eT}{m}\frac{\hat{C}}{\hat{C}\varepsilon}\left[\tau_{\mathrm{tr}}(\varepsilon)v(\varepsilon)\varepsilon\right]_{\varepsilon=\mu} G(\Delta/T). \tag{102}$$

Here $r(\varepsilon)$ is the density of states while τ_{tr} is the so-called transport relaxation time describing relaxation of the function $n_p^{(1)}$ proportional (for an isotropic excitation spectrum) to the first spherical harmonic. For the case of impurity scattering it is given by

$$\frac{1}{\tau_{\mathrm{tr}}} = \frac{\pi N_i (2\pi)^4}{m^2} \int (\,\mathrm{d}p)_p \left|f_{pp'}\right|^2 \left(u_p u_{p'} - v_p v_{p'}\right)^2 \delta\left(\tilde{\varepsilon}_p - \tilde{\varepsilon}_{p'}\right)\left[1 - \cos\left(p, p'\right)\right].$$

The function $G(x)$ is defined by the integral

$$G(x) = \frac{3}{2\pi^2}\int_x^\infty \frac{y^2\,\mathrm{d}y}{\cosh^2(y/2)} \tag{103}$$

If $x \ll 1$, we have

$$G(x) = 1 - 2x^2/\pi^2 \tag{104}$$

Thus, for $T \to T_{\mathrm{c}}$ we get for the transport coefficient η the well-known expression for normal metals. For large values of the argument, $x \gg 1$, we have

$$G(x) = \frac{24}{\pi^2}x^2 e^{-x} \tag{105}$$

so for low temperatures ($T \ll T_{\mathrm{c}}$) the coefficient η is exponentially small.
Ginzburg (1944) was the first to suggest the existence of such a normal thermoelectric current

in superconductors. He concluded that in anisotropic or inhomogeneous superconductors the normal thermoelectric current can produce a magnetic field proportional to the temperature gradient. He also pointed out that in the bulk of a homogeneous isotropic superconductor the total current vanishes because the normal current is offset by the supercurrent. This makes it impossible to observe the thermoelectric effect in a simpleconnected isotropic superconductor directly.

However, one can make an independent measurement of the supercurrent which manifests itself by the creation of a phase difference $\delta\chi$ in the order parameter across the sample's boundaries (Gal'perin et al. 1973b, 1974a). The most effective way to observe the phase difference is to make the superconductor a part of bimetallic loop that may also contain weak links (Gal'perin et al. 1973b, 1974b, Garland and Van Harlingen 1974). Such a system may be, for instance, a superconducting quantum interferometer which measures $\delta\chi$ directly. It may also be a usual thermoelectric loop made of two different superconductors; in this case a non-quantized part of magnetic flux proportional to the temperature gradient appears in the cavity of the loop. Thus, the coefficient η in superconductors is measureable. It should give valuable information about the relaxation processes.

A number of experiments was made to observe the thermoelectric magnetic flux (see, for example, Zavaritskii 1974, Selzer and Fairbank 1974, Pegrum et al. 1975, Van Harlingen and Garland 1978). But in most of these experiments (except that of Zavaritskii 1974) the observed temperature-dependent magnetic flux was by several orders of magnitude larger than the theoretically predicted one. We do not intend to discuss in this chapter possible sources of these discrepancies. Some discussion was given by Pegrum and Gunault (1976), and by Kozub (1978); they considered, in particular, an important masking effect. It is due to temperature dependence of the penetration depth which leads to T -
dependent redistribution of the magnetic flux between the cavity and the surface layer with a width of the order of the penetration depth.

Several theoretical papers were also published, where the influences of some specific features of quasi particle transport on the thermoelectric effect were studied [phonon drag (Gurevich and Krylov 1975), scattering on magnetic impurities (Kon 1975, Kon and Nika 1976, Gelikman and Reizer 1975)].

One may also expect a specific thermoelectric effect in the situation where a temperature gradient exists in the presence of a supercurrent. Taking symmetry considerations into account one may conclude that a contribution to the quasiparticle distribution function proportional to $(v_s\nabla T)$ and a corresponding contribution to the current density should exist in this case (Aronov 1974). Noting that $v_{\rm s}\nabla T$ does not depend on p one might also come to conclusion that this part of the nonequilibrium distribution function relaxes only through collisions with phonons and, as a result, the corresponding contribution to the current density should be proportional to $\tau_{\rm ph}v_{\rm s}\,(v_{\rm s}\nabla T)$ (Aronov 1974). Unfortunately, such reasoning, employed in several papers (Aronov 1974, Kozub 1978, Gal'perin et al., 1978) seems to be erroneous. Indeed, it can be shown that such an effect should be proportional, apart from $\tau_{\rm ph}$, to the integral

$$\int ({\rm d}p)\frac{\partial\tilde{\varepsilon}_p}{\partial p}\delta\left(\varepsilon-\tilde{\varepsilon}_p\right) \tag{106}$$

which, as we have seen in section 6 , vanishes. Thus, we come to the conclusion that in the case of comparatively strong impurity scattering no thermoelectric effect proportional to $\tau_{\rm ph}$ exists. This means that all the additional terms in the nonequilibrium distribution function proportional to $v_c\nabla T$ are also proportional to $\tau_{\rm im}$. As a consequence, the corresponding contribution to the thermoelectric current can be estimated as

$$\left(p_{\rm F}v_{\rm s}/T\right)^2\eta\nabla T \tag{107}$$

and may be discarded in standard experimental situations, where $pv_s \ll T$.
Nevertheless, a specific v_--dependent thermoelectric effect does exist in superconductors. It manifests itself by the appearance of the branch imbalance discussed above, and, consequently, of the potential ϕ in the presence of ∇T and v, (Schmid and Schön 1979). The corresponding thermoelectric potential ϕ is proportional to $(v, \nabla T)$; it can be homogeneous if this quantity is constant along the sample. It was shown (Schmid and Schön 1979) that this effect is also connected with the impurity scattering rather than with the phonon scattering. This fact is in accordance with the considerations discussed above.

One may also mention, in conclusion, the effect considered recently by Shelankov (1980) which is analogous to the well-known Nernst effect in normal conductors. If an external magnetic field is parallel to the surface of a superconducting plate supercurrent flows near the surface because of

Meissner-Oxenfeld screening. If a temperature gradient exists along the plate, it produces, in combination with the supercurrent, branch imbalance accompanied by the transverse potential difference $\delta\phi = \phi_1 - \phi_2$, where ϕ_1 and ϕ_2 are the values of the nonequilibrium covariant potential on the surfaces of the plate.

21.8 8. Acoustical properties of superconductors

21.8.1 8.1. Deformational perturbations

In this section we are going to consider another important class of perturbations, i.e. those due to the strain of a superconductor. They appear, for instance, if sound propagates through a superconductor.

The electron dispersion law is affected by the strain. To describe this effect one shoud choose the proper reference frame. For this purpose either Lagrangian or Eulerian coordinates can be used. Consider some point of the elastic continuum. Let us specify its initial position by the vector r; its position after the strain is $r' = r + u$, u being the displacement vector. The strained state of the elastic medium can be described by the vector u as a function of either the Lagrangian coordinates r, t or the Eulerian coordinates r', t. The Lagrangian reference frame "follows" the strained continuum, and the interaction Hamiltonian in this system has the simplest form. It is the system we shall use hereafter in this section to formulate the transport equation. The noninertiality and curvilinearity of the system can properly be taken into account by adding extra terms to the interaction Hamiltonian.

The strain field being a slowly-varying function of r and t, we shall use the well-known effective-mass approach. Along the lines of this approach we shall consider an electron as a quasiparticle with the Hamiltonian $E_0(-\mathrm{i}\hbar\hat{c}/\hat{c}r)$ where $E_0(p)$ is the unperturbed energy spectrum (here we, of course, are to reject the previously formulated assumption of isotropy of the electron spectrum). The strain tensor

$$u_{ik} = \left(\frac{1}{2}\right)\left(\frac{\partial u_i}{\partial x_k} + \frac{\partial u_k}{\partial x_i}\right) \tag{108}$$

is considered to be small: $|u_{ik}| \ll 1$. In this approximation the one-electron Hamiltonian of a normal metal has the form (see Akhieser 1938, Akhieser et al. 1957)

$$\hat{H} = E_0(\hat{p}) + \lambda_{ik}(\hat{p})u_{ik} - m_0 v\frac{\partial u}{\partial t}, \tag{109}$$

where $\hat{p} = -\mathrm{i}\hbar\hat{d}/\hat{c}r$. Here λ_{ih} is the tensor of deformational potential. The third term describes the well-known Stuart-Tolman effect due to acceleration of the lattice, m_0 being the mass of the free electron.

To obtain the spectrum of the excitations in the superconducting state one should insert the Hamiltonian (108) in the Bogoliubov-De Gennes equation which gives

$$\tilde{\varepsilon}(p,r) = \sqrt{\left[E_0(p) + \lambda_{ik}u_{ik} + \phi - \mu\right]^2 + \Delta^2} + p_s v - m_0 v\dot{u}. \tag{110}$$

One can see that the deformational perturbation contributes both to the potential ϕ as the term $\lambda_{ik}u_{ik}$ and to the term $p_s v$ as the item $-m_0 v\dot{u}$. Note that the term $\lambda_{it}\,(p)u_{ik}$, depending on the electron quasimomentum p, is different for different electrons. The potential ϕ should satisfy the neutrality condition. For instance, for the case of stationary deformation this condition has the form

$$u_{ik}\overline{\lambda_{ik}(p)} + \phi = 0. \tag{111}$$

(Here the bar denotes the average over the Fermi surface.)
To obtain the expression for the acoustic power density $\mathscr{P}$ absorbed per second in a unit volume of a superconductor one should differentiate the expression for the entropy density over time, then use the Boltzmann equation, and finally average the expression over the period of the sound wave. In such a way we get the following expression for $\mathscr{P}$ (Gal'perin 1974):

$$\mathscr{P} = \left\langle \int (\mathrm{d}p)\dot{\tilde{\varepsilon}}(p,r)n_p \right\rangle, \tag{112}$$

where $\tilde{\varepsilon}(p,r)$ is given by eq. (110), angular brackets mean the time average over the period.

21.8.2 8.2. Nonlinear acoustic phenomena in superconductors

Acoustic absorption in superconductors was studied in a number of papers. It was shown that investigation of acoustical properties can give valuable information about the excitation spectrum and other properties of superconductors.

We shall concentrate ourselves on nonlinear acoustic phenomena. On the one hand, the problem of the linear response of a superconductor to acoustic perturbation is relatively simple and has been studied extensively. On the other hand, the problem of nonlinear acoustic phenomena is much more complicated and it is the transport equation approach that permits one to solve it and at the same time to get clear physical understanding at every step of its solution. This problem is interesting also from the experimental point of view, because nowadays it is possible to observe nonlinear effects in normal metals. (For the theory of nonlinear acoustic phenomena in normal metals see the review article by Gal'perin et al. 1979, where some experimental data are also discussed.)

Therefore, one can hope that experimental observation of the effects of the same nature in superconductors is also possible.

Of a number of possible nonlinear acoustic effects we shall discuss only two here: nonlinear absorption and the acousto-electric effect. In the linear theory the absorption coefficient Γ is independent of sound intensity S. We determine the nonlinear absorption as the physical situation where the coefficient Γ depends on S and it is this dependence that we shall discuss below.

The absorption mechanism depends strongly on the relation between sound wavelength $2\pi/q$ and electron mean free path l. Nonlinear effects in absorption are much more pronounced provided $q\,|\gg 1$, and we shall confine ourselves to this case.

The second, acousto-electric, effect exists irrespective of the value of the quantity ql. This effect has no direct analogue in normal conductors. It amounts to the following. A travelling acoustic wave drags the quasiparticles, which produces a.d.c. normal current, $j^{(a)}$, which is known as the acoustoelectric current. In an isolated sample the normal current is offset by a

supercurrent $j^{(s)}$ which is proportional to $\nabla\chi$. The sum $j^{(a)}+j^{(s)}$ being zero one may conclude that a travelling acoustical wave creates a stationary phase difference in a superconductor. The phase difference can be measured in different ways discussed in several papers (Gal'perin et al. 1973a,b, 1974a,b, 1978).

Therefore, the purpose of the theory is to calculate the acousto-electric current $j^{(a)}$.

Let us describe the physics of nonlinear ultrasonic absorption at $ql \gg 1$. To understand this, we shall describe briefly the situation in normal conductors. Let us for simplicity consider interaction with longitudinal acoustic waves. In this case electrons interact with the sound wave only via the deformational potential. Consequently, the sound wave is accompanied by a wave of the electric field acting on the electrons which propagates with the sound velocity w. Such a wave of the effective field materially affects only those electrons whose velocities in the direction of sound propagation, ι_1, are close to the sound velocity, w, because the mean field acting on the rest of the electrons is small. Therefore the interaction of the electrons with the sound wave is determined by the properties of the distribution function in the "resonance" region of velocities and also by the width of this region. In the linear regime the characteristic width of the "resonance region" is of the order of $|v_x - w| \simeq v_{\mathrm{F}}(ql)^{-1}$ and the characteristic interaction time is of the order of τ, τ being the mean free time of the resonance electrons. Consequently, the linear absorption coefficient Γ_0 is independent of the mean free path l. Therefore, this mechanism is known as collisionless damping; it is analogous to the well-known Landau damping of plasma waves (see Landau 1946).

If the sound intensity is sufficiently high the structure of the resonance region is changed. Some of the resonance electrons become "captured" by the
sound wave: their motion in the coordinate system following the travelling wave is finite in the direction of the wave propagation, x. The captured electrons oscillate in the potential wells produced by the acoustic wave. The frequency of the oscillations is of the order

$$\omega_0 \simeq q\tilde{v} = q\sqrt{U_0/m} \tag{113}$$

where $U_0 = \left(\hat{\lambda}_{ik} - \bar{\lambda}_{ik}\right) u_{ik}^{(0)}, \tilde{v} = \sqrt{U_0/m}$ is the characteristic velocity of the oscillatory motion, while $u_{ik}^{(0)}$ is the amplitude value of the tensor u_{ik}. Each scattering event changes the direction of the electron velocity and removes it from the captured group. Therefore, in order that such a group would perform oscillatory motion the inequality

$$\omega_0\tau \gg 1 \tag{114}$$

should be satisfied. This inequality means that the captured electrons perform many oscillations in the potential wells during the time between collisons, τ.

The formation of a group of captured electrons leads to distortion of the electron distribution in the resonance region of velocities, the width of which is of the order of $\tilde{v}$, and, consequently, to the appearance of nonlinear effects in sound absorption. The distribution function of the untrapped electrons is also changed by the sound wave. However, its variation is relatively large only in the resonance region, i.e. the width of the corresponding region of velocities is also of the order of i. In other words, the number of untrapped resonance electrons is of the order of the number of trapped electrons.

Note that the relative number of resonance electrons is small: it is of the order of $U_0/\mu \ll 1$. Nevertheless, the inequality (114) can be satisfied if the product ql is large enough. Indeed, we have

$$\omega_0\tau \simeq ql\sqrt{U_0/\mu}.$$

The parameter $\omega_0\tau$ can be large even if the actual value of the sound intensity is relatively small.

This physical picture is based implicitly on classical consideration. It is valid if (1) the number of quantum levels in each potential well is large or (2) if these levels are smeared by the collisions. It means that our picture is valid if

$$\frac{\hbar^2 q^2}{m} \ll U_0 \quad \text{or} \quad \frac{\hbar^2 q^2}{m} \ll \frac{\hbar}{\tau}. \tag{115}$$

In what follows we shall consider at least one of these conditions to be satisfied.

Now let us turn to our immediate purpose, i.e to a superconductor. Normal excitations in a superconductor behave essentially in the same manner as electrons in normal metals. So one can expect that a similar mechanism of nonlinearity in superconductors exists as a consequence of bunching of normal excitations discussed above.

This situation can be described quantitatively with the help of the transport equation, where one should use as the excitation energy the expression given in the previous section. There are two gauge-covariant potentials, ϕ and p , that enter this expression.

For longitudinal sound we are interested in they both should be determined from the neutrality condition. General results of such an analysis depend on the ratio ω/q in comparison to v_{F}, i.e. on the relative importance of the time and spatial dispersion (see, for instance, Aronov and Gurevich 1976). If the spatial dispersion is more important than the time dispersion, i.e. if $\omega/q < \iota_F$, one may discard the term $p_{\mathrm{s}}v$ from eq. (110). Then the neutrality condition gives

$$\phi = -\lambda_{ik} u_{ik}$$

This is why the quantity

$$\bar{\xi}_p = \xi_p + U = \check{\zeta}_p + \left[\lambda_{ik}(p) - \tilde{\lambda}_{ik}\right] u_{ik} \tag{116}$$

enters the expression

$$\dot{\varepsilon}_p = \sqrt{\xi_p^2 + \Delta^2}$$

for the excitation energy. In this case the effective potential U depends on the quasimomentum p (cf. eq. 5).

To calculate the ultrasonic absorption coefficient, one should obtain the nonequilibrium distribution function n_p by solving the transport equation. Let us divide the distribution function n_p into the sum of two parts $n_p = n^{(0)}\left(\hat{\varepsilon}_p\right) + n_p^{(1)}$, where the first part is averaged over a constant-energy surface. Let us assume that the function $n^{(0)}\left(\tilde{\varepsilon}_p\right)$ to be the equilibrium one (we shall discuss below when this is the case). Then, as can be established on the basis of eq. (15), no essential corrections to the gap are necessitated by the nonequilibrium character of the distribution function. The transport equation for this case has the form:

$$\left(v_x \frac{\tilde{\xi}_p}{\varepsilon_p} - w\right) \frac{\partial n_p^{(1)}}{\partial x} - \frac{\partial U}{\partial x} \frac{\tilde{\xi}_p}{\varepsilon_p} \frac{\partial n_p^{(1)}}{\partial p_x} + \frac{n_p^{(1)}}{\tau} \frac{|\tilde{\xi}|}{\varepsilon_p} = w \frac{\partial U}{\partial x} \frac{\tilde{\xi}_p}{\varepsilon_p} \frac{\partial n^{(0)}}{\partial \tilde{\varepsilon}_p}. \tag{117}$$

Here we use two approximations. First, we have considered $n_p^{(1)}$ to depend on x and t in the combination ($x - wt$) only. A sufficient criterion for this assumption is $\Gamma 1 \ll 1$, which usually holds. Secondly, we have discarded the "in" term of the collision operator. Such a procedure can be justified if one takes into account that the resonance group is small. This is why the probability for an electron to escape from this group is much larger than the probability for a nonresonant electron to join this group.

We shall analyse the eq. 117 with the help of the method of characteristics. One can see that equations to determine the quasiparticle trajectory have the energy integral.

$$\sqrt{\xi_p^2 + \Delta^2} - p_x w = \mathscr{E}. \tag{118}$$

Let us compare this equation with the corresponding one for the normal state, which can be written in the form

$$\tilde{\xi}_p - p_x w = E. \tag{119}$$

One can see that in the normal state the potential $U(x)$ leads to coordinate dependence of the x-component of the quasimomentum, p, i.e. to distortion of the shape of electron trajectory. In the presence of a sound wave it becomes curvilinear rather than a straight line. The absorption coefficient Γ is determined by "group velocity" $v_{gx} = \partial E/\partial p_x$, which in the normal state is $v_x - w$; this quantity should be calculated from eq. (119) and its characteristic value is, as we have already seen, of the order of $\tilde{v}$.

The corresponding group velocity in the superconducting state is equal to $v_x \xi_p/\varepsilon_p - w$. Thus, there are two sources of the influence of the potential U on the group velocity v_g. One of them is the distortion of the shape of electron trajectories (just as in the normal state). This mechanism, as we shall see later, is characterized by the same quantity $\omega_0\tau$ as in the normal state. Thus, the threshold value of U_0, describing the onset of the nonlinear effects, is of the order of $U_0^{(th)} \simeq m/(q\tau)^2$. The second source is specific for the superconducting state. One can see that the group velocity may change even if the trajectory remains a straight line. due to the change of the quantity Ξ_p. i.e. of the modulus of the quasimomentum p. Furthermore, it can even change its sign without a change of the sign of v_x. It is clear that this effect can lead to specific localization of a quasiparticle in the field of an acoustic wave. This effect is somewhat similar to the well-known Andreev reflection of quasiparticles by inhomogeneities of the order parameter.

The influence of such Andreev-like localization on the sound absorption was studied by Galako et al. (1981).

Our immediate purpose is to illustrate the application of the transport equation approach to acoustic phenomena rather than a detailed discussion of different mechanisms of nonlinear acoustic absorption. This is why we shall restrict ourselves to the first mechanism, which is the simplest. To understand the region of parameters where this mechanism is dominant let us analyse the energy integral (118).

Note that if one may neglect the second term in eq. (118) it leads to the equality $\widetilde{\xi}_p = \xi =$ const. In this case

$$v_x = p_x/m = (2U_0/m)^{1/2} \sqrt{A - \left[\overline{U(x)}/U_0\right]}, \tag{120}$$

where we have introduced the notation

$$\mu - \frac{p_\perp^2}{2m} + \xi \equiv U_0 A$$

(we shall see that the characteristic value of A is of the order of unity).
To estimate the corrections due to the finite value of the term $p_x w$ in comparison with $\sqrt{\xi_p^2 + \Delta^2}$ let us expand the last term in powers of the quantity $\delta\xi_p = \tilde{\xi}_p - \tilde{\zeta}$ up to first order:

$$(\xi\varepsilon)\delta_p \pm \left(2mU_0 w^2\right)^{12} \sqrt{A - \frac{U(x)}{U_0} + \frac{\delta\xi_p}{U_0}} = 0.$$

Here $\varepsilon = \sqrt{\xi^2 + A^2}$. It can be seen from this equation that one can neglect the quantity $\delta\xi_p$ in the second term if

$$\left(2mw^2/U_0\right)^{1/2} \ll \zeta\check{\zeta}/\varepsilon. \tag{121}$$

If this condition is satisfied one can still use eq. (120) for $v_x(x)$, and we have

$$\delta\check{\zeta}_p = \frac{\varepsilon}{\xi} mwv_x(x). \tag{122}$$

To estimate the role of this correction to ξ one should compare the quantity $\delta_{\zeta_p}\mu(\ \mathrm{d}\ \mathrm{d}\ \xi_{\xi'})(\xi')$ to the velocity $r_{\gamma'}$. Indeed, dividing the transport equation eq. (117) by $\hat{=} i_p$ we obtain an equation similar to that for the normal case. The only difference is that the quantity $w\%_p, \tilde{\zeta}_p$ rather than w enters this equation. The first source of nonlinearity is the change of v_x along the trajectory, the second source is the change of $1\omega_p\tilde{\Xi}_p$ due to the change of $\tilde{\Xi}_p$. Using eq. (122) for $\delta\xi_p$ and comparing the term $\delta\xi_p\ \mathrm{w}(\mathrm{d}\ \mathrm{d}\ \xi\ )\ (\ \delta\ )$ with l', we get the following criterion for the range of applicability of the theory we shall discuss below

$$\frac{mw^2}{T}\min\left(\frac{\Delta}{T}, \frac{\Delta^2}{T^2}\right) \ll 1 \tag{123}$$

[here we have taken into account that $\xi \simeq \max(\sqrt{\Delta T}, T)$]. Combining eq. (121) with the expression for the threshold amplitude $U_0^{(\mathrm{th})}$ we get the second criterion of applicability of our theory:

$$\left(U_0/U_0^{(th)}\right)^{1/2} > \max(1, \omega\tau\varepsilon/\xi). \tag{124}$$

Let us now discuss when it is justified to consider the function $n^{(0)}(\varepsilon)$ as the equilibrium one. There are two kinds of corrections to the function $n^{(0)}\varepsilon$: stationary corrections and corrections with the period of the sound wave. One can verify that only corrections of the first kind may be important. The corresponding upper limit can be obtained by comparison of the energy transfer to a quasiparticle during the energy relaxation time $\tau_{\mathrm{ph}} \simeq \hbar^3\omega_{\mathrm{D}}^2/T^3$ with the characteristic energy scale, $\min(T, T_c - T)$. The resulting estimate has
the form

$$S \ll \frac{NT}{\Gamma\mu\tau_{\mathrm{ph}}}\min\left(T_{\mathrm{c}} - T, T_{\mathrm{c}}\right). \tag{125}$$

This condition is met for most of the interesting cases.
The problem is somewhat more complicated for the case of transverse sound which is not discussed here in detail. For this situation the changes in $n^{(0)}(\varepsilon)$ by intensive acoustic wave were studied by Bulyzhenkov and Ivlev (1976a,b)*. These changes may be of the same nature as in the case of superconductivity stimulation; they are discussed by Eliashberg and Ivlev (1985).

Now let us turn to the calculation of the nonlinear sound absorption coefficient for the case $(\omega_0\tau \gg> 1$. It can be shown (see Gal'perin et al. 1973a) that the absorption coefficient Γ, can be expressed in terms of the nonequilibrium distribution function:

$$\Gamma_{\mathrm{s}} = \left(\rho\omega^2u^2\right)^{-1}\int(\ \mathrm{d}p)\left\langle\frac{\xi_p}{\varepsilon_p}n_p\frac{\partial U}{\partial x}\right\rangle_\eta \tag{126}$$

where $\langle\cdots\rangle_\eta$ denotes averaging over the wave coordinate $\eta = qx - wt$, and ρ is the crystal density.**

To obtain the nonequilibrium part $n_p^{(1)}$ of the distribution function one may rewrite eq. (117) in terms of the dimensionless quantities

$$\eta, \quad \tilde{v}_x \equiv v_x/\left(U_0/m\right)^{1/2}, \quad \tilde{U} \equiv U(x)/U_0$$
$$\tilde{v}_x \frac{\hat{i}n_p^{(1)}}{\partial \eta} - \frac{\mathrm{d}\tilde{U}}{\mathrm{d}\eta}\frac{\hat{i}n_p^{(1)}}{\partial \tilde{v}_\mathrm{x}} + \frac{\operatorname{sign}\xi_p}{u_0\tau}u_p^{(1)} = \tilde{U}\frac{w'}{\sqrt{U_0/m}}\frac{\hat{i}n^{(0)}(\varepsilon)}{\partial\varepsilon}. \tag{127}$$

To solve this equation one should formulate the appropriate boundary conditions. The distribution function of the untrapped quasiparticle should satisfy the periodicity condition in the wave coordinate η while the distribution function of the trapped quasiparticles should satisfy the condition of specular reflection from the walls of the potential wells produced by the sound wave. The general solution was obtained by Gal'perin et al. (1972), and has a rather complicated form. However, in the case of strong nonlinearity ($\omega_0\tau \gg 1$ it can be expanded in powers of the small parameter $1/\omega_0\tau$, and the main contribution to the absorption coefficient appears to be of the first order in $1/\omega_0\tau$. One can

obtain the following result

$$\frac{\Gamma_\mathrm{S}}{\Gamma_{\mathrm{S}0}} = 1.1\overline{\left[\frac{\Lambda_{xx}^2}{q\tau\left(U_0/m\right)^{1/2}}\frac{2}{\mathrm{e}^{d/T}+1}\right]\cdot\left[\frac{2\Lambda_{xx}^2}{\mathrm{e}^{d/T}+1}\right]^{-1}}, \tag{128}$$

where $\Gamma_{\mathrm{S}0}$ is the linear absorption coefficient in the superconductor, and $\Lambda_{xx} = \lambda_{xx} - \bar{\lambda}_{xx}$.

21.8.3 8.3. Acousto-electric current and field

For the calculation of the d.c. current generated by a traveling acoustic wave it is natural to seek the solution of the Boltzmann equation (6) in the form

$$n_p = n^{(0)}\left(\varepsilon_p + pv_s\right) + n_p^{(1)} \tag{129}$$

Using the general expression for the current density (see eq. 40) one can obtain, in linear approximation in the small parameter pv_s/Δ,

$$j = j^{(a)} + eN_\mathrm{s}v_\mathrm{s},$$

where

$$j^{(a)} = \frac{e}{2}\int(\,\mathrm{d}p)_p v\left\langle\left(n_p^{(1)} - n_{-p}^{(1)}\right)\right\rangle_\eta \tag{130}$$

is the current of the dragged normal excitations. To calculate this current, one may neglect the motion of the condensate.

We shall calculate $j^{(a)}$ without solving eq. (6), using the method developed for this purpose by Kagan (1967). Let us multiply eq. (6) by the electron velocity v and integrate it over the surface of constant energy $\varepsilon_p = \varepsilon$ and over the wave period. By definition, for elastic collisions

$$\int(\mathrm{d}p)vIn_p^{(1)}\dot{\delta}\left(\varepsilon-\varepsilon_p\right) = \frac{\left|\breve{\zeta}_p\right|}{\varepsilon_p}\int(\,\mathrm{d}p)I^{(\mathrm{n})}vn_p^{(1)}\delta\left(\varepsilon-\varepsilon_p\right).$$

[0]*It can be shown that the nonlinear effects due to changes in $n^{(0)}$ discussed by Bulyzhenkov and Ivlev are suppressed if the nonlinearity discussed above in detail is well pronounced.

**This expression is valid if one can neglect the nonlinear distortion of the acoustic wave itself so that the wave can be represented by single harmonic. This assumption may be justified if $U_0 \ll \mu$ (see Gal'perin and Kozub 1977).

The only other term of eq. (6) that does not vanish with the accepted accuracy after averaging over the period of the wave is

$$-\int (\mathrm{d}p) v \left\langle \frac{\partial U}{\partial \boldsymbol{r}} \frac{\xi_p}{\varepsilon_p} \frac{\partial n_p^{(1)}}{\partial \boldsymbol{p}} \right\rangle_\eta \delta\left(\varepsilon - \varepsilon_p\right)$$

As a result, we get for $j^{(a)}$ in the time-of-relaxation approximation

$$\begin{aligned} j^{(\mathrm{a})} &= e \int_\Lambda^\infty \mathrm{d}\varepsilon \tau_{\mathrm{tr}} \frac{\varepsilon}{|\xi|} \int (\mathrm{d}p) v \frac{\xi_p}{e_p} \left\langle \frac{\partial U}{\partial r} \frac{\partial n_p^{(1)}}{\partial p} \right\rangle_\eta \delta\left(\varepsilon - \varepsilon_p\right) \\ &= -e \int (\ \mathrm{d}p) \tau_{\mathrm{tr}}(\varepsilon) m^{-1} \left\langle n_p^{(1)} \frac{\partial U}{\partial r} \right\rangle_\eta \operatorname{sign} \xi_p. \end{aligned} \tag{131}$$

Inasmuch as the electrons contributing to the last integral are mainly close to the Fermi surface while the scale of variation of $\tau_{\mathrm{im}}^{(\mathrm{n})}$ is μ, one can take the relaxation time outside the integral. As a result, we get the following relation connecting the acousto-electric current $j^{(a)}$, the absorption coefficient Γ, the sound intensity S and the electron mobility in the normal state, μ_n

$$j^{(a)} = \frac{\mu_{\mathrm{n}} \Gamma_{\mathrm{n}} S}{w} \frac{N_0 - N_{\mathrm{s}}}{N_0} = \mu_{\mathrm{n}} \frac{\Gamma_{\mathrm{s}} S}{w} \mathscr{F}\left(\frac{\Delta}{T}\right), \tag{132}$$

where

$$\begin{aligned} \mathscr{F}\left(\frac{\Delta}{T}\right) &= \left(\int_\Delta^\infty \frac{\varepsilon}{\sqrt{\varepsilon^2 - \Delta^2}} \frac{\partial n^{(0)}}{\partial \varepsilon} \mathrm{d}\varepsilon\right) / \left(\int_\Delta^\infty \mathrm{d}\varepsilon \frac{\partial n^{(0)}}{\partial \varepsilon}\right) \\ &= \frac{1}{4}\left(\mathrm{e}^{\Delta/T} + 1\right) \int_0^\infty \mathrm{d}x \frac{x + (\Delta/T)}{\sqrt{x(x + 2\Delta/T)}} \cosh^{-2}\left(\frac{x}{2} + \frac{\Delta}{2T}\right) \end{aligned} \tag{133}$$

The relation (132) is the generalization of the well-known Weinreich relation (see Weinreich 1957) for superconductors.

Thus, we have calculated the normal acousto-electric current. Inasmuch as the total current in the bulk of a superconductor should vanish we have the following expression for p_{s} :

$$\frac{1}{2}\hbar \nabla \chi = p_{\mathrm{s}} = -\frac{1}{w N_{\mathrm{s}}} \tau \mathscr{F}(\Lambda/T) \Gamma_{\mathrm{s}} S \tag{134}$$

Integrating this equation along the length of the sample and taking into account the law of acoustic intensity spatial variation because of the absorption,

$$\mathrm{d}S\ \mathrm{d}x = -\Gamma S$$

we obtain the following relation for the phase difference across a sample of length L

$$|\delta\chi| = \frac{2\tau \mathscr{F}(\Delta/T)}{\hbar w N_s} \left(S|_{x=0} - S|_{x=L}\right). \tag{135}$$

We think that the simplest experimental arrangement to observe this phase difference is a monometallic superconducting loop, the travelling acoustic wave propagating along a part of the loop. The measured quantity may be the magnetic flux through the loop which equals

$$\phi_{\mathrm{m}} = \phi_0(n + \delta\chi/2\pi), \tag{136}$$

where n is an integer while $\phi_0 = \pi\hbar c/e$ is the magnetic flux quantum.
Now let us turn to the acousto-electric field in superconductors (Aronov 1976) we have mentioned briefly in section 6 . As we have seen from eq. (92), if the normal current is spatially inhomogeneous the potential ϕ becomes inhomogeneous too. Indeed, the rhs of eq. (92) can be written as $-(1/e)\,\mathrm{div}\, j^{(n)}$,
and in the stationary case the quantity $\nabla^2\phi$ is nonvanishing. This means that the presence of an inhomogeneous normal current leads to an electric field $E = -(1/e)\nabla\phi$. One of the sources of such a field can be a travelling acoustic wave which drags quasiparticles of a superconductor. As a result, the d.c. acousto-electric normal current we have discussed above appears. Because of sound attenuation this current is coordinate-dependent. Thus, to obtain the acousto-electric field one should add $-(1/e)\,\mathrm{div}\, j^{(n)}$ to the rhs of eq. (92).

Another important thing is that the acousto-electric field leads to a contribution $\sigma_{ik}^{(\mathrm{n})} E_k$ to the electric current, so the total current density near T_c is equal to

$$j_i = eN_\mathrm{s} v_{\mathrm{s}i} + j_i^{(\mathrm{a})} + \sigma_{ik}^{(\mathrm{n})} E_k. \tag{137}$$

In a stationary state this current must vanish. As a result, the superflow velocity becomes coordinate dependent, and the equality $eN_\mathrm{s} v_{\mathrm{s}i} + j_i^{(a)} = 0$ we have employed above is valid only at distances from the sample boundaries much larger than L_b. One should take this fact into account when analysing the conditions for the observation of acousto-electric effects. Making use of eq. (132) for $j^{(a)}$ and taking into account that $\partial S/\partial x = -\Gamma_\mathrm{s} S$ we have at $T_\mathrm{c} - T \ll T_\mathrm{c}$

$$\left(-\frac{\partial^2}{\partial x^2} + L_\mathrm{b}^{-2}\right)\phi = \frac{l}{wN}\Gamma_\mathrm{s}\frac{\partial S(x)}{\partial x}. \tag{138}$$

This equation as well as eq. (92) is valid in the vicinity of T_c.
Usually the attenuation length Γ_s^{-1} is much larger than L_b. In such a case one obtains from eq. (138) the following expression for the acousto-electric field $E^{(\mathrm{a})}$

$$E_\mathrm{x}^{(\mathrm{a})} = -\frac{1}{e}\frac{\partial\phi}{\partial x} = -\frac{1}{wNe}\Gamma_\mathrm{s} S_0 \left(\Gamma_\mathrm{s} L_\mathrm{b}\right)^2 \mathrm{e}^{\Gamma_\mathrm{s}\mathrm{x}}. \tag{139}$$

Thus, an acoustic wave produces the acousto-electric field $E^{(\mathrm{a})}$ in the bulk of a superconductor.

21.9 9. Derivation of the transport equations for slowly varying external fields

In this section we shall demonstrate the derivation of a basic set of equations describing transport in superconductors. It is convenient to use for this purpose the Keldysh diagram technique (Keldysh 1964). In the course of the derivation we shall follow papers by Gal'perin et al. (1973a) and Aronov and Gurevich (1974).

Let us start from the Dyson equation for the electron Green function. To account for the specific features of the superconducting state one should
introduce, besides the normal matrix Green function

$$\hat{G}^{\alpha\beta} = \begin{pmatrix} G_\mathrm{c} & G_+ \\ G_- & \widetilde{G}_\mathrm{c} \end{pmatrix} = \begin{pmatrix} -\mathrm{i}\left\langle\, \mathrm{T}\psi_\alpha(x)\psi_\beta^+(x')\right\rangle & \mathrm{i}\left\langle\psi_\beta^+(x')\,\psi_\alpha(x)\right\rangle \\ -\mathrm{i}\left\langle\psi_\alpha(x)\psi_\beta^+(x')\right\rangle & -\mathrm{i}\left\langle\, \mathrm{T}\psi_\alpha(x)\psi_\beta^+(x')\right\rangle \end{pmatrix}, \tag{140}$$

also the anomalous matrix Green function

$$\hat{F}^{\alpha\beta} = \begin{pmatrix} \langle \mathrm{T}\psi_\alpha(x)\psi_\beta(x')\rangle & -\langle\psi_\beta(x')\,\psi_\alpha(x)\rangle \\ \langle\psi_\alpha(x)\psi_\beta(x')\rangle & \left\langle \widetilde{\mathrm{T}}\psi_\alpha(x)\psi_\beta(x')\right\rangle \end{pmatrix}. \tag{141}$$

In the same way one should also introduce the matrix ${}^{+}F^{x\beta}$, which differs from (141) by replacement of ψ by ψ^{+}. Here α and β are the spin indices, $\psi^{+}$and ψ are the electron creation and annihilation operators, x denotes the combination (r,t), and T and $\tilde{\mathrm{T}}$ are the time-ordering and antitime-ordering symbols. In this section the angular brackets represent the average over the equilibrium ensemble, external fields being included in the unperturbed Hamiltonian. The interaction is considered to be spin-independent. Therefore

$$\begin{aligned} &\hat{G}^{\alpha\beta} = \delta_{\alpha\beta}\hat{G}, \qquad {}^{+}\hat{\mathrm{F}}^{\alpha\beta} = \hat{\mathrm{I}}_{\alpha\beta}{}^{+}\mathbf{F}, \\ &\hat{F}^{\alpha\beta} = -\hat{I}_{\alpha\beta}\hat{F}, \quad \hat{I}_{\alpha\beta} \equiv \begin{pmatrix} 0 & 1 \\ -1 & 0 \end{pmatrix}. \end{aligned} \tag{142}$$

The Dyson equations for $\hat{G}$ and ${}^{+}\hat{F}$ have the form

$$\begin{aligned} \hat{\sigma}_z G_0^{-1}(x_1)\,\hat{G}(x_1x_2) =& \hat{1}\delta(x_1-x_2) + \mathrm{i}\int \mathrm{d}^4x_3\hat{\Sigma}(x_1x_3)\,\hat{G}(x_3x_2) \\ &+ \mathrm{i}\int \mathrm{d}^4x_3\hat{\Delta}'(x_1x_3)^{+}\,\hat{F}(x_3x_2) \end{aligned} \tag{143}$$

$$\begin{aligned} \hat{\sigma}_z G_0^{*-1+\hat{F}(x_1,x_2)=} &\mathrm{i}\int \mathrm{d}^{+}x_3\hat{\Sigma}^{\mathrm{T}}(x_3x_1)^{+}\,\hat{F}(x_3x_2) \\ &+ \mathrm{i}\int \mathrm{d}^4x_3{}^{+}\hat{\Delta}'(x_1x_3)\,\hat{G}(x_3x_2). \end{aligned} \tag{144}$$

We omit the analogous equation for $\widehat{F}(x_1x_2)$. Here

$$G_0^{-1}(x_1) = \mathrm{i}\hbar\frac{\partial}{\partial t_1} - \left(\frac{1}{2m}\right)\left[\hat{p}_1 - \frac{e}{c}A(x_1)\right]^2 - e\varphi(x_1) + \mu \tag{145}$$

$\hat{p}_1 = -i\hbar\hat{c}/\partial r_1$ being the canonical momentum operator. The self-energy parts $\hat{\Sigma}$ and $\hat{A}'$ are 2×2 matrices in the Keldysh technique. The matrix $\hat{\Sigma}$ is defined according to the rules of the usual Feynman technique in terms of $\hat{G}$ and the phonon Green function matrix $\hat{D}$, which is defined in the same way as eqs. (140). The electron phonon vertex is represented by the matrix $\Gamma^h_{\prime\prime\prime}(x,x',y)$ with phonon index k and electron indices j,j'; the simple vertex has the matrix structure $\delta_{jj}(\hat{\sigma}_z)_{jj'k}$. Here

$$\hat{\sigma}_z = \begin{pmatrix} 1 & 0 \\ 0 & -1 \end{pmatrix}$$

is the operator which acts on the corresponding matrix indices; we call them the Keldysh indices (not to be confused with the spin indices). The self-energy matrix $\hat{\Delta}'$ differs from $\hat{\Sigma}$ by the replacement of $\hat{G}$ by $\hat{F}$.

We consider the case of slowly varying (in time and space) external fields. To employ this condition it is natural to seek the solutions of Dyson equations (143) and (144) in the form

$$\hat{G}(x_1x_2) = \hat{\mathscr{G}}\exp\left[\frac{1}{2}\mathrm{i}\chi(\mathrm{x}_1) - \frac{1}{2}\mathrm{i}\chi(\mathrm{x}_2)\right] \tag{146}$$

$$+{}^{+}F(x_1x_2) = {}^{+}\mathscr{F}(x_1x_2)\exp\left[-\frac{1}{2}\mathrm{i}\chi(x_1) - \frac{1}{2}\mathrm{i}\chi(x_2)\right] \tag{147}$$

$${}^{+}\hat{\Delta}'(x_1x_2) = {}^{+}\Delta(x_1x_2)\exp\left[-\frac{1}{2}\mathrm{i}\chi(x_1) - \frac{1}{2}\mathrm{i}\chi(x_2)\right] \tag{148}$$

The functions $\hat{\mathscr{G}}$ and $\hat{\mathscr{F}}$ are slowly varying functions of the central coordinate $x = (x_1+x_2)\,2$ and rapidly varying functions of the difference coordinate $X = x_1 - x_2$, where X represents the

set of spatial coordinates ρ and time τ. In accordance with the semiclassical approximation, we neglect the higher-order derivatives of the phase $\chi(x)$.

Performing transformation to the Fourier components in terms of the difference variable X we get from eqs. (143) and (144) the following equation for $\hat{g}(p,x)$:

$$\hat{\sigma}_z\left[\mathscr{G}_0^{-1}\left(p+p_s,\varepsilon-\phi\right)+\frac{1}{2}\mathrm{i}\hbar B\left(p+p_s\right)\right]\hat{\mathscr{G}}(p,x)$$
$$=\hat{1}+\mathrm{i}\hat{\Sigma}(p)\hat{\mathscr{G}}(p,x)+\mathrm{i}\hat{\Delta}(p)^{+}\mathscr{F}(p,x)-\frac{1}{2}\{\hat{\Sigma},\hat{\mathscr{G}}\}-\frac{1}{2}\left\{\hat{\Delta},{}^{+}\hat{\mathscr{F}}\right\} \tag{149}$$

Here

$$\{A,B\}=\frac{\hat{i}A\hat{i}B}{\hat{i}x\hat{i}p}-\frac{\hat{i}A\hat{i}B}{\hat{i}p},$$

p denotes the set of variables p and ε,

$$g_0^{-1}(\boldsymbol{p},\varepsilon)=\varepsilon-\mu-\boldsymbol{p}^2/2m \tag{150}$$

and

$$B\left(p+p_s,x\right)=\frac{\partial}{\partial t}-\frac{\partial\phi}{\partial r}\frac{\partial}{\partial p}+\frac{p+p_s}{m}\frac{\partial}{\partial r}-\frac{\partial}{\partial r}\frac{\left(p+p_s\right)^2}{2m}\frac{\partial}{\partial p}. \tag{151}$$

The corresponding equation for ${}^{+}\mathscr{F}(p,x)$ differs from eq. (149) by the replacement $\mathscr{G}\to{}^{+}\mathscr{F}, p_{\mathrm{s}}\to-p_{\mathrm{s}}, \varepsilon\to-\varepsilon, {}^{+}\hat{\Delta}\to\hat{\Delta}, \hat{\Sigma}(p)\to\hat{\Sigma}^{\mathrm{T}}(-p)$. Note that these equations are gauge-covariant because external fields enter them through the gauge-covariant combinations p_{s} and ϕ only.

In the course of derivation of eq. (149) and the corresponding equation for ${}^{+}\mathscr{F}$ we have used inequalities (1) and (2).

To find the functions $\mathscr{G}_{\mathrm{c}}$ and $\mathscr{F}_{\mathrm{c}}$, i.e. the " 11 " components of the matrices $\mathscr{G}$ and $\mathscr{F}$, it is sufficient to retain in the corresponding equations only those terms which do not themselves contain derivatives with respect to x, and we can discard the terms of the type $\Sigma_{+}\mathscr{G}_{-}$which are proportional to the small parameter $1/4\tau$. Assuming that the electron energy spectrum of the normal metal has already been renormalized by the normal self-energy part Σ_c, we have

$$\mathscr{G}_c(p,x)=u_p^2A(p)-v_p^2A(-p) \tag{152}$$
$$+\mathscr{F}_c(p,x)=-iu_pv_p[A(p)+A(-p)] \tag{153}$$

where

$$A(p)=\frac{n_p}{\varepsilon-\tilde{\varepsilon}_p-\mathrm{i}\delta}+\frac{1-n_p}{\varepsilon-\tilde{\varepsilon}_p+\mathrm{i}\delta}$$

and n_p is a function of the quasimomentum p. We shall see that it has the physical meaning of the quasiparticle distribution function.

The order parameter Δ is represented by the " 11 " matrix element of the anomalous self-energy matrix. One can find the following equation for the element

$${}^{+}\Delta(\varepsilon,p,x)=\int(\mathrm{d}p)_{p'}\int\frac{\mathrm{d}\varepsilon'}{2\pi}\left|c_q\right|^2D_c\left(p'-p,-\varepsilon'\right)+\mathscr{F}_c\left(\varepsilon-\varepsilon',p',x\right) \tag{154}$$

where D_c is the phonon causal Green function (in order to obtain this equation one should set the electron-phonon vertex equal to the simple vertex $\Gamma^k_{0jj'}=c_q\delta_{p'-p-hq}\left(\hat{\sigma}_z\right)_{j'k}$. One can

see that ${}^{+}\Delta_c(\varepsilon, p_{\mathrm{F}})$ has dispersion, i.e. is essentially dependent on ε at ε of the order of $\hbar\omega_{\mathrm{D}}$. For the usual transport phenomena the energies of the order of T or 1 are important, which are much smaller than the Debye energy $\hbar(\omega_1)$. Taking this into account we may assume that $\Lambda(\varepsilon, p, x)$ is independent of the energy in the energy interval we are interested in. Thus, we can assume ${}^{+}\Delta_c(\varepsilon, p) \equiv \Delta$ Making use of eqs. (152) and (153) and the criteria (1) and (2), as well as of the spectral representation

$$\mathscr{G}_{\mathrm{c}} = \int^{x} \frac{\mathrm{d}\varepsilon'}{2\pi\mathrm{i}} \left[\frac{\mathscr{G}_{+}}{\varepsilon - \varepsilon' - \mathrm{i}\delta} - \frac{\mathscr{G}_{-}}{\delta - \varepsilon' + \mathrm{i}\delta} \right] \tag{155}$$

and the analogous expression for ${}^{+}\overline{\mathscr{F}}$, we get the following expressions for "!, and $\mathscr{F}_{+}$

$$\mathscr{G}_{+} = 2\pi\mathrm{i}\left[u_p^2 n_p \delta(\varepsilon - \tilde{\varepsilon}_p) + v_p^2(1 - n_{-p})\,\delta(\tilde{\varepsilon}_{-p} + \varepsilon)\right], \tag{156}$$

$$+\mathscr{F}_{+} = \mathscr{F}_{+} = -2\pi u_p v_p \left[(1 - n_{-p})\,\delta(\varepsilon + \tilde{\varepsilon}_{-p}) - n_p \delta(\varepsilon - \tilde{\varepsilon}_p)\right]. \tag{157}$$

The expression for $\mathscr{G}_{?}$ differs from eq. (156) by the replacement $n_{+.p} \leftrightarrows -n_{\pm p} + 1$ and by the sign; $\mathscr{F}_{-}(p, x) =^{+} \mathscr{F}_{+}(-p, x)$.

$$n_p(x) = \int_0^{\infty} \frac{\mathrm{d}\varepsilon}{2\pi\mathrm{i}} \left[\mathscr{G}_{+}(\varepsilon, p) - \mathscr{G}_{-}(\varepsilon, -p)\right]. \tag{158}$$

The Green functions $\mathscr{G}_{+}$and $\mathscr{G}_{-}$being imaginary, one can find the equation for $n_p(x)$ by adding the Dyson equations for $\mathscr{G}_{+}$an $\mathscr{G}_{-}$to the corresponding Hermitian-conjugate equations. Besides, one can neglect in the rhs of eq. (149) and of the corresponding equation for $\mathscr{G}_{-}$:
(1) the terms containing the space and time derivatives of the normal Green function $\mathscr{G}$, as well as of the normal selfenergies Σ,
(2) the terms proportional to the derivatives of $\Delta_{\pm}$and ${}^{+}\Delta_{+}$(these are proportional to the small parameter d/l).

The terms proportional to $\partial\Delta/\partial p$ can be also discarded. Thus, the only term with derivatives that should be taken into account on the rhs of the Dyson equation for $\mathscr{G}_{+}$ is

$$\frac{\hbar\hat{c}A_c\hat{c} + \mathscr{F}}{\partial p}.$$

As a result, the Dyson equation for $\mathscr{G}_{+}$ acquires the following form

$$\left[\mathscr{G}_0^{-1}(p + p_{\mathrm{s}}, \varepsilon - \phi) + \frac{\mathrm{i}\hbar B(p + p_{\mathrm{s}})}{2}\right]\mathscr{G}_{+}(p, x) + \frac{\hbar}{2}\frac{\partial\Delta_{\mathrm{c}}}{\partial r}\frac{\partial + \mathscr{F}_{+}}{\partial p}$$
$$= \mathrm{i}\left(\sum_{\mathrm{c}} \mathscr{G}_{+} + \sum_{+} \hat{\mathscr{G}}_{\mathrm{c}} + \Delta_{\mathrm{c}} + \mathscr{F}_{+} + \Delta_{+} + \mathscr{F}_{\mathrm{c}}\right). \tag{159}$$

Taking into account the identities

$$\hat{\mathscr{H}}^{+} = \hat{\sigma}_1\hat{\mathscr{H}}_1, \quad \hat{j}^{+} = -\hat{\sigma}_1{}^{+}\hat{A}_0\hat{\sigma}_1 \quad \hat{\sigma}_1 = \begin{pmatrix} 0 & 1 \\ 1 & 0 \end{pmatrix}.$$

one can show that the Hermitian-conjugate equation for " 4 , differs from cq. (159) by the replacement $\mathscr{G}_0^{-1} \to -\mathscr{G}_0^{-1}$ in the lhs and $\Sigma \rightleftarrows \mathscr{G}, \Delta \rightleftarrows \mathscr{F}$ in the rhs. Combining this equation with eq. (159) and taking into account the Keldysh identity (Keldysh 1964)

$$\Sigma_{\mathrm{c}} + \widetilde{\Sigma}_{\mathrm{c}} + \Sigma_{+} + \Sigma = 0$$

and the analogous identity for $\triangle$ one can find

$$\hbar B\,(p+p_{\rm s})\,\mathscr{G}_{+}+{\rm i}\hbar\frac{\partial\Delta_{\rm c}}{\partial r}\frac{\partial^{+}\mathscr{F}^{+}}{\partial p}=\Sigma_{+}\mathscr{G}_{-}-\Sigma_{-}\mathscr{G}_{+}+\Delta_{\rm c}^{+}\mathscr{F}_{+}+{}^{+}\tilde{\Delta}_{\rm c}\mathscr{F}_{+}+\Delta_{+}{}^{+}\mathscr{F}_{\rm c}+{}^{+}\Delta_{+}\mathscr{F}_{\rm c}. \tag{160}$$

Similarly, we have for $\mathscr{G}_{-}$

$$-\hbar B\,(p+p_{\rm s})\,\mathscr{G}_{-}+{\rm i}\hbar\frac{\partial\Delta_{\rm c}}{\partial r}\frac{\partial^{+}\mathscr{F}}{\partial p}=\Sigma_{-}\mathscr{G}_{+}-\Sigma_{+}\mathscr{G}_{-}+\tilde{\Delta}_{\rm c}{}^{+}\mathscr{F}_{-}+{}^{+}\Delta_{\rm c}\mathscr{F}_{-}+\Delta_{-}{}^{+}\mathscr{F}_{\rm c}+{}^{+}\Delta_{-}\mathscr{F}_{\rm c}. \tag{161}$$

Replacing p by $-p$ in eq. (161) and taking into account the identities

$$\Delta_{\rm c}+\tilde{\Delta}_{\rm c}+\Delta_{+}+\Delta_{-}=0,\quad \Delta_{+}(-p)=\Delta_{+}(p),\quad \mathscr{F}_{\pm}(p)=\mathscr{F}_{+}(-p) \tag{162}$$

and analogous identities for ${}^{+}\Delta$ and ${}^{+\mathscr{F}}$ (which can be derived from the Dyson equations and the definitions of $\mathscr{F}$ and Δ) we obtain as the sum of eqs. (160) and (161)

$$\begin{aligned}\hbar\Big[B\,(p+p_s)\,\mathscr{G}_{+}(p,x)-B\,(-p+p_v)\,\mathscr{G}_{(-p,x)}+2{\rm i}\frac{\partial\Delta_c}{\partial r}\frac{\partial^{+}\mathscr{F}_{+}}{\partial p}\Big]\\ =\left(\Sigma_{+}\mathscr{G}_{-}-\Sigma_{-}\mathscr{G}_{+}\right)_{p}+\left(\Sigma_{-}\mathscr{G}_{+}-\Sigma_{+}\mathscr{G}\right)_{-p}\\ +\left(\Delta_{+}{}^{+}\mathscr{F}_{-}-\Delta_{-}{}^{+}\mathscr{F}_{+}+{}^{+}\Delta_{+}\mathscr{F}_{-}-{}^{+}\Delta_{-}\mathscr{F}_{+}\right)_{p}.\end{aligned} \tag{163}$$

Substituting the explicit expressions for the Green functions into eqs. (163) we find that the function of the momentum, n_p. obeys the Boltzmann equation (6) and thus has the physical meaning of the distribution function of the quasiparticles.

We have mentioned above that the criteria for the applicability of this theory turn out to be the most stringent near $T_{\rm c}$. These criteria appear in the course of analysis of the equations for the anomalous Green functions and the self-consistency condition (154). This condition was derived in the zeroth approximation in the function ${}^{+}\mathscr{F}_{\rm c}(p)$ [and ${}^{+}\overline{\mathscr{F}}_{\pm}(p)$]. Inserting eqs. (152) and (153) into eq. (154), we can transform the latter to the form of eq. (15).

To determine the range of its applicability let us make estimates of the discarded terms. For this purpose, one should write the equation for ${}^{+\mathscr{F}_{+}}(p)$ taking into account terms proportional to the time derivative and to the derivatives with respect to the central coordinates, as well as terms containing the collision operator. As a result, an additional term appears in the equation for the gap. This term is of the order of

$$\left(\bar{\Xi}_{p}\right)^{-1}(\hat{c}\Delta/\partial t),$$

where $\widetilde{\xi}_{p}$ is the characteristic value of $\widetilde{\xi}_{p}$ for the problem under consideration.

If, for instance, the state is shifted not too far from equilibrium we have $\widetilde{\zeta}_{p}\simeq T_{c}$.
The criterion of applicability of the equation for the gap is found by comparison of the terms of the type $\left(\hbar/\Delta\tilde{\xi}_{p}\right)(\partial\Delta/\partial t)$ with the lhs of the equation

$$1+(\lambda_{\rm e}/2)\int({\rm d}p)_{p}\frac{1-2n_{p}}{\varepsilon_{p}}=0$$

The latter is of the order of $\Delta^{2}/T_{\rm c}^{2}$ near equilibrium. Accordingly, for a state not far from equilibrium the neglect of the terms with time derivatives may be justified only if

$$\hbar\omega/\xi_{p}\simeq\hbar\omega/T_{\rm c}\ll\Delta^{2}/T_{\rm c}^{2}.$$

This condition was found by Gorkov and Eliashberg (1968, 1969).

21.10 10. Conclusion

We have discussed the transport-equation approach to the description of transport phenomena in superconductors and demonstrated its applications to various problems. One can see that this approach is by many aspects analogous to the classical transport approach successfully employed in normal conductors. Indeed, the transport equation is similar to the corresponding Boltzmann equation in the normal state and the expressions for the transport coefficients are similar as well (see sections 6, 7). So we have formulated a scheme for description of the response of a superconductor to slowly varying (in time and space) external perturbations which is very close to the classical one. Nevertheless, the full set of equations for a superconductor is rather complicated and one should not overestimate the similarity of the two schemes. Indeed, there is the Cooper pair condensate in a superconductor, which is a dynamical system interacting strongly with the normal excitations.

New degrees of freedom call for additional variables: as we have seen, the full set of equations contains extra variables and extra equations as compared to the normal conductors. The condensate motion, as well as the normal excitation distribution, influences the energy gap. Thus, the full set of equattions should be treated self-consistently, which is in general a rather complicated problem. However, even in this case the transport-equation approach seems to be much less involved than more general schemes.

There is another advantage of this approach - it is comparatively easy to interpret its results qualitatively because they are expressed in terms of a quantity with clear physical meaning, i.e. the excitation distribution function.

The most important question concerns the range of applicability of the approach. The corresponding conditions have been formulated in section 2. It should be mentioned, however, that these conditions are dependent on the character of the problem in question, i.e. on the characteristic quantum time
and space parameters of a system. So it is difficult to give universal criteria for the applicability of the transport-equation approach. One should estimate the characteristic quantum parameters of the system under consideration before applying this approach and one should take care not to break the inequalities of section 2. We have tried to demonstrate this procedure in section 6 (logarithmic term in conductivity). Sometimes, one can see from the final result that the limits of applicability of the transport equation are violated, for instance, the corresponding integrals may diverge. But even in such a case one can usually guess which quantum quantity cuts the integral off. That means that order-of-magnitude estimations can be obtained even in this case: the transport-equation approach has a heuristic value.

We believe that in the future the approach discussed in this review article may prove to be useful for the analysis of many problems connected with transport phenomena in superconductors.

22 The Kinetic Theory of Superconductors with Excess Quasiparticles by Galitskii, Elesin, Kopaev (!!!!!!)

22.1 Introduction

The influence of an electromagnetic field and tunnel injection on superconductors leads to the creation of quasiparticles so that their number is greater than in thermal equilibrium. This situation takes place if the field frequence ω or the voltage across the junction V exceeds the gap 24*. Thus, a nonequilibrium state of the superconductor arises, which is accompanied by a number of interesting phenomena observed experimentally, namely: first-order transitions of the type superconductor-normal metal (or Δ_1-superconductor- Δ_3 superconductor), instabilities

and hysteresis effects, the formation of spatially inhomogeneous states of a new type, etc. Quite a large number of papers and reviews deal with the theoretical investigation of superconductors with excess quasiparticles (Tremblay 1981, Elesin and Kopaev 1981). The shape of the energy distribution of quasiparticles created by an electromagnetic field or tunnel injection is the most important parameter of the theory. It appears that the order parameter, the stability of the state and the response to an external magnetic field may be very sensitive to the quasiparticle energy distribution. Therefore, a correct determination of the shape of the quasiparticle distribution function (QDF) is the fundamental task of the theory.

The general problem of simultaneously describing the dynamic and kinetic properties of quasiparticles was solved by Keldysh (1964). The Keldysh technique has made it possible to derive systems of equations for an exciton and a photon dielectric (semiconductor in a strong electromagnetic field, Elesin 1970a) and for superconductors (Elesin et al. 1973, Aronov and Gurevich 1973). Gor'kov and Eliashberg (1968) developed another method for describing nonequilibrium systems; using this method, Eliashberg (1970, 1971a) derived a system of equations for a superconductor. This system includes the equation for the order parameter $A(r,t)$, and kinetic equations for the QDF $n(\xi,r,t)$ and phonons $N(\varepsilon,r,t)$ (Chang and Scalapino 1977).

The purpose of this review is to describe the present state of the theory of these phenomena and to show how the theoretical results agree with experimental data obtained for superconductors with excess quasiparticles. Most attention is given to a consistent knetic theory, which makes it possible to

describe unambiguously a wide range of phenomena using solutions of the kinetic equations.

The review claims in no way to provide a complete bibliography, because it relies mainly on papers dealing with the kinetic theory and also on papers, which have appeared in recent years. Earlier papers are considered in detail in the reviews by Tremblay (1981), Elesin and Kopaev (1981), Langenberg (1975), and Aronov and Spivak (1978).

The present review consists of two parts. Section 1 deals with the singleband approximation, which assumes that the field frequency is less than the energy gap E_g between the conduction band and the valence band; section 2 considers the opposite case $\omega > E_g$, where the electromagnetic field induces transitions between the bands (the two-band approximation).

The basic equations for the gap Δ, QDF$n(\xi,r,t)$ and phonons $N(\varepsilon,r,t)$ are presented in section 1.1. The electromagnetic field appears on the right-hand side of the kinetic equation for quasiparticles and acts as a source of excess quasi-particles. A similar role is played by tunnel injection.

Irrespective of the nature of the sources, it is convenient to divide them into two classes (Elesin 1974): "wide sources" create quasiparticles with energies in the range $\Delta\langle\varepsilon\langle\bar{\varepsilon},\bar{\varepsilon}\rangle\rangle$ (these are realized under optical pumping $\omega \geqslant \Delta$, tunnel injection $V \gg \Delta$, ionization by charged particles, etc.); "narrow sources" create quasiparticles in a small energy range $\varepsilon - 2\Delta \ll \Delta$ (these are realized at threshold values of the frequency and voltage).

Section 1.2 is devoted to the most interesting class of states - those of superconductors with wide quasiparticle sources.

Experimental investigations in this field began after the work of Testardi (1971), in which he reported the measurement of the resistance of superconducting films irradiated with laser pulses. Testardi came to the conclusion that the superconductor normal metal transition observed was caused by excess quasiparticles, created by the electromagnetic field, rather than by "simple heating". Later on, Sai-Halasz et al. (1974), Hu et al. (1974) and Golovashkin et al. (1975) discovered that the resistance of a superconductor irradiated with light appeared gradually, starting at a certain critical power β_c, and reaching normal values in a fairly wide range of β

0

- We assume $\hbar = c = 1$.

(but not in a jump-like manner as in the equilibrium case). Those authors have assumed that a new type of nonequilibrium intermediate state may be possible, in which the superconducting and normal phases co-exist.

Further investigations of superconductors with optical (Golovashkin et al. 1978, 1979a,b, 1980, Mitsen 1981) and especially tunnel injection (Iguchi 1977, Fush et al. 1977, Mitsen 1979, Pan and Rudenko 1981, Mitsen et al. 1981) have confirmed the existence of an inhomogeneous state in nonequilibrium superconductors, and also have revealed other phenomena such as first-order phase transitions (Iguchi 1977, Fush et al. 1977), broadening of current-voltage characteristics, hysteresis effects, etc.

It should be noted that all these phenomena are observed in thin films (3003000Å). Such a small thickness is necessary in order to ensure that nonequilibrium phonons are removed before they come into equilibrium with the lattice and quasiparticles. Otherwise, the external action leads just to heating of the superconductor.

The first theoretical model was suggested by Owen and Scalapino (1972); this model was further developed in several papers (Baru and Sukhanov 1975, Scalapino and Huberman 1977, Hida 1978a,b) and was called the μ^*-model. It is assumed in the μ^*-model that the QDF can be represented in the form

$$n_{\mu^*} = \left[\exp\left(\frac{\varepsilon - \mu^*}{T}\right) + 1\right]^{-1} \tag{1}$$

where μ^* is the positive chemical potential and T is the lattice temperature. The μ^*-model predicted the inverse population of quasiparticles ($n > \frac{1}{2}$), firstorder transition at a certain critical concentration, diffusive instability, anomalous paramagnetism, and other effects. Comparison of the μ^*-model with experiment has revealed a number of essential difficulties (Golovashkin et al. 1979b, Tremblay 1981). Some time later Parker (1975) suggested a thermal model (the so-called T^*-model), in which the QDF was used in the form

$$n_{T^*} = \left[\exp\frac{\varepsilon}{T^*} + 1\right]^{-1} \tag{2}$$

The Parker function differs from the function of thermal (equilibrium) quasiparticles

$$n_{\mathrm{T}} = \left[\exp\frac{\varepsilon}{T} + 1\right]^{-1} \tag{3}$$

in that the lattice temperature is replaced by a certain effective temperature T^* determined from balance relations. The T^*-model describes well the dependence of A on the pumping power β in a certain range of β values, but it does not predict first-order transitions and instabilities, and is, therefore, insufficient to describe phenomena near the phase transition region, for example, the inhomogeneous state.

A third model was suggested by Elesin (1974, 1976, 1979a) and was developed further in papers by Elesin (1977b), Elesin et al. (1977a, b, 1979). Elesin and Levchenko (1978), Eckern et al. (1979) and Imai (1980). It is based on the analysis and solution of the kinetic equations for quasiparticles. It was shown in those papers that the QDF differed significantly from the corresponding functions in the μ^* - and T^*-models, the specific features of $n(\xi)$ being of general character and having a clear physical meaning.

Specific features of the QDF are caused by the fact that quasiparticle relaxation is a coherent process. The energy distribution of excess quasi-
particles decays slower than that of thermal quasiparticles, so $n(\xi)$ satisfies the conditions (Elesin 1976)

$$n(\xi = 0) < n_T(\xi = 0), \tag{4}$$

$$n(\xi) < \frac{1}{2}. \tag{5}$$

Here n_T is the thermal QDF taken with the same Δ and temperature $T(\Delta)$ according to the BCS theory.

This means in terms of the quasiequilibrium distribution (1) that μ^* is negative and T^* exceeds T_c, i.e. the quasiparticle distribution is as if it were "overheated" (Elesin and Kopaev 1981).

The function $n(\xi)$ is less than $\frac{1}{2}$ and leads to an ambiguous dependence of the gap on the pumping power (Elesin 1976), characteristic of coherent instability (Elesin 1977a), which in turn gives rise to a laminated inhomogeneous state. This laminated state represents alternating superconducting and normal regions.

The model described [called the E-model by Eckern et al. (1979) and Tremblay (1981)] predicts a first-order transition into the normal or inhomogeneous state provided the optical pumping power (or voltage across the junction) exceeds a certain critical value.

The E-model makes it possible to predict and describe a wide range of phenomena, in particular the unsteady intermediate state under optical pumping, and the steady state under tunnel injection. In section 1.3.5 conclusions deduced from the μ^*-, T^*- and E-models are compared with experimental results.

The kinetic theory of superconductors with a narrow quasiparticle source is briefly outlined in section 1.3, following mainly the papers by Elesin (1974, 1979b), Aronov and Spivak (1976), Schön and Tremblay (1979), and Gray and Willemsen (1978). In this case specific features of the QDF are determined by the effect of the order parameter on the source type, since the rate of threshold quasiparticle production is proportional to the difference $\omega - 24$. As in the E -model, the order parameter is an inhomogeneous function and the state appears to be unstable against the so-called "threshold instability" predicted by Elesin (1974) and leading to a laminated inhomogeneous state. The difference is, however, that in the latter case the state is laminated into phases with different but finite values of the order parameter.

Experimental investigations of the threshold tunnel injection were performed by Dynes and Narayanamurti (1972) and by Gray and Willemsen (1978) who proved the existence of a two-gap inhomogeneous state.

The second part of this review presents the theory for the case of the twoband model. Both the bands should be taken into account here because an electromagnetic field with a frequency higher than the energy gap E_g gives rise to interband transitions. Besides interband transitions discussed in sections 1.1 and 1.3, the electromagnetic field leads to two additional effects.

First, nonequilibrium electrons in the conduction band and holes in the valence band are created due to absorption of the field. This shifts the Fermi level in metals and doped semiconductors. In pure semiconductors and insulators the electrons occupy (under the action of the field) the bottom of the conduction band.

Second, interband transitions may result in a dynamic effect-a change in the electron spectrum. In fact, as was shown by Galitskii et al. (1969), a gap $2\hat{i}$, proportional to the product of the interband transition dipole moment and the field amplitude, arises in the spectrum of electrons in the valence and conduction bands.

Electrons and holes form field-coupled pairs, which are similar in many respects to Cooper pairs and electron-hole pairs of an exciton insulator.

The appearance of a gap in the electron spectrum, and, hence singularities in the density of states, significantly affects the state of a superconductor.

Depending on the concentration of equilibrium electrons in the conduction band, the field may either suppress superconductivity (Elesin and Kopaev 1972) or increase the critical temperature (Elesin and Kopaev 1974). The net result depends on the relative position of the Fermi level and the gap 2λ created by the field.

The electromagnetic field may also lead to a change in the quasi-particle energy distribution. In particular, the function may become asymmetric or even inverse ($n > \frac{1}{2}$) (Elesin 1975).

In fact, if the field is sufficiently strong so that the gap 2% exceeds the Debye frequency (ω_{D}. the quasiparticles cannot recombine through the gap and are accumulated at energies larger than E_{F}. The inverse distribution may, in turn, create conditions for the appearance of a superconducting state with repulsion between the electrons (Kirzhnits and Kopaev 1973, Galitskii et al. 1973) and also for abnormal paramagnetism (Galitskii et al. 1973).

22.2 1.1. The dynamic and kinetic equations in Single-band approximation

The treatment of nonequilibrium processes in superconductors requires a system of equations which simultaneously describes both dynamic and kinetic properties. In the weak-coupling approximation this system is reduced to the order parameter equation and kinetic equations for the distribution functions of quasiparticles and phonons (Elesin 1977a).

22.2.1 1.1.1. The order parameter equation

In the spatially homogeneous case the order parameter equation is of the form (Eliashberg, 1970, 1971, Elesin et al. 1973)

$$\Delta = -g\int_0^{\omega_{\mathrm{D}}} \frac{\mathrm{d}\xi}{\varepsilon}(1-2n(\xi))\Delta, \quad n(\xi) = \int \frac{n_p\,\mathrm{d}\Omega}{4\pi}, \quad \varepsilon = \sqrt{\xi^2+\Delta^2} \tag{6}$$

where g is the electron phonon coupling constant $(g<0), n(\check{\zeta})$ is the QDF satisfying the kinetic equation (9), and ω_{D} is the Debye frequency; hereafter by Δ we mean the modulus of the order parameter.

The spatial variation of $\Delta(r)$ in a nonequilibrium superconductor is described by an equation similar to the Ginzburg-Landau equation:

$$\xi_0^2\left(\frac{\partial}{\partial r} - 2\mathrm{i}e\mathscr{A}\right)^2\Delta(r) = \frac{\partial U}{\partial\Delta} \tag{7}$$

$$U(\Delta) = \int_0^{\Delta}\Delta'\mathrm{d}\Delta'\left[\frac{1}{|g|} - \int_0^{\omega_{\mathrm{D}}}\mathrm{d}\xi\frac{1-2h(\xi,r)}{\left(\xi^2+(\Delta')^2\right)^{1/2}}\right] \tag{8}$$

which is obtained (Elesin 1977a) under the assumption that Δ is small and varies slowly within the coherence length $\check{\zeta}_0$: here $\check{\zeta}_0$ is a functional of the QDF of the normal metal $n_0(\xi)$:

$$\xi_0^2 = \frac{p_0^2}{3m}\int_0^{\infty}\frac{\mathrm{d}\xi}{\xi}\left(\frac{\mathrm{d}}{\mathrm{d}\xi}\frac{2n_0-1}{\xi}\right)$$

The description of unsteady processes requires, in general, a time equation for A. But in most cases the analysis can be restricted to equation (7), because the time needed for the establishment of a steady state in the system of Cooper pairs is much less than that for a system of quasiparticles.

The vector potential $\mathscr{A}$ includes also the potential of a electromagnetic field of a frequency ω. The inclusion of $\mathscr{A}$ into the dynamic equation (7) for Δ makes it possible to describe the direct

influence of the field on the order parameter. This influence was studied in detail by Gorkov and Eliashberg (1969) [see also the review by Dmitriev and Khristenko (1978)], and it was shown that the effect is significant at low frequencies satisfying the condition ($\omega^2 < \omega_c^2 = A\tau_{ph}$ (τ_{ph} is the phonon energy relaxation time of quasiparticles). Let us note that since the values of τ_{ph} are large ($\tau_{ph}\Delta \gg 1$) the above condition is met at frequencies much lower than $2A$.

At frequencies $\omega > 2\Delta > \omega_c$ the main contribution is due to the second channel, where the electromagnetic field acts as a source of quasiparticles. Therefore, in further consideration we can neglect the contribution of the electromagnetic field in eq. (7) and take it into account only in the kinetic equation (9).

22.2.2 1.1.2. The kinetic equation for the quasiparticle distribution function

The kinetic equation for the QDF is of the form

$$\frac{\partial n(p,r,t)}{\partial t} + \frac{\partial n}{\partial r}\frac{\partial \varepsilon}{\partial p} - \frac{\partial \mathrm{n}}{\partial p}\frac{\partial \varepsilon}{\partial r} = I_{imp} + I_{ph} + I_{ee} + Q, \tag{9}$$

where ε is the quasiparticle energy, Q is the quasiparticle source, and I_{ph}, I_{ce}, I_{imp} are the collision integrals of quasiparticles with phonons, quasiparticles and impurities, respectively; the last integral can be written in the form

$$I_{imp} = -\frac{\xi}{\varepsilon\tau_{imp}}\{n(p,r,t) - n(\xi,r,t)\}, \tag{10}$$

where τ_{imp} is the relaxation time at the impurity.
The equation for the QDF $h(\xi,r,t)$ integrated over angles is obtained from eq. (9) in an ordinary way, if we take into account that τ_{imp}/τ_{ph} is small:

$$\frac{\partial}{\partial t}n(\xi,r,t) + \frac{|\xi|}{\varepsilon}L^2\left\{\frac{\partial}{\partial r_i}\left[-\frac{\partial h}{\partial r_i} + \frac{\partial \varepsilon}{\partial r_i}\frac{\partial h}{\partial \varepsilon}\right] + \frac{\partial \varepsilon}{\partial r_i}\frac{\partial}{\partial \varepsilon}\left[\frac{\partial n}{\partial r_i} - \frac{\partial \varepsilon}{\partial r_i}\frac{\partial n}{\partial \varepsilon}\right]\right\} = I_{ph} + I_{ee} + Q. \tag{11}$$

The phonon collision integral (Eliashberg 1971) is

$$I_{ph} = S^+ - S^- - S^R \tag{12}$$

$$S^+ = \frac{1}{\tau_{ph}\Delta_0^{k+2}}\int_\xi^{\omega_D+\xi} d\xi' \left(\varepsilon' - \varepsilon\right)^{k+1} v1 - \eta\frac{\Delta^2}{\varepsilon\varepsilon'}\Big) \times \left[(1-n)n'\left(1+N_{n'-\varepsilon}\right) - h\left(1-h'\right)N_{\varepsilon'-\varepsilon}\right] \tag{13}$$

$$S^- = \frac{1}{\tau_{ph}\Delta_0^{k+2}}\int_0^{\zeta} d\xi' \left(\varepsilon' - \varepsilon\right)^{k+1}\left(1 - \eta\frac{\Delta^2}{\varepsilon\varepsilon'}\right) \times \left[n\left(1-n'\right)\left(1+N_{\varepsilon-\varepsilon'}\right) - (1-n)n'N_{\varepsilon-k'}\right] \tag{14}$$

$$S^R = \frac{1}{\tau_{ph}\Delta_0^{k+2}}\int_0^{\omega^{-\xi}} d\xi'' \left(\varepsilon + \varepsilon'\right)^{k+1}\left(1 + \eta\Delta^2\right) \times \left[nn'\left(1+N_{\varepsilon+\varepsilon'}\right) - (1-n)\left(1-k'\right)N_{\varepsilon+\varepsilon'}\right] \tag{15}$$

$$\frac{1}{\tau_{ph}} = \frac{\eta|g|\Delta_0}{2}\left(\frac{\Delta_0}{\omega_D}\right)^{k+1}, \quad n\left(\xi'\right) \equiv n', \quad \varepsilon\left(\xi'\right) \equiv \varepsilon'. \tag{16}$$

Here N_r is the phonon distribution function, k is a factor describing the dependence of the matrix element of the electron phomon interaction on q $\left(M_{\mathrm{q}}^2 \sim q^{\mathrm{k}}\right)$, η is a parameter taking the values +1 for a superconductor (Eliashberg 1971, 1970) and -1 for an exciton and photon insulator (Elesin

1970a). The first two terms in eq. (12) describe the energy relaxation of quasiparticles (S^+, "arrival"; S^-, "leaving"), the third term S^{R} describes quasiparticle recombination with the emission (absorption) of phonons. The coherence factors ($1 \pm \eta\Delta^2/\varepsilon\varepsilon'$) appear due to coherence of the interaction between quasiparticles and phonons and play very important roles in the phenomena discussed below.

In the one-band model $n(\zeta)$ is an even function in the case of electromagnetic pumping and symmetric tunnel injection. The collision integral (12) has been written with due account for this fact. In the general case the coherence factors ($1 \mp \eta\left(\Delta^2/\varepsilon\varepsilon'\right)$) should be replaced by

$$\left(1 \pm \eta\frac{\xi\xi'}{\varepsilon\varepsilon'} \mp \eta\frac{A^2}{\varepsilon\varepsilon'}\right).$$

In the two-band model of a superconductor in a strong electromagnetic field of frequency $\omega > E_{\mathrm{g}}$ the kinetic equation (12) is modified as follows.

The quasiparticle energy ε is replaced by $\tilde{\varepsilon} = \sqrt{\varepsilon^2 + \lambda^2}$, and a term is introduced which describes recombination of electrons and holes through the forbidden band (Elesin 1970a).

The quasiparticle collision integral for superconductors I_{ee} was found by Eliashberg (1970) and can be represented in the form

$$\begin{aligned}
&I_{\mathrm{ee}} = S_{\mathrm{ee}}^+ - S_{\mathrm{ee}}^- \qquad (17)\\
&S_{\mathrm{ee}}^+ = \frac{1}{\tau_{\mathrm{ec}}\Delta_0^2}\iiint_0^1 \mathrm{d}\xi_1\ \mathrm{d}\xi_2\ \mathrm{d}\xi_3\\
&\times\{M_1(1-n)n_1n_2n_3\delta\left(\varepsilon-\varepsilon_1-\varepsilon_2-\varepsilon_3\right)\\
&\quad + 3M_2(1-n)n_1n_2\left(1-n_3\right)\delta\left(\varepsilon-\varepsilon_1-\varepsilon_2+\varepsilon_3\right)\\
&\quad +3M_3(1-n)n_1\left(1-n_2\right)\left(1-n_3\right)\delta\left(\varepsilon-\varepsilon_1+\varepsilon_2+\varepsilon_3\right)\},\\
&S_{\mathrm{ee}}^- = \frac{1}{\tau_{\mathrm{ec}}\Delta_0^2}\iiint_0^\infty \mathrm{d}\xi_1\ \mathrm{d}\xi_2\ \mathrm{d}\xi_3\\
&\quad\times\{M_1n\left(1-n_1\right)\left(1-n_2\right)\left(1-n_3\right)\delta\left(\varepsilon-\varepsilon_1-\varepsilon_2-\varepsilon_3\right)\\
&\quad + 3M_2n\left(1-n_1\right)\left(1-n_2\right)n_3\delta\left(\varepsilon-\varepsilon_1-\varepsilon_2+\varepsilon_3\right)\\
&\quad +3M_3n\left(1-n_1\right)n_2n_3\delta\left(\varepsilon-\varepsilon_1+\varepsilon_2+\varepsilon_3\right)\},\\
&M_1 = \left(1-\frac{\Delta^4}{\varepsilon\varepsilon_1\varepsilon_2\varepsilon_3}\right) - \frac{b\Delta^2}{3a\varepsilon}\left(\frac{1}{\varepsilon_1}+\frac{1}{\varepsilon_2}+\frac{1}{\varepsilon_3}-\frac{\varepsilon^2}{\varepsilon_1\varepsilon_2\varepsilon_3}\right),\\
&M_2 = M_1\left(-\varepsilon_3\right). \quad M_3 = M_1\left(-\varepsilon_1,-\varepsilon_2\right), \quad \frac{1}{\tau_{\mathrm{ec}}} = \frac{a\Delta_0^2}{E_F},
\end{aligned}$$

where a and b are dimensionless quantities of the order of unity dependent on the electron-electron interaction matrix element; M_i are the coherence factors, which describe the coherence of quasiparticle interaction.

It is useful to derive the law of conservation of the number of quasiparticles $\bar{n}$; this law can easily be found by integrating eq. (11) with respect to ξ :

$$\frac{\partial \bar{n}}{\partial t} + L^2 \frac{\partial}{\partial r_\mathrm{i}} \int_\varepsilon \frac{\xi}{\varepsilon} \left(\frac{\partial n}{\partial r_\mathrm{i}} - \frac{\partial \varepsilon}{\partial r_\mathrm{i}} \frac{\partial n}{\partial \varepsilon} \right) \frac{\mathrm{d}\xi}{\Delta_0}$$
$$+ \frac{1}{\tau_\mathrm{ph}} \int_0^{\omega_\mathrm{D}} \frac{\mathrm{d}\xi}{\Delta_0^{k+3}} \int_0^{\omega_\mathrm{D}-\xi} \mathrm{d}\xi' \left(\varepsilon + \varepsilon'\right)^{k+1} \left(1 + n \frac{\Delta^2}{\varepsilon\varepsilon'}\right) \varphi_\mathrm{ph}\left(\xi, \xi'\right)$$
$$- \int_0^\infty I_\mathrm{ee} \frac{\mathrm{d}\xi}{\Delta_0} = \bar{Q} \tag{18}$$

$$\varphi_\mathrm{ph}\left(\xi, \xi'\right) = n(\xi) n\left(\xi'\right) - N_{\varepsilon+\varepsilon'}\left(1 - n(\xi) - n\left(\xi'\right)\right)$$

$$\bar{n} = \frac{1}{\Delta_0} \int_0^\infty \mathrm{d}\xi n(\xi, r, t), \quad \bar{Q} = \frac{1}{\Delta_0} \int_0^\infty \mathrm{d}\xi Q \tag{19}$$

22.2.3 1.1.3. Sources of nonequilibrium quasiparticles

The nonequilibrium states considered in this review, are formed due to the production of quasiparticles by external sources (electromagnetic and ultrasonic fields with $\omega > 2\Delta$, tunnel injection with $V > 2\Delta$, ionizing particles, etc.). Although the results obtained below are valid, to a certain extent, for all those sources, we shall consider in detail only two of them: electromagnetic pumping Q_ω and symmetric tunnel injection Q_V. According to Eliashberg (1970a), Q_ω can be represented in the form

$$Q_\omega = Q_\omega^{(1)} + Q_\omega^{(2)} + Q_\omega^{(3)}, \tag{20}$$
$$Q_\omega^{(1)} = \alpha_\omega \rho^\omega(\omega - \varepsilon)\left(1 - n_\varepsilon - n_{\omega-\varepsilon}\right),$$
$$Q_\omega^{(2)} = Q_{-\omega}^{(3)} = \alpha_\omega \rho^\omega(\varepsilon - \omega)\left(n_{\varepsilon-\omega} - n_\varepsilon\right),$$
$$\rho^{(\omega)}(\omega - \varepsilon) = \frac{(\omega - \varepsilon) - \left(\Delta^2/\varepsilon\right)^{(1+k\omega)/2}}{\sqrt{(\omega - \varepsilon)^2 - \Delta^2}} - 0(\omega - \ddot{-}\Delta), \quad 0(x) = \begin{cases} 1, & x \geqslant 0 \\ 0, & x < 0 \end{cases} \tag{21}$$

where

$$\alpha_\omega = \frac{E^2 e^2 L^2}{2m\omega^2\pi\left(1 + \omega^2\tau_\mathrm{imp}^2\right)\tau_\mathrm{ph}} \tag{22}$$

$$L^2 = \frac{v_\mathrm{F}^2 \tau_\mathrm{imp} \tau_\mathrm{ph}}{3} \tag{23}$$

$k_\omega = +1, \alpha_{(1)}$ is the electromagnetic injection parameter, L is the quasiparticle diffusion length, and v_F is the velocity of electrons at the Fermi surface.

Note that expression (22) corresponds to absorption at free electrons. In certain superconductors other mechanisms, for instance interband absorption, may give the main contribution. Since the film thickness d usually exceeds the reciprocal absorption coefficient, its explicit form is insignificant and it can be taken as $1/d$.

The source which really creates quasiparticles is described by the quantity $Q_\omega^{(1)}$, while $Q_{(2,3)}^{(2,3)}$ describes the energy redistribution of quasiparticles present in the system, since $\int_0^x \mathrm{d}\xi \left(Q^{(2)} + Q^{(3)}\right) = 0$.

In the case of tunnel injection through the symmetric SIS junction eq. (19) may be used for Q_V, in which, however, one should put $\omega = V, k_\mathrm{V} = -1, \alpha_\omega = \alpha_\mathrm{V}$ (Kirichenko et al. 1976):

$$\alpha_v = \frac{2\sigma_N \tau_\mathrm{ph}}{d e^2 v(0)}, \tag{24}$$

where σ_N is the junction conductivity in the normal state, d is the film thickness, and $r(0)$ is the density of electron states. An essential difference between Q_V and Q_c is that the coherence factor $\lambda^2\varepsilon$ does not appear in Q_V.

As was already noted in the Introduction, the sources can be divided, irrespective of their nature, into two classes: wide sources and narrow sources. This classification appeared to be quite convenient for understanding the physics of the phenomena and analytically solving the equations in the limiting cases of wide and narrow sources. The fact is that in these cases one can separate the processes through which the order parameter affects the QDF formation.

Indeed, in the case of a wide source Δ disappears from the expression for the source $Q^{(1)}$, that is, $Q^{(1)} = \alpha_\omega\theta(\omega - \varepsilon)$, and it affects only the relaxation processes. Since the "density of source action" is small (Elesin 1974), the kinetic equation may be assumed homogeneous (one may take $Q = 0$), so the relationship between n and Q can be found from the condition (18) that the number of quasiparticles is conserved.

In the case of a narrow source the order parameter has a decisive effect on the source. Note that $Q^{(2)}$ and $Q^{(3)}$ do not play an essential role in the phenomena considered if $(1) > 2A$. One should bear in mind that the concept of a narrow source has a meaning only if the injection intensity is sufficiently low, so that the change in the parameter $\delta A^{\text{is small, } \delta A \ll A_0}$. On the contrary, in the case of intensive injection where $\Delta_0 - \delta\Delta \ll \Delta_0$, a source with frequency $\omega - 2A_0 \ll 1_0$ becomes wide because the energies of quasiparticles produced are $\omega \sim 2A_0 \ll 1$. In the case of tunnel injection the equation for an external circuit should be taken into account:

$$\mathscr{E} = V + JR, \quad \bar{J} = \int \mathrm{d}^2 r J(V, d)$$

$$J(V, \Delta) = J_1 + J_2$$
$$J_1 = \alpha_V \int_\Delta^{\vee - \Delta} \mathrm{d}\varepsilon\rho(\varepsilon)Q_V^{(1)}, \quad J_2 = 2\alpha_V \int_\Delta^\infty \mathrm{d}\varepsilon\rho(\varepsilon)Q_V^{(3)} \tag{25}$$

where $\mathscr{E}$ is the emf, R is the external resistance, J is the current flowing through the SiS junction, and $\rho(\varepsilon) = \varepsilon/\sqrt{\varepsilon^2 - \Delta^2}$.

22.2.4 1.1.4. The kinetic equation for phonons

The phonon distribution function $N(\varepsilon)$ may differ from the equilibrium one

$$N_T(\varepsilon) = \left[\exp\frac{\varepsilon}{T} - 1\right]^{-1} \tag{26}$$

and it can be found from the following kinetic equation (Chang and Scalapino 1977):

$$\frac{\partial N}{\partial t} + \frac{N - N_T}{\tau_{\text{es}}} = \frac{1}{\tau_B}\int_\Delta^{\varepsilon - \Delta} \frac{\mathrm{d}\varepsilon'}{\Delta_0}\rho(\varepsilon')\,\rho(\varepsilon - \varepsilon')$$
$$\times \left[n_{\varepsilon'}n_{\varepsilon-\varepsilon'} - N(1 - n_{\varepsilon'} - n_{\varepsilon-\varepsilon'})\right]\left(1 + \frac{\Delta^2}{\varepsilon'(\varepsilon - \varepsilon')}\right) + \frac{2}{\tau_\beta}\int_\Delta^\infty \frac{\mathrm{d}\varepsilon'}{\Delta_0}\rho(\varepsilon)\rho(\varepsilon + \varepsilon')$$
$$\times \left[n_{\varepsilon+\varepsilon'}(1 - n_{\varepsilon'}) - N(n_{\varepsilon'} - n_{\varepsilon+\varepsilon'})\right]\left(1 - \frac{\Delta^2}{\varepsilon'(\varepsilon + \varepsilon')}\right), \tag{27}$$

$$\tau_{\text{es}} = \frac{4d}{s}, \quad \frac{1}{\tau_\beta} = \frac{\pi|g|\Delta_0\omega_D}{2E_F}, \tag{28}$$

where s is the acoustic velocity. The second term in eq. (27) takes into account the fact that phonons can penetrate from the film into the substrate; the third and fourth terms account for the production of phonons under recombination and scattering of quasiparticles, respectively.

22.2.5 1.1.5. The kinetics of quasiparticles in superconductors

The energy distribution of excess quasiparticles is formed due to the source and relaxation processes. The effect of the source $Q^{(1)}$ lies in the break of a Cooper pair and production of two quasiparticles. A wide source creates quasiparticles with high energies $\varepsilon \ll \Delta$. The quasiparticle created gives its energy to the electron gas the lattice.

In the first case the quasiparticle energy is consumed to increase the energy of quasiparticles already produced and to create new quasiparticles via impact ionization through the gap 24 . This is the way multiple production of quasi-
particles occurs, the process being characterized by the multiplication coefficient $r_{\rm cc}$.

In the second case the energy is consumed for the emission of nonequilibrium phonons. Eventually, the quasiparticles reach the bottom of the band and recombine with emission of a phonon ($\Delta \ll \omega_{\rm D}$), forming a Cooper pair again. Nonequilibrium phonons may either leave the film within a time $\tau_{\rm es}$ or undergo reabsorption within a time τ_β, producing a pair of quasiparticles (or increasing their energy) and thereby leading to multiplication with the coefficient $r_{\rm ph}$. The relative probability for phonons to leave and to be reabsorbed is characterized by the parameter $\gamma = \tau_{\rm es}\,/\tau_\beta$, which is limited to the right by phonon-phonon interaction.

The kinetics of quasiparticles in superconductors is similar, in certain respects, to the kinetics of electrons in semiconductors in which electron-hole pairs are produced (Ryvkin 1963). Indeed, the parameter 24 acts here as the energy gap and quasiparticles as electrons and holes. However, nonequilibrium processes in superconductors have essential distinctive features.
(1) The gap 24 in superconductors is very sensitive to the concentration and energy distribution of quasiparticles and may even become zero.
(2) Since the ratio $2\Delta/\omega_{\rm D}$ is small, scattering and recombination are singlephonon processes and occur at approximately the same rate (Elesin 1974). This means that recombination and scattering times are approximately equal, so the QDF must differ from the quasiequilibrium functions (occurring if the recombination time is large in comparison with the scattering time) and, in particular, from the functions in the μ^*-model (Owen and Scalapino 1972) (except for the case of low T and β).
(3) The order parameter significantly affects the relaxation and production of quasiparticles.

22.3 1.2. Superconductors with a wide quasiparticle source. Optical pumping and tunnel injection at high voltages in Single-band approximation

22.3.1 1.2.1. The distribution function of excess quasiparticles

Consider first a spatially homogeneous case.
At present, there are many papers in which the QDF $n(\xi)$ has been determined analytically (Vardanyan and Ivlev 1973, Elesin 1974, 1976, 1977a,b, Eckern et al. 1979) and numerically (Elesin et al. 1977a,b, Imai 1980) for a wide range of the parameters. The main properties and specific features of $n(\xi)$ are of general character and have a clear physical meaning.

Let us first discuss the properties of $n(\xi)$, which satisfy the kinetic equation with phonon relaxation. The contribution of electron-electron collisions is usually small (Eliashberg 1970, Vardanyan and Ivlev 1973) and will be considered below.

As was established by Elesin (1974, 1976), $n(\xi)$ is a monotonously decaying
function localized mainly in the energy range $\xi \sim \Delta_0$, which does not exceed $\frac{1}{2}$. Moreover, the QDF is not only less than $\frac{1}{2}$, it satisfies the more strict "overheating" condition (4) (Elesin et al. 1979).

Condition (4) is very important and permits the classification of QDF. In particular, the

"overcooled" QDF satisfying a condition inverse to eq. (4) lead to essentially different consequences (the so-called NE-model) (Eckern et al. 1979, Elesin 1976, 1977a). The thermal function serves as if it were a limiting boundary separating the functions $n(\zeta)$ in the E- and NE-models (Elesin 1977b).

The "overheating" character of the QDF is closely related to the coherence factors ($1 \pm \eta\,(\Delta^2/\varepsilon\varepsilon')$) in the integral of collisions between quasiparticles and phonons (12). According to Elesin (1976), a coherence correction n_1 can be separated in the QDF, so $n(\xi)$ is represented in the form

$$n(\xi) = n_0(\varepsilon) + n_1(\xi) \tag{29}$$

where $n_0(\varepsilon)$ statisfies eq. (11) with the coherence factors equal to zero ($\eta = 0$), and the function n_1 is proportional to the coherence factors $\eta\Delta^2/\varepsilon\varepsilon'$.

To elucidate the specific features of $n(\xi)$, it is convenient to consider the simplest model, assuming in eq. (12) $k = -1, T = 0, \gamma = 0$. This model implies an exact solution (Elesin 1976, 1977a) for $\Delta/\Delta_0 \ll 1$:

$$n_0(\varepsilon) \equiv n_0(\xi) = \frac{1}{2}\left(1 - \frac{\xi}{\sqrt{\xi^2 + 4\Delta_0^2\bar{n}^2}}\right), \tag{30}$$

$$n_1 = -\frac{\Delta^2}{\varepsilon}\left(\frac{1}{4\bar{n}\Delta_0}\ln\frac{2\bar{n}\Delta_0}{\Delta}\right), \quad \eta = 1. \tag{31}$$

Substitution of $n_0(\xi)$ into the equation (6) for the gap yields a critical concentration of quasiparticles $\bar{n}_\mathrm{c}$, at which the gap vanishes ($\Lambda = 0$).

$$\bar{n}_\mathrm{c} = \frac{1}{2}. \tag{32}$$

Using then the normalization conditions (18), we find the critical power

$$\beta_\mathrm{c} = n_\mathrm{c}^2 = \frac{1}{4}$$

It can be seen from eqs. (30) and (31) that $n(\xi) < \frac{1}{2}$ and satisfies the overheating condition (4) for $\eta = 1$ due to the coherence correction.

A decrease in $n(\xi)$ near small $\xi \sim \Delta$ is caused by an increase in the quasiparticle recombination rate proportional to $(1 + \Delta^2/\varepsilon\varepsilon')$, which is especially pronounced as $\zeta \to 0$. Note that if η were equal to -1 , the distribution would be "overcooled" (Elesin 1976, Eckern et al. 1979) (the NE-model).

In the general case of finite temperatures, the actual matrix elements are $M_\mathrm{q}^2 \sim q, k = 1$, and if the effect of phonon reabsorption is taken into account, the specific features of $n(\xi)$ remain unchanged.

The main properties of $n(\xi)$ were formulated by Elesin (1976, 1977*b*). Let us first recall those properties of the function $n_0(\varepsilon)$ which are close to those of $n_T(\varepsilon)$.
(1) Expansion of the integrals of $n_0(\varepsilon)$ includes only even powers of Δ^2 [as in the case of $n_T(\varepsilon)$].
(2) The value of $n_0(\varepsilon)$ is less than $\frac{1}{2}, n_0(0) = \frac{1}{2}$ (as for n_T).
(3) The asymptotic behaviour of $n_0(\varepsilon)$ for large ε has a power form (Vardanyan and Ivlev 1973, Elesin 1976),

$$n_0(\varepsilon) \sim \varepsilon^{-(k+3)}, \quad \varepsilon \to \infty \tag{33}$$

unlike the exponential decay for $n_T = e^{-\varepsilon/T}$.
(4) The functions $n_0(\varepsilon)$ for $\Delta = 0$ pass into "critical" functions $n_0(\breve{\zeta})$ satisfying the kinetic equation with $\Lambda = 0$. These functions are characterized by a single parameter ${a_1}^{1/2}$,

$$n_0(\xi) \equiv n_0\left(\xi/a_1^{1/2}\right), \quad a_{\mathrm{i}} = \int_0^\infty \xi^i n_0(\xi)\mathrm{d}\xi \tag{34}$$

which plays the role of effective temperature. Substitution of the function $n_0(\xi)$ into the gap equation makes it possible to find a critical value a_{1c} at which the gap becomes zero:

$$\frac{1}{|g|} = \int_0^{\omega_{\mathrm{D}}/{a_{1\mathrm{c}}}^{1/2}} \frac{1-n_0(x)}{x}\,\mathrm{d}x.$$

In particular, for $\gamma = 0, T = 0$ we have (Elesin et al. 1977)

$${a_{lc}}^{1/2} = 0,58\Delta_0 \simeq T_c, \quad a_{0c} = 0.4\Delta_0 \tag{35}$$

Once $n_0(x)$ is known, one can find the critical concentration of quasiparticles

$$\bar{n}_{\mathrm{c}} = a_0/\Delta_0 = 0.4 \tag{36}$$

or in the dimensionless form

$$N_{\mathrm{c}} = v(0)A_0\bar{n}_{\mathrm{c}}. \tag{37}$$

The quantity $\bar{n}_c$ practically coincides with the concentration of thermal quasiparticles $\bar{n}_f = T_{\mathrm{c}} \ln 2 = 0.4$, indicating once more that the properties of n_0 and n_T are close for $\xi \leqslant \Delta_0$.

Substituting $n_0(\xi)$ into the normalization condition (18), we find the critical power $\beta_{\mathrm{c}} = \bar{Q}$, which corresponds to the vanishing of the gap (see section 1.2.4).

The coherence correction n_1 for small $\Lambda_/\Delta_0$ can be found in the general form and expressed as

$$n_1 = \ddot{-}\eta\frac{\Lambda^2}{\pi\varepsilon}\varphi, \tag{38}$$

$$\varphi = \frac{\pi}{a_2}\int_0^\infty \xi\mathrm{d}\xi\varphi_{\mathrm{ph}}(\xi,0) \tag{39}$$

where $\varphi_{\mathrm{ph}}(\xi,0)$ is the function (19), into which the "critical" distribution functions of quasiparticles $n_0(\xi)$ and phonons $N_0(\xi)$ are substituted.

Relations (38), (39) and (19) imply the following properties of n_1 :
(1) The sign of the "coherence" correction n_1 is determined by the sign of $\eta = (\pm 1)$ in the coherence factors. In superconductors $\eta = 1, n_1 < 0$; in an exciton insulator $\eta = -1, n_1 > 0$.
(2) The correction n_1 is proportional to $\varphi\,(\xi,\xi')$ (see eq. 19), which is a measure of the "nonequilibrium of the system". The function $\varphi\,(\xi,\xi')$ represents the recombination collision integral, which vanishes in equilibrium. The maximum of φ is reached at $T = 0, \gamma = 0$ and is equal to (Elesin et al. 1977a)

$$\varphi_{\mathrm{m}} = \frac{\pi a_1}{2a_2} = \frac{0.71}{\Delta_0} \tag{40}$$

Obviously, as T and the film thickness (i.e. γ) increase, the number of nonequilibrium phonons N, grows and φ correspondingly decreases, tending to zero but always remaining a positive quantity. From the physical viewpoint this is related to the fact that $\varphi\,(\xi,\xi')$ is proportional to the difference between the quasiparticle recombination rate (the first term) and the production rate due to reabsorption of thermal and nonequilibrium phonons. For $\beta > 0$ the number of recombining particles always exceeds the number of particles produced due to reabsorption of non-equilibrium phonons, so $\varphi > 0$.

(3) Subtracting from $n(0)$ (eq. 29) the function $n_7(0)$ and taking into account that $n_0(0) = n_T(0)^*$, we obtain the "overheating" condition (4)

$$n(\xi = 0) - n_T(\xi = 0) = n_1(\xi = 0) < 0 \tag{41}$$

It can be seen from eq. (41) that the difference between the QDF $n(\xi = 0)$ and the equilibrium one $n_T(\xi = 0)$ is caused by the coherence correction n_1. It is obvious therefore that as γ and T grow, when $\varphi \to 0$ and $n_1 \to 0, n(\xi)$ tends to $n_0(\varepsilon)$.

The above properties and the form of $n\,(\xi')$ were confirmed by computeraided numerical solution of the complete system of equations for A, n and N (eqs. 6, 11, 12, 36) (Elesin et al. 1977a,b, 1979, Imai 1980).

Elesin et al. (1979) calculated the functions $n(\xi)$ for a wide range of the parameters β, Δ, T and γ. It was assumed in solving the equations that the source acts in the energy range $9A_0 < \omega < 10A_0$ and it was shown that its shape does not influence the results obtained (if $\omega \gg \Delta_0$).

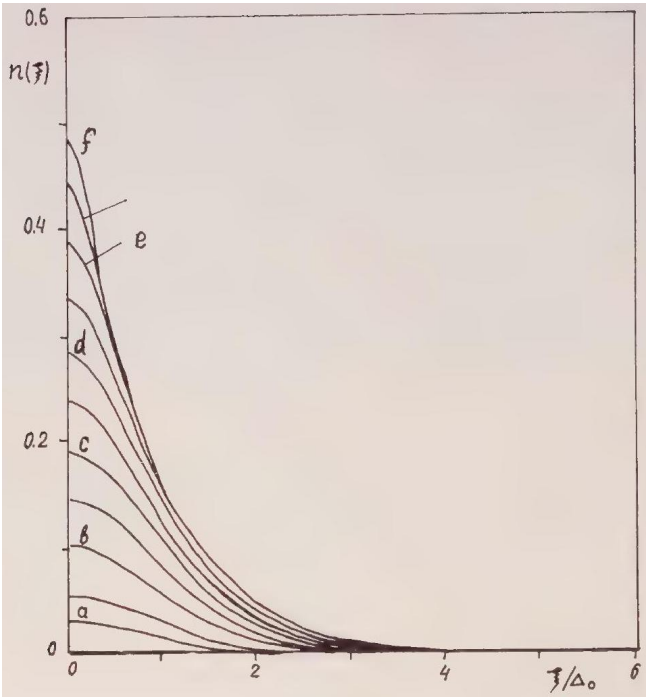


Fig. 1. Dependence of the quasiparticle distribution function on energy, for $T = 0$ and $\gamma = 0.15$ and the following values of the order parameter Δ / Δ_{0} (and correspondingly β): (a) 0.95 ; (b) 0.8 ; (c) 0.6 ; (d) 0.4 ; (e) 0.5 ; (f) 0.01 . (Elesin et al. 1979.)

Figure 1 shows a typical form of the QDF $n\,(\xi\Lambda_0)$ for various β, with $T = 0$, $\gamma = 0.15$.

In order to illustrate that the "overheating" condition (4) is really satisfied for the distribution function at $\xi = 0$, fig. 2 plots the values of $n(\xi = 0)$ as a function of Δ and, for comparison, the values of the thermal QDF $n_{\mathrm{T}}(\xi = 0)$. As can be seen from fig. 2, $n(\xi = 0)$ is less than $n_{\mathrm{T}}(\xi = 0)$ for any γ and T, in accordance with condition (4).

Numerical solution of the system $(6, 11, 12, 26)$ has been performed by Imai (1980), confirming the results of Elesin et al. (1979). Imai (1980) performed his calculations, using the general

[0]*This equality can easily be demonstrated for the simple case $N_\varepsilon = 0$. Then, according to Elesin (1976), $n_0(s) = \frac{1}{2}\,(1 - 2\Delta a_1/a_2)$, the ratio $2a_1/a_2$ is equal to $1/2T_{\mathrm{c}}$ (Elesin et al. 1977a), so we arrive at the equality in question.

formula for a quasiparticle source Q. for frequencies (1)$\Delta_0 = 2, 1$ and 8, 20, reabsorption parameters $\gamma = 0, 1, 10$, and different temperatures. The QDF for (1) $\Delta_0 = 8, 20$ (wide source) differ little from each other (see fig. 3) and from those obtained by Elesin et al. (1979). This con-

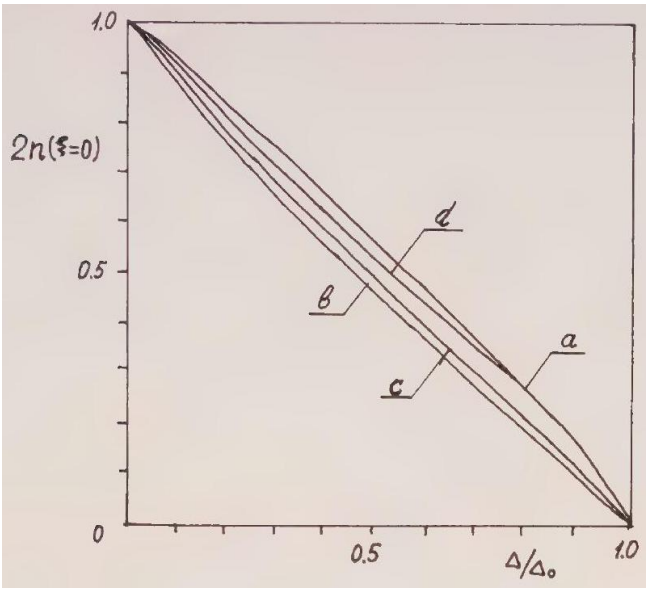


Fig. 2. Dependence of $2n(\xi = 0)$ on the order parameter: (a) according to the BCS theory; $(b - d)$ nonequilibrium distribution function with (b) $\gamma=0$, $T / \Delta_{0} =0$, (c) $\gamma = 0.15, T/\Delta_0 = 0$, (d) $\gamma = 0.15$, $T/\Delta_0 = 0.44$. (Elesin et al. 1979.)}

firms the conclusion, substantiated by Elesin (1974), that the shape of a wide source is insignificant. The reason is that $n(\xi)$ is formed mainly for $\xi \leqslant \Delta_0$ due to rapid relaxation of quasiparticles with $\xi \gg \Delta_0$.

Figure 3 clearly shows the effect of the reabsorption coefficient γ on $n(\zeta)$. The function n with $\gamma = 1$ decays faster with increasing ξ than n with $\gamma = 0$.

It would be of interest to approximate the monotonous function n by the quasiequilibrium QDF

$$n_{\mathrm{F}}(\xi) = \left[\exp\left(\frac{\varepsilon - \mu^*}{T^*}\right) + 1\right]^{-1} \tag{42}$$

considering μ^* and T^* as fitting parameters*. It should be noted first of all that for any values of μ^* and T^* the functions n and n_{F} cannot be fitted to each other exactly in the whole energy range (the discrepancy is especially large for $\gamma \to 0, T \to 0$).

If approximation is performed with respect to the minimum of the deviation $(n - n_{\mathrm{F}})$ within the entire energy range, μ^* and T^* can be found to $5 - 10\%$ for

any set of the parameters β, γ and T (Elesin et al. 1979). The dependences of μ^* and T^* on β for various T and γ are shown in fig. 4.

As can be seen from the figure, both parameters are different from zero, the effective chemical potential always being negative, $\mu^* < 0$, and the effective temperature T^* can exceed T_c. Both parameters are functions of $T_{,\gamma}$ and β, and in the interval $\beta_{\mathrm{c}} < \beta < \beta_{\mathrm{H}}$ they are two-valued functions of β. Negative values of μ^* mean, obviously, that the value of the function n is less than $\frac{1}{2}$. For small A the chemical potential can be related to the coherence correction:

[0]*The fact that this is only an approximation is clearly seen from the following example. At $T = 0, \gamma = 0, n(\xi)$ is determined from eq. (12) when neither of the terms S^+(or S), S^{R} vanishes separately (as it must be in equilibrium).

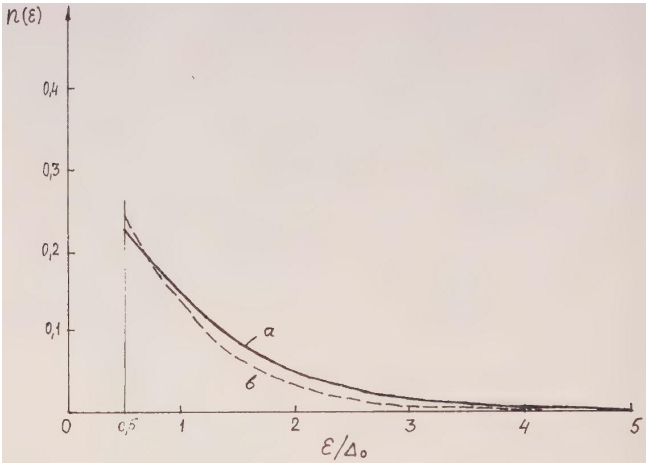


Fig. 3. Dependence of the QDF $n(\varepsilon)$ on ε / Δ_{0} for $T/T_c = 0.5, \Delta/\Delta_0 = 0.5$: (a) $\omega/\Delta_0 = 8.20, \gamma = 0$; (b) $\omega/\Delta_0 = 8, \gamma = 1$. (Imai 1980.)

$$\mu^*/4T_c = n_1(\xi = 0), \tag{43}$$

which makes quite clear why μ^* has a negative value in superconductors.
It is interesting to note that the "effective temperature" T^* exceeds T_c (the ratio T, T, may be as high as 1.55), but at the same time the order parameter is nonzero ($1.A_0 \geqslant 0.3$). This means that T^* cannot be considered as a temperature and also clearly indicates (together with $\mu^* < 0$) that quasiparticles are "overheated".

The conclusions that μ^* is negative and $T^* > T_c$ were confirmed by Imai (1980) who obtained (by approximating n for two points $\varepsilon = A$ and $\varepsilon = 3A$ with

$\omega/\Delta_0 = 20, \gamma = 0$) the following values:

$$\mu^* = -0.91\Delta, T^*/T_c = 1.4.^*$$

Let us compare the QDF in the E-model with the QDF in the μ^*- and T^*-models. [The μ^* - and T^*-models have been analysed in detail by Tremblay (1981).] It should be stressed that although in the E-model the quasiparticle distribution function can be parametrized in an approximate manner, using μ^* and T^*, the fact that both these parameters must change simultaneously means that the predictions of this theory differ significantly from those of the μ^* - and T^*-models. This has to be clear from the above considerations and the discussion which follows.

Equation (43) shows that if the coherence correction is neglected, the chemical potential μ^* can be put equal to zero, to give the function $n_0(\varepsilon)$ close to that in the T^*-model. Hence, the T^*-model does not allow for the coherence of interaction. Obviously, the T^*-model becomes a good approximation for $; \gg 1, T \to T_c$. A similar conclusion was made by Chang et al. (1979). As far as the μ^*-model is concerned, the function (1) possesses the properties $n_{\mu^*}(0) > n_1(0), n_{\mu^*}(0) > \frac{1}{2}, \mu^* > (T \to 0)$, which differ significantly from those for $n(\xi)$ in the E-model, the discrepancy being related to the fact that the QDF (1) satisfies the kinetic equation under the condition (Vardanyan and Ivlev 1973, Elesin 1976)

$$\bar{n} < \tilde{n} = \frac{1}{28} (T/\Delta_n)^{7/2} \ll 1. \tag{44}$$

This means that the μ^*-model is inapplicable for $T = 0$ [see the paper by Elesin et al. (1976b) where the solution has been found for $T = 0$ and $\ddot{n} \to 0$] and also for $\bar{n} > \tilde{n}$. And it is this region, into which the non-trivial predictions of the μ^*-model fall.

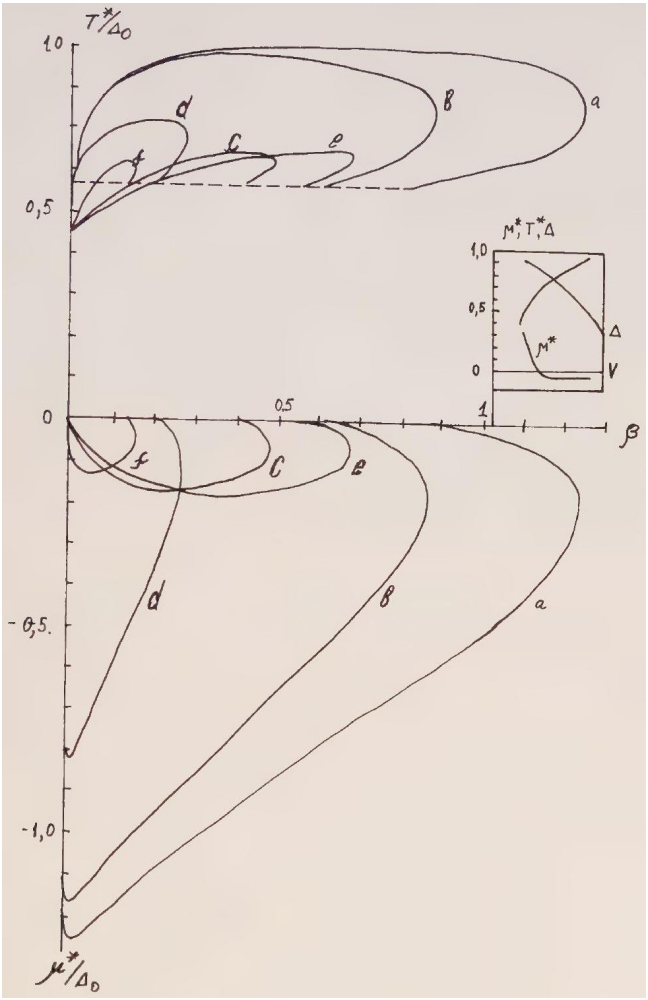


Fig. 4. Dependence of the parameters $T^{*} and μ^* on the source power β. The values of the parameters γ and T : (a) $\gamma = 0, T = 0$; (b) $\gamma = 0.02, T = 0$; (c) $\gamma = 0.02, T/\Lambda_0 = 0.44$; (d) $\gamma = 0.15, T = 0$; (e) $\gamma = 0, T/\Delta_0 = 0.44$; (f) $\gamma = 0.15, T/\Delta_0 = 0.44$. (Elesin et al. 1979.)}

As was noted by Elesin (1976, 1977b, 1979a) and Eckern et al. (1979), a model alternative to the E-model is, in principle, possible, if one takes $\eta = -1$ in the coherence factors (the NE-model, where N stands for negative). In this model the function satisfies the condition

$$\frac{1}{2} > n_{\mathrm{NE}}(\xi = 0) > n_{\mathrm{T}}(\xi = 0) \tag{45}$$

that is, the distribution is "overcooled" (as in the μ^*-model), but n_{NF} does not exceed $\frac{1}{2}$. The NE-model leads to predictions significantly different from those of the μ^*-model, though in the former model the chemical potential is positive by virtue of eq. (43).

Let us consider the effect of electron-electron collisions. It is usually accepted (Eliashberg 1970, Vardanyan and Ivlev 1973) that electron electron collisions have only a small effect on the form of the QDF for $\xi < A_0$ because

the ratio C of the constants of electron-electron and electron-phonon interactions,

$$C = \frac{\tau_{\mathrm{ph}}}{\tau_{\mathrm{ee}}} = \frac{a\omega_{\mathrm{D}}^2}{\pi |g| E_{\mathrm{F}} \Delta_0}, \tag{46}$$

[0]*"Overheating" of quasiparticles has been observed experimentally by Willemsen and Gray (1978) (see section 1.2.11).

is small.
However, corrections to $n(\xi)$ due to electron-electron (e-e) interaction may, in general, be significant even for small C since the nonequilibrium state is very sensitive to the form of $n(\xi)$. Moreover, in certain superconductors $C > 1$, for instance, in aluminium [see the Tables in the articles by Aronov and Spivak (1978) and Elesin and Kopaev (1981)].

The effect of e e interaction on the form of $n(\xi)$ has been studied by Aronov and Spivak (1979) and Elesin (1981).

Elesin (1981) studied the behaviour of $n(\check{\zeta})$ near the phase transition region ($A/A_0 \ll 1$) with due account for e-e collisions, and showed that this behaviour remains qualitatively unchanged, at least for not too large G.

In fact, it follows from eq. (17) that the function $n(\xi)$ has the properties

$$n_0(\xi) < \frac{1}{2}, \quad n_0(0) = \frac{1}{2}, \quad (\text{ any } C)$$

and

$$\xi \to \infty, \quad n_0(\xi) \sim \xi^{-4}.$$

If the electron-phonon and electron-electron interactions are taken into account, the coherence correction can be represented in the form

$$n_1 = -\frac{\Delta^2 a_1}{2\varepsilon\pi\tilde{a}_2}\left(\varphi_{\text{ph}} - G\varphi_{\text{ee}}\right) \tag{47}$$

where

$$\varphi_{\text{ee}} = \iint_0 \mathrm{d}x_1\ \mathrm{d}x_2 \frac{x_1^2 + x_2^2 + x_1 x_2}{x_1\left(x_1 + x_2\right) x_2}\varphi_{\text{ee}}\left(x_1, x_2\right) \tag{48}$$

$$\varphi_{\text{ec}}\left(x_1, x_2\right) = n_0\left(x_1 + x_2\right)\left[1 - n_0\left(x_1\right)\right]\left[1 - n_0\left(x_2\right)\right] - n_0\left(x_1\right) n_0\left(x_2\right)\left[1 - n_0\left(x_1 + x_2\right)\right] \tag{49}$$

$$\tilde{a}_2 = a_2 + C S_{\text{ee}}^{+}\left(n_0, 0, 0\right) \tag{50}$$

Let us note first of all that the contribution to $n(\xi)$ from the coherence factors due to electron-electron interaction appears to be opposite to that due to electron-phonon interaction. This means that inclusion of electron electron collisions leads to a positive correction to the chemical potential.

The nonequilibrium function φ_{ee} is proportional to the difference of recombination and production rates, so the equilibrium QDF n_{T} makes φ_{ec} vanish, as well as φ_{ph} .

Yet, there is an essential difference between φ_{ph} and φ_{ee}. This lies in the fact that in thin films (and for $T \to 0$), when the number of phonons is small, quasiparticle production processes due to phonons are suppressed and φ_{ph} reaches a value of the order of unity. A second term describing quasiparticle production is always present in φ_{ee}, so this function is small and, probably, always less than φ_{ph}.

Hence, for not very large values $C < 1$ the main contribution is due to φ_{ph}, so we obtain the earlier results, but with a certain renormalization (Elesin 1981).

If C is sufficiently large (which is unlikely to occur in practice), the situation appears to be more complicated because the problem of finding $n_0(\zeta)$ for large C and calculating φ_{ph} and φ_{ee} is difficult to solve. Although estimates performed with due account for the fact that φ_{ce} has to decrease with increasing C indicate that the phonon contribution should dominate, it is not excluded that n_1 may change sign (which would lead to the NE-model). Only particular calculations may give the final answer.

Aronov and Spivak (1979) investigated the effect of electron-electron collisions on $n(\xi)$; this function was sought in the form

$$n = \exp\left(\frac{\mu^* - \varepsilon}{T^*}\right) \tag{51}$$

and μ^* and T^* were found from the conservation laws for the number of quasiparticles and for the energy (for details see Aronov and Spivak 1978). These authors conclude that the chemical potential may become negative in a certain pumping power range. if electron-electron collisions are taken into account. This contradicts, in general, the result obtained by Elesin (1981) (see eq. 47), because the contribution of the coherence factors to the function n_1 due to electron-electron interaction leads to a positive correction to μ^* as well. Direct comparison of the results is, however, difficult because the function (51) is applicable only for very low pumping intensities.

22.3.2 1.2.2. The order parameter

The order parameter is quite sensitive to the energy distribution of quasiparticles, especially for $\breve{\xi} = 0$. "Overheating" of quasiparticles leads, as Elesin (1976) was the first to show, to an ambiguous dependence of the order parameter A on the pumping power β, starting with a certain critical value β_c. Following the paper by Elesin (1976), let us derive an equation for A, assuming that AA_0 is small. Using the properties of $n_0(\delta)$ and relation (34), we obtain from eq. (6) to within Δ^2

$$\Delta\left(\delta + \alpha\Delta^2 + 2\int \frac{n_1}{\varepsilon}\,\mathrm{d}\xi\right) = 0 \tag{52}$$

$$\delta = \frac{a_1 - a_{1c}}{a_{1c}} \tag{53}$$

where α is a numerical coefficient to be defined below. Note that the expansion in eq. (52) appears to be a good approximation in a wide range of Δ (Elesin 1977b). Substituting n_1 into eq. (52), we obtain the equation for the order parameter and the expression for the energy (8) of a non-equilibrium superconductor (Elesin 1976, 1977b):

$$\Delta\left(\delta + \alpha\Delta^2 - \varphi\Delta\right) = 0 \tag{54}$$

$$U(\Delta, \delta) = \Delta^2\left(\frac{\delta}{2} - \frac{\varphi\Delta}{3} + \frac{\alpha\Delta^2}{4}\right) \tag{55}$$

This result was confirmed in subsequent papers (see, for example, Eckern et al. 1979). Equations (54) and (55) differ from the Ginzburg-Landau equation by the presence of a term, linear in Δ, with the coefficient of "non-equilibrium" φ (and also by the form of coefficients δ and α). The solution of eq. (54) is

$$\Delta_1 = 0, \quad \Delta_{2,3} = \frac{\varphi}{2\alpha}\left(1 \mp \sqrt{1 - \frac{4\alpha\delta}{\varphi^2}}\right), \tag{56}$$

i.e. for $\varphi \neq 0$ two more solutions exist besides the trivial solution $\Delta_1 = 0$: one solution, Δ_3, decays with increasing β; the other, Λ_2, grows with β and appears for $\delta > 0$ or $\beta > \beta_c$. Both solutions merge at $\delta = \delta_H = \varphi^2/4\alpha$ so the "two-value" interval of $\Delta(\beta)$ is equal to $\varphi^2/4\alpha$. The coefficients $\delta = c\,(\beta - \beta_c)\,, \beta_c, \alpha$ and φ depend, in general, on T,;and k. They have been determined by Elesin et al. (1977a,b, 1979) and have been presented by Elesin and Kopaev

(1981). In particular, for $\gamma = 0, T = 0, k = 1$ we have $\varphi = 1, \alpha = 1.9, C = 0.37, \beta_c = 0.83$; and for $\gamma = 0, T \to T_c, k = 1$ one obtains (Elesin 1976)

$$\varphi = \beta\zeta_3, \quad \delta = \frac{T - T_c}{T_c} + 2\beta\zeta_2 \tag{57}$$

where ζ_i is a coefficient of the order of unity.
It is also useful to consider the dependence of Δ on temperature for $\beta \neq 0$ (Elesin 1976). It can easily be seen that for

$$T > T_c\,(1 - 2\beta\zeta_2)$$

the dependence $\Delta(T)$ becomes two-valued. Numerical calculations (Elesin et al. 1977a,b, 1979) made it possible to find $A(\beta)$ in a wide range of β, γ and T. The dependences $\Delta(\beta)$ for $k = 1$ are shown in fig. 5. It can be seen from this figure that for all T and γ there is a branch of the solution $A(\beta)$, increasing with β, which appears at a power exceeding the critical one. As T and γ grow, the two-value region of $\Delta(\beta, T)$ get narrower, but the slope of $\mathrm{d}\Delta\mathrm{d}\beta$ remains positive.

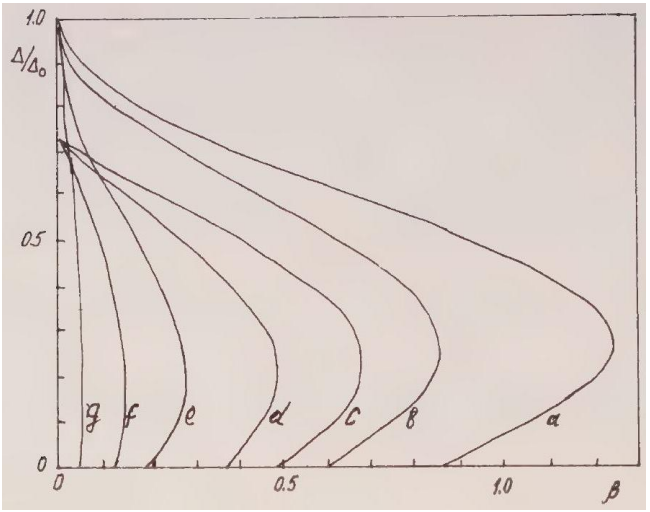


Fig. 5. Dependence of the order parameter on the source power β for different values of the parameters γ and T : (a) 0,0 ; (b) $0.02, 0$; (c) $0, 0.44$; (d) $0.02, 0.44$; (e) $0.15, 0$; (f) $0.15, 0.44$; (g) $1.0, 0$.

(Elesin et al. 1979.)

Even more detailed calculations of $\Delta(\beta)$ have been performed by Imai (1980). For the same values of the parameters they agree completely with those of Elesin et al. (1977b, 1979). Figure 6 presents the dependences of Δ/Δ_0 on β/β_c for $T/T_c = 0.5$ and different values of ω/Δ_0 and γ. The cases $\omega/\Delta_0 = 8$ or 20, $\gamma = 0$ differ little and coincide with the corresponding cases in fig. 4. A decrease in (1) A_0 leads to a considerable increase in Δ on the upper branch. This is illustrated by the curve with $\omega/\Delta_0 = 2.1$. In particular, the value of $\Delta\,(\beta_c)\,/\Delta_0$ reaches 0.72 . The curves $\Delta(\beta)$ with $\gamma = 1$ in fig. 6, and also with $\gamma = 1, 10$, show the effect of phonon reabsorption on the dependence $\Delta(\beta)$. It can be seen that the ambiguity region remains considerable even for large $\gamma = 10$, the decay being slower for smaller values of $(\omega), A_0$. These results agree with conclusions of Elesin (1977b) that $\mathrm{d}A\ \mathrm{d}\beta > 0$ for whatever large γ. The conclusions are based on the fact that the nonequilibrium function φ, which determines the derivative $\mathrm{d}\Delta/\mathrm{d}\beta$ (or $\mathrm{d}\Delta/\mathrm{d}\delta$), is positive

$$\left.\frac{\mathrm{d}\Delta}{\mathrm{d}\delta}\right|_{A=0} = \frac{1}{\varphi}. \tag{58}$$

Relation (58) implies several important consequences. If $\varphi < 0$, the anomalous solution disappears and A vanishes for $\beta = \beta_c$ with a finite negative derivative $\mathrm{d}\Delta/\mathrm{d}\beta$ (or $\mathrm{d}\Delta/\mathrm{d}\delta$). In the limiting case $\varphi = 0$ (equilibrium or

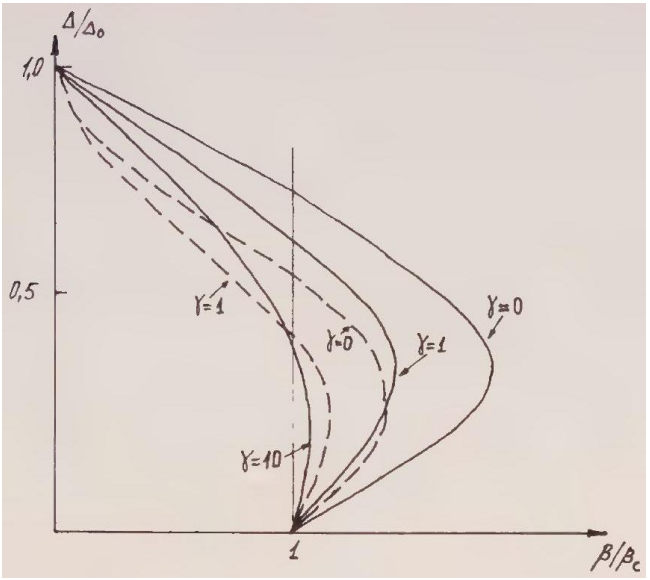


Fig. 6. Dependence of $\Delta / \Delta_{0} on β/β_c for $\gamma = 0, 1, 10$. Solid curve: $\omega/\Delta_0 = 2.1$; dashed curve: $\omega/\Delta_0 = 8.$}

disregard of coherence) a second-order transition with infinite derivative occurs.
Such a strong dependence of Δ on n_1 can be explained by the fact that n_1 appears in the gap equation together with the function $1-2n_0(\varepsilon)$, which is small near $\xi = 0$. And it is this interval of small ξ, where $n_0(0) = \frac{1}{2}$, which contributes mainly to the integral (6).

Figure 7 presents the dependences for three cases:
(1) $\eta = 1, \varphi > 0$ (this case corresponds to the E-model, first-order transition);
(2) $\eta = 0, \varphi = 0$ (second-order transition);
(3) $\eta = -1, \varphi < 0$ (the NE-model, second-order transition with a finite derivative).

Now compare the results with those of the μ^* - and T^*-models. Obviously, case (2) corresponds to the T^*-model, in which $\Delta(\beta)$ is single-valued.

In the μ^*-model Δ is a two-valued function for any β (Tremblay 1981) (for $T \to 0$), while in the E -model the second solution appears only for $\beta > \beta_{\mathrm{c}}$. Note that the prediction of the μ^*-model differs also from that of the NE-model, in which $\Delta(\beta)$ is single-valued (case 3). The above consideration referred to a spatially homogeneous state. Inhomogeneous states are described by the general system of equations (7, 11). In a number of cases they can be reduced

to one order-parameter equation. To this end, one has to find a solution of the kinetic equation (11), substitute it into the gap equation (7) and integrate with respect to ζ.

This calculation procedure was performed in the works of Elesin (1977b) and Eckern et al. (1979). In the general case, an inhomogeneous nonequilibrium state of a superconductor is characterized by two lengths: the coherence length ξ_0 and the quasiparticle diffusion length L.

The equation for Δ in the limiting case $\xi_0 \gg L$ and also for any ξ_0 and L under the assumption that Δ varies slowly was derived by Elesin (1977a) [for details see the review by Elesin and Kopaev (1981)]. Eckern et al. (1979) derived a similar equation for any L and $\check{\zeta}_0$ (as $T \to T_{\mathrm{c}}$) without assuming slow variation of A. This can be done by passing, in the

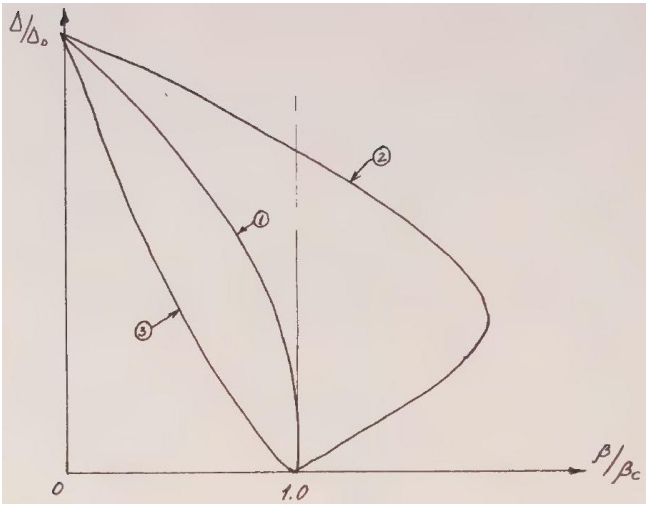


Fig. 7. Dependence of $\Delta / \Delta_{0
$ on β/β_c for (1) the T*-model, (2) the E -model and (3) the NE-model.
(Elesin 1977b.)}

kinetic equation (11), to a new representation, in which quasiparticle diffusion occurs under the condition $\varepsilon(r) = \text{const}$ [i.e. n depends on r only through $A(r)$]. The importance of this representation was noted by Smith (1977).

Using the method suggested by Eckern et al. (1979), Elesin and Kopaev (1981) derived a closed equation for Δ

$$\hat{\Pi}\left(\xi_0, L\right)\Delta = \frac{\partial U(\Delta, \delta)}{\partial \Delta}, \tag{59}$$

where the differential operator is given by $\hat{\Pi}\left(\xi_0, L\right)$,

$$\hat{\Pi}\left(\xi_0, L\right)\Delta = \left[\xi_0^2\nabla^2 + L^2\nabla^2\left(\delta + \alpha\Delta^2\right) - L^2\xi_0^2\nabla^4\right]\Lambda, \tag{60}$$

and U is the energy of a superconductor (eq. 55).
For $\xi_0 \gg L$ eq. (59) coincides with the equation obtained by Elesin (1977a); for $T \to T_c$ it coincides with the equation derived by Eckern et al. (1979).

For $\xi_0 \gg L$ eq. (59) has a structure similar to that of the Ginzburg-Landau equation, an essential difference being the presence of a third-power term proportional to the nonequilibrium function φ.

Time derivatives of Δ (needed for stability analysis) can be of two types. First, there is a term $\tau_\Delta(\partial\Delta/\partial t)$, which takes into account the variation of Δ with the order parameter relaxation time τ_1 (Eckern et al. 1979). This term is significant only for the analysis of the stability of the normal state. Second, there is a derivative which allows for a change in Δ due to variation of the quasiparticle distribution function. In the general case, this term is nonlinear in $\delta/\partial t$. But to analyse the stability, we are interested in small decrements $\tilde{\gamma}$ (near the stability limit), i.e. only in the term linear in $\hat{c}/\hat{c}t$. In this approximation the following equation for $\hat{c}\Delta$, $\hat{c}t$ can be obtained (Elesin 1977b, Eckern et al. 1979, Elesin and Kopaev 1981):

$$-\left(\tau_A + D\right)\partial\Delta/\partial t + \hat{\Pi}\Delta = \partial U/\partial\Delta, \tag{61}$$

$$D = \Lambda^2\int_0^\infty \frac{1-2n}{\varepsilon^3}\,\mathrm{d}\xi. \tag{62}$$

For $\gamma = 0, T = 0, D = \pi\Delta a_1/a_2$, eq. (61) coincides with that in the article by Elesin et al. (1980a); for $\gamma = 0, T \to T_c, D = \pi\Delta/4T_c$ it coincides with the equation derived by Eckern et al. (1979).

22.3.3 1.2.3. The number of superconducting electrons and magnetic properties

The magnetic properties of superconductors are closely related to the number of superconducting electrons N_S, because the linear response to a weakly varying magnetic field is (Abrikosov and K halatnikov 1958)

$$J = -\frac{e^2 N_0}{mc} N_S, \tag{63}$$

where N_S is given by

$$N_S = 1 + 2\int_0^\infty \frac{dn}{d\varepsilon}\, d\xi. \tag{64}$$

In equilibrium superconductors N_S is positive, in particular $N_S \sim \Delta^2$ for $T \to T_c$, which corresponds to anomalous diamagnetism.

The sign of $N_{S'}$ determines also the stability of a superconductor against inhomogeneous perturbations (see section 1.2.6), the case $N_s > 0$ corresponding to stability.

The sign of N_S has long been a debatable problem, but now it can be considered as solved, to a great extent: in all cases studied $N_S > 0$ for superconductors.

Let us prove first of all, following the papers by Elesin (1977a,b), that the sign of N_S is related to the sign of the coherence correction to the ODF n_1. Substituting $n(\xi)$ into N_S and using the general properties of $n_0(\varepsilon)$ (see section 1.2.1), we obtain the expression for N_S to within Δ^2

$$N_S = 1 + 2\int_0^\infty \frac{dn_0(\xi)}{d\xi}\, d\xi + 2\int_0^\infty \frac{dn_1}{d\varepsilon}\, d\xi = 2\int_0^\infty \frac{dn_1}{d\varepsilon}\, d\xi. \tag{65}$$

Since $n_0(0) = \frac{1}{2}$, the first two terms in eq. (65) cancel, and N_S is determined only by the coherence correction n_1.

Since the derivative $dn_1/d\varepsilon = -n_1/\varepsilon$ (see eq. 38), the expression for N_S can be rewritten in the form

$$N_s = \eta\varphi\Delta, \tag{66}$$

which implies that in the nonequilibrium case ($\varphi > 0$) the sign of N_S is determined by the sign of the coherence factor η. If $\eta = 1$ (superconductor), $N_s > 0$, that is, nonequilibrium superconductors with excess quasiparticles remain diamagnetic, and $N_S \sim \Delta$. The positive sign of $N_{S'}$ was confirmed in subsequent papers (Eckern et al. 1979, Elesin et al. 1979, Imai 1980) both analytically and numerically for the whole interval of Δ values and for a wide range of the other parameters.

Obviously, in the NE-model ($\eta = -1$) the sign of N_s becomes negative. This possibility was discussed by Elesin (1977b, 1979a) and by Eckern et al. (1979).

In the μ^*-model N_S is negative (Chang and Scalapino 1974, Baru and Sukhanov 1975), i.e. the μ^*-model predicts anomalous paramagnetism.* From the mathematical point of view this is related to a more rapid, in comparison with n_T, decay of the QDF with energy in the μ^*-model (the property of "supercooling").

The study of the effect of magnetic field and superconducting current on the state of superconductors with excess quasiparticles is an important problem. The fact is that a current is

usually passed through a film to measure the voltage across the film in the resistive state, as, for example, is the case with optical pumping or injection. In a number of cases the currents needed are almost equal to the critical ones. Therefore, Elesin (1980) considered the effect of magnetic field H and current state on the character of the phase transition in a superconductor with a wide source of quasiparticles. If the film is thin $\left(d < \tilde{\lambda}_3, \zeta_0; \tilde{\lambda}\right.$ is the London length) and the magnetic field is parallel to it, the

dependence $\Delta(\beta)$ retains its ambiguous character and the critical value β_c decreases with increasing magnetic field:

$$\beta_{\mathrm{c}}(H) = \beta_{\mathrm{c}} - \tilde{h}^2, \quad \tilde{h}^2 = \frac{1}{24}\left(\frac{H}{\tilde{H}_{\mathrm{c}}}\right)^2\left(\frac{d}{\tilde{\lambda}^2}\right)^2, \quad \tilde{H}_{\mathrm{c}} = 4\pi v(0)\Delta_0\zeta, \tag{67}$$

where $\hat{H}_{\mathrm{c}}$ is the "critical magnetic field", ζ is of the order of unity.
By varying the superconductor free energy (55), which allows for the contribution due to superconducting current and magnetic field, one can find the expression for the order parameter of a thin film:

$$\Delta = \frac{\varphi}{2\alpha}\left[1 \mp \sqrt{1 - \frac{4\alpha\delta(H)}{\varphi^2}}\right], \quad \delta(H) = \delta + \hat{h}. \tag{68}$$

It can be seen that the dependence $\Delta(\beta)$ has two branches, which appear for $\beta > \beta_{\mathrm{c}}(H)$, given by eq. (67).

Thus, the dependence $\Delta(\beta)$ retains its ambiguous character in a magnetic field. Note that as the magnetic field H increases at fixed β, the ordinary solution Δ_3 decreases, while a new solution Δ_2 grows. The diminishing of the critical power $\beta_{\mathrm{c}}(H)$ is of interest for experimental investigations because it permits the reduction of overheating of irradiated films.

It can also be shown (Elesin 1977a) that the value $\delta_0(H)$, at which the Gibbs energies of the normal and superconducting phases become equal to each other, is

$$\delta_0(H) = \delta_0 - \hat{h}. \tag{69}$$

In other words, the dependence $\Delta(\beta)$ shifts as a whole with increasing H. It should be noted that the results obtained here (and subsequent results) may find quantitative application for small δ.

Now let us consider the current state. If the current J is specified, expressing then the velocity in terms of Δ and J, we arrive at the following equation for Δ :

$$\Delta\left(\delta + \alpha\Delta^2 - \varphi A + \frac{\tilde{J}^2}{\Delta^2}\right) = 0, \quad \hat{J}^2 = \frac{J^2}{J_{\tilde{h},}^2}. \tag{70}$$

In this case the solution, which grows with β, does exist for all δ since the main contribution for small Δ is due to the term $\widetilde{J}^2/\Delta^2$, which is present in the equation also for $\beta = 0$.

Let us find the quantity $\delta_0(J)$. Using the expression for the energy and eq. (70), we easily obtain

$$\delta_0(J) = \delta_0 - \frac{9}{4}\alpha\tilde{J}^2. \tag{71}$$

Thus, the power needed for the first-order transition or for the transition of a superconductor into the inhomogeneous state decreases with increasing current.

[0]*It should be noted that the possibility of anomalous paramagnetism in nonequilibrium superconductors ($N_{\mathrm{S}} < 0$) with inverse quasiparticle distribution was first pointed out by Galitskii et al. (1973) (see section 2.5).

The decrease in the power becomes appreciable, if the current and magnetic field attain the values

$$J \simeq \frac{2\sqrt{2}}{9\alpha} J_{k\rho}, \quad H \simeq \tilde{H}_{\mathrm{c}} \left(24\beta_{\mathrm{c}}\right)^{1/2} \frac{\tilde{\lambda}}{d} \tag{72}$$

The critical current of a film vanishes at $\delta = \varphi/4\alpha$.
As was noted by Elesin (1976) the QDF determines the sign of the superconducting current in an external alternating electric field E_0 of frequency Ω. It can be shown (Elesin et al. 1973) that the expression for this current (if scattering from impurities is taken into account) is, for $\Omega \ll \Delta$:

$$J_{\mathrm{S}} = \mathrm{i}\sigma_{\mathrm{S}} E_0, \quad \sigma_S = \frac{\pi A}{\Omega} \sigma_{\mathrm{N}} (1 - 2n(\xi = 0)) \tag{73}$$

If the functions satisfy the condition (5), $n(0) < \frac{1}{2}$ (the E-, NE- and T^*-models), the conductivity is positive, typical of equilibrium superconductors. In the μ^* model σ_{S} changes its sign. Note that the change in the sign can be verified experimentally.

Moreover, if σ_{s} were negative, this would lead to a specific electrical instability (Elesin and Kopaev 1981), which arises as soon as $n(0) > \frac{1}{2}$. Indeed, the fluctuation of the charge would give rise to an electric field, which in turn would produce a current enhancing the charge fluctuation. The development of this instability would lead to the destruction of the superconducting state or to the formation of a certain inhomogeneous state.

22.3.4 1.2.4. The critical power of optical pumping

As was shown by Elesin (1974) (see section 1.2.2), the order parameter vanishes at a certain critical power β_c. This is the boundary from where a second solution for Δ appears. The critical power can be found by substituting the "critical" QDF $n_0(\xi)$ into the normalization condition (18):

$$\begin{aligned} \beta_{\mathrm{e}} (T, \gamma') = & \frac{1}{\Lambda_0^4} \int_0^{(\omega_1)} \mathrm{d}\xi \int_0^{(\omega_1)^-} \mathrm{d}\xi' \left(\xi + \xi'\right)^2 \\ & \times \left[n_0 n_0' - N_{\xi+\xi'} \left(1 - n_0 - n_0'\right)\right] + C \int_0^{\infty} \frac{\mathrm{d}\xi}{\Delta_0} I_{\mathrm{ee}}(\xi) \end{aligned} \tag{74}$$

This expression for β_{c} includes two terms having different physical meaning.
The last term, with a negative sign, describes the impact ionization of quasiparticles by high-energy quasiparticles, that is, it describes the multiplication of quasiparticles. Large ξ contribute to this term (see Vardanyan and Ivlev 1973), where the QDF $n_0(\xi) \sim \beta/\xi^4$ is proportional to the source power β. Transferring the last term to the left-hand side, we obtain instead of β_{c}

$$\beta_{\mathrm{c}} \to \beta_{\mathrm{c}} \left(1 + r_{\mathrm{ee}}\right) \tag{75}$$

where r_{ee} is the multiplication coefficient. For $C \ll 1, r_{\mathrm{ee}}$ has been found by Vardanyan and Ivlev (1973).

The addend $N\left(1 - n - n'\right)$ in the first term describes the production of quasiparticles due to equilibrium N_T and non-equilibrium $N = N_0(\xi) + N_v(\xi)$ phonons, where $N_0(\xi)$ stands for phonons produced under recombination and scattering of low-energy particles ($\xi \lesssim \Delta_0$) and N_{V} denotes phonons produced under scattering of high-energy quasiparticles. The contribution of these quasiparticles depends directly on the intensity β and describes the multiplication of

quasiparticles due to phonon absorption (the multiplication coefficient is $r_{\rm ph}$). In the remaining integral those energies $\xi \leqslant \Delta_0$ are significant, at which $n_0(\xi)$ is close to the thermal one (see section 1.2.1), so the following substitution is possible (Elesin 1977a):

$$\varphi_{\rm ph}\left(\check{\zeta}, \xi', T, , \eta'\right) = \frac{\varphi_{\rm ph}\left(\xi, \xi', T, \gamma = 0\right)}{1 + \gamma'\left(\xi + \xi'\right)/\Lambda_0} \tag{76}$$

The factor $\left(1 + \gamma\left(\xi + \xi'\right)/\Delta_0\right)$ accounts for an increase in the quasiparticle lifetime due to reabsorption processes. Obviously, it can be taken out of the integral sign in the form $(1 + \eta_i)$ where η_i is a quantity of the order of unity. Summarizing the results for $\beta_c(T, \gamma)$, we obtain

$$\beta_{\rm c}(T, \gamma) = \beta_{\rm c}(T)\left(1 + r_{\rm ec} + r_{\rm ph}\right)^{-1}\left(1 + \gamma\eta_\gamma\right)^{-1} \tag{77}$$

$$\beta_{\rm c}(T) = \frac{1}{\Delta_0^4}\int_0^\infty {\rm d}\xi \int_0^\infty {\rm d}\xi'\left(\xi + \xi'\right)^2 \times \left[n_0(\xi) n_0\left(\xi'\right) - N_{\rm T}\left(\xi + \xi'\right)\left(1 - n_0(\xi) - n_0\left(\xi'\right)\right)\right] \tag{78}$$

The coefficient $r_{\rm ph}$ is insensitive to ; and the dependence $\beta_{\rm c}\left(\gamma'\right)$ is mainly determined by the factor $(1 + \gamma\eta_i)$.

The temperature dependence of the critical power is given by a universal function $\beta_c(T)$. At $T = 0$ it reaches a maximum of 0.84 (Elesin et al. 1977a). As T grows, $\beta_{\rm c}$ decreases due to the production of thermal quasiparticles and for $T \to T_{\rm c}$ it is described by the expression $\beta_{\rm c}(T) = A\left(T_{\rm c} - T\right)$ (Elesin 1976). The dependence $\beta_{\rm c}(T)$ in the entire temperature range was found by Elesin et al. (1979) and is shown in fig. 8. The relationship between the measured power $W_{\rm c}\,({\rm W/cm^2})$ and dimensionless power $\beta_{\rm c}$ is given by the expression (Golovashkin et al. 1980)*

$$W_{\rm c} = \beta_{\rm c}(T)\frac{N_{\rm c}\hbar\omega}{4\tau_{\rm ph}\left(1 + \tau_{\rm ee} + \tau_{\rm ph}\right)\left(1 + \gamma\eta_\gamma\right)k_1^2 k(\omega)} \tag{79}$$

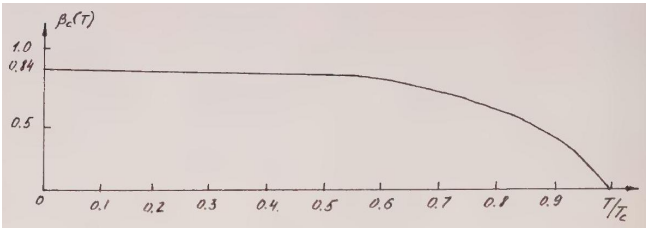


Fig. 8. Theoretical dependence of the dimensionless pumping $\beta_{\rm c}$ on $T/T_{\rm c}$. (Golovashkin et al. 1980.)

where $k(\omega), k_1^2$ are the coefficients of absorption and reflection of electromagnetic field. If one takes into account that usually in superconductors the thickness $d \gg k^{-1}(\omega), d^{-1}$ can be substituted for $k(\omega)$.

Comparison of $W_{\rm c}$ with experimental data is performed in section 1.2.11.

22.3.5 1.2.5. Current-voltage characteristics of tunnel junctions

The variation of Δ due to quasiparticle injection in tunnel junctions with a sufficiently low resistance may lead to a radical change in their currentvoltage characteristics.

[0]*Note that there is a misprint in the corresponding equation in the article by Elesin and Kopaev (1981); instead of $r_{\rm e} r_{\rm f}$ their formula should read $r_{\rm ee} + r_{\rm ph}$.

The effect of weak injection on the energy gap has been considered theoretically in several papers (see, for example, Kirichenko and Seminozhenko 1977).

Strong injection in SiS junctions at high voltages ($V \gg A$, wide source) has been studied by Elesin and Levchenko (1978) and Elesin et al. (1980a, b).

It was shown by Elesin et al. (1977b) that the order parameter vanishes at a critical voltage V_c, which satisfies the condition

$$\alpha_V \int_0^{\gamma_c} \frac{\mathrm{d}\xi}{\Delta_0} (1 - 2n_0) = \beta_c(T, \gamma) \tag{80}$$

In particular, for $T = 0, \alpha_V \ll 1$, the critical voltage

$$\frac{V_c}{\Delta_0} = \frac{\beta_c(0)}{\alpha_v} \gg 1 \tag{81}$$

is large in comparison with Δ, so under these conditions tunnel injection is equivalent to the effect of a wide source. Therefore, for $V > V_\mathrm{c}$ the dependence $\Delta(V)$ becomes many-valued. The multiplicity of $\Delta(V)$ leads, naturally, to multiplicity of the current voltage characteristics $J(V)$. Depending on the values of the parameters $\alpha_V, \hat{\gamma}$ and T, three types of $I - V$ characteristics (shown in fig. [9)] may exist. They may be classified according to relationships between the characteristic values of the currents J_c, J_0 and J_th (Elesin et al. 1980a.b):

$$J_\mathrm{c} = J\left(V_\mathrm{c}, \Delta = 0\right), \quad J_0 = J\left(V_0, \Delta = 0\right), \quad J_\mathrm{th} = J\left(V_\mathrm{H}, \Delta_\mathrm{H}\right), \tag{82}$$

where V_0 is the voltage at which the energies of the normal and superconducting phases become equal. Current-voltage characteristics of the first type correspond to the condition $J_0 > J_c > J_\mathrm{th}$, those of the second type to $J_0 > J_\mathrm{th} > I_\mathrm{c}$, and those of the third type to $J_\mathrm{th} > J_0 > J_\mathrm{c}$. As was shown by Elesin et al. (1980a) (see below, section 1.2.10), current voltage characteristics of types I and II lead to transition into the inhomogeneous state (with $d_3 \neq 0$ and $J_1 = 0$), while characteristics of type III lead to a first-order transition into the normal state.* The conditions for characteristics of each type to occur have been derived by Elesin et al. (1980b). Note that growth of T and γ may cause characteristics of type III to become those of type II.

The temperature dependence of the critical voltage $V_c(T)$ and the corresponding critical dimensionless current $J_c(T)$

$$\begin{aligned} J_c(T) &= \alpha_1 \int_0^1 \frac{d\xi}{d_0} (1 - 2n_0) + 2\alpha_1 \int_0^1 \frac{d}{d_0} \left[n_0(\xi) - n_0\left(\xi + I_c\right)\right] \\ &= \beta_c(T) + 2\alpha_V \frac{T_c}{A_0} \ln\left[1 + \exp\left(-\frac{V_c}{T_c}\right)\right] \end{aligned} \tag{83}$$

differs slightly from $\beta_c(T)$:

$$V_c(T) = \begin{cases} \beta_c(0)/\alpha_V, & T \to 0, \\ 2\sqrt{\frac{T_c \beta_c(T)}{\alpha_V \Delta_0}} \sim \sqrt{1 - T/T_c}, & T \to T_c, \end{cases} \tag{84}$$

Equations (83). (84) imply that I_c and J_c should decrease with increasing T. that is, the dependence is qualitatively similar to that of the power under optical pumping (cf. section 1.2.4).

22.3.6 1.2.6. Stability analysis. Coherent instability under optical pumping

The stability of nonequilibrium superconductors has been studied with respect to two classes of perturbations: fast perturbations (at times much less than the phonon relaxation time τ_{ph}) and slow perturbations (at times of the order of τ_{ph}).

The stability with respect to fast inhomogeneous perturbations was studied in several articles (Kemoklidze and Pitaerskii 1967. Aronor and Gurevich 1973. Chang and Scalapino 1974. Baru and Sukhanov 1975. Elesin 1977. Eckern et al. 1979. Imai 1980). The criteria obtained were identical, though

different in form. and in the limit $yl. = 1$ ig is the perturbation wave sector) they reduce to the following expression for the decrement $\tilde{\%}$ (Elesin and Kopaev 1981, Eckern et al. 1979)

$$\tilde{\gamma} = -q^2 L^2 \frac{N_{\text{s}}}{D}. \tag{85}$$

The sign of ; 1s determined by the signs of the number of superconducting electrons. 1 isee sectoon 1.2 .3) and of the quantit: 1) lisee eq. 621 . which are the functionals of steady-state QDF.

In the E-model X is prositive (see 1.2 .3) and J) - (1) bi wrtue of the properts (5) (n-in - is) the decrement is negatioe. - 11. Thus. the s.stem is stable against fast perturbatuns. and instabilittes are stabilized due to quasi-particle diffusion. This result as abotained b; Elesin 199-69 and confirmed by Flesm 11977a.b). and alor in papers by Feckern et al. 119'y) and Imal 11geron by somew hat different methods. I mas has performed computer-aded calculatoms in a wide range of the parameters.

In the NE-model $N - ()$ isce section 1.2.3) and D remains positive $\left(n - \frac{1}{2} \cdot 1\right.$. so the decrement ; is posstrie. In this case anomalous diffuston of quasiparticles a ould lead io the erhancement of inhomogenerous perturbations. that 13. to the so-called diffusion instability (see below, section 1.2.7).

The μ^*-model, in which $1, -1$). also predicts diffusion instability. I Chang and Scalapino 1974. Baru and Sukhano: 1975). It should be noted. however. that in the μ^*-model D mas becrme negative $\left(n - \frac{i}{2}\right)$ (for example. for $T \to (1)$ and $\mu^* > \sqrt{\frac{4}{3}A}$).

In the T^*-model $N_{\text{S}} > 0, D > 0, \tilde{\gamma} < 0$, and the superconductor is stable.
The stability; against sion perturbaturs has been studied b; Elesin 119-al. Eckern et al. (1979) and Imai (198()).

A tope of instabilit: pecific of superconductors atth a aide quasiparticle source was predicted b: Fiesm 19'GTai. aho called it coherent mstability. since it is related to the coherence of the interactum betseen quasiparticle and phomons. The instabilit: arroes in the state with $1 = 1$. corresponding to the increasing solutions lef. sectoon 1.2.21. To study coherent instabilit: one can proceed from the hinctic equation iflesin $19^{\top -}$ a. imal 1 yxon. ar the kinetic equation modified for $T \to T$. If.ckern et al. 1979). or equation iffi, for 1 1Elesin and Kopaes 19811. Let usconsider. following the paper by Elesin and Kopaev (1981), a homogeneous perturbation

$$\Delta(t) = \Delta + \dot{\Delta} \exp(\dot{r}t). \tag{86}$$

Substituting eq. $|xf_1|$ into eq. $|6|$ 1. ae obtain for the dimensoniev decrement

$$\tilde{i} = -\frac{1}{D} \frac{\hat{c}^2 U}{Di1^2}, \tag{87}$$

[0]*Transition into the inhomogeneous state for type-III characteristics is possible, if the injection current is reduced after the transition into the normal state (see fig. 9).

or using expression (55) for $U(\Delta, \delta)$

$$\tilde{\gamma} = \frac{2}{\Delta\delta}, \quad \Delta\delta \equiv \frac{\hat{c}\Delta}{\hat{c}\delta}. \tag{88}$$

Equation (88) shows that the increasing solution Δ_2 is unstable, while the solution Δ_3 is stable (the stability of the solution $\Delta_1 = 0$ is discussed below). It is a simple matter to demonstrate that the system passes into the normal state for $\Delta(t=0) < \Delta_2(\delta)$ and into the superconducting state for $\Delta(t=0) > \Delta_2(\delta)$.

The physical meaning of instability is as follows. Suppose that the gap in the state with A_2 on the increasing branch slightly decreases due to a fluctuation. Then the probability of quasiparticle recombination ($1+A^2/\varepsilon\varepsilon'$) will decrease and, hence, the number of quasiparticles (near $\xi \sim \Delta$) will increase. The equation for Δ implies that this will lead to a further diminishing of the gap, and so on.

It is interesting to note that when the system passes into the normal state (at a fixed β) an additional number of quasiparticles δn are produced due to a decrease in the re-combination rate.

It would be useful to relate the stability of a system to peculiarities of the energy $U(\Delta)$ by virtue of eq. (87). The dependence $U(\Delta)$ is shown in fig. 10 .

It can be seen that $U(\Delta)$ has three extrema Δ_1, Δ_2 and Δ_3, the values Δ_1 and Δ_3 corresponding to the minimum of $U(\Delta)$ and Δ_2 to the maximum. It is natural, therefore, that the solution Δ_2 is unstable.

Different energies $U(A_1)$ and $U(A_3)$ may correspond to the stable solution

A_1 and A_3. Thus, one of these states (with a higher energy) will be metastable and the other will be really stable. At a certain pumping power $\delta = \delta_0$ the energies of the states become equal and co-existence of the superconducting and normal phases, i.e. an inhomogeneous state, is possible. As was shown by Eckern et al. (1979), the time needed for a system to pass from the metastable to the stable state for $\delta \neq \delta_0$ is very long, if strong fluctuations and the nuclei of the stable phase are absent. Therefore, depending on the external conditions, a superconductor may undergo a first-order transition into the normal state either at $\delta = \delta_0$ or at $\delta = \delta_{\mathrm{H}}$ and $\delta = 0$, the transition in the latter case being accompanied with a hysteresis.

Using eq. (61), it is not difficult to obtain the decrement for inhomogenous perturbations:

$$\tilde{\gamma} = \frac{2}{\Delta\delta} - q^2 L^2 \tag{89}$$

The instability decrement is maximal at $q = 0$, but it remains positive also for inhomogeneous perturbations for $q^2L^2 <^2 /\Delta\delta$. This means that lamination into the superconducting and normal phases, i.e. transition into an inhomogeneous state, is possible under appropriate conditions. Figure 10 shows descriptively the lamination process. Suppose that an inhomogeneous fluctuation $\Delta(x)$ arises in a superconductor, which is in the state with Δ_2. Due to coherent instability, the order parameter in the state with $\Delta(x) < \Delta_2$ will drop down to $\Delta_1 = 0$, while in the state with $\Delta(x) > \Delta_2$ it will increase to Δ_3.

Equation (61) permits the analysis of stability of the normal state $\Delta_1 = 0$. The corresponding decrement $\tilde{\gamma}$ is (Elesin et al. 1981, Eckern et al. 1979)

$$\tilde{\gamma} = -\delta - q^2\xi_0^2 - \delta q^2 L^2 - L^2\xi_0^2 q^4 \tag{90}$$

that is, the normal state $A_1 = 0$ is stable for $\delta > 0$. The diffusion of quasiparticles and the order parameter leads to an additional stabilization. This result was obtained earlier by Elesin et al. (1976a) for the case of $\check{s}_0 \gg L$ and any $\check{s}_0 q$. Equation (61) permits also the study of stability of inhomogeneous solutions

$$\Delta(r,t) = \Delta(r) + \tilde{\Delta}\exp(\tilde{\gamma}t), \delta(t) = \delta + \tilde{\delta}\exp(\tilde{\gamma}t) \tag{91}$$

In this case we obtain for $\tilde{\Delta}(r)$ the equation

$$\left(\hat{\Pi} + \frac{\partial^2 U}{\partial \Delta^2}\right)\tilde{\Delta}(r) + \left(\frac{\partial^2 U}{\partial \Delta \partial \delta}\right)\tilde{\delta} = -\tilde{\gamma}D \tag{92}$$

the decrement $\tilde{\gamma}$ being an eigenvalue of this equation.
The conditions of coherent instability may be satisfied under tunnel injection at high voltages $V \gg \Delta_0$ (Elesin and Levchenko 1978). The possibility of fixing the current is an essential difference from the case of optical pumping (Elesin and Levchenko 1978). In the regime of a given current (corresponding
to large R) eq. (25) should be added and a change in the voltage,

$$V(t) = V + \tilde{V}\exp(\tilde{\gamma}t), \tag{93}$$

should be taken into account. We then obtain for $\hat{i}$ (Elesin and Kopaev 1981)

$$\tilde{\gamma} = \frac{1}{\Delta_{\mathrm{V}}}\frac{1 + R\,\mathrm{d}J/\mathrm{d}V}{1 - RJ_{\mathrm{V}}} - q^2L^2, \quad J_{\mathrm{V}} = \left(\frac{\partial J}{\partial V}\right)_{\Delta} \tag{94}$$

$$\frac{\mathrm{d}J}{\mathrm{d}V} = J_{\mathrm{V}} + J_{\Delta}\Delta_{\mathrm{V}}, \quad J_{\Delta} = \left(\frac{\partial J}{\partial \Delta}\right)_{\mathrm{V}}, \quad \Delta_{\mathrm{V}} = \frac{\partial \Delta}{\partial V}. \tag{95}$$

Consider the current-voltage characteristic of type I (see fig. 9). If the current exceeds J_{th} , we are first at the descending portion of the current-voltage characteristic corresponding to $A = A_2$. The homogeneous solution is stable against homogeneous perturbations for a fixed current. Indeed, since on the descending portion of the current-voltage characteristic $\mathrm{d}J/\mathrm{d}V < 0$ (but $J_V > 0$ and $1 + RJ_{\mathrm{V}} > 0$), $\tilde{\gamma}$ is negative for R satisfying the condition $|\mathrm{d}J/\mathrm{d}V|R > 1$. This is how, for example, the state with $\Delta = \Delta_2$ is approached in a superconductor.

This state, however, appears to be unstable against inhomogeneous perturbations which do not alter the total current, i.e. satisfy the condition

$$\int \mathrm{d}^2 r\tilde{\Delta}(r) = 0 \tag{96}$$

In this case the decrement $\tilde{\gamma}$ becomes positive for perturbations which vary in space sufficiently slow, $\tilde{\gamma} = \Delta_{\mathrm{V}}^{-1} - q^2L^2$, and the sample is laminated into the normal $\Delta_1 = 0$ and superconducting Δ_3 phases (see above) along the current direction, the regions with smaller Δ and higher currents alternating with those of larger Δ and lower currents.

A similar lamination occurs for current voltage characteristics of types II and III.

22.3.7 1.2.7. Diffusion instability

Diffusion instability caused by possible anomalous diffusion of quasiparticles has been predicted by Chang and Scalapino (1974) and by Baru and Sukhanov (1975). The diffusion of quasiparticles is assumed to proceed from the region with large order parameter land correspondingly low quasiparticle concentration $\bar{n}$) to the region with small Δ (and large $\bar{n}$).

Instability develops in the following way. Suppose that Δ decreased in a certain region of space. Then, the gradient of Δ leads to a flow of quasiparticles, which further diminishes A, and so on. The conditions under which diffusion instability may occur. (85), are determined by the sign of the quantities N_{S} and D (eq. 64), which is a functional of $n(\xi)$. As was already noted, the QDF in the μ^* - and NE-models satisfy the condition $n(0) > n_T(0)$ ("super-

cooled" QDF) and yield $N_S < 0, D > 0$ to meet the conditions for the occurrence of diffusion instability. However, in superconductors with optical and tunnel pumping the quasiparticle distribution is "overheated" and $N_S > 0$, so diffusion instability cannot take place.*

At the same time, in an exciton insulator where the signs of the coherence factors are opposite to those in superconductors (see section 1.1.2) the NEmodel is applicable. The possibility of diffusion instability occurring in an exciton insulator was pointed out by Elesin (1979a) who derived the conditions for diffusion instability to take place and calculated the wave vector with which the spatial variation of $\Delta(r)$ is modulated.

22.3.8 1.2.8. Inhomogeneous states in the E-model

The development of coherent instability leads to the formation of an inhomogeneous laminated state (Elesin 1977a) described by the steady-state equation (59). The structure of the inhomogeneous state in the E-model was studied by Elesin (1977a), Elesin et al. (1980a, b) and by Eckern et al. (1979).

It is a simple matter to understand the situation in the one-dimensional case when quasiparticle diffusion is neglected ($\xi_0 \gg L$). In this case eq. (59) takes the form (Elesin 1977a)

$$\frac{\mathrm{d}^2\Delta}{\mathrm{d}x^2} = \frac{\partial U}{\partial \Delta}, \quad x \equiv \frac{x'}{\xi_0}, \tag{97}$$

$$\left.\frac{\mathrm{d}\Delta}{\mathrm{d}x}\right|_{x=+1/2} = 0, \tag{98}$$

where l is the film length.
The first integral of this equation is

$$\frac{1}{2}\left(\frac{\mathrm{d}\Delta}{\mathrm{d}x}\right)^2 = C - U(\Delta), \quad C = U\left(\Delta^{(2)}\right) = U\left(\Delta^{(3)}\right) \tag{99}$$

where C is a constant and $A^{(i)}(i = 1, 2, 3, 4)$ are the roots of the equation

$$C - U\left(\Lambda^{(i)}\right) = 0.$$

Analysis of the trajectories leads to the following possible spatially inhomogeneous solutions for Δ (Elesin 1977a; see also Eckern et al. 1979, and Tremblay 1981):
(1) oscillating from $\Delta^{(2)}$ to $\Delta^{(3)}$;
(2) narrow layers with $\Delta \neq 0$ or $\Delta = 0$ (soliton-type solutions):
(3) monotonous solutions.

In order to find out which of these solutions are stable, one has to analyse their stability with the help of eq. (92). This analysis shows (Elesin and Kopaev 1981, Eckern et al. 1979, Tremblay 1980) that only the monotonous solutions are stable, with stability for $\delta \neq \delta_0$ and under the additional conditions

$$\frac{\mathrm{d}\bar{J}}{\mathrm{dV}} < 0, \quad R > \left|\frac{\mathrm{d}\bar{J}}{\mathrm{dV}}\right| \tag{100}$$

0

- Yet, it is not forbidden, in principle. For example, the possibility is not excluded for diffusion instability to occur in superconductors with strong electron electron interaction (see section 1.2.1). The assumption has been made (Eckern et al. 1979) that the case $N_S < 0$ is possible under phonon pumping.

which are satisfied for a given tunnel injection current.
Among the monotonous solutions there is a specific one (connecting the singular points $A_{10} = 0$ and $\Delta_{30} \neq 0$), which is called the laminated solution. This solution occurs for a certain value of $\delta_0, C = 0$, at which the energies of the phases are equal

$$U(\Delta_{10}) = U(\Delta_{30}), \quad \delta_0 = {}^{2/9}\,\mathrm{d}, \quad \Delta_{30} = {}^{2/3}\alpha, \tag{101}$$

$$\Delta(x) = \frac{\Delta_{30}}{1 + \exp\left[-\sqrt{\delta_0}\,(x + x_0)\right]}, \tag{102}$$

where x_0 is the position of the junction boundary. It is noteworthy that the boundary conditions do not fix the position x_0.

The monotonous solutions for $\delta \neq \delta_0$ were found by Elesin et al. (1980b). In particular, for long films ($l \gg \xi_0$) and $\delta > \delta_0$ we have

$$\Delta(x) = \Delta_3 - \frac{4by}{y^2 - 2by + (\Delta_2 - \Delta_1)^2}, \tag{103}$$

$$y = (\Delta_2 - \Delta_1) \exp \sqrt{\frac{\alpha b}{2}} \left(x + \frac{1}{2}l\right) \tag{104}$$

$$b = (\Delta_3 - \Delta_2)(\Delta_3 - \Delta_1), \quad b = \Delta_1 + \Delta_2 - 2\Delta_3.$$

The order parameter $\Delta(x)$ increases monotonously from its minimal value $\Delta_{\min} = \Delta\left(-\frac{1}{2}l_2\right)$ to the maximal one $\Delta_{\max} = \Delta\left(\frac{1}{2}l\right)$, and for $\delta \to \delta_0$

$$\Delta_{\min} = \frac{2}{3}\sqrt{\frac{\delta - \delta_0}{\delta_0}} \tag{105}$$

and $\Delta_{\max} = \Delta_3$ increases slowly to $2/3\alpha$.
Let us now take into account the diffusion of quasiparticles, considering, for simplicity, the inverse limiting case $L \gg \xi_0$. It was shown (Elesin 1977a, Eckern et al. 1979, Elesin and Kopaev 1981), for the one-dimensional case, that the inclusion of quasiparticle diffusion does not qualitatively alter the structure of the inhomogeneous state. The width of the intermediate region $\check{\zeta}_0$ is replaced by L, and the parameter δ_0 changes slightly (by $5^\circ{}_0$). According to Eckern et al. (1979) and to Elesin and Kopaev (1981), the pumping value at which the
phase energies become equal is

$$\delta_0(L) = \frac{15}{64\alpha} = \frac{2.5}{9\alpha} \tag{\prime}$$

In the two-dimensional and three-dimensional cases the problem is much more complicated and cannot be solved completely. Although assumptions have been made that the qualitative results must be the same (see Volkov and Kogan 1968), it is quite possible that geometrical factors may affect the structure of the inhomogeneous state.

The effect of spatial inhomogeneities of the original films and also of boundary conditions on the structure and stability of inhomogeneous states requires further investigation. In particular, the boundary condition corresponding to a superconductor-insulator interface has been used in eq. (98). In particle, however, this choice of the boundary condition is not unique. For example, under optical pumping current metal contacts are placed at the ends of the sample. A superconductor-metal interface requires, of course, another boundary condition.
1.2.9. Inhomogeneous unsteady state in superconductors with optical pumping In superconductors with optical pumping the frequencey ω is fixed ($R = 0!$). Therefore, according to eq. (100) a steady-state inhomogeneous solution exists for a single value of the pumping power δ_0.

For $\delta \neq \delta_0$ the phase boundary will move at a velocity proportional to the difference $\delta - \delta_0$ (Elesin 1977a). In particular, for $L \ll \xi_0$ the phase boundary velocity is

$$v_c = \frac{(\delta - \delta_0)}{\delta_0} \frac{3\xi_0 \delta_0^{1/2}}{\tau\Delta} \tag{106}$$

In fact, we seek a solution of eq. (61) in the form of a travelling wave $\Delta(x - v_c t)$. The equation for $\Delta(x - v_c t)$ will differ from eq. (97) by the term

$$\frac{v_c \tau \Delta}{\xi_0} \frac{\partial \Delta}{\partial x}$$

which has the meaning of a friction force. Multiplying the modified equation by $\mathrm{d}\Delta/\mathrm{d}x$ and integrating it along the "motion trajectory", we find the velocity given by eq. (106). For $\delta > \delta_0$ a stationary wave is propagated, which causes the sample to pass from the superconducting into the normal phase. On the contrary, for $\delta > \delta_0$ the wave transforms the normal phase into the superconducting phase.

In the opposite limiting case $L > \breve{\zeta}_0$, the phase boundary travels at a velocity (Elesin 1977a)

$$v_c = \frac{L}{\tau_{ph}} \frac{\delta - \delta_0(L)}{\delta_0(L)} \zeta \tag{107}$$

where ζ is of the order of unity. The motion of the boundary is similar, to a certain extent, to the motion of combustion wave boundaries in gaseous mixtures (or to a liquid-vapour interface). Indeed, a transition into the normal phase, accompanied by the production of excess quasiparticles (an analog of reaction heat), takes place at the interface, since the state with $\Delta < \Delta_2$ (for $\delta > \delta_0$) is unstable. The excess quasiparticles diffuse into the neighbouring region to reduce the gap there to $\Delta < \Delta_2$. In this region the transition into the normal phase occurs again and so on, that is, a wave of "combustion" of the superconducting phase propagates at a velocity $\sim L/\tau_{ph}$. Obviously, after some time the sample gets filled with a single phase, so the inhomogeneous state under optical pumping can be observed in an unsteady regime.

In most of the experiments known to us the inhomogeneous state is observed (for example, as an increase in the resistance) in a pulsed, i.e. unsteady regime, the pulse duration τ_u being of the order of filling time. Therefore, Elesin (1977a) suggested to interprete a gradual transition, observed as a change in the resistance (and other phenomena) within the framework of the unsteady inhomogeneous state model. According to this model, the resistance appears after the normal phase (spanning the film over its width b) arises, the size of this phase growing at a velocity v_c (107). The value of the total film resistance by the end of the pulse, R_1, can be written as

$$\frac{R_J}{R_N} = \frac{v_c \tau_u}{l} = \frac{\tau_u L(\delta - \delta_0(L))}{\tau_{ph} l \delta_0} \delta = \frac{\tau_u L}{\tau_{ph} l} \frac{\beta - \hat{\beta}_0}{2\delta_0 \beta_c} \zeta, \tag{108}$$

where R_N is the film resistance in the normal state, l is the film length, $\widetilde{\beta}_0 = (1 + \delta_0)^2 \beta_c$. It can be seen from eq. (108) that the resistance appears at a power exceeding β (which almost coincides with β_c, since $\delta_0 \ll 1$) and grows linearly with β. The time needed to span the width of the film gives rise to a time delay in the appearance of the resistance relative to the pumping pulse:

$$\tau_{delay} = v_c / b \tag{109}$$

This time delay must decrease with increasing power and temperature.

The model suggested permits a wide range of experimental facts to be explained, though it encounters certain difficulties. Comparison with experiment has been performed in a number

of papers and reviews (see, for example, Tremblay 1981) and will be discussed below (section 1.2.11).

While making comparisons, one has to remember that the model does not allow for certain experimental complications. Some of them were already mentioned in section 1.2.8.

Special attention should be drawn to a possible peculiar "pinning" of phase boundaries at film inhomogeneities. Indeed, if the film contains regions, with a size of the order of L, with a higher value of the order parameter Δ_0 (and hence, with a lesser τ_{ph}), the motion of the phase boundary may cease until the power increases to $\bar{\beta}_0(r)$, the critical power in the inhomogeneity region.

It should be noted that the unsteady inhomogeneous state may be observed under electromagnetic pumping with $\omega > 2A$, and also under tunnel injection with a constant voltage.

22.3.9 1.2.10. The inhomogeneous state of superconductors with tunnel injection

Steady-state inhomogeneous states in the E-model are possible for a given tunnel injection current (Elesin and Levchenko 1978). The current determines the phase boundary.

In order to prove that the stability conditions (100) are satisfied, one has to find the current-voltage characteristic of the transition in the inhomogeneous state $\bar{J} = \bar{J}(V)$. This was done in the papers by Elesin et al. (1980a, b), in which the following expressions were obtained for the dimensionless current $\bar{J}$ and the derivative $\mathrm{d}\bar{J}/\mathrm{d}V$ for $V > V_0$:

$$\bar{J} = \alpha_V \left(V - 2\bar{A}^2/V\right) \tag{110}$$

$$\bar{\Delta}^2 = \Delta_3^2 - \frac{1}{l\sqrt{2\alpha\bar{b}}}\left[1 - 2\sqrt{b}\left(\Delta^{(1)} + \Delta^{(2)} + \Delta^{(3)}\right)\ln\left|\frac{2\sqrt{b}+b}{2\sqrt{b}-b}\right|\right] \tag{111}$$

$$\frac{\mathrm{d}\bar{J}}{\mathrm{d}V} = \alpha_V\left(1 - \frac{2^{2/3}\Delta_3}{\sqrt{\alpha}V_0 l\,(V - V_0)}\right). \tag{112}$$

The derivative $\mathrm{d}J\ \mathrm{d}\,V$ is positive everywhere (in particular for $V < V_\mathrm{c}$), except for the region $V - V_0 \ll V_0$ where it becomes negative and tends to $-\infty$. The current-voltage characteristic $J(V)$ of the SiS junction in the inhomogeneous state is shown in fig. 9 (section 1.2.5).

The stability conditions (100) imply that such a characteristic is unstable. In fact.

$$\text{if } J > J_\mathrm{th}\ (V < V_\mathrm{c})\text{, then} \quad \mathrm{d}J,\ \mathrm{d}V > 0$$

and the state is unstable for $V \leqslant V_\mathrm{c}$.

Consider a current-voltage characteristic of the type I. For $J > J_\mathrm{th}$ the voltage of the system decreases jumpwise (J is fixed!) to $V \geqslant V_0$, where $\mathrm{d}\bar{J}/\,\mathrm{d}V|_{\mathrm{v}\geqslant\mathrm{v}_0} < 0$, so the system is stable, according to eq. (100).

For long films stability is attained at $V = V_0$, so the inhomogeneous distribution is described by the laminated solution (102). The sample is laminated into phases $A_1 = 0$ and $\Delta_{30} \neq 0$.

As the current increases, the volume of the normal phase grows fand that of the superconducting phase diminishes) for a fixed voltage $I - I_0$ (the vertical portion of the $I - V$ characteristic).

For $J = J_0$ the system passes completely into the normal state. The corresponding $I - V$ characteristic is shown in fig. 9 by a solid line.

The inhomogeneous state described is possible for $I - V$ characteristics of types I and II only. For I-V characteristics of type III the system passes into
the normal state before the junction voltage reaches the value V_0, since $J_\mathrm{H} > J_0$. Therefore,

for type-III characteristics the sample goes over jumpwise, at $J = J_H$, from the homogeneous superconducting into the homogeneous normal state. However, as the current decreases the system passes, at $J = J_0$ and $V = V_0$, into the inhomogeneous state of the type described above.

A qualitatively similar behaviour may be expected in the two-dimensional case where current pinching occurs and the parameters of the system are of the order of Δ. Consider, for example, a solution in the form of a superconducting radially symmetric pinch of the radius ρ_0. If $\rho_0 \ll l$, the boundary conditions are satisfied automatically. The order parameter A varies from a certain value $\Delta = \Delta_{max}$ at the centre of the pinch to $\Delta = 0$ at the periphery.

As in the case of superconductors with an S -shaped $I-V$ characteristic (Volkov and Kogan 1968), the superconducting pinch is stable at the descending portion of the $I-V$ characteristic in the given current regime, that is under conditions (100). It is a simple matter to verify that the derivative dJ/dV becomes negative and tends to $-\infty$ as $V \to V_0$. Thus, the IV characteristic has a vertical portion at $V = V_0$.

22.3.10 1.2.11. Comparison of theory and experiment. Conclusion

The main predictions which follow from the models considered in this review, are listed in table 1. As can be seen from the table, the T^* - and BCS models are very close to each other, as far as certain properties are concerned. These models seem to be intermediate between the E- and NE-models, which appear to give opposite results with respect to properties 1, 2, and 4-8.

The properties 3,7 and 10 are common for the E- and NE-models.
All ten properties can be verified experimentally, to a certain accuracy. It seems useful to recall the temporal and spatial scales characteristic of experiments. The relaxation times of quasiparticles τ_{ph} near $\xi \sim A_0$ are of the order of $10^{-8} - 10^{-10}$ s. The length of typical light pulses is $10^{-7} - 10^{-5}$ s. This is enough for quasiparticles and phonons to relax to their steady-state value. Tunnel experiments are usually performed under steady-state conditions.

The typical lengths: the coherence length at $T = 0$ is $\xi_0 = (10^{-6} - 10^{-4})$ cm; the quasiparticle diffusion length $L = \sqrt{D\tau_{ph}} = (10^{-4} - 10^{-3})$ cm; the approximate dimensions of the samples: width 10^{-1} cm, length 1 cm , thickness 10^{-5} cm.

Determination of the form of the QDF and $A(\beta)$ (properties 2-4). The number of works dealing with direct experimental determination of the QDF is rather scanty (Balkashin et al. 1977, Jaworsky and Parker 1979, Kaplan et al. 1977, Willemsen and Gray 1978). The last work is the most comprehensive; it is devoted to the determination of $n(\xi)$ in thin aluminium films with tunnel injection.

Willemsen and Gray processed their data with the help of the function (42).

They showed that at a high junction voltage (corresponding to the wide-source criterion) the parameters μ^* and T^* aro nonzero and depend on V' (see fig. 4), the chemical potential μ^* being negative and T^* exceeding T_c. The ratio T^*/T_c is higher than unity and reaches 1.5, while $A_1 A_0 > 0.3$. These data as well as the dependence of μ^* and T^* on the voltage agree well (both qualitatively and quantitatively) with the predictions of the E-model (Elesin et al. 1979) (see section 1.2.1), indicative of "overheating" of quasiparticles (property 2). The
dependence $A(V)$ coincides with that shown in fig. 5. Note that the dependence of Δ on pumping power up to $V = V_c$ agrees quantitatively with the corresponding dependence predicted by the T^*-model. Therefore, the results of a number of papers exhibiting good agreement with the T^*-model can also be considered as confirming the E-model. (More careful measurements are needed to distinguish the E-model from the T^*-model.) One has to remember that the results presented usually refer to Δ values below a certain Δ_c, and then the transition into the normal or inhomogeneous state occurs (properties 4, 5). [Willemsen and Gray (1978) report

Table 1
Main predictions of models considered.

Property		
	E-model	T*-model
(1) Kinetic equation for $n(\zeta)$	Satisfied for $\eta = 1$	Satisfied for η
(2) $n(\zeta)$	$n(0) < n_{\mathrm{T}}(0)$ overheating	Equilibrium w
(3) $n(\xi)$	$n < 1/2$	$n < 1/2$
(4) Form of $\Delta(\beta)$	two-valued	singlevalued
(5) Type of phase transition	1st-order	2nd-order
(6) Magnetic properties	$N_{\mathrm{S}} > 0$ diamagn.	$N_{\mathrm{S}} > 0$ diama
(7) Sign of supercon. current	$\sigma_{\mathrm{S}} > 0$	$\sigma_{\mathrm{S}} > 0$
(8) Instability	coherent	absent
(9) Inhomogeneous state	laminated: unsteady (ω = const.), steady (I = const.)	absent
(10) Critical power	$\beta_c(0) \neq 0, \beta_c$ drops with T	$\beta_c(0) \neq 0, \beta_c$ d

$\Delta_{c'}\Delta_0 = 0.3$, in the paper by Lambert et al. (1977) $\Delta_c/\Delta_0 = 0.3$, etc.]

Lambert et al. (1977) determined $n(\check{\zeta} = 0)$ by ultrasonic absorption measurements. The corresponding dependence is presented in the paper by Elesin and Kopaev (1981) and illustrates good agreement with the theory. It is also shown that $n(0) < \frac{1}{2}$ (property 3).

Fuchet et al. (1977) showed that $n < \frac{1}{2}$ and $\Delta_c/\Delta_0 = 0.6$.

Thus, experiment confirms properties (2-4) of the E-model.

Inhomogeneous state under optical pumping. A rather detailed comparison between theory and experiment was performed by Tremblay (1981) who concluded that the E-model permits a consistent and also the most complete explanation of some experimental results.

At the same time, certain problems arose, first of all the problem of stationarity. The fact is that the E-model predicts a change in the film resistance with time (see section 1.2.8). Yet, some experiments revealed stationarity, as reported, for example, in the paper by Sai-Halasz et al. (1974). The reflection coefficient does not change during the laser pulse $\tau_{\mathrm{u}} = 10^{-8}$ s.

Such stationarity was also observed by Golovashkin et al. (1975) for short laser pulses, while for long pulses ($\tau_{\mathrm{u}} > 10^{-6}$ s) those authors found that the film resistance increased with time, in accordance with the E-model, and suggested an explanation of the stationarity observed.

According to Mitsen (1981), the stationarity is caused by the small duration of the laser pulse. The distance travelled by the normal phase during the pulse is very small, so the increase in the resistance cannot be detected.

Below we shall describe the results reported by Golovashkin et al. (1975. 1978, 1979a,b, 1980), which are interpreted by those authors within the framework of the E-model, and also of certain more recent works concerning optical pumping.

Many important results have been obtained by Golovashkin et al. (1975, 1978. 1979a,b, 1980) who studied the behaviour of lead, niobium. Nb_3Sn and V_3Si films irradiated by pulses of semiconductor, argon and neodymium lasers. At powers W exceeding a certain critical value $W_c(T)$ (dependent on temperature) a gradually increasing resistance appeared that gave rise to a measurable voltage V. Figure 11 shows the typical time dependence of V across

the lead film for different temperatures, and also the trace of the laser pulse with the length 10μ s; $W = 30$ W/cm^2. It can be seen from the figure that the signal across the sample appears at a temperature much lower than $T_6 = 7.2$ K. As the temperature increases, the signal amplitude grows to reach the value V_N across the film in the normal state.

During the laser pulse, the voltage across the sample is not constant, but increases with time reaching a maximum by the end of the pulse. Golovalshkin et al. have estimated, using

the dependence $V(t)$, the velocity of the normal phase boundary to obtain the value $v_c = 2.5 \times 10^4$ cm/s $(W/W_c = 1.5)$, which agrees within an order of magnitude with eq. (107).

Using the value of the velocity v_c, one can find a minimal pulse length τ_0 at which "stationarity" is still observed

$$\tau_0 = \frac{0,1\bar{d}}{v_c} = 10^{-6} \text{ s},$$

where $\bar{d} = 0.1$ cm is the characteristic size of the normal region. It is clear from this point of view that for $\tau_u = 10^{-8}$ s "stationarity" had to be observed by SaiHalasz et al. (1974). The signal delay $\delta\tau$ with respect to the beginning of the laser pulse is an essential effect. It follows from fig. 11 that $\delta\tau$ drops linearly with increasing T (or W), in accordance with the prediction of the E-model (see properties $1, 2, 4$). Substitution of $b = 10^{-1}$ cm and $v_c = 2.5 \times 10^5$ cm/s into eq. (109) yields $\delta\tau = 4\mu$ s, which agrees with experiment.

The growth of the resistance with time and the signal delay effect confirm properties 8,9 of the E-model.

Figure 12 shows the typical voltage-power dependence $V(\tau_u)$. It can be seen that the film resistance at the end of the pulse increases with power, in accordance with eq. (108). The dependence $V(W)$ (fig. 11) is of threshold character. The film passes into the resistive state for $W > W_c$.

A detailed comparison of the dependences of W_c on T and film thickness d with the existing models was performed by Golovashkin et al. (1979a,b, 1980) (see fig. 13a,b). They observed not only qualitative, but also good quantitative agreement with the E -model (property 10). The μ^*-model leads to qualitatively different dependences (Golovashkin et al. 1979a, b, 1980).

Inhomogeneous states with similar properties have been discovered by Janik et al. (1975) and by Buisson et al. (1978).

Buisson et al. (1978) observed the occurrence of a resistive state in Al films ($d = 500$ and 800Å) irradiated with pulses of a dye laser with a duration of 6 ns and energy (in the pulse) 0.5μ J. Dynes et al. (1977) irradiated aluminium films of $d = 200$Å by an argon laser with a maximal power of 0.5 W , and measured the change in the transmission coefficient at microwave frequencies (100 GHz) under optical pumping. They assumed that an intermediate state in the form of

superconducting and normal phases occurred in the film, the normal phase volume increasing with W.

Smith (1980) studied inhomogeneous states in a uniform geometry [for details see the review by Tremblay (1981)].

We have not come across publications concerning direct experimental verification of diamagnetism (property 6) and the sign of the superconducting current (property 7). But we are neither acquainted with communications on these anomalies, which are easy to observe. As far as the effect of current is concerned, several papers reported a decrease in the critical power W_c with increasing J, in accordance with the predictions of the E-model (see section 1.2.3).

In summary, one may conclude that the E-model explains the main experimental facts. The T^* - and μ^*-models have been discussed in detail by Tremblay (1981). We note only that the T^*-model agrees qualitatively with the E-model for powers W below the critical value W_c.

The experimental data presented above are at variance with the μ^*-model for properties $2, 3, 8, 9, 10$ and, probably, 6 and 7 . It should be noted that the μ^* model is difficult to compare with experiment. The fact is that the μ^*-model does not provide an expression for experimentally determined W_c, but gives the value n_c at which instability occurs, and this value n_c does not correspond to the moment when the resistance appears (Tremblay 1981).

Tunnel injection at high voltages. According to the E-model, the injection of quasiparticles in SiS junctions at $V >\Rightarrow$ must lead to a multi-valued dependence of Δ and I on V, and also

to a first-order transition into the normal or inhomogeneous state (see section 1.2.10).

The E-model predicts these phenomena, in principle, for any α_V. It should be noted, however, that they are difficult to observe for very small α_v and, correspondingly, large V. Indeed, in this case the S-shaped portion of the IV characteristic is rather difficult to detect against the high-voltage background, and moreover intensive heat release ($\sim 1/\alpha_V$) masks the effect. The values $\alpha_v \gtrsim 0.1$ are the most suitable for observation.

Tunnel injection for $V \gg A$ was studied in a number of works (see the reviews by Tremblay 1981 and by Elesin and Kopaev 1981), but we shall concentrate here on the most typical ones.

Junctions with double injection (e.g. Al-I-Al-I-Al) of the size $10^{-1} \times 10^{-1} \times 10^{-5}$ cm are usually employed in experiment.

One of the junctions with "high" resistance ($10^{-2} - 10^{-4}$Ohmcm^2) acts as a detector and controls the properties of the middle sample perturbed by the injector junction with a low resistance ($10^{-4} - 10^{-6}$Ohmcm^2). Most tunnel experiments are carried out under steady-state conditions. Since the total contact resistance is small, the given current regime is practically always realized in these experiments.

First-order transitions into the normal state were observed by Fush et al. (1977) in tin films for $T < T_\lambda$, and also by Mitsen (1979) ($T > T_\lambda$) when the current exceeded a certain critical value. Their results are not at variance with the E-model, which predicts the first-order transition for type-III IV characteristics (see section 1.2.10), and also with the μ^*-model. However, Fush et al. (1977) believe that the attainment of the film critical current could be the cause of the transition.

The inhomogeneous state was observed by Iguchi (1977) at a temperature $T > T_\lambda$ (as a gradual change in the resistance).

A transition into the inhomogeneous state very close to that predicted by the E-model was observed by Mitsen (1979) and by Pan and Rudenko (1981).

Mitsen (1979) studied the junction Sn − I − Sn. Its current-voltage characteristic is shown in fig. 14. Curves 1 and 2 refer to different values of α_V. At a certain injection current J_{th}, to which the voltage V_H corresponds, a negative voltage jump to $V = V_0$, followed by a vertical portion of the $I - V$ characteristic, is observed across the junction. (The currents J_{th} are less than the critical ones.) As the current decreases, hysteresis is observed. The results obtained are in good qualitative agreement with the E-model (see section 1.2.10) and correspond to $I-V$ characteristics of types I or II. In particular, V_H, J_0, J_{th} grow with the decreasing α_v. Mitsen has estimated, using experimental data, the critical concentration of quasiparticles from the relation

$$\frac{N_c v'}{\tau_{ph}} = \frac{J_{th}}{e}$$

to obtain $N_c = 0.4 \times 10^{19}$ cm^{-3}, which is in good agreement with the theoretical estimate (see eq. 37) for tin

$$N_c = v(0)a_0 = v(0)\Delta_0 \cdot 0.4 = 0.31 \times 10^{19} \text{ cm}^{-3}.$$

Note that Mitsen's 1979 paper contains a misprint; the theoretical formula used therein overestimates N_c by a factor of 4 .

According to Mitsen (1979) heating, which occurs in such experiments, does not affect the results.

Pan and Rudenko (1981) investigated the $I - V$ characteristic of the junction Nb − I − Nb (see fig. 15). For $J > J_{th}$, a voltage jump across the junction was observed, and a voltage appeared across the Nb. The voltage increased linearly with current, indicative of a transition into the normal state at $J = J_{th}$. As the current was decreased, a vertical portion (i.e. the inhomogeneous state) appeared (see fig. 15a).

This behaviour corresponds to the third-order transition in the E-model. Pan and Rudenko (1981) measured the temperature dependence $J_{\text{th}}(T)$ (see fig. 15b) and showed that it agrees qualitatively with $\beta_c(T)$, that is, with the prediction of the E-model. Using a sophisticated technique, they eliminated the effect of overheating on the dependence $J_{\text{th}}(T)$. Otherwise, experiment reveals a nonmonotonous dependece $J_{\text{th}}(T)$ similar to that observed by Iguchi (1977). In this respect, the work of Iguchi can also be interpreted within the framework of the E-model, especially if allowance is made for the fact that Iguchi (1977) observed the inhomogeneous state at temperatures up to T_c, whereas according to the μ^*-model diffusion instability disappears at $T > 0.6T_c$.

There are works, besides the aforementioned ones, which neither fit the Emodel. For example, Iguchi et al. (1981) state that they have observed an inhomogeneous state with four gaps.

Thus, one may conclude that at present the E-model is the most satisfactory, both from the theoretical and from the experimental point of view. This model represents the kinetic theory of superconductors with excess quasiparticles.

At the same time, one has to remember that the E-model does not take into account experimental complications associated with inhomogeneities of films and radiation, with heating, and so on. Therefore, only detailed quantitative comparison between theory and experiment, with due account for specific experimental conditions, can decide between one model or another.

22.3.11 1.3. Superconductors with a narrow quasiparticle source. Threshold electromagnetic pumping and tunnel injection in Single-band approximation

If the frequency of the electromagnetic field (or the voltage V) is close to the threshold, the state of a superconductor appears to be essentially nonequilibrium. The QDF differs significantly from the quasiequilibrium one (especially for $T = 0, \hat{i} = 0$) and grows with ξ. The dependence of the gap on

frequency (voltage) becomes three-valued. The state is unstable against "threshold instability", which may lead to a first-order transition of the superconductor from the state with Δ_0 into the state with lesser gap A_3 or into the inhomogeneous state. The latter represents an alternation of phases with Δ_0 and A_3, different from zero. In other words, a superconductor with threshold injection exhibits a behaviour very close to that described by the E-model for a wide source. Therefore, let us consider the basic phenomena, using the analogy just mentioned. The theory of a narrow source was developed in papers by Elesin (1974, 1979b), Aronov and Spivak (1976), Schön and Tremblay (1979), Elesin et al. (1980a, b), Gray and Willemsen (1980), and Hida (1978a, b), and inhomogeneous states with two values of the gap were observed experimentally by Dynes et al. (1977) and by Gray and Willemsen (1978).

22.3.12 1.3.1. The quasiparticle distribution function

Let us confine ourselves to the case $\gamma = 0 (T = 0)$. The kinetic equation for a narrow source can be simplified significantly if one takes into account that scattering processes are strongly suppressed as compared to recombination, due to the factors $(\varepsilon - \varepsilon')^2$ and coherence factors $(1 - \Delta^2/\varepsilon\varepsilon')$. At $T = 0$ when the terms $Q^{(2,3)}$ describing the energy redistribution of quasiparticles can be neglected in the expression for the source, we arrive at the following equation (Elesin 1974, Aronov and Spivak 1976):

$$n_z \bar{n} = \alpha_\omega (\hat{\delta})^{K(\omega)} \frac{1 - n_z - n_{1-z}}{\sqrt{1-z}} \Theta(z)\Theta(1-z) \tag{113}$$

where

$$\bar{\delta} = \frac{\omega - 2\Delta}{2\Lambda}, \quad z = (\varepsilon - \Delta)/\Delta\bar{\delta}$$

In the case of tunnel injection, $\alpha_V \bar{\delta}^{-1/2}$ must be substituted for $\alpha_\omega \bar{\delta}^{-1/2}$ because the coherence factor is absent (see eq. 21).

Equation (113) shows that the shape of the source has a major effect on the QDF. Aronov and Spivak (1976) have obtained an exact solution of eq. (113):

$$n_z = A\frac{\sqrt{z}\Theta(z)\Theta(1-z)}{\sqrt{z(1-z)} + A(\sqrt{z} + \sqrt{1-z})} \tag{114}$$

where the coefficient A satisfies the normalization condition. It can easily be seen that $n(z)$ is different from zero in the interval $0 < z < 1$ and takes the values $n(0) = 0$ and $n(1) = 1$, i.e., in the case of a narrow source the distribution function differs significantly from the equilibrium one, has a positive derivative, and can reach unity. The coefficients $A_{(1)}, A_\vee$ appear to be essentially different. For example, for small $\alpha_{(1)} A_{(1)}$ is also small, while A_V may become large as $\widehat{\delta} \to 0$. Therefore, the QDF for electromagnetic pumping is nonzero in a

narrow interval near $z = 1$, and for tunnel injection n_z is of the order of unity almost in the whole interval $0 < z < 1$. An exact solution for n_z has been found for $T \to T_\mathrm{c}$ as well, and it can be represented in the form (Elesin et al. 1980a)

$$n = n_\mathrm{T} + n_2 + \hat{n}$$

where n_2 is a smooth function due to the action of $Q^{(2)}$, and the "narrow" part $\hat{n}$ is given by

$$\hat{n} = n_z(T = 0)\psi_\mathrm{T}, \quad \psi_\mathrm{T} = 1 - n_\mathrm{T}(z) - n_\mathrm{T}(1-z) \tag{115}$$

The correction $\hat{n}$ possesses the property (114). If reabsorption is taken into account, the QDF becomes smoother and tends to the equilibrium one in the limit $\gamma \to \infty$. Figure 16, taken from a paper by Imai (1980), shows the QDF for $\gamma = 1, 10$.

22.3.13 1.3.2. The order parameter

A narrow source produces quasiparticles with energies in a narrow interval $\omega - 2\Delta$, so the quasiparticles are localized near $\varepsilon \sim A$. The local character of $n(\xi)$ makes it possible to find, by virtue of eq. (6), a universal relationship
between A and $\bar{n}$, the quasiparticle concentration (see, for example, Elesin 1977b):

$$\Delta = \Delta_0(1 - 2\bar{n}), \quad \bar{n} \ll 1. \tag{116}$$

In order to obtain a closed system for Δ and $\bar{n}$ in the case of small α_ω, it is sufficient to use the normalization condition (18). Taking into account the local character of $n(\xi)$, we arrive at the relation (Elesin 1974)

$$\bar{n}^2 = \alpha_{()}\frac{\omega - 2A}{2\Delta_0}\Theta(\omega - 2\Delta) \quad (\text{ at } T = 0) \tag{117}$$

which expresses the equality of the quasiparticle recombination rate (the lefthand side) and the rate of production of quasiparticles due to the electromagnetic field (since the $\alpha_{()}$are small, the $n(\zeta)$ in Q are put equal to zero). It is important to note that the production rate is proportional to the interval $\omega - 2\Delta$ and depends significantly on A. In other words, in the case of a narrow source the order parameter controls the quasiparticle production rate. This leads,

as was shown by Elesin (1974), to a characteristic threshold instability (see section 1.3.3) and a multi-valued dependence of Δ on ω (Elesin 1979b, Schön and Tremblay 1979).

Indeed, eliminating $\bar{n}$ from eqs. (115) and (116) we obtain an equation for A whose solution in the interval $-\alpha_\omega < \delta < 0$ is of the form

$$\Delta_5 = \Delta_0, \quad \Delta_{4,3} = \Delta_0 \left[1 - 2\alpha_\omega \left(1 \mp \sqrt{1 + \delta/\alpha_\omega}\right)\right]. \tag{118}$$

Three solutions, Δ_5, Δ_4 and Δ_3, exist in this interval.
The existence of three solutions is related to the fact that Δ influences the quasiparticle production rate. The solution $A_5 = A_0$ corresponds to the case where the source is switched off ($\omega < 2\Delta_0$). If, on the contrary, $\Delta = \Delta_{4.3} < \Delta_0, \Delta$ decreases and the source produces quasiparticles; then solutions increasing with ω and solutions, Δ_4, decaying with ω are possible. Qualitatively similar results are also obtained under tunnel injection ($\omega \to V$):

$$\Delta_5 = \Delta_0, \quad \Delta_4 = V/2, \quad \Delta_3 = \Delta_0 \left(1 - 2\sqrt{\frac{1}{2}\pi\alpha_V}\right) \tag{119}$$

But now the solution Δ_3 is constant and Δ_4 depends "universally" on the voltage (see fig. 17a). This relation is different from eq. (118) because the coherence factors are absent in the source for tunnel injection.

Note that multiplicity of $\Delta(\omega)$ occurs for any α_ω. The conclusion on the existence of three solutions $\Delta(V)$ (Elesin 1979b) was simultaneously made also by Schön and Tremblay (1979). They solved graphically the equation for Δ for $T \to T_c$. The case of finite temperatures was also considered by Elesin et al. (1980c), where the contribution due to the terms $Q_v^{(2)}$ and $Q_v^{(3)}$ was taken into account.

The multiplicity of $\Delta(\omega)$ and $\Delta(V)$ must lead to a multi-valued dependence of the absorbed electromagnetic power and of current through the tunnel junc-

tion $J(V)$ [for details see Elesin and Kopaev (1981)]. Indeed, it was shown by Elesin (1979b) and by Schön and Tremblay (1979) that the IV characteristic is S-shaped near $V = 2A$.

Figure 17 shows the dependence $\Delta(V)$ and the $I - V$ characteristics in the entire voltage range for different α_V, as calculated analytically (Elesin 1979b, Schön and Tremblay 1979) and numerically (Elesin et al. 1980a, b). The second portion of the S-shaped $I - V$ characteristic is due to the coherent mechanism (see section 1.2). Qualitative concepts on IV characteristics with a negative slope at $V = 24$ have been used by Gray and Willemsen (1978).

22.3.14 1.3.3. Threshold instability

Elesin (1974) predicted a type of instability, for the case of a narrow source
($\omega \approx 24$), that was called "threshold instability". This occurs as follows. Suppose that at an initial moment $\Delta = \Delta_0, \bar{n} = 0$ and $\omega \leqslant 2\Delta_0$. A fluctuation of $\bar{n}$ leads to a decrease in Δ (see eq. 116) and, hence, to an increase in the width of the source action, which is proportional to $\omega - 24$ (see eq. 117). This, in turn, increases n, and so on. A similar instability can arise in superconductors with tunnel injection (Elesin 1979b, Schön and Tremblay 1979) for $V \leqslant 24$, and was observed experimentally (Dynes et al. 1977, Gray and Willemsen 1978).

To find the decrement, we shall use the equation for Δ, the deviation of Δ from A_0, which coincides with the quasi-particle concentration $\bar{n}$ (see eq. 116) (Elesin 1979, Elesin and Kopaev 1981) ($L \gg \zeta_0$ at $T = 0$)

$$\bar{\Delta} = \frac{\Delta_0 - \Delta}{2\Delta_0} = \bar{n}, \quad \frac{\partial \bar{n}}{\partial t} - L^2 \frac{\partial^2 \bar{n}}{\partial r^2} = \frac{\partial U(\bar{n}, \delta)}{\partial \bar{n}}$$
$$U(\bar{n}, \delta) = -\int_0^{\bar{n}} \alpha \bar{n}' \left(2\bar{n}'^2 - \bar{Q}_\omega\right), \quad \bar{Q}_\omega = \alpha_\omega(\delta + 2\bar{n})\Theta(\delta + 2\bar{n}) \tag{120}$$

Here $U(\bar{n}(\Delta))$ is the energy of the system, similar to that in the E-model, which has minima at Δ_5 and Δ_3 and a maximum at Δ_4. The corresponding decrement is (Elesin 1979b)

$$\tilde{\gamma} = \frac{1}{2\Delta} \frac{\partial^2 U}{\partial \Delta^2} - q^2 L^2 = \alpha_\omega \left(\frac{\partial \Delta}{2\Delta \partial \delta}\right)^{-1} - q^2 L^2 \tag{121}$$

This relation implies that the increasing solution Λ_4 (corresponding to the maximum of $U(\bar{n}(\Delta))$ is unstable, and quasiparticle diffusion stabilizes the perturbations. Thus, the situation is completely analogous, in qualitative respect, to that in the E-model (see sections 1.2.6 and 1.2.8) if we make the substitutions $A_1 \to A_5, A_2 \to A_4, A_3 \to A_3$, so we can use the above results.

In particular, one is to observe first-order transitions $A_5 = A_0 \to A_3$ at $\delta = \delta_0$, hysteresis ($\Delta_3 \to \Delta_0$ at $\delta = -\alpha_\omega$) or the inhomogeneous state.

22.3.15 1.3.4. Inhomogeneous states

Threshold instability leads to an inhomogeneous state, which is described by the steady-state equation (119).

The steady-state inhomogeneous solution is laminated, it separates the homogeneous regions with $\Delta_5 = \Delta_0$ and $\Delta_3 \neq 0$ and is realized at a certain frequency ($_0$ or voltage V', [which corresponds to the equality $U(A_3) = U(A_5)$]. For an electromagnetic field the laminated solution is of the form (Elesin 1979b)

$$\bar{\Delta}(x) = \begin{cases} 3\left[x - x_0 - 4\sqrt{2/\alpha(1)}\right]^2, & x \leqslant x_0 \\ \bar{\Delta}_{30} \tanh^2\left[\sqrt{\alpha\omega/2}\,(x - x_0) + C_2\right], & x > x_0 \end{cases} \tag{122}$$

where $\tanh C_2 = \frac{1}{2}$, x_0 is the coordinate of the transition boundary, and

$$\nearrow_{30} = \frac{3\alpha_\omega}{2}, \quad \frac{\omega_0}{2A_0} = 1 - \frac{3\alpha_\omega}{4}. \tag{123}$$

Qualitatively similar results are also obtained for tunnel injection. In particular, the quantities V_0 and A_{30} are given by (Elesin 1979b)

$$\frac{A_0 - A_{30}}{\Delta_0} = \sqrt{\pi\alpha_{\mathrm{V}}}, \quad \frac{V_0}{2A_0} = 1 - \sqrt{\frac{\pi\alpha v}{4}}. \tag{124}$$

Analogous results have been obtained by Gray and Willemsen (1978), Hida (1978), and Schön and Tremblay (1979).

The $I-V$ characteristics of an SiS junction resemble those considered in section 1.2. Indeed, for currents J exceeding J_{th} ($\mathrm{d}J/\mathrm{d}V < 0$) threshold instability arises, which leads to lamination into pinches with Δ_5 and Δ_3, and is accompanied, by virtue of eqs. (100) and (125), with a jumpwise voltage decrease to V_0. A laminated solution with $\Delta_{50} = \Delta_0$ and Δ_{30} is formed. The position of the phase boundary x_0 is determined by the total current.

As the current grows further, the volume of the phase with Δ_{30} increases at a constant voltage V_0 (vertical portion of the $I - V$ characteristic), until the sample is completely filled with the phase A_{30}.

22.3.16 1.3.5. Comparison with experiment. Conclusion

The model considered agrees well with experimental data concerning the observation of the "two-gap state" under threshold tunnel injection (Dynes et al. 1977, Gray and Willemsen 1978).

It explains the form of the $I-V$ characteristics for a "detector" and a "generator" (see fig. 18), in particular, the vertical portion at $V=V_0$, jumps and hysteresis of the generator $I-V$ characteristic, and the form of the $I-V$ characteristic of the "detector" (lamination of the phase with A_{30}). The model describes quantitatively the relationship between the difference $\Delta_0-\Delta_{30}$ observed and the injection coefficient α_V and V_0 (see eq. 124); it also explains the non-threshold character of the effect, and so on.

It is believed at present that experiment is described well, at least qualitatively, by the theory considered above (Tremblay 1981, Elesin and Kopaev 1981).

22.4 2. Effect of electromagnetic field on superconductors in the two-band approximation

If the field frequency ω exceeds the energy gap, the valence band should be taken into account besides the conduction band. The theory of such an effect was developed by Galitskii et al. (1969, 1973), Elesin and Kopaev (1972, 1974), Elesin (1975), and Kirzhnits and Kopaev (1973).

22.4.1 2.1. The electron spectrum of a crystal in a strong electromagnetic field

Consider a crystal in the field of a strong electromagnetic wave with the vector potential

$$\mathscr{A}=\mathscr{A}_0\cos(\omega t-kr),\quad k\mathscr{A}_0=0. \tag{125}$$

Suppose that the frequency ω exceeds the energy gap between the valence and conduction bands, which have a maximum and a minimum, respectively, at the centre of the Brillouin zone.

In this case the field induces resonant electron transitions between the valence band and the conduction band, which satisfy the condition $E_{\mathrm{c}}(p)-E_{\mathrm{v}}(p+k)-\omega=0$. If the photon wave vector k is neglected in comparison with the electron quasimomentum p, the resonant transitions will occur with conservation of the quasimomentum (direct transitions).

Assuming the field to be sufficiently strong [see below for the corresponding condition, eq. (127)], we can include the resonance portion of the interaction with electromagnetic field into the zero-order Hamiltonian, whose eigenstates can be determined exactly (Galitskii et al. 1969):

$$H_0(t)=\sum_p E_p\left(a_p^+a_p+b_{-p}^+b_{-p}\right)+\lambda_p\left(a_p^+b_{-p}^+\mathrm{e}^{-\mathrm{i}\omega t}+b_{-p}a_p\mathrm{e}^{\mathrm{i}\omega t}\right) \tag{126}$$

Here $a_p^+$and $b_{-p}^+$are the operators of production of an electron in the conduction band and a hole in the valence band, respectively,

$$\lambda_p=\frac{1}{2}eA_0v_{\mathrm{cv}}(p),\quad v_{\mathrm{cv}}(p)=\frac{1}{m}\int\psi_{\mathrm{c}p}^*\hat{p}\psi_{\mathrm{v}p}\,\mathrm{d}^3r,$$

v_{cv} is the matrix element of the interband transition rate, and ψ_{cp} and ψ_{vp} are the Bloch functions of electrons in the conduction and valence bands.

The use of the Hamiltonian (126) as the zero-order approximation is valid if the frequency of transitions between the bands due to the field is much higher than the collision frequency $1/\tau$

$$\lambda \gg 1/\tau, \tag{127}$$

where by τ we mean the smallest among the electron-phonon collision time, electron electron collision time and annihilation time τ_A. The Hamiltonian $H_0(t)$ depends on time. Using the unitary transformation (Galitskii et al. 1969)

$$U(t) = \exp\left\{-\frac{1}{2}i\omega t \sum_p \left(a_p^+ a_p + b_{-p}^+ b_{-p}\right)\right\} \tag{128}$$

it is convenient to go over to a representation in which the Hamiltonian is time independent:

$$\begin{aligned} H_0 &= U^+(t)H_0(t)U(t) - \mathrm{i}U^+\frac{\partial U}{\partial t} \\ &= \sum_p \left[\xi_p\left(a_p^+ a_p + b_p^+ b_p\right) + \lambda(p)\left(a_p^+ b_p^+ + b_p a_p\right)\right], \\ \xi_p &= \frac{1}{2m}\left(p^2 - p_0^2\right), \quad \frac{p_0^2}{2m} = \mu_0 = \frac{\omega - E_\mathrm{g}}{2}. \end{aligned} \tag{129}$$

The canonical transformation

$$a_p = u_p\alpha_p + v_{-p}\beta_{-p}^+, \quad b_{-p} = u_p\beta_{-p} - v_{-p}\alpha_p^+ \tag{130}$$

reduces the Hamiltonian (129) to the diagonal form

$$H_0 = \sum_p \varepsilon_p\left(\alpha_p^+\alpha_p + \beta_{-p}^+\beta_{-p}\right). \tag{131}$$

The ordinary anticommutation relations for Fermi particles hold true for the operators of new quasiparticles, and the functions u_p, ι_p and the quasiparticle energy are given by

$$\left.\begin{matrix} u_p^2 \\ v_p^2 \end{matrix}\right\} = \frac{1}{2}\left(1 + \frac{\xi}{\varepsilon_p}\right), \tag{132}$$

$$\varepsilon_p = \sqrt{\xi_p^2 + \lambda_p^2}. \tag{133}$$

The operators $\alpha_p\left(\alpha_p^+\right)$and $\beta_p\left(\beta_p^+\right)$are the parameters of annihilation (production) of quasiparticles of species α and β, which describe the superposition of electrons and holes.

The quasiparticle spectrum has a gap at $p = p_0$. Thus, an electromagnetic field of a frequency exceeding the energy gap leads to an essential dynamic effect, namely the occurrence of a gap in the energy spectrum of electrons of the conduction and valence band.

This result was first derived by Galitskii et al. (1969) when they considered the interaction of a strong resonance field with pure semiconductors (i.e. semiconductors in which the concentration of conduction band electrons tends to zero for $T \to 0$). Obviously, this result is also valid for doped semiconductors and metals.

22.4.2 2.2. The quasiparticle distribution function

Consider now the kinetics of quasiparticles, described by the quasiparticle distribution functions

$$n_\alpha = \left\langle \alpha_p^+ \alpha_p \right\rangle, \quad n_\beta = \left\langle \beta_p^+ \beta_p \right\rangle \tag{134,135}$$

The equations for these functions have been derived by Galitskii et al. (1969) using the Bogolyubov method and by Elesin (1970a) using the Keldysh technique. These equations differ from eqs. (12) and (13 15) by the sign of the coherence factors and by the presence of a collision term accounting for annihilation between electrons and holes

$$I_{\mathrm{A}} = \frac{1}{\tau_{\mathrm{A}}} \left[v_p^4 (1 - k_p)^2 - u_p^4 n_p^2 \right], \quad \frac{1}{\tau_{\mathrm{A}}} = \frac{4}{3} e^2 \omega \left| v_{\mathrm{cv}} \right|^2. \tag{136}$$

First we consider the simplest case where the concentration of equilibrium electrons is small as compared with that of electrons produced by the field ($E_{\mathrm{F}} \to 0$). If annihilation (136) is disregarded (usually $\tau_{\mathrm{ph}} \ll \tau_{\mathrm{A}}$), the QDF for this case is (Galitskii et al. 1969)

$$n_\alpha(p) = n_\beta(p) = n_{\mathrm{T}} = \left[\exp \frac{\varepsilon}{T} + 1 \right]^{-1}. \tag{137}$$

At zero temperature $n_p = 0$ and the so-called saturation state is reached. In this state the energy distribution of electrons and holes

$$f_p = \left\langle a_p^+ a_p \right\rangle = \left\langle b_p^+ b_p \right\rangle = v_p^2 \tag{138}$$

has the form of the Fermi step smeared out near the boundary energy μ_0 by the value i. (it is assumed that $i \ll \mu_0$). In other words, the electrons (holes) occupy the portion of the conduction (valence) band from $p = 0$ to $p = p_0$. This is easy to explain.

Indeed, the law of conservation of momentum implies that electrons with momentum p_0 must pass from the valence band into the conduction band.

When interacting with the lattice, the electrons emit phonons and occupy the states with lesser momenta up to p_0.

In the saturation state the absorption coefficient of the electromagnetic field vanishes (Galitskii et al. 1969). A nonzero value of the absorption coefficient is obtained if annihilation (136) is taken into account. An allowance for annihilation, by virtue of the condition $\tau_{\mathrm{A}} > \tau_{\mathrm{ph}}$, changes n_p in a small region near $\xi = 0$, this change being dependent on the parameter (Elesin 1975)

$$\eta_{\mathrm{A}} = \frac{\tau_{\mathrm{ph}}}{\tau_{\mathrm{A}}} \left(\frac{\mu_0}{\lambda} \right)^2 \tag{139}$$

and on the ratio $2\lambda/\omega_{\mathrm{D}}$.

Solutions of the kinetic equation for quasiparticles have been studied in detail for both steady-state and unsteady cases (Elesin 1970a, 1975, Galitskii and Elesin 1973, Galitskii et al. 1978).

For example, in the case $\lambda \ll \omega_{\mathrm{D}}, \eta_{\mathrm{A}} \ll 1, n(\xi)$ is no longer an even function and can be represented in the form

$$n(\xi) = \begin{cases} v_p^2, & -a_0 \, (\omega_{\mathrm{D}} < \xi < \infty \\ 0, & \xi < a_0 \omega_{\mathrm{D}}, \quad a_0 = \int_{-\infty}^{\infty} \frac{\mathrm{d}\xi n(\xi)'}{\omega_{\mathrm{D}}} \end{cases} \tag{140}$$

where a_0 is proportional to the annihilation rate.

If $2\lambda > \omega_{\mathrm{D}}, \eta_{\mathrm{A}} \ll 1$, the solution of the kinetic equation will be (Elesin 1975)

$$n(\varepsilon) = \left[\exp \frac{\varepsilon - \mu^*}{T} + 1 \right]^{-1}, \quad n(\varepsilon) = \begin{cases} 1, & \varepsilon < \mu^* \\ 0, & \varepsilon > \mu^*, \end{cases} \quad T = 0, \tag{141}$$

where $\mu^*(0)/\mu_0 = \tau/3, T$ is the lattice temperature.

An inverse population exists in the conduction (valence) band. This form of the distribution

is related to the fact that the gap $2\lambda > \omega_{\rm D}$ forbids electron transitions (the rate of single band recombination is zero) into the state with $\xi < 0$ from the state with $\xi > 0$, where the electrons are accumulated due to indirect virtual transitions in the strong field (cf. the μ^*-model).

If we take into account the presence in the conduction band of equilibrium electrons with concentration n_d, we have to use the kinetic equation for each QDF $n_\alpha = n_\beta$; the QDFs are now related by

$$n_{\rm d} = \int \frac{{\rm d}^3 p}{(2\pi)^3} \left(n_\alpha(p) - n_\beta(p)\right) \tag{142}$$

22.4.3 2.3. The decay and spectrum of interacting quasiparticles

The results obtained above are valid if $\lambda\tau > 1$. The point is, which τ actually appears in this condition.

This problem was considered in a number of papers, using the efficient methods developed in superconductivity theory (Abrikosov et al. 1962) and the approach suggested by Keldysh (1964).

The spectrum and decay of quasiparticle excitations were found by Elesin (1969, 1970a) when sufficiently strong electron-phonon interaction was taken into account. It was shown that the gap in the excitation spectrum does remain, whatever strong the electron-phonon interaction be, and the decay is small.

A similar result has been obtained for electron-electron interaction.
The most significant effect on the spectrum was found to be due to scattering from charged (nonmagnetic!) impurities considered by Elesin (1970b). The impurity lamination was shown to lead to the destruction of an electron hole pair and to vanishing of the gap in the excitation spectrum at a certain time of scattering from an impurity $\lambda_{\rm imp}$:

$$\tau_{\rm imp} = 1/\lambda. \tag{143}$$

The reason is that the field of a charged impurity acts on the pair components with oppositely directed forces, due to the different signs of the electron and hole charges. The situation resembles that for a superconductor with magnetic impurities.

In pure crystals the decay of excitations is mainly determined by annihilation processes (interband recombination of electrons), the contribution being of two types. First, there is a contribution $\sim 1/\tau_A$, which is related to the probability of the direct escape of an electron from a state near the gap into the valence band. It is usually small because $\tau_{\rm A} \geqslant \tau_{\rm ph}$.

Second, there is a contribution (Elesin 1970a)

$$\gamma_{\rm A} = \frac{1}{\tau_{\rm A}} \frac{\mu_0}{\lambda} \gg \frac{1}{\tau_{\rm A}}, \tag{144}$$

which is essentially nonequilibrium.
Expression (144) is obtained if the QDF (140) is substituted into the decay formula (Elesin 1970a)

$$\gamma_{\rm A} = \frac{\pi\zeta_0}{2\omega_{\rm D}^2} \int_{-\mu_0}^{\infty} {\rm d}\xi \xi^2 n(\xi) \tag{145}$$

where ζ_0 is the constant of electron-phonon interaction.
The result has a simple physical meaning. The electrons, which find themselves, due to the field, in the conduction band at $p = p_0$ in the energy range $i.$ escape rapidly (as compared with interband recombination, since $\tau_{\rm ph} \ll \tau_{\rm A}$) into the energy range μ_0, from which they recombine at a rate of $1, \tau_{\rm A}$. Since the resultant rate of electron escape from the energy range μ_0 is limited

by recombination, the phonon time disappears from eq. (144), but a factor μ_0/λ.
appears. It takes into account that recombination occurs from the whole energy range μ_0.

Thus, the gap does exist if the following condition is satisfied:

$$\lambda > \frac{1}{\tau_{\rm A}} \frac{\mu_0}{\lambda}, \tag{146}$$

which can be rewritten in the form

$$Ik(\omega) > \frac{n_0}{\tau_{\rm A}}, \tag{147}$$

where I is the field intensity, $k(\omega)$ is the absorption coefficient. Condition (147) means that the rate of electron production must exceed the rate of electron annihilation. This is the condition needed for electrons to occupy the bottom of the conduction band up to the energy μ_0 (the saturation state) and this condition is relatively easy to realize ($I \sim 10^5$ W/cm^2) (Elesin 1970a).

22.4.4 2.4. The effect of a strong electromagnetic field on the properties of superconductors

The effect on superconductors of an electromagnetic field giving rise to interband transitions has been studied in several papers (Buimistrov 1968, Kumar and Sinha 1968, Blazhin and Selivanenko 1970, Aronov and Gurevich 1972, Elesin and Kopaev 1972, 1974).

Buimistrov (1968), Kumar and Sinha (1968) and Blazhin and Selivanenko (1970) considered the effect of a field on T_c due to renormalization of the matrix element of electron-phonon interaction caused by the mixing of wave functions.

The paper by Aronov and Gurevich (1972) considers the effect of a resonance field, which causes electrons above the gap ($\xi > 0$) to pass into an empty band. In this case a decrease in the number of thermal electrons near $\xi = 0$ and, hence, an increase in $T_{\rm c}$ was expected.

Aronov and Gurevich (1972) assumed that the QDF is of the form (1) with $\mu^* < 0$ and came to the conclusion that $T_{\rm c}$ must tend to infinity. Unfortunately, this conclusion has not been confirmed by the corresponding calculations of $n(\xi)$ and is, therefore, open to doubt.

The effect of simultaneous dynamic and kinetic action of the field was studied by Elesin and Kopaev (1972, 1974) for the cases of absence and presence of electrons in the conduction band, respectively.

According to (Elesin and Kopaev 1972), the kinetic action lies in the formation of a Fermi sphere of nonequilibrium electrons in the conduction band.

In this state superconductivity may arise due to an ordinary phonon
mechanism and to the formation of a superconducting gap at the Fermi surface μ_0.

The dynamic action means that a field gap 2λ (see section 2.1) is formed at the Fermi surface. As is shown by Elesin and Kopaev (1972), the field suppresses superconductivity if λ exceeds the energy of the Cooper pair A_0 :

$$\lambda \geqslant \Delta_0, \quad \Delta_0 = 2\omega_{\rm D} \exp\left(-\frac{1}{|g|}\right). \tag{148}$$

If $\lambda < \Delta_0$, the superconducting gap decreases,

$$\Delta = \sqrt{\Delta_0^2 - \lambda^2} \tag{\prime}$$

Consider this problem for $T = 0$ and $1/\tau_A = 0$, following Elesin and Kopaev (1972). The initial Hamiltonian of the system represents the Hamiltonian H_0 (129). The system is described

by Green's functions $G_{\|}$and ${F_{\|}}^{+}$(i is the band number) and also by the function G_{12}, which corresponds to electron-hole pairing. Solving the system, we obtain

$$G_{11}(p,\omega)=\frac{\omega+\xi}{\tilde{D}},\quad F_{11}^{+}=\frac{-i\Lambda^{*}}{\tilde{D}},\quad G_{21}=\frac{i\lambda}{\tilde{D}} \tag{149}$$

$$\tilde{D}=\omega^{2}-\tilde{\varepsilon}_{p}^{2},\quad \tilde{\varepsilon}_{p}=\sqrt{\xi^{2}+\Delta^{2}+\lambda^{2}} \tag{150}$$

$$1=|g|\int\frac{\mathrm{d}\xi}{\sqrt{\xi^{2}+\lambda^{2}+\Delta^{2}}} \tag{151}$$

The equation for the gap (151) yields the solutions (148) and (148'). Interestingly, the dispersion relation for quasiparticles (150) includes the gap $\sqrt{\xi^{2}+\lambda^{2}}=\Delta_{0}$, which remains constant for $0\leqslant\lambda<\Delta_{0}$.

The field suppresses the Meissner effect, reducing the number of superconducting electrons (Elesin and Kopaev 1974):

$$N_{\mathrm{S}}=1-\left(\lambda/\Delta_{0}\right)^{2},\quad 0\leqslant\lambda\leqslant\Delta_{0}. \tag{152}$$

At the same time, T_{c} almost does not change. This can be explained by the fact that the gap makes the production of thermal excitations difficult, which must lead to an effective increase in T_{c}. Indeed, the ratio $T_{\mathrm{c}}/\Delta(0)$ is

$$\frac{T_{c}}{\Delta(0)}=0.57\frac{1-0.3\lambda^{2}/\Delta_{0}^{2}}{1-\lambda^{2}/\Delta_{0}^{2}}, \tag{153}$$

i.e. it coincides with that in the BCS theory for $\lambda=0$ and exceeds 0.57 if $\lambda\neq 0$.

For crystals with equilibrium electrons in the conduction band the effect of the field is different.

As was shown by Elesin and Kopaev (1974), in this case T_{c} may rise significantly because the field gap does not coincide with the Fermi level. Therefore, the field gap does not suppress the superconducting gap. On the
contrary, renormalization of the electron spectrum due to λ leads to an increase in the density of states at the Fermi level, which corresponds to a rise in T_{c}. Elesin and Kopaev (1974) obtained the following expression for T_{c} :

$$T_{\mathrm{c}}=2.28\frac{\tilde{n}^{2}}{\lambda}\exp\left(-\frac{\tilde{n}}{\lambda}g_{0}\right),\quad g_{0}=\ln\frac{0.57\lambda}{T_{\mathrm{c}0}},\quad \tilde{n}=\frac{Nd}{3n_{0}}\mu_{0}. \tag{154}$$

It is assumed here that $i\gg T_{\mathrm{c}0},T_{\mathrm{c}}\ll 4\hat{n}^{2}/\lambda$. Note that the density of states at the Fermi level is proportional to the ratio $\lambda/\tilde{n}\gg 1$, so the factor $\tilde{n}/\lambda$ in the exponential in eq. (154) accounts for an increase in the density of states at the Fermi level; the pre-exponential factor $\tilde{n}^{2}/\lambda$ is related to a decrease in the energy region of interelectron attraction due to the formation of the gap 2λ.

The maximum value of T_{c} is

$$T_{\mathrm{cm}}=2.28\lambda_{\mathrm{m}}\left(\ln\frac{\lambda_{\mathrm{m}}0.57}{T_{\mathrm{c}0}}e\right)^{-1},\quad \frac{\lambda_{\mathrm{m}}}{\tilde{n}}+1=\ln\frac{0.57\lambda_{\mathrm{m}}}{T_{\mathrm{c}0}}. \tag{155}$$

Note that for a field intensity $\sim 10^{5}$ W/cm^{2} the value of λ_{m} is of the order of 10^{13} cm^{-1} and corresponds to $T_{\mathrm{cm}}\sim 100$ K.

22.4.5 2.5. Superconductivity in systems with repulsion and inverse quasiparticle distribution

An inverse distribution of quasiparticles may give rise to superconductivity of a new type-superconductivity with repulsion between electrons. Indeed, if in eq. (6) we change the sign both in $(1-2n)$ and in g, the equation will have a non-trivial solution. This was noted by Kirzhnits and Kopaev (1973).

In order to understand the nature of a bound state thus formed, it is convenient to use the concept of quasiholes (Elesin et al. 1973), for which the distribution is not inverse, the potential energy of interaction is positive (repulsion), and the kinetic energy is negative due to the negative sign of the hole mass. Obviously, since the potential and kinetic energies have opposite signs, the bound state may, in principle, occur.

The main difficulty for this state to occur lies in the initial creation and upkeep of the inverse quasiparticle population.

To avoid this difficulty, Kirzhnits and Kopaev (1973) suggested a "semiconductor model", in which the dielectric gap is assumed to make the inverse distribution possible. In this case the gap arises near the band extrema, rather than at the Fermi surface.

Another possibility was suggested by Galitskii et al. (1973) where a "selfsustained" superconducting state with $2A > (\theta_1)$ and $n\,(\xi_1^2) > \frac{1}{2}$ was shown to exists in a metal within a certain energy range near the Fermi level in the case of repulsion between electrons.

The inverse population near the Fermi surface is created due to a resonance electromagnetic field at a frequency of $\omega > E_g$. As was shown above (see section 2.1), the gap 2λ arises in this case near the Fermi surface. If $2\hat{\lambda} > \omega_{\mathrm{D}}$, the QDF becomes inverse* (see section, 2.2). In this case the equation

$$1 = g_{\mathrm{ee}} \int_0^{\omega} \frac{\mathrm{d}\xi(2n-1)}{\tilde{\varepsilon}} \tag{156}$$

has the solution

$$\Delta = \begin{cases} \sqrt{\Delta_0^2 - \lambda^2}, & 0 \leqslant \lambda \leqslant \Delta_0 \\ 0 \qquad\quad , & \lambda > \Delta_0 \end{cases} \tag{157}$$

$$\Delta_0 = \frac{2\mu^2}{\tilde{\omega}} \exp\left(-\frac{1}{g_{\mathrm{ee}}}\right)\left(1 - \exp\left(-\frac{2}{g_{\mathrm{ee}}}\right)\right)^{-1}.$$

This solution implies that λ should be chosen so as to be larger than $\omega_{\mathrm{D}}/2$ but less than Δ_0. Obviously, the condition

$$2\Delta_0 > \omega_{\mathrm{D}} \tag{158}$$

must also be satisfied, which is quite real due to large values of the constants g_{ee}.

Since the gap in the quasiparticle spectrum is $\sqrt{\lambda^2 + \Delta^2} = \Delta_0$, we can let λ adiabatically tend to zero (i.e. switch off the field), retaining, nevertheless, condition (158).

This means that in the nonequilibrium state and in the presence of a source transferring quasiparticles from the state below the gap into the state above it (in order to compensate for a certain recombination of quasiparticles due to multiphonon and electron-electron processes) the solution with the gap A_0 is self-sustained-the gap creates an inverse quasiparticle distribution, which in turn gives rise to a gap.

Conditions needed for such a state to be stable and the power of an additional source were considered in detail by Galitskii et al. (1973), Elesin (1970a), and Elesin and Kopaev (1981). The properties of inverse superconductivity were also studied in those papers at greater length.

Here we shall only touch upon the effect of anomalous paramagnetism of such superconductors, first discovered by Galitskii et al. (1973). This effect is closely related to the sign of N_S (see section 1.2.2).

Indeed, the current which arises due to a slowly varying magnetic field is expressed by eq. (63) where N_s is given by eq. (64). Using the expression for $n(\xi)$, we find that $N_s < 0$ and is equal to

$$N_S = -\left[\frac{2\mu}{\sqrt{\mu^2 - \Delta^2}} - 1\right] \simeq -1, \quad \mu \gg \Delta. \tag{159}$$

Obviously, the negative sign of N_S is associated with "supercooling" of the inverse distribution (and with the fact that $n(0) > \frac{1}{2}$).

0

- Note that this state does arise without an additional source, which transfers quasiparticles from the state below the gap into the state above it (Elesin 1975).

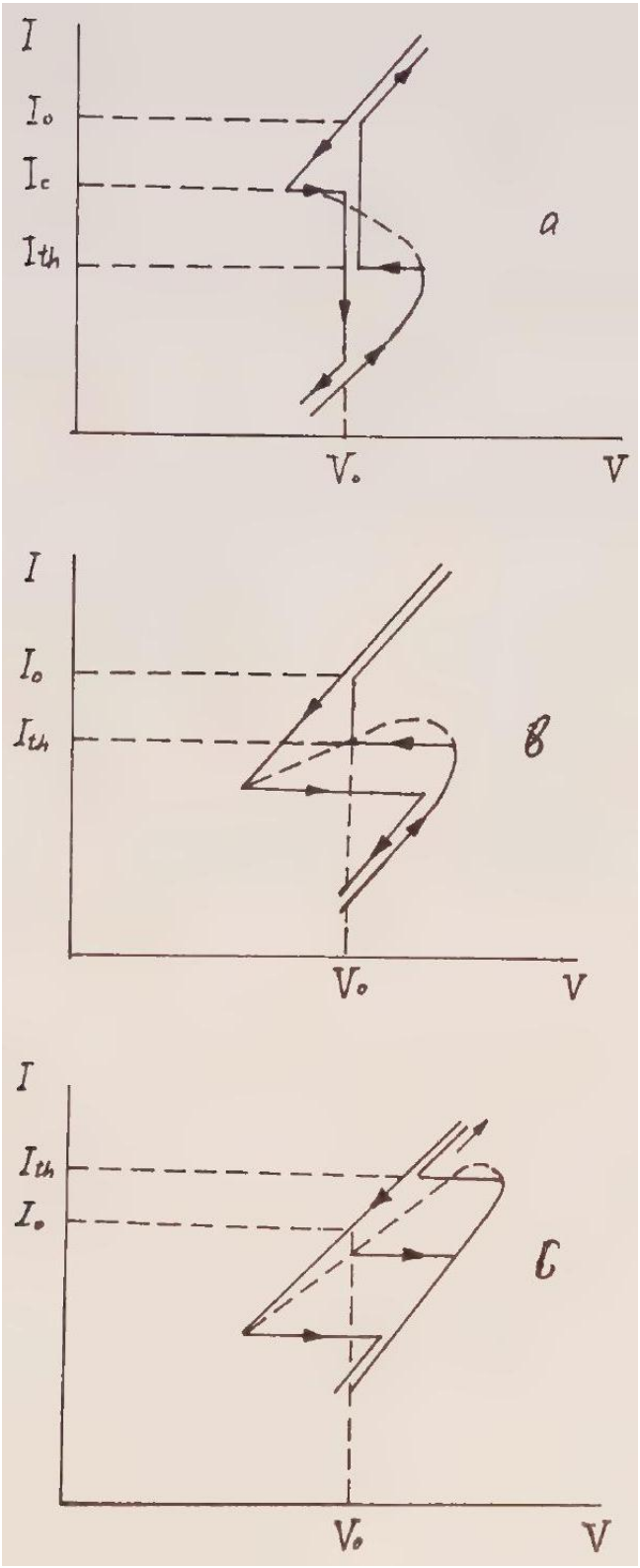


Fig. 9. Current voltage characteristics of junctions for high voltages: (a) type I; (b) type II; (c) type III. The dashed line corresponds to a homogeneous junction, the solid line to an inhomogeneous junction. (Elesin et al. 1980a,b.)

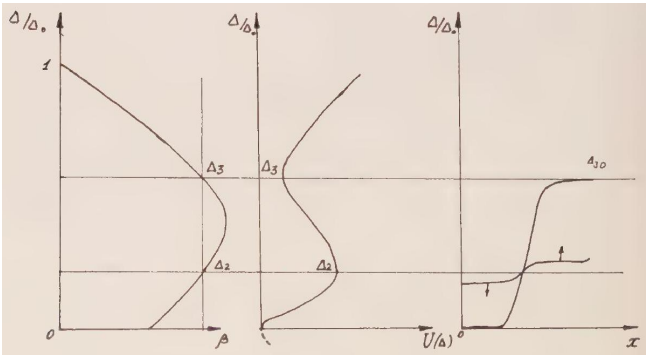


Fig. 10. (a) The dependence $\Delta(\beta)$; (b) dependence of energy $U(\Delta)$ on Δ; (c) dependence of Δ on the coordinate (laminated solution). (Elesin 1977a.)

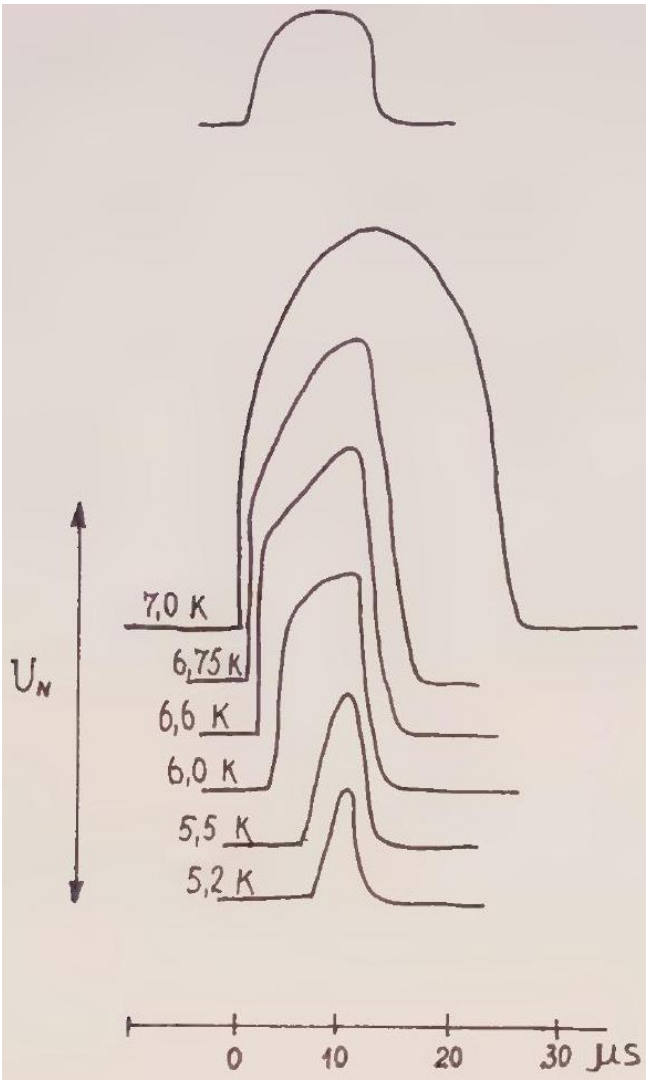


Fig. 11. Voltage across a Pb film under illumination with laser light for different temperatures (top: oscillogram of the laser pulse); $V_{\mathrm{N
}}$ is the voltage across the sample in the normal state. (Mitsen 1981.)}

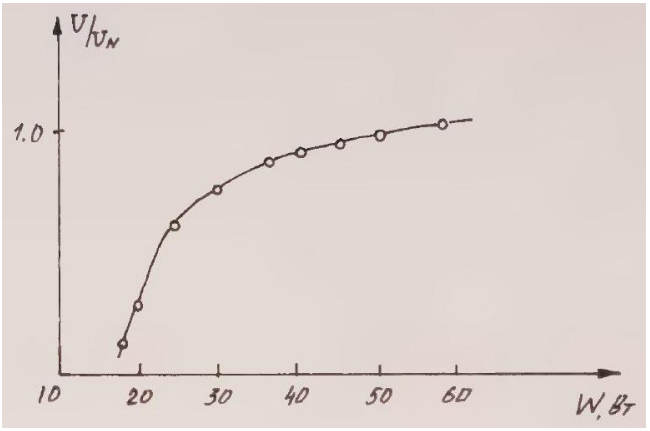


Fig. 12. Dependence on pumping power of the reduced voltage across a Pb sample under laser illumination; $\tau_{\mathrm{u
}}=1 \mu \mathrm{~s}, T=6.75 \mathrm{~K}$. (Mitsen 1981.)}

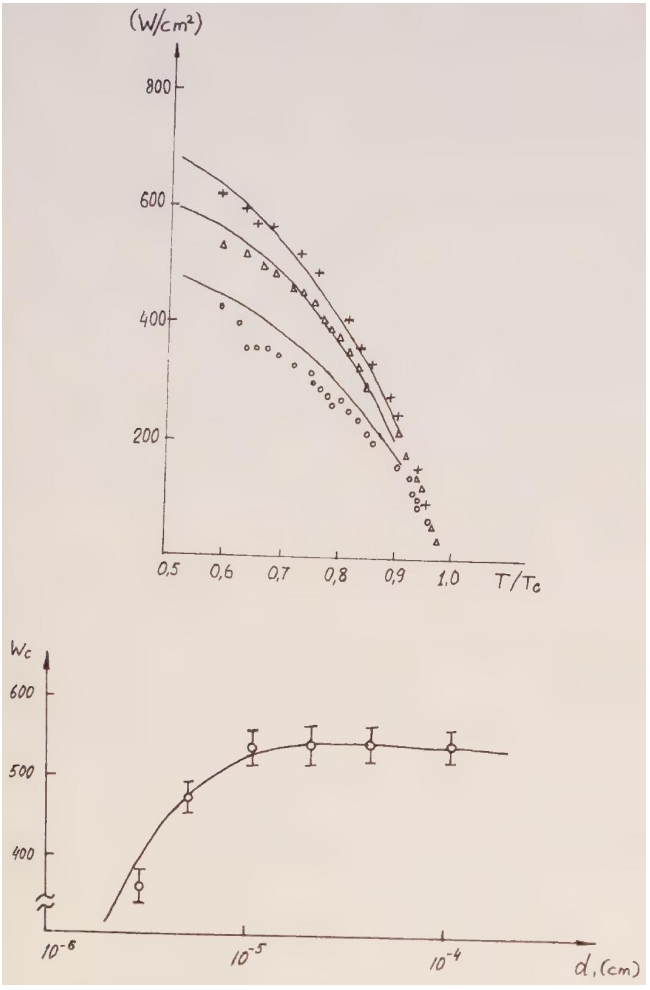


Fig. 13. (a) Dependence of the critical power on reduced temperature for Pb films of different thickness. Solid lines represent theoretical dependences $W_{1
\left(T T_{1}\right)$ according to eq. (79): (1300∧ : (A) 500Å : (x) 1000Å. (b) Dependence of the critical power on the thickness of a Pb film for $T/T_{\mathrm{c}} = 0.7$. Solid line: theoretical dependence $W_{\mathrm{c}}(d)$ according to eq. (79). (Golovashkin et al. 1980.)}

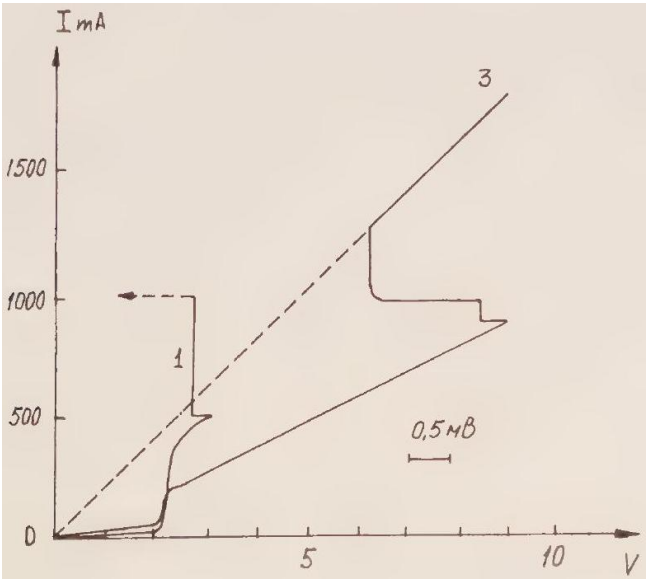


Fig. 14. Current-voltage characteristics of $\mathrm{Sn -\mathrm{I}-\mathrm{Sn}}$ junctions: (1) $\eta_T = 2.8 \times 10^{-3}\Omega, S = 0.16$ mm^2, $T = 1.7$ K, $d = 1200$Å; (2) $\eta_\mathrm{T} = 5.5 \times 10^{-3}\Omega, d = 2600$Å, $T = 1.7$ K. (Mitsen 1979.)}

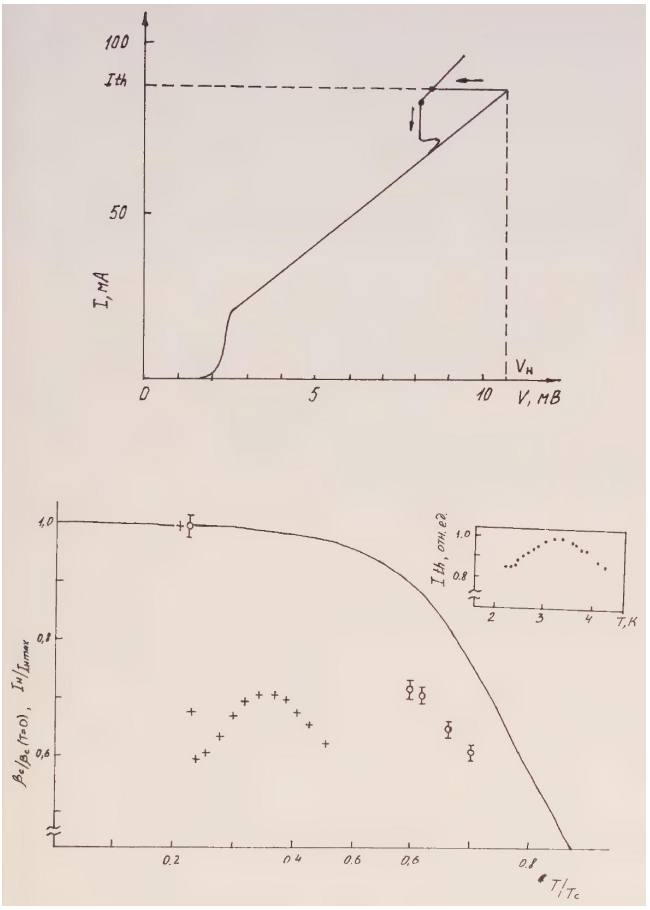


Fig. 15. (a) Current-voltage characteristic for $\mathrm{Nb -\mathbf{I ~ P b}}$ junction. (Pan and Rudenko 1981.) (b) Dependence of J_H on the local temperature $T_1(+)$ and on the bath temperature $\mathrm{T_b}(\bar{s})$. Solid line is the temperature dependence of $\mathrm{J_H}(T)/J_\mathrm{H}(0) = \beta_\mathrm{c}(T)/\beta_\mathrm{c}(0)$ taken from the article by Pan and Rudenko (1981).}

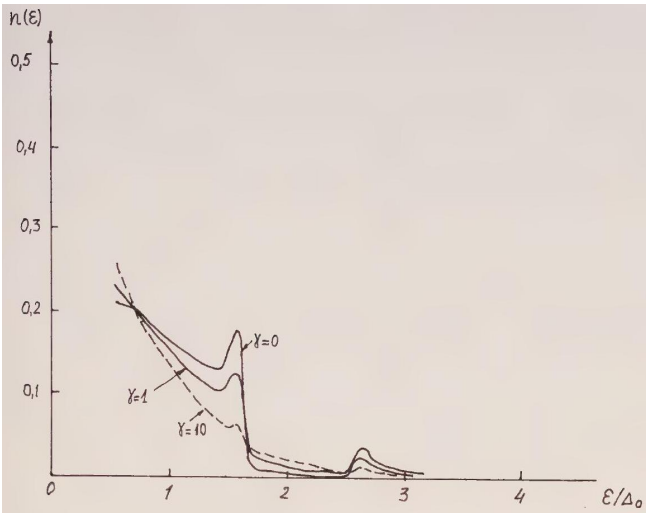


Fig. 16. The dependence $n(\varepsilon)$ for $\omega / \Delta_{0 =2.1, T / T_{\mathrm{c}}}=0.5, \Delta / \Delta_{0}=0.5$, and $\gamma = 0, 1, 10$. (Imai 1980.)}

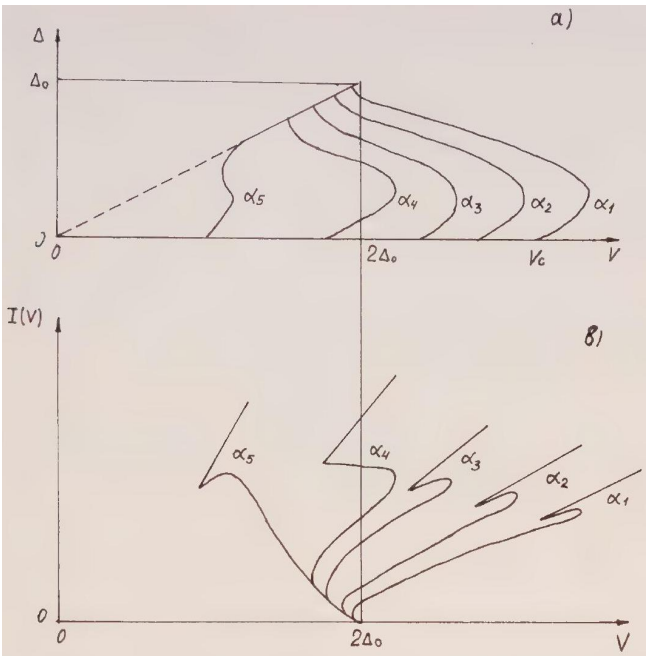


Fig. 17. (a) Dependence of the order parameter Δ on the junction voltage for different values of the injection parameter $\alpha_{V : \alpha_{1}<\alpha_{2}<\alpha_{3}<\alpha_{4}<\alpha_{5}$. (b) Dependence of the tunnel junction current $J(\ V)$ on the voltage for different α_{v}. (Elesin 1979b.)}

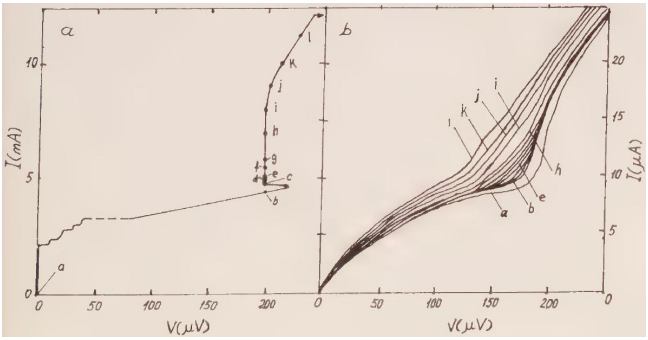


Fig. 18. Current-voltage characteristic of (a) generator and (b) detector; $T=1.169 \mathrm{˜K}$. (Gray and Willemsen 1978.)

23 Kinetic Equations in Superconducting Thin Films by Chang

23.1 1. Introduction

Within the frame work of the BCS theory (Bardeen et al. 1957), a superconductor is a system of three components: the quasiparticles, the phonons, and the paired electrons. Because of the strong interactions among the three components, disturbing any one component also drives the other two out of equilibrium. In order to understand the nonequilibrium phenomena to be discussed in this chapter, we need a means of describing the response of the three components to an external driving source. We have adopted the kineticequation approach. The excitation spectra of the quasiparticles and the phonons are described by a set of coupled kinetic equations (Bardeen et al. 1959, Ambegaokar and Tewordt 1964, Prange and Kadenoff 1964, Chang 1981). Following the treatment of Eliashberg (1970), the paired electrons are characterized by an energy gap using a modified BCS gap equation that relates the energy gap to the energy spectra of the quasiparticles in a nonequilibrium state.

In general, a superconducting state under driven condition depends upon not only the relaxation times of the sample and the strength of the driving source but also on the specific nature of the driving mechanism. For a given power input, various driving mechanisms excite quasiparticles and phonons differently, i.e., they produce different excitation spectra. The different signatures of the driving sources, as we will see, can be responsible for many interesting phenomena.

In the next section, we will introduce the coupled kinctic equations for the quasiparticle and phonon distributions. We begin by discussing the injection rates, i.e., the excitation rates of quasiparticles and phonons due to four kinds of external sources: quasiparticle injection through a tunnel junction, microwave radiation, light radiation, and phonon radiation. We will show that due to the singularity in the quasiparticle density of states at the gap edge, sharp structures in the quasiparticle and phonon spectra can occur. We also discuss the various relaxation processes and calculate the corresponding collision integrals.

How far away from equilibrium a system can be driven is determined by the relaxation time of the system and the strength of the source. However, in general, the relaxation time depends upon the specific nature of the non-
equilibrium state. Only when a system is driven into a state close to the original equilibrium state, can the relaxation times be expressed in terms of macroscopic dynamic variables and hence be of interest for consideration. In section 3, we will calculate the relaxation times of quasiparticles and phonons associated with various relaxation processes. These relaxation times are microscopic in nature and depend upon the ambient temperature and the energy of the quasiparticle or phonon states. We will show that the macroscopic relaxation times measured by various techniques are different weighted averages of these microscopic times. We also describe a technique which can measure the microscopic quasiparticle lifetimes. Superconductors driven far from equilibrium are considered in section 4 . We will consider three interesting phenomena. First, the generation of narrow-band phonons. We show that nearly monochromatic phonons of frequency $v \sim 2\Delta/h$ can be generated from a superconductor-insulator-superconductor tunnel junction. Since the energy gap is typically of order 1 meV , the phonon frequency is of order 500 GHz . Next, we consider the enhancement of superconductivity by microwave irradiation and quasiparticle tunnel injection. Finally, we will discuss two simple analytic models: the μ^* and T^* models which have been widely used to describe a superconductor with poor thermal coupling with the ambience. Stability of the driven homogeneous steady state will be discussed briefly using these models.

23.2 2. Basic equations

We will be interested in nonequilibrium states driven in a uniform and steady state manner. The kinetic equations which govern the quasiparticle and phonon distributions, $f(E_k)$ and $n(\Omega_q)$, have the following forms:

$$\frac{\mathrm{d}f(E_k)}{\mathrm{d}t} = I_{\mathrm{qp}}(E_k) + \left.\frac{\partial f(E_k)}{\partial t}\right|_{\mathrm{collision}} \tag{2.1a}$$

and

$$\frac{\mathrm{d}n(\Omega_q)}{\mathrm{d}t} = I_{\mathrm{ph}}(\Omega_q) + \left.\frac{\partial n(\Omega_q)}{\partial t}\right|_{\mathrm{collision}} \tag{2.1b}$$

Here $I_{\text{чр}}(E_{\mathrm{h}})$ and $I_{\mathrm{ph}}(\Omega_{\mathrm{q}})$ are respectively the energy spectra of the quasiparticle and phonon injection rates. The contributions to the rate of change of the quasiparticle and phonon distributions due to the various interaction mechanisms, are represented by $\left(\hat{\partial} f(E_h), \hat{\partial} t\right)_{\mathrm{coll}}$ and $\left(\hat{\partial} n(\Omega_q)/\hat{c}t\right)_{\mathrm{coll}}$. We calculate each term in eq. (2.1) by Fermi's Golden Rule. This method is the simplest and brings out the physics clearly. Furthermore, it has been shown (Eliashberg 1972, Entin-Wohlman and Orbach 1979a) that as long as the energy gap is well formed, the result of this method is the same as that obtained from a more rigorous Green function approach.

23.2.1 2.1. Injection rates

Here we first discuss the injection rates due to the various driving mechanisms. Collision rates are discussed in section 2.2.

23.2.2 2.1.1. Quasiparticle tunneling injection

Consider a tunnel junction formed by two superconducting thin strips separated by an insulating layer. The tunneling of quasiparticles can be described by the Hamiltonian (Bardeen 1961, 1962, Cohen et al. 1962)

$$H_{\mathrm{T}} = \sum_{k\cdot q,\sigma} T_{kq} C^{+}_{k\sigma} C_{q\sigma} + \text{ Hermitian conjugates.} \tag{2.2}$$

Here we use $k(q)$ for the wavevector of a quasiparticle state in the left (right) film of the junction, and $C^{+}_{k\sigma}(C_{k\sigma})$ is the creation (destruction) operator for an electron of wavevector k and spin σ. In terms of the quasiparticle operators γ and γ^{+}(see e.g. Schrieffer 1964):

$$\gamma^{+}_{k\uparrow} = u_k C^{+}_{k\uparrow} - v_k S^{+} C_{-k\downarrow}, \tag{2.3a}$$

$$\gamma_{k\downarrow} = u_k C_{-k\downarrow} + v_k S C^{+}_{k\uparrow}, \tag{2.3b}$$

the tunneling Hamiltonian becomes

$$H_{\mathrm{T}} = \sum_{k,q} T_{kq} \left(u_k \gamma^{+}_{k^*} + v_k \gamma_{-k_\downarrow} S^{+}\right)\left(u_q \gamma_{q\uparrow} + v_q S \gamma^{+}_{q\downarrow}\right) + \text{Hermitian conjugates.} \tag{2.4}$$

Here $S^{+}(S)$ is the pair creation (destruction) operator and u and v are the wellknown coherence factors. The four terms in eq. (2.4) give four distinct tunneling processes. It can

be easily shown that the Hermitian conjugate represents the reverse processes of these four direct processes. The four processes are shown in fig. 1. Their contribution to the quasiparticle injection can be calculated using the Golden-Rule approximation. We have for the right-hand film, the injection rates due to the four processes:

$$W_q^{\mathrm{a}} = \frac{2\pi}{\hbar\Omega_{\mathrm{R}}} \sum_k |T_{kq} u_k u_q|^2 (f_k - f_q)\, \delta(E_q - E_k - eV),$$
$$W_q^{\mathrm{b}} = \frac{2\pi}{\hbar\Omega_{\mathrm{R}}} \sum_k |T_{kq} v_k v_q|^2 (f_k - f_q)\, \delta(E_q - E_k + eV),$$
$$W_q^{\mathrm{c}} = \frac{2\pi}{\hbar\Omega_{\mathrm{R}}} \sum_k |T_{kq} v_k u_q|^2 (1 - f_k - f_q)\, \delta(E_q + E_k - eV),$$
$$W_q^{\mathrm{d}} = \frac{2\pi}{\hbar\Omega_{\mathrm{R}}} \sum_k |T_{kq} u_k v_q|^2 (1 - f_k - f_q)\, \delta(E_q + E_k + eV). \tag{2.5}$$

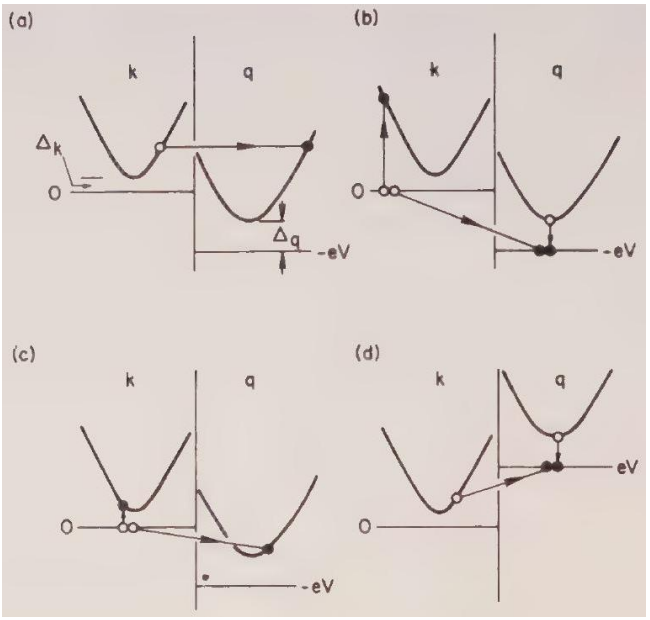


Fig. 1. Four quasiparticle tunneling channels in a superconductor-insulator junction, illustrated by their $T_{q k
$ terms, i.e., those which transfer an electron from k to q. (From Kirtley et al. 1980.)}

Here, the junction voltage is defined to be $V = V_q - V_k$, and Ω_{R} is the volume of the right-hand film under injection.

We first notice that the injection rates depend upon the non-equilibrium quasiparticle distribution. They also depend upon the coherence factors:

$$\mathrm{u}_k^2 = \frac{1}{2}(1 + \xi_k/E_k) \tag{2.6a}$$

and

$$v_k^2 = \frac{1}{2}(1 - \xi_k/E_k), \tag{2.6b}$$

with $\check{\zeta}_h$ being the electron energy measured from the chemical potential and $E_k = \left(\check{\xi}_k^2 + A^2\right)^{1/2}$. Since the coherence factors are not symmetric with respect to the

chemical potential, the injection rates for quasiparticle states of the same energy E but residing on the two different branches of $\xi_h > 0$ and $\xi_h < 0$ will be different. Therefore the steady-state quasiparticle distribution function will not only depend upon the energy of the state but also upon which branch the state is on. We use $f_{>}(E_h)$ and $f_{<}(E_h)$ to represent the distribution of quasiparticles on the $\xi_k > 0$ and $\xi_k < 0$ branches, respectively.

To put the injection rates into a more practical form, we carry out the sum over the wavevector k and eliminate T_{kq} in favor of the normal state conductance for the junction $G_{\rm nn}$. We obtain

$$W^{\rm a}_{\gtrless}(E_{\rm R}) = \frac{G_{\rm nn}}{2e^2 N_{\rm R}(0)\Omega_{\rm R}}\rho_{\rm L}(E_{\rm R}-eV)\left\{u^2_{\rm L>}(E_{\rm R}-eV)u^2_{\rm R\gtrless}(E_{\rm R})\left[f_{\rm L>}(E_{\rm R}-eV)\right.\right.$$
$$\left.\left. -f_{\rm R\gtrless}(E_{\rm R})\right] + u^2_{\rm L<}(E_{\rm R}-eV)\,u^2_{\rm R\gtrless}(E_{\rm R})\left[f_{\rm L<}(E_{\rm R}-eV) - f_{\rm R\gtrless}(E_{\rm R})\right]\right\}$$

$W^{\rm b}_{\gtrless}(E_{\rm R}) = {\rm W}^{\rm a}_{\gtrless}(E_{\rm R})$ with the replacements of V by $(-V)$ and u by v.

$$W^{\rm c}_{\gtrless}(E_{\rm R}) = \frac{G_{\rm nn}}{2e^2 N_{\rm R}(0)\Omega_{\rm R}}\rho_{\rm L}(-E_{\rm R}+eV)\left\{v^2_{\rm L} > (-E_{\rm R}+eV)\,u^2_{\rm R\gtrless}(E_{\rm R})\right.$$
$$\left[1 - f_{\rm L} > (-E_{\rm R}+eV) - f_{\rm R\gtrless}(E_{\rm R})\right] + v^2_{\rm L<}(-E_{\rm R}+eV)\,u^2_{\rm R\gtrless}(E_{\rm R})$$
$$\left.\left[1 - f_{\rm L<}(E_{\rm R}+eV) - f_{\rm R\gtrless}(E_{\rm R})\right]\right\}$$

$W^{\rm d}_{\gtrless}(E_{\rm R}) = W^{\rm c}_{\gtrless}(E_{\rm R})$ with replacements of V by ($-V$) and interchanged roles of u and v.

Here $G_{\rm nn} = (4\pi e^2/\hbar)\,T^2 N_{\rm L}(0)N_{\rm R}(0)\Omega_{\rm L}\Omega_{\rm R}, T$ is the effective tunneling matrix element, Ω is the volume under injection, and $\rho_{\rm L}(E_{\rm L}) \equiv \theta(E_{\rm L}-\Delta_{\rm L})\,|E_{\rm L}|\,/\,(E_{\rm L}-A_{\rm L})^{1/2}$ is the normalized BCS density of states function for the quasiparticles in the left film. The total quasiparticle injection rate into the right film for the two $\xi_k \gtrless 0$ branches are

$$I_{\rm qp}\overset{>}{<}(E_{\rm R}) = W^{\rm a}_{\gtrless}(E_{\rm R}) + W^{\rm b}_{\gtrless}(E_{\rm R}) + W^{\rm c}_{\gtrless}(E_{\rm R}) + W^{\rm d}_{\gtrless}(E_{\rm R})\,. \tag{2.8a}$$

When the injection rate is not too strong, we can approximate the distribution function in the right-hand side by the equilibrium distribution, i.e. $f_{>}(E) \sim f_{<}(E) \sim f_0(E,T)$ with $f_0(E,T) = 1/\left(\exp\left[(E-\mu)/k_{\rm B}T\right]+1\right)$. The injection rates for a film in a symmetric junction of $A_{\rm L} = A_{\rm R} = A$ and biased at voltages of $V = Ae$ and $3A/e$ are shown in fig. 2 . The quantitative difference in the excitation rates for the $\xi_k > 0$ branch ($I_{\rm qp} >$), and the $\xi_k < 0$ branch ($I_{\rm qp} <$), is apparent. For negative voltages, the solid and dotted curves interchange roles due to the electron-hole symmetry. Furthermore, the injection spectrum due to tunneling from a normal metal can be obtained from eqs. (2.7, 8a) with $\Lambda_{\rm L} = 0$.

Finally, since, no phonons are injected into the films,

$$I_{\rm ph}(\Omega_q) = 0 \tag{2.8b}$$

23.2.3 2.1.2. Microwave irradiation

We consider a film irradiated by microwaves of frequency (1). If the electromagnetic field is described by the vector potential

$$A(r,t) = A_\omega e^{{\rm i}(q\cdot r-\omega t)} + \text{ c.c.} \tag{2.9}$$

The coupling Hamiltonian is of the form (Mattis and Bardeen 1958)

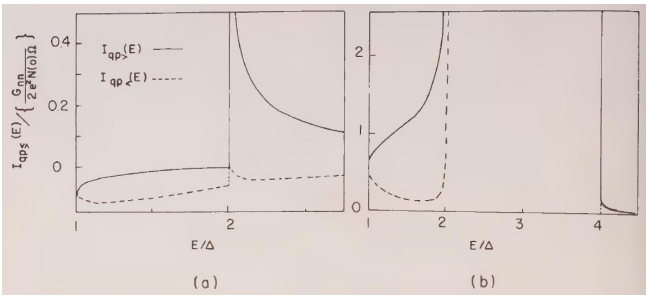


Fig. 2. The energy spectra of the quasiparticle injection rate in the film of a symmetric superconductor-insulator superconductor tunnel junction. (a) Ambient temperature $T_{a =0.9 T_{c}$ and bias voltage $V = \Delta(T)/e$. (b) $T_a = 0.5T_c$ and $V = 3\Delta(T)/e$.}

$$
\begin{aligned}
H(t) =& -\frac{1}{c}\int j(r)\cdot A(r,t)\mathrm{d}^3 r \\
=& \frac{e}{2mc}\sum_{k,\sigma} A_\omega\cdot(2k+q)C^+_{k+q,\sigma}C_{k,\sigma}\mathrm{e}^{-\mathrm{i}\omega t} + \text{ Hermitian conjugate} \\
=& \sum_k \frac{eA_\omega\cdot(2k+q)\mathrm{e}^{-\mathrm{i}\omega t}}{2mc}\left\{L(k+q,k)\left[\gamma^+_{(k+q)\uparrow}\gamma_{k\uparrow}-\gamma^+_{-k\downarrow}\gamma_{-(k+q)\downarrow}\right]\right. \\
& \left. -P(k+q,k)\left[\gamma^+_{(k+q)\uparrow}\gamma^+_{-k\downarrow}S+\gamma_{k\downarrow}\gamma_{-(k+q)\downarrow}S^+\right]\right\} \\
& + \text{Hermitian conjugate,}
\end{aligned}
\tag{2.10}
$$

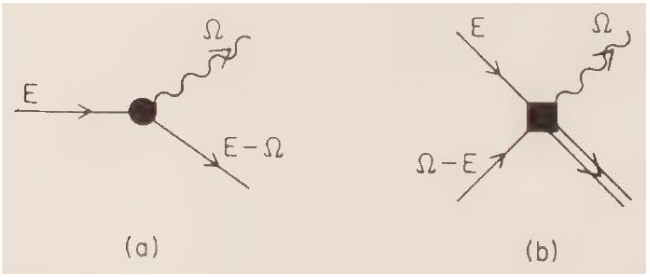


Fig. 3. Basic processes of the electron-microwave interaction. The solid lines represent electrons and the wavy lines represent photons. (a) Scattering process; (b) recombination process or pairbreaking process. The same diagrams can also describe the electron-phonon interaction if the wavy lines are considered representing phonons. (From Chang and Scalapino 1978.)

where the coherence factors L and P are given by

$$L(p',p) = u_{p'}u_p + v_{p'}v_p \tag{2.11a}$$

and

$$P(p',p) = u_{p'}v_p - u_p v_{p'}. \tag{2.11b}$$

Therefore the interaction Hamiltonian provides two processes for exciting the quasiparticles. These are shown in fig. 3. The injection rates due to the two processes can again be calculated from the Golden Rule. After eliminating the matrix element in favor of the more practical quantity R_N, the normal-state surface resistance, we obtain

$I_{\rm qp}(E) = \frac{2R_{\rm N}H^2}{{\rm dN}(0)\omega^2}$
$\times \Big\{\rho(E-\omega)\left(1+\frac{A^2}{E(E-\omega)}\right)[f(E-\omega)(1-f(E))-f(E)(1-f(E-\omega))]\theta(E-\omega-\Delta)$
$+\rho(E+\omega)\left(1+\frac{\Delta^2}{E(E+\omega)}\right)[f(E+\omega)(1-f(E))-f(E)(1-f(E+\omega))]\theta(E+\omega-\Delta)$

$$+\rho(\omega-E)\left(1-\frac{\Delta^2}{E(\omega-E)}\right)[(1-f(E))(1-f(\omega-E)) \tag{2.12a}$$

$-f(E)f(\omega-E)]\theta(E-\Delta)\theta(\omega-E-\Delta)\}$.

Here H is the RF magnetic field. The first two terms in the curly brackets are due to process (a). The last term is contributed by process (b) and is nonzero only when $\hbar\omega > 2\Delta$. We notice that in this case both branches of $\breve{\zeta}_h \gtrless 0$ are excited equally.

Since the coupling of the microwaves to the phonons is usually quite weak, we will assume for this case

$$I_{\rm ph}\left(\Omega_q\right) = 0. \tag{2.12b}$$

23.2.4 2.1.3. Heat pumping and light irradiation

For a superconducting thin film attached to a heater at temperature $T_{\rm H}$, the phonon injection current is given by (Little 1959)

$$I_{\rm ph}(\Omega) = \frac{\Gamma_s}{2d}\left[n\left(\Omega, T_{\rm H}\right) - n(\Omega)\right]. \tag{2.13a}$$

Here Γ is an angularly averaged phonon transmission coefficient between the film and the heater, s is the averaged speed of sound in the film, and d is the film thickness. Since the phonon frequency of interest is of the order 2.1 h . which is much smaller than the Debye frequency $v_{\rm D}, \Gamma$ and s can be taken to
be constants independent of Ω. Obviously

$$I_{\rm qp}\left(E_k\right) = 0 \tag{2.13b}$$

for the case of heat pumping.

As for the case of films under laser irradiation, it has been shown (Chang and Scalapino 1977c) that pseudoinjection terms can be used. They have the forms:

$$I_{\rm qp}\left(E_k\right) = 0 \tag{2.14a}$$

and

$$I_{\rm ph}\left(\Omega_q\right) = \text{ constant }. \tag{2.14b}$$

23.2.5 2.2. Relaxations

We will consider three relaxation processes: (a) the electron-phonon interaction, which is inelastic, (b) the electron-impurity scattering, which is elastic, and (c) the "relaxation" of phonons by escape from the sample film. Usually, these are the most important relaxation mechanisms. Other processes such as electron-magnetic impurities scattering have been discussed by many authors (Schmid and Schön 1975, Entin-Wohlman and Orbach 1979b, Pethick and Smith 1980, Lemberger and Clark 1981), and will not be discussed here.

23.2.6 2.2.1. Electron-phonon collisions

The Hamiltonian for the electron-phonon interaction has the well-known form (see e.g. Schrieffer 1964)

$$H_{ep\ \mathrm{h}} = \sum_{pq\sigma i} g_{q\lambda} \mathrm{C}^{+}_{(p+q),\sigma} \mathrm{C}_{p\sigma} \left(a_{q\lambda} + a^{+}_{-q\lambda} \right) \tag{2.15}$$

In terms of the quasiparticle operators (eq. 2.3) it becomes

$$\begin{aligned} H_{\mathrm{e-ph}} = & \sum_{pq\lambda} g_{q\lambda} \left(a_{q\lambda} + a^{+}_{-q\lambda} \right) \left\{ N(p+q,p) \left[\gamma^{+}_{(p+q)\uparrow} \gamma_{p\uparrow} + \gamma^{+}_{-p\downarrow} \gamma_{-(p+q)\downarrow} \right] \right. \\ & \left. + M(p+q,p) \left[\gamma^{+}_{(p+q)\uparrow} \gamma^{+}_{-p\downarrow} S - \gamma_{p\uparrow} \gamma_{-(p+q)\downarrow} S^{+} \right] \right\} \end{aligned} \tag{2.16}$$

where

$$N\left(p',p\right) \equiv u_{p'}u_p - \iota_{p'}\iota_p = \frac{1}{2}\left(1 - \left(\Delta^2 - \xi_p\xi_{p'}\right)/E_pE_{p'}\right) \tag{2.17a}$$

and

$$M\left(p',p\right) \equiv u_{p'}v_p + v_{p'}u_p = \frac{1}{2}\left(1 + \left(\Delta^2 - \xi_p\xi_{p'}\right)/E_pE_{p'}\right). \tag{2.17b}$$

Therefore the basic processes are the same as for the microwave case (fig. 3) although the matrix elements and the coherence factors involved are different. These processes can change both the quasiparticle and phonon distributions.

Their contribution to the rate of change of the distributions $\hat{c}f\left(E_p\right)/\hat{c}t$ and $\partial n\left(\Omega_q\right)/\partial t$, can be easily calculated using the Golden-Rule approximation. If we further assume strong elastic interactions between the quasiparticle and the impurities, the treatment of Eliashberg in dealing with strong superconductors can be adopted (Eliashberg 1960, Scalapino, 1969) to average out the angular dependence and to eliminate g_q in favor of $x^2F(\Omega)$. We obtain for the quasiparticle relaxation rate

$$\begin{aligned} & \left.\frac{\partial f(\xi)}{\partial t}\right|_{\mathrm{eph}} = \frac{2\pi}{\hbar}\int_{-\infty}^{\infty}\mathrm{d}\xi'\int_{0}^{\infty}\mathrm{d}\Omega\alpha^2F(\Omega) \\ & \times\left\{\frac{1}{2}\left(1-\frac{\Delta^2-\xi\xi'}{EE'}\right)\left[f\left(\xi'\right)\left(1-f(\xi)\right)(n(\Omega)+1)-\left(1-f\left(\xi'\right)\right)f(\xi)n(\Omega)\right]\delta\left(\Omega+E-E'\right)\right. \\ & -\frac{1}{2}\left(1-\frac{\Delta^2-\xi\xi'}{EE'}\right)\left[f(\xi)\left(1-f\left(\xi'\right)\right)\left(n(\Omega)+1\right)-\left(1-f(\xi)\right)f\left(\xi'\right)n(\Omega)\right]\delta\left(\Omega+E'-E\right) \\ & \left.+\frac{1}{2}\left(1+\frac{\Delta^2-\xi\xi'}{EE'}\right)\left[\left(1-f(\xi)\right)\left(1-f\left(\xi'\right)\right)n(\Omega)-f(\xi)f\left(\xi'\right)\left(n(\Omega)+1\right)\right]\delta\left(\Omega-E-E'\right)\right\} \end{aligned} \tag{2.18}$$

where the subscript "e-ph" stands for inelastic electron-phonon interactions. The first two terms are contributed by the scattering process (a) with the first (second) term due to the scattering of a quasiparticle from a state of energy $E = \left(\xi^2+\Delta^2\right)^{1/2}$ to a state of $E' > E\left(E' < E\right)$ and vice versa. They are proportional to the effective-interaction matrix element squared, α^2; the effective phonon density of states, $F(\Omega)$; the coherence factor $N^2 = \frac{1}{2}\left[1-\left(\Delta^2-\xi\xi'\right)/EE'\right]$, and the various quasiparticle and phonon distribution functions. The last term is due to the recombination process and its reverse, the pairbreaking process. We notice that the

coherence factor involved is $M^2 = \frac{1}{2}[1+ (\Delta^2 - \xi\xi')/EE']$ which is different from the previous case. Furthermore, only phonons of energy $\Omega = E + E' \geqslant 24$ give a nonzero contribution to the last term.

Similarly, the contribution of the electron phonon interaction to the rate of change of the phonon distribution is

$$\begin{aligned}\left.\frac{\partial n(\Omega)}{\partial t}\right|_{\text{eph}} &= \frac{2\pi}{\hbar}\int_{-}^{\prime} \mathrm{d}\xi \int^{\prime} \mathrm{d}\xi' \frac{2N(0)}{N}\alpha^2 \\ &\times \left\{\frac{1}{2}\left(1 - \frac{\Delta^2 - \xi\xi'}{EE'}\right)[f(\xi)(1 - f(\xi'))n(\Omega) - f(\xi')(1 - f(\xi))(n(\Omega)+1)]\,\delta(\Omega + E - E')\right. \\ &+ \frac{1}{4}\left(1 + \frac{\Delta^2 - \xi\xi'}{EE'}\right)[(1 - f(\xi))(1 - f(\xi'))n(\Omega) \\ &\left. - f(\xi)f(\xi')(n(\Omega)+1)]\,\delta(\Omega - E - E')\right\} \end{aligned} \tag{2.19}$$

where N and $2N(0)$ are respectively the ion density and the electron density of states on the Fermi surface. The first term is due to the scattering process while the second is due to the pair-breaking process as can be clearly seen by noticing the different coherent factors and the different combinations of the distribution functions involved.

23.2.7 2.2.2. Electron-impurity interactions

We assume that this interaction is elastic and spin independent. It has been shown (Eliashberg 1970a) that the effect of a strong electron-impurity interaction is to average out the angular dependence of states with the same energy. However, for a superconductor with an isotropic gap, because the relevent coherence factor $N(p', p)$ for elastic scattering vanishes with $\xi_{\text{p}} = -\xi'_p$, quasiparticles on the $\xi_p > 0$ branch cannot be scattered to the $\xi'_p < 0$ branch and vice versa. This means that the effect of elastic scatterings is to average out the population of states residing on the same branch only, and in general the populations of the two branches with $\check{\zeta}_p > 0$ and $\check{\zeta}_p < 0$ are different. Therefore, instead of considering $f(E)$ alone we have to consider $f_>(E)$ and $f_<(E)$ separately when a population imbalance on the branches exists such as in the case of quasiparticle tunnel injections discussed in section 2.1.1.

For superconductors with an anisotropic energy gap, the coherence factor $N(p', p)$ associated with the elastic scattering is not zero. Therefore, elastic scattering will contribute to the reduction of the branch imbalance, which can be measured by the function $f_-(E) = f_>(E) - f_<(E)$. Tink ham (1972) calculated the contribution to the rate of change of the distribution function $f(E)$ and found a term of the form

$$\left.\frac{\partial f_-(E)}{\partial t}\right|_{\text{e-i}} = -\frac{2f_-(E)}{\tau_{\text{el}}(E)} \tag{2.20a}$$

with the energy-dependent elastic branch-mixing rate $\tau_{\text{el}}^{-1}(E)$ given by

$$\tau_{\text{el}}^{-1}(E) = \tau_{\text{i}}^{-1}\frac{\Delta^2 E}{(E^2 - \Delta^2)^{3/2}} \tag{2.20b}$$

where $\tau_i{}^1$ is an energy-independent time rate proportional to the mean squared deviation of the anisotropic gap as well as the impurity concentration, and A is the averaged gap energy in the equilibrium state.

In the presence of a branch imbalance, it is found more convenient to consider, instead of $f_>(E)$ and $f_<(E)$, the functions:

$$f_+(E) \equiv \frac{1}{2}\left[f_>(E) + f_<(E)\right] \tag{2.21a}$$

and

$$f_-(E) \equiv \left[f_>(E) - f_<(E)\right], \tag{2.21b}$$

which are respectively symmetric and antisymmetric with respect to the populations of the two branches. The rate of change of these functions due to electron phonon interactions can be easily obtained from eq. (2.18). We have

$$\begin{aligned}
&\partial f_+(E)|_{eph} = -\frac{2\pi}{h}\int_0^{'} \mathrm{d}E'\rho\left(E'\right) \\
&\partial \int_{x^2} F\left(E-E'\right)\left[\theta(E-E')(1-\frac{\Delta^2}{EE'})\left(f_-(E)\left(1-f_-\left(E'\right)\right)\left(n\left(E-E'\right)\right)\right.\right. \\
&\left.\left.-\left(1-f_+(E)\right)f_+\left(E'\right)n\left(E-E'\right)\right)+\frac{|\xi\xi'|}{4EE'}f_-(E)f_-\left(E'\right)\right] \\
&-\left[E\to E' \text{ and } E'\to E\right] \\
&+\alpha^2F\left(|E+E'|\right)\left[(1+\frac{\Delta^2}{EE'})\left(f_+(E)f_+\left(E'\right)\left(n\left(E+E'\right)+1\right)\right.\right. \\
&\left.\left.-\left(1-f_+(E)\right)\left(1-f_+\left(E'\right)\right)n\left(E+E'\right)\right)+\frac{|\xi\xi'|}{4EE'}f_-(E)f_-\left(E'\right)\right]\Bigg\}
\end{aligned} \tag{2.22a}$$

and

$$\begin{aligned}
&\left.\frac{\partial f_-(E)}{\partial t}\right|_{e-\text{ ph}} = -\frac{2\pi}{\hbar}\int_0^{\infty}\mathrm{d}E'\rho\left(E'\right)f_-(E)\left\{\alpha^2F\left(E-E'\right)\left(1-\frac{\Delta^2}{EE'}\right)\right. \\
&\times\left[\theta\left(E-E'\right)\left(1+n\left(E-E'\right)-f_+\left(E'\right)\right)+\theta\left(E'-E\right)\left(f_+\left(E'\right)+n\left(E'-E\right)\right)\right] \\
&\left.+\alpha^2F\left(|E+E'|\right)\left(1+\frac{\Delta^2}{EE'}\right)\left(f_+\left(E'\right)+n\left(E+E'\right)\right)\right\} \\
&+\frac{2\pi}{\hbar}\int_0^{\infty}\mathrm{d}E'\rho\left(E'\right)f_-\left(E'\right)\frac{|\xi\xi'|}{EE'}\left\{\alpha^2F\left(|E-E'|\right)\right. \\
&\times\left[\theta\left(E-E'\right)\left(f_+(E)+n\left(E-E'\right)\right)+\theta\left(E'-E\right)\left(1+n\left(E'-E\right)-f_+(E)\right)\right] \\
&\left.-\alpha^2F\left(|E+E'|\right)\left(f_+(E)+n\left(E+E'\right)\right)\right\}
\end{aligned} \tag{2.22b}$$

23.2.8 2.2.3. Phonon escape

Through this mechanism the sample gets rid of the energy injected by the external source. We use a phenomenological term

$$\left.\frac{\hat{c}n(\Omega)}{\hat{c}t}\right|_{\text{cs}} = -\frac{n(\Omega)-n^-\left(\Omega,T_{\text{a}}\right)}{\tau_{\text{c}}} \tag{2.23a}$$

to simulate the escape of excess phonons.
Here $n\left(\Omega.T_a\right)$ is the equilibrium phonon distribution at the ambient temperature. T_a. The phonon escape time. $\tau_{...}$. depends strongly upon the genmetry and the acoustic match between the sample and the environment. In fact, the situation here is similar to the case of heat pumping discussed in section 2.1.3, and the phonon escape time is given by

$$\tau_{\text{es}} = 2d/\Gamma s. \tag{2.23b}$$

23.2.9 2.3. Summary on the kinetic equations

From the above discussion it is clear that a superconductor can be disturbed in many different ways. If the "characteristic frequency" associated with the external source (for tunnel junction of quasiparticles the characteristic frequency is eV/h) exceeds 24/h, pair-breaking can occur and the nonequilibrium state would have a quasiparticle density larger than that in equilibrium. However, if the characteristic frequency of the source is small, the primary effect of the external source is to redistribute the quasiparticles by exciting them into higher-energy states (e.g., microwave irradiation with $v < 2\Delta/h$) or to extract quasiparticles out of the film (e.g., tunneling in an asymmetric junction). Furthermore, quasiparticle injection through tunnel junction can create population imbalance on the two quasiparticle branches of $\zeta_k > 0$ and $\zeta_k < 0$.

As for the relaxation back to equilibrium, only the quasiparticle recombination process can reduce the quasiparticle density. When this process takes effect, phonons of energy $\Omega \geqslant 2A/e$ will be created. The effect of the elastic electron impurity scattering is to average out the angular dependence for states of the same energy. However, it is ineffective for the relaxation of the branch imbalance if the gap anisotropy is small. If this is the case, we have to consider the two branches of $\xi_k \gtrless 0$ separately.

Putting all the pieces together, we have three coupled kinetic equations for the distribution functions of the quasiparticles and phonons. Their detailed forms are

$$\frac{\mathrm{d}f_+(E)}{\mathrm{d}t} = I^+_{\mathrm{qp}}(E) + \left.\frac{\partial f_+(E)}{\partial t}\right|_{\mathrm{e-ph}}, \tag{2.24a}$$

$$\frac{\mathrm{d}f_-(E)}{\mathrm{d}t} = I^-_{\mathrm{qp}}(E) + \left.\frac{\partial f_-(E)}{\partial t}\right|_{\mathrm{e-ph}} + \left.\frac{\partial f_-(E)}{\partial t}\right|_{\mathrm{e-i}} \tag{2.24b}$$

$$\frac{\mathrm{d}n(\Omega)}{\mathrm{d}t} = I_{\mathrm{ph}}(\Omega) + \left.\frac{\partial n(\Omega)}{\partial t}\right|_{\mathrm{e-ph}} + \left.\frac{\partial n(\Omega)}{\partial t}\right|_{\mathrm{esc}} \tag{2.24c}$$

with

$$I^+_{\text{чр}}(E) = \frac{1}{2}\{I_{\text{чр}} > (E) + I_{\text{чр}} < (E)\}$$

and

$$\mathrm{I}_{\mathrm{qp}}(E) = I_{\mathrm{qp}} > (E) - I_{\mathrm{qp}} < (E).$$

The terms $\partial f_\pm(E)/\,\partial t|_{e\mathrm{ph}}$ and $\partial n(\Omega)/\,\partial t|_{e\mathrm{ph}}$ are given by eqs. (2.22) and (2.19).

23.2.10 2.4. Modified gap equation

To solve the kinetic equations, we need to know the energy gap. It has been shown that the energy gap in a nonequilibrium state is governed by the modified BCS gap equation (Eliashberg 1970b), which can be put into the form

$$\ln\left(\Delta/\Delta_0\right) = -\int_1^\infty \mathrm{d}E \frac{2f_+(E)}{\sqrt{(E^2-\Delta^2)}} \tag{2.25}$$

where A_0 is the zero-temperature energy gap.

In summary, the coupled kinetic equations (eq. 2.24) along with the modified gap equation (eq. 2.25) form the basis of our discussion. For a given driving situation, these coupled equations have to be solved simultaneously. Let us first apply these equations to a system driven into a state near equilibrium.

23.3 3. Systems near equilibrium

In a system slightly away from equilibrium, the deviations of the quasiparticle and phonon distributions, $\delta f_{\gtrless}(E)$ and $\delta n(\Omega)$, as well as the energy gap are small compared with their respective equilibrium values. This means that we can use the coupled equations linearized with respect to

$$\delta f_+(E) \equiv f_+(E) - f^\circ(E), \tag{3.1a}$$
$$\delta f_-(E) \equiv f_-(E), \tag{3.1b}$$
$$\delta n(\Omega) \equiv n(\Omega) - n^\circ(\Omega), \tag{3.1c}$$

to describe the system, where $f(E)$ and $n(\Omega)$ are, respectively, the quasiparticle and phonon distributions in the equilibrium state at an ambient temperature T_a. The only terms in the kinetic equations that need to be linearized are those contributed by the electron phonon interaction. In the linear approximation, they have the forms:

$$\begin{aligned}\left.\frac{\partial f_+(E)}{\partial t}\right|_{e-\mathrm{ph}} = &-\int_0^\infty \mathrm{d}E' 4N(0)\rho(E') \\ &\times \{\delta f_+(E)\left[K_1(E,E') + K_1(-E,-E') + K_1(E,-E')\right] \\ &+\delta f_+(E')\left[K_1(E',E) + K_1(-E',-E) - K_1(E',-E)\right]\} \\ &-\int_0^\infty \mathrm{d}\Omega N F(\Omega)\delta n(\Omega)\left[K_2(\Omega,E) + K_2(-\Omega,E) - K_2(\Omega,-E)\right]\end{aligned} \tag{3.2a}$$

$$\begin{aligned}\left.\frac{\partial f_-(E)}{\partial t}\right|_{\mathrm{e\cdot ph}} = &-\int_0^\infty \mathrm{d}E' 4N(0)\rho(E') \\ &\times \{\delta f_-(E)\left[K_1(E,E') + K_1(-E,-E') + K_1(E,-E')\right] \\ &+\delta f_-(E')\left[K_3(E,E') + K_3(-E,-E') + K_3(E,-E')\right]\}\end{aligned} \tag{3.2b}$$

$$\begin{aligned}\left.\frac{\partial n(\Omega)}{\partial t}\right|_{e-\mathrm{ph}} = &-\int_0^\infty \mathrm{d}E 4N(0)\rho(E)\delta n(\Omega)\left[K_2(\Omega,E) + \frac{1}{2}K_2(\Omega,-E)\right] \\ &-\int_0^\infty \mathrm{d}E 4N(0)\rho(E)\delta f_+(E)\frac{4N(0)}{NF(\Omega)} \\ &\times [-\rho(E-\Omega)K_1(E,E-\Omega) + \rho(\Omega+E)K_1(-E,-(E+\Omega)) \\ &-\rho(\Omega-E)K_1(E,-(E-\Omega))]\end{aligned} \tag{3.2c}$$

where the functions K_1, K_2 and K_3 in the integrands are defined to be

$$K_1(E,E') \equiv \frac{2\pi}{\hbar}\frac{\alpha^2 F(E-E')}{4N(0)}\left(1 - \frac{\Delta^2}{EE'}\right)\theta(E-E')\left[1 + n^\circ(E-E') - f^\circ(E')\right],$$
$$K_2(\Omega,E) = \frac{2\pi}{\hbar}\frac{\alpha^2 F(\Omega)}{NF(\Omega)}\rho(\Omega+E)\left(1 - \frac{\Delta^2}{E(\Omega+E)}\right)\theta(\Omega+E-\Delta)\left[f^\circ(E) - f^\circ(\Omega+E)\right],$$
$$K_3(E,E') = \frac{2\pi}{\hbar}\frac{\alpha^2 F(\Omega)}{4N(0)}\left(\rho(E)\rho(E')\right)^{-1}\theta(E-E')\left[f^\circ(E) + n^\circ(E-E')\right].$$

We notice that $\delta f_+(E)$ and $\delta f_-(E)$ are decoupled. Furthermore the phonon equation depends upon δf_+only. This set of coupled equations has been solved, with the assumption

$\delta f'(E) = 0$ (Chang and Scalapino 1977c), for the four different driving mechanisms discussed in the previous section. We will not discuss the results for $\delta f_+(E)$ and $\delta n(\Omega)$ here. The more interesting cases of strongly driven systems will be discussed in section 4 . Here we first discuss the derivation and the measurement of the various microscopic relaxation times which are of interest in their own right.

23.3.1 3.1. Microscopic lifetimes: calculation

The quasiparticle and phonon lifetimes in superconductors, due to the electron phonon interaction, have been calculated by Kaplan et al. (1976) using the Green function method. Here we derive them from the linearized kinetic equations (3.2).

23.3.2 3.1.1. Quasiparticle lifetimes

Consider a superconductor with perturbed distributions $\delta f_\pm(E)$ for states of energy E. All other energy states are assumed to be in thermal equilibrium.

The relaxation of the distribution functions due to the electron-phonon interaction is given by

$$\frac{\partial f_\pm(E)}{\partial t} = -\delta f_\pm(E) \int_0^\infty \mathrm{d}E' 4N(0)\rho(E') \left[K_1(E,E') + K_1(-E,-E') + K_1(E,-E')\right] \quad (3.3)$$

where the first two terms in the square brackets are due to the scattering process while the last term is due to the recombination process. Therefore, it is natural to define the inelastic quasiparticle relaxation rates for $\delta f_\pm(E)$ by

$$\left[\tau_{\mathrm{qp}}^+(E)\right]^{-1} = \left[\tau_{\mathrm{qp}}^-(E)\right]^{-1} = \left[\tau_*^{-1}(E) + \tau_{\mathrm{r}}^{-1}(E)\right], \quad (3.4)$$

with

$$\tau_{\mathrm{s}}^{-1}(E) \equiv \int_0^\infty \mathrm{d}E' 4N(0)\rho(E') \left[K_1(E,E') + K_1(-E,-E')\right]$$

and

$$\tau_{\mathrm{r}}^{-1}(E) \equiv \int_0^\infty \mathrm{d}E' 4N(0)\rho(E') K_1(E,-E')$$

This expression for the relaxation rates only differs from that obtained by Kaplan et al. by an overall phonon renormalization factor Z_1^{-1}. The scattering lifetime and the recombination lifetime are plotted in figs. 4 and 5, respectively, where the simple form $x^2F(\Omega) = b\Omega^2$ is assumed. This is quite adequate for all materials except Pb and Hg . The characteristic quasiparticle lifetime τ_0 is given by

$$\tau_0 = \frac{\hbar Z_1}{2\pi b (k_{\mathrm{B}}T_{\mathrm{c}})^3}. \quad (3.5)$$

It has been calculated and tabulated, and found to be orders of magnitude different for various materials (Kaplan et al. 1976).

Figure 4 shows the temperature dependence of τ_{s} for quasiparticles of different energies. We see that τ_{s} increases for a quasiparticle of energy $\omega \sim \Delta(T)$ as the temperature decreases, because a quasiparticle at the gap edge cannot emit a phonon and scatter when it is in the lowest quasiparticle energy state. Thus it can only be scattered by thermal phonons whose population decreases as the temperature decreases, therefore τ increases. As for quasiparticles of higher

energy, spontaneous phonon emission sets a limit to the scattering lifetime and τ_s saturates at low temperatures. On the other hand, as shown in fig. 5, the recombination lifetime for all quasiparticles increases as the temperature decreases. This is because the recombination process is a binary reaction which requires two quasiparticles. At low temperatures the quasiparticle density decreases exponentially as the temperature is lowered and hence τ_{r} increases.

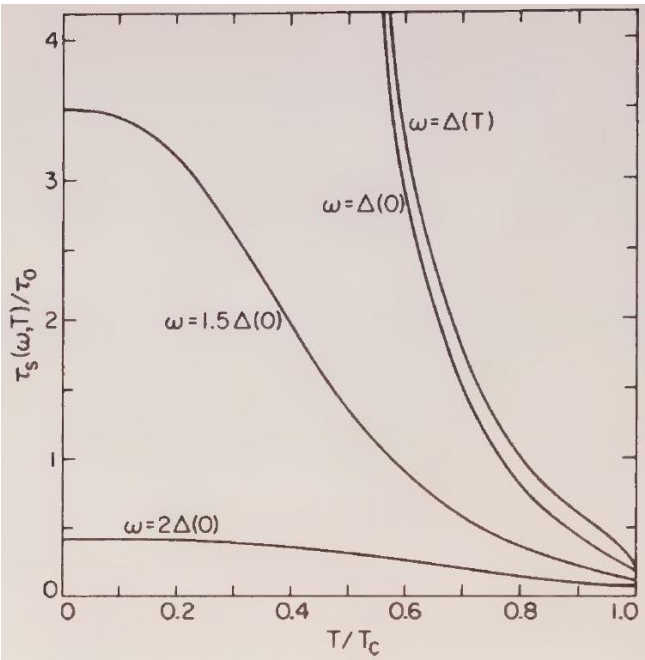


Fig. 4. Temperature and energy dependences of the quasiparticle scattering lifetime. (From Chang and Scalapino 1978.)

A comparison of these two lifetimes is shown in fig. 6 where curves for various fixed ratios of τ_s/τ_r are plotted in the quasiparticle-energy-ambienttemperature space for an equilibrium superconductor. For $T \leqslant 0.2T_{\mathrm{c}}$, the scattering process dominates. For $T \gtrsim 0.2T_{\mathrm{c}}$, the scattering process dominates the relaxation of the high-energy quasiparticles, while the recombination process dominates the relaxation of the low-energy quasiparticles. Therefore, a high-energy quasiparticle is most likely to relax by scattering into a low-energy state where it goes through a recombination process to create a pair.

Another quasiparticle lifetime of interest is the lifetime associated with the relaxation of the charge in quasiparticle excitations. Since a quasiparticle of wavevector k is a combination of u_k^2 electron and v_k^2 hole, the net charge of the excitation (in units of $-e$) is

$$q_k = u_k^2 - v_k^2 = \xi_k/E_k. \tag{3.6}$$

Therefore in general, an imbalance in the branch population implies a nonzero quasiparticle charge density

$$Q^* \equiv \sum_{k,\sigma} q_k f_k = \int_0^\infty \mathrm{d}E 2N(0)\delta f_-(E) \tag{3.7}$$

The quasiparticle charge relaxation rate that characterizes the relaxation of Q^* is defined as

$$\tau_{Q^*}^{-1} \equiv I_{Q^*}/Q^* \tag{3.8}$$

Here I_{Q^*} is the quasiparticle charge injection rate and is given by

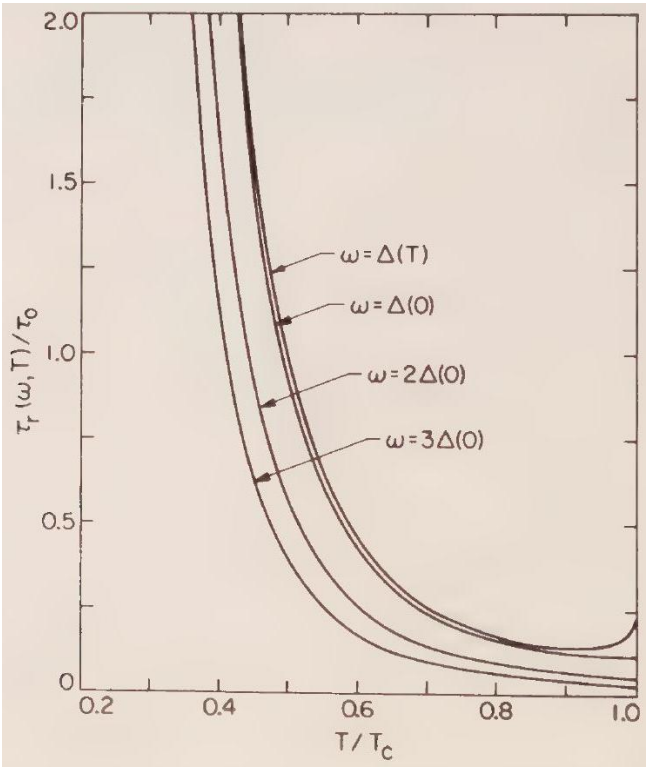


Fig. 5. Temperature and energy dependences of the quasiparticle recombination lifetime. (From Chang and Scalapino 1978.)

$$I_{Q^*} \equiv \sum_{k,\sigma} q_k I\left(E_k\right) = \int_0^\infty \mathrm{d}E 2N(0) I_{\mathrm{qp}}^-(E) \tag{3.9}$$

Utilizing eqs. (2.24b) and 3.2b) we find

$$\tau_{Q^*}^{-1} = \int_\Delta' \mathrm{d}E 2N(0) f_-(E) \left[\tau_{Q^*}^{-1}(E,T) + \tau_{\mathrm{el}}^{-1}(E)\right] / \int_1^\infty \mathrm{d}E 2N(0) f_-(E) \tag{3.10}$$

with the microscopic inelastic charge relaxation rate given by

$$\begin{aligned}\tau_{\mathrm{Q}^*}^{-1}(E) \equiv & \frac{2\pi}{\hbar} \int_0^\infty \mathrm{d}E' \rho\left(E'\right) \\ & \times \left\{ \left[\alpha^2 F\left(|E'-E|\right) \theta\left(E'-E\right) \left(1 - \frac{\Delta^2}{EE'} - \rho^{-2}\left(E'\right)\right) \left(f^\circ\left(E'\right) + n^\circ\left(E'-E\right)\right)\right] \right. \\ & \left. + \left[E \to -E, E' \to -E'\right] + \left[E \to -E\right]\right\}\end{aligned} \tag{3.11}$$

which is the same expression as that obtained by Chang (1979). The temperature dependence of τ_{Q^*} for five different quasiparticle energies is shown in fig. 7. All curves diverge as T approaches T_c. Otherwise τ_{Q^*} is of the same order as τ_s and τ_{r}.

23.3.3 3.1.2. Phonon lifetimes

Now consider an excess distribution of phonons with energy Ω in a superconductor otherwise at equilibrium. The decay of the excess phonons due to the electron-phonon interaction is governed by [from eq. (3.2c)]

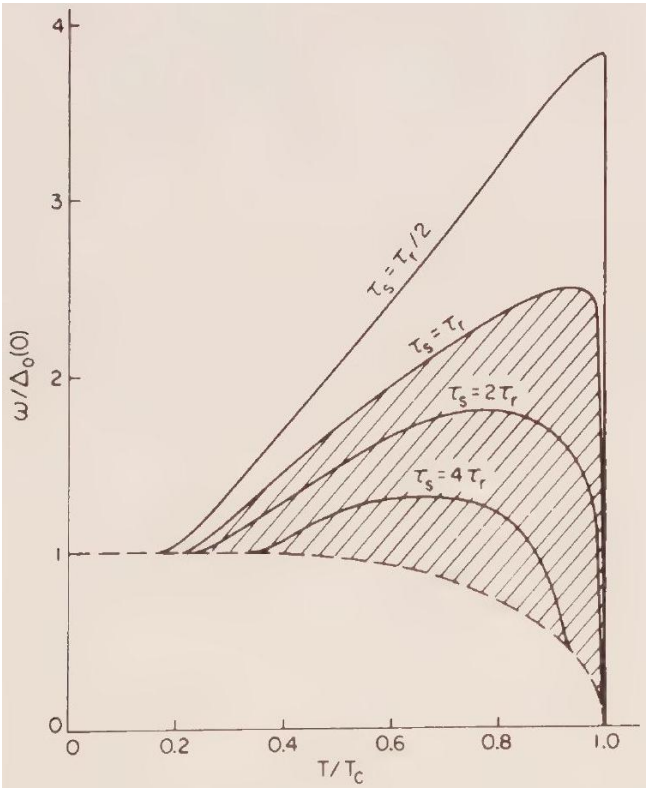


Fig. 6. Locus of points on the energy -temperature plane where $\tau_{\mathrm{s} } / \tau_{\mathrm{r}}=0.5,1,2$, and 4 . The dashed curve represents $\Delta(T)/\Delta_0$, so that all quasiparticle states lie above this curve. (From Kaplan et al. 1976.)}

$$\left.\frac{\partial n(\Omega)}{\partial t}\right|_{\mathrm{eph}} = -\int_0^\infty \mathrm{d}E 4N(0)\rho(E)\delta n(\Omega)\left[K_2(\Omega,E)+\frac{1}{2}\,\mathrm{K}_2(\Omega,-E)\right] \tag{3.12}$$

where the first term in the square brackets is due to the scattering process and the second term is due to the pair-breaking process. Therefore, the inelastic phonon relaxation rate is

$$[\tau_{\mathrm{ph}}(\Omega)]^{-1} = \left[\tau_{\mathrm{s}}^{\mathrm{ph}}(\Omega)\right]^{-1} + \tau_{\mathrm{B}}^{-1}(\Omega), \tag{3.13}$$

where the phonon scattering rate and pair-breaking rate are defined, respectively, as

$$\left[\tau_{\mathrm{s}}^{\mathrm{ph}}(\Omega)\right]^{-1} \equiv \int_0^\infty \mathrm{d}E' 4N(0)\rho\left(E'\right) K_2\left(\Omega,E'\right) \tag{3.14a}$$

and

$$\tau_{\mathrm{B}}^{-1}(\Omega) \equiv \int_0^\infty \mathrm{d}E' 4N(0)\rho\left(E'\right)\frac{1}{2}K_2\left(\Omega,-E'\right) \tag{3.14b}$$

The phonon scattering and pair-breaking rates are plotted in fig. 8. The most significant feature of the phonon relaxation rate is the dominance of the pair-breaking process over the scattering process for phonons with energy $\Omega \geqslant 24$. The characteristic phonon time

$$\tau_0^{\mathrm{ph}} = \frac{\hbar N}{4\pi^2 N(0)\alpha^2\Delta(0)}, \tag{3.15}$$

with $\Delta(0)$ the zero temperature energy gap, is typically of order 10^{-10} s. Values of τ_0^{ph} for various materials are also calculated and tabulated by Kaplan et al. (1976).

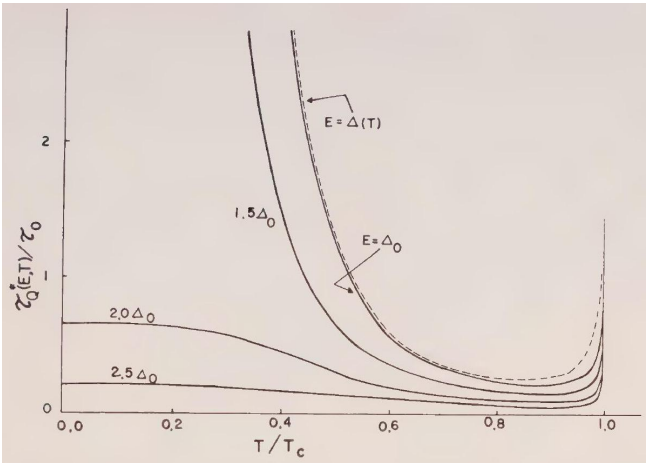


Fig. 7. Temperature and energy dependences of the quasiparticle charge-imbalance relaxation time. (From Chang 1979.)

23.3.4 3.2. Microscopic lifetime: measurement

Due to the lack of a high-resolution phonon spectrometer, the phonon distribution in a nonequilibrium superconductor is difficult to measure directly. However, various means have been developed to make indirect measurements. These have been reviewed by Eisenmenger (1981). On the other hand, the quasiparticle distribution can be probed quite accurately by the quasiparticle-tunneling technique (Chang and Scalapino 1976, Willemsen and Gray 1978, Horstman et al. 1981). Furthermore, using a double-junction structure, the tunneling technique has been shown to be capable of measuring the microscopic quasiparticle lifetime due to inelastic collisions as well as elastic collisions (Kaplan et al. 1977, Chang 1977).

Details of the measurement and analysis are given by Kirtley et al. (1980). Here we briefly outline the physics behind the technique, and discuss the result obtained for Al films.

Consider an $Al/Al/Pb-Bi$ junction. The Al/Al junction has a low re-

(From Kirtley et al. 1980.)

sistance and serves as an injector to drive the center Al film out of equilibrium. The driven state of this film is probed by the high resistance $Al/Pb-Bi$ detector junction. When the Al/Al junction is biased at zero voltage, four well-known structures in the $I-V$ curve of the detector junction occur at $V_{\mathrm{d}}=\pm\left(\Delta_{\mathrm{Pb}}\pm\Delta_{\mathrm{A1}}\right)/e$. When $V_{\mathrm{i}}>2A/e$, four additional structures are observed at $\mathrm{V_d}=\pm\left[\Delta_{\mathrm{Pb}}\pm\left(\Delta_{\mathrm{A1}}-|eV_{\mathrm{i}}|\right)\right]/e$. To bring out the details of these structures, $I_{\mathrm{d}}(2\omega)$ (which is proportional to $\mathrm{d}^2I_{\mathrm{d}}/\mathrm{d}V^2$) versus V, instead of I versus V, is shown in fig. 9. These curves indicate that there are small steps in the detector $I-V$ characteristics at $V_{\mathrm{d}}=\pm\left(\Delta_{\mathrm{Pb}}+\Delta_{\mathrm{A1}}-|eV_{\mathrm{i}}|\right)/e$ and a small peak and dip at $V_{\mathrm{d}}=\left(\Delta_{\mathrm{Pb}}-\Delta_{\mathrm{A1}}+|eV_{\mathrm{i}}|\right)/e$. We note that for these structures (occurring at voltages of equal magnitude but opposite sign) the amplitudes are different. This asymmetric effect increases with increasing injection voltage V_{i}.

It has been shown that these structures result from the sharp structure in the quasiparticle injection rate at energy $E_{\mathrm{s}}=eV_{\mathrm{i}}-\Lambda_{\mathrm{A1}}$ (fig. 2). Effects due to the structure at (eV_i+A_{A1}) are too small to be detected. The injected quasiparticles relax and give a steady state distribution which, for the most part, resembles a thermal distribution with an effective temperature $T^*>T_{\mathrm{a}}$. However, the steady-state distribution also contains a small residue from the sharp structure in the injection spectrum. Figure 10 shows schematically the effects of this

sharp structure on the detector-junction current. The excess quasi-particles enhance the currents contributed by processes (a) and (d) as shown in (c|a) and (c|d). They also block processes (b) and (c), and reduce the currents contributed by them as shown in (c|b) and (c|c). We note that the most effective enhancement and reduction corresponding to each process

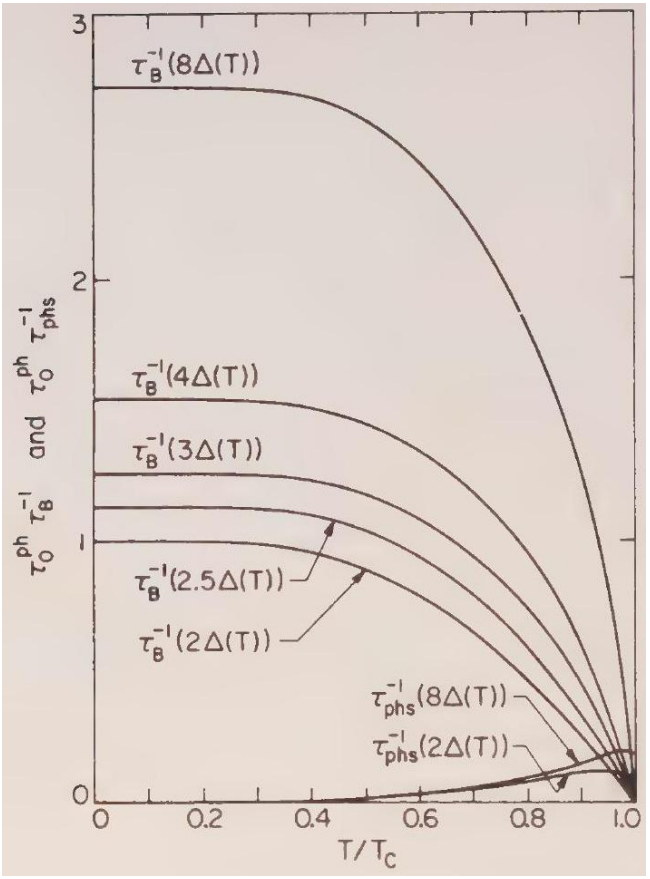


Fig. 8. Phonon decay rates due to scattering and pair-breaking processes. (From Chang and Scalapino 1978.)

occur at different detector voltages. This results in the four measured structures in the detector $\mathrm{d}^2 I, \mathrm{dV}^2$ curve, shown in fig. 9 , each corresponding to a different
process. The asymmetry in the detector junction $I - V$ curve is due to the imbalance in the injection rate on the two $\xi \gtrless 0$ branches. We also note that, since the magnitudes of the $I - V$ structures depend only on the magnitude of the sharp structure of the steady-state quasiparticle distribution at $E_\mathrm{s} = eV_\mathrm{i} - \Delta_\mathrm{A1}$ (which in turn is governed by the relaxation times of the quasiparticles of that particular energy), the quasiparticle relaxation time at energy E_s can be obtained from a quantitative analysis of the magnitudes of the $I \cdot V$ structures. Furthermore, by sweeping the injector junction voltage and changing the temperature, the energy and temperature dependences of the relaxation time can be mapped out.

The magnitudes of the current-step heights at $\pm V_\mathrm{d}^\mathrm{s} = \pm\left(\Delta_\mathrm{Pb} + \Delta_\mathrm{A1} - eV_\mathrm{i}\right)/e$ for the injector voltage $V_\mathrm{i} > 2\Delta_\mathrm{A1}/e$ can be readily calculated. We obtained (Chang 1977)

$$\Delta I_\mathrm{d}\left(\pm V_\mathrm{d}^\mathrm{s}\right) = \frac{\pi G_\mathrm{nn}^\mathrm{i} G_\mathrm{nn}^\mathrm{d}\left(\Delta\Delta_\mathrm{Pb}\right)^{1/2}}{8e^2 N(0)\Omega}\tau_\mathrm{qp}\rho\left(eV_\mathrm{i} - \Lambda\right)$$
$$\times\left[1 - f^\circ\left(\Delta, T^*\right) - f^\circ\left(eV_\mathrm{i} - \Delta, T^*\right)\right]\left[1 \pm \left(1 - \frac{\Delta^2}{\left(eV_\mathrm{i} - \Lambda\right)^2}\right)\frac{\tau_\mathrm{el}}{2\tau_\mathrm{qp} + \tau_\mathrm{cl}}\right] \tag{3.16}$$

Here all the unsubscripted functions and parameters such as ρ, Δ, Ω, etc. are those for the center Al film. The inelastic relaxation time τ_qp and the elastic relaxation time τ_{e1} are to be evaluated at the energy $E = eV_i - A_{A1}$ and at the temperature T^*. Clearly, the inelastic quasiparticle relaxation time $\tau_\mathrm{qp}\left(eV_\mathrm{i} - A_\mathrm{A1}\right)$ can be obtained from the sum, and the elastic

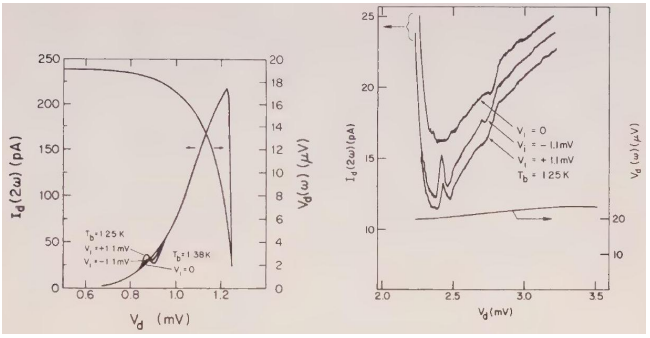


Fig. 9. Left-hand figure: second-harmonic current signal and first harmonic voltage modulation versus detector bias voltage, with injection at bath temperature $T_{\mathrm{B}}=1.25$ K, and with no injection at a higher bath temperature $T_\beta = 1.38$ K. The cusp in the detector $I-V$ characteristic at $(\Delta_{\mathrm{Pb}}-\Delta_{\mathrm{A1}})/e$ occurs at $V_{\mathrm{d}} = 1.22$mV. The nonequilibrium structure appears at $V_{\mathrm{d}} = (\Delta_{\mathrm{Pb}}+\Delta_{\mathrm{A1}}-|eV_i|)/e = 0.84$mV. The background signal curves for the injection and no-injection conditions match exactly, indicating an effective film temperature under injection $T^* = 1.38$ K. Right-hand figure: same experiment with detector voltage biased above the current step at $(\Delta_{\mathrm{pb}}-\Delta_{\mathrm{A1}}+|eV|,)/e$.}

branch mixing time $\tau_{\mathrm{e1}}(eV_{\mathrm{i}}-\Delta_{\mathrm{A1}})$ can be obtained from the difference of the current-step magnitudes at $V_{\mathrm{d}} = \pm(\Delta_{\mathrm{Pb}}+\Delta_{\mathrm{A1}}-eV_{\mathrm{i}})/e$. Experimental data for a dirty A1 film have

been obtained by Kirtley et al. (1980). The inelastic quasiparticle relaxation time as a function of the quasiparticle energy for four different ambient temperatures is shown in fig. 11 (left). The corresponding curves calculated from eq. (3.4) are shown in fig. 11 (right). The agreement is good. However, the elastic quasiparticle-impurity scattering time obtained using this technique is independent of both energy and temperature within the uncertainty of the measurement. This is different from the theoretical prediction (Tinkham 1972) of a $(E^2-\Delta^2)^{3/2}/E\Delta^2$ energy dependence, although the magnitude of the predicted τ_{c1} is consistent with the experimental value. At the moment, there is no explanation of this. Data for a clean Al film have been obtained by Moody and Paterson (1981). The same conclusion can be drawn from their data.

23.3.5 3.3. Macroscopic lifetimes

23.3.6 3.3.1. The quasiparticle density relaxation time

In a thin superconducting film under a driven situation, excess quasiparticles can be created. The relaxation time of the excess quasiparticle density, τ_{d}, has long been an interesting subject (Rothwarf and Taylor 1967, Gray et al. 1969). Letting δN and I_{qp} be, respectively, the excess quasiparticle density and the injection rate of the quasiparticle, we have

$$\begin{aligned}\delta N &= \sum_{k\pi}\delta f_k \\ &= \int_d^\infty \mathrm{d}E 4N(0)\rho(E)\delta f_+(E)\end{aligned} \tag{3.17}$$

and

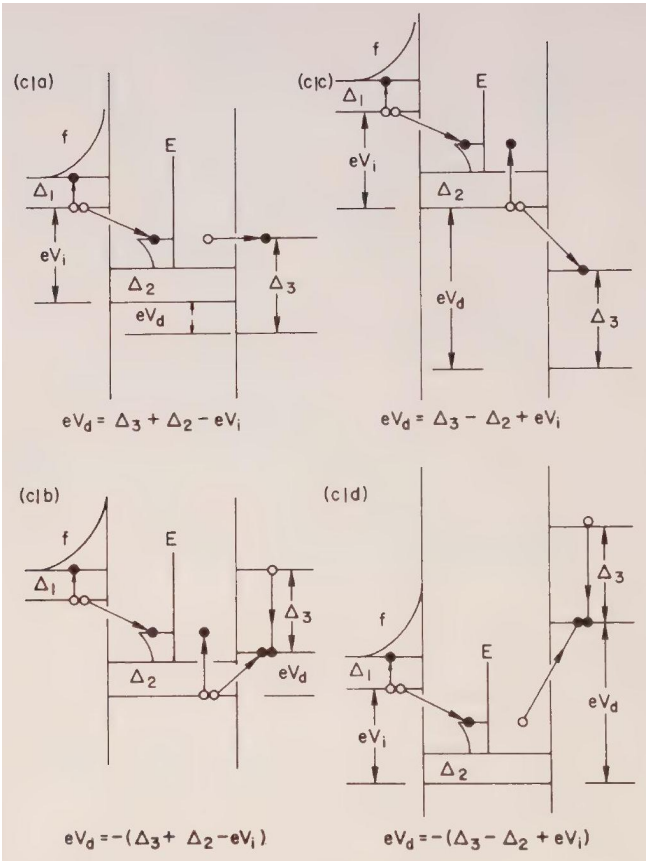


Fig. 10. Four detector bias situations which give rise to the singularities in the detector currentvoltage curve due to the injector channel c. (From Kirtley et l. 1980.)

$$I_{\mathrm{qp}}^{+} = \sum_{k\sigma} I_h$$
$$= \int_A^\infty \mathrm{d}E 4N(0)\rho(E)I^{+}(E) \tag{3.18}$$

The quasiparticle density relaxation time is defined as

$$\tau_{\mathrm{d}} = \delta N / I_{\mathrm{qp}}^{+} \tag{3.19}$$

It has been shown that the excess quasiparticle density δN can be extracted from tunneling data (Chang and Scalapino 1976). For example, at low temperature, the tunneling current of a symmetric superconductor -insulatorsuperconductor junction is proportional to the sum of the quasiparticle densities in the two films which form the junction if the junction voltage is biased at a value slightly below 21. Also, to a good approximation, the gap suppression from its equilibrium value is directly proportional to the excess quasiparticle density in a nonequilibrium film.

Intuitively, one would expect that the relaxation time τ_{d} would be related to the quasiparticle recombination time $\tau_{\mathrm{r}}(E,T)$ and the phonon pair-breaking time $\tau_{\mathrm{B}}(E,T)$ since these processes change the quasiparticle density. Also important will be the phonon escape time τ_{cs} because it governs the relaxation of the energy injected into the system by an external source. To examine how these times are related to the quasiparticle density relaxation time τ_{d}, we first find a relationship between I_{qp} and δN from the kinetic equation (2.23a). Substituting eq. (3.3) into eq. (2.22a) and summing over the quasiparticle states, we have

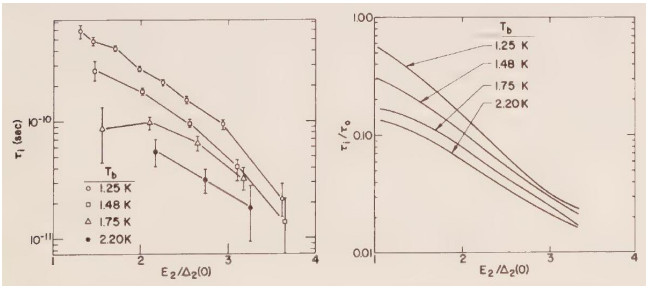


Fig. 11. Left-hand figure: experimental values of the inelastic relaxation time versus the normalized quasiparticle energy for four bath temperatures. Right-hand figure: theoretical calculation of the same quantities. (From Kirtley et al. 1980.)

$$I_{\mathrm{qp}}^{+}=2\delta N\left\langle\tau_{\mathrm{r}}^{-1}\right\rangle_{\mathrm{qp}}-2\delta N_{\omega}\left\langle\tau_{\mathrm{B}}^{-1}\right\rangle_{\mathrm{ph}} \tag{3.20}$$

Here

$$\delta N_{\omega}\equiv\int_{2,\Delta}^{\infty}\mathrm{d}\Omega NF(\Omega)\delta n(\Omega) \tag{3.21}$$

is the excess density of phonons with energy $\Omega\geqslant 2\Delta$, while

$$\left\langle\tau_{\mathrm{r}}^{-1}\right\rangle_{\mathrm{qp}}\equiv\int_{\Delta}^{\infty}\mathrm{d}E4N(0)\rho(E)\delta f^{+}(E)\tau_{\mathrm{r}}^{-1}(E)/\int_{\Delta}^{\infty}\mathrm{d}E4N(0)\rho(E)\delta f^{+}(E) \tag{3.22a}$$

and

$$\left\langle\tau_{\mathrm{B}}{}^{1}\right\rangle_{\mathrm{ph}}\equiv\int_{21}^{1}\mathrm{d}\Omega NF(\Omega)\delta n(\Omega)\tau_{\mathrm{B}}{}^{1}(\Omega)/\int_{21}^{1}\mathrm{d}\Omega NF(\Omega)\delta n(\Omega) \tag{3.22b}$$

are, respectively the quasiparticle recombination rate and phonon pairbreaking rate averaged over the excess distribution. $\delta N_{,}$ can be calculated by substituting eq. (3.12) into the phonon kinetic equation (2.22c). We obtain

$$\delta N_{\omega}=\delta N\left(\left\langle\tau_{\mathrm{sA}}^{-1}-\tau_{\mathrm{sE}}^{-1}-\tau_{\mathrm{r}}^{-1}\right\rangle_{\mathrm{qp}}\right)/\left\langle\left(\tau_{\mathrm{s}}^{\mathrm{ph}}\right)^{-1}+\tau_{\mathrm{B}}^{-1}+\tau_{\mathrm{cs}}^{-1}\right\rangle_{\mathrm{ph}}. \tag{3.23}$$

Here

$$\tau_{\mathrm{sE}}^{-1}\equiv\int\mathrm{d}E'4N(0)\rho\left(E'\right)K_{1}\left(e,E'\right)\theta\left(E-E'-2\Delta\right)$$
$$\tau_{\mathrm{sA}}^{-1}\equiv\int\mathrm{d}E'4N(0)\rho\left(E'\right)K_{1}\left(-E,-E'\right)\theta\left(E'-E-2\Delta\right)$$

are the quasiparticle scattering rates associated with, respectively, the emission and absorption of a phonon of energy $\Omega\geqslant 2.1$. Eliminating is $N_{,}$ from ecls. (3.20 and 3.23), we obtain

$$\tau_{\mathrm{d}}^{-1}=2\left\langle\tau_{\mathrm{r}}^{-1}\right\rangle_{\mathrm{qp}}\left\{1-\frac{1+\left\langle\tau_{\mathrm{sE}}^{-1}-\tau_{\mathrm{sA}}^{-1}\right\rangle_{\mathrm{qp}}/\left\langle\tau_{\mathrm{r}}^{-1}\right\rangle_{\mathrm{qp}}}{1+\left[\left\langle\left(\tau_{\mathrm{s}}^{\mathrm{ph}}\right)^{-1}+\tau_{\mathrm{es}}^{-1}\right\rangle_{\mathrm{ph}}\right]/\left\langle\tau_{\mathrm{B}}^{-1}\right\rangle_{\mathrm{ph}}}\right\}. \tag{3.24}$$

The above expression for $\tau_{\rm d}^{-1}$ can be simplified if the excess quasiparticles have low energies and quasiparticle states of energy $E \geqslant 3\Delta$ are not disturbed. In this case the effect of the quasiparticle scattering process can be neglected and we have

$$\tau_{\rm d}^{-1} = 2\left\langle \tau_{\rm r}^{-1}\right\rangle_{\rm qp} / \left[1 + \left\langle \tau_{\rm B}^{-1}\right\rangle_{\rm ph} / \left\langle \tau_{\rm es}^{-1}\right\rangle_{\rm ph}\right]. \tag{3.25}$$

We see that the macroscopic charge density relaxation rate ${\tau_{\rm d}}^{-1}$ is a direct measure of the microscopic quasiparticle recombination rate averaged over the excess quasiparticle distribution. For the phonon escape time $\tau_{\rm es} = 0$, we have $\tau_{\rm d}^{-1} = 2\left\langle \tau_{\rm r}^{-1}\right\rangle_{\rm qp}$, with the factor of 2 due to the fact that each recombination event reduces two quasiparticles. When $\tau_{\rm es}$ is finite, the well known phonon trapping factor $\left\langle \tau_{\rm B}^{-1}\right\rangle_{\rm ph} / \left\langle \tau_{\rm e}^{-1}\right\rangle_{\rm ph}$ first pointed out by Rothwarf and Taylor (1967) reduces $\tau_{\rm d}^{-1}$ from the average quasiparticle recombination rate.

23.3.7 3.3.2. Quasiparticle charge relaxation time

The time τ_{Q^*} that governs the quasiparticle charge relaxation is of interest because it is related to many physical quantities that can be directly measured. (See, for example, Clarke 1981.) For example, it has been shown that for a superconductor-insulator superconductor tunnel junction in which one of the films has a charge imbalance Q^* there is a finite quasiparticle tunneling current at zero-bias voltage (Clarke 1972, Tinkham and Clark 1972, Moody and Paterson 1978, Chi and Clarke 1979a). Specifically one has

$$I(V=0) = \frac{G_{n1}\Omega}{2dN(0)e} Q^* \tag{3.26}$$

The quasiparticle injection rate I_{Q^*} can be easily calculated from eq. (3.9) using the $I_{\gtrless}(E)$ obtained in section 2 . Therefore, measuring $I(V=0)$ yields immediately the charge relaxation rate

$$\tau_{Q^*}^{-1} = I_{Q^*}/Q^* = \frac{2dN(0)e}{G_{\rm nn}\Omega} \frac{I_{Q^*}}{I(V=0)} \tag{3.27}$$

which from eq. (3.10) is just the microscopic rate $\tau_{Q^*}^{-1}(E) + \tau_{\rm e1}^{-1}(E)$ averaged over the excess quasiparticle charge distribution $q_k f_k$.

Details of the measurement and the analysis can be found in the articles by Chi and Clarke (1979a) and Clarke (1981).

23.4 4. Systems far from equilibrium

The strength of external sources required to drive a superconductor far from equilibrium has been worked out for different driving situations (Chang and Scalapino 1977b). For example, in the quasiparticle tunnel-injection case, the driving strength is characterized by $G_{\rm nn}/2N(0)e^2\Omega$, while the relaxation time
for the quasiparticle is characterized by τ_0. Therefore the parameter

$$A = \frac{G_{\rm nn}\tau_0}{2N(0)e^2\Omega}\left(\frac{k_{\rm B}T_{\rm c}}{\Delta_0}\right)^3 \tag{4.1}$$

is a good measure of how strongly the system is driven. For Al films of thickness $d \sim 10^3$Å, it is found that the conductance per unit area $G_{\rm nn}d/\Omega$ needs to be greater than $10^4\Omega^{-1}$ cm^{-2} to make $A \sim 0.01$. For Sn , due to the shorter relaxation time τ_0, the required conductance per area would be larger ($\sim 2\times 10^6\Omega^{-1}$ cm^{-2}).

However, the above consideration neglects the phonon-trapping effect discussed in section 3.3.2 where it is shown that, if the thermal coupling between the sample and the environment is weak, the effective quasiparticle relaxation time will be longer than the intrinsic time τ_0. Therefore, in the actual experimental situation, the required strength may be smaller than those given above. Also, in this case of weak thermal coupling, the injected energy will be transferred between the quasiparticle and phonon systems many times before it is finally released from the sample. This will tend to smear out the sharp structures in the injected quasiparticle spectrum and the specific signature of the driving mechanisms may be washed out. We will discuss this case later. First, let us discuss the properties of films with strong thermal coupling where the signatures of the driving sources are significant and contribute to interesting phenomena.

23.4.1 4.1. Narrow band phonon generation

The physics behind narrow-band phonon generation using a nonequilibrium superconducting thin film is easy to understand. Consider a symmetric superconductor-insulator superconductor tunnel junction biased at a voltage slightly above $24/e$. From figs. 1 and 2 it is easy to see that the dominant tunneling process at low temperature is either process (c) or (d), depending upon whether V is positive or negative. Quasiparticles are predominantly injected into states of energy ranging from A to $eV - A$ for both films in the junction. Energy conservation forbids the excitation of quasiparticles with energy greater than $eV - A$ by process (c) or (d). The excited quasiparticles then relax and recombine into pairs with the emission of phonons of energy ranging from 2Δ to $2(eV - \Delta)$. When the voltage is set at a value just above $2\Delta/e$ the bandwidth, $2(eV - A) - 2A = 2(eV - 2A)$, can be very narrow.

Eisenmenger and Dayem (1967) were the first to suggest the use of tunnel junctions in the generation of high-frequency narrow-band phonons ($v = 24/h \sim 10^{12}$ Hz). The energy spectra of phonons emitted from a symmetric superconductor insulator -superconductor tunnel junction have been investigated experimentally by Dayem and Wiegand (1972) and Dynes et al. (1971, 1972).

Theoretical work to calculate the emitted-phonon energy spectra was first attempted by Dayem and Wiegand (1972). They used a set of linearized kinetic equations. However, in a real situation, it is more likely that, to generate high intensity phonons in narrow energy ranges, the system needs to be driven into nonequilibrium states for which the linear approximation is not valid. Therefore, the full set of nonlinear kinetic equations has to be solved along with the modified gap equation (eqs. 2.23, 24). This work has been carried out by Chang and Scalapino (1977a, 1978) and here we go through their results briefly.

The steady-state quasiparticle and phonon energy spectra are shown in fig. 12. We have neglected the effect associated with the branch imbalance which is unimportant in this case since most of the quasiparticles are injected into states of $E \sim \Delta$. The ambient temperature is set at $T = 0$, the bias voltage is $V = 2A_0/e$, and the phonon trapping factor is $\tau_{es}/\tau_B(2A_0) = 1, 4,$ and 8 . The parameter A which characterizes the strength of the driving source is set at 0.01 . Here $\tau_B(2A_0)$ is the pair-breaking time of a phonon with energy $2A_0$ in an equilibrium superconductor at zero temperature. We notice that as expected

the energy gap is suppressed by the injected auasiparticles and the suppression is large for a large phonon-trapping factor. Furthermore, a large phonontrapping factor tends to smear the sharp structure in the quasiparticle spectra at $E = eV - \Delta$ somewhat. As for the phonon spectra, fig. 12 shows that there is an intense narrow band of phonons of energy $\Omega \sim 24$. The width is indeed approximately given by $2(eV - 2\Delta)$ which can be made small by adjusting the voltage V close to the steady state value of $2\Delta/e$. These curves may give the wrong impression that a high phonon-trapping factor generates a high density of narrow-band phonons. The fact that this is not the case can be seen by an examination of the energy spectra of the emitted

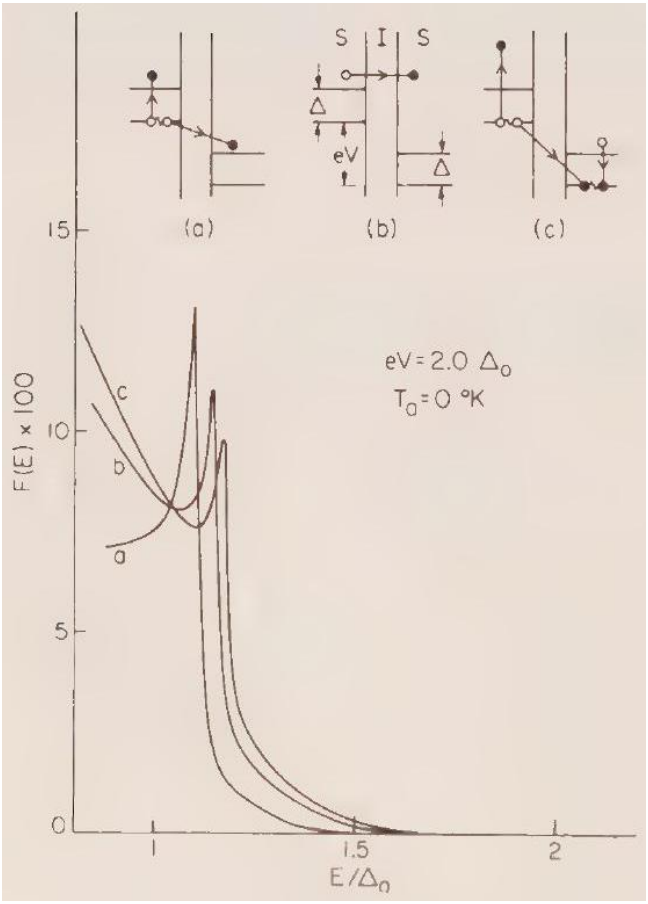


Fig. 12. Steady state quasiparticle (left-hand figure) and phonon (right-hand figure) distributions in thin films under quasiparticle tunnel injection through a symmetric junction. The ambient temperature is $T=0 \mathrm{˜K
$ and the voltage is $V = 2\Delta_0/e$. Curves a-c correspond to $\tau_{es}/\tau_B = 1, 4$ and 8 , respectively. Inset shows the three processes that contribute to the tunneling current. (From Chang and Scalapino 1978.)}

phonons, which is proportional to $\Omega^2 n(\Omega)/\tau_{es}$ (fig. 13). It can be seen clearly that indeed high phonon-trapping factors tend to smear the sharp structures and broaden the bandwidth of the emitted phonons.

We want to emphasize that the narrow energy bandwidth of the emitted phonons is the result of a nonlinear effect. In fact, for thin films under weakly driven conditions, the scattering process dominates the relaxation of quasiparticles, as can be seen in fig. 6. Since the scattering process necessarily tends

to smear out the quasiparticle energy distribution, the emitted phonons will not have a sharp energy dependence. The reason that we do have narrow-band phonons emitted is because of the large number of quasiparticles injected into the film, so that in the nonequilibrium state a quasiparticle can find a partner to recombine with into a pair with relative ease. Therefore, the recombination process, instead of the scattering process, dominates the relaxation.

Attempts to generate narrow-band phonons using a thin film driven by heat pulses (Narayanamurti and Dynes 1971, Dynes and Narayanamurti 1972) and microwaves (Rutledge et al. 1979) have also been made. However, the results are not as favorable as in the case using tunnel junctions. In the heat pumping case, this is due to the lack of a mechanism to cut off the generation of phonons on the high-energy side. In the microwave case, this is because the coherence factor of the scattering process is larger than that of the recombination

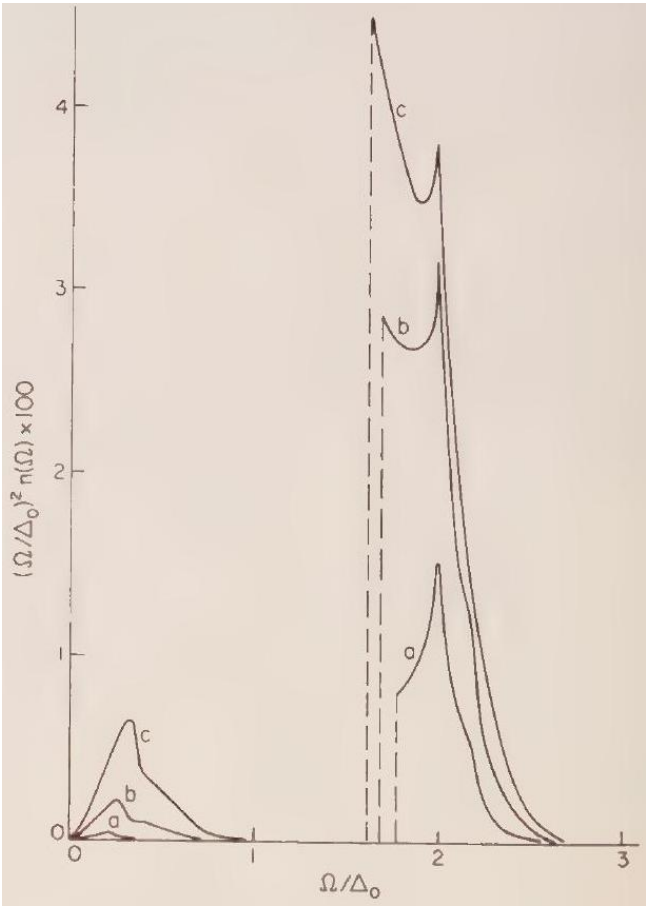


Fig. 12. Steady state quasiparticle (left-hand figure) and phonon (right-hand figure) distributions in thin films under quasiparticle tunnel injection through a symmetric junction. The ambient temperature is $T=0 \mathrm{˜K
$ and the voltage is $V = 2\Delta_0/e$. Curves a-c correspond to $\tau_{es}/\tau_B = 1, 4$ and 8 , respectively. Inset shows the three processes that contribute to the tunneling current. (From Chang and Scalapino 1978.)}

process for the quasiparticle-microwave interactions. This means that before a large quasiparticle density of $E \sim \Delta$ is achieved by strong microwave irradiation of frequency $v \sim 24/\mathrm{h}$, many of them will already be scattered again by microwave photons into states of $E \sim 3A$. The relaxation of these quasiparticles is dominated by the scattering process with the emission of phonons which will not give phonons of narrow bandwidth.

23.4.2 4.2. Enhancement of superconductivity

The energy gap of a superconducting thin film is observed to increase when the film is under microwave irradiation (Kommers and Clarke 1977, Hall et al. 1980, 1981, Horstman et al. 1981), quasiparticle tunnel injection (Gray 1978, Chi and Clarke 1979), and low-frequency phonon injection (Seligson and Clarke 1982).

The enhancement of the energy gap using quasiparticle tunnel injection was first proposed by Parmenter (1961). He noticed that when an asymmetric junction is biased at a voltage smaller than the difference of the gap voltages of the two films, the quasiparticle density in the film with the smaller gap will be reduced and hence superconductivity enhanced. Later, Wyatt et al. (1966) and Dayem and Wiegand (1967) observed enhancement of the critical current in microbridges irradiated by microwaves. Eliashberg (1970), inspired by their results, suggested

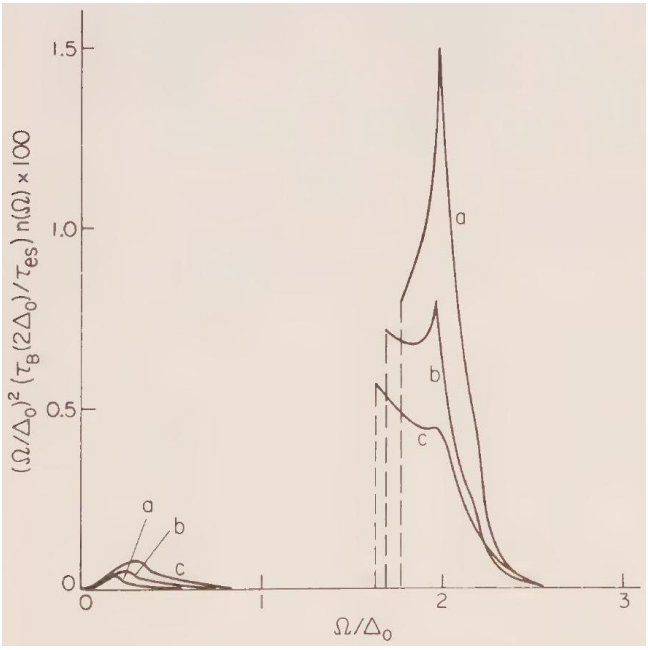


Fig. 13. Energy spectra of the emitted phonons shown in the previous figure. (From Chang and Scalapino 1978.)

that the enhancement was due to the shoveling of quasiparticles from low-energy states to high-energy states. He noticed that it is the occupation of the low-energy states that most severely interferes with the pair correlation of the electrons (see eq. 2.24). Since microwaves of frequency $y < 24/h$ cannot break a pair, it can only excite the low-energy quasiparticles into high-energy states. This results in an enhanced gap and hence an enhanced critical current.

Eliashberg (1970, 1972) and Ivlev and co-workers (1971, 1973) have studied the gap enhancement due to microwave irradiation using the quasiparticle

$$A = \frac{2R_{\mathrm{N}}H^2}{dN(0)\omega^2}\left(\frac{k_{\mathrm{B}}T_{\mathrm{c}}}{\Delta_0}\right)^3\tau_0.$$

kinetic equation. Chang and Scalapino (1976, 1978) have included nonequilibrium phonon effects by solving the full set of quasiparticle and phonon kinetic equations selfconsistently. They found that the shoveling of quasiparticles into higher energy states by the microwaves can result in a reduction in the quasiparticle density and hence an enhancement of the energy gap. This can be achieved because higher-energy quasiparticles can recombine into pairs faster than the lower-energy ones. To be more specific, we note first that the phonon density of states in the Debye approximation varies as the phonon energy squared. Thus for phonons emitted by recombination of quasiparticles
near the gap edge, the final phonon density of states involved is proportional to $(2\Delta)^2$. However, if the two quasiparticles are shoveled into states of energy $\Delta + hv$ before they recombine into a pair, the recombination phonon would have energy $2(A + hv)$ and the final phonon density of states involved would be proportional to $4(4 + hv)^2$. Therefore tunneling excitation of quasiparticles can lead to faster quasiparticle recombination and a net reduction of the quasiparticle density in the steady state.

Numerical solutions of the variations of the gap and the quasiparticle density N_{qp} with microwave coupling for the four different phonon trapping factors $\tau_{\mathrm{es}}\,/\tau_{\mathrm{B}}\,(2A_0) = 0.2, 2, 8$, and 16 are shown in fig. 14. These curves clearly show that the gap enhancement is related to the quasiparticle-density reduction at small driving amplitudes. When the driving force is

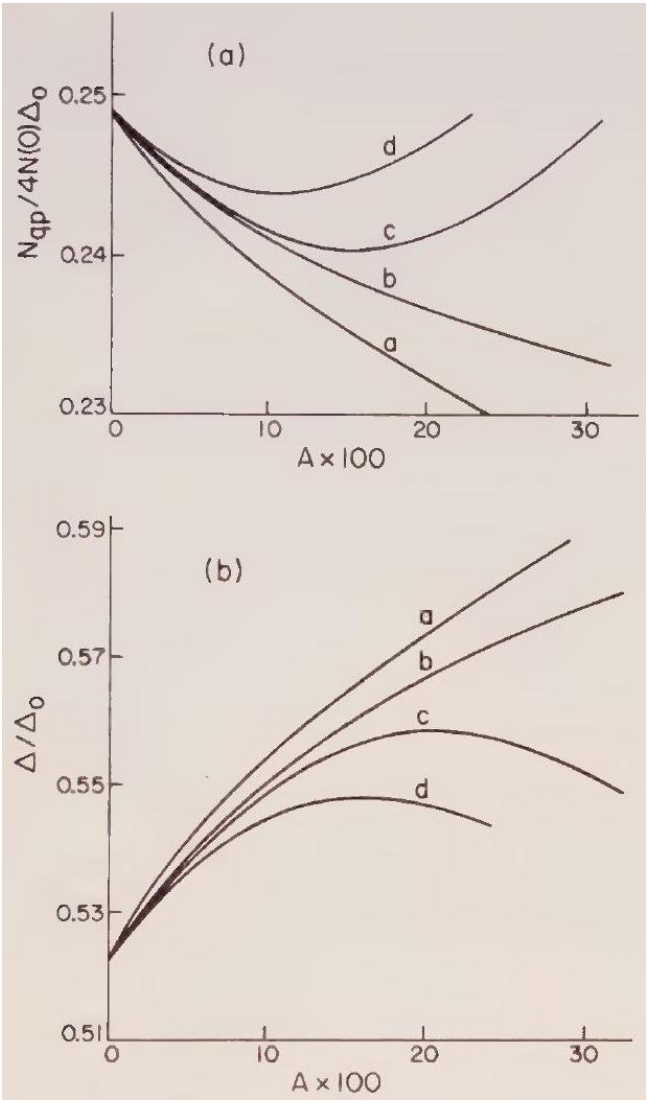


Fig. 14. The microwave coupling dependences of (a) the steady-state quasiparticle density and (b) the energy gap. (From Chang and Scalapino 1978.) The bath temperature is $T=0.9 T_{c $. The microwave frequency is $v = \Delta_0/2h$. Curves a-d correspond to $\tau_{es}/\tau_B = 0.2, 2, 8$ and 16 , respectively. The parameter that represents the coupling strength is}

strong [e.g. $A \sim 0.2$ in case (d)], nonlinear effects set in and the quasiparticle density can be larger than its equilibrium value. In this case, the gap enhancement is completely due to the redistribution of the quasiparticles.

Theoretical work on the gap enhancement in superconducting films of a symmetric tunnel junction due to quasiparticle tunnel injection has been carried out by Peskovatskii and Seminozenko (1976) and Chang (1978). The reason that the energy gap can be enhanced for both films is similar to the case of microwave irradiation. A junction biased at $V < 2A/e$ can have process (a) and (b) (fig. 1) contribute to the current. The effect of these processes is to shovel quasiparticles from low-energy states to high-energy states as the lowfrequency microwave do (see, for example, fig. 1).

Although the physics behind the gap enhancement is the same for microwave irradiation as for quasiparticle tunnel injection, the experimental situations are quite different. In the tunneling case, the coupling constant is fixed for a given junction, however the bias voltage can be adjusted at will. In the case of microwave irradiation, the coupling amplitude can be changed at will by changing the imput power, but the frequency of the microwaves is difficult

to adjust. Experimental studies of the gap enhancement have been carried out by Gray (1978) using a symmetric A1, A1 junction and by Chi and Clarke (1979) using an asymmetric A1/A1 junction.

In fig. 15 the energy gap as a function of the junction bias voltage is shown for coupling constants of $A = 0.05$ and 0.1 and an ambient temperature of $T = 0$. These curves are obtained (Chang 1978) by assuming that there is no branch imbalance. Nonequilibrium phonons are taken into account. The phonon trapping factor is set equal to $\tau_{cs}, \tau_B\,(2A_0) = 8$, which is typical for an Al film on sapphire in liquid Helium. It is interesting to note that the energy gap begins to decrease before the bias voltage reaches $2A, h$ when the pair breaking process sets in. This is different from the result of Peskovatskii and Seminozenko (1976) who ignored the nonequilibrium phonon effect and found that the gap increases with increasing voltage. The curves shown in fig. 15 are in good qualitative agreement with the experimental data (Gray 1978). The

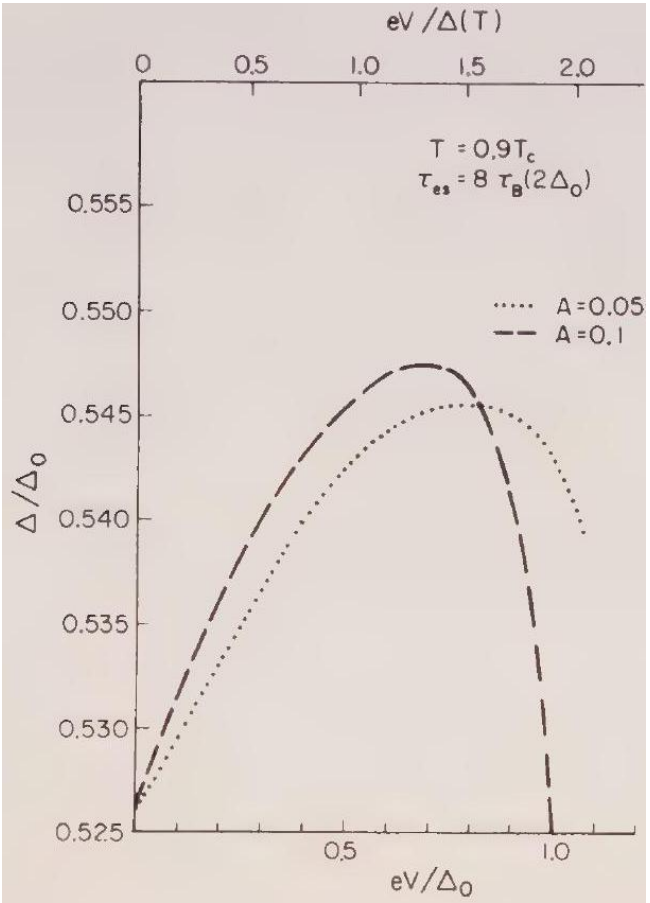


Fig. 15. Voltage dependence of the gap enhancement due to quasiparticle tunnel injections using a symmetric junction. (From Chang 1978.)

magnitude of the maximum gap enhancement calculated is to be slightly less than 4% using these parameters. The experimental value of a maximum enhancement is slightly larger than 1%. Among other things, this could be due to the magnetic field generated by the current or the neglect of the quasiparticle branch imbalance.

Before we leave this subject, I would like to emphasize that this effect can be observed only in samples with good thermal coupling. For a sample with severe phonon trapping, "heating" effects will be important and the energy gap will be suppressed instead of enhanced. A simple heating model has been developed to take the nonequilibrium phonons into account (Mooij 1981). Both the redistribution and the reduction of quasiparticles have been observed

in a microwave-driven film which shows gap enhancement (Horstman et al. 1981). What is the maximum amount of the enhancement that can be achieved experimentally, and which mechanism is more responsible for this effect. remain as intriguing questions.

23.4.3 4.3. Analytical models and instability

As mentioned before, only when the thermal coupling between the sample and its environment is strong do the energy distributions of the quasiparticles show the specific structures associated with the external driving source. For weak thermal coupling, the quasiparticle distribution is smooth and can be described by an analytic model. There are two well-known models: the μ^* model by Owen and Scalapino (1972) and the T^* model first proposed by Parker (1975) and later modified by Chang et al. (1979). In the μ^* model it is assumed that the phonons are in thermal equilibrium with the ambience, while the quasiparticles thermalize rapidly to the ambient temperature, but because of a recombination bottleneck these are excess quasiparticles in the steady state. The presence of excess quasiparticles is taken into account by using an effective chemical potential μ^* which is greater than its equilibrium value. In the T^* model, on the other hand, Parker (1975) has assumed that phonons of energy $\Omega < 24$ are in thermal equilibrium with the environment. This is based upon the fact that these phonons cannot break pairs so that their lifetime associated with the electron-phonon interaction is long compared with the phonon-escape time for the usual situation. This means they have stronger coupling to the environment than to the quasiparticles. Quasiparticles and phonons of energy $\Omega \geqslant 2\Delta$ are assumed to be in equilibrium at a temperature higher than the ambient temperature. Later, Chang et al. (1979) have shown that if the quasiparticles can be described by a Fermi function with an effective temperature T^*, the kinetic equations can be solved exactly to give the phonon distribution

$$n(\Omega) = \frac{\left\{\left[\tau_{\mathrm{s}}^{\mathrm{ph}}\left(\Omega, T^*\right)\right]^{-1} + \tau_{\mathrm{B}}^{-1}\left(\Omega, T^*\right)\right\} n\left(\Omega, T^*\right) + \tau_{\mathrm{es}}^{-1} n\left(\Omega, T_{\mathrm{a}}\right)}{\left[\tau_{\mathrm{s}}^{\mathrm{ph}}\left(\Omega, T^*\right)\right]^{-1} + \tau_{\mathrm{B}}^{-1}\left(\Omega, T^*\right) + \tau_{\mathrm{es}}^{-1}}. \tag{4.2}$$

This distribution function is a weighted average of two Bose functions and has a discontinuity at $\Omega = 24$ because the pair-breaking process can happen to phonons with $\Omega \geqslant 24$ only. The quasiparticle and phonon distributions given by the modified T^* model have been confirmed by numerical solution of the full set of kinetic equations in the limit of high phonon trapping, typically $\tau_{\mathrm{es}}/\tau_{\mathrm{B}}(2A) \geqslant 20$. Experimental measurements of the quasiparticle distribution have been carried out by various groups (e.g., Willemsen and Gray 1978, Jaworski and Parker 1979. Smith et al. 1980). It is found that they can be well approximated by a Fermi function with a T^*, except for the cases in which the quasiparticles are predominantly injected into states near the gap edge (such as the case of tunnel injection with a bias voltage $V \sim 2A/e$). In such cases a Fermi function with two parameters: μ^* and T^*, improves the fitting greatly.

The application of the μ^* model is found good only at low temperatures and for systems with good thermal coupling to the environment. Nevertheless, it has attractive features. It is easy to handle and it predicts an instability for a spatially uniform nonequilibrium state at a sufficiently large driving amplitude (Chang and Scalapino 1974). To understand why this can occur, consider a thin film at $T = 0$. When the driving source is turned on, quasiparticles are created increasing the chemical potential μ^* above the gap edge. The increased quasiparticle density increases μ^* measured from the gap edge and at the same time suppresses the energy gap. If the gap suppression exceeds the increase of μ^* measured from the gap edge, the net result is a decrease of μ^* due to the increased quasiparticle density. Since $\delta\mu^*/\delta N < 0$ implies a flow of quasiparticles from regions of low density to regions of high density, a uniform distribution of quasiparticles cannot be restored by diffusion.

The effect of quasiparticle diffusion has been considered by Scalapino and Huberman (1977) using the μ^* model. Other theoretical attempts to investigate the instability of a homogeneous nonequilibrium steady state have been made (Schmid 1977, Hida 1978, Elesin 1979, Tremblay 1981). Comparison with experimental results shows that more work, both on theory and experiments, needs to be done. This is a fast developing area. The problem of instabilities in nonequilibrium superconductors is intriguing and far from being completely solved.

24 Vortex Motion in Superconductors by Larkin, Ovchinnikov

24.1 1. Introduction

According to their behaviour in a magnetic field all the superconductors can be classified under two large groups: type-I and type-II superconductors. In a sufficiently strong magnetic field type-II superconductors transfer into a special state, in which superconducting properties, for instance, magnetic moment, weaken with increasing magnetic field. This state is called the mixed state or the Shubnikov phase (Shubnikov et al. 1937). As has been shown by Abrikosov (1957), a magnetic field penetrates into a superconductor in the mixed state in the form of separate threads. In this case the threads form a regular triangular lattice. The magnetic field breaks the space homogeneity of the order parameter and generates vortices.

In an electric field flux lines move with a velocity proportional to the electric field strength. With such a motion the distribution function of normal excitations deviates from its equilibrium value, which results in energy dissipation.

In a weak electric field the deviation of the distribution function from the equilibrium value is proportional to the electric field $\boldsymbol{E}$.

In an ideal homogeneous superconductor the transport current is also proportional to $\boldsymbol{E}$. However, nonlinearity of the $I-V$ characteristic of a superconductor sets in rather early. This can be accounted for by the fact that in metals energy relaxation is slow and the distribution function is thus strongly dependent on the electric field. In a normal metal the conductivity is determined by the total number of electrons and is independent of details of their distribution with energy. Therefore, the IV' characteristic of a normal metal remains linear up to large fields. In a superconductor the conductivity depends on the order parameter, which is very sensitive to the shape of the distribution function. As a result, the $I-V$ characteristic of a superconductor becomes nonlinear at a current density much below the depairing critical current.

The initial part of the IV characteristic is determined by inhomogeneities always present in real samples. Inhomogeneities distort the vortex lattice and lead to arising of metastable current states. In such a state a current below some critical value does not lead to the motion of flux lines and energy
dissipation. The value of the critical current, its dependence on magnetic field and temperature, and also the $I-V$ characteristic for current densities exceeding the critical one, depend essentially on the type of inhomogeneities.

In section 2, the equation of motion of a vortex structure is derived. Each term in this equation has a simple physical meaning and describes a force acting on the vortex. Here the viscosity force is expressed through variation of the Green function and the distribution function of excitations in an electric field.

In section 3 we consider ideal homogeneous superconductors in a weak electric field. The dependence of the conductivity of a superconductor on the values of magnetic field, temperature and the electron free path has been determined. The conductivity of superconductors has been

investigated theoretically for all the cases when the solution of a static equation for the order parameter is known.

Section 4 is devoted to investigation of nonlinear effects arising upon motion of flux lines. In the vicinity of the transition temperature excitations are put out of the region of the vortex core. The vortex compresses and viscosity shows a drastic drop. At low temperatures the process of generation of new excitations is more essential, which may result in an intensive emission of almost monochromatic phonons.

Section 5 presents a description of elastic properties of a vortex lattice, which are important for understanding the phenomenon of pinning. Unlike the common elastic media, the elastic moduli of a vortex lattice have a strong space dispersion (Brandt 1977). Another difference is that even weak inhomogeneities cause the vanishing of the long-range order in the vortex lattice (Larkin 1970).

In section 6, pinning processes are investigated. If the interaction of a defect with the lattice is sufficiently strong, then metastable states may form on a single defect (strong pinning). In this case the critical current is proportional to the defect concentration (Labusch 1969b). For defects weakly interacting with the vortex lattice, the critical current arises due to collective effects and is proportional to the square of the concentration (Larkin and Ovchinnikov 1973c).

The friction force depends on the velocity of the vortex motion, which results in deviation of the $I - V$ characteristic from the linear law. When the pinning is strong, the friction in motion is less than the friction at rest. When the pinning is weak, the friction force grows with increasing vortex lattice velocity.

The Appendix presents a derivation of kinetic equations for the excitation distribution function. These equations are used for studying the dynamic characteristics of superconductors.

24.2 2. Equation of flux line motion in inhomogeneous superconductors

24.2.1 2.1. Phenomenological derivation

Many phenomena arising on the flux line motion in superconductors have a macroscopic character.

In this case a flux line lattice can be regarded as a continuous medium. The equations of motion of such a medium can be obtained by averaging microscopic equations over the volume containing a large number of flux lines. After such averaging the state of a flux line lattice is described by a two-dimensional displacement vector u. The forces acting on an isolated unit volume are different in physical nature and have different dependences on the displacement vector $\boldsymbol{u}$. The viscosity force $\boldsymbol{f}_{\mathrm{v}}$ at small velocities $\boldsymbol{v}$ of the flux line lattice is proportional to the velocity

$$f_v = -n_v \eta v, \quad v = \partial u/\partial t \tag{1}$$

where n_v is the flux line density related to the induction B by the formula

$$B = n_i \phi, \quad \phi = \pi\hbar/e \tag{2}$$

ϕ is the flux quantum. A mean electric field is associated with the motion of flux lines:

$$E = -\frac{1}{c}[v \times B]. \tag{3}$$

In the coordinate system moving together with flux lines, the mean electric field is zero.

The viscosity coefficient η in eq. (1) is, generally speaking, a tensor. The nondiagonal elements of the tensor describe the Hall effect. With increasing velocity, the viscosity coefficient

decreases. The value η changes essentially at a comparatively small velocity, when the transport current j is essentially less than the critical current of depairing. This phenomenon is connected with the fact that the electron distribution function becomes nonequilibrium upon flux line motion.

If a transport current with the density $\langle j \rangle$ passes through a superconductor, then the Lorentz force acts on the flux lines:

$$f_{\mathrm{L}} = \frac{1}{c}[j \times B]. \tag{4}$$

In homogeneous superconductors the Lorentz force is equal to the viscosity force. This allows us to express the current density through the electric field
intensity

$$j = \sigma E, \quad \sigma = \phi\eta/B. \tag{5}$$

In real superconductors there always exist inhomogeneities of different kinds: pores, dislocation loops, grain boundaries and other phase regions. Such inhomogeneities are called pinning centres and lead to a dependence of the free energy F on the position of the flux line lattice and, namely, to a pinning force arising,

$$f_{\mathrm{pin}} = -\delta F_{\mathrm{pin}}/\delta u \tag{6}$$

Usually the distances between pinning centers are large. This makes it possible to distinguish the volume containing a separate defect and the pinning force (6) connected with it.

In the space between the pinning centers the flux line lattice is deformed. Its deformation is weak and may be described by means of the theory of elasticity. The elastic force is equal to (Labusch 1967)

$$f_{\mathrm{el}} = -\frac{\delta F_{\mathrm{el}}}{\delta u} = (C_{11} - C_{66})\,\frac{\partial}{\partial \rho}\left(\frac{\partial u}{\partial \rho}\right) + \left(C_{66}\frac{\partial^2}{\partial \rho^2} + C_{44}\frac{\partial^2}{\partial z^2}\right) u; \tag{7}$$

the z axis is chosen in the direction of the magnetic field, ρ is a twodimensional vector in the xy plane, and C_{1K} are elastic moduli. In many cases elasticity theory is applicable in all the volume involving the vicinities of the pinning center. When the centers are very strong, plastic deformation arises in their vicinity. In this case eq. (7) is applicable at sufficiently large distances from the pinning center. A triangular lattice has only three independent moduli. They may be considered to be constant only in the case when the displacement vector varies slowly at distances of the order of the magnetic field penetration depth. Otherwise, the bending of the lattice is stronger than that of magnetic lines of force. This effect results in a strong space dispersion of the elastic moduli C_{11} and C_{44} (Brandt 1977).

The sum of all the forces acting on the flux line lattice should be zero. Substituting for these forces eqs. (1), (4), (6) and (7) we get an equation of motion of the flux line lattice:

$$f_{\mathrm{el}} + f_{\mathrm{v}} + f_{\mathrm{L}} + f_{\mathrm{pin}} = 0 \tag{8}$$

$$(C_{11} - C_{66})\,\frac{\partial}{\partial \boldsymbol{\rho}}\left(\frac{\partial \boldsymbol{u}}{\partial \boldsymbol{\rho}}\right) + \left(C_{66}\frac{\partial^2}{\partial \boldsymbol{\rho}^2} + C_{44}\frac{\partial^2}{\partial z^2}\right) u - \sigma B^2 \frac{\partial u}{\partial t} + [j \times \boldsymbol{B}] + f_{\mathrm{pin}} = 0 \tag{9}$$

(Schmid and Hauger 1973, Larkin and Ovchinnikov 1973c). The parameter which is most difficult to determine, both theoretically and experimentally, is the pinning force f_{pin} . Usually, microscopic parameters of the pinning center are known poorly. In the most interesting case, strong pinning, the lattice deformation is plastic and quantitative calculation is difficult. But even when

the force of interaction with one pinning center is known, the problem of summing arises as well. The problem is that f_{pin} depends on the relative positions of the lattice and the pinning center. When the interaction force with one pinning center achieves a maximum, the interaction force with other centers may be less or even may have an opposite direction. Therefore, the mean pinning force is less than the sum of the maximum values of individual forces. To calculate the mean force it is necessary to solve eq. (9). Therefore, the mean force may depend on the vortex velocity, i.e., on the electric field. The friction of motion is not equal to that of the state of rest. Averaging eq. (9) over the volume containing a large number of pinning centers, one may get the I V characteristic of the sample

$$\langle j(\boldsymbol{E})\rangle = \sigma(\boldsymbol{E})\boldsymbol{E} + \left[\langle f_{\text{pin}}\rangle \times \boldsymbol{B}\right]/\boldsymbol{B}^2 \tag{10}$$

where σ is the conductivity without pinning.
At zero electric field the superconducting current may be nonzero. The state with a current is metastable. Thermal fluctuations lead to the damping of a superconducting current with time. At temperatures not very close to the critical one, the energy of the vortex interaction with the pinning centers far exceeds the temperature. Such damping ("creep") is thus exponentially small and will not be taken into account below.

24.2.2 2.2. Microscopic derivation of the equation of motion

Equation (9) can be derived from microscopic equations of the theory of superconductivity. Therewith, the microscopic nature of the parameters involved in eq. (9) is elucidated and in many cases it is possible to find their dependence on temperature, magnetic field and on microscopic characteristics of the superconductor.

The microscopic equations for the order parameter Δ and for the vector potential A have the form of eqs. (A.20) and (A.21):

$$\begin{aligned}
&\frac{1}{\lambda_{\text{eff}}}\Lambda_{1,2} = \pm\frac{1}{8}\int \mathrm{d}\Omega_p \left(g_p^{\mathrm{K}}(t,t)\right)_{12,21} \\
&\operatorname{rot}\operatorname{rot} A = \frac{4\pi}{c}j = -\frac{\mathrm{e}\pi v}{2}\int \mathrm{d}\Omega_p \operatorname{Tr}\tau_2 \frac{p}{m} g_p^{\mathrm{K}}(t,t)
\end{aligned} \tag{11}$$

where $\nu = mp/2\pi^2$ is the density of states on the Fermi surface, λ_{eff} is the effective constant of the electron electron interaction, and y_p^K is the matrix composed of single-particle Green functions. The equation expressing $y_{,}^{\mathrm{K}}$ through Δ and $\boldsymbol{A}$ is given in the Appendix (A.12).

Suppose the solutions of the system of equations (11) in the static case $A_0(r)$, $A_0(r)$ are known. The change in the free energy δF at small static deviations
from equilibrium is

$$\delta F = v\int \mathrm{d}^3 r \int \frac{\mathrm{d}\Omega_p}{4\pi} \operatorname{Tr}\left(\frac{\hat{\Delta}}{\lambda_{\text{eff}}} - \frac{\pi}{2} g_p^{\mathrm{K}}(t,t)\right)\delta\hat{\Delta} + \frac{1}{4\pi}\int \mathrm{d}^3 r \delta A(\operatorname{rot}\operatorname{rot} A - 4\pi j), \tag{12}$$

where $\hat{A}$ is determined by eq. (A.20).
At small velocities $\boldsymbol{V}$ of the vortex lattice motion, the solution of eqs. (11) may be written in the form

$$\Delta^{(1,2)}(r,t) = \Delta_0^{(1,2)}(r-u)\exp(\pm 2\mathrm{i}e\chi) + \Delta_1^{(1,2)}$$
$$A(r,t) = A_0(r-u) + \frac{\partial\chi}{\partial r} + \tilde{A} + A_1$$
$$\frac{\partial\chi}{\partial t} = \frac{\partial u}{\partial t}A_0(r-u) \tag{13}$$

The vector potential $\tilde{A}$ describes the magnetic field created by the transport current $\langle j\rangle$. This field varies only slightly at distances of the order of the lattice period. Therefore, one may regard it as included into the induction $\boldsymbol{B}$, so that Δ_0 and A_0 are determined by the local value of the induction $\boldsymbol{B}$ at each point of the sample.

The phase χ of the gauge transformation is chosen so that at an infinitesimal displacement u the increment of the order parameter A would not contain terms increasing with distance. The small corrections Δ_1 and A_1 do not contain increasing terms either and satisfy the complicated equations obtained by linearization of system (11). It is shown that for calculating the mean forces involved in eq. (9), it is not required to find A_1 and A_1. This method is similar to the perturbation theory in quantum mechanics, where it is sufficient to know the wave functions of a zero-order approximation to calculate the energy in first order. The function y may be presented in the form $g_0 + g_1$ with an accuracy up to the first-order term in velocity. The function g_0 is found by solving eqs. (A.12) in a static case. In these equations instead of Δ and A one should insert their expansion (13) together with the zero- and firstorder terms. The function g_1 is found by solving eqs. (A.12) to first order with respect to velocity of motion, using a zero-order approximation for the potentials Δ and A.

Then this expansion and (13) are substituted into system (11), the first equations of system (11) are multiplied by $\partial_+ A^*$ and $\partial_- A$, the latter is multiplied by rot A_0 vectorially and the summation of all equations is performed. As a result, taking into account formula (12), we arrive at

$$\frac{\delta}{\delta \boldsymbol{U}}\left[F + \left(\frac{\delta F}{\delta\Delta^{(1)}}\Delta_1^{(1)} + \frac{\delta F}{\delta\Delta^{(2)}}\Delta_1^{(2)} + \frac{\delta F}{\delta \boldsymbol{A}}\boldsymbol{A}_1\right)\right] + [j\times\boldsymbol{B}]$$
$$-\frac{mp}{4\pi}\int\frac{\mathrm{d}\varepsilon}{2\pi}\int\frac{\mathrm{d}\Omega_p}{4\pi}\left\langle \mathrm{Tr}\left(e[\boldsymbol{H}\times\boldsymbol{v}]\tau_z - \left(\frac{\partial}{\partial\boldsymbol{r}} - 2\mathrm{i}e\boldsymbol{A}\tau_z\right)\hat{\Delta}\right) g_1^{\mathrm{K}}(\boldsymbol{\rho},\varepsilon,t)\right\rangle = 0. \tag{14}$$

The free energy F of a homogeneous superconductor does not change when the flux line lattice is subjected to a homogeneous displacement. The first term in eq. (14) is thus nonzero only due to inhomogeneities and elastic deformations and is equal to the sum of the pinning forces f_{pin} and the elastic force f_{el} . The second and third terms in square brackets give small corrections, proportional to the velocity, to these forces and are not taken into account in this chapter. Therefore, to calculate f_{el} and f_{pin} it is necessary to obtain the deformation dependence of the free energy. The next term in eq. (14) is equal to the Lorentz force and arises due to the term $\tilde{A}$ in eq. (13).

The last term in eq. (14) gives a microscopic expression for the viscosity force. In this expression the Green function g_1 appears due to the motion of flux lines. The viscosity force at small velocities is proportional to velocity.

The relationship of the mean electric field with the flux line velocity is obtained from eq. (13) for the vector potential. Differentiating A with respect to time and averaging over the volume, we have

$$\boldsymbol{E} = -\left\langle\frac{\partial\boldsymbol{A}}{\partial t}\right\rangle = -\left[\frac{\partial\boldsymbol{u}}{\partial t}\,\mathrm{rot}\,\boldsymbol{A}\right] = [\boldsymbol{B}\times\boldsymbol{v}]. \tag{15}$$

24.3 3. Conductivity of superconductors in a mixed state

In this section we consider the vortex motion in homogeneous superconductors free from pinning forces. Actually this means that the transport current passing through a superconductor much exceeds the pinning critical current.

When the transport current flows, a Lorentz force arises, causing flux line motion. The flux line motion is accompanied by heating of normal excitations and energy dissipation. Two mechanisms of energy dissipation can be considered. One of the dissipation mechanisms is related with the Joule heating of normal excitations by an electric field (Strnad et al. 1964, Bardeen and Stephen 1965). The second mechanism is connected with inhomogeneity of the absolute value of the order parameter in the flux line (Tinkham 1964). Such inhomogeneity leads to a force affecting normal excitations. Therefore, the moving flux line drags the normal component.

The conductivity of a superconductor in a mixed state can be found from the condition of equality of the Lorentz and viscosity forces. The Lorentz force is proportional to the transport current density, the viscosity force to the velocity of the flux line lattice. As follows from eq. (15), the flux line velocity is
proportional to the electric field $\boldsymbol{E}$. So, in the region of weak currents we have

$$j = \sigma \boldsymbol{E} \tag{16}$$

In homogeneous superconductors the pinning force and elastic deformation of a vortex lattice are absent. Therefore, the first term in eq. (14) is zero. Making a cross-product of eq. (14) by $\boldsymbol{B}$ we get:

$$j = -\frac{mp}{4\pi B^2} \int \frac{\mathrm{d}\varepsilon}{2\pi} \int \frac{\mathrm{d}\Omega_p}{4\pi} \left\langle \mathrm{Tr} \left(\mathrm{e}v(\boldsymbol{B} \times \boldsymbol{H})\tau_z + \left[\boldsymbol{B}, \left(\frac{\partial}{\partial r} - 2\mathrm{i}e\boldsymbol{A}\tau_z \right) \hat{\Delta} \right] \right) g_1^{\mathrm{K}}(p, r, t) \right\rangle . \tag{17}$$

Equation (17) expresses the transport current through the Green function $g_1^K(p, t)$.

Equations for the Green function $y_1^K(p, r, t)$ are derived in the Appendix. It is possible to obtain an analytical expression for the conductivity for some limiting cases only.

24.3.1 3.1. Temperatures close to T_{c}

In the vicinity of the transition temperature the order parameter Δ can be found from the Ginzburg Landau equation. For superconductors with a small electron free path the range within which the order parameter varies is of the order of $\xi(T) = (\pi D/8\,(T_c - T))^{1/2}$. Therefore, the Green functions of the local approximation (A.39) satisfy eq. (A.37).

The omitted gradient terms are small with respect to the parameter $(1 - T/T_{\mathrm{c}})^{1/2}$. In a local approximation the contribution to the current arising from the distribution function f is anomalously large. Retaining only this contribution in the Green function g_ρ^{K} (eq. A.47), eq. (17) is reduced to

$$j = \frac{mp}{4\pi B^2} \left\langle \int_{|\varepsilon|>|\Delta|} \frac{\mathrm{d}\varepsilon}{2\pi} \left(\varepsilon^2 - |\Delta|^2 \right)^{1/2} f \cdot \left[\boldsymbol{B} \frac{\partial |\Delta|^2}{\partial r} \right] \right\rangle . \tag{18}$$

For fields close to $H_{\mathrm{c}2}$ the term $\sigma_{\mathrm{N}}\boldsymbol{E}$ arising from the current part of the Green function should be added to the right-hand side of cq. (18): $\sigma_{\swarrow} = e^2 p^2 l_{\mathrm{tr}}/3\pi^2$ is the conductivity of a metal in the normal state, with $l_{1,}$ the electron mean free path of transport. The distribution function f is determined from eqs. (A.43) and (A.44), in which $\partial/\partial t$ should be substituted by $-(v\partial/\partial r)$. Applying formula (15) the lattice velocity v is expressed through the electric field E. As a result, from eq. (18) we find the conductivity of a superconductor in a mixed state:

$$\frac{\sigma}{\sigma_N} - 1 = \frac{1}{4e^2 D^2 T B^2} \int_0^x d\varepsilon \phi(\varepsilon) \tag{19}$$

where

$$\phi(\varepsilon) = \frac{eB}{\pi} \int_{V_j} d^2\boldsymbol{r} \frac{\partial \left(\varepsilon^2 - |\Delta|^2\right)^{1/2}}{\partial \boldsymbol{r}} \left(-\frac{\partial^2}{\partial \boldsymbol{r}^2}\right)^{-1} \frac{\partial \left(\varepsilon^2 - |\Delta|^2\right)^{1/2}}{\partial \boldsymbol{r}}, \tag{20}$$

π/eB is the volume of an elementary cell, V_ε is the region where $|\varepsilon| > |\Delta|$. The boundary condition in expression (20) for $(-\hat{c}^2/\hat{c}r^2)^{-1}$ is given by eq. (A.42). For $|\varepsilon| > |\Delta|_{\max}$ the volume V_ε coincides with the whole cell and for $\phi(\varepsilon)$ we get

$$\phi(\varepsilon) = \left\langle \left(\left(\varepsilon^2 - |\Delta|^2\right)^{1/2} - \left\langle \left(\varepsilon^2 - |\Delta|^2\right)^{1/2} \right\rangle \right)^2 \right\rangle, \quad |\varepsilon| > |\Delta|_{\max}. \tag{21}$$

In eqs. (19) and (20), only ε of the order of Δ are important so $\phi(\varepsilon) \sim A^2 B/H_{c2}$. Expression (19) for the conductivity has thus the form

$$\frac{\sigma}{\sigma_N} - 1 = \frac{1}{(1 - T/T_c)^{1/2}} \frac{H_{c2}}{B} \tilde{f}\left(B/H_{c2}\right). \tag{22}$$

We now substitute into formulas (19), (21) the value of the order parameter Δ, found from the Ginzburg Landau equation in a weak magnetic field $B \ll H_{c2}$ and for fields close to H_{c2}. As a result, for the function $\tilde{f}$ we have

$$\tilde{f}(x) = \begin{cases} 4.04, & x \ll 1, \quad \kappa \gg 1, \\ 0.31 \left(\frac{1 - H/H_{c2}}{1 - \frac{1}{2}\kappa^2}\right)^{3/2}, & 1 - x \ll 1, \end{cases} \tag{23}$$

where κ is the Ginzburg-Landau parameter. The numerical coefficients in formula (23) differ from those obtained in earlier papers (Gorkov and Kopnin 1973a, Larkin and Ovchinnikov 1973b), since in these papers an erroneous boundary condition for the operator $(-\partial^2/\partial r^2)^{-1}$ was used. To calculate the function $\tilde{f}$ in an arbitrary magnetic field, the hexagonal lattice is replaced by a round cell. Such an approximation is exact for weak fields. Even for fields close to H_{c2} the error in determining the derivative of $|\Delta|$ at $|\Delta| = 0$ is less than 1% in the round-cell method. One may thus hope that the error is small in calculation of the conductivity as well.

In the approximation of a round cell the expression for conductivity has been derived by Danilov et al. (1974). However, in their paper erroneous boundary conditions were used. In the present chapter, we applied the boundary condition (A.42) for $|\varepsilon| < |\Delta|_{\max}$, and for $|\varepsilon| > |\Delta|_{\max}$ we used expression (22) for the function $\phi(\varepsilon)$. The results of numerical calculation are presented in table 1. These values can be given by an interpolation formula

$$\tilde{f}(x) = \begin{cases} 4.04 - \left(\frac{B}{H_{c2}}\right)^{1/4} \left(3.96 + 2.38 \frac{B}{H_{c2}}\right), & \frac{B}{H_{c2}} < 0.315, \\ \left(1 - \frac{B}{H_{c2}}\right)^{3/2} \left(0.43 + 0.69 \left(1 - \frac{B}{H_{c2}}\right)\right), & \frac{B}{H_{c2}} > 0.315. \end{cases} \tag{24}$$

It should be noted that the function $\tilde{f}$ essentially decreases already in weak fields.

Growth of conductivity on approaching the transition temperature is caused by a strong change in the distribution function of excitations. Such growth continues while the size of a flux line is not too large, and the time of diffusion of excitation through the core of the flux line is smaller than the time of the energy relaxation. These time scales become of the same order when $T_c - T \sim \tau_\varepsilon^{-1}$. With further approaching T_c the deviation of the distribution function from equilibrium decreases. In this case the first term in eq. (A.40) is small as compared to I^{ph}.

Table 1
Numerical results for the function $f(x)$, calculated with eq. (24).

B/H_{c2}	$\tilde{f}(x)$	B/H_{c2}	$\tilde{f}(x)$
0	4.04	0.1633	1.2
0.02	2.53	0.2222	0.92
0.0247	2.449	0.32	0.604
0.03125	2.347	0.5	0.2776
0.04082	2.214	0.08889	0.0182
0.05556	2.036	0.9512	$4.987 \cdot 10^{-3}$
0.08	1.814	0.978	$1.473 \cdot 10^{-3}$
0.125	1.435	0.99187	$3.179 \cdot 10^{-4}$

The collision integral I^{ph} in this case can be taken in the form of a τ_ε-approximation (formula eq. A.34), because the essential ε in eq. (19) for the conductivity are of the order of Δ and are thus much smaller than T_c. In a linear expansion in the velocity from eq. (A.40) we find

$$f = \tanh\left(\frac{\varepsilon}{2T}\right) + \frac{\tau_\varepsilon}{2\varepsilon}\frac{\partial \tanh(\varepsilon/2T)}{\partial\varepsilon}\left(v\frac{\partial|\Delta|^2}{\partial \boldsymbol{r}}\right). \tag{25}$$

Substituting expression (25) for the distribution function into eq. (18), we get the following expression for the conductivity:

$$\sigma - \sigma_{\mathrm{N}} = \frac{mp\tau_\varepsilon}{8\pi T B^2}\langle|\Delta\left|\left(\frac{\partial|\Delta|}{\partial r}\right)^2\right\rangle. \tag{26}$$

For small fields the solution for A for a single flux line can be inserted into eq. (26). As a result, we have (Larkin and Ovchinnikov 1977)

$$\begin{aligned}\frac{\sigma}{\sigma_{\mathrm{N}}} &= \frac{H_{c2}}{B}\frac{\pi^2\tau_\varepsilon}{16T\,(T_c - T)}\int_0^\infty \mathrm{d}\rho\rho|\Delta|\left(\frac{\partial|\Delta|}{\partial\rho}\right)^2 \\ &= 2.73\frac{H_{c2}}{B}\tau_\varepsilon T_c\,(1 - T/T_c)^{1/2}\end{aligned} \tag{27}$$

While approaching T_c the conductivity determined by eq. (26) decreases. Therefore, there is a maximum at $T_c - T \sim \tau_\varepsilon^{-1}$ in the temperature dependence of the conductivity.

24.3.2 3.2. Fields close to H_{c2}

Let us consider now fields close to H_{c2}. As follows from eq. (24), the contribution to the conductivity connected with a change of the distribution function decreases as $(1 - H/H_{c2})^{3/2}$. The change of the Green function $g^{\mathrm{R.A}}$ becomes more essential. In the vicinity of H_{c2} the order parameter Δ is small and the Green functions can be found by expanding eq. (A.37) in powers of Δ. In main approximation $\alpha^{\mathrm{R.A}} = \pm 1$, and eq. (A.37) becomes a linear equation for the function $\beta^{\mathrm{R.A}}$. The coordinate dependence of the function $\beta^{\mathrm{R.A}}$ is the same as that of the order parameter Δ. They are eigenfunctions of the operator $-\partial_-^2$, corresponding to the minimal eigenvalue equal to $2eH_{c2}$:

$$\beta_1^{\mathrm{R,\ A}} = -\frac{\mathrm{i}\Lambda}{\tilde{\lambda} \mp \mathrm{i}\varepsilon}, \quad \beta_2^{\mathrm{R,\ A}} = -\frac{\mathrm{i}\Delta^*}{\tilde{\lambda} \mp \mathrm{i}\varepsilon}, \tag{28}$$

where

$$\tau = eH_{c2}D + \tau_s^{-1} + (2\tau_\varepsilon)^{-1}. \tag{29}$$

Approximation (A.38) for the collision integral holding in the vicinity of T_c has been applied for deriving formulas (28) and (29). At low temperatures, in eq. (29) the last term should be omitted completely, since it is small compared to the first term. Now insert expressions (28) into eq. (A.47) for the function g^K. As a result, for the conductivity σ from eq. (17) we get

$$\frac{\sigma}{\sigma_N} - 1 = \frac{\langle|\Delta|^2\rangle}{4\pi T}\left\{\frac{1}{eH_{c2}D}\psi'\left(\frac{1}{2}+\frac{\tilde\lambda}{2\pi T}\right) + \frac{1}{\tilde\lambda}\psi'\left(\frac{1}{2}+\frac{\tilde\lambda}{2\pi T}\right) + \frac{1}{2\pi T}\psi''\left(\frac{1}{2}+\frac{\tilde\lambda}{2\pi T}\right)\right\} = \tilde\alpha\,(1-H/H_{c2}). \tag{30}$$

The first term in eq. (30) (Maki 1966) arises from the first term in expression (A.47) for y^K. This term is related with drag of electrons by the moving lines of constant absolute value of the order parameter. Magnetic impurities and energy relaxation only weakly affect this term. The last two terms are connected with changes in the spectrum of excitations at small energies (Thompson 1970). Magnetic impurities and energy relaxation decrease this contribution.

The expression for $\langle|\Delta|^2\rangle$ near H_{c2} can be obtained by expanding eqs. (A.20) and (A.37) into series in Δ (Caroli et al. 1966). As a result, for the value $\tilde\alpha$
determined by formula (30) we have (Ovchinnikov and Brandt 1975)

$$\tilde\alpha = \frac{2}{\beta_A}\psi'(x)\frac{\psi'(x) + \frac{eH_{c2}D}{\tilde\lambda}\psi'(x) + \frac{eH_{c2}D}{2\pi T}\psi''(x)}{-\psi''(x) - \frac{1}{6\pi T}\left(\frac{1}{\tau_s}+\frac{1}{2\tau_\varepsilon}\right)\psi'''(x) - \frac{8e^2p^2l_{tr}^2v}{9\pi}\left(\psi'(x)\right)^2}, \tag{31}$$

where $\beta_A = 1.1596, \quad x = 0.5 + \tilde i/2\pi T$.
In the vicinity of the transition temperature eq. (31) simplifies to

$$\tilde\alpha = \frac{2.496}{1-\frac{1}{2}\kappa^2}\left[1 + \left(1 + \frac{\pi}{4\,(T_c - T)}\left(\tau_s^{-1} + (2\tau_\varepsilon)^{-1}\right)\right)^{-1}\right] \tag{32}$$

where

$$\kappa^2 = 63\zeta(3)/2\pi^3e^2p^2l_{tr}^2v$$

Equation (30) is valid for superconductors with a small electron mean free path. Near the transition temperature the limitation for the free path is weaker: $l \ll \xi(T)$. In this case $\langle|\Delta|^2\rangle$ should be found from the Ginzburg-Landau static equation, its coefficients depending on the ratio $//\zeta(0)$ (Gor'kov 1959).

The expression for the conductivity near H_{c2}, valid at an arbitrary temperature and the ratio $l/\xi(0)$, has been obtained by Ovchinnikov (1974).

The first terms in eqs. (30) and (32) depend only slightly on the energy relaxation time. The second term in eq. (32) decreases rapidly on approaching T_c.

Figure 1 shows the dependence of the coefficient $\bar\alpha$ on the reduced temperature T/T_c at $\kappa^2 \gg 1$ and different values of the parameter

$$\Gamma = \left(\tau_s^{-1} + (2\tau_\varepsilon)^{-1}\right)/2\pi T_c$$

The same figure shows experimental data (Meier-Hirmer et al. 1976) on the conductivity in the vicinity of H_{c2} for $Pb_{0.8}\,In_{0.2}$ and $Pb_{0.9}\,In_{0.1}$. It follows from fig. 1 that for the energy relaxation time

$$(T_c\tau_\varepsilon)^{-1} \sim 0.2$$

24.3.3 3.3. Low temperatures

Consider now the case of low temperatures $T \ll T_c$, weak fields, and a small electron free path (Gor'kov and Kopnin 1973b). At low temperatures, in eqs. (17) and (A.48) low energies $\varepsilon \sim T$ are essential. Therefore, it is sufficient to solve eqs. (A.37) for the Green functions $\beta^{R,A}, \alpha^{R,A}$ at $\varepsilon = 0$. In this case

$$\alpha^R = -\alpha^A = \sin\psi, \quad \beta^R = \beta^A = -i\cos\psi\exp(i\varphi), \tag{33}$$

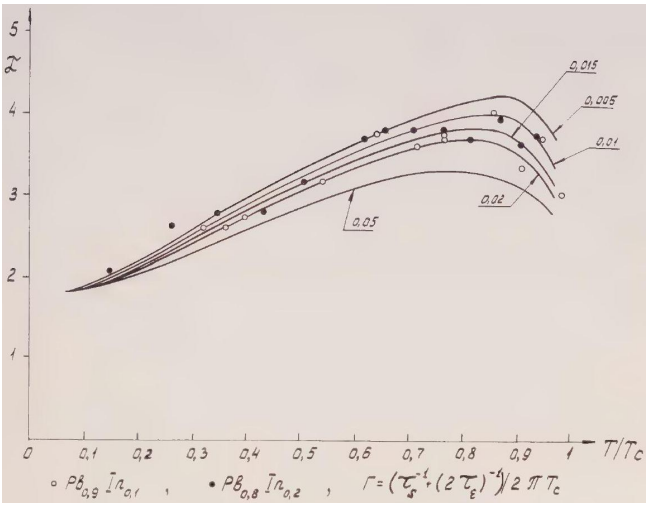


Fig. 1. Solid lines: dependence of $\tilde{x}$ on reduced temperature according to eqs (30)-(32), for different Γ. Symbols: experimental results of Meier-Hirmer et al. (1976).}

where φ is the phase of the order parameter, and ψ is a real function of the coordinates, satisfying the equation

$$\frac{r^2\psi}{\partial r^2} + \frac{\sin 2\psi}{2r^2} - \frac{2|A|}{D}\sin\psi = 0 \tag{34}$$

with the boundary condition

$$\psi(\infty) = 0. \tag{35}$$

From eqs. (17) and (A.48), taking account of eq. (33), we find

$$j = \mathrm{mp}_{2\pi\boldsymbol{B}^2}\int_{2\pi}^{\mathrm{d}\varepsilon}\left\langle D\left[\boldsymbol{B}^{i\varphi}\frac{i\varphi}{\partial\boldsymbol{r}}\right]_{\partial r^2}^{\hat{r}^2 f_1} + \frac{if}{\partial\varepsilon}\left[\boldsymbol{B}^{i|\cdot 1|}\left|\left(v^i\frac{\cos\psi}{\partial\boldsymbol{r}}\right)\right\rangle\right.\right. . \tag{36}$$

where v is the velocity of the flux line lattice.
It should be noted that in eq. (36) the distribution function f should be taken in zero approximation. The function f_1 is found from eq. (A.32), which, taking account of eq. (33), is reduced to

$$-D\left[\frac{1}{\rho}\frac{\partial}{\partial\rho}\left(\rho\frac{\partial}{\partial\rho}\right) - \frac{1}{\rho^2}\right]\tilde{f}_1 + 2|\Delta|\cos\psi\tilde{f}_1 = \frac{2|\Delta|\cos\psi}{\rho}, \tag{37}$$

where

$$f_1 = -\frac{\partial f}{\partial \varepsilon}\frac{\rho}{2}\left(\frac{\partial \varphi}{\partial \boldsymbol{r}}v\right)\tilde{f}_1 \tag{38}$$

From eq. (36) we find (Gor'kov and Kopnin 1973).

$$\frac{\sigma}{\sigma_{\mathrm{N}}} = \frac{H_{\mathrm{c2}}(0)}{B}\tilde{\beta}, \tag{39}$$

$$\tilde{\beta} = \frac{D}{\Delta_\infty}\frac{\partial \tilde{f}_1}{\partial \rho}\bigg|_0 + \frac{1}{\Delta_\infty}\int_0^\infty \mathrm{d}\rho\rho\frac{\partial|\Delta|}{\partial\rho}\frac{\partial\cos\psi}{\partial\rho} = 0.9. \tag{40}$$

The conductivity of superconductors with a large electron mean free path has been less investigated. By order of magnitude the vortex viscosity at low temperatures for pure and dirty superconductors has the same form (39) (Bardeen and Stephen 1965). In pure superconductors the derivative $\partial\Delta/\partial\rho$ at $\rho \to 0$ increases with decreasing temperature (Kramer and Pesch 1974). One may assume that a decrease in temperature causes a compression of the vortex up to the size of vT/T_{c}^2. The conductivity is determined by the behaviour of the absolute value of the order parameter Δ at distances $r \sim v/T_{\mathrm{c}}$. From the assumption on the compression of the flux line core it follows that conductivity grows logarithmically with decreasing temperature (Bardeen and Sherman 1975, Larkin and Ovchinnikov 1976). The Green function of a superconductor with a large electron free path at low energies is

$$g^{\mathrm{R,\ A}} = \chi^{\mathrm{R,\ A}}\begin{pmatrix} 1 & -\mathrm{i}\exp(\mathrm{i}\varphi + \mathrm{i}\eta(t)) \\ \mathrm{i}\exp(-\mathrm{i}\varphi - \mathrm{i}\eta(t)) & -1 \end{pmatrix} \tag{41}$$

(Kramer and Pesch 1974), where the phase $\eta(t)$ is

$$\eta(t) = \frac{2e}{v\sin\theta}\int_{-\infty}^{t}\mathrm{d}t_1\nu\left(A - \frac{1}{2e}\frac{\partial\varphi}{\partial r}\right), \tag{42}$$

$t/\sin\theta$ is the distance on the trajectory counted from the point which is nearest to the axis of the flux line, and θ is the angle between the velocity and the magnetic field.

$$\begin{aligned}\chi^{\mathrm{R,\ A}} =& \frac{\mathrm{i}v\sin\theta}{2}\exp\left(-\frac{2}{v\sin\theta}\left|\int_0^{\mathrm{t}}\Delta\cos\eta\ \mathrm{d}t_1\right|\right) \\ &\times\left(\varepsilon\varphi_1(\theta,x) - \varphi_2(\theta,x) \pm \mathrm{i}\delta\right)^{-1}\end{aligned} \tag{43}$$

where x is the impact parameter,

$$\begin{aligned}\varphi_1(\theta,x) &= \int_0^\infty \mathrm{d}t\exp\left(-\frac{2}{v\sin\theta}\left|\int_0^{\mathrm{t}}\ \mathrm{d}t_1\Delta\cos\eta\right|\right) \\ \varphi_2(\theta,x) &= \int_0^\infty \mathrm{d}t\Delta\sin\eta\exp\left(-\frac{2}{v\sin\theta}\left|\int_0^{\mathrm{t}}\ \mathrm{d}t_1\Delta\cos\eta\right|\right)\end{aligned} \tag{44}$$

It follows from the system of equations (A.52) that the distribution function f_1 is small, and the function f is constant on the trajectory. Integrating the first equation (A.52) along the trajectory we get

$$\mathrm{i}\frac{\partial f}{\partial \varepsilon}\int_{-\infty}^{\infty}\mathrm{d}l\,\mathrm{Tr}\,\frac{\partial \hat{H}}{\partial t}\left(g_p^{\mathrm{R}}-g_p^{\mathrm{A}}\right)$$
$$=\frac{m}{2}\int_{-\infty}^{\infty}\mathrm{d}l\int\mathrm{d}\Omega_{p_1}\sigma_{pp_1}\left(f_p-f_{p_1}\right)\mathrm{Tr}\left(g_p^{\mathrm{R}}-g_p^{\mathrm{A}}\right)\left(g_{p_1}^{\mathrm{R}}-g_{p_1}^{\mathrm{A}}\right) \tag{45}$$

where

$$\hat{H}(t)=-\frac{\mathrm{i}e}{m}(p\cdot A)\tau_z-\mathrm{i}\hat{\Delta}.$$

The current density is determined by eq. (17) in which

$$g_1^{\mathrm{K}}(p)=\left(g_p^{\mathrm{R}}-g_p^{\mathrm{A}}\right)f(p).$$

It follows from eq. (43) that $g_p^R-g_p^A$ is proportional to $\delta\left(\varepsilon\varphi_1-\varphi_2\right)$. Therefore, for $|\varepsilon|\ll|\Delta|,\varphi_2$ is small, which corresponds to the trajectories passing at small impact parameters from the flux line axis.

Provided the Kramer and Pesch (1974) hypothesis is valid and compression of the flux line core takes place, then essentially at distances of the order of v/Δ from the flux line axis the order parameter may be regarded to be constant equal to Δ_∞. To logarithmic accuracy eq. (45) for isotropic scattering is reduced to an algebraic equation, and for the distribution function we get the expression

$$f_p=\tanh\left(\frac{\varepsilon}{2T}\right)+\frac{2\tau\Delta^2}{v}\partial\frac{\tanh(\varepsilon/2T)}{\partial\varepsilon}\frac{e(v\cdot\boldsymbol{E})}{|e[\boldsymbol{B}\times v]|}\ln\begin{pmatrix}v\sin\theta\\ \Delta|\bar{X}|\end{pmatrix}. \tag{46}$$

Substituting this distribution function into expression (17) for the current, we have (Larkin and Ovchinnikov 1976).

$$\sigma/\sigma_{\mathrm{N}}=0.23\left(H_{c2}/B\right)\ln\left(\Delta_0/T\right) \tag{47}$$

In case the hypothesis on the compression of the flux line core is invalid, then in eq. (47) the logarithm is replaced by a number of the order of unity. For determining this number it is required to know the coordinate dependence of the order parameter.

Thus, the problem of the flux line lattice conductivity is solved for all the cases when the solution of a static problem for the order parameter Δ is known.

24.4 4. Nonlinear effects in the motion of vortices in superconductors

In metals at low temperatures the energy relaxation time $\tau_\varepsilon\sim\theta_D^2/T^3$ is large. Therefore, in comparatively weak electric fields a strong change of the energy distribution function of electrons takes place. In a normal metal such a change does not affect the conductivity. In superconductors the energy gap strongly depends on the shape of the distribution function, hence, deviation from Ohm's law occurs even for slowly moving flux lines.

24.4.1 4.1. Nonlinear conductivity

-For a rough estimation of the dependence of the conductivity on the electric field we consider the case when the time of inelastic electron electron collisions is small, as compared to the time of electron phonon or phonon thermostat interactions. In this case the temperature

of electrons may noticeably differ from the thermostat temperature T. Thus, the conductivity, which is determined by the electron temperature, is

$$\sigma(E,T) = \sigma\left(0, T + \sigma E^2 \tau^*/c\right) \tag{48}$$

where c is the electron heat capacity. It may be seen from this expression that at large τ^* nonlinear effects may be strong in a rather weak electric field.

Below we consider another limiting case, when heat is removed effectively and the lattice is in equilibrium with the thermostat, and the time of energy relaxation due to interelectron collisions is larger than that of the electronphonon interaction or of the same order. In this case, due to the slow energy relaxation, the change in conductivity is large and is determined by the variation of the distribution function which now is not reduced to variation in the electron temperature and is more complicated.

The effect is strongest at temperatures close to the critical one, when a slight variation in the distribution function causes a large variation in the order parameter or in its coordinate dependence. This in turn causes a decrease in conductivity, and the voltage dependence of the current has an N-type shape. The parameters of the IV characteristic depend essentially on the magnetic field value and on the magnetic impurity concentration. The strongest nonlinear effects arise in weak magnetic fields at low concentrations of magnetic impurities, when there is a gap in the excitation spectrum and the excitation is captured in the core of the vortex.

In the vicinity of the transition temperature strong variations of conductivity and of the order parameter arise in a weak electric field, when the distribution function varies only slightly. This is connected with the fact that a nonequilibrium correction to the distribution function in the equation for Δ must be compared with the terms proportional to $T_c - T$. In this case the distribution function $\langle f(\varepsilon)\rangle$, in the left-hand side of eq. (A.45) can be replaced by $\tanh(\varepsilon/2T)$. The time derivative in eq. (A.45) should be replaced by $-(v\partial/\partial\mathbf{r})$. Equations (A.45), (A.46) and (A.50) form a closed system of equations for the functions $\Delta(r)$ and $f(\varepsilon)$. However, to determine the function $f(\varepsilon)$ at $\varepsilon \ll \Delta$ it is sufficient to know the shape of the function $A(r)$ near the flux line axis, where $|\Delta(\rho)| = A\rho$. The left- and right-hand sides of formula (A.45) are proportional to A^{-2}, and so the correction to the distribution function at $\varepsilon \ll |\Delta|$ is independent of the slope A and is equal to

$$f(\varepsilon) - \tanh(\varepsilon/2T) = \frac{17}{36}\tau_\varepsilon v^2 \varepsilon/DT \tag{49}$$

In a weak magnetic field $B \ll H_{c2}$ it is possible to find the analytical dependence of $f(\varepsilon)$ at $\varepsilon \to \Delta_\infty$. In this case in eq. (A.45) the essential distances much exceed the correlation length where $\Delta(r) = \Delta_\gamma\left(1 - A/\rho^2\right)$. Substituting such value into eq. (A.45) yields

$$f(\varepsilon) - \tanh(\varepsilon/2T) = \tau_\varepsilon v^2 \left(\Delta_\infty^2 - \varepsilon^2\right)^{1/2}/\pi DT \tag{50}$$

At $\varepsilon > A_\gamma$ in a weak magnetic field $B \ll H_{c2}$, ihe correction to the distribution function is small, since the heating occurs in the region $\rho \sim \xi$, and relaxation proceeds in the whole volume.

In the region $\varepsilon < \Delta_\infty$ we use the interpolation formula

$$f(\varepsilon) - \tanh(\varepsilon/2T) = 0.4\tau_\varepsilon v^2 \frac{\varepsilon\left(\Delta_\infty^2 - \varepsilon^2\right)^{1/2}}{\Delta_\infty DT}. \tag{51}$$

The chosen form of the function $f(\varepsilon)$ has a correct dependence at $\varepsilon \ll \Delta$ and near the threshold $\varepsilon = \Delta_\infty$.

The numerical coefficient 0.4 is equal to the average of the limiting values 0.32 and 0.48 . For the distribution function determined by eq. (51) the nonequilibrium correction to the Ginzburg Landau equation (A.50) is calculated analytically and equals

$$\int_{\Delta}^{A_\infty} \frac{\mathrm{d}\varepsilon\Delta}{\left(\varepsilon^2-\Delta^2\right)^{1/2}}(f(\varepsilon)-\tanh(\varepsilon/2T)) = 0.314\tau_\varepsilon v^2 \frac{\Delta\left(\Delta_\infty^2-\Delta^2\right)}{\Delta_\infty DT}. \tag{52}$$

The correction determined by eq. (52) has the same form as the non-gradient terms in the Ginzburg-Landau equation. The coordinate dependence of the order parameter is thus retained, $\Delta(r)=\Delta(\rho/\xi)$ with the substitution

$$\xi^2 \to \xi^2(v) = \xi^2(0)\left[1+\left(E/E^*\right)^2\right]^{-1} \tag{53}$$

where

$$\left(E^*\right)^2 = D\left(1-\frac{T}{T_c}\right)^{1/2}\left(\frac{B}{C}\right)^2\tau_\varepsilon^{-1}, \quad \xi_{(0)}^2 = \frac{\pi D}{8\left(T_c-T\right)} \tag{54}$$

So, the motion of flux lines leads to a decrease of the vortex core. The physical reason for this is in the following: normal excitations inside the vortex are heated and diffuse into the energy range $\varepsilon > \Delta$. Their effective pressure on the walls of the vortex drops and the vortex compresses. At temperatures close to T_c generation of excitations in the center of the vortex appears inessential. It should be noted that strong compression of the vortex takes place in a comparatively weak electric field, when the correction to the distribution function is still small. Therefore, for the conductivity one may apply eqs. (19) and (20) of the linear approximation. The order parameter $\Delta(r)$ in these formulas should be found with allowance made for an electric field. In an approximation, when the compression of vortex is described by a decrease in the correlation length ξ (eq. 53), in eq. (20) it is possible to use dimensionless variables. Since the function $\phi(\varepsilon)$ is proportional to ξ^2, the expression for conductivity in weak magnetic fields acquires the form

$$\frac{\sigma}{\sigma_\mathrm{N}} = \frac{4.04}{\left(1-T/T_\mathrm{c}\right)^{1/2}}\frac{H_{\mathrm{c}2}}{B}\frac{1}{1+\left(E/E^*\right)^2}. \tag{55}$$

It follows from eq. (55) that with increasing electric field the conductivity decreases. This decrease continues up to fields of the order

$$E = E^*/\left(1-T/T_\mathrm{c}\right)^{1/4} \tag{56}$$

With further increase of the electric field the diffusion of excitations in the energy inside the vortex becomes strong and the distribution function for $0 < \varepsilon < A_x$ acquires a value independent of the electric field. The compression of the vortex stops at the size

$$\xi = \check{\zeta}(T)\left(1-T,T_\mathrm{c}\right)^{1/4}.$$

In this case the conductivity becomes independent of the electric field:

$$\sigma/\sigma_\mathrm{N} = CH_{\mathrm{c}2}/B, \tag{57}$$

where the constant C is of the order of unity. For such small sizes of the vortex one cannot use the local approximation equations (A.38) for the Green functions. The conductivity determined by eq. (57) exceeds that of a normal metal. A complete destruction of superconductivity occurs at a larger electric field, when the distribution function changes not only for the electrons captured in vortices, but also for the electrons in the whole volume. From eq. (48) for this field we get

$$eE = T\left(1-T/T_c\right)^{1/2}/\left(D\tau_\varepsilon\right)^{1/2}. \tag{58}$$

To determine the numerical coefficient in eq. (58) it is necessary to solve the integral equation for the electron distribution function in a normal metal. In this case one cannot use the τ_ε approximation for the collision term.

From eqs. (55) and (57) it follows that the I-V characteristic has an N-type shape,

$$j = \sigma_{\rm N}\frac{H_{\rm c2}}{B}\left\{\frac{4.04}{(1-T/T_{\rm c})^{1/2}}\frac{1}{1+(E/E^*)^2}+C\right\}\boldsymbol{E} \tag{59}$$

and on the dependence $j(E)$ there is a maximum lying in the vicinity of the point $E = E^*$. In the regime of a given current a hysteresis should be observed. A jump in the $I-V$ characteristic has been observed experimentally (Musienko et al. 1980). By the location of the jump the value of E^* was determined, its dependence on the magnetic field and temperature coinciding with the theoretical one (eq. 54). For the energy relaxation time the following values are obtained:

$$\tau_\varepsilon({\rm Sn}) = 6.6\times10^{-10}\ {\rm s}, \quad \tau_\varepsilon({\rm Al}) = 4-7\times10^{-8}\ {\rm s}$$

Equations (55)-(59) are valid for the case of a weak magnetic field. As follows from eqs. (22) and (24), the linear conductivity decreases rapidly with increasing magnetic field. Such a decrease is described by the function $\hat{f}\,(B/H_{\rm c2})$. In weak magnetic fields the action of a magnetic field is reduced to compression of the vortex. Therefore, besides the effect of a decrease in conductivity described above, the change in the argument of the function $\hat{f}$ should also be taken into account,

$$\frac{\sigma}{\sigma_{\rm N}} = \frac{1}{(1-T/T_{\rm c})^{1/2}}\frac{H_{\rm c2}}{B}\frac{1}{1+(E/E^*)^2}\tilde{f}\left(\frac{B}{H_{\rm c2}}\frac{1}{1+(E/E^*)^2}\right) \tag{60}$$

Equation (60) is valid in magnetic fields which are small compared to $H_{\rm c2}$. As the magnetic field grows, not only the cooling of electrons captured by the vortex, but also the heating of electrons with energy $\varepsilon > \Delta$ becomes essential. In magnetic fields close to $H_{\rm c2}$, the heating of electrons and the decrease in $T_{\rm c}$ and in $H_{\rm c2}$ caused by this heating, becomes most essential. This region of magnetic fields has been considered in detail by Larkin and Ovchinnikov (1975). In this case the electric field suppresses essentially the superconducting addition to conductivity. However, the main contribution, coinciding with the conductivity of a normal metal, is not sensitive to the electric field. Therefore, the $I-V$ characteristic in magnetic fields close to $H_{\rm c2}$ displays only slight deviation from the linear dependence. At low temperatures the conductivity is weakly sensitive to a change in the distribution function. Therefore, nonlinear effects in the $I-V$ characteristic are weak (Larkin and Ovchinnikov 1977).

24.4.2 4.2. Emission of monochromatic phonons in the motion of vortices

As a result of the vortex motion there arises a nonequilibrium distribution of electrons with energies causing emission of nonequilibrium phonons. The most interesting phenomena arise at low temperatures. In rather weak electric fields the dependence of the distribution function on ε is determined by the electric field and not by the temperature. As long as the energy of heated electrons is low as compared with the gap 4 , they do not leave the core of the vortex, and a wide spectrum of phonons with a frequency ω of the order of the nonequilibrium excitation energy is emitted. In a sufficiently strong electric field, electrons heated inside the vortex reach the energy $\varepsilon = A$. Then they leave the region of the vortex core and, if the vortex density is low, they are, essentially, not heated further. Accumulation of excitations with energy ε near Δ takes place, and these excitations recombine with emission of phonons with a frequency close to 24 . The width and intensity of emission can be found from eq. (A.45) for the distribution

function. In the narrow region essential for us, in the vicinity of the threshold $\varepsilon = A$, the energy diffusion coefficient D_ε depends logarithmically on energy and we replace it by the constant

$$D_\varepsilon = \begin{cases} 2\tau\Delta^2 eB(E/B)^2, & \tau\Delta > 1, \\ \Delta eB(E/B)^2, & \tau\Delta < 1. \end{cases}$$

For widely spaced flux lines, the recombination of excitations accompanied by emission of a phonon with energy close to 24 is the main relaxation process in eq. (A.45) at $\varepsilon > \Delta$. Equation (A.45) for $\varepsilon > \Delta$ is reduced to

$$\frac{\partial}{\partial\varepsilon}\left(D_\varepsilon \frac{\partial f}{\partial\varepsilon}\right) = -\frac{2\Lambda^3 m g_{\text{eff}}^2}{\pi(sp)^2(\varepsilon-\Delta)^{12}}(1-f(\varepsilon))\int_1^\infty \frac{\mathrm{d}\varepsilon_1}{(\varepsilon_1-\Delta)^{1/2}}\left(1-f\left(\varepsilon_1\right)\right). \tag{61}$$

The solution of eq. (61) is the Bessel function

$$1 - f = Ay^{2/3}K_{2/3}(y), \tag{62}$$

where

$$y^{4/3} = \frac{\varepsilon-\Delta}{\tilde{\mu}}, \quad \tilde{\mu}^{-2} = \frac{\Delta^3 mpg_{\text{eff}}^2}{(sp)^2 D_\varepsilon} A \cdot 2.55$$
$$A = (1 - f(\Delta)) \cdot 2.33 \tag{63}$$

The boundary value of the distribution function $f(\Delta)$ is determined by the diffusion of excitations inside the flux line.

The distribution of phonons with frequencies in the vicinity of $\omega = 2\Delta$ has
the form

$$\frac{\partial N_\omega}{\partial t} = \frac{2\Delta^3 mp}{\pi(sp)^2}\lambda_{\text{eff}} \iint_\Delta^\infty \frac{\mathrm{d}\varepsilon\ \mathrm{d}\varepsilon_1}{(\varepsilon-\Delta)^{1/2}\left(\varepsilon_1-\Delta\right)^{1/2}}\delta\left(\varepsilon+\varepsilon_1-\omega\right)(1-f(\varepsilon))\left(1-f\left(\varepsilon_1\right)\right) \tag{64}$$

The characteristic width of this distribution is of the order of $\tilde{\mu}$.
If the energy of heated electrons is small, as compared to Δ, the number of electrons leaving the vortex core is exponentially small (Larkin and Ovchinnik ov 1977):

$$1 - f = A\exp\left[-\left(\varepsilon/T^*\right)^{5/2}\right] \tag{65}$$

where

$$T^* \sim \Delta\left[T_{\text{c}}\tau_\varepsilon\left(T_{\text{c}}\right)\left(j/j_{\text{c}}\right)^2\right]^{1/5} \tag{66}$$

and j_{c} is the critical depairing current. In this case the number of monochromatic phonons with energy 24 and the phonon distribution width are exponentially small. For T^* of the order of Δ the distribution width is

$$\tilde{\mu}^3 = \left(\frac{0.5T^*}{\Delta}\right)^5 \frac{T_{\text{c}}T^*}{\tau}\frac{B}{H_{\text{c2}}}, \quad \tau\Delta > 1 \tag{67}$$

Equations (65)-(67) are valid for superconductors with a large electron mean free path $\tau\Delta \gg 1$.

Therefore, at low temperatures and widely spaced flux lines the total energy of the electric field is converted into the energy of almost monochromatic phonons with frequency $\omega = 24$.

24.5 5. Elasticity of a vortex lattice

24.5.1 5.1. Elastic moduli

Smooth deformations of a vortex lattice can be described by means of elasticity theory. For a triangular lattice only three elastic moduli are nonzero: the compression modulus $C_1 = C_{11} - C_{66}$, shear modulus C_{66}, and tilting modulus C_{44}. The correction to the free energy resulting from elastic deformations of a vortex lattice is equal to

$$\delta F_{\rm el} = \frac{1}{2}\int d^3r \left\{ (C_{11}-C_{66}) \left(\frac{\partial u}{\partial r}\right)^2 + C_{66}\left(\frac{\partial u_\beta}{\partial r_x}\right)^2 + C_{44}\left(\frac{\partial u}{\partial z}\right)^2 \right\}. \tag{68}$$

Upon compression and tilting deformation, the shape of a vortex lattice does not change and the free energy of a deformed lattice is equal to that of an undeformed lattice in the renormalized magnetic field. On compression we
have $\boldsymbol{B} = \boldsymbol{B}_0(1 + \operatorname{div} \boldsymbol{u})$, on tilting we have

$$H_\perp^2 = H_\parallel^2 \left(\frac{\partial u}{\partial z}\right)^2 \tag{69}$$

Therefore, for C_{11} and C_{44} we get (Labusch 1967)

$$C_{44} = \frac{\boldsymbol{H}\cdot\boldsymbol{B}}{4\pi}, \quad C_{11} - C_{66} = \frac{B^2}{4\pi}\frac{\partial H}{\partial \boldsymbol{B}}. \tag{70}$$

The shape of a triangular lattice changes with shear deformations. And the elastic modulus C_{66} is expressed through the free energy of the lattice, in which the angle between the vectors of an elementary cell is not 60° (Labusch 1967, 1969a, Brandt 1976).

24.5.2 5.2. Space dispersion of elastic moduli

As a rule, elasticity theory is applicable when the size of a deformed region is large as compared to the lattice period. For the vortex lattice there exist physical reasons for the moduli C_{11} and C_{44} having a strong space dispersion at rather small wave vectors (Brandt 1977). This comes about as a result of trapping the magnetic field by a long-wave deformation of the lattice and the fact that the elastic energy is determined by variation of the magnetic field energy. But the magnetic field cannot vary at distances less than the effective penetration depth $\delta_{\rm eff}$. So, under deformation of a lattice with the wave vectors $\boldsymbol{K}$ exceeding $\delta_{\rm eff}^{-1}$, the magnetic field does not vary and the magnetic force lines break away from the vortex lattice. In this case the elastic energy does not increase with K. For description of such deformations the vector potential and the displacement vector u should be regarded as independent variables. In fields close to H_{c2} there exists another reason for there to arise space dispersion in the elastic modulus C_{11}. The thing is that the shape of a vortex lattice is determined by terms of the order of Δ^2 in the free energy, and the value Δ itself by terms of the order of Δ^4. Thus, the absolute value of Δ should also be regarded as an independent variable. We seek the order parameter Δ and the vector potential in the form

$$\Delta(r) = \Delta_0(r-u)\exp\left[2ie\,(\boldsymbol{u}\cdot\boldsymbol{A}_0) + i\chi + s\right], \quad \boldsymbol{A} = \boldsymbol{A}_0 + \boldsymbol{A}_1. \tag{71}$$

Expanding expression (12) for the free energy in a power series of u, s, χ and A_1 up to quadratic terms we get

$$\delta F_{\rm el} = \frac{k_{\rm h}^2}{8\pi}\int \mathrm{d}^3r \left\{ \frac{1}{k_{\rm h}^2}\left(\mathrm{rot}\, A_1\right)^2 + \left(A_1 + [\boldsymbol{B}\cdot u] - \frac{1}{2e}\frac{\partial\chi}{\partial r}\right)^2 \right.$$
$$+ a_1\left(A_{\rm z}^{(1)} - \frac{1}{2e}\frac{\partial\chi}{\partial z}\right)^2 + a_2\left(\left(\frac{\partial s}{\partial r}\right)^2 + k_\psi^2 s^2\right) + a_3\left(\frac{\partial s}{\partial z}\right)^2$$
$$\left. -a_4\left(s\frac{\partial \boldsymbol{u}}{\partial \boldsymbol{r}}\right) - a_5 s\left(\frac{\partial}{\partial \boldsymbol{r}}\left[\boldsymbol{B}\cdot\boldsymbol{A}_1\right]\right)\right\}$$
$$+ \int d^3r \left\{ \langle j_1\rangle \boldsymbol{A}_1 + \frac{C_{66}}{2}\frac{\partial u_\alpha}{\partial r_\beta}\frac{\partial u_\alpha}{\partial r_\beta} + \frac{a_6}{2}\left(\frac{\partial u}{\partial z}\right)^2\right\}, \quad \alpha,\beta = 1,2. \tag{72}$$

The coefficients in this formula have been found for T close to $T_{\rm c}$:

$$\begin{aligned} &a_1 = a_3 = a_5 = 0, && a_6 = \boldsymbol{B}(\boldsymbol{H}-\boldsymbol{B})/4\pi, \quad a_2 = 1/4e^2 \\ &a_4 = B/e, && k_{\rm h}^2 = \tfrac{2e^2p^2l_{\rm tr}}{3T}\eta\left\langle|\Delta\right|^2\Big\rangle \\ &k_\psi^2 = k_{\rm h}^2\left[1 - \tfrac{\partial H}{\partial B}\right]^{-1}, && \eta = 1 - \tfrac{8T\tau_{\rm tr}}{\pi}\left(\psi\left(\tfrac{1}{2} + \tfrac{1}{4\pi T\tau_{\rm tr}}\right) - \psi\left(\tfrac{1}{2}\right)\right) \end{aligned} \tag{73}$$

and for magnetic fields close to $H_{\rm c2}$ (Larkin and Ovchinnikov 1979)

$$\begin{aligned} k_{\rm h}^2 &= \frac{8\pi ev\langle|\Delta|^2\rangle}{B}\gamma_1, \quad k_\psi^2 = \frac{eB\langle|\Delta|^2\rangle}{2\pi^2T^2}\gamma_{\gamma_1} \\ a_2 &= 1/4e^2, \quad a_1 = 4e^2a_3 = \gamma_3/\gamma_1, \quad a_4 = B/e \\ a_5 &= \gamma_3/eB\gamma_1, \quad a_6 = B(H-B)/4\pi \\ C_{66} &= 0.48\frac{v\langle|\Delta|^2\rangle^2}{32\pi^2\beta_{\rm A}T^2}\left\{1 - \frac{8e^2p^2v^3\tau_{\rm tr}^2}{9\pi\gamma_2}\left(\psi'\left(\frac{1}{2}+\frac{eBD}{2\pi T}\right)\right)^2\right\} \\ \gamma_1 &= \psi\left(\frac{1}{2}+\frac{3eBD}{2\pi T}\right) - \psi\left(\frac{1}{2}+\frac{eBD}{2\pi T}\right) \\ \gamma_2 &= -\beta_{\rm A}\psi''\left(\frac{1}{2}+\frac{eBD}{2\pi T}\right) - \frac{8e^2p^2v^3\tau_{\rm tr}^2}{9\pi}\left(\beta_{\rm A}-1\right)\left(\psi'\left(\frac{1}{2}+\frac{eBD}{2\pi T}\right)\right)^2, \\ \gamma_3 &= \frac{eBD}{\pi T}\psi'\left(\frac{1}{2}+\frac{eBD}{2\pi T}\right) - \gamma_1, \\ \langle|\Delta|^2\rangle &= \frac{2\pi T}{\gamma_2}eD\left(H_{\rm c2}-B\right)\psi'\left(\frac{1}{2}+\frac{eBD}{2\pi T}\right) \end{aligned} \tag{74}$$

Minimizing expression (72) for the free energy with respect to variables s and $A_1 - (1/2e)(\partial\chi/\partial r)$ yields

$$\delta F_{\rm el} = \frac{1}{2}\int \frac{\mathrm{d}^3\boldsymbol{K}}{(2\pi)^3}\left\{\left(C_{11}(\boldsymbol{K}) - C_{66}\right)K_\alpha K_\beta \right.$$
$$\left. + \left(C_{66}\boldsymbol{K}_\perp^2 + C_{44}(\boldsymbol{K})K_{\rm z}^2\right)\delta_{\alpha\beta}\right\}U_\alpha(\boldsymbol{K})U_\beta(-\boldsymbol{K}) \tag{75}$$

$$C_{44} = \frac{B^2 k_{\rm h}^2}{4\pi}(1+a_1)\left[\boldsymbol{K}^2 + k_{\rm h}^2 + a_1\left(\boldsymbol{K}_{\rm z}^2 + k_{\rm h}^2\right)\right]^{-1} + a_6$$

$$C_{11} - C_{66} = \frac{B^2 k_{\rm h}^2}{4\pi}\{\left(\boldsymbol{K}^2 + k_{\rm h}^2(1+a_1)\right)\left[\boldsymbol{K}^2 + k_{\rm h}^2\right) \times \left(\boldsymbol{K}^2 + k_{\rm h}^2 + a_1\left(K_{\rm z}^2 + k_{\rm h}^2\right)\right)\right]^{-1}$$
$$- \left(1 + \frac{a_5}{a_4}\frac{B^2 k_{\rm h}^2}{\boldsymbol{K}^2 + k_{\rm h}^2}\right)\left(\frac{a_4^2}{4B^2 a_2} + \frac{a_4 a_5}{4a_2}\frac{k_{\rm h}^2}{\boldsymbol{K}^2 + k_{\rm h}^2}\right)$$
$$\times \left(\boldsymbol{K}^2 + k_\psi^2 + \frac{a_3}{a_2}K_z^2 - \frac{a_5}{4a_2}\boldsymbol{K}_\perp^2\frac{B^2 k_{\rm h}^2}{\boldsymbol{K}^2 + k_{\rm h}^2}\right)^{-1}\Bigg\} \tag{76}$$

The space dispersion of the elastic modulus C_{66} is small and the elastic moduli C_{44} and C_{11} decrease rapidly with increasing K, provided $K > \delta_{\rm eff}^{-1}$. Plastic deformation of a vortex lattice is often observed experimentally. Particularly, separate dislocations in such a lattice have been observed (Truble and Essmann 1968). The relative easiness of formation of plastic deformations is likely to be a consequence of the fact that the minimum of the free energy F for a triangular lattice is shallow and its energy is only 2°_0 less than that of a square lattice. Plastic deformation has hardly been studied theoretically.

24.5.3 5.3. Absence of long-range order in a vortex lattice

Vanishing of the long-range order due to weak inhomogeneities (Larkin 1970) is an important property of a vortex lattice. And it is this property that distinguishes the vortex lattice from an ordinary solid body, in which the point defects do not break the long-range order. This results from the fact that defects shift together with the lattice in a solid body. The energy of interaction of defects with the lattice is independent of homogeneous shift and is determined by deformation. The vortex lattice does not drag the defects of an atomic structure. And the shift of vortices caused by such a defect decreases slowly with the distance from the defect. At large distances the shifts caused by different defects accumulate and increase with distance so that the long-range order vanishes.

Proceeding from simple energy considerations it is possible to estimate the size of the region where there exists short-range order. Suppose the force of interaction of a lattice with one pinning center is $\tilde{f}_{\rm pin}$. Then the interaction energy changes by the value $\tilde{f}_{\rm pin}\, a$, if the lattice is shifted by the period a. Pinning centers are located in random points and forces are randomly orientated. Therefore, upon shifting a region containing N pinning centers, the change in energy is determined by fluctuations and is equal to

$$\delta F_{\rm pin} = -\widetilde{f}_{\rm pin} a N^{1/2} = -\widetilde{f}_{\rm pin} a\,(nV_{\rm c})^{1/2} \tag{77}$$

where n is the concentration of pinning centers, V_c is the volume of the region where a short-range order exists and the relative shift is less than a period. The shift of the region results in an increase of the elastic energy. Thus, the change of the unit volume energy δF due to inhomogeneities is

$$\delta F = C_{66}\,(a/R_{\rm c})^2 + C_{44}\,(a/L_{\rm c})^2 - f_{\rm pin}\,a\,(n/V_{\rm c})^{1/2}\,, \tag{78}$$

where $R_{\rm c}$ and $L_{\rm c}$ are the transverse and longitudinal dimensions of the region in which there is a short-range order, $V_{\rm c} = R_{\rm c}^2 L_{\rm c}$. Let us find $R_{\rm c}$ and $L_{\rm c}$ from the condition that expression (78) has a minimum

$$R_{\rm c} = 32^{1/2}\frac{C_{66}^{3/2}C_{44}^{1/2}a^2}{n\tilde{f}_{\rm pin}^2}, \quad L_{\rm c} = \frac{8a^2C_{66}C_{44}}{n\tilde{f}_{\rm pin}^2}$$
$$V_{\rm c} = \frac{256a^6c_{44}^2c_{66}^4}{n^3\tilde{f}_{\rm pin}^6} \tag{79}$$

For weak inhomogeneities the pinning force can be found with perturbation theory. For superconductors with randomly varying electron electron interaction we have

$$\lambda_{\rm eff}^{-1} = \left\langle \lambda_{\rm eff}^{-1} \right\rangle + \lambda_1, \tag{80}$$

where λ_1 is a random value, its correlator being

$$\varphi\left(\boldsymbol{r}-\boldsymbol{r}_1\right) = \left\langle \hat{\lambda}_1(\boldsymbol{r})\hat{\lambda}_1\left(\boldsymbol{r}_1\right)\right\rangle. \tag{81}$$

The variation of the free energy δF in first order with respect to λ_1 is equal to

$$\delta F = v\int \mathrm{d}^3 r\lambda_1(r)|\Delta(r)|^2. \tag{82}$$

The free energy (82) implies the following local force of interaction of the pinning center with the vortex lattice:

$$f_{\rm pin} = v\hat{\nu}_1(r)\frac{i|\Delta|^2}{ir}. \tag{83}$$

Equation (9) makes it possible to express the correlation function of shifts $U(r)$ through the correlator $\varphi(r)$

$$\left\langle (u(r)-u(0))^2\right\rangle = \int \frac{\mathrm{d}^3\boldsymbol{K}}{(2\pi)^3}W(\boldsymbol{K})(1-\cos\boldsymbol{K}\cdot\boldsymbol{r})$$
$$\times\left\{\left(C_{66}\boldsymbol{K}_\perp^2 + C_{44}(\boldsymbol{K})K_{\rm z}^2\right)^{-2} + \left(C_{11}(\boldsymbol{K})K_\perp^2 + C_{44}(\boldsymbol{K})K_{\rm z}^2\right)^{-2}\right\}, \tag{84}$$

where

$$W(\boldsymbol{K}) = v^2\int \mathrm{d}^3\boldsymbol{r}\varphi(\boldsymbol{r})\left\langle \frac{\partial\left|\Delta\left(r_1\right)\right|^2}{\partial\boldsymbol{r}_1}\frac{\partial\left|\Delta\left(r+\boldsymbol{r}_1\right)\right|^2}{\partial\boldsymbol{r}}\right\rangle\exp(-\mathrm{i}\boldsymbol{K}\cdot\boldsymbol{r}). \tag{85}$$

The elastic modulus C_{11} always exceeds the modulus C_{66}, and the second term in formula (84) is small as compared to the first term. Using expression (76) for the modulus C_{44} and calculating the integral in formula (84) to logarithmic accuracy, yields

$$\left\langle (u(r)-u(0))^2\right\rangle = \frac{w(0)}{4\pi^{1/2}BC_{66}^{3/2}}$$
$$\times\left\{\left(\rho^2+\frac{4\pi C_{66}}{B^2}z^2\right)^{1/2} + \frac{1}{2k_{\rm h}}\ln\left(\frac{\rho^2}{\xi^2}+\frac{4\pi C_{66}z^2}{B^2k_{\rm h}^2\xi^4}\right)\right\} \tag{86}$$

The region of the vortex lattice in which the relative shift is less than the interaction radius of pinning forces r_f is called a correlation region. The linear dimensions $R_{\rm c}$ of the correlation region are determined by eq. (86):

$$\left\langle \left(u\left(R_{\mathrm{c}}\right)-u(0)\right)^{2}\right\rangle = r_{\mathrm{f}}^{2}. \tag{87}$$

If the linear dimensions R_{c} of the correlation region satisfy the condition

$$R_{\mathrm{c}} k_{\mathrm{h}} \gg 1 \tag{88}$$

then the dispersion of elastic moduli is inessential. In this case the values L_{c} and R_{c} determined by eqs. (86) and (87) go into expression (79) with the substitution

$$a \to r_{\mathrm{f}}, \quad n\widetilde{f}_{\mathrm{pin}}^{2} = W(0). \tag{89}$$

In another limiting case,

$$\xi < R_{\mathrm{c}} < k_{\mathrm{h}}^{-1}, \tag{90}$$

the second term in eq. (86) is essential. In this case the volume of the correlation region V_{c} depends exponentially on the magnetic field

$$V_{\mathrm{c}} \sim \exp\left\{ b \frac{12\pi^{1/2} B C_{66}^{3/2} k_{\mathrm{h}} r_{\mathrm{f}}^{2}}{W(0)} \right\} \tag{91}$$

where b is a number of the order of unity.

24.6 6. Pinning

24.6.1 6.1. Critical current

In superconductors with atomic lattice inhomogeneities (hard superconductors) the transport current may flow without flux line motion and energy dissipation. The Lorentz force in this case is balanced against the interaction with defects (pinning force f_{pin}). The current state arising from this interaction is metastable.

The problem of calculating the mean pinning force can be divided into two parts: calculation of the force of interaction of the vortex lattice with a separate defect and averaging the force over different randomly arranged pinning centers. To linear approximation in the defect concentration it is sufficient to calculate the mean force with which one defect acts on the vortex lattice. Averaging eq. (9) over coordinates we get

$$[j_{\mathrm{c}} \cdot \boldsymbol{B}] = -n \left\langle \int f_{\mathrm{pin}} \, \mathrm{d}^{3} r \right\rangle \tag{92}$$

where n is the concentration of defects, and $\left\langle \int f_{\mathrm{pin}} \, \mathrm{d}^{3} r \right\rangle$ is the mean force of interaction of one defect with the vortex lattice. On the other hand, the force arising when the defect shifts relative to the lattice is

$$-\partial \boldsymbol{F} / \partial \boldsymbol{u}_{\infty} \tag{93}$$

where F is the free energy of a superconductor with a defect. From eq. (93) it follows that the mean force is nonzero only when there exist metastable states and, consequently, F is a many-valued function of the displacement (Labusch 1969b). Averaging eq. (93) over the value of displacement yields

$$j_{\mathrm{c}} B = n \delta F / \tilde{a}_{1} \tag{94}$$

where δF is the free energy jump on passing from one metastable state to another, and $\tilde{a}_1$ is the mean distance where such a transition takes place.

For sufficiently weak interaction of pinning centers with the vortex lattice the interaction energy can be found with perturbation theory (eq. 82) and is a single-valued function of the vortex lattice location. In this case the critical current is determined by collective effects, and the term proportional to the concentration of defects is zero.

A qualitative picture of the formation of metastable states can be obtained. if eq. (83) of the perturbation theory is utilized for the pinning force, but account is taken of a change of the argument of the order parameter as a result of a shift caused by the defect. Then

$$u = C^{-1} f_{\text{pin}}\,(r-u), \quad C^{-1} = \int \frac{d^3\boldsymbol{K}}{(2\pi)^3}\left[C_{66}\boldsymbol{K}_\perp^2 + C_{44}(\boldsymbol{K})K_2^2\right]^{-1} \tag{95}$$

is the displacement of the lattice caused by the force.
If the force f_{pin} is small, eq. (95) has only one solution and metastable states are absent. Another case is realized for a sufficiently large force f_{pin} . If the maximum shift exceeds some critical value u_c, the dependence $u(r)$ and, consequently, the functions of $f(\boldsymbol{r}-\boldsymbol{u})$ become many-valued. In this case the pinning force depends on history, i.e., hysteresis appears.

If the range where the function f_{pin} changes is equal to r_r, the solution of eq. (95) becomes many-valued under the condition that

$$u > r_{\text{f}}, \quad f_{\text{pin}} > C r_{\text{f}} \tag{96}$$

Condition (96) can be fulfilled in the whole range of magnetic fields. In this case the dependence of the pinning force on the magnetic field has a smooth dome-shaped form.

There exist superconductors for which condition (96) is satisfied only in weak magnetic fields or in fields close to H_{c2}, where elastic moduli are small. In this case in the dependence of the critical current on the magnetic field a sharp maximum is observed near H_{c2} (peak-effect). Estimates for the pinning force f_{pin} and the position of the critical-current maximum for different types of defects have been obtained by Larkin and Ovchinnikov (1979). With increasing temperature the position of the current maximum may be invariable or moves in the direction of large or small fields. All these types of temperature dependence have been observed in experiment (Osborne and Kramer 1974, Borka et al. 1977, Vinnikov et al. 1976).

A quantitative expression for the value of the free energy jump and, hence, for the critical current density, has been obtained for some particular cases only.

For large-size defects, whose properties differ from those of the matrix, the metastable state of a vortex lattice can be studied by elasticity theory (Larkin and Ovchinnikov 1981). The critical current is high for cases where there is a barrier for the vortex to enter into the defect region. In this case the layer of vortices is adjacent to the surface of a defect in a large area. The vortex-defect interaction force is

$$f_{\text{pin}} = \frac{2}{3}\pi a b p_{\text{c}}, \tag{97}$$

where the adjoining area is

$$\pi a b = \frac{\pi p_c^2 R_2^{3/2} R_1^{1/2}}{4 C_{44} C_{11}^{3/4} C_{66}^{1/4}}, \quad R_1/R_2 > \left(C_{66}C_{11}\right)^{1/2}/C_{44} \tag{98}$$

where a, b are radii of the adjacent ellipse in the x,z directions, respectively, p_c is the maximum pressure exerted by the defect boundary onto the vortex layer,

$$p_{\text{c}} = \int f_{\text{pin}}\,\mathrm{d}y \tag{99}$$

and $R_{1,2}$ are the radii of the defect curvature.
If the maximum displacement of vortices, u, is large compared to the lattice period, the force of interaction of each defect with the lattice is close to the maximum one, and averaging over defect positions is reduced to simple summation. In the general case the averaging of the force leads to eq. (94). Therefore, for calculating the mean force it is necessary to find the free energy of the vortex lattice with a defect as a function of a u, -displacement of the lattice at large distances relative to the defect and calculate the jump of this function.

If the size of a defect is comparable with or less than the lattice period, then
metastable states on a single defect may arise, provided the properties of the defect are considerably different from those of the matrix. In this case distortion of the vortex lattice near the defect is strong and cannot be found by means of elasticity theory. To calculate the functions $F(u,\ )$ it is necessary to solve numerically the Ginzburg-Landau equation or the more general eqs. (11) and (12). Such calculations have been performed for cylindrical pores of small radius in a field close to H_{c2} (Ovchinnikov 1980). The dependence of the critical current on the magnetic field in this case turns out to be nonmonotonous and by order of magnitude is

$$j_c B \sim (1 - T/T_c)^{1,5} (1 - H/H_{c2})^2 . \tag{100}$$

In case no metastable states arise on a separate pinning center, the pinning force is much weaker and appears due to collective effects, when a large volume of the order of V_c turns into a metastable state (eqs. 79, 80).

If the flowing current is less than the critical one, each of the volumes V_c shifts independently by a distance less than the size of the vortex core under the Lorentz force, so that the arising pinning force would compensate the Lorentz force. Since inside the volume V_c the lattice is almost regular, and the pinning centers are randomly arranged, the pinning forces acting on the lattice from each center almost compensate each other. The maximum force acting on the volume V_c is equal to $\widetilde{f}_{\rm pin}\, N^{1/2}$, where $N = nV_c$ is the number of pinning centers in the volume V_c. The critical current is

$$Bj = \widetilde{f}_{\rm pin} \frac{n}{N^{1/2}} = \widetilde{f}_{\rm pin}\, (n/V_c)^{1/2} \tag{101}$$

When the space dispersion of elastic moduli is not important, the volume V_c is determined by eq. (79), and the critical current (Larkin and Ovchinnikov 1973) is

$$Bj = \frac{n^2 \widetilde{J}_{\rm pin}^4}{16 a^3 C_{44} C_{66}^2}. \tag{102}$$

In a magnetic field close to H_{c2} the elastic modulus C_{44} reaches a constant limit, $C_{66} \sim (H_{c2} - B)^2$, and the force $\tilde{f}_{\rm pin}$ is in many cases proportional to Δ^2, i.e. $H_{c2} - B$. As a result, the critical current only slightly depends on the magnetic field.

While the magnetic field approaches H_{c2}, its effective penetration depth $\delta = {k_h}^{-1}$ increases and exceeds the correlation radius R_c. In this case one should take into account the space dispersion of the modulus C_{++}, and for the volume V_c expression (91) must be used. The critical current increases sharply (peak-effect) with increasing magnetic field (Larkin and Orchinnikov 1978). The current stops increasing as R_c becomes less than the lattice period a. There is no further decrease in the volume V_c, and due to the decrease in the force $\tilde{f}_{\rm pin}$ the current decreases proportionally with $H_{c2} - B$. Another. more reasonable
cause of the peak-effect has been described in the foregoing and is connected with the fact that in the vicinity of H_{c2} the elastic modulus C_{66} drops, the lattice softens and strong pinning with formation of metastable states on a single defect becomes possible.

Above, the case is considered when defects only slightly distort the vortex lattice in the main part of the volume. In case the field or temperature is close to the critical one and there

are many defects, the phase transition is smeared and in the area of smearing there arises a structure strongly distinguished from the periodic one (Ioffe and Larkin 1981). In this case superconductivity arises in separate, widely spaced regions connected thanks to the proximity effect. The real transition temperature and the critical current in such a structure are found by means of percolation theory.

The transport current or thermal fluctuations break the weakest bonds. The critical current is determined from the condition that unbroken bonds form a continuous cluster. In the region of a smeared phase transition the critical current decreases exponentially with increasing magnetic field. For instance, for defects which are inclusions of another phase with a critical magnetic field H_{c2}, exceeding the critical field of the matrix $H_{\rm m}$, for magnetic fields $H > H_{\rm m}$ the critical current is

$$j = j_0 \zeta_c^{-1,8} \xi \xi_{11} n^{2/3} \exp(-\zeta_c) \tag{103}$$
$$\zeta_c^{-2} = 2,7\pi n \xi^2 \breve{\zeta}_{11}, \quad \breve{\zeta}_{11}^2 = \zeta^2 \frac{H_{\rm m}}{H - H_{\rm m}}$$

where n is the concentration of inclusions, ξ is the size of a pair (correlation radius) of the matrix and j_0 is the depairing current in the inserted substance.

Two types of critical current dependence on the magnetic field value have been observed experimentally. In the case of strong pinning this dependence has a smooth maximum at a magnetic field (0.3-0.5) H_{c2}. Usually in the case of weak pinning, generally in a wide range of magnetic fields the pinning force only slightly depends on the magnetic field and only in the vicinity of H_{c2} there is a narrow high maximum (peak-effect). In magnetic fields not close to H_{c2}, a collective pinning is likely to be realized. This fact is indicated both by the small value of the critical current and by its nonlinear dependence on the concentration of defects (Kpfer and Manuel 1979).

It would be natural to suppose that in the region of magnetic fields beyond the peak strong pinning is realized in the current density, as in the case of the dome-shaped dependence of the current density on the magnetic field. A most simple picture of strong pinning has been described above and consists in formation of metastable states on a single pinning center. In this case the mean force is obtained by simple summation. However, such a simple picture does not always agree with experiment. A quantitative comparison of theory and experiment can be carried out for the pinning centers produced as a result of
irradiation. Under irradiation it is possible to check the number and the magnitude of defects. In some cases (Kramer 1978) a linear dependence of the mean pinning force on concentration of small-size defects is observed, for which the Labusch criterion is not fulfilled even when allowance is made for the space dispersion of elastic moduli. In other cases (Kpfer and Manuel 1979, Reichert et al. 1981) the pinning force does not generally depend on the concentration of defects. May be in this case plastic flow of the vortex lattice takes place.

24.6.2 6.2. I-V characteristic

At a transport current density exceeding the critical value flux lines start moving, and in a superconductor there arises a voltage proportional to the velocity of the flux line motion. The transport current in this case is determined by the sum of the pinning and viscous forces. The viscous force has been considered above and for a weak electric field $\boldsymbol{E}$ is proportional to $\boldsymbol{E}$. The pinning force is also dependent on the velocity of the flux line motion which affects the shape of the $I - V$ characteristic. If metastable states are formed on a single defect (strong pinning), the pinning force decreases with increasing velocity, since the moving lattice badly fits the defect shape. The mutual influence of defects diminishes with increasing velocity. This

usually decreases the mean pinning force. Therefore, the collective part of the pinning force increases with velocity.

Let us first consider weak pinning. Quantitative results in this case can be obtained at a sufficiently high velocity of the flux line motion, when the pinning force in eq. (9) can be taken into account by perturbation theory (Larkin and Ovchinnikov 1973c, Schmid and Hauger 1973). It is convenient to write eq. (9) in the integral form

$$\begin{aligned} u =& u_0 + u_1 \\ u_1(r,t) =& \int_{-\infty}^{t} \mathrm{d}t_1 \int \mathrm{d}^3 r M\left(t-t_1, r-r_1\right) \\ & \times \left\{ f_{\mathrm{pin}}\ \left(r_1, r_1 - u_0\left(t_1\right) - u_1\left(r_1,t_1\right)\right) + \left[\langle j\rangle \boldsymbol{B}\right] - \sigma B^2 \frac{\partial u_0}{\partial t} \right\}. \end{aligned} \tag{104}$$

The retarded Green function M satisfies the equation

$$\begin{aligned} & -\left[\left(C_{11}-C_{66}\right)\frac{\partial}{\partial\rho}\left(\frac{\partial M}{\partial\rho}\right) + \left(C_{66}\frac{\partial^2}{\partial\rho^2} + C_{44}\frac{\partial^2}{\partial z^2}\right) M\right] + \sigma B^2 \frac{\partial M}{\partial t} \\ & = \delta\left(t-t_1\right)\delta\left(r-r_1\right). \end{aligned} \tag{105}$$

In a time-independent electric field $\boldsymbol{E}$ the lattice moves with a constant velocity v and $u_0 = vt$. The electric field E is connected with the velocity v by eq. (15) and the current density $\langle j\rangle$ is expressed in $\boldsymbol{E}$ and the pinning force by eq. (10).

In zero order with respect to u_1 the mean force f_{pin} is zero and the current density $\boldsymbol{j} = \sigma\boldsymbol{E}$. In first order with respect to $\boldsymbol{u}_1$ we have

$$\left[j_1 \boldsymbol{B}\right] = \left\langle \left(u_1 \frac{\partial}{\partial u_0}\right) f_{\mathrm{pin}} \right\rangle. \tag{106}$$

For the pinning force determined by inhomogeneities of the interaction constant, eq. (83) can be easily rewritten as

$$f_{\mathrm{pin}}\left(r, r-u_0\right) = \mathrm{i}\nu\lambda_1(r) \sum_{\mathrm{n}} \boldsymbol{K}_n |\Delta|_n^2 \exp\left(\mathrm{i}\boldsymbol{K}_n\left(r-u_0\right)\right) \tag{107}$$

where $\boldsymbol{K}_n$ are reciprocal lattice vectors and $|\Lambda|_n^2$ are the Fourier components of the function $|\Delta(r)|^2$. Substituting expression (107) into eqs. (104) and (106) yields

$$\begin{aligned} \left[j_1 \boldsymbol{B}\right] =& \frac{\mathrm{i}v^2}{2} \sum_n \int \frac{\mathrm{d}^3 g}{(2\pi)^3} \varphi_n \left|\left(|\Delta|_n^2\right)\right|^2 \left\{ \left(C_{66}\boldsymbol{g}_\perp^2 + C_{44} g_z^2 + \mathrm{i}\sigma B^2\left(\boldsymbol{K}_n v\right)\right)^{-1} \right. \\ & \left. + \left(C_{11} g_\perp^2 + C_{44} g_z^2 + \mathrm{i}\sigma B^2\left(\boldsymbol{K}_n v\right)\right)^{-1} \right\}, \end{aligned} \tag{108}$$

where

$$\varphi_n = \int \mathrm{d}^3 r \exp\left(-\mathrm{i}\boldsymbol{K}_n \cdot r\right) \left\langle \lambda_1(r)\lambda_1(0)\right\rangle \tag{109}$$

At small velocities v in the integral (108) small g are essential:

$$C_{66} g_1^2 \sim \sigma B^2 v / a, \tag{110}$$

where a is the linear size of the cell. If the value $\boldsymbol{g}_-^2$ determined by formula (110) satisfies the condition

$$g_\perp^2 < k_\mathrm{h}^2 \tag{111}$$

then the space dispersion of the elastic modulus C_{44} is unimportant and the correction j_1 to the current density is proportional to $v^{1/2}$

$$\begin{aligned}[j_1\boldsymbol{B}] =& \frac{v^2}{8\pi\left(2C_{44}\right)^{1/2}}\left(\frac{1}{C_{66}}+\frac{1}{C_{11}}\right)\sum_n \varphi_n\left|\left(|\Lambda|_n^2\right)\right|^2\boldsymbol{K}_n\boldsymbol{K}_n^2 \\ &\times\left(\sigma\boldsymbol{B}^2\left|\left(\boldsymbol{K}_n v\right)\right|\right)^{1/2}\operatorname{sign}\left(\boldsymbol{K}_n v\right).\end{aligned} \tag{112}$$

It should be noted that the pinning force increases with velocity.
With increasing velocity, the value $g_\perp$ increases, condition (111) is not satisfied anymore and space dispersion of the elastic modulus C_{44} becomes important. In this case the correction to the current density depends logarithmically on velocity

$$[j_1\boldsymbol{B}] = \frac{v^2\sigma B}{16\pi^{1/2}k_\mathrm{h}C_{66}^{3/2}}\sum_n \varphi_n\left|\left(|\Delta|_n^2\right)\right|^2\boldsymbol{K}_n\boldsymbol{K}_n^2\left(\boldsymbol{K}_n v\right)\ln\left(\frac{C_{66}}{a^2\sigma B^2\left|\left(\boldsymbol{K}_n v\right)\right|}\right). \tag{113}$$

Equations (112) and (113) are obtained by expanding in $\boldsymbol{u}_1$. Such an expansion is valid for sufficiently high velocities. Investigation of the subsequent terms of the expansion shows that the IV characteristic of a superconductor with a weak pinning can be presented in the form

$$j(\boldsymbol{E}) = j_\mathrm{c}\mathscr{T}\left(\sigma E/j_\mathrm{c}\right), \tag{114}$$

where $\mathscr{T}(x)$ is some universal function. The critical current density j_c is determined by eq. (101).

Now we would like to find the $I-V$ characteristic for strong pinning. As has been shown above, the critical current in this case is determined by the free energy of a superconductor with one defect. The free energy is a function of lattice shift relative to defect.

The shape of the $I-V$ characteristic in some region of the electric field is also determined by the dependence of the free energy on the value of the displacement.

When the lattice moves with a small velocity, its deformation far from the defect is described by the elasticity equation (9), even if in the vicinity of the defect the deformation is plastic and this equation is inapplicable. It is important that in the vicinity of the defect deformation is the same as that in the static case and the force of interaction of the defect with the lattice is determined by expression (93). However, the argument in this formula is not the displacement at infinity $\boldsymbol{u}$, , but the displacement that would have existed in a static problem. The difference in these displacements is determined by eq. (104) and is equal to

$$u_1(t) = \int \mathrm{d}t_1\left(M_v\left(t-t_1\right) - M_{t-0}\left(t-t_1\right)\right)\tilde{f}_\mathrm{pin}\ \left(t_1\right) \tag{115}$$

where the Green function M is determined by eq. (105). We are interested in the displacement u_1 at the location of the defect. At this point expression (115) is reduced to the form

$$u_1(t) = -\frac{1}{8\pi C_{44}^{1/2}}\left(\frac{1}{C_{66}}+\frac{1}{C_{11}}\right)\left(\frac{\sigma B^2}{\pi}\right)^{1/2}\frac{\partial}{\partial t}\int_{-,}^{t}\frac{\mathrm{d}t_1}{\left(t-t_1\right)^{1/2}}\hat{f}_\mathrm{pin}\left(t_1\right). \tag{116}$$

The mean force is

$$[j\boldsymbol{B}] = -\frac{n}{T}\int_0^T \mathrm{d}t f_{\mathrm{pin}}\left(vt - u_1(t)\right) \tag{117}$$

where $T = \hat{a}_1/v$ is the time between jumps. In zero-order approximation at $u_1 = 0$ we obtain eq. (94) for the current density from eqs. (93) and (117). In this approximation the time-averaged value coincides with the result of averaging over a random distribution of defects. To calculate the next approximation we perform a substitution of the argument in eq. (117)

$$vt - u_1(t) \to v\tilde{t}$$

Using expression (116) for $\boldsymbol{u}_1$, we find the correction to the current density which depends on the velocity of the vortex lattice motion

$$\begin{aligned}[j_1\boldsymbol{B}] = &-\frac{1}{8\pi C_{44}^{1/2}}\left(\frac{1}{C_{66}}+\frac{1}{C_{11}}\right)\left(\frac{\sigma B^2}{\pi}\right)^{1/2}\frac{n}{v^2T}\\ &\times\int_0^T \mathrm{d}t\left(\tilde{f}_{\mathrm{pin}}(vt)-\tilde{f}_{\mathrm{pin}}(0)\right)\frac{\partial^2}{\partial t^2}\int_{-\infty}^{t}\frac{\mathrm{d}t_1}{(t-t_1)^{1/2}}\left(v\tilde{f}_{\mathrm{pin}}\left(vt_1\right)\right)\end{aligned} \tag{118}$$

where $\tilde{f}_{\mathrm{pin}}\left(0\right)$ is the value of the force at the moment immediately after the jump. The subtraction in eq. (118) has been performed to eliminate spurious divergence. It follows from eq. (118) that the correction to the current density is proportional to v^{12}. The proportionality coefficient depends on the explicit form of the function $\tilde{f}_{\mathrm{pin}}$. For large-size defects the force $\tilde{f}_{\mathrm{pin}}$ is always close to its maximum value. Deviation from the maximum value for the whole period of motion is a linear function of time.

$$\tilde{f}_{\mathrm{pin}}(t) = \mathcal{J}_{\mathrm{m}}\left(1-\frac{T-t}{T}C_1\right), \quad 0<t<T \tag{119}$$

The coefficient C_1 is of the order of the ratio of the lattice period to the displacement caused by the defect. The IV characteristic is obtained from the formulas (118) and (119):

$$j = \sigma E + j_c\left\{1-\frac{\tilde{f}_m C_1^2}{8\cdot 2^{1/2}\frac{\pi^2\hat{a}_1^{3/2}}{C_{44}^{1/2}}}\left(\frac{1}{C_{66}}+\frac{1}{C_{11}}\right)\left(-\check{\zeta}_{112}\right)\left(\sigma B^2 2\pi i\right)^{12}\right\} \tag{120}$$

Equation (120) has also been obtained by another method (Larkin and Ovchinnikov 1981). There the dependence of the coefficient C_1 on the defect characteristics has been found as well.

Thus, with increasing velocity of the lattice motion the mean pinning force decreases. This decrease in the pinning force at small velocities exceeds the viscosity force. So, voltage jumps should exist on the $I-V$ characteristic. This has been observed in experiment (Chang and McKinnon 1968, Chang et al. 1969).

The square root dependence of the current density on the velocity of the flux line lattice motion is connected with deformation of the lattice at large distances of order $v^{-1/2}$. While deriving eq. (120) the concentration of defects has been assumed to be small and their mutual effect is not taken into consideration. The initial part of the $I-V$ characteristic is determined by collective effects. Therefore, at sufficiently high defect concentration no jumps on the $I-V$ characteristic can be observed.

An interesting phenomenon may occur when a high-frequency current is passing through a superconducting film. In this case the $I-V$ characteristic can be obtained, provided in eqs. (104) and (107) the mean velocity v is regarded as a function of time

$$\frac{\partial u_0}{\partial t} = v_0 + v_1 \cos \omega t \tag{121}$$

Analogously as eq. (108) has been obtained, we derive the following equation for the current density in an alternating field (Schmid and Hauger 1973, Larkin and Ovchinnikov 1973c)

$$[j_i \boldsymbol{B}] = \frac{v^2}{16 d C_{66}} \sum_{n,m} \varphi_m \boldsymbol{K}_m \boldsymbol{K}_m^2 I_n^2 \left(\frac{(\boldsymbol{K}_m \boldsymbol{v}_1)}{\omega} \right) \left| \left(|\Lambda|_m^2 \right) \right|^2 \operatorname{sign} \left((\boldsymbol{K}_m v_0) - n\omega \right). \tag{122}$$

Therefore on the $I-V$ characteristic steps arise at voltages satisfying the Josephson relation $2\pi E m = B\omega n a$ (a is the lattice period, m, n are integers). The value of these steps is proportional to the critical current. Such steps have been observed experimentally (Fiory 1971).

24.7 7. Conclusion

In this chapter the theory of flux line motion in superconductors has been reviewed. Experimental results have been mentioned only when they could provide information confirming or contradicting the theoretical results.

The theory of flux line motion in homogeneous superconductors without pinning forces has been developed fairly well. The dependence of conductivity on temperature and magnetic field and non-linear effects on an electric field are investigated for all the cases where the solution of a static cquilibrium problem is known. Usually, these results are in agreement with experiment, provided the pinning force effect is separated. The experimental data on critical pinning currents are very numerous, but they are poorly systematized because no fundamental theory of this phenomenon is yet available. The pinning theory is developed sufficiently well for those cases where the lattice deformation may be assumed to be elastic. In this case it is possible to explain
the peak on the dependence of a critical current on a magnetic field near H_{c2} ("peak-effect") and some singularities on the I V characteristic. In many cases the vortex lattice deformation is likely to be plastic. The theory of plastic deformation exists only for some simple cases. A quantitative comparison of theory and experiment is also difficult, since in most cases the character of defects and the force of the single-defect interaction with a vortex lattice is unknown.

24.8 Appendix. Kinetic equation for dirty superconductors

In normal metals the classical kinetic equation is applicable when the electron mean free path is large in comparison with the wavelength of electrons. In superconductors, in addition to the excitation wavelength there is another parameter: the size of a pair or the correlation length. Therefore, the standard kinetic equation is applicable only in the cases when the mean free path and the range in which the order parameter changes, greatly exceeds the correlation length.

Here we obtain a more general but more complicated quasi-classical equation. While deriving this equation we use only the smallness of the electron wavelength compared to all other characteristic lengths (Eliashberg 1971, Larkin and Ovchinnikov 1973a, 1975, 1977, Shelankov 1980, Schmid 1981, Watts-Tobin et al. 1981). This equation is a generalization of static quasi-classical equations for the Green functions (Eilenberger 1968, Larkin and Ovchinnikov 1968).

It is convenient to represent the Green functions of a superconductor in matrix form, the elements of the matrix being ordinary and anomalous Green functions:

$$G^{>}(1,2) = -i\left\langle \begin{pmatrix} \psi_\uparrow(1)\psi_\uparrow^+(2) & \psi_\uparrow(1)\psi_\downarrow(2) \\ -\psi_\downarrow^+(1)\psi_+^+(2) & -\psi_\downarrow^+(1)\psi_\downarrow(2) \end{pmatrix} \right\rangle,$$
$$G^{<}(1,2) = i\left\langle \begin{pmatrix} \psi_\uparrow^+(2)\psi_\uparrow(1) & \psi_\downarrow(2)\psi_\uparrow(1) \\ -\psi_\uparrow^+(2)\psi_\downarrow^+(1) & -\psi_\downarrow(2)\psi_\downarrow^+(1) \end{pmatrix} \right\rangle. \tag{A.1}$$

The averaging is performed over the dynamic state. It is supposed that at $t \to -x$ the system is in equilibrium, and then the external field transforms it into some dynamic state. In a static case, using the functions $G^{>}$and $G^{<}$it is possible to compose chronologically ordered averages; the equations for these have been obtained by Gorkov (1958). In the dynamic case we apply the methods proposed by Keldysh (1964) for deriving the kinetic equation in a normal metal. Keldysh showed that for the dynamic case the Dyson equation
is replaced by a system of equations for three values:

$$G^{\mathrm{R}}(1,2) = \theta(t_1 - t_2)\left\{G^{>}(1,2) - G^{<}(1,2)\right\},$$
$$G^{\mathrm{A}}(1,2) = -\theta(t_2 - t_1)\left\{G^{>}(1,2) - G^{<}(1,2)\right\},$$
$$G^{\mathrm{K}}(1,2) = G^{>}(1,2) + G^{<}(1,2). \tag{A.2}$$

This system can be written in matrix form, provided the following matrices are introduced:

$$\check{G} = \begin{pmatrix} G^{\mathrm{R}} & G^{\mathrm{K}} \\ 0 & G^{\mathrm{A}} \end{pmatrix}, \quad \check{\Sigma} = \begin{pmatrix} \Sigma^{\mathrm{R}} & \Sigma^{\mathrm{K}} \\ 0 & \Sigma^{\mathrm{A}} \end{pmatrix}. \tag{A.3}$$

Each element of the matrix (A.3) in the Keldysh space is a matrix in the Gor'kov space as well. These matrices satisfy the equation

$$\left(\breve{G}_0^{-1} - \breve{\Sigma}\right)\breve{G} = \breve{1}. \tag{A.4}$$

Here the product means multiplication of matrices and convolution with respect to the coordinates and time,

$$\int \mathrm{d}^4 x_3 \left(\breve{G}_0^{-1} - \breve{\Sigma}\right)(x_1, x_3)\,\breve{G}(x_3, x_2) = \check{\delta}(x_1 - x_2) \tag{A.5}$$

where

$$\breve{G}_0^{-1}(x_1, x_2) = \left(i\check{\tau}_z \frac{\partial}{\partial t_1} - e\varphi + \mu + \frac{1}{2m}\check{\partial}^2\right)\check{\delta}(x_1 - x_2), \tag{A.6}$$
$$\check{\partial} = \frac{\partial}{\partial r} - ieA\check{\tau}_z, \tag{A.7}$$

where φ is the scalar potential, $\boldsymbol{A}$ is the vector potential, and μ is the chemical potential.

The two-row Pauli matrices τ act in the space of the Gor'kov matrices and are unit matrices in the space of the Keldysh matrices. In a normal metal the quasiclassical approximation makes it possible to obtain an equation for the density matrix which is equal to the Green function in coinciding times $t_1 = t_2$. In superconductors the equation for the Green function at close coordinate points is more general. As is seen from eq. (A.5), the Green function is a rapid function of the relative variable $r_1 - r_2$, and it is convenient to perform the Fourier transformation with respect to this variable:

$$\check{G}(\boldsymbol{p},\boldsymbol{r}) = \int \mathrm{d}^3\boldsymbol{r}'\check{G}\left(\boldsymbol{r}_1,\boldsymbol{r}_2\right)\exp\left(-\mathrm{i}\boldsymbol{p}\cdot\boldsymbol{r}'\right)$$
$$\boldsymbol{r}_{1,2} = \boldsymbol{r} \pm \frac{1}{2}\boldsymbol{r}' \tag{A.8}$$

After such a transformation the main term in G_0^{-1} is $p^2, 2m-\mu$. Therefore, $\check{G}(p)$ has a sharp maximum near the Fermi surface. To cancel large terms we subtract from eq. (A.5) the equation conjugated to it,

$$\left(\check{G}_0^{-1} - \check{\Sigma}\right)\check{G} - \check{G}\left(\check{G}_0^{-1} - \check{\Sigma}\right) = 0. \tag{A.9}$$

In this equation only $\check{G}$ has a sharp dependence on p^2. Therefore, it can be integrated with respect to $\xi_p = p^2/2m - \mu$ and one may obtain an equation for the quasiclassical Green function,

$$\check{g}(\boldsymbol{p},\boldsymbol{r}) = \frac{i}{\pi}\int \mathrm{d}\xi_p\check{G}(\boldsymbol{p},r) \tag{A.10}$$

The dependence on p in the left-hand side of formula (A.10) means only the dependence on the directions of the vector p, its value being equal to $p = p_\mathrm{F}$;

$$\left[\tau_\mathrm{z}\frac{\partial}{\partial t}\delta\left(t-t_1\right) + \mathrm{i}e\varphi(t) + \frac{p}{m}\check{\partial} + \mathrm{i}\check{\Sigma}, \circ\check{g}\right]_- = 0 \tag{A.11}$$

$[\ ,\ ]$ denotes a commutator, and the sign $\circ$ is convolution with respect to time, so that in detailed notation eq. (A.11) has the form

$$\check{\tau}_z\frac{\partial\check{g}}{\hat{C}t} + \frac{\partial\check{g}}{\partial t'}\check{\tau}_z + \frac{p}{m}\left(\frac{\partial\check{g}}{\partial r} - \mathrm{i}e\boldsymbol{A}(t)\check{\tau}_z\check{g} + \mathrm{i}e\boldsymbol{A}\left(t'\right)\check{g}\check{\tau}_z\right) + \mathrm{i}e\varphi(t)\check{g} - \mathrm{i}\check{y}\varphi\left(t'\right)$$
$$+\mathrm{i}\int_{-\infty}^{\infty}\mathrm{d}t_1\left\{\check{\Sigma}\left(t,t_1\right)\check{g}\left(t_1,t'\right) - \check{g}\left(t,t_1\right)\check{\Sigma}\left(t_1,t'\right)\right\} = 0 \tag{A.12}$$

Equation (A.12) is homogeneous relative to the function $\dot{g}$. An additional condition fixing normalization of the function and essentially simplifying the solution of the equation is

$$\check{g}\circ\check{g} = \check{1}. \tag{A.13}$$

Direct calculation shows that this condition is fulfilled in the equilibrium case and that it is compatible with eq. (A.12). It is possible to express the self-energy operator $\check{\Sigma}$ in $\check{g}$, taking into account the interaction with phonons and impurities by perturbation theory. To first order we have

$$\Sigma^{>}(1,2) = G^{>}(1,2)D^{<}(1,2), \quad \Sigma^{<}(1,2) = G^{<}(1,2)D^{>}(1,2),$$
$$D^{>}(1,2) = D^{<}(2,1) = -\mathrm{i}\left\langle\phi\left(x_1\right)\phi\left(x_2\right)\right\rangle, \tag{A.14}$$

where ϕ is the potential of the interaction of electrons with phonons or impurities. The impurity field is time-independent and classical. Therefore, $D^{>}_{\mathrm{imp}} = D^{<}_{\mathrm{imp}}$,

$$\check{\Sigma}_p^{imp}\left(t,t'\right) = -\frac{1}{2}\mathrm{i}nv\int \mathrm{d}\Omega_{p_1}\sigma_{pp_1}\check{g}_{p_1}\left(t,t'\right) \tag{A.15}$$

where $\sigma_{pp'}$ is the impurity scattering cross-section, and n is the impurity concentration.

If there exist spin-flip impurities, then these would contribute to the selfenergy

$$\check{\Sigma}_{\rm s}\left(t,t'\right)=-\frac{\rm i}{2\tau_{\rm s}}\int\frac{{\rm d}\Omega_{p_1}}{4\pi}\check{\tau}_{=}\check{g}_{p_1}\left(t,t'\right)\check{\tau}_{=}$$

Representing in formula (A.14) $G^{\gtrless}$ and $D^{\gtrless}$ through $G^{\rm R.A.K}$, $D^{\rm R.A.K}$ we obtain

$$\begin{aligned}
&\sum_{p}^{\rm ph(R,\ A)}\left(t,t'\right)=\frac{1}{8}\lambda_{\rm eff}\int{\rm d}\Omega_{p1}\left\{D^{\rm K}_{p-p1}\left(t'-t\right)g^{\rm R,\ A}_{p1}\left(t,t'\right)+D^{\rm A,R}_{p-p1}\left(t'-t\right)g^{\rm K}_{p1}\left(t,t'\right)\right\}\\
&\sum_{p}^{\rm ph(\ K)}\left(t,t'\right)=\frac{1}{8}\lambda_{\rm eff}\int{\rm d}\Omega_{p_1}\left\{D^{\rm K}_{p-p1}\left(t'-t\right)g^{\rm K}_{p1}\left(t,t'\right)\right.\\
&\left.-\left(D^{\rm R}_{p-p_1}\left(t'-t\right)-D^{\rm A}_{p-p_1}\left(t'-t\right)\right)\left(g^{\rm R}_{p_1}\left(t,t'\right)-g^{\rm A}_{p_1}\left(t,t'\right)\right)\right\}
\end{aligned}\tag{A.16}$$

where $i_{\rm eff}=vg^2_{\rm eff}$, and $g_{\rm eff}$ is the constant of the electron-phonon interaction. The phonon Green functions $D^{\rm R,A}$ are equal to

$$D^{\rm R}_k(\omega)=D^{\rm A}_k(\omega)^*=-\frac{\omega^2(\boldsymbol{k})}{\omega^2(\boldsymbol{k})-(\omega+{\rm i}\delta)^2}\tag{A.17}$$

In thermodynamic equilibrium the phonon function $D^K(k,\omega)$ is given by the expression

$$D^{\rm K}(k,\omega)=\left(D^{\rm R}_k(\omega)-D^{\rm A}_k(\omega)\right)\coth(\omega/2T)\tag{A.18}$$

If the phonons are not in a thermodynamic equilibrium state, then in eq. (A.18) one should substitute $\coth(\omega/2T)$ by $1+2n(\omega)$, where $n(\omega)$ is the phonon distribution function. The terms in $\Sigma^{\rm ph}$, proportional to $D^{\rm R}-D^{\rm A}$ or to $D^{\rm K}$, describe the processes accompanied by emission or absorption of phonons. The term proportional to $D^{\rm R}+D^{\rm A}$ corresponds to virtual phonon exchange. The frequencies of virtual phonons are of the order of $\omega_{\rm D}$ and are large compared to the external field frequency and temperature. Therefore,

$$D^R_k\left(t-t'\right)+D^A_k\left(t-t'\right)=-2\delta\left(t-t'\right)\tag{A.19}$$

Such a term is inserted with the same coefficient into $2^{\rm ph(R.A)\ (R.}$ and is absent from $\Sigma^{\rm ph(K)}$. The contribution of virtual phonons to $\Sigma^{\rm ph}$ is thus proportional to a unit matrix in the Keldysh space and equals $-\delta\left(t-t'\right)\bar{\Delta}$, where

$$\check{\Delta}=\left(\begin{array}{cc}\hat{\Delta}&0\\0&\hat{\Delta}\end{array}\right),\quad\hat{\Delta}(t)=\frac{1}{8}\lambda_{\rm eff}\int{\rm d}\Omega_p g^{\rm K}_p(t,t).\tag{A.20}$$

The current density is also expressed through the Green function, integrated over the energy variable

$$j=-\frac{1}{8}ev\int{\rm d}\Omega_p\,{\rm Tr}\,\tau_z\frac{p}{m}g^{\rm K}_p(t,t).\tag{A.21}$$

The diagonal elements $y^K(t,t)$ in formula (A.21) give renormalization of the chemical potential and velocity on the Fermi surface. Below, these effects are neglected.

For superconductors with a small electron free path the system of equations (A.12) can be simplified and reduced to an equation in the Green function $\check{g}$, averaged over the directions of the vector p.

In this case the Green function $\check{g}_p$ can be presented in the form

$$\check{g}_p=\check{g}+p\check{g}\check{g}_1,\quad p\check{g}_1\ll\check{g},\tag{A.22}$$

where the functions $\check{g}$ and $\check{g}_1$ are independent of the direction of the vector p. From the normalization conditions (A.13) it follows that

$$\check{g} \circ \check{g} = \check{1}, \quad \check{g} \circ \check{g}_1 + \check{g}_1 \circ \check{g} = 0. \tag{A.23}$$

Substituting expression (A.22) for the function $\check{}_p$ into eq. (A.12) and taking into account relation (A.23) we get

$$\check{g}_1 = -\frac{\tau_{\rm tr}}{m} \left\{ \mathrm{i}e\boldsymbol{A}\tau_z \delta\left(t - t'\right) + \check{g} \circ \check{\partial} g \right\}. \tag{A.24}$$

Substituting expressions (A.22) and (A.24) for the function $\check{g}_p$ into eq. (A.12) and averaging over the directions of the vector $\boldsymbol{p}$ yields

$$\begin{aligned} &- D\frac{\partial}{\partial r}\left\{ \mathrm{i}e\boldsymbol{A}\check{\tau}_z \delta\left(t - t'\right) + \check{g} \circ \check{\partial}\check{g} \right\} + \check{\tau}_z \frac{\partial \check{g}}{\partial t} + \frac{\partial \check{g}}{\partial t'}\check{\tau}_z + (-\mathrm{i}\check{\Delta}(t) + \mathrm{i}e\varphi(t))\check{g} \\ &- \check{g}\left(-\mathrm{i}\check{\Delta}\left(t'\right) + \mathrm{i}e\varphi\left(t'\right)\right) + \mathrm{i}eD\left\{ \boldsymbol{A}(t)\check{\tau}_z\check{g} \circ \check{\partial}\check{g} - (\check{g} \circ \check{\partial}\check{g})\boldsymbol{A}\left(t'\right)\check{\tau}_z \right\} \\ &= -\mathrm{i}\left(\check{\Sigma}^{\rm ph} \circ \check{g} - \check{g} \circ \check{\Sigma}^{\rm ph}\right) \end{aligned} \tag{A.25}$$

where $D = vl_{\rm tr}, 3$ is the diffusion coefficient. Equation (A.25) contains equations for $y^{R.A}$ and y^K. The diagonal elements of the matrix equation (A.25) give equations for $g^{\rm K.A}$. They have the same form as eq. (A.25), with $\check{g}$ substituted by $g^{R,A}$. The normalization equation (A.25) denotes that

$$g^{\rm R,\ A} \circ g^{\rm R,\ A} = 1, \quad g^{\rm R} \circ g^{\rm K} + g^{\rm K} \circ g^{\rm A} = 0. \tag{A.26}$$

Any matrix satisfying the second condition of eq. (A.26) can be presented in the form

$$g^K = g^R \circ \hat{f} - \hat{f}^{\circ} \circ g^A. \tag{A.27}$$

The non-diagonal element of the matrix equation (A.25) determines the matrix y^K. We insert it into this equation in the form of (A.27). From the equation obtained we subtract the equation for y^R. multiplied by $\hat{f}$, from the
right-hand side, and add the equation for $g^{\rm A}$, multiplied by $\hat{f}$, from the left-hand side. As a result we have

$$
\begin{aligned}
&-D\frac{\partial}{\partial r}\left(\frac{\partial \hat{f}}{\partial r}-g^{\mathrm{R}}\circ\frac{\partial \hat{f}}{\partial r}\circ g^{\mathrm{A}}\right)+g^{\mathrm{R}}\circ\left(\tau\frac{\partial \hat{f}}{\partial t_{\mathrm{i}}}+\frac{\partial \hat{f}}{\partial t'}\tau_z\right)-\left(\tau_z\frac{\partial \hat{f}}{\partial t}+\frac{\partial \hat{f}}{\partial t_{\mathrm{i}}}\tau_z\right)\circ g^{\mathrm{A}}\\
&\quad+D\frac{\partial \hat{f}}{\partial r}\circ g^{\mathrm{A}}\circ\partial g^{\mathrm{A}}-D\left(g^{\mathrm{R}}\circ\partial g^{\mathrm{R}}\right)\circ\frac{\partial \hat{f}}{\partial r}+\left[\hat{f}-\mathrm{i}\hat{\Delta}+\mathrm{i}e\varphi)-(-\mathrm{i}\hat{\Delta}+\mathrm{i}e\varphi)\hat{f}\right]\circ g^{\mathrm{A}}\\
&\quad+g^{\mathrm{R}}\circ[(-\mathrm{i}\hat{\Delta}+\mathrm{i}e\varphi)\hat{f}-\hat{f}(-\mathrm{i}\hat{\Delta}+\mathrm{i}e\varphi)]+\mathrm{i}eD\left(\boldsymbol{A}\tau_z\frac{\partial \hat{f}}{\partial \boldsymbol{r}}-\frac{\partial \hat{f}}{\partial \boldsymbol{r}}\boldsymbol{A}\tau_z\right)\\
&\quad+\mathrm{i}eD\left(g^{\mathrm{R}}\circ\frac{\partial \hat{f}}{\partial \boldsymbol{r}}\circ g^{\mathrm{A}}\boldsymbol{A}\tau_z-\boldsymbol{A}\tau_z g^{\mathrm{R}}\circ\frac{\partial \hat{f}}{\partial \boldsymbol{r}}\circ g^{\mathrm{A}}\right)\\
&\quad+\mathrm{i}eD\left(\hat{f}\boldsymbol{A}\tau_z-\boldsymbol{A}\tau_z\hat{f}\right)\circ g^{\mathrm{A}}\partial g^{\mathrm{A}}-\mathrm{i}eD\left(g^{\mathrm{R}}\circ\partial g^{\mathrm{R}}\right)\circ\left(\hat{f}\boldsymbol{A}\tau_z-\boldsymbol{A}\tau_z\hat{f}\right)\\
&\quad+\mathrm{i}eD\left(\frac{\partial A}{\partial \boldsymbol{r}}\tau_z\hat{f}-\hat{f}\frac{\partial \boldsymbol{A}}{\partial \boldsymbol{r}}\tau_z\right)\\
&=-\mathrm{i}\left\{-\sum^{\mathrm{ph(R)}}\circ\hat{f}\circ g^{\mathrm{A}}+\sum^{\mathrm{ph(\ K)}}\circ g^{\mathrm{A}}-g^{\mathrm{R}}\circ\sum^{\mathrm{ph(\ K)}}\right.\\
&\quad\left.-g^{\mathrm{R}}\circ\hat{f}\circ\sum^{\mathrm{ph(\ A)}}+g^{\mathrm{R}}\circ\sum^{\mathrm{ph(R)}}\circ\hat{f}+\hat{f}\circ\sum^{\mathrm{ph(\ A)}}\circ g^{\mathrm{A}}\right\}.
\end{aligned}
\tag{A.28}
$$

Of the four equations for the matrix $\hat{f}$ only two are linearly independent. Following the papers by Schmid and Schön (1975) and Larkin and Ovchinnikov (1977), we choose the matrix $\hat{f}$ to be diagonal,

$$\hat{f}=f+f_1\tau_{=}. \tag{A.29}$$

In a paper by Shelankov (1980) another choice for the matrix $\hat{f}$ has been proposed:

$$\hat{f}=f+g^{\mathrm{R}}f_1. \tag{A.30}$$

For fields slowly varying with time (frequency $(1)\ll 1$), the Green functions $y^{\mathrm{R},\uparrow}$ and the distribution function $\hat{f}$ are sharp functions of time difference and slowly varying functions of the half-sum of times. Therefore, it is convenient to perform the Fourier transformation over the time difference. The Fourier component of convolution over the time variable is determined by the formula

$$A\circ B=\exp\left[\frac{1}{2}i\left(\partial_\varepsilon^A\partial_t^B-\partial_t^A\partial_\varepsilon^B\right)\right]A(\varepsilon,t)B(\varepsilon,t), \tag{A.31}$$

where the differential operator λ^4 affects A only. Substituting expression (A.29) for $\hat{f}$ into eq. (A.28) we get

$$-D\frac{\hat{c}}{\partial r}\,\mathrm{Tr}\left(\frac{\partial f}{\partial r}\left(1-g^{\mathrm{R}}g^{\mathrm{A}}\right)\right)+\frac{\partial f}{\partial t}\,\mathrm{Tr}\left(g^{\mathrm{R}}\tau_z-\tau_z g^{\mathrm{A}}\right)$$

$$
\begin{aligned}
&- D\frac{\partial f_1}{\partial \boldsymbol{r}} j_\varepsilon - \frac{\partial f}{\partial \varepsilon}\,\mathrm{Tr}\,\frac{\partial \hat{\Delta}}{\partial t}\left(g^{\mathrm{R}} - g^{\mathrm{A}}\right) - 2\mathrm{i} f_1\,\mathrm{Tr}\,\hat{\Delta}\tau_z\left(g^{\mathrm{R}} - g^{\mathrm{A}}\right)\\
&+ \frac{\partial f_1}{\partial t}\,\mathrm{Tr}\,\hat{\Delta}\tau_z\frac{\partial\left(g^{\mathrm{R}} + g^{A}\right)}{\partial \varepsilon} + eD\frac{\partial A}{\partial t}\frac{\partial f}{\partial \varepsilon} j_\varepsilon = -4I_1^{\mathrm{ph}}(f)\\
&- D\frac{\partial}{\partial \boldsymbol{r}}\,\mathrm{Tr}\left(\frac{\partial f_1}{\partial z}\left(1 - g^{\mathrm{R}}\tau_z g^{\mathrm{A}}\tau_z\right)\right) + \frac{\partial f_1}{\partial t}\,\mathrm{Tr}\left(g^{\mathrm{R}}\tau_z - \tau_z g^{\mathrm{A}}\right)\\
&- D\frac{\partial f}{\partial \boldsymbol{r}} j_\varepsilon + e\frac{\partial \varphi}{\partial t}\frac{\partial f}{\partial \varepsilon}\,\mathrm{Tr}\left(g^{\mathrm{R}}\tau_z - \tau_z g^{\mathrm{A}}\right)\\
&+ \frac{\partial f}{\partial \varepsilon}\,\mathrm{Tr}\,\tau_z\frac{\partial \hat{\Delta}}{\partial t}\left(g^{\mathrm{R}} + g^{\mathrm{A}}\right) + \frac{\mathrm{i}}{2}\frac{\partial f}{\partial \varepsilon}\,\mathrm{Tr}\,\tau_z\frac{\partial^2 \Delta}{\partial t^2}\frac{\partial\left(g^{\mathrm{R}} - g^{\mathrm{A}}\right)}{\partial \varepsilon}\\
&- 2\mathrm{i} f_1\,\mathrm{Tr}\left(g^{\mathrm{R}}\hat{\Delta} + \hat{\Delta} g^{\mathrm{A}}\right) + \frac{\partial f_1}{\partial t}\,\mathrm{Tr}\left(\hat{\Delta}\frac{\partial\left(g^{\mathrm{R}} - g^{\mathrm{A}}\right)}{\partial \varepsilon}\right)\\
&+ 2eD\frac{\partial^2 A}{\partial \boldsymbol{r}\partial t}\frac{\partial f}{\partial \varepsilon} = -4I_2^{\mathrm{ph}}\left(f_1\right)
\end{aligned}
\tag{A.32}
$$

where

$$
j_\varepsilon = \mathrm{Tr}\,\tau_z\left(g^{\mathrm{R}}\partial g^{\mathrm{R}} - g^{\mathrm{A}}\partial g^{\mathrm{A}}\right)
$$

The collision integrals $I_1^{\mathrm{ph}}, I_2^{\mathrm{ph}}$ in formula (A.32) are rather cumbersome and we shall not write them out. They are presented in the paper by Larkin and Ovchinnikov (1977). In the static case the solution of eq. (A.32) has the form

$$
f = \tanh(\varepsilon/2T), \quad f_1 = 0 \tag{A.33}
$$

The dependence of the distribution function on energy is determined from the condition that the electron -phonon collision integral should be zero. Near the transition temperature, for energies $\varepsilon \ll T$ the collision integral I_1^{ph} is equal to

$$
I_1^{\mathrm{ph}}(f) = \tau_\varepsilon^{-1}\frac{|\varepsilon|}{\left(\varepsilon^2 - |\Delta|^2\right)^{1/2}}\left(f(\varepsilon) - \tanh\left(\frac{\varepsilon}{2T}\right)\right), \quad |\varepsilon| > |\Delta|, \tag{A.34}
$$

where

$$
\tau_\varepsilon^{-1} = \frac{\pi\lambda_{\mathrm{eff}}}{2(sp)^2}\int_0^\infty \frac{\mathrm{d}\varepsilon\varepsilon^2}{\cosh\left(\frac{\varepsilon}{2T}\right)\sinh\left(\frac{\varepsilon}{2T}\right)} = \frac{7\zeta(3)\pi\lambda_{\mathrm{eff}}T^3}{2(sp)^2} \sim T^3 \tag{A.35}
$$

where s is the velocity of sound, and θ_{D} is the Debye temperature. τ_ε is large; consequently, in relatively weak electric fields a strong change arises in the electron distribution function.

In many problems the electric field acts stronger on the distribution function than on the Green function $g^{\mathrm{R,A}}$. In these cases it is possible to restrict oneself to a static approximation for the functions $g^{\mathrm{R.A.}}$. Writing down the Green function $g^{\mathrm{R,A}}$ in the form

$$
g^{\mathrm{R,\ A}} = \begin{pmatrix} \alpha & \beta_1 \\ -\beta_2 & -\alpha \end{pmatrix}^{\mathrm{R,\ A}} \tag{A.36}
$$

then from formula (A.25) we get the following system of equations for the functions $\alpha, \beta_{1,2}$:

$$
-D\partial \mp \left(\alpha^{\mathrm{R,\ A}}\partial \mp \beta_{1,2}^{\mathrm{R,\ A}} - \beta_{1,2}^{\mathrm{R,\ A}}\frac{\partial \alpha^{\mathrm{R,\ A}}}{\partial r}\right) + 2\mathrm{i}\Delta_{1,2}\alpha^{\mathrm{R,\ A}} - 2\mathrm{i}\varepsilon\beta_{1,2}^{\mathrm{R,\ A}} + \frac{2}{\tau_\varepsilon}\alpha^{\mathrm{R,\ A}}\beta_{1,2}^{\mathrm{R,\ A}} = -I_{1,2}^{\mathrm{ph(R,\ A)}}. \tag{A.37}
$$

The electron-phonon collision integral $I_{1,2}^{\mathrm{ph(R,A)}}$ is determined by formula (A.25). In the vicinity of T_c and for $\varepsilon \ll T_\mathrm{c}$ it is equal to

$$I_{1,2}^{\mathrm{ph(R)}} = \frac{\beta_{1,2}^{\mathrm{R}}}{\tau_\varepsilon}, \quad I_{1,2}^{\mathrm{ph(\ A)}} = -\frac{\beta_{1,2}^{\mathrm{A}}}{\tau_\varepsilon}. \tag{A.38}$$

If the gradient terms in eq. (A.37) are small, one may use a local approximation for the functions $\alpha, \beta_{1,2}$:

$$\frac{\alpha^{\mathrm{R,\ A}}}{\varepsilon \pm \mathrm{i}/2\tau_\varepsilon} = \frac{\beta_{1,2}^{\mathrm{R,\ A}}}{\Delta_{1,2}} = \pm \left(\left(\varepsilon \pm \frac{\mathrm{i}}{2\tau_\varepsilon} \right)^2 - |\Delta|^2 \right)^{-1/2}. \tag{A.39}$$

In such cases the kinetic equation for the function f acquires the form (Larkin and Ovchinnikov 1977)

$$-D\frac{\partial^2 f}{\partial r^2} + \frac{\partial f}{\partial t}\frac{\partial \left(\varepsilon^2 - |\Delta|^2\right)^{1/2}}{\partial \varepsilon} - \frac{\partial f}{\partial \varepsilon}\frac{\partial \left(\varepsilon^2 - |\Delta|^2\right)^{1/2}}{\partial t} = -I_1^{\mathrm{ph}}(f). \tag{A.40}$$

For the distribution function f in eq. (A.40) it is necessary to obtain a boundary condition at $|\varepsilon| = |\Delta|$. Integrating eq. (A.32) we obtain that in the narrow region near the boundary the value

$$\frac{\partial f}{\partial r} \operatorname{Tr}\left(1 - g^R g^A\right) \tag{A.41}$$

is continuous. Expression (A.41) under the barrier is zero. Consequently,

$$\left.\frac{\partial f}{\partial n}\right|_{\text{on bound.}} = 0. \tag{A.42}$$

In many problems the range of variation of the order parameter Δ is much less than the energy relaxation length $R_\varepsilon = (D\tau_\varepsilon)^{1/2}$. In this case it is possible to obtain an equation for the coordinate-averaged distribution function $\langle f \rangle$. The
distribution function f in this case has the form

$$f = \langle f \rangle + \tilde{f} \tag{A.43}$$

The coordinate-dependent $\widetilde{f}$ is small and can be found in a linear approximation in the electric field without the phonon collision integral.

When eq. (A.40) is valid, $\tilde{f}$ satisfies the equation

$$-D\frac{\partial^2 \tilde{f}}{\partial r^2} = \frac{\partial \langle f \rangle}{\partial \varepsilon}\frac{\partial \left(\varepsilon^2 - |\Delta|^2\right)^{1/2}}{\partial t}. \tag{A.44}$$

Averaging eq. (A.40) over coordinates and using the expression for $\widetilde{f}$ determined by eq. (A.44), we obtain

$$\frac{\partial}{\partial \varepsilon}\left(D_\varepsilon \frac{\partial \langle f \rangle}{\partial \varepsilon}\right) = \left\langle I_1^{\mathrm{ph}}(f) \right\rangle, \tag{A.45}$$

where

$$D_\varepsilon = \frac{eB}{\pi}\int_{V_t} \mathrm{d}^2 r \frac{\partial \left(\varepsilon^2 - |\Delta|^2\right)^{1/2}}{\partial t}\left(-D\frac{\partial^2}{\partial r^2}\right)^{-1}\frac{\partial \left(\varepsilon^2 - |\Delta|^2\right)^{1/2}}{\partial t}, \tag{A.46}$$

V_ε is the region in which $|\varepsilon| > |\Delta|$.
In the general case, eq. (A.45) for the function $\langle f \rangle$ retains its form. However, for the function D_ε a more complicated expression is obtained (Larkin and Ovchinnikov 1975, 1977).

All the physical values are determined by the Green function g^K. By means of eqs. (A.24), (A.27), (A.29) and (A.31) g^{K} is expressed through the distribution function. In slowly varying fields in the convolution operation (A.31) it is possible to retain only the first time-derivatives. As a result we get

$$
\begin{aligned}
& g_p^{\mathrm{K}} = g^{\mathrm{K}} + p g_1^{\mathrm{K}} \\
& g^{\mathrm{K}} = g^{\mathrm{R}} \hat{f} - \hat{f} g^{\mathrm{A}} - \frac{\mathrm{i}}{2} \frac{\partial f}{\partial \varepsilon} \frac{\partial}{\partial t} \left(g^{\mathrm{R}} + g^{\mathrm{A}} \right) \qquad \text{(A.47)} \\
& g_1^{\mathrm{K}} = -\frac{\tau_{1r}}{m} \left\{ \frac{\partial \hat{f}}{\partial r} - g^{\mathrm{R}} \frac{\partial \hat{f}}{\partial r} g^{\mathrm{A}} + \left(g^{\mathrm{R}} \partial g^{\mathrm{R}} \right) \hat{f} - \hat{f} \left(g^{\mathrm{A}} \partial g^{\mathrm{A}} \right) \right. \\
& + \frac{e}{2} \frac{\partial A}{\hat{\imath} t} \left[\frac{\partial g^{\mathrm{R}}}{\hat{\imath} \varepsilon} \tau = g^{\mathrm{K}} - g^{\mathrm{R}} \tau = \frac{\partial g^{\mathrm{K}}}{\partial \varepsilon} + \frac{\partial g^{\mathrm{K}}}{\hat{\imath} \varepsilon} \tau = g^{\mathrm{A}} - g^{\mathrm{K}} \tau = \frac{\partial g^{\mathrm{A}}}{\hat{\imath} \varepsilon} \right] \\
& \left. + \frac{\mathrm{i}}{2} \left[-\frac{\partial g^{\mathrm{R}}}{\partial t} \frac{\partial g^{\mathrm{K}}}{\partial \varepsilon} + \frac{\partial g^{\mathrm{R}}}{\partial \varepsilon} \hat{\imath} \frac{\partial g^{\mathrm{K}}}{\partial t} - \frac{\partial g^{\mathrm{K}}}{\partial t} \partial \frac{\partial g^{\mathrm{A}}}{\partial \varepsilon} + \frac{\partial g^{\mathrm{K}}}{\partial \varepsilon} \partial \frac{\partial g^{\mathrm{A}}}{\partial t} \right] \right\}. \qquad \text{(A.48)}
\end{aligned}
$$

Near the transition temperature, from eqs. (A.21), (A.37) for the order parameter Δ one may obtain a Ginzburg Landau type equation with an additional term arising due to deviation of the distribution function $\langle f \rangle$ from
the equilibrium one:

$$
\begin{aligned}
& \left\{ (1 - T/T_{\mathrm{c}}) + \frac{\pi D}{8T} \partial_-^2 - \frac{7\zeta(3)|\Delta|^2}{8\pi^2 T^2} \right\} \Delta + \\
& \quad + \frac{1}{4} \int_{-\infty}^{\infty} \mathrm{d}\varepsilon (\langle f(\varepsilon) \rangle - \tanh(\varepsilon/2T)) \left(\beta_1^{\mathrm{R}} - \beta_1^{\mathrm{A}} \right) = 0 \qquad \text{(A.49)}
\end{aligned}
$$

In the particular case of a weak current and a coordinate-independent absolute value of the order parameter we have

$$
\begin{aligned}
& \{ (1 - T/T_{\mathrm{c}}) - \frac{7\zeta(3)|\Delta|^2}{8\pi^2 T^2} - \frac{\pi D e^2 A^2}{2T} \\
& \quad + \int_{|\Delta|}^{\infty} \frac{\mathrm{d}\varepsilon}{(\varepsilon^2 - |\Delta|^2)^{1/2}} \left(\langle f(\varepsilon) \rangle - \tanh \left(\frac{\varepsilon}{2T} \right) \right) \Bigg\} \Delta = 0 \\
& j = -\frac{e^2 p^2 I_{\mathrm{tr}}}{3\pi} \Delta f(\Delta) A \qquad \text{(A.50)}
\end{aligned}
$$

Let us consider now in short the case of an arbitrary electron mean free path. As in the case of superconductors with a small electron mean free path, we search for the Green function g^K in the form of eq. (A.27). However, now the Green function $g^{\mathrm{R.A}}$ and the distribution function f, f_1 depend also on the direction of momentum p.

Analogously as eq. (A.28) has been obtained, from formula (A.12) we get an equation for the distribution function $\hat{f}_p$:

$$
\begin{aligned}
&g^{\mathrm{R}}\circ\left(\boldsymbol{v}\frac{\partial\hat{f}}{\partial\boldsymbol{r}}\right)-\left(\boldsymbol{v}\frac{\partial f}{\partial\boldsymbol{r}}\right)\circ g^{\mathrm{A}}+g^{\mathrm{R}}\circ\left(\frac{\partial}{\partial t}+\frac{\partial}{\partial t'}\right)\hat{f}\tau_z-\tau_z\left(\left(\frac{\partial}{\partial t}+\frac{\partial}{\partial t_1}\right)\hat{f}\right)\circ g^{\mathrm{A}}\\
&\quad+g^{\mathrm{R}}\cdot\left(\hat{H}\left(t_1\right)\hat{f}-\hat{f}\hat{H}\left(t'\right)\right)+\left(\hat{f}\hat{H}\left(t_1\right)-\hat{H}(t)\hat{f}\right)g^{\mathrm{A}}\\
&\quad+i\left\{\sum^{\mathrm{Ph(\ K)}}\circ g^{\mathrm{A}}-g^{\mathrm{R}}\circ\sum^{\mathrm{Ph(\ K)}}-\sum^{\mathrm{Ph(R)}}\circ\hat{f}\circ g^{\mathrm{A}}-g^{\mathrm{R}}\circ\hat{f}\circ\sum^{\mathrm{Ph(\ A)}}\right.\\
&\quad\left.+g^{\mathrm{R}}\circ\sum^{\mathrm{Ph(R)}}\circ\hat{f}+\hat{f}\circ\sum^{\mathrm{Ph(\ A)}}\circ g^{\mathrm{A}}\right\}=0 \qquad \text{(A.51)}\\
&\hat{H}(t)=-\frac{\mathrm{i}e}{m}(pA(t))\tau_z-\mathrm{i}\hat{\Delta}(t)+\mathrm{i}e\varphi(t)
\end{aligned}
$$

Using eq. (A.31) for the convolution operation, from eq. (A.51) in a slowly-varying electromagnetic field we get

$$
\begin{aligned}
&\mathrm{Tr}\{\left[\left(v\frac{\partial f_1}{\partial\boldsymbol{r}}\right)+\frac{\partial f}{\partial t}-\frac{\partial f}{\partial\varepsilon}e\left(v\frac{\partial\boldsymbol{A}}{\partial t}\right)\right]\tau_z\left(g^{\mathrm{R}}-g^{\mathrm{A}}\right)-\frac{\partial f}{\partial\varepsilon}\frac{\partial\hat{\Delta}}{\partial t}\left(g^{\mathrm{R}}-g^{\mathrm{A}}\right)\\
&\quad+2\mathrm{i}f_1\hat{\Delta}\left(\tau_z g^{\mathrm{A}}+g^{\mathrm{R}}\tau_z\right)\\
&\quad+\frac{nv}{2}\int\mathrm{d}\Omega_{p_1}\sigma_{pp_1}\left(\hat{f}_p-\hat{f}_{p_1}\right)\left[g_p^{\mathrm{R}}g_{p_1}^{\mathrm{R}}+g_{p_1}^{\mathrm{A}}g_p^{\mathrm{A}}-g_p^{\mathrm{A}}g_{p_1}^{\mathrm{R}}-g_{p_1}^{\mathrm{A}}g_p^{\mathrm{R}}\right]\Big\}=\mathrm{St}_1^{\mathrm{Ph}}\\
&\mathrm{Tr}\{\left[\left(v\frac{\partial f}{\partial r}\right)+\frac{\partial f_1}{\partial t}+e\frac{\partial\varphi}{\partial t}\frac{\partial f}{\partial\varepsilon}\right]\tau_z\left(g^{\mathrm{R}}-g^{\mathrm{A}}\right)+\frac{\partial f_1}{\partial t}\hat{\Delta}\frac{\partial\left(g^{\mathrm{R}}-g^{\mathrm{A}}\right)}{\partial\varepsilon}\\
&\quad+\frac{\partial f}{\partial\varepsilon}\left[\frac{\partial\hat{\Delta}}{\partial t}\left(g^{\mathrm{A}}\tau_z-\tau_z g^{\mathrm{R}}\right)-\frac{\mathrm{i}}{2}\frac{\partial^2\hat{\Delta}}{\partial t^2}\left(\frac{\partial g^{\mathrm{A}}}{\partial\varepsilon}\tau_z+\tau_z\frac{\partial g^{\mathrm{R}}}{\partial\varepsilon}\right)\right]-2\mathrm{i}f_1\hat{\Delta}\left(g^{\mathrm{R}}+g^{\mathrm{A}}\right)\\
&\quad+\frac{nv}{2}\int\mathrm{d}\Omega_{p_1}\sigma_{pp_1}\left(\hat{f}_p-\hat{f}_{p_1}\right)\left(\tau_z g_p^{\mathrm{R}}g_{p_1}^{\mathrm{R}}+\tau_z g_{p_1}^{\mathrm{A}}g_p^{\mathrm{A}}-g_p^{\mathrm{A}}\tau_z g_{p_1}^{\mathrm{R}}-g_{p_1}^{\mathrm{A}}\tau_z g_p^{\mathrm{R}}\right)\Big\}=\mathrm{St}_2^{\mathrm{Ph}}. \qquad \text{(A.52)}
\end{aligned}
$$

The kinetic equations (A.51) are written as applied to the problem on the flux line motion. More complete equations with electron-phonon collision integrals have been presented by Larkin and Ovchinnikov (1977).

25 Theory of the Resistive State in Narrow Superconducting Channels by Galaiko, Kopnin

25.1 1. Introduction

The resistive state is the state in which the superconductor has a finite resistance to a d.c. current. Despite the apparent peculiarity of such a state (since superconductivity is usually understood as zero resistance to d.c. current) it can be observed rather frequently and indicates that the lack of resistance itself is not a fundamental property of superconductivity.

Resistive states can be observed in a wide variety of phenomena. One of the well-known examples is the mixed state of type-II superconductors where an electric field is generated by vortex motion due to the transport current through the sample (see the reviews by Gorkov and Kopnin 1975 and Larkin and Ovchinnikov 1985). One can note the growing interest to a

related phenomenon where a finite resistance appears when the transport current passes along the magnetic field direction so that the vortex motion is much more complicated (see for example Brandt 1980 and Clem 1980). Resistive states can be observed also in type-I superconductors. One can mention the intermediate state of superconducting cylinders in the current-carrying state and also the two-dimensional mixed state at the inner surface of a hollow cylinder when the superconductivity is destroyed by the current (Landau and Sharvin 1969). These problems are reviewed by Dolgopolov and Landau (1985) in this volume. A finite resistance is observed also in wide and thick superconducting strips with dimensions larger than the characteristic superconducting lengths: the coherence length $\xi(T)$ and the magnetic field penetration depth $\hat{\lambda}(T)$. The electric field is generated in this case by the motion of flux tubes which are created near the sample surface.

Finally, the resistive state is observed in long narrow superconducting channels (including long superconducting microbridges) and whiskers with lateral dimensions less than the coherence length and the magnetic field penetration depth. It is this type of resistive states which is considered in the present review.

This choice is not fortuitous. We shall see later that this problem has a fundamental character, and its explanation requires some new (as compared with the classical understanding of superconductivity) ideas and the very recent achievements of the time-dependent microscopic theory. On the other hand, this type of resistive state is well studied experimentally and presents
more interest for theoreticians, due to its effective one-dimensionality (all the quantities depend only on the coordinate along the channel) which reduces the mathematical complexity considerably and makes the physical picture more transparent. The major physical effects involved have a close similarity with the processes taking place in Josephson junctions and weak links (see the review by Aslamazov and Volkov 1985, this volume) and with the processes of the electric field penetration into a superconductor near the normalsuperconducting interface (Artemenko and Volkov 1979).

The present review describes only the theory of the resistive state of narrow superconducting channels. The experimental results are given with the only purpose to outline qualitatively the main features of the phenomenon and do not claim any completeness. Moreover, we do not intend to survey all the available literature on this problem, which is very extensive, but would like to concentrate on the basic ideas and results of the theory which help to understand this interesting and unusual phenomenon.

The review has the following structure. In the second part of the present section we give briefly the main experimental results characterizing the major properties of the resistive state of narrow superconducting channels. In section 2, the general results are discussed which follow from the fact that superconductivity and electric field coexist in the sample. Here the concept of "phase slip centers" (PSCs) is introduced, and the so-called "quantization rule" is derived, which is a generalization of the well-known Josephson relation. Section 3 deals with the Langer and Ambegaokar fluctuation theory of PSC describing the thermodynamical activation of PSCs in the immediate vicinity of the critical temperature. Some other qualitative models of the resistive state are also described in this section. In sections 4 and 5 we discuss the results of solutions of time-dependent microscopic superconductivity equations by means of numerical and analytical methods, respectively. The theory of the voltage steps in the current voltage characteristics of superconducting channels with a finite length is considered in section 6. Finally, in section 7 we discuss the overall state of the theory and its correspondence to the experimental data.

25.1.1 1.1. Basic experimental results

By narrow superconducting channels we mean samples of which the lateral dimensions are less than (or in practice, of the order of) the characteristic superconducting lengths: the coherence length $\xi(T)$ and the magnetic field penetration depth $i(T)$. Such conditions are met by narrow strips and whiskers. For example, the lateral dimensions for tin must be on the order of some tenths of μm. The length of the samples must be sufficient (tens or hundreds of μm). The purity of the samples influences, comparatively slightly, the main features of their resistive state, and the current voltage characteristics of narrow evaporated strips and whiskers are qualitatively rather similar.

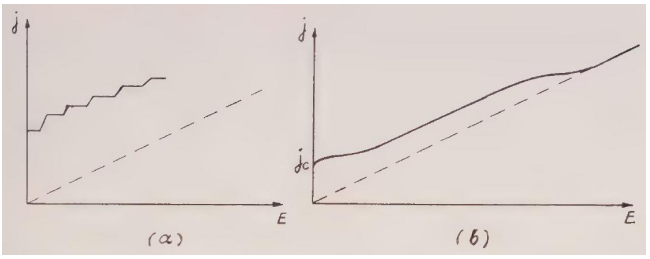


Fig. 1. The schematic current-voltage characteristics of narrow superconducting channels for: (a) channels with a finite length and (b) for long channels. The dashed line is Ohm's law.

Experiments are usually done at temperatures close to the critical one since in this case one can reduce the Joule heating which is quite large in the resistive state.

The major characteristic of the resistive state is its current-voltage characteristic (CVC). Qualitatively, for not very long channels, it has the form represented in fig. la (Meyer and von Minnigerode 1972, Skocpol et al. 1974, Smith 1980, Galako et al. 1976).

One can compare the experimental CVC with the characteristic obtained from the Ginzburg Landau theory, shown in fig. 2. The Ginzburg-Landau theory predicts that the superconductivity should disappear and the sample should go into the normal state when the current exceeds some value known as the Ginzburg Landau critical current j_c (for a review of Ginzburg Landau theory see. e.g.. De Gennes 1966). The principal difference between the CVC in fig. 1 and that in fig. 2 is that a broad region in currents and voltages exists, in practice. where superconductivity and a d.c. electric field are present simultaneously. This state is what we call the resistive state of the superconductor.

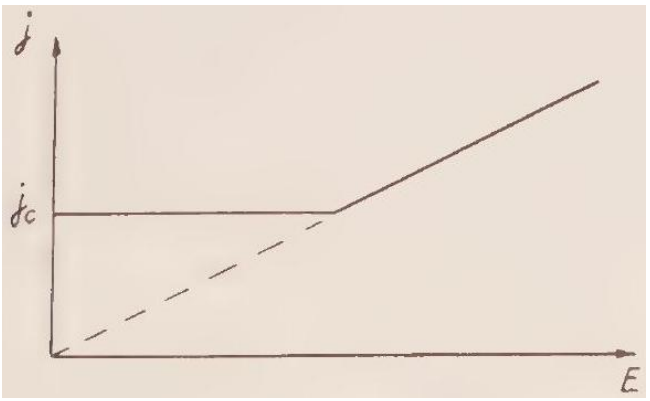


Fig. 2. Current-voltage characteristic of a narrow channel in the Ginzburg-Landau theory. The dashed line is Ohm's law.

Note that it is absent in the classical Ginzburg-Landau theory.
The important feature of CVCs of channels with a finite length is the voltage steps observed for both whiskers (Meyer and von Minnigerode 1972) and narrow strips (Skocpol et al. 1974, Smith 1980). Samples in the resistive state have also essential nonstationary properties. First of all, the a.c. Josephson effect can be observed in these samples under external microwave irradiation (Skocpol et al. 1974). The generation of lower frequencies is also observed (Churilov et al. 1969, Galaiko et al. 1973), the generation being localized at the ends of the sample.

We can see that the behavior of narrow superconducting channels in the resistive state differs significantly from the classical picture of the currentcarrying superconductor. Moreover, small lateral dimensions make impossible the explanation of resistivity in the usual terms of vortex motion or normal phase regions through the sample. We can state therefore that the resistive state in narrow superconducting channels is a new type of superconducting state.

25.2 2. The general picture of the resistive state. Phase slip centers

The theory has to explain first of all the most striking point, namely, how superconductivity can exist in a sample in which a d.c. electric field is present. The Cooper pairs are charged and should therefore be accelerated in presence of an electric field until they reach the critical velocity and the superconductivity disappears. As we have seen, however, this is not the case in practice. The point is that the motion of Cooper pairs in a superconductor and, generally, the behavior of a superconductor in an electromagnetic field is governed not by the vector, $\boldsymbol{A}$, and scalar, ϕ,-potentials of the electromagnetic field but by the so-called gauge invariant potentials (see, e.g., Larkin and Ovchinnikov 1985).

$$\boldsymbol{Q} = A - \frac{\hbar c}{2e}\nabla\chi, \quad \Phi = \phi + \frac{\hbar}{2e}\frac{\partial\chi}{\partial t}. \tag{1}$$

Here χ is the phase of the complex order parameter $\Delta\exp(\mathrm{i}\chi)$. In contrast to the potentials A and ϕ the gauge invariant potentials Q and Φ have real physical meaning. For example, the potential Q is related to the velocity of Cooper pairs:

$$V_\mathrm{s} = -\frac{e}{mc}Q.$$

The meaning of the potential Φ will be discussed below. With the potentials (1) one can write that

$$\boldsymbol{E} = -\frac{1}{c}\frac{\partial\boldsymbol{Q}}{\partial t} - \nabla\Phi,$$

and hence

$$\frac{\partial v_s}{\partial t} = \frac{e}{m}(\boldsymbol{E} + \nabla\Phi). \tag{2}$$

Equation (2) describes the above-mentioned process of Cooper pair acceleration. The last term in the right-hand side of eq. (2) plays a very important role. Note the gauge invariant potential Φ can be considered as the difference between the chemical potentials of quasiparticles $\mu_\mathrm{e} = -e\phi$ and Cooper pairs (per particle) $\mu_\mathrm{p} = \frac{1}{2}\hbar(\hat{c}\chi/\hat{c}t)$. In equilibrium $\mu_\mathrm{e} = \mu_\mathrm{p}$ and $\Phi = 0$. To restrict the velocity of Cooper pairs from growing to infinity, the electric field $\boldsymbol{E}$ has to be averaged out by the term $\nabla\Phi$. It means that the resistive state of a superconductor should be essentially nonequilibrium with $\Phi \neq 0$. The potential Φ in a superconductor, however, cannot be too large either, otherwise the conductivity also would be destroyed. We suppose that the sample is sufficiently long. Then the potential difference $\delta\phi$ between two points which are far enough apart can take up rather large values. In order to keep the potential Φ limited,

the difference $\delta\phi$ has to be compensated by a corresponding difference of the pair chemical potentials $\delta\mu_{\rm p}$ or, which is the same, by a corresponding growth rate of the phase difference between the two points.

The resulting picture can, in principle, be visualized in two different ways. The first, static, model suggests that a periodic structure develops along the sample, the order parameter being equal to zero in points of maximum $|\Phi|$. The neighboring superconducting regions have chemical potentials $\mu_{\rm p}$ which differ from each other by the potential difference $\delta\phi$ between these regions. Therefore, within each superconducting region $\boldsymbol{E} = -\nabla\Phi, \left(\partial\boldsymbol{Q}_{/}\partial t\right) = 0, \mu_{\rm p} = \text{const}$. The finite magnitude of Φ results from the compensation of the voltage drop $\delta\phi$ by the difference $\delta\mu_{\rm p}$ of the pair chemical potentials between the neighboring superconducting regions. In the points where the order parameter is zero the macroscopic phase coherence is broken, and $\mu_{\rm p}$ and Φ experience jumps. This is illustrated schematically in fig. 3 where A is the modulus of the order parameter and x is the coordinate along the sample. This static model was proposed by Fink (1973a,b), Fink and Poulsen (1974a,b, 1975) and by Galako (1974, 1975, 1976a,b, 1977), Galako and Shumeko (1976), Galako et al. (1976) and Bezuglyi et al. (1977).

Such a picture ignores, however, a very important point, namely, that the neighboring superconducting regions have different pair chemical potentials $\mu_{\rm p} = \frac{1}{2}\hbar(\partial\chi/\partial t)$. This implies that the phase difference between the neighboring regions will grow with time and the order parameters in them will strongly interact with each other. Indeed, let us write the complex order parameter

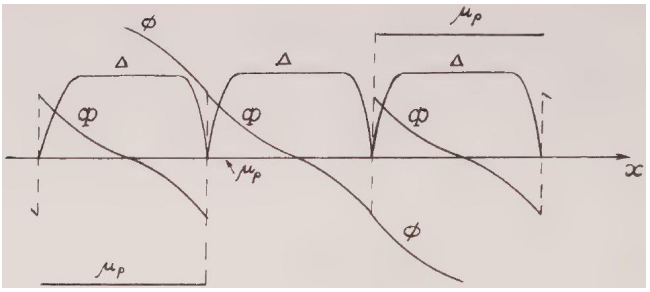


Fig. 3. The schematic behavior of the order parameter Δ and the potentials $\mu_{\rm e}, \mu_{\rm p}$ and Φ in the static model of the resistive state.

$\psi = \Delta e^{ix}$ in the form

$$\psi = \Delta^{(1)}(x)\exp\left(2i\mu_{\rm p}^{(1)}t/\hbar\right) + \Delta^{(2)}(x)\exp\left(2i\mu_{\rm p}^{(2)}t/\hbar\right),$$

where $\Delta^{(1,2)}\exp\left(2i\mu_{\rm p}^{(1,2)}t/\hbar\right)$ are the order parameters in the two neighboring superconducting regions. It is clear that the modulus of the order parameter $\Delta = |\psi|$ will strongly oscillate in regions of overlaps of $\Delta^{(1)}(x)$ and $\Delta^{(2)}(x)$ and the static model will not be valid here. The question arises, whether the static model is applicable at all. This problem is discussed in more detail in section 5; for now we note only that, as we shall see later, the oscillations, fortunately, take place only in quite narrow regions near points of broken phase coherence; practically the order parameter oscillates only slightly over the whole interval between the two neighboring points.

In the present review we choose another approach which suggests the nonstationary behavior from the very beginning. As has been said above, the potential difference $\delta\phi$ between two points x_1 and x_2 far enough apart has to be compensated by the growth rate of the phase difference between the two points in order to maintain a finite magnitude of the gauge invariant potential Φ, i.e.,

$$\delta\phi + \frac{\hbar}{2e}\frac{\partial}{\partial t}(\delta\chi) \simeq 0. \tag{3}$$

This can be conveniently illustrated in the space where the real and imaginary parts of the order parameter $\psi = \psi_1 + \mathrm{i}\psi_2$ are plotted on two coordinate axes and the third axis is the x-coordinate along the sample (Langer and Ambegaokar 1967, Rieger et al. 1972) (see fig. 4). In the uniform state the modulus $A = (\psi_1^2 + \psi_2^2)^{1,2}$ is constant and the loops of the helix in fig. 4 have the same radius. The phase difference $\delta\chi$ grows with time and the loops of the helix become more dense. This can not, however, continue for infinitely long

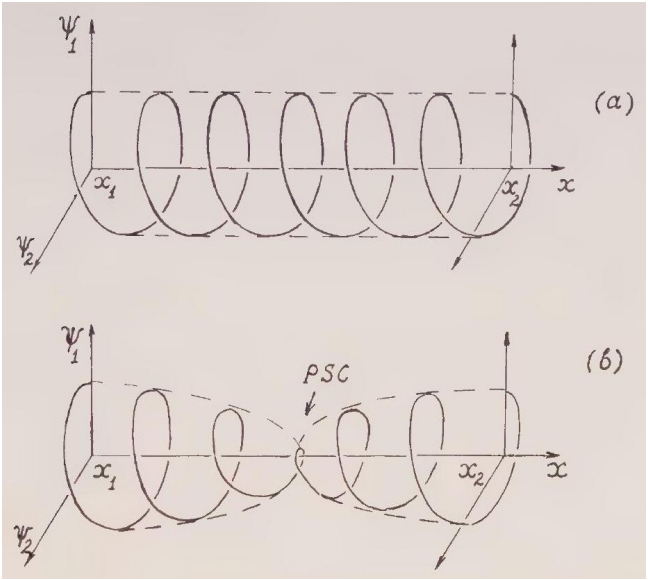


Fig. 4. A representation of the complex order parameter $\psi=\psi_{1 +\mathrm{i} \psi_{2}$ in the space $\{\psi_1, \psi_2, x\}$. The only possibility for the helix to loose a loop is to turn its radius to zero at some point.}

since the phase difference $\delta\chi$ determines the velocity of the condensate

$$v_\mathrm{s} \sim \frac{\hbar\delta\chi}{m\,(x_2 - x_1)}$$

which, therefore, will grow, thus resulting again in destruction of superconductivity. For the phase difference to be restricted some mechanism of reduction is required. It can be seen from fig. 4 that the helix could lose one or more loops if its radius A would become zero in some point between x_1 and x_2.

The points where the order parameter turns to zero and its phase experiences jumps by multiples of 2π are known as phase slip centers (PSCs).

To maintain the superconductivity in the sample the phase slip process has to repeat in time, the average period t_0 between phase slips being related to the average voltage V across the points x_1 and x_2 by eq. 3 . Since the phase difference changes by 2π when one loop is thrown off, we get after averaging eq. (3) over time

$$2eV = \frac{2\pi\hbar}{t_0} \tag{4}$$

i.e., the usual Josephson relation. Later we shall give a more formal derivation of such an equation, on the basis of the topological properties of PSCs.

Two different mechanisms of PSC formation are possible. First, PSCs can be formed as a result of thermodynamic fluctuations in the system. The probability of such an event is proportional to $\exp(-\delta F/T)$ where δF is the freeenergy barrier between two uniform states before and after the phase slippage. It is clear that this process is more probable near the critical temperature where the barrier is small. This mechanism was proposed by Langer and Ambegaokar (1967); they suggested also the general picture of phase slippage described above.

When the temperature is lowered from the critical temperature, the probability of fluctuation formation of PSC decreases rapidly and this process is replaced by the intrinsic, and therefore more fundamental, process. One can visualize the process of PSC excitation due to a sufficiently large d.c. current as being similar to the excitation of string vibrations due to the motion of a bow with a constant velocity. From a more formal point of view, this means that the processes of PCS formation, i.e., the order parameter oscillations in some points of the channel, are the result of nonlinearities of limiting-cycle type, which are characteristic for the system.

If the superconducting channel has structure defects the formation of PSCs will take place most probably in "weak points" where the order parameter is suppressed by external causes. In sufficiently long and uniform samples, however, PSCs should be formed periodically in time and in coordinate along the channel because of the space and time homogeneity.

The process of PSC formations can be conveniently represented in twodimensional space-time $\{x; ct\}$ (Ivlev and Kopnin 1978). In fig. 5 the dots designate PSCs, i.e., the points in space-time where the modulus of the order

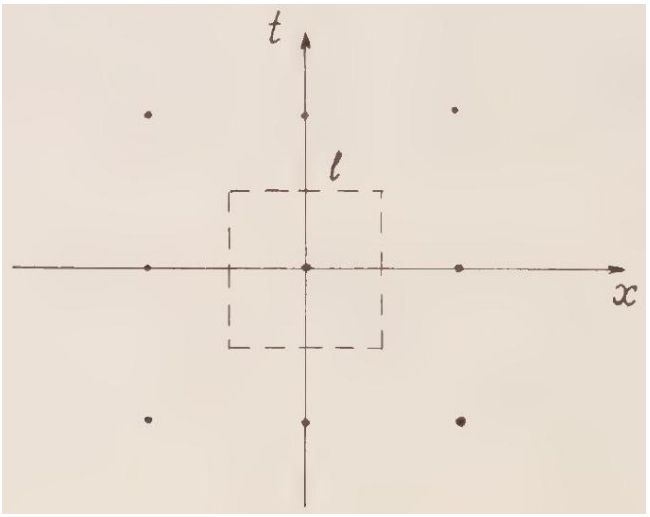


Fig. 5. The space-time ${x ; c t\
$. The solid dots indicate PSCs (see text). The contour ℓ encloses a unit cell of the PSC structure in the space-time $\{x; ct\}$.}

parameter is zero, $\Delta = 0$. We assume that these points form a periodic structure in the space $\{x; ct\}$. It can be easily seen that the process of throwing off n loops when A goes to zero in fig. 4 is equivalent to the condition that the phase of the order parameter should change by $2\pi n$ after going along a closed contour around a PSC in the space time $\{x; ct\}$ in fig. 5, n being an integer. Therefore, the phase slip centers can be considered as vortex-like topological singularities in the space-time $\{x; ct\}$.

For these topological singularities, one can derive (Ivlev and Kopnin 1978) a "quantization rule" for the electric field "flux" in the space-time $\{x; ct\}$, which is analogous to the quantization of the magnetic flux in the usual space. We introduce the two-dimensional vectors

$$\rho = \{x, ct\}, \quad q = \{Q_x, -\Phi\}, \quad a = \{A_x, -\phi\},$$

which are related by

$$q = a - \frac{\hbar c}{2e}\frac{\partial \chi}{\partial \rho} \tag{5}$$

After integration of the vector $\boldsymbol{q}$ along a closed contour around a PSC one gets, with eq. (5),

$$\oint_\ell q \, \mathrm{d}p = \oint a \, \mathrm{d}\rho - \frac{\hbar c}{2e} \oint \frac{\partial \chi}{\partial \rho} \, \mathrm{d}\rho. \tag{6}$$

With the obvious formula

$$E = -\left(\frac{1}{c}\right)\left(\frac{\hat{c}A}{\hat{\partial} t}\right) - \left(\frac{\hat{c}\phi}{\partial x}\right) = (\mathrm{curl}\, a)_3,$$

the first integral in the right-hand side can be transformed according to the Stokes theorem into an integral of $(\mathrm{curl}\ a)_3$ over the area enclosed by the contour ℓ. The second integral in the right-hand side of eq. (6) gives the phase change $2\pi n$ after going around a PSC. So we have

$$\oint_t q \, \mathrm{d}\rho = \int_S E \, \mathrm{d}xc \, \mathrm{d}t - \frac{2\pi\hbar c}{2e} n.$$

If we consider a separate PSC the integral in the left-hand side, along the infinitely remote contour, vanishes. In case of a periodic array of PSCs, this integral vanishes also if one chooses the boundary of a unit cell of the PSC lattice in the space-time $\{x; ct\}$ as the contour of integration. So we get

$$\int_{S_0} E \, \mathrm{d}S = \phi_0 n, \tag{7}$$

where $\phi_0 = \pi\hbar c/e$ is the "flux quantum" which is formally equal to the quantum of magnetic flux in the ordinary space. The integration in eq. (7) extends over
the unit cell area S_0 in the space $\{x; ct\}$: $\mathrm{d}S = \mathrm{d}xc \, \mathrm{d}t$. The "quantization rule" (7) is the generalization of the Josephson relation to the case of a spatially distributed a.c. potential. When E is time-independent, eq. (7) immediately gives the usual Josephson relation (4). The quantization rule (7) is very useful since it gives the space- and time-averaged electric field (the one which is measured experimentally) in terms of the periods of the PSC structure in time, t_0, and in the coordinate, L,

$$\langle E \rangle = \frac{\phi_0 n}{c t_0 L}. \tag{8}$$

25.3 3. The phenomenological theories of the resistive state

25.3.1 3.1. Fluctuation-induced phase slip centers

In this section we discuss briefly basic qualitative theories suggested for the resistive state.

When the current through a sample is very small (the exciting force is small) the thermodynamic fluctuations in the system are the main mechanism for the PSC formation. Their probability is proportional to $\exp(-\delta F/T)$ and they are significant only in the close vicinity of T_c where the activation energy is low,

$$\delta F \sim (F_{\rm n} - F_{\rm s})\, \xi(T) S \propto (T_{\rm c} - T)^{3/2}$$

Experimental evidence is now available which verifies that thermodynamic fluctuations are responsible for the resistive state in the temperature range very close to the critical one: $1 - T/T_{\rm c} \leqslant 10^{-4}$ (Webb and Warburton 1968, Lukens et al. 1970. Newbower et al. 1972). The theory of this phenomenon was considered first by Little (1967). A more comprehensive theory was proposed by Langer and Ambegaokar (1967) and was developed further by McCumber and Halperin (1970) and by Tucker and Halperin (1971). We describe here the main results of the Langer and Ambegaokar (LA) theory.

As it was said above, the rate of phase "throw-off"'s or the frequency of PSC formation is related to the voltage across the region of the superconducting channel, where the PSC is formed, by eq. (8) or by eq. (4). To find the resistivity of the superconducting channel, one has to express the frequency of the fluctuation formation of PSCs in terms of the current through the channel. The LA theory treats this problem in the following way.

Let us consider a channel with length L_0 and suppose for definiteness that the order parameter satisfies cyclic boundary conditions at its ends, i.e., that the helix in fig. 4 has an integer number of loops. The wave function of the superconducting electrons, which is proportional to the complex order parameter, has the form

$$\psi_k = \Delta_k \exp(ikx) \tag{9}$$

in the uniform current-carrying state. Here $k = 2\pi m/L_0$. The corresponding current density

$$j = \frac{2e}{i\hbar}\left(\psi^* \nabla\psi - \psi \nabla\psi^*\right)$$

is equal to $j_k = (4e/h)k\Delta_k^2$. The free energy

$$F = \int {\rm d}^3 r \left[|\nabla\psi|^2 - \alpha|\psi|^2 + \frac{1}{2}\beta|\psi|^4\right] \tag{10}$$

[where $\alpha = \alpha_0\,(T_{\rm c} - T)$] in the current-carrying state (9) is

$$F\{\psi_k\} = SL_0\left[\left(k^2 - \alpha\right)\Delta_k^2 + \frac{1}{2}\beta\Delta_k^4\right], \tag{11}$$

where S is the cross-sectional area of the channel. One can easily calculate the free-energy difference between the state (9) with m loops and the state with ($m - 1$) loops:

$$\delta F_1 = \frac{\partial F}{\partial k}\frac{2\pi}{L_0} = \frac{S\pi k}{e} j.$$

Hence the transition frequency between the states $k \leftrightarrows k - (2\pi/L_0)$ is

$$\hat{\gamma} = \Omega(T) \exp\left(-\frac{\delta F_0}{T} \pm \begin{array}{c}\dot{\delta} F_1 \\ 2T\end{array}\right). \tag{12}$$

The prefactor $\Omega(T)$ in the LA theory has the form

$$\Omega(T) = \frac{2\pi N_{\rm e}}{\tau},$$

where $N_{\rm e} = SL_0 n$ is the number of electrons in the sample (n is the electron density) and τ is a characteristic time of microscopic processes remaining undetermined in the LA theory. δF_0 is the free-energy barrier between the states ψ_k and $\psi_{k(2\pi L_0)}$. After calculating the probability

flux of the system from the state ψ_k into the state $\psi_{k-(2\pi/L_0)}$ and equating it to $2eV/\hbar$ in accordance with eq. (4), we find

$$\frac{2eV}{\hbar} = \frac{4\pi n S L_0}{\tau} \sinh\left(\frac{\delta F_1}{2T}\right) \exp\left(-\frac{\delta F_0}{T}\right).$$

Langer and Ambegaokar assumed that the time τ entering this expression is the mean free time characterizing the conductivity of the normal metal
$\sigma_{\rm n} = ne^2\tau/m$. Then the resistivity of the sample in the limit $j \to 0$ is

$$\frac{\rho_{\rm s}}{\rho_{\rm n}} = \frac{\pi^2\hbar^2 n^2 S^2}{mT} \exp\left(-\frac{\delta F_0(j \to 0)}{T}\right) \tag{13}$$

For a complete calculation of the resistivity in eq. (13) one has to find the free-energy barrier δF_0 between two states which have different numbers of loops. The free-energy barrier is the saddle point of the functional (10) in the space of functions $\psi(x)$. This implies that the function $\psi_0(x)$, corresponding to the "pass" solution, must satisfy the condition $\delta F/\delta\psi = 0$, i.e., must be a solution of the Ginzburg-Landau equation

$$\nabla^2\psi + \psi - |\psi|^2\psi = 0. \tag{14}$$

Equation (14) is written in the dimensionless units of Ginzburg Landau theory, where x is measured in $\xi(T)$ and ψ is measured in $\psi_{\rm GL} = (\alpha/\beta)^{1/2}$. The current density in these units has the form

$$j = (1/2{\rm i})\left(\psi^*\nabla\psi - \psi\nabla\psi^*\right) \tag{15}$$

It is convenient to separate modulus and phase of the order parameter $\psi = \Delta\exp({\rm i}\chi)$ and introduce the gauge invariant variables $\Delta = |\psi|$ and $Q = -\nabla\chi$ (here $A = 0$). Equations (14) and (15) become

$$\frac{\partial^2\Delta}{\partial x^2} + \left(1 - \Delta^2 - Q^2\right)\Delta = 0 \tag{16}$$

$$j = -\Delta^2 Q, \quad \operatorname{div} j = 0 \tag{17}$$

Equations (16), (17) have the first integral

$$\left(\frac{\partial\Delta}{\partial x}\right)^2 + \Delta^2 - \frac{1}{2}\Delta^4 + \frac{j^2}{\Delta^2} = \text{ const.} \tag{18}$$

The solution $\Delta(x)$ can be easily obtained if one uses the analogy with particle motion in the potential

$$U(\Delta) = \Delta^2 + \frac{j^2}{\Delta^2} - \frac{1}{2}\Delta^4. \tag{19}$$

In this analogy Δ corresponds to the coordinate of the particle and x to time. The potential $U(\Delta)$ is shown in fig. 6. Bounded solutions for Δ are possible only when the constant in the right-hand side in eq. (18) is less than or equal to $U_{\max}(j)$ (see fig. 6). The solution $\Delta(x)$ represents in this case a function, periodic in x, which can be written in the implicit form

$$x = \int_{\Delta_0}^{\Delta} \frac{{\rm d}\Delta}{[C - U(\Delta)]^{1/2}} \tag{20}$$

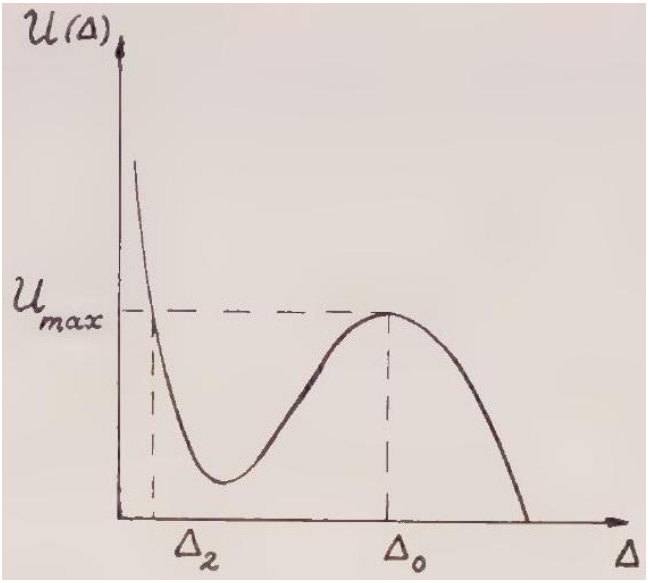


Fig. 6. The schematic form of the "potential" $U(\Delta)$ for eq. (18).

where the zero of x is chosen in the point $A = A_2$. We need a solution which transforms into the uniform solution $\Delta = \Delta_2$ with the given current j as $x \to \pm\infty$. One can obtain such a solution taking $C = U_{\max}$:

$$x = \int_{1,2}^{\Delta} \frac{\mathrm{d}\Delta}{[U_{\max} - U(\Delta)]^{1/2}}. \tag{21}$$

This function is schematically shown in fig. 7 . The order parameter A_0 in the uniform current-carrying state is related to the current j by

$$j = \Delta_0^2 \sqrt{1 - \Delta_0^2}. \tag{22}$$

Equation (22) has solutions only if $j \leqslant j_c = 2/3\sqrt{3}$. The value j_c is known as the Ginzburg-Landau critical current. When $j > j_c$ a uniform superconducting state is impossible.

The solution (21), shown in fig. 7 , represents the function corresponding to the maximum of the free-energy functional $F\{\psi\}$ in the space of functions ψ,

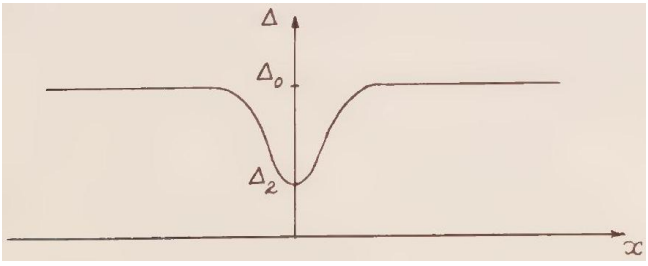


Fig. 7. The LA solution (21) for eq. 18.

along the line which connects the two states before and after the formation of a PSC and passes through the states with minimum possible free energies.

We are interested here in small currents, $j \to 0$. In this case eq. (21) takes the form

$$\Delta(x) = \tanh \frac{|x|}{\sqrt{2}} \tag{23}$$

This solution passes through zero at $x = 0$ and corresponds directly to a PSC.
With eq. (23) and eq. (10) it is easy to calculate the free-energy barrier

$$\delta F_0(j=0) = \frac{8\sqrt{2}}{3}\frac{\alpha_0^{3/2} S}{2\beta}\left(T_c - T\right)^{3/2} \tag{24}$$

Equations (13) and (24) are the main result of the LA theory.
It should be noted, however, that the LA estimation of the prefactor $\Omega(T)$ in eq. (12) gives rise to very serious doubts. Its exact calculation requires direct knowledge of the dynamics of the system's transition through the potential barrier. This problem was considered by McCumber and Halperin (1970) on the basis of the time-dependent Ginzburg-Landau equations supplemented by the Langevin random forces describing fluctuations. According to the results of McCumber and Halperin the prefactor $\Omega(T)$ in eq. (12) appears to be

$$\Omega(T) = \frac{N(T)}{\tau(T)},$$

where $\tau(T) = \pi\hbar/8\left(T_c - T\right)$ is the characteristic relaxation time in the Ginzburg-Landau theory for the modulus of the order parameter, and $\mathrm{N}(T)$ is the effective number of statistically independent subsystems within the length of the sample, which is proportional to $L_{0/}\check{\zeta}(T)$. At small currents they get for the prefactor

$$\Omega(T) = \frac{\sqrt{3}L_0}{2\pi^{3/2}\xi(T)\tau(T)}\left(\frac{\delta F_0}{T}\right)^{1/2}$$

The estimation of this expression shows that the prefactor in the theory of McCumber and Halperin is about 10 orders of magnitude smaller than that in the LA theory.

25.3.2 3.2. Spontaneous formation of phase slip centers

As was said previously, the fluctuation mechanism of PSC formation plays a role only in a very narrow interval around of T_c. If one goes beyond this special interval the probability of fluctuations becomes extremely small. Moreover, if the current through a sample is sufficiently small there will be no mechanism of formation of PSC and the voltage across the channel will be
zero, i.e., the sample will be in a purely superconducting state. When the current exceeds a limiting value (dependent on the sample length) the conditions for spontaneous formation of PSC are satisfied (the system falls in a region of attraction to a limiting cycle) and one PSC appears in the sample. This is reflected as a voltage step in the CVC (see fig. 1a). When the current is increased further, two, three and more PSCs may appear in the sample, accompanied by corresponding voltage steps in the CVC. This happens in samples of finite length. In an infinitely long sample, the total number of PSCs is always large and the density increases smoothly with the current; the corresponding CVC has the form of a smooth curve (fig. 1b).

It is clear from the discussion above that the nonlinearity of a system must play the main role in the resistive state. This inevitably leads to the conclusion that it is very complicated to obtain the exact solution of the problem, if this is possible at all. For this reason we first outline some qualitative theories of the resistive state.

The qualitative picture of PSC formation is the following: the velocity of the superconducting condensate increases under the action of an electric field. Then at some time and place in the sample the velocity reaches such a value (not necessarily equal to the critical velocity) that the superconducting state becomes unstable and the order parameter falls to zero at this place. When Δ turns to zero the phase coherence is destroyed. Then the formation of the superconducting condensate starts again in the vicinity of this point since the sample is at a

temperature below T_c. The superconductivity is restored, however, with a different phase, so that the phase difference between the superconducting regions to the right and to the left of a PSC is changed by 2π compared to the phase difference in the initial state. This process repeats in the time determined by eq. (4).

Rieger et al. (1972) have proposed a numerical model for PSC formation. They defined the moment of PSC formation as the moment when the free energy of a sample section, which increases due to the acceleration of Cooper pairs by an electric field, becomes higher than the free energy of the state which this section would have if the phase difference between the ends were 2π less. This condition is, of course, quite artificial and the model proposed by Rieger et al. is useful only as a first step in solving the problem of the resistive state.

We postpone the consideration of the PSC dynamics to later sections and discuss now a qualitative picture of formation of the voltage across the PSC: we shall follow here the model suggested by Skocpol. Beasley and Tinkham (1974) (SBT-model).

The total current density can be represented as a sum of the supercurrent j_s and the normal current $j_n = \sigma E$:

$$j = \sigma E + j_s = -\sigma \left(\frac{\partial \Phi}{\partial x} + \frac{1}{c} \frac{\partial Q}{\partial t} \right) + j_s. \tag{25}$$

All the quantities in the right-hand side of eq. (25) depend on time, varying periodically with the period $t_0 = 2\pi/\omega_J$, where ω_J is the Josephson frequency. We are interested in the time-averaged voltage which is measured experimentally. After averaging eq. (25) over time the term $\partial Q/\partial t$ vanishes due to periodicity and we have

$$j = -\sigma \frac{\partial \bar{\Phi}}{\partial x} + \bar{j}_s \tag{26}$$

It was said in section 2 that the gauge invariant potential Φ can be considered as the difference between the chemical potentials of Cooper pairs, $\mu_p = (\hbar/2)\partial\chi/\partial t$, and quasiparticles, $\mu_e = -e\phi$, i.e. $\Phi = (\mu_p = \mu_e)/e$. In an equilibrium superconductor, it always holds that $\mu_e = \mu_p$ and $\Phi = 0$.

As we have seen Φ has to be nonzero in the resistive state. This type of nonequilibrium results from the possibility, characteristic for a superconductor, of imbalance between the occupation numbers of electron-like and hole-like branches in the energy spectrum (the so-called "branch imbalance"). We shall not consider the physical nature of this effect in detail since it goes beyond the scope of this review. Numerous original literature is available on this question (see, e.g., Tinkham and Clarke 1972, Tinkham 1972, Schmid and Schön 1975, Artemenko et al. 1978, also the review by Artemenko and Volkov 1979). The important point here is that this nonequilibrium, just as any other nonequilibrium, has a characteristic relaxation time, τ_Q (Tinkham and Clarke 1972, Tinkham 1972). Due to the quasiparticle diffusion, the nonequilibrium created in some place of a superconductor is transferred to other places and decays with a characteristic diffusion length $l_E = \sqrt{D\tau_Q}$, where D is the diffusion coefficient. The length l_E is the relaxation length of branch imbalance, i.e of Φ, in case this nonequilibrium does not depend on time (i.e., is maintained by external sources). This length is known as the electric field penetration depth. since $\boldsymbol{E} = -\nabla\Phi$ in the static case. The relaxation process of the difference $\mu_p - \mu_e$ occurs by means of interaction of excitations with the condensate through phonons (see, e.g., Artemenko and Volkov 1979) and that is why the relaxation time, τ_Q, contains the long electron-phonon collision time $\tau_{ph} \sim T_D^2\, \hbar/T^3$ where T_D is the Debye temperature. As a result, the electric field penetration depth appears to be quite large. Calculations of the length l_E near the critical temperature (Schmid and Schön 1975, Artemenko et al. 1978) yield $l_E = (4DT\tau_{ph}/\pi\Delta)^{1,2}$; this considerably exceeds the coherence length $\check{\zeta}(T)$.

Now we can write down the equation for $\bar{\Phi}$ in the form

$$\hat{c}^{\hat{2}}\bar{\Phi}=\frac{1}{l_E^2}\bar{\Phi} \tag{27}$$

The simplest approximation is to consider l_E independent of x. The solution of eq. (27) is then

$$\bar{\Phi}=C\sinh\left(\frac{x-x_1}{l_{\mathrm{E}}}\right)$$

where C is a constant and x is the point where $\bar{\Phi}=0$. We assume for simplicity that the ends of the superconducting channel are connected with the bulk superconducting "banks" which are in equilibrium so that $x=x_1$ corresponds to the end of the channel. From eq. (27) we get

$$j-j_{\mathrm{s}}(x)=-\frac{\sigma}{l_{\mathrm{E}}}C\cosh\left(\frac{x-x_1}{l_{\mathrm{E}}}\right)$$

Let us suppose that the sample has a finite length and there is only one PSC in it, at the point $x=x_0$. The potential drop from x to the PSC is

$$\bar{\Phi}_1=C\sinh\left(\frac{x_0-x_1}{l_{\mathrm{E}}}\right)$$

Adding here the potential drop $\bar{\Phi}_2$ from the point x_0 to the point x_2 where $\bar{\Phi}=0$ (the other end of the channel) we get

$$\bar{V}=\bar{\Phi}_1+\bar{\Phi}_2=\frac{l_{\mathrm{E}}}{\sigma}\left[\tanh\left(\frac{x_0-x_1}{l_{\mathrm{E}}}\right)+\tanh\left(\frac{x_2-x_0}{l_{\mathrm{E}}}\right)\right]\left(\mathrm{j}-\bar{\mathrm{j}}_{\mathrm{s}}\left(\mathrm{x}_0\right)\right). \tag{28}$$

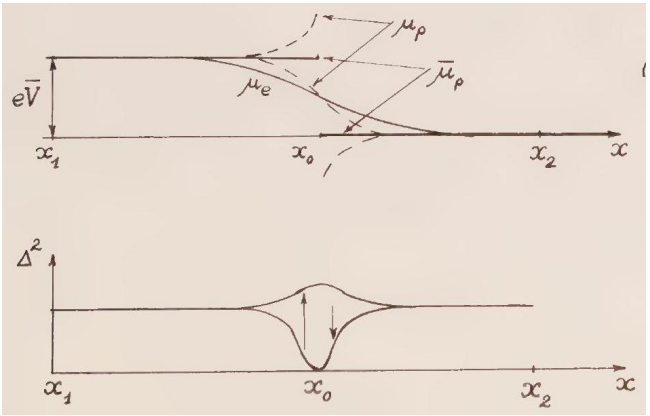


Fig. 8. The behavior of (a) the potentials μ_{p} and μ_{e} and (b) the order parameter Δ in the SBT model. The bars indicate time-averaged values.}

(a)
(b)

If $|x_0-x_1|, |v_2-x_0| \gg l_{\mathrm{E}}$ then $\bar{v}=\frac{2l_{\mathrm{E}}}{\sigma}\left(j-\bar{j}_{\mathrm{s}}\left(x_0\right)\right)$, and the differential resistivity for one PSC is

$$\rho_{\mathrm{d}}=2l_{\mathrm{E}}/\sigma$$

The voltage $\bar{V}$ is the difference between the time-averaged chemical potentials of Cooper pairs to the right and to the left of the PSC. The schematic behavior of the potentials and of the order parameter in the SBT-model is shown in fig. 8. The fine experiment by Dolan and Jackel (1977) verified perfectly the spatial distribution of the potentials shown in fig. 8a.

If a superconducting channel has a uniform structure the first PSC appears in the middle and we get from eq. (28)

$$\bar{\Phi} = -\left(j - j_{\mathrm{s}}\left(x_0\right)\right) \frac{l_{\mathrm{E}}}{\sigma} \sinh\left[\left(x - x_1\right)/l_{\mathrm{E}}\right] / \cosh\left(L_0/2l_{\mathrm{E}}\right)$$

where $L_0 = (x_2 - x_1)$ is the length of the channel. The supercurrent is

$$j_{\mathrm{s}}(x) = j + \sigma \frac{\partial \bar{\Phi}}{\partial x} = j - \left[j - \bar{j}_{\mathrm{s}}\left(x_0\right)\right] \cosh\left(\frac{x - x_1}{l_{\mathrm{E}}}\right) / \cosh\left(\frac{L_0}{2l_{\mathrm{E}}}\right)$$

The supercurrent reaches its maximum at the ends of the channel (connected with the superconducting banks) where it is equal to

$$j_{\mathrm{s}\,\max} = j\left[1 - \operatorname{sech}\left(\frac{L_0}{2l_{\mathrm{E}}}\right)\right] + \bar{j}_{\mathrm{s}}\left(x_0\right) \operatorname{sech}\left(\frac{L_0}{2l_{\mathrm{F}}}\right)$$

The supercurrent cannot exceed the Ginzburg Landau critical current j_c. On the other hand, when the total current is increased the condition $j_{s\,\max} \leqslant j_c$ will not be valid, starting with some value of the total current. In this case the solution with one PSC only becomes impossible. This means that one more PSC should appear in the sample, accompanied by a voltage step in the CVC. When the current is increased further there would appear a third and more PSCs, each formation of a new PSC being accompanied by a corresponding voltage step. We see that the simple SBT-model can also give a qualitative explanation for the voltage steps in the CVC (Tinkham 1979). This question will be discussed in more detail in section 6 on the basis of the microscopic equations.

The simple physical considerations discussed above give a key to the understanding of the nature of the resistive state. They must be compatible, however, with the known dynamic properties of superconductors which follow from the microscopic theory. This problem is treated in other sections of the present review.

25.4 4. The microscopic theory: results of numerical solutions of timedependent superconductivity equations

25.4.1 4.1. Time-dependent superconductivity equations

The formation of PSCs is an essentially dynamic process and should be described by time-dependent superconductivity equations. Unfortunately, a system of time-dependent equations for superconductors is in general very complicated. It contains, in addition to equations for the superconducting variables Δ, Q and Φ, generalized kinetic equations for "distribution functions" of excitations (see, e.g., Larkin and Ovchinnikov 1985). To get a closed set of equations for $\Delta, \boldsymbol{Q}$ and Φ is possible only in some special cases. We write down here dynamic equations which can be derived from the microscopic theory if all variations in the quantities are sufficiently slow in space and time. We require that $Dk^2, \omega \ll \tau_{\mathrm{ph}}^{-1}$ where D is the diffusion coefficient, τ_{ph} is the electron-phonon relaxation time, and ω and k are the characteristic frequency and wavevector of the problem, respectively.* In spite of these restrictions the equations which we shall use here have a sufficiently general form and are valid in a quite reasonable temperature range, from the experimental point of view. These equations have been obtained in the most

general case by Kramer and Watts-Tobin (1978a) and by Watts-Tobin et al. (1981) (see also Golub 1976 and Schön and Ambegaokar 1979). They are as follows

$$-\frac{\pi}{8T}\left(4\tau_{\rm ph}^2A^2+1\right)^{1/2}\frac{\partial\Delta}{it}+\frac{\pi D}{8T}\left(\nabla^2\Lambda-\frac{4e^2}{c^2}Q^2\Lambda\right) \tag{29}$$
$$+\frac{T_c-T}{T_c}\Delta-\frac{7\zeta(3)\Delta^3}{8\pi^2T^2}=0$$

$$\left(4\tau_{\rm ph}^2\Delta^2+1\right)^{-1/2}\Delta^2\Phi+\frac{D}{c}\,\mathrm{div}\left(\Delta^2Q\right)=0 \tag{30}$$

$$j=-\sigma\left(\frac{1}{c}\frac{\partial Q}{\partial t}+\nabla\Phi\right)-\frac{\pi\sigma\Lambda^2Q}{2cT} \tag{31}$$

One can easily get from eq. (31) and the electroneutrality condition $\mathrm{div}\, j=0$, that

$$D\nabla^2\Phi+\frac{D}{c}\,\mathrm{div}\,\frac{\partial\boldsymbol{Q}}{\partial t}=\frac{\pi}{2T}\frac{\Lambda^2\Phi}{\left(4\tau_{\rm ph}^2\Delta^2+1\right)^{1/2}} \tag{32}$$

Equation (32) describes the branch imbalance relaxation mentioned above.
When Δ is constant, it determines the penetration depth

$$l_{\rm E}=\left(\frac{2DT}{\pi\Delta^2}\right)^{1/2}\left(4\tau_{\rm ph}^2\Delta^2+1\right)^{1/4}$$

for a d.c. electric field.
In the gapless case $\tau_{\rm ph}\Delta\ll 1$, eqs. (29)-(32) transform into the timedependent Ginzburg-Landau equations (TDGL) (Abrahams and Tsuneto 1966, Schmid 1966). In the opposite case $\Delta\tau_{\rm ph}\gg 1$, eq. (29) coincides with the dynamic equation for a superconductor with a gap, which has been obtained first by Gor'kov and Eliashberg (1969), and eq. (32) defines the electric field penetration depth

$$l_{\rm E}=\left(D\tau_{\rm ph}\frac{4T}{\pi\Delta}\right)^{1/2} \tag{33}$$

which coincides with the results of Schmid and Schön (1975) and Artemenko et al. (1978).
We can see from these equations that the characteristic frequency scale is of the order of

$$\omega_0=\frac{\pi\Delta_{\rm GL}^2}{2T}, \tag{34}$$

where

$$\Lambda_{\rm GL}=\left[\frac{8\pi^2T\left(T_{\rm c}-T\right)}{7\zeta(3)}\right]^{1/2} \tag{35}$$

is the equilibrium order parameter. The characteristic scale for spatial variations of Δ is the coherence length

$$\xi(T)=\left[\frac{\pi D}{8\left(T_c-T\right)}\right]^{1/2} \tag{36}$$

0

- From now on we put $\hbar=1$.

The ratio $l_{\rm E}/\xi(T)$ is of the order of $\left(\Delta^2\tau_{\rm ph}^2+1\right)^{1/4}$ and is always larger than unity. Equations (29) (32), are, therefore, valid in the temperature range $1-T_1T_{\rm c}\ll(\tau_{\rm ph}T_{\rm c})^{-1}$. We shall see later, however, that the Josephson frequency of oscillations in the resistive state is larger than the ω_0 from eq. (34) so that the actual temperature range of validity of eqs. (29)-(32) will be somewhat narrower.

It will be convenient to use dimensionless variables. We shall measure distances in $\xi(T)$, the order parameter in $\Delta_{\rm GL}$, frequencies in ω_0, and currents in units of $\sigma\omega/2e\xi$. In the new units the potentials are $\Phi=\varphi+(\partial\chi/\partial t)$, $Q=A_x-(\partial\chi/\partial x)$ and the equations take the form

$$-u\left(\frac{\Delta^2}{\Gamma^2}+1\right)^{1,2}\frac{\lambda A}{\partial t}+\frac{\hat{\imath}^2\Delta}{\partial x^2}+\left(1-\Delta^2-Q^2\right)\Delta=0, \tag{37}$$

$$u\Delta^2\left(\frac{\Delta^2}{\Gamma^2}+1\right)^{-1/2}\Phi+\frac{\partial\left(\Delta^2Q\right)}{\partial x}=0 \tag{38}$$

$$j=-\frac{\partial Q}{\partial t}-\frac{\partial\Phi}{\partial x}-\Delta^2Q \tag{39}$$

$$\frac{\partial^2\Phi}{\partial x^2}+\frac{\partial^2 Q}{\partial x\partial t}=u\Delta^2\left(\frac{\Delta^2}{\Gamma^2}+1\right)^{-1/2}\Phi. \tag{40}$$

Here Γ is the pair-breaking term

$$\Gamma=(2\tau_{\rm ph}A_{\rm GL})^{-1}=\frac{\pi}{8\sqrt{u}\,(\tau_{\rm ph}T_{\rm c})\,(1-T/T_{\rm c})^{1/2}}. \tag{41}$$

The coefficient $u=\pi^4,14\zeta(3)=5.79$. The electric field penetration depth in the new units is, from eq. (40),

$$l_{\rm E}=\left(\frac{\Delta^2}{\Gamma^2}+1\right)^{1/4}/u^{1/2}\Delta,$$

and for $\Gamma\ll1$ it will be

$$l_{\rm E}=(u\Gamma\Delta)^{-1/2}. \tag{42}$$

The equations (29)-(33) or (37)-(40) form the basis for our analysis of the resistive state.

25.4.2 4.2. Numerical results

We have said previously that phase slip processes have essential nonlinear nature so it is very difficult to obtain a mathematically exact analytical solution even for the comparatively simple time-dependent equations (29)(32), and such a solution is not yet found. Numerical methods of solving these equations can be very helpful here.

The first results in this line have been obtained by Kramer and Baratoff (1977). They investigated the TDGL equations which are valid in case of gapless superconductivity. In terms of eqs. (37)-(40) this corresponds to the limit $\Gamma\gg1$, when the lack of a gap in the energy spectrum is due to strong electron-phonon interaction:

$$-u\frac{\partial\Delta}{\partial t}+\frac{\partial^2\Delta}{\partial x^2}+\left(1-\Delta^2-Q^2\right)\Delta=0 \tag{43}$$

$$u\Delta^2\Phi+\frac{\partial\left(\Delta^2Q\right)}{\partial x}=0 \tag{44}$$

$$j=-\frac{\partial Q}{\partial t}-\frac{\partial\Phi}{\partial x}-\Delta^2Q \tag{45}$$

$$\frac{\partial^2 \Phi}{\partial x^2} + \frac{\partial^2 Q}{\partial x \partial t} = u\Delta^2 \Phi. \tag{46}$$

The system of equations (43)-(46) can be represented in a complex form if one introduces the complex order parameter $\psi = \Delta \exp(\mathrm{i}\chi)$. We can ignore the magnetic field produced by a current since the lateral dimensions of the sample are small, and put $A = 0$. Then we have

$$\begin{aligned} &- u\left(\frac{\partial}{\partial t} + \mathrm{i}\phi\right)\psi + \frac{\partial^2 \psi}{\partial x^2} + \left(1 - |\psi|^2\right)\psi = 0, \\ &j = -\frac{\partial \phi}{\partial x} + \frac{1}{2\mathrm{i}}\left(\psi^* \frac{\partial \psi}{\partial x} - \psi \frac{\partial \psi^*}{\partial x}\right). \end{aligned} \tag{48}$$

Similar equations appear for gapless superconductors with large concentrations of magnetic impurities (Gor'kov and Eliashberg 1968), one has to put $u = 12$ in the latter case. The TDGL equations (47), (48) differ from the usual Ginzburg-Landau equations (14), (15) by the term with the time derivative in the gauge invariant form in eq. (47) and by the additional term with the normal current in eq. (48).

Kramer and Baratoff (1977) solved eqs. (47), (48) for two values of the parameter u : $u = 5.79$ and $u = 12$; they obtained the following results:
(1) When the current is less than some value j_1 ($j_1 = 0.326$ for $u = 5.79$ and $j_1 = 0.284$ for $u = 12$) perturbations with respect to the purely superconducting state decay, and the superconductor returns to a uniform current-carrying state with the order parameter from eq. (22). Note that in this case $j_1 < j_c$, where $j_c = (2/3\sqrt{3}) = 0.385$ is the Ginzburg-Landau critical current.
(2) When the current is larger than a threshold value j_2 (where $j_2 = 0.335$ for $u = 5.79$ and $j_2 = 0.291$ for $u = 12$) the superconducting current-carrying state transforms into an expanding domain of the normal phase and finally disappears. Thus, the superconducting state appears to be unstable for $j > j_2$. The threshold current j_2 coincides with the stability limit of the normal-superconducting interface studied by Likharev (1974).
(3) In the interval between j_1 and j_2 there exists a solution which corresponds to phase slippage. This solution behaves as follows. The channel remains superconducting over its length, but at some point local oscillations of the order parameter Δ take place. When Δ turns to zero the phase χ experiences a jump of 2π. When the current approaches j_1 the oscillation period tends to infinity and the solution transforms into the Langer and Ambegaokar solution (20) asymptotically as $t \to \pm x$. The amplitude of oscillations decreases with increasing current. The Kramer and Baratoff solution for $u = 5.79$ and $j = j_1$ is shown in fig. 9.

These results were the first direct verification of the existence of a solution with phase slippage and have given evidence for the existence of a limiting

cycle with oscillations of the required type for a system described by eqs. (47), (48) or eqs. (43)-(45).

Equations (43)-(45) were also investigated more recently by Ivlev et al. (1980a,b). They use the gapless equations for modelling the processes in superconductors with a gap in the energy spectrum. The main idea was as follows. When there is a gap (i.e. when $\Gamma \ll 1$) the electric field penetration depth (42) is large: $1_E \sim \Gamma^{-1/2} \gg 1$. This situation can be simulated in terms of eqs. (44) and (46) by giving a small value to the parameter u : since l_{E} in eq. (46) is proportional to $u^{-1/2}$ this will ensure $l_{\mathrm{E}} \sim u^{-1/2} \gg 1$. Therefore, by means of the simplest TDGL equations (43)-(46), it turns out that it is possible to describe the most important feature (with respect to the resistive state) of real superconductors (i.e., superconductors with a gap), namely, the large value of the electric field penetration depth $l_E/\xi \gg 1$.

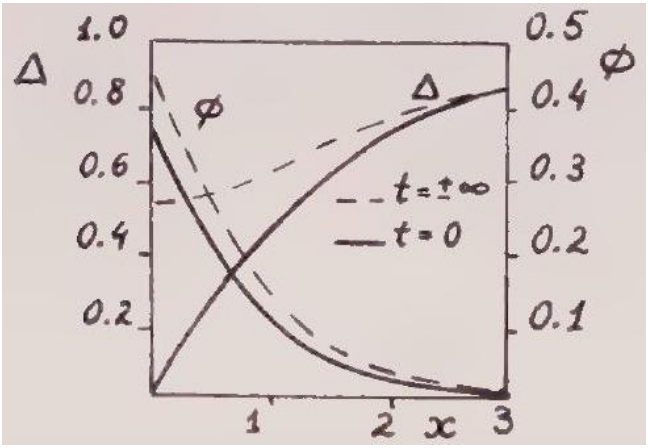


Fig. 9. The behavior of Δ and $\mu_{\mathrm{e
}}$ at different times according to numerical computations by Kramer and Baratoff (1977) for the TDGL equations. The parameters are $u = 5.79$ and $j = j_1 = 0.326$.}

Ivlev et al. (1980a,b) solved eqs. (43)-(46) numerically with $u = 0.01$. The total length of the channel was divided into equal segments with length L and the equations were solved on one segment $0 \leqslant x \leqslant L$ with $L = 40$. The boundary conditions $\hat{c}\Delta^2/\hat{r}x = 0$ and $\Phi = \phi + (\partial\chi/\partial t) = 0$ were imposed, which follow from the periodicity of the structure with period L and from the symmetry of the problem with respect to the points $x = 0, L$ taking account for the even parity of A and j_ς and the odd parity of Φ. The length L represents, therefore, the distance between the neighboring PSCs which form a periodic structure along the channel. The solution describing the oscillations in A is shown in fig. 10.

These results have one important feature: the oscillations of the order parameter are localized in a rather narrow region around a PSC while the variables A, Q and Φ are practically independent of time for the greatest part of the distance between two PSCs. The reasons why this is so will be discussed in the next section.

The numerical investigations were then continued by Kramer and WattsTobin (1978a,b) and by Watts-Tobin et al. (1981) directly for eqs. (37)-(40)

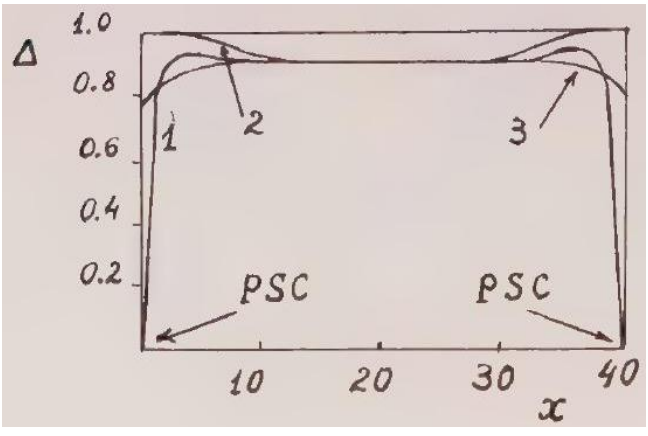


Fig. 10. The coordinate dependence of Δ at different times according to numerical results of Ivlev et al. (180a,b) for TDGL equations. The parameters are $u = 0.01$ and $j = 0.4$. The curves 1,2 , and 3 are for $t = 0, t = 0.053$, and $t = 2.188$, respectively. The period of oscillation $t_{0
=2.52$.}

with different values of the parameter Γ. It was found that the range of currents where the solution with phase slippage exists is broadened with decreasing Γ, the current j_2 being proportional to Γ^{-1} at small Γ. The oscillations of the order parameter occur qualitatively in the same way as in the case of the simple TDGL equations. The results of Watts-Tobin et al. (1981) for Δ, with $L = 6, j = 0.4$ and different values of Γ, are represented in fig. 11. Watts-Tobin et al. mentioned the fact that, with decreasing in Γ, the curves $\Delta(x,t)$ approach the curve which corresponds to the steady-state dependence of the order parameter near the boundary with a normal phase, i.e., the curve, satisfying the boundary condition $\Delta(x=0)=0$. The explanation for this will be given in section 5.2.

The described numerical results are of great importance. They prove first of all the very fact of the existence of solutions which correspond to phase slippage and verify thereby the validity of the general understanding of the nature of the resistive state. The numerical methods, however, cannot give complete information on the resistive state properties and how they depend on the various sample parameters and the real experimental conditions. Therefore, analytical solutions of time-dependent equations are needed since only they can answer these questions. The recent progress in the microscopic theory of the resistive state along this line will be discussed in the following sections.

25.5 5. The microscopic theory: results of analytical solutions of timedependent superconductivity equations

25.5.1 5.1. The stability analysis of the current-carrying normal state

In this section we investigate the stability of the current-carrying normal state with respect to infinitely small fluctuations of the order parameter. When the

order parameter is infinitely small we have always the gapless situation $\Delta\tau_{\rm ph} < 1$, so that a superconductor will be described by eqs. (47) and (48). The linearized eqs. (47) and (48) have the form

$$u\frac{\partial\psi}{\partial t} - \mathrm{i}ujx\psi - \frac{\partial^2\psi}{\partial x^2} - \psi = 0. \tag{49}$$

The solution of this equation can be written in the form (Ivlev et al. 1980b)

$$\psi(x,t) = \left(\frac{u}{4\pi t}\right)^{1/2} \exp\left(\frac{t}{u} - \frac{\mathrm{j}^2\mathrm{t}^3}{12u}\right) \int_{-\alpha}^{\infty} \mathrm{d}y\psi(y,0) \exp\left\{\begin{array}{c}\mathrm{i}jt\\ 2\end{array}(x+y) - \frac{u(x+y)^2}{4t}\right\}. \tag{50}$$

The term t^3 in the exponent accounts for the acceleration of the Cooper pairs
by an electric field, and results in the destruction of superconductivity. This leads to the conclusion that, according to Gor'kov (1970) and Kulik (1970), the normal state is stable with respect to infinitely small fluctuations.

This conclusion, however, does not apply to fluctuations with a finite magnitude. The point is that the behavior of a superconductor depends significantly on how an electric field is created in it. In a circuit with a given voltage the normal state is stable at any electric field, independent of how small it is. In a circuit with a given current, however, expulsion of the electric field from the superconductor may take place either totally or partially, the result being either the pure superconducting or the resistive state. This can occur if the order parameter reaches a value of the order of unity in some place of a superconducting channel. This can be spoken of as a nucleus of the superconducting phase in the normal state. This nucleus will either grow or decrease, depending on the current, and the normal state will be

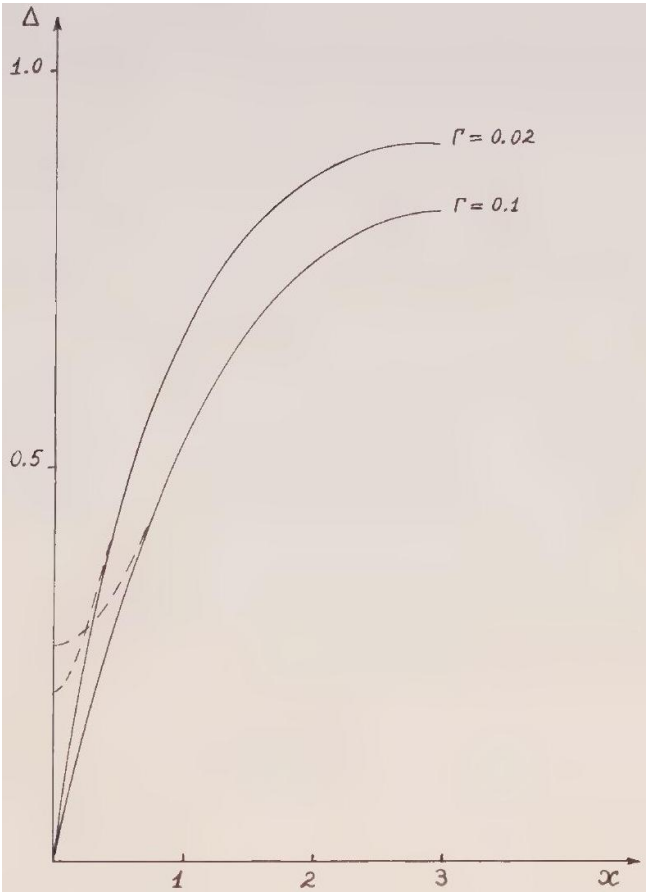


Fig. 11. The coordinate dependence of Δ for different values of Γ according to Watts-Tobin et al. (1981). The full lines correspond to minima of $\Delta(x = 0)$ and the dashed lines to maxima of $\Delta(x = 0)$.

either unstable or stable. Interesting numerical results concerning the stability of both the normal and the superconducting state have been obtained by WattsTobin et al. (1981).

Suppose that a fluctuation of Δ appears with amplitude.$_1$ and size larger than ξ. Then, as can be seen from eq. (50), it will evolve according to

$$\Delta \simeq \Delta_0 \exp\left(\frac{t}{u} - \frac{j^2 t^3}{3}\right)$$

passing through a maximum $A_{\max} = A_0 \exp(2, 3uj)$. Thus, if the amplitude of an initial fluctuation is larger than or of the order of

$$\Delta_c = \exp\left(-\frac{2}{3uj}\right) \tag{51}$$

it can reach a value of the order of unity during its further evolution, after which the system can go either into a uniform current-carrying superconducting state locally stable at $j < j_c$, or into the resistive state.

From eq. (50) one can draw an important conclusion about the static model of the resistive state discussed in section 2 . In the static model the order parameter is equal to zero at some points in the sample and $\mu_p = \frac{1}{2}(\hat{c}\chi, \hat{c}t)$ experiences jumps at these points (see fig. 3). Such a solution for eqs. (47) and (48) has been obtained by Fink (1973a, b) and Fink and Poulsen (1974a, b, 1975). We examine now, using eq. (50), what will happen to this static solution if one does not impose the special condition $\psi(0, t) = 0$. Near the point $x = 0$ and at the initial

instant of time, $\Delta = \alpha|x| \ll 1$. We find from eq. (44) that $Q = \frac{1}{3}u|\Phi(x = \pm 0)||x|$. Therefore, the order parameter near a static PSC should have the form

$$\psi_{\rm st}(x,t) = \alpha|x| \exp\left\{ \mathrm{i}|\Phi(x=\pm 0)| \left(t - \frac{x^2 u}{6} \right) \operatorname{sgn} x \right\} \tag{52}$$

If we now compare expression (52) with the solution (50) of the timedependent equation (49) when $\Delta \ll 1$, we can see that $\psi_{\rm st}$ from eq. (52) is not a solution of eq. (49), actually, and that the true solution of eq. (49), with the initial condition $\Delta = \alpha|x|$, gives $|\psi(0,t)| = (t\alpha/u)^{1/2}$, which is nonzero at any time $t \neq 0$. This means that a PSC cannot exist as a static object since there is no way to fulfil the condition $\psi(0,t) = 0$, and also that the solution of Fink and Poulsen is unstable near a PSC. This conclusion is supported also by the numerical results of Ivlev et al. (1980a,b). Indeed, curve 1 in fig. 10 corresponds to the solution of Fink and Poulsen. In this case, however, there was no condition $\Delta = 0$ imposed at $x = 0, L$ and the curve does not pass through zero at $x = 0, L$ at subsequent moments of time but oscillates from zero to unity.

25.5.2 5.2. The structure of the phase slip centers

We consider below the time-dependent equations (37)-(42) in the most interesting case, from both the experimental and the theoretical point of view, when there is a gap in the energy spectrum of the superconductor, $\Gamma \ll 1$, which corresponds to temperatures $(T_{\rm c}\tau_{\rm ph})^{-2} \ll 1 - T/T_{\rm c}$. We remind ourselves that the electric field penetration depth is large in this case: $l_E \sim \Gamma^{-1/2} \gg 1$. The following analysis will be based on the results of Ivlev et al. (1980a,b) and Ivlev and Kopnin (1981a).

According to the quantization rule (7) the time- and space-averaged electric field is related to the periods of the PSC structure. In the dimensionless units of section 4.1 this relation has the form

$$\langle E \rangle = \frac{2\pi n}{L t_0}. \tag{53}$$

The integer n indicates how many times 2π the phase looses after formation of each PSC. We choose $n = 1$ as is the case for the ordinary vortices in type-II superconductors.

When a uniform sample (without any defects) is considered, it is clear that the only mechanism which determines the distance between PSCs is the relaxation of the potential Φ, i.e., the relaxation of the imbalance between the chemical potentials of the Cooper pairs, $\mu_{\rm p}$. and quasiparticles, $\mu_{\rm c}$ (the imbalance being created during phase slippages). This means that the distance should be of the order of the electric field penetration depth $|_1$. If the current through the sample is not too large, i.e., $j \sim \sigma E \sim j_{\rm c}(j \sim 1$ in our units) the period of oscillations t_0 should be of the order of $L^{-1} \sim \Gamma^{1/2}$ according to eq. (53).

When $\Gamma \ll 1$ one can write eqs. (38) and (39) in the form

$$j = -\frac{\partial Q}{\partial t} + \frac{1}{u\Gamma}\frac{\partial}{\partial x}\left[\frac{1}{\Delta}\frac{\partial}{\partial x}\left(\Delta^2 Q\right) \right] - \Delta^2 Q. \tag{54}$$

Estimation of the first term in the right-hand side of eq. (54) gives $Q t_0^{-1} \sim Q_{\sim}\Gamma^{-1/2}$, where $Q_{\sim}$ is the oscillating part of $Q : Q = Q + Q_{\sim}$, and the bar indicates averaging over time. The second and the third term are of the order Q at distances of order $I_E \sim \Gamma^{-1/2}$. It follows that the oscillating part of Q should be small, $Q_{\sim} \sim \Gamma^{1/2}\bar{Q}$ so that $Q \simeq \bar{Q}$. The oscillating part $Q_{\sim}$ will be of the same order as $\bar{Q}$ only at shorter distances from a PSC where the first and the second term in eq. (54) will be of the same order, i.e., at distances from a PSC of the order of $x_1 = \Gamma^{-1/4} \ll L$. In ordinary units we have $x_1 = [\xi(T) l_E]^{1/2}$. It is important that the

oscillations of the order parameter remain small at such distances. This can be seen from the estimation of the relevant terms in eq. (37), which gives

$$\frac{\Delta}{\Gamma}\frac{\partial\Delta}{\partial t} \sim \Delta$$

at distances $x \gtrsim 1$. Hence, the oscillating part of the order parameter $\Delta_\sim \sim \Gamma t_0 \sim \Gamma^{3/2}$. This swing of oscillations in Δ is not sufficient to drive the order parameter to zero in the region where $\Delta \sim 1$. This means that oscillations in Δ could result in Δ going to zero at some moments in time only in the region where $\bar{A}$ is small: $\bar{\Delta} \ll 1$. This region of very small Δ determines the characteristic size of a PSC, i.e., of that region of the sample where the order parameter oscillates strongly. We designate the size of this region as x_2. Since in this region $\Delta \sim x_2(\partial\Delta/\partial x)$ and $(\partial\Delta/\partial x) \sim 1$, the size x_2 is of order Δ, therefore $x_2 \ll 1$.

We see that all the variables A, Q, and Φ oscillate only slightly at distances far enough from a PSC: $x \gg x_1$. Note that x_1 is still much shorter than the distance L between two neighboring PSCs. At distances $x_1 \ll x \ll L$ where all variables are practically static one can use eqs. (37)-(39) in the form

$$\frac{\partial^2\Delta}{\partial x^2} + \left(1 - \Delta^2 - \frac{j_\mathrm{s}^2}{\Delta^4}\right)\Delta = 0 \tag{55}$$

$$j = -\frac{\hat{c}\Phi}{\partial x} + J_\mathrm{s} \tag{56}$$

$$u\Gamma\Delta\Phi = \frac{\hat{\partial} j_\mathrm{s}}{\partial x} \tag{57}$$

where one has averaged over time. In these equations the supercurrent $j_\mathrm{s} = -\Delta^2 Q$ is introduced. The second-derivative term $\lambda^2\Delta/\lambda x^2$ can be omitted in eq. (55) at distances $x \gg 1$; so

$$j_\mathrm{s} = \Delta^2\sqrt{1-\Delta^2}. \tag{58}$$

Equations (56)-(58) can be integrated easily:

$$\Phi^2 = \frac{2}{u\Gamma}\int_j^{s_{\mathrm{s}0}} \frac{(j - j_\mathrm{s})\,\mathrm{d}j_\mathrm{s}}{\Delta\,(j_\mathrm{s})} = \frac{2}{u\Gamma}\int_{\Delta_0}^{\Delta} \frac{\left(j - \Delta^2\sqrt{1-\Delta^2}\right)(3\Delta^2-2)\,\mathrm{d}\Delta}{\sqrt{1-\Delta^2}} \tag{59}$$

$$\frac{L}{2} - x = \frac{1}{u\Gamma}\int_{j_\mathrm{s}}^{j_{\mathrm{s}0}} \frac{\mathrm{d}j_\mathrm{s}}{\Delta\,(j_\mathrm{s})\,\Phi\,(j_\mathrm{s})} = \frac{1}{u\Gamma}\int_{\Delta_0}^{1} \frac{(3\Delta^2-2)\,\mathrm{d}\Delta}{\sqrt{1-\Delta^2}\Phi(\Delta)} \tag{60}$$

Here Δ_0 and j_{s0} are related by eq. (58) and represent the values of Δ and j_s midway between two PSCs. The integration limits are chosen on the basis of the fact that the potential Φ is equal to zero at the point $x = \frac{1}{2}L$ due to the symmetry of the structure with respect to the midpoint between two PSCs and due to the odd parity of Φ.

Thus, $j_{\mathrm{s}0}$ is the maximum value of the supercurrent which is achieved in the midpoint between two PSCs. The integration in eqs. (59), (60) should be carried out on the branch of the function $\Delta\,(j_s)$ which is thermodynamically stable, i.e., corresponds to $0 \leqslant j_\mathrm{s} \leqslant j_\mathrm{c}$ and $1 \geqslant \Delta \geqslant \sqrt{\frac{2}{3}}$ (see fig. 12).

Now we consider the region closely around a PSC: $x \ll L \sim \Gamma^{-1/2}$. Estimating the derivative $\hat{c}j_\mathrm{s}/\partial x$ according to eq. (38) we have $\hat{\lambda}j_\mathrm{s}/\hat{\lambda}x \sim I\Phi$, and

$$(\partial j_\mathrm{s}/\partial x) \sim \Gamma^{1/2} \tag{61}$$

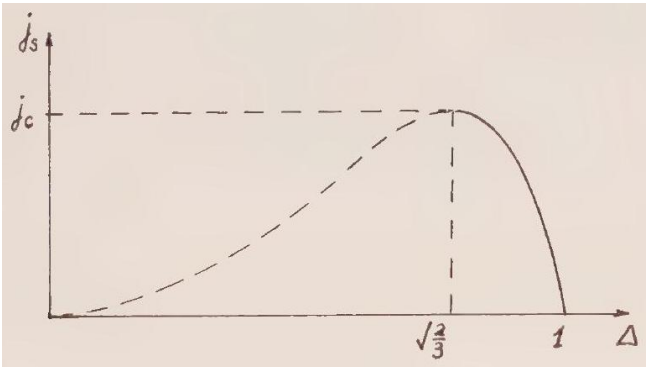


Fig. 12. The function $j_{s (1)$. The thermodynamically stable branch is shown by the solid curve and the unstable one is shown by the dashed curve.}

since $\Phi = \pi t_0{}^1 \sim \Gamma^{-1/2}$. Due to eq. (61) one can consider j_s independent of x at distances $x \ll \Gamma^{-1/2}$. After averaging eq. (37) over time one can write it in the region of static Δ, i.e., at $x \gg x_2$, in the form

$$\frac{\partial^2 \Delta}{\partial x^2} + \left(1 - \Delta^2 - \frac{\overline{j_s^2}}{\Delta^4}\right)\Delta = 0 \tag{62}$$

With the condition (61), the solution of eq. (62) can be obtained similarly to the LA solution (20) (see section 3.1) where the potential will be

$$U(A) = \Delta^2 - \frac{1}{2}\Delta^4 + \frac{\overline{j_s^2}}{\Delta^2}$$

(see figs. 6, 7). This solution has to match at $x \geqslant 1$ with solution (60) which has a very small derivative $\hat{C}A_1\hat{C}x \sim \Gamma^{1/2}$. Extending solution (20) to $x \gg 1$ with zero derivative corresponds to $C = U_{\max}$. Thus, the proper solution has the form

$$x = \int_{\Delta_2}^{\Delta} \frac{\mathrm{d}\Delta}{\sqrt{U_{\max} - U(\Delta)}} \tag{63}$$

Here $x = 0$ corresponds to the minimal value $\Delta = A_2$.
As has been shown previously, the order parameter has to reduce to very small values when approaching a PSC within the static region of A. This corresponds to $\Delta_2 \ll 1$. A small value of Δ_2 is possible only when $j_s^2 \ll 1$. It is clear from the potential $U(A)$ that $A_2 = \sqrt{2\overline{j_c^2}}$. In this case eq. (63) reduces approximately to

$$\Delta = \tanh(|x|/\sqrt{2}) \tag{64}$$

which holds at $\Delta \gg \sqrt{\overline{j_s^2}}$.
The value Δ_2 is, by order of magnitude, the average Δ in the oscillation region. Since $\Delta \sim j_s$ in this region the value of Δ can be easily estimated from eq. (37). Since $Q \sim j_s/\Delta^2 \sim \Delta^{-1}$ we have

$$\frac{\Delta}{\Gamma}\frac{\partial \Delta}{\partial t} \sim \frac{1}{\Lambda}$$

and, hence, $A \sim (\Gamma t_0)^{1/3} \sim \Gamma^{1/2}$. For the size of the oscillation region we find $x_2 \sim \Gamma^{1/2}$. In ordinary units this gives

$$x_2 = \xi(T)\sqrt{\Gamma}.$$

It is interesting to follow the behavior of the potential Φ in the dynamic region. The time-averaged potential Φ does not practically vary at distances small compared with l_E. This is seen from eq. (38) averaged over time:

$$\frac{r^2\bar{\Phi}}{r^2} = u\Gamma \cdot 1\bar{\Phi}$$

(if $x \geqslant x_2$). Thus the change in Φ is small at distances $x \ll \Gamma^{-12}$ and Φ remains finite when $x \to 0$. Its value $\Phi(x = \pm 0) = \pm\Phi_0$ is given by eq. (59) where one should put $\Delta = 1$ at $x \ll l_E$. On the other hand, the instantaneous values of Φ $(x = 0; t)$ must be zero at any time except for the moments of phase slip, $t = 0$, $t_0, \ldots$, when they go to infinity. This follows from the symmetry of the PSC
structure with respect to the point $x = 0$ and the odd parity of Φ. From eq. (39) one easily concludes that the growth of Φ from zero to values of the order of $\Phi_0 \sim t_0^{-1}$ occurs within the dynamic region $x \sim x_2$.

Thus we obtain the following results:
(1) A phase slip region has a size of the order of $\xi(T)\Gamma^{1/2}$. Here all the variables oscillate strongly. At the moments when $\Delta = 0$ the phase χ experiences jumps of 2π and $\Phi(x = 0)$ goes to infinity. The amplitude of oscillations in Δ is of order $\Delta_{\mathrm{GL}}\sqrt{\Gamma}$.
(2) As one goes away from a PSC the oscillations in Δ decay rapidly and Δ becomes practically independent of time at distances $x \gg x_2 = \zeta(T)\Gamma^{1/2}$. Here $\Phi = \bar{\Phi}$, where $\bar{\Phi}$ is equal to $\bar{\Phi}\,(x \ll l_E) = \Phi_0$ from eq. (59). The behavior of $\Delta(x)$ is given by eq. (64). The order parameter takes its equilibrium value $\Delta = A_{\mathrm{GL}}$ (in dimensionless units $\Delta = 1$) at $x \gtrsim \xi$. The supercurrent oscillates but remains still small so that the whole current is practically due to the normal excitations.
(3) At distances $(\xi l_E)^{1/2} \ll x \sim L$ oscillations of all the quantities are negligible. Here relaxation of $\Phi = (\mu_{\mathrm{p}} - \mu_{\mathrm{e}})/e$ takes place. This kind of inequilibrium is created in a PSC region as a result of phase slips. As the potential Φ and the normal current $j_{\mathrm{n}} = -\sigma(\hat{C}\Phi/\hat{C}x)$ decrease, the supercurrent j_{s} increases and Δ diminishes. The supercurrent j_{s} reaches its maximum at the midpoint between two PSCs.

The behavior of the order parameter Φ and the currents j_{s} and j_{n} is shown in fig. 13. The behavior of the order parameter near PSCs is in good agreement with the results of numerical computations by Watts-Tobin et al. (1981).

At the end of this subsection we outline the temperature range of validity of our results. The Josephson frequency of oscillations ω_{j} is of the order of $(\Delta^2/T)\,\Gamma^{-1/2}$. Since our equations are valid if $\Gamma \ll 1$ and $\omega_{\mathrm{J}} \ll \tau_{\mathrm{ph}}^{-1}$, one has to use temperatures in the interval

$$(\tau_{\mathrm{ph}}T_{\mathrm{c}})^{-2} \ll 1 - T/T_{\mathrm{c}} \ll (\tau_{\mathrm{ph}}T_{\mathrm{c}})^{-6/5}.$$

25.5.3 5.3. The current-voltage characteristic

Having averaged the expression for the electric field $E = -iQ, it - i\Phi/ix$ over time, one obtains $\bar{E} = -\partial\bar{\Phi}/\partial x$. Hence the time- and space-averaged electric field, which will also be designated by E, has the form

$$E = 2\Phi_0/L, \tag{65}$$

where Φ_0 and L are given by eqs. (59) and (60), with the boundary conditions found above: $\Delta = 1$ at $x \ll l_E$. We have for the structure period L from eq. (60)

$$L = \frac{2}{u\Gamma} \int_{\Delta_0}^{1} \frac{(3\Delta^2 - 2)\,\mathrm{d}\Delta}{\sqrt{(1-\Delta^2)\Phi(\Delta)}}, \tag{66}$$

where $\Phi(\Delta)$ is taken from eq. (59). For the current-voltage characteristic

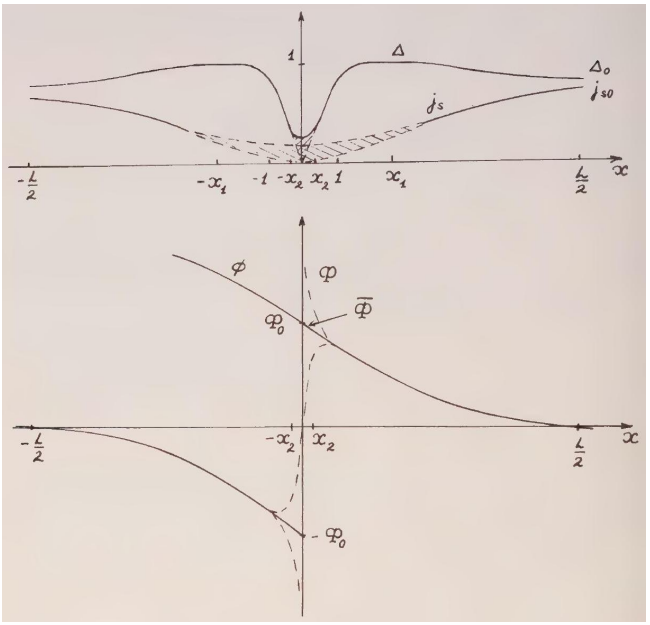


Fig. 13. The behavior of (a) Δ and j_{s, and (b) Φ and $\bar{\Phi}$ in the (solid lines) static and (dashed lines) dynamic regions. The values which Δ and j_s can take during oscillations are shaded. (Ivlev and Kopnin 1981.)}

(CVC) we finally obtain

$$E \int_{\Delta_0}^{1} \frac{(3\Delta^2 - 2)\,\mathrm{d}\Delta}{(1-\Delta^2)^{1/2} f(\Delta;\Delta_0)} = 2f(1;\Delta_0) \tag{67}$$

where

$$f^2(\Delta;\Delta_0) = \int_{\Delta_0}^{\Delta} \frac{\left(j - x^2\sqrt{1-x^2}\right)(3x^2-2)\,\mathrm{d}x}{(1-x^2)^{1/2}} \tag{68}$$

Therefore only a solution of the equations for the potential in the static region is needed to calculate the CVC. At this point, the results of the dynamic theory of the resistive state (Ivlev and Kopnin 1972, 1981a, Ivlev et al. 1976a,b) become istry closes io that of the statuc model developed by Csalark (1974. 1975, 1976a.b, 19-7 (salare et al. (1976). and (salaikes and Shumeikes (1976). One can see from a comparares of fig. 3. zhich illustrates the static model. anth fig 13 that the potentials $\mathcal{I}$ in both cater behave ser; simularly coer aimset the whole distance: between Ps C. except for a narroz regron rear the PSC. In the static model, the formation of a wollage across a PSC, has the came possual nature an in the dynamic theor? and occurs through reiaxatoms of the branch imbalance $\mathcal{L} - 1\mu_0 - \mu_0$) e over distances larger than the coher ence length () new thould note. However, that the results of the statue model of Csalaiks and co-zosters taken as they: samd have one shordermung. The thing is that Csalaiks and cro-mreks integrate "yuators for she protential of the pe of eq. in and 1571 using the thermodynamically unstable branch 11/1 ahan corresponde to $0 - 1-$ fisee fig. 12). Thes soluton cannot exast in a real phyucal outem Theresure, the results of these works have to be corrected accordingly.

Further consideratoons derend on the ratus of the channel iergeth. L. . to the distance. L. methosen PSC. If I, $\sim L$, there is room only for a finite rumber of PSCA in the channel and the behaver)? of the C.VC is determened by the creation, of new Pses ath increasing current. Than problem and be discussed in sation - ffere we cronsider the opposite case. "Lo. In the case the number of P'st. an the channel as large and one can consider theor density to merease amouthly with increasing current. Flquatums 167 and 1641 represent a set of carves deermired by the froe parameter 1_0 for /h. I . These curves are shown in fig. 14. Addumai physical consideratums are necessar; for a proper chooe of the parameter 1. Here one can use the princhple of minimum entropy production iminimum dissupatoral. According to thas principle. a regme with the mununum prossible E should be realized in the system a nen the current is fines. This ersure: the minimum disapation ijE. Thes regme corresponds to the upper curve in fig. 14. characteriad hy 1, = 0.8 wor is $\therefore 0 \to 6.1$. This choice is equisalent to the conditon that ite supercarren thould have the maximum possible :alue. We thall assume that 1 , in aha: follows.

In order to return to ordinar: Lones in ey: iffl and ifil one should reprece E by $\left(2\sigma E 3\sqrt{3} j_c\right)$ and j by $\left(2j3\sqrt{3} j_c\right)$. As a result we get

$$\frac{\sigma E}{h} \int^{1} \frac{(3x^2-2)\,\mathrm{d}x}{|t-x^2|\,\pi|\sqrt{2}|} = 3\sqrt{3} f\left(1 : \sqrt{\frac{2}{3}}\right). \tag{69}$$

The function $f\left(x; \sqrt{\frac{2}{3}}\right)$ is defined by eq. (68).

I wis acparate regors can be distungulshed in the CTr figl Now fig. 141

(1) The initial part, $j - j_c \ll j_c$. The structure period is logarithmically large in.

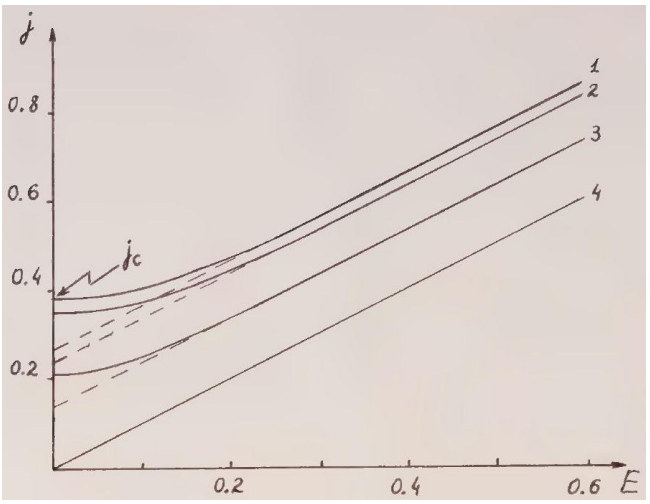


Fig. 14. The CVC calculated according to eqs. (67), (68) with different values of Δ_{0}. The parts of CVCs with excess currents $j_{\mathrm{exc}} = a j_{\mathrm{c}}$ are seen: curve (1) $\Delta_0 = \sqrt{\frac{2}{3}}, a = 0.68$; (2) $\Delta_0 = 0.9, a = 0.61$; (3) $A_0 = 0.975, a = 0.35$; (4) Ohm's law.}

this case:

$$L = 2 l_E \left(\frac{\Delta_{\mathrm{GL}}}{\Delta_0}\right)^{1/2} \ln\left(\frac{C j_{\mathrm{c}}}{j - j_{\mathrm{c}}}\right),$$

where $C \sim 1$, and the CVC has the form

$$j - j_{\mathrm{c}} \simeq j_{\mathrm{c}} \exp\left(-0.91\,(j_{\mathrm{c}}/\sigma E)\right).$$

It has zero slope as $E \to 0$, resulting from the infinite length of the channel.
(2) The region of large currents: $j \gg j_c$. Here the CVC proceeds parallel to Ohm's law: $j = \sigma E + j_{exc}$ with the excess current $j_{exc} = a j_c$, where

$$a = \frac{3^{3/2}}{4}\left[\int_{\sqrt{\frac{2}{3}}}^{1} \frac{x^2\,(3x^2-2)\,\mathrm{d}x}{p\left(x:\sqrt{\frac{2}{3}}\right)}\right] / p\left(1;\sqrt{\frac{2}{3}}\right)$$

and

$$p^2\,(x;x_0) = \int_{x_0}^{x} \frac{3y^2-2}{\sqrt{1-y^2}}\,\mathrm{d}y.$$

The CVC of eq. (69) has been obtained by Ivlev et al. (1980b). They calculated also the CVC for the more general case when the supercurrent j_s influences the branch-imbalance relaxation. As we have said previously only a
solution of the static equations for the potential distribution is needed to calculate the CVC. In the static region the equation for the potential Φ looks like eq. (32) with the difference that its right-hand side contains a factor describing the effect of the supercurrent (Bulyzhenkov and Ivlev 1979):

$$D\nabla^2\Phi = \frac{\pi\Delta}{4T\tau_{ph}} q(z)\Phi$$

where

$$q(z) = 1 + \frac{2z}{\pi}\int_1^\infty \frac{\sqrt{x^2-1}\,\mathrm{d}x}{x\left[\mathrm{x}\sqrt{x^2-1}+z\right]} = \begin{cases} 1 & \text{if} \quad z \ll 1 \\ \sqrt{z} & \text{if} \quad 1 \ll z \ll T^2/\Delta_{GL}^2 \end{cases}$$

and $z = (4De^2, c^2)\,Q^2\tau_{ph}$. In the units of eqs. (34)-(36) this equation can be written in a form similar to eq. (57):

$$\frac{\partial j_s}{\partial x} = u\Gamma\Delta q(z)\Phi, \tag{70}$$

where now $z = 8\,(T_c - T)\,\tau_{ph}Q^2/\pi$. Equations (55), (56) and (70) can be integrated easily. As a result we have $(Q^2 = 1-\Delta^2)$:

$$\Phi^2 = \frac{2}{u\Gamma}\int_{\Delta_0}^{\Delta} \frac{\left(j - \Delta^2\sqrt{1-\Delta^2}\right)(3\Delta^2-2)}{\sqrt{1-\Delta^2}\,q(z)}\mathrm{d}\Delta,$$
$$\frac{1}{2}L - x = \frac{1}{u\Gamma}\int_{\Delta_0}^{\Delta} \frac{(3\Delta^2-2)\,\mathrm{d}\Delta}{\sqrt{(1-\Delta^2)\Phi(\Delta)q(z)}}$$

instead of eqs. (59), (60). The CVC determined by eq. (65) looks like the one considered above and its behavior is qualitatively similar to that in fig. 14.

These results are valid in a wider temperature range:

$$(\tau_{ph}T_c)^{-2} \ll 1 - T/T_c \ll (\tau_{ph}T_c)^{-1/2}$$

It can be seen from the data in table 1 that this temperature range corresponds
to temperatures at which actual experiments are carried out. Therefore, these CVCs allow not only qualitative but even quantitative comparison with experiment.

Table 1
Values of the parameter $\tau_{\mathrm{ph}} k_{\mathrm{B}} T_{\mathrm{c}} / \hbar$ for various superconductors.

Material	$\frac{T_c}{(K)}$	$\frac{\tau_{ph}}{(s)}$	$\tau_{\mathrm{ph}} k_{\mathrm{B}} T_{\mathrm{c}} / \hbar$
Pb	7.2	2×10^{-11}	2×10^{1}
In	3.4	10^{-10}	4×10^{1}
Sn	3.8	3×10^{-10}	10^{2}
Al	1.2	10^{-8}	10^{3}

25.5.4 5.4. The upper boundary of the resistive state

The resistive state of narrow superconducting channels occupies a rather broad region of currents, experimentally (see fig. 1a,b). The lower boundary of this region, as we have seen, is of the order of the critical Ginzburg-Landau current j_c and has the temperature dependence $(T_c - T)^{3/2}$. More difficult is the question of the resistive state's upper boundary, i.e., the lowest current for which deviations from Ohm's law can be observed. Strictly speaking, there should always be deviations from Ohm's law due to fluctuation-induced creation of Cooper pairs in the normal state, the Cooper pairs then being accelerated and destroyed by the electric field (Gorkov 1970, Kulik 1970). These fluctuation corrections should be, however, extremely small for currents as large as those for which deviations are observed, experimentally.

The first attempt to obtain the boundary at which the normal state of a channel transforms into the resistive one was made by Galaiko (1974, 1976, 1977) in the framework of the static model of the resistive state. He studied the nucleation of the superconducting phase on the background of the normal state of a current-carrying channel. According to his results the normal state becomes unstable below some critical current

$$j_2 = \frac{4\sigma\,(T_c - T)}{e} \left(\frac{2\pi T_c}{7\zeta(3) D} \right)^{1/2}. \tag{71}$$

This result, however, has the same shortcoming as the static model itself; it does not account for the inevitable oscillations of the order parameter in the overlapping region of the nuclei of the superconducting phase. As a result of these oscillations, the static equation for the modulus of the order parameter which has been used in obtaining eq. (71) would fail, so eq. (71) seems not to solve the problem of the upper boundary of the resistive state.

Since the normal current-carrying state is stable with respect to infinitely small fluctuations, the resistive state should appear and vanish through a transition of first-order type. This means that, when the current is increased above some critical current j_2, the dynamic resistive state described in section 5.2 should vanish in a jump-like way and the sample should become normal. We estimate here the upper boundary of the dynamic state (Ivlev et al. 1980b). According to eqs. (59) and (66), the structure period decreases with increasing current and is of the order of $L \sim \xi(T)\,(j_c/j\Gamma)^{1/2}$. When the current j is of the order of j_c/Γ the distance between PSCs would be of the order of $\check{\zeta}(T)$.

The order parameter has to be small at PSCs and of the order of unity in the midpoints between PSCs. It is clear that such a solution cannot exist if the distance between PSCs is less than $\check{\zeta}(T)$. We conclude that the resistive state would vanish when the current is larger than

$$j_2 \sim \frac{j_c}{\Gamma} \propto \frac{\sigma T^{1/2} \tau_{\mathrm{ph}}}{e D^{1/2}} (T_c - T)^2 \tag{72}$$

This estimation of the critical current j_2 is in good agreement with the results of numerical

computations by Watts-Tobin et al. (1981).

Joule heating of the sample plays an important role in the destruction of the resistive state. This heating can produce hot-spots in the sample where superconductivity is locally destroyed, these hot spots developing then into purely normal state (Volkov and Kogan 1974). Moreover, Joule heating can cause the destruction of superconductivity merely due to overheating the sample. These effects depend, however, on the conditions of sample cooling and the structural homogeneity of the channel, and we will not consider them here. We note, however, that, even with ideal cooling which keeps the temperature of the crystal lattice of the sample equal to that of the external medium, the electron system will be overheated with respect to phonons. This would result in an effective decrease in T_c, and the superconductivity can vanish completely if the current is large enough. An estimation of such a current can be made if in eq. (29) one takes into account the correction to the distribution function produced by the overheating of electrons. This correction is proportional to $\tau_{\rm ph} D e^2 E^2 \left(\partial^2 f_\varepsilon / \partial \varepsilon^2\right)$, where f_α is the equilibrium distribution function. As a result, eq. (29) will also contain a term

$$\frac{7\zeta(3)\tau_{\rm ph} D e^2 E^2 \Delta}{2\pi^2 T^2}.$$

The critical field E_2 is found from equating this term to $(T_{\rm c} - T)\,\Delta/T$ which gives

$$j_2 = \frac{\sigma\pi}{e}\left[\frac{2T_{\rm c}\,(T_{\rm c}-T)}{7\zeta(3)\tau_{\rm ph} D}\right]^{1/2} \tag{73}$$

This result has been obtained by Galaiko (1976b, 1977) and is valid at temperatures $1 - T/T_{\rm c} \gg (\tau_{\rm ph} T_{\rm c})^{-1}$. At higher temperatures, $1 - T/T_{\rm c} \ll (\tau_{\rm ph} T_{\rm c})^{-1}$, the role of heating decreases, and the current j_2 will be determined by eq. (72).

It should be noted that the described results concerning j_2 are mainly qualitative, and therefore the problem of the upper critical current still remains unsolved.

25.6 6. Voltage steps in the current-voltage characteristics of superconducting channels with finite length

Voltage steps can be observed in the CVC of a not very long superconducting channel. They are related to the creation of new PSCs in a channel when the current through the sample is increased. The qualitative picture of voltage steps based on the SBT model (Skocpol et al. 1974, Tinkham 1979) was described in section 3.2. We consider here a more thorough approach based on the microscopic theory. The problem of voltage steps was solved first by Bezuglyi et al. (1977), we outline their results below.

Since the dynamic region of oscillations is very narrow and is localized near PSCs one can use here, just as in the case of the long channels in section 5.3, the static equations only. We assume that a superconducting channel with the length L_0 is connected with the current source by means of normal contacts (see fig. 15). When the current is less than $j^{(1)}$, where $j^{(1)}$ corresponds to the creation of the first PSC, the voltage across the channel is determined by the penetration of the electric field into the superconducting channel from the normal contacts (see, e.g., Artemenko et al. 1978, Ivlev et al. 1980d.e). This state is represented in fig. 15a. The order parameter is sharply depressed from the equilibrium value $\Delta_{\rm GL}$ to zero at distances of order $\xi(T)$ near the SN interface. Going further away from the interface, Φ and $j_{\rm n}$ decrease. $j_{\rm s}$ increases and Δ diminishes at distances of order of l_E.

When the current is increased above $j^{(1)}$ the first PSC appears in the middle of the channel (fig. 15b). This state remains in the interval $j^{(1)} < j < j^{(2)}$ and then the second PSC appears, and so on. The conditions near the SN-boundary (Ivlev et al. 1980d,e) at distances larger than ξ but small compared to I_E and those at the boundary of the static region near a PSC (see

section 5.2) are the same: $j_\mathrm{s} = 0$ and $\Delta = 1$, hence, we can use eq. (59) directly to determine the voltage across the channel.

Suppose that there are n PSCs in the channel, then the potential formed across one PSC is

$$\Phi_n^2(A) = \tfrac{2}{u\Gamma} \int_{\Lambda_{0\mathrm{n}}}^{A} \frac{\left(j - \Delta^2\sqrt{1-\Delta^2}\right)(3\Delta^2 - 2)}{\sqrt{1-\Delta^2}}\,\mathrm{d}\Delta \tag{74}$$

Here A_{0n} is the value of Δ at the midpoint between the neighboring PSCs (or at the midpoint between the SN-boundary and the nearest PSC). The parameter $\Delta_{0\mathrm{n}}$ is related now to the channel length L_0 by

$$\frac{L_0}{2(n+1)} = \frac{1}{u\Gamma} \int_{\Delta_{0\mathrm{n}}}^{1} \frac{(3\Delta^2 - 2)\,\mathrm{d}\Delta}{\sqrt{1-\Delta^2}\Phi(\Delta)} \tag{75}$$

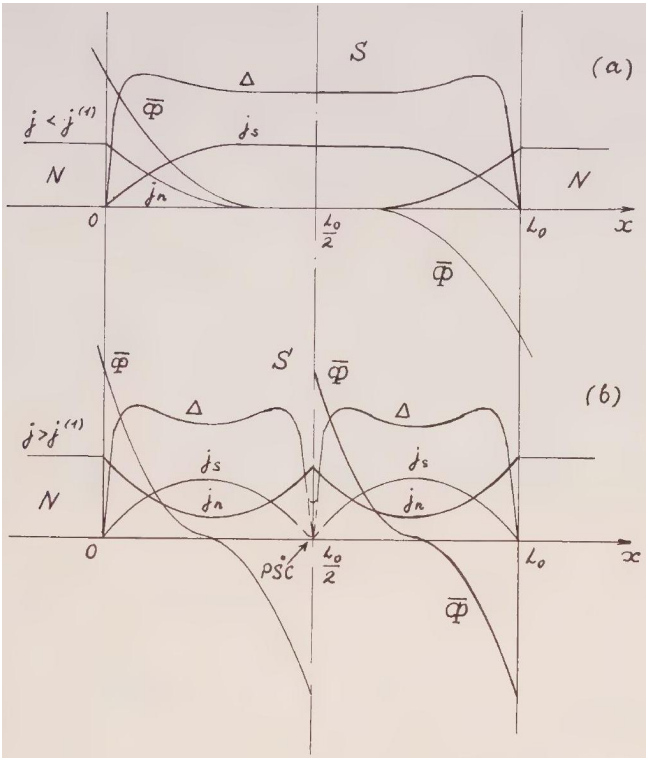


Fig. 15. The behavior of A, the currents \$j_{\mathrm{s}}\$ and j_n, and $\bar{\Phi}$ in a superconducting channel with normal contacts. (a) $j < j^{(1)}$ and PSC is absent. (b) $j^{(1)} < j < j^{(2)}$, there is one PSC in the middle.}

The total voltage drop across the channel is

$$V = 2(n+1)\Phi_n(\Delta = 1). \tag{76}$$

Equations (74)-(76) describe the CVC of a channel completely, but their explicit form is very complicated. We restrict ourselves to the case of weak currents, $j - j_\mathrm{c} \ll j_\mathrm{c}$ and $n \sim 1$, and suppose that $L_0 \gg l_E$. We get from eqs. (74) and (75)

$$\frac{L_0}{2(n+1)} = \frac{1}{(u\Gamma A_{0\mathrm{n}})^{1/2}} \ln \frac{Cj_\mathrm{c}}{j - j_{\mathrm{s}0}^{(n)}}. \tag{77}$$

Here $C \sim 1$, and $j_{\mathrm{s}0}^{(n)} = \Delta_{0\mathrm{n}}^2\sqrt{1-\Delta_{0\mathrm{n}}^2}$ is the supercurrent in the midpoints between PSCs.

If one increases the total current j keeping the number n of PSCs in the channel constant then the current $j_{so}^{(n)}$ will also increase according to eq. (77). When $j_{so}^{(n)}$ reaches the critical current j_c the solution with n PSCs becomes impossible and the $(n+1)$ th PSC appears. The current $j^{(n)}$ at which the nth PSC forms, i.e., when the nth step in the CVC appears, is determined by eq. (77):

$$j^{(n)} - j_c = j_c \exp\left\{-\frac{\sqrt{u\Gamma}L_0}{2n}\left(\frac{2}{3}\right)^{1/4}\right\}; \quad n = 1, 2, \ldots \tag{78}$$

The magnitude of a step does not practically depend on n and is equal to the voltage $2\Phi_0$ across one PSC, where

$$\Phi_0^2 = \frac{2}{u\Gamma}\int_{\sqrt{\frac{2}{3}}}^{1} \frac{\left(j_c - \Delta^2\sqrt{(1-\Delta^2)}\right)(3\Delta^2-2)}{\sqrt{(1-\Delta^2)}}\mathrm{d}\Delta \simeq \frac{0.150}{u\Gamma} \tag{79}$$

if n is of order of unity. The current dependence of the voltage Φ_n across one PSC in the interval between the nth and the $(n+1)$ th step has the form

$$\Phi_n^2 = \Phi_0^2 + \frac{2}{u\Gamma}(j - j_c)\int_{\sqrt{\frac{2}{3}}}^{1} \frac{3\Delta^2-2}{\sqrt{(1-\Delta^2)}}\mathrm{d}\Delta. \tag{80}$$

Hence, the CVC in this interval has a constant slope with differential resistance

$$\left(\frac{\partial V}{\partial j}\right)_n = \frac{2(n+1)}{u\Gamma\Phi_0}p^2\left(1;\sqrt{\frac{2}{3}}\right) \simeq 2.06\frac{n+1}{\sqrt{u\Gamma}}. \tag{81}$$

The CVC is shown in fig. 16.

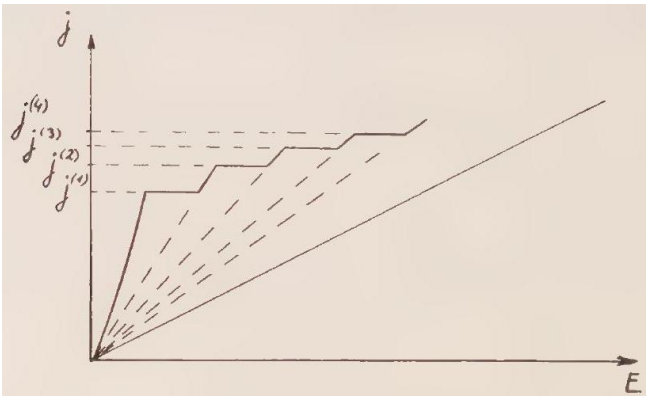


Fig. 16. The schematic CVC of a channel with finite length according to Bezuglyi et al. (1977).

In ordinary units we get for the differential resistance

$$\left(\frac{\partial V}{\partial j}\right)_n = 2.06(n+1)\frac{l_E}{\sigma},$$

where l_E is given by eq. (33). One can note that the numerical value $2.06 l_E/\sigma$ of the differential resistance produced by one PSC agrees surprisingly well with the phenomenological result of the SBT-model (Skocpol et al. 1974), which gives

$$\left(\frac{\partial V}{\partial j}\right)_n = 2l_E/\sigma$$

(see section 3.2).
The initial part of the CVC from $j = 0$ to $j = j^{(1)}$ corresponds to the superconducting state of the channel and is determined by the electric field penetration from normal contacts into the superconductor. This part of the CVC is described in the general case by the results obtained by Ivlev et al. (1980 d, e). When the channel is connected with superconducting banks the voltage will not be observed in the initial part of the CVC and one should replace ($n + 1$) by n in eqns. (75)-(81).

25.7 7. Conclusions

We can generally state that the main features of the resistive state in narrow superconducting channels find their explanation in the recent theory. This concerns first of all the over-all behavior of a CVC and the voltage steps in it. The a.c. Josephson effect observed experimentally by Skocpol et al. (1974) is without doubt related to PSC oscillations with the Josephson frequency (Ivlev and Kopnin 1982). As to the generation of lower frequencies (Churilov et al. 1969, Galaiko et al. 1973, 1976), there is as yet no satisfactory explanation for this effect. It seems to be due to the motion of the PSC structure as a whole (Galaiko et al. 1976) but final conclusions are still difficult to draw. Also there are insufficient data for the verification of the temperature dependence of the upper critical current j_2. Experimental data obtained by Galako et al. (1976) suggest a linear dependence of $j_2\gamma\,(T_c - T)$ which does not agree with either eq. (72) or eq. (73).

Despite these and some other questions still open, the general picture of the resistive state as a structure of PSCs is established quite reliably. Experiments verify not only the overall shape of the CVC, but also such fine features as the spatial distribution of the potentials μ_e and μ_p (Dolan and Jackel 1977) and the temperature and magnetic field dependence of the differential resistance of a PSC (Kadin et al. 1978).

The concept of phase slippage in the resistive states of different types, of superconductors turns out to be very useful. The vortex motion in type-II superconductors and in superfluid helium and the motion of flux tubes in typeI superconductors are also mechanisms of phase slippage. These are the processes for which the term "phase slippage" has been introduced (Anderson 1966). We face, however, a qualitatively new type of phase slippage in narrow superconducting channels. The point is that phase slippage in bulk superconductors is carried out by means of moving defects of a superconducting structure, which exist in the system even when dissipation is absent. In narrow superconducting channels, however, PSCs exist only in the presence of dissipation. A system with PSCs is essentially dissipative and methods based on thermodynamic considerations are not suitable here.

The concept of phase slippage also proves to be very useful for the description of the two-dimensional mixed state and the intermediate state of a superconducting wire in a current-carrying state (see the review by Dolgopolov and Landau (1985) in this volume). Ivlev and Kopnin (1980) and Ivlev et al. (1980c) have shown that the coexistence of electric field and superconductivity in these cases is also due to a phase slippage mechanism like PSC in the resistive state in narrow superconducting channels.

26 Collective Modes in Superconductors by Shon

26.1 1. Introduction

The dynamic properties of superconductors have been the subject of an extensive research for many years. Various relaxation processes have been investigated which reveal much about the macroscopic order and the microscopic interaction typical for the superconducting state.

Collective oscillations, in particular those of low frequencies, are interesting for the same reasons. In neutral superfluids a large variety of sound-like (propagating) collective oscillations, which have a linear dispersion relation, are well established. However, in superconductors none of these modes has been observed. The main reason is that the particles in the superconductor are charged. Hence, the frequency of density waves is shifted to the plasma frequency, which is little modified by the superconducting transition. Furthermore, the electrons in the superconductor move in a lattice, which in practice is always distorted. Hence, their motion is subject to (Ohmic) damping. It was only after a long lasting search, both theoretically and experimentally, that a sound-like collective mode in superconductors was detected, in the experiments of Carlson and Goldman (1973, 1975). They investigated the order parameter structure factor and found resonant peaks at finite frequencies $\pm\omega_q$, where (ω_4 depends linearly on the wave vector.

Early theoretical descriptions, based on the two-fluid model or the phenomenological time-dependent Ginzburg Landau theory gave neither a proper description of the collective modes nor of the relaxation mechanisms. The discussion of collective modes was incited particularly after the establishment of the microscopic theory by Bardeen, Cooper and Schrieffer (1957). In the original form it failed to account for the Meissner effect in a gauge-invariant way. The remedy of this flaw also leads to the prediction of a soundlike collective density oscillation in a (hypothetical) neutral superconductor (Anderson 1958, Bogoliubov et al. 1959). This mode, which involves oscillations of the phase of the order parameter, is also predicted by the Goldstone theorem. In a (real) charged superconductor, however, the frequency of this density mode is shifted to the plasma frequency and of little physical interest.

In the following years many investigations were concerned with the response of the superconductor to perturbations like electromagnetic response or attenuation of ultrasound. These descriptions involved only the order parameter and the thermal quasiparticles, thus precluding many nonequilibrium features. More recently, however, it became clear that the deviations of the quasiparticle distribution in superconductors from equilibrium may be significant. One reason is that the inelastic scattering times in superconductors are comparatively long. A complete description has to incorporate both degrees of freedom: the quasiparticles and the order parameter. It has to establish a kinetic theory for the quasiparticle distribution function in the superconducting state and to specify the influence of a nonequilibrium distribution on the order parameter. It turns out that in clean superconductors a sufficient theory is of a rather transparent form. The central part is a Boltzmann equation for the distribution function $f(p;r,t)$ (Aronov and Gurevich 1974). It is of the same form as in the normal metal with some rather obvious modifications due to the characteristic superconducting properties. Also in dirty superconductors, where the majority of experiments is performed, one finds a Boltzmann type of equation for the quasiparticle distribution as a function of the energy $f'(E;r,t)$ (Schmid and Schön 1975a). One of the consequences of the coupling between the order parameter and the quasiparticles is that the order parameter relaxation becomes rather slow. Furthermore, the theory accounts for the phenomenon of charge imbalance (Clarke 1972, Tinkham 1972) and its relaxation.

The microscopic description being developed, the collective mode observed by Carlson and Goldman quickly found a theoretical interpretation both in dirty (Schmid and Schön 1975b,c) as well as in clean superconductors (Artemenko and Volkov 1975). The main features are: the collective mode is a high frequency, collisionless oscillation of the supercurrent which is compensated by a counterflow of the normal current. Since the frequency is high a hydrodynamic description is not possible and, in principle, the full energy and/or momentum dependence of the distribution function has to be taken into account. In certain limits, simple approximate descriptions can be developed (see e.g. Pethick and Smith 1979 or Kadin et al. 1980). In the following, we will indicate these approximate pictures. However, the main purpose of this article is to describe quantitatively the collective modes in superconductors on the basis of the

full microscopic theory. Because of its experimental relevance we will consider the dirty limit in more detail.

The plan of the chapter is as follows. Section 2 contains a short review of various collective modes. We contrast charged and uncharged systems, the hydrodynamic and collisionless frequency range, superfluids and superconductors. Also we present a qualitative, simple picture of the Carlson Goldman collective mode. In section 3 we present the microscopic theory and evaluate it further in order to describe collective modes at general frequencies. The order parameter structure factor is calculated in section 4. Analytic expressions covering various limits near T_c are presented, and a comparison with experiments is performed. In section 5, we derive further results from the microscopic theory, which are relevant for a complete understanding of the collective modes. We discuss the charge imbalance relaxation, consider neutral superconductors and low temperatures. We review the theoretical literature concerned with the Carlson-Goldman mode and other collective modes. We also discuss the physical manifestation of the collective modes. Section 6 contains some conclusions. In the Appendix we extend the calculation of the order parameter structure factor to cover a larger range of temperatures near the transition temperature.

26.2 2. Review of collective sound-like modes

26.2.1 2.1. Two-fluid hydrodynamics of helium II

Sound-like collective oscillations in superfluids were first investigated in the superfluid phase of helium (He II) in a range of parameters where a hydrodynamic description applies (Landau and Lifshitz 1959, Khalatnikov 1965): In this case, He II can be thought as consisting of two interpenetrating liquids: a superfluid which moves with zero viscosity, and a normal viscous fluid. Both liquids may move relative to one another without friction. The two components are characterized by their densities n_s and n_n, and their velocities v and v_n. The sum $n = n_\mathrm{s} + n_\mathrm{n}$ is the total (number) density and $j = n_\mathrm{s} v_\mathrm{s} + n_\mathrm{n} v_\mathrm{n}$ is the total (number) current density. The superfluid flow does not carry entropy, and it is a potential flow ($\mathrm{curl}\, v_\mathrm{s} = 0$). These properties and the local conservation laws form the basis of the hydrodynamic theory of He II.

From the hydrodynamic description one finds that in bulk He II three different types of propagating collective modes exist: first, second, and fourth sound. (The third sound is a surface wave.) First sound is the density wave familiar from normal systems. In the superfluid both components move in phase with the same velocity $v_\mathrm{n} = v$. (We ignore thermal expansion.) The phase velocity of this mode $c_1^2 = \hat{\imath} p / \hat{\partial}(mn)$ is nearly independent of the temperature. In the second sound mode the normal and the superfluid component move in opposite directions such that the total current vanishes and the density remains constant in space. However, the local entropy density is modulated and hence, the second sound is also called entropy wave. Its phase velocity is $c_2^2 = T s^2 n_\checkmark / c n_\mathrm{n}$ (s is the entropy per unit mass, o the specific heat per unit mass). Fourth sound is found if there exists a strong damping mechanism for the motion of the normal component, e.g. if the He II is immersed in a medium with fine pores. In this case, only the superfluid component performs density oscillations. The phase velocity depends on the superfluid density

$$c_4^2 = \frac{n_n}{n} c_1^2 + \frac{n_n}{n} c_2^2,$$

where the second term in this expression is usually small.

An essential assumption in the derivation of the hydrodynamic equations is that the system is in local thermal equilibrium and that the state of the system can be described completely by the local values of the thermodynamic variables, the superfluid density and velocity. Thus,

consistency requires that the frequencies of collective modes found from these equations are small compared to internal relaxation rates $\omega \ll 1/\tau_{\rm eq}$.

26.2.2 2.2. Hydrodynamic description of superfluid Fermi systems

In the hydrodynamic regime the superfluid Fermi systems, superfluid ^{3}He and superconductors, can also be described in terms of a two-fluid picture (Bardeen 1958). The superfluid component represents the Cooper pairs and the normal component the thermally excited quasiparticles. However, in certain respects, the Fermi systems differ significantly from He II.

The superfluid ^{3}He is an anisotropic superfluid with strong interatomic forces. A successful description is based on Landau's theory of Fermi liquids (Landau 1956, 1957, 1958, Leggett 1965, 1966, 1975). First. second, and fourth sound exist (Wölfle 1973), with phase velocities depending on the Landau parameters and the orientation. In addition, the structure of the order parameter leads to a rich variety of further collective modes.*

In superconductors, because of the long-range Coulomb interaction, no hydrodynamic sound-like collective oscillation exists.** First and fourth sound are associated with density oscillations, and hence their frequencies are shifted up to the plasma frequencies depending on the total electron density n or the superfluid density $n_{,}$, respectively. The velocity of the second sound mode remains unchanged. However, second sound is practically always overdamped (Bardeen 1958, Ginzburg 1961, Enz 1974). In a superfluid liquid, the damping is due to friction between the normal component and walls, and may be negligible under suitable conditions. In a superconductor, the quasiparticles forming the normal component always have a finite scattering rate $1, \tau_{cc}$ due to elastic electron-impurity and inelastic electron-phonon scattering. This leads to a damping of the second sound mode given by $\gamma = n_{\rm s}/n_{\rm n}\tau_{\rm sc}$. The collective mode can only be observed if γ is small compared to the resonant frequency $\gamma \ll \omega$. Furthermore, a hydrodynamic description is sufficient only if the frequencies and wave vectors are small*** $\omega \ll 1/\tau_{\rm eq}$ and $q \ll 1/\lambda_{\rm eq} = 1/v_{\rm F}\tau_{\rm eq}$ (Enz 1974). Since the Fermi velocity is much larger than the velocity of second sound c_2, the second of these conditions is more restrictive. Hence, a window

condition for the frequency of second sound results, which can only be met at temperatures extremely close to the critical temperature $T_{\rm c}$ (in a range of order $10^{-5}T_{\rm c}$).

26.2.3 2.3. Collisionless modes

In contrast to the hydrodynamic regime characterized by $\omega \ll 1/\tau_{\rm eq}$, the regime $\omega \gg 1, \tau_{\rm eq}$ is called collisionless. For any fixed frequency one enters this regime when the temperature is lowered, since then the inelastic scattering of quasiparticles and the establishment of local thermal equilibrium become increasingly slower. While in the hydrodynamic region the quasiparticle distribution is always of a thermal form (corresponding to the local values of the thermodynamic variables and the superfluid density and velocity), it may differ significantly from a thermal distribution in the collisionless region. It is therefore essential to take into account the detailed energy and momentum dependence of the distribution function of the quasiparticles.

0

- A detailed discussion is given by Wölfle (1977, 1978).
  **A systematic discussion is given by Enz (1974).
  ***In section 3 we will express $1/\tau_{\rm eq}$ in terms of microscopic parameters. Relaxation to a local equilibrium requires inelastic scattering processes, hence $\tau_{\rm eq} \geqslant \tau_{\rm sc}$.

A familiar example of a collisionless collective mode is zero sound, which exists at low temperatures in uncharged normal Fermi systems, provided that the quasiparticle interaction is repulsive (Landau 1957). The velocity of zero sound c_0 for weak coupling is $c_0 = c_F$, and it increases with coupling strength. The Fermi surface in this mode performs rather complex oscillations.

26.2.4 2.4. The Bogoliubov-Anderson mode

26.2.5 2.4.1. The problem of gauge invariance in superconductors

There has been an extensive discussion of collective oscillations in superconductors in the literature*, starting with the development of the microscopic theory by Bardeen, Cooper and Schrieffer (1957). The reason for this was that the original BCS description gave a correct account of the Meissner effect only when the response to a vector potential A was calculated in a gauge where div $A = 0$. It failed to do so in an arbitrary gauge. (The same problem appears in neutral superfluid Fermi systems where expressions for the current may be obtained which do not satisfy the continuity equation, while the reduction of the moment of inertia - the analogue to the Meissner effect is described correctly.) This insufficiency in the original BCS description arises from the fact that only quasiparticle excitations were included among the excited states. It was pointed out by Bardeen (1957) and demonstrated first in the work of Anderson (1958) that a vector potential with div $A \neq 0$ also couples to a collective density fluctuation mode. Inclusion of this mode in a consistent way leads to a gauge invariant and current conserving theory. This can be done

most systematically by working within a conserving approximation, a procedure eludicated by Baym and Kadanoff (1961) and Baym (1962) and applied to superconductors by Ambegaokar and Kadanoff (1961). An equivalent way of handling the problem was suggested by Nambu (1960) who made use of a generalized Ward identity.

26.2.6 2.4.2. Uncharged Fermi systems

In all treatments on this subject a low temperature collective mode was found. It can be described as a state in which the phase of the order parameter varies periodically in space and time. Thus, supercurrents are flowing, resulting in a spatial variation of the superfluid density. In an uncharged Fermi system, this mode has a sound-like dispersion relation. The phase velocity is formally equal to the phase velocity of hydrodynamic first sound c_1, although the frequency may be rather large and the mode is not a hydrodynamic mode. The reason is that, in a superconductor, the existence of the energy gap prevents transitions to excited states as long as the frequency is small $\omega < 2\Delta$. The system follows adiabatically the compression and expansion due to the sound wave. Thus, a local equilibrium distribution is maintained although the mechanism is completely different from the relaxation processes occurring in a hydrodynamic first sound situation. The mode was first discovered by Bogoliubov et al. (1959) and is called Bogoliubov-Anderson mode in the literature. It already exhausts the conductivity sum rule (Kadanoff and Martin 1961), thus one can conclude that it is only sound-like collective oscillation of the system at $T = 0$.

The investigations were extended to finite temperatures first by Kadanoff and Martin (1961) and generalized to include strong interactions i.e., the Fermi liquid effects, by Larkin and Migdal (1963) and by Leggett (1965, 1966). The result is that at zero temperature for arbitrary strength of the interaction, the Bogoliubov-Anderson mode has a phase velocity equal to that of first sound. At finite temperatures the existence of the mode depends on the strength of the

[0]*For a review see Martin (1969).

interaction:
(i) For weak attraction the collective mode is only well defined at $T = 0$. As the temperature is raised, the velocity increases-never reaching ι_F - and the oscillation becomes rapidly damped, disappearing altogether when the average velocity of the quasiparticles becomes of order $v_F/\sqrt{3}$.
(ii) For weak repulsive interaction the mode exists at zero temperature and in the vicinity of the transition temperature. There it merges with the predictions of normal fluid kinetic theory, i.e. it becomes zero sound. The velocity depends strongly on the temperature.
(iii) For strong repulsive interactions the mode exists at all temperatures. The velocity depends only weakly on the temperature. (In this limit also the velocity of zero and first sound do not differ much.) This limit applies to ^{3}He. Indeed the predicted small change in velocity of sound was found experimentally in superfluid ^{3}He (Paulson et al. 1973).

26.2.7 2.4.3. Superconductors

In charged superconductors the frequency of the Bogoliubov Anderson mode is shifted to the plasma frequency, due to the long range Coulomb forces. Since the plasma frequency is barely modified by the superfluid transition we cannot expect experimental evidence of this mode. The plasmon mode, however, is still necessary to maintain gauge invariance. The nature of the BogoliubovAnderson mode in superfluids can also be understood on the basis of Goldstone's theorem. It states that if an infinitesimal uniform change of the ground state of a system produces a new ground state degenerate with it, then an infinitesimal change in the state varying slowly in space will generate an eigenstate of low energy. This means the system must have an excitation branch with no energy gap. In the superfluid Fermi systems the degeneracy is connected with the phase of the order parameter of the condensed phase. In the collective mode the phase varies periodically in space. In a neutral superfluid, the Bogoliubov-Anderson sound mode is the gapless collective excitation required by the Goldstone theorem. In a charged super-conductor, however, the singular nature of the long-range Coulomb forces renders the theorem inconclusive.

26.2.8 2.5 The Carlson-Goldman mode

The first experimental demonstration of the existence of a collective mode with a phonon-like dispersion relation in a superconductor was given by Carlson and Goldman (1973, 1975, 1976). They investigated the frequency and wavevector dependence of the order-parameter structure factor

$$S(q,\omega) = \langle \Delta^*(r,t)\Delta(0,0)\rangle_{q,(\omega)} \tag{2.1}$$

of a short mean free path superconducting aluminium film using a method suggested by Ferrell (1969) and Scalapino (1970).

Above T_c, only one peak in the structure factor centered at $\omega = 0$ was seen (Anderson et al. 1972). Below T_c, an additional symmetric pair of peaks at finite frequencies shows up. It results from a propagating order parameter collective mode. The resonant frequency is almost proportional to the wave vector. It also depends on the temperature. This peak was identified to originate from fluctuations in the phase in the order parameter, whereas the central peak results from fluctuations in the magnitude of the order parameter. When the temperature is lowered, the propagating mode is increasingly damped and the peak is leveled off. Furthermore, there appears a structure at $\omega = 24$.

The experimental values of the structure factor above T_c are in good agreement with the results from the diffusive time-dependent GinzburgLandau equation (Schmid 1966, Abrahams and Tsuneto 1966). But it is not possible to explain the existence of a propagating mode below

T_c by this
equation. Nor is a hydrodynamic description in terms of a two-fluid model sufficient, since the resonant frequency is not small in comparison to internal relaxation rates. We will find below that the mode is characterized by a charge imbalance between the quasiparticles and the condensed phase. Hence, the characteristic relaxation rate is the charge imbalance relaxation rate $1/\tau_{Q*}$ (Clarke 1972, Tinkham 1972). In fact, the mode is a collisionless mode, in the sense that the frequency is much larger than the inelastic electron-phonon collision rate, $\omega \gg 1/\tau_{\mathrm{E}}$, but the elastic electron impurity scattering rate is even larger, $\omega \ll 1/\tau_{\mathrm{imp}}$.

One can find a rather simple physical description of the collective mode in the limit*

$$\Gamma, Dq^2 \ll |\omega| \ll \Delta \ll T_{\mathrm{c}}, \tag{2.2}$$

where Γ measures the pair breaking (which results from inelastic electronphonon scattering, scattering at paramagnetic impurities, magnetic field, supercurrent, ...) D is the diffusion coefficient, and Δ is the energy gap. In this case, one finds from the microscopic theory that the chemical potential of the Cooper pairs Φ obeys the relation

$$\frac{\pi\Delta}{4T}\dot{\Phi} + \frac{1}{2eN_0}\operatorname{div} j_{\mathrm{s}} = 0 \tag{2.3}$$

We will comment further on this relation in section 5. At present, we merely mention that it can be interpreted as a "continuity equation for the superfluid" (Pethick and Smith 1979) with coefficients determined by the microscopic theory.

Space charges are minimized in this collective mode by a counterflow of supercurrent and normal current. Hence, we are led to consider a situation where

$$\operatorname{div}(j_{\mathrm{s}} + j_{\mathrm{n}}) \approx 0. \tag{2.4}$$

We express the supercurrent as

$$j_{\mathrm{s}} = en_{\mathrm{s}}v_{\mathrm{s}}, \tag{2.5}$$

where the superfluid velocity obeys the acceleration equation

$$m\dot{v}_{\mathrm{s}} = -\operatorname{grad}\Phi + eE. \tag{2.6}$$

Since the frequencies considered are still small in comparison to the elastic electron impurity scattering rate, $\omega \ll 1/\tau_{\mathrm{imp}}$, the normal current is proportional to the driving force. Near T_c, in a rough approximation, it is the same as in the
normal state

$$j_{\mathrm{n}} = \sigma E \tag{2.7}$$

These equations allow for longitudinal collective oscillations $\propto \mathrm{e}^{-\mathrm{i}\left(\omega_{\varphi 1} - q\cdot r\right)}$ with dispersion relation

$$\omega_4 = -\frac{1}{2}\mathrm{i}\gamma \pm \sqrt{c_{\mathrm{CG}}^2 q^2 - \gamma^2/4} \tag{2.8}$$

The phase velocity and the damping of this propagating mode are given by

$$c_{\mathrm{CG}}^2 = \frac{n_{\mathrm{s}}}{n}\frac{4T}{\pi\Delta}\frac{v_{\mathrm{F}}^2}{3}, \quad \because = \frac{n_{\mathrm{s}}}{n}\frac{1}{\tau_{\mathrm{imp}}} \tag{2.9}$$

[0*] We use units where $\hbar = k_{\mathrm{B}} = c = 1$.

Although normal current and supercurrent are flowing in opposite directions, this mode is not a second sound mode. It is neither a hydrodynamic mode, nor does it involve temperature or entropy fluctuations. It is primarily a longitudinal oscillation of the condensate, the restoring force being given by the gradient of the Cooper pair chemical potential. This is most apparent if we consider a hypothetical uncharged superconductor where a similar but undamped mode is found with $\omega_q = \pm c_{\mathrm{CG}} q$. There the normal current j_{n} remains zero and hence, the mode involves local density fluctuations. In a charged superconductor, the supercurrent oscillation produces an electric field which drives the normal current to perform a counteroscillation. It turns out that the resulting total space charges are small and can be ignored in the continuity equation (2.4). However, the normal current is subject to Ohmic losses, which is the origin of the damping γ. Close to T_{c} where the superfluid density n_{s} is small, the superfluid oscillations can be compensated by small oscillations of the normal current, and hence the damping is small. At lower temperatures the superfluid density and the damping increase. (In order to avoid misinterpretations, we stress the point that the superfluid density n_{s} is merely a coefficient relating superfluid velocity and supercurrent. It depends on the temperature and impurity concentration. It is not related to the fluctuations of the local charge density.)

We note that the phase velocity of the collective mode is larger than that of hydrodynamic fourth sound by a factor $4T/\pi\Lambda$, but is still small in comparison to the Fermi velocity. Near $T_{\mathrm{c}}, n_{\mathrm{s}}$ is given by

$$\frac{n_{\mathrm{s}}}{n} = \frac{7\zeta(3)}{4\pi^2}\frac{\Delta^2}{T^2}\chi\left(\frac{1}{2\pi T_{\mathrm{c}}\tau_{\mathrm{imp}}}\right) \tag{2.10}$$

where Gor'kov's function expresses the dependence on the impurity concentration. It is defined as

$$\chi(x) = \frac{8}{7\zeta(3)}\sum_{v=0}^{\infty}(2v+1)^{-2}(2v+1+x)^{-1} \tag{2.11}$$

In clean superconductors $T_{\mathrm{c}}\tau_{\mathrm{imp}} \gg 1$, when $\chi \approx 1$, we recover the results of Artemenko and Volkov (1975). In the simple description given above, we neglected quasiparticle diffusion processes which lead to an additional damping of order Dq^2. Thus, in clean superconductors, the collective mode only exists if the conditions

$$\frac{\Delta^2}{T^2}\frac{1}{\tau_{\mathrm{imp}}}, \Gamma \ll |\omega_q| \ll \frac{\Delta}{T}\frac{1}{\tau_{\mathrm{imp}}} \tag{2.12}$$

are satisfied, where the upper frequency limit guarantees that $Dq^2 \ll \omega_q$.
In dirty superconductors, where $T_{\mathrm{c}}\tau_{\mathrm{imp}} \ll 1$, the superfluid density reduces to $n_{\mathrm{s}}/n = \pi\Delta^2/2T\tau_{\mathrm{imp}}$ and the phase velocity is

$$c_{\mathrm{CG}} = \sqrt{2\Delta D}. \tag{2.13}$$

This result (Schmid and Schön 1975b) explains well the experimental findings of Carlson and Goldman (1975) as far as the absolute value and temperature dependence of the phase velocity is concerned. The result (2.9) also gives a qualitative account of the damping, which increases with decreasing temperature. Because of the damping, the collective mode in dirty samples propagates only if

$$\frac{\Delta^2}{T}, \Gamma \ll |\omega| \ll \Delta. \tag{2.14}$$

The virtue of the presentation given above is to provide a physical picture of the propagating mode. However, we still have to justify the relation (2.3), and we have to investigate in

more detail the effect of various damping mechanisms, in particular the effect of quasiparticle diffusion. We also will derive in the following the complete order-parameter structure factor of a superconductor near T_c for general frequencies and wave vectors including also fluctuations in the magnitude of the order parameter.

26.3 3. The microscopic theory

26.3.1 3.1. Some remarks

Nonequilibrium phenomena in superconductors can be described on various levels. Under certain conditions a rather simple kinetic theory based on the BCS theory is sufficient. It consists of a Boltzmann equation for the distribution function of the excitations (Aronov and Gurevich 1974) which includes collisions of the excitations, e.g. with impurities and with phonons (Bardeen et al. 1959). Furthermore, the excitations are coupled to the condensate. In order for this description to be valid, variations in space and time have to be sufficiently slow $qv_{\mathrm{F}} \ll \Delta$ and $\omega \ll A$. In addition, all scattering processes have to be weak.

In connection with the collective mode larger frequencies and wave-vectors are of interest. This means that we need a more general description, e.g. in terms of microscopic Green functions. We also need the general theory if the interactions with impurities, phonons, or other pair breaking effects are not weak. On the other hand, the characteristic wavelengths of interest are still much larger than the Fermi wavelength. This fact permits significant simplifications. A theory which systematically incorporates this limit from the beginning was developed by Eilenberger (1968) and independently by Larkin and Ovchinnikov (1968). They found that it is sufficient to consider the quasiclassical Green function which is obtained from the full Green function $G(p, E)$ by integration over the magnitude of the momentum. The concept was extended by Eliashberg (1971) for retarded interactions such that inelastic electron-phonon collisions can be included. Later Schmid and Schön (1975a) introduced in this context the quasiparticle distribution. A very compact formulation of the problem based on the Keldysh (1964) technique was given by Larkin and Ovchinnikov (1977, 1981), Hu (1980) and Schmid (1981).

In the following subsection, we will summarize the quasiclassical theory and we will evaluate the equation of motion further in order to describe the collective mode and to calculate the order-parameter structure factor. This means we allow for sufficiently general frequencies and wave vectors. On the other hand, it is sufficient to linearize the theory. Since the propagating collective mode is a collisionless mode, inelastic electron-phonon collisions are relatively weak. They provide, however, an important relaxation and damping mechanism, and we will point out their effect. We will present the explicit calculation only in the dirty limit ($T_{\mathrm{c}}\tau_{\mathrm{imp}} \ll 1$), since most experiments are performed with samples having short mean free paths. Explicit expressions are given for temperatures close to T_c.

26.3.2 3.2. Dirty limit theory

In the dirty limit ($T_{\mathrm{c}}\tau_{\mathrm{imp}} \ll 1$) the quantities of interest can be expressed by the part of the quasiclassical Green function which is isotropic in momentum space (Usadel 1970). This function

$$\bar{\hat{g}}(E; r, t) = \frac{\mathrm{i}}{\pi \overline{\mathrm{N}_0}} \int \frac{\mathrm{d}^3 p}{(2\pi)^3} \hat{G}(p, E; r, t)$$

obeys the equation of motion*

$$\left[\overline{\hat{\tau}}_3 E - \overline{\hat{1}}_{e\varphi} - \overline{\hat{\Sigma}}_{\rm ph} - \overline{\hat{\Sigma}}_{\rm sf} \coloneqq \overline{\hat{g}}\right] = \frac{1}{2}\mathrm{i}D\left[\hat{\partial}_\rho[\hat{g};[\hat{\partial};\overline{\hat{g}}]]\right], \tag{3.1}$$

where $[,]$ *is a commutator. The function* $\hat{g}$ is normalized,

$$\dot{\hat{g}} \circ \overline{\hat{g}} = \hat{1} \tag{3.2}$$

Apart from the retarded and the advanced Green function, in nonequilibrium situations also a third function $\hat{g}^{\rm K}$, introduced by Keldysh (1964), is needed, which can be combined with $\hat{g}^{\rm R}$ and $\hat{g}^{\rm A}$ to form a matrix in "Keldysh space"

$$\overline{\hat{g}} = \begin{pmatrix} \hat{g}^{\rm R} & \hat{g}^{\rm K} \\ 0 & \hat{g}^{\rm A} \end{pmatrix}. \tag{3.3}$$

The caret indicates that the quantities are still matrices in particle-hole (Nambu) space. The dot product is defined as

$$A \circ B = \exp\left[\frac{1}{2}\mathrm{i}\left(\partial_E^A \partial_t^B - \partial_t^A \partial_E^B\right)\right] A(E,t)B(E,t), \tag{3.4}$$

where ∂^A acts on A only, ...** In two cases it may be expressed in simple terms: (i) If the external frequencies are small, $\omega \ll \Delta, T$ we can expand the exponential and restrict ourselves to the first few derivatives (see e.g. Schmid 1981). (ii) If we proceed in a linearized theory one of the quantities A or B is a static function and we may use a Fourier transformation to our advantage, e.g.

$$[A(E,t) \circ B(E)]_\omega = A(E,\omega)B(E-\omega/2). \tag{3.5}$$

The gauge-invariant spatial derivative is

$$\overline{\hat{\delta}} = \overline{\hat{1}}\frac{\partial}{\partial r} - i\overline{\hat{\tau}}_3 eA(r,t) \tag{3.6}$$

and φ and A are the electromagnetic potentials. The scattering at magnetic impurities leads to a self energy

$$\hat{\Sigma}_{\rm ff} = -\frac{\mathrm{i}}{2\tau_{\rm s}}\overline{\hat{\tau}}_3\overline{\hat{g}\hat{\tau}}_3. \tag{3.7}$$

The electron phonon interaction is described by $\hat{\Sigma}_{ph}$. It plays a twofold role: inelastic collisions are contained in the components $\hat{\Sigma}^{\rm K}_{\rm ph}$ and $\hat{\Sigma}^{\rm R}_{\rm ph} - \hat{\Sigma}^{\rm A}_{\rm ph}$, pair correlations are contained in $\hat{\Sigma}^R_{ph} + \hat{\Sigma}^A_{ph}$. If we ignore renormalization effects we have

$$\left(\hat{\Sigma}^{\rm R}_{\rm ph} + \hat{\Sigma}^{\rm A}_{\rm ph}\right)/2 = -\mathrm{i}\Delta\hat{\tau}_\theta; \quad \hat{\tau}_\theta = \mathrm{e}^{-\mathrm{i}\theta\hat{\tau}_3}\hat{\tau}_1, \tag{3.8}$$

where Δ and θ are the magnitude and the phase of the complex order parameter $\Delta = \Delta \mathrm{e}^{-\mathrm{i}\theta}$. The order parameter satisfies the self-consistency relation

$$\Delta(r,t) = \frac{1}{4\mathrm{i}}\lambda\int \mathrm{d}E\left\{\hat{g}^{\rm K}(E;r,t)\right\}_{12} \tag{3.9}$$

[0]*For further details see e.g. Schmid (1981). We use the notation introduced in this reference.

[0]*In general, spatial variations require an equivalent operation (see Eckern and Schmid, 1981). However, since the wavelengths considered are large in comparison to the Fermi wavelength $1/p_{\rm F}$, we can neglect this generalization for most purposes.

where λ is the electron-phonon coupling constant.
The Keldysh component of the Green's function can be related to a distribution function as follows

$$\hat{g}^{\mathrm{K}} = \hat{g}^{\mathrm{R}} \circ \hat{h} - \hat{h} \circ \hat{g}^{\mathrm{A}}, \quad \hat{h} = \left(1 - 2f^{(\mathrm{L})}\right) \hat{1} - 2f^{(\mathrm{T})} \hat{\tau}_3, \tag{3.10}$$

where in equilibrium $f^{(L)}(E; r, t)$ is equal to the Fermi distribution $f_0(E)$ and $f^{(T)}\ (E; r, t) = 0$. The superscripts refer to two degrees of freedom, the longitudinal and the transverse mode. This terminology refers to the fact that the two modes are associated with changes in the magnitude and the phase of the complex order parameter, respectively. Another distinction between the two modes is that they involve changes either in the energy or in the charge. Thus, they are also called energy mode (L) and charge mode (T), respectively.

The charge density and the current density, finally, are given by

$$\rho(\boldsymbol{r}, t) = -2eN_0 \left\{ \frac{1}{8} \int \mathrm{d}E \, \mathrm{Tr} \left[\hat{g}^{\mathrm{K}}(E; \boldsymbol{r}, t) \right] + e\varphi \right\} \tag{3.11}$$

and, omitting the arguments ($E; r, t$) in $\hat{h}$ and $\hat{g}$,

$$j(r,t) = \frac{\sigma}{8e} \int \mathrm{d}E \, \mathrm{Tr} \, \tau_3 \Big\{ [\hat{\partial}, \hat{h}] - \hat{g}^{\mathrm{R}} \circ [\hat{\partial}, \hat{h}] \circ \hat{g}^{\mathrm{A}} + \frac{1}{2} \left[\hat{g}^{\mathrm{R}}; \left[\hat{\partial}, \hat{g}^{\mathrm{R}} \right] \right] \circ \hat{h} - \frac{1}{2} \hat{h} \circ \left[\hat{g}^{\mathrm{A}}; \left[\hat{\partial}, \hat{g}^{\mathrm{A}} \right] \right] \Big\} \tag{3.12}$$

Both satisfy the continuity equation $\dot{\rho} + \mathrm{div}\, j = 0$. Furthermore, since in metals the space charges are suppressed almost entirely by Coulomb forces, we have with good accuracy $\rho = 0$ and $\mathrm{div}\, j = 0$. The density of states per spin at the Fermi surface N_0 and the normal state conductivity are related by $\sigma = 2e^2 N_0 D$.

The equilibrium Green function can be chosen to contain only a $\hat{\tau}_3$ and $\hat{\tau}_\theta$ component

$$\hat{g}_0^{R(A)}(E; r) = \alpha^{R(A)}(E; r)\hat{\tau}_3 + \beta^{R(A)}(E; r)\hat{\tau}_0. \tag{3.13}$$

The retarded (advanced) components satisfy

$$\begin{aligned} &\alpha^2 + \beta^2 = 1 \\ &-\mathrm{i}\left(E \pm \frac{\mathrm{i}}{2\tau_{\mathrm{E}}}\right)\beta + \Delta\alpha = \alpha\beta\Gamma_0 - \frac{D}{2}\left[\alpha\left(\frac{\partial}{\partial \boldsymbol{r}}\right)^2 \beta - \beta\left(\frac{\partial}{\partial \boldsymbol{r}}\right)^2 \alpha\right]. \end{aligned} \tag{3.14}$$

Here we have omitted the superscript R(A). The inelastic electron phonon collision rate enters with a plus (minus) sign in the equation for the retarded (advanced) quantities. Further pair breaking effects are represented by Γ_0. These are for example, scattering at magnetic impurities, supercurrent flow, or a magnetic field applied parallel to a thin film of thickness d. In these cases one has $\Gamma_0 = 1/\tau_{\mathrm{s}}, 2m^2 D v_{\mathrm{s}}^2, \frac{1}{6} e^2 D d H^2$, respectively. We can relate α and β to spectral quantities. In particular, the reduced density of states in superconductors is

$$N_1(E) = \frac{1}{2}\left[\alpha^{\mathrm{R}}(E) - \alpha^{\mathrm{A}}(E)\right] \tag{3.15}$$

Analytic solutions for α and β can be obtained in different limits. For example, in a homogeneous superconductor with no pair breaking effects other than inelastic electron-phonon scattering, we find

$$\alpha^{\mathrm{R(\ A)}}(E) = (E \pm \mathrm{i}/2\tau_{\mathrm{E}}) \,/ \sqrt{(E \pm \mathrm{i}/2\tau_{\mathrm{E}})^2 - \Delta^2}$$
$$\beta^{\mathrm{R(\ A)}}(E) = \mathrm{i}\Delta / \sqrt{(E \pm \mathrm{i}/2\tau_{\mathrm{E}})^2 - \Delta^2} \tag{3.16}$$

where $\mathrm{Im}\,\sqrt{\ldots} > 0$. In certain cases, it is also sufficient to know the large energy expansions for $E \gg \Delta$

$$\alpha^{\mathrm{R(\ A)}}(E) = \pm \left[1 + \frac{\Delta^2}{2(E \pm \mathrm{i}\Gamma)^2}\right]$$
$$\beta^{\mathrm{R(\ A)}}(E) = \pm \frac{\mathrm{i}\Delta}{E \pm \mathrm{i}\Gamma} \left[1 + \frac{E\Delta^2}{2(E \pm \mathrm{i}\Gamma)^3}\right] \tag{3.17}$$

Here Γ contains all pair breaking mechanisms (i.e. it also includes the effect of electron-phonon collisions); e.g.

$$\Gamma = \frac{1}{\tau_{\mathrm{s}}} + \frac{1}{2\tau_{\mathrm{E}}} + \frac{1}{2} D \left(4m^2 v_{\mathrm{s}}^2 - \frac{1}{\Delta} \frac{\partial^2}{\partial \boldsymbol{r}^2} \Delta\right) \tag{3.18}$$

The expansion (3.17) is also valid for strong pair breaking $\Gamma \gg \Delta$. The complete theory is gauge invariant. We can make this explicit by using only the gaugeinvariant quantities

$$\Phi = \frac{1}{2}\hat{\theta} - e\varphi, \quad v_{\mathrm{s}} = -\frac{1}{2m}\left(\frac{\partial}{\partial r}\theta + 2eA\right) \tag{3.19}$$

Since $\dot{\theta}/2$ is the Cooper pair electrochemical potential, Φ has the meaning of a pair chemical potential. Furthermore, v_{s} is the superfluid velocity. On the other hand, the gauge where Δ is real ($\theta = 0$) has particular virtues. If one resorts to an expansion of the dot product in terms of time derivatives, this gauge ensures the fastest convergence. In the linearized theory, the real Δ gauge is still a convenient gauge.

26.3.3 3.3. Linearized theory

If the deviations from equilibrium are small, we may proceed in a linearized theory. We split according to

$$f^{\mathrm{L}} = f_0 + f_1^{\mathrm{L}}, \quad f^{\mathrm{T}} = f_1^{\mathrm{T}}$$

$$\hat{g}^{\mathrm{R}} = \hat{g}_0^{\mathrm{R}} + \hat{g}_1^{\mathrm{R}}, \text{ (similarly for A, K)}$$
$$\Delta = \Delta_0 + \Delta_1, v_{\mathrm{s}} = v_{\mathrm{s}0} + v_{\mathrm{s}1}$$

Also Φ is a small quantity. For convenience, we will omit the subscript 0 at $A_0 \equiv \Delta$ in the following. After Fourier transformation with respect to time in order to express the dot product in simple terms we obtain from the K component of eq. (3.1) for general frequencies two (coupled) linearized Boltzmann equations for the two distribution functions $f_1^{\mathrm{L}}(E; r, \omega)$ and $f_1^{\mathrm{T}}(E; \boldsymbol{r}, \omega)$. (Actually, we consider the following combinations of the components of (3.1) : $\{\ldots\}^{\mathrm{K}} - \{\ldots\}^{\mathrm{R}} \circ h + h \circ \{\ldots\}^{\mathrm{A}}$.)

$$
\begin{aligned}
&N_1\dot{f}_1^{\mathrm{L}} - D\frac{\partial}{\partial r}\left[M^{\mathrm{L}}\left(\frac{\partial}{\partial r}f_1^{\mathrm{L}}\right)\right] - 4Dmv_{\mathrm{s}0}\left(\frac{\partial}{\partial r}f_1^{\mathrm{T}}\right)N_2R_2 \\
&\quad + \dot{d}_1R_2\frac{\partial f_0}{\partial E} - 4Dm^2v_{\mathrm{s}0}\cdot v_{\mathrm{s}1}N_2R_2\frac{\partial f_0}{\partial E} - K^{\mathrm{L}}\left(f_1^{\mathrm{L}}\right) = 0 \\
&N_1\dot{f}_1^{\mathrm{T}} + 2\Delta N_2 f_1^{\mathrm{I}} - D\frac{\partial}{\partial r}\left[M^{\mathrm{T}}\left(\frac{\partial}{\partial r}f_1^{\mathrm{T}} + m\dot{v}_{\mathrm{s}1}\frac{\partial f_0}{\partial E}\right)\right] \\
&\quad - 4Dmv_{\mathrm{s}0}\left(\frac{\partial}{\partial r}f_1^{\mathrm{L}}\right)N_2R_2 - N_1\dot{\Phi}\frac{\partial f_0}{\partial E} - K^{\mathrm{T}}\left(f_1^{\mathrm{T}}\right) = 0
\end{aligned}
\tag{3.20}
$$

Here, we have written for short $f_1^{\mathrm{L}} = -i\omega f_1^{\mathrm{L}}(E;r,\omega),\ldots$, and $N_1 = N_1(E;\omega),\ldots$. We have introduced generalized spectral quantities, depending on frequency shifted equilibrium Green's functions, by

$$
\begin{aligned}
N_1(\mathrm{E};\omega) &= \frac{1}{2}\left[\alpha^{\mathrm{R}}\left(E+\frac{1}{2}\omega\right) - \alpha^{\mathrm{R}}\left(E-\frac{1}{2}\omega\right)\right], \\
N_2(E;\omega) &= \frac{1}{2}\left[\beta^{\mathrm{R}}\left(E+\frac{1}{2}\omega\right) + \beta^{\mathrm{A}}\left(E-\frac{1}{2}\omega\right)\right], \\
R_2(E;\omega) &= (1/2\mathrm{i})\left[\beta^{\mathrm{R}}\left(E+\frac{1}{2}\omega\right) - \beta^{\mathrm{A}}\left(E-\frac{1}{2}\omega\right)\right],
\end{aligned}
\tag{3.21}
$$

and

$$
M^{\mathrm{T}}(E;\omega) = N_1^2(E;\omega) + N_2^2(E;\omega), \quad M^{\mathrm{L}}(E;\omega) = N_1^2(E;\omega) - R_2^2(E;\omega)
$$

In the following, we will always write the arguments of the spectral quantities to remind ourselves of this frequency shift, whereas we will drop the arguments of the distribution functions and other quantities where no confusion can occur.

The Boltzmann equations are of the form (3.20) for frequencies satisfying $\omega \ll T$ since we approximated the expression $\frac{1}{2}\mathrm{i}\left\{\tanh\left[\left(E+\frac{1}{2}\omega\right)/2T\right] - \tanh\left[\left(E-\frac{1}{2}\omega\right)/2T\right]\right.$, by $i\omega\left(\hat{c}f_0/\hat{c}E\right)$. The electron-phonon collision integrals are denoted by K^T and K^L. We do not give here their detailed form. Rather, we only mention that they consist of a "scattering out" term $-(1/\tau_{\mathrm{E}})$ $\times N_1(E;\omega)f_1^{\top(L)}$ proportional to the inelastic electron-phonon collision rate;* and a "scattering in" term involving integrals of f_1. An important property is that K^{T} conserves the charge $\int \mathrm{d}EK^{\mathrm{T}}\left(f_1^{\mathrm{T}}\right) = 0$.

Simple expression for the current can be worked out in limiting cases. Near T_{c}, to leading order in Δ/T we find

$$
j_0 = \frac{\sigma}{e}\frac{\pi\Delta^2}{2T}mv_{\mathrm{s}0}\left[\frac{2}{\pi^2}\psi'\left(\frac{1}{2}+\rho\right)\right] \tag{3.22}
$$

where $\rho = \Gamma/2\pi T$ and ψ' is the derivative of the digamma function [e.g. $\psi'\left(\frac{1}{2}\right) = \pi^2/2$]. The linear terms in leading order in Δ/T and $\omega/T, Dq^2/T$ are

$$
\begin{aligned}
j_1(r,\omega) = &-\frac{\sigma}{e}\int \mathrm{d}E\left\{M^{\mathrm{T}}(E;\omega)\left[\left(\frac{\partial}{\partial r}f_1^{\mathrm{T}}\right) + m\dot{v}_{\mathrm{i}1}\frac{\partial f_0}{\hat{c}E}\right]\right. \\
&\left.+4mv_{\mathrm{s}0}\ \mathrm{N}_2(\mathrm{E};\omega)\mathrm{R}_2(\mathrm{E};\omega)f_1^{\mathrm{L}}\right\} \\
&+\mathrm{Lin}\left\{\frac{\sigma}{e}\frac{\pi\Delta^2}{2T}mv_{\mathrm{s}}\left[\frac{2}{\pi^2}\psi'\left(\frac{1}{2}+\rho\right)\right]\right\}
\end{aligned}
\tag{3.23}
$$

By Lin{...} we denote the linear part of {...}, linearized with respect to variations of Δ and v_s. (Also ρ depends on v_s.) In the evaluation of j_0 and of the last term in j_1 we encountered integrals involving the factor $1-2f_0(E)$ in combination with products of retarded quantities only (or advanced only). This fact allowed us to use the expansion (3.17) of α and β, if Δ/T and ω/T are small.

The charge density in the same limit becomes

$$\rho = 2eN_0 \left\{ \int \mathrm{d}E N_1(E;\omega) f_1^{\mathrm{T}} + \Phi \right\} \tag{3.24}$$

The magnitude of the order parameter obeys, near T_c, a generalized Ginzburg-Landau equation. In nonequilibrium situations it depends strongly on the nonequilibrium distribution function. We find

$$\frac{\pi}{8\ \mathrm{T}}\gamma\dot{A}_1 - \Psi A = -\operatorname{Lin}\left\{ \left[\alpha + \beta\frac{\Delta^2}{T^2} + \gamma\xi^2(0)\left(4m^2v_{\mathrm{s}}^2 - \frac{\partial^2}{\partial r^2}\right)\right] A \right\} \tag{3.25}$$

with coefficients depending on the pair breaking strength. For $\Gamma \ll T$ one has $\gamma = 1, \alpha = (T-T_{\mathrm{c}})/T_{\mathrm{c}}$, (notice however, that T_{c} is depressed by pair breaking: in the limit considered $T_{\mathrm{c}} = T_{\mathrm{c0}} - \frac{1}{4}\pi\Gamma\big), \beta = 7\zeta(3)/8\pi^2$ and the coherence length in the dirty limit is related to D by $\zeta^2(0) = \pi D/8T_c$. For the general strength of the

pair breaking one has (Entin-Wohlman and Orbach 1978)

$$\alpha = \frac{T-T_{\mathrm{c}}}{T_{\mathrm{c}}}\left[1-\rho\psi'\right], \quad \beta = \frac{\psi'' + (\rho/3)\psi'''}{(4\pi)^2},$$

and $\gamma = \frac{1}{2}\pi^2\psi'$, where the argument of all $\psi^{(n)}$ is $\frac{1}{2}+\rho$ and $\rho = \Gamma/2\pi T$ contains all pair breaking effect except those written explicitly in (3.25). The distribution function enters in an important way in (3.25) in the gap control function

$$\Psi = -\frac{1}{\Delta}\int \mathrm{d}E R_2(E;\omega) f_1^{\mathrm{L}} \tag{3.26}$$

26.4 4. The order-parameter structure factor

26.4.1 4.1. The formal solution

The order parameter structure factor (2.1) in a superconductor is composed of two contributions reflecting fluctuations in the magnitude and in the phase of the order parameter,

$$S(\mathrm{q},\omega) = S^{\mathrm{L}} + S^{\mathrm{T}}. \tag{4.1}$$

It is connected to a pair field susceptibility by the fluctuation dissipation theorem

$$S(q,\omega) = \frac{2T}{\omega}\operatorname{Im}[\chi(q,\omega)]. \tag{4.2}$$

We, therefore, calculate the response of the system to an applied perturbation. The contribution from the magnitude fluctuations is obtained from the linearized Ginzburg Landau equation (3.25) where on the right-hand side an additional normalized drive term $1/2N_0$ is added. Then $\chi^{\mathrm{L}}(q,\omega) = \Lambda_1(q,\omega)$.

Similarly, we can proceed using a generalized Ginzburg - Landau equation for the phase, which yields $\chi^{\top}(q,\omega) = -A()_1(q,\omega)$ (Schmid and Schön 1975c). In the real Δ gauge, we

[0]*Strictly, $1/\tau_{\mathrm{E}}$ depends on the energy and on the frequency ω. However, near T_{c} we may replace it by its normal state value at T_{c} for $E = \omega = 0$.

correspondingly calculate the response of v_s to a source term, which we add in the continuity equation

$$\dot{\rho} + \operatorname{div} j = -2e\Delta. \tag{4.3}$$

Then $\chi^{\mathrm{T}}(q,\omega) = -\mathrm{i}(2m\Delta/q)v_{\mathrm{s}1}(q,\omega)$ for longitudinal oscillations of $v_{\mathrm{s}1}$.
If we insert the expressions for ρ and j_1, (3.24) and (3.23), and make use of the Boltzmann equation (3.10) we find that the continuity equation to leading order in Δ/T takes the form

$$2\Delta \int \mathrm{d}E N_2(E;\omega) f_1^{\mathrm{T}}(E;q,\omega) + \mathrm{i}D \operatorname{Lin}\left\{ mq \cdot v_{\mathrm{s}} \frac{\pi\Delta^2}{2T}\left[\frac{2}{\pi^2}\psi'\left(\frac{1}{2}+\rho\right)\right]\right\} = \frac{\Delta}{N_0}. \tag{4.4}$$

Furthermore, in Maxwell's equation $\operatorname{div} \boldsymbol{E} = 4\pi\rho$ we can neglect the left-hand side as long as the characteristic wavelengths are small in comparison to the Thomas-Fermi screening length $\lambda_{\mathrm{TF}} = (8\pi e^2 N_0)^{-1/2} \approx 10^{-8}$ cm. This means we have approximate charge neutrality, i.e.

$$\int \mathrm{d}E N_1(E;\omega) f_1^{\mathrm{T}} + \Phi = 0 \tag{4.5}$$

Finally, f_1^{L} and f_1^{T} are found as solutions of the Boltzmann equations (3.20).
We consider first situations where no or only a small static supercurrent is flowing in the superconductor, i.e. $v_{\mathrm{s}0} \approx 0$. In this case, the (L)- and (T)-modes decouple. For transparency, we also restrict ourselves in the following to the important case of not too strong pair breaking, i.e. Γ/T is small. We make no assumption on Γ/Δ, and the generalization to strong pair breaking $\Gamma \gtrsim T$ is straightforward (see Entin-Wohlman and Orbach 1978). We are mainly interested in high frequency phenomena where $\omega \gg 1/\tau_{\mathrm{E}}$. In this context we can neglect the electron-phonon collisions, which in turn allows a straightforward (exact) solution of the Boltzmann equation for f_1^{L} and f_1^{T}. On the other hand, near T_{c} we can easily generalize the result to include the effect of electronphonon scattering in an approximate way. To leading order in A/T the collision operator K^T can be replaced by a reduced operator

$$K_{\mathrm{red}}^{\mathrm{T}} = -\frac{1}{\tau_{\mathrm{E}}} N_1(E;\omega)\left[f_1^{\mathrm{T}}(E) + \frac{\partial f_0}{\partial E}\int \mathrm{d}E' N_1(E';\omega) f_1^{\mathrm{T}}(E')\right] \tag{4.6}$$

which, like the exact operator, conserves the charge $\int \mathrm{d}E K_{\mathrm{red}}^{\top} = 0$. Also, we can replace K^{L} by the scattering-out term only,

$$K^{\mathrm{L}} \approx -(1/\tau_{\mathrm{E}}) N_1(E;\omega) f_1^{\mathrm{L}}$$

With these approximations and use of (4.5) the solutions of the Boltzmann equations are

$$\begin{aligned} f_1^{\mathrm{L}} =& \frac{1}{Q^{\mathrm{L}}} \frac{1}{4T\cosh^2(E/2T)} (-\mathrm{i}\omega)\Delta_1 R_2(E;\omega) \\ f_1^{\mathrm{T}} = \frac{1}{\mathrm{Q}^{\mathrm{T}}} \frac{1}{4T\cosh^2(E/2T)} [& -(-\mathrm{i}\omega + 1/\tau_{\mathrm{E}})\,\Phi N_1(E;\omega) \\ & - D\omega mq \cdot v_{\mathrm{s}1} M^{\mathrm{T}}(\mathrm{E};\omega)] \end{aligned} \tag{4.7}$$

where

$$\begin{aligned} Q^{\mathrm{L}} &= (-\mathrm{i}\omega + 1/\tau_{\mathrm{E}})\, N_1(E;\omega) + Dq^2 M^{\mathrm{L}}(E;\omega) \\ Q^{\mathrm{T}} &= (-\mathrm{i}\omega + 1/\tau_{\mathrm{E}})\, N_1(E;\omega) + 2\Delta N_2(E;\omega) + Dq^2 M^{\mathrm{T}}(E;\omega) \end{aligned} \tag{4.8}$$

(Notice, also in the generalized densities of states the combination $-i\omega + 1/\tau_{\rm E}$ appears.) We now define the integrals

$$X_{ij} = \int_{+\infty}^{\infty} \mathrm{d}E \frac{1}{\cosh^2 E/2T} \frac{N_i(E;\omega)N_i(E;\omega)}{Q^{\rm T}} \quad i,j = 1,2$$
$$X_{\rm L} = \int_{-\infty}^{\infty} \mathrm{d}E \frac{1}{\cosh^2 E/2T} \frac{R_2^2(E;\omega)}{Q^{\rm L}} \tag{4.9}$$

In X_{11} we split off the leading term

$$X_{11} = \frac{4T}{-i\omega + 1/\tau_{\rm E} + Dq^2} + \tilde{X}_{11} \tag{4.9'}$$

The wave vector dependence thus written explicitly in (4.9') turns out to be most important. Furthermore, we encounter the integral $\int_{-\infty}^{\infty} N_2(E;\omega)\mathrm{d}E = \pi A$.

With these definitions we readily obtain

$$\chi^{\rm L}(q,\omega) = \frac{4T}{\pi N_0}\left[-\frac{16T_{\rm c}}{\pi}\alpha - \mathrm{i}\omega + Dq^2 - \frac{2\mathrm{i}\omega}{\pi}X_{\rm L}\right]^{-1} \tag{4.10}$$

$$\chi^{\rm T}(q,\omega) = \frac{4T}{\pi N_0}\left\{-\mathrm{i}\omega + Dq^2 + \mathrm{i}\omega\frac{2}{\pi}\left[X_{22} - \frac{(X_{12})^2}{\tilde{X}_{11} - \frac{4TDq^2}{(\mathrm{i}\omega+1/\tau_{\rm E}+Dq^2)(-\mathrm{i}\omega+1/\tau_{\rm E})}}\right]\right\}^{-1}$$

26.4.2 4.2. Analytic expressions

It remains to evaluate the integrals X_{ij}. We find analytic expressions in several limits. In the considered order in Δ/T we may set in the integrals X_{12}, X_{22}, $\widetilde{X}_{11}$ and $X_{\rm L}$ the factor $\cosh^{-2}(E/2T) = 1$. In context with the collective mode an important case is that of negligible pair breaking $\Gamma \ll \omega$. In this limit we find

$$X_{12} = -\frac{i}{2}\frac{v\delta}{v^2+\delta^2}(I + rJ) + \frac{\delta^2}{v^2+\delta^2}L$$
$$X_{22} = -\frac{\delta}{2}(I - rJ) + \mathrm{i}\frac{\delta^2}{v}L + \frac{\pi}{2}$$
$$\tilde{X}_{11} = -\mathrm{X}_{22} + \frac{1}{2}\frac{\delta}{v^2+\delta^2}\left[H + \left(s - 2v^2 - 2\right)I + r^2 J\right] + \mathrm{i}\frac{r\delta^2}{v\left(v^2+\delta^2\right)}L + \frac{\pi}{2}$$
$$X_{\rm L} = \frac{\delta}{2}\left(1 + \frac{1}{v^2+\delta^2}\right)I + \frac{sr}{2\delta}J + \frac{\mathrm{i}s}{v}L - \frac{\pi}{2} \tag{4.12}$$

We used the notation $v = \omega/(24)$ and $\delta = D\mathrm{q}^2/(24)$ and introduced

$$s = \frac{\delta^2}{v^2+\delta^2} - \delta^2, \quad r = \delta^2 + v^2 - \frac{v^2}{v^2+\delta^2}$$

The functions, I, J, H are combinations of complete elliptic integrals of the first kind $K(k)$, the second kind $E(k)$, and third kind $\Pi\left(\alpha^2, k\right)$. They are, using the notation of Byrd and Friedman (1971)

$$
\begin{aligned}
I &= \frac{2}{1+v}K(k)\theta(1-v) + \frac{\mathrm{i}}{1+v}K\left(k'\right) \\
J &= \frac{-2}{s(1+v)}\Pi\left(\frac{(1-v)^2}{s}, k\right)\theta(1-v) + \frac{\mathrm{i}}{(1+v)\left[(1+v)^2-s\right]}\Pi\left(\frac{4v}{(1+v)^2-s}, k'\right) \\
H &= 2(1+v)[K(k)-E(k)]\theta(1-v) + \mathrm{i}(1+v)E\left(k'\right)
\end{aligned}
\tag{4.12'}
$$

with $k = (1-v)/(1+v), k' = \sqrt{1-k^2}$. The real parts of I, J and H vanish for $v > 1$. Finally, for $v \leqslant \sqrt{1-\delta^2}$, where $s \geqslant 0$, the functional L is given by

$$
L = \frac{\pi}{4}\frac{v}{\delta^2}\left[\frac{v-\delta^2/\sqrt{s}}{\sqrt{1-(\sqrt{s}+v)^2}} + \frac{v+\delta^2/\sqrt{s}}{\sqrt{1-(\sqrt{s}-v)^2}}\right] \tag{II}
$$

while for $v > \sqrt{1-\delta^2}$, where $s < 0$, it is

$$
L = -\mathrm{i}\frac{\pi v}{4\delta\sqrt{-s}}\left[1 - \frac{r}{\sqrt{\left(1-s-v^2\right)^2 - 4sv}}\right] + \frac{\pi v}{2\delta^2}\frac{\left(v+\mathrm{i}\delta^2/\sqrt{-s}\right)}{\sqrt{1-(\mathrm{i}\sqrt{-s}+v)^2}}. \tag{III}
$$

All square roots are positive real numbers except for the expression $\sqrt{1-(\mathrm{i}\sqrt{-s}+v)^2}$, which has a positive real and negative imaginary part.

Another interesting limit is the case of small wave vectors $Dq^2 \ll \omega$ or $Dq^2 \ll 1/\tau_{\mathrm{E}}$. In this case, we find for general strength of the pair breaking (but still $\Gamma \ll \mathrm{T}$)

$$
\begin{aligned}
X_{12} &= \frac{\pi}{2}\frac{\sqrt{(-\mathrm{i}\omega+2\Gamma)/\left(-\mathrm{i}\omega+1/\tau_{\mathrm{E}}\right)}}{\sqrt{1+\left(-\mathrm{i}\omega+2\Gamma\right)\left(-\mathrm{i}\omega+1/\tau_{\mathrm{E}}\right)/(2A)^2}} \\
X_{22} &= \frac{\pi}{2} - \frac{\left(-\mathrm{i}\omega+1/\tau_{\mathrm{E}}\right)}{2\Delta}X_{12} \\
\tilde{X}_{11} &= \frac{-2\Delta}{-\mathrm{i}\omega+1/\tau_{\mathrm{E}}}X_{12} \\
X_{\mathrm{L}} &= \frac{\pi\Delta}{-\mathrm{i}\omega+1/\tau_{\mathrm{E}}}\left\{\sqrt{1+\frac{(-\mathrm{i}\omega+2\Gamma)^2}{(2\Delta)^2}} - \frac{(-\mathrm{i}\omega+2\Gamma)}{2\Delta}\right\}
\end{aligned}
\tag{4.13}
$$

where for $\omega = 0$ the square roots are positive. More precisely, we find the forms (4.13) in both the limits $\Gamma = 1/2\tau_{\mathrm{E}}$ and $\Gamma \gg \Delta$. Furthermore, they differ only by a few percent from the result of a first order expansion in $\Gamma_i\Delta$. Therefore, we use (4.13) as interpolation formulas for all values of Γ.

Although (4.13) is the small Dq^2 limit of the integrals X_{ij}, we stress again that the dominant wave vector dependence is taken into account by splitting X_{11} into two contributions in eq. (4.9') and keeping the Dq^2 written explicitly there.

Finally, we give the results for small wave vectors and weak pair breaking Γ, $Dq^2 \ll \omega \ll \Delta \ll T$, including first order corrections in Dq^2/ω and Γ/ω. In this case

$$
\begin{aligned}
X_{12} &= \frac{\pi}{2}\left(1 + \mathrm{i}\frac{\Gamma_0}{\omega} + \frac{2}{\pi}\mathrm{i}\frac{Dq^2}{\omega}\right) \\
X_{22} &= \frac{\pi}{2} - \mathrm{i}\frac{\omega}{2A}\frac{\pi}{2}\left(1 + \mathrm{i}\frac{\Gamma_0}{\omega} + \mathrm{i}\frac{1}{\omega\tau_\mathrm{E}}\right) - \frac{Dq^2}{2\Delta}\left(\ln\frac{8\Delta}{\omega} - 1 + \mathrm{i}\frac{\pi}{2}\right) \\
\tilde{X}_{11} &= -\mathrm{i}\frac{\pi\Delta}{\omega}\left(1 + \mathrm{i}\frac{1/\tau_\mathrm{E} - \Gamma_0}{\omega} - \mathrm{i}\frac{4}{\pi}\frac{Dq^2}{\omega}\right) \\
X_\mathrm{L} &= -\frac{\pi}{2} + \frac{\pi\Delta}{-\mathrm{i}\omega + 1/\tau_\mathrm{E}} - \frac{Dq^2\Delta}{\omega^2}\left(\ln\frac{8\Delta}{\omega} - 4 + \mathrm{i}\frac{\pi}{2}\right)
\end{aligned}
\tag{4.14}
$$

where Γ_0 represents the pair breaking effects other than inelastic electron phonon scattering ($\Gamma = \Gamma_0 + 1/2\tau_\mathrm{E}$).

26.4.3 4.3. Results

The order-parameter structure factor $S(q,\omega) = S^\mathrm{L}(q,\omega) + S^\mathrm{T}(q,\omega)$ is plotted in figures 1 to 4 as a function of the frequency for different wave vectors and temperatures near T_c. We used both the weak pair breaking expressions (4.12) and the small wave-vector expansion (4.13). Several features are quite conspicuous.

First, there is a central peak at small frequencies resulting mainly from the longitudinal structure factor. For vanishing wave vectors q $\to$ 0, this peak reflects the order parameter relaxation with characteristic time τ_1. For instance, for weak pair breaking due to electron-phonon scattering only ($\Gamma = 1/(2\tau_\mathrm{E}) \ll \Delta$), we find (Schmid 1968, Schmid and Schön 1975a)

$$
\frac{1}{\tau_\Delta} = \frac{7\zeta(3)}{\pi^3}\frac{\Delta}{T}\frac{1}{\tau_\mathrm{E}}. \tag{4.15}
$$

The generalization to arbitrary pair breaking follows in a straightforward manner from (4.13) (Eckern and Schön 1978). On the other hand, for finite wave-vectors, considered here, the central peak is broader, reflecting the existence of a diffusive mode. From eq. (4.14) we find that to lowest order in Δ/T for $\Gamma \ll Dq^2 \ll \omega \ll \Delta$

$$
\chi^\mathrm{L}(q,\omega) = \frac{4T}{\pi N_0}\frac{\omega}{2\Delta}\left[\omega + \mathrm{i}\frac{Dq^2}{\pi}\ln\frac{8\Delta}{\omega}\right]^{-1}. \tag{4.16}
$$

Second, for finite wave vectors, the transverse part of the structure factor at temperatures close to T_c shows a peak at finite frequencies. In the limit Γ, $Dq^2 \ll \omega \ll \Delta \ll T$ we can use the expansion (4.14) and find a simple expression*:

$$
\chi^\mathrm{T}(q,\omega) = A\left\{\omega^2 + \mathrm{i}\omega\left[\frac{\pi A^2}{2T} + \frac{Dq^2}{\pi}\left(2\ln\frac{8\Delta}{\pi} - 2\right) + \frac{1}{\tau_\mathrm{E}} + \Gamma_0\right] - 2\Delta Dq^2\right\}^{-1}, \tag{4.17}
$$

where the prefactor depends strongly on Dq^2

$$
A = \frac{4T}{\pi N_0}\frac{1}{Dq^2}\left(i\frac{\pi\Delta^2\omega}{2T} - 2\Delta Dq^2\right). \tag{4.18}
$$

In the form (4.17), we easily see that this peak in the structure factor results from a pole of χ^T at

$$
\omega_q = -\frac{1}{2}i_\gamma \pm \sqrt{c^2q^2 - \frac{1}{4}\gamma^2}.
$$

which reflects a propagating collective mode. The bare phase velocity of this mode (in the dirty limit) is

$$c_{CG} = \sqrt{2AD}. \tag{4.19}$$

The mode is damped. The mode damping in the dirty limit is given by

$$\gamma = \frac{n_s}{n}\frac{1}{\tau_{imp}} + \frac{Dq^2}{\pi}\left(2\ln\frac{8\Delta}{\omega} - 2\right) + \frac{1}{\tau_E} + \Gamma_0. \tag{4.20}$$

Clearly, the propagating mode only exists at temperatures close to T_c as long as the damping $n_s\,((n\tau_{imp}) = \pi A^2, (2T)$, which is due to ohmic losses of the normal current, is small. On the other hand, the mode is damped due to

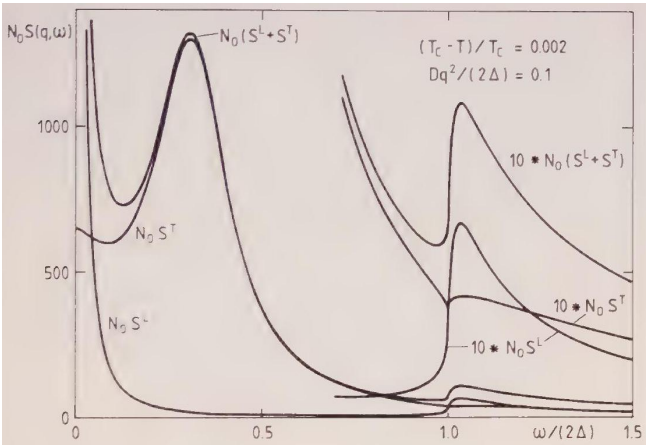


Fig. 1. The structure factors representing fluctuations of the magnitude and the phase of the order parameter \$S\^{}\{L
\$ and $S^{\bar{T}}$, and the total structure factor, i.e the sum of $S^L + S^T$, are plotted as a function of the frequency ω. The results are those of short mean free path superconductors, the wavevector is fixed at $Dq^2/(2\Delta) = 0.1$ and the reduced temperature is $(T_c - T)/T_c = 0.002$. Pair breaking effects are small, $\Gamma, 1/\tau_E \approx 0$, i.e. the expansion (4.12) is used. The structure factors are shown for positive frequencies only, they are symmetric in ω. They are multiplied by N_0, the density of states at the Fermi surface. The parts with large frequencies are also shown enhanced by a factor 10 in order to resolve better the resonance of S^L at $\omega = 2\Delta$. The central peak of S^L represents a diffusive mode, the peak of $S^\top$ the Carlson-Goldman propagating collective mode.}

diffusion processes of the quasiparticles which is reflected by the second term in %. Hence. the mode propagates only if $Dq^2 \ll \omega\ |$. As long as the resonant frequency $|\omega| \approx c_{CG}q$ is small in comparison to Δ this condition is always satisfied. Finally. we see that inelastic electron

0

- Various authors, concerned with different limits, have derived this result, extensions, or parts of it before. Schmid and Schön (1975b) and Artemenko and Volkov (1975) considered the case of small Dq^2 and $\Gamma = 0$ in the dirty and clean limits, respectively. Schmid and Schön (1975c) and Dinter (1978a,b) considered general Dq^2 and $\Gamma = 0$. Ovchinnikov (1977) included Dq^2 and Γ_0 to first order and, in addition, allowed for general impurity concentrations. Schön and Ambegaokar (1979) considered small Dq^2, but general Γ as long as $\Gamma/T \ll 1$, and included the effect of an imposed supercurrent. Entin-Wohlman and Orbach (1978) formulated the problem for general Γ/T, but in their final expressions for the damping left out the leading correction in Γ_0/ω [included in eq. (4.17)]. Also Artemenko and Volkov (1979), Kulik et al. (1981) and Cheishvili (1982) discussed the problem for general impurity concentrations.

phonon collisions and any other pair breaking mechanism further increase the damping. (See also Cheishvili 1977, 1982 and Galaiko et al. 1978). Summarizing, we conclude that in a short mean free path superconductor the collective mode propagates if the following conditions are satisfied:

$$\Gamma_0, \quad \frac{1}{\tau_E}, \quad \frac{\Delta^2}{T} \ll |\omega| \ll \Delta. \tag{4.21}$$

The qualitative features which we obtain from the expansion (4.18) are also borne out by the analysis of the more complete results shown in the figures.

In this context it should be added that in superconductors with longer mean free path, the propagating mode is also found (Artemenko and Volkov 1975.

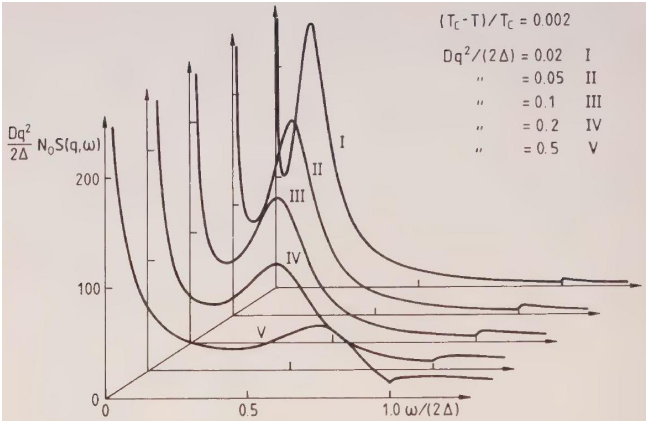


Fig. 2. The (total) order-parameter structure factor is shown as a function of the frequency for different wavevectors: (curve I) $D q^{2}/(2 \Delta)=0.02$, (II) 0.05 , (III) 0.1 , (IV) 0.2 , and (V) 0.5 . The other parameters are the same as in fig. 1. For easier comparison the structure factors are plotted reduced by a factor $Dq^2/(24)$. Notice the following features: (i) the diffusive central peak broadens with increasing Dq^2; (ii) the peak at finite frequency is shifted roughly proportional to q, i.e. it represents a propagating mode; (iii) the damping of the propagating mode becomes stronger with increasing Dq^2; (iv) the resonance at $\omega = 24$ becomes less pronounced as Dq^2 increases.}

1979; Dinter 1978a; Ovchinnikov 1977). The same physical damping mechanisms exist. But, since the superfluid density depends on the impurity concentration the phase velocity and the strength of the damping are different. In clean superconductors the restriction of weak diffusive damping $Dq^2 \ll |\omega|$ results in an upper limit to the frequency $|\omega| \ll \Delta_1 \, (T\tau_{\mathrm{imp}})$ (Ovchinnikov 1977).

Third, we find that the order parameter structure factor strongly increases at frequencies above $2A$. This is again due to the longitudinal part $S^{\mathrm{L}}(\mathrm{q}, \omega)$. In the limit of very weak pair breaking and very small wave vectors, the structure factor S^{L} vanishes for $\omega \leqslant 24$ and sets in proportional to $\sqrt{(\omega/2\Delta)^2 - 1}$ above $\omega = 24$. Hence, this structure is a resonance. It differs from the structures discussed so far which result from poles of the susceptibility in the complex frequency plane. In the time domain, this resonance corresponds to an oscillation at frequency $\omega = 2\Delta$ which is damped according to a power law in $1/(\Delta t)$. This means the damping is never small. In contrast a pole corresponds to an oscillation damped exponentially. The effect of pair breaking is to smear out this structure (Schön and Ambegaokar 1979) and S^L becomes proportional

to $-\operatorname{Im} \sqrt{1 + [(-i\omega + 2\Pi)/24]^2}$ (see eq. 4.13). Spatial variations have a similar effect (Dinter 1978a,b): From the expansion of (4.12) we find that near $\omega = 2A$ the structure factor

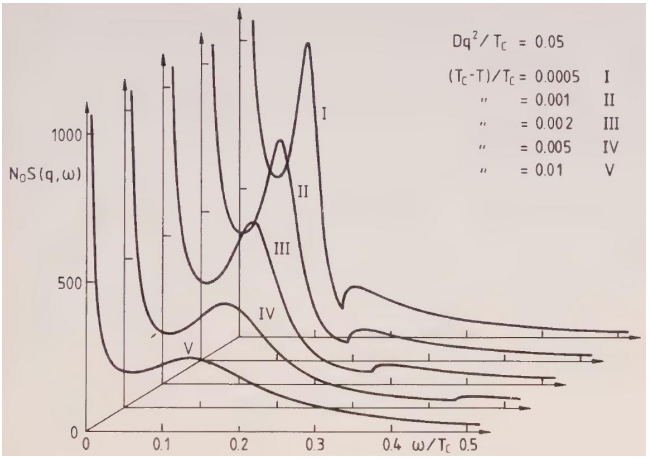


Fig. 3. The (total) order-parameter structure factor is shown as a function of the frequency for different (reduced) temperatures: (curve I) $\left(T_{\mathrm{c}}-T\right) / T_{\mathrm{c}}=0.0005$, (II) 0.001 , (III) 0.002 , (IV) 0.005 , (V) 0.01 . The wavevector is fixed at $Dq^2/T_{\mathrm{c}} = 0.05$, the other parameters are the same as in fig. 1. Notice the following features: (i) the peak representing the propagating mode is shifted roughly proportional to $\sqrt{\Delta(T)}$; (ii) the damping of this mode increases with decreasing temperature; (iii) there is a resonance at $\omega = 2\Delta(T)$.}

S^{L} is proportional to $\sqrt{(\omega/2\Delta)^2 - 1}\theta(\omega - 2\Delta) + Dq^2/2\Delta$.

In a superconductor where a finite supercurrent is flowing in equilibrium already, i.e. $v_{\mathrm{s0}} \neq 0$, the fluctuations in the magnitude and phase of the order parameter are coupled. In other words, the longitudinal (energy) mode and the transverse (charge) mode are no longer independent. We can still proceed as before, to calculate the response to an external drive [compare e.g. eq. (4.3)], and obtain the pair field susceptibilities. A technical complication arises from the coupling of the two Boltzmann equations. The problem has been dealt with in the limit of small wave vectors $Dq^2 \ll |-i\omega + 1/\tau_E|$ by Schön and Ambegaokar (1979). We merely quote some of the results. The most important effects of the imposed supercurrent are: (i) The gap relaxation time becomes longer and it diverges (mode softening) if the imposed supercurrent approaches the Ginzburg-Landau critical current j_{c}. For $\Gamma \ll \Delta$ one finds that a spatially

(q) modulated fluctuation of Δ relaxes with rate

$$1/\tau_A = \frac{1}{2\Delta\tau_{\mathrm{E}}}\left(\frac{14\zeta(3)\Delta^2}{\pi^3 T} + Dq^2 - 16Dm^2v_{\mathrm{s0}}^2\right), \tag{4.22}$$

where Δ is reduced due to the supercurrent. Hence, at j_{c} homogeneous fluctuations ($q = 0$) of Δ become unstable first. (ii) Both phase velocity and damping of the propagating collective mode are affected. The phase velocity is reduced,

$$c_{\mathrm{CU}}^2 = 2AD\left(1 - \frac{2Dm^2v_{\mathrm{s0}}^2}{\Delta}\right), \tag{4.23}$$

while the damping is increased due to the pair breaking effect of the imposed supercurrent (see eq. 4.20).

26.4.4 4.4. Comparison with experiment*

In many systems exhibiting a second-order phase transition, the order parameter can be directly coupled to a classical external field. The response of the order parameter to this

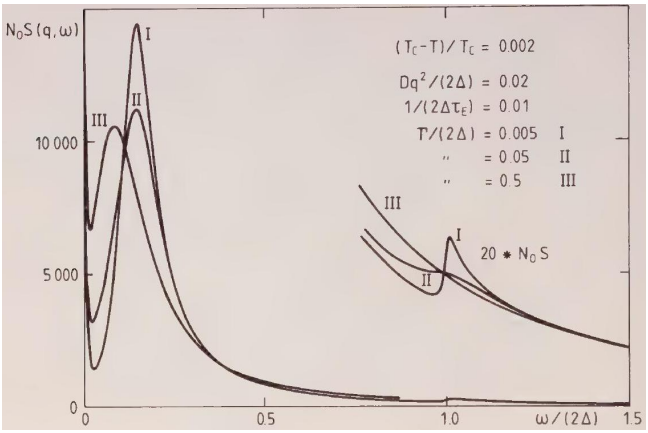


Fig. 4. The (total) order-parameter structure factor is shown as a function of the frequency for different strength of the pair breaking. The parts with large frequencies are also/only shown enhanced by a factor 20 . Curve I represents the situation where the pair breaking is due to inelastic phonon collisions only i.e. $\Gamma=1 /\left(2 \tau_{\mathrm{E }}\right)$, with rate assumed to be $1/(2\Delta\tau_{\mathrm{E}}) = 0.01$. Curves II and III represent the situation with additional stronger pair breaking mechanisms. The expansions (4.13) are used. Hence, the result is correct only for $\omega \gg Dq^2$. (The expansions can also be applied if $1/\tau_E \gg Dq^2$, but the parameters are chosen differently.) The comparison shows the following features: (i) pair breaking effects act as a damping mechanism for the collective mode and reduce the peak frequency; (ii) the resonance at $\omega = 2\Delta$ is washed out by pair breaking effects. Since the expansion (4.13) is used, the damping of the collective mode due to diffusion is not accounted for in fig. 4 . This effect can be seen by comparing curve I of fig. 2 and curve I of fig. 4 , which have roughly the same parameters.}

field determines the characteristic susceptibility and correlation function. In a superconductor however, the order parameter A is off-diagonal in electron number representation. For this reason one cannot couple to Δ with a classical field. Nevertheless, following a suggestion of Ferrell (1969) the pair field susceptibility can be determined by measuring the conductivity of a Josephson junction. The metal of interest which is near its transition temperature forms one side of the junction. The metal on the other side is well below its transition temperature. The order parameter of the high T_c superconductor provides the off-diagonal coupling to the fluctuating order parameter of the superconductor near T_c. These fluctuations give rise to Josephson currents which appear as an excess conductivity.

The geometry of the junctions used in the experiments is shown in fig. 5. On one side is the superconductor of interest, a film of thickness d, with transition

temperature T_c. Since $T \approx T_c$ the penetration depth $\dot{\lambda}(T)$ is large and an applied parallel magnetic field completely penetrates the film. On the other side is a superconductor well below its transition temperature T_c' with penetration depth λ'. The order parameter of this superconductor has a well defined value with negligible fluctuations. The state of the Josephson junction depends on the phase difference across the barrier, which is a function of both the magnetic field and the DC voltage applied to the junction. A field H, in the y-direction, produces a variation of the phase difference in the z-direction characterized by a wave vector

$$q = (2eH/c)\,(\lambda' + d/2)\,, \tag{4.24}$$

A DC voltage V, applied to the junction, produces time variations with frequency

[0]*For a detailed review see also Goldman (1981).

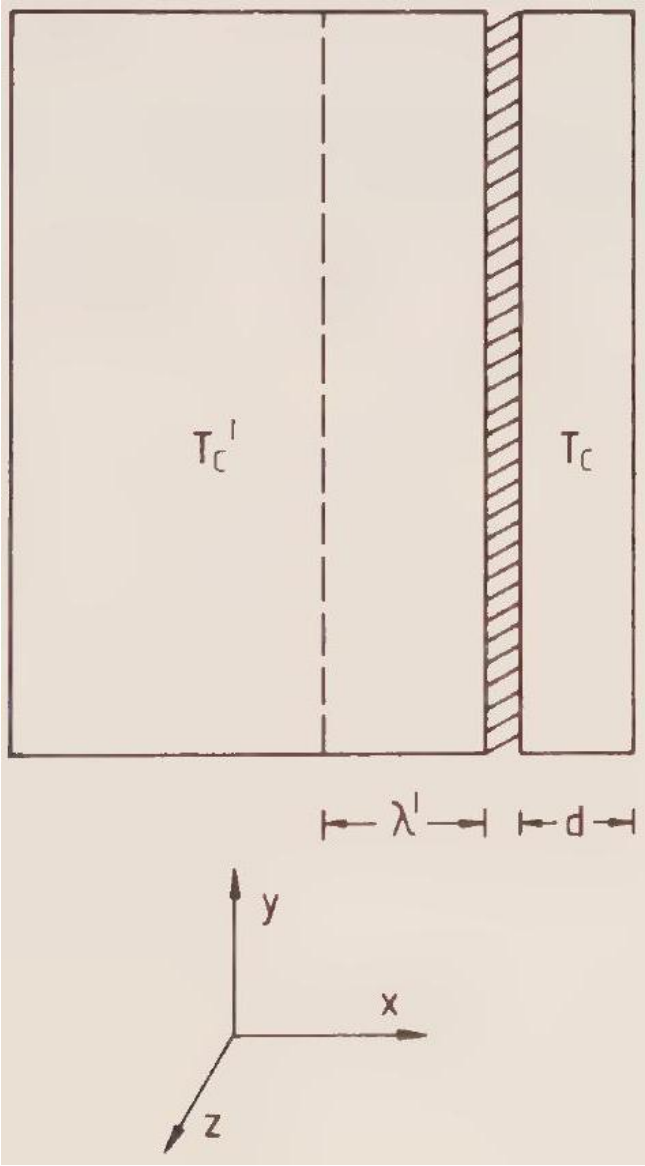


Fig. 5. The tunneling junction geometry is shown which is used in the experiments to measure the order-parameter structure factor of the superconducting film.

$$\omega = 2\mathrm{eV}. \tag{4.25}$$

Even above T_c an excess current due to pair tunneling is flowing. It turns out to be related to the pair field susceptibility by

$$I_{ex}(H,V) = \text{ const } \cdot \mathrm{Im}[\chi(q,\omega)]. \tag{4.26}$$

The constant in (4.26) is proportional to $|T|^4$ where T is the tunneling matrix element. Scalapino (1970) derived this result starting from a model Hamiltonian for the pair tunneling. Takayama (1971) and Shenoy and Lee (1974) confirmed this result by microscopic calculations.

Also below T_c, the pair current may serve as a probe for the fluctuations and the pair field susceptibility (see e.g. Dinter 1978a). However, since the expectation value of the fluctuating order parameter is nonzero, also the usual Josephson current (proportional to $|T|^2$) is flowing. This contribution is usually larger than I_{cx}, but can be quenched by applying a magnetic field. Another large contribution to the current results from quasiparticle tunneling. It has

to be subtracted numerically from the experimental data. In the experiments of Carlson and Goldman (1975, 1976) short mean free path superconducting aluminium films were investigated. Pair breaking effects were weak. The resulting order-parameter structure factor is shown in fig. 6 (full lines). It is compared with the theoretical result derived above (broken lines) in the limit of vanishing pair breaking (i.e. using 4.12), corrected to include second order contributions in $\Delta/T, \omega/T$, and Dq^2/T given in the Appendix (Schön 1976). Except at very small frequencies we find very good quantitative agreement between both results with no adjustable parameter. We confirm that the central peak results from fluctuations in the magnitude of the order parameter. It is a diffusive peak of the type following from eq. (4.16). Notice that the resolution of the experiments is too rough to detect a homogenous ($q \approx 0$) gap relaxation with rate $1/\tau_1$ (compare eq. 4.15). The peak at finite frequencies results from fluctuations in the phase of the order parameter. The

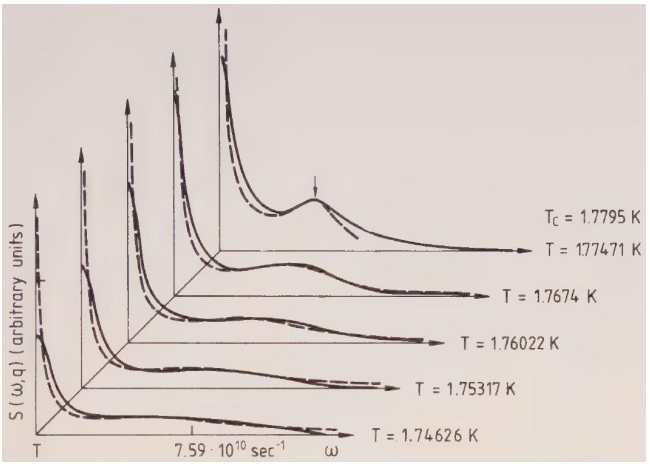


Fig. 6. The order-parameter structure factor measured in the experiment of Carlson and Goldman (1975) (solid line) is compared with the theoretical result (including corrections in \$\Delta / \mathrm{T , \omega / \mathrm{T}\$, Dq^2/T) (broken line). The parameters of the calculated curves are the same as in the experiments. The wavevector is $q = 4 \times 10^4$ cm^{-1}, the diffusion coefficient is $D = 18.6$ s^{-1} cm^2, and the transition temperature is $T_c = 1.7795$ K. Only the absolute value of the structure factor, which is uncertain in the experiments, is scaled to fit at one point, indicated by the arrow.}

frequency where the peak due to the collective mode is found is much larger than the charge imbalance relaxation rate $1/\tau_{Q^*}$ (see below). Hence, the mode is definitely not a hydrodynamic mode, rather it is a collisionless mode.

A magnetic field is applied to create the spatially periodic structure. The data shown in fig. 6 were obtained in a field of 125 G which leads to a wave vector $q = 4 \times 10^4$ cm^{-1}. This field also leads to pair breaking of strength $\Gamma_0 = 1.95 \times 10^9$ s^{-1}, which may account for the difference between experimental and plotted theoretical results at small frequencies. It has no noticeable direct effect on the propagating mode.

Since the magnetic field also lowers the transition temperature, a comparison of the resonance frequencies for different wave vectors should be performed at the same reduced temperature

$$\alpha(T,H) = \frac{[T - T_c(H)]}{T_c(H)} \approx \alpha(T,0) + \frac{\pi e^2 D d^2}{24 T_c(0) c^2} H^2. \tag{4.27}$$

In fig. 7 the dispersion relation $\omega(q)$ at fixed $\alpha(T,H)$ found from the

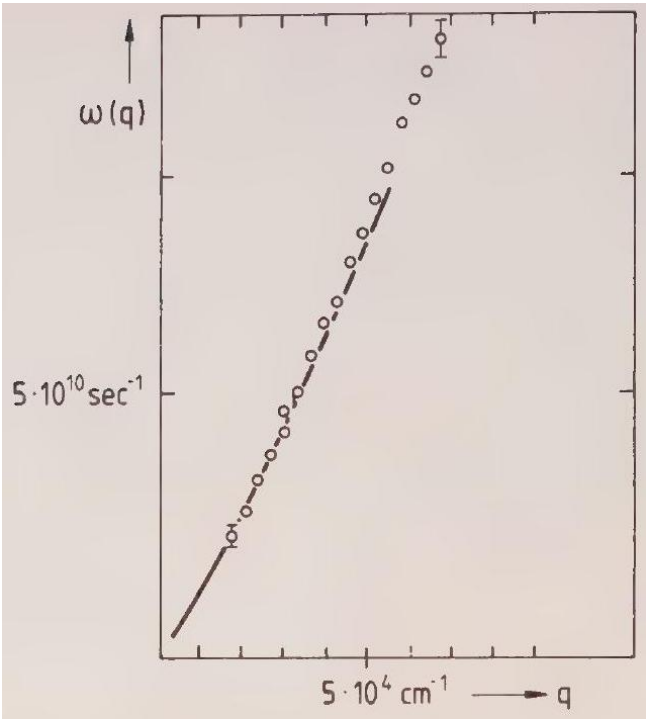


Fig. 7. The dispersion relation $\omega(q)$ at fixed reduced temperature $-\alpha(T, H)=6.32 \times 10^{-3}$ obtained experimentally (Carlson and Goldman 1975) and from the calculated structure factor is compared.}

experiment is shown and compared with the theoretical result. Over the range of wave vectors where the experiment was performed, ω(q) is almost proportional to q, which means the resonant peak results from a sound-like mode. The phase velocity of this mode, which is obtained from the slope of the curves, depends on the reduced temperature. It is typically of the order $c \approx 10^6$ cm/s. The temperature dependence of the resonant frequency $\omega(q)$ at fixed values of the wave vector is shown in fig. 8. Again the agreement between theoretical and experimental result with no adjustable parameter is excellent.

The effect of the various damping mechanisms on the collective mode, including the pair breaking effect of paramagnetic impurities, was examined in more detail by Aspen and Goldman (1979, 1981). The temperature dependence of γ due to ohmic losses of the normal current (4.20) was confirmed quantitatively. Furthermore, the experiments demonstrate qualitatively the influence of additional pair breaking effects. However, no quantitative systematic agreement, as far as the pair breaking effects are concerned, was obtained. In the same work also the resonance in the structure factor at $\omega \approx 2\Delta$ was investigated in more detail. The smearing of the step seems to be in reasonable agreement with the predictions of the theory.

26.5 5. Extensions and further collective modes

26.5.1 5.1. Space and time dependent conversion

Although there is no unique prescription how to separate the total current into a normal and a supercurrent part, it appears natural to call the contributions to j_1 in (3.23) which contain f_1^{T} and $m\dot{v}_{s_1}$ the normal current. The familiar linear response to an applied homogeneous electric field

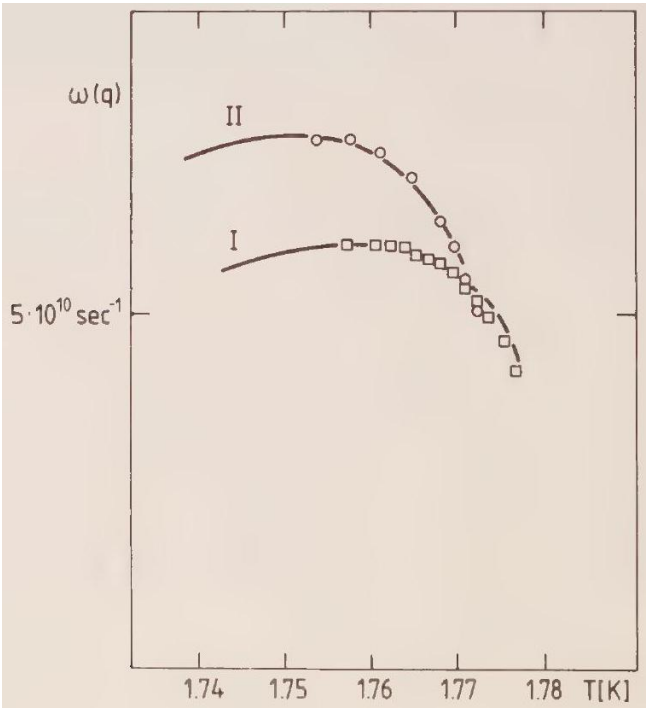


Fig. 8. The dependence of the resonant frequency on the reduced temperature $\left(T_{\mathrm{c}}-T\right) / T_{\mathrm{c}}$ as measured in the experiment and calculated is compared. The parameters of curve I are the same as in fig. 6. In curve II the wavevector is $q = 4.8 \times 10^4$ cm^{-1} and $T_{\mathrm{c}} = 1.775$ K.}

$$j(\omega) = [\sigma_1(\omega) + \mathrm{i}\sigma_2(\omega)]\, E(\omega)$$

suggest a slightly different identification, namely $j_{\mathrm{n}}(\omega) = \sigma_1(\omega)E(\omega)$, where

$$\sigma_1(\omega) = \sigma \frac{1}{2\omega} \int_{-\infty}^{\infty} \mathrm{d}E \left[N_1\left(E + \frac{1}{2}\omega\right) \mathrm{N}_1\left(E - \frac{1}{2}\omega\right) + \mathrm{R}_2\left(E + \frac{1}{2}\omega\right) \mathrm{R}_2\left(E - \frac{1}{2}\omega\right) \right] \times \left(\tanh \frac{E + \frac{1}{2}\omega}{2T} - \tanh \frac{E - \frac{1}{2}\omega}{2T} \right) \tag{5.1}$$

Here the usual generalized densities of states appear $N_1(E) \equiv N_1(E; \omega = 0)$ [compare eqs. (3.15) and (3.21)] and $R_2(E) \equiv R_2(E; \theta) = 0$). Both identifications differ by small terms of order $\omega L^2/T^3$ only. By combining the continuity equation $\dot{\rho} + \operatorname{div} j = 0$ and the Boltzmann equation we find [compare eq. (4.4)]

$$2\Delta \int N_2(E;\omega) f_1^{\mathrm{T}} - \frac{1}{2eN_0} \operatorname{div} j_{\mathrm{s}} = 0 \tag{5.2}$$

We consider situations with temperatures near T_c (which allow us to use the reduced electron phonon collision operator), weak spatial variations ($Dq^2 \ll \omega$ or $Dq^2 \ll 1/\tau_{\mathrm{E}}$) and $v_{\mathrm{s}0} = 0$. We can then easily solve the Boltzmann equation in terms of the pair chemical potential Φ. In the limit considered we have

$$2\Delta \int N_2 f_1^{\mathrm{T}} = 2\Delta \frac{X_{12}}{X_{11}} \int N_1 f_1^{\mathrm{T}} \tag{5.3}$$

The expansion (4.13) is the appropriate limit of X_{12} and in the order considered we may set $X_{1\mathrm{i}} \approx 4T/\left(-i\omega + 1/\tau_{\mathrm{E}}\right)$. Thus, we have

$$-\frac{\pi\Delta}{4T_{\mathrm{c}}}\left[\frac{\left(-\mathrm{i}\omega+2\Gamma\right)\left(-\mathrm{i}\omega+1/\tau_{\mathrm{E}}\right)}{1+\left(-\mathrm{i}\omega+2\Gamma\right)\left(-\mathrm{i}\omega+1/\tau_{\mathrm{E}}\right)/(2\Delta)^2}\right]^{1/2}\Phi-\frac{1}{2eN_0}\operatorname{div} j_{\mathrm{s}}=0 \tag{5.4}$$

In the frequency range $\Gamma, 1/\tau_{\mathrm{E}} \ll \omega \ll \Delta$ this relation reduces to eq. (2.3) which was an essential ingredient of the approximate description of the CarlsonGoldman collective mode in section 2.5. Furthermore, eq. (5.4) describes the conversion of currents. The charge neutrality fixes $\operatorname{div}\left(j_{\mathrm{n}}+j_{\mathrm{s}}\right)=0$. Near $T_{\mathrm{c}}, j_{\mathrm{n}}$ is roughly equal to the normal state value $j_n \approx \sigma E$. Thus in a stationary experiment with a normal current flowing into a superconductor, the electric field penetrates to a depth

$$\lambda_{Q*}=\sqrt{D\tau_{Q*}} \tag{5.5}$$

The rate $1/\tau_{Q*}$ is the charge imbalance relaxation rate describing the conversion of an injected normal current into supercurrent (Clarke 1972, Tinkham 1972; Schmid and Schön 1975a)

$$\frac{1}{\tau_{Q*}}=\frac{\pi\Delta}{4T}\left(\frac{2\Gamma}{\tau_{\mathrm{E}}}\right)^{1/2}\left(1+\frac{\Gamma}{2\Delta^2\tau_{\mathrm{E}}}\right)^{-1/2} \tag{5.6}$$

Finally, we find from (5.4) that in a spatially homogeneous situation, with no external perturbation, the free decay of a charge imbalance, i.e. a nonequilibrium pair chemical potential, occurs on a time scale τ_{F} (Kadin et al. 1980).

26.5.2 5.2. The "neutral" superconductor

Although of hypothetical nature, the neutral superconductor is an interesting theoretical object since the absence of Coulomb interactions allows for a richer variety of low frequency collective modes. The pair chemical potential and the superfluid velocity are now related directly by

$$\frac{\partial}{\partial r}\phi=-m\dot{v}_{\mathrm{s}} \tag{5.7}$$

Again, a continuity equation is satisfied where now ρ and j are the number density and the corresponding current density. They are given by the same expressions as in the charged case except for an obvious replacement. As before, we find from the continuity equation and the Boltzmann equation

$$2\Delta\int \mathrm{d}E N_2(E;\omega) f_1^{\mathrm{T}}-\frac{1}{2N_0}\operatorname{div} j_{\mathrm{s}}=0 \tag{5.8}$$

but the distribution differs from the result in the charged case. We consider again the case near T_{c}, small wave vectors $Dq^2 \ll \omega$ or $Dq^2 \ll 1/\tau_{\mathrm{E}}$ and $v_{\mathrm{s}0}=0$ and solve the Boltzmann equation for f_1^T in terms of Φ. We now find

$$\frac{\Delta}{2T}X_{12}\frac{\left(-\mathrm{i}\omega\right)\left(-\mathrm{i}\omega+1/\tau_{\mathrm{E}}\right)}{-\mathrm{i}\omega+\frac{\Delta}{2T}\frac{1}{\tau_{\mathrm{E}}}X_{12}}\Phi+\frac{n_{\mathrm{s}}}{n}\frac{v_{\mathrm{F}}^2}{3}m\operatorname{div} v_{\mathrm{s}}=0, \tag{5.9}$$

where we used the free electron connection $2N_0=3n/mv_{\mathrm{F}}^2$. With (5.7) we immediately find that at small frequencies $\omega \ll 1/\tau_{\mathrm{E}}$ a propagating solution exists with frequency ω satisfying

$$\omega^2=c_4^2q^2\left(1-\mathrm{i}\omega\tau_{Q*}\right), \tag{5.10}$$

where $c_4^2 = n_s v_F^2/3n$ and τ_{Q*} is given in eq. (5.6). This mode, for ω small in comparison to the charge imbalance relaxation rate $1/\tau_{Q^*}$, is the hydrodynamic fourth sound, familiar from neutral superfluids. For finite frequencies, it is damped due to the charge conversion processes. In phenomenological treatments this process is described by a second viscosity.

There are in general several such coefficients. However, in a superconductor where the normal current is dissipative, like clamped superfluids, only one coefficient ζ appears (see e.g. Khalatnikov 1969, Putterman 1974, and Schmid 1980). Hence, we can identify

$$\zeta = \tau_{Q*}/2N_0. \tag{5.11}$$

Furthermore, we find from (5.9) that also at large frequencies $\omega \gg \Gamma$ there exist a propagating solution, satisfying

$$\omega^2 + \mathrm{i}\omega\begin{pmatrix}1\\ \tau_E + \Gamma_0\end{pmatrix} - \frac{4T}{\pi A}c_4^2 q^2 = 0. \tag{5.12}$$

This is again the Carlson Goldman mode. The phase velocity $c^2_{(C'_G)} = 4Tc_+^2\pi A$ is the same as in the charged case. Pair breaking effects again lead to damping. However, there is no damping $xn_s/n\tau_{imp}$ since in the uncharged system the normal component remains at rest and is not subject to ohmic losses*. Although the phase velocity of the Carlson-Goldman mode is larger than that of fourth sound by the factor $\sqrt{4T,(\pi\Lambda)}$ we cannot find simultancously two

propagating solutions at fixed q. The conditions $c_4 q \ll 1/\tau_{Q*} = \pi\Delta/4T\tau_E$ and $1/\tau_E \ll c_{CG}q$ cannot be met simultaneously.

26.5.3 5.3. Low temperatures

So far we have restricted our attention to temperatures close to T_c. However, we can extend our description to lower temperatures as well, starting from the formal theory presented in section 3. We find that the distribution functions obey the Boltzmann equations (3.20) at all temperatures. The only generalization is that if the frequencies are comparable to T or larger than T we have to retain, here and in other places below, the expression $\frac{1}{2}\left\{\tanh\left[E+\frac{1}{2}\omega\right)/2T\right] - \tanh\left[\left(E-\frac{1}{2}\omega\right)/2T\right]\right\}$ instead of the expansion $-i\omega\left(\partial f_0/\partial E\right)$. At lower temperatures the inelastic electron-phonon collision rate becomes smaller (see e.g. Kaplan et al. 1976) and hence the collisionless regime ($\omega \gg 1/\tau_E$) gains more importance. Whereas near T_c we relied on expansions in $A/T, \omega/T$ and Dq^2/T, at low temperatures $T \ll \Delta$ we find simple results if $\omega, Dq^2 \ll A$. If the frequencies and wave-vectors considered satisfy these conditions the charge density is given by eq. (3.24) at all temperatures. Also the current density is given by the expression (3.23) encountered before, with one rather obvious replacement: the last term (if $\omega, Dq \ll \Delta$) becomes, at low temperatures $T \ll \Delta$ for not too strong pair breaking $\Gamma < A$:

$$\mathrm{Lin}\left\{\frac{\sigma}{e}\pi\Delta m v_s\left(1-\frac{4\Gamma}{3\pi\Delta}\right)\right\} = \mathrm{Lin}\left\{e n_s \boldsymbol{v}_s\right\}. \tag{5.13}$$

Notice, that Γ depends on ι_s too. Although we consider here explicitly only the dirty limit, generalizations are possible, as indicated by the second general form of (5.13). For example, the dependence of n_s on the impurity concentrations at low temperatures and weak pair breaking ($\Gamma, T \ll \Delta$) is (Abrahams and Tsuneto 1966)

[0]*In superfluid ^{3}He this mode is overdamped as a consequence of the Fermi-liquid interaction.

$$\frac{n_s(x)}{n} = \begin{cases} \frac{1}{x}\left(\frac{\pi}{2} - \frac{\arccos x}{\sqrt{1-x^2}}\right) & \text{for } x \leqslant 1 \\ 1 & \\ x\left(\pi - \frac{\operatorname{arccosh} x}{\sqrt{x^2-1}}\right) & \text{for } x \geqslant 1 \end{cases} \tag{5.14}$$

where $x = 1, (2\Delta\tau_{\rm imp}\,)$. Or, in the dirty limit for weak pair breaking and $Dq^2,\ \omega \ll \mathrm{Max}\{\Delta, T\}$ the temperature dependence of n_s is

$$n_{\rm s}(T) = \frac{\sigma}{e^2}\pi\Delta m \tanh\frac{\Delta}{2T}. \tag{5.15}$$

From the self-consistency relation one finds at low temperatures the following relation from small frequencies and wave vectors ($\omega, Dq^2 \ll \Delta$), which replaces
the Ginzburg-Landau equation found near T_c

$$\Delta_1(1 - \pi\Gamma/4\Lambda) + \pi D m^2 v_{\rm s0}\cdot v_{\rm s1} - \int {\rm d}E R_2(E) f_1^{\rm L}(E) = 0 \tag{5.16}$$

where $R_2(E) \equiv R_2(E; \omega = 0)$.
As far as the transverse (charge) mode is concerned, we again start from the continuity equation which we compare to the Boltzmann equation, integrated over the energy. Hence, for $\omega, Dq^2 \ll \Delta$

$$\begin{aligned} &\dot\Phi + \frac{1}{2N_0}\,\mathrm{div}\,(n_{\rm s}v_{\rm s}) - 2\Delta\int N_2(E) f_1^{\rm T} \\ &\quad + \frac{\rm i}{2}\Phi\int\left[\tanh\frac{E+\frac{1}{2}\omega}{2T} - \tanh\frac{E-\frac{1}{2}\omega}{2T}\right] N_1(E) = 0 \end{aligned} \tag{5.17}$$

In general, this result differs from those obtained near $T_{\rm c}$ since the last term no longer cancels $\dot\Phi$. At low temperatures and small frequencies $T, \omega \ll \Delta$ it becomes $(\omega^2/2\Delta)\,\Phi$, i.e. it is small. In this limit also the term $2\Delta\int N_2(E)\int_1^T(E)$, which is most important near $T_{\rm c}$, is negligible. In fact if the wavevectors are small and inelastic scattering is weak $1/\tau_{\rm E}, Dq^2 \ll \omega$ it is also $(\omega^2/2\Delta)\,\Phi$ and hence cancels the last term.

From (5.17) we immediately see that in an uncharged superconductor, where $\partial\Phi/\partial\boldsymbol{r} = -m\dot v_{\rm s}$, at low temperatures $T \ll \Delta$ a propagating collective mode exists for not too large wavevectors and frequencies $\omega, Dq^2 \ll \Delta$ with phase velocity

$$c^2 = \frac{n_{\rm s}}{n}\frac{v_{\rm F}^2}{3} \tag{5.18}$$

This is the Bogoliubov-Anderson mode. The phase velocity is formally equal to that of hydrodynamic fourth sound, although the frequency may take arbitrary values in comparison to the inelastic scattering rate $1/\tau_{\rm E}$. In the dirty limit for weak pair breaking $c^2 = \pi\Delta D$. In most treatments concerned with the Bogoliubov Anderson mode, clean superconductors were considered, where at low temperatures $n_{\rm s}/n \approx 1$. Hence, the phase velocity was found to be formally equal to that of hydrodynamic first sound. For general impurity concentration the phase velocity follows from eqs. (5.14) and (5.18). At higher temperatures both integrals in (5.17) have to be evaluated. If the frequency is large in comparison to the inelastic scattering rate $1/\tau_{\rm f}$, which of course increases with the temperature, we expect the collective mode to exist at all temperatures. The phase velocity changes with temperature. Near $T_{\rm c}$ we recover the Carlson-Goldman mode of the neutral superconductor discussed in section 5.2.

The Bogoliubov-Anderson mode involves local density fluctuations. Hence it does not exist in a real charged superconductor at most temperatures. A

counterflow of the normal current makes approximate charge neutrality possible. However, we have seen that only very close to T_c the resulting Ohmic losses are small enough for the mode not to be overdamped.

26.5.4 5.4. Further theoretical work on the Carlson-Goldman collective mode

From the early data of Carlson and Goldman (1973) a large pair breaking parameter ($\Gamma \approx 10^{11}$ s^{-1}) was erroneously inferred. This would imply that in the temperature range where the experiments were performed, the superconductor is gapless since $\Lambda \leqslant \Gamma$ and the time-dependent GinzburgLandau theory of Gor'kov and Eliashberg (1970) would yield an appropriate description. Motivated by this interpretation Maki and Sato (1974) and Brieskorn et al. (1974) calculated the order-parameter structure factor of a neutral gapless superconductor. Apart from a central diffusive peak centered at $\omega = 0$, they found a resonant peak at finite frequency, resulting from a fourth sound mode. The frequency of this mode follows from the relation (5.10). However, the superfluid density and hence the phase velocity are reduced by the pair breaking. For general Γ/T in the dirty limit c_4 is given by

$$c_4^2 = \frac{\Delta^2 D}{\pi T}\psi'\left(\frac{1}{2}+\rho\right) \tag{5.19}$$

In the extreme gapless case $\Gamma \gg T$ this reduces to $c_4^2 = 2A^2D/\Gamma$ and τ_{Q*} becomes $\tau_{Q*} = \Gamma/(2\Delta^2)$. Clearly, these results do not apply to the experimental situation, both because of the effect of the charge and because the pair breaking Γ in the experiments was rather weak (Carlson 1975). Nevertheless, the work of Maki and Sato (1974) and Brieskorn et al. (1974) provided the first insight into the physical processes responsible for the peaks in the structure factor.

Later, Bray and Schmidt (1975b) postulated ad hoc a phenomenological description of charged superconductors. They put up a set of rate equations for the normal and superfluid densities and currents, allowing also for conversion between the two components. Their description is similar in spirit to that presented in section 2.5, but in some respects without justification goes beyond it. For example, they postulated that the normal current is driven also by a gradient of a normal chemical potential μ_n. It is not clear a priori that in the high frequency regime such a chemical potential is a sensible concept. Moreover, their acceleration equation for the supercurrent differs from eq. (2.6). If they identify certain phenomenological parameters with results of the microscopic theory they reproduce the Carlson Goldman collective mode. However, they stress that the phase velocity is slightly larger than the results quoted above, namely $c^2 = c_{CG}^2 + c_4^2$. The difference results from the not so well motivated -inclusion of $\lambda\mu_n$ ir , which represents a restoring force due to a compression of the normal liquid. In any case, the difference is small (c_4^2 is smaller than $c_{(G,G}^2$ by a factor $\pi \lrcorner /4T$) and hence consistently does not show up
in the results presented above. In the clean limit, Dinter (1978a) quotes such a correction. However, in the dirty limit, by extending our microscopic analysis, we find further corrections, reversing the effect. Also, the damping terms found by Bray and Schmidt do not agree with those derived from the microscopic theory. In gapless superconductors, Bray and Schmidt (1975a) in a model description find some evidence of a soundlike collective mode with phase velocity $c = \sqrt{2}c_4$. The increase in comparison to the fourth sound in neutral gapless superconductors is again due to the compression of the normal fluid, which compensates the superfluid oscillation. However, even within the model the conditions for this mode to exist, are (nearly) impossible to meet.

Another phenomenological approach, based on the established thermodynamic theory of irreversible processes as applied to clamped superfluids, was put forward by Putterman (1977). (Superconductors, where the motion of the normal component is subject to Ohmic losses, correspond for frequencies $\omega\tau_{\rm imp} \ll 1$ to superfluids where the normal component is clamped.) The conversion of normal and supercurrents at low frequencies is accounted for in this description by a coefficient of second viscosity $\zeta(0) = \tau_{Q*}/2N_0$ [compare eq. (5.11)], (Landau and Lifshitz 1959, Khalatnikov 1965, Putterman 1974). The underlying physical processes, the inelastic electron phonon-collisions in superconductors, are rather slow. At finite frequencies, one is led to the substitution

$$\zeta(\omega) = \zeta(0)/\left(1 - \mathrm{i}\omega\tau_{\rm E}\right) \tag{5.20}$$

As a result, at high frequencies $\omega\tau_{\rm E} \gg 1$ a soundlike collective mode is found with phase-velocity (Putterman 1977, Schmid 1980)

$$c^2 = n_{\rm s}\zeta(0)/\tau_{\rm E} = \frac{n_{\rm s}2T}{mN_0\pi\Delta} \tag{5.21}$$

Also the most important damping proportional to $n_{\hookrightarrow}, (n\tau_{\rm imp})$ is found. Clearly, this mode is the Carlson-Goldman mode. In a neutral superconductor the substitution (5.20) roughly corresponds to the transition from (5.10) to (5.12).

A relatively simple description of many nonequilibrium phenomena in clean superconductors, which resembles somewhat a two-fluid picture, was developed by Pethick and Smith (1979). It is based on the Boltzmann equation description of the excitations in the superconductor of Aronov and Gurevich (1974), and hence is restricted to small wavevectors and frequencies $v_{\rm F}q, \omega \ll \Delta$, and weak collision processes and pair breaking. Pethick and Smith split (somewhat artificially) changes of the electric charge into a normal and a superfluid charge $\rho_{\rm n}$ and $\rho_{\rm s}$-not to be confused with the coefficients $n_{\rm n}$ and $n_{\rm s}$ which they relate to the deviation of a normal and a superfluid chemical potential $\mu_{\rm n}$ and $\mu_{\rm s} \equiv \Phi$ from the equilibrium value $\mu_{\rm eq} : \rho_{\rm s} = \chi_{\rm s}\left(\mu_{\rm s} - \mu_{\rm eq}\right)$ and $\rho_{\rm n} = \chi_{\rm n}\left(\mu_{\rm n} - \mu_{\rm eq}\right)$. Near $T_{\rm c}$ the coefficients are found to be $\chi_{\rm s} = \pi\Delta 2eN_0/4T$ and $\chi_{\rm n} = 2eN_0$. In this context it is important to realize that in some static or low frequency situations, the distribution function of the excitations can be parametrized with good accuracy by a chemical potential μ_n. The two kinds of charges and the corresponding currents obey two continuity equations, with source terms of opposite signs describing the conversion of charges. At high frequencies $\omega \gg 1/\tau_{\rm E}$ superfluid and normal charges are separately conserved. If we impose the charge neutrality requirement and assume again the normal current to be given by $j_n = \sigma\boldsymbol{E}$ we recover the approximate macroscopic description presented in section 2.5. Quantitatively, however, the description applies at most for parameters restricted by the conditions (2.2). Damping effects are not well accounted for and the temperature has to be very close to $T_{\rm c}$.

Another compact formulation describing collective modes and other charge imbalance phenomena was developed by Kadin et al. (1980). They derived, for clean superconductors, from the Boltzmann equation for the excitations in the appropriate limit a single differential equation for the charge imbalance Q^*. We can easily derive the equivalent formulation for dirty superconductors in the present framework. From eq. (5.4) and the charge neutrality it follows that in the limit $Dq^2 \ll \mathrm{Max}\left\{\omega, 1/\tau_{\rm E}\right\} \ll \Delta$ the charge imbalance

$$Q^* \equiv 2eN_0 \int \mathrm{d}E N_1(E) f_1^{\Upsilon}(E) = -2eN_0\Phi \tag{5.22}$$

obeys the relation

$$\frac{\pi\Delta}{4T}\left(-i\omega + \frac{1}{\tau_{\rm E}}\right) Q^* + \mathrm{div}\, j_{\rm n} = 0$$

For simplicity, we ignore pair breaking effects other than the inelastic electron-phonon scattering. Furthermore, near T_c the normal current is approximately

$$j_{\mathrm{n}} \approx \sigma E = \frac{\sigma}{e}\left(\frac{m}{e n_{\mathrm{s}}} j_{\mathrm{s}} - \frac{1}{2eN_0}\nabla Q^*\right)$$

Combining these relations and $\operatorname{div} j = 0$ yields (Kadin et al. 1980)

$$\left\{\frac{4Tn_{\mathrm{s}}}{\pi\Delta}\frac{v_F^2}{3}\nabla^2 - \frac{\partial^2}{\partial t^2} - \left(\frac{n_{\mathrm{s}}}{n}\frac{1}{\tau_{\mathrm{imp}}} + \frac{1}{\tau_{\mathrm{E}}}\right)\frac{\partial}{\partial t} - \frac{n_{\mathrm{s}}}{n}\frac{1}{\tau_{\mathrm{imp}}}\frac{1}{\tau_{\mathrm{E}}}\right\} Q^* = 0 \tag{5.23}$$

In this form one easily recovers the Carlson Goldman mode and further properties mentioned in section (5.1). Kadin et al. (1980) further pointed out
the equivalence of the result (5.23) and the telegraph equation, which describes the propagation of electromagnetic waves down a transmission line with series inductance and resistance, as well as shunt capacitance and leakage conductance.

26.5.5 5.5. Manifestation of the Carlson-Goldman collective mode

The existence of the Carlson Goldman mode as a collective excitation in the superconductor being established. the natural question to ask is, how it can be excited and which physical properties are affected by it. So far the most convincing experimental manifestation of the collective mode is its influence on the excess pair current in Josephson tunnel junctions*, which we discussed in section 4.4.

The collective mode also affects the dielectric function $\varepsilon(q,\omega)$ of the superconductor (Dinter 1978b. Bezuglyi and Bratus' 1981, Bezuglyi et al. 1982). In particular Im[1 &(q. (%)] has a minimum at the resonant frequency. This suggests the possibility of exciting the collective mode in a superconductor by electromagnetic waves incident on its boundary (Bezuglyi et al. 1982). However. the coupling is rather weak: the electric field inside the superconductor at the boundary is smaller by orders of magnitude than that applied from outside. As another example we mention that also the properties of the phonons in the system are affected by the collective mode (Dinter 1978 b). As a result, at fixed wavevector the ionic correlation function shows, besides the resonant peak due to ordinary sound, a second though much smaller peak at the resonant frequency (y_4 of the Carlson-Goldman mode. (Typical values in clean samples are $q \sim 10^2$ cm^{-1} and $\omega_q \sim 10^{10}$ s^{-1}.) So far neither the effect on the dielectric function nor that on the phonons is verified experimentally.

The effect of the Carlson Goldman collective mode is much more likely to be seen near phase slip centers in superconductors. These spatially localized centers exist in quasi-onedimensional superconductors when a current close to the critical current I_c is imposed. In the core of the center the order parameter collapses periodically in time allowing the phase to reset by 2π (Skocpol et al. 1974). During this brakdown the supercurrent $I.\ (\ x,t\ )$ is locally reduced. in fact vanishes periodically in the core ($x = 0$), and hence part of the imposed current I is carried as normal current. Since the conversion of currents is rather slow. the normal current (in particular the time-averaged normal current) is flowing to distances of the order of $i_{1/2\%}$ (see eq. 5.5) away from the core. The frequency of the oscillations is equal to the time-averaged voltage ($\omega_{\mathrm{g}} = 2eV$. This in turn depends on the effective resistance of the phase slip center $\overline{V'} = R_{\mathrm{eff}}\left(I - \bar{I}_{\mathrm{c}}\right)$ where

$R_{\mathrm{eff}} = 2\lambda_{Q*}/\sigma A$ and A is the cross-section of the superconductor. One expects qualitatively that the periodic oscillations of normal and supercurrent in the phase slip center also excite the Carlson-Goldman collective mode. However, a quantitative discussion is rather complicated.

[0]*Compare also Kadin and Goldman (1982).

We mention here the numerical analysis of Kadin et al. (1980). These authors combined in a model treatment the transmission line (eq. 5.23) with an ideal Josephson element to represent the core of the phase slip center. They have to make assumptions on the supercurrent in the core; also the transmission line model ignores all effects of the spatially varying order parameter. Nevertheless they demonstrate rather convincingly the propagation of the collective mode. The mode is strongly damped and only propagates to short distances.

We can easily estimate the decay length $i.$ for the collective mode. It is approximately

$$i_\gamma \approx 2c_{\mathrm{CG}}/\gamma \approx \left[\left(32/\pi^2\right) DT^2/\Delta^3\right]^{12}$$

in the dirty limit. Since in most situations, except very close to T_c, the inelastic scattering rate $1/\tau_{\mathrm{E}}$ is small compared to Λ^2/T the decay length λ_γ, is shorter than the conversion length $\lambda_{Q*} = [(4/\pi)D\tau_E T/\Delta]^{1/2}$. In clean samples,

$$\lambda_\gamma \approx \left[(64\pi/7\zeta(3))D\tau_{\mathrm{imp}}T^3/\Delta^3\right]^{1/2}$$

is short in comparison to λ_{Q*} as long as $1\tau_E \ll \Delta^2\,(20T^2\tau_{\mathrm{imp}}\,)$. This condition is still realized in most situations, although the opposite limit is conceivable. We conclude that in most cases the waves propagate only to distances which are short in comparison to the distance the time-averaged normal current is flowing. It has been conjectured that these waves may propagate between phase slip centers and synchronize their oscillations, resulting in a voltage locking. This locking has been observed experimentally in closely spaced microbridges (Jillie et al. 1977, Palmer and Mercereau 1977, Lindelof and Bindslev Hansen 1977). However, in view of the different length scales $i_{\ldots} \ll i_{Q*}$, more direct coupling mechanisms may be more important. In fact, a thorough numerical analysis based on the complete theory of (weakly) gapless ($\Gamma \gtrsim \Delta$) superconductors (Baratoff 1982) reveals that neighbouring phase slip centers synchronize even in the gapless superconductor where the propagating mode is overdamped.

In another experiment (Kadin et al. 1981) a phase slip center near a boundary, which can reflect the waves back to the phase slip center, was investigated. The current-voltage characteristic shows several peaks which may be related to resonances of the waves in this arrangement. So far, no quantitative explanation could be given, but the idea is interesting and further work is desirable.

For completeness, we mention the work of Kulik (1979). He considered the interaction of electrons with the Carlson Goldmann collective oscillation. He
quantizes this oscillator according to the usual rules, calling the quantized particles bogolons. The electron-bogolon interaction then is investigated further, in particular its effect on the conversion of charges and on the penetration depth of an electric field into a superconductor. The penetration depth is found to be temperature independent, if the electron-bogolon interaction is the dominant interaction. We doubt whether it makes sense to quantize the -strongly damped-Carlson-Goldman oscillation and whether the bogolons represent a useful particle concept. Also, because the CarlsonGoldman mode frequency must be small $\omega_q \approx c_{\mathrm{CG}}q \lesssim \Delta$, the number of bogolons ought to be smaller than that of excited phonons by a factor of order $(\Delta/T)^{3/2}$. Hence, most likely the electron-phonon scattering is more important than electron-bogolon scattering.

26.5.6 5.6. Amplitude oscillations and further collective modes

It is well known that many superconducting response functions show a marked frequency dependence at the threshold of the creation of quasiparticle pairs at $\omega = 24$. This is an important result of the BCS theory. A number of response functions were calculated, e.g. by Mattis and Bardeen (1958), and further functions for more general parameters by Ovchinnikov

(1970). In the present chapter we have found a branch cut in the pair field susceptibility near T_c extending to $\omega = 2\Delta$. In the time domain, this implies that the magnitude (amplitude) of the order parameter may oscillate at a frequency 24 . This can be interpreted as virtual decay of Cooper pairs into pairs of quasiparticles due to the quantum-mechanical energy-time uncertainty (Schmid 1968). However, this oscillation is not a collective mode, rather it is a resonance. It is damped according to some power of $1/t$ even in the absence of any collision process. The oscillation is a quantum-mechanical effect related to the gap in the spectrum and the damping is a consequence of the fact that the excitation spectrum is continuous beyond 24 . In the response functions the resonance is represented by a branch cut extending to $\omega = 2A$. In contrast a collective mode corresponds to a pole in the complex ω plane.

As an illustration, we consider a homogenous superconductor at low temperatures $T \ll A$. A supercurrent is imposed which at time $t = 0$ is switched from j_0 to $j_0 + j_1$ (where j_1 is small). Because of the pair breaking effect of the supercurrent, this change requires an adjustment of the order parameter from Δ to eventually $\Delta + \Delta_1(\infty)$ and of the superfluid velocity from v_{s0} to $v_{s1}(\infty)$. This adjustment takes place in two stages on two very different time scales: Δ^{-1} and the inelastic collision time τ_E. In the first fast stage $\Delta_1(t)$ and $v_{s1}(t)$ perform damped oscillations, reaching after times long compared to Δ^1 but still small compared to τ_E intermediate values $\bar{\Delta}_1$ and $\tilde{v}_{s1}$, which are very close to $\Delta_1(\infty)$ and $v_{s1}(\infty)$, respectively. The difference is proportional to $e^{-d/T}$. Using the response functions derived by Ovchinnikov (1970) we find for 1. $\lesssim t \ll \tau_E$ (Ovchinnikov and Schön 1981)

$$\Delta_1(t) = \tilde{\Delta}_1 \left\{ 1 - \frac{1}{\sqrt{\pi^3 \Delta t}} [(\ln(64\Delta t) + \gamma) \cos(2\Delta t + \pi/4) \right.$$

$$\left. + \pi/2 \sin(2\Delta t + \pi/4)] \right\}$$

$$v_{s1}(t) = \tilde{v}_{s1} \left\{ 1 + \frac{\pi}{2} \frac{1}{(2\Delta t)^2} \cos(2\Delta t) \right\} \tag{5.24}$$

where Euler's constant is $\gamma = 0.577$. After these oscillations are damped out the quasiparticle distribution is still out of equilibrium. It relaxes by inelastic scattering and recombination processes (total rate $1/\tau_E$) which is the second slow stage. Because of the coupling between the distribution function and the order parameter and the superfluid velocity the quasiparticle relaxation results in a further, though smaller ($\propto e^{-\Delta T}$) adjustment of Δ and v_s. This may be detected and used in turn to investigate the relaxation processes (Ovchinnikov et al. 1981).

Littlewood and Varma (1981) observed that in those superconductors where a charge density wave is established, this wave modulates the density of states at the Fermi surface and hence couples to the superconducting order parameter. In the coupled system they find a collective mode with frequency close to, but slightly smaller than 24

$$\omega_g = 2\Delta \left[1 - \frac{2\alpha^2}{\pi^2} \left(1 - \frac{4\Delta^2}{\omega_0^2} \right) \right], \tag{5.25}$$

where α is the dimensionless coupling strength and ω_0 the phonon frequency. The mode called "gap" mode shows up as a very sharp peak in the phonon spectral function $S_{ph}(\omega)$ at the frequency ω_g. In order for it to be observable $\omega_0/24$ must not be too large. In addition $S_{ph}(\omega)$ has a broadened peak at ω_0, and a foot extending down to $\omega = 2\Delta$ reflecting the excitation of quasiparticles. With increasing coupling strength ω_g decreases, the ω_0 peak broadens, the foot becomes larger and the oscillator strength in the gap mode increases. Littlewood and Varma stress that the gap mode involves modulations of the magnitude (amplitude) of the superconducting order parameter. This means that the modulation of a low frequency (ω_0

) phonon, coupled suitably to the superconducting order parameter, allows for a long lived collective mode of the order parameter. In contrast, without this coupling we found only a resonance as discussed above, i.e. an oscillation which is strongly damped according to a power law.

The gap mode may be the mode which Sooryakumar and Klein (1980) observed in Raman-scattering experiments on $2H - NbSe_2$ (where $\omega_0/\Delta \approx 5$) as
sharp lines below the superconducting transition temperature $T_c = 7.2$ K. Balseiro and Falicov (1980) explained this peak as a phonon-quasiparticle pair bound state. Beyond the usual BCS interaction they included only the interaction of the ω_0 phonon with the electronic charge. Littlewood and Varma (1981) pointed out that this interaction can only lead to effects close to the plasma frequency of the electron system and since $\omega_{p_1} \gg \omega_0$ has no effect on the phonon self energy near ω_0.

For completeness we mention the possibility of exciton-like modes (see e.g. Martin 1969). They may arise due to electron-electron interactions in angular momentum channels with $l \neq 0$. Crudely they correspond to excited pair states. Their energy may lie in the energy gap of the quasiparticles. However, no conclusive experimental evidence for these modes exists.

26.6 6. Conclusions

In the investigation of the Carlson-Goldman collective mode, similarly as in the case of many relaxation phenomena in superconductors near T_c, a rather good, even quantitative agreement between theory and experiment has been found. This confirms further that the microscopic description summarized in section 3 is correct and complete, at least in the vicinity of the transition temperature. We mention, however, that the analysis of relaxation processes at lower temperatures revealed some unresolved discrepancies between theory and experiment (see e.g. Lemberger and Clarke 1981).

In the literature several descriptions of the collective modes have been presented, which in part appear quite simple. For instance, Artemenko and Volkov (1975) proceed similarly as we do, but start from the clean limit theory of Aronov and Gurevich (1974). It should be kept in mind that this theory is valid only under several restrictions: the system has to be clean, $1/\tau_{\text{imp}} \ll \Delta$, pair breaking effects have to be weak, $\Gamma \ll \Delta$, and only small wavevectors and frequencies are allowed, $\imath_F q, \omega \ll A$. In contrast, the experiments are performed in dirty superconductors, and in connection with the collective modes frequencies of order Δ or larger are interesting, too.

A simple description which resembles a two-fluid picture was deduced by Pethick and Smith (1979) from the clean limit theory. It reproduces the most prominent features of the Carlson-Goldman mode near T_c. It does not include various damping effects-e.g. due to diffusion or inelastic scattering. Since the derivation is rather unsystematic, it is not clear how these effects could be incorporated.

It should be kept in mind, that the Carlson-Goldman collective mode is a rather subtle effect. The currents nearly cancel but still some electric field driving the normal current is left. The damping is proportional to Δ^2/T whereas the approximate descriptions require $\Delta/T \ll 1$. In view of this it appears
fortuitous that any simple macroscopic description of the mode can be developed. We also stress that the concept of a normal chemical potential which has proven a rather accurate parametrization of a nonequilibrium distribution in homogenous, static charge imbalance phenomena (see e.g. Chi and Clarke 1979) no longer does so in high frequency or inhomogenous problems. Descriptions of the collective modes based on this parametrization, e.g. of Kadin et al. (1981), are therefore only approximate. (The transmission line model for example does not account for the damping due to quasiparticle diffusion.) A complete theory has to keep the full

functional form of the quasiparticle distribution. It is on this level that the good quantitative agreement with experiments is obtained.

Several of the investigations, based on the microscopic theory (Ovchinnikov 1977, Dinter 1978a,b, Artemenko and Volkov 1979. Kulik et al. 1981) derive the properties of the collective mode directly in a Green function formulation without introducing the concept of the distribution function. In fact, unless ω/A is small the distribution function $f(E;\omega)$ depending on the generalized densities of states like $N_1(E;\omega)$ which we used in our description, is no longer a classical concept. However, the present formulation has the advantage that it makes contact with the familiar Boltzmann equation description in the low frequency limit. In particular, the inclusion of collision processes appears transparent in this form.

We have restricted the explicit discussion in this article to temperatures close to T_c or to low temperatures. As far as the sound-like collective mode found by Carlson and Goldman is concerned, temperatures very close to T_c are most interesting, but for the quantitative comparison with the experiments (fig. 6,7 and 8) we found it necessary to include corrections in an expansion in Δ/T and ω/T. Since in the high frequency phenomena the inelastic electronphonon collision play only a minor role, the corrections can be determined analytically by straightforward higher order expansion (see the Appendix). Similarly, we could extend the analysis to general temperatures. This requires finding the supercurrent at general temperatures for the space and time dependent problem and to evaluate the integrals $x_{1/}$ (generalized if ω/T is not small). The problem is an integration problem only.

By calculating the order parameter structure factor we have given a complete account of the collective excitations in a superconductor, however, subject to several restrictions. We considered only small (linear) deviations from the equilibrium. The equilibrium state is homogenous in space. We only indicated some of the effects of an imposed supercurrent, which couples amplitude and phase fluctuations of the order parameter. We did not consider coupling to other degrees of freedom in the material, for example, the phonons. These restrictions permit a complete and still rather simple theoretical description, but also exclude many most interesting examples of collective phenomena in superconductors. One which is most intriguing is the existence
of a phase slip center in an otherwise homogenous one-dimensional superconductor. This is clearly a nonlinear phenomenon, involving both magnitude and phase oscillations, which appears if the imposed current is of the order of the critical current. As another example, we mention the Josephson plasma oscillations in a tunnel junction. Here the spatial structure and the Coulomb interaction between charges on the two sides of the junction play a prominent role. This list could be continued, but clearly we could not even try to cover all these collective excitations.

26.7 Appendix. Correction terms in the description of the CarlsonGoldman mode

We have restricted the explicit discussion in the main part of the text to temperatures very close to T_c and to low temperatures. In fact, as far as the sound-like collective mode of Carlson and Goldman is concerned, temperatures near T_c are most interesting. For a quantitative comparison with experiment, deviations from the lowest order expansion in A/T and ω/T may become noticeable. As long as inclastic electron phonon scattering processes can be ignored, i.e. for $\omega \gg 1/\tau_E$, the generalization to lower temperatures is straightforward, in particular we can easily find the next order corrections in $\Delta/T, \omega/T$, and Dq^2/T.

In this order, the Boltzmann equation and the expression for the charge remain unchanged. Corrections, e.g. from the expansion of $\tanh\left[\left(E+\frac{1}{2}\omega\right)/(2T)\right] - \tanh\left[\left(E-\frac{1}{2}\omega\right)/(2T)\right]$, appear in higher order only. However, the supercurrent acquires additional terms. The corrections to

expression (3.23) are

$$j_1' = \frac{\sigma}{e}\frac{\pi\Delta^2}{2T} m v_{\mathrm{s}1} \left[-\frac{1}{2\pi^3}\psi''\left(\frac{1}{2}+\rho\right)\right] \frac{\mathrm{i}\omega - Dq^2/2}{T}, \tag{A.1}$$

where ψ'' is the second derivative of the digamma function, e.g. $\psi''\left(\frac{1}{2}\right) = -14\zeta(3)$. When calculating the pair field susceptibility we again start from the continuity equation, including a drive term, and make use of the Boltzmann equation. The result is a relation similar to eq. (4.4) but modified in an obvious way to account for div j_1'. Furthermore, the ϕ terms no longer cancel. In the following, we consider only $\Gamma/T \ll 1$.

As long as we can ignore inelastic electron-phonon collisions, the solution of the Boltzmann equation is still of the form (4.7) with $1/\tau_{\mathrm{E}} = 0$. Inclusion of the electron-phonon collision integral operator at temperatures not close to T_c is complicated. The reduced collision operator is sufficient only to lowest order in Δ/T. In general, one has to resort to a numerical solution of the integral equation.

When solving for $v_{\mathrm{s}1}$, the evaluation of $\int N_1 f_1^{\top}$ and $\int N_2 f_1^{\top}$ again suggests to consider the integrals X_{ij} defined in eq. (4.9). In their evaluation we now have to retain the factor $\cosh^{-2}(E/2T)$. Also we encounter the integrals

$$X_2 = \int \mathrm{d}E N_2(E;\omega)/\cosh^2(E/2T), \quad X_1 = \int \mathrm{d}E N_1(E;\omega)/\cosh^2(E/2T)$$

Analytic expressions of the integrals X_{ij} for different cases in leading order in Δ/T and ω/T were given in section 4.2. The correction terms are

$$\begin{aligned} X_{12}' &= \frac{\mathrm{i}\omega}{-\mathrm{i}\omega + Dq^2}\frac{7\zeta(3)}{\pi^2}\frac{\Delta}{T} \\ X_{22}' &= 0\left(\frac{\omega\Delta^2}{T^3}\right) \approx 0 \\ X_{11}' &= -\frac{\mathrm{i}\omega\Lambda}{\left(-\mathrm{i}\omega + Dq^2\right)^2}\frac{7\zeta(3)}{\pi^2}\frac{\Delta}{T} \end{aligned} \tag{A.2}$$

Furthermore, we have to retain the correction to X_2

$$X_2 = \pi\Delta + i\omega\frac{7\zeta(3)}{\pi^2}\frac{\Delta}{T} \tag{\prime}$$

and in the limit considered we have $X_1 = 4T\mathrm{Y}$, where Y is the Yoshida function. Near T_c it is $\mathrm{Y} = 1 - (7\zeta(3)/4\pi^2)\,(\Delta^2/T^2)$. We thus find

$$\begin{aligned} \chi^{\mathrm{I}} = \frac{4T}{\pi N_0}\Bigg\{ &-\mathrm{i}\omega\left[\frac{X_2}{\pi\Delta} - \mathrm{i}\omega\frac{2T}{\pi\Delta^2}(1-\mathrm{Y})\right] + Dq^2\left[1 + \left(\mathrm{i}\omega - Dq^2/2\right)\frac{7\zeta(3)}{\pi^3 T}\right] \\ &+\mathrm{i}\omega\frac{2}{\pi}\left[X_{22} - \frac{\left(X_{12} + \frac{2T}{4}(1-\mathrm{Y})\right)^2}{\tilde{X}_{11} - \frac{4TDq^2}{(-\mathrm{i}\omega+Dq^2)(-\mathrm{i}\omega)}}\right]\Bigg\}^{-1}, \end{aligned} \tag{A.3}$$

where the integrals X_{ij} include the correction (A.2).

Note added in proof

(?????)

In restricted geometries the Coulomb forces are weaker than in the bulk and hence do not shift the frequency of density oscillations to the bulk plasma frequencies. For example in

superconducting filaments of cross-section smaller than about 10^{-14} m^2, in a large frequency range at all temperatures below T_c, a collective density oscillation exists with a sound-like dispersion relation and weak damping. See

Mooij, J.E., and G. Schön, 1985, Phys. Rev. Lett. 55, 114.

27 Resistive States of Type-I Superconductors by Dolgopolov

27.1 1. Introduction

In this chapter we shall consider the resistive states which arise in bulk samples of type-I superconductors. The main factor which governs the structure of resistive states in bulk samples is the magnetic field distribution in the bulk of a sample, and this distinguishes, in principle, the present case from resistive states in thin superconducting channels or films. The intermediate state, the twodimensional mixed state and the resistive state of the surface superconductivity layer, which may be observed in superconductors with Ginzburg-Landau parameter $\kappa > 0.42$, all refer to the resistive states in type-I superconductors.

The first part of this chapter considers the problem related to resistive phenomena in the intermediate state, and the second one deals completely with the study of the two-dimensional mixed state of type-I superconductors. The problems regarding the resistive state of the surface superconductivity layer will not be considered here because they have been discussed in detail in the review by Park (1969).

The intermediate state has now been under investigation for several decades. After the first experiments it became clear that a sample in the intermediate state represents a more or less dispersed mixture of regions of superconducting and normal phases; several years later, after the Meissner effect had been discovered (Meissner and Ochsenfeld 1933), a macroscopic theory of the static intermediate state was developed (Peierls 1936, London 1936). A year later L. Landau (1937) solved the problem of the shape of interphase boundaries and obtained an expression for the period of the layered structure of the intermediate state in a plate in a transverse magnetic field. Then, World War II interrupted rapid progress in the study of the intermediate state, and the structure of this state was discoverd only after WWII in experiments performed by Meschkovskii and Shal'nikov (1947).

The period of the intermediate state structure is determined by the surface tension at the boundary between superconducting and normal phases, so study of the structures of the intermediate state can yield the coefficient of surface tension, which is an important parameter of a superconductor. Yet, the structures which arise in an external magnetic field appeared to be much more complicated than the idealized pattern of plane-parallel layers used in theoretical calculations. For instance, layers which are plane-parallel in the bulk of a sample can twist and branch out quaintly near the surface* (Balashova and Sharvin 1956, Faber 1958), and if the concentration of one of the phases is small, the normal or superconducting layers may be in the form of filaments extended along the magnetic field. The crystallographic anisotropy of the surface tension also significantly affects the formation of structures of the intermediate state.

While studying the intermediate state in a spherical tin sample, Balashova and Sharvin (1956) noticed that near the equatorial line where the magnetic field is strongly tilted to the sample surface the structure is in the form of parallel layers. Using then a magnetic field tilted to the surface of plane samples at an angle of 10°15°, Sharvin (1957, 1960) obtained sufficiently regular layered structures of the intermediate state to determine the interphase surface tension for tin (1957) and indium (1960). As was shown theoretically by Dzyaloshinskii (1955), such structures in a tilted magnetic field correspond to a minimal energy.

Thus, in the middle of the fifties the phenomenon of the destruction of superconductivity by an external magnetic field seemed to be understood almost completely. The resistance of samples in the intermediate state was associated with a current flowing perpendicular to the boundaries between the phases, and the electric current was assumed to align the domains appropriately. However, a paper by Gorter appeared in 1957, in which he noticed that even in the presence of a direct current a continuous motion of the domains is possible - a dynamic intermediate state. The dynamic intermediate state was discovered experimentally by Sharvin (1965b).

The discovery of the dynamic intermediate state stimulated a large number of theoretical and experimental works dealing with resistive states in type-I superconductors, because rather specific features of the intermediate state are fully manifested precisely under such nonequilibrium conditions. Below we shall try to elucidate the present state of the art in this field of physics of superconductors.

Of course, in a single chapter it is impossible to give equal attention to all the aspects of the problem, so we shall concentrate, above all, on the least studied processes occurring in the destruction of superconductivity by a current; more briefly we shall touch upon such phenomena as the dynamic intermediate state and propagation of electromagnetic waves**; problems concerning the resistance of the phase boundaries will not be considered at all, i.e. we shall confine ourselves to sufficiently low temperatures where the Andreev reflection of electrons at the boundary with the superconducting phase (Andreev 1966) leads to the fact that the conductivity tensor of the normal domains coincides with the conductivity tensor for a bulk normal metal, even if the free path of the charge carriers exceeds the thickness of the normal regions.

The two-dimensional mixed state of type-1 superconductors has been observed experimentally quite recently (I. Landau and Sharvin 1969). This specific resisitive state plays a rather essential role in many cases where superconductivity is destroyed by a current. Unfortunately, so far even the qualitative picture of processes occuring in the mixed state of type-1 superconductors is unclear, not to say about a consistent theory of this state. Therefore, we shall concentrate on the discussion of experimental results, and at the end of the paper will present a brief analysis of theoretical models now available.

27.2 2. Resistive phenomena in the intermediate state

27.2.1 2.1. The dynamic intermediate state

As was already noted, Gorter (1957) was the first to point out the possibility of a continuous motion of the domains in the intermediate state in the presence of a direct current. He considered the case where the superconductivity of a cylindrical sample is destroyed by a current. Problems concerning the destruction of superconductivity by a current will be discussed below; here we shall dwell upon the dynamic intermediate state, which arises when a relatively weak current flows through a sample whose superconductivity is partly destroyed by an external magnetic field.

Let us consider how the domains are to move in the simplest case where the structure of the intermediate state is in the form of alternating layers of superconducting and normal phases extended along the current (fig. 1). It may seem at first sight that all the current must flow in the superconducting layers and the resistance of the sample must be zero. However, had

[0]*Thus, a large dispersity of the structure is attained near the sample surface, which leads to a decrease in the energy related to an inhomogeneity of the magnetic field above the surface.

** Problems concerning the propagation of electromagnetic waves in the intermediate state have been considered in detail in the review by Krylov (1980).

such a current distribution taken place, the magnetic field due to the current flowing in the superconducting layer would have been added to the external magnetic field on the one side and would have been cancelled out of it on the other side (fig. 1b). Under such conditions the superconducting layer cannot, obviously, remain at rest, but will start moving to the side where the magnetic field is weaker, which. in turn, leads to an electric field and a current in the normal regions.

The velocity of the interphase boundaries, v, can easily be determined from the continuity equation for the tangential component of the electric field at the phase boundary, which must be satisfied in the boundary-fixed coordinate system. In the superconducting region the electric field vanishes and the boundary condition can be written in the form

$$\left(e + \frac{1}{c} v \times h\right) \times n = 0 \tag{1}$$

where e and h are the values of the electric and magnetic fields in the normal region, and n is a vector normal to the boundary. Since in the intermediate state

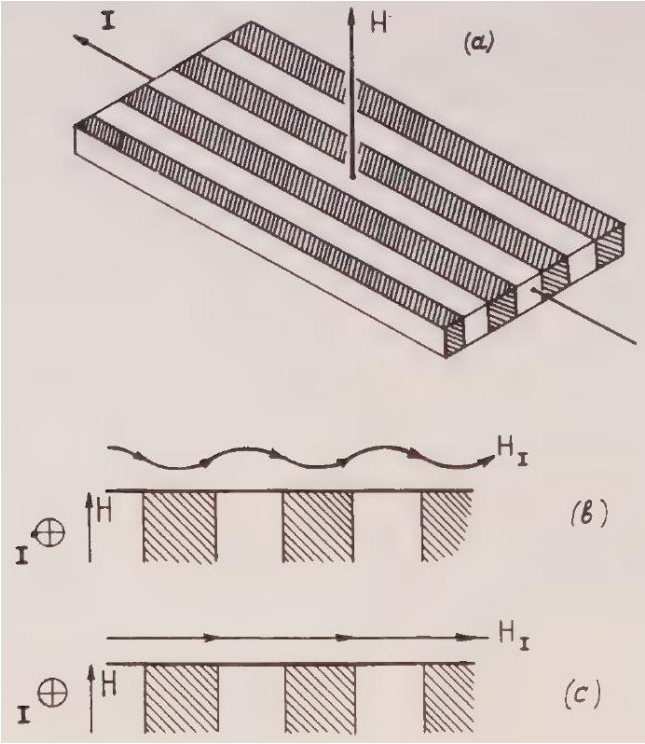


Fig. 1. Motion of the layers oriented parallel to the transport current: (a) Diagram of the experiment. ($\mathrm{b
, \mathrm{c}$) Distribution of the magnetic field due to the current (curve H_I) near the sample surface; (b) in the case where the current flows only through superconducting layers; (c) in the case where the current density in the normal domains is I/S.}

$|h| = H_\mathrm{c}$, we obtain

$$v = c\frac{\boldsymbol{e} \times \boldsymbol{h}}{H_c^2}. \tag{2}$$

The electric field in the normal regions is $\boldsymbol{e} = \rho j_\mathrm{n}$ where ρ is the resistivity of the normal metal, and j_n is the current density in the normal phase. The equality between the values of the magnetic field on the opposite sides of a superconducting layer implies that $|j_n| = I/S$ where I is the total current in the sample, and S is its cross-section (see fig. 1c)*.

Observation of the domain motion requires a regular structure of the intermediate state of a known configuration and a technique which makes it possible to detect the motion of superconducting and normal layers; moreover, the samples must be sufficiently perfect (otherwise, the domain boundaries will be hold up by the defects, which may cause the domains to turn and stop). All these conditions have been satisfied in the experiments performed by Sharvin (1965b).

In those experiments a tilted magnetic field was used to create a layered structure of the intermediate state extended along the current, and a microcontact technique designed by Sharvin (1965a) was employed to detect the domain motion.

The microcontacts were obtained by touching the sample surface with a thin ($20 - 50\mu$ m in diameter) wire. When the sample goes over (under the contact) from the superconducting to the normal state the contact increases its resistance by $10^{-1} - 10^{-3}$ Ohm, which corresponds to contact diameters $\sim 0.1 - 1\mu$ m (Sharvin 1965a). Such microcontacts appeared to be a simple and convenient tool for recording domain motion in the intermediate state. Mounting several microcontacts on the sample surface, one could observe the motion of the domains from one contact to another and, thus, determine the domain velocity and the structure period. Figure 2 shows simultaneous recording of temporal oscillations of the resistance of two contacts when a moving structure of the intermediate state is present in the sample.

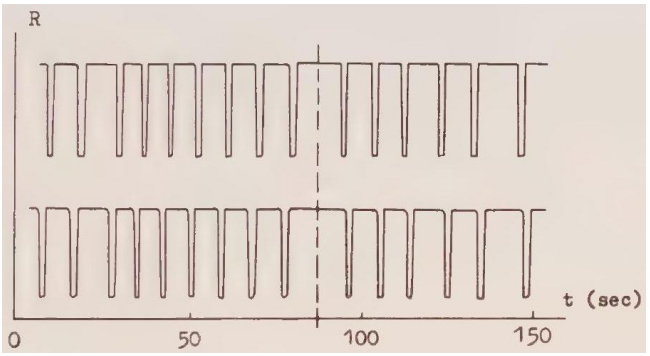


Fig. 2. Simultaneous recording of voltage oscillations across two contacts 0.1 mm apart in the direction of the layer motion. A tin sample at $T=2.93 \mathrm{˜K , H=105 \mathrm{Oe}, I=2 \mathrm{˜A}$. At the moment shown by the dashed line the current in the sample is reversed. (Sharvin and I. Landau 1970.)}

A theory of the dynamic intermediate state has been constructed by Andreev and Sharvin (1967). They showed, in particular, that the motion of the domain should necessarily take place if an electric field component tangential to the interface exists in the normal regions. For instance, the layers aligned normally to the current can move due to the Hall effect in the normal domains*; substituting the Hall electric field in the form $\boldsymbol{e}_{\mathrm{x}} = j_{\mathrm{n}} \times \boldsymbol{h}/Nq$ (N is the difference between the number of electrons and holes per unit volume, q is the electron charge) into eq.

(2), we obtain for the velocity of motion in the current direction

$$v = j_{\mathrm{n}}/Nq. \tag{3}$$

Thus, in this case the layers move at a velocity equal to the charge carrier drift velocity.

[0]*This statement refers only to the case where the current in the sample is perpendicular to the magnetic field (for a more rigorous derivation see the paper by Andreev 1966).

[0]*Such a motion of the layers is also possible in anisotropic metals, provided the current direction does not coincide with the direction of one of the principal axes of the conductivity tensor.

An arbitrary configuration of the superconducting and normal domains will be displaced as a whole in the direction normal to the resultant electric field at the velocity defined by eq. (2), and the only possible static structure is a layered structure of the intermediate state with the layers aligned perpendicular to the electric field. The main conclusions of the theory of the dynamic intermediated state have been confirmed experimentally in the work of Sharvin and I. Landau (1970).

Thus, the motion of the domains in the intermediate state, when a direct current flows through the sample, is the rule rather than the exception. Let us emphasize once more that sufficiently perfect samples are required to observe the dynamic intermediate state*. By perfectness of the samples we mean in this case the homogeneity at distances of the order of the coherence length $\xi(T)$, rather than chemical purity of sample material. So, uniformly distributed impurities should not hinder the motion of domains; this was actually observed in the experiments of Sharvin and Gal'perina (1971), in which they found that even a significant amount of tin introduced into indium samples did not lead to any obstacles for the motion of the domains.

It should also be noted that in imperfect samples the pinning of layers extended along the current may lead to a decrease in the sample resistance or even to its vanishing. The opposite effect would be observed if in a metal with nonzero Hall effect the layers perpendicular to the transport current are at rest. Actually, the continuity of the tangential component of the electric field at the interface will lead to transverse currents in the normal layers that are shortened through the superconducting regions, and this should result in an increase of dissipation in the sample.

In the first work on the observation of the dynamic intermediate state Sharvin pointed out that the motion of domains in the intermediate state could, in principle, be used for constructing a continuously operating refrigerating machine. In fact, at low temperatures almost all the entropy is connected with the conduction electrons and, therefore, is confined to the normal regions, while the superconducting layers play the part of sufficiently effective heat insulators. Hence, the motion of the layers should lead to entropy transfer from one edge of a sample to the other. If one makes use of the motion of layers caused by the Hall effect, the dissipation due to the release of Joule heat can be reduced by employing

samples with lower residual resistance; in this case, owing to the specific mechanism of electron reflection at the interface (Andreev 1966) the scattering of charge carriers at the sample surface is practically eliminated in the intermediate state. Such a "freezing" effect has been observed in the work of Sharvin and Bronevoi (1977); it should, however, be noted that practical use of this effect requires samples whose residual resistance must be several orders of magnitude less than that obtained by present-day experimental techniques.

At present, the dynamic intermediate state has been observed in most of the type-I superconductors*. Microcontacts, magnetic field micro-probes and, probably the most obvious, the magneto-optic method were used to observe the motion of domains. The work of Lebedev and Khotkevich (1980) is worth mentioning here, in which they observed softening of lead in the intermediate state caused by the motion of domains under the flow of a direct current.

27.2.2 2.2. Macroscopic electrodynamics of the intermediate state

Since the surface tension at the boundaries between the normal and superconducting phases is small, the period of the structure of the intermediate state is also small in comparison with the sample size**. This makes it possible to use a macroscopic description of the intermediate

[0]*Apparently, Chandrasekhar et al. (1967) failed to observe the dynamic intermediate state in experiments similar to those of Sharvin because of the imperfection of the samples used.

state. The complete system of macroscopic equations describing the electromagnetic properties of the intermediate state has beeen derived by Andreev (1966).

The macroscopic approach employs quantities averaged over regions whose dimensions are large in comparison with the thickness of the layers, but small in comparison with distances over which the structure changes significantly; these quantities are the magnetic induction $\boldsymbol{B}$ and the electric field intensity $\boldsymbol{E}$. They are defined as mean values of h and $\boldsymbol{e}$, the "microscopic" intensities of the magnetic and electric fields. The fields h and e themselves are quantities which have already been averaged over volumes whose dimensions are much larger than the interatomic distances, but smaller than the thickness of the layers. In the superconducting phase h and e vanish; in the normal phase one may not distinguish between the microscopic magnetic induction and h. because the magnetic susceptibility of the normal metal is small.

The fields e and h in the normal domains obey ordinary Maxwell's equations. and $|h| = H_{\mathrm{c}}$. Following the paper by Andreev, let us introduce the macroscopic magnetic field intensity H in such a way that in normal layers the value of H at a given "point" coincides with the value of h. The vectors of magnetic induction B

and magnetic moment per unit volume $\boldsymbol{M}$ will be in this case:

$$B = x_{\mathrm{n}} H, \quad M = \frac{1 - x_{\mathrm{n}}}{4\pi} H, \quad |H| = H_{\mathrm{c}}, \tag{4}$$

where x_n is the concentration of the normal phase. The averaged microscopic equations yield the ordinary (for any conducting medium) formulae, which relate B, H and the mean value of the electric field $E = x_{\mathrm{n}} e$ by

$$\operatorname{div} B = 0, \quad \operatorname{rot} E = -\frac{1}{c}\frac{\partial \boldsymbol{B}}{\partial \boldsymbol{t}}, \quad \operatorname{rot} B = \frac{4\pi}{c}\bar{i}. \tag{5}$$

Here $\bar{i}$ denotes the macroscopically averaged total current density in the intermediate state. Separating, as usual, out of the total current density the term $c \operatorname{rot} M$, which is related to magnetization currents but does not lead to actual charge transfer through the sample, we can rewrite the last of eqs. (5) as

$$\operatorname{rot} H = \frac{4\pi}{c} j \tag{6}$$

where $j = \bar{i} - c \operatorname{rot} M$ is the transport current density in the sample*. Let us emphasize that besides currents in the normal regions j also includes superconducting currents flowing along the phase boundaries.

The electrodynamics of the intermediate state differs, in principle, from the electrodynamics of a normal metal in that there is not a universal relationship between the transport current density j and the intensities of the fields E and H. However, there exists a relationship between the field intensities and the component of the transport current perpendicular to the magnetic field, $j_\perp$

$$j_{\perp\alpha} = \frac{1}{x_{\mathrm{n}}} \sigma_{\alpha\beta} E_\beta \tag{7}$$

where $\sigma_{\alpha\beta}$ is the two-dimensional conductivity tensor of a bulk normal metal placed in the magnetic field $\boldsymbol{H}$. The subscripts α and β take two values in the plane perpendicular to the magnetic field.

[0]*See, for example, Salomon and Harris (1971), Farrel (1972), Farrel and Isett (1972), Gupta and Farrel (1973), Chien and Farrel (1974), Wolf et al. (1974), Farrel and Chien (1975), Laeng et al. (1975), and Lerski (1975).

**The surface tension is usually written in the form $\Delta \cdot H_c^2/8\pi$ where the parameter Λ has the dimension of length and lies in the range $10^{-6} - 10^{-4}$ cm.

In order to obtain a closed system of equations, Andreev used the transversality of the electric and magnetic fields in the intermediate state, $\boldsymbol{E}\cdot\boldsymbol{H}=0$, which directly follows from the "microscopic" boundary conditions for the electric (eq. 1) and magnetic ($h\times n=0$) fields.

Since the component of the transport current $j_{\|}$along the magnetic field is not directly related to the field intensities, j should be eliminated from the equations. To this end, eq. (6) has to be vector-multiplied by $\boldsymbol{H}$. Thus, the

complete system of electrodynamic equations of the intermediate state is

$$\begin{aligned}&\operatorname{div}\boldsymbol{B}=0,\quad \operatorname{rot}\boldsymbol{E}=-\frac{1}{c}\frac{\partial\boldsymbol{B}}{\partial t},\quad (\boldsymbol{H}\cdot\boldsymbol{\nabla})\boldsymbol{H}=\frac{4\pi}{c}j_{\perp}\boldsymbol{H},\\&\boldsymbol{E}\cdot\boldsymbol{H}=0,\quad |\boldsymbol{H}|=H_c,\quad \boldsymbol{B}=x_{\mathrm{n}}\boldsymbol{H},\quad j_{\perp\alpha}=\frac{1}{x_{\mathrm{n}}}\sigma_{\alpha\beta}E_{\beta}.\end{aligned}\tag{8}$$

Let us note that this is non-linear even if σ does not depend on $\boldsymbol{H}$. Once these equations are solved, the total transport current density can be found by calculating (c /4π) rot $\boldsymbol{H}$.

Solution of system (8) makes it possible to determine macroscopic characteristics of the intermediate state in samples of various geometry for different configurations of external magnetic fields and current in the sample; for instance, Andreev (1966) has solved the problem for a plate with a current in a transverse magnetic field for an arbitrary relationship between the current and the intensity of the external magnetic field. Yet, of the most interest is the possibility to solve in a general way the problem of propagation of electromagnetic waves in the intermediate state. The results of such calculations are presented in the next section.

27.2.3 2.3. Propagation of electromagnetic waves and hydrodynamic effects in the intermediate state

The general equations of macroscopic electrodynamics (8) have been used by Andreev (1966) to study the propagation of electromagnetic waves. He showed that weakly decaying electromagnetic waves can propagate in the intermediate state of a sample with a unequal number of electrons and holes. These waves are circularly polarized and are similar, in their properties, to helicons, which exist in normal metals (see, for instance, the review by Kaner and Skobov 1966).

Following Andreev (1966), we put

$$\boldsymbol{H}=\boldsymbol{H}_0+\boldsymbol{H}',\quad x_{\mathrm{n}}=x_{\mathrm{n}}^{(0)}+x_{\mathrm{n}}',\quad |\boldsymbol{H}_0|=\boldsymbol{H}_{\mathrm{c}}\tag{9}$$

to explain the dispersion law of the waves. Small increments to the equilibrium values, $\boldsymbol{H}', x_{\mathrm{n}}'$ and also $\boldsymbol{E}$, are due to the presence of the wave and proportional to $\exp\{\mathrm{i}\,(k'z-\omega t)\}$. We shall assume that the equilibrium values H_0 and $x_{\mathrm{n}}^{(0)}$ themselves change at distances much larger than $|k|^{-1}$ and linearize the equations (8) with respect to $x_{\mathrm{n}}', \boldsymbol{H}'$ and $\boldsymbol{E}$:

$$\begin{aligned}&k\cdot\boldsymbol{H}_0x_{\mathrm{n}}'+x_{\mathrm{n}}^{(0)}k\cdot\boldsymbol{H}'=0,\quad k\times\boldsymbol{E}=-{}_c^1\left(\omega\left(\boldsymbol{H}_0x_{\mathrm{n}}'+x_{\mathrm{n}}^{(0)}\boldsymbol{H}'\right),\right.\\&\boldsymbol{E}\cdot\boldsymbol{H}_0=0,\quad \boldsymbol{H}'\cdot\boldsymbol{H}_0=0,\quad (\boldsymbol{k}\cdot\boldsymbol{H}_0)\,\boldsymbol{H}'=-\frac{4\pi}{c}\mathrm{i}\,(j_{\perp}\times\boldsymbol{H}_0)\,.\end{aligned}\tag{10}$$

Taking vector products of the second and last of eqs. (10) with H_0 and eliminating H' from the relations thus obtained, we find

[0]*Here we employ the now common term "transport current", instead of the term "conduction current" used in the original paper by Andreev.

$$E_\alpha = \frac{4\pi \mathrm{i}\omega}{c^2 \left(k \cdot H_0\right)^2} H_\mathrm{c}^2 \sigma_{\alpha\beta} E_\beta. \tag{11}$$

Equating the determinant of this system to zero, we obtain the dispersion relation

$$\omega^2 \left(\sigma_{\alpha\beta}\sigma_{\beta\alpha} - \sigma_{\alpha\alpha}\sigma_{\beta\beta}\right) - i\omega \frac{c^2 \left(k \cdot H_0\right)^2}{4\pi H_c^2} \left(\sigma_{\alpha\alpha} + \sigma_{\beta\beta}\right) + \left(\frac{c^2 \left(k \cdot H_0\right)^2}{4\pi H_c^2}\right)^2 = 0. \tag{12}$$

Weakly decaying waves arise in the case where the non-diagonal elements of the conductivity tensor are large as compared to the diagonal elements, i.e. if

$$\sigma_{\alpha\beta} = -\sigma_{\beta\alpha} = \frac{Nqc}{H_c} \gg \sigma_{\alpha\alpha}, \sigma_{\beta\beta}. \tag{13}$$

The spectrum of helicons in the intermediate state can be written in the form

$$\omega = \frac{cH_\mathrm{c}}{4\pi Nq} k_z^2 \tag{14}$$

where $k_z = \left(k \cdot H_0\right)/H_\mathrm{c}$ is the projection of the wave vector of the wave onto the magnetic field direction. The attenuation of electromagnetic waves,

$$\gamma = 2\pi \quad \frac{\mathrm{Im}\{\omega\}}{\omega} = \frac{\sigma_{\alpha\alpha} + \sigma_{\beta\beta}}{\sigma_{\alpha\beta}}, \tag{15}$$

is determined by the two-dimensional conductivity tensor of a bulk normal metal in the plance perpendicular to the magnetic field.

These calculations correspond to the case where the macroscopic description is applicable, and this means that the helicon wavelength must be large in comparison with the period of the intermediate state structure. Thus, the propagation of electromagnetic waves is associated with the motion of interphase boundaries, and their experimental investigation as well as the study of other dynamic effects in the intermediate state require sufficiently perfect samples.

Helicons in the intermediate state were first observed by Maxfield and Johnson (1965): a more detailed investigation was then performed by Kushnir et al. (1971). In those works, however, samples of poor quality were used, which led to difficulties in the interpretation of the experimental results and apparent discrepancy with the theory. These experimental difficulties were overcome by Krylov (1976) who studied helicons in high-purity single-crystal indium samples. All the experimental results obtained by Krylov are in excellent agreement with Andreev's theory. Let us note here the work of

Krylov, Bronevoi and Sharvin (1974), in which the measurement of helicon attenuation was used to examine indium purity by determining the free path of charge carriers; this method appeared to be especially convenient for highpurity samples where the mean free path of the electrons is comparable with the sample size, because the attenuation of helicons in the intermediate state (see eq. 15) is determined by the conductivity tensor of the bulk metal.

Andreev (1967) has also considered the effect of a direct current on the spectrum of helicons in the intermediate state. In fact, the electrodynamic equations of the intermediate state are nonlinear and the presence of a direct current alters the spectrum of helicons in such a way that their erenkov radiation from sample inhomogeneities becomes possible. As a result, a fraction of the energy of the current is transferred to the energy of radiated waves and dissipated, which leads to an increase in the sample resistance. Andreev has called this additional resistance "wave resistance"*. Let us emphasize that the wave resistance does not vanish when the free path of charge carriers increases infinitely, so it must dominate for sufficiently pure samples.

If inhomogeneities in a sample are distributed regularly, the current-voltage characteristic of the sample should exhibit a large number of resonance peaks**. In fact there exists only a

discrete set of wavelengths λ_n of helicons, which may be radiated from static inhomogeneities, these wavelengths being dependent on the current value. If one of the values λ_n coincides with the period of the inhomogeneity distribution, the radiation is especially intensive. It should be noted, however, that the observation of resonance wave resistance is rather difficult, because this requires that the mode of oscillations excited from the inhomogeneities should be attenuated little in the time the structure is displaced by one inhomogeneity period. This period must be large in comparison to that of the intermediate state structure and small in comparison with the sample thickness.

So far, only nonresonant increase in the sample resistance in the intermediate state has been observed in the presence of regularly distributed inhomogeneities (Krylov 1974, 1975a,b); also, the "hydrodynamic" character of the flow of a moving intermediate state structure around a stationary obstacle has been observed directly by magneto-optic techniques (Laeng et al. 1978).

27.2.4 2.4. On the structure of the intermediate state under the destruction of superconductivity by a current

Let us now turn to the case where the superconductivity of a bulk cylindrical sample is destroyed by a current flowing through it. In this case the destruction of superconductivity starts when the magnetic field (due to the current) at the surface exceeds a critical value– Silsbee's rule (1916)*. For currents I exceeding the critical value $I_c = cr_0H_c/2$ (r_0 is the sample radius) one or another structure of the intermediate state must exist in the sample.

The first model of the structure of the intermediate state for this case was suggested by London (1937). In this model the intermediate state represents a periodic (along the sample axis) system of alternating superconducting and normal layers (fig. 3). However, the conclusions of the London model agreed

poorly with experimental results, and twenty years later Gorter (1957) and Gorter and Potters (1958) suggested an entirely new model of the intermediate state. The Gorter structure is dynamic, and represents a system of coaxial cylindrical layers of superconducting and normal phases, which arise at the boundary of the intermediate-state core and collapse at the sample axis (fig. 4).

It will be shown below that it is the Gorter structure that must be observed in experiment. So, we shall concentrate on processes taking place in a sample in the presence of the Gorter structure of the intermediate state. The magnetic field in the normal metal outside the intermediate-state core, $H(r)$, is the sum of the magnetic field due to the current flowing through the intermediate-state core and the magnetic field due to the current in the normal part of the sample. If the current in the normal part is distributed uniformly, then

$$H(r) = Ar + B/r. \tag{16}$$

0

- The nonlinearity $(\boldsymbol{H}\cdot\boldsymbol{\nabla})\boldsymbol{H}$, which appears in the electrodynamic equation of the intermediate state, is similar to the term $(v\cdot\nabla)v$ in Euler's hydrodynamic equations, and the radiation of helicons from sample inhomogeneities resembles the radiation of sound when a supersonic flow goes round an obstacle. This analogy will be even more complete if we introduce the velocity of the structure in the current direction $v = j/Nq$ (see eq. 3); then the radiation of helicons from static inhomogeneities can be considered as the formation of waves under the motion of the intermediate state structure. In this case, radiation of helicons of wavelength λ necessarily takes place when the velocity v becomes equal to that of propagation of electromagnetic waves of this wavelength.
  **Andreev (1967) has solved this problem for a plate in a transverse magnetic field.

[0]*The accuracy to which this rule is to be fulfilled will be considered at the end of this section.

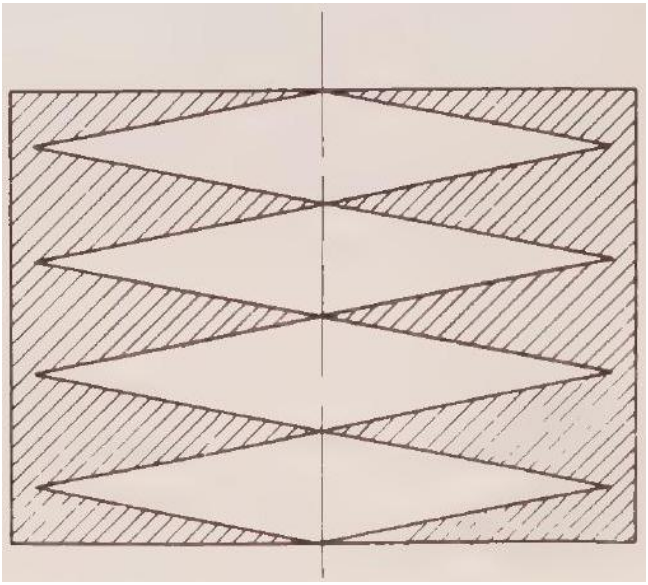


Fig. 3. Schematic diagram of the London structure (normal domains are hatched).

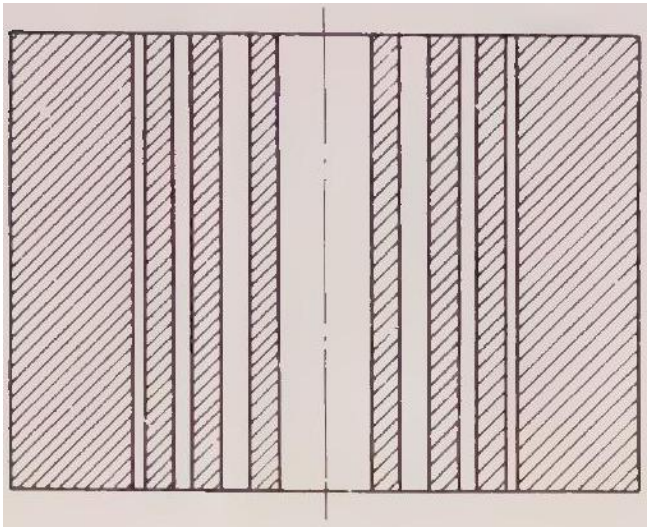


Fig. 4. Schematic diagram of the Gorter structure (normal domains are hatched).

The constants A and B are determined from the conditions $H = H_c$ at the boundary of the intermediate-state core (at $r = r_i$), and $H = (I/I_c)\, H_c$ at the sample surface. It can easily be seen that the radius of the intermediate state region cannot exceed the value

$$r_{i0} = r_0 \left[I/I_c - \left(I^3/I_c^2 - 1 \right)^{1/2} \right]. \tag{17}$$

In this case the magnetic field, which is equal to H_c at the boundary of the region of the intermediate state, increases towards the sample surface, and $(\hat{c}H/\hat{c}r) \mid r = r_{i0} = 0$. For the Gorter structure the radius of the intermediate-state core cannot remain constant, but must decrease because of the motion of the outer boundary of the external superconducting layer towards the sample axis. If the radius of the intermediate-state core $r_1 < r_{i0}$, a region is formed in the normal part of the sample (for $r > r_i$) where the magnetic field is less than the critical one (fig. 5), and the difference $H_c - H_m$ and the size of the region in which $H < H_c$ increase with decreasing r_i. This process goes on until a new superconducting layer is formed in the normal part of the sample at the minimum of the magnetic field.

Out of the two above-mentioned structures only the London structure can be calculated completely. The condition that the magnetic field intensity everywhere in the normal metal must not be less than the critical value makes it possible to obtain (London 1937) the radius of the intermediate-state core in a sample carrying a current I (eq. 17), the dependence of the concentration of the normal phase on the distance from the sample axis $x_{\mathrm{n}} = r/r_{\mathrm{i}0}$, and the resistance of the sample in the intermediate state

$$R = \frac{R_{\mathrm{n}}}{2}\left[1 + \left(1 - I_{\mathrm{c}}^2/^2\right)^{1/2}\right] \tag{18}$$

(R_{n} is the sample resistance in the normal state). In particular, for $I = I_{\mathrm{c}}$ we have $R = 0.5R_{\mathrm{n}}{}^*$.

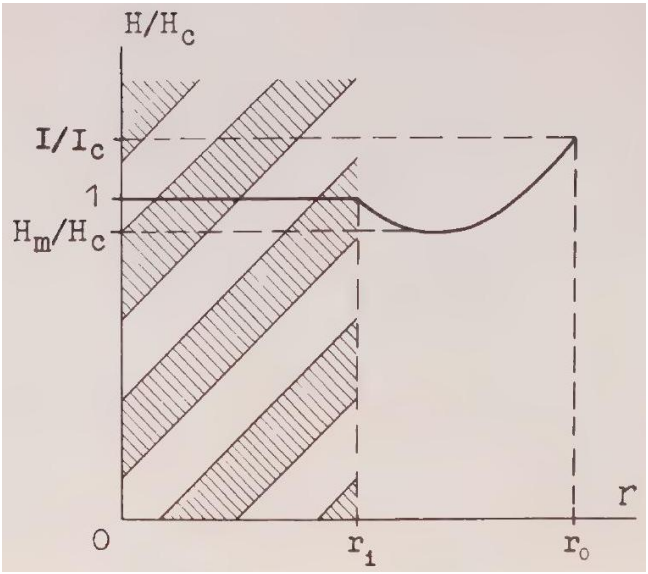


Fig. 5. Diagram of the distribution of the magnetic field in the sample; region $r<r_{\mathrm{i}}$ is occupied by the intermediate state.

The Gorter structure implies continuous formation of new superconducting layers in the bulk of a normal metal, and this occurs with some delay, relative to the equilibrium situation, due to supercooling effects. Therefore, the average (in time) radius of the intermediate-state core, for the Gorter structure, is always less than $r_{\mathrm{i}0}$, and the resistance is larger than the value determined by eq. (18). The exact values of these quantities cannot, however, be calculated.

The experimental value of the resistance jump at $I = I_{\mathrm{c}}$ (see fig. 6) is always much higher than the value $0.5R_{\mathrm{n}}$, which follows from the London model; since the Gorter model can, in principle, give any value of the resistance jump (higher than $0.5R_n$) one might conclude that the Gorter model is more suitable here. However, some modifications of the London model of the periodic structure have appeared (Andreev 1968, Baird and Mukherjee 1968) which agree much better with experimental resistance values.

It is worth noting here that no conclusion should be made about the validity of one or another model only on the basis of data on the resistance in the intermediate state. For instance, Andreev (1968) and Baird and Mukherjee (1968) have suggested models for the structures of

0

- The same results can be obtained by solving the system of equations (8).

the intermediate state based on quite different ideas and assumptions, but these models give practically the same dependences $R(I)$ for actual experiments*. Another important fact is the

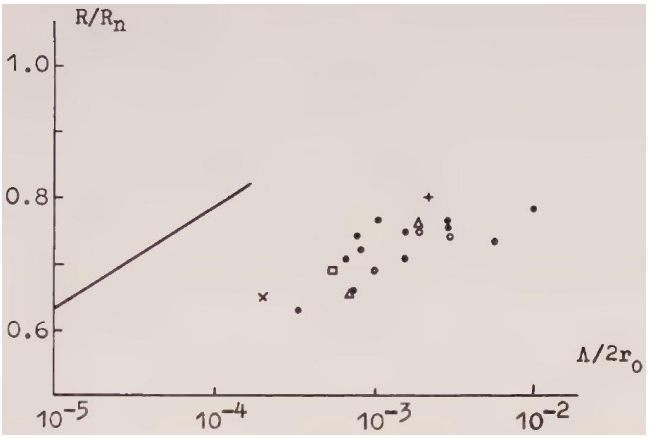


Fig. 6. Resistance jump at $I=I_{\mathrm{c}}$ as a function of surface tension. Solid line is calculation for a rounded-off periodic structure (I. Landau 1979). Symbols correspond to various experimental data: (+) Alekseevskii (1938), ( ) H. Meissner (1958), H. Meissner and Zdanis (1958), (△) E. Troinar (1960); (□) Freud et al. 1968), (×) I. Landau (1973), () Watson and Huebener (1974.)}

large scatter of experimental data on the resistance jump obtained by various authors, which considerably exceeds possible experimental errors (see fig. 6)*. This fact is usually ignored, though it seems obvious that a correct model of the structure of the intermediate state must not only agree with individual experimental results but also explain the scatter of experimental data**.

The London structure of the intermediate state has been developed for zero surface tension at the phase boundary. However, in type-I superconductors the phase boundaries have a positive surface tension, and this circumstance is so important here that it makes impossible the existence of any periodic structures under ordinary exerpimental conditions. In the London structure the interface has a break at point A (see fig. 7). Surface tension prevents the existence of breaks, so the interface near point A must be rounded. At a curved interface the magnetic field must satisfy the following condition:

$$H = H_{\mathrm{c}}\left(1 - \Lambda/2r_{\mathrm{c}}\right), \tag{19}$$

where r_{c} is the radius of curvature of the interface at a given point. Thus, at point A' the magnetic field must be slightly less than the critical one; and the closer the rounded interface is to point A , the larger is the difference $H_{\mathrm{c}} - H\left(A'\right)^{*}$.

Here it is pertinent to recall that under the destruction of superconductivity by a current the magnetic field at a distance r' from the sample axis is determined by the total current flowing in the region $r < r'$. Hence, the relationship between the shape of the interface and

[0]*A considerable discrepancy between the curves corresponding to these models presented in the paper by Mukherjee (1973), is connected with the fact that the wrong value of one of the parameters was used in constructing the curve corresponding to Andreev's theory (see the paper by I. Landau 1978).

[0]*In this figure the values of R/R_{n} are plotted as a function of the parameter $A/2r_0$; it is worth emphasizing that the scatter depends weakly on the way of representation of experimental data.

** Let us note that for the Gorter structure a considerable scatter of experimental data is quite natural because the degree of magnetic supercooling of the normal phase, necessary for the formation of a new superconducting layer, determines the resistance of a sample, and this degree may change significantly from sample to sample, depending on the preparation method, the presence and composition of impurities, etc.

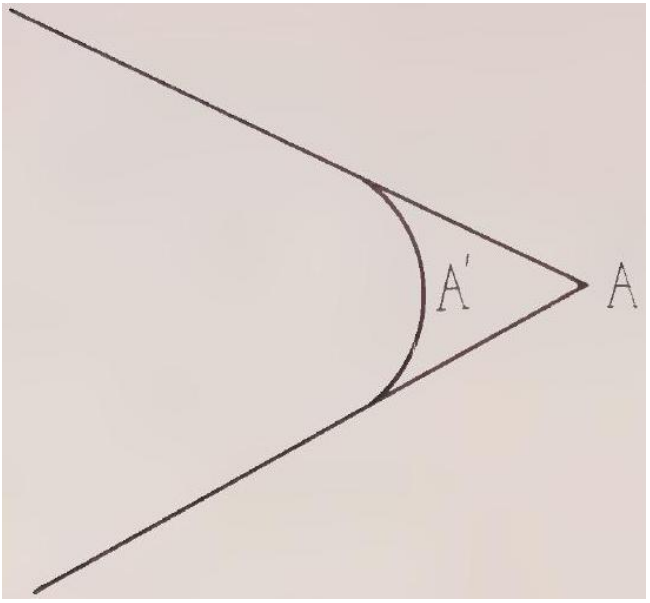


Fig. 7. Schematic diagram of a superconducting layer near the edge of the intermediate state core.

the magnetic field on it is essentially nonlocal, so in order to alter the magnetic field near the boundary of the intermediate-state core, one has to rearrange, to a greater or lesser extent, the structure in the central part of the sample**.

The shape of the interface, at which the magnetic field obeys condition (19) and the currents in the normal phase are distributed in accordance with the conditions at the boundary with the superconducting phase, can be calculated only numerically. Such calculations were performed by I. Landau (1978) for several values of surface tension and it was found that in all actual situations the radius of the intermediate-state core for the rounded structure, r_{i}, is appreciably less then $r_{\mathrm{i}0}$. This means that in the normal metal outside the intermediate-state core, like the case of the Gorter structure, there is a region in which $H < H_{\mathrm{c}}$ (see fig. 5). Therefore, the periodic structure of the intermediate state is unstable relative to the appearance of new superconducting

domains in the normal part of the sample, so it might exist only as a metastable state. Comparison of calculated values of the sample resistance with experiment (see fig. 6) has shown, however, that the Gorter-type structure occurs in practice*.

Let us briefly consider other models of the intermediate state now available. In the models suggested by Andreev (1968) and by Baird and Mukherjee (1968), as well as in the London model, interfaces have breaks, which makes the existence of such structures impossible. In a paper by Mel'nikov (1981) dealing with the same problem, the rounded periodic structure of the intermediate state was calculated numerically. But in these calculations surface tension was not taken into account; the radius obtained for the intermediatestate core is not only much smaller than the sample radius, but also much smaller than the radius of the rounded periodic structure considered above**. So, that paper seems to be of mathematical rather than physical interest.

[0]*The important role of surface tension in the formation of the structure of the intermediate state under the destruction of superconductivity by a current was noted by Sharvin (1977).

**This case differs, in principle, from the situation where superconductivity is destroyed by an external magnetic field. In the latter case the relationship between the shape of the interface and the magnetic field on it is local and difficulties similar to those mentioned above (e.g., the presence of breaks at the interface when the domains exit onto the surface of the sample) are not significant.

Let us now discuss why it was determined experimentally, which structure of the intermediate state arises under the destruction of superconductivity by a current. The main difficulty is that the intermediate-state core is covered with a layer of the normal metal, and the structure can only be judged from various indirect data. As was already noted, data on the sample resistance carry little information. Observation of the periodic structure of the intermediate state on the surface of a sample in the presence of a transverse magnetic field is, in fact, a different experimental situation, since the transverse magnetic field will, naturally, lead to a considerable rearrangement of the structure. From this point of view, the work of Kan and Frolov (1974) was of interest, in which the periodic structure of the intermediate state in the bulk of a sample seemed to have been observed directly. However, as was established later by the same authors (Frolov and Kan 1978), the work appeared to be erroneous, and the oscillations observed were caused by inhomogeneity of the sample parameters along its length. Thus, so far there have been no experimental observations yielding direct, or even indirect, evidence of the existence of a periodic structure of the intermediate state; moreover, some experimental results agree poorly with this assumption.***.

On the other hand, direct indications of the existence of the Gorter structure are not available either (if experiments with a longitudinal magnetic field are not considered****). Indeed, if the Gorter structure were present the periodic

formation of new superconducting layers would lead to oscillations of the sample resistance. This circumstance, noted in Gorter's first work (1957) seemed to lead to a prompt discovery of the Gorter structure. However, even experiments specially designed to observe resistance oscillations (see, for example, the paper by Watson and Huebener 1974) yielded, in fact, negative results: though some samples did reveal an alternating component of the voltage, its amplitude was much lower than theoretical predictions. The absence of clearly pronounced resistance oscillations in the intermediate state is, apparently, one of the main arguments against the existence of the Gorter structure.

In practice, however, a small amplitude of the alternating component of the voltage across the sample is by no means an indication that there is no Gortertype structure in the sample. The fact is that in actual samples such a structure may differ significantly from the idealized system of coaxial cylindrical layers of superconducting and normal phases. As was already noted at the beginning of this section, a new superconducting region arises when the magnetic field in the normal metal decreases to a certain value $H_1 < H_c$. If the sample is sufficiently homogeneous, then for $H < H_1$ a large number of nuclei of the superconducting phase arise simultaneously in the bulk of the normal metal; these merge and form a circular superconducting layer, so we have the case of a typical Gorter structure. If the sample is far from perfect, the nuclei of the superconducting phase will be formed in various regions of the sample at different degrees of supercooling, i.e. at different moments. Small superconducting regions, which arise in this case. simultaneously grow and move to the axis of the sample, so the structure formed in the sample will not even be axially symmetric, and the amplitude of resistance oscillations may be many order of magnitude less than what follows from theoretical calculations.

Most of the experiments dealing with the destruction of superconductivity by a current

0

- A rounded periodic structure may, probably, exist only in samples of a very large diameter (with the ratio $\Lambda/2r_0 \lesssim 10^{-5}$). Experiments on such samples have not been performed because of considerable experimental difficulties.

  ** In the model suggested by Mel'nikov, the region in which $H < H_c$ for $I = I_c$ occupies more than 95% of the sample volume, and the minimal value of the magnetic field in the normal metal is less than $0.2H_c$.

  *** A detailed analysis of various experimental results has been presented by I. Landau (1978).

  ****These experiments will be discussed below, in the section dealing with the paramagnetic effect in type-I superconductors.

have been performed with thin wires made by extruding through draw plates. Such samples are polycrystalline, and since ordinary objects of investigation have a considerable anisotropy of the thermal expansion coefficient, this leads to the concentration of stresses at grain boundaries and makes such samples absolutely unfit for studying the dynamic intermediate state.

Let us touch upon another circumstance to be taken into account in the experimental study of the intermediate state appearing under the destruction of superconductivity of a cylindrical sample by a current. The fact is that an ideal Gorter structure is unstable with respect to a longitudinal magnetic field. Obviously, even a very weak longitudinal field will be pumped into a sample through successive motions of superconducting layers; as time goes on, this process will lead to the destruction of the intermediate state and the formation of a more complicated structure, in which the layers of the two-dimensional mixed state of type-I superconductors play an important role. This situation
will be considered in greater detail below; here we shall only estimate the value of an external longitudinal magnetic field, which is sufficient to destroy the intermediate state in the bulk of the sample.

The longitudinal field will not be pumped into the sample only in the case where the external field is so weak that the normal regions cannot contain even one magnetic flux quantum, $\phi_0 = 2 \times 10^{-7}\text{Oecm}^2$. For a sample several millimetres in diameter (one can hardly imagine a high-quality single crystal of much smaller diameter) this estimate yields a value of the external longitudinal field $H < 10^{-6}$ Oe. Thus, the ideal Gorter structure can occur only under thorough screening and compensation of external magnetic fields. However, the time during which the structure of the intermediate state in the bulk of the sample is destroyed by pumping of a longitudinal magnetic field, can be very long. For instance, in pure samples ~ 1 cm in diameter this time can reach several days for reasonable values of the external magnetic field, $H_{||} = 10^{-4}H_c = 10^{-2}$ Oe; in other words, the structure which arises under such conditions practically does not differ from the purely Gorter structure during the time of an ordinary experiment.

Let us now determine the corrections to the critical current connected with the surface tension at the interfaces having a finite value. Surface tension causes the destruction of superconductivity not to start at exactly the critical value of the magnetic field at the surface of the sample, but at somewhat stronger currents. In a cylindrical sample the destruction of superconductivity should start with the formation of a normal shell along the cylinder circumference. The correction to the critical current can easily be found from the condition that the gain due to the energy of magnetic field in the normal metal must be equal to the surface energy of the cylindrical interface formed:

$$\Delta I_c = 0.5\,(\Lambda/r_0)^{2/3}\,I_c \tag{20}$$

After the transition of the surface to the normal state the intermediate state structure is gradually formed in the bulk of the sample, and the free energy of the samples increases due to the work done by the current supply. However, although the free energy of the sample in the intermediate state is appreciably greater than in the superconducting state, the inverse transition to the superconducting state is impossible because the radius of the intermediate state region is smaller than the sample radius.

The calculated value of ΔI_c is very small, which is in excellent agreement with experiments of Posada and Rinderer (1975) and also of I. Landau (1980). There it was shown that the destruction of superconductivity with increasing current occurs practically at $I = I_c$, while the restoration of superconductivity with decreasing current may be "delayed" down to currents considerably lower than I_c. The existence of the intermediate state for $I < I_c$ is further evidence of the fact that the radius of the intermediate state region at $I = I_c$ is less than the sample radius.

Andreev (1968) calculated a similar correction to the critical current, by comparing the total energy of the sample in the intermediate state with the energy of the superconducting sample, and obtained, naturally, a much larger value $\Lambda I_c = 0.8\,(\Lambda/r_0)^{4/9}\,I_c$. These calculations would be applicable if an intermediate state structure existed in the sample whose radius tended to the sample radius as $I \to I_c$. Let us also note that these calculations are inconsistent with experimental data because such corrections to I_c exceed possible experimental errors (see I. Landau 1980).

27.3 3. Two-dimensional mixed state of type-I superconductors

27.3.1 3.1. Introductory remarks

In the preceding sections we have considered resistive phenomena associated with the existence of the intermediate state, but it was found that under the destruction of superconductivity by a current a resistive state may exist in type-I superconductors, which is not the intermediate one, i.e. which does not represent a mixture of macroscopic regions of superconducting and normal phases*.

Let us consider, for example, the destruction of superconductivity of a hollow cylindrical sample by a current. If the axial symmetry conditions are satisfied, the magnetic field due to the current is zero in the sample hole and, hence, remains small inside the metal near the internal surface. Therefore, the normal state for $T < T_c$ must be unstable even if the current in the sample considerably exceeds the critical value $I_c = cr_2H_c/2$ (r_2 is the radius of the external surface of the sample). On the other hand, the sample has a resistance for $I > I_c$, so an uninterrupted superconducting layer cannot be formed along the internal surface. It may be assumed that in this case a thin macroscopically homogeneous layer of a certain special state arises at the internal surface of the sample. The thickness of this layer must be of the order of $\xi(T)$. The existence of a special resistive state under such conditions was first proposed by **L.** Landau (1938) who called this a mixed state.

In this case the term "mixed state" means a certain new state in which superconducting and normal properties are "mixed up" so intimately that it does not make sense to speak about individual regions of superconducting or normal phases. It was assumed initially that the mixed state should also arise under the destruction of superconductivity by an external magnetic field as a result of infinite branching of normal domains near the surface of the sample (L. Landau 1943).

The possibility of the existence of the mixed state under the destruction of superconductivity by a current has not been considered until recently, and after it has been found that a non-branched intermediate state structure arises in the destruction of superconductivity by an external magnetic field (Lifshits and Sharvin 1977), the term "mixed state" was used to denote the Shubnikov phase in type-II superconductors. Therefore, to avoid confusion, and taking into account that the mixed state of type-I superconductors is in the form of thin layers, we shall call it the two-dimensional mixed state or, in brief, the tm state.

A number of experiments have been performed so far to study the tm state. The macroscopic properties of tm layers have been investigated and some effects have been observed caused by the existence of such layers. It has been shown experimentally that the thickness of a tm layer is, in fact, of the order of the coherence length. Nevertheless, it is impossible to reconstruct, even qualitatively, the picture of processes occurring in the layer only on the basis of experimental results. It seems to us that progress in the study of the tm state is held back by the absence of a theory capable to describe the actual experimental situation.

[0]*In the present section the term "macroscopic" will be used to describe regions whose size considerably exceeds the coherence length $\xi(T)$.

Let us also note that at currents only slightly exceeding the critical one a region occupied by the intermediate state may, in principle, exist in the bulk of the sample. However, if the current increases up to the values

$$I > I_{\mathrm{i}} = I_{\mathrm{c}} \frac{r_1^2 + r_2^2}{2 r_1 r_2}$$

(r_1 is the radius of the hole) the intermediate state cannot exist in the bulk of the sample. Here we shall consider only this relatively simple case, where the difference between the properties of the sample and a normal metal is only due to the presence of the tm layer.

27.3.2 3.2. The tm state in hollow cylinders

The tm state was first observed in the work of I. Landau and Sharvin (1969). The existence of this state is revealed most clearly in the current-voltage characteristics of hollow cylindrical samples (fig. 8). As can be seen from the figure, at $T < T_{\mathrm{c}}$ and $I > I_{\mathrm{c}}$ the sample carries an excess current in comparison with that of the normal sample. It is natural to assume that this excess current flows through the tm layer (we shall denote it by $I_{1\ \mathrm{m}}$). The value of I_{tm} can easily be determined from experimental current voltage characteristics as the difference between the abscissae of curves 2 and 3 (or curves 1 and 3 for a lower temperature). Within the accuracy of those experiments the current in the tm layer was $I_{\mathrm{c}} r_1 / r_2$, i.e. the surface density of the current in the layer is

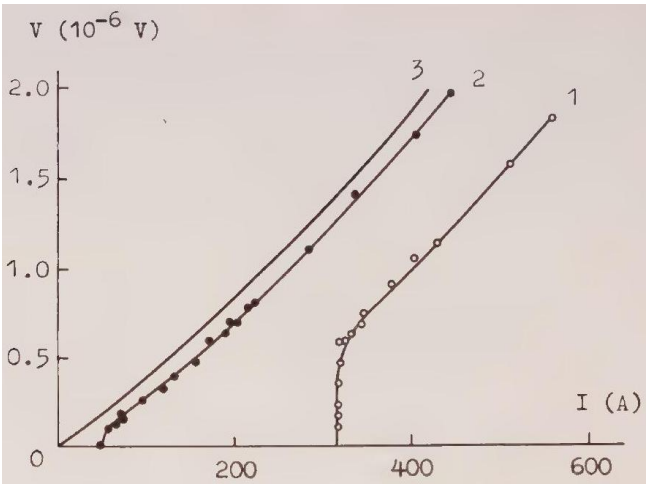


Fig. 8. Current-voltage characteristics of a hollow cylindrical sample: (1) \$T=1.39 \mathrm{˜K \$; (2) $T = 3.16$ K; (3) extrapolation of the current-voltage characteristic in the normal state to $T = 3.16$ K. The deviation of the characteristic from a straight line is due to the dependence of the resistance of the normal metal on the magnetic field of the current. (I. Landau and Sharvin 1969.)}

close to $H_{\mathrm{c}}/4\pi$, which allows the metal adjacent to the tm layer to be in the normal state*.

In the experiments of I. Landau and Sharvin (1972) conditions were realized under which the tm layer could be created not only on the inner surface of a hollow cylindrical sample, but also on the outer surface and in the bulk of the sample at an arbitrary distance from the axis. To this end, a superconducting wire extended along the cylinder axis was placed in the cavity of the sample. The current in this central wire (it will be denoted by I_{b}) could flow independently of the current in the sample. Small inductance coils were placed near the inner and outer surfaces of the cylinder to monitor the state of the sample surface. These coils made

it possible to observe changes in the surface impedance, thereby detecting the appearance or disappearance of the tm layer**.

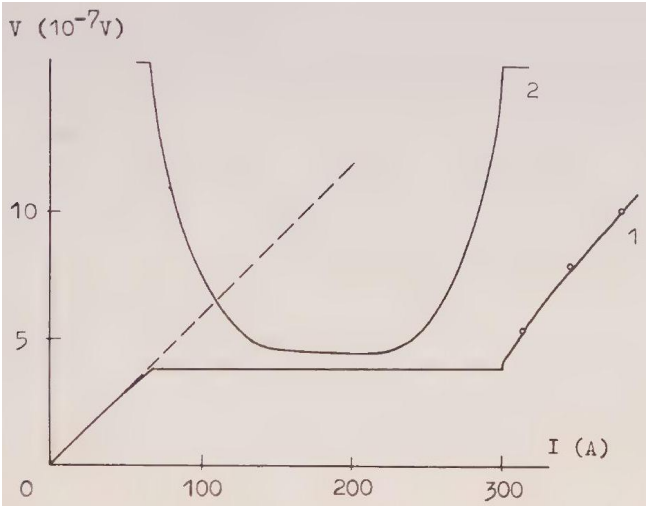


Fig. 9. Dependence on the current of (curve 1) the voltage across the sample and (curve 2) the impedance of the outer surface of the sample. $T=2.95 \mathrm{˜K , I_{\mathrm{b}}=-181 \mathrm{˜A}$. Points are calculated values of the voltage across the sample. (I. Landau and Sharvin 1972.)}

The most interesting is the case where the currents in the central wire and the sample flow in opposite directions. Figure 9 shows the current voltage characteristic of the sample at constant $I_{\mathrm{b}} < 0$ (curve 1) and the dependence on the current of the impedance of the outer surface of the sample (curve 2). The experimental conditions were such that $|I_{\mathrm{b}}| > I_{\mathrm{c}}$, so in the current range $0 \leqslant I < -(I_{\mathrm{b}} + I_{\mathrm{c}})$ the sample was completely in the normal state and its resistance and impedance were practically constant. As the current flowing through the sample increased further, a tm layer occurred on the outer surface of the sample, and the impedance of this surface then dropped rapidly. reaching practically the value for a purely superconducting surface near the point $I = -I_{\mathrm{b}}$ where the magnetic field at the outer surface vanishes. As the current varied in the range

$$-(I_{\mathrm{b}} + I_{\mathrm{c}}) < I < -(I_{\mathrm{b}} - I_{\mathrm{c}})\,.$$

the voltage across the sample remained constant, hence the current flowing through the normal part of the sample was also constant, and the magnetic field at the boundary between the normal metal and the tm layer remained equal to H_c. At the same time, the current in the tm layer increased from zero to $2I_{\mathrm{c}}$ and the field at the outer surface of the sample varied from $-H_{\mathrm{c}}$ to H_{c}. At point $I + I_{\mathrm{f}} = I_{\mathrm{c}}$ the surface of the sample passed to the normal state, yet the tm layer did not disappear but started moving into the bulk of the sample, continuing to carry a considerable portion of the current. The points in fig. 9 represent the calculation of the

0

- More accurate measurements performed later (I. Landau 1976, 1979) have shown that at currents slightly exceeding I_{c} the difference between I_{tm} and $I_{\mathrm{c}} r_1/r_2$ is negligible, but an increase in the current density in the normal part of the sample leads to a decrease in I_{tm}, this decrease being more considerable in samples of metal with a larger resistivity.

**These coils were connected in the tank circuit of a RF oscillator, so the change in frequency of the oscillator, Δf (the measured value), was proportional to change in the imaginary part of the surface impedance.

current-voltage characteristic under the assumption that the tm layer is a cylindrical surface of radius r' and carries a current $cr'H_c$, so the magnetic field jumps from $-H_c$ to H_c at the layer.

The foregoing assumptions that the tm state should exist on the inner surface of hollow cylindrical samples remain, in principle, valid for any value of the current. On the other hand, it is obvious that sufficiently strong current will destroy the tm state and the entire sample will become normal. The current I_{c2} corresponding to the destruction of the tm state was measured by I. Landau and Svistov (1980) for two single-crystal indium samples. The samples had the same geometrical dimensions and crystallographic orientation, but different residual resistance. The results of the experiments are shown in fig. 10. As can be seen from the figure, the tm state is destroyed at sufficiently strong currents and different factors had to be taken into account, which might lead to considerable errors in determining I_{c2}. So, the temperature of the samples was monitored directly during the measurements, and the transverse magnetic field, which appeared in the hole of the sample because the geometry of the sample and current leads was not ideally axisymmetric, was compensated. The high value of I_{c2} restricted the possibility of measuring its temperature dependence, and although sufficiently strong currents (up to 1200 A) were used

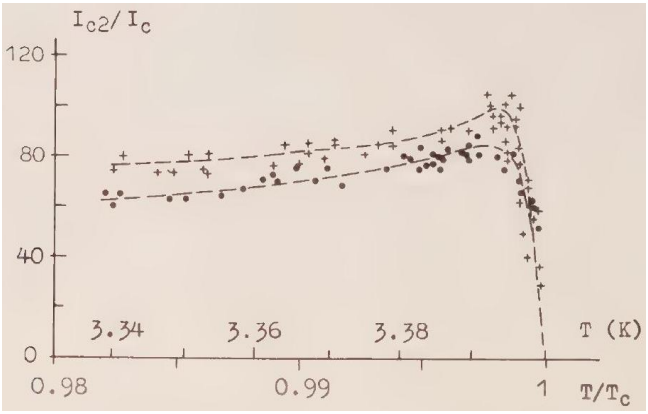


Fig. 10. Dependence of I_{c2} / I_c on temperature; ( ) sample 1, (+) sample 2. (I. Landau and Svistov 1980.) The results presented in figs. 10 and 13-17 are obtained with four single-crystal indium samples with a slight admixture of tin; the dimensions of the samples were $r_1 = 2$ mm, $r_2 = 4$ mm; the resistance ratio $R(300\ \mathrm{K})/R(0\ \mathrm{K})$ was 1700 for sample 1,3300 for sample 2,1800 for sample 3 and 2200 for sample 4.}

in the experiments the current at which the tm state was destroyed could be measured only near T_c.

The sharp decrease in the ratio I_{c2}/I_c on approaching T_c can be explained by the following simple considerations. In fact, a tm layer must, at any rate, be destroyed if the current density in the sample is so high that the magnetic field due to the current flowing in the completely normal sample reaches the critical value for a thickness equal to that of the tm layer. This condition can be written in the form

$$I_{c2} \sim I_c \frac{r_2^2 - r_1^2}{2 r_1 d_m}, \tag{21}$$

where d_m is the minimum possible thickness of a tm layer. The value of d_m cannot be less than $\zeta(T)$, so it grows when T_c is approached, thereby causing I_{c2}/I_c to decrease. Such an estimate gives, obviously, too high values. More interesting is a slight decrease in I_{c2}/I_c as the temperature falls below $0.998T_c$ and the electric field rises (for sample with higher resistance).

27.3.3 3.3. Paramagnetic effect in type-I superconductors

The paramagnetic effect observed by Steiner and Schoeneck (1943) originates from the fact that the magnetic permeability of a bulk cylindrical sample whose superconductivity is destroyed by a current exceeds unity for a magnetic field parallel to the sample axis.

Here we shall not touch upon various attempts to explain the paramagnetic effect by the formation of special intermediate state structures, since it can easily be shown from the general equations of electrodynamics of the intermediate state (8) that no intermediate state structure can arise in a cylindrical sample with a current placed in a longitudinal magnetic field*.

In a cylindrical coordinate system the fourth of equations (8) can be written in the form

$$E_\varphi H_\varphi + E_r H_r + E_z H_z = 0 \tag{22}$$

The mean value, with respect to time, of E_φ is zero ($\bar{E}_\varphi \neq 0$ would mean a continuous increase or decrease of the longitudinal magnetic field in the sample); the components E_r and H_r are also zero. Thus, we obtain from eq. (22) $E_z H_z = 0$, but since $E_z \neq 0$ we have $H_z = 0$, i.e. the intermediate state cannot describe the situation which arises in a sample in the presence of a longitudinal magnetic field.

On the other hand, the Gorter structure of the intermediate state** that

must take place in the destruction of superconductivity by a current seems to be quite suitable for explaining the paramagnetic effect. Actually, a successive motion of cylindrical superconducting regions must lead to a pumping of longitudinal magnetic flux into the sample, which, in fact, is observed in the paramagnetic effect. It can easily be seen, however, that using only superconducting and normal domains one cannot describe a steady-state situation where the mean longitudinal magnetic flux does not change with time.

Quite a natural way out is to suggest that a cylindrical superconducting layer, in its motion towards the sample axis, is transformed into a tm layer before a new superconducting layer is formed around it* (here we mean a steadystate situation). As long as the superconducting layer exists the longitudinal magnetic flux is pumped into the sample; after the superconducting layer is transformed into a tm layer the magnetic flux starts decreasing (because the tm state is resistive) and the tm layer moves further on towards the sample axis. The decrease in the longitudinal magnetic flux in the sample proceeds until a new superconducting layer is formed. Thus, in the model considered the magnetic flux in the sample and its resistance must oscillate with time**.

Regular oscillations of the magnitude of the longitudinal magnetic flux and resistance were observed by I. Landau (1973) in the study of the paramagnetic effect in indium samples (fig. 11). The above-considered model of the paramagnetic effect does not allow the magnitude of the longitudinal magnetic flux to be calculated for any sample because the moment of formation of a new superconducting layer cannot be determined exactly from a priori considerations. However, quite simple ideas (see I. Landau 1973) make it possible to relate the observed resistance of the sample and its effective permeability for a longitudinal magnetic field $\mu^* = \phi/\pi r_0^2 H_\mathrm{e}$ (ϕ is the longitudinal magnetic flux in the sample, H_e is the external magnetic field); as is frequently the case, calculations can be performed only for two limiting cases: weak external field ($H_\mathrm{e}/H_\mathrm{c} \ll 1$) and strong external field ($1 - H_\mathrm{e}/H_\mathrm{e} \ll 1$). The calculated curves are compared with experimental values of μ^* in fig. 12.

The observation of correlated oscillations of the resistance and magnetic moment of a sample, and also the good agreement between the calculated and experimental values of μ^*, are

[0]*The simple proof of this statement given below comes from Andreev (1972).

**In this paragraph we shall discuss only an ideal Gorter structure, assuming that new superconducting regions arise already in the form of cylindrical surfaces.

convincing evidence of the validity of the dynamic model of the paramagnetic effect.

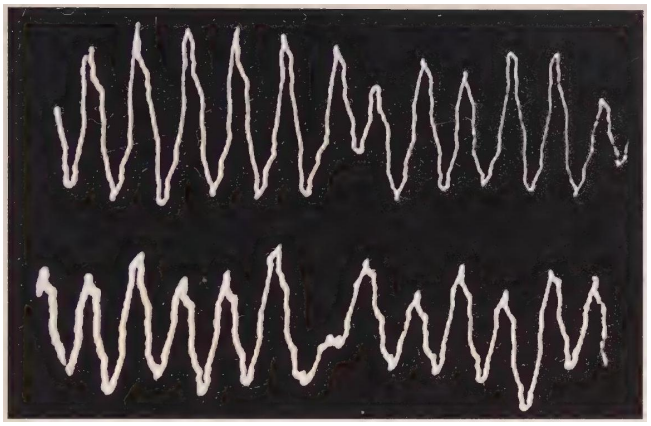


Fig. 11. Oscillations of magnetic flux (upper curve) and resistance (lower curve) of indium sample 7.8 mm in diameter, $R(300 \mathrm{˜K
) / R(0 \mathrm{˜K})=2500, T=3.24 \mathrm{˜K}, H_{e}=0.18 H_{\mathrm{c}}=4.5 \mathrm{Oe}, I=1.05 I_{\mathrm{c}}=44 \mathrm{˜A}$. Oscillation frequency is 10 Hz ; amplitude of magnetic flux oscillations is $\sim 4\%$ of mean magnetic flux in the sample; amplitude of resistance oscillations is $\sim 2\%$ of the mean value. (I. Landau 1973.)}

27.3.4 3.4. Study of the tm state in a longitudinal magnetic field

There are two types of external magnetic fields which do not distort the axial symmetry in the study of the tm state in hollow cylindrical samples, namely, circular and longitudinal magnetic fields. In section 3.2 we have already discussed the results obtained in the presence of an external circular magnetic field. In this paragraph we shall consider the results of experimental investigations of the tm state in hollow cylindrical samples in the presence of a longitudinal magnetic field and also under simultaneous action of a longitudinal and a circular magnetic field (I. Landau 1974, 1979; I. Landau and Svistov 1980).

Figure 13 shows how the longitudinal magnetic field H_{i} in the hole of the sample depends on the external longitudinal magnetic field H_{e}. As can be seen from the figure, H_{i} considerably exceeds H_{e} in the entire range of external

magnetic fields up to $H_{\mathrm{e}} \approx H_{\mathrm{c}}$ when the whole sample becomes normal. At $H_{\mathrm{e}} \approx 0.65 H_{\mathrm{c}}$ the $H_{\mathrm{i}}\left(H_{\mathrm{e}}\right)$ curve revealed a sharp drop of H_{i} with the increasing H_{e}, and hysteresis was observed for this part of the curve. Measurements of the impedance of the inner surface showed that the singularity in the $H_{\mathrm{i}}\left(H_{\mathrm{e}}\right)$ curve corresponds to a sharp increase in the surface impedance (fig. 14). As the magnetic field increased further, the impedance started oscillating with time at a frequency of $1-2$ Hz (traces presented in the figure were obtained at a constant sweep rate of the magnetic field).

The dependences of the ratio $H_{\mathrm{i}}/H_{\mathrm{e}}$ on the current in the sample and the temperature are shown in figs. 15 and 16.

[0]*Let us emphasize that this assumption follows directly from the analysis of the motion of a cylindrical superconducting layer in the presence of a longitudinal magnetic field. The fact is that as this superconducting layer moves the longitudinal magnetic field $H_{\|}$increases at the inner surface of the layer; an increase in $H_{\|}$must, in turn, lead to a decrease in the velocity of the interface, and sine the velocity of the outer boundary of the layer remains unchanged the thickness of the layer will decrease until it is transformed into a tm layer.
**The tm state is resistive, so the coexistence in a sample of longitudinal electric and magnetic fields in the presence of a structure of tm layers is not in contradiction with the laws of electrodynamics.

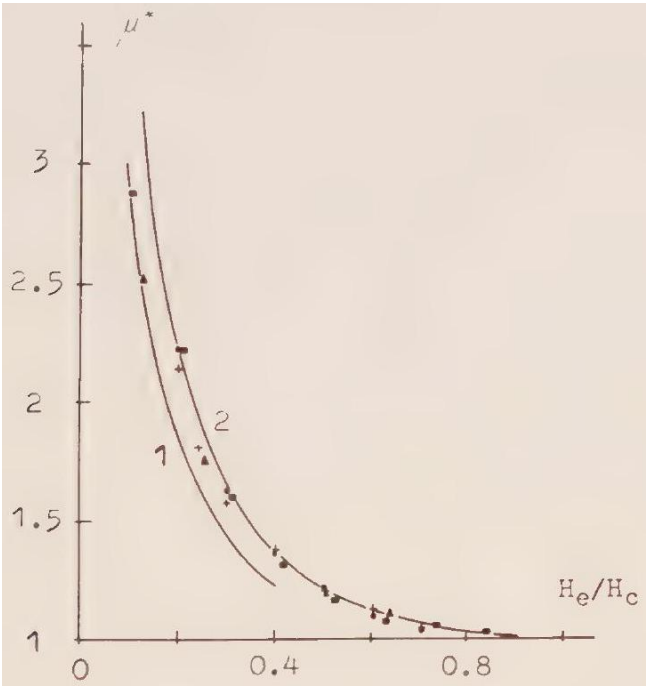


Fig. 12. The dependence $\mu^{*}\left(H_{c}\right)$ for two indium samples. First sample: () $T = 3.335$ K, $T = 3.27$ K, $(-)T = 3.24$ K. Second sample: $(+)T = 3.24$ K. Solid curves: calculation based on the observed values of the sample resistance: (1) for $H_e/H_c \ll 1$; (2) for $1 - H_c/H_c \ll 1$. (I. Landau 1973.)}

Figure 17 presents the longitudinal magnetic field in the hole of the sample as a function of current in the central wire. In that interval of I_b values for which the tm layer is on the inner surface of the sample, $H_i > H_e$; the tm layer in the bulk of the sample did not affect the magnetic field in the hole, so $H_i = H_e$; when the layer reached the outer surface the effect changed its sign and $H_i < H_e$. The dependence $H_i\,(H_e)$ for the latter case is also shown in fig. 13.

The results presented in this section show that in the presence of a longitudinal magnetic field the current in the layer is not parallel to the electric field. Lines of current are in the form of helixes whose sign is determined by the mutual orientation of the electric and magnetic fields at the boundary between the layer and the normal metal, the helical pitch decreasing with increasing longitudinal magnetic field.

27.3.5 3.5. The tm state under non-stationary external conditions

What was considered above referred to the tm state which arise when a direct current flows through a sample. It was found, however, that tm layers may arise under fast changes in an external magnetic field.

The first experiments of such kind were those of Dolgopolov and Murzin (1976, 1977, 1979) in which they studied the behaviour of cylindrical tin samples placed in a longitudinal magnetic field that varied as $H_e = H_= + H_\sim \sin(\omega)$. At all frequencies ω used in the experiments the skin-layer depth in the normal state δ was small in comparison with the sample radius r_0. It was shown in those experiments that superconductivity in the bulk of the sample is destroyed even in the case where $H_= < H_c$ (provided $H_= + H_- > H_c$), and the magnetic flux through the sample may even exceed $\pi r_0^2 H_0$ (fig. 18).

This pumping of the longitudinal magnetic flux into the sample is related to the fact that

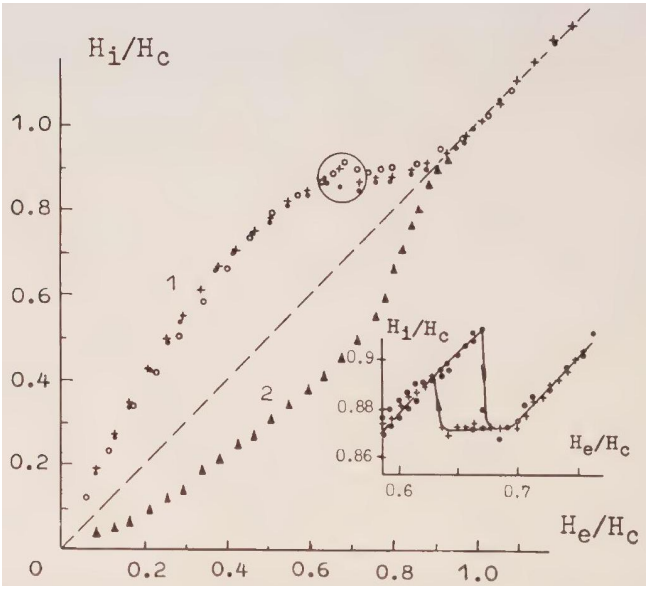


Fig. 13. Dependence on the external magnetic field of the longitudinal magnetic field in the hole of sample. Curve 1: the tm layer is on the inner surface of the sample ($I_{\mathrm{b }}=0$): (◯) sample 3, $T = 3.194$ K, $I = 1.25I_{\mathrm{c}} = 81$ A; $(+, -)$ sample 4, $T = 3,27$ K; (+) corresponds to $I = 1.15I_{\mathrm{c}} = 51$ A and ( ) to $I = 2.08I_{\mathrm{c}} = 85$ A. Curve 2: the tm layer is on the outer surface of sample 4, $I = 85$ A, $I_{\mathrm{b}} = -93$ A, $T = 3.27$ K. The insert is a large-scale view of the part in the circle; sample 4 , $T = 3.194$ K, $I = 81$ A. (I. Landau 1974.)}

during the time when $H_e > H_c$ the surface of the sample becomes normal and the external magnetic field can freely penetrate into the sample,

while for the time when the external magnetic field decreases to values less than H_{c} a tm layer is formed on the surface, which makes it difficult for the magnetic field to get out of the central part of the sample. At the boundary between the tm layer and the normal metal the magnetic field is equal to the critical one, therefore, the magnetic field for the normal region inside the sample never drops below H_{c} (fig. 19).

Measurements of the average (over the sample surface) electric field have shown that at least for sufficiently large values of $H_$the layer which arises on the sample surface, is really a resistive one. Arrow A in fig. 20 indicates the formation of the layer and arrow B to its destruction. As can be seen from the figure, the electric field inside the layer (region AB) is not zero.

The peak at B (fig. 20) is due to the penetration of the magnetic field into the region that was previously occupied by the tm layer. The thickness of the layer, d, can be estimated from the area of the peak. Figure 21 shows the experimental dependence of d on ω. In the frequency range investigated the thickness of the layer decreased with the increasing ω and amounted to about $3\xi(T)$ at maximum frequencies. This character of the dependence $d(\omega)$ was caused, most likely, by the nonequilibrium conditions under which the tm layer was formed. In fact, the formation of a tm layer of the on the surface of a normal sample, like any phase transition of the first order, proceeds with a certain delay relative to the equilibrium situation (at high frequencies the layer is, probably, to arise only after the magnetic field decreases to a value corresponding to absolute instability of the normal phase). At that moment the magnetic field in the normal metal is less than H_{c} inside a region of the order

of the skin-layer thickness and the time the tm layer exists on the sample surface is too short for the layer to reach equilibrium.

More equilibrium conditions can be obtained if a strong external magnetic field ($H_{\mathrm{e}} > H_{\mathrm{c}}$

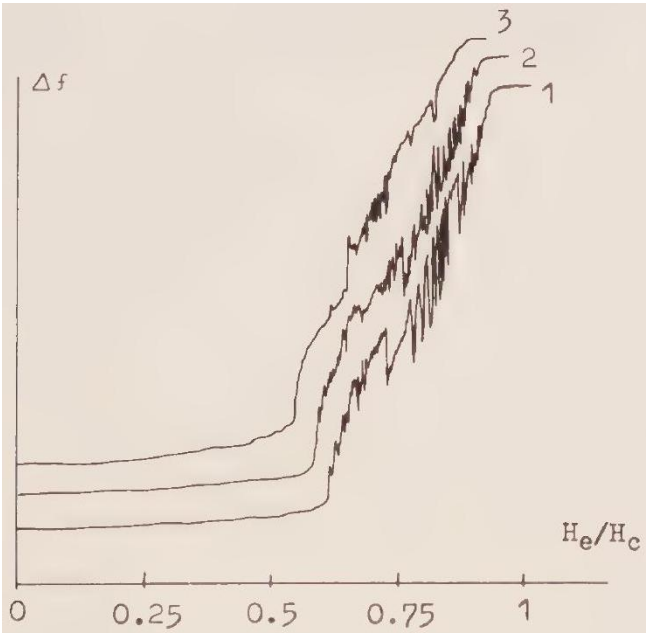


Fig. 14. Dependence of the inner-surface impedance of sample 4 on the longitudinal magnetic field. $T=3.375 \mathrm{˜K
$: (1) $I = 8.6$ A, (2) $I = 15$ A, (3) $I = 29$ A; $I_c = 6.6$ A. (I. Landau 1974.)}

) parallel to the sample surface is switched off. After the external field is switched off eddy currents are induced in the sample and initially the magnetic field in the bulk of the sample remains larger than H_c; the magnetic field outside the sample is zero and conditions on the sample surface are completely analogous to those on the inner surface of hollow cylinders when superconductivity is destroyed by a current. Under such experimental conditions suggested by Dolgopolov and Dorozhkin (1978) there is no need for strong currents, which makes the experiment much simpler from a technical viewpoint. On the other hand, the attenuation of eddy currents leads to the fact that the tm layer appears to be under nonstationary external conditions, and this restricts, to some extent, experimental possibilities.

The tm state arising on switching off the external magnetic field was studied by Dorozhkin and Dolgopolov (1979a,b) and by I. Landau and Svistov (1980). The experimental conditions of these investigations were somewhat different: Dorozhkin and Dolgopolov's measurements were performed with a rectangular aluminium sample with dimensions $1 \times 1 \times 2$ cm (the larger dimension being directed along the magnetic field), while I. Landau and Svistov investigated a long cylindrical indium sample (the diameter of the sample was 8 mm). The main goal of those experiments was to study the structure of the layer with the aid of microcontacts.

If a magnetic field component perpendicular to the surface under investigation was present, the tm layer was inhomogeneous, that is, it contained
a structure of moving normal domains. When these normal domains passed under the microcontacts the resistance of the contacts oscillated. By placing several microcontacts on the surface of the sample and comparing the signals from different contacts one could observe the motion of the normal regions between them and determine the direction and velocity of motion, and the characteristic dimensions of the structure.

The results obtained for aluminium and indium were slightly different. Two types of structures, namely layered and island, were observed in experiments with aluminium. The structure of the first type appeared on switching off a relatively weak external field $[(H_e - H_c)/H_c \lesssim 3]$. The normal regions in this case were in the form of strips extended along the projection of the external magnetic field on the sample surface; the direction of motion of these regions coincided

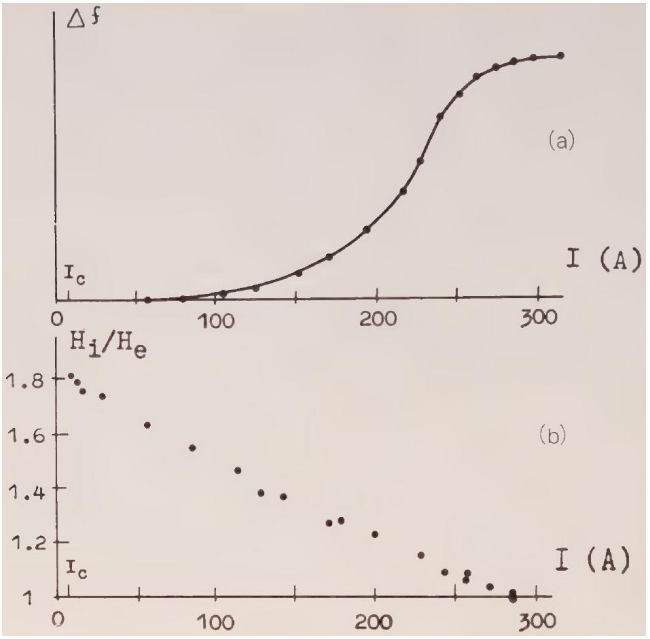


Fig. 15. Dependences of (a) the inner-surface impedance and (b) the magnitude of the paramagnetic effect on the current in the sample. Sample \$4, T=3.375 \mathrm{˜K
, H_{\mathrm{e}}=0.22 H_{\mathrm{c}}=0.73 \mathrm{Oe}\$. (I. Landau 1974.)}

with that of the currents flowing in the sample.

After switching off stronger magnetic fields H_{e} island structures were observed in aluminium, as well as in indium, which moved perpendicular to the current*. The velocity of the normal regions increased with decreasing transverse component of the magnetic field approximately as $1/H_{\perp}$. At small values of $H_{\perp}$ the signals from different contacts were not correlated any more, so the parameters of the structure could not be measured. Figure 22 shows several oscillograms of the voltage across the contacts.

In the absence of a transverse magnetic field no structure in the tm layer was observed in experiments with indium. In aluminium, under similar conditions, voltage pulses across the contacts were observed that corresponded to the motion of normal regions. The pulses from different contacts did not correlate in this case, and asymmetric pulses were frequently observed. This behaviour was interpreted as the formation of non-stationary structure with spontaneously appearing and annihilating normal regions carrying transverse magnetic fields of opposite signs. The measurements on aluminium, however, were performed with relatively short samples, so it is quite probable that the normal regions observed for the field H_{e} parallel to the surface were due to edge effects.

In experiments with aluminium the thickness of the tm layer was also measured. The measurements were performed as follows. After a strong magnetic field had been switched off, a tm layer appeared on the surface of the sample; the magnetic field was then switched on and the voltage across a coil wound around the sample was measured. The signal from this coil revealed a characteristic voltage pulse associated with the destruction of the layer and penetration of the magnetic field into this region. Determining the magnetic flux penetrating into the sample, one could estimate the thickness of the layer.

The experiments performed yielded the value $\sim \xi(T)$ for the thickness of the layer.

0

- The absence of the layered structure in indium samples is most likely to be related to the fact that measurements for small values of H_e were not performed in these experiments.

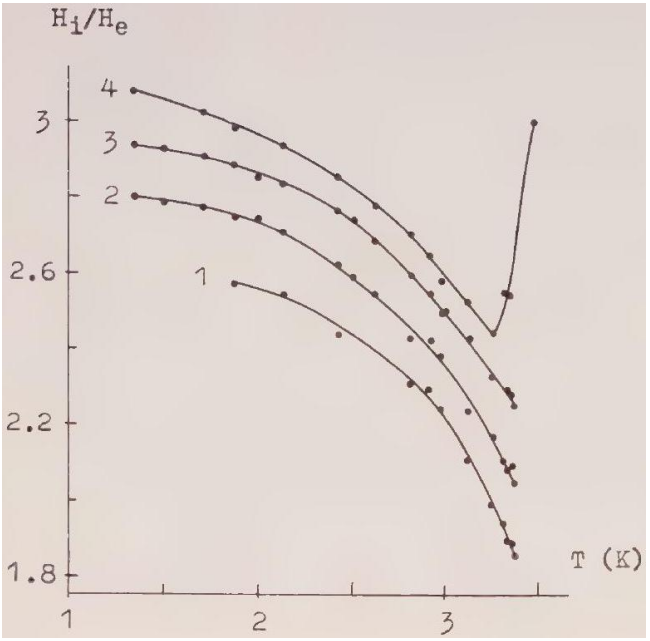


Fig. 16. The magnitude of the paramagnetic effect as a function of temperature. Sample 1, $H_{\mathrm{e}}=0.05 H_{\mathrm{c}}$: (curve 1) $I = 4I_c$; (2) $I = 2.8I_c$; (3) $I = 1.9I_c$; (4) $I = 1.2I_c$. (I. Landau and Svistov 1980.)}

Among the results concerning the structure arising in the tm layer in the presence of a transverse magnetic field one should note the relatively large period of the structure (fig. 23), which considerably exceeds $\xi(T)$*. This means that an electric field should also exist between the normal regions because the arguments that a resistive layer exists on the surface of a sample as a whole are completely applicable to individual "superconducting" regions in the tm layer whose dimensions are much larger than the layer thickness. Thus, the case where a transverse magnetic field is present can be interpreted as a peculiar intermediate state, in which regions occupied by the tm state play the role of superconducting regions.

27.3.6 3.6. Discussion of theoretical models

At present there are a number of theoretical papers dealing with the tm state, the theoretical concepts being developed via the construction of various models. In some papers periodic structures are proposed for the tm layer, which consist, in analogy with the intermediate state, of purely superconducting and purely normal domains; models of a homogeneous tm layer also exist. Nevertheless, all these models either are inconsistent with experimental results or have a region of applicability of the theoretical calculations which is far from actual experimental situation.

Let us first consider the models with periodic structures (Gor'kov and Dorokhov 1974, Andreev and Dzhikaev 1977). These structures are shown in fig. 24. As can be seen from the figure, both the structures have breaks on the

interface, which makes the existence of such structures impossible (see section 2.4). For the structure in a thin tm layer this circumstance appears to be much more essential than for the structure of the intermediate state in a bulk cylindrical sample. Let us consider an

[0]*This fact by no means contradicts the estimates of the thickness of the tm layer because in superconducting films with a thickness of the order of the coherence length an island-type structure is observed whose characteristic dimensions significantly exceed the thickness of the films (Goren and Tinkham 1971).

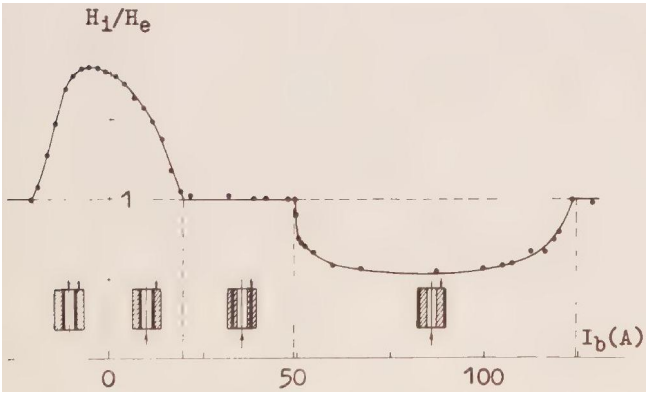


Fig. 17. Dependence on the current in the central wire of the longitudinal magnetic field in the hole of sample $4 ; T=3.27 \mathrm{˜K
, I=-85 \mathrm{˜A}, H_{\mathrm{e}}=0.4 H_{\mathrm{c}}=8.2 \mathrm{Oe}$. The bottom part of the figure is a schematic diagram of the sample cross-section, arrows show directions of the currents, bold-face line indicates the position of the im layer. (I. Landau 1974).}

arbitrary superconducting region at the inner surface of a hollow cylindrical sample (fig. 25). The magnetic field in a

hole of the sample is zero, while the magnetic field at the boundary between the superconducting region and the normal part of the sample is determined by currents flowing into this region; therefore this field increases when moving from point 1 to point 2 . In the case of a periodic structure of the intermediate state under the destruction of superconductivity of a bulk cylindrical sample such inflow of the currents is compensated by the increasing distance from the sample axis (for the cylindrical geometry the magnetic field decreases as $1/r$). In the case of the tm state the change in the distance from the sample axis can be neglected and equilibrium at the interface can be attained only if the equilibrium magnetic field at the interface also increases when moving from point 1 to point 2 . There are, probably, only two ways to alter equilibrium conditions at the interface: first, one can use the dependence of the equilibrium magnetic field on the thickness of the superconducting layer (this possibility was employed by Gor'kov and Dorokhov 1974); second, one can use the fact that the equilibrium magnetic field at the interface depends on the curvature of the interface at a given point (this way of constructing the structure of the tm state was employed by Andreev and Dzhikaev 1977). Both these ways lead to acute angles at the interface where the concentration of the superconducting phase vanishes; and this is impossible, as was mentioned above.

Let us also note that the absence of a regular periodic structure in the tm layer directly follows from experimental study of the layer by microcontacts (see section 3.5).

Ivlev and Kopnin (1980) have suggested a model of the tm layer constructed in analogy with the resistive state of thin superconducting channels. In this model the layer consists of "superconducting" regions separated by narrow regions in which the order parameter vanishes (phase-slip centres). Quotation marks have been put around the word superconducting here, because in these regions an electric field exists along with the superconducting condensate current and, hence, in these regions energy is consumed from a current supply. This model is not truly periodic, since the phase-slip centres do not exist permanently but arise from time to time in various parts of the layer. Unfortunately, the applicability of this model requires electric fields and current densities considerably exceeding those used in real experiments. The restriction on the current density is most essential here, because the structure of the above type cannot exist for the relatively small current densities attained in experiments.

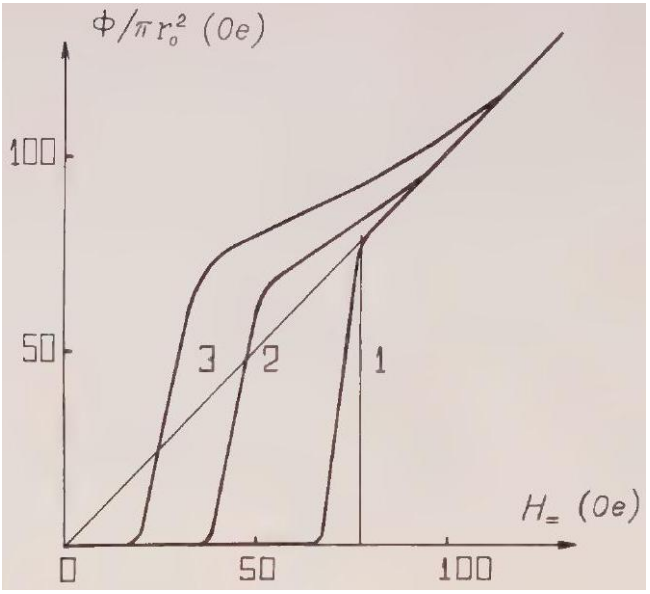


Fig. 18. Dependence on external magnetic field of the longitudinal magnetic flux in a sample: (1) $H_{\sim}=0$; (2) $H_{=} = 45.5$Oe; (3) $H_{\sim} = 67.5$Oe. (Dolgopolov and Murzin 1974.)

As far as the models of homogeneous tm layers are concerned, they cannot be compared with experiment because the region of their applicability is very far from the real experimental situation. For instance, the model developed by Andreev and Tekel (1972) corresponds to the case where the electric field in the sample $E \equiv 0$ and describes, in fact, a thin superconducting layer. The model developed by Andreev and Bestgen (1973) refers to the opposite limiting case where the superconductivity in the tm layer is destroyed to such a degree that the small amount of superconducting pairs in the layer can be considered as fluctuations; in this case the superconducting current in the layer $I_{\rm s}^*$ must be significantly less than the normal current $I_{\rm n}^*$, while in experiments, on the contrary, we have $I_{\rm s}^* \gg I_{\rm n}^*$.

Nevertheless, it is interesting to note that Bestgen (1973, 1979) considered the effect of a longitudinal magnetic field on the tm layer within the framework of the model of Andreev and Bestgen (1973), and showed that many of the theoretical conclusions are in qualitative agreement with experiment. Among these conclusions one may note the correct sign of the effect when a tm layer is either on the inner or on the outer surface of the sample, the absence of the effect when the tm layer is in the bulk of the sample, instabilities observed for large values of the longitudinal magnetic field (see fig. 14), and, finally, a decrease in the magnitude of the paramagnetic effect with increasing temperature (see fig. 16). Although the theoretical calculations are formally not applicable to the experimental situation, it is difficult to believe that the aforementioned qualitative agreement between theory and experiment for various aspects of the behaviour of the tm layer in a longitudinal magnetic field is simply occasional. It is, probably, an indication of the fact that such a behaviour of the superconducting condensate in the presence of parallel
electric and magnetic fields is, in essence, a more general circumstance, and is retained for any relationship between $I_{\rm s}^*$ and $I_{\rm n}^*$.

The structure of the tm state is of great interest because it represents a certain new type of resistive state of superconductors. Probably, kinetic and non-stationary process, related to the coexistence in the tm layer of superconductivity and electric field, should play an important role.

Let us also note that experimental investigations alone, without a profound development of

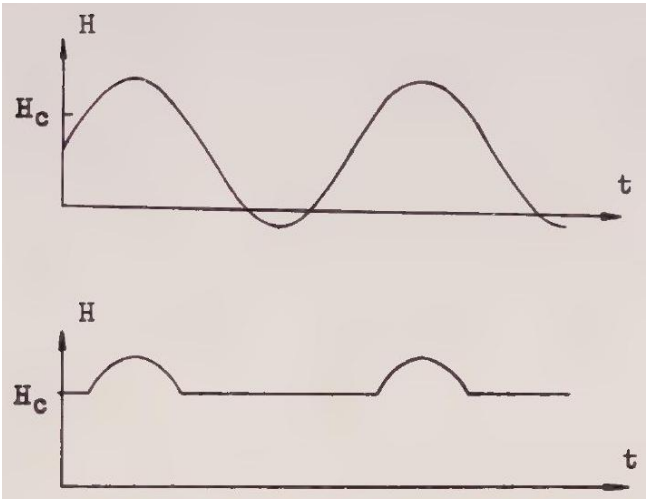


Fig. 19. Temporal dependence of (top) the external magnetic field and (bottom) the magnetic field at the boundary of the normal region.

the theoretical concepts, are unlikely to lead to considerable progress in the understanding of processes occurring in the tm layer. The fact is that of most interest here are rather sophisticated and laborious experiments, for example, creation of a tunnel or Josephson junction on the surface of a sample and investigation of the characteristics of such junctions in the presence of the tm layer. Such experiments, however, usually yield rather complicated results which, apparently, are difficult to interpret unambiguously without an appropriate theoretical model. On the other hand, experimental data now available are, of course, quite sufficient to verify the validity of one theoretical model or another.

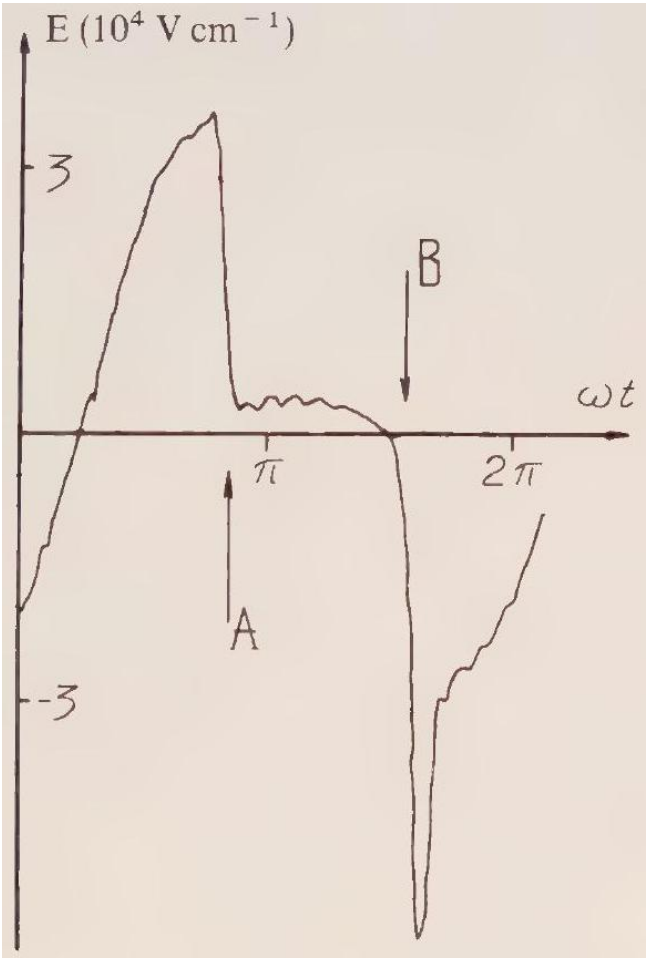


Fig. 20: Electric field strength, averaged over the sample surface, as a function of the phase of the alternating field. $\omega / 2 \pi=146 \mathrm{kHz
, H_{=}=40 \mathrm{Oe}, H_{\mathrm{c}}=54 \mathrm{Oe}, H_{\sim}=40
\mathrm{Oe}$. (Dolgopolov and Murzin 1979.)}

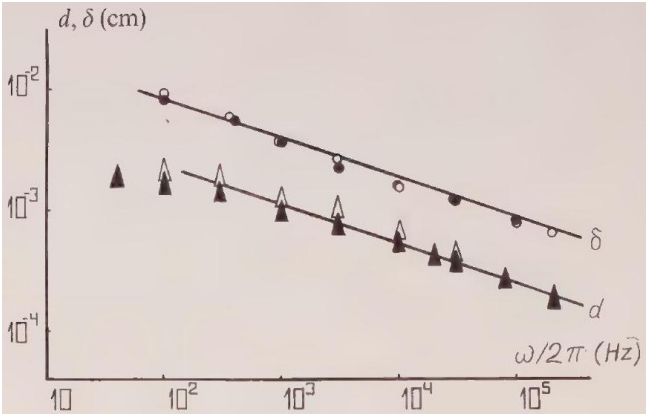


Fig. 21. Skin-layer depth and the thickness of the tm layer as functions of the alternating field frequency. Dots for d are obtained at $H_{\sim
=225 \mathrm{Oe}, H_{\mathrm{c}}=230 \mathrm{Oe}, H_{=}=37 \mathrm{Oe}$.
Straight lines correspond to the dependence $\omega^{1/3}$. (Dolgopolov and Murzin 1979.)}

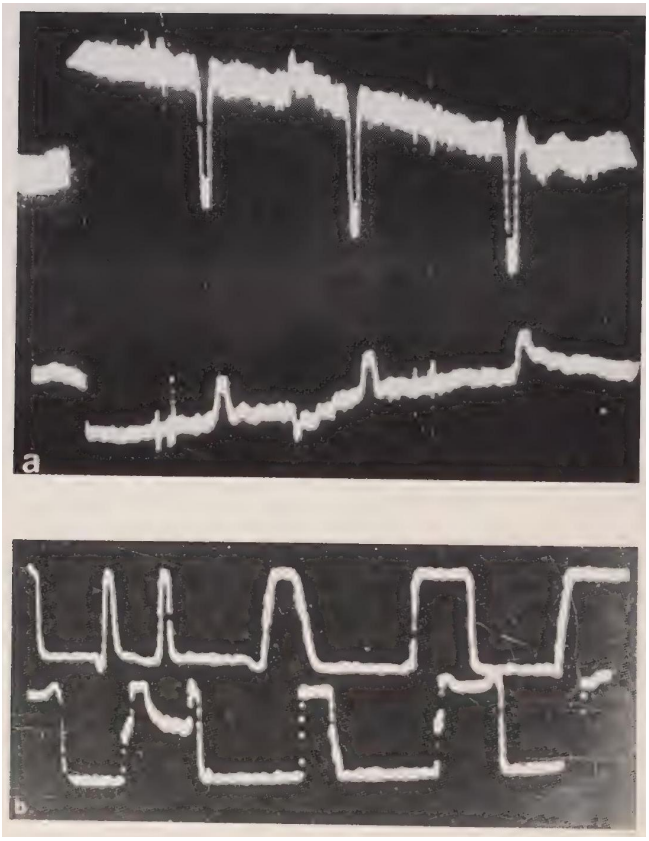


Fig. 22. Oscillograms of the voltage across the microcontacts. (a) From Dorozhkin and Dolsopolon i 1970 i The magnetic field II, that somithed off ated to the sample surface at an angle of 111.11 II $2.7-04 \mathrm{˜K
-1 \mathrm{n}$ the light an incleste in the sample resistance corresponds to deflection of the tas upward tor the lawe wallestam and to deflection downward for the upper oscillogram. (b) From I. Landau and Svistov (1980) H_e is parallel to the sample surface; $H_e/H_c = 8.4$; the external static magnetic-field normal to the sample surface is $H_\perp = 19$Oe; $T = 2.8$ K (sweep width is 15 ms).}

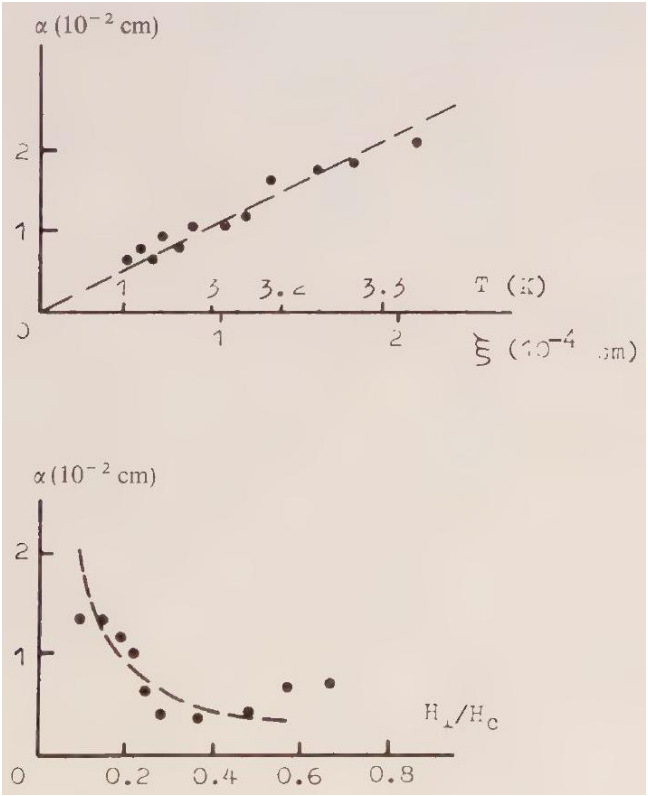


Fig. 23. Dependence of the mean period of the structure on temperature and the transverse magnetic field; (a) $\alpha(T)$ at $H_{\perp}=0.18\ H_{\mathrm{c}}$; (b) $\alpha\,(H_{\perp})$ at $T = 3.06$ K; $H_{\mathrm{c}} = 700$Oe; $H_{\mathrm{c}} = 52$Oe; the density of the circular current near the sample surface is $6.9cH_{\mathrm{c}}/4\pi r_0$. The dashed curve corresponds to the dependence $\alpha \times 1/H_{\perp}$. (1. Landau and Svistov 198().)}

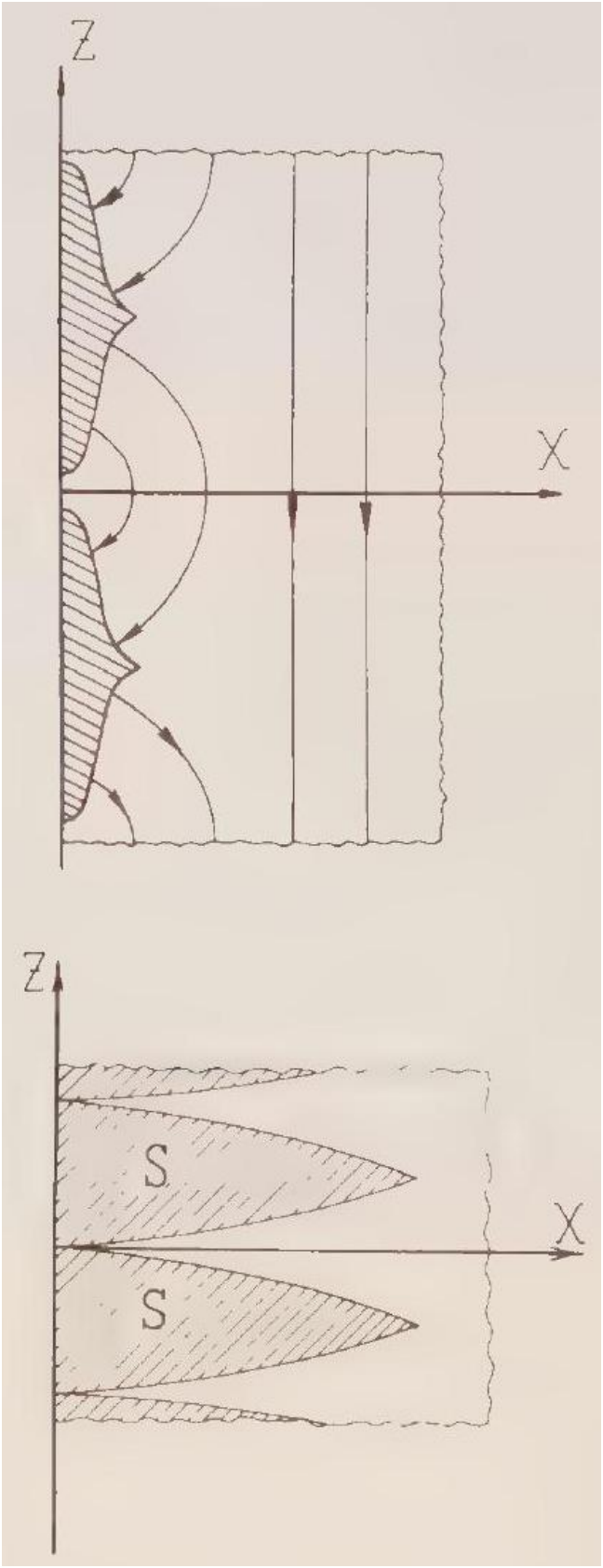


Fig. 24. Patterns of periodic structures suggested for the tm layer: (a) Gor'kov and Dorokhov (1974); (b) Andreev and Dzhikaev (1977). Superconducting domains are hatched. Arrows schematically show the direction of lines of the current.

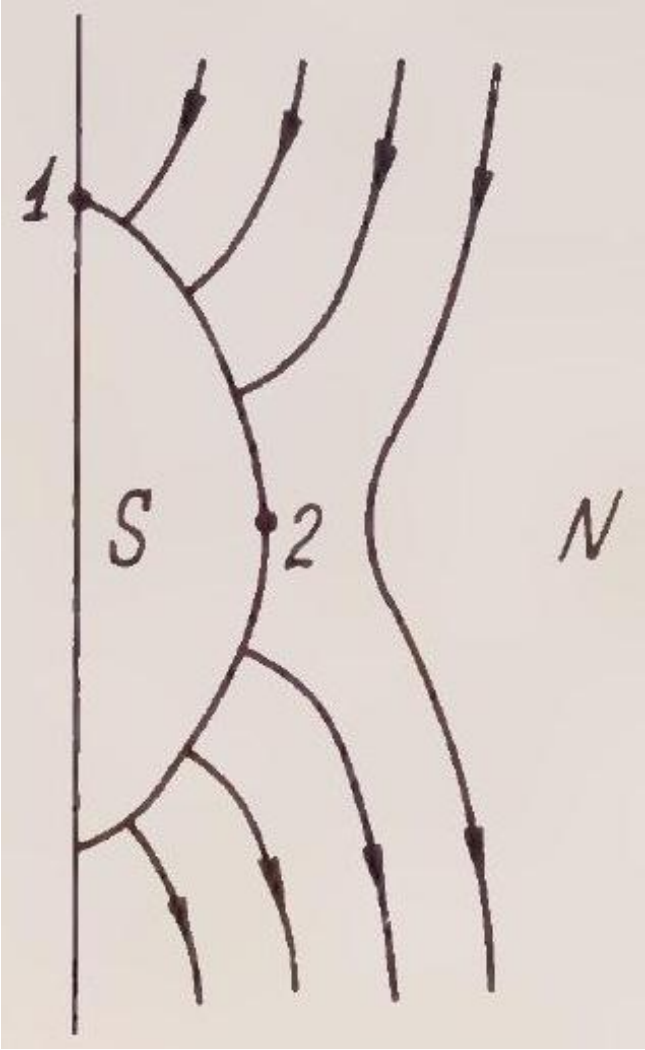


Fig. 25. Schematic diagram of the superconducting region on the inner surface of a hollow cylindrical sample; arrows show the direction of lines of current.

28 Collisionless relaxation of the energy gap in superconductors by Volkov, Kogan, 1973

(it is not written, physically why the perturbation relax and why can they appear? these are the main questions)

Abstract

Equations are derived for equal-time Green's functions and describe the dynamics of superconductors during a time that is short in comparison with the electron energy relaxation times τ_{ph} and τ_{ee}.

(which exactly these times are? it means $t < \tau_{ph}, \tau_{ee}$)

The time evolution of small initial perturbations of the order parameter Δ is investigated.

(what physically happens when there are these initial perturbations????)

It is established that following initial perturbations of a definite type (which type?) the energy gap relaxes only as a result of inelastic collisions of the electrons during a time on the order of τ_{ph}, τ_{ee}.

(only! why only?..)

In the general case which???, the order parameter at $t < \tau_{ph}, \tau_{ee}$ oscillates with a frequency $\sim 2\Delta$ and with an amplitude that attenuates asymptotically with time in accord with a power law.

(so in particular case gap decreases and in general case it also oscillates?)

(still don't understand the physics behind this formulas...)

28.0.1 1. Introduction

Much progress has been made recently in the problem of the nonstationary phenomena in superconductors. Equations describing the kinetics of superconductors were obtained. These equations are of simplest form in the case of gapless superconductivity [1–3].

(why for gapless?? and how is it??)

In this case they are closed equations for the order parameter Δ and generalize the Ginzburg-Landau equations.

At the same time, there are many problems in which an important role is played precisely by the presence of the finite gap in the energy spectrum of the superconductor (I thought it is important for all problems...).

One such problem arises in the problem of perturbation relaxation in superconductors.

It is easy to verify that in gapless superconductors the perturbations of Δ decrease exponentially to zero.

(how to verify it??? well, if SC is gapless, then there should be no gap, so it should decrease...)

What remains unclear is the character of the relaxation of Δ in the absence of external field in superconductors with gaps.

(why we need an absence of external field?)

In particular, one can conceive of a situation in which the perturbations of Δ experience natural undamped oscillations [4] (within a time short in comparison with the inelastic relaxation times).

(was it discovered in [4]??? B. I. Ivlev, ZhETF Pis. Red. 15, 441 (1972))

The kinetics of superconductors with finite gaps is described by sufficiently complicated equations, obtained by Éliashberg [5] for equal-time Green's functions.

In this paper we examine, on the basis of equations derived from the Eliashberg equations, the behavior of a small initial perturbation of Δ in the absence of fields, and in a time interval small in comparison with the electron energy-relaxation times

$$\tau_{ph} \approx \hbar\Theta_D^2/T^3, \qquad \tau_{ee} \approx \hbar\varepsilon_F/T^2,$$

which reach 10^{-8} sec in order of magnitude.
(it is interesting to find why these times are such, but now it is better to just believe it)

It will be shown below that for a definite type of perturbation, the characteristic time of variation of the initial perturbation is Δ^{-1}, which is small in comparison with τ_{ph} and τ_{ee}.

Then the inelastic collisions of the electrons do not influence the evolution of the perturbation during the course of times that are short in comparison with τ_{ph} and τ_{ee}, and the corresponding collision integrals can be neglected.

This enables us to simplify greatly the initial Eliashberg equations for the equal-time Green's functions and to change over to equations relative to Green's functions with coinciding times (accurate to $\sim \omega_{\text{D}}^{-1}$).

The derived equations can be regarded as "collisionless" kinetic equations for the superconductor.
(what is kinetic here if there are no collisions??)

In Sec. 2 we derive first the Eliashberg equations by a different method, which in essence is a generalization of the Keldysh technique [6] to the case of superconductors. This approach is simplest and most lucid.

28.0.2 2. Derivation of the Fundamental Equations

(here, there is an introduction of functions and equations in a complicated notation. without reading the works before, it is impossible to understand it.)

Keldysh's method consists of ordering the secondquantization operators in the Green's functions on a double time-dependent contour consisting of two axes, one extending from $-\infty$ to $+\infty$, and the other from $+\infty$ to $-\infty$. The time on the second axis is assumed to be longer (in the sense of ordering of the operators) than any time on the first axis, while the ordering of the operators on the second axis is in antichronological order, i.e., the operator with the smallest time, closest to $-\infty$, is located to the left. In accordance with the fact that the time of each of the two ψ operators in the Green's function can be either on the first or on the second axis of the contour, four functions making up the matrix are possible. In the case of generalization to include superconductors, it is necessary to introduce also the spin indices of the operators (the Gor'kovNambu technique [7]):

$$\psi_\uparrow(1_i) \equiv \psi_1(1_i), \quad \psi_\downarrow^+(1_i) \equiv \psi_2(1_i),$$

where 1 is the aggregate of the spatial coordinates and time, and i is the index of the temporal axis.
(this is a very strange notation)

Thus, the single-particle Green's function of the electrons

$$G_{\alpha\beta}^{\prime k}(11') = i^{-1}\left\langle T\psi_\alpha(1_i)\,\psi_\beta{}^+(1_k{}')\right\rangle \tag{1}$$

constitutes a matrix both in the spin indices (α, β) and in the temporal indices (i, k) (it is meant space-time indices???), while the angle brackets denote averaging with the density

matrix taken at the instant t_o at which the Heisenberg operators coincide with the Schrödinger operators.

(if we have two times, by which we average???)

In addition to the functions (1), we define also the retarded and advanced functions, and also the function introduced by Keldysh [6] :

$$\begin{aligned} G_{\alpha\beta}{}^{n}(11') &= i^{-1}\theta(t_1 - t_1')\left\langle\left\{\psi_\alpha(1), \psi_\beta{}^{+}(1')\right\}_{+}\right\rangle, \\ G_{\alpha\beta}{}^{A}(11') &= i\theta(t_1' - t_1)\left\langle\left\{\psi_\alpha(1), \psi_\beta{}^{+}(1')\right\}_{+}\right\rangle, \\ G_{\alpha\beta}{}^{K}(11') &= G_{\alpha\beta}{}^{12} + G_{\alpha\beta}{}^{21} = i^{-1}\left\langle\left[\psi_\alpha(1), \psi_\beta{}^{+}(1')\right]_{-}\right\rangle. \end{aligned} \tag{2}$$

From the definitions (1) and (2) we get the following relations [6] (the spin indices have not been written out):

$$\begin{aligned} G^{11} + G^{22} &= G^{12} + G^{21}, \\ G^{4} = G^{11} - G^{21} &= G^{12} - G^{22}, \\ G^{8} = G^{11} - G^{12} &= G^{21} - G^{22}. \end{aligned} \tag{3}$$

If the system contains no fields acting directly on the electron spins, and if the spin-orbit interaction can be neglected, then

$$G_{\alpha\beta}^{ij*}(11') = (-1)^{\alpha+\beta} G_{\bar{\alpha}\bar{\beta}}^{\bar{i}\bar{j}}(11') \tag{4}$$

where the bar over the index denotes its replacement by the opposite: $\bar{1} = 2$ and $\bar{2} = 1$.

(??????? I don't understand what exactly is meant here??? what is 1,2?)

From (4) and (3) it follows that

$$\begin{aligned} G_{\alpha\beta}^{A(R)*}(11') &= -(-1)^{\alpha+\beta} G_{\bar{\alpha}\bar{\beta}}^{A(R)}(11'), \\ G_{\alpha\beta}^{K*}(11') &= (-1)^{\alpha+\beta} G_{\bar{\alpha}\bar{\beta}}^{K}(11'). \end{aligned} \tag{5}$$

In addition, it is easy to verify that

(?????)

$$\begin{aligned} G_{\alpha\alpha}{}^{K*}(11') &= -G_{\alpha\alpha}{}^{K}(1'1), \\ G_{\alpha\beta}{}^{K}(11') &= G_{\alpha\beta}{}^{K}(1'1), \quad \alpha \neq \beta. \end{aligned} \tag{6}$$

In Dyson's equation for the Green's function

$$\hat{\sigma}_z \hat{G}_0^{-1}(1) G(11') - \Sigma(12) G(21') = 1 \cdot \delta(1 - 1') \tag{7}$$

(???? there should be in some articles this equation but in comprehensible notation)

the operator

$$\left(G_0^{-1}(1)\right)_{\alpha\beta} = \delta_{\alpha\beta} i\partial/\partial t_1 - (H(1))_{\alpha\beta}$$

is a matrix in the space of the spin indices, with

$$\hat{H} = \begin{pmatrix} H & 0 \\ 0 & -H^* \end{pmatrix},$$

where $H(1)$ is the single-electron operator of the energy, reckoned from the Fermi energy, with allowance for the external fields. In addition, $(\ \sigma_{\mathrm{Z}})_{\mathrm{ik}}$ in (7) is a Pauli matrix, while $(1)^{\mathrm{ik}}_{\alpha\beta} = \delta_{\alpha\beta}\delta_{\mathrm{ik}}$.

In the phonon model, the mass operator is given by a well known sum of diagrams [8] in which, however, each vertex is set in correspondence with the matrix

$$\left(\mathscr{T}^{(0)}(12;3)\right)^{ij;k}_{\alpha\beta} = (\sigma_z)_{ij}\,\delta_{jk}\,(\sigma_z)_{\alpha\beta}\,\delta(1-2)\delta(1-3).$$

(so, below the results of the previous articles are used. the only way to understand them is to read that articles)

In the first-order approximation we have

$$\Sigma^{ij}_{\alpha\beta}(12) = i(-1)^{\alpha+\beta+i+j} G^{ij}_{\alpha\beta}(12) D^{ji}(21) \tag{8}$$

The contribution made to Σ by the direct interaction is also given by the usual sum of diagrams [8], in which each elementary four-corner vertex is set in correspondence with the matrix

$$\begin{aligned}\left(\Gamma^{(1)}(12;34)\right)^{h_1h_2h_4}_{\alpha_1\alpha_2\alpha_3\alpha_4} = -iv(12)\,(\sigma_z)_{k_1k_2}\,\delta_{k_1k_3}\delta_{k_2k_4}\left\{(\sigma_z)_{\alpha_1\alpha_3}\,\delta(1-3)\,(\sigma_z)_{\alpha_2\alpha_4}\,\delta(2-4)\right.\\ \left.-\,(\sigma_z)_{\alpha_1\alpha_4}\,\delta(1-4)\,(\sigma_z)_{\alpha_3\alpha_3}\,\delta(2-3)\right\}.\end{aligned} \tag{9}$$

The mass operators are connected by a relation [6] that follows from (3):

$$\Sigma^{11} + \Sigma^{22} + \Sigma^{12} + \Sigma^{21} = 0$$

The equations for $\mathrm{G^R}, \mathrm{G^A}$, and $\mathrm{G^K}$ follow from (7):

$$G_0^{-1}(1)G^{R(A)}\,(11') - \Sigma^{R(A)}(12)G^{R(A)}\,(21') = \delta\,(1-1') \tag{10}$$

$$G_0^{-1}(1)G^{K}\,(11') - \Sigma^{R}G^{K} + \Omega G^{A} = 0$$

where

$$\Sigma^{R(A)} = \Sigma^{11} + \Sigma^{12(21)} = -\Sigma^{22} - \Sigma^{21(12)}$$

$$\Omega = \Sigma^{12} + \Sigma^{21} \tag{11}$$

These equations differ from the corresponding equations of Keldysh's paper [6] only in that all the quantities are matrices in the spin indices.

Relations (4) and (5) for the Green's functions correspond to the following relations for the mass operators:

$$\begin{aligned}\Sigma^{ij}_{\alpha\beta} &= (-1)^{\alpha+\beta}\Sigma^{\bar{i}\bar{j}}_{\bar{\alpha}\bar{\beta}} \\ \Sigma^{R(A)*}_{\alpha\beta} &= -(-1)^{\alpha+\beta}\Sigma^{R(A)}_{\bar{\alpha}\bar{\beta}}, \quad \Omega^*_{\alpha\beta} = -(-1)^{\alpha+\beta}\Omega_{\bar{\alpha}\bar{\beta}}\end{aligned} \tag{12}$$

(I have no idea what is the meaning of these relations)

If we write out the spin indices in (10) explicitly and use (5) and (12) then, as can be easily verified, we obtain the Eliashberg equations [5]1). It is necessary to bear in mind here the following correspondence between the notation of our paper and [5] :

$$G_{11}^{R(A)} = -G^{R(A)}, \quad G_{12}^{R(A)} = -F^{R(A)}, \quad G_{11}{}^{K} = -G, \quad G_{12}{}^{K} = -F,$$
$$\Sigma_{11}^{R(A)} = -\Sigma_{1}^{R(A)}, \quad \Sigma_{12}^{R(A)} = \Sigma_{2}^{R(A)}, \quad \Omega_{11} = -\Sigma_{1}, \quad \Omega_{12} = \Sigma_{2}.$$

We write out explicitly only the equations for $\mathrm{G}_{11}^{\mathrm{K}}$ and $\mathrm{G}_{12}^{\mathrm{K}}$, which we shall need later on (together with the conjugate equations):

$$(i\partial/\partial t_1 - H(1))\, G_{11}{}^{K}(11') - \Sigma_{11}{}^{R} G_{11}{}^{K} + \Sigma_{12}{}^{K} G_{12}{}^{K*} + \Omega_{11} G_{11}{}^{A} + \Omega_{12} G_{12}{}^{A*} = 0,$$
$$(i\partial/\partial t_1' + H^*(1'))\, G_{11}{}^{K}(11') + G_{11}{}^{K}\Sigma_{11}{}^{A} + G_{12}{}^{K}\Sigma_{12}{}^{A*} - G_{11}{}^{R}\Omega_{11} + G_{12}{}^{R}\Omega_{12}{}^{*} = 0, \quad (13)$$
$$(i\partial/\partial t_1 - H(1))\, G_{12}{}^{K}(11') - \Sigma_{11}{}^{R} G_{12}{}^{K} - \Sigma_{12}{}^{R} G_{11}{}^{\kappa *} + \Omega_{11} G_{12}{}^{A} - \Omega_{12} G_{11}{}^{A*} = 0,$$
$$(i\partial/\partial t_1' - H(1'))\, G_{12}{}^{K}(11') - G_{12}{}^{K}\Sigma_{11}{}^{A*} + G_{11}{}^{K}\Sigma_{12}{}^{A} - G_{12}{}^{R}\Omega_{11}{}^{*} - G_{11}{}^{R}\Omega_{12} = 0. \quad (14)$$

As is well known, $\left(\Sigma_{12}^{\mathrm{R}} + \Sigma_{12}^{\mathrm{A}}\right)/2$ plays the role of the operator of the energy gap Δ of the superconductor. We represent Σ_{12}^{R} and Σ_{12}^{A} in the form

$$\Sigma_{12}^{R(\boldsymbol{A})}(12) = \Delta(12) + 1/2\left(\Sigma_{12}^{R(\boldsymbol{\Lambda})}(12) - \Sigma_{12}^{\boldsymbol{\Lambda}(R)}(12)\right). \quad (15)$$

We add Eqs. (13) for $\mathrm{G}_{11}^{\mathrm{K}}$ and, in similar fashion, Eqs. (14) for $\mathrm{G}_{12}^{\mathrm{K}}$. The result can be represented in the following form (we neglect renormalization effects described by $\mathrm{Re}\,\Sigma_{11}(\mathrm{A})$[5]):

$$(i\partial/\partial t - H(1) + H^*(1'))\, G_{11\kappa}{}^{K}(11') + \Delta(12) G_{12}{}^{K*}(21') + G_{12}{}^{K}(12)\Delta^*(21') = I_{11}(11')$$

$$(i\partial/\partial t - H(1) - H(1'))\, G_{12}{}^{K}(11') - \Delta(12) G_{11}{}^{K*}(21') + G_{11}{}^{K}(12)\Delta(21') = I_{12}(11') \quad (16)$$

Here $t = (t_1 + t_1')/2$, and the form of the "collision integrals " I_{11} and I_{12} can be easily obtained from (13)(15).

(some complicated equations....)

From the expressions for Σ_{12}^{R} and Σ_{12}^{A} (see (11) and (8)) follows the well known results [5]

$$\Delta(12) = 1/4 i^{-1} G_{12}{}^{K}(12)\left[D^A(21) + D^R(21)\right]$$

Here the sum of the phonon functions $D^A + D^R$, regarded as the function $\tau = t_1 - t_2$, is a narrow peak of width $\sim \omega \bar{D}^{-1}$. Therefore the energy gap is

$$\Delta(\mathbf{R}t) = \int d\mathbf{r} d\tau \Delta(12) = \frac{ig^2}{2} \int \frac{d\mathbf{p}}{(2\pi)^3} \int_{-\omega_D}^{\omega_D} \frac{d\varepsilon}{2\pi} G_{12}{}^{K}(\mathbf{R}t; \mathbf{p}\varepsilon) \quad (17)$$

where

$$\mathbf{R} = (\mathbf{r}_1 + \mathbf{r}_2)/2, \quad \mathbf{r} = \mathbf{r}_1 - \mathbf{r}_2$$
$$G_{12}{}^{K}(\mathbf{R}t; \mathbf{p}\varepsilon) = \int d\mathbf{r} d\tau e^{-i\mathbf{p}\mathbf{r} + i\varepsilon\tau} G_{12}{}^{K}(12)$$

In a number of problems, the reciprocal of relaxation times in a superconductor are much smaller than Δ and then the characteristic frequencies of all the quantities as functions of t. In

this case I_{11} and I_{12} can be discarded in (16). We can simplify the obtained collisionless kinetic equations further by using the already mentioned narrowness of $\Delta(12)$ as a function of τ, and by using the fact that to determine $\Delta(\mathrm{Rt})$ we need the function $\mathrm{G}_{12}^{\mathrm{K}}$ at practically equal times ($\tau \lesssim \omega_{\mathrm{D}}^{-1}$). This makes the system of collisionless equations (Eqs. (16) without the right-hand sides) for $\mathrm{G}_{11}^{\mathrm{K}}$ and $\mathrm{G}_{12}^{\mathrm{K}}$ with $\tau \lesssim \omega_D^{-1}$, together with expression (17) for Δ (Rt), a closed system.

We introduce the notation

$$g(\mathbf{p};\mathbf{R}t) = \frac{1}{2\pi}\int_{-\omega_D}^{\omega_D} d\varepsilon {G_{11}}^K(\mathbf{R}t;\mathbf{p}\varepsilon)$$
$$f(\mathbf{p};\mathbf{R}t) = \frac{1}{2\pi}\int_{-\omega_D}^{\omega_D} d\varepsilon {G_{12}}^K(\mathbf{R}t;\mathbf{p}\varepsilon) \tag{18}$$

Taking into account the approximations made above, we obtain from (16)

$$[i\partial/\partial t - H(\mathbf{r}_1 t) + H^*(\mathbf{r}_1{}' t)]\, g(\mathbf{r}_1\mathbf{r}_1{}' t) + \Delta(\mathbf{r}_1 t)\, f^*(\mathbf{r}_1\mathbf{r}_1{}' t) + \Delta^*(\mathbf{r}_1{}' t)\, f(\mathbf{r}_1\mathbf{r}_1{}' t) = 0,$$
$$[i\partial/\partial t - H(\mathbf{r}_1 t) - H(\mathbf{r}_1{}' t)]\, f(\mathbf{r}_1\mathbf{r}_1{}' t) - \Delta(\mathbf{r}_1 t)\, g^*(\mathbf{r}_1\mathbf{r}_1{}' t) + \Delta(\mathbf{r}_1{}' t)\, g(\mathbf{r}_1\mathbf{r}_1{}' t) = 0. \tag{19}$$

We note that these equations are obtained in the BCS model without additional assumptions. In accordance with formula (9) for $\Gamma^{(1)}$ in the self-consistent field approximation we have

$${\Sigma_{\alpha\beta}}^{ij}(12) = -i\,(\sigma_z)_{ij}\left\{(\sigma_z)_{\alpha\beta}\, v(13){G_{\gamma\gamma}}^{ij}(33) - (-1)^{\alpha+\beta}{G_{\alpha\beta}}^{ij}(12)v(21)\right\}.$$

In this approximation $\sum_A^{\mathrm{ij}} = 0$ at $\mathrm{i} \neq \mathrm{j}$ and $\Omega = 0$, and the mass operators $\Sigma_{\alpha\beta}^{\mathrm{R}}$ and $\Sigma_{\alpha\beta}^{\mathrm{A}}$ reduce to $\Sigma_{\alpha\beta}^{11}$ or $-\Sigma_{\alpha\beta}^{22}$.

Next, as usual, we include Σ_{11}^{R} and Σ_{11}^{A} in the chemical potential.

(?????? why???)

And express $\Delta(12) = 1/2\,(\Sigma_{12}^{11} - \Sigma_{12}^{22})$ in the form

$$\Delta(12) = -1/2i{G_{12}}^K(12)v(21) = 1/2ig\delta(12){G_{12}}^K(11) = \Delta(1)\delta(12)$$

When relations (5) are taken into account, we arrive at (19).

It should be noted that the obtained equations (19) describe the behavior of the Green's functions integrated with respect to ϵ (see (18)), and not with respect to $\xi = (p^2 - p_0^2)/2m$ as in Eliashberg's paper [5]. Therefore the first equation of (19) goes over at $\Delta = 0$ into the usual collisionless kinetic equation.

(I'll think about this statement not soon)

28.0.3 3. Collisionless Evolution of Perturbations in a Superconductor

We use Eqs. (19) to investigate the evolution of the initial perturbations in a superconductor during times that are short in comparison with the energy-relaxation times τ_{ph} and τ_{ee}.

(again, physically what happens when there is a perturbation and when relaxation of them happens???)

We confine ourselves to the spatially homogeneous case and assume that all the quantities are independent of the direction of p, and that there are no fields. After applying a Fourier transformation with respect to the difference coordinate $r - r_1 - r_1'$, Eqs. (19) and (17) take the form

$$i\partial g(\xi t)/\partial t + \Delta(t) f^*(\xi t) + \Delta^*(t) f(\xi t) = 0 \tag{20a}$$
$$(i\partial/\partial t - 2\xi) f(\xi t) + 2\Delta(t) g(\xi t) = 0 \tag{20b}$$
$$\Delta(t) = i\frac{\lambda}{2}\int d\xi f(\xi, t) \tag{20c}$$

(comment that this is how we always see the gap, as $\Delta(t) = i\frac{\lambda}{2}\int d\xi f(\xi, t)$. why, by the way???? is it written in Gorkov's papers???)

We took into account here the fact that in accordance with (6) g is pure imaginary. Assume that arbitrary initial perturbations $\delta g_0(\xi)$ and $\delta f_0(\xi)$ have occurred in the superconductor and are described by the deviations of the functions f and g from their stationary values g_0 and f_0. The perturbations can be produced either by electromagnetic radiation or by injecting quasiparticles or pairs into the superconductor. Let us find the evolutions of the perturbations with the aid of the linearized system (20). We see that the problem is quite analogous in its formulation with the Landau problem of evolution of perturbations in a collisionless plasma [9]. The electric self-consistent field in the plasma corresponds in the superconductor to the "field" Δ(t).

The stationary functions f_0 and g_0 can be represented, according to (20), in the form

$$f_0(\xi) = -i\Delta\chi(\xi), g_0(\xi) = -i\xi\chi(\xi), \tag{21}$$

where the form of $\chi = \chi^*$ is determined by the particular conditions for the production of the stationary state. Under thermodynamic equilibrium we have

$$\chi = [\mathrm{th}(\varepsilon/2T)]/\varepsilon,$$

where $\epsilon = (\xi^2 + \Delta^2)^{1/2}$. We linearize (20) with respect to the stationary values in (21):

$$(i\partial/\partial t - 2\xi)\delta f(\xi t) - 2i\xi\chi\delta\Delta(t) + 2\Delta\delta g(\xi t) = 0$$
$$i\partial\delta g/\partial t - 2\Delta\chi\delta\Delta'' + 2\Delta\delta f'(\xi t) = 0$$

The prime and double prime denote here the real and imaginary parts of the function, respectively. We note that, at small perturbations, $\delta\Delta'$ is the change of the gap $|\Delta|$, while $\delta\Delta''/\Delta$ is the change of the phase of the order parameter.

We separate the imaginary and real parts of the equation:

$$\begin{gathered}\partial\delta f''/\partial t + 2\xi\delta f' - 2\xi\chi\delta\Delta'' = 0\\ \partial\delta f'/\partial t - 2\xi\delta f'' - 2\xi\chi\delta\Delta' + 2\Delta\delta g'' = 0\\ \partial\delta g''/\partial t + 2\Delta\chi\delta\Delta'' - 2\Delta\delta f' = 0\end{gathered} \tag{22}$$

For the Laplace transforms of the sought functions $\delta F(s)$ we obtain from (22)
(maybe here, there is a nontrivial mathematics, but in general it is clear what happens)

$$\left(s^2 + 4\varepsilon^2\right)\delta \mathrm{r}'(s) - 4\varepsilon^2\chi\delta\Delta''(s) + 2\xi\chi s\delta\Delta'(s) = \delta\dot{f}_0' + s\delta f_0' - 2\xi\chi\delta\Delta';$$
$$\left(s^2 + 4\varepsilon^2\right)\delta f''(s) - 2\xi\chi s\delta\Delta''(s) + 4\xi^2\chi\delta\Delta'(s) = -\frac{2\xi}{s}\left(\delta\dot{f}_0' + s\delta f_0'\right) + \frac{4\xi^2 v}{s}\delta\Delta_0' + \frac{\delta f_0''}{s}\left(s^2 + 4\varepsilon^2\right) \tag{23}$$

Here $\delta\Delta_0' = [\delta\Delta'(\mathrm{t})]\,\mathrm{t} = 0$, etc. In the derivation of (23) we have expressed δg_0 with the aid of the section equation of (22) in terms of $[\ \mathrm{d}\delta f'/\mathrm{dt}]_{\mathrm{t}=0} \equiv \delta\dot{f}_0'$ and $\delta f_0''$.

We multiply (23) by $\lambda/2$ and integrate with respect to ξ. We confine ourselves to the case of functions χ that are even in ξ. Then, taking (23) into account, we obtain

$$s^2 F(s)\delta\Delta''(s) = \left\langle \frac{\delta\dot{f}_0' + s\delta f_0'}{s^2+4\varepsilon^2} \right\rangle, \tag{24a}$$

$$\left(s^2+4\Delta^2\right) F(s) \left(\delta\Delta'(s) - \frac{\delta\Delta_0'}{s}\right) = \frac{1}{s}\left\langle \frac{2\xi\left(\delta\dot{f}_0' + s\delta f_0'\right)}{s^2+4\varepsilon^2} \right\rangle. \tag{24b}$$

We have introduced here the notation

$$F(s) = \left\langle \frac{\chi}{s^2+4\varepsilon^2} \right\rangle, \quad \langle \ldots \rangle = \frac{\lambda}{2}\int_{-\omega_D}^{\omega D} d\xi \ldots$$

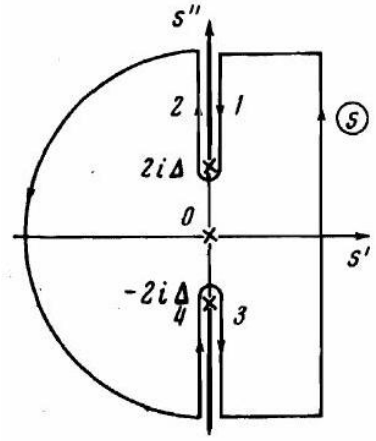
and used the equality $\chi = 1$, which follows from (20c) and (21).
(is it the same as in Eliashberg's work???)

If $\delta\dot{f}_0' = 0$ and $\delta f_0' = 0$ (but $\delta f_0'' \neq 0$) then as seen from (24b), $\delta\Delta'(s) = \delta\Delta_0'/s$, meaning that $\delta\Delta'(\mathrm{t}) = \delta\Delta_0' = \mathrm{const}$ and that the energy gap relaxes only as a result of inelastic collisions during a relaxation time much larger than Δ^{-1}. If $\Delta\dot{f}_0' + s\delta f_0' \neq 0$, then that part of this function which is even in ξ determines the time variation of $\delta\Delta''(\mathrm{t})$, i.e., the change of the phase of the order parameter, while the odd part determines the variation of $\delta\Delta'(\mathrm{t})$, i.e., of the modulus of the gap.

Let us investigate the analytic properties of $F(s)$ in the complex s plane. Near the imaginary axis $s = i\Omega + \delta$, where $\delta \to 0$, we have

$$F(s) = \frac{\lambda}{2}\left\{ \int_{-\omega_D}^{\omega D} \frac{d\xi\chi(\varepsilon)}{4\varepsilon^2 - \Omega^2} - i\frac{\pi}{2}\,\mathrm{sgn}(\Omega\delta)\frac{\chi(\Omega/2)}{\left(\Omega^2-4\Delta^2\right)^{1/2}}\theta\left(\Omega^2-4\Delta^2\right) \right\} \tag{25}$$

At $|\Omega| > 2\Delta$, the imaginary part of $F(s)$ experiences a discontinuity when s crosses the imaginary axis. Therefore $F(s)$ has a branch point at $s = \pm 2\mathrm{i}\Delta$, and the single-valued branch $F(s)$ should be chosen by drawing the cuts as shown in the figure.



The functions in the right-hand side of (24) have the same branch points as $F(s)$. Therefore $\delta\Delta''(s)$ has in the general case branch points at $s = \pm 2i\Delta$, and in addition poles of first and second order at zero, while $\delta\Delta'(s)$ has, in addition to these branch points, also a first-order pole at zero. It is important to emphasize that $\delta\Delta'(s)$ has no poles at the point $s = \pm\mathrm{i}2\Delta$.

Indeed, the right-hand side of (24b) differs from zero if $\delta\dot{f}_0' + s\delta f_0'$ has a part that is odd in ξ. At the same time, from the continuity of this part at the point $\xi = 0$ it follows that it can be represented in the form $\xi\eta(\xi)$, where $\eta(\xi)$ is an even function having no singularities at zero. Then the right-hand part of (24b) can be transformed into

$$\langle\eta\rangle - \left(s^2 + 4\Delta^2\right)\left\langle\frac{\eta}{s^2 + 4\varepsilon^2}\right\rangle.$$

The first term does not depend in general on s, and the second factor at $s^2 + 4\Delta^2$ has the same singularities as $F(s)$.

Since the function $\delta\Delta'(s)$ has no poles at the points $s = \pm i2\Delta$, it follows that the energy gap, even if we neglect the inelastic collisions, has no natural undamped oscillations with frequency 2Δ (cf. [4]).

Let us illustrate the behavior of $\delta\Delta$(t) under the following concrete initial conditions

$$\delta f_0' = 2\alpha_1\xi\chi + \alpha_2\chi, \qquad \delta\dot{f}_0' = 2\beta_1\xi\chi + \beta_2\chi,$$

where α_i and β_i are small constants. It follows then from (24), with allowance for (23), that

$$\delta\Delta''(s) = \frac{\beta_2}{s^2} + \frac{\alpha_2}{s} = \frac{\dot{\Delta}_0''}{s^2} + \frac{\Delta_0''}{s},$$
$$\delta\Delta'(s) = \frac{\Delta_0'}{s} + \frac{\beta_1 + \alpha_1 s}{s\left(s^2 + 4\Delta^2\right)F(s)} - \frac{\beta_1 + \alpha_1 s}{s}$$

Taking the inverse Laplace transform, we find that the imaginary part of the gap, which is proportional to the phases, increases linearly with time:

$$\delta\Delta''(t) = \delta\dot{\Delta}_0''t + \delta\Delta_0'',$$

while the real part is given by

$$\delta\Delta'(t) = \delta\Delta_0' - \beta_1 + \frac{1}{2\pi i}\int_{-i\infty+\sigma}^{i\infty+\sigma}\frac{ds\left(\beta_1 + \alpha_1 s\right)e^{st}}{s\left(s^2 + 4\Delta^2\right)F(s)}. \tag{26}$$

The integral can be represented here in the form of a difference of the integral over the entire closed contour in the figure and the integrals over sections $1, 2, 3$, and 4 of the second contour. As a result we obtain

(I'll check math later, a good problem in complex analysis)

$$\frac{1}{2\pi i}\int_{-i\infty+\sigma}^{i\infty+\sigma}\frac{ds\left(\beta_1 + \alpha_1 s\right)e^{st}}{s\left(s^2 + 4\Delta^2\right)F(s)} = \frac{\beta_1}{4\Delta^2 F(0)} - \frac{2}{\pi}\int_{2\Delta}^{\infty}d\Omega\frac{\operatorname{Im}F(\Omega)}{|F(\Omega)|^2}\frac{1}{\Omega^2 - 4\Delta^2}\left[\beta_1\frac{\cos\Omega t}{\Omega} - \alpha_1\sin\Omega t\right]. \tag{27}$$

In the calculation we took into account the fact that the imaginary part of $F(s)$ on opposite sides of the cut along the imaginary axis (see the figure) differ in sign, and that $F(s) = F(-s)$.

It is easy to verify that at t = 0 the integral in (26) is equal to β_1 and that $\delta\Delta'(0) = \delta\Delta_0'$, as should be the case. To understand the character of the time variation of the gap perturbation, let us find the asymptotic value of the integral in (27) at $2t\Delta \gg 1$. It is determined by the behavior of the integrand at $\Omega \approx 2\Delta$. It can be shown that $\operatorname{Re}F(s)$ has no singularities as $s \to 2i\Delta$ (see (25)) and that $\operatorname{Im}F/|F|^2 = (\operatorname{Im}F)^{-1}$ near this point. Substituting Im F from (25) and taking the equilibrium value of χ, we obtain

$$\delta\Delta'(t) = \delta\Delta'_0 - \beta_1 + \frac{\beta_1}{4\Delta^2 F(0)} + \left(\frac{2}{\pi}\right)^{3/2} \frac{1}{\lambda \,\mathrm{th}(\Delta/2T)} \times (2t\Delta)^{-1/2} \left[\beta_1 \cos\left(2\Delta t + \frac{\pi}{4}\right) - 2\alpha_1 \Delta \sin\left(2\Delta t + \frac{\pi}{4}\right)\right].$$

We see that the perturbation of the gap, as a function of the time, take the form of oscillations having a frequency $\sim 2\Delta$ and an amplitude that attenuates like $t^{-1/2}$. It is important that with increasing t (but at $\mathrm{t} \ll \tau_{\mathrm{ee}}, \tau_{\mathrm{ph}}$) in the considered collisionless approximation the gap perturbation $\delta\Delta'(\mathrm{t})$ tends.generally speaking neither to zero nor to $\delta\Delta'_0$.

28.0.4 My questions about work by Volkov, Kogan

(?)

29 Coherent Excited States in the Theory of Superconductivity: Gauge Invariance and the Meissner Effect by Anderson, 1958

Abstract

We discuss the coherent states generated in the Bardeen, Cooper, and Schrieffer theory of superconductivity by the momentum displacement operator $\rho_{\mathrm{Q}} = \Sigma_n \exp(i\mathbf{Q}\cdot\mathbf{r}_n)$. Without taking into account plasma effects, these states are like bound Cooper pairs with momentum $\hbar\mathbf{Q}$ and energies lying in the gap, and they play a central role in the explanation of the gauge invariance of the Meissner effect. Long-range Coulomb forces recombine them into plasmons with equations of motion unaffected by the gap. Central to the argument is the proof that the non-gauge-invariant terms in the Hamiltonian of Bardeen, Cooper, and Schrieffer have an effect on these states which vanishes in the weak-coupling limit.

29.0.1 I. Introduction

Buckingham [1] has questioned whether an energygap model of superconductivity, such as that of Bardeen, Cooper, and Schrieffer, [2] can explain the Meissner effect without violating a certain identity derived by Schafroth [3] on the basis of gauge invariance, and by Buckingham using essentially an f-sum rule. This identity is what causes the insulator, which also has an energy gap, to fail to show a Meissner effect; thus, Buckingham and Schafroth [4] argue, a proof of gauge invariance lies at the core of the problem of superconductivity, especially since the Hamiltonian used in BCS is not gauge-invariant.

Bardeen [5] argues that the matrix elements and energy states involved in the gauge problem bring in coherent excitations which will be strongly coupled to the plasma modes, a high-frequency phenomenon presumably unaltered by superconductivity. Unfortunately, while we find that this is indeed exactly the situation, the insulator also often has normal plasma modes. Thus, while the BCS calculation in the London gauge is probably entirely correct, and justifiable on physical grounds, it throws little light on the basic differences between the three cases-insulator, metal, and superconductor.

We also noticed that the operator which is central in the gauge problem as well as the plasma theory,

$$\rho_{\mathbf{Q}} = \sum_n \exp\left(i\mathbf{Q}\cdot\mathbf{r}_n\right)$$
$$= \sum_{\mathrm{k},\sigma} {c_{\mathrm{k}+\mathbf{Q},\sigma}}^* c_{\mathrm{k},\sigma}, \tag{1}$$

has another interesting property: its separate components ${c_{\mathrm{k}+\mathrm{Q},\sigma}}^* c_{\mathrm{k},\sigma}$, when applied to the BCS groundstate wave function Ψ_g, create excited pairs of electrons $\mathbf{k}_1, \mathbf{k}_2$ with momentum pairing

$$\mathbf{k}_1 + \mathbf{k}_2 = \mathbf{Q} \tag{2}$$

[5] J. Bardeen, Nuovo cimento 5, 1765 (1957).
instead of zero. The total operator applied to Ψ_g leads to a linear combination of such states, which can be thought of as equivalent to a Cooper bound state [6] of a pair of electrons with nonzero momentum, superimposed on the BCS ground state.

Our discussion of these problems is based on the following physical picture: any transverse excitation involves breaking up the phase coherence over the whole Fermi surface of at least one pair in the superconducting ground state, and so involves a loss of attractive binding energy. This causes the Meissner effect. Longitudinal excitations, however, such as those generated by ρ_{Q}, do not break up phase coherence in the superconducting state, and so their energies involve only kinetic energy, or electromagnetic energy when plasma effects are included. Thus longitudinal and transverse excitations are different in the superconductor, in a sense in which they are not in either the metal or the insulator, and it turns out to be this difference which allows a gaugeinvariant explanation of the Meissner effect.

We proceed further in two stages. First, we discuss the fictitious problem in which the only plasma effect is the screening of the long-range repulsion. In this stage gauge invariance requires, and we indeed find, that the states

$$\Psi_{\mathrm{Q}} = \rho_{\mathrm{Q}}\Psi_g \tag{3}$$

have energies in the energy gap and proportional to Q^2. In a perfectly gauge-invariant theory, their energy would be just the kinetic energy

$$E_{\mathrm{Q}} = \left(\hbar^2 Q^2/2m\right)\left(2\epsilon_f/3\pi\epsilon_0\right), \tag{4}$$

but we find a small correction going to zero in the weakcoupling limit. Equation (4) follows from the same f sum rule which leads to gauge invariance.

There is a fundamental difference, which we demonstrate, between the ways in which superconducting and normal substances satisfy this sum rule. Both normal metals and insulators (leaving out the rather confusing effects of long-range Coulomb forces which can be studied later) satisfy this rule with ordinary excitations in such a way that the more familiar optical sum rule-

which in turn leads to normal diamagnetism-also follows. In these normal cases the states (3) can be shown not to exist separately from the ordinary excitations. In the superconductor,

[01] M. J. Buckingham, Nuovo cimento 5, 1763 (1957).
[2] Bardeen, Cooper, and Schrieffer, Phys. Rev. 106, 162 (1957); 108, 1175 (1957). The latter we call BCS, and we shall follow its notation as far as possible.
[3] M. R. Schafroth, Helv. Phys. Acta 24, 645 (1951).
[4] M. R. Schafroth (private communication). I am indebted to G. Wentzel for an elegant presentation of these questions in a series of discussions, to which M. Lax and C. Herring also contributed.
[06] L. N. Cooper, Phys. Rev. 104, 1189 (1956).

however, the rule is satisfied by matrix elements involving only the longitudinal excitations (3), while the optical sum rule and Meissner effect involve transverse excitations with entirely different behavior from the longitudinal ones. Basically, these transverse excitations involve combinations of pair states which have a finite angular as well as linear momentum and cannot be bound into quasi "Cooper pairs" like the longitudinal excitations. This difference is the basis for the electromagnetic properties of superconductivity.

At this stage any number of $\mathbf{Q} \neq 0$ pairs could be incorporated into the state with little loss of energy. This alleviates the rigidity of the BCS ground state to some extent, making it easier to fit physical boundary conditions. On the other hand, we will find that when plasma effects are included the $\mathbf{Q} = 0$ pairing condition is again enforced, except possibly in particular geometrical situations for very long wavelengths.

In the second stage of the calculation we discuss these plasma effects. Our procedure corresponds to that of Nozières and Pines, [7] who find that the f-sum rules, and particularly the relationship of the optical and longitudinal forms, are best discussed prior to including the long-range Coulomb effects. Appealing to the random-phase approximation, which allows separation of the different momenta $\mathbf{Q}$, we show that the longitudinal f-sum rule becomes the commutation rule of plasma coordinates and momenta, while the transverse behavior is unaffected, whether normal or superconducting, when the long-range Coulomb interactions are included. The states Ψ_{Q} are recombined to make the plasma excitations, which now have large excitation energies and do not affect the energy gap.

29.0.2 II. Commutators and Energies of Coherent States

In this section we carry out the first stage of the program in the introduction. We naively ignore plasma effects and subsidiary conditions and study the energies of coherent excited states, and the f-sum rules, using the BCS ground state derived from phonon and screened Coulomb interactions.

The initial Hamiltonian used by BCS contains the kinetic energy and the second-order phonon interaction between electrons, but ignores the self-energy as well as higher-order terms. It is

$$\begin{aligned} H = & \sum_{\mathbf{k},\sigma} \epsilon_{\mathrm{k}} n_{\mathrm{k},\sigma} + \frac{1}{2} \sum_{\mathrm{k},\mathrm{k}',\sigma,\sigma',\kappa} 2\hbar\omega_\kappa \left|M_\kappa\right|^2 \\ & \times \left[\left(\epsilon_{\mathrm{k}} - \epsilon_{\mathrm{k}+\kappa}\right)^2 - \left(\hbar\omega_\kappa\right)^2\right]^{-1} c_{\mathrm{k}'-\kappa,\sigma'} * c_{\mathrm{k}',\sigma'} \\ & \times {c_{\mathrm{k}+\kappa,\sigma^*}}^* c_{\mathrm{k},\sigma} + H_{\mathrm{Coul}} \,. \end{aligned} \tag{5}$$

Almost immediately BCS drop, except for later perturbation calculations, all terms except $\mathbf{k}' = -\mathbf{k}, \sigma' = -\sigma$; and they replace the coefficient by a constant unless either $|\epsilon_{\mathrm{k}}|$ or $|\epsilon_{\mathrm{k}+\kappa}| > \hbar\omega$, in which case it is zero. The resulting Hamiltonian is their H_{red} .

The Hamiltonian (5) is already not gauge-invariant, if it is to be used with the usual expressions for the current and for the perturbation of an electromagnetic field, because it depends on $\mathbf{k}$ as well as $\boldsymbol{\kappa}$. Fortunately, however, we shall show that the important difficulties are not connected with the momentum dependence of (5) but with the simplification to H_{red} . The difficulty is that in calculating the properties of coherent excited states of the BCS theory one must take into account more than just the $\mathbf{k}' - \mathbf{k}$ terms of the interaction.

When this is done we shall show that the corrections caused by the $\mathbf{k}$ dependence of (5) in the important sum rules and energies become negligible in a well-defined limit which is that applying to most superconductors.

[07] P. Nozières and D. Pines, Phys. Rev. 109, 741 (1958).

The entire argument is based on a commutation relation used by Buckingham [1] in this connection and by Nozières and Pines [7] for other reasons:

$$\begin{aligned}[H_K, \rho_{\mathbf{Q}}] = &\left(-\hbar^2/2m\right) \\ &i\mathbf{Q}\cdot\sum_n \left[\nabla_n \exp\left(i\mathbf{Q}\cdot\mathbf{r}_n\right) + \exp\left(i\mathbf{Q}\cdot\mathbf{r}_n\right)\nabla_n\right] \\ &= \left(\hbar^2/2m\right)\sum_{\mathbf{k},\sigma}\mathbf{Q}\cdot(2\mathbf{k}+\mathbf{Q}) {c_{\mathbf{k}+\mathbf{Q},*}}^* c_{\mathbf{k},\sigma},\end{aligned} \tag{6}$$

where H_K is the kinetic energy and ρ_{Q} is defined in (1). 1 In the case of most simple kinds of forces, which are functions only of coordinates or at most of relative momenta, ρ_{Q} commutes with the potential energy. Then (6) may be written, using

$$[H, \rho_Q] = [H_K, \rho_Q]\,,$$

as

$$\begin{aligned}&\left(E_m - E_{m'}\right)\left(m\left|\rho_{\mathrm{Q}}\right|m'\right) \\ &\quad = \left(\hbar^2/2m\right) \\ &\quad \mathbf{Q}\cdot\sum_j \left(m\left|\nabla_j \exp\left(i\mathbf{Q}\cdot\mathbf{r}_j\right) + \exp\left(i\mathbf{Q}\cdot\mathbf{r}_j\right)\nabla_j\right|m'\right)\end{aligned} \tag{7}$$

We may also deduce from (7) the basic f-sum rule:

$$\begin{aligned}\left[\left[H, \rho_{\mathrm{Q}}\right], \rho_{-\mathrm{Q}}\right] &= N\hbar^2 Q^2/m; \\ \sum_{m'}\left(E_m - E_{m'}\right)\left|\left(m\left|\rho_{\mathrm{Q}}\right|m'\right)\right|^2 &= \frac{1}{2}N\hbar^2Q^2/m,\end{aligned} \tag{8}$$

or

$$\begin{aligned}\sum_{m'}\left|\left(m\left|\mathbf{Q}\cdot\sum_j\left[\nabla_j\exp\left(i\mathbf{Q}\cdot\mathbf{r}_j\right) + \exp\left(i\mathbf{Q}\cdot\mathbf{r}_j\right)\nabla_j\right]\right|m'\right)\right|^2 \\ \times\left(E_{m'} - E_m\right)^{-1} = 2mNQ^2/\hbar^2\end{aligned} \tag{9}$$

Now in the case of (5) the potential energy does not commute with ρ_{Q}. However, what we can show is that the commutator can be made arbitrarily small compared to (7).

In doing this we shall not use the explicit form (5) but shall carry out the first stage-the cutoff-of the simplification to H_{red} , in full confidence that the results would be practically the same if we used (5) itself, because the new potential is no less k-dependent than the old in the region of interest. One can then show that the full interaction energy, corresponding to the $\mathbf{k}' = -\mathbf{k}$ terms
of the BCS H_{red} , is

$$H_V = -\frac{1}{2}V\sum_{\mathbf{q}}\left[\sum_{\mathbf{k}'\neq\mathbf{k}}\sum_{(\mathbf{k}_{\mathbf{k}'}<\hbar\omega)}\sum_{\mathbf{k}(\epsilon_{\mathbf{k}}<\hbar\omega)} + \sum_{\mathbf{k}'\neq\mathbf{k}(\epsilon_{\mathbf{k}'}-\mathbf{q}<\hbar\omega)}\sum_{\mathbf{k}(\epsilon_{\mathbf{k}}-\mathbf{q}<\hbar\omega)}\right]\left(c_{\mathbf{k}'\uparrow} * c_{-\mathbf{k}'+\mathbf{q}\downarrow} * c_{-\mathbf{k}+\mathbf{q}\downarrow} c_{\mathbf{k}}\uparrow\right). \tag{10}$$

(All notations are as used in BCS) Then first of all we have to calculate the commutator of this with ρ_{Q}. This is done in the Appendix, and the result is:

$$[H_V, \rho_Q] = \frac{1}{2}V \left[\sum_{\mathbf{k}' \neq \mathbf{k}} \sum_{\mathbf{k}\left(\epsilon_{\mathbf{k}} < \hbar\omega, \epsilon_{\mathbf{k}+Q} > \hbar\omega\right)} - \sum_{\mathbf{k}' \neq \mathbf{k}} \sum_{\mathbf{k}\left(\epsilon_{\mathbf{k}} > \hbar\omega, \epsilon_{\mathbf{k}+Q} < \hbar\omega\right)} + (\text{ same with } \mathbf{k} \to \mathbf{k}', \mathbf{k}' \to \mathbf{k}) \right]$$
$$\times \left({c_{\mathbf{k}'+Q\uparrow}}^* {c_{-\mathbf{k}'+\mathbf{q}\downarrow}}^* c_{-\mathbf{k}+\mathbf{q}\downarrow} c_{\mathbf{k}\uparrow} - {c_{\mathbf{k}'-q\uparrow}}^* {c_{-\mathbf{k}'\downarrow}}^* c_{-\mathbf{k}-Q\downarrow} c_{\mathbf{k}-q\uparrow} \right). \quad (11)$$

These terms already refer only to $\mathbf{k}$ states within $\mathbf{Q}$ of the cutoff surface, and contain subtractions which make them depend on only the derivatives of the wave function near this surface. Thus, (11) will always be small acting on states close to the ground state, at least for small Q.

We shall see that the most important measure of this smallness is the scalar product.

$$(\rho_{\mathrm{Q}} \Psi_g, [H_V, \rho_{\mathrm{Q}}]\, \Psi_g)\,, \quad (12)$$

where Ψ_g is the BCS ground state. This will be computed in the Appendix also, but first we will need to compute the wave function

$$\Psi_{\mathrm{Q}} = \rho_{\mathrm{Q}} \Psi_g \quad (13)$$

and its normalization. Consider a particular term of ρ_{Q},

$$\left(\rho_{\mathrm{Q}^k}\right)_+ = c_{\kappa+\mathrm{Q}\uparrow} * c_{\kappa\uparrow} \quad (14a)$$

or

$$\left(\rho_Q{}^k\right)_- = c_{-\kappa\downarrow} * c_{-\kappa-Q\downarrow} \quad (14b)$$

Then

$$\left(\rho_{\mathrm{Q}}{}^{\kappa}\right)_+ \Psi_g = \prod_{\mathrm{k} \neq \kappa, \kappa+Q} \left[(1 - h_{\mathrm{k}})^{\frac{1}{2}} + h_{\mathrm{k}}^{\frac{1}{2}} {b_{\mathrm{k}}}^* \right]$$
$$\times (1 - h_{\kappa+Q})^{\frac{1}{2}}\, h_\kappa^{\frac{1}{2}}\, {c_{\kappa+Q\downarrow}}^* c_{-\kappa} \uparrow \Psi_v$$

Ψ_v being the vacuum state. Thus

$$\left(\rho_{\mathrm{Q}}\right)_+ \Psi_g = h_\kappa^{\frac{1}{2}} \left(1 - h_{\kappa+\mathrm{Q}}\right)^{\frac{1}{2}} \Psi_{-\kappa,\kappa+\mathrm{Q}} \quad (15)$$

where the last notation refers to the presence of a pair of real "single" excitations in the BCS sense in states $-\kappa \downarrow$ and $\kappa + \mathrm{Q} \uparrow$. Similarly,

$$\left(\rho_{\mathrm{Q}}{}^{\kappa}\right)_- \Psi_g = h_{\kappa+\mathrm{Q}^{\frac{1}{2}}} \left(1 - h_\kappa\right)^{\frac{1}{2}} \Psi_{-\kappa,\kappa+Q} \quad (16)$$

and

$$\Psi_Q = \rho_Q \Psi_g \cong 2 \sum_\kappa h_\kappa^{\frac{1}{2}} \left(1 - h_\kappa\right)^{\frac{1}{2}} \Psi_{-\kappa,\kappa+Q}. \quad (17)$$

Thus Ψ_{Q} is indeed a certain linear superposition of pair excitations with momentum $\mathbf{Q}$. Its normalization factor is

$$(\Psi_{\mathrm{Q}}, \Psi_{\mathrm{Q}}) = 4 \sum_{\mathrm{k}} h_{\mathrm{k}} (1 - h_{\mathrm{k}})$$
$$\cong 2\pi\epsilon_0 N(0) \tag{18}$$

which is finite-a vital point, since the corresponding quantity in metal or insulator approaches zero with $\mathbf{Q}$. Equation (18) already implies the presence of longrange order in the ground state, as we shall see.

Now we can compute the quantity (12) in the Appendix. The result is

$$(\rho_{\mathrm{Q}}\Psi_g, [H_V, \rho_{\mathrm{Q}}]\, \Psi_g) = \frac{2}{3}\epsilon_0^2 N(0)\hbar^2 k_F^2 Q^2/m^2\omega^2. \tag{19}$$

In order to get a measure of the magnitude of (19), and for later work, let us also calculate the kinetic energy commutator (6). This is also done in Appendix I, and the result is

$$\begin{aligned}
&(\rho_{\mathbf{Q}}\Psi_g, [H_K, \rho_{\mathrm{Q}}]\, \Psi_g) \\
&\quad = \frac{\hbar^2}{2m}\left(\rho_{\mathrm{Q}}\Psi_g, \sum_{\mathbf{k},\sigma} \mathbf{Q}\cdot(2\boldsymbol{\kappa} + \mathbf{Q}) {c_{\kappa+Q,\sigma}}^* c_{\kappa,\sigma}\Psi_g\right) \\
&\quad = \frac{4}{3}\left(\hbar^2 Q^2/2m\right) N(0)\epsilon_F
\end{aligned} \tag{20}$$

This value is shown there to be essentially independent of the exact structure of the wave function if it resembles a Fermi sea at all.

We can now, first of all, get a numerical measure of the relative magnitude of the ordinary terms (6) and the non-gauge-invariant terms (11) by taking the ratio of (19) to (20). The result is

$$(19)/(20) = 2\epsilon_0^2/\hbar^2\omega^2 = 2\exp[-2/N(0)V] \tag{21}$$

which is completely negligible for most superconductors, and zero in the weak-coupling limit (when, of course, in principle superconductivity still exists). Thus we have proved our first contention: that, although exact gauge invariance is still not present except in the weakcoupling limit, the inclusion of the $\mathrm{Q} \neq 0$ terms of H_V restores gauge invariance well enough so that no difficulties of principle are encountered by ignoring the terms (11).

We now can use (19), (20), and (18) to show that in this stage, before the introduction of specific plasma effects, states closely related to $\rho_Q\Psi_g$ must lie in the energy gap. To show this we use the identity

$$\begin{aligned}
E_{\mathrm{Q}}\,(\rho_{\mathrm{Q}}\Psi_g, \rho_{\mathrm{Q}}\Psi_g) &= (\rho_{\mathrm{Q}}\Psi_g, H\rho_{\mathrm{Q}}\Psi_g) \\
&= (\rho_{\mathrm{Q}}\Psi_g, [H\rho_{\mathrm{Q}} - \rho_{\mathrm{Q}}H]\, \Psi_g) \\
&\quad + E_0\,(\rho_{\mathrm{Q}}\Psi_g, \rho_{\mathrm{Q}}\Psi_g)
\end{aligned} \tag{22}$$

using the fact that the ground state is an eigenstate. (The first equality defines E_{Q} as the energy of Ψ_{Q}.)

Thus

$$\begin{aligned}
(E_{\mathrm{Q}} - E_0) = (\rho_{\mathrm{Q}}\Psi_g, \rho_{\mathrm{Q}}\Psi_g)^{-1}\,(\rho_{\mathrm{Q}}\Psi_g,\ [H, \rho_{\mathrm{Q}}]\, \Psi_g) \\
\simeq \frac{2}{3\pi}\left(\frac{\epsilon_F}{\epsilon_0}\right)\frac{\hbar^2 Q^2}{2m}.
\end{aligned} \tag{23}$$

Since ρ_{Q} is a state of momentum $\hbar\mathbf{Q}$, it is orthogonal to the ground state; thus some eigenstate must lie below E_{Q}. One guesses that Ψ_{Q} is really a very good approximation to this state. [8]

These states, if they existed, would have interesting properties. Their effective mass is about 10^{-4} electron mass. Therefore the specific heat would be tiny and probably below the accuracy of present measurements. The states would exist distinct from the individual particles only up to the energy gap, so that the maximum $\mathbf{Q}$ would be about $m\epsilon_0/\hbar^2 k_F \simeq 10^4/\mathrm{cm}$. Another fact about them is that they cannot be correctly calculated directly from the excitation energies of the pair states and the appropriate matrix elements of H_V. This is because the BCS ground state, while nearly exact, does not diagonalize H well enough for this purpose; we shall discuss this point later.

It is the uniqueness of the states Ψ_{Q} which will be the central feature in the explanation of the Meissner effect. Ψ_Q is a longitudinal excitation; the corresponding transverse excitations are of a completely different character. Study of the steps which lead to Eq. (11), or a little thought about the properties of Cooper pairs, quickly convinces us that no energy advantage is gained by making an excitation which does not have the

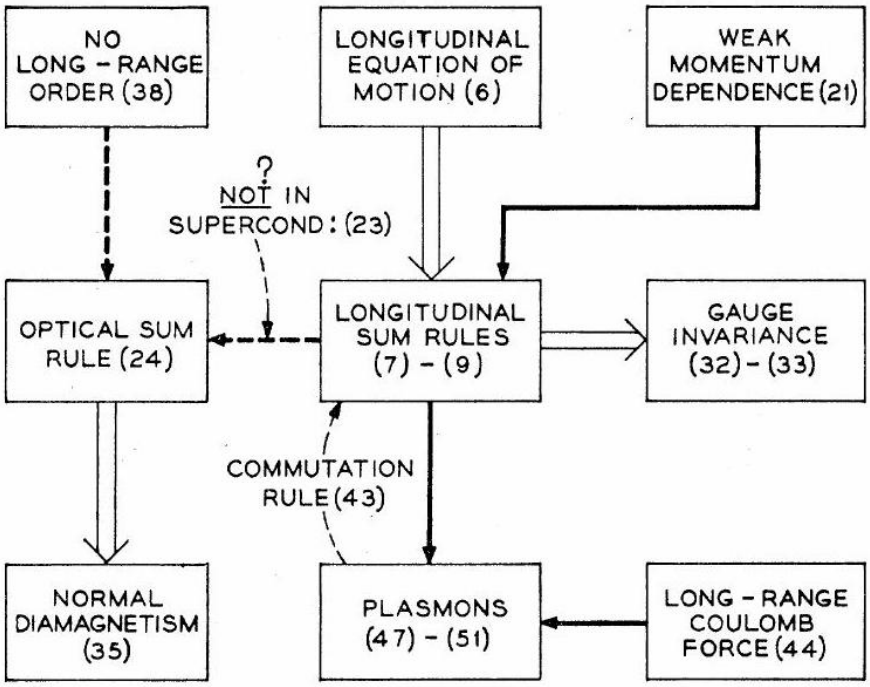


Fig. 1. Logical relations among diamagnetism, sum rules, gauge invariance, and plasmons. Wide arrows are general theorems, solid arrows mean "valid for superconductors at least," and heavy dashed arrows are theorems for normal but not superconducting cases. The numbers in parentheses refer to equations in the text.

same amplitude at all points of the Fermi surface. Any transverse excitation is of this form, and thus necessarily has a finite excitation energy as its wave number approaches zero. An equivalent statement is that no excitation possessing a finite angular momentum exists in the energy gap, since Cooper pairs have no bound state with nonzero angular momentum.

To understand the effect of these statements let us return to the fundamental sum rule (8). [From here on, we consider the question of the gauge invariance of the Hamiltonian itself closed.

[08] J. Bardeen has pointed out to me that (23) could also be derived by the method of R. P. Feynman [Phys. Rev. 94, 262 (1954)] using the BCS calculation of the correlation function. Feynman also presents arguments that $\rho_Q \Psi_g$ is nearly the eigenstate.

All statements are exactly true only in the weak coupling limit in which (11) $\equiv 0$.] Equations (8) and (9) are general statements, and indeed are used in the Nozières-Pines plasmon theory, [7] since they involve only longitudinal excitations. Actually, in the solid as in the atom the more familiar form of (9) is the optical (i.e., transverse) sum rule, to derive which one takes the limit as $Q \to 0$ and assumes

$$\begin{aligned}\frac{2mN}{\hbar^2} &= \lim_{Q\to 0} Q^{-2} \sum_{m'} (E_{m'} - E_m)^{-1} \\ &\quad \times \left| \left(m \left| \mathbf{Q} \cdot \sum \left[\nabla_j \exp\left(i\mathbf{Q}\cdot\mathbf{r}_j\right) + \exp\left(i\mathbf{Q}\cdot\mathbf{r}_j\right) \nabla_j \right] \right| m' \right) \right|^2 \\ &= \frac{1}{3} \sum_{m'} (E_{m'} - E_m)^{-1} \left| \left(m \left| 2 \sum_j \nabla_j \right| m' \right) \right|^2 . \end{aligned} \tag{24}$$

The condition for the validity of this limit process has not been previously discussed; we shall find that it involves the absence of a certain type of long-range order, which is, however, present in a superconductor, in that there is a qualitative difference between transverse and longitudinal excitations even as $\mathbf{Q} \to 0$ and in the absence of Coulomb forces.

29.0.3 III. Relationship of Sum Rules and Electromagnetic Properties; Comparison of Normal and Superconducting Cases

In this section we shall show how the mathematical questions of the sum rules (6)-(9) and (24) are related to the physical questions of gauge invariance and the Meissner effect. Figure 1 is a schematic diagram of the rather complex relationships involved. The core of the argument is that it is the longitudinal sum rule (9) which implies gauge invariance. As we have pointed out (9) is always true. On the other hand, normal diamagnetism is a consequence of the optical sum rule (24). We shall then show that the normal cases obey the optical sum rule, while the BCS superconductor need not because of the distinction between the states Ψ_Q and the transverse excitations. BCS have in fact shown, in deriving the Meissner effect, that it does not, and there is no need to repeat their calculation here.

To do this we must write down the two quantities involved in the calculation of electromagnetic effects, the current operator:

$$\begin{aligned}\mathbf{J}(r) &= (ie\hbar/2m)\left(\Psi^*\nabla\Psi - \Psi\nabla\Psi^*\right) - (e^2/mc)\,\Psi^*\mathbf{A}\Psi \\ &= \mathbf{J}_p + \mathbf{J}_d\end{aligned} \tag{25}$$

and the perturbation to the Hamiltonian caused by the vector potential A:

$$H_1 = (ie\hbar/2m) \int dr \Psi^*(\mathbf{A}\cdot\nabla + \nabla\cdot\mathbf{A})\Psi \tag{26}$$

The vector potential may be expanded in Fourier series:

$$\mathbf{A} = \sum_{\mathrm{Q}} \mathbf{a}_{\mathrm{Q}} \exp(i\mathbf{Q}\cdot\mathbf{r}),$$

and one can calculate the appropriate Fourier components of the current $\mathbf{J}_\mathbf{Q}$. If we set

$$\mathbf{J}_{\mathrm{Q}} = -K_{\mathrm{Q}}\mathbf{a}_{\mathrm{Q}} \tag{27}$$

then it is well known that the Meissner effect follows when in the London gauge:

$$\nabla \cdot \mathbf{A} = 0$$
$$\lim_{\mathrm{Q}\to 0} K_{\mathrm{Q}} = \text{ finite} \tag{28}$$

On the other hand, in a longitudinal gauge there can be no physical current:

$$\nabla \times \mathbf{A} = 0$$
$$K_{\mathrm{Q}} \equiv 0 \tag{29}$$

The problem is to reconcile these two [(28) and (29)].
In an energy-gap model, (28) is true because the $\mathbf{J}_p$ term of (25) either is small or vanishes, as a result of small matrix elements and finite energy denominators in perturbation theory. But the finite energy denominators must not cause $\mathbf{J}_p$ to vanish in the longitudinal case (29) (see reference 4).
Let us take up the longitudinal case first. Then a typical component is

$$\mathbf{A} = \nabla \exp(i\mathbf{Q}\cdot\mathbf{r}) \tag{30}$$

The Qth Fourier component of the resulting paramagnetic current is, in perturbation theory,

$$\begin{aligned}\mathbf{J}_p = &\sum_{m'} \left(\frac{e^2\hbar^2}{4m^2c}\right) \\ &\times \left(0 \left| \sum_n \left[\exp\left(i\mathbf{Q}\cdot\mathbf{r}_n\right)\nabla_n + \nabla_n \exp\left(i\mathbf{Q}\cdot\mathbf{r}_n\right)\right] \right| m'\right) \\ &\times \left(m' \left| i\mathbf{Q}\cdot \sum_n \left[\exp\left(i\mathbf{Q}\cdot\mathbf{r}_n\right)\nabla_n + \nabla_n \exp\left(i\mathbf{Q}\cdot\mathbf{r}_n\right)\right] \right| 0\right) \\ &\times \left(E_{m'} - E_0\right)^{-1} + \text{ complex conj.}\end{aligned} \tag{31}$$

From the sum rule (9),

$$\mathbf{Q}\cdot\mathbf{J}_p = iQ^2 Ne^2/mc \tag{32}$$

which is exactly the negative of

$$\mathbf{Q}\cdot\mathbf{J}_d = -\left(Ne^2/mc\right)(\mathbf{Q}\cdot\mathbf{A}) \tag{33}$$

Thus (9) ensures gauge invariance, and our proof that
to a certain order of accuracy (7) is maintained in BCS is a proof of gauge invariance to that order.

Now consider the real diamagnetism problem in which

$$\mathbf{A} = \mathbf{a}_{\mathrm{Q}} \exp(i\mathbf{Q}\cdot\mathbf{r}); \quad \mathbf{a}_{\mathrm{Q}}\cdot\mathbf{Q} = 0 \tag{34}$$

Now,

$$\begin{aligned}\mathbf{J}_p = &\sum_{m'} \left(e^2\hbar^2/4m^2c\right) \\ &\times \left(0 \left| \sum_n \left[\exp\left(i\mathbf{Q}\cdot\mathbf{r}_n\right)\nabla_n + \nabla_n \exp\left(i\mathbf{Q}\cdot\mathbf{r}_n\right)\right] \right| m'\right) \\ &\times \left(m' \left| \sum_n \left[\exp\left(i\mathbf{Q}\cdot\mathbf{r}_n\right)\mathbf{a}_\mathbf{Q}\cdot\nabla_n + \nabla_n \cdot \mathbf{a}_\mathbf{Q} \exp\left(i\mathbf{Q}\cdot\mathbf{r}_n\right)\right] \right| 0\right) \\ &\times \left(E_{m'} - E_0\right)^{-1} + \text{ complex conj.}\end{aligned} \tag{35}$$

As far as possible constant terms are concerned, if the optical sum rule (24) is valid, then (35) is also equal to the corresponding $\mathbf{J}_d$ and normal diamagnetism follows.

Having thus shown how the gauge invariance and sum rule questions are the same, let us compare how the three cases-superconductor, insulator, and normal metal-obey the sum rules (7) and (9). In the normal metal, the ground state may be approximated by a Fermi sea. The appropriate excited states are singleparticle excitations from $\mathbf{k}$ to $\mathbf{k}+\mathbf{Q}$, whose excitation energies are proportional to $\mathbf{Q}$. Equation (7) is satisfied by finite matrix elements of ρ_Q and small excitation energies. However, we can see from (8) that the sum

$$\sum_{m'} \left|\left(0\left|\rho_\mathrm{Q}\right|m'\right)\right|^2 = \left(\Psi_\mathrm{Q}, \Psi_\mathrm{Q}\right) \tag{36}$$

vanishes as Q when $Q \to 0$, as a result of the small number of possible excitations as $Q \to 0$. This means that the identity (22) does not cause any anomalous excited states to appear as $Q \to 0$.

The insulator behaves in an even more regular way. In the insulator there is an automatic energy gap between the ground state and all excitations, but (7) can be satisfied because $\left(0\left|\rho_\mathrm{Q}\right|m\right) \to 0$. This in turn is simply a consequence of the fact that excited states are orthogonal to the ground state. The sum (36) in the insulator vanishes as Q^2, and again (22) does not cause any special excited states to appear.

We see, then, that the failure of (36) to vanish in the superconductor is the major difference from the normal state. We now show that this is related to the presence of a kind of long-range order in the electrons' wave function. A unified way to prove that (36) vanishes in the normal cases is to write the wave function as a determinant of localized one-electron functions:

$$\Psi_0 = \sum_P (-1)^P \prod_{j=1}^N \Psi\left(\mathbf{r}_j - \mathbf{R}_{P(j)}\right) \tag{37}$$

In the insulator case, the Ψ 's are the usual Wannier functions. Equation (37) is not in the literature for the case of the Fermi sea, but may be derived as a limit from the insulator by increasing the lattice spacing and combining more and more Brillouin zones to approximate a sphere. Then, as we approach $Q = 0$,

$$\rho_{\mathbf{Q}}\Psi_0 = \sum_i \sum_{\boldsymbol{P}} (-1)^P \exp\left(i\mathbf{Q}\cdot\mathbf{r}_j\right) \prod_{j=1}^{N} \Psi\left(\mathbf{r}_j - \mathbf{R}_{P(j)}\right)$$
$$= \left[\sum_j \exp\left(i\mathbf{Q}\cdot\mathbf{R}_j\right)\right] \Psi_0 + \sum_{P,j} (-1)^P$$
$$\times \exp\left(i\mathbf{Q}\cdot\mathbf{R}_{P(j)}\right) \mathbf{Q}\cdot\left(\mathbf{r}_j - \mathbf{R}_{P(j)}\right)$$
$$\times \prod_j \Psi\left(\mathbf{r}_j - \mathbf{R}_{P(j)}\right) \cdots = 0 + o(Q) \tag{38}$$

In the real physical case, one-electron determinants
are only an approximation. Nonetheless, if we retain the definition of "no long-range order" as meaning that the wave function is really a properly symmetrized product of factors, each referring to a volume small in comparison to the whole specimen, then the above proof still holds.

Now we come to the question of showing that (24) holds in the metal and insulator but not in the superconductor. The proof for one-electron function representations of metal and insulator is trivial, but we shall give it here in a form using (37) which indicates how it might easily be generalized to any case without long-range order.

The sum rule we start from may also be written in the mixed form

$$\sum_m \left(0 \left| \mathbf{Q}\cdot\sum_j \left[\nabla_j \exp\left(-i\mathbf{Q}\cdot\mathbf{r}_j\right) + \exp\left(-i\mathbf{Q}\cdot\mathbf{r}_j\right)\nabla_j\right] \right| m\right) \left(m\left|\exp\left(i\mathbf{Q}\cdot\mathbf{r}_j\right)\right| 0\right) + \text{ c.c.} \;= 2NQ^2. \tag{39}$$

The above is simply the scalar product

$$\left(\sum_{P,j} (-1)^P \exp\left(i\mathbf{Q}\cdot\mathbf{R}_{P(j)}\right) 2\mathbf{Q}\cdot\nabla_j \Pi\Psi\left(\mathbf{r}_j - \mathbf{R}_{P(j)}\right), \sum_{P,j} (-1)^P \exp\left(i\mathbf{Q}\cdot\mathbf{R}_{P(j)}\right) \mathbf{Q}\cdot\left(\mathbf{r}_j - \mathbf{R}_{P(j)}\right) \Pi\Psi\left(\mathbf{r}_j -\right.\right.$$

Here we have already used (38). In any case in which the Wannier functions may be taken even or odd, this is the same as

$$\sum_j \left(\sum_P (-1)^P \exp\left(i\mathbf{Q}\cdot\mathbf{R}_{P(j)}\right) 2\mathbf{Q}\cdot\nabla_j \Psi\left(\mathbf{r}_j - \mathbf{R}_{P(j)}\right), \sum_{P'} (-1)^{P'} \exp\left(i\mathbf{Q}\cdot\mathbf{R}_{P'(j)}\right) \mathbf{Q}\cdot\left(\mathbf{r}_j - \mathbf{R}_{P'(j)}\right) \Psi\left(\mathbf{r}_j -\right.\right. \tag{40}$$

Since the Ψ are localized, the scalar product will vanish for all but nearby $\mathbf{R}_{P(j)}$'s, which means that at small $\mathbf{Q}$ the exponentials all approach unity. Clearly the only property of the wave function which has been used is the absence of long-range order. The above proof fails completely for the BCS ground state, simply because (37) and (38) are not true. The matrix elements which enter in the current in the BCS case can be shown to lead to states with finite angular momentum, which are orthogonal to the states Ψ_Q which satisfy the sum rule (9). For details of the actual calculation see the BCS paper.

29.0.4 IV. Plasma Considerations

So far all our work has ignored the long-range order and correlations caused by the plasma effect. The reason is now obvious: that a certain special type of long-range order is required

to explain the Meissner effect, which is not at all similar to the order enforced by long-range Coulomb forces. That latter order would only serve to obscure the relationships. Prior to plasma effects, the derivation of (24) from (9) is trivial, as in the NozièresPines paper [7]; afterwards, it is not at all simple.

In fact, we shall simply repeat the Nozières-Pines work here, but must first briefly explain the philosophy of what we do. The interaction used in BCS includes both the phonon and repulsive Coulomb interactions, the latter appropriately screened, so that our procedure does require justification, in that this screening implies that in the ground-state wave function the plasma effects have already been included.

The basis of our justification is provided by the observation of Sawada, Brueckner, Fukuda, and Brout [9]

that the plasma properties of the free-electron gas follow from a Hamiltonian in which the different $\mathbf{Q}$'s are completely decoupled. This observation provides a deeper justification for the "random-phase approximation" of Bohm and Pines. [10] What we shall do is to retain the random-phase approximation in the superconductor.

As Sawada et al. show, the random-phase approximation is equivalent to assuming it more probable that Coulomb interactions return an excited particle into the Fermi sea than that they excite still another. Such terms, as shown by Brueckner and Gell-Mann, [11] always lead to the most singular parts of the interactions. Our rather physical argument is that we can show that the part of the interaction retained by these authors is practically unchanged by the energy gap. It is then very hard to see why the less singular parts of the Coulomb interaction would take on a new importance and overwhelm the more singular terms in the superconducting, but not the normal case.

Our procedure is in principle the following: the original BCS Hamiltonian is assumed to contain all the Coulomb interaction except that part involving ρ_{Q} itself. Thus most of the screening is present, while all momenta except $\mathbf{Q}$ have corresponding subsidiary conditions and plasma terms. For Q, however, we can still prove (7) and (9) and study the transition from (9) to (24) as we did in the last section; the random-phase approximation tells us there is no strong coupling of $\mathbf{Q}$ and other momenta (we shall discuss the explicit point where this is introduced later). We then show that the plasma properties follow from the sum rules, practically

unaffected by the gap. On the other hand, the states Ψ_Q disappear and are replaced by the plasma states at $E = \hbar\omega_p$. This means that, in a sense, the pairing criterion $\mathbf{Q} = 0$ of BCS is enforced only by the subsidiary condition associated with the plasma.

To derive the plasma effects, we shall use the method of the appendix of reference 9 . Define a quantity

$$\Pi_{\mathbf{Q}} = \left(NQ^2\right)^{-1} 2i\mathbf{Q}\cdot\sum_j \left[\nabla_j \exp\left(i\mathbf{Q}\cdot\mathbf{r}_j\right) + \exp\left(i\mathbf{Q}\cdot\mathbf{r}_j\right)\nabla_j\right] \tag{41}$$

The commutation rule (7) gives us

$$[H, \rho_{\mathrm{Q}}] = \left(N\hbar^2Q^2/mi\right)\Pi_{\mathrm{Q}}, \tag{42}$$

while (9) gives

$$[\Pi_{\mathrm{Q}}, \rho_{-\mathrm{Q}}] = i, \tag{43}$$

[09] Sawada, Brueckner, Fukuda, and Brout, Phys. Rev. 108, 507 (1957).

[010] D. Bohm and D. Pines, Phys. Rev. 85, 338 (1952).

[11] K. A. Brueckner and M. Gell-Mann, Phys. Rev. 106, 367 (1957).

so that $\Pi_{\mathrm{Q}}{}^{*}$ plays the role of a momentum conjugate to the coordinate ρ_{Q}, and the sum rule becomes their commutation relation. Now we must introduce the interaction

$$H_c = \frac{2\pi e^2}{Q^2}\left(\rho_{\mathrm{Q}}\rho_{-\mathrm{Q}} + \rho_{-\mathrm{Q}}\rho_{\mathrm{Q}}\right) \tag{44}$$

of which we write only the **Q** terms. We also assume the existence of a ground state of energy E_0, which we expect to be perturbed from the Ψ_g so far discussed in such a way as to give the part of the long-range correlation energy associated with ρ_{Q}, and the subsidiary condition. Finally, we observe that if ρ_Q and Π_Q are to play the role of plasma oscillation coordinates, the first excited state Ψ_1 is obtainable by

$$\Psi_1 = \left(\alpha\rho_{\mathrm{Q}} + \beta\Pi_{\mathrm{Q}}\right)\Psi_0 \tag{45}$$

while the energy condition

$$E_1\Psi_1 = \left(H_0 + H_c\right)\Psi_1 \tag{46}$$

is just

$$\left[H, \left(\alpha\rho_{\mathrm{Q}} + \beta\Pi_{\mathrm{Q}}\right)\right]\Psi_0 = E_1\left(\alpha\rho_{\mathrm{Q}} + \beta\Pi_{\mathrm{Q}}\right)\Psi_0 \tag{47}$$

and, as Sawada et al. show, [9] the condition that Ψ_0 be the ground state is the subsidiary condition:

$$\left(\alpha\rho_{\mathrm{Q}} + \beta\Pi_{\mathrm{Q}}\right)^{\dagger}\Psi_0 \equiv 0 \tag{48}$$

The commutator in (47) with Π_{Q} is made up of

$$\left[H_c, \Pi_{\mathrm{Q}}\right] = +4\pi e^2 Q^{-2} i\rho_{\mathrm{Q}} \tag{49}$$

and of

$$\begin{aligned}\left[H_0, \Pi_{\mathrm{Q}}\right] &= mi\left(N\hbar^2Q^2\right)^{-1}\left[H_0, \left[H, \rho_{\mathrm{Q}}\right]\right] \\ \left[H_0, \Pi_{\mathrm{Q}}\right]_{mm'} &= mi\left(N\hbar^2Q^2\right)^{-1}\left(E_m - E_{m'}\right)^2\left(m\left|\rho_{\mathrm{Q}}\right|m'\right)\end{aligned} \tag{50}$$

in the representation in which H_0 is diagonal. The sum rules (7) and (8) show us that this is of lower order in Q than (49) except in the insulator (for which a complete discussion has been given by Nozières and Pines [7]).

The random-phase approximation consists in assuming that (49) is the only important commutator of Π_Q with any of the Coulomb terms. A discussion of this was given earlier.

We can now solve (47).

$$\alpha\left(\frac{N\hbar^2Q^2}{mi}\right)\Pi_{\mathrm{Q}} + \beta\left(\frac{4\Pi e^2}{Q^2}i\right)\rho_{\mathrm{Q}} = E_1\left(\alpha\rho_{\mathrm{Q}} + \beta\Pi_{\mathrm{Q}}\right).$$

Since ρ_{Q} and Π_{Q} are independent, this can be solved to give

$$E_1^2 = 4\pi ne^2\hbar^2/m = \left(\hbar\omega_p\right)^2 \tag{51}$$

$$\alpha/\beta = im\omega_p/N\hbar Q^2 \tag{52}$$

and the subsidiary condition, from (48),

$$\left(\alpha\rho_{-Q} - \beta\Pi_{-Q}\right)\Psi_0 = 0 \tag{53}$$

which is the same as that of Bohm and Pines [10] as $Q \to 0$, since $\alpha \gg \beta$, and the no-plasmon states have almost no $Q \neq 0$ pairs present. 'The old states Ψ_g and Ψ_Q have disappeared; they are related to Ψ_0 and Ψ_1 more or less as eigenfunctions of momentum are to the harmonic oscillator eigenfunctions. The derivation of (51) and (53) completes our program of showing that only (7) and (44) are necessary to normal plasmon behavior.

29.0.5 V. Conclusion

The above is by no means a rigorous and complete answer to the original question of whether the BCS theory satisfies gauge invariance and the sum rules and still shows a Meissner effect. Although most of it is fairly rigorous, a few parts have to be considered as a map for how things might be, rather than a proof of how they are. A few points which would bear further discussion follow.

The first one is the question of rigorous rather than approximate gauge invariance. To show rigorous gauge invariance we would have to show that the corrections to $\mathbf{J}$ and H_1 always canceled the momentum dependence of H_0. Many arguments indicate that this is not a basic difficulty. For instance, one can always make a superconductor of arbitrarily large transition temperature by letting $\hbar\omega \to \infty$ and $\exp[-1/N(0)V] \to 0$ simultaneously, thus satisfying gauge invariance arbitrarily well.

Second is the random-phase approximation in the superconductor. As this is an incompletely solved question for normal metals, we have little hope of making much more headway here.

The most serious question revolves around the correctness of calculating E_{Q} by the commutator argument rather than directly from BCS excited-state energies and matrix elements. These latter are all calculated ignoring the higher order corrections of $\mathbf{Q} \neq 0$ interactions as well as the fact that the BCS ground state is not the exact solution of the reduced Hamiltonian. We believe that the argument is as sound as that of any such intermediate coupling method, in that what has to be assumed is that certain properties of the ground statethe energy commutator, which is very insensitive, and the normalization of Ψ_Q, equivalent to the correlation function of the electrons [8]-are more stable against perturbations than the actual matrix elements themselves. In calculating frequencies of other coherent elementary excitations, such as sound waves or spin waves in metals, the same situation often arises-the energy calculated directly from what appears to be the correct wave function is not the same as that calculated from the equations of motion.

29.0.6 Appendix. Computations of Commutators

The interaction H_V is given in Eq. (10). We divide ρ_{Q} into two parts:

$$\rho_{\mathrm{Q}} = \rho_{\mathrm{Q}}^{+} + \rho_{\mathrm{Q}}^{-} = \sum_{\mathrm{K}} \left(c_{\mathrm{K+Q}\uparrow}{}^{*} c_{\mathrm{K}\uparrow} + c_{-\mathrm{K}\downarrow}{}^{*} c_{-\mathrm{K-Q}\downarrow} \right) \tag{A1}$$

and by direct computation:

$$H_V \rho_Q + -\rho_Q + H_V = V \sum_q \left(\sum_{k(\epsilon_k < \hbar\omega)} \sum_{k' \neq k(\epsilon_{k'} < \hbar\omega)} + \sum_{k(\epsilon_k - q < \hbar\omega)} \sum_{k' \neq k(\epsilon_{k'} - q < \hbar\omega)} \right) \tag{A2}$$

$$\times \left(c_{k'+Q\uparrow}{}^{*} c_{-k'+q\downarrow}{}^{*} c_{-k+q\downarrow} c_{k\uparrow} - c_{k'\uparrow}{}^{*} c_{-k'+q\downarrow}{}^{*} c_{-k+q\downarrow} c_{k-Q\uparrow} \right).$$

In the case of ρ_{Q^-}, the summations are the same but the last parentheses read:

$$\left(c_{\mathrm{k}'\uparrow}{}^{*}c_{-\mathrm{k}'+\mathrm{q}+\mathrm{Q}\downarrow}{}^{*}c_{-\mathrm{k}+\mathrm{q}\downarrow}c_{\mathrm{k}\uparrow}-c_{\mathrm{k}'\uparrow}{}^{*}c_{-\mathrm{k}'+\mathrm{q}\downarrow}{}^{*}c_{-\mathrm{k}+\mathrm{q}-\mathrm{Q}\downarrow}c_{\mathrm{k}\uparrow}\right). \tag{A3}$$

In both (A2) and (A3) the second term can be made to correspond with the first by the appropriate substitutions: in (A2) by

$$\mathbf{k}'-\mathbf{Q}\to k',\quad \mathbf{k}-\mathbf{Q}\to\mathbf{k},\quad \mathbf{q}-\mathbf{Q}\to\mathbf{q} \tag{A4}$$

and in (A3) simply by

$$\mathbf{q}-\mathbf{Q}\to\mathbf{q}. \tag{A5}$$

If Q is small, (A4) and (A5) have no effect on the large majority of terms, so that the appropriate parts of the second term cancel the first. Near the cutoff surface, the substitutions affect the presence or absence of the terms: (A4) when the cutoff depends on $\mathbf{k}$ and $\mathbf{k}'$, (A5) when it depends on $\mathbf{k}-\mathbf{q},\mathbf{k}'-\mathbf{q}$. The resulting terms near the cutoff surface are given in (11) of the text.

It is also necessary to use Eq. (11) to compute $(\ \rho_{\mathrm{Q}}\Psi_g,[H_V,\rho_{\mathrm{Q}}]\,\Psi_g\ )$. Equation (17) of the text shows us that only terms of the commutator which break up only two pairs can contribute to the scalar product. Examination of (11) reveals that two types of term can appear. These are the terms involving $\mathbf{q}=0$ or $\mathbf{q}=-\mathbf{Q}$. Upon taking this into account, the important part of (11) becomes

$$\frac{1}{2}V\left\{\sum_{k'\neq k}\left[\sum_{k(\epsilon_k<\hbar\omega,\epsilon_k+Q>\hbar\omega)}-\sum_{k(\epsilon_k>\hbar\omega,\epsilon_k+Q<\hbar\omega)}\right]+\text{ same with }\mathbf{k}'\to\mathbf{k},\mathbf{k}\to\mathbf{k}'\right\}$$
$$\times\left(c_{k'+Q\uparrow}c_{-k'\downarrow}{}^{*}c_{-k\downarrow}c_{k\uparrow}+c_{k'+Q\uparrow}{}^{*}c_{-k'-Q\downarrow}{}^{*}c_{-k-Q\downarrow}c_{k\uparrow}-c_{k'\uparrow}{}^{*}c_{-k'\downarrow}{}^{*}c_{-k-Q\downarrow}c_{k\uparrow}-c_{k'+Q\uparrow}c_{-k'\downarrow}{}^{*}c_{-k-Q\downarrow}c_{k+Q\uparrow}\right). \tag{A6}$$

The effect of the terms in parentheses in this equation on the BCS Ψ_g may now be computed:

$$\begin{aligned}()\Psi_g=\Bigg\{&\prod_{\mathrm{K}\neq\mathrm{k}',\mathrm{k}'+\mathrm{Q},\mathrm{k}}\left[(1-h_{\mathrm{K}})^{\frac12}+h_{\mathrm{K}}{}^{\frac12}b_{\mathrm{K}}{}^{*}\right]h_{\mathrm{k}\frac12}\,(1-h_{\mathrm{k}'})^{\frac12}\,(1-h_{\mathrm{k}'+\mathrm{Q}})^{\frac12}\,c_{\mathrm{k}'+\mathrm{Q}\uparrow}{}^{*}c_{-\mathrm{k}'\downarrow}{}^{*}\\&-\prod_{\mathrm{K}\neq\mathrm{k},\mathrm{k}+\mathrm{Q},\mathrm{k}'+\mathrm{Q}}\left[(1-h_{\mathrm{K}})^{\frac12}+h_{\mathrm{K}\frac12}b_{\mathrm{K}}{}^{*}\right](1-h_{\mathrm{k}'+\mathrm{Q}})^{\frac12}\,h_{\mathrm{k}\frac12}h_{\mathrm{k}+\mathrm{Q}\frac12}b_{\mathrm{k}'+\mathrm{Q}}{}^{*}c_{\mathrm{k}+Q\uparrow}c_{-\mathrm{k}\downarrow}{}^{*}\\&+\prod_{\mathrm{K}\neq\mathrm{k},\mathrm{k}+\mathrm{Q},\mathrm{k}'}\left[(1-h_{\mathrm{K}})^{\frac12}+h_{\mathrm{K}\frac12}b_{\mathrm{K}}{}^{*}\right]h_{\mathrm{k}\frac12}h_{\mathrm{k}+\mathrm{Q}\frac12}\,(1-h_{\mathrm{k}'})^{\frac12}\,b_{\mathrm{k}'}{}^{*}c_{\mathrm{k}+\mathrm{Q}\uparrow}{}^{*}c_{-\mathrm{k}\downarrow}{}^{*}\\&-\prod_{\mathrm{K}\neq\mathrm{k}',\mathrm{k}+\mathrm{Q},\mathrm{k}'+\mathrm{Q}}\left[(1-h_{\mathrm{K}})^{\frac12}+h_{\mathrm{K}\frac12}b_{\mathrm{K}}{}^{*}\right]h_{\mathrm{k}+\mathrm{Q}\frac12}\,(1-h_{\mathrm{k}'})^{\frac12}\,(1-h_{\mathrm{k}'+\mathrm{Q}})^{\frac12}\,c_{\mathrm{k}'+Q\uparrow}c_{-\mathrm{k}'\downarrow}{}^{*}\Bigg\}\,\Psi_v\end{aligned}$$

Now we combine this with (23) and (24) to compute the scalar product:

$$\begin{aligned}(\rho_Q\Psi_g,[H_V,\rho_Q]\,\Psi_g)=\frac12V\Bigg[&\sum_{\mathbf{k}(\epsilon_{\mathbf{k}}<\hbar\omega,\epsilon_{\mathbf{k}}+Q>\hbar\omega)}\sum_{\mathbf{k}'\neq\mathbf{k}}-\sum_{\mathbf{k}(\epsilon_{\mathbf{k}}>\hbar\omega,\epsilon_{\mathbf{k}}+Q<\hbar\omega)}\sum_{\mathbf{k}'\neq\mathbf{k}}+\sum_{\mathbf{k}'(\epsilon_{\mathbf{k}'}<\hbar\omega,\epsilon_{\mathbf{k}'}+Q>\hbar\omega}\sum_{\mathbf{k}\neq\mathbf{k}'}-\cdots\Bigg]\\&\times\Bigg\{\left[h_{\mathbf{k}'}^{\frac12}\,(1-h_{\mathbf{k}'+Q})^{\frac12}+h_{\mathbf{k}'+Q\frac12}\,(1-h_{\mathbf{k}'})^{\frac12}\right](1-h_{\mathbf{k}'})^{\frac12}\,(1-h_{\mathbf{k}'+Q})^{\frac12}\\&\times\left[h_{\mathbf{k}^2}^{\frac12}\,(1-h_{\mathbf{k}})^{\frac12}-h_{\mathbf{k}+Q\frac12}\,(1-h_{\mathbf{k}+Q})^{\frac12}\right]+\left[h_{\mathbf{k}^2}^{\frac12}\,(1-h_{\mathbf{k}+Q})^{\frac12}+h_{\mathbf{k}+Q\frac12}\,(1-h_{\mathbf{k}})^{\frac12}\right]\\&\times h_{\mathbf{k}\frac12}h_{\mathbf{k}+Q\frac12}\left[h_{\mathbf{k}'}{}^{\frac12}\,(1-h_{\mathbf{k}'})^{\frac12}-h_{\mathbf{k}'+Q\frac12}\left(1-h_{\mathbf{k}'+Q\frac12}\right)\right]\Bigg\}.\end{aligned}$$

If in the first term we interchange the labels $\mathbf{k}$ and $\mathbf{k}'$, it becomes very similar to the second, and the whole sum is symmetric in $\mathbf{k}$ and $\mathbf{k}+\mathbf{Q}$, and antisymmetric in $\mathbf{k}'$ and $\mathbf{k}'+\mathbf{Q}$. We therefore have left only twice the limited sum over $\mathbf{k}'$:

$$\begin{aligned}(\rho_{\mathrm{Q}}\Psi_g,[H_V,\rho_{\mathrm{Q}}]\,\Psi_g) &= V\left[h_{\mathrm{k}}^{\frac{1}{2}}\left(1-h_{\mathrm{k+Q}}\right)^{\frac{1}{2}}+h_{\mathrm{k+Q}^{\frac{1}{2}}}\left(1-h_{\mathrm{k}}\right)^{\frac{1}{2}}\right]\\ &\times\left[h_{\mathrm{k}^2}^{\frac{1}{2}}h_{\mathrm{k+Q}^{\frac{1}{2}}}+\left(1-h_{\mathrm{k}}\right)^{\frac{1}{2}}\left(1-h_{\mathrm{k+Q}}\right)^{\frac{1}{2}}\right]\left[h_{\mathrm{k}'}\frac{1}{2}\left(1-h_{\mathrm{k}'}\right)^{\frac{1}{2}}-h_{\mathrm{k}'}+\mathrm{Q}^{\frac{1}{2}}\left(1-h_{\mathrm{k}'+\mathrm{Q}}\right)^{\frac{1}{2}}\right]. \quad \text{(A7)}\end{aligned}$$

In view of the symmetry in $\mathbf{k}$ and $\mathbf{k}+\mathbf{Q}$ and the fact that Q is very small, the $\mathbf{k}$ sum may be simplified to $2V\sum_{\mathrm{k}}\left[h_{\mathrm{k}}\left(1-h_{\mathrm{k}}\right)\right]^{\frac{1}{2}}=2\epsilon_0$. The $\mathbf{k}'$ sum is an integral over the cutoff surface $|\epsilon|=\hbar\omega$. When $\mathbf{k}'$ points at an angle θ to $\mathbf{Q}$, the energy difference is

$$\delta\epsilon=\epsilon_{\mathrm{k}'+\mathrm{Q}}-\epsilon_{\mathrm{k}'}=\left(\hbar^2k_FQ\cos\theta\right)/m \quad \text{(A8)}$$

and the number of states in the surface element at this angle is $\frac{1}{2}\sin\theta d\theta N(0)\delta\epsilon$. Thus

$$\begin{aligned}\sum_{\mathbf{k}}\Delta\left[h_{\mathbf{k}^{\frac{1}{2}}}\left(1-h_{\mathrm{k}}\right)^{\frac{1}{2}}\right] &= 4N(0)\frac{1}{2}\int_0^{\pi/2}\sin\theta d\theta\left[\left(\frac{\hbar^2}{m}\right)k_FQ\cos\theta\right]^2\frac{d}{d\epsilon}\left[\frac{1}{2}\epsilon_0\left(\epsilon^2+\epsilon_0^2\right)^{-\frac{1}{2}}\right]_{\epsilon=\hbar\omega}=\\ &=\frac{1}{3}\frac{N(0)\hbar^2k_F^2Q^2\epsilon_0}{(m^2\omega^2)} \quad \text{(A9)}\end{aligned}$$

which gives the value (19) of the text.

Finally, we compute the commutator involved in the kinetic energy:

$$\begin{aligned}\sum_{\mathrm{K},\sigma}\mathbf{Q}\cdot(2\mathbf{K}+\mathbf{Q})c_{\mathrm{K+Q},\sigma}{}^*c_{\mathrm{K},\sigma}\Psi_g &= \mathbf{Q}\cdot\sum_{\mathrm{K}}(2\mathbf{K}+\mathbf{Q})\left(c_{\mathrm{K+Q}\uparrow}{}^*c_{\mathrm{K}\uparrow}-c_{-\mathrm{K}\downarrow}{}^*c_{-\mathrm{K}-\mathrm{Q}\downarrow}\right)\Psi_g\\ &=\mathbf{Q}\cdot\sum_{\mathrm{K}}(2\mathbf{K}+\mathbf{Q})\left[h_{\mathrm{K}^{\frac{1}{2}}}\left(1-h_{\mathrm{K+Q}}\right)^{\frac{1}{2}}-h_{\mathrm{K+Q}^{\frac{1}{2}}}\left(1-h_{\mathrm{K}}\right)^{\frac{1}{2}}\right]\Psi_{-\mathrm{K},\ \mathrm{K+Q}}, \quad \text{(A10)}\end{aligned}$$

using (14)-(16). Again using (15) and (16), we get

$$(\rho_{\mathrm{Q}}\Psi_g,[H_{\mathrm{K}},\rho_{\mathrm{Q}}]\,\Psi_g)=\left(\hbar^2/2m\right)\sum_{\mathrm{K}}\mathbf{Q}\cdot(2\mathbf{K}+\mathbf{Q})\left(h_{\mathrm{K}}-h_{\mathrm{K+Q}}\right). \quad \text{(A11)}$$

For small Q, this is almost exactly

$$-\left(\hbar^2/m\right)\sum_{\mathbf{k}}(\mathbf{Q}\cdot\mathbf{k})\mathbf{Q}\cdot\nabla_{\mathbf{k}}\left(h_{\mathrm{k}}\right)=\left(\hbar^2/m\right)^2\sum_{\mathbf{k}}(\mathbf{Q}\cdot\mathbf{k})^2(dh/d\epsilon). \quad \text{(A12)}$$

In this form it is clearly independent of the exact form of the distribution, and thus is practically the same as the identical quantity for a Fermi sea. Evaluating (A12) (the assumption must be made that ϵ_0 is small), we get the result quoted as (20) of the text.

30 A Time Dependent Ginzburg-Landau Equation and its Application to the Problem of Resistivity in the Mixed State by A. Schmid, 1966

Abstract

A time dependent modification of the Ginzburg-Landau equation is given which is based on the assumption that the functional derivative of the Ginzburg-Landau free energy expression with respect to the wave function is a generalized force in the sense of irreversible thermodynamics acting on the wave function. This equation implies an energy theorem, according to which the energy can be dissipated by i) production of Joule heat; ii) irreversible variation of the wave function. The theory is a limiting case of the BCS theory, and hence, it contains no adjustable parameters. The application of the modified equation to the problem of resistivity in the mixed state reveals satisfactory agreement between experiment and theory for reduced temperatures higher than 0.6 .

30.0.1 I. Introduction

In the theory of superconductivity, the Ginzburg-Landau equation [1] has proven to be very successful. The most interesting consequences of this equation have been found by Abrikosov [2] who investigated the behavior of superconductors of the second type - mostly metals of short mean free path in the normal state - in a magnetic field. He found that the magnetic field will penetrate in the superconductor in quantized units of flux (fluxoids, flux lines), if the field is greater than a critical field H_{c1}, and that a second order phase transition takes place at a field $H_{c2} > H_{c1}$. This particular state of a superconductor is called the mixed state. Ginzburd and Landau proposed their equation on a phenomenological basis; it was later shown by Gorkov [3] that this equation can be derived from the BCS theory [4] in the case of thermodynamic equilibrium and for temperatures close to the transition temperature.

Recently Kim, Hempstead and Strnad [5] found in experiments that the voltage-current ratio doesn't vanish for a type II superconductor in a magnetic field, that Ohm's law applies, and that the resistivity depends on the magnetic field. Since fluxoids experience a Lorentz force exerted by the transport current, they thought of a frictional force due to the uniform motion of the fluxoids (flux flow) which counterbalances this driving force. Subsequently, Stephen and Bardeen [6] treated this problem theoretically on the basis of a local model that is a generalization of the London theory. Their calculations agree well with the experimental results, at least in the case of low temperatures. As far as the energy dissipation in this resistive state of type II superconductors is concerned, Stephen and Bardeen consider only losses due to Joule heat of the normal electrons. According to Tinkham [7], an additional dissipative mechanism due to the finite relaxation time of the superelectrons should be taken into account.

Since the Ginzburg-Landau equation deals only with thermodynamic equilibrium (where each physical quantity is constant in time), it cannot be applied to the above mentioned problem. Yet, one may ask whether there exists a generalization of the Ginzburg-Landau equation where the effective wave function (proportional to the gap) is allowed to change in time such that the problem of flux flow would be included in the solutions.

Generalizations of the Ginzburg-Landau equation, which include time dependent terms, have already been proposed by Stephen and Suhl [8], by Anderson et al. [9], and by Jakeman and Pike [10].

The same problem will be discussed here, since the author feels that there may be different approaches to that problem. In particular, the aim of this paper is to present the simplest type of time dependent equation which allows the superconductor to relax in its equilibrium state if no external driving forces are present. The effects of impurity scattering will be included in this equation. Keeping in mind this aim, we will derive a set of equations in section II, using the Gorkov formulation [11] of the BCS theory. Of course, we will have to limit ourselves to the case of small and slowly varying gap. This set allows to determine all field quantities; and it will be shown in section III that these equations imply a theorem on energy conservation. In section IV the consequences of these equations will be discussed for flux flow in type II superconductors in the cases where the magnetic induction is small (H_{c1}) or close to the upper critical field (

H_{c2}); and satisfactory agreement will be found with experiment.

30.0.2 II. A Time Dependent Ginaburg-Landau Equation

In the field free case, the simplest equation which allows the Ginzburg-Landau wave function ψ to relax to its equilibrium value is given by

$$\gamma\hbar\frac{\partial\psi}{\partial t} = \frac{1}{2m}(\hbar\nabla)^2\psi + \alpha\psi - \beta|\psi|^2\psi. \tag{II.1}$$

This type of equation has already been considered by Landat and Khalatnikov [12] in connection with superfluid helium. Eq. (II.1) implies that a deviation of ψ from its equilibrium value $\sqrt{\alpha/\beta}$ has to vanish proportional to $\exp(-t/\tau_{\mathrm{R}})$, where
the relaxation time τ_{R} is given by

$$\tau_{\mathbb{R}} = \frac{\hbar\gamma}{2\alpha} \tag{II.2}$$

provided that γ is real and positive *.
In order to determine γ which appears in eq. (II.1), we start from the Gorkov equation [11] without external fields and consider the approximation

$$\begin{aligned}\Delta^*(x) = -ig\int dx_1 G_0(x_1,x)\,\Delta^*(x_1)\,G_0(x_1,x) + \\ + ig\int dx_1dx_2dx_3 G_0(x_1,x)\,\Delta^*(x_1)\,G_0(x_1,x_2)\times \\ \times\,\Delta(x_2)\,G_0(x_3,x_2)\,\Delta^*(x_3)\,G_0(x_3,x)\end{aligned} \tag{II.3}$$

which is sufficient for a small gap $\Delta(x)$[3].$G_0(x,x')$ is the Green's function of the metal in the normal state, and x stands for $\boldsymbol{r},t$.

Since the superconductor is supposed to be not in thermodynamic equilibrium, we have to be careful about the integration with respect to time. We follow the procedure given by Kadanoff and Baym [13]. This implies that, at the time $-\infty$, the equilibrium state of the metal is the normal state. This seems to be contradictory at first sight, because the metal is superconducting in the temperature range of interest. However, we imagine that we are able to switch the electronelectron interaction responsible for superconductivity such that the interaction constant is zero at $t=-\infty$, and then, assumes slowly its usual value. Since this switching process will be completed long before the times of interest, it doesn't affect the results and hence, should be considered merely a mathematical trick **. This procedure amounts to the replacement of the coupling constant g by $e^{\delta t}g$ (δ small and positive), and of $\Delta(x)\,(=gF^+(x,x))$ by $e^{\delta t}\Delta(x)$.

We now expand $\Delta(x_1)$ in the first integral of the r.h.s. of eq. (II.3) as follows

$$\begin{aligned}\Delta(\boldsymbol{r}_1t_1) = \Delta(\boldsymbol{r}t) + \frac{\partial\Delta(\boldsymbol{r}t)}{\partial q_j}(q_{1j}-q_j) + \frac{1}{2}\frac{\partial^2\Delta(\boldsymbol{r}t)}{\partial q_j\partial q_k}(q_{1j}-q_j)(q_{1k}-q_k) + \\ + \frac{\partial\Delta(\boldsymbol{r}t)}{\partial t}(t_1-t)\,;\quad (q_1,q_2,q_3)=\boldsymbol{r}\end{aligned} \tag{II.4}$$

In the second integral we take the $\Delta(x_j)$ just equal to $\Delta(x)$. This approximation is the same used by Gorkov [3], with the exception of the last term in eq. (II.4), which takes the time dependence of $\Delta(x)$ approximately into account. All the integrals which do not depend on the

time integration variable (except by the factors G_0), turn out to be identical with Gorkov's result [3] in the case of no time dependence. The additional term,

$$-ig\frac{\partial\Delta^*(\boldsymbol{r}t)}{\partial t}\int dx_1 G_0\left(x_1,x\right)e^{\delta t_1}\left(t_1-t\right)G_0\left(x_1,x\right) \tag{II.5}$$

is the same for superconductors with and without impurities. We assume the latter to be the case, where the Fourier transform of G_0 with respect to the space

coordinate is given by

$$G_0^{>}\left(\boldsymbol{k};t_1,t\right)=-\frac{i}{\hbar}\frac{e^{-\frac{i\varepsilon_k}{\hbar}(t_1-t)}}{e^{-\beta\varepsilon_k}+1};\quad G_0^{<}=\frac{i}{\hbar}\frac{e^{-\frac{i\varepsilon_k}{\hbar}(t_1-t)}}{e^{+\beta\varepsilon_k}+1},$$

where $\beta=1/kT$ and $\varepsilon_k=\hbar^2k^2/2m-\varepsilon_{\mathbf{F}}$ ($\varepsilon_{\mathbf{F}}$ is the Fermi energy). Following the procedure of ref. [13], we find the expression (II.5) to be equal to

$$\begin{aligned}&-ig\frac{\partial A^*}{\partial t}\int\frac{d^3\boldsymbol{k}}{(2\pi)^3}\int_{-\infty}^{i}dt_1\left(\left(G_0^{<}\left(\boldsymbol{k};t_1,t\right)\right)^2-\left(G_0^{>}\left(\boldsymbol{k};t_1,t\right)\right)^2\right)e^{\delta t_1}\left(t_1-t\right)\\&=\frac{\partial A^*}{\partial t}-igN(0)\\&=-\frac{\partial\Delta^*}{\partial t}\frac{\pi\hbar gN(0)}{8kT_{\mathrm{c}}};*\end{aligned} \tag{II.6}$$

$N(0)$ being the density of states at the Fermi surface.
Following Gorkov, we put

$$\psi(\boldsymbol{r}t)=\frac{7\zeta(3)n_0\chi(\varrho)}{16\pi^2k^2T_{\mathrm{c}}^2}\cdot\Delta(\boldsymbol{r}t);\quad\zeta(3)=1.202 \tag{II.7}$$

where $\chi(\varrho)$ is defined by eq. (15) of ref. [3b] and obtain eq. (II.1) as a substitute of eq. (II.2). The coefficients of eq. (II.1) are given by

$$\alpha=\frac{1}{\eta}\frac{T_{\mathrm{c}}-T}{T_{\mathrm{c}}};\beta=\frac{1}{\eta}\frac{2}{n_0\cdot\chi(\varrho)};\quad\gamma=\frac{1}{\eta}\cdot\frac{\pi}{8kT_{\mathrm{c}}};\quad\eta=\frac{7\zeta(3)\varepsilon_{\mathrm{F}}}{12\pi^2k^2T_{\mathrm{c}}}\chi(\varrho); \tag{II.8}$$

where n_0 is the density of electrons. Using these values, we find the relaxation time τ_{R}, eq. (II.2), equal to

$$\tau_{\mathrm{R}}=\frac{\pi}{16}\frac{\hbar}{kT_{\mathrm{c}}}\left(1-T/T_{\mathrm{c}}\right)^{-1}\approx 0.7\frac{\hbar}{\Delta(T=0)}\left(1-T/T_{\mathrm{c}}\right)^{-1}$$

which is very close to the relaxation time considered by Tinkham [7].
In the case of external fields, we include the effects of a vectorpotential $\boldsymbol{A}(\boldsymbol{r}t),\operatorname{curl}\boldsymbol{A}=\boldsymbol{H}$, by replacing $\hbar\nabla$ in eq. (II.1) by $\hbar\nabla+(2ie/c)\boldsymbol{A}(\boldsymbol{r}t)^{\star\star}$. In order to have a gauge invariant equation, we have to substitute $\hbar\partial/\partial t$ by a term of the form $\hbar\partial/\partial t-2ie\tilde{\Phi}(\boldsymbol{r}t)$. A gauge transformation consists in the simultaneous substitutions

$$\psi\to\psi e^{(2ie/\hbar c)p};\quad A\to A+\nabla\varphi;\quad\tilde{\Phi}\to\tilde{\Phi}-\frac{1}{c}-\frac{\partial p}{\partial t}.$$

0

- Actually, it is only necessary to have $\operatorname{Re}\gamma>0$; we will find, however, γ to be real. γ cannot be purely imaginary, since then a stationary solution $|\psi|=$ const. can be found arbitrarely far off from the equilibrium value.

$\star\star$ Stephen and Surll [7] expand the Gorkov equation in a power series of $\Delta(x)-\Delta_0$, where Δ_0 is the zero field equilibrium value of the gap and avoid thereby this switching process. On the other hand, for a type II superconductor near $H_{c2},\Delta(x)-\Delta_0$ might be quite large whereas $\Delta(x)$ is small.

This form of a gauge transformation indicates a relationship between the effective potential $\tilde{\Phi}$ and the electric potential Φ. We propose the relation

$$\tilde{\Phi} = \Phi - \mu/e \tag{II.9}$$

where μ is the local chemical potential of the superconductor ***. We have implicitly assumed that a local thermodynamic equilibrium can be defined.

Considering the modifications discussed above, we obtain the final form of eq. (IT.1) :

$$\gamma\left(\hbar\frac{\partial}{\partial t} - 2ie\tilde{\Phi}\right)\psi = \frac{1}{2m}\left(\hbar\nabla + \frac{2ie}{c}\boldsymbol{A}\right)^2\psi + \alpha\psi - \beta|\psi|^2\psi \tag{A}$$

In order to obtain equations for the quantities $\boldsymbol{A}$ and Φ, we have to determine expressions for the sources of the electromagnetic field, the current density $\boldsymbol{j}$ and the charge density ϱ.

The current density is given by

$$\boldsymbol{j}(\boldsymbol{r}t) = \left[\frac{\hbar e}{m}\left(\nabla_{\boldsymbol{r}} - \nabla_{\boldsymbol{r}'}\right)G\left(x, x'\right) + \frac{2ie}{mc}\boldsymbol{A}(x)G\left(x, x'\right)\right]_{\boldsymbol{r}=\boldsymbol{r}';t=t'-0}$$

where $G\left(x, x'\right)$ is the Green's function in the superconducting state. Considering the Gorkov equation, we find $G\left(x, x'\right)$ in sufficient approximation equal to

$$\begin{aligned} G\left(x, x'\right) &= G_0\left(x, x'\right) - \\ &- \int dx_1 dx_2 G_0\left(x, x_1\right)\Delta\left(x_1\right)G_0\left(x_2, x_1\right)A^*\left(x_2\right)G_0\left(x_2, x'\right) \end{aligned} \tag{II.10}$$

The first term of the r.h.s. of eq. (II.10) is the Green's function of the metal in the normal state and, consequently, the current density $\boldsymbol{j}_{\mathrm{n}}$ resulting from this term is the same as the current density in the normal state. By Ohm's law, we have

$$\boldsymbol{j}_{\mathrm{n}} = \sigma\tilde{\boldsymbol{E}}$$

where the effective field strength $\tilde{\boldsymbol{E}}$ is given by

$$\tilde{\boldsymbol{E}}(\boldsymbol{r}t) = -\frac{1}{c}\frac{\partial}{\partial t}\boldsymbol{A}(\boldsymbol{r}t) - \nabla\tilde{\Phi}(\boldsymbol{r}t) \tag{TI.11}$$

In the second term, we expand

$$\Delta\left(\boldsymbol{r}_{\mathrm{n}}t_{\mathrm{n}}\right) = \Delta(\boldsymbol{r}t) + \left(\boldsymbol{r}_{\mathrm{n}} - \boldsymbol{r}\right)\nabla\Delta(\boldsymbol{r}t); \tag{II.12}$$

omitting terms as $\frac{\partial^2 A}{\partial q_j \partial q_k}$ and $\frac{\partial A}{\partial t}$, which, according to the treatment above, should be considered of the same order of magnitude. In this way, we get the second contribution to the current density equal to the expression given by Ginzburg and Landau*. We insert these results in Maxwell's second equation and get a second basic equation:

0

- Calculating the coefficient of the next order term $\partial^2\Delta/\partial t^2$, we are led to the assumption that the expansion parameter of this series is of the order $\hbar/kT_{\mathrm{c}}$.
  ** See the discussion given by Maki [14].
  *** The chemical potential μ is the energy necessary to add an electron in thermodynamic equilibrium (for instance, at constant temperature), whereby the electromagnetic fields have to be kept fixed. It is a rather unphysical concept, which is shown by the fact that μ appears only in the combination (II.9). In the case $\mathbf{A} = \mathbf{0}, \mu - e\boldsymbol{\Phi}$ is the electrochemical potential.

$$\begin{aligned}
&\frac{1}{c^2}\frac{\partial^2}{\partial t^2}\boldsymbol{A}+\frac{1}{c}\frac{\partial}{\partial t}\nabla\Phi+\operatorname{curl}\operatorname{curl}\boldsymbol{A}=\frac{4\pi}{c}\left(\boldsymbol{j}_{\mathrm{n}}+\boldsymbol{j}_{\mathrm{s}}\right)\\
&\boldsymbol{J}_{\mathrm{n}}=-\sigma\left[\frac{1}{c}\frac{\partial}{\partial t}\boldsymbol{A}+\nabla\tilde{\Phi}\right]\\
&\boldsymbol{j}_{\mathrm{s}}=\frac{ie\hbar}{m}\left(\psi^*\nabla\psi-\psi\nabla\psi^*\right)-\frac{4e^2}{mc}\boldsymbol{A}|\psi|^2
\end{aligned}\tag{B}$$

We now derive an expression for the charge density $\varrho(\boldsymbol{r}t)$ of the electrons. Subtracting the positively charged background, we have

$$\varrho=2ieG\left(x,x'\right)_{r=r';t=t'-0}+en_0$$

where $G\left(x,x'\right)$ is given by eq. (II.10). Corresponding to the two parts of G, we put $\varrho=\varrho_{\mathrm{n}}+\varrho_{\mathrm{s}}{}^{\star}$.

The charge density ϱ_n in the normal state is proportional to the change of the chemical potential and, therefore, by eq. (II.9), proportional to $\Phi-\tilde{\Phi}$. We put

$$\varrho_{\mathrm{n}}=-\frac{1}{4\pi}\lambda_{\mathrm{D}}^{-2}(\Phi-\tilde{\Phi})$$

where λ_{D} is the Debye screening length, $\lambda_{\mathrm{D}}=\left[8\pi e^2N(0)\right]^{-1/2}$.
In the expression of ϱ_s, which is proportional to the second term of the r.h.s. of eq. (II.10) when $x=x'$, we expand $\Delta\left(\boldsymbol{r}_{\mathrm{n}}t_{\mathrm{n}}\right)$ according to eq. (II.3) and obtain in the case of no external fields

$$\varrho_{\mathrm{S}}=c_1|\nabla\Delta(\boldsymbol{r}t)|^2+c_2\left[\Delta^*\nabla^2\Delta(\boldsymbol{r}t)+\Delta\nabla^2\Delta^*(\boldsymbol{r}t)\right]+ic_3\left[\Delta^*\frac{\partial\Delta}{\partial t}-\Delta\frac{\partial\Delta^*}{\partial t}\right].$$

As far as the time dependence in this problem is concerned, the calculation of the coefficients c_j follows the prescription given above. The coefficients c_1 and c_2 depend on the presence of impurities and can be calculated using Gorkov's method [3b]. For simplicity, we consider only the case of isotropic scattering where $c_2=\frac{1}{2}c_1$; then

$$c_1|\nabla\Delta|^2+c_2\left[\Delta^*\nabla^2\Delta+\Delta\nabla^2\Delta^*\right]=\frac{1}{2}c_1\nabla^2|\Delta|^2.$$

We put the expressions for the charge densities in Maxwell's third equation and obtain:

$$\begin{aligned}
-\frac{1}{c}\frac{\partial}{\partial t}\nabla\boldsymbol{A}-\nabla^2\Phi&=4\pi\left(\varrho_{\mathrm{n}}+\varrho_{\mathrm{s}}\right);\\
\varrho_{\mathrm{n}}&=-\frac{1}{4\pi}\lambda_{\mathrm{D}}^{-2}(\Phi-\tilde{\Phi});\\
\varrho_{\mathrm{s}}&=\frac{e}{2\varepsilon_{\mathrm{F}}}\cdot\frac{\hbar^2}{2m}\nabla^2|\psi|^2+\frac{3}{\varepsilon_{\mathrm{F}}\chi(\bar{\varrho})}\times\\
&\quad\times\left[\frac{i\hbar}{2}\left(\psi^*\frac{\partial\psi}{\partial t}-\psi\frac{\partial\psi^*}{\partial t}\right)+2e\tilde{\Phi}|\psi|^2\right].
\end{aligned}\tag{C}$$

0

- One may wonder why the magnitude of the normal current is unaffected by the presence of superconductivity, since one expects the normal conductivity to decrease by increasing magnitude of the gap. One can obtain such corrections by expanding $\Delta(rt)$, eq. (II.12), to higher orders in the derivatives.

It may be interesting to note that even in the equilibrium case, where $\frac{\partial \psi}{\partial t} = \tilde{\Phi} = 0$, the charge density is not necessarily zero **.

The set of eqs. (A), (B), and (C) corresponds to 6 independent equations. In principle it is, therefore, possible to determine the 7 unknown quantities $|\psi(\boldsymbol{r}, t)|$,

$\arg \psi(\boldsymbol{r}, t), A_i(\boldsymbol{r}, t), \Phi(\boldsymbol{r}, t)$, and $\tilde{\Phi}(\boldsymbol{r}, t)$, if one takes into account the irrelevance of the gauge of the wave function and of the electromagnetic field.

Eq. (C) has some features in common with the "additional Ginzburg-Landau equation" proposed by Anderson et al. [9]. However, this equation does not give a direct physical insight, mainly because it contains both Φ and $\tilde{\Phi}$, of which only $\tilde{\Phi}$ is of physical importance. We derive a more appropriate equation, starting from the continuity equation

$$\operatorname{div} \boldsymbol{j} = \operatorname{div} (\boldsymbol{j}_{\mathrm{n}} + \boldsymbol{j}_{\mathrm{s}}) = -\frac{\partial}{\partial t} \boldsymbol{o}.$$

Considering the definitions of $\boldsymbol{j}_{\mathrm{n}}$ and $\boldsymbol{j}_{\mathrm{s}}$, eq. (B), and transforming div $\boldsymbol{j}_{\mathrm{s}}$ by means of eq. (A), we obtain

$$\begin{aligned} 1 - \frac{\partial}{\partial t} \nabla \boldsymbol{A} + \nabla^2 \tilde{\Phi} &= \frac{1}{\sigma} \operatorname{div} \boldsymbol{j}_{\mathrm{s}} - \frac{1}{\sigma} \frac{\partial}{\partial t} \varrho; \\ \operatorname{div} \boldsymbol{j}_{\mathrm{s}} &= \frac{4\gamma e}{\hbar} \left[\frac{i\hbar}{2} \left(\psi^* \frac{\partial}{\partial t} \psi - \psi^{-\frac{\partial}{\partial t}} \psi^* \right) + 2e\tilde{\Phi} |\psi|^2 \right]. \end{aligned} \tag{II.13}$$

In many cases, $\frac{\partial}{\partial t} \varrho$ is a quantity which can be neglected (we will meet only this situation in the following calculations). Then, eq. (II.13) has a structure similar to eq. (B). In correspondence to the London penetration depth λ_{L} of the magnetic field, a penetration depth $\lambda_{\tilde{\Phi}}$ of the effective potential $\tilde{\Phi}$ can be defined which is given by

$$\lambda_{\tilde{\Phi}} = \sqrt{\frac{\hbar \sigma \beta}{8e^2 \gamma \alpha}}$$

For superconductors of short mean free path in the normal state, $\lambda_{\tilde{\Phi}}$ is equal to

$$\lambda_{\tilde{\Phi}} = 0.42 \xi$$

where $\xi = \frac{\lambda_{\mathrm{L}}}{x}$ is the coherence length *.

0

- We emphasize that ϱ_n is the charge density in a corresponding normal state and, therefore, the meaning of ϱ_n is quite different from the concept of the density of normal electrons used in the two fluid model. Consequently, ϱ_{s} is not the density of super electrons; for instance, we will find $\varrho_{\mathrm{s}} = 0$ in the zero field equilibrium case.

  ** We may calculate the charge density using eq. (C), by noting that $\nabla^2 |\psi|^2$, and hence Φ will vary over distances approximately equal to the coherence length ξ (about 10^{-6} to 10^{-7} cm). Therefore, $\nabla^2 \Phi \leqslant \lambda_D^{-2} \Phi$ $(\lambda_{\mathrm{D}} \approx 10^{-7}$ cm), and in a first step we have

$$\Phi = \lambda_{\mathrm{D}}^2 \cdot \frac{2\pi e}{\varepsilon_{\mathrm{F}}} \cdot \frac{\hbar^2}{2m} \nabla^2 |\psi|^2$$

Using this result, we get

$$\varrho = -\frac{1}{4\pi} \nabla^2 \Phi = -\lambda_{\mathrm{D}}^2 \frac{e}{2\varepsilon_{\mathrm{F}}} \cdot \frac{\hbar^2}{2m} \nabla^4 |\psi|^2$$

ϱ may be estimated to be less than 10^4 esu $\approx 10^{-5}$Coul/cm^3, and the variations of Φ should be less than 10^{-6} esu $\approx 10^{-3}$ volts.

30.0.3 III. The Energy Theorem

In this section the balance of the free energy density of a superconductor in an electromagnetic field will be discussed on the basis of eqs. (A), (B) and (C). The free energy is the appropriate thermodynamic potential since the process discussed in this paper are at constant temperature.

The free energy density of the electromagnetic field F_{em} is given by

$$F_{\text{em}} = \frac{1}{8\pi}\left[\boldsymbol{H}^2 + \boldsymbol{E}^2\right] = \frac{1}{8\pi}\left[(\operatorname{curl}\boldsymbol{A})^2 + \left(\frac{1}{c}\frac{\partial}{\partial t}\boldsymbol{A} + \nabla\Phi\right)^2\right]. \tag{III.1}$$

The free energy density of the superconductor may be considered as consisting of two parts:
(i) the free energy density F_n of the metal in a normal state corresponding to the same values of its variables (temperature and density);
(ii) the free energy difference F_{sn} between superconducting and normal state.
F_{sn} is given by the expression of Ginzburg and Landau [1]

$$F_{\text{sn}} = \frac{1}{2m}\left|\left(\hbar\nabla + \frac{2ie}{c}\boldsymbol{A}\right)\psi\right|^2 - \alpha|\psi|^2 + \frac{\beta}{2}|\psi|^4 \tag{III.2}$$

since this relation is correct even in the case where the Ginzburg-Landau equation (II.1) is not fulfilled. We only have to remember that eq. (II.1) can be derived by minimizing F_{sn}, which means that F_{sn} displays the correct functional dependence on its variables in the neighborhood of the equilibrium states.

In the normal state, the only parameter which can be varied at constant temperature, is the density - ϱ/e. Using the thermodynamic relation $\frac{\partial F_{\text{n}}}{\partial(-\varrho/e)} = \mu^*$, we find

$$F_{\text{n}} = -\frac{1}{e}\int \mu d\varrho' \tag{III.3}$$

where some constant part has been discarded.
We calculate the change of the total energy density in time

$$\frac{dF}{dt} = \frac{dF_{\text{em}}}{dt} + \frac{dF_{\text{n}}}{dt} + \frac{dF_{\text{sn}}}{dt} \tag{III.4}$$

According to standard electrodynamies, the first term on the r.h.s. of eq. (III.4) can be written as follows

$$\frac{dF_{\text{em}}}{dt} = -\operatorname{div}\boldsymbol{S} - \boldsymbol{j}\cdot\boldsymbol{E}; \tag{III.5}$$
$$\boldsymbol{S} = \frac{c}{4\pi}\boldsymbol{E}\times\boldsymbol{H};$$

where $\boldsymbol{S}$ is the Pointing vector.
Using $\frac{\partial\varrho}{\partial t} = -\operatorname{div}\boldsymbol{j}$, we find the second term equal to

$$\frac{dF_{\text{n}}}{dt} = \frac{1}{e}\operatorname{div}\mu\boldsymbol{j} - \frac{1}{e}\boldsymbol{j}\nabla\mu \tag{III.6}$$

In calculating the last term, we obtain in a first stage

[0] $\star\lambda_{\text{L}}$ and $\varkappa$ are defined in ref. [1].

$$\frac{dF_{\rm sn}}{dt} = -j_{\rm s}\frac{1}{c}\frac{\partial}{\partial t}\boldsymbol{A} + 2\,\mathrm{Re}\,\frac{\partial\psi}{\partial t}\left[-\frac{1}{2m}\left(\hbar\nabla - \frac{2ie}{c}\boldsymbol{A}\right)^2 - \alpha + \beta|\psi|^2\right]\psi^* + \\ + 2\,\mathrm{Re}\,\frac{\hbar}{2m}\,\mathrm{div}\,\frac{\partial\psi}{\partial t}\left[\hbar\nabla - \frac{2ie}{c}\boldsymbol{A}\right]\psi^* \qquad \text{(III.7)}$$

where the definition of $\boldsymbol{j_s}$, eq. (B), has been used. Considering eqs. (II.13) and (B), we find that

$$-\boldsymbol{j}_{\rm s}\nabla\tilde{\Phi} + 2\,\mathrm{Re}\left(\frac{1}{\hbar}2ie\tilde{\Phi}\psi\right)\gamma\left[\hbar\frac{\partial}{\partial t} + 2ie\tilde{\Phi}\right]\psi^* + \\ + 2\,\mathrm{Re}\,\frac{1}{2m}\,\mathrm{div}(-2ie\tilde{\Phi}\psi)\left[\hbar\nabla - \frac{2ie}{c}\boldsymbol{A}\right]\psi^* \\ = -\boldsymbol{j}_{\rm s}\nabla\tilde{\Phi} - \tilde{\Phi}\nabla\boldsymbol{j}_{\rm s} + \nabla\left(\boldsymbol{j}_{\rm s}\tilde{\Phi}\right) = 0$$

The left hand expression will be added to r.h.s. of eq. (III.7). Using eq. (A), we put eq. (III.7) in the following form

$$\frac{dF_{\rm sn}}{dt} = -\boldsymbol{j}_{\rm s}\left[\frac{1}{c}\frac{\partial}{\partial t}\boldsymbol{A} + \nabla\tilde{\Phi}\right] - \frac{2\gamma}{\hbar}\left|\left(\hbar\frac{\partial}{\partial t} - 2ie\tilde{\Phi}\right)\psi\right|^2 + \\ + \mathrm{div}\,\mathrm{Re}\,\frac{1}{m}\left|\left[\hbar\nabla - \frac{2ie}{c}\boldsymbol{A}\right)\psi^*\right]\left[\left(\hbar\frac{\partial}{\partial t} - 2ie\tilde{\Phi}\right)\tilde{\psi}\right] \qquad \text{(III.8)}$$

Adding up the results (III.5, III. 6 and III.8), we finally obtain

$$\frac{dF}{dt} = -W - \mathrm{div}\,\boldsymbol{J}_{\rm E}$$
$$W = \sigma\left[\frac{1}{c}\frac{\partial}{\partial t}\boldsymbol{A} + \nabla\tilde{\Phi}\right]^2 + \frac{2\gamma}{\hbar}\left|\left(\hbar\frac{\partial}{\partial t} - 2ie\tilde{\Phi}\right)\psi\right|^2 \qquad \text{(D)}$$
$$\boldsymbol{J_E} = \boldsymbol{S} - \mu\boldsymbol{j}/e - \mathrm{Re}\,\boldsymbol{1}\,\frac{1}{m}\left[\left(\hbar\nabla - \frac{2ie}{c}\boldsymbol{A}\right)\psi^*\right]\left[\left(\hbar\frac{\partial}{\partial t} - 2ie\tilde{\Phi}\right)\psi\right]$$

We interprete this relation in the following way. The increase of the free energy density is always less than the energy accumulated by the energy current $\boldsymbol{J_E}$. The quantity W obviously represents a loss in reversible energy and, therefore, is the power dissipated in irreversible processes. The first part of W corresponds to the production of Joule heat of the normal electrons, whereas the second part is due to the finite relaxation time ($\gamma \neq 0$) of the wave function ψ. In terms of irreversible thermodynamics, this last part can be considered as the product of the time variation of a generalized coordinate, namely $\frac{\partial\psi}{\partial t} - \frac{2ie}{\hbar}\tilde{\Phi}_\psi$, times the force acting on it, which is given by the r.h.s. of eq. (A)*.

0

- Since the derivative is taken at fixed electromagnetic field, μ is the chemical, not the electrochemical potential.

30.0.4 IV. The Resistivity of Type II Superconductors

According to Abrikosov [2], there are two limiting cases for type II superconductors in the mixed state:
(i) the vicinity of the point of second order phase transition, where the magnetic field is close to H_{c2}, and $|\psi|^2$ is small;
(ii) the magnetic field is so small that only few fluxoids are in the superconductor.

In these two cases, we will determine that solution of eqs. (A), (B) and (C) which corresponds to the experimental situation in the investigations of Kim, Hempstead and Strnad [5]. The usual way of thinking of this situation is that a fixed transport current causes the fluxoids to move, which in turn gives rise to a voltage drop across the superconductor. On the other hand, one can equally well consider the voltage drop fixed, which maintains a transport current and forces the fluxoids to move. The latter picture is appropriate in case (i), where the superconductor is close to the normal state; and the first one is good in case (ii), where one is not far from ideal superconductivity.

According to the idea of a steady flow of fluxoids [5,6], we assume, in both cases, the time dependence of all quantities $X(\boldsymbol{r}, t)$ to be of the form $X(\boldsymbol{r} - \boldsymbol{v}t)$, where $\boldsymbol{v}$ is the drift velocity of the fluxoids. This implies that

$$\frac{\partial}{\partial t} X(\boldsymbol{r}, t) = -\boldsymbol{v} \cdot \nabla X(\boldsymbol{r}, t). \tag{IV.1}$$

Since the demagnetisation factors of the samples used in experiment are fairly high, we take the mean magnetic field in the superconductor, the induction B, as variable. The cases (i) and (ii) correspond to $B \to H_{c2}$ and $B \to 0$, respectively.

- The contribution to W which is connected with the time variation of the modulus of ψ, namely $2\gamma\hbar \left(\frac{\partial}{\partial t}|\psi|\right)^2$, is similar to the expression proposed by Tinkham [7] in order to account for relaxation effects in superconductors.

The ratio $R = \varrho_{\mathrm{i}}/\varrho_{\mathrm{n}}$, where ϱ_{f} and ϱ_{n} are the resistivities of the considered mixed state and of the normal state, respectively, will be a function of B such that $R\,(H_{\mathbf{c2}}) = 1$ and $R(0) = 0$. The restriction to the limiting cases (i) and (ii) means that we will determine dR/dB when $B = H_{c2}$ and $B = 0$. We note that $\varrho_{\mathrm{r}} = \langle \tilde{H} \rangle / \langle j \rangle (\langle \cdots \rangle$ means the average value) has to be calculated for vanishing small $\langle \tilde{H} \rangle$, which allows to simplify the calculations considerably.

Conveniently, we rewrite eqs. (A), (B) and (C) using reduced units. We put

$$\boldsymbol{r} = \lambda_{\mathrm{L}} \boldsymbol{r}'; \quad \boldsymbol{A} = \sqrt{2}\lambda_{\mathrm{L}} H_{\mathrm{cb}} \boldsymbol{A}'; \quad \psi = \sqrt{\frac{\alpha}{\beta}}\psi';$$

$$t = \frac{\hbar\gamma}{\alpha} t'; \quad \Phi(\tilde{\Phi}) = \frac{\alpha}{2e\gamma} \Phi'\left(\tilde{\Phi}'\right);$$

where $\lambda_{\mathrm{L}} \left(= \sqrt{mc^2\beta/16\pi e^2\alpha}\right)$ is the zero field penetration depth, $H_{\mathrm{cb}}\,(= 4\pi\alpha^2/\beta)$ the thermodynamic critical field. The substitutions in the first line are the usual ones; in the second line the scaling factors $\frac{\hbar\gamma}{\alpha}\,(= 2\tau_{\mathrm{R}})$ and $\frac{\alpha}{2e\gamma}$ are about $10^{-11}\frac{T_c}{T_c - T}$ sec, and $10^{-7}\frac{T_c - T}{T_c}$ esu. Using these substitutions and dropping the primes on the newly introduced quantities, we obtain

$$\left(\frac{1}{\varkappa}\nabla + i\boldsymbol{A}\right)^2 \psi + \psi - \left(\frac{\partial}{\partial t} - i\tilde{\Phi}\right)\psi - |\psi|^2\psi = 0 \qquad (\prime)$$

$$\nu_1\left(\frac{\partial^2}{\partial t^2}\boldsymbol{A} + \frac{1}{\varkappa}\frac{\partial}{\partial t}\nabla\Phi\right) + \operatorname{curl}\operatorname{curl}\boldsymbol{A} =$$

$$= -\Sigma\left(\frac{\partial}{\partial t}\boldsymbol{A} + \frac{1}{\varkappa}\nabla\tilde{\Phi}\right) + \frac{i}{2\varkappa}\left(\psi^*\nabla\psi - \psi\nabla\psi^*\right) - \boldsymbol{A}|\psi|^2 \qquad (\prime)$$

$$\frac{1}{\varkappa}\frac{\partial}{\partial t}\nabla\boldsymbol{A} + \frac{1}{\varkappa^2}\nabla^2\Phi = \nu_2(\Phi - \tilde{\Phi}) - \nu_3\nabla^2|\psi|^2 -$$

$$-\nu_4\left[\frac{i}{2}\left(\psi^*\frac{\partial\psi}{\partial t} - \psi\frac{\partial\psi^*}{\partial t}\right) + \tilde{\Phi}|\psi|^2\right] \qquad (\prime)$$

where $\varkappa$ is the Ginzburg-Landau constant, and

$$\begin{array}{ll} \nu_1 = \frac{14\zeta(3)}{\pi^4}\left(\frac{\varkappa\lambda_{\mathrm{D}}}{\lambda_{\mathrm{L}}}\right)^2; & \nu_2 = \left(\frac{\lambda_{\mathrm{L}}}{\varkappa\lambda_{\mathrm{D}}}\right)^2; \\ \nu_3 = \frac{1}{6}\frac{e^2 p_{\mathrm{P}}}{\hbar k T_{\mathrm{e}}}\frac{\chi(\varrho)}{x^2}; & \nu_4 = \frac{14\zeta(3)}{3}\frac{e^2 p_{\mathrm{F}}}{\hbar k T_{\mathrm{c}}}\frac{\varepsilon_{\mathrm{F}}}{kT_{\mathrm{c}}}\cdot\chi(\varrho); \\ \Sigma = \frac{m\beta}{4e^2\hbar\gamma}\cdot\sigma. & \end{array} \qquad \text{(IV.2)}$$

Concerning the order of magnitude of these coefficients, we observe that $v_1\,(v_2; \nu_3; \nu_4)$ is roughly about $10^{-4}\,(10^4; 10^5; 10^{10})$.Σ decreases with decreasing σ; in the limit of small σ (mean free path shorter than the coherence length ξ_0), Σ assumes a constant value

$$\Sigma_0 = \frac{14\zeta(3)}{\pi^4} = 0.173 \qquad \text{(IV.3)}$$

In these reduced units, the energy balance takes the form (the unit of energy is $H_{\mathrm{cb}}^2/4\pi$)

$$\frac{1}{2}\frac{dF}{dt} = -W - \operatorname{div}\boldsymbol{J}_{\mathrm{E}}$$

$$W = \Sigma\left(\frac{\partial}{\partial t}\boldsymbol{A} + \frac{1}{\varkappa}\nabla\tilde{\Phi}\right)^2 + \left(\left(\frac{\partial}{\partial t} - i\tilde{\Phi}\right)\psi\right|^2 \qquad (\prime)$$

$$\boldsymbol{J}_{\mathrm{E}} = \boldsymbol{E}\times\boldsymbol{H} - \frac{1}{\varkappa e}\mu\boldsymbol{j} - \operatorname{Re}\frac{1}{\varkappa}\left[\left(\frac{1}{\varkappa}\nabla - i\boldsymbol{A}\right)\psi^*\right]\left[\left(\frac{\partial}{\partial t} - i\tilde{\Phi}\right)\psi\right].$$

We are interested in the approximation linear in the driving field $\langle\tilde{E}\rangle$. In this approximation, eq. (II.13) allows to determine $\tilde{\Phi}$ directly provided the equilibrium values of $\psi, \boldsymbol{A}$, and Φ are known. Since we may safely assume the drift velocity to be proportional to $\langle\tilde{E}\rangle$, a quantity $\frac{\partial X}{\partial t} = -\boldsymbol{v}\cdot\nabla X$ can be replaced by - $\boldsymbol{v}\cdot\nabla X_{\mathrm{e}}$, where X_{e} is the equilibrium value of X. Therefore, we write eq. (II.13) in the following form *

$$-\frac{\Sigma}{x^2}\nabla^2\tilde{\Phi} + \tilde{\Phi}\,|\psi_{\mathrm{e}}|^2 =$$

$$= \frac{i}{2}v\cdot\left(\psi_{\mathrm{e}}^*\nabla\psi_{\mathrm{e}} - \psi_{\mathrm{e}}\nabla\psi_{\mathrm{e}}^*\right) - v\cdot\nabla\left(\frac{\Sigma}{\varkappa}\nabla\cdot\boldsymbol{A}_{\mathrm{e}}\right) - v\cdot\nabla\left(\frac{v_1}{x^2}\nabla^2\Phi_{\mathrm{e}}\right); \qquad \text{(IV.4)}$$

where, according to eq. (C′),

$$\frac{1}{\varkappa^2}\nabla^2\Phi_{\mathrm{e}} = v_2\Phi_{\mathrm{e}} - v_3\nabla^2\,|\psi_{\mathrm{e}}|^2\,. \qquad \text{(IV.5)}$$

(i) Vicinity of phase transition. If $B \to H_{c2}, |\psi|^2 \to 0$. Therefore, a zero order solution of eqs. (B') and (IV.4) is

$$\begin{aligned} \boldsymbol{A}^{(0)} &= \left(0, H^{(0)}x, 0\right) \\ \tilde{\Phi}^{(0)} &= -\varkappa \tilde{E}_x^{(0)} x \end{aligned} \tag{IV.6}$$

which corresponds to an effective electric field $\tilde{\boldsymbol{E}}^{(0)} = \left(\tilde{E}_x^{(0)}, v_x H^{(0)}, 0\right)$ perpendicular to the magnetic field $\boldsymbol{H}^{(0)} = \left(0, 0, H^{(0)}\right)$. Thereby, we have neglected the magnetic field due to the transport current, which is supposed to be compensated.

We insert the quantities (IV.6) in (A'), perform the time derivative according to eq. (IV.1), and neglect the cubic term. Since there is no dependence on z, the general solution of this equation is

$$\psi^{(0)} = \sum_k C_k e^{iky} \varphi_k(x) \tag{IV.7}$$

where

$$\frac{1}{\varkappa^2}\frac{\partial^2}{\partial x^2}\varphi_k + \left(\frac{ik}{\varkappa} + iH^{(0)}x\right)^2 \varphi_k + \varphi_k + v_x \frac{\partial}{\partial x}\varphi_k + ikv_y\varphi_k - i\varkappa \tilde{E}_x^{(0)} x \varphi_k = 0$$

Putting $\varphi_k = u_k \exp\left(-\frac{1}{2}\varkappa^2 v_x x\right)$, we find a harmonic oscillator type equation for $u_k(x)$ [15]. In order to have φ_k bounded, we have to put $v_y = -\tilde{E}_x^{(0)}/H^{(0)}$. Furthermore, we have to require that $H^{(0)}$ is as large as possible. This implies $v_x = 0$; and, therefore, $\tilde{\boldsymbol{E}}(0) = \left(\tilde{E_x^{(0)}}, 0, 0\right)$. These results may be put in the following form

$$\tilde{E}(0) = -v \times H^{(0)} \tag{IV.8a}$$

which, in ordinary units, corresponds to *

$$c\tilde{\boldsymbol{E}}^{(0)} = -\boldsymbol{v} \times \boldsymbol{H}^{(0)} \tag{IV.8b}$$

In addition, we have

$$\begin{aligned} H^{(0)} &= \varkappa \left[1 - \left(\varkappa E_x^{(0)}/2H^{(0)}\right)^2\right] \\ \varphi_k &= \exp\left(-\frac{1}{2}\varkappa H^{(0)}\left[x + \frac{1}{\varkappa H^{(0)}}\left(k + i\varkappa \tilde{E}_x^{(0)}/2H^{(0)}\right)\right]^2\right) \end{aligned} \tag{IV.9}$$

In the next step, we determine $\boldsymbol{j}_\delta^{(1)}$, which is obtained by inserting $\boldsymbol{A}^{(0)}$ and $\psi^{(0)}$ in the corresponding expression:

0

- One may doubt whether eq. (IV.1) can be applied to quantities as $A, \Phi, \tilde{\Phi}$ and ψ, which have no direct physical meaning. However, if one uses the relation (IV.1) for all these quantities simultaneously, possible mistakes will cancel (this implies for instance that the electric field is now defined by $\boldsymbol{E} = (\boldsymbol{v}\cdot\nabla)\boldsymbol{A} - \frac{1}{\varkappa}\nabla\Phi\big)$. One may convince oneself that, indeed, eq. (IV.4) is gauge invariant.

$$j_{sx}^{(1)} = \frac{\varkappa}{2H^{(0)}}\tilde{E}_x^{(0)}\left|\psi^{(0)}\right|^2 \qquad -\frac{1}{2\varkappa}\frac{\partial}{\partial y}\left|\psi^{(0)}\right|^2$$

$$j_{sy}^{(1)} = \qquad +\frac{1}{2\varkappa}\frac{\partial}{\partial x}\left|\psi^{(0)}\right|^2 \tag{IV.10}$$

The mean value $\left\langle \boldsymbol{j}_{\mathrm{s}}^{(1)} \right\rangle$ has only a component in x direction equal to

$$\frac{x}{2\tilde{H}^{(0)}}\langle|\psi^{(0)}\Big|^2\Big\rangle\tilde{E}_x^{(0)}.$$

The ratio R is given by

$$R = \frac{\varrho_{\mathrm{f}}}{\varrho_n} = \frac{\Sigma\langle\tilde{E}\rangle}{\Sigma\langle\tilde{E}\rangle + \langle j_{\mathrm{s}}\rangle} = \left(1 + \langle j_{\mathrm{s}}\rangle / \Sigma\langle\tilde{E}\rangle\right)^{-1}.$$

For the purpose of calculating $\frac{dR}{dB}\big|_{B=H_{c^2}}$, we can neglect terms of higher order than $\left|\psi^{(0)}\right|^2$ in $\langle j_{\mathrm{s}}\rangle \mid \Sigma\langle\tilde{E}\rangle$ and, therefore, we are allowed to replace $\langle j_{\mathrm{s}}\rangle$ by $\left\langle j_{\mathrm{s}}^{(1)}\right\rangle$, and $\langle\tilde{E}\rangle$ by $\left\langle \tilde{E^{(0)}}\right\rangle$. Hence

$$R = 1 - \frac{x}{2\Sigma\ddot{H}(0)}\langle|\psi^{(0)}\Big|^2\Big\rangle. \tag{IV.11}$$

In the linear approximation, $\langle|\psi^{(0)}\big|^2\rangle$ may be replaced by its equilibrium value, which, according to Abrikosov [2], is given by**

$$\langle|\psi^{(0)}\big|^2\rangle = \frac{2\varkappa^2}{1 + 1.16\,(2\varkappa^2 - 1)}\left(1 - \frac{B}{H_{\mathrm{c}2}}\right). \tag{IV.12}$$

Considering eqs. (IV.11, IV.12), we find the slope of $R(B), B = H_{\mathrm{c}2}$, equal to

$$\left.\frac{dR(B)}{dB}\right|_{B=H_{c2}} = \frac{x^2}{\Sigma\left[1 + 1.16\,(2\varkappa^2 - 1)\right]}\frac{1}{H_{c2}(\bar{T})}. \tag{IV.13a}$$

This equation holds equally in ordinary units. For superconductors of short mean free path ($l < \xi_0$), the value of $\sum$ is given by eq. (IV.3); then we have

$$\left.\frac{dR(B)}{d\bar{B}}\right|_{B=H_{c2}} = \frac{2.5}{H_{\mathrm{c}2}(T)} \tag{IV.13b}$$

We compare relation (IV.13) with experimental results. For different reduced temperatures T/T_{c}, a plot $R = R(B)$ of experimental data is given in Fig. 4 of ref. [5a], and in Fig. 2a of

0

- More generally, this equation reads

$$c\langle\tilde{\boldsymbol{E}}\rangle = -\boldsymbol{v}\times\langle\boldsymbol{H}\rangle.$$

Sometimes, $\langle\tilde{\boldsymbol{E}}\rangle$ is referred to as the electric field induced by moving fluxoids [5]. However, this argument has not always been found to be convincing [16]. An alternative possibility toexplain this equation is to state that, if not subject to extra forces, the superconductive wave function moves with a drift velocity such that the mean electric field in the moving frame of reference vanishes.

** Concerning the value 1.16 see ref. [17].

ref. [5b]. According to relation (IV.13), the slope of R changes discontinuously at $B = H_{c2}$, whereas the experimental curves have a rounded knee in the transition region. Our assumption is that this rounded knee results from experimental circumstances. Therefore, we will neglect the rounded part of the experimental curve and take $\frac{dR}{dB}\big|_{B=H_{c2}}$ equal to the steepest slope of $R(B)$, just before it reaches the value 1 . Using this prescription, we find
a) sample $Nb_{0.5}Ta_{0.5}$

T/T_c		0.7	0.6	0.5	0.3
$H_{c2}\frac{dR}{dB}\big\|_{B=H_{c2}}$	2.2	2.0	2.0	2.5	

b) sample $Nb_{0.1}Ta_{0.9}$

T/T_c		0.92	0.79	0.64	0.44	0.35
$H_{c2}\frac{dR}{dB}\big\|_{B=H_{c2}}$	2.8	3.0	3.0	4.4	6.3	

The data confirm relation (IV.13) in so much, as $H_{c2}\frac{dR}{dB}\big|_{B=H_{c2}}$ does not depend on temperature, if the temperature is not too low, say $T/T_c \geqq 0.6$. We find $H_{c2}\frac{dR}{dB}\big|_{B=H_{c2}}$ equal to 2.1 ± 0.1, and 2.9 ± 0.1 for superconductor a) and b), respectively. In both cases, the mean free path of the superconductors is short enough such that the theoretical value 2.5 should be appropriate for $H_{c2}\frac{dR}{dB}\big|_{B=H_{ea}}$. Within 20%, this value agrees with the experimental result. This should be considered a good agreement on account of the uncertainties in defining the final slope of the experimental curves. As far as the low temperature behavior is concerned, there is no doubt that in this case the equations (A), (B) and (C) cannot be considered as accurate enough.
(ii) Small fields. In this case, the calculation follows in principle the procedure of Stephen and Bardeen [6]. We will calculate the energy dissipated by a moving fluxoid. This energy has to be equal to the energy input via transport current, since the total free energy of the superconductor is constant in a state of steady flow.

Considering eq. (D′), the total dissipated power (per unit volume) is given by $D = \frac{1}{V}\int d^3\boldsymbol{r} W(\boldsymbol{r}, t)$, where V is the volume of the superconductor. Reasoning in the same way as done in deriving eq. (IV.4), we find that the leading part of D, which is proportional to the square of the drift velocity $\boldsymbol{v} = (0, v, 0)$ is obtained by replacing A and ψ by their equilibrium values. Therefore,

$$D = \frac{1}{V}\int d^3\boldsymbol{r}\Sigma\left(v\frac{\partial}{\partial y}A_e - \frac{1}{\varkappa}\nabla\tilde{\Phi}\right)^2 + \frac{1}{V}\int d^3\boldsymbol{r}\left|\left(-v\frac{\partial}{\partial y} - i\tilde{\Phi}\right)\psi e\right|^2; \tag{IV.14}$$

where $\tilde{\Phi}$ is defined by eq. (IV.4).

In equilibrium, the wave function of a single fiuxoid is, in cylindrical coordinates, of the form

$$\psi_e = f(r)e^{i\varphi}$$

We do not know $f(r)$ exactly; however, the approximation

$$f(r) = \frac{\varkappa r}{\sqrt{\varkappa^2 r^2 + 2}}$$

is reasonable and allows simple calculations. When $x \gg 1$, this ansatz yields the energy per unit length of the fluxoid $\varepsilon = 2\pi[\ln\varkappa + 0.52]/\varkappa^2$, which agrees sufficiently with Abrikosov's value $\varepsilon = 2\pi[\ln x + 0.08]/x^2$.

We put

$$\boldsymbol{Q} = \boldsymbol{A}_e + \frac{1}{\varkappa}\nabla\varphi = Q(r)[-\sin\varphi, \cos\varphi, 0]; \tag{IV.1.5a}$$

and in equilibrium, eq. (B′) becomes

$$\frac{d}{dr}\frac{1}{r}\frac{d}{dr}rQ(r) = f^2Q(r) \tag{IV.16}$$

The appropriate solution of this equation is

$$Q(r) = \frac{\sqrt{x^2r^2/2+1}}{xr}\frac{K_1\left(\frac{1}{x}\sqrt{x^2r^2+2}\right)}{K_1(\sqrt{2}/x)} \tag{IV.15b}$$

where K_n is the modified Bessel function of second kind and order n.
Concerning eq. (IV.4), which determines $\tilde{\Phi}$, we can discard the last term of the r.h.s. of this equation. Since $\varkappa^2\nu_2 \gg 1$, it follows from eq. (IV.5) that $\Phi_\mathrm{e} = \frac{\nu_3}{\nu_2}\nabla^2 f^2$. Therefore, $v\frac{\partial}{\partial y}\frac{\nu_1}{x^2}\nabla^2\Phi_\mathrm{e}$ is equal to $v\frac{\partial}{\partial y}\frac{\nu_1\nu_3}{x^2\nu_2}\nabla^4 f^2$ and hence, it is smaller than the first term by roughly the factor $\frac{\nu_1\nu_3}{\nu_2} \approx 10^{-3}$. This result has an interesting consequence. It actually means that in sufficient approximation the total current $\boldsymbol{j}_\mathrm{n} + \boldsymbol{j}_\mathrm{s}$ is free of divergences.

Since $\operatorname{div}\boldsymbol{A}_\mathrm{e} = 0$, eq. (IV.4) becomes

$$-\frac{\Sigma}{x^2}\nabla^2\tilde{\Phi} + f^2\tilde{\Phi} = -vf^2\frac{\partial}{\partial y}\varphi = -vf^2\frac{\cos\varphi}{r} \tag{IV.17}$$

$\tilde{\Phi}$ is obviously proportional to $\cos\varphi$. Putting

$$\tilde{\Phi} + v\frac{\partial}{\partial y}\varphi = P(r)\cos\varphi \tag{IV.18a}$$

we obtain the differential equation of $P(r)$ quite similar to eq. (IV.16). From there we get the solution

$$P(r) = v\frac{\sqrt{x^2r^2/2+1}}{xr}\frac{K_1\left(\sqrt{x^2r^2+2/\Sigma}\right)}{K_1(\sqrt{2/\Sigma})} \tag{IV.18b}$$

Corresponding to eqs. (IV.15, IV.18), the magnetic and electric fields vanish proportional to e^{-r} as $r \gg 1$ and, therefore, fluxoids which are sufficiently separated will not influence each other. If there are N fluxoids per unit area, the resulting field is the sum of the fields of the individual fluxoids. Calculating the mean effective electric field in this way, we obtain

$$\left\langle \tilde{\boldsymbol{H}}_x \right\rangle = N\int dxdy\left[v\frac{\partial}{\partial y}\left(A_\mathrm{e}\right)_x - \frac{1}{x}\frac{\partial}{\partial x}\tilde{\Phi}\right] = -\frac{2\pi}{x}Nv \tag{IV.19}$$

and $\left\langle \tilde{E}_y \right\rangle = 0$. Furthermore, the mean magnetic field B is $-\frac{2\pi}{\varkappa}N$ such that - (see eq. (IV.8)
-

$$\left\langle \tilde{E}_x \right\rangle = -vB \tag{IV.20}$$

We found the divergence of the total current to be zero. Since the internal currents of the superconductor are free of divergences, we conclude, that the transport current $\boldsymbol{j}_T$ is constant in space, equal to $\langle \boldsymbol{j} \rangle$. We assume $\boldsymbol{j}_T$ parallel to the mean electric field. Therefore, the energy input per unit volume via the transport current is given by

$$\left\langle \boldsymbol{J}_\mathrm{T} \cdot \tilde{\boldsymbol{E}} \right\rangle = j_\mathrm{T}\left\langle \tilde{\boldsymbol{E}}_x \right\rangle. \tag{IV.21}$$

The expression (IV.21) has to be equal to the dissipated power. Considering eq. (IV.14), we put $D = N\eta v^2 = N\eta_1 v^2 + N\eta_2 v^2$, and using the results (IV.15, IV.18), we obtain

$$\eta_1 = \frac{\pi}{2}\left(\frac{\Sigma}{\varkappa^2} - \frac{K_1^2(\sqrt{2}/\varkappa) - K_0^2(\sqrt{2}/\varkappa)}{K_1^2(\sqrt{2}/\varkappa)} + \frac{K_1^2(\sqrt{2}/\Sigma) - K_0^2(\sqrt{2}/\Sigma)}{K_1^2(\sqrt{2/\Sigma})}\right); \tag{IV.22a}$$

$$\eta_2 = \frac{\pi}{2}\left(\frac{1}{2} + \frac{K_2(\sqrt{2/\Sigma})K_0(\sqrt{2/\Sigma}) - K_1^2(\sqrt{2/\Sigma})}{K_1^2(\sqrt{2/\Sigma})}\right).$$

In the limit of show mean free path, we have $\sqrt{2/\Sigma} = 3.4$, and hence,

$$\eta_1 = 0.11\pi; \quad \eta_2 = 0.43\pi \tag{IV.22b}$$

We are now able to calculate the ratio R. Using eqs. (IV.21, IV.22), we obtain

$$R = \Sigma\frac{\langle\tilde{E}\rangle}{\langle\tilde{j}\rangle} = \Sigma\frac{\langle\tilde{E}\rangle^2}{N\eta v^2} = \frac{2\pi\Sigma}{\eta}B$$

where B has to be a positive quantity. From there, we find the slope of R at $B = 0$ equal to

$$\left.\frac{dR}{dB}\right|_{B=0} = \frac{2\pi}{\eta}\cdot\frac{1}{H_{c2}(T)} \tag{IV.23a}$$

which reduces to

$$\left.\frac{dR}{dB}\right|_{B=0} = \frac{0.64}{H_{c2}(T)} \tag{IV.23b}$$

in the above mentioned limit.
Kim, Hempstead and Strnad [5a] have represented their experimental results by the following formula

$$\left.\frac{dR}{d\bar{B}}\right|_{B=0} = \frac{1}{H_{c2}(T=\bar{0})}\cdot f\left(T/T_c\right)$$

where $f\left(T/T_c\right)$ is a universal function practically independent of T and such that $f(0) = 1$. For $T/T_c \approx 0.6$, experimental and theoretical results coincide; however, the general temperature dependence is different. As far as the lack of agreement at lower temperatures is concerned (at $T = 0$, the theoretical value is about 40%
too low), it may be explained very well by the restricted validity of the eqs. (A-C). In the high temperature range, however, we do not think the experimental formula to be very reliable. The initial slope of R cannot remain finite as $T \to T_c$, since the B values for which R has to reach unity ($B = H_{c2}$) will approach zero. (Note that the behavior of the sample $Nb_{0.1}Ta_{0.9}$ of ref. [5b] seems to indicate an appreciable variation of the initial slope and thus does not confirm the assumption $f \approx 1$.)

Most of this work was done during a stay at the University of Illinois, Urbana; and I wish to thank very much for the hospitality. In particular, I gratefully acknowledge the stimulating discussions with Professor J. Bardenn, which led to the idea of this work. Furthermore, I take the opportunity to thank Professor G. Falk for many helpful comments.

31 Stability of nonequilibrium Fermi distributions with respect to Cooper pairing by Aronov, Gurevich

(current conclusion: I don't understand this article, because it uses Keldysh's formalism, which I don't know yet)

Abstract

The stability of normal and superconducting nonequilibrium Fermi systems relative to Cooper pairing and Cooper pair decay, respectively, is investigated. If the inequality $\hbar/\tau\Delta \ll 1$ is obeyed, where Δ is the superconducting gap thickness and τ is the electron-phonon collision time, the stability condition does not depend explicitly on the method whereby the imbalance is produced, and is expressed only in terms of the superconducting excitation distribution function $m(\epsilon)$. It is shown that if the sign of the difference $1-2m(\epsilon)$ is constant throughout the complete energy region ϵ, the superconducting state will be stable. The stability condition obtained in the paper is used to analyze a number of concrete cases.

31.0.1 1. Introduction

The question of the possibility of Cooper pairing of electrons under strongly nonequilibrium conditions has recently evoked considerable interest from the experimental point of view [1,2] as well as from the point of view of theoretical developments. [3–12]

As Éliashberg has shown, [6] in a number of interesting cases even in nonequilibrium systems the gap parameter Δ is determined from the BCS equation, in which it is only necessary to replace the equilibrium distribution function of the superconducting excitations by the nonequilibrium one:

$$\Delta = -\lambda N(0) \int_{\Delta}^{\omega_D} \Delta \frac{n(-\varepsilon) - n(\varepsilon)}{(\varepsilon^2 - \Delta^2)^{1/2}} d\varepsilon \tag{1.1}$$

where λ is the effective coupling constant of the electron-electron interaction, N(0) is the density of electron states near the Fermi surface, ω_D is the limiting frequency of the Debye phonons, and $n(\epsilon)$ is the (nonequilibrium) distribution function of the superconducting excitations. It is determined by the type of external perturbation creating the nonequilibrium state, and it also depends on Δ as a parameter. If the distribution function is anisotropic, then n(ϵ) should be understood as the corresponding average value over a surface of constant energy. In the so-called symmetric case, which we shall mainly be occupied with in what follows, one has

$$n(-\varepsilon) = 1 - n(\varepsilon). \tag{1.2}$$

Let Eq. (1.1) have a nontrivial solution. For the sake of definiteness, we first assume this solution to be unique. In addition, a solution with $\Delta = 0$ also exists. Thus arises the necessity of comparing these two solutions and ascertaining which of them will actually be realized.

In the equilibrium case this question can be resolved on the basis of simple energy considerations. The solution with $\Delta \neq 0$ would correspond to a smaller energy of the ground state (or, at finite temperatures below the critical temperature-it would correspond to a smaller value of the free energy) than the solution with $\Delta = 0$. In nonequilibrium cases simple energy considerations do not permit us to compare these two states since the energy of the superconductor is not conserved: it interacts with the external system creating the nonequilibrium. Therefore, in order to solve the problem which has been posed, it is natural to investigate the stability of these two states: the state with $\Delta = 0$ with regard to Cooper
pairing, and the state with $\Delta \neq 0$ with regard to the destruction of the pairs. In order to do this it is necessary to calculate the two-particle retarded Green's function of the electrons in a conductor for small total momentum and energy of the electrons. If the Green's function, regarded as a function of the total energy, has a pole in the upper half-plane, this implies instability. The instability of a normal Fermi system with attractive interactions for T = 0 is established in such a manner. [13a] The stability of the normal, nonequilibrium Fermi distribution was first investigated by Batyev [4] in the same way, using Keldysh's diagram technique. [14]

The stability of the state with $\Delta \neq 0$ with respect to small fluctuations of the order parameter Δ is investigated in the present article. The solution of the stability problem is greatly facilitated owing to the fact that here the nonequilibrium distribution function of the excitations can be regarded as fixed. The point is that in order to investigate the stability of the system with regard to pairing, it is sufficient to trace its evolution during a time interval of order $\hbar/\Delta$. This time interval is assumed to be much smaller than the characteristic elec-tron-phonon collision time τ, during which pronounced changes occur in the average values of the quasi-particle distribution functions. We substantially utilize the inequality $\hbar/\tau\Delta \ll 1$ in the construction of the theory. It is found that the superconducting nonequilibrium state is stable in all cases when Eq. (1.1) has a nontrivial solution and the difference $\mathrm{n}(-\epsilon) - \mathrm{n}(\epsilon)$ keeps the same sign for all $\epsilon > 0$.

However, if the sign of the difference $n(-\epsilon) - n(\epsilon)$ is not constant, then the system generally possesses a number of nontrivial properties. Thus, additional modes of collective oscillations, which are not present in the equilibrium superconductor, may exist in it. Furthermore, the system may turn out to be unstable with respect to fluctuations of the order parameter Δ, where the instability manifests itself as an increase in the amplitude of these collective oscillations. An example of such an instability is considered in Sec. 4.

For a system in an external field, the investigation of stability is valid only when the momentum acquired by a Cooper pair during the field's period $1/\Omega$ (or, in the case of a constant field, over the length of the sample) is small in comparison with the coherence length ξ : [1)]

$$eE/\Omega \ll \hbar/\xi = \hbar m\Delta/p_F,$$

where $\mathrm{p_F}$ is the "Fermi momentum," that is, the momentum corresponding to the middle of the energy gap. This criterion turns out to be substantially more stringent than the requirement that $e^2E^2/\mathrm{m}\Omega^2$ be small in comparison with Δ; it characterizes the accuracy of our theory in determining the critical value Δ_c, corresponding to the boundary of the stability region.

In the case of a normal conductor one can show that the influence of the field can be neglected if its work on a pair during one period of the field is small in comparison with the increment of growth of the amplitude of the Cooper pair wave function. The theory can actually be applied to the case when the electron distribution function is noticeably perturbed near the Fermi surface whereas the influence of the field on the dynamics of the electrons is negligible-for example, if the nonequilibrium distribution appeared in connection with the illumination of a thin metal film.

Hitherto the question has only been the dynamical stability of the system with respect to Cooper pairing. However, since the topic of discussion is strongly nonequilibrium systems it is necessary in general to also investigate their stability with respect to perturbations of the quasi-particle distribution functions. This investigation is carried out mainly by standard methods with the help of the kinetic equation. It is only necessary to keep the following point in mind. It turns out to be possible to investigate the dynamical stability of the system for a fixed quasi-particle distribution function. On the other hand, it is impossible to investigate the stability of the distribution function for a fixed spectrum because the magnitude of the gap Δ and together with it the transition probabilities as well depend on the shape of the distribution function. Therefore, a perturbation of the distribution function must lead to a perturbation of the order parameter, and therefore also leads to a perturbation of the transition probabilities.

We shall use the results of the general theory in order to investigate the stability in a number of specific cases. In particular, one unusual example is consid-ered-the so-called inverse Fermi distribution. We want to explain [2)] the fact (which appears to be paradoxical at first glance) that Eq. (1.1) has a nonvanishing solution Δ for $\lambda > 0$ (repulsion) for the case when the distribution function $n(\epsilon)$ has the following form in the energy range of interest to us: $n(\epsilon) = 1$

for $\epsilon > 0$ and $n(\epsilon) = 0$ for $\epsilon < 0$. In this case the solution with $\Delta = 0$ turns out to be unstable with respect to pairing, and the solution with $\Delta \neq 0$ turns out to be stable.

One might describe the physics of this bound state in the following way. The inverse distribution of Fermi particles is equivalent to an ordinary distribution of Fermi holes with a negative effective mass. But, as is clear from an analysis of the corresponding Schrödinger equation, particles with negative effective mass form bound states in the presence of repulsion. The case of the bielectron [15] is a well-known example of this.

The bound states, which arise in the present case, form a Bose condensate, a gap appears in the spectrum of the single-particle excitations, and the total energy of the system increases upon pairing. One can verify this, in particular, by calculating the energy of the system as a function of Δ. The energy has a maximum at the value of Δ determined from condition (1.1).

Thus, in the present example we verify that energy considerations in general do not permit us to judge the dynamical stability of a nonequilibrium system. It should be noted that it is necessary to consider the inverse Fermi distribution as a purely model example because of the following reason. If it is assumed that, upon a further increase of the energy ϵ within the limits of the same band, the function $n(\epsilon)$ again vanishes, then even though such a scheme is stable with respect to the generation of plasmons and other longitudinal oscillations, [13 b] the characteristic electron-electron collision time τ_e in it turns out to be so small that the parameter $\hbar/\tau_e\Delta$ turns out to be of the order of unity in the best case. However, if $n(\epsilon) = 1$ right up to the edge of the forbidden band, then the corresponding system is unstable with respect to the generation of plasmons and other longitudinal oscillations.

We shall use the diagram technique developed by Keldysh. [14] It permits us to determine simultaneously the energy spectrum of a nonequilibrium system and also its kinetic characteristics, that is, in our case we can determine the nonequilibrium distribution function of the superconducting excitations. In particular, an expression for the operator describing the collisions of the excitations with phonons is obtained by such a method. The corresponding expression was previously obtained by Éliashberg. [6]3) However, our expression (2.18) is applicable to any anisotropic, nonequilibrium distribution function, and is not averaged over angles, as was done in [6].

31.0.2 2. Derivation of the Kinetic Equation

Following Keldysh, [14] we define the normal Green's function of the electrons in the following way:

$$\hat{G^{\alpha\beta}}(x,x') \equiv \begin{pmatrix} G_c^{\alpha\beta}(x,x') & G_+^{\alpha\beta}(x,x') \\ G_-^{\alpha\beta}(x,x') & G_c^{\alpha\beta}(x,x') \end{pmatrix} = \begin{pmatrix} G_{11}^{\alpha\beta} & G_{12}^{\alpha\beta} \\ G_{21}^{\alpha\beta} & G_{22}^{\alpha\beta} \end{pmatrix} = \\ = \begin{pmatrix} -i\left\langle T\psi_\alpha(x)\psi_\beta{}^+(x')\right\rangle, & i\left\langle \psi_\beta{}^+(x')\,\psi_\alpha(x)\right\rangle \\ -i\left\langle \psi_\alpha(x)\psi_\beta{}^+(x')\right\rangle, & -i\left\langle \tilde{T}\psi_\alpha(x)\psi_\beta{}^+(x')\right\rangle \end{pmatrix} \tag{2.1}$$

Here α and β are spin indices, T and $\tilde{\mathrm{T}}$ denote T-products and anti-T-products, respectively, and the angular brackets denote averages with respect to the unperturbed Hamiltonian.

In analogous fashion we introduce the matrix functions $\hat{\mathbf{F}}$ and ${}^+\hat{\mathbf{F}}$:

$$F^{\alpha\beta}(x,x') = \begin{pmatrix} \left\langle T\psi_\alpha(x)\psi_\beta(x')\right\rangle, & -\left\langle \psi_\beta(x')\,\psi_\alpha(x)\right\rangle \\ \left\langle \psi_\alpha(x)\psi_\beta(x')\right\rangle, & \left\langle \tilde{T}\psi_\alpha(x)\psi_\beta(x')\right\rangle \end{pmatrix} \equiv \begin{pmatrix} F_c^{\alpha\beta}(x,x') & F_+^{\alpha\beta}(x,x') \\ F_-^{\alpha\beta}(x,x') & F_c^{\alpha\beta}(x,x') \end{pmatrix} \tag{2.2}$$

The function ${}^{+}\hat{F}$ is obtained from $\hat{F}$ by replacing all of the operators ψ in Eq. (2.2) by ψ^{+}. As is usually done, let us assume that the interaction does not depend on the spins. Then

$$\hat{G}_{\alpha\beta}^{\alpha\beta}(x,x') = \hat{G}(x,x')\,\delta_{\alpha\beta}, \quad \hat{F}^{\alpha\beta}(x,x') = -\hat{F}(x,x')\,I_{\alpha\beta}$$
$$\hat{I} = \begin{pmatrix} 0 & 1 \\ -1 & 0 \end{pmatrix} i\sigma_y$$

(there is no explanation here, for understanding why we are working this way, one needs to see other articles or books!)

Similarly we find:

$${}^{+}F^{\alpha\beta} = {}^{+}FI_{\alpha\beta}$$

The phonon Green's function is given by

$$\hat{D} = \begin{pmatrix} D_c D_+ \\ D_- \widetilde{D}_c \end{pmatrix} = \begin{pmatrix} -i\left\langle T\varphi(x)\varphi(x')\right\rangle, & -i\left\langle \varphi(x')\varphi(x)\right\rangle \\ -i\left\langle \varphi(x)\varphi(x')\right\rangle, & -i\left\langle \tilde{T}\varphi(x)\varphi(x')\right\rangle \end{pmatrix} \tag{2.3}$$

Later we shall be interested in the case of a spatially homogeneous system, where the Green's functions depend on the difference between the spatial coordinates. Then, assuming that the Green's functions are slowly varying functions of the total time t, and evaluating the Fourier component with respect to the difference of coordinates and times, we obtain the following result in the zero-order approximation (furthermore, we take $\hbar = 1$):

$$\hat{G}_0^{-1} = \left(\frac{i}{2}\frac{\partial}{\partial t} + \varepsilon - \xi_{\mathrm{p}}\right)\hat{\sigma}_z, \tag{2.4}$$

where σ_Z is a matrix which acts on the lower indices (not the spin indices) of the Green's function, $\xi_{\mathrm{p}} = (\mathrm{p}^2/2\ \mathrm{m}) - \mu$, μ denotes the origin with respect to which the energy is measured; later on we choose this to coincide with the middle of the superconducting energy gap.

The Feynman diagram technique can be used for the functions $\hat{G}$ and $\hat{F}$, and consequently the corresponding system of Dyson equations has the form

$$\left(\frac{i}{2}\frac{\partial}{\partial t} + \varepsilon - \xi_{\mathrm{p}}\right)\sigma_z\hat{G}(p,t) = \hat{1} + i\hat{\Sigma}(p,t)\hat{G}(p,t) + i\hat{\Delta}(p,t)^{+}\hat{F}(p,t)$$
$$\left(\frac{i}{2}\frac{\partial}{\partial t} - \varepsilon - \xi_{\mathrm{p}}\right)\sigma_z{}^{+}\hat{F}(p,t) = i\hat{\Sigma}^{T}(-p,t)^{+}\hat{F}(p,t) + i^{+}\hat{\Delta}(p,t)\hat{G}(p,t) \tag{2.5}$$

(???? why???)

One can isolate the system of equations for $G_c(p,t)$ and ${}^{+}F_c(p,t)$ from the system (2.5) by taking the 11-component in the matrix equations. In this connection we discard the time derivative and also all terms which contain the functions G_+, D_+, and ${}^{+}F_+$. The latter step is permissible if the parameter $1/\tau\Delta$ is small, where τ is the characteristic time for electron-phonon collisions.

(??? why this approach works for noneqSC??? how does it generalizes eq sc approach???)

As an example let us present the expression for the self-energy part Δ_c, which appears in the right-hand side of the equation

$$\Delta_{\mathrm{c}}(\varepsilon,\mathbf{p}) = \int\frac{d^3q}{(2\pi)^3}\int\frac{d\omega}{2\pi}\left|c_{\mathbf{q}}\right|^2 D_c(-\mathbf{q},-\omega)F_{\mathrm{c}}(\mathbf{p}-\mathbf{q},\varepsilon-\omega), \tag{2.6}$$

where c_q is the electron-phonon coupling constant (I'll change notation later). Just as in the equilibrium case, the dispersion $\Delta_c(\epsilon, p, t)$ arises for $\epsilon \sim \omega_D$. For our purposes, however, as will be clear from what follows below, energies $\epsilon \ll \omega_D$ are important. In addition, just like in the equilibrium case, frequencies $\omega \approx \Delta(0, p_F) \ll \omega_D$ are essential in Eq. (2.6). Taking these inequalities into account, we obtain, just as in the equilibrium case, the following equation for $\Delta_c(0, p_F)$:

(??? I don't understand how the transformation is done???)

$$\Delta = -\frac{\lambda}{2}\int \frac{d^3p}{(2\pi)^3}\int \frac{d\varepsilon}{2\pi}F_c(\varepsilon, \mathbf{p}) \tag{2.7}$$

where λ is a constant.

For values of $\epsilon \ll \omega_D$ the solution of the system of equations (2.5) for the functions G_c and F_c has the form

(derive!!!)

$$\begin{aligned} G_c(\varepsilon, \mathbf{p}) &= u_{\mathbf{p}}^2\left(\frac{m_{\mathbf{p}}}{\varepsilon - \varepsilon_{\mathbf{p}} - i\delta} + \frac{1-m_{\mathbf{p}}}{\varepsilon - \varepsilon_{\mathbf{p}} + i\delta}\right) + v_{\mathbf{p}}^2\left(\frac{m_{-\mathbf{p}}}{\varepsilon + \varepsilon_{\mathbf{p}} + i\delta} + \frac{1-m_{-\mathbf{p}}}{\varepsilon + \varepsilon_{\mathbf{p}} - i\delta}\right), \\ {}^+F_c(\varepsilon, \mathbf{p}) = F_c(\varepsilon, \mathbf{p}) &= -iu_{\mathbf{p}}v_{\mathbf{p}}\left(\frac{m_{\mathbf{p}}}{\varepsilon - \varepsilon_{\mathbf{p}} - i\delta} + \frac{1-m_{\mathbf{p}}}{\varepsilon - \varepsilon_{\mathbf{p}} + i\delta} - \frac{m_{-\mathbf{p}}}{\varepsilon + \varepsilon_{\mathbf{p}} + i\delta} - \frac{1-m_{-\mathbf{p}}}{\varepsilon + \varepsilon_{\mathbf{p}} - i\delta}\right) \end{aligned} \tag{2.8}$$

$$u_{\mathbf{p}}^2 = \frac{1}{2}\left(1 + \frac{\xi_{\mathbf{p}}}{\varepsilon_{\mathbf{p}}}\right), \quad v_{\mathbf{p}}^2 = \frac{1}{2}\left(1 - \frac{\xi_{\mathbf{p}}}{\varepsilon_{\mathbf{p}}}\right), \quad \varepsilon_{\mathbf{p}} = \left(\Delta^2 + \xi_p^2\right)^{1/2}.$$

Here m_p is an undetermined (for the time being) positive function whose absolute value does not exceed unity. We shall call it the distribution function of the excitations, and we shall write down a kinetic equation for it below. One can verify that it is related to the distribution function of the quasi-electrons by the following equations:

$$\begin{aligned} m_{\mathrm{p}} &= n_{\mathrm{p}} \text{ for } \xi_{\mathrm{p}} > 0, \\ m_{\mathrm{p}} &= 1 - n_{\mathrm{p}} \text{ for } \xi_{\mathrm{p}} < 0. \end{aligned} \tag{2.9}$$

By substituting expressions (2.8) into Eq. (2.7) we obtain Eq. (1.1) of the BCS theory.

(do it!!!)

Using the definitions of the Green's functions, it is not difficult to obtain the following spectral representations for the causal functions:

$$\begin{aligned} G_c(\mathbf{p}, \varepsilon) &= \int_{-\infty}^{\infty}\frac{d\varepsilon'}{2\pi i}\left[\frac{G_+(\varepsilon', \mathbf{p})}{\varepsilon - \varepsilon' - i\delta} - \frac{G_-(\varepsilon', \mathbf{p})}{\varepsilon - \varepsilon' + i\delta}\right], \\ {}^+F_c(\mathbf{p}, \varepsilon) &= \int_{-\infty}^{\infty}\frac{d\varepsilon'}{2\pi i}\left[\frac{{}^+F_-(\varepsilon', p)}{\varepsilon - \varepsilon' - i\delta} - \frac{{}^+F_+(\varepsilon', \mathbf{p})}{\varepsilon - \varepsilon' + i\delta}\right]. \end{aligned} \tag{2.10}$$

One can write down a similar relationship for $F_c(\epsilon, p)$. The relationships for the anti-causal functions are obtained if we interchange the positions of the functions with plus and minus subscripts on the right-hand side of (2.10).

Comparing expressions (2.10) with (2.8), we find

$$G_+(\varepsilon,\mathbf{p}) = 2\pi i\left[u_p^2 m_p \delta(\varepsilon-\varepsilon_p) + v_p^2(1-m_{-p})\,\delta(\varepsilon+\varepsilon_p)\right],$$
$$G_-(\varepsilon,p) = -2\pi i\left[u_p^2(1-m_p)\,\delta(\varepsilon-\varepsilon_p) + v_p^2 m_{-p}\delta(\varepsilon+\varepsilon_p)\right], \tag{2.11}$$
$${}^+F_+(\varepsilon,\mathbf{p}) = {}^+F_-(-\varepsilon,-\mathbf{p}) = F_+(\varepsilon,\mathbf{p}) = -2\pi u_p v_p\left[(1-m_p)\,\delta(\varepsilon-\varepsilon_p) - m_{-p}\delta(\varepsilon+\varepsilon_p)\right]. \tag{2.12}$$

It is clear from (2.11) that

$$m_{\mathrm{p}} = \int_0^\infty \frac{d\varepsilon}{2\pi i}\left[G_+(p) - G_-(-p)\right]. \tag{2.13}$$

(?? I am lost, what are we doing???)

Thus, in order to derive the kinetic equation for the function m_p, it is necessary to obtain equations for $G_+(p)$ and G_(p). Since these functions are purely imaginary, by taking the real part of the matrix component 12 of the first equation of (2.5) we obtain

$$\frac{\partial}{\partial t}\operatorname{Im} G_+ = \operatorname{Im}\left\{\Sigma_+ G_- - \Sigma_- G_+ + \Delta_+^+ F_- - \Delta_-^+ F_+\right\} \tag{2.14}$$

Here, in connection with the transformation of the right-hand part, it is convenient to use the Lehmann representations for the self-energy parts, which have the form

$$\Sigma_{\mathrm{c}}(\mathbf{p},\varepsilon) = -\int \frac{d\varepsilon'}{2\pi i}\left[\frac{\Sigma_+(\mathbf{p},\varepsilon')}{\varepsilon-\varepsilon'-i\delta} - \frac{\Sigma_-(\mathbf{p},\varepsilon')}{\varepsilon-\varepsilon'+i\delta}\right]. \tag{2.15}$$

This can easily be checked in lowest-order perturbation theory, which is the approximation of interest to us.

As an example, let us write down the perturbation theory expression for one of the self-energy parts, namely Δ_-:

$$\Delta_-(\varepsilon,\mathbf{p}) = \int \frac{d^3q}{(2\pi)^3}\int \frac{d\omega}{2\pi}\left|c_{\mathbf{q}}\right|^2 D_-(\omega,\mathbf{q}) F_-(\varepsilon-\omega,\mathbf{p}-\mathbf{q}). \tag{2.16}$$

Here D_(ω, q) is the phonon propagator. In the lowest-order approximation we find

$$D_\pm(\omega,\mathbf{q}) = -2\pi i\left[(N_{\mp\mathbf{q}}+1)\,\delta(\omega\pm\omega_{\mathbf{q}}) + N_{\pm\mathbf{q}}\delta(\omega\mp\omega_{\mathbf{q}})\right], \tag{2.17}$$

where $\mathrm{N_q}$ is the phonon distribution function.

(??? below, I am fully lost)

A similar relationship is also obtained for $G_-(-p)$. Subtracting one from the other, substituting the explicit expressions for the propagators and the self-energy parts into the right-hand side, and then integrating over ϵ in the semi-infinite limits, we obtain the following expression for the collision integral:

$$\left(\frac{\partial m_{\mathrm{p}}}{\partial t}\right)_{\mathrm{coll}} = 2\pi\sum_{\mathrm{q}}\left|c_{\mathrm{q}}\right|^2\Big\{(1-m_{\mathrm{p}})\,m_{\mathrm{p-q}}\,(u_{\mathrm{p}}u_{\mathrm{p-q}} - v_{\mathrm{p}}v_{\mathrm{p-q}})^2$$

$$\times \left[\left(1+N_{-\mathrm{q}}\right)\delta\left(\varepsilon_{\mathrm{p}}-\varepsilon_{\mathrm{p-q}}+\omega_{\mathrm{q}}\right)+N_{\mathrm{q}}\delta\left(\varepsilon_{\mathrm{p}}-\varepsilon_{\mathrm{p-q}}-\omega_{\mathrm{q}}\right)\right]-m_{\mathrm{p}}\left(1-m_{\mathrm{p-q}}\right)$$
$$\times\left(u_{\mathrm{p}}u_{\mathrm{p-q}}-v_{\mathrm{p}}v_{\mathrm{p-q}}\right)^{2}\left[N_{-\mathrm{q}}\delta\left(\varepsilon_{\mathrm{p}}-\varepsilon_{\mathrm{p-q}}+\omega_{\mathrm{q}}\right)+\left(1+N_{\mathrm{q}}\right)\delta\left(\varepsilon_{\mathrm{p}}-\varepsilon_{\mathrm{p-q}}-\omega_{\mathrm{q}}\right)\right]$$
$$+\left(1-m_{\mathrm{p}}\right)\left(1-m_{\mathrm{-p+q}}\right)\left(u_{\mathrm{p}}v_{\mathrm{p-q}}+u_{\mathrm{p-q}}v_{\mathrm{p}}\right)^{2}\Big[\left(1+N_{-\mathrm{q}}\right)\delta\left(\varepsilon_{\mathrm{p}}+\varepsilon_{\mathrm{p-q}}+\omega_{\mathrm{q}}\right)$$
$$+N_{\mathrm{q}}\delta\left(\varepsilon_{\mathrm{p}}+\varepsilon_{\mathrm{p-q}}-\omega_{\mathrm{q}}\right)\Big]-m_{\mathrm{p}}m_{\mathrm{-p+q}}\left(u_{\mathrm{p}}v_{\mathrm{p-q}}+u_{\mathrm{p-q}}v_{\mathrm{p}}\right)^{2}$$
$$\times\left[N_{\mathrm{q}}\delta\left(\varepsilon_{\mathrm{p}}+\varepsilon_{\mathrm{p-q}}+\omega_{\mathrm{q}}\right)+\left(1+N_{-\mathrm{q}}\right)\delta\left(\varepsilon_{\mathrm{p}}+\varepsilon_{\mathrm{p-q}}-\omega_{\mathrm{q}}\right)\right]\Big\}. \tag{2.18}$$

The first two terms on the right-hand side describe processes which conserve the number of excitations, that is, the scattering of excitations accompanied by the absorption or emission of phonons. The third and fourth terms describe the creation of a pair of quasi-particles from the condensate with the absorption of a phonon and the annilation of a pair with the emission of a phonon. The terms containing δ-functions of the form $\delta\left(\epsilon_p+\epsilon_{p-q}+\omega_p\right)$ vanish identically since in the quasiparticle representation we are using $\epsilon_p>0$. However, instead of quasi-electrons above the gap and quasi-holes below the gap, as we are now doing, one can write down the kinetic equation in another representation used by us earlier, [10,11] which operates by using the quasielectron distribution function $\mathrm{n_p}$ both above and below the gap. [4)] In this representation the form of the collision operator remains the same, but since for $\xi_p<0$ the energy of the quasi-electrons in this representation is negative, all of the δ-functions give a contribution to the collision operator.

31.0.3 3. The Two-Particle Green's Function and the Conditions for Stability

In order to investigate stability, it is necessary to determine the two-particle retarded Green's function associated with a small total momentum q and total frequency ω. Here we shall use an effective four-fermion Hamiltonian with an effective coupling constant λ.

In the normal metal the problem reduces to a summation of the series which is graphically shown in Fig. 1 (see [13a]). The vertex part

$$\hat{\Gamma}_{\alpha\beta,\gamma\delta}(q)=\hat{\Gamma}(q)\left(\delta_{\alpha\gamma}\delta_{\beta\delta}-\delta_{\alpha\delta}\delta_{\beta\gamma}\right)$$

satisfies the following matrix equation:

$$\hat{\Gamma}(q)=\hat{\Gamma}_0+i\hat{\Gamma}_0\hat{S}(q)\hat{\Gamma}(q) \tag{3.1}$$

where $\hat{\Gamma}_0=\lambda\hat{\sigma}_Z$. The quantity $\hat{\Gamma}$ has the properties of a boson Green's function and is a 2×2 matrix, and $\widehat{\mathrm{S}}$ is the self-energy part, which is given by

$$\hat{S}=\begin{pmatrix} S_c & S_+ \\ S_- & \hat{S}_c \end{pmatrix}=\begin{pmatrix} \int\frac{d^4p}{(2\pi)^4}G_c(p)G_c(q-p), & \int\frac{d^4p}{(2\pi)^4}G_+(p)G_+(q-p) \\ \int\frac{d^4p}{(2\pi)^4}G_-(p)G_-(q-p), & \int\frac{d^4p}{(2\pi)^4}G_c(p)G_c(q-p) \end{pmatrix}, \tag{3.2}$$

In order to obtain the retarded Green's function $\Gamma_{\mathbf{r}}$ we make a unitary transformation of Eq. (3.1) with the help of the matrix $U=\left(1+i\sigma_y\right)/\sqrt{2}$. Finally we have

$$U^{-1}\hat{\Gamma}U=\begin{pmatrix} 0 & \Gamma_a \\ \Gamma_r & \Gamma_d \end{pmatrix},\quad \Gamma_d=\Gamma_++\Gamma_-,\quad \Gamma_{r,a}=\Gamma_c-\Gamma_\pm \tag{3.3}$$

Furthermore, we find

$$U^{-1}\hat{S}U=\begin{pmatrix} S_d & S_r \\ S_a & 0 \end{pmatrix},\quad S_d=S_++S_-,\quad S_{r,a}=S_c+S_\pm \tag{3.4}$$

In deriving these formulas we have used the identities [14]

$$\Gamma_{\mathrm{c}} + \widetilde{\Gamma}_{\mathrm{c}} = \Gamma_{+} + \Gamma_{-} \tag{3.5}$$

$$S_{\mathrm{c}} + S_{\mathrm{c}} + S_{+} + S_{-} = 0 \tag{3.6}$$

Hence

$$\Gamma_r = \lambda + i\lambda S_r \Gamma_r \tag{3.7}$$

Thus, the constructive method of evaluating Γ_{r_1} consists in writing down the graphical equation Fig. 1 directly for the retarded Green's function Γ_r. One can evaluate the self-energy part $\mathrm{S_r}$ appearing in it with the aid of the relationship (3.4).

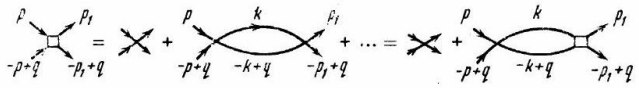


FIG. 1

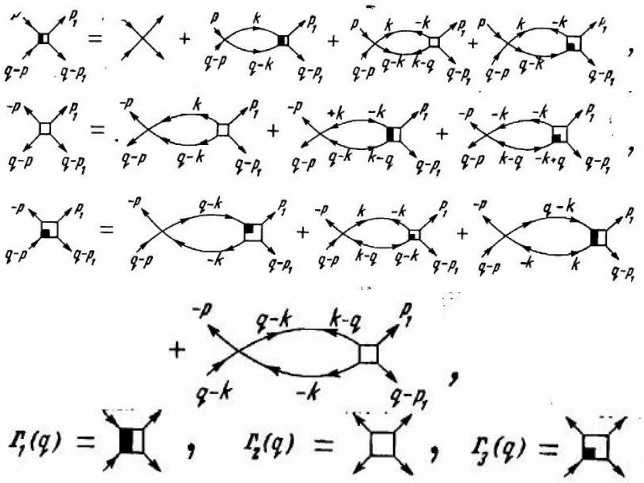


FIG. 2

Anomalous electron Green's functions exist in the case of a superconductor. Therefore, in calculating the self-energy parts, the system of equations, which is represented graphically in Fig. 2, arises for the quantities Γ_1, Γ_2 and Γ_3 :

$$\left(\hat{1} - i\lambda\hat{S}_T\right)\begin{pmatrix} I_{1r} \\ I_{2r} \\ I_3 \end{pmatrix} = \begin{pmatrix} \lambda \\ 0 \\ 0 \end{pmatrix} \tag{3.8}$$

Here the elements of the matrix $\hat{\mathrm{S}}_{\mathrm{c}}$ are given by

$$S_{11}(q) = S_{22}(-q) = \int \frac{d^4k}{(2\pi)^4} G_{\mathrm{c}}(k) G_{\mathrm{c}}(q-k),$$

$$S_{12}(q) = S_{21}(q) = \int \frac{d^4k}{(2\pi)^4} F_{\mathrm{c}}(k) F_{\mathrm{c}}(q-k),$$

$$S_{13}(q) = S_{31}(q) = S_{23}(-q) = S_{32}(-q) = -\int \frac{d^4k}{(2\pi)^4} F_{\mathrm{c}}(k) G_{\mathrm{c}}(q-k),$$

$$S_{33}(q) = -\int \frac{d^4k}{(2\pi)^4} \left[G_{\mathrm{c}}(k) G_i(k+q) + F_{\mathrm{c}}(k)^{+} F_{\mathrm{c}}(k+q)\right]. \tag{3.9}$$

By doing the calculation and then analytically continuing the answer, we obtain the following results (the subscript **r** is omitted):

$$S_{11}(q) = \sum_{\mathbf{k}} \left[u^2_{\mathbf{k+q}/2} u^2_{\mathbf{k-q}/2} f_q(\mathbf{k}) + v^2_{\mathbf{k+q}/2} v^2_{\mathbf{k-q}/2} f_{-q}(\mathbf{k}) + 2u^2_{\mathbf{k+q}/2} v^2_{\mathbf{k-q}/2} \varphi_q(\mathbf{k})\right] \tag{3.10}$$

$$S_{12}(q) = -\sum_{\mathbf{k}} u_{\mathbf{k+q}/2} v_{\mathbf{k+q}/2} u_{\mathbf{k-q}/2} v_{\mathbf{k-q}/2} \left[f_q(\mathbf{k}) + f_{-q}(\mathbf{k}) - 2\varphi_q(\mathbf{k})\right]$$

$$S_{13}(q) = -i \sum_{\mathbf{k}} u_{\mathbf{k+q}/2} v_{\mathbf{k-q}/2} \left[u_{\mathbf{k+q}/2} u_{\mathbf{k-q}/2} \left[\varphi_q(\mathbf{k}) - f_q(\mathbf{k})\right]\right.$$
$$\left. - v_{\mathbf{k+q}/2} v_{\mathbf{k-q}/2} \left[\varphi_q(\mathbf{k}) - f_{-q}(\mathbf{k})\right]\right\}$$

$$S_{33}(q) = -S_{12}(q) + \sum_{\mathbf{k}} \left[\left(u^2_{\mathbf{k-q}/2} u^2_{\mathbf{k+q}/2} + v^2_{\mathbf{k-q}/2} v^2_{\mathbf{k+q}/2}\right) \varphi_q(\mathbf{k})\right.$$
$$\left. + u^2_{\mathbf{k+q}/2} v^2_{\mathbf{k-q}/2} \left[f_q(\mathbf{k}) + f_{-q}(\mathbf{k})\right]\right]$$

$$f_q(\mathbf{k}) = i \frac{m_{\mathbf{k+q}/2} + m_{-\mathbf{k+q}/2} - 1}{\omega - \varepsilon_{\mathbf{k+q}/2} - \varepsilon_{\mathbf{k-q}/2} + i\delta} = f_q(-\mathbf{k}) \tag{3.11}$$

$$\varphi_q(\mathbf{k}) = i \frac{m_{\mathbf{k+q}/2} - m_{\mathbf{k-q}/2}}{\omega - \varepsilon_{\mathbf{k+q}/2} + \varepsilon_{\mathbf{k-q}/2} + i\delta} = \varphi_{-q}(\mathbf{k}) \tag{3.12}$$

We obtain the dispersion equation by setting the determinant of the system of equations (3.8) equal to zero:

$$\left\| \hat{1} - i\lambda \hat{S}_r(q) \right\| = 0 \tag{3.13}$$

It follows from Eq. (3.13) that the dispersion equation is invariant under the substitutions $\lambda \to -\lambda$ and $\mathrm{m_k}$
$\to 1 - \mathrm{m_k}$, that is, the spectrum of the collective oscillations and of the two-particle excitations in a system having the usual Fermi distribution and attractive interactions turns out to be the same as in a system with the inverse Fermi distribution and repulsion.

Let us start with an analysis of the stability conditions for the normal metal. For $\Delta = 0$ and $\mathrm{q} = 0$ the dispersion equation (3.13) gives

$$1 = \lambda N(0) \int_{-\omega_D}^{\omega D} d\xi \frac{1 - 2n(\xi)}{\omega - 2\xi + i\delta} \tag{3.14}$$

For the given form of the distribution function $n(\xi)$, this equation has complex roots. If the roots are located in the lower half-plane, then the state is stable. If the function $\mathrm{n}(\xi)$ depends on some external parameter (and in the equilibrium case, it would depend on the temperature), then a root may intersect the real axis for a certain value of this parameter. This is therefore the stability boundary of the normal state. It is determined from the condition that Eq. (3.14) has a real root. In this case, by separating out the imaginary part in Eq. (3.14), we find

$$n(\omega/2) = 0 \tag{3.15a}$$

By choosing the origin with respect to which the energy ξ is measured, and hence the quantity $\omega/2$, to coincide with the point at which $\mathrm{n}(\xi) = 1/2$, we obtain the condition $\omega = 0$ from Eq. (3.15a). By isolating the real part in Eq. (3.14) we obtain the following equation for the determination of the stability boundary:

$$1 = -\frac{1}{2} \lambda N(0) \int_{-\omega_D}^{\omega_D} \frac{d\xi}{\xi} [1 - 2n(\xi)] \tag{3.15b}$$

Here $n(\xi)$ is the average of n_k over the corresponding constant-energy surface. In the case of equilibrium, Eq. (3.15b) goes over into the well-known equation for the determination of the critical temperature T_c. In so far as we are able to judge, Eqs. (3.15) differ somewhat from the corresponding stability conditions derived by Batyev. [4]

Let us proceed to the investigation of a superconductor. When $q = 0$ Eq. (3.13) takes the form

$$\left[\gamma + \left(4\Delta^2 - \omega^2\right) Z\right] \left[\gamma - \left(4\Delta^2\gamma + \omega^2\right) Z + 2\Delta^2\omega^2 Z^2\right] = 0 \tag{3.16}$$

$$Z(\omega) = \lambda N(0) \int_\Delta^\infty \frac{1 - 2m(\varepsilon)}{\left(\varepsilon^2 - \Delta^2\right)^{1/2}} \frac{d\varepsilon}{\omega^2 - 4\varepsilon^2 + i\omega\delta} \tag{3.17}$$

$$\gamma = 1 + \lambda N(0) \int_\Delta^\infty \frac{d\varepsilon}{\left(\varepsilon^2 - \Delta^2\right)^{1/2}} [1 - 2m(\varepsilon)] \tag{3.18}$$

So that the stationary value, Δ_S, of the parameter Δ is determined from the equation $\gamma = 0$. The relationship $n(-\xi) = 1 - n(\xi)$ was used in the derivation of Eq. (3.16).

When $\gamma = 0$ the left part of Eq. (3.16) breaks up into a product of factors, two of which give the real roots $\omega^2 = 0$ and $\omega = \pm 2\Delta_S$, and the other two factors lead to the equations

$$Z(\omega) = 0, \tag{3.19}$$

$$Z(\omega) = +1/2\Delta_s^2. \tag{3.20}$$

Equation (3.20) doesn't have any solutions. In fact, one can rewrite it in the form

$$\frac{\lambda N(0)}{2} \int_1^\infty dx \frac{1 - 2m(x\Delta)}{\left(x^2 - 1\right)^{1/2} \left(x^2 - \omega^2/4\Delta_2^2 - i\omega\delta\right)} = 1$$

The small factor $\lambda N(0)$ appears to the left; in order of magnitude this factor is equal to $\ln^{-1}(\omega_D/\Delta_0)$, where Δ_0 denotes the equilibrium gap for $T = 0$. As one can easily verify, the smallness of this factor can not be compensated by the integral, whose order of magnitude does not exceed unity.

Thus, the stability boundary of the superconducting state is determined by Eq. (3.19). In this equation we set $\omega = \omega' - \mathbf{i}\omega''$. The stability boundaries are determined from the condition that ω'' becomes an infinitesimal negative quantity. By isolating the imaginary part in Eq. (3.19), we find that this condition is satisfied provided that one of the following two conditions is fulfilled:

$$\omega' = 0, \tag{3.21a}$$

$$m\left(\omega_i'/2\right) = 1/2. \tag{3.22a}$$

These are also those values of the frequency at which an instability may begin.

We note that Eq. (3.22a) may, in general, have several solutions, in which case we shall distinguish them by the subscript i. The real part of Eq. (3.19) together with conditions (3.21a) or (3.22a) determine those values of the external parameters, characterizing the nonequilibrium nature of the distribution, at which the instability begins. The corresponding equation for case (3.21a) has the form

$$\int_{\Delta_\varepsilon}^\infty \frac{d\varepsilon}{\varepsilon^2} \frac{1 - 2m(\varepsilon)}{\left(\varepsilon^2 - \Delta_\varepsilon^2\right)^{1/2}} = 0 \tag{3.21b}$$

and for case (3.22a)

$$\int_{\Delta_i}^{\infty} \frac{d\varepsilon}{(\varepsilon^2-\Delta_i^2)^{1/2}} \frac{1-2m(\varepsilon)}{\varepsilon^2-\omega_i'^2/4} = 0 \tag{3.22b}$$

We see that in order for Eqs. (3.21) and (3.22) to have a solution, the function $1-2\ \mathrm{m}(\xi)$ must be alternating in sign. [5)]

Thus, if the function $\mathrm{m}(\epsilon)$ in the important range of variation of ϵ does not pass through the value 1/2, then the superconducting state is stable.

Furthermore, if the function $1-2\ \mathrm{m}(\epsilon)$ has only one change of sign, then Eq. (3.22) doesn't have a solution. In this case the stability boundary is determined by Eq. (3.21b). Undamped, collective oscillations with frequencies $\omega^2 < 4\Delta_S^2$ exist in a system in its region of stability; these are determined by the following dispersion equation:

$$\int_{\Delta_\varepsilon}^{\infty} \frac{d\varepsilon}{(\varepsilon^2-\Delta_\varepsilon^2)^{1/2}} \frac{1-2m(\varepsilon)}{\varepsilon^2-\omega^2/4} = 0 \tag{3.23}$$

Thus, we see that in this case the instability is related to the vanishing of the frequency of one of these undamped, collective modes.

However, if the function $1-2\ \mathrm{m}(\epsilon)$ changes sign more than once, then a solution of Eq. (3.22) may also exist. And the actual boundary of the stability region is determined by the most stringent condition out of all the conditions which are obtained in this manner. In this case weakly-damped modes with frequencies, whose dispersion equation has the form $\mathrm{Z}(\omega)=0$, may also exist near the boundary of the stability region. The instability may
appear as a change in the sign of the attenuation coefficient for one of these modes.

Now let us explain the principle used in selecting the diagrams associated with the derivation of the system of equations (3.8). When $\gamma = 0$ the dispersion equation (3.16) has, in particular, the roots $\omega = \pm 2\Delta_{\mathrm{S}}$. But, as $\omega \to \pm 2\Delta_S$ each of the self-energy parts S_{ik} diverges logarithmically, and the problem reduces to the summation of an infinite sequence of diagrams, that is, it reduces to the solution of the system of equations shown in Fig. 2.

On the other hand, in order to obtain the pole associated with small values of ω and q , that is, the acoustic mode, it is sufficient (to within terms of order $\lambda \mathrm{N}(0) \ll 1$) to sum the same sequence of diagrams. In connection with satisfying the self-consistency condition $\gamma = 0$ the principal terms of the series, which do not depend on ω and q , cancel each other, and consequently a pole appears as $\omega \to 0$ and $\mathrm{q} \to 0$.

The summation of the sequence of diagrams, permitting us to obtain the roots $\omega = 0$ and $\omega = \pm 2\Delta$, has been carried out in the articles by Migdal and Maleev [17] for the equilibrium superconductor at $\mathrm{T} = 0$.

Now let us investigate the acoustic solution of the dispersion equation, which tends to zero as $\mathrm{q} \to 0$[18,19], for values of $q \neq 0$. Carrying out an expansion of the dispersion equation (3.13) correct to terms of order q^2, we obtain the following result for an isotropic distribution:

$$\omega^2 = c^2 q^2, \tag{3.24}$$

At $\mathrm{T} = 0$ and for the equilibrium case, [19] one finds

$$c^2 = v_F^2/3. \tag{3.25}$$

Expression (3.25) is calculated to the zero-order approximation with respect to the small parameter $\lambda N(0)$. The accuracy of our calculation permits us, in principle, to also derive the next approximation in powers of this parameter. There is no attenuation of sound as long as $\omega^2(\mathrm{q}) < 4\Delta_{\mathrm{S}}^2$. We emphasize that this result also pertains to the inverse Fermi distribution.

31.0.4 4. Examples of the Investigation of Stability

Now let us discuss the stability of the nonequilibrium superconducting states which were previously considered in articles [5,7,8–12]. The nonequilibrium distribution function m(ϵ) in the presence of an ultrahigh-frequency field is found in the article by Ivlev and Éliashberg. [7] The state is stable whenever the corresponding equation for the gap has a solution. Under the same external conditions, i.e., at the same temperature and for the same power of the high-frequency field, the normal state is also stable (in any event, if the temperature is above the superconducting transition point in equilibrium). Thus, one of these two states must be metastable.

A completely analogous situation occurs in the case when the nonequilibrium state of the superconductor can be described with the aid of a quasifield, analyzed by the authors in [9].

A different situation is considered in [8], that of the strongly nonequilibrium state which appears when a conductor is illuminated by light of a definite spectral composition. Here the Fermi step becomes more abrupt than in equilibrium at the given temperature, and the corresponding superconducting state is stable, since the difference $1-2n(\epsilon)$ has a constant sign for $\epsilon > 0$.

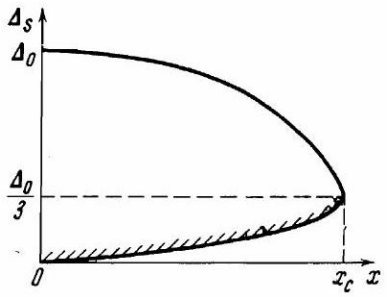


FIG. 3 The dependence of Δ_S on the concentration of excitations, $x\ \left(x_c = 1/3\sqrt{3}\right)$.

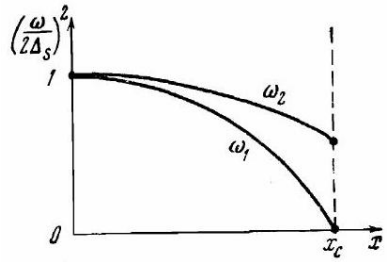


FIG. 4. The dependence of the frequencies of the collective modes on the concentration of excitations ($x_c = 1/3\sqrt{3}$).

However, the normal state is unstable in the presence of sufficiently intense illumination. The easiest way to see this is to note that the distribution which appears differs very little from the equilibrium distribution at T = 0. Thus, there is an important distinction between the present case and the situations which we were talking about above.

The superconducting state with an inverse Fermi distribution (with a repulsive interaction between the particles) is also stable, because $n(\epsilon) > 1/2$ in the essential range of positive energies. However, the normal state associated with the inverse Fermi distribution is unstable.

Owen and Scalapino [12] have recently studied the nonequilibrium state of a superconductor having an excess (in comparison with its equilibrium value) concentration of superconducting excitations. [6)] They confine their discussion to the stability in this model at T = 0. Introducing ν, the chemical potential of the excitations, we may write the equation of state (1.1) in the following form:

$$v + \left(v^2 - \Delta_s^2\right)^{1/2} = \left(\Delta_0 \Delta_s\right)^{1/2}. \tag{4.1}$$

Here Δ_0 denotes the half-width of the equilibrium gap, that is, the half-width for zero

concentration of the excitations. It is convenient to rewrite expression (4.1) by introducing the dimensionless concentration of excitations:

$$x \equiv \frac{1}{2\Delta_0 N(0)} \sum_{\mathbf{p}} n_{\mathbf{p}} = \frac{1}{\Delta_0} \left(\nu^2 - \Delta_s^2\right)^{1/2} \tag{4.2}$$

Then Eq. (4.1) can be written down in the form [7)]

$$\Delta_0 \left(\Delta_0 - \Delta_0\right)^2 = 4x^2 \Delta_0^3 \tag{4.3}$$

The dependence of Δ_S on x is schematically shown in Fig. 3.

The stability criterion (3.25) gives the following result for the critical value of the quantity ν :

$$v_c = 2\Delta_0/3\sqrt{3} \tag{4.4}$$

which corresponds to the following result for the critical concentration of excitations

$$x_c = 1/3\sqrt{3} \tag{4.5}$$

and for the gap

$$\Delta_{c'} = \Delta_0/3 \tag{4.6}$$

In order to understand which branch of the curve shown in Fig. 3 is unstable, let us consider the dispersion equation (3.19). Its solution has the form

$$\omega_1^2 = 4\Delta_3^2 \left[1 - x^2 \left(\Delta_0/\Delta_3\right)^3\right] \tag{4.7a}$$

$$\omega_2^2 = 4\Delta_3^2 \left\{1 - x^2 \left(\Delta_0/\Delta_3\right)^3 \left[1 - 2x \left(\Delta_0/\Delta_3\right)^{1/3}\right]^2\right\} \tag{4.7b}$$

For $x = x_c$ and $\Delta_s = \Delta_c$ the solution ω_1^2 tends to zero like $(x_c - x)^{1/2}$, and $\omega_2^2 = 32\Delta_c^2/9$. Using the equation of state (4.3), we see that $\omega_1^2 < 0$ for $x < x_c$ and $\Delta_S < \Delta_c$, and therefore this branch of the solution is unstable. The dependences of ω_1^2 and ω_2^2 on the concentration in the stable region are schematically shown in Fig. 4.

Thus, two collective modes exist in the strongly nonequilibrium state in a superconductor, and for $q = 0$ the frequencies of these modes are determined by formulas (4.7). Such modes are not present in equilibrium. The instability which we have been considering-this is an instability of that collective mode which appears in the nonequilibrium state. Since the given state is a state of incomplete equilibrium, it is clear that the criterion that the energy be a minimum should also define, and actually does define in this case, the stability region of the superconducting state.

32 The Behavior of a Superconductor in a Variable Field by Gor'kov, Eliashberg

Abstract

The dynamical equations previously found for the model of a gapless superconductor are used for the calculation of some nonlinear high-frequency effects.

The high-frequency region is primarily considered here, the parameter Δ mainly being determined by the time average of the square of the field intensity.

Actually, the results do not depend on the choice of model. In each individual case, the boundary of the high frequency region should be specified.

For type I superconductors, the behavior of Δ near the boundary is calculated for the presence of a large-amplitude high-frequency field. The case of the simultaneous effect of a constant and a varying field is also considered. Special interest attaches to the effect of a high frequency field on the hysteresis pattern calculated for a stationary Ginzburg field. Formulas are derived which describe the destruction of the superconductivity of films of various thicknesses in a variable field.

For type II superconductors, the destruction of surface superconductivity by a high-frequency field is calculated. In particular, the dependence of the field strength H_{c3} on the variable field amplitude is found, and equations are obtained for the description of the dynamics of the surface layer.

(so, in a nutshell, we shine a laser on a SC, what will be??? this is what should be answered in this article)

32.0.1 1. Introduction

The properties of superconductors in a nonstationary electromagnetic field have thus far been inadequately studied.

On the one hand, experimental difficulties connected with heating in a strong variable field do not permit us to outline a clear picture of the phenomena, and on the other hand, theoretical results based on modern microscopic representations are virtually nonexistent.

(why inadequately??)

A general approach to the problem of nonstationary properties of a superconductor was proposed previously by the authors in [1], but it was noted at the same time that the general arrangement of the problem, independent of the experimental conditions, is possible in the region in which there are sufficient normal carriers to guarantee heat elimination, and the superconductivity is a relatively small effect. This is, above all, the region near the critical temperature or, for example, the case considered in detail in [1] of gapless superconductivity in alloys with paramagnetic impurities.

For the latter problem, the generalization of the Ginzburg-Landau equation in a varying field was written in [1] :

$$\dot{\Delta} + \frac{\tau_s}{2}\left\{\pi^2\left(T^2 - T_c^2\right) + \frac{|\Delta|^2}{2}\right\}\Delta + D\left(-i\nabla - \frac{2e}{c}\mathbf{A}\right)^2\Delta = 0, \tag{1}$$

$$\mathbf{j} = \sigma\mathbf{E} - \frac{2\sigma\tau_s}{c}|\Delta|^2(\mathbf{A} - \nabla\varphi).$$

Equations (1) are valid in the region of frequencies comparable with the characteristic scale frequency $\omega_0 = 2\tau_S\left|\Delta_0\right|^2$ (Δ_0 is the equilibrium value of the gap). These equations, obtained in [1] for the special case of paramagnetic alloys, nevertheless allows us to understand the qualitative picture of the phenomena taking place in superconductors in a variable field. In this connection, we note that the parameter κ of the Ginzburg-Landau theory in this system

$$\varkappa^2 = c^2/48\pi\sigma D \tag{2}$$

can be either small or large, depending on which initial pure metal was chosen for the preparation of the alloy. In other words, we shall regard below the system (1) as a reasonable

model, which allows us to study the properties of both Pippard ($\kappa \ll 1$) and London ($\kappa \gg 1$) superconductors.

We transform to the dimensionless variables used in the Ginzburg-Landau theory: [2]

$$H' = -\frac{H}{\sqrt{2}H_{cm}}, \quad A' = \frac{A}{\sqrt{2}H_{cm}\delta_L}, \quad \Delta' = \frac{\Delta}{\Delta_0}, \tag{3}$$

and to the nondimensional time parameter

$$t' = \omega_0 t. \tag{1'}$$

(Here, we shall omit the primes for the nondimensional quantities. The transition to the ordinary variables is everywhere indicated in the corresponding places.) In what follows, we shall limit ourselves to the consideration of one-dimensional situations (films, half-space), where one can assume Δ to be real. In terms of the new variables for all quantities, which depend only on a single coordinate, the set of equations for Δ and the field A has the form

$$12\Delta + \left(\dot{\Delta}^2 - 1\right)\Delta - \frac{1}{x^2}\frac{\partial^2\Delta}{\partial z^2} + A^2\Delta = 0,$$
$$\frac{\partial^2\Delta}{\partial z^2} = \dot{A} + \Delta^2 A. \tag{1'}$$

32.0.2 2. Pippard Superconductors ($\kappa \ll 1$)

For slow changes in the field, up to the point at which the amplitudes of the magnetic field is no longer smaller than the critical value, the change in Δ is small. If the fields exceed critical, then a first-order transition takes place in thick samples, as a result of which a moving separation boundary appears between the normal and superconducting phases. The kinetics of such a transition was considered by I. Lifshitz. [3] We shall therefore not linger over the details of the situation. We only note that the criteria of slowness of change in the field depends on the degree of perfection of the sample and of its surface, inasmuch as precisely these circumstances determine the formation of the boundary. We shall therefore study below the case of high frequencies ($\omega \gg 1$) where the formation and motion of the separation boundary are impossible.

For proof of the latter assertion, we recall that, as is well known, the structure of the boundary separating the two phases is characterized by two lengths: the London penetration depth and the scale of change in Δ (in dimensionless units, these are 1 and $1/\kappa$, respectively). Thus, for $\kappa \ll 1$, the location of the boundary is fixed with an accuracy to within a length ~ 1. At the same time, it is seen from the second of Eqs. (1') that, during the period of change of the field, the boundary cannot go out from the surface a distance greater than $\omega^{-1/2} \ll 1$.

If $\omega \gg 1$, then $\Delta(\mathrm{t}) = \Delta + \Delta_1(\mathrm{t})$, where the time average $\overline{\Delta_1(t)} = 0$ and the value of Δ_1 is small (see below). Therefore, the equation for the static part of the gap has the usual form of Ginzburg-Landau theory:

$$\left(\Delta^2 - 1\right)\Delta - \frac{1}{v^2}\frac{\partial^2\Delta}{\partial\tau^2} + \overline{A^2\Delta} = 0, \tag{4}$$

where, however, the variable part of A, A_1 (before time averaging) is determined from the usual equations of the normal skin effect:

$$\partial^2 A_1/\partial z^2 = \dot{A}_1. \tag{1'}$$

Assuming that the skin depth is less than all the characteristic dimensions of the problem, we find for A_1, in the case of a monochromatic field,

$$A_1 = \frac{h_1}{\sqrt{2}}\delta_s \exp\left(-\frac{z}{\delta_s}\right)\cos\left(\omega t - \frac{z}{\delta_s} - \frac{\pi}{4}\right),$$
$$\overline{A_1^2} = \frac{h_1^2\delta_s^2}{4}\exp\left(-\frac{2z}{\delta_s}\right),$$

where h_1 is the amplitude of the alternating field, $\delta_S = \sqrt{2/\omega}$.
If a constant field h_0 also figures in the problem, then its penetration depth is Δ^{-1}.

32.0.3 A. Boundary of a Bulk Superconductor

Let us consider the superconducting half-space $z > 0$ and assume that the field is sufficiently small so that one can determine the change of Δ by perturbation theory: $\Delta = 1 + \Delta_1$ ($\Delta_1 \ll 1$). Then

$$2\Delta_1 - \frac{1}{x^2}\frac{\partial^2\Delta_1}{\partial z^2} + \frac{{h_1}^2}{4}{\delta_s}^2\exp\left(-\frac{2z}{\delta_s}\right) + {h_0}^2 e^{-2z} = 0.$$

The solution of this equation with the boundary condition $(\partial\Delta/\partial\mathbf{z})_{\mathbf{z}=0} = 0$ is

$$\Delta_1(z) = \frac{{h_1}^2{\delta_s}^4x^2}{8\,(2 - x^2{\delta_s}^2)}\left[\exp\left(-\frac{2z}{\delta_s}\right) - \frac{\sqrt{2}}{x\delta_s}\exp(-x\sqrt{2}z)\right] + \frac{{h_0}^2x^2}{2\,(2-x^2)}\left[e^{-2z} - \frac{\sqrt{2}}{x}\exp(-x\sqrt{2}z)\right] \tag{5}$$

or, for $\kappa \ll 1$ and z = 0,

$$\Delta(0) = 1 - \left(\frac{x{h_1}^2{\delta_s}^3}{8\sqrt{2}} + \frac{x{h_0}^2}{2\sqrt{2}}\right). \tag{5'}$$

Solving the first of Eqs. (1') for the variable part Δ_1(t), we find that the component $\Delta_{1,2\omega}$ is equal to ($\kappa \ll 1$)

$$\Delta_{1,2\omega}(z) = \frac{h_1^2\delta_s^4x^2}{16}\left[\exp\left(-\frac{2z}{\delta_s}\right) - \frac{e^{i\pi/4}}{2\sqrt{3}x}e^{-kz}\right],$$

where $k = 4\sqrt{3}\,(\kappa/\delta_S)\,e^{-i\pi/4}$. In other words, in the absence of a constant component, $\Delta_{12\omega}$ has a diffusion "tail" at comparatively small distances $z \sim \delta_S/\kappa$ and its value

$$\Delta_{1,2\omega}(z) \approx -\frac{{h_1}^2{\delta_s}^4\chi}{32\sqrt{3}}e^{i\pi/4}e^{-kz}$$

is smaller by the factor $\delta_S \ll 1$ than the constant component Δ_1(z) of (5'). Therefore, we see that in the region where $h_1^2\delta_s^3\kappa \le 1$, the stationary part of Δ is actually large in comparison with $\Delta_1(t)$, the rapidly oscillating part of the gap, which justifies our assumption in the derivation of the averaged equations (4).

Equations (5) and (5') are naturally valid only so long as $h_1^2\delta_S^2\kappa \ll 1$ and $h_0^2\kappa \ll 1$. Continuation of the solution into the region of stronger fields when $\kappa \lesssim 1$ generally requires numerical calculations similar to those which were carried out by Ginzburg [4] in the determination of the supercooling field. In the region $\kappa^{\ll 1}$, however, an analytical approach is possible, which was not noted in [1]. Having it in mind to study the qualitative picture, we now make use of it. The essential fact is that the field arises in the superconductor at a distance from the surface $\sim_{\delta_0}$ for

the variable and $1/\Delta(0)$ for the constant component of the magnetic field. If these distances are small in comparison with $1/\kappa$, then there is no field at great distances from the surface of the sample and the solution for Δ(z) is [2]

$$\Delta = \text{th}[\varkappa(z+C)/\sqrt{2}]. \tag{6}$$

The problem consists of connecting the solution in the region of change of the field with the solution (6). Taking it into account that in the region of the field itself, the function Δ and its derivative

$$\frac{\partial\Delta}{\partial z} = x^2\left\{\left(\Delta^2(0)-1\right)\Delta(0)z + \Delta(0)\int_0 \bar{A}^2 dz\right\} \tag{7}$$

are slowly changing, we can "join" (7) and (6) together at $z \ll 1/\kappa$. This is possible if

$$h_1{}^2\delta_s{}^3 > 1, \quad h_0{}^2/\Delta^2(0) \gg 1. \tag{8}$$

The conditions (8) overlap for $\kappa \ll 1$ with the region of applicability of (5) and (5'). Thus the "joining" conditions are

$$\begin{gathered}\Delta(0) = \text{th}(\varkappa C/\sqrt{2}) \\ \varkappa\Delta(0)\int_0^\infty \overline{A^2}dz = \frac{1}{\sqrt{2}\,\text{ch}^2(\varkappa C/\sqrt{2})} = \frac{1}{\sqrt{2}}\left(1-\Delta(0)^2\right).\end{gathered} \tag{9}$$

Comparing the first of the conditions (9), as $C \to \infty$,

$$\Delta(0) = 1 - 2e^{-x\sqrt{2}C}$$

with the expression (5′), we see that C is logarithmically large for small $\kappa h_1^2\delta_S^3$ and $h_0^2\kappa$.

We now undertake a detailed study of the general case of (8). The second of Eqs. (9), in which C is contained, can be written in the form

$$h_0^2 = \frac{\sqrt{2}}{x}\Delta(0)^2\left(1-\Delta(0)^2\right) - \frac{h_1^2\delta_s^3\Delta(0)^3}{4}. \tag{10}$$

If there is no constant field ($h_0 = 0$), it then follows from (10) that

$$\Delta(0) = -\frac{xh_1^2\delta_s^3}{8\sqrt{2}} + \left(1 + \frac{x^2h_1^4\delta_s^6}{128}\right)^{1/2}. \tag{11}$$

For small fields (11) coincides with (5'); in the limit of large field amplitudes,

$$\Delta(0) \approx 64/\varkappa h_1{}^2\delta_s{}^3 \tag{11'}$$

asymptotically approaches zero. Therefore, in the superconductor for $\Delta(x)$ in the limit of extremely strong fields, we obtain essentially the dependence

$$\Delta(z) = \text{th}(xz/\sqrt{2}).$$

Thus, for the infinite half-space, the superconductivity is not destroyed in a high-frequency field. There is only one stationary regime. Once again, we recall that we assume a small Joule heating of the boundary, for which it is necessary to remove heat from the surface of the same.

Before concerning ourselves with the case of the complete Eq. (10), let us first make more precise the results obtained in [4], which pertain to the superheating field. Let $h_1 = 0$; then $h_0^2 = \sqrt{2}\kappa^{-1}\Delta(0)^2\,(1-\Delta(0)^2)$. This is a curve with a maximum, i.e., $\Delta(0)$ as a function of

h_0 is not well defined. The location of the maximum determines the superheating field H_S for $\kappa \ll 1$:

$$H_s = \frac{H_{cm}}{2^{1/4}\sqrt{x}} \approx \frac{0.84}{\sqrt{x}} H_{cm},$$

which differs somewhat from the result obtained in [4] by numerical calculation. Another circumstance is much more interesting. In Fig. 5 of [4] is given the curve $\psi(0)$ (i.e., $\Delta(0)$) of the field h_0. When inverted as a plot of h_0 vs. $\Delta(0)$, this curve has a single maximum, while the important fact is that this curve must reach the point (in our variables) $\Delta(0) = 0,\ h_0 = 1/\sqrt{2}$, which corresponding to a first order phase transition (formation of a boundary between the normal and superconducting phases). The region $\Delta(0) \to 0$ cannot be considered by our method, inasmuch as, along with the condition $h_0^2/\Delta^2(0) \gg 1$, the condition of the localization of the field near the boundary $1 \ll \Delta(0)/\kappa$ must be satisfied. However, upon satisfaction of the latter condition as $\kappa \to 0$ Eq. (10) ($h_1 = 0$) is still valid in the region $h_0 \ll 1, \Delta(0) \ll \sqrt{\kappa}$, i.e., curve (10) enters into the region of fields smaller than critical.

In Fig. 1 a graph is constructed of the dependence of $2\kappa h_0^2$ on $\Delta^2(0)$, from which it is seen that in the region indicated by the dashed line, $\Delta(0)$ has four values as a function of h_0. In the usual scale of critical fields, this region is shown schematically in Fig. 2. It is evident that the portion of the curve AB will also be metastable.

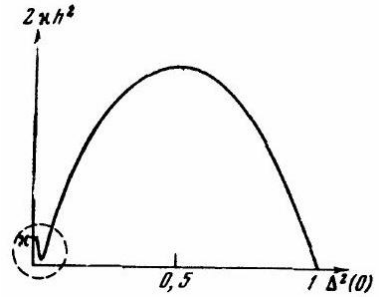


FIG. 1

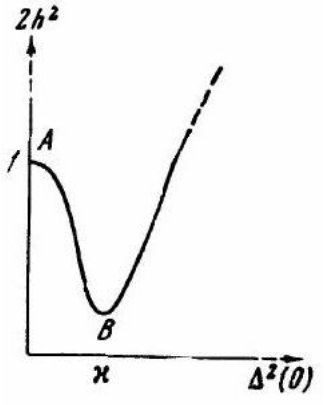


FIG. 2

It is physically probable that this portion corresponds to a certain surface current which screens the external field.

Our discussion refers to the limiting case $\kappa \to 0$. Now, assuming h_0 to be given in Eq. (10), we shall consider the destruction of the superconductivity by an alternating field in the presence of a constant field less than critical ($h_0 < 1/\sqrt{2}$). The dependence of $\Delta(0)$ on h_1, in contrast with (11) becomes non-single valued. The maximum of h_1^2 corresponds to the value

$$\Delta cr^2 = \frac{3\sqrt{2}\varkappa h_0^2}{1 + \left[1 + 6\sqrt{2}\varkappa h_0^2\right]^{1/2}} \approx \frac{3}{\sqrt{2}} x h_0^2,$$

which generally corresponds to much larger amplitudes of the variable field

$$\frac{{h_1}^2{\delta_s}^3}{4} = \frac{2{h_0}^2}{\Delta_{\mathrm{cr}^3}} \sim \frac{1}{h_0 \mathrm{x}^{3/2}}.$$

The value of $\Delta^2_{\mathbf{cr}}$ still satisfies our criterion of the localizability of the field

$$1 < \Delta_{\mathrm{cr}}/x \sim h_0/\sqrt{x}.$$

The existence of ambiguity of $\Delta(0)$ as a function of h_1 means that in the region $\Delta^2(0)$ there exists still another branch, similar to the case in a constant field discussed above, which is stable in the sense that $\Delta(0)$ falls off with increase in amplitude of the alternating fields. We did not succeed in analyzing this branch analytically. However, it can be established that in the presence of a constant magnetic field, an increase in the amplitude of the alternating field can produce a "collapse" of the regime, described by Eqs. (5), (5') and (11). This confirmation generally refers only to sufficiently small $\kappa(\sqrt{\kappa} \ll 1)$.

32.0.4 B. Superconducting Plates

As before, let $\kappa \ll 1$. We consider the case of a film with thickness $2d \ll 1/\kappa$. Then, as is known, we can neglect the dependence of Δ on the coordinate, as a result of which, we can omit in (1) terms with second derivative in z, and the set (1) is considerably simplified. In [1] the destruction of superconductivity by an alternating field was studied in detail for the case in which the dimensions of the layer are small in comparison with the penetration depth ($d \ll 1$). Such films in a magnetic field experience a second-order phase transition. In particular, it was discovered in [1] that in the case of a high-frequency field, the destruction of the superconductivity is determined by the mean-square field. Here we would wish only to add several observations, which touch on the properties of such a film in a slowly changing, strong field.

It was shown in [1] that generally, in a slow field, the change of $\Delta(\mathrm{t})$ follows the field change adiabatically. However, if we want to obtain a steady solution (one not depending on the initial conditions), in which a periodic behavior of Δ takes place in a periodically changing magnetic field then, in accord with [1], the condition $1 - \mathrm{h}^2 > 0$ is always necessary (notation from [1]). In other words, the regime, even in a suitably slow field, in which the plate undergoes periodic transition from the superconducting state to the normal, cannot always be established and must "collapse" for sufficiently large amplitude.

The new regime is determined by the value of the random fluctuations which arise during the time when the field is less than critical and the normal phase of the film is made absolutely unstable. Such a regime will certainly be aperiodic. The discovery of a collapse of the periodic regime and the study of the new regime is of considerable interest to us. We have based our arguments above on the formulas of [1], but it is clear that a similar "turbulent" regime will exist for all films with $2\,\mathrm{d} < \sqrt{5}$, for which the phase transition in the magnetic field is of second order. [2] We are dealing here with variable fields with amplitude of the order of the value of the critical field $\mathrm{H_{cm}}$.

We now proceed to the case of high frequencies $\omega \gg 1$ ($\delta_{\mathrm{S}} \ll 1$) and $1 \ll \mathrm{d} \ll 1/\kappa$. We shall assume that a constant magnetic field $\mathrm{h_0}$ is applied to the film from both sides. So far as the variable field with amplitude h_1 is concerned, let it be applied only from one side. Inasmuch as $\delta \ll 1$, the variable skin field penetrates only very slightly into the layer. Averaging the field (4) over the z coordinate (from $-d$ to $+d$), we obtain by a direct solution of the Ginzburg-Landau equations [2] the relation

$$\frac{[\Delta^2-(1-\alpha_1)]\cdot 2\Delta^2\mathrm{ch}^2\Delta d}{1-(\mathrm{sh}\,2\Delta d)/2\Delta d}=h_0^2, \tag{12}$$

where

$$\alpha_1=\frac{1}{2d}\int_{-d}^{+d}\overline{A_1^2}dz=\frac{h_1^2}{16d}\delta_s^3$$

By the substitution of variables

$$\Delta'=\frac{\Delta}{\sqrt{1-\alpha_1}},\quad d'=d\sqrt{1-\alpha_1},\quad h_0'=\frac{h_0}{1-\alpha_1} \tag{13}$$

we reduce it to an equation similar to that studied for films in [2,4].

If $h_0^2=0$, then $\Delta^2=1-\alpha_1$ falls off monotonically to zero with increase in the power of the variable field. We see that (comparable with [1]) the superconductivity for films with $d\ll 1/\kappa$ exists only if the amplitude of the field does not exceed some limit

$$h_1{}^2<4\sqrt{2}d\omega^{3/2} \tag{14}$$

Let a certain level of power of the variable field be given. Then the phase transition of the film in the constant magnetic field is significantly changed. For $\mathrm{d}'<\sqrt{5/2}$, this transition is of second order. In other words, according to (13), in the presence of radiation a second order phase transition takes place in a constant field for larger thicknesses:

$$\alpha_{\mathrm{cr}}=\sqrt{5}/2\sqrt{1-\alpha_1}. \tag{15}$$

The dependence of the critical field on the thickness is determined now by the relation

$$h_{\mathrm{c2}}=\sqrt{3}d^{-1}\sqrt{1-\alpha_1}. \tag{16}$$

For $\mathrm{d}>\mathrm{d_{cr}}$, from (15), the phase transition is a first order transition. Equation (16) has the meaning of a supercooling field. The superheating field is determined by the maximum of the curve (12). For $\mathrm{d}'\gg 1$, the field h′ was determined in [4] : $\mathrm{h_S'}=0.6\sqrt{\mathrm{d}'}$. Therefore, from (13),

$$h_{\mathrm{s}}=0.6\sqrt{d}\,(1-\alpha_1)^{5/4}\,. \tag{17}$$

The relations (16) and (17) determine the region of hysteresis (the region of ambiguity of the dependence of Δ on h_0). It is evident that this region contracts. However, in the presence of an alternating field, we cannot establish the criterion which corresponds to the thermodynamic criterion determining that field $\mathrm{h_{ocr}}$ in which the first order phase transition will be actually established. Similar experiments on the displacements of the critical field can easily be conducted.

In turn, by fixing the constant field $\mathrm{h_0}$ in the limits between (16) and (17), we conclude, inasmuch as h_0' in this range has associated with it two values of Δ, that the ambiguity of Δ exists also with respect to the dependence on the power of the variable field for fixed $\mathrm{h_0}$. It is seen from (16) that this ambiguity, i.e., the possibility of collapse of the superconducting steady state, arises for

$$\alpha_1=1-\frac{h_0^2d^2}{3}\quad(d<d_{\mathrm{cr}})\,.$$

The new regime obviously corresponds to the skin effect in the normal phase.

We have shown above that in the semi-infinite sample, the superconductivity does not vanish in a rapidly alternating field up to very high powers. On the contrary, according to (14), there is always a limiting value of the power in a thin film, above which the superconducting state cannot exist. We shall show that for thin films κd ~ 1, a transition takes place from the first situation to the second.

For this case, we consider a thick film (κd ~ 1) in a rapidly changing field ($\delta_S \ll 1$), applied from one side ($z = 0$). Then, as also for the case of an infinite halfspace, there is no field in the greater part of the film thickness. However, the gap is not equal to unity on the second wall (at $z = 2d$). We shall denote its value $\Delta(2d) \equiv \Delta_1$; then the first integral of Eq. (4) without a field can be written in the form

$$\frac{d\Delta}{dz} = x\left[\left(\Delta_1^2 - \Delta^2\right)\left(1 - \frac{\Delta_1^2 + \Delta^2}{2}\right)\right]^{1/2},$$

where we used the fact that $(\partial\Delta/\partial z)_{z=2d} = 0$. Assuming as in Sec. A that

$$\int_0^\infty \overline{A^2} dz = \alpha \gg \delta_s$$

and joining the results, we obtain two conditions

$$\int_{\Delta_0}^{\Delta_1} d\Delta \left[\left(\Delta_1^2 - \Delta^2\right)\left(1 - \frac{\Delta_1^2 + \Delta^2}{2}\right)\right]^{-1/2} = 2xd$$

$$\left[\left(\Delta_1^2 - \Delta_i^2\right)\left(1 - \frac{\Delta_1^2 + \Delta_0^2}{2}\right)\right]^{1/2} = \Delta_0 x\alpha$$

(where $\Delta_0 = \Delta(0), \alpha = \mathrm{h}_1^2\delta_\mathrm{S}^3/8$). Introducing the variable $\Delta/\Delta_1 = \cos \mathrm{z}, 0 < \mathrm{x} < \pi/2$, we transform both conditions to the much more convenient form

$$\int_0^u \frac{dx}{\sqrt{k^2 + \sin^2 x}} = \frac{2xd}{\sqrt{k^2+2}}, \qquad (18)$$

$$\sqrt{k^2 + \sin^2 u} = \alpha x\sqrt{k^2+2}\,\mathrm{ctg}\, u,$$

while

$$u = \arccos\left(\Delta_0/\Delta_1\right), \quad \Delta_1 = \sqrt{2}/\left(k^2+2\right). \qquad (20)$$

Equation (19) can be solved relative to u :

$$\cos^2 u = 1 + 1/2\left\{k^2 + \alpha x - \left[\left(k^2 + \alpha x\right)^2 + 4\alpha x\right]^{1/2}\right\}$$

After this, the problem of the determination of Δ_0 and Δ reduces to the numerical solution of Eq. (18). However, we shall not deal with this, bearing in mind only to show that there exists some critical thickness, above which no increase in the power can destroy the superconductivity over the entire volume of the film. For this purpose, we note that the destruction of superconductivity means k $\to \infty$ ($\Delta_1 \to 0$). It then follows from (18) that u $= 2\kappa$ d, while

$$xd < \pi/4 \qquad (21)$$

Here the threshold power that destroys superconductivity is determined by

$$1 = \alpha_{\mathbf{cr}} x\,\mathrm{ctg}\, 2xd \qquad (22)$$

For $\kappa d \ll 1$, we again get (13). For $\kappa d \sim 1$, we see that for destruction of the superconductivity in the film by the alternating field alone, high powers are necessary ($\kappa \ll 1$):

$$h_1^2 \varkappa \omega^{-3/2} \sim 1$$

Summing up what has been said about type I superconductors, we note only that although the majority of the formulas were obtained by us in the limiting case $\kappa \ll 1$, the phenomena described above undoubtedly are also valid for $\kappa \sim 1$. In this case, the situation deals with entirely realistic powers of the alternating field.

32.0.5 3. London Superconductors (Alloys with $\kappa \gg 1$)

The case of low frequencies of the alternating field for alloys is even more complicated in comparison with type I superconductors. If the amplitude of the variable field exceeds the critical value of the field H_{C_1}, for which vortices are formed, then the penetration of the field into the superconductor is connected with the motion of the quantized vortices. This effect has always had a hysteresis character, both because of the presence of the surface barrier and because of the imperfection of the sample. Therefore, it seems to us that one should consider the general picture of a similar nature rather on a phenomenological basis rather than on the basis of a microtheory constructed for the homogeneous alloy. In this connection, we limit ourselves to the remark that the "motion" of the boundary of the field, for the reasons given, takes place with a velocity v that is less than follows from the second of Eqs. (1'): $v < \sqrt{\omega}$, and in what follows, we shall study the case of high frequencies $\delta_S \ll 1/\kappa$, where the motion of the vortices is practically non-existent. [1)]

In weak fields we have (5') for the correction to the gap as before ($\kappa \gg 1$, but $\kappa \delta_S \ll 1$). For strong fields, we can apply the method of "joining" the two solutions described by Eqs. (7), (9) of the previous section. The joining together of the two solutions (7) and (6) takes place at distances $z \sim \delta \ll 1/\kappa$. Therefore, the criterion of applicability of the method is

$$h_1^2 \delta_s^3 \gg 1 \tag{23}$$

and Eq. (5') ($\kappa \delta_0 \ll 1$) can be obtained from (11) as the limiting case.

Thus, in this limiting high-frequency case, all the results of the previous section are valid. These were obtained for the half-space and film (if $h_0 = 0$). Once again, however, we note the fact that for films with $d > 1/\kappa$ for type II superconductors, there is the possibility of a new solution with the formation of vortices inside the film.

We now proceed to the inverse situation, where $\delta_s \gg 1/\kappa$.

$$\Delta^2(z) = 1 - \overline{A^2}(z) \tag{24}$$

The applicability of the quasiclassical solution (24) is limited to the vicinity of x_0, where $\Delta(z_0) = 0$. If the field is large enough,

$$h_1^2 \delta_s^2 / 4 \gg 1 \tag{25}$$

[01)] In experiments in a variable field, the amplitude of which is greater than H_{cl}, it is naturally always possible to have the existence of a finite vortex density in the sample which is oriented in a different way from these, so that the mean field connected with them was equal to zero. The formation of vortices is always possible, since this is one of the mechanisms of Joule loss. The regime in the variable field in the present of vortices, which are formed in fluctuating fashion, will necessarily be aperiodic (it is possible that a similar picture was observed in [[5,6]]; however, theoretical investigation of it is too complicated, and we shall in what follows digress from the possibility of a similar mechanism of collapse of the established regime.

and such a point exists, one must connect the solution (24) with the solution of the equation ($x = z - z_0$)

$$\frac{1}{x^2}\Delta'' + \frac{4x}{\delta_s}\Delta - \Delta^3 = 0 \tag{26}$$

with the conditions for the latter

$$\partial\Delta/\partial x \to 0, \quad x \to -\infty, \quad \Delta\infty x^{1/2}, \quad x \to +\infty.$$

By the substitution

$$x = \left(\delta_s/4x^2\right)^{1/3}\xi, \quad \Delta = \Delta\left(4/\delta_s x\right)^{1/3}$$

we reduce (26) to the form

$$\bar{\Delta}'' + \xi\bar{\Delta} - \Delta^3 = 0 \tag{\prime}$$

Equation (26') is the transcendental equation of Painleve (see [7]), relative to which it is shown that this solution is always a single-valued function of the complex variable ξ. Thus, even in this case, the superconductivity in a strong variable field for the half-space changes monotonically with increase in the power. However, in contrast with the type I superconductors (see [6]), to the left of the point z_0 there arises a region of normal phase. The very point z_0 moves to the right with increase in the field. Without solving (26) and (26'), we can see that, to the left of z_0, Δ decays according to the law

$$\Delta\infty \exp\left\{-\frac{4}{3}\frac{x}{\sqrt{\delta_s}}\left|z - z_0\right|^{3/2}\right\}. \tag{27}$$

The two latter problems, considered below in this section, pertain to the surface superconducting layer in fields $H_{C2} < H < H_{C_3}$, the existence of which was shown first by Saint-James and de Gennes [8]. We shall first show that a sufficiently large varying field destroys the surface layer. According to [8], we ought to study the existence of an infinitely small localized solution of Eq. (1) for Δ in a constant field h_0 and an alternating field $h_1(t)$. Let $\delta_S \gg 1/\kappa$ and the solution $\Delta(z, y)$ is sought in the form $\Delta(x, y) = \Delta(z)e^{iky}$. In correspondence with [8], we get for $\omega \gg 1$ Eq. (4) in the form

$$-\frac{1}{x^2}\frac{\partial^2\Delta_0}{\partial z^2} + \left[{h_0}^2\left(z - z_0\right)^2 + \frac{h_1^2}{4}\delta_s^2\exp\left(-\frac{2z}{\delta_s}\right)\right]\Delta_0 = \Delta_0 \tag{28}$$

The region of change of $\Delta_0(z)$ is of the order of $z \sim z_0 \sim 1/\kappa$ (see below). Therefore the exponent above can be replaced by unity. By the change of variables

$$z' = z\left(1 - \frac{h_1^2\delta_s^2}{4}\right)^{1/2}, \quad h'^2 = h_0^2\left(1 - \frac{h_1^2\delta_s^2}{4} -\right)^{-3/2} \tag{29}$$

we transform (28) to the form studied in [8]. This equation has its first solution for $h' = 1.7\kappa$. Then

$$h_{c3} = 1.7x\left(1 - \frac{h_1^2\delta_s^2}{4}\right)^{3/4}$$

As soon as h_{c_3} becomes equal to $\kappa\,(H = H_{c_2})$, the superconducting state becomes absolutely unstable in the bulk of the sample. Thus the condition for the vanishing of the surface layer is

$$1,7\left(1 - 1/4h_1^2\delta_s^2\right)^{3/4} = 1 \tag{30}$$

In conclusion, we consider a problem of unquestioned methodological interest-the derivation of equations which control the superconductivity in the surface layer for a varying field. We shall consider the case of small subcriticalities:

$$H(t) - H_{c3} \ll H_{c3} \tag{31}$$

and low frequencies. Thus, let $h(t) = h_{c_3} + h_1(t)$. Then, assuming that $\Delta_{=c}(t)\Delta_0(z)$, where $\Delta_0(z)$ is the solution of (28) for $h_1 = 0$, and multiplying the first of Eqs. (1) by this expression, integrating over z , we get

$$12c\overline{\dot{\Delta}_0{}^2} + c^4\overline{\Delta_0{}^4} - c^2\overline{\Delta_0{}^2} - \frac{c^2}{\lambda^2}\left(\overline{\Delta_0\frac{\partial^2\Delta_0}{\partial z^2}}\right) + \left(A' + h_{c3}\,(z - z_0)\right)^2\Delta_0{}^2c^2 = 0 \tag{32}$$

Here integration over z is indicated by the bar, A′ is the field composed of the external field h_1 and the field of the superconducting currents. By virtue of the smallness of h_1 we can expand (31) in Eq. (32) in terms of A' :

$$12c\dot{c}\overline{\Delta_0^2} + c^4\overline{\Delta_0^4} + 2h_{c3}\overline{A'(z)\,(z - z_0)\,\Delta_0^2(z)}c^2 = 0 \tag{33}$$

The field A' satisfies the equation

$$\partial^2 A'/\partial z^2 = \dot{A}' + c^2\Delta_0^2(z)\left\{h_{c3}\,(z - z_0) + A'(z)\right\} \tag{34}$$

Equation (34) must be solved by the method of successive approximations, taking it into account that c is small. For this purpose, we introduce the notation

$$A'(z) = A_1'(z) + A_S(z)$$

where

$$\partial^2 A_S/\partial z^2 = c^2 h_{c3}\Delta_0^2(z)\,(z - z_0)$$

Then, following [9], we integrate the last term in (33) by parts:

$$2\overline{A'(z)h_{c3}\,(z - z_0)\,\Delta_0^2(z)}c^2 = -2\overline{h'(z)h_S(z)} \tag{35}$$

where $\mathrm{h}' = \partial \mathrm{A}_1'/\partial \mathrm{z} + \partial \mathrm{A}_S/\partial \mathrm{z}$ and we have used the property noted in [8] that the total current in the superconducting layer is equal to zero:

$$h_{S,z} = 0 = h_{c3}c^2\int_0^\infty \Delta_0^2(z)\,(z - z_0)\,dz = 0 \tag{36}$$

For A_1', we have, according to (34), the equation

$$\frac{\partial^2 A_1'}{\partial z^2} = \dot{A}_1' + \dot{A}_S + c^2\Delta_0^2(z)\,[A_S + A_1'] \tag{\prime}$$

In Eq. (33), the term with the time derivative is substantial in the region $\omega \sim c^2$. We shall be guided by this scale of frequencies. It is then seen from (36) that the screening currents are small and the field h' in the first approximation can be set equal to $h' = h_1(t) + h_S$. Thus (35) is transformed to the form

$$-2h_1(t)\overline{h_S(z)} - 2\overline{h_S^2(z)} \tag{37}$$

where

$$h_S(z) = -c^2 h_S \int_z^\infty \Delta_0^2(z)\,(z - z_0)\,dz$$

The calculation of all the integrals entering into (33) and (37) is generally possible only numerically. However, in the limit $\kappa \gg 1$, the calculation can be greatly simplified. In particular, it is possible to omit the term $\overline{h_S^2}$ in (37). Actually, this term makes a contribution to the coefficient before c^4 in (33). Let $\overline{\Delta_0^2} = 1$. Then, inasmuch as the characteristic length dimension is $1/\kappa$, while the field is $h_{c3} \sim \kappa$, we have

$$\overline{h_S(z)} \overset{\overline{\Delta_0^4} \sim x,\quad h_S(z) \sim c^2/\varkappa \sim c^2/h_{c3},}{\sim} \quad \overline{h_S^2(z)} \sim c^4/\varkappa.$$

Final formulas are conveniently obtained by using the variational method of determination of $\Delta_0(z)$ proposed by Kittel (see [9]). Choosing $\Delta_0(z)$ in the form e^{-rz^2}, we find

$$r = \frac{x h_{c3}}{2}\sqrt{1 - \frac{2}{\pi}}, \quad z_0 = \frac{1}{\sqrt{2\pi r}}, \quad h_{c3} \approx 1.66$$

Using the latter expression, after simple calculations, we get

$$12\dot{c} + \frac{c^3}{\sqrt{2}} + \frac{h_1(t)}{h_{c3}} c = 0 \tag{38}$$

The general solution of an equation of the type (38) is given in [1]. By means of it one can, from Eqs. (34'), find the corrections, for example, to the impedance in a metal, arising from the surface layer.

33 Inelastic Electron Collisions and Nonequilibrium Stationary States in Superconductors by Eliashberg

Abstract

A derivation of the dynamic equations for superconductors is presented, in which inelastic collisions between electrons or between electrons and phonons are taken into account explicitly. It is assumed that the phonons are in equilibrium (play the role of a thermostat). The conditions for which this assumption is valid are discussed. The equations are written in a form which is analogous to the kinetic equation but their structure is much more complex than for a normal metal. This complication is mainly due to the need for taking into account changes induced in the excitation spectrum density by an alternating external field. For thin films taken as an example, it is shown that under certain conditions the alternating field effect consists mainly of a redistribution of the excitations with respect to energy, the spectrum density remaining constant. In this case the set of equations reduces to an equation for the energy gap, which is identical in form to the BCS equation but has a nonequilibrium distribution function, and to a nonlinear kinetic equation for this function.

33.0.1 1. Choice of Model

ONE of the important problems of the dynamic theory of superconductivity is the investigation of the nonequilibrium stationary states of the superconductor that are produced by continuous application of an alternating field. It is clear that the existence of such states is possible only because of the coupling between the electrons and the thermostat, the role of

which is played in final analysis by the cooling medium. The mechanism of this coupling can be quite complicated, but it is realized in any case by the inelastic collisions of the electrons with the phonons, with the walls of the sample, and also with one another. Such collisions, however, are not considered in the simplified BCS model [1], on which the greater part of the dynamictheory investigations is based. This is justified by the relatively low probability of the inelastic electron scattering processes in metals. The corresponding damping of the excitations γ in the normal state is, as is well known, of the order of $\mathrm{T}^3/\Theta_{\mathrm{D}}^2$ and $\mathrm{T}^2/\mathrm{E_F}$ in electron-phonon and electron-electron scattering, and is comparable with the energy scale characteristic of superconductors, namely the value of the parameter Δ, only in a very small neighborhood of the transition temperature:

$$(T_{\mathrm{c}} - \mathrm{T})/T_{\mathrm{c}} \sim (T_{\mathrm{c}}/\Theta_D)^4, \quad (T_{\mathrm{c}}/E_F)^2.$$

In the case of bulky superconductors, the perturbation connected with the action of the alternating field is localized near the surface, and the kinetics of the process is determined mainly by the diffusion relaxation mechanism. Of course, such a mechanism by itself does not lead to a stationary regime. Nonetheless, if the time-averaged deviation from equilibrium is small in the stationary state, then the final results do not contain the characteristics of the inelastic processes. On the other hand, it is precisely by virtue of the slowness of the energy relaxation of the electrons that the dynamic properties of the superconductors are strongly influenced by the deviation from equilibrium in the energy distribution of the electrons; at a small average value, the collision amplitude becomes appreciable. The hydrodynamic approximation is therefore not suitable here, and there is no simple generalization of the Ginzburg-Landau theory for the nonequilibrium case [2–4].

Moreover, the large value of the electron-energy relaxation time gives rise to a noticeable stationary deviation in the energy distribution of the electrons even for relatively weak excitation. A study of the effects that may be connected with this calls for explicit allowance for the inelastic processes. Such an allowance is essential, in particular, for the investigation of the dynamics of superconductors of small dimensions, when the entire volume of the sample is in the nonequilibrium state, and there is no diffusion relaxation.

Before we proceed to derive the equations, we must dwell on the choice of the model. We consider below the simplest case, when the role of the thermostat is played by the lattice, so that the coupling of the electrons with the thermostat is effected by electronphonon interaction. A definite role can be played here also by electron-electron collisions, which we shall also take into consideration.

Let us discuss now the degree to which this assumption can be regarded as justified in different cases.

The simplest situation in this sense occurs in the case of samples of small dimensions, particularly for thin films, which will be discussed here for concreteness. We are interested in films whose thickness is of the same scale as the correlation radius $\xi_0 \sim \hbar \mathrm{v}/\mathrm{T_c}$ (v is the electron velocity on the Fermi surface), i.e., much larger than the wavelength of the thermal phonon at $\mathrm{T} \sim \mathrm{T_c}$. If the $\rho \mathrm{s}$ (ρ-density, s -speed of sound) in the metal and in the cooling medium are of the same order of magnitude, then the phonon will give up its energy practically in each collision with the wall (see, for example, [5]). On the other hand, the free-path time of a thermal phonon in a bulky sample, connected with its interaction with the electrons, is of the order of $\hbar \mathrm{v}/\mathrm{sT}$[6], so that the corresponding free path is $\sim \xi_0$ at $\mathrm{T} \sim \mathrm{T_c}$. Thus, at a film thickness $\mathrm{d} < \xi_0$, the phonon distribution will be determined by the collisions with the walls and its deviation from equilibrium will be small. On the other hand, if ρs is much smaller in the medium than in the metal, then to satisfy this condition it is necessary to have correspondingly thinner films. In the case of relatively thick films, when the phonons relax mainly on electrons, their distribution function will align itself

to the distribution of the electrons. Since the phonon specific heat is small compared with that of the electrons, the phonons in this case exert no direct influence at all on the stationary distribution of the electronic excitations, which in this method of excitation is determined by the electron-electron collisions and by the condition that determines the equality of the energy flux absorbed by the electrons to the flux carried away through the walls. In this case, generally speaking, the situation does not reduce at all to simple heating: the electron distribution, and with it the phonon distribution, can differ noticeably from the temperature distribution.

All the foregoing pertains to some intermediate temperature region, when $\Delta \sim T$. The situation can change greatly at low temperatures and in the vicinity of $\mathrm{T_c}$. If $\mathrm{T} \ll \Delta$, then at not too intense an irradiation, the number of the excitations is small and they therefore exert a small influence on the phonon system, so that the latter remains at equilibrium also in the case of films thicker than indicated above. The same takes place, albeit for another reason, when $\mathrm{T} \gg \Delta$: if the field frequency is comparable with Δ, then it can be shown [7] that the nonequilibrium excitations are concentrated in the energy region $\epsilon \sim \Delta \ll T$, and the bulk of the excitations remains in equilibrium and plays, together with the phonons, the role of the thermostat.

These last considerations, which pertain to extreme temperatures, remain in force also for a bulky superconductor: the region of low temperatures and the vicinity of T_c are here, too, favorable for the use of the chosen model. At the same time, when the problem is formulated in greater detail, it must be borne in mind that in the case of a bulky sample we deal with a picture that is essentially inhomogeneous in space. The nonequilibrium excitations produced in the region δ of field penetration can then proceed from the surface to a greater or a smaller depth, which depends on the ratio of the transport path time τ, which we shall assume to be determined by the impurities, to the energy relaxation time τ_0. If $\tau \ll \tau_0$, then we have diffusion of the nonequilibrium excitation to a depth $L \sim (l\mathrm{v}\tau_0)^{1/2}$, which, depending on the impurity concentration, on the temperature, and on the field frequency, can be either larger or smaller than δ. Owing to the large value of τ_0, the inequality $L \gg \delta$ can be satisfied also under the condition $l \ll \xi_0$, and we therefore confine ourselves here to a discussion of only this case. The form of the electron distribution will change with increasing distance from the surface. At distances small compared with L, this change is due mainly to the dependence of the diffusion coefficient of the excitations in the superconductor on the energy:
$\mathrm{D}_\epsilon = \left(l\mathrm{v}_\epsilon/3 \sim \sqrt{\epsilon^2 - \Delta^2}\right.$, At distances comparable with L , inelastic processes come into play. If the phonon mean free path connected with their interaction with the electrons is larger than L, as can occur at low temperatures, then the phonons remain in equilibrium, and the electrons relax over a length L to the tem perature of the phonon thermostat. A similar situation arises, for the reason indicated above, also near T_c. In these cases, the mechanism whereby the heat is carried away does not enter explicitly into the problem.

In the intermediate temperature interval, and also at low temperatures under conditions of sufficiently strong pumping, the number of excitations is large and the equilibrium in their distribution is violated in the entire energy interval. Therefore, as in the foregoing example of a relatively thick film, the phonons have time to align themselves to the electron distribution and drop out of the game. In this case, owing to the electron-electron collisions, thermalization of the excitation gas takes place over distances $\sim_L$, but the corresponding temperature may differ from the initial one, and the heat removal must be taken into account explicitly for its determination.

The foregoing estimates, of course, are schematic and need refinement as applied to concrete problems. Nonetheless, they show that there exists a sufficiently wide circle of problems the investigation of which can be carried out on the basis of the chosen model and does not require explicit allowance for the heat-removal mechanism.

33.0.2 2. Dynamic Equations in the Phonon Model

In order to take the electron-phonon collisions into account in a consistent manner, we derive the dynamic equations on the basis of the phonon model. As in the paper of Gor'kov and the author [3], the starting point is the concept of discrete imaginary frequencies, in which the expansion of the Green's function in powers of the external field has a simple diagram structure. The essential complication that arises when working with the phonon model is that it is necessary to deal here with energy-dependent self-energy parts, which will be determined by the same diagram approximation as in the equilibrium case [8] (Fig.1). ($\mathrm{P} = \{\xi, \mathrm{p}\}, \mathrm{K} = \{\omega, \mathrm{k}\}$) :

$$\Sigma_1(P, P-K) = T\sum_{\varepsilon'} \int \frac{d^3\mathbf{p}'}{(2\pi)^3} D\left(P'-P\right) G\left(P', P'-K\right), \tag{1}$$

$$\Sigma_2(P, P-K) = T\sum_{\varepsilon'} \int \frac{d^3\mathbf{p}'}{(2\pi)^3} D\left(P'-P\right) F\left(P', P'-K\right).$$

The functions G and F are assumed to be exact in the sense that they include, besides the external alternating field, also the self-energies Σ_1 and Σ_2. In contrast, the Green's function of the phonons is assumed to be free:

$$D\left(P'-P\right) = g^2 \frac{{}'_{\ldots} n^2_{n'-\mathbf{p}}}{\omega^2_{\mathbf{p}'-\mathbf{p}} - \left(\varepsilon' - \varepsilon\right)^2} \tag{2}$$

corresponding to the assumption that the phonons are

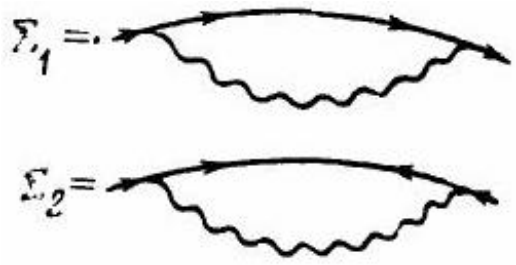


FIG. 1

in equilibrium. (The renormalization of the phonon spectrum can be regarded as taken into account in (2), since it is practically independent of the smearing region near the Fermi surface, which is affected by violation of the equilibrium.)

We shall carry out an analytic continuation of (1) by regarding G and F as sums of diagrams of different order in the alternating field. Since the entire procedure is independent of whether we are dealing with Σ_1 or Σ_2, we shall set the function G in correspondence with the electron line and will not mark the directions of the arrows on the diagrams.

Let us consider a diagram of N -th order in the field. It depends on the frequencies of its extreme electron lines ϵ and $\epsilon - \omega$, and in addition it depends on the frequencies ωl corresponding to the field vertices ($\sum_{l=1}^{N} \omega_l = \omega$). Since in the approximation (1) = (2) a single electron line passes through any diagram G , the field vertices can be numbered in the sequence in which they follow along this line from left to right, regardless of whether this diagram contains the insert Σ or not (Fig. 2). Let us ascertain the analytic structure of G(N) as a function of the variable ϵ at fixed $\omega_l = 2\ \mathrm{m}_l \pi \mathrm{Ti}$. We are interested in the final analysis in the continuation of each of the ω_l from the upper halfplane, and we can therefore assume that all the $\mathrm{m}_l > 0$. The diagram of Fig. 1a (i.e., the one not containing Σ), is a product of the zeroth-approximation functions $\mathrm{G(P)} = (\xi - \epsilon)^{-1}, \xi = \mathrm{v}\left(\mathrm{p} - \mathrm{p}_0\right)$:

$$G^{(N)}_{\varepsilon,\varepsilon-\omega} \infty G_\varepsilon G_{\varepsilon-\omega_1} G_{\varepsilon-\omega_1-\omega_2} \ldots G_{\varepsilon-\omega}$$

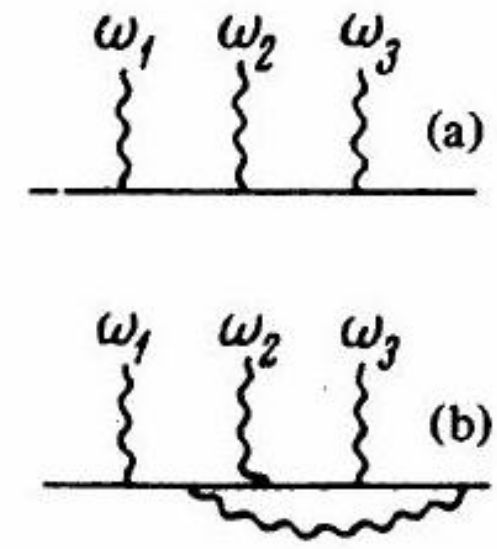
and its singularities as functions of ϵ (in this case, poles), located on lines parallel to the real axis: $\operatorname{Im}\epsilon = 0, \operatorname{Im}(\epsilon-\omega_1) = 0, \ldots, \operatorname{Im}(\epsilon-\omega) = 0$. We shall show now that the same lines are singular also for a diagram $G(N)$ of arbitrary form (for example, Fig 2b). To this end, obviously, it suffices to verify that $\Sigma^{(}\mathrm{N}\big)$ has the same analytic structure as its internal electron line.

To do so, we transform the sum in (1) into a contour intergral, drawing the cuts in the ϵ' plane along the indicated singular lines $\mathrm{G}^{(\mathrm{N})}_{\epsilon',\epsilon'-\omega}$ and along the singular line of the D-function $\operatorname{Im}(\epsilon'-\epsilon) = 0 (\epsilon = (2\mathrm{n}+1)\pi\mathrm{Ti})$, and choosing the integration contour as shown in Fig. 3. We denote the jump of the $\mathrm{G}^{(N)}$ function on its l-th cut by $\delta_l\left(\mathrm{G}^{(\mathrm{N})}\right)$, numbering these cuts in the upward direction. We then obtain the following representation for $\Sigma^{(N)}$:

$$\Sigma^{(N)}_{\varepsilon,\varepsilon-\omega} = \int_{-\infty}^{\infty} \frac{dz}{4\pi i} \Big\{ \operatorname{cth}\frac{z}{2T} \left(D^R - D^A\right)_z G^{(N)}_{z+\varepsilon,z+\varepsilon-\omega}$$
$$+ \operatorname{th}\frac{z}{2T} \left[D(z-\varepsilon)\delta_0\left(G^{(N)}\right) + D\left(z-\varepsilon+\omega_1\right)\delta_1\left(G^{(N)}\right) \right.$$
$$\left. \ldots + D(z-\varepsilon+\omega)\delta_N\left(G^{(N)}\right)\right]\Big\} \tag{3}$$

Since the integration variable z is real, we see that $\Sigma(N)$ contains the same combinations of ϵ and ω_l as $G^{(N)}$, thus proving the statement made above.

Continuing (3) with respect to ϵ from the regions $\operatorname{Im}(\epsilon-\omega) > 0$ and $\operatorname{Im}\epsilon < 0$, we obtain the contributions of N -th order in the field to Σ^{R} and Σ^{A}, respec-



tively. In these cases, all the combinations of ϵ with ω_l that enter in (3) have imaginary parts of definite sign, and therefore the successive continuation with respect to each of the ω_l does not depend on the order. Shifting then the integration variables in each term of (3) in a simple manner, so as to restore the initial designation of the arguments, and summing over all the N , we arrive at the following formulas:

$$\Sigma_1^{R(A)}(P, P-K) = \int_{-\infty}^{\infty} \frac{d\varepsilon'}{4\pi i} \int \frac{d^3\mathbf{p}'}{(2\pi)^3} \Big\{ \operatorname{cth}\frac{\varepsilon'-\varepsilon}{2T} \left(D^R - D^\Lambda\right)_{P'-P}$$
$$\times G^{R(\Lambda)}\left(P', P'-K\right) + D^{\Lambda(R)}\left(P'-P\right) G\left(P', P'-K\right)\Big\} \tag{4}$$

where

$$G(P,P-K)=\sum_{N=0}^{\infty}\sum_{l=0}^{N}\delta_l\left(G^{(N)}\right)\operatorname{th}\frac{\varepsilon_l}{2T},\quad \varepsilon_l=\varepsilon-\omega_1-\ldots-\omega_l \tag{5}$$

Expressions for $\Sigma_2^{\mathrm{R(A)}}$ are obtained from this by replacing $G^{R(A)}$ and G by $F^{R(A)}$ and F. Since all the free lines and the proper spectra forming the diagrams $\mathrm{G^{R(A)}}$ are retarded (advanced), it follows that $\mathrm{G^{R(A)}}$ and $F^{R(A)}$ can be expressed in the usual manner in terms of $\Sigma_1^{\mathrm{R(A)}}$ and $\Sigma_2^{\mathrm{R(A)}}$:

$$\left\{\begin{pmatrix}\xi-\varepsilon-\Sigma_1+H_1 & -\Sigma_2\\ \Sigma_2^{+} & \xi+\varepsilon-\bar{\Sigma}_1+\bar{H}_1\end{pmatrix}\begin{pmatrix}G\\ -F^{+}\end{pmatrix}\right\}_{P,P-K}^{R(A)}=\hat{1}(2\pi)^4\delta(\omega)\delta(\mathbf{k})$$
$$H_1=-\frac{e}{c}(\mathbf{vA})+e\varphi,\quad \bar{H}_1=\frac{e}{c}(\mathbf{vA})+e\varphi. \tag{6}$$

The function G , introduced by the relation (5), and the analogous function F, play the principal role in the theory of nonequilibrium phenomena. We shall soon show that all the physical quantities, namely the current, Δ, etc., are expressed directly in their terms.

To establish the connection between G and Σ, we rewrite (5) in a somewhat different form, namely, we separate from the contribution of each diagram the terms corresponding to the upper edge of the upper cut and the lower edge of the lower cut (Fig. 3). The separated terms obviously define the retarded and advanced Green's functions, so that we obtain the following definition of the new quantity $\mathrm{G^{(a)}}$:

$$G(P,P-K)=G^R(P,P-K)\operatorname{th}\frac{\varepsilon-\omega}{2T}-\operatorname{th}\frac{\varepsilon}{2T}G^A(P,P-K)$$
$$+G^{(a)}(P,P-K) \tag{7}$$

It is easy to verify that, in the case of the BCS model, in which Δ enters in the diagrams in analogy to the external field, $\mathrm{G^{(a)}}$ coincides with the anomalous part of the Green's function introduced earlier [3]. All the terms making up $\mathrm{G^{(a)}}$ have a common property in that they have $G^R(P)$ as the incoming free line and $\mathrm{G^A(P-K)}$ as the outgoing line. The difference from the BCS model consists here in the fact that (5) has a part connected with the self-energy cuts. From (5) and

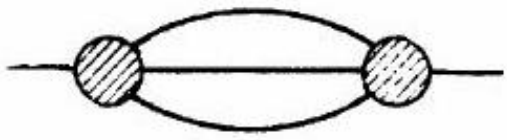


FIG. 3

(7), taking into account the fact that G contains the self-energies Σ_1 and Σ_2 (and with inverted arrow directions), we readily find that

$$G^{(a)}_{\varepsilon,\varepsilon-\omega}=\left\{G^R\left(-h+\Sigma_1^{(a)}\right)G^4-F^{\mathrm{q}}\left(-\bar{h}+\bar{\Sigma}_1^{\prime a}\right)F^{+A}\right.$$
$$\left.-G^R\Sigma_2^{(a)}F^{+A}-F^R\Sigma_2^{+(a)}\bar{G}^A\right\}_{\varepsilon,\varepsilon-\omega} \tag{8}$$

where

$$h_{e,\varepsilon-\omega}=\left(\operatorname{th}\frac{\varepsilon}{2T}-\operatorname{th}\frac{\varepsilon-\omega}{2T}\right)H_1(\omega)$$

and $\Sigma_1^{(a)}, \bar{\Sigma}_1^{(a)}, \Sigma_2^{(a)}, \bar{\Sigma}_2^{+(a)}$ are expressed in terms of the discontinuities on the cuts of the corresponding self-energies with the aid of relations of the type (5) and (7):

$$\Sigma_{\varepsilon,\varepsilon-\omega} = \Sigma^R_{\varepsilon,\varepsilon-\omega} \operatorname{th} \frac{\varepsilon-\omega}{2T} - \operatorname{th} \frac{\varepsilon}{2T} \Sigma^A_{\varepsilon,\varepsilon-\omega} + \Sigma^{(a)}_{\varepsilon,\varepsilon-\omega}$$
$$= \sum_{N=0}^{\infty} \sum_{l=0}^{N} \delta_l \left(\Sigma^{(N)}\right) \operatorname{th} \frac{\varepsilon_l}{2T}. \tag{9}$$

The superior bar denotes an inversion of the arrow directions in the diagrams. In a coordinate representation we have identities of the type

$$\bar{G}^A(x,x') = G^R(x',x), \quad \bar{G}^{(a)}(x,x') = G^{(a)}(x',x); x = \{t, \mathbf{r}\}$$

Finally, we note that in (8) we have used the abbreviated notation [1)] :

$$\{ABC\}_{\mathrm{s,e}-\omega} = \iint_{-\infty}^{\infty} \frac{d\omega_1 d\omega_2}{(2\pi)^2} A_{\mathrm{e,e}-\omega_1} B_{\mathrm{e}-\omega_1,\mathrm{e}-\omega_2} C_{\mathrm{e}-\omega_2,\mathrm{e}-\omega} \tag{10}$$

In exactly the same manner, we can obtain expressions for $\mathrm{F^{(a)}}$, $\mathrm{F^{+(a)}}$, and $\overline{\mathrm{G}}^{(\mathrm{a})}$. For example,

$$F^{(a)}_{\varepsilon,\varepsilon-\omega} = \left\{ G^R \left(-h + \Sigma_1^{(a)}\right) F^A + F^R \left(-\bar{h} + \bar{\Sigma}_1^{(a)}\right) \bar{G}^A \right. \tag{11}$$
$$\left. + G^R \Sigma_2^{(a)} \bar{G}^A - F^R \Sigma_2^{+(a)} F^A \right\}_{\varepsilon,\varepsilon-\omega}.$$

It remains for us to express Σ, defined in accordance with (9), in terms of the Green's functions, as was done above for $\Sigma^{R(A)}$ (see Fig. 4). From (3) we obtain, with the aid of the identity $\coth(\mathrm{x}' - \mathrm{x})(\tanh \mathrm{x}' - \tanh \mathrm{x} = 1 - \tanh \mathrm{x} \tanh \mathrm{x}'$,

$$\Sigma_1(P, P-K) = \int_{-\infty}^{\infty} \frac{d\varepsilon'}{4\pi i} \int \frac{d^3\mathbf{p}'}{(2\pi)^3} \left\{ \operatorname{cth} \frac{\varepsilon'-\varepsilon}{2T} G(P', P'-K) \right. \tag{12}$$
$$\left. - \left(G^R - G^A\right)_{P',P'-K} \right\} \left(D^R - D^A\right)_{P'-P}$$

Formulas for Σ_2 and $\Sigma_2^+$are obtained from this by replacing G with F and F^+. We now have a complete system of equations describing, on the basis of the Fröhlich model, the behavior of a superconductor in an alternating field.

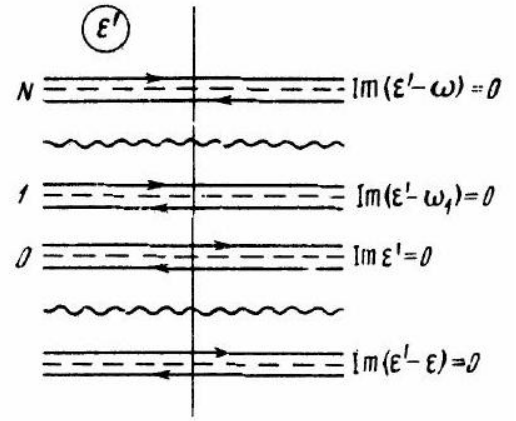


FIG. 4

[01)] Depending on the representation, integration is implied here with respect to the intermediate coordinates or with respect to the momenta.

33.0.3 3. Kinetic Equations

Let us eliminate from the equations of the preceding section the anomalous functions $\mathrm{G}^{(\mathrm{a})}, \Sigma^{(\mathrm{a})}$, etc. To this end, we note that $G^{(\mathrm{a})}$ (Eq. (8)) satisfies the following Dyson equation, which is obtained by separating on the left the free line $G^R(P) = (\xi - \epsilon - i\delta)^{-1}$:

$$(\xi - \varepsilon)G^{(a)}(P, P-K) = \left\{\left(-H_1 + \Sigma_1^R\right) G^{(a)} - \Sigma_2^R F^{+(a)}\right\}_{P,P-K} + \left\{\left(-h + \Sigma_1^{(a)}\right) G^A - \Sigma_2^{(a)} F^{+A}\right\}_{P,P-K}$$

(the notation is the same as in (8) and (10)). Substituting here in place of the anomalous functions their expressions from (7) and (9) and using Eqs. (6) for $\mathrm{G}^{\mathrm{R(A)}}$ and $\mathrm{F}^{\mathrm{R(A)}}$, we obtain an equation for G(5) :

$$(\xi - \varepsilon)G(P, P-K) = \left\{\left(-H_1 + {\Sigma_1}^R\right) G - {\Sigma_2}^R F^+ + \Sigma_1 G^A - \Sigma_2 F^{+A}\right\} + (2\pi)^4 \delta(\omega)\delta(\mathbf{k}) \tag{13}$$

In exactly the same manner, we obtain an equation for F:

$$(\xi - \varepsilon)F(P, P-K) = \left\{\left(-H_1 + {\Sigma_1}^R\right) F + {\Sigma_2}^R \bar{G} + \Sigma_1 F^A + \Sigma_2 \bar{G}^A\right\} \tag{14}$$

and, analogously, for $F^+$and $\bar{G}$. An important property of Eqs. (13) and (14) is the fact that only the Σ of formulas (4) and (12) depend explicitly on the temperature, and we see that T enters in these formulas as the temperature of the phonon thermostat. The situation here is in full correspondence with that demonstrated by Keldysh [9], whose method could be used in our case. The method chosen by us to obtain the dynamic equations makes it possible to retain the direct connection with the previously described diagram technique [3].

We call attention now to the fact that, as noted a number of times [6,8], the self energies Σ are practically independent of the momentum, i.e., of $\xi = \mathrm{v}\,(\mathrm{p} - \mathrm{p}_0)$. In fact, p enters only in the D function, and since both the external momentum p and the internal momentum p' are close to the Fermi momentum p_0, it follows that $D\,(p - p')$ depends mainly on the angle between them. This enables us to go over in (4) and (12) from integration with respect to p to integration with respect to ξ and the angles

$$\frac{d^3\mathbf{p}}{(2\pi)^3} \approx \frac{mp_0}{2\pi^2}\frac{dO_{\mathbf{p}}}{4\pi}d\xi$$

and to integrate the electron functions in these formulas with respect to ξ. Introducing the notation

$$g_{\varepsilon,\varepsilon-\omega}(\mathbf{p},\mathbf{k}) = \int_{-\infty}^{\infty} d\xi G(P, P-K),\ f_{\varepsilon,\varepsilon-\omega}(p,k) = \int_{-\infty}^{\infty} d\xi F(P, P-K) \tag{15}$$

we rewrite Σ in the form

$$\Sigma^{R(A)}_{i\varepsilon,\varepsilon-\omega}(\mathbf{p},\mathbf{k}) = \int_{-\infty}^{\infty}\frac{d\varepsilon'}{4\pi i}\int\frac{dO_{\mathbf{p}}}{4\pi}\left\{\mathrm{cth}\,\frac{\varepsilon'-\varepsilon}{2T}\left(D^R - D^A\right)g^{R(A)} + D^{A(R)}g\right\} \tag{I}$$

$$\Sigma_{1\varepsilon,\varepsilon-\omega}(\mathbf{p},\mathbf{k}) = \int_{-\infty}^{\infty}\frac{d\varepsilon'}{4\pi i}\int\frac{dO_{\mathbf{p}}}{4\pi}\left\{\mathrm{cth}\,\frac{\varepsilon'-\varepsilon}{2T}g - \left(g^R - g^A\right)\right\}\left(D^R - D^A\right) \tag{I}$$

and analogously, for $\Sigma_2{}^{2)}$; $\mathrm{D}^{\mathrm{R(A)}} \equiv \mathrm{D}^{\mathrm{R(A)}}_{\epsilon'-\epsilon}\,(\mathrm{p}' - \mathrm{p})$, $\mathrm{g} \equiv \mathrm{g}_{\epsilon'}, \epsilon' - \omega(\mathbf{p},\mathbf{k})$.

We see now that ξ enters explicitly only in the lefthand sides of (13) and (14), and we can therefore obtain equations directly for g and f. To do so, we write out for G and F equations

analogous to (13) and (14), but obtain from (8) and (11) by separating the free righthand line: $\mathrm{G^A(P-K)} = (\xi - \mathrm{vk} - \epsilon + \omega + \mathrm{i}\delta)^{-1}$ in the case of G and $\overline{\mathrm{C}}^{\mathrm{A}}(\mathrm{P-K}) = (\xi - \mathrm{vk} + \epsilon - \omega - \mathrm{i}\delta)^{-1}$ in the case of F :

$$(\xi - \mathbf{vk} - \varepsilon + \omega)G(P, P-K) = \left\{G\left(-H_1 + {\Sigma_1}^A\right) - F{\Sigma_2}^{+A}\right.$$
$$\left. + G^R\Sigma_1 - F^R{\Sigma_2}^+\right\} + (2\pi)^4\delta(\omega)\delta(\mathbf{k})$$
$$(\xi - \mathbf{vk} + \varepsilon - \omega)F(P, P-K) = \left\{F\left(-\bar{H}_1 + {\bar{\Sigma}_1}^A\right) + G{\Sigma_2}^A\right.$$
$$\left. + F^R\bar{\Sigma}_1 + G^R\Sigma_2\right\}$$

Combining these equations with (13) and (14), so as to exclude ξ from the left-hand side, and integrating with respect to ξ, we obtain

$$(\omega - \mathbf{vk})g_{\varepsilon,\varepsilon-\omega} = \left\{H_1 g - gH_1 + g{\Sigma_1}^\Lambda - {\Sigma_1}^R g - f{\Sigma_2}^{+\Lambda}\right. \tag{16}$$
$$\left. + {\Sigma_2}^R f^+ + g^R\Sigma_{\cdot} - \Sigma_1 g^\Lambda - f^R{\Sigma_2}^+ + \Sigma_2 f^{+\Lambda}\right\}_{\varepsilon,\varepsilon-\omega}$$
$$(2\varepsilon - \omega - \mathbf{vk})f_{\varepsilon,\varepsilon-\omega} = \left\{H_1 f - f\bar{H}_1 + \bar{f}{\bar{\Sigma}_1}^\Lambda - {\Sigma_1}^R f + g{\Sigma_2}^\Lambda\right. \tag{17}$$
$$\left. - {\Sigma_2}^R\bar{g} + f^R\Sigma_1 - \Sigma_1 f^\Lambda + g^R\Sigma_2 - \Sigma_2\bar{g}^\Lambda\right\}_{\varepsilon,\varepsilon-\omega}$$

Besides the processes of scattering and decay of excitations, Eqs. (16) and (17) take into account also the renormalization effects. The latter are determined by the quantity $\Sigma_1^{\mathrm{R}} + \Sigma_1^{\mathrm{A}}$ and are practically insensitive to violation of the equilibrium [3)]. We shall disregard them and retain in the equations only the dissipative part Σ_1^{R} :

$$2i\gamma_{\varepsilon,\varepsilon-\omega} \equiv {\Sigma_{\mathrm{t}}}^{\mathrm{R}} - {\Sigma_{\mathrm{t}}}^{\mathrm{A}} = \int_{-\infty}^{\infty}\frac{d\varepsilon'}{4\pi i}\int\frac{dQ_{p'}}{4\pi}\left[\operatorname{cth}\frac{\varepsilon'-\varepsilon}{2T}\left(g^{\mathrm{R}} - g^{\mathrm{A}}\right) - g\right]\left(D^R - D^A\right)$$

With the same accuracy, the role of Δ is assumed by the quantity

$$\Delta = 1/2\left(\Sigma_2^R + \Sigma_2^A\right) \tag{19}$$

which varies as a function of ϵ in an interval $\sim \omega_D$, so that when $\epsilon \sim \Delta$ and $T \ll \omega_D$ this dependence is immaterial. The first term under the integral sign in (4') for Σ_2 introduces in Δ a contribution $\sim \Delta\,(T/\omega_D)^2$. We can therefore use for the determination of Δ the simplified equation

$$\Delta_\omega(k) = \lambda\int_{-\omega_D}^{\omega_D}\frac{d\varepsilon}{4\pi i}\int\frac{dO_P}{4\pi}f_{e,\varepsilon-\omega}(\mathbf{p},\mathbf{k}) \tag{20}$$

At the same time, for $\Sigma_2^{\mathrm{R}} - \Sigma_2^{\mathrm{A}}$ it is necessary to retain the exact expression:

$$2i\delta_{e,\varepsilon-\omega} \equiv \Sigma_2^R - {\Sigma_2}^\Lambda = \int_{-\infty}^{\infty}\frac{d\varepsilon'}{4\pi i}\int\frac{dO_p}{4\pi}\left[\operatorname{cth}\frac{\varepsilon'-\varepsilon}{2T}\left(f^R - f^\Lambda\right)\right.$$
$$\left. - f\right]\left(D^R - D^\Lambda\right) \tag{21}$$

After these simplifications, Eq. (16) takes the form

$$(\omega - \mathrm{vk})g_{\varepsilon,\varepsilon-\omega} = \left\{H_1 g - gH_1 - f\Delta^* + \Delta f^+\right\}_{e,e-\omega} + I_{\varepsilon,\varepsilon-\omega} \tag{22}$$

[02)] We have included the factor $\mathrm{mp_0}/2\pi^2$ in the D function (2), where now $\mathrm{g^2 mp_0}/2\pi^2 \equiv \lambda \sim 1$.

[3)] As is well known [6,8] in the equilibrium case $\mathrm{Re}\,\Sigma_{1\epsilon}^{\mathrm{R}} \approx \mathrm{a}\epsilon$, where a ~ 1 has the same value in the normal and in the superconducting states, accurate to within $(\Delta/\omega_{\mathrm{D}})^2$.

where

$$I = \left\{-i(g\gamma + \gamma g) + i\left(f\delta^+ + \delta f^+\right) + g^R\Sigma_1 - \Sigma_1 g^\Lambda - f^R\Sigma_2^+ + \Sigma_2 f^{+\Lambda}\right\} \tag{23}$$

It is easy to verify that the collision integral (23) vanishes when the equilibrium expressions are substituted for $g_{\epsilon,\epsilon-\omega} = 2\pi\delta(\omega)g_\epsilon$ and $f_{\epsilon,\epsilon-\omega} = 2\pi\delta(\omega)f_\epsilon$:

$$g_\varepsilon = \left(g^R - g^\Lambda\right)_\varepsilon \operatorname{th}\frac{\varepsilon}{2T}, \quad f_\varepsilon = \left(f^R - f^\Lambda\right)_\varepsilon \operatorname{th}\frac{\varepsilon}{2T} \tag{24}$$

i.e., Eq. (16) describes relaxation to the equilibrium.

Even more significant simplifications can be made in Eq. (17) for f. The point is that here the right-hand side contains the variable $\epsilon \sim \Delta, T$, whereas the dissipative parts γ and δ ((18) and (21)) are much smaller in the entire significant temperature interval, with the exception of a very small vicinity of T_c, an estimate for which was given in the beginning of the article. Their role here, as in the expressions for $g^{R(A)}$ and $f^{R(A)}$ consists, roughly speaking, in the fact that they lead to a certain smearing of the singularity in the density of the excitation spectrum near $\epsilon = \Delta$, and are, as a rule, by no means the principal source of such smearing. Therefore such quantities should be neglected in (17) (as also in $g^{R(A)}$ and $f^{R(A)}$, which enter in (23)). As a result we obtain for f the equation

$$(2\varepsilon - \omega - \mathbf{vk})f_{\varepsilon,\varepsilon-\omega}(\mathbf{p},\mathbf{k}) = \left\{H_1 f - f\bar{H}_1 + g\Delta - \Delta\bar{g}\right\}_{e,\varepsilon-\omega} \tag{25}$$

The system (22)-(25) plays the role of the kinetic equation in the case of the superconducting state. In the variant linearized with respect to the external field, equations of this type have already been used by a number of authors (see, in particular, [10]). It should be noted however, that it was possible to obtain nonlinear equations only because of the procedure of integration with respect to ξ, [4)], whereas the true kinetic equation would correspond to equations for the Green's functions integrated with respect to ϵ. But it is precisely for this reason that the equations given here remain valid also when the concept of the excitation spectrum becomes meaningless. Such a situation will occur, for example, if Δ is a sufficiently rapid function of the coordinates and of the time.

In the next sections we shall obtain for the electronimpurity and electron-electron collision integrals expressions that should be added to (23).

33.0.4 4. Scattering by Impurities

The interaction with impurities is included in the general scheme of the theory, as well as the interaction with the external field [3]. In the imaginary-frequency representation, self-energy parts σ_1, σ_2, and σ_2^+appear in the Green's-function diagrams after averaging over the impurity positions. As a result of analytic continuation, each of them, as in the case of phonons, generates three quantities $\sigma R(A)$ and σ, expressions for which will be derived here under the assumption that the scattering is isotropic:

[4)] Equations for the functions integrated with respect to ξ were obtained for the equilibrium case by Eilenberger [[11]].

$$\sigma_1^{R(A)} = \frac{1}{2\pi\tau}\left\langle g^{R(A)}\right\rangle, \quad \sigma_1 = \frac{1}{2\pi\tau}\langle g\rangle,$$
$$\sigma_2^{R(A)} = \frac{1}{2\pi\tau}\left\langle f^{R(A)}\right\rangle, \quad \sigma_2 = \frac{1}{2\pi\tau}\langle f\rangle,$$
$$\langle \ldots\rangle = \int \frac{dO_{\mathrm{p}}}{4\pi}, \tag{26}$$

where τ is the transport free-path time of the electron [5)], and g and f are the functions defined above, calculated with allowance for the impurities. Adding (26) to the corresponding phonon self-energies in (16) and (17), we obtain the integrals for collisions with impurities:

$$I_p^{(imp)} = \int \frac{dO_{p'}}{4\pi}\left\{\left[g^R g\right]_{pp'} + \left[g g^{\Lambda}\right]_{pp'} - \left[f^R f^{+}\right]_{pp'} - \left[f f^{+\Lambda}\right]_{pp'}\right\} \tag{27}$$

$$K_p^{(imp)} = \int \frac{dO_{p'}}{4\pi}\left\{\left[g^R f\right]_{pp'} + \left[g f^{\Lambda}\right]_{pp'} + \left[f \bar{g}^{\Lambda}\right]_{pp'} + \left[f^R \bar{g}\right]_{pp'}\right\} \tag{28}$$

$$[gf]_{pp'} \equiv g_p f_{p'} - g_{p'} f_p$$

which must be included respectively in the right-hand sides of (22) and (25). These expressions possess the property that their averages over the directions of p vanish, as a consequence of the elasticity of the scattering by impurities.

33.0.5 5. Electron-Electron Interaction

We are interested in the interaction between electrons only to the extent that it leads to collision processes that are of importance for the kinetics. In addition, it makes its own contribution to the kernel of the equation for Δ. However, within the framework of the model equation (20) we can simply assume that λ is defined with allowance for all the interactions. Finally, the electron-electron interaction necessitates, generally speaking, that the electronic system be regarded as a Fermi liquid. We note in this connection that the renormalized quantities that arise in the theory of Fermi liquids are practically insensitive to the transition of the metal into the superconducting state, and it can therefore be assumed that they are accounted for in the employed characteristics of the normal metal, such as the spectrum density, the vertex of the interaction with the external field, etc. On the other hand, we shall not consider effects connected with the possible existence of excitations of the zero-sound type.

In the derivation of the equation for the electronelectron collision integral, we shall start from the fact that in a superconductor, as in a normal metal, only paired collisions are significant: processes in which a large number of excitations take part have a low probability because of degeneracy. Just as in the calculation of the damping of the excitations in a normal Fermi liquid [13], we should pick out in each diagram Σ in succession all the cross sections with three lines (Fig. 4), and take into account the dependence on the discrete imaginary frequencies (and by the same token on the temperature), on the external field, and in the given case on the parameter Δ of the superconducting state only in these cross sections. This

procedure makes it necessary for us to regard both vertices on the diagram of Fig. 4 as the true amplitudes for the scattering of two excitations on the Fermi surface, containing no dependences on the aforementioned parameters which characterize the smearing region.

[05)] If paramagnetic impurities are also present, then σ_1 and σ_2 contain respectively the relaxation times τ_1 and τ_2 [12].

Since superconductivity is taken into account in the separated lines of the diagram of Fig. 4, Σ_1 and Σ_2 are actually determined by several diagrams of this type, which differ in the disposition of the arrows. Each such diagram corresponds to a different combination of amplitudes. In the imaginary-frequency representation, Σ_1 and Σ_2 can be expressed as follows:

$$\Sigma_1(P, P-K) = T^2 \sum_{\varepsilon_1,\varepsilon_2} \iint \frac{d^3\mathbf{p}_1 d^3\mathbf{p}_2}{(2\pi)^6} \left\{ AG_1G_2\bar{G}_3 - BF_1F_2{}^+G_3 \right\},$$
$$\Sigma_2(P, P-K) = T^2 \sum_{\varepsilon_1,\varepsilon_2} \iint \frac{d^3\mathbf{p}_1 d^3\mathbf{p}_2}{(2\pi)^6} \left\{ BG_1\bar{G}_2F_3 - AF_1F_2F_3{}^+ \right\}, \tag{29}$$

where A and B are two different quadratic forms of the amplitudes, the explicit form of which we do not need. For clarity, we present here expressions for A and B in perturbation theory, when the amplitudes can be replaced by a certain effective potential $\mathrm{V_q}$:

$$A = -2\left|V_{p-p_2}\right|^2 + V_{p-p_2}V_{p-p_1},$$
$$B = -2\left|V_{p_1+p_2}\right|^2 + V_{p-p_1}V_{p-p_2} + V_{p_1+p_2}V_{p-p_i} + V_{p-p_1}V_{p_1;p_2}. \tag{30}$$

We have taken into account the fact that, depending on the method of joining the vertices in Σ, an additional electron loop may or may not arise. The sign of the diagram also changes when a pair of lines $\mathrm{FF}^+$is added. The internal lines correspond to the complete Green's functions including the alternating field, $\mathrm{G_1} = \mathrm{G}\left(\mathrm{P_1}, \mathrm{P_1} - \mathrm{K_1}\right)$, etc., and in order to write down the succeeding formulas in symmetrical form, we have determined the internal variables by starting from the "decay" conservation law $\mathrm{P} = \mathrm{P_1} + \mathrm{P_2} + \mathrm{P_3}$ and $\mathrm{K} = \mathrm{K_1} + \mathrm{K_2} + \mathrm{K_3}$. This is the reason for the appearance of $\overline{\mathrm{G}}$ in (29).

Regarding the diagram $\Sigma\,(\Sigma_1$ or $\Sigma_2)$ of definite order in the external field as a function of the complex variable ϵ at fixed imaginary frequencies of the field vertices, we can verify, just as in the case of the phonons, that it corresponds to cuts on the lines $\mathrm{Im}\,(\epsilon - \Omega_\mathrm{k}) = 0$, located between the extreme lowest cut $\mathrm{Im}\,\epsilon = 0$ and the highest cut $\mathrm{Im}(\epsilon - \omega) = 0$. The values of Ω_k represent here, too, certain combinations of the frequencies of the field vertices, but the set of these combinations and their total number depend in this case on the distribution of the field vertices over the internal lines of the diagram of Fig. 4. Let us as sume that the G functions of these lines correspond to the sets of cuts $\mathrm{Im}\,(\epsilon_1 - \omega_{1\mathrm{i}}) = 0, \mathrm{Im}\,(\epsilon_2 - \omega_{2\mathrm{k}}) = 0$, $\mathrm{Im}\,(\epsilon_3 - \omega_3 l) = 0$, and let us transform the sum over the frequencies in (29) into a contour integral (a double integral in this case). The transformation is carried out here in two steps: we first replace with an integral the sum over one of the variables, say ϵ_2, at a fixed imaginary value of ϵ_1, and then go over to the integral in the sum over ϵ_1. The external variable ϵ and the field frequencies remain imaginary to the end. The result takes the form

$$\Sigma\infty T^2\sum_{\varepsilon_1,\varepsilon_2}G_{\varepsilon_1}G_{\varepsilon_2}G_{\varepsilon-\varepsilon_1-\varepsilon_2}$$

$$=\iint_{-\infty}^{\infty}\frac{dz_1dz_2}{(4\pi i)^2}\left\{\sum_{i,k}\delta_i\left(G_{x_1+\omega_{1i}}\right)\delta_k\left(G_{z_2+\omega_{2k}}\right)G_{\varepsilon-\omega_{1i}-\omega_{2k}-z_1-z_2}\,\mathrm{th}\,\frac{z_1}{2T}\,\mathrm{th}\,\frac{z_2}{2T}\right.$$
$$-\sum_{k_1,l}G_{z_1+\varepsilon-\omega_{2k}-\omega_{3l}}\delta_k\left(G_{z_2+\omega_{2k}}\right)\delta_l\left(G_{-z_1-z_2+\omega_{3l}}\right)\mathrm{cth}\,\frac{z_1}{2T}\,\mathrm{th}\,\frac{z_2}{2T}$$
$$+\sum_{kl}G_{z_1+\varepsilon-\omega_{2_k}-\omega_{3l}}\delta_k\left(G_{z_2-z_1+\omega_{2k}}\right)\delta_l\left(G_{-z_2+\omega_{3l}}\right)\mathrm{cth}\,\frac{z_1}{2T}\,\mathrm{th}\,\frac{z_2}{2T}$$
$$\left.-\sum_{i,l}\delta_i\left(G_{z_1+\omega_{1i}}\right)G_{z_2-z_1+\varepsilon-\omega_{1i}-\omega_{3l}}\delta_l\left(G_{-z_2+\omega_{3l}}\right)\mathrm{th}\,\frac{z_1}{2T}\,\mathrm{th}\,\frac{z_2}{2T}\right\}\tag{31}$$

In order not to clutter the formulas, we have omitted the second index of the G functions. The combinations obtained here of ϵ with $\omega_{1\mathrm{i}},\omega_{2\mathrm{k}}$, and $\omega_3 l$ form the set of cuts of the given diagram Σ. Continuing (31) with respect to ϵ from the regions $\mathrm{Im}(\epsilon-\omega)>0$ and $\mathrm{Im}\,\epsilon<0$, and then with respect to all the field frequencies from the upper half-plane we obtain without difficulty Σ^{R} and Σ^{A}. We are interested only in the dissipative part $\Sigma^R-\Sigma^A$, for which we obtain the expression

$$\Sigma^R-\Sigma^A\propto\iint_{-\infty}^{\infty}\frac{d\varepsilon_1d\varepsilon_2}{(4\pi i)^2}\left\{G_1G_2\left({G_3}^R-{G_3}^A\right)+G_1\left({G_2}^R-{G_2}^A\right)G_3\right.$$
$$\left.+\left({G_1}^R-{G_1}^A\right)G_2G_3+\left({G_1}^R-{G_1}^A\right)\left({G_2}^R-{G_2}^A\right)\left({G_3}^R-{G_3}^A\right)\right\}\tag{32}$$

Using a definition of the type (9)

$$\Sigma_{\varepsilon,\varepsilon-\omega}=\sum_{N=0}^{\infty}\sum_k\delta_k\left(\Sigma^{(N)}_{\varepsilon,\varepsilon-\omega}\right)\mathrm{th}\,\frac{\varepsilon-\Omega_k}{2T}$$

we obtain

$$\Sigma\infty\int_{-\infty}^{\infty}\frac{d\varepsilon_1d\varepsilon_2}{(4\pi i)^2}\left\{G_1G_2G_3+G_1\left({G_2}^R-{G_2}^A\right)\left({G_3}^R-{G_3}^A\right)\right.$$
$$\left.+\left({G_1}^R-{G_1}^A\right)G_2\left({G_3}^R-{G_3}^A\right)+\left({G_1}^R-{G_1}^A\right)\left({G_2}^R-{G_2}^A\right)G_3\right\}\tag{33}$$

Then applying these formulas to (29), we obtain expressions for the quantities $\Sigma_1^R-\Sigma_1^A,\Sigma_1$ and $\Sigma_2^R-\Sigma_2^A,\Sigma_2$ of interest to us. Before we present the results, we note that all these quantities are expressed in fact in terms of the Green's functions integrated with respect to ξ, and do not depend on ξ themselves. The point is that owing to the short-range character of the effective interaction, the amplitudes in (30) can be regarded as dependent on the angles only. We can therefore write, for example,

$$\iint\frac{d^3\mathbf{p}_1d^3\mathbf{p}_2}{(2\pi)^6}AG_1G_2G_3$$
$$=\left(\frac{mp_0}{2\pi^2}\right)^2\iint\frac{dO_{\mathbf{p}_1}dO_{\mathbf{p}_2}}{(4\pi)^2}A\iiint d\xi_1d\xi_2d\xi_3\delta\left(\xi_3-v\left(p_3-p_0\right)\right)G_1G_2G_3$$

The δ function limits here, in the main, the integration with respect to the angle, requiring that $p_3\equiv\mid p-p_1\ -p_2\mid\approx p_0$, and thus

$$\iint \frac{d^3\mathbf{p}_1 d^3\mathbf{p}_2}{(2\pi)^6} AG_1G_2G_3 = \left(\frac{mp_0}{2\pi^2}\right)^2 \frac{1}{p_0 v} \iint \frac{dO_{\mathbf{p}_1} dO_{\mathbf{p}_2}}{(4\pi)^2} \delta\left(\frac{p_3}{p_0} - 1\right) Ag_1g_2g_3 \tag{34}$$

Taking all these formulas into account, we can now write

$$\begin{aligned} 2i\gamma &= \hat{L}\left[A\left\{g_1g_2\bar{g}^3\right\}_1 - B\left\{f_1f_2{}^+g_3\right\}_1\right] \\ \Sigma_1 &= \hat{L}\left[A\left\{g_1g_2\bar{g}_3\right\}_2 - B\left\{f_1f_2{}^+g_3\right\}_2\right] \\ 2i\delta &= \hat{L}\left[B\left\{g_1\bar{g}_2f_3\right\}_1 - A\left\{f_1f_2f_3{}^+\right\}_1\right] \\ \Sigma_2 &= \hat{L}\left[B\left\{g_1\bar{g}_2f_3\right\}_2 - A\left\{f_1f_2f_3{}^+\right\}_2\right] \\ \hat{L} &= \left(\frac{mp_0}{2\pi^2}\right)^2 \frac{1}{p_0 v} \iint_{-\infty}^{\infty} \frac{d\varepsilon_1 d\varepsilon_2}{(4\pi i)^2} \iint \frac{dO_{p_1} dO_{p_2}}{(4\pi)^2} \delta\left(\frac{p_3}{p_0} - 1\right) \end{aligned} \tag{35}$$

where $\{\ldots\}_1$ and $\{\ldots\}_2$ are forms patterned after the curly brackets in (32) and (33), respectively. Substitution of these formulas in (23) leads to an expression for $I^{(e)}$.

33.0.6 6. Charge and Current Densities. Electroneutrality Condition

In the preceding sections we obtained equations for the Green's functions integrated with respect to ξ. It is clear that they can be used to calculate only quantities that are determined completely by the electrons near the Fermi surface. It is therefore necessary to exercise a certain caution when writing down the expressions for the current densities and the electron numbers. If we start from the expressions for j and N in the imaginary-frequency representation, then a direct application of the continuation procedure employed above, with allowance for the definition (5) of the function G, leads to the formulas

$$\mathbf{j}_\omega(k) = -\frac{2e}{m} \int_{-\infty}^{\infty} \frac{d\varepsilon}{4\pi i} \int \frac{d^3\mathbf{p}}{(2\pi)^3} \mathbf{p} G_{e,\,-\,-\omega}\left(\mathbf{p}_+, \mathbf{p}_-\right) - \frac{e^2}{mc}(NA)_{\omega,k} \tag{36}$$

$$N_\omega(k) = -2 \int_{-\infty}^{\infty} \frac{d\varepsilon}{4\pi i} \int \frac{d^3\mathbf{p}}{(2\pi)^3} G_{e,\varepsilon-\omega}\left(\mathbf{p}_+, \mathbf{p}_-\right); \quad \mathbf{p}_\pm = \mathbf{p} \pm \frac{\mathbf{k}}{2} \tag{37}$$

We shall assume that in the absence of an external field the medium is homogeneous. We stipulate that in the presence of a field the density of the number of electrons remain the same as before. The electroneutrality requirement frees us of the need for taking into account the Coulomb character of the interaction under conditions when the frequencies, gradients, and field amplitudes are small compared with quantities of atomic scale. To formulate this condition explicitly, we separate that part of the function G which is connected with the contribution made to (36) and (37) by the remote regions, and therefore cannot be calculated by integration with respect to ξ. This part, obviously, should not depend on Δ. It is determined by the regular terms (see (7)) of the function of the normal state, since all of them, with the exception of the free line, vanish upon integration with respect to ξ. Correct allowance for the contribution of these terms to N in first order in the electrochemical potential $\varphi_\omega(\mathrm{k})$[6)] leads to the following expression:

$$\begin{aligned} &N_\omega(k) - N_0(2\pi)^4\delta(\omega)\delta(\mathbf{k}) \\ &= -\frac{mp_0}{\pi^2}\mathbf{r}e\varphi_\omega(k) + \int_{-\infty}^{\infty} \frac{d\varepsilon}{4\pi i} \int \frac{dO_{\mathbf{p}}}{4\pi} g'_{\varepsilon,\varepsilon-\omega}(\mathbf{p},\mathbf{k})\Bigg], \quad N_0 = \frac{p_0^3}{3\pi^2} \end{aligned}$$

where the prime denotes that it is necessary to subtract from g the contribution of the free line $2\pi\mathrm{i}\tanh(\epsilon/2\ \mathrm{T})$. By virtue of the neutrality condition we have

$$e\varphi_\omega(k) = -\int_{-\infty}^{\infty}\frac{d\varepsilon}{4\pi i}\int\frac{dO_{\mathbf{p}}}{4\pi}g'_{\varepsilon,\varepsilon-\omega}(\mathbf{p},\mathbf{k}). \tag{38}$$

A similar separation of the contribution made to j by the regions far from the Fermi surface leads to a cancellation of the second term in (36) (see also [3]):

$$\mathbf{j}_\omega(k) = -\frac{p_0 e}{\pi^2}\int_{-\infty}^{\infty}\frac{d\varepsilon}{4\pi i}\int\frac{dO_{\mathbf{p}}}{4\pi}\mathbf{p}g_{e,e-\omega}(\mathbf{p},\mathbf{k}) \tag{39}$$

Using the equations obtained above for g and f, we can easily verify that (38) coincides with the equation $\mathrm{div}\,\mathbf{j} = 0$.

33.0.7 7. Thin Films in a High-Frequency Field

We apply here the obtained equations to description of a thin film in the field of a wave incident normally onto its surface. We choose a gauge with a vector potential in the plane of the film, and confine ourselves to the case when the film is so thin that $\mathrm{A}_\omega, \Delta$, and the other quantities with them are constant over its cross section. We assume at the same time that the electron mean free path determined by scattering from impurities is small compared with the film thickness, making it possible to disregard the singularities of electron reflection from the walls. This condition also ensures satisfaction of the inequalities $\Delta\tau \ll 1$, $\mathrm{T}\tau \ll 1, \omega\tau \ll 1$ and leads to a weak dependence of g and f on the angle ϑ between p and $\mathbf{A}_\omega$:

$$g = g^{(0)} + g^{(1)}\cos\vartheta, \quad f = f^{(0)} + f^{(1)}\cos\vartheta \tag{40}$$

From (22) and (25), in which in this case it is necessary to put k = 0, we readily obtain equations for the individual components. The equations averaged over the angles do not contain terms corresponding to collisions with impurities, whereas in the equations for $g^{(1)}$ and $f^{(1)}$ these collisions play the principal role, and therefore the inelastic processes can be neglected here. In spite of these simplifications, the equations still retain a rather complicated structure, in accord with the complicated character of the action of the alternating field on the superconducting state.

Let us discuss first the case of the normal state, when $\Delta = 0$ and $g^{R(A)} = \pm\pi\mathrm{i}$. The last equation means that, within the framework of the approximation connected with the integration with respect to ξ, the field has no influence on the level density of the normal electrons. We write out, assuming the field to be monochromatic, an equation for the element $g^{(0)}_{\epsilon,\epsilon} \equiv g_\epsilon$, which is diagonal in the energy:

$$0 = \frac{ev}{3c}\left\{A_\omega\left(g^{(1)}_{\varepsilon,\varepsilon+\omega} - g^{(1)}_{\varepsilon-\omega,\varepsilon}\right) + A_{-\omega}\left(g^{(1)}_{\varepsilon,\varepsilon-\omega} - g^{(1)}_{\varepsilon+\omega,\varepsilon}\right)\right\} + I_\varepsilon \tag{41}$$

Here I_ϵ takes the inelastic collisions into account, and its order of magnitude is $I_\epsilon \sim i\tau_0^{-1}(g\epsilon - g_\epsilon)$, where τ_0 is a certain effective energy relaxation time, and $g_{\epsilon_0} = 2\pi i\tanh(\epsilon/2T)$. If the field frequency is sufficiently high so that $\omega\tau_0 \gg 1$, then the nondiagonal elements $g^{(0)}_{\epsilon,\epsilon-2\omega}$ etc. are small compared with g_ϵ relative to the parameter $(\omega\tau_0)^{-1}$. Therefore $g^{(1)}$ can be expressed only in terms of $g\epsilon$. Since it follows for a normal metal from (27) that $\mathrm{I}^{(\mathrm{imp})} = -(\mathrm{i}/\tau)\mathrm{g}^{(1)}$, we obtain, inasmuch as $\omega\tau \ll 1$,

[06] It is obviously necessary to include in φ both the scalar potential of the field and the variation of the chemical potential. Allowance of terms of higher order in φ lead to corrections $\sim \mathrm{e}\varphi/\mathrm{E_F}$. The latter pertains also to terms with the vector potential.

$$g^{(1)}_{\varepsilon,\varepsilon-\omega} = i\tau\frac{ev}{c}A_\omega\left(g_{\varepsilon-\omega} - g_\varepsilon\right)$$

Substituting in (41), we obtain an equation for g_ϵ :

$$0 = 2i\left(\frac{e}{c}\right)^2\frac{vl}{3}A_\omega A_{-\omega}\left(g_{e-\omega} - 2g_e + g_{e+\omega}\right) + I_e. \tag{42}$$

Introducing the notation

$$g_e = 2\pi i\left(1 - 2n_\varepsilon\right), \tag{43}$$

we can easily verify that the electron-phonon and electron-electron collision integrals obtained above have a canonical form with n_ϵ as the distribution function.

As seen from (42), when $\omega \lesssim \mathrm{T}$ the correction to n ∈ linear in the field intensity is of the order of magnitude

$$\delta n_e \sim \frac{\alpha\omega^2\tau_0}{T^2}, \quad \alpha = D\left(\frac{e}{c}\right)^2 A_\omega A_{-\omega}, \quad D = \frac{lv}{3}, \tag{44}$$

which indeed determines the field intensity at which a noticeable deviation from equilibrium takes place in the energy distribution of the electrons [7] : $\alpha \sim \mathrm{T}^2/\omega^2\tau_0$. We note that although (42) contains effects that are nonlinear in the field intensity, they are limited to those corresponding to successive single-quantum transitions. The probability of simultaneous absorption of two quanta has a small factor $(\omega\tau)^{-2}$ compared with cascade absorption.

In the case of the superconducting state at not too low temperatures, when there are enough excitations already in equilibrium ($\mathrm{T} \sim \Delta$), it is natural to expect the field intensity at which an appreciable change in the energy distribution of the excitations takes place to be determined, as before, from (44). The situation is made more complicated, however, by the fact that here the field also influences the density of the spectrum. Formally this is taken into account by the functions $gR(A)$ and $fR(A)$, which enter in the equations, and are altered by the turning on of the field in the case of the superconducting state. The situation here is analogous to that obtaining in the case of a constant magnetic field, although it is made more complicated by retardation effects. Consequently, substantial changes in the spectrum should be expected in fields whose amplitude is comparable with the critical magnetic field of the film, meaning $\alpha \sim \Delta, T$ in the notation (44) [8]. Since τ_0 is quite large (for example, $\tau_0\ \mathrm{T_C} \sim (\mathrm{T_c}/^{\omega}\mathrm{D})^2$), it follows that $\omega^2\tau_0 > \mathrm{T}$ even at not too high frequencies, and the changes in the excitation distribution become significant in fields which are still small compared with $\mathrm{H_c}$. Under such conditions, when calculating the energy distribution of the excitations, we can regard the field in the first approximation only as the source of transition at a constant spectrum density. We shall simplify the equations further as applied to this situation, confining ourselves, as in the example with the normal metal, to single-photon transitions ($\omega\tau_0 \gg 1$).

The diagonal element $g\epsilon$ is determined here, too, from (41), and in Eq. (25) for f ∈ we should leave out

the field term, since the field enters here alongside with $\epsilon \sim \Delta$, unlike in (41), where it enters in combination with τ_0^{-1}. We thus have simply [9]

$$f_\varepsilon = (\Delta/\varepsilon)g_\varepsilon. \tag{45}$$

[07] Since we are dealing with a thin film in which, as noted in Sec. 1, the phonons are close to equilibrium, the effect under consideration does not reduce to simple heating, although it has the same scale.

[8] Actually, the superconductivity of the films is destroyed by the current [[14]], but the parameters of the superconducting state nevertheless change in the scale of $\mathrm{H_c}$: the destruction by the current occurs abruptly.

In the equations for $g^{(1)}$ and $f^{(1)}$, which follow from (22) and (25) with allowance for (27) and (28), it is necessary to retain only the diagonal elements g_ϵ and f_ϵ. As to $gR(A)$ and $f^{R(A)}$, their averages over the angles should be replaced by the unperturbed values

$$g_e^{R(A)} = \frac{\varepsilon}{\Delta} f_e^{R(A)} = \pi i \frac{\varepsilon}{\xi_e^{I(A)}},$$

$$\xi_e{}^R = -\left(\xi_e{}^\Lambda\right)^* = \begin{cases} \sqrt{\varepsilon^2 - \Delta^2}\,\operatorname{sign}\varepsilon + i\delta, & \varepsilon^2 > \Delta^2, \\ i\sqrt{\Delta^2 - \varepsilon^2}, & \varepsilon^2 < \Delta^2, \end{cases}$$

and the angle parts should be calculated in first order in the field:

$$g^{(1)R(A)}_{\varepsilon,\varepsilon-\omega} = \frac{ev}{c} A_\omega \frac{\pi i}{\left(\xi_\varepsilon + \xi_{\varepsilon-\omega}\right)^{R(\Lambda)} + i/\tau} \left[1 - \frac{\varepsilon(\varepsilon-\omega) + \Delta^2}{\left(\xi_\varepsilon \xi_{\varepsilon-\omega}\right)^{R(\Lambda)}}\right],$$

$$f^{(1)R(A)}_{\varepsilon,\varepsilon-\omega} = -\frac{ev}{c} \frac{\pi i}{\left(\xi_\varepsilon - 1 - \xi_{\varepsilon-\omega}\right)^{R/(\lambda)} + i/\tau} \frac{2\varepsilon - \omega}{\left(\xi_\varepsilon \xi_{\varepsilon-\omega}\right)^{R(\Lambda)}}.$$

Taking all the foregoing into account, we obtain after simple manipulations

$$g^{(1)}_{\varepsilon,\varepsilon-\omega} = i\tau \frac{ev}{c} A_\omega \left[\varepsilon(\varepsilon-\omega) + \Delta^2\right] \left[\frac{g_{\varepsilon-\omega}}{(\varepsilon-\omega)\xi_\varepsilon{}^K} + \frac{g_\varepsilon}{\varepsilon \xi^A_{\varepsilon-\omega}}\right], \quad l < \xi_0 \tag{46}$$

and, substituting (46) in (41), we arrive at an equation for gϵ. We write down the result, introducing the notation

$$g_\varepsilon = 2\pi i \frac{\varepsilon}{\sqrt{\varepsilon^2 - \Delta^2}} \theta\left(\varepsilon^2 - \Delta^2\right)(1 - 2n_\varepsilon) \tag{47}$$

where n_ϵ is defined as an even function of the energy, the equation for which is ($\epsilon \geq \Delta$)

$$0 = 2\alpha\left[U_-\left(n_{\varepsilon-\omega} - n_\varepsilon\right) - U_+\left(n_\varepsilon - n_{\varepsilon+\omega}\right) + V\left(1 - n_\varepsilon - n_{\omega-\varepsilon}\right)\right] + J_\varepsilon$$

$$U_\pm = \frac{\left[\varepsilon(\varepsilon \pm \omega) + \Delta^2\right]\theta(\varepsilon \pm \omega - \Delta)}{\sqrt{\left(\varepsilon^2 - \Delta^2\right)\left[(\varepsilon \pm \omega)^2 - \Delta^2\right]}}$$

$$V = \frac{\left[\varepsilon(\omega - \varepsilon) - \Delta^2\right]\theta(\omega - \varepsilon - \Delta)}{\sqrt{\left[(\omega - \varepsilon)^2 - \Delta^2\right]\left(\varepsilon^2 - \Delta^2\right)}} \tag{48}$$

The expression for $J_\epsilon = I_\epsilon/4\pi$ follows directly from (23), (18), (21), and (35) with allowance for the simplifications listed here:

$$J = J^{(ph)} + J^{(e)},$$

$$J_e^{(ph)} = \frac{\pi\lambda}{2\left(sp_0\right)^2} \int_\Delta^\infty d\varepsilon' \int_0^\infty d\omega \frac{\omega^2 \varepsilon\varepsilon'}{\left[\left(\varepsilon^2 - \Delta^2\right)\left(\varepsilon'^2 - \Delta^2\right)\right]^{1/2}}$$

$$\times \left\{ \left[n'(1-n)\left(1 + N_\omega\right) - n\left(1 - n'\right)N_\omega\right]\left(1 - \frac{\Delta^2}{\varepsilon\varepsilon'}\right)\delta\left(\varepsilon' - \varepsilon - \omega\right) \right.$$

$$+ \left[n'(1-n)N_\omega - n\left(1-n'\right)\left(1 + N_\omega\right)\right]\left(1 - \frac{\Delta^2}{\varepsilon\varepsilon'}\right)\delta\left(\varepsilon - \varepsilon' - \omega\right)$$

$$\left. + \left[(1-n)\left(1-n'\right)N_\omega - nn'\left(1 + N_\omega\right)\right]\left(1 + \frac{\Delta^2}{\varepsilon\varepsilon'}\right)\delta\left(\varepsilon + \varepsilon' - \omega\right) \right\}$$

$$J_e^{(e)} = \frac{1}{p_0 v} \iint_\Lambda^\infty \int \frac{N_\omega = \left(e^{\omega/T} - 1\right)^{-1}}{\left[\left(\varepsilon^2 - \Delta^2\right)\left(\varepsilon_1^2 - \Delta^2\right)\left(\varepsilon_2^2 - \Delta^2\right)\left(\varepsilon_3^2 - \Delta^2\right)\right]^{1/2}}$$

$$\times \{M_1 [(1-n)n_1n_2n_3 - n(1-n_1)(1-n_2)(1-n_3)]\,\delta(\varepsilon-\varepsilon_1-\varepsilon_2-\varepsilon_3)$$
$$+3M_2 [n_1n_2(1-n)(1-n_3) - nn_3(1-n_1)(1-n_2)]\,\delta(\varepsilon+\varepsilon_3-\varepsilon_1-\varepsilon_2)$$

$$+3M_3 [n_1(1-n)\ (1-n_2)(1-n_3) - (1-n_1)nn_2n_3]\,\delta(\varepsilon+\varepsilon_2+\varepsilon_3-\varepsilon_1)\}$$
$$M_1 = a\left(\varepsilon\varepsilon_1\varepsilon_2\varepsilon_3 - \Delta^4\right) - \frac{b}{3}\left(-\varepsilon^2+\varepsilon_1\varepsilon_2+\varepsilon_1\varepsilon_3+\varepsilon_2\varepsilon_3\right)\Delta^2 \tag{50}$$
$$M_2 = -M_1(-\varepsilon_3) \quad M_3 = M_1(-\varepsilon_2,-\varepsilon_3)$$

where a and b are numbers of the order of unity, obtained from (30) by averaging over the angles:

$$a = -2\pi\left(\frac{mp_0}{2\pi^2}\right)^2 \iiint \frac{dO_{\mathbf{p}}dO_{\mathbf{p}_1}dO_{\mathbf{p}_2}}{(4\pi)^3}\delta\left(\frac{|\mathbf{p}-\mathbf{p}_1-\mathbf{p}_2|}{p_0}-1\right)A$$

and b is similarly connected with B. We emphasize that the equations contain the nonequilibrium value of Δ, which should be determined in accordance with (20) and (45) from the BCS equation:

$$1 = \lambda\int_{\Delta}^{\omega_D}\frac{d\varepsilon}{\sqrt{\varepsilon^2-\Delta^2}}(1-2n_\varepsilon) \tag{51}$$

with the nonequilibrium distribution function n_ϵ.

In conclusion, we note that the estimates given at the beginning of the section pertained to the temperature region $T \sim \Delta$. Using the results of the direct calculation of the correction to Δ, linear in the field intensity [15,17], we can show that in the vicinity of T_c the condition for the applicability of (48)-(51) is $\omega^2\tau_0 \approx \Delta$, which coincides with the condition given above for $\Delta \sim T$. The case of low temperatures calls for a special investigation.

09) In this case $\Delta = \Delta^*, f = f^+, \overline{g} = -g$.

Part VI
Special Effects: Useful, Selected Articles

Part VII

Experiments: Main Articles about Superconductors

Part VIII
Experiments: Main Articles about Simulators, Not Superconductors

34 Observing Dynamical Phases of BCS Superconductors in a Cavity QED Simulator by Young et al.

Abstract

In conventional Bardeen-Cooper-Schrieffer (BCS) superconductors [Bardeen *et al.*(1957)], electrons with opposite momenta bind into Cooper pairs due to an attractive interaction mediated by phonons in the material.

While superconductivity naturally emerges at thermal equilibrium, it can also emerge out of equilibrium when the system's parameters are abruptly changed [Yuzbashyan *et al.*(2006), Barankov and Levitov(2006), Yuzbashyan and Dzero(2006), Gurarie and Radzihovsky(2007), 36, 93, Yuzbashyan *et al.*(2015)].

The resulting out-of-equilibrium phases are predicted to occur in real materials and ultracold fermionic atoms but have not yet all been directly observed.

(in which articles there was statement that it is impossible to observe them?)

Here we realise an alternate way to generate the proposed dynamical phases using cavity quantum electrodynamics (cavity QED).

Our system encodes the presence or absence of a Cooper pair in a long-lived electronic transition in ^{88}Sr atoms coupled to an optical cavity and represents interactions between electrons as photon-mediated interactions through the cavity [Lewis-Swan *et al.*(2021), Kelly *et al.*(2022)].

(how???)

To fully explore the phase diagram, we manipulate the ratio between the single-particle dispersion and the interactions after a quench and perform real-time tracking of subsequent dynamics of the superconducting order parameter using non-destructive measurements.

We observe regimes where the order parameter decays to zero (phase I) [Barankov and Levitov(2006), Yuzbashyan and Dzero(2006)], assumes a non-equilibrium steady-state value (phase II) [Barankov and Levitov(2006), Yuzbashyan *et al.*(2006)], or exhibits persistent oscillations (phase III) [Barankov and Levitov(2006), Yuzbashyan *et al.*(2006)].

This opens up exciting prospects for quantum simulation, including the potential to engineer unconventional superconductors and to probe beyond mean-field effects like the spectral form factor [Stewart(2017), Sato and Ando(2017)], and for increasing coherence time for quantum sensing.

(which prospects? beyond mean-field effects???)

Conclusion

The demonstrated capability to emulate dynamical phases of superconductors in optical cavities opens exciting prospects for quantum simulation. For example, it will be interesting to see if our cavity simulator can engineer and probe topological superfluid phases [93, Black-Schaffer(2012), Nandkishore *et al.*(2012), Kiesel *et al.*(2012), Kiesel *et al.*(2013), Fischer *et al.*(2014), Shankar *et al.*(2022)]

(topological superfluid phases???)

and understand competing superconducting orders [Laughlin(1998), Balatsky *et al.*(2006)] in a single system

(competing superconducting orders ????),

or else enable simulation of superfluidity in phenomena relevant to high energy physics [Schäfer and Teaney(2009), Pehlivan *et al.*(2011)].

34.1 Introduction

Quantum simulation offers a path to understand a broad range of phenomena, from high-temperature superconductivity and correlated quantum magnetism in condensed matter physics [Zhou *et al.*(2021)] (???)to quarks and gluons in nuclei and matter under extreme conditions [Shuryak(2017)] (???), as well as the black hole information paradox in gravitational physics [Harlow(2016)] (???).

A fascinating and promising case is the prethermal dynamical phases [Marino *et al.*(2022)] predicted to emerge from quenches of superconductors and superfluids [Yuzbashyan *et al.*(2006), Barankov and Levitov(2006), Yuzbashyan and Dzero(2006), Gurarie and Radzihovsky(2007), 36, 93, Yuzbashyan *et al.*(2015), Volkov,Kogan (1973), Yuzbashyan *et al.*(2005), Barankov *et al.*(2004), Yuzbashyan(2008), Foster *et al.*(2014), Collado *et al.*(2023)], systems that feature Cooper pairing of electrons or neutral fermions.

(just a collection of relevant citations)

While there has been great progress in pump-probe experiments of superconductors to induce such fast quenches using THz technology, and signs of phases I and II have been observed, the intense pulses couple nonlinearly to the Cooper pairs in the superconductor and complicate a clean observation of the dynamical phases [Mansart *et al.*(2013), Matsunaga *et al.*(2013), Matsunaga *et al.*(2014)].

(I'll read it, I don't know yet, why is it so?)

For these reasons, the realisation of fermionic superfluids in ultracold atomic gases [Randeria and Taylor(2014)] has generated great excitement [Yuzbashyan *et al.*(2006), Barankov and Levitov(2006), Yuzbashyan and Dzero(2006), Gurarie and Radzihovsky(2007), 36, 93, Yuzbashyan *et al.*(2015)]; however, to date observations have been limited to spectroscopic signatures rather than the full time dynamics [Behrle *et al.*(2018)].

(spectroscopic signatures ???)

In neither system has a systematic scan of the dynamical phase diagram been performed, and in fact phase III has not been observed. (why by the way? people didn't try?)

(dynamical phase diagram ????)

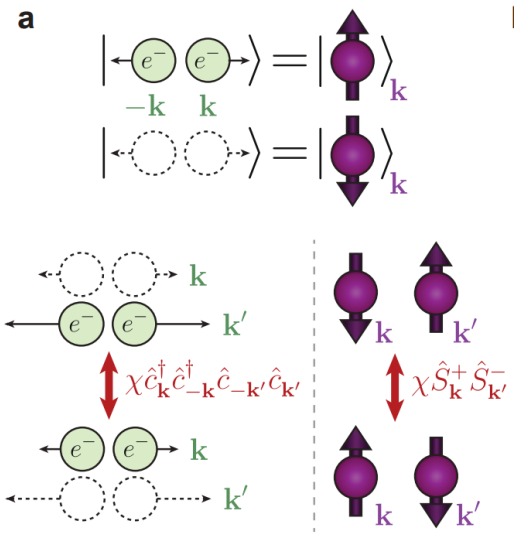


Figure 34.1: **a**, The Anderson pseudospin mapping encodes the presence and absence of a Cooper pair as the up and down states of a spin-1/2 system, respectively (???). Under this mapping, the attractive interaction $\chi \hat{c}^\dagger_{\mathbf{k}} \hat{c}^\dagger_{-\mathbf{k}} \hat{c}_{-\mathbf{k}'} \hat{c}_{\mathbf{k}'}$ between electrons is equivalent to an all-to-all exchange interaction $\chi \hat{S}^+_{\mathbf{k}} \hat{S}^-_{\mathbf{k}'}$ between pseudospins.

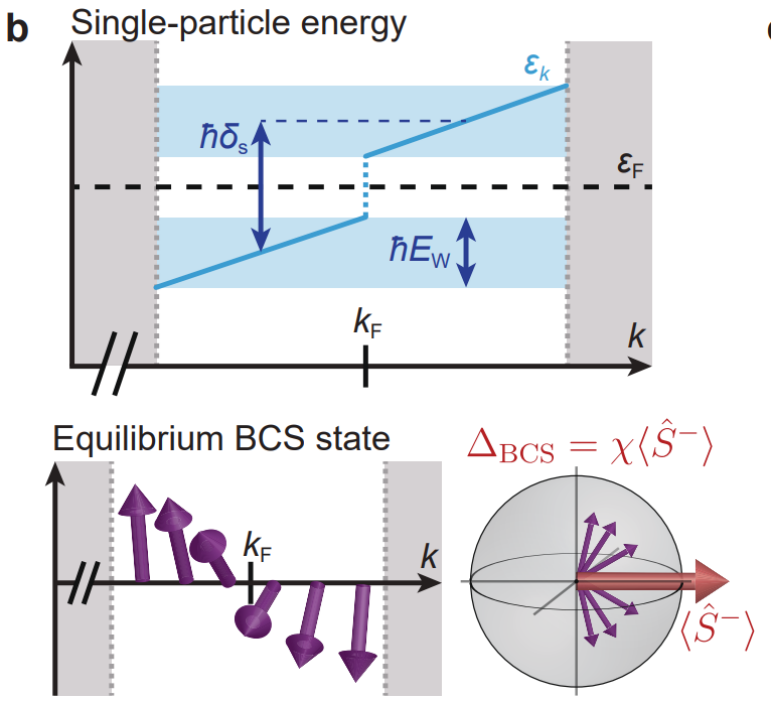


Figure 34.2: **b**, Model parameters. The top plot shows the effective dispersion relation near the Fermi surface engineered in our system as a function of parameters δ_s and E_W, controlled using AC Stark shifts. The bottom plot visualises the ground state of a BCS superconductor using Anderson pseudospins (still haven't understood them fully...). Near the Fermi momentum, the pseudospins develop a phase-coherent superposition at a scale set by a nonzero BCS pairing gap Δ_{BCS}. This gap is self-consistently defined from the spin coherence as shown on the Bloch sphere.

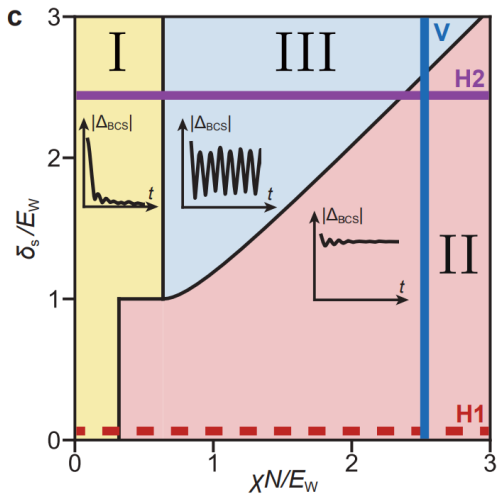


Figure 34.3: **c**, Dynamical phase diagram. The three dynamical phases can be realised by varying parameters χN, δ_s, and E_W. (what is the meaning of moving through vertical or horizontal axes??) Representative dynamics of the BCS order parameter $|\Delta_{BCS}|$ for each phase are shown as insets. We explore cut H1 (dashed line) in Fig. **??** using a single ensemble of atoms and cuts V and H2 (solid lines) in Figs. 34.9 and 34.10 using two separately controlled sub-ensembles.

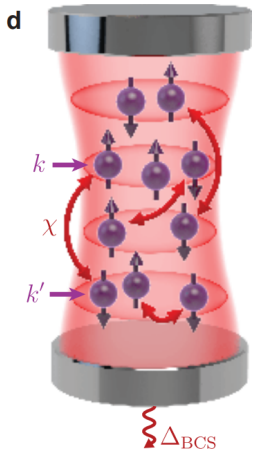


Figure 34.4: **d**, Cavity QED implementation of the BCS interaction. Coupling many strontium atoms to a detuned optical cavity generates infinite-range spin-exchange interactions mediated by a virtual exchange of cavity photons. This interaction also causes a field proportional to Δ_{BCS} to leak out of the cavity, providing a real-time probe of the dynamics.

(it is not clear, what were the results before?) Here, we take a step forward towards this challenge by using internal electronic states to encode effective Cooper pairs. (= do simulation)

At the heart of this implementation is the Anderson pseudospin mapping [Anderson(1958)] by which the presence or absence of Cooper pairs in a momentum mode is encoded in a pseudo spin-1/2 system. We simulate Anderson pseudospins using a long-lived electronic transition in ^{88}Sr with interactions between the spins mediated by a high finesse optical cavity. (how????)

As proposed in Refs. [Lewis-Swan *et al.*(2021), Kelly *et al.*(2022)] (read these papers!!), the scattering between Cooper pairs in condensed matter systems can be engineered in our system via the exchange of photons through the cavity (see Fig. **??d**).

(read their article, tell why it can be so??? I have no idea now)

In this way, the dynamics of a collection of interacting spin-1/2 systems maps onto the low-energy physics of a superconductor or superfluid.

We probe all three dynamical phases (phases I, II, and III) predicted to exist in BCS superconductors
(where was this prediction made???)
by utilising the high degree of control and flexibility in state initialisation, interaction control, and non-destructive measurements available when coupling long-lived atoms to an optical cavity. Behaviours intrinsic to phase I (normal phase) and phase II (finite steady-state superconductivity) have previously been observed in spin systems realized in optical cavities [Davis *et al.*(2020), Norcia *et al.*(2018a)] (read these articles!!!) and in two-level atoms interacting via collisions [Allred *et al.*(2002), Kleine *et al.*(2008), Deutsch *et al.*(2010), Smale *et al.*(2019)] (read these articles!!!).

We build on this work by clarifying the connection between these dynamical phases from the BCS model and the physics of many-body gap protection in spin systems.
(what is the second, gap protection??)
Our results also provide the first demonstration of phase III (a self-generated Floquet phase featuring persistent oscillations of the order parameter), which is predicted to dynamically emerge in superconductors via quenches from weak to strong interactions [Barankov and Levitov(2006), Yuzbashyan *et al.*(2015)]. In our system, we instead engineer this phase using flexible control of the single-particle dispersion [Lewis-Swan *et al.*(2021), Collado *et al.*(2023)] (to understand it, I would need to read these articles), dynamically resembling the low-energy condition of a BCS superconductor.
For all experiments, we perform real-time tracking of the superconducting order parameter, enabling fast readout of the dynamics.

34.2 Experimental setup and model system

To realise dynamical phases of the BCS model, we laser cool (how is it by the way?) an ensemble of $N = 10^5 - 10^6$ ^{88}Sr atoms and trap them inside a $\lambda_L = 813$ nm 1D optical lattice supported by a high-finesse optical cavity.
(what is an optical lattice?)
A spin-1/2 system is encoded in the electronic ground state $|\downarrow\rangle = |^1S_0, m_J = 0\rangle$ and a long-lived optical excited state $|\uparrow\rangle = |^3P_1, m_J = 0\rangle$.
Along this transition, we define spin operators $\hat{S}_k^- = |\downarrow\rangle\langle\uparrow|_k$ and $\hat{S}_k^z = (|\uparrow\rangle\langle\uparrow|_k - |\downarrow\rangle\langle\downarrow|_k)/2$ for single atoms with labels $k \in \{1, ..., N\}$, as well as the collective lowering operator $\hat{S}^- = \sum_k \hat{S}_k^-$ and raising operator $\hat{S}^+ = (\hat{S}^-)^\dagger$.

Assuming homogeneous atom-light coupling in the cavity and unitary dynamics, our system can be described by the Hamiltonian

$$\hat{H} = \hbar\chi\hat{S}^+\hat{S}^- + \sum_k \varepsilon_k \hat{S}_k^z. \tag{34.1}$$

The first term represents an infinite-range spin-exchange interaction described by a frequency scale χ [Norcia *et al.*(2018a)], realised using the collective coupling between the atomic ensemble and a detuned optical cavity mode.
(why????? what is the meaning of these spins?? need to study [Norcia *et al.*(2018a)] to find the derivation of this model for the gas!!)

Inhomogeneous atom-light coupling and dissipative processes (including, foremost, single-particle spontaneous decay) are present in the current implementation but do not largely change

the qualitative behaviour of the targeted dynamical phases under our experimental conditions (see Methods). Previously, we have characterised this interaction [Norcia *et al.*(2018a)](read!!!) and studied collective dynamics by applying an external drive [Muniz *et al.*(2020)] (read!!!).

In this work, we go beyond the fully collective manifold by engineering a spread in single-particle energies $\varepsilon_k = \hbar\omega_k$ using applied AC Stark shifts ω_k [Baghdad *et al.*(2023), Sauerwein *et al.*(2023)]. (read!!!)

These shifts form the second term in the Hamiltonian and compete with the spin-exchange interaction.

Equation (34.1) is the so-called Richardson-Gaudin spin model [Richardson and Sherman(1964), Gaudin(1976)], which describes the low-energy physics of Bardeen-Cooper-Schrieffer (BCS) superfluids and superconductors using the Anderson pseudospin mapping [Anderson(1958)]. (read their paper!!??)

This mapping relates the presence (or absence) of a Cooper pair formed by a pair of electrons with momenta $\pm\mathbf{k}$ to a spin-up (or down) at momentum $\mathbf{k}$, as shown in Fig. **??a**.

Correspondingly, annihilating a Cooper pair maps to a spin lowering operator by the relation $\hat{S}^-_{\mathbf{k}} \coloneqq \hat{c}_{\mathbf{k}}\hat{c}_{-\mathbf{k}}$, where $\hat{c}_{\pm\mathbf{k}}$ are fermionic annihilation operators.

Similarly, the spin operator $2\hat{S}^z_{\mathbf{k}} + 1 \coloneqq \hat{c}^\dagger_{\mathbf{k}}\hat{c}_{\mathbf{k}} + \hat{c}^\dagger_{-\mathbf{k}}\hat{c}_{-\mathbf{k}}$ counts the number of electrons with momentum $\mathbf{k}$ or $-\mathbf{k}$. (I guess, this is explained in Anderson's paper) Our cavity system therefore manifestly implements a BCS superconductor if one identifies the label k of an atom in the cavity with the momentum $\mathbf{k}$ of the electrons in a Cooper pair.

In this way, the first term in Eq. (34.1) is equivalent to the attractive interaction between electrons in the superconductor, and the second term can be associated with the kinetic energy or dispersion relation of the electrons. Note that the BCS model, described by Eq. (34.1), only accounts for the zero momentum collective excitations present in conventional superfluids and superconductors [Anderson(1958)].

The BCS order parameter in the Anderson mapping is defined by $\Delta_{\mathrm{BCS}} = \chi\langle\sum_{\mathbf{k}} \hat{c}_{\mathbf{k}}\hat{c}_{-\mathbf{k}}\rangle = \chi\langle\hat{S}^-\rangle$, as depicted in Fig. **??b**.

In equilibrium, it plays the role of the BCS pairing gap, which energetically favours many-body states where the electrons arrange in a coherent superposition between Cooper pairs and holes for states close to the Fermi energy.

Away from equilibrium, Δ_{BCS} is also predicted to characterise the three dynamical phases (I, II, and III) that arise after quenches in superconductors and superfluids [Marino *et al.*(2022)] (what is in this article?). Such dynamical phases represent distinct regimes of dynamical behaviour that arise after a sudden perturbation of a control parameter in a closed many-body system.

They are described using a time-averaged or steady-state order parameter that demonstrates non-analytic behaviour at the boundary between phases.

(a very unclear sentence. regimes use some secret steady-state order parameter? what is it??)

In particular, the BCS model is predicted to exhibit second-order dynamical phase transitions.

(what is it??)

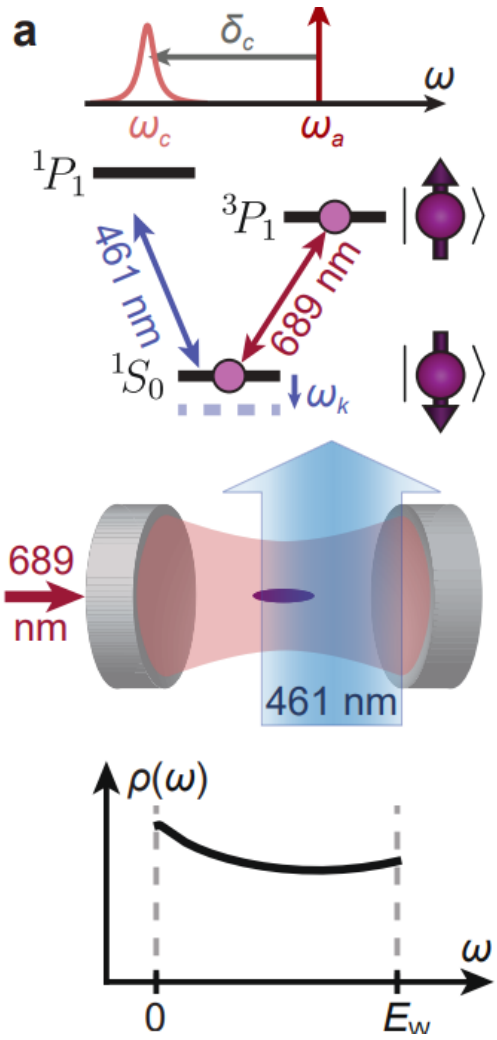


Figure 34.5: **a**, Tuning the single-particle dispersion. We shine an off-resonant 461 nm beam onto the atoms from outside the cavity. This generates a distribution of AC Stark shifts representing a roughly uniform density of states $\rho(\omega)$ (bottom plot).

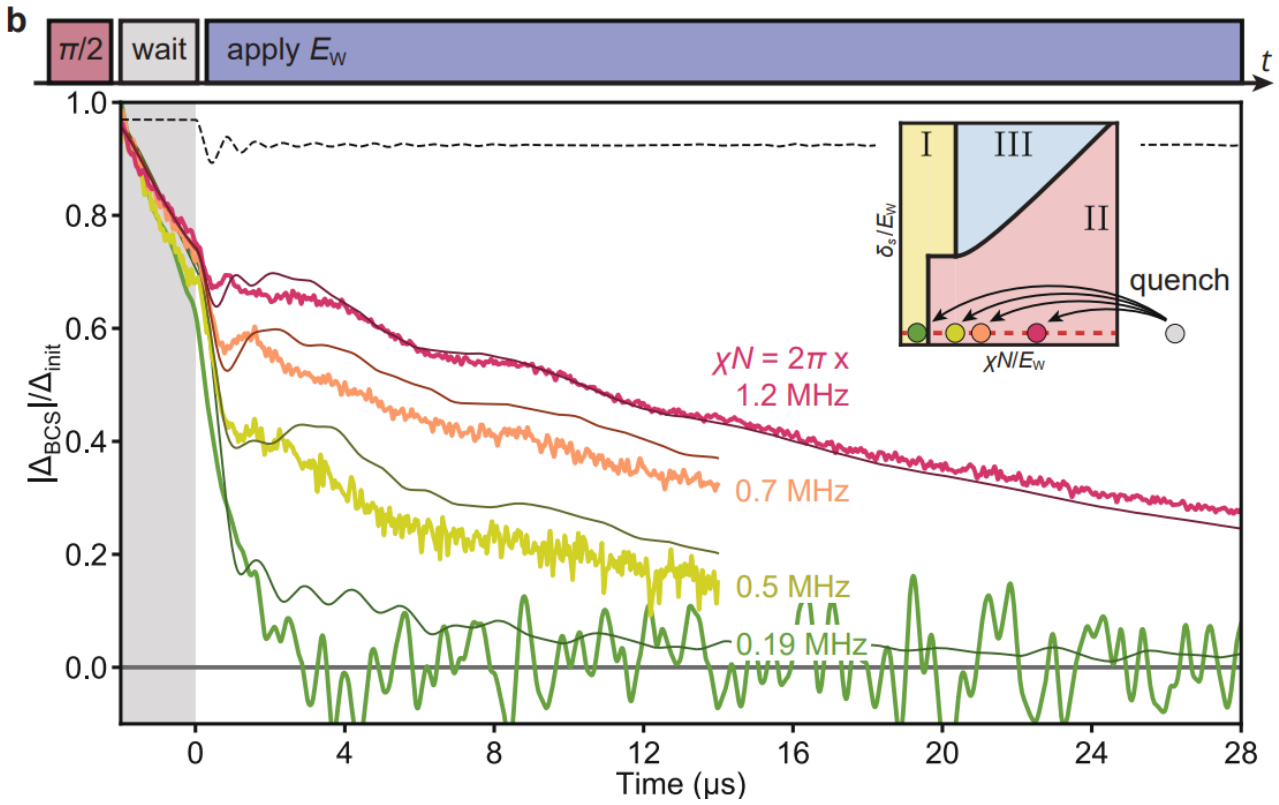


Figure 34.6: **b**, Probing phase I and phase II. We perform a rapid $\pi/2$ pulse to prepare a highly coherent initial state, wait for 2 μs, quench to a variable $\chi N/E_W$ with $\delta_s = 0$, and then let the system evolve. The inset shows the explored parameter cut and identifies post-quench $\chi N/E_W$ values with coloured dots. The main plot shows experimental time traces of $|\Delta_{BCS}|$ (coloured curves) accompanied by numerical simulations (darker lines). Two curves are extended to demonstrate long-time coherence protection, with the $\chi N/2\pi = 0.19$ MHz trace smoothed for clarity. For $\chi N/2\pi = 1.2$ MHz, we show an ideal simulation neglecting dissipation and motional effects (dashed line), which exhibits transient Higgs oscillations. Hints of these oscillations are present in experimental data with additional damping.

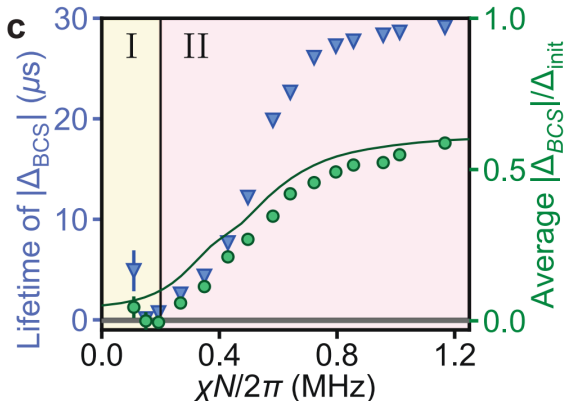


Figure 34.7: **c**, Characterising the phase transition. Blue triangles show the fitted coherence time of $|\Delta_{BCS}|$ from $t = 1$ μs to 30 μs. Green circles show the time-averaged $|\Delta_{BCS}|$ between $t = 3$ μs and 8 μs, with the dark green line representing numerical simulations. In all cases, we identify a phase transition at $\chi N/2\pi = 0.2$ MHz. Error bars in all plots represent the s.e.m. of boostrap resamplings on experimental shots.

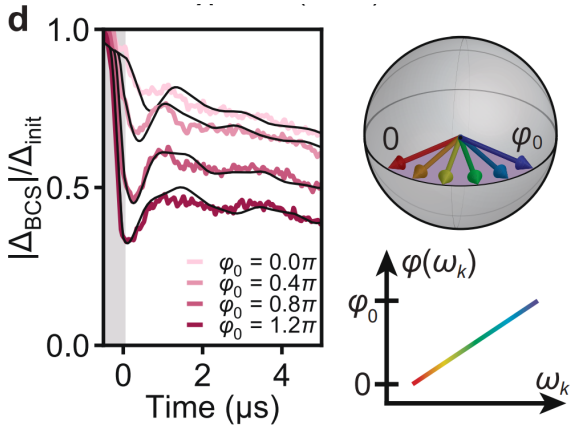


Figure 34.8: **d**, Varying initial conditions. Before $t = 0$, we shine a high-intensity 461 nm beam within 300 ns, engineering an initial phase spread $\varphi(\omega_k) \in [0, \varphi_0]$ depicted on the Bloch sphere. The phase $\varphi(\omega_k)$ applied to atom k is proportional to the post-quench frequency shift ω_k. Traces represent different φ_0 and show enhanced oscillations with increasing φ_0.

Phase I is characterised by a steady state with a vanishing order parameter $|\Delta_{\mathrm{BCS}}(t)| \to 0$ at long times. Phase II exhibits a steady state with a constant nonzero order parameter $\Delta_\infty := \lim_{t\to\infty} |\Delta_{\mathrm{BCS}}(t)| > 0$. Finally, phase III features oscillations in $|\Delta_{\mathrm{BCS}}(t)|$ that persist to long times, realising a Floquet superfluid despite not being periodically driven [Foster *et al.*(2014), 93, Yuzbashyan *et al.*(2015), 36]. The long-time behaviour of these dynamical phases admits a simpler description in terms of the Lax-reduced Hamiltonian, which is an effective Hamiltonian taking the same form of Eq. (34.1) but with rescaled parameters and a reduced number of spins [Yuzbashyan *et al.*(2015), Marino *et al.*(2022)]. Under this formulation, phases I, II, and III emerge when the Lax-reduced Hamiltonian describes effective zero-spin, one-spin, and two-spin systems respectively.

Inspired by the Lax-reduced Hamiltonian, and in order to explore all three dynamical phases, we engineer two sub-ensembles of atoms with separate control over energy shifts within each sub-ensemble. For practical convenience, we introduce experimental control in the form of an overall frequency splitting δ_s between two sub-ensembles and an effective frequency width E_W of each sub-ensemble to engineer a tunable dispersion relation ε_k as in Fig. **??b**. Phase I and phase II can also be observed using a single ensemble of atoms as shown in Fig. **??**. Both experimental setups can nonetheless be described by a common phase diagram as shown in Fig. **??c**.

We initialise all the atoms in the $|\downarrow\rangle$ state and then apply a coherent $\pi/2$ pulse through the cavity in 100 ns such that $\Omega \gg \chi N$, where Ω is the pulse Rabi frequency and χN is the characteristic interaction strength for an ensemble of N atoms. This establishes a large BCS order parameter Δ_{BCS} on a timescale faster than any other relevant dynamics, mimicking the ground state of a Hamiltonian with an infinite interaction strength χ. We then quench the system by rapidly turning on ε_k, which sets a finite ratio $\chi N/E_W$ and a variable δ_s/E_W, allowing us to explore the dynamical phase diagram shown in Fig. **??c**.

We measure both the pre- and post-quench dynamics of $|\Delta_{\mathrm{BCS}}|$ by monitoring light emitted by the atoms into the cavity as a function of time (see Fig. **??d**).

This light arises from a superradiance process which is suppressed when the cavity resonance is detuned from the atomic transition frequency by much more than κ, the cavity power decay linewidth [Weiner *et al.*(2012), Bohnet *et al.*(2013), Norcia *et al.*(2016)].

(what it the superradiance? what is going on in the cited articles??)

In this limit, the established cavity field adiabatically follows $\langle \hat{S}^- \rangle$, which is proportional to Δ_{BCS}. By measuring the leakage of light from the cavity in heterodyne with a local oscillator, we therefore obtain a real-time probe of Δ_{BCS}.

(how is it???)

Importantly, at the chosen detuning this probe is quasi-nondestructive, since only a small fraction of the atoms emit light over relevant timescales. In plots of $|\Delta_{\mathrm{BCS}}|$ over time, we normalise traces to the initial gap size Δ_{init} measured right after the $\pi/2$ pulse.

34.3 Phase I to phase II

We probe the phase I to phase II transition by varying the ratio $\chi N/E_{\mathrm{W}}$ between the interaction strength and the width of the single-particle energy distribution. As shown in Fig. **??a**, we shine an off-resonant 461 nm beam onto a single atomic ensemble from the side of the cavity that generates a distribution of AC Stark shifts with a spread E_{W}. Careful shaping of the 461 nm beam allows us to realise a roughly flat density of states (see Methods), resulting in a setup consistent with the $\delta_{\mathrm{s}} = 0$ line in Fig. **??c** (see Supplemental Online Material). After the initial $\pi/2$ pulse, we wait for 2 μs to let transient dynamics settle and then turn on the 461 nm beam to quench on $E_{\mathrm{W}}/2\pi = 0.83$ MHz from an initial value $E_{\mathrm{W}}^{(0)}/2\pi \ll 0.1$ MHz. The beam exhibits a rise time of roughly 50 ns, much faster than the relevant dynamics. To scan across the phase diagram in the inset of Fig. **??b**, we vary the interaction strength χN between shots by changing the atom number N.

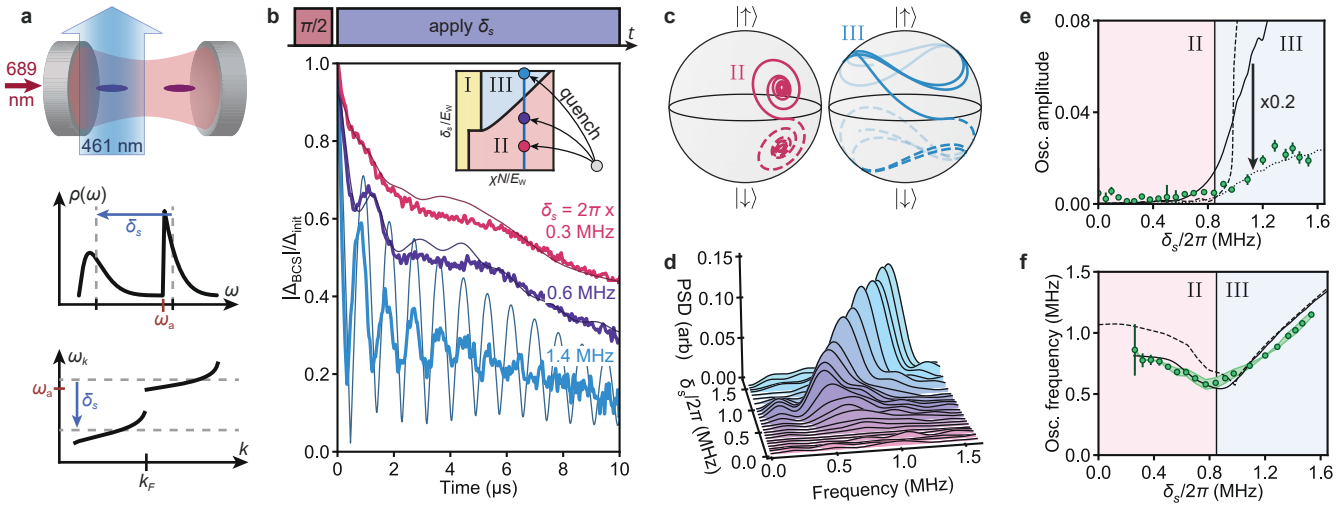


Figure 34.9: **Phase II to phase III transition.** **a**, Engineering a bimodal energy distribution. We prepare two atomic clouds with centres separated by 3 mm and shine an off-resonant 461 nm beam centred on one cloud. This generates a density of states $\rho(\omega)$ (middle plot), equivalent to a dispersion relation $\varepsilon_k = \hbar\omega_k$ (bottom plot). **b**, Probing phase II and phase III. We prepare the same initial state as in Fig. **??b** with a $\pi/2$ pulse, quench to a finite δ_s/E_W, and then let the system evolve. The inset shows the explored parameter cut and identifies post-quench δ_s/E_W values with coloured dots. As before, coloured traces represent experimental time traces of $|\Delta_{BCS}|$, and darker lines represent numerical simulations. **c**, Ideal simulations of mean-field trajectories for the two sub-ensembles (solid and dashed curves) in phase II (magenta) and phase III (blue). The trajectories are projected onto the surface of the Bloch sphere for visual clarity. **d**, Fourier response of $|\Delta_{BCS}|^2$ for different δ_s, plotted as power spectra of the dynamics from $t = 0.5$ μs to 4 μs after subtracting slow-moving behaviour. **e**, Average oscillation amplitude between $t = 3$ μs and 8 μs. For the remaining plots, dashed lines represent ideal simulations (ignoring dissipation or motional effects), and solid dark lines correspond to full simulations. The additional dotted line represents numerical simulations rescaled by $\times 0.2$, plotted to show similar trend behaviour between experimental data and simulations. We identify a phase transition around $\delta_s/2\pi = 0.85$ MHz. **f**, Oscillation frequency of $|\Delta_{BCS}|$, measured using power spectra calculated in (**d**). We correct for systematics inferred from our data analysis and assume this correction has an uncertainty of 100%, shown by the green band. The phase transition point observed in data in panels (**e**) and (**f**) agrees well with simulations.

As shown in Fig. **??b** and **c**, we observe two distinct dynamical behaviours corresponding to phases I and II, signalled by the decay rate of $|\Delta_{BCS}|$. For experiments with sufficiently small χN, such as $\chi N/2\pi = 0.19$ MHz, $|\Delta_{BCS}|$ decays with a $1/e$ coherence time of 0.9 ± 0.1 μs. This coherence time is consistent with single-particle dephasing of $\langle \hat{S}^- \rangle$ set by the energy spread $\hbar E_W$ and is nearly constant throughout this regime. We identify the fast decay of $|\Delta_{BCS}|$ as an experimental signature of phase I. For larger interaction strengths, we observe a rapid increase in coherence time up to a maximum of 29 μs when $\chi N/2\pi = 1.2$ MHz; this constitutes an improvement of more than a factor of 30. We identify this extended coherence time regime as phase II. The residual decay of $|\Delta_{BCS}|$ in this regime can be attributed to intrinsic dissipative processes including spontaneous emission, off-resonant superradiant emission, and scattering of 461 nm light [Norcia *et al.*(2016), Norcia *et al.*(2018a)], which set a maximum predicted coherence time of 29 μs (see Methods). All experimental observations (coloured traces) are in good agreement with numerical simulations based on experimental conditions (dark lines—see Methods).

Due to the separation of timescales in the decay of $|\Delta_{\mathrm{BCS}}|$, we are able to determine the boundary between phase I and phase II in our experiment by calculating the average $|\Delta_{\mathrm{BCS}}|$ in a time window from 3 μs to 8 μs as a function of χN (see Fig. **??c**). In this analysis, phase I features a vanishing average $|\Delta_{\mathrm{BCS}}|$, while phase II sees a nonzero $|\Delta_{\mathrm{BCS}}|$ that increases with χN. The sharp rise of average $|\Delta_{\mathrm{BCS}}|$ around $\chi N/2\pi = 0.2$ MHz indicates a dynamical phase transition, which agrees with the point predicted by numerical simulations. In a spin-model picture, the BCS pairing gap corresponds to the energy gap between collective angular momentum states, which exists due to the spin-exchange interaction $\chi\hat{S}^{+}\hat{S}^{-}$ [Rey *et al.*(2008)]. Phase II corresponds to the parameter region where such interactions are sufficiently strong to protect against single-particle dephasing. As a result, the observed transition directly relates to previous experiments exploring coherence protection in other systems [Davis *et al.*(2020), Norcia *et al.*(2018a), Smale *et al.*(2019), Deutsch *et al.*(2010), Kleine *et al.*(2008), Allred *et al.*(2002)].

In BCS superconductors, the excitation of a Higgs mode is predicted to occur in phase II. This mode can be characterised by a collective damped oscillation of the order parameter $|\Delta_{\mathrm{BCS}}|$ with a characteristic frequency of $2\Delta_{\infty}$ [Yuzbashyan *et al.*(2015)]. We observe hints of Higgs oscillations by comparing the experimental trace of $|\Delta_{\mathrm{BCS}}|$ at $\chi N/2\pi = 1.2$ MHz (red curve in Fig. **??b**) with the dissipation-free simulation (dashed line in Fig. **??b**) and noticing that the first dip in the experimental trace coincides with the first cycle of Higgs oscillations (see Methods). The size of this feature can be increased experimentally by engineering an initial phase spread $\varphi(\omega_k) \in [0, \varphi_0]$ between atoms which is correlated with the post-quench frequency shifts ω_k of the atoms, as shown in Fig. **??d**. The initial state with a nonzero opening angle φ_0 shares qualitative features with the BCS ground state at finite χ up to a $\pi/2$ rotation on the Bloch sphere [Lewis-Swan *et al.*(2021)], in contrast to the initial state mimicking the BCS ground state with infinite χ in Fig. **??b**.

34.4 Phase II to phase III

We probe the phase II to phase III transition using a vertical cut through the dynamical phase diagram. To realise this, we introduce an energy splitting $\hbar\delta_{\mathrm{s}}$ between two individually addressable clouds of atoms along the cavity axis using AC Stark shifts from our 461 nm beam, as shown in Fig. 34.9**a**. In combination with a background energy spread $\hbar E_{\mathrm{W}}$ associated with lattice shifts (see Methods), this produces a bimodal density of states and a dispersion relation similar to the one proposed in Fig. **??b**. As before, we begin the experiment with a highly coherent state and with $\delta_{\mathrm{s}} = 0$. Then, we quench on a nonzero δ_{s} and let the system evolve. Between shots, we scan δ_{s} while fixing $\chi N/2\pi = 0.9$ MHz and $E_{\mathrm{W}}/2\pi \approx 0.34$ MHz to explore the vertical cut.

The resulting dynamics show a marked change in the dynamical evolution of $|\Delta_{\mathrm{BCS}}|$ over the scan as shown in Fig. 34.9**b**, which we attribute to a transition between phase II and phase III dynamics. For small δ_{s}, we either see Higgs-like oscillations which are damped after 3 μs (the trace where $\delta_{\mathrm{s}}/2\pi = 0.6$ MHz) or, for very small splittings, no oscillations resolvable above the noise floor ($\delta_{\mathrm{s}}/2\pi = 0.3$ MHz). We associate this regime with phase II since it overlaps with the previously observed phase II dynamics in parameter space. For larger δ_{s}, curves instead show large-amplitude oscillations that persist for more than 5 μs ($\delta_{\mathrm{s}}/2\pi = 1.4$ MHz). We identify the long-lived oscillations in this parameter regime as an experimental signature of phase III.

Intuitively, we can understand the difference between the two phases by identifying the two sub-ensembles of atoms with two Bloch vectors (see Fig. 34.9**c**). In phase II, a finite δ_{s} causes the Bloch vectors to precess in different directions, but the dominant scale χN locks them together to form the solid and dashed magenta orbits. In the presence of a finite E_{W}, the orbits decay, but the Bloch vectors maintain phase coherence. On the other hand, in phase III δ_{s} is large enough that the two Bloch vectors accrue an unbounded relative phase, as in the blue

orbits. The presence of interactions locks each sub-ensemble separately against a finite E_{W}, leading to persistent oscillations. This effective beating of two large spins in a macroscopic array of spin-1/2 particles is truly an interaction-driven effect since the interactions are strong enough to lock the spins within each sub-ensemble but not strong enough to lock both sub-ensembles together. In our implementation of phase III, the bimodal distribution allows us to dynamically separate the Bloch vectors of the two sub-ensembles, instead of starting with an already split distribution like in weakly interacting BCS ground states featuring a sharp Fermi edge. Despite their qualitative differences, these two situations can be dynamically connected (see Methods).

We can experimentally define a boundary between phase II and phase III using the separation of timescales observed for oscillations in $|\Delta_{\mathrm{BCS}}|$. Fig. 34.9**e** shows the average oscillation amplitude in a time window from $t = 3$ μs to 8 μs. In this analysis, we observe a sharp rise in oscillation amplitude at $\delta_{\mathrm{s}}/2\pi = 0.85$ MHz $\approx \chi N/2\pi$ as we increase δ_{s}, which we identify as a dynamical phase transition. Numerical simulations plotted in Fig. 34.9**e** agree fairly well with data in capturing trend behaviour and estimating the phase transition point. However, we see a discrepancy in the absolute size of the observed and predicted oscillation amplitudes. We attribute this to an extra dephasing mechanism (likely residual motional effects) in our system or other imperfections in the experimental sequence not captured by the theory model.

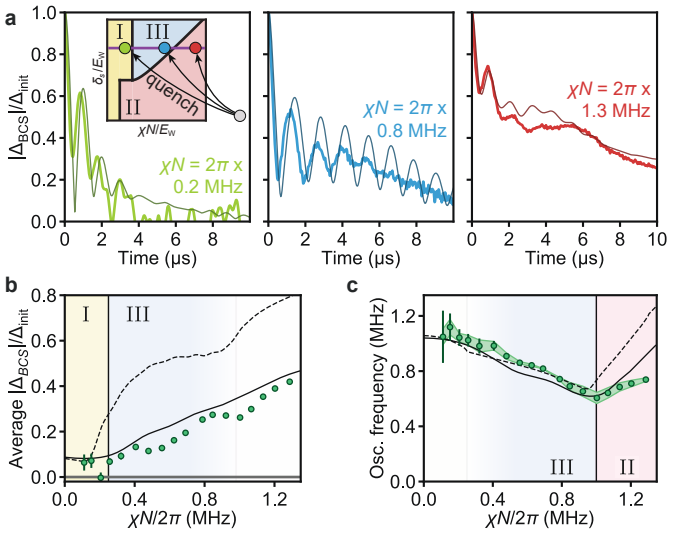


Figure 34.10: **Scan across three dynamical phases. a**, Probing phase I, II and III dynamics using time traces of $|\Delta_{\mathrm{BCS}}|$. Quenches are performed in the same manner as in Fig. 34.9**b**, except between shots we hold post-quench values of δ_{s} fixed and vary χN instead. The inset shows the explored cut through the phase diagram and identifies final $\chi N/E_{\mathrm{W}}$ values with green (phase I), blue (phase III), and red (phase II) dots. The $\chi N/2\pi = 0.2$ MHz trace is smoothed for clarity. **b**, Time average of $|\Delta_{\mathrm{BCS}}|$ in a bin from $t = 3$ μs to 8 μs vs. interaction strength. The experimental data shows signatures of a phase I to phase III transition at $\chi N/2\pi = 0.25$ MHz. **c**, Oscillation frequency of $|\Delta_{\mathrm{BCS}}|$ vs. interaction strength in a bin from $t = 0.5$ μs to 4 μs. Again, we correct for systematics inferred from our data analysis and assume this correction has an uncertainty of 100%, shown by the green band. This data identifies a phase III to phase II transition at $\chi N/2\pi = 1.0$ MHz. Experimental data and transitions in both plots are consistent with numerical simulations.

We verify the location of the phase II to phase III transition using the short-time oscillation frequency (from $t = 0.5$ μs to 4 μs) as an additional experimental signature. As can be seen in the Fourier responses in Fig. 34.9**d** and quantified in Fig. 34.9**f**, the oscillation frequency exhibits a dip vs. δ_{s} at the previously-identified phase boundary. This dip is present in roughly

the same location for experiment and theory and is expected to coincide with the phase II to phase III transition (see Supplemental Online Material).

34.5 Scan across three dynamical phases

Finally, we observe all three dynamical phases in a single cut through parameter space, as shown in Fig. 34.10**a**. We run the same experimental sequence described in Fig. 34.9, but instead scan χN between shots with $\delta_s/2\pi = 1.1$ MHz and $E_W/2\pi = 0.46$ MHz fixed. This allows us to probe phase I, phase III and then phase II by increasing atom number N.

Using order parameters established in Figs. **??** and 34.9, we determine boundaries between the three phases. As shown in Fig. 34.10**b**, the long-time average of $|\Delta_{BCS}|$ rises suddenly around $\chi N/2\pi = 0.25$ MHz in both data and simulations. This transition marks the boundary between phase I and phase III. Additionally, at $\chi N/2\pi = 1.0$ MHz we observe a dip in the short-time oscillation frequency of $|\Delta_{BCS}|$ (Fig. 34.10**c**), marking a transition between phase III and phase II. For this scan, we do not use the long-time oscillation amplitude as an order parameter due to poor signal-to-noise for smaller values of χN.

34.6 Methods

34.6.1 Experimental setup: phase I to phase II transition

To explore the phase diagram cut in Fig. **??**, we first load $10^5 - 10^6$ ^{88}Sr atoms from a magneto-optical trap into an 813 nm optical lattice supported by a high-finesse optical cavity, similar to previous experiments [Norcia *et al.*(2016), Norcia *et al.*(2018b), Norcia *et al.*(2018a), Muniz *et al.*(2020)]. The resulting atomic cloud has a temperature of roughly 15 μK, resulting in a Gaussian distribution transverse to the cavity axis with standard deviation $\sigma_y = \sigma_z = 16$ μm (coordinates defined in Extended Data Fig. 34.11**a**). Further, the cloud is extended over thousands of lattice sites, forming a distribution along the cavity axis with a standard deviation $\sigma_x = 430$ μm. We measure an axial trapping frequency of $\omega_x/2\pi = 165$ kHz, giving a Lamb-Dicke parameter of $\eta = 0.17$ for excitation with 689 nm light. At the measured temperature, $\eta^2(2\bar{n}+1) = 0.11 \ll 1$, placing the atoms in the Lamb-Dicke regime. We set a quantisation axis along $\hat{y}$ with a 2.4 G magnetic field and tune the lattice polarisation to a "magic angle" relative to this axis, such that the differential lattice shift between ground ($|^1S_0\rangle$) and excited ($|^3P_1, m_J = 0\rangle$) states vanishes [Muniz *et al.*(2020)]. Using piezoelectric actuators, we stabilise the cavity length to set the closest TEM_{00} resonance to be 51 MHz red-detuned from the atomic transition.

After loading into the lattice, we initialise the atoms with a $\hat{y}$-polarised drive through the cavity which is nominally resonant with the atomic transition. Because the drive is far off-resonance from the cavity (which has linewidth $\kappa/2\pi = 153$ kHz at 689 nm), the induced Rabi frequency is somewhat suppressed. Nonetheless, we find that roughly 5 mW of power before the cavity is sufficient to drive the atoms with a $\pi/2$ pulse in 100 ns. We allow the atoms to settle for 2 μs in order to distinguish the desired physics from transient dynamics observed after state initialisation, which we attribute to undesired excitation of sideband transitions. We then shine a 461 nm beam from the side of the cavity along the $\hat{y}$ direction, detuned from the $|^1S_0\rangle - |^1P_1\rangle$ transition by more than 10 GHz, in order to induce AC Stark shifts on the ground state. The beam has waists $(w_x, w_z) = (1030\ \mu\text{m}, 75\ \mu\text{m})$ along the $\hat{x}$ and $\hat{z}$ directions at the plane of the atoms, and its centre is displaced from the centre of the atomic cloud by $x_0 = 580$ μm along the cavity axis. From these dimensions, we calculate an atomic density of states $\rho(\omega)$ as a function of frequency shift which is roughly uniform between 0 and a maximum shift $\hbar E_W$. We estimate

that for the power and detuning used in this cut, the 461 nm beam scatters off the atoms with an average rate of $R_{sc}/2\pi = 1.3$ kHz, roughly a factor of six smaller than $\gamma/2\pi = 7.5$ kHz, the spontaneous emission rate. Combined with collective emission from the atoms as described in the Readout section of the Methods, these dissipation processes set a maximum predicted coherence time in the system of 29 μs.

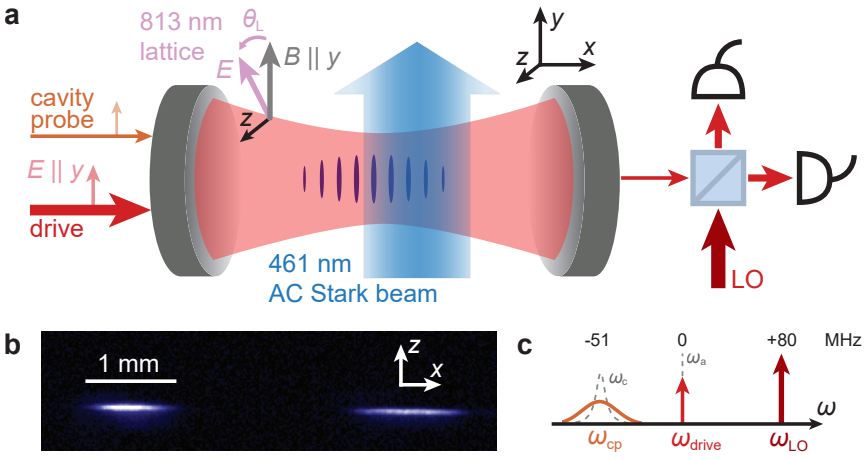


Figure 34.11: **Experimental configuration. a**, Detailed diagram of the cavity and all relevant beams. A magnetic field along $\hat{y}$ sets the quantisation axis. The 813 nm optical lattice supported by the cavity has a tunable linear polarisation. We drive a $\pi/2$ pulse with a beam polarised along $\hat{y}$ through the cavity, and during the experiment we probe the cavity resonance frequency using a second $\hat{y}$-polarised beam to measure atom number. A 461 nm beam far-detuned from the $|^1S_0\rangle - |^1P_1\rangle$ transition shines on the atoms from the side of the cavity, inducing AC Stark shifts. We probe signals transmitted through the cavity using a balanced heterodyne detector. **b**, Fluorescence image of the two atomic clouds used when scanning through phase III in Figs. 34.9 and 34.10. **c**, Frequency landscape of 689 nm beams. The atomic drive frequency ω_{drive} is resonant with the atomic transition. The cavity probe frequency ω_{cp} is nominally centred with the cavity resonance frequency, 51 MHz red-detuned from the atomic transition. The local oscillator used in heterodyne detection has frequency ω_{LO} and is 80 MHz blue-detuned from the atomic transition.

34.6.2 Experimental setup: cuts through phase III

For the two cuts through phase III described in Figs. 34.9 and 34.10, we load the atoms in two clouds separated by 3 mm, as shown in Extended Data Fig. 34.11**b**. The left cloud has an extent described by standard deviations $(\sigma_x, \sigma_z) = (200\ \mu\text{m}, 16\ \mu\text{m})$. The right cloud has a similar extent along σ_z but is broader along the cavity axis. We tune the lattice polarisation to point along $\hat{z}$, which breaks the magic angle condition and introduces a differential trap depth between ground and excited states of 0.47 MHz for atoms experiencing peak lattice intensity. Due to their finite temperature, the atoms experience a spread in lattice intensities which leads to an inhomogeneous trap depth. We estimate the induced distribution of energy shifts by assuming the atoms occupy a 2D Gaussian distribution radially with standard deviation $\sigma_y = \sigma_z = 16\ \mu$m, compared to the lattice waist $w_y = w_z = 80\ \mu$m. This produces a peaked distribution equivalent to the narrow peak in Fig. 34.9**a**.

In these experiments, we perform a $\pi/2$ pulse as before and then immediately shine a 461 nm beam centred on the left ("bright") atomic cloud. Unlike in the previous cut, we do not wait for transient dynamics to settle after state initialisation, for the sake of simplicity. We do not see major differences between observed and expected behaviour when omitting the wait period. The beam has waists $(w_x, w_z) = (1700\ \mu\text{m}, 80\ \mu\text{m})$. We install a beam block just

before the chamber that clips the beam tail that would otherwise hit the right ("dark") atomic cloud. The 3 mm separation between clouds is sufficiently large to ensure the beam does not significantly diffract around the beam block. The beam shifts the mean energy of the bright cloud away from that of the dark cloud, introducing a tunable δ_s. While nominally, we hold E_W fixed while scanning δ_s to explore the phase II to phase III transition, in reality the finite size of the blue beam introduces an additional contribution to E_W on the bright cloud. As δ_s increases, therefore, both the size and shape of the single-particle energy distribution changes. We calculate E_W in a consistent manner by estimating the standard deviation of the bright cloud distribution and matching the result to a uniform distribution with the same standard deviation (see Supplemental Online Material). In the main text, we report the value of E_W obtained at the phase transition point for the phase II to phase III transition. As we increase the 461 nm beam power, the atoms also scatter more blue photons. At the largest applied AC Stark shift, we estimate that the bright cloud experiences a scattering rate of $R_{sc}/2\pi = 3.4$ kHz, resulting in lower coherence times for traces with large δ_s. However, this excess decoherence does not bias our measurements of oscillation amplitude and frequency at times $t \leq 8$ μs.

34.6.3 Readout

After initialisation in all experiments, the atomic ensemble establishes a small electric field inside the cavity which adiabatically follows $\langle \hat{S}^- \rangle$ [Norcia *et al.*(2018a)]. Assuming homogeneous atom-light coupling (see next section for modifications due to inhomogeneous coupling), the complex amplitude of the electric field leaking out of the cavity is given by

$$\alpha_{out}(t) = -\frac{g}{\delta_c}\sqrt{\kappa_m}\langle \hat{S}^-(t) \rangle, \tag{34.2}$$

where α_{out} has units of $\sqrt{\text{photons/s}}$. Here, $2g/2\pi = 10.6$ kHz is the single-photon Rabi frequency for an atom maximally coupled to the cavity, $\delta_c/2\pi = (\omega_c - \omega_a)/2\pi = -51$ MHz is the detuning between the cavity resonance frequency ω_c and the atomic transition frequency ω_a, and $\kappa_m/2\pi = 41$ kHz is the rate at which photons incident on the cavity mirror are transmitted. α_{out} is a form of dissipation in the system equivalent to superradiance in a detuned cavity limit. Over the region of parameter space explored in this work, we estimate that the dissipation rate never exceeds $\gamma_{SR}/2\pi = 2.3$ kHz. We measure the detuned superradiant light as it leaks out of the cavity using balanced heterodyne detection, providing us with a real-time probe of $\langle \hat{S}^- \rangle \propto \Delta_{BCS}$. In plots of $|\Delta_{BCS}|$ in the main text, we calculate the square magnitude of this quantity and average over 400-1600 shots of the experiment, taken within 2-10 minutes. We then perform background subtraction to remove vacuum noise power from the heterodyne signal. Finally, we take a signed square root of the result to return an estimate of $|\Delta_{BCS}|$ which averages to zero in the absence of a real signal. This explains why some traces dip below zero despite representing a nonnegative quantity.

Additionally, the cavity experiences a (dispersive) shift in its resonance frequency proportional to the number of atoms. We use this fact to measure atom number by sending a pulsed probe tone through the cavity and measuring the frequency shift using the transmitted light. Since this light is spectrally resolved from the light emitted by the atoms, we are able to measure both signals independently on our heterodyne detector. The different optical frequencies involved in the heterodyne beat are compared in Extended Data Fig. 34.11**c**.

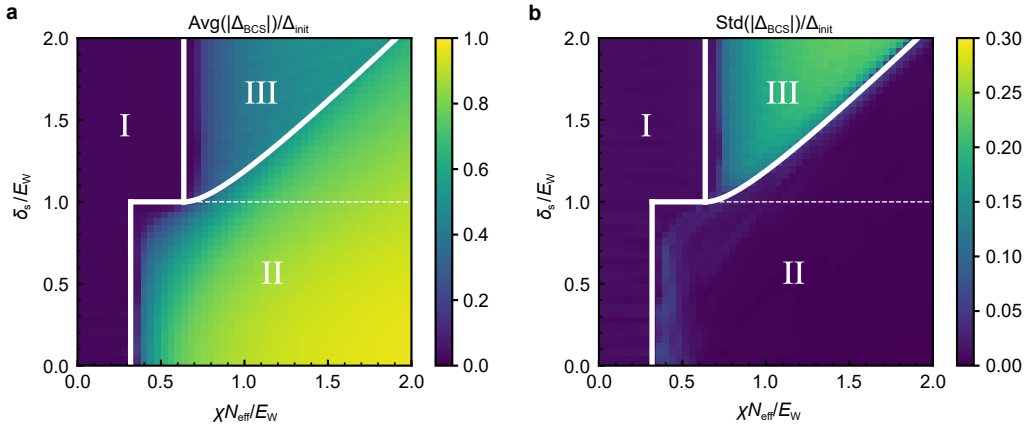


Figure 34.12: **Numerical simulation of the dynamical phase diagram based on Eq. (34.3).** We identify the dynamical phases based on the long-time average (**a**) and the long-time standard deviation (**b**) of $|\Delta_{\mathrm{BCS}}(t)|$, normalised by its initial value $\Delta_{\mathrm{init}} \equiv |\Delta_{\mathrm{BCS}}(0)|$. The white solid lines mark the corresponding dynamical phase boundaries, analytically derived from Eq. (34.1), which agree with the numerical results based on Eq. (34.3). The white dashed lines mark an extra dynamical phase transition that only exists for Eq. (34.1).

34.6.4 Dynamical phase diagram

The unitary dynamics of our system is modelled by an effective atom-only Hamiltonian, given by

$$\hat{H} = \hbar\chi \sum_{jk} \zeta_j \zeta_k \hat{S}_j^+ \hat{S}_k^- + \sum_k \varepsilon_k \hat{S}_k^z, \tag{34.3}$$

where $\hat{S}_k^{+,-}, \hat{S}_k^{x,y,z}$ are the standard spin-1/2 operators on atom k. We define $\chi = -g^2\delta_c/(\delta_c^2 + \kappa^2/4)$, where g and δ_c are as defined in the previous section, and κ is the cavity linewidth. The spatial dependence of the interaction term is characterised by $\zeta_j = \cos(j\phi)$ with $\phi = \pi\lambda_L/\lambda_c$, which arises because the lattice wavelength $\lambda_L = 813$ nm is incommensurate with the cavity wavelength $\lambda_c = 689$ nm. In contrast to Eq. (34.1), Eq. (34.3) becomes non-integrable due to the inhomogeneity in the interaction term. Nevertheless, as shown in Extended Data Fig. 34.12, Eq. (34.3) leads to a similar dynamical phase diagram as Eq. (34.1) if we

1. Use a generalised superconducting order parameter $\Delta_{\mathrm{BCS}} = \chi \sum_k \zeta_k \langle \hat{S}_k^- \rangle$;
2. Interpret the $\pi/2$-pulse as a pulse along the cavity axis under the Hamiltonian $\hat{H}_{\mathrm{drive}} = \hbar\Omega \sum_k \zeta_k S_k^y$ that generates the maximum possible $|\Delta_{\mathrm{BCS}}|$, which occurs when $\Omega t = 0.586\pi$;
3. Replace the atomic number N by an effective atom number $N_{\mathrm{eff}} = N/2$, such that χN_{eff} represents the averaged interaction strength of Eq. (34.3).

We can still measure the generalised order parameter Δ_{BCS} using the field leaking out of the cavity as in the previous section, since with inhomogeneous coupling the transmitted field takes the form $\alpha_{\mathrm{out}}(t) = -\frac{g}{\delta_c}\sqrt{\kappa_m} \sum_k \zeta_k \langle \hat{S}_k^-(t) \rangle \propto \Delta_{\mathrm{BCS}}$. The dynamical phase diagram in Extended Data Fig. 34.12 is numerically calculated based on unitary evolution under Eq. (34.3), with a single-particle dispersion $\varepsilon_k/\hbar$ sampled from a uniform distribution in the frequency range $[-\delta_s/2 - E_W/2, -\delta_s/2 + E_W/2]$ and $[\delta_s/2 - E_W/2, \delta_s/2 + E_W/2]$. There χN corresponds to the averaged interaction strength of Eq. (34.3). We identify the dynamical phases based on the long-time average of $|\Delta_{\mathrm{BCS}}|$, given by

$$\mathrm{Avg}(|\Delta_{\mathrm{BCS}}|) = \lim_{T\to\infty} \frac{1}{T} \int_0^T |\Delta_{\mathrm{BCS}}(t)| dt, \tag{34.4}$$

as well as the long-time oscillation amplitude of $|\Delta_{\mathrm{BCS}}|$. Since the oscillations in $|\Delta_{\mathrm{BCS}}|$ might deviate from a sinusoidal form, for theoretical simulations it is easier to use the standard deviation as a measure of the oscillation amplitude:

$$\begin{aligned}&\mathrm{Std}(|\Delta_{\mathrm{BCS}}|)\\&=\left[\lim_{T\to\infty}\frac{1}{T}\int_0^T\Big(|\Delta_{\mathrm{BCS}}(t)|-\mathrm{Avg}(|\Delta_{\mathrm{BCS}}|)\Big)^2dt\right]^{1/2}.\end{aligned}\tag{34.5}$$

When comparing to experimental data, we measure oscillation amplitude using the Fourier spectrum because technical noise in the experiment contributes to the standard deviation of the time traces (see Fig. 34.9**d**). The dynamical phases can be characterised in theoretical simulations by

- Phase I: $\mathrm{Avg}(|\Delta_{\mathrm{BCS}}|)=0$, $\mathrm{Std}(|\Delta_{\mathrm{BCS}}|)=0$.
- Phase II: $\mathrm{Avg}(|\Delta_{\mathrm{BCS}}|)>0$, $\mathrm{Std}(|\Delta_{\mathrm{BCS}}|)=0$.
- Phase III: $\mathrm{Avg}(|\Delta_{\mathrm{BCS}}|)>0$, $\mathrm{Std}(|\Delta_{\mathrm{BCS}}|)>0$.

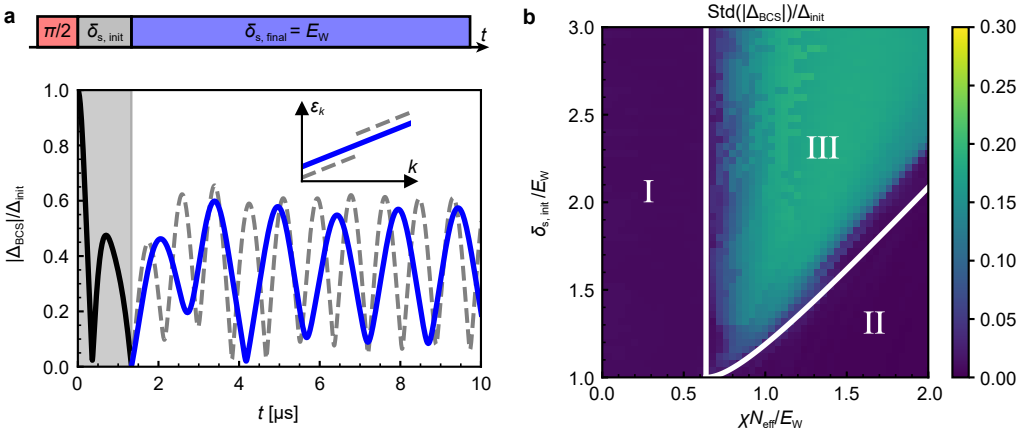


Figure 34.13: **Alternative approach for phase III. a**, Simulation of an alternative experimental sequence. As described by the timing sequence at the top, we simulate an experiment that prepares the initial state using a $\pi/2$ pulse, lets the system evolve under a bimodal distribution of single-particle energy (see the inset) until $|\Delta_{\mathrm{BCS}}|$ reaches its minimum value, and then quenches the system back to a continuous distribution of single-particle energies (see the inset). The theoretically predicted time trace of $|\Delta_{\mathrm{BCS}}|$ with $\chi N/E_{\mathrm{W}}=1.0$ and $\delta_{\mathrm{s,init}}/E_{\mathrm{W}}=1.6$ is shown at the bottom. The blue (grey dashed) line shows phase III dynamics under a continuous (bimodal) distribution. **b**, Long-time standard deviation of $|\Delta_{\mathrm{BCS}}(t)|$ after quenching to the continuous distribution shown in **a**. The white lines are dynamical phase boundaries for bimodal distributions (see Extended Data Fig. 34.12). Nearly all the choices of parameter for phase III using bimodal distributions can lead to phase III behaviours after quenching to the continuous distribution.

The dynamical phase boundaries (white solid lines) in Extended Data Fig. 34.12 are analytically calculated using a Lax analysis applied to Eq. (34.1), similar to the one discussed in [Lewis-Swan *et al.*(2021), Marino *et al.*(2022)], and take the following form (see Supplemental Online Material for a detailed derivation):

- Phase I to phase II:

$$\begin{aligned}&\frac{\chi N}{E_{\mathrm{W}}}=\frac{1}{\pi}\quad\text{with}\quad\frac{\delta_{\mathrm{s}}}{E_{\mathrm{W}}}\in[0,1],\\&\frac{\delta_{\mathrm{s}}}{E_{\mathrm{W}}}=1\quad\text{with}\quad\frac{\chi N}{E_{\mathrm{W}}}\in\left[\frac{1}{\pi},\frac{2}{\pi}\right].\end{aligned}\tag{34.6}$$

- Phase I to phase III:

$$\frac{\chi N}{E_{\mathrm{W}}} = \frac{2}{\pi} \quad \text{with} \quad \frac{\delta_{\mathrm{s}}}{E_{\mathrm{W}}} > 1. \tag{34.7}$$

- Phase II to phase III:

$$\frac{\delta_s}{E_{\mathrm{W}}} = \csc\left(\frac{E_{\mathrm{W}}}{\chi N}\right) \quad \text{with} \quad \frac{\chi N}{E_{\mathrm{W}}} > \frac{2}{\pi}. \tag{34.8}$$

The analytical results agree with the numerical simulations for Eq. (34.3). The only difference is that Eq. (34.1) predicts an extra dynamical phase transition marked by the white dashed line. The dynamical phase boundaries shown in Fig. **??c** are constructed by the analytical formulas above.

34.6.5 Phase III dynamics: the case of a continuous single-particle dispersion

In this manuscript, we generate phase III using a bimodal single-particle dispersion, represented with idealized assumptions by Fig. **??b** and with actual experimental conditions by Fig. 34.9**a**. Here we show that this experimentally convenient approach generates similar phase III dynamics to the one obtained in the case of a continuous dispersion but with different initial conditions.

This is done by the protocol shown in Extended Data Fig. 34.13**a**, which uses a bimodal distribution ($\delta_{\mathrm{s,init}} > E_{\mathrm{W}}$) just to generate a state with minimum $|\Delta_{\mathrm{BCS}}|$. At this point the system's dispersion is restored to be continuous by setting $\delta_{\mathrm{s,final}} = E_{\mathrm{W}}$. This approach more closely resembles the phase III quench discussed in actual BCS superconductors, where phase III is observed by quenching from a state with weak BCS paring gap $|\Delta_{\mathrm{BCS}}|$ to one with a strong pairing gap [Yuzbashyan *et al.*(2015)]. Numerical simulations based on Eq. (34.3) show that nearly all choices of parameters that lead to phase III using a bimodal distribution also lead to phase III dynamics when quenching to a continuous distribution. The only exception is a small parameter regime close to the boundary between phase III and phase II (see Extended Data Fig. 34.13**b**). Note that here we use definitions for Δ_{BCS}, the $\pi/2$ pulse, and χN which correspond to Eq. (34.3), as explained in the previous section.

34.6.6 Numerical simulations

The black dashed lines in Figs. **??**, 34.9, and 34.10 are computed from unitary evolution under Eq. (34.3) using a single-particle dispersion ε_k, sampled from the experimentally engineered distribution.

The black solid lines in the same figures are obtained by adding dissipative processes and axial motion to Eq. (34.3). The system dynamics is described by the following master equation for the density matrix $\hat{\rho}$:

$$\frac{d\hat{\rho}}{dt} = -\frac{i}{\hbar}[\hat{H}, \hat{\rho}] + \mathcal{L}(\hat{L}_c)[\hat{\rho}] + \sum_k \mathcal{L}(\hat{L}_{s,k})[\hat{\rho}] + \sum_k \mathcal{L}(\hat{L}_{\mathrm{el},k})[\hat{\rho}]. \tag{34.9}$$

The Lindblad superoperator takes the form $\mathcal{L}(\hat{L})[\hat{\rho}] = \hat{L}\hat{\rho}\hat{L}^\dagger - \frac{1}{2}(\hat{L}^\dagger\hat{L}\hat{\rho} + \hat{\rho}\hat{L}^\dagger\hat{L})$. Superradiance through the cavity is described by the jump operator

$$\hat{L}_c = \sqrt{\Gamma}\sum_k \zeta_k \hat{S}_k^-, \tag{34.10}$$

where $\Gamma = \chi\kappa/\delta_c$. Spontaneous emission from the atomic excited state is described by the jump operator

$$\hat{L}_{s,k} = \sqrt{\gamma}\hat{S}_k^-, \tag{34.11}$$

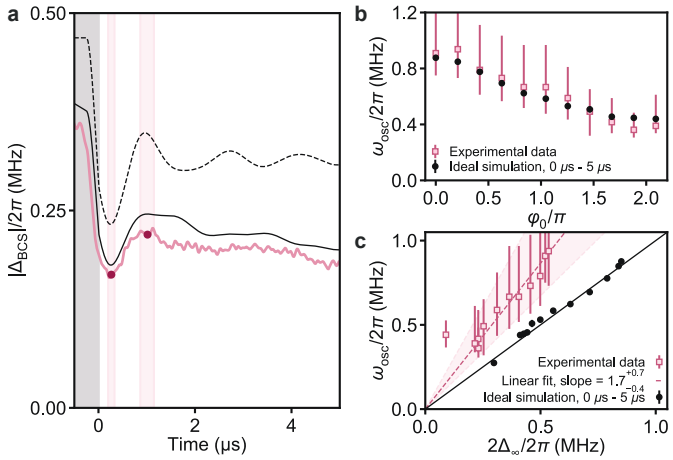
where $\gamma/2\pi = 7.5$ kHz is the spontaneous emission rate out of $^3P_1$. Single-particle decoherence is described by the jump operator

$$\hat{L}_{\mathrm{el},k} = \sqrt{2\gamma_{\mathrm{el}}}\hat{S}_k^z, \tag{34.12}$$

where γ_{el} is a fitting parameter taking into account free space scattering from the AC Stark shift beam, as well as other decoherence processes in the experiment (see Supplemental Online Material). These are the dominant dissipative processes in our system.

The axial trapping frequency of the lattice is 165 kHz and is therefore smaller than the spin-exchange interaction rate χN for most of the experiments. As a consequence, in contrast to the idealised model where atoms are assumed to be frozen, motional processes need to be accounted for, even though they are suppressed in the Lamb-Dicke regime. As shown in the Supplemental Online Material, axial motion can lead to a faster damping rate of $|\Delta_{\mathrm{BCS}}|$ oscillations. The predicted dynamical phase boundaries are nevertheless unaffected by the axial motion.

All the numerical simulations are computed using the mean-field approximation, which replaces the operators $\hat{S}_k^{x,y,z}$ by their expectation values $\langle\hat{S}_k^{x,y,z}\rangle$ in the Heisenberg equation of motion. The mean-field treatment of the BCS model is predicted to be exact in the thermodynamic limit due to the infinite-range nature of the interactions [Yuzbashyan *et al.*(2015)]. The atom number for numerical simulation is set to 5000 for the ideal conditions and 2000 for actual experimental conditions. We rescale χ to match χN with experimental values.



[H]

Figure 34.14: **Collective scaling in damped phase II oscillations. a**, Time dynamics of $|\Delta_{\mathrm{BCS}}|$ measured after engineering an initial phase spread over $[0, \varphi_0]$ where $\varphi_0 = 0.8\pi$ as in Fig. 2**d**, plotted in absolute frequency units (pink trace). The solid black curve represents a numerical simulation of the full system, whereas the dashed curve represents an ideal simulation neglecting dissipation and motional effects. We obtain a crude estimate of oscillation frequency in the experimental data by fitting a trough and peak to smoothed data (after subtracting slow-moving behaviour) within the first couple μs (magenta points), using these points to infer a half period of oscillation, and with uncertainties determined using a 90% amplitude threshold (pink bands). **b**, Comparing oscillation frequency estimates of experimental data (pink squares) with those of ideal simulations (black dots) for different φ_0. Theory oscillation frequencies are calculated using a Fourier transform from $t = 0$ μs to $t = 5$ μs. Error bars for experimental data are set by the minimum and maximum frequencies implied by uncertainties in the half period shown in **a**. The two frequency estimates agree within error bars. **c**, Collective scaling of oscillation frequency. For each φ_0 measured in the experiment, we plot the oscillation frequency against the long-time BCS gap Δ_∞, calculated at $t = 18$ μs for ideal simulations and at $t = 3$ μs for experimental data. The solid black line is defined by $\omega_{\mathrm{osc}} = 2\Delta_\infty$, demonstrating the expected scaling for Higgs oscillations. The dashed pink line represents a linear fit to the experimental data. The pink band shows the uncertainty in the slope assuming correlated error in ω_{osc}, such that its bounds are defined by linear fits to the data assuming maximum and minimum values for ω_{osc} as defined by the error bars.

34.6.7 Higgs-like behaviour in short-time phase II dynamics

When quenching into phase II, we observe highly damped oscillations in $|\Delta_{\mathrm{BCS}}|$, reminiscent of the Higgs oscillations predicted to arise in this regime of the BCS model. Here, we analyse traces from Fig. **??d**, in which we engineer a variable phase spread $\varphi(\omega_k) \in [0, \varphi_0]$ before quenching into phase II, to study this potential connection.

In the BCS model, Higgs oscillations can be characterised by their frequency, which should scale with the long-time BCS order parameter Δ_∞ as $\omega_{\mathrm{osc}} = 2\Delta_\infty$ [Yuzbashyan *et al.*(2015)]. We confirm this scaling in theory by measuring the oscillation frequency from $t = 0$ μs to $t = 5$ μs in idealised numerical simulations ignoring dissipation and motional effects (black dashed line in Extended Data Fig. 34.14**a**). For different values of the phase spread extent φ_0, the system reaches its steady state at a different long-time BCS gap Δ_∞. By parametrically plotting the oscillation frequency vs. $2\Delta_\infty$ as a function of φ_0 in panel **c**, we observe the expected scaling.

As discussed in the main text, oscillations in $|\Delta_{\mathrm{BCS}}|$ are consistently smaller and decay more quickly in experiment than in theory. Nonetheless, we obtain a crude estimate of the experimental oscillation frequency by measuring a half period from the first trough and peak

of $|\Delta_{\mathrm{BCS}}(t)|$, as shown in panel **a**. In panel **b**, we compare the frequency in experimental data to that of ideal simulations for different φ_0 and show that the frequencies agree within error bars. This suggests that the transient dynamics observed in $|\Delta_{\mathrm{BCS}}|$ are related to the Higgs oscillations present in theory.

Although the experimental oscillation frequency agrees with simulations, the steady-state order parameter Δ_∞ is much smaller, as can be seen in Extended Data Fig. 34.14**a**. As a result, the measured frequencies scale linearly with Δ_∞ but with a different prefactor. In panel **c**, we fit a linear relation of $\omega_{\mathrm{osc}} = (1.7^{+0.7}_{-0.4}) \times 2\Delta_\infty$ to the data, where the slope uncertainty bounds are calculated assuming errors in ω_{osc} are perfectly correlated. Most of the reduction in Δ_∞ can be captured in theory by considering dissipation and motional effects (solid black trace). We see an additional small difference in $|\Delta_{\mathrm{BCS}}|$ between full numerical simulations and experimental data, which we attribute to drifts in experimental alignments and calibration factors over time. This difference is not apparent in Fig. **??d** because we plot $|\Delta_{\mathrm{BCS}}|$ in normalised units.

34.7 Dynamical phase diagram

In this section, we perform detailed analysis of the dynamical phase diagram shown in Fig. 1**c** in the main text. We start from analytic calculation in the case of homogeneous couplings, and then generalize to the case of inhomogeneous couplings. Finally we discuss the application of our findings to experimental conditions.

34.7.1 Homogeneous model

(??? I don't understand this at all right now)

First we discuss the dynamical phases for the BCS Hamiltonian with homogeneous couplings,

$$\hat{H} = \hbar\chi \hat{S}^+ \hat{S}^- + \sum_k \varepsilon_k \hat{S}^z_k. \tag{34.13}$$

We will set $\hbar = 1$. As shown in Ref. [Yuzbashyan *et al.*(2015), Lewis-Swan *et al.*(2021)], the dynamical phases can be determined using a mean-field Lax vector analysis. The Lax vector is defined as $\vec{L}(u) = L^x(u)\hat{x} + L^y(u)\hat{y} + L^z(u)\hat{z}$ with components,

$$L^x(u) = \sum_k \frac{S^x_k(0)}{u - \varepsilon_k/2}, \quad L^y(u) = \sum_k \frac{S^y_k(0)}{u - \varepsilon_k/2}, \quad L^z(u) = -\frac{1}{\chi} - \sum_i \frac{S^z_k(0)}{u - \varepsilon_k/2}, \tag{34.14}$$

where $S^{x,y,z}_k(0)$ are the expectation value of operators $\hat{S}^{x,y,z}_k$ in the initial state.

Here we consider the initial state as $S^x_k(0) = 1/2$, $S^y_k(0) = S^z_k(0) = 0$, and ε_k is chosen from a uniform distribution in the frequency range $[-\delta_{\mathrm{s}}/2 - E_{\mathrm{W}}/2, -\delta_{\mathrm{s}}/2 + E_{\mathrm{W}}/2]$ and $[\delta_{\mathrm{s}}/2 - E_{\mathrm{W}}/2, \delta_{\mathrm{s}}/2 + E_{\mathrm{W}}/2]$ (why this is the range???).

In this case, the mean-field Lax vector takes the following form: (??? there is an idea of averaging here??? not clear how MF leads to this expression.... what is N?)

$$\begin{aligned}
\chi L^x(u) &\approx \frac{\chi N}{2}\left[\frac{1}{2E_{\mathrm{W}}}\int_{-\delta_{\mathrm{s}}/2-E_{\mathrm{W}}/2}^{-\delta_{\mathrm{s}}/2+E_{\mathrm{W}}/2}\frac{dx}{u - x/2} + \frac{1}{2E_{\mathrm{W}}}\int_{\delta_{\mathrm{s}}/2-E_{\mathrm{W}}/2}^{\delta_{\mathrm{s}}/2+E_{\mathrm{W}}/2}\frac{dx}{u - x/2}\right] \\
&= \frac{\chi N}{2E_{\mathrm{W}}}\left[\ln\left(u + \frac{\delta_{\mathrm{s}}}{4} + \frac{E_{\mathrm{W}}}{4}\right) - \ln\left(u + \frac{\delta_{\mathrm{s}}}{4} - \frac{E_{\mathrm{W}}}{4}\right) + \ln\left(u - \frac{\delta_{\mathrm{s}}}{4} + \frac{E_{\mathrm{W}}}{4}\right) - \right. \\
&\qquad \left. - \ln\left(u - \frac{\delta_{\mathrm{s}}}{4} - \frac{E_{\mathrm{W}}}{4}\right)\right], \\
\chi L^y(u) &= 0, \\
\chi L^z(u) &= -1.
\end{aligned} \tag{34.15}$$

Note that $\ln z$ in the complex plane is a multivalued function. Here we take the principal value $\ln z = \ln|z| + i\mathrm{Arg}(z)$, where $\mathrm{Arg}(z)$ is the argument of z restricted in the interval $(-\pi, \pi]$. Directly combining the logarithm functions might lead to moving out of the principal branch.

One can define the dynamical phases based on the number of complex roots of equation $\vec{L}(u)\cdot\vec{L}(u) = 0$ (read Yuzbashyan): Phase I has zero complex roots, phase II has a pair of complex roots, phase III has two pairs of complex roots. Whether the complex roots have non-zero or vanishing real parts could be used for further separation of the phases. In our case, the equation $\vec{L}(u)\cdot\vec{L}(u) = 0$ takes the following form,

$$\frac{\chi N}{2E_{\mathrm{W}}}\left[\ln\left(u+\frac{\delta_{\mathrm{s}}}{4}+\frac{E_{\mathrm{W}}}{4}\right)-\ln\left(u+\frac{\delta_{\mathrm{s}}}{4}-\frac{E_{\mathrm{W}}}{4}\right)+\ln\left(u-\frac{\delta_{\mathrm{s}}}{4}+\frac{E_{\mathrm{W}}}{4}\right)-\ln\left(u-\frac{\delta_{\mathrm{s}}}{4}-\frac{E_{\mathrm{W}}}{4}\right)\right]=\pm i. \tag{34.16}$$

We find four dynamical phases based on analyzing the roots of Eq. (34.16):

- Phase I: No complex roots, which exist in the regime

$$\frac{\delta_{\mathrm{s}}}{E_{\mathrm{W}}}<1,\quad \frac{\chi N}{E_{\mathrm{W}}}<\frac{1}{\pi}\qquad\text{or}\qquad \frac{\delta_{\mathrm{s}}}{E_{\mathrm{W}}}>1,\quad \frac{\chi N}{E_{\mathrm{W}}}<\frac{2}{\pi}. \tag{34.17}$$

- Phase II: A pair of complex roots,

$$\frac{u}{E_{\mathrm{W}}}=\pm\frac{i}{4}\left[\cot\left(\frac{E_{\mathrm{W}}}{\chi N}\right)+\sqrt{\csc^2\left(\frac{E_{\mathrm{W}}}{\chi N}\right)-\frac{\delta_s^2}{E_{\mathrm{W}}^2}}\right], \tag{34.18}$$

  which exist in the regime

$$\frac{\delta_{\mathrm{s}}}{E_{\mathrm{W}}}<1,\quad \frac{\chi N}{E_{\mathrm{W}}}>\frac{1}{\pi}. \tag{34.19}$$

- Phase IIIa: Two pairs of complex roots with vanishing real parts,

$$\frac{u_1}{E_{\mathrm{W}}}=\pm\frac{i}{4}\left[\cot\left(\frac{E_{\mathrm{W}}}{\chi N}\right)+\sqrt{\csc^2\left(\frac{E_{\mathrm{W}}}{\chi N}\right)-\frac{\delta_s^2}{E_{\mathrm{W}}^2}}\right], \tag{34.20}$$

$$\frac{u_2}{E_{\mathrm{W}}}=\pm\frac{i}{4}\left[\cot\left(\frac{E_{\mathrm{W}}}{\chi N}\right)-\sqrt{\csc^2\left(\frac{E_{\mathrm{W}}}{\chi N}\right)-\frac{\delta_s^2}{E_{\mathrm{W}}^2}}\right], \tag{34.21}$$

  which exist in the regime

$$\frac{\delta_{\mathrm{s}}}{E_{\mathrm{W}}}>1,\quad \frac{\chi N}{E_{\mathrm{W}}}>\frac{2}{\pi},\quad \frac{\delta_{\mathrm{s}}}{E_{\mathrm{W}}}<\csc\left(\frac{E_{\mathrm{W}}}{\chi N}\right). \tag{34.22}$$

  In phase IIIa, the order parameter, Δ_{BCS} oscillates around a non-zero value (non-ZOPA) as pointed out in Ref. [Collado *et al.*(2023), Lewis-Swan *et al.*(2021)].

- Phase IIIb: Two pairs of complex roots with non-zero real parts,

$$\frac{u_1}{E_{\mathrm{W}}}=\frac{1}{4}\left[\sqrt{\delta_s'^2-\csc^2\left(\frac{1}{\chi' N}\right)}\pm i\cot\left(\frac{1}{\chi' N}\right)\right],\quad \frac{u_2}{E_{\mathrm{W}}}=\frac{1}{4}\left[-\sqrt{\delta_s'^2-\csc^2\left(\frac{1}{\chi' N}\right)}\pm i\cot\left(\frac{1}{\chi' N}\right)\right], \tag{34.23}$$

  which exist in the regime

$$\frac{\delta_{\mathrm{s}}}{E_{\mathrm{W}}}>1,\quad \frac{\chi N}{E_{\mathrm{W}}}>\frac{2}{\pi},\quad \frac{\delta_{\mathrm{s}}}{E_{\mathrm{W}}}>\csc\left(\frac{E_{\mathrm{W}}}{\chi N}\right). \tag{34.24}$$

  In phase IIIb, Δ_{BCS} oscillates with zero order parameter average (ZOPA) as explained in Ref. [Collado *et al.*(2023), Lewis-Swan *et al.*(2021)] (read these articles!).

The dynamical phases derived from the Lax analysis above are supported by numerical evidences, as shown in Fig. 34.15**a** and Fig. 34.15**b**. We numerically solve the dynamics of $\Delta_{\mathrm{BCS}} = \chi\langle\hat{S}^{-}\rangle$ under Eq. (34.13) based on mean field approximation, and then identify dynamical phases based on long-time average of $|\Delta_{\mathrm{BCS}}|$,

$$\mathrm{Avg}(|\Delta_{\mathrm{BCS}}|) = \lim_{T\to\infty}\frac{1}{T}\int_0^T |\Delta_{\mathrm{BCS}}(t)|dt, \tag{34.25}$$

and long-time oscillation amplitude of $|\Delta_{\mathrm{BCS}}|$. Since the oscillations in $|\Delta_{\mathrm{BCS}}|$ might deviates from a sinusoidal form, it is easier to use the standard deviation as a measure of the oscillation amplitude,

$$\mathrm{Std}(|\Delta_{\mathrm{BCS}}|) = \left[\lim_{T\to\infty}\frac{1}{T}\int_0^T \Big(|\Delta_{\mathrm{BCS}}(t)| - \mathrm{Avg}(|\Delta_{\mathrm{BCS}}|)\Big)^2 dt\right]^{1/2}, \tag{34.26}$$

although experimentally it's better to use the peak of Fourier spectrum to suppress the noise (see Fig. 3**d** in the main text). The dynamical phases can be characterized by

- Phase I: $\mathrm{Avg}(|\Delta_{\mathrm{BCS}}|) = 0$, $\mathrm{Std}(|\Delta_{\mathrm{BCS}}|) = 0$.
- Phase II: $\mathrm{Avg}(|\Delta_{\mathrm{BCS}}|) > 0$, $\mathrm{Std}(|\Delta_{\mathrm{BCS}}|) = 0$.
- Phase III: $\mathrm{Avg}(|\Delta_{\mathrm{BCS}}|) > 0$, $\mathrm{Std}(|\Delta_{\mathrm{BCS}}|) > 0$.

Since ε_k is chosen from a distribution with particle-hole symmetry (symmetric about 0), Δ_{BCS} becomes a real number in this case. One can further separate phase IIIa and phase IIIb by the behavior of Δ_{BCS} shown in Fig. 34.15**e** and Fig. 34.15**f**.

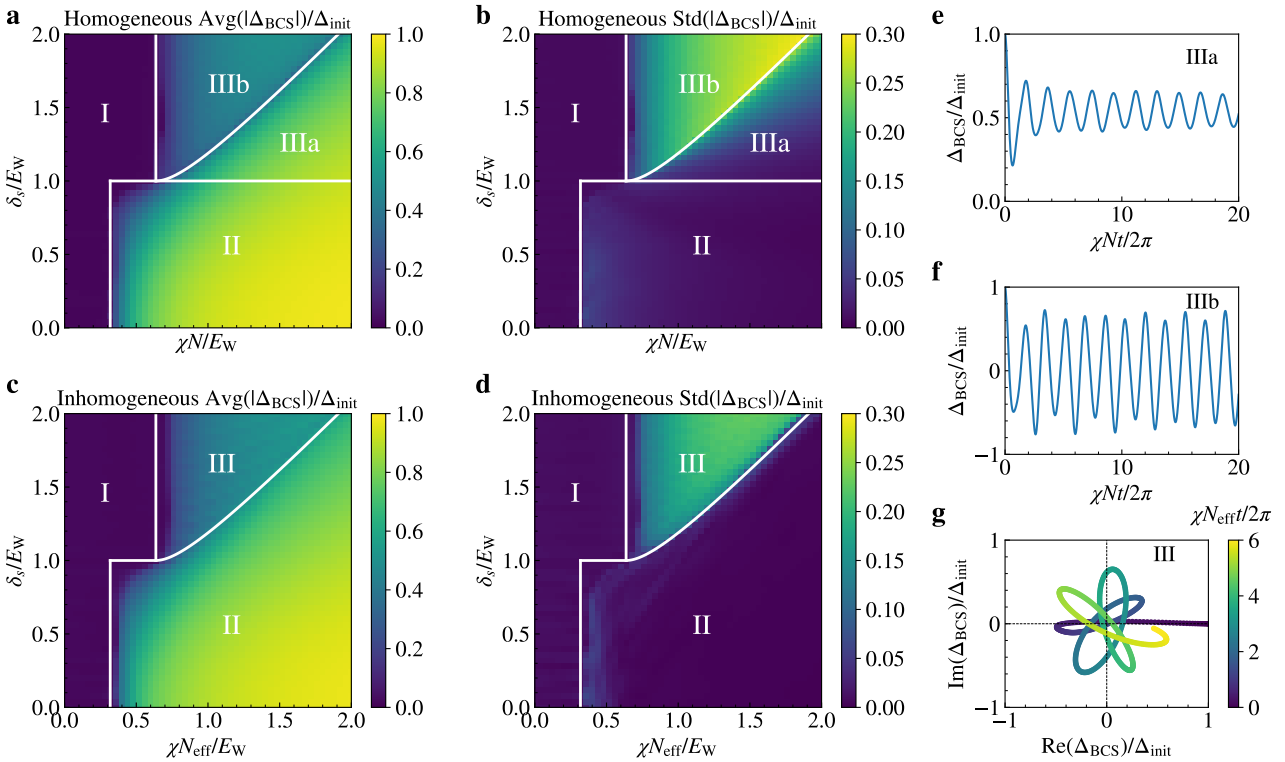


Figure 34.15: **Dynamical phase diagrams.** **a** and **b**, Dynamical phase diagram of the homogeneous model normalized by $\Delta_{\text{init}}/\chi N = 1/2$, where Δ_{init} is the initial value of $|\Delta_{\text{BCS}}|$. The white lines are the dynamical critical points derived from the Lax analysis. **c** and **d**, Dynamical phase diagram of the inhomogeneous model normalized by $\Delta_{\text{init}}/\chi N_{\text{eff}} = \mathcal{J}_1(\Omega\tau)$. The white lines are the same as the homogeneous model. **e**, Time evolution of Δ_{BCS} at $\delta_{\text{s}}/E_{\text{W}} = 1.1$, $\chi N/E_{\text{W}} = 1.0$ under the homogeneous model (phase IIIa). **f**, Time evolution of Δ_{BCS} at $\delta_{\text{s}}/E_{\text{W}} = 1.6$, $\chi N/E_{\text{W}} = 1.0$ under the homogeneous model (phase IIIb). **g**, Time evolution of Δ_{BCS} at $\delta_{\text{s}}/E_{\text{W}} = 1.6$, $\chi N/E_{\text{W}} = 1.0$ under the inhomogeneous model (phase III).

34.7.2 Inhomogeneous model

Here we discuss the dynamical phases for the BCS Hamiltonian with inhomogeneous coupling,

$$\hat{H} = \hbar\chi \sum_{jk} \zeta_j \zeta_k \hat{S}_j^+ \hat{S}_k^- + \sum_k \varepsilon_k \hat{S}_k^z, \tag{34.27}$$

where ζ_k is generated by random sampling of $\cos(x)$, with x chosen from a uniform distribution in the interval $[0, 2\pi)$. Similar to the homogeneous model, $\varepsilon_k/\hbar$ is still chosen from a uniform distribution in the frequency range $[-\delta_{\text{s}}/2 - E_{\text{W}}/2, -\delta_{\text{s}}/2 + E_{\text{W}}/2]$ and $[\delta_{\text{s}}/2 - E_{\text{W}}/2, \delta_{\text{s}}/2 + E_{\text{W}}/2]$. In this case, we explore the dynamical phases numerically since the Lax analysis is not applicable. As shown in Fig. 34.17**c** and Fig. 34.17**d**, one can obtain similar dynamical phases as the homogeneous model: Phase I remains the same, Phase IIIa merges into Phase II, and Phase IIIb becomes the new Phase III. The phase boundary can be roughly captured by the analytical solution of the homogeneous model. Note that χN_{eff} is the averaged interaction strength in the inhomogeneous case, where $N_{\text{eff}} = N/2$. The superconducting order parameter is defined as $\Delta_{\text{BCS}} = \chi \sum_k \zeta_k \langle \hat{S}_k^- \rangle$. The initial condition is chosen as the maximum $|\Delta_{\text{BCS}}|$ one can achieved by an external drive along the cavity axis, $\hat{H}_{\text{drive}} = \Omega \sum_k \zeta_k \hat{S}_k^y$. Assuming the initial state can be prepared by applying $\hat{H}_{\text{drive}}$ for a time τ, we have

$$\frac{\Delta_{\text{init}}}{\chi N_{\text{eff}}} \approx \frac{1}{2\pi} \int_0^{2\pi} dx \cos(x) \sin(\Omega\tau \cos(x)) = \mathcal{J}_1(\Omega\tau), \tag{34.28}$$

where $\mathcal{J}_n$ is the Bessel function of the first-kind, and the maximum of $\mathcal{J}_1(\Omega\tau)$ can be achieved at $\Omega\tau = 0.586\pi$. It is worth to mention that $\Delta_{\rm BCS}$ is a real number initially, but it becomes a complex number during the time evolution, as shown in Fig. 34.17**g**.

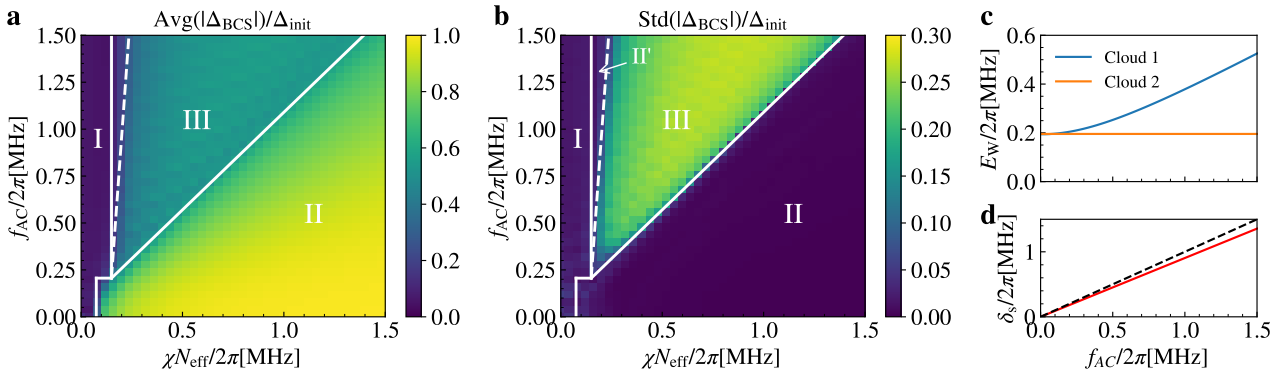


Figure 34.16: **Experimental control of dynamical phases.** **a** and **b**, Dynamical phase diagram for the experiment with two atomic ensembles, in terms of averaged spin-exchange interaction strength $\chi N_{\rm eff}$ and peak AC Stark shift $f_{\rm AC}$. The white lines show the predicted dynamical phase boundaries to guide the eye. The white dashed line marks a small region of phase II' due to the imbalance of $E_{\rm W}$ for the two atomic ensembles. **c**, $E_{\rm W}$ as a function of peak AC Stark shift $f_{\rm AC}$, with AC Stark shift applying to atomic cloud 1. **d**, $\delta_{\rm s}$ as a function of peak AC Stark shift $f_{\rm AC}$ (red line). The dashed line marks the place where $\delta_{\rm s} = f_{\rm AC}$.

34.7.3 Experimental control of dynamical phases

Here we elaborate on the experimental implementation of the Hamiltonian Eq. (34.27). As discussed in the previous section, we would like to approximately engineer single-particle energies $\varepsilon_k/\hbar$ sampled from a uniform distribution in the frequency range $[-\delta_{\rm s}/2 - E_{\rm W}/2, -\delta_{\rm s}/2 + E_{\rm W}/2]$ and $[\delta_{\rm s}/2 - E_{\rm W}/2, \delta_{\rm s}/2 + E_{\rm W}/2]$. The two different experimental schemes used in the main text to explore the energy distribution are summarized in the following table:

	Description	Approx. $\varepsilon_k/\hbar$
Scheme I (Fig. 2, main text)	1) Single atomic cloud 2) AC Stark shift	$[-\tilde{E}_{\rm W}/2, \tilde{E}_{\rm W}/2]$
Scheme II (Fig. 3, 4, main text)	1) Two atomic clouds 2) AC Stark shift to cloud 1	Cloud 1: $[-\delta_{\rm s}/2 - E_{\rm W}/2, -\delta_{\rm s}/2 + E_{\rm W}/2]$ Cloud 2: $[+\delta_{\rm s}/2 - E_{\rm W}/2, +\delta_{\rm s}/2 + E_{\rm W}/2]$

The first scheme is used to probe the phase I to phase II transition. We use a single atomic ensemble and apply an AC Stark shift beam with a gradient to approximately engineer $\varepsilon_k/\hbar$ from a uniform distribution $[-\tilde{E}_{\rm W}/2, \tilde{E}_{\rm W}/2]$, as discussed in the Methods. As shown in Fig. 2**a** in the main text, the distribution of atomic frequencies is not exactly uniform, so we calculate the variance of the frequency distribution experimentally. Theoretically we assign a spread $\tilde{E}_{\rm W}$ such that the uniform distibution over $[-\tilde{E}_{\rm W}/2, \tilde{E}_{\rm W}/2]$ matches the measured experimental variance. We use this scheme to probe the dynamical phase diagram at $\delta_{\rm s} = 0$ (see Fig. 1**c** in the main text).

It is worth mentioning that the uniform distribution $[-\tilde{E}_{\rm W}/2, \tilde{E}_{\rm W}/2]$ can be interpreted in two different ways: 1) $\delta_{\rm s} = 0$ and $E_{\rm W} = \tilde{E}_{\rm W}$; 2) $\delta_{\rm s} = E_{\rm W} = \tilde{E}_{\rm W}/2$. Here we prefer the first interpretation $\delta_{\rm s} = 0$ because in this scheme we only have a single control parameter

(the strength of AC Stark shift beam). Additionally, the line $\delta_s = E_W$ in the dynamical phase diagram has an implication that a small perturbation of δ_s can generate a gap in atomic frequency, which is prohibited under this mapping between experimental controls and the model parameters.

In the second scheme that probes transitions into phase III, we use two atomic ensembles and apply an AC Stark shift beam (peak AC Stark shift f_{AC}) to the first ensemble to generate a frequency splitting δ_s between the two ensembles. In contrast to the first scheme, as discussed in the Methods, here we instead use the differential lattice light shifts to engineer a frequency spread E_W for each ensemble. As shown in Fig. 3**a** in the main text, in this case we define δ_s as the mean frequency difference between the two ensembles, and E_W as the width of a uniform distribution generating the same variance.

It is worth mentioning that the Gaussian profile of the AC Stark shift beam leads to an increase in E_W for the first atomic ensemble, as well as a reduction of the expected splitting of the two ensembles $\delta_s < f_{AC}$, as shown in Fig. 34.16**c** and **d**. Using experimental parameters, we get the dynamical phase diagram as depicted in Fig. 34.16**a** and **b**. The imbalance of E_W for the two atomic ensembles can lead to a small region of phase II' marked by the white dashed line. This occurs because the spin-exchange interaction is able to lock the ensemble with smaller E_W, while the ensemble with larger E_W remains unlocked, which leads to $|\Delta_{BCS}|$ approaching a small but nonzero constant value. In the experiment, due to other dissipative processes and reduced signal-to-noise ratio for small χN, we do not observe a difference between phase I and phase II'. This is the cause of a small discrepancy between theory and experiment in Fig. 4**b** in the main text in identifying the position of the phase transition.

34.8 Short-time signatures of dynamical phases

In this section, we discuss the properties of the dynamical phases using short-time observables, since dissipative processes and noise in the experiment lead to difficulties in measuring long-time observables. In the following, we show that phase I can be characterized by the fast decay of $|\Delta_{BCS}|$, phase II can be characterized by Higgs oscillations. We further show that the phase II to phase III transition can be captured by the dip in the short-time oscillation frequency of $|\Delta_{BCS}|$. Finally, we provide an explanation of the frequency dip using an analytical solution of the two-spin BCS model.

34.8.1 Phase I: fast decay

In phase I, the single-particle energy term $\sum_k \varepsilon_k \hat{S}_k^z$ dominates over the spin-exchange interaction. To leading order, one can calculate $|\Delta_{BCS}|$ in the homogeneous model by dropping the interaction term, which gives

$$\begin{aligned}\frac{|\Delta_{BCS}|}{\chi N} &\approx \frac{1}{2N}\left|\sum_k e^{-i\varepsilon_k t/\hbar}\right| = \frac{1}{2}\left|\frac{1}{2E_W}\int_{-\delta_s/2-E_W/2}^{-\delta_s/2+E_W/2} e^{-ixt}dx + \frac{1}{2E_W}\int_{\delta_s/2-E_W/2}^{\delta_s/2+E_W/2} e^{-ixt}dx\right| \\ &= \frac{1}{2}\left|\cos\left(\frac{\delta_s}{2}\right)\right| \cdot \left|\frac{\sin(E_W t/2)}{E_W t/2}\right|.\end{aligned} \tag{34.29}$$

The decay profile of $|\Delta_{BCS}|$ is set by a sinc function with a $1/e$ coherence time t satisfying $E_W t/2\pi \approx 0.7$. For the inhomogeneous model a similar fast decay time scale of the order of $E_W t/2\pi \sim 1$ can be derived. As shown in Fig. 2**b** in the main text, we observe fast decay of $|\Delta_{BCS}|$ within 1 μs in phase I. The decay time scale for the other dynamical phases can be more than 10 times longer.

34.8.2 Phase II: Higgs oscillation

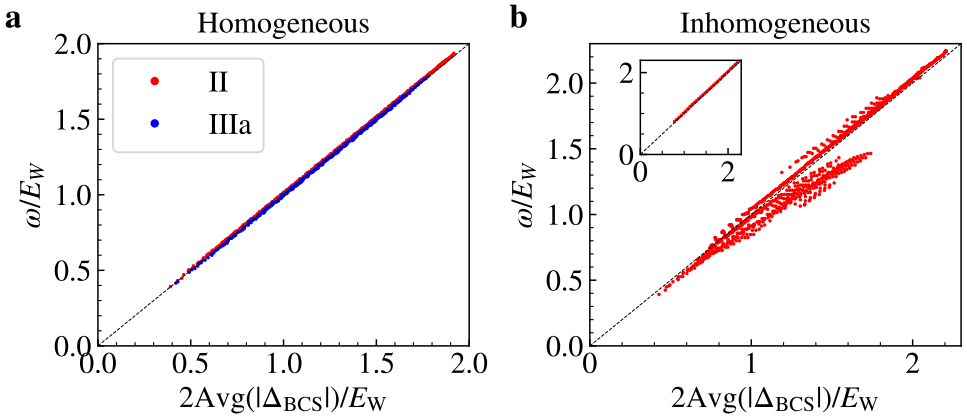


Figure 34.17: **Relation between oscillation frequency and averaged order parameter in Higgs oscillations. a**, Homogeneous model where each point is a choice of $(\chi N, \delta_s)$ in phase II (red) and phase IIIa (blue). The dashed line represents $\omega = 2\mathrm{Avg}(|\Delta_{\mathrm{BCS}}|)$. **b**, Inhomogeneous model where each point is a choice of $(\chi N_{\mathrm{eff}}, \delta_s)$ in phase II. The inset shows the points with $\delta_s = 0$.

Higgs oscillation, generated by collective excitation of the Higgs mode in BCS superconductor, is characterized by the oscillation of $|\Delta_{\mathrm{BCS}}|$ at frequency $\omega = 2\mathrm{Avg}(|\Delta_{\mathrm{BCS}}|)$ [Yuzbashyan *et al.*(2015)]. For the homogeneous model (see Fig. 34.17**a**), we numerically confirmed this relation for all the points in phase II and phase IIIa. For the inhomogeneous model (see Fig. 34.17**b**), this relation is approximately satisfied in phase II. In experiment, we observe hints of Higgs oscillation (see Fig. 2 in the main text), which can be ideally described by the inhomogeneous model with $\delta_s = 0$ (see the inset in Fig. 34.17**b**).

34.8.3 Transition to phase III: frequency dip

In the main text, we discuss a way to understand the phase II to phase III transition by visualising the two atomic ensembles as two large spins. For the inhomogeneous model, phase II exists in the small δ_s regime, where the two spins lock to each other and form a single large spin through spin-exchange interactions. In this case the many-body gap protection leads to the damped oscillations observed in phase II. Increasing δ_s in phase II leads to the reduction of the many-body gap, and hence to a decrease of the corresponding oscillation frequency. Phase III exists in the large δ_s regime, where the spin locking occurs separately in each ensemble, and the two large spin are instead precessing around each other, with a rate set by the splitting δ_s and the spin-exchange interaction. Increasing δ_s in phase III leads to a speed up of the oscillation frequency. Therefore one expects the existence of a frequency dip separating between phase II and phase III. Indeed as shown in Fig. 34.18**c** and **d**, we find good agreement between the frequency dip and the corresponding dynamical critical point. For small δ_s, the oscillation frequency approaches the Higgs oscillation frequency discussed in the previous subsection. For large δ_s, the oscillation frequency approaches δ_s. The reduction of oscillation frequency compared to δ_s indicates many-body effects in phase III. It's worth to mention that in contrast to the inhomogeneous model, the frequency dip indicates the phase IIIa to phase IIIb transition for the homogeneous model.

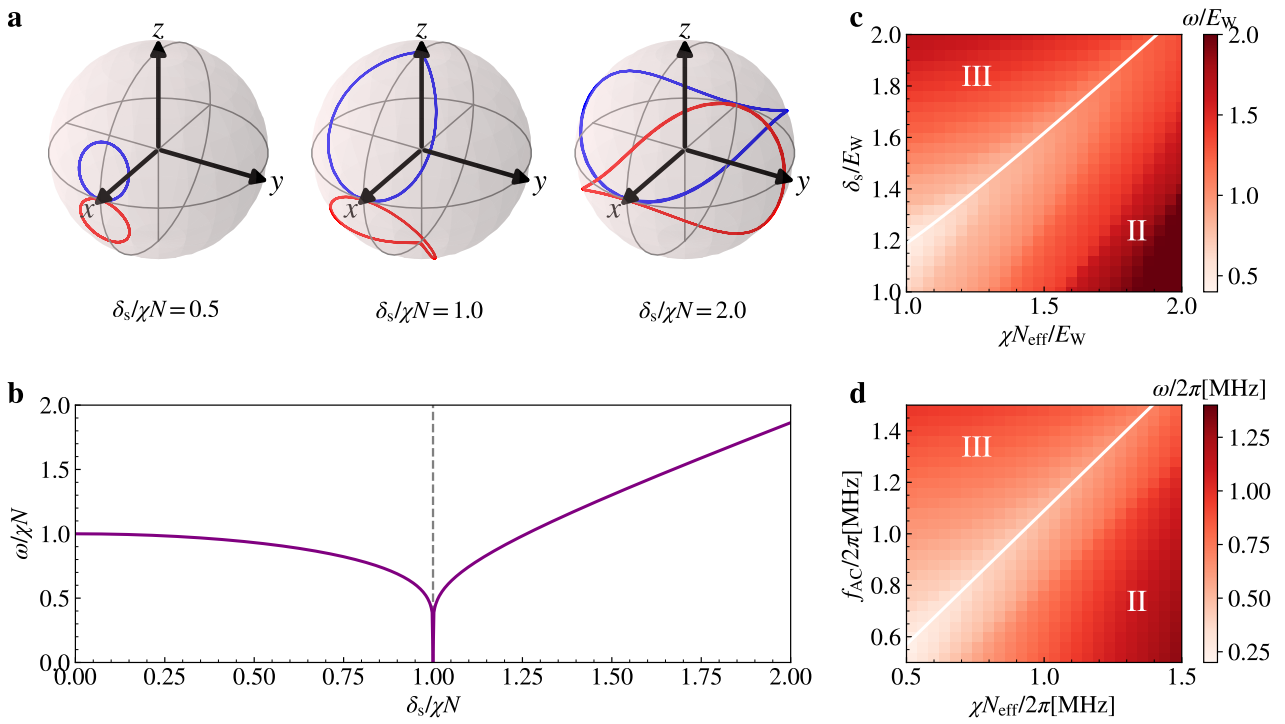


Figure 34.18: **Frequency dip as a signature of the phase II to phase III transition.** **a**, Mean field trajectories of the two large spin model evolving under Eq. (34.30). From left to right, Bloch spheres display trajectories with $\delta_s/(\chi N) = 0.5, 1$, and 2 respectively. **b**, Oscillation frequency of $|\Delta_{BCS}|$ in the two-spin BCS model Eq. (34.30) as a function of $\delta_s/\chi N$. The frequency dip at $\delta_s/\chi N = 1$ marks the dynamical phase transition point. **c**, Short-time frequency ω of the dynamics under inhomogeneous atom-light coupling (see Eq. (3) in the Methods). The white line marks the phase II to phase III transition, the same boundary as shown in Extended Data Fig. 2 from the Methods. **d**, Short-time frequency ω of the dynamics using experimental control parameters. The white line marks the phase II to phase III transition and represents the same boundary as in Fig. 34.16. The frequency dips match the dynamical critical points for both cases.

34.8.4 Frequency dip in the two-spin BCS model

Here we use the analytical mean field solution of the BCS Hamiltonian with two large spins ($S = N/4$ for each spin) to understand the frequency dip discussed above. In this case, the Hamiltonian simplifies to

$$\hat{H}/\hbar = \chi \hat{S}^+ \hat{S}^- + \frac{\delta_s}{2}\hat{S}_1^z - \frac{\delta_s}{2}\hat{S}_2^z, \tag{34.30}$$

where $\hat{S}^\pm = \hat{S}_1^\pm + \hat{S}_2^\pm$. The mean field equations of motion for the Hamiltonian above can then be written as

$$\begin{aligned} &\frac{d}{dt}S_1^x = 2\chi S^y S_1^z - \frac{\delta_s}{2}S_1^y, \quad \frac{d}{dt}S_1^y = -2\chi S^x S_1^z + \frac{\delta_s}{2}S_1^x, \quad \frac{d}{dt}S_1^z = -2\chi(S_2^y S_1^x - S_2^x S_1^y), \\ &\frac{d}{dt}S_2^x = 2\chi S^y S_2^z + \frac{\delta_s}{2}S_2^y, \quad \frac{d}{dt}S_2^y = -2\chi S^x S_2^z - \frac{\delta_s}{2}S_2^x, \quad \frac{d}{dt}S_2^z = -2\chi(S_1^y S_2^x - S_1^x S_2^y). \end{aligned} \tag{34.31}$$

The spin components without the hat represent the expectation value of the corresponding spin operators.

In the following, we assume an initial state satisfying $S_1^x = S_2^x = N/4$, $S_1^y = S_2^y = S_1^z = S_2^z = 0$. The conserved quantities of the two-spin BCS model are the total magnetisation

$$S^z = S_1^z + S_2^z = 0, \tag{34.32}$$

the total energy

$$E/\hbar = \chi S^+S^- + \frac{\delta_s}{2}S_1^z - \frac{\delta_s}{2}S_2^z = \chi\left(\frac{N}{2}\right)^2, \tag{34.33}$$

as well as the spin length of each of the large spins, $(S_1^x)^2 + (S_1^y)^2 + (S_1^z)^2 = (N/4)^2$, $(S_2^x)^2 + (S_2^y)^2 + (S_2^z)^2 = (N/4)^2$. Using these conserved quantities, one can derive from the mean field equations in Eq. (34.31) an equation of motion for the BCS order parameter, $\Delta_{\rm BCS} = \chi S^-$. To simplify the notation, we define $\Delta \equiv |\Delta_{\rm BCS}|/\chi N$, i.e. $\Delta^2 = S^+S^-/N^2$. From Eq. (34.32) and Eq. (34.33), we obtain

$$\frac{d}{dt}\Delta^2 = -\frac{\delta_s}{\chi N^2}\frac{d}{dt}S_1^z = \frac{2\delta_s}{N^2}(S_2^yS_1^x - S_2^xS_1^y), \tag{34.34}$$

which leads to

$$\begin{aligned}\frac{d^2}{dt^2}\Delta^2 &= \frac{2\delta_s}{N^2}\left(S_1^x\frac{d}{dt}S_2^y + S_2^y\frac{d}{dt}S_1^x - S_1^y\frac{d}{dt}S_2^x - S_2^x\frac{d}{dt}S_1^y\right)\\ &= 4\delta_s\chi\Delta^2S_1^z - \frac{2\delta_s^2}{N^2}(S_1^xS_2^x + S_1^yS_2^y).\end{aligned} \tag{34.35}$$

From the above conserved quantities, we can create the equivalent expressions $\delta_s S_1^z = -\chi N^2(\Delta^2 - 1/4)$, $2(S_1^xS_2^x + S_1^yS_2^y) = N^2\Delta^2 - 2\times(N/4)^2 + 2(S_1^z)^2$. Plugging these into the equation of motion gives

$$\frac{d^2}{dt^2}\Delta^2 = -6(\chi N)^2(\Delta^2)^2 + \left(2(\chi N)^2 - \delta_s^2\right)\Delta^2 + \frac{\delta_s^2 - (\chi N)^2}{8}. \tag{34.36}$$

The equation above can be further simplified to

$$\frac{1}{2}\left(\frac{d}{dt}\Delta\right)^2 + V(\Delta) = 0, \tag{34.37}$$

where

$$V(\Delta) = \frac{1}{2}(\chi N)^2\left(\Delta^2 - \frac{1}{4}\right)\left(\Delta^2 - \frac{1-(\delta_s/\chi N)^2}{4}\right), \tag{34.38}$$

with an initial condition $\Delta = 1/2$. Eq. (34.37) can be understood as a classical particle with position Δ oscillating in the potential $V(\Delta)$. For $\delta_s < \chi N$, we find Δ oscillating between $\Delta_{\max} = 1/2$ and $\Delta_{\min} = \sqrt{1-(\delta_s/\chi N)^2}/2$. This is equivalent to phase II in the cases of many spins with inhomogeneous atom-light couplings, because all the oscillations damp in the large χN limit. For $\delta_s > \chi N$, we find Δ oscillating between $\Delta_{\max} = 1/2$ and $\Delta_{\min} = 0$, since the definition of Δ requires $\Delta \geq 0$. This is equivalent to phase III in the cases of many spins because the phase connects to single-particle oscillations in the large δ_s limit. Therefore, a dynamical phase transition occurs at $\delta_s/\chi N = 1$, which is equivalent to the phase II to phase III transition in the many-spin system.

The analytical solution of Eq. (34.37) can be written in terms of Jacobian elliptic funtions dn and cn:

$$\Delta(t) = \begin{cases} \frac{1}{2}\mathrm{dn}\left(\frac{1}{2}\chi N t\middle|(\delta_s/\chi N)^2\right) & \text{if } \delta_s < \chi N \\ \\ \frac{1}{2}\left|\mathrm{cn}\left(\frac{1}{2}\delta_s t\middle|(\chi N/\delta_s)^2\right)\right| & \text{if } \delta_s > \chi N \end{cases}. \tag{34.39}$$

The frequency of $\Delta(t)$ can be written in terms of the complete elliptic integral of the first kind $K(k^2)$:

$$\frac{\omega}{\chi N} = \begin{cases} \dfrac{\pi}{2K\Big((\delta_s/\chi N)^2\Big)} & \text{if } \delta_s < \chi N \\ \dfrac{\delta_s}{\chi N}\dfrac{\pi}{2K\Big((\chi N/\delta_s)^2\Big)} & \text{if } \delta_s > \chi N \end{cases}. \tag{34.40}$$

The mean-field trajectories on the Bloch sphere are shown in Fig. 34.18**a**, and the oscillation frequency Eq. (34.40) is shown in Fig. 34.18**b**. The dynamical phase transition can also be understood from the mean field trajectories. For $\delta_s < \chi N$, the two large spins lock to each other and oscillate near the x axis of the Bloch sphere. For $\delta_s > \chi N$, the two large spins are unlocked and precess around the whole Bloch sphere. Near the dynamical critical point, the mean field trajectories are close to the north pole or south pole of the Bloch sphere, which leads to a slow down of the oscillations because they approach stable fixed points of the Hamiltonian.

34.9 Axial Motion

In this section, we elaborate on how to take into account axial motion present in the experimental system. Similar discussions can be found in Ref. [Muniz *et al.*(2020)]. We start with the one-dimensional Hamiltonian of our cavity QED system with two internal atomic levels ($|\uparrow\rangle$ and $|\downarrow\rangle$), given by

$$\begin{aligned}\hat{H} = &\sum_{\sigma=\{\uparrow,\downarrow\}} \int dx\ \hat{\psi}^\dagger_\sigma(x)\left[\frac{\hat{p}^2}{2M} + V_0\sin^2(k_L x)\right]\hat{\psi}_\sigma(x) + \int dx\ \hat{\psi}^\dagger_\uparrow(x)\Big[\hbar\omega_0 + U_{ac}(x)\Big]\hat{\psi}_\uparrow(x) \\ &+ \hbar g_c \int dx\ \cos(k_c x)\left[\hat{\psi}^\dagger_\uparrow(x)\hat{\psi}_\downarrow(x)\hat{a} + \hat{a}^\dagger\hat{\psi}^\dagger_\downarrow(x)\hat{\psi}_\uparrow(x)\right] + \hbar\omega_c\hat{a}^\dagger\hat{a},\end{aligned} \tag{34.41}$$

where $k_L = 2\pi/\lambda_L$ is the wavenumber of the lattice beams ($\lambda_L = 813$nm), k_c is the wavenumber of the cavity mode ($\lambda_c = 689$nm), ω_0 is the atomic transition frequency between $|\uparrow\rangle$ and $|\downarrow\rangle$ states, $U_{ac}(x)$ is the AC Stark shift applied to the atoms (including the differential light shift from the lattice beams and the transverse AC Stark shift beam), and ω_c is the frequency of cavity resonance.

Since the atoms are trapped in an optical lattice with lattice depth on the order of $10^3 E_R$, we can approximate each lattice site as an harmonic trap with axial trapping frequency $\hbar\omega_T = \sqrt{4V_0E_R}$, where $E_R = \hbar^2k_L^2/2M$ is the lattice recoil energy. We also ignore tunnelling processes between lattice sites. In this case, one can expand the atomic field operator in terms of lattice site index j and harmonic oscillator levels n:

$$\hat{\psi}_\sigma(x) = \sum_{jn} \hat{c}_{jn,\sigma}\phi_n(x - ja_L). \tag{34.42}$$

Here, $a_L = \lambda_L/2$ is the lattice spacing, and ϕ_n is the harmonic oscillator wave function for mode n, given by

$$\phi_n(x) = \frac{1}{\sqrt{2^n n!}}\left(\frac{M\omega_T}{\pi\hbar}\right)^{1/4} \mathrm{e}^{-M\omega_T x^2/2\hbar} H_n\left(\sqrt{\frac{M\omega_T}{\hbar}}x\right) \tag{34.43}$$

where $H_n(x)$ are the Hermite polynomials. Plugging this expansion into the Hamiltonian and transforming to the rotating frame of the atoms, we obtain

$$\hat{H}/\hbar = \sum_{jn\sigma} n\omega_T\hat{c}^\dagger_{jn,\sigma}\hat{c}_{jn,\sigma} + \sum_{jn}\varepsilon_{jn}\hat{c}^\dagger_{jn,\uparrow}\hat{c}_{jn,\uparrow} + g_c\sum_{jnm}\zeta^{nm}_j(\hat{c}^\dagger_{jn,\uparrow}\hat{c}_{jm,\downarrow}\hat{a} + \hat{a}^\dagger\hat{c}^\dagger_{jm,\downarrow}\hat{c}_{jn,\uparrow}) + \delta_c\hat{a}^\dagger\hat{a} \tag{34.44}$$

where $\delta_c = \omega_c - \omega_a$. For simplicity, we assume $U_{ac}(x)$ is either small or slowly varying in space and thus does not change the trap geometry. This term gives rise to an inhomogeneous transition frequency $\varepsilon_{jn} = \int dx U_{ac}(x)[\phi_n(x - ja_L)]^2/\hbar$. We calculate ζ_j^{nm} in the following way:

$$\begin{aligned}\zeta_j^{nm} &= \int dx\ \cos(k_c x)\phi_n(x - ja_L)\phi_m(x - ja_L) = \int dx\ \cos(k_c x + k_c j a_L)\phi_n(x)\phi_m(x) \\ &= \cos(j\varphi)\int dx\ \cos(k_c x)\phi_n(x)\phi_m(x) - \sin(j\varphi)\int dx\ \sin(k_c x)\phi_n(x)\phi_m(x) \\ &= \cos(j\varphi)\,\mathrm{Re}\left[(i\eta)^s e^{-\eta^2/2}\sqrt{\frac{n_<!}{n_>!}}L_{n_<}^s(\eta^2)\right] - \sin(j\varphi)\,\mathrm{Im}\left[(i\eta)^s e^{-\eta^2/2}\sqrt{\frac{n_<!}{n_>!}}L_{n_<}^s(\eta^2)\right].\end{aligned} \tag{34.45}$$

where $\varphi = \pi k_L/k_c$, $s = |n - m|$, $n_< = \min(n, m)$, $n_> = \max(n, m)$, $L_n^\alpha(x)$ are the generalised Laguerre polynomials, and $\eta = k_c\sqrt{\hbar/2M\omega_T}$ is the Lamb-Dicke parameter. In our case $\omega_T/2\pi = 165$ kHz, implying that $\eta = 0.17$. This places us in the Lamb-Dicke regime where ζ_j^{nm} is negligible for $|n - m| > 1$. It can be convenient to rewrite the Hamiltonian in terms of operators $\hat{S}^j_{n\sigma,m\sigma'} = \hat{c}^\dagger_{jn,\sigma}\hat{c}_{jm,\sigma'}$, resulting in the following form:

$$\hat{H}/\hbar = \sum_{jn\sigma} n\omega_T \hat{S}^j_{n\sigma,n\sigma} + \sum_{jn}\varepsilon_{jn}\hat{S}^j_{n\uparrow,n\uparrow} + g_c\sum_{jnm}\zeta_j^{nm}(\hat{S}^j_{n\uparrow,m\downarrow}\hat{a} + \hat{a}^\dagger\hat{S}^j_{m\downarrow,n\uparrow}) + \delta_c\hat{a}^\dagger\hat{a}. \tag{34.46}$$

In addition to the Hamiltonian dynamics, we also consider dissipation processes such as cavity loss with a rate $\kappa/2\pi = 153$ kHz, as well as spontaneous emission with a rate $\gamma/2\pi = 7.5$ kHz. The full dynamics of this open system can be described by the following Lindblad master equation:

$$\frac{\mathrm{d}}{\mathrm{d}t}\hat{\rho} = -\frac{i}{\hbar}[\hat{H}, \hat{\rho}] + \left[\hat{L}_{\mathrm{cav}}\hat{\rho}\hat{L}^\dagger_{\mathrm{cav}} - \frac{1}{2}\{\hat{L}^\dagger_{\mathrm{cav}}\hat{L}_{\mathrm{cav}}, \hat{\rho}\}\right] + \sum_{jn}\left[\hat{L}_{j,n}\hat{\rho}\hat{L}^\dagger_{j,n} - \frac{1}{2}\{\hat{L}^\dagger_{j,n}\hat{L}_{j,n}, \hat{\rho}\}\right], \tag{34.47}$$

where the jump operator for cavity loss is given by $\hat{L}_{\mathrm{cav}} = \sqrt{\kappa}\hat{a}$, and the single-particle jump operators for spontaneous emission are given by $\hat{L}_{j,n} = \sqrt{\gamma}\hat{S}^j_{n\downarrow,n\uparrow}$. Here, we assume that spontaneous emission is in the Lamb-Dicke regime.

In the experiment, δ_c is the largest frequency scale ($\delta_c \gg g_c\sqrt{N}, \kappa$), so we can adiabatically eliminate the cavity photons [Reiter and Sørensen(2012)] and obtain the following effective atom-only master equation:

$$\frac{\mathrm{d}}{\mathrm{d}t}\hat{\rho} = -\frac{i}{\hbar}[\hat{H}_{\mathrm{eff}}, \hat{\rho}] + \left[\hat{L}_{\mathrm{col}}\hat{\rho}\hat{L}^\dagger_{\mathrm{col}} - \frac{1}{2}\{\hat{L}^\dagger_{\mathrm{col}}\hat{L}_{\mathrm{col}}, \hat{\rho}\}\right] + \sum_{jn}\left[\hat{L}_{j,n}\hat{\rho}\hat{L}^\dagger_{j,n} - \frac{1}{2}\{\hat{L}^\dagger_{j,n}\hat{L}_{j,n}, \hat{\rho}\}\right]. \tag{34.48}$$

Here, the effective Hamiltonian is given by

$$\hat{H}_{\mathrm{eff}}/\hbar = \sum_{jn\sigma} n\omega_T\hat{S}^j_{n\sigma,n\sigma} + \sum_{jn}\varepsilon_{jn}\hat{S}^j_{n\uparrow,n\uparrow} + \chi\sum_{jnm}\sum_{kpq}\zeta_j^{nm}\zeta_k^{pq}\hat{S}^j_{n\uparrow,m\downarrow}\hat{S}^k_{p\downarrow,q\uparrow}, \tag{34.49}$$

and effective collective jump operator generating superradiant decay takes the form

$$\hat{L}_{\mathrm{col}} = \sqrt{\Gamma}\sum_{jnm}\zeta_j^{nm}\hat{S}^j_{m\downarrow,n\uparrow}, \tag{34.50}$$

where $\chi = -g_c^2\delta_c/(\delta_c^2 + \kappa^2/4)$ and $\Gamma = g_c^2\kappa/(\delta_c^2 + \kappa^2/4)$. The equivalent superconducting order parameter takes the following form:

$$\Delta_{\mathrm{BCS}} = \chi\sum_{kpq}\zeta_k^{pq}\langle\hat{S}^k_{p\downarrow,q\uparrow}\rangle. \tag{34.51}$$

One can recover the inhomogeneous model discussed in the previous section by removing the axial harmonic oscillator level labels.

Similarly, the Hamiltonian for initial state preparation takes the form

$$\hat{H}_{\text{drive}}/\hbar = \sum_{jn\sigma} n\omega_T \hat{S}^j_{n\sigma,n\sigma} + \frac{1}{2}\sum_{jnm} \zeta_j^{nm}(\Omega \hat{S}^j_{n\uparrow,m\downarrow} + \Omega^* \hat{S}^j_{m\downarrow,n\uparrow}). \tag{34.52}$$

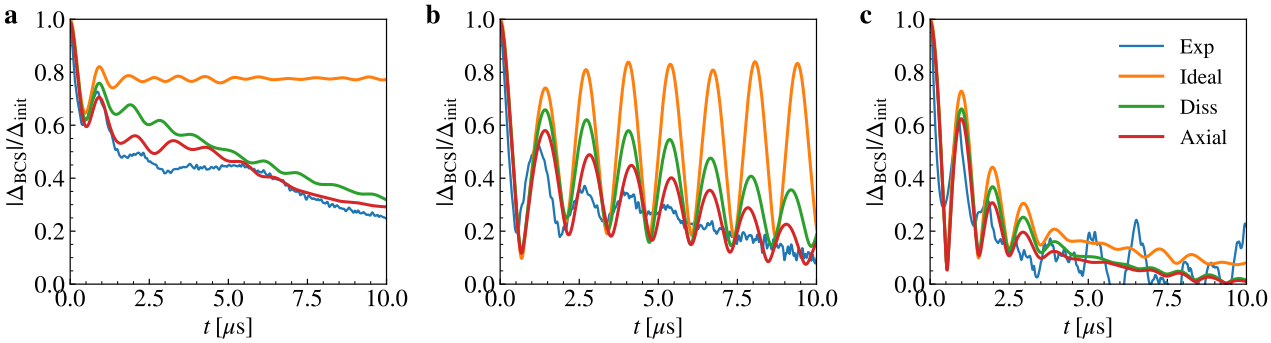


Figure 34.19: **Understanding experimental results with axial motion effects. a** Example phase II traces with $\chi N/2\pi = 1.29$MHz, $f_{\text{AC}}/2\pi = 1.1$MHz. **b** Example phase III traces with $\chi N/2\pi = 0.79$MHz, $f_{\text{AC}}/2\pi = 1.1$MHz. **c** Example phase I traces with $\chi N/2\pi = 0.15$MHz, $f_{\text{AC}}/2\pi = 1.1$MHz. The blue points are experimental data, the orange lines represent numerical simulations under ideal conditions (see Eq. (3) in the Methods), the green lines include dissipative processes on top of the ideal simulations, and the red lines consider both dissipative processes and axial motion effects.

In numerical simulations, we perform a mean-field approximation, which replaces the operators $\hat{S}^j_{p\sigma,q\sigma'}$ by their expectation values $\langle \hat{S}^j_{p\sigma,q\sigma'} \rangle$ in the Heisenberg equation of motion. We perform a random sampling of the axial harmonic oscillator mode n for each atom based on a thermal distribution of 15 μK, and we only include the modes n and $n \pm 1$ into our calculation due to the Lamb-Dicke parameter. The atom number in our simulations is set to 2000; to match χN to experimental values, we rescale χ accordingly. We also empirically take into account two additional dissipation processes to quantitatively capture the behavior of $|\Delta_{\text{BCS}}|$ at longer time scales. The first is a single-particle decoherence between electronic states, described by the jump operators $\hat{L}^{\text{el}}_{j,\sigma} = \sqrt{\gamma_{\text{el}}} \sum_n \hat{S}^j_{n\sigma,n\sigma}$ with $\gamma_{\text{el}}/2\pi < 1$kHz for Fig. 2 starting from $t = 0\mu$s, and by $\gamma_{\text{el}}/2\pi = 0.0036(f_{\text{AC}}/2\pi) + 4$kHz for Fig. 3 and Fig. 4 in the main text. The second is a single-particle decoherence between motional states, described by the jump operators $\hat{L}^{\text{mo}}_{j,n} = \sqrt{\gamma_{\text{mo}}} \sum_\sigma \hat{S}^j_{n\sigma,n\sigma}$ with $\gamma_{\text{mo}}/2\pi = 15$kHz.

Some example traces including axial motion effects are depicted in Fig. 34.19. Generally speaking, accounting for these effects allows us to more accurately predict features present in the experimentally measured evolution of $|\Delta_{\text{BCS}}|$, at the same time leaving the predicted dynamical phase boundaries unchanged. As shown in Fig. 34.19a, including axial motion effects in phase II traces allows us to capture the faster damping rate of the Higgs oscillations, as well as a slow oscillation in $|\Delta_{\text{BCS}}|$ at the axial trapping frequency. Likewise, as shown in Fig. 34.19b, including axial motion effects in phase III traces allows us to capture the faster damping rate of the oscillations in $|\Delta_{\text{BCS}}|$, although the observed damping rate is still faster than the rate predicted by theory. Finally, as shown in Fig. 34.19c, all the theory simulations of phase I dynamics are similar to the simulation under ideal conditions, indicating that axial motion does not play an significant role in this regime.

34.10 Questions about “Observing Dynamical Phases ..” by Young et al.

Why it is non-destructive?

(????)

Why the dynamical phase diagram is such?

(???? it looks very not smooth... is there an intuitive understanding of it???)

Bibliography

References

34.11 Bibliography from Old, Fundamental Artiles

Bibliography from Experiments on charge imbalance in superconductors by John Clarke

Abrahams, E., P.W. Anderson, P.A. Lee and T.V. Ramakrishnan, 1981, Phys. Rev. B24, 6783.
Abrikosov, A.A., and L.P. Gor'kov, 1960, Zh. Eksp. Teor. Fiz. 39, 1781 [Sov. Phys. JETP 12, 1243]
Anderson, P.W., 1959, J. Phys. Chem. Solids 11, 26.
Andreev, A.F., 1964, Zh. Eksp. Teor. Fiz. 46, 182 [Sov. Phys. JETP 19, 1228].
Aponte, J.M., and M. Tinkham, 1983, J. Low Temp. Phys. 51, 189.
Aronov, A.G., 1974, Zh. Eksp. Teor. Fiz. 67, 178 [Sov. Phys. JETP 40, 90].
Artemenko, N., and A.F. Volkov, 1976, Zh. Eksp. Teor. Fiz. 70, 1051 [Sov. Phys. JETP 43, 548].
Artemenko, N., and A.F. Volkov, 1977, Zh. Eksp. Teor. Fiz. 72, 1018 [Sov. Phys. JETP 45, 533].
Artemenko, N., A.F. Volkov and A.V. Zaitsev, 1978, J. Low Temp. Phys. 30, 487.
Bardeen, J., L.N. Cooper and J.R. Schrieffer, 1957, Phys. Rev. 108, 1175.
Battersby, S.J., and J.R. Waldram, 1984, Phys. F14, 109.
Beyer Nielsen, J., Y.A. Ono, C.J. Pethick and H. Smith, 1980, Solid State Commun. 33, 925.
Beyer Nielsen, J., C.J. Pethick, J. Rammer and H. Smith, 1982, J. Low Temp. Phys. 46, 565.
Blonder, G.E., and M. Tinkham, 1983, Phys. Rev. B27, 112.
Blonder, G.E., M. Tinkham and T.M. Klapwijk, 1982, Phys. Rev. B25, 4515.
Chambers, R.G., 1952, Proc. Roy. Soc. (London) 215, 481.
Chang, J.-J., 1977, Phys. Rev. Lett. 39, 1352.
Chang, J.-J., 1979, Phys. Rev. B19, 1420.
Chang, J.-J., and D.J. Scalapino, 1977, Phys. Rev. B15, 2651.
Chi, C.C., and J. Clarke, 1979, Phys. Rev. B19, 4495.
Chi, C.C., and J. Clarke, 1980, Phys. Rev. B21, 333.
Christian, J.W., J.P. Jan, W.P. Pearson and I.M. Templeton, 1958, Proc. Roy. Soc. (London) A245, 213.
Clarke, J., 1972, Phys. Rev. Lett. 28, 1363.
Clarke, J., 1976, in: Superconductor Applications: SQUIDs and Machines, eds. B.B. Schwartz and S. Foner (Plenum, New York) p. 67.
Clarke, J., 1981, in: Nonequilibrium Superconductivity, Phonons, and Kapitza Boundaries (Proc. NATO ASI), ed. K.E. Gray (Plenum, New York) ch. 5.
Clarke, J., and J.L. Paterson, 1974, J. Low Temp. Phys. 15, 491.
Clarke, J. and M. Tinkham, 1980, Phys. Rev. Lett. 44, 106.
Clarke, J., U. Eckern, A. Schmid, G. Schön and M. Tinkham, 1979a, Phys. Rev. B20, 3933.
Clarke, J., B.R. Fjordbge and P.E. Lindelof, 1979b, Phys. Rev. Lett. 43, 642.
Craven, R.A., G.A. Thomas and R.D. Parks, 1971, Phys. Rev. B4, 2185.
De Gennes, P.G., 1966, Superconductivity of Metals and Alloys (Benjamin, New York).
Dolan, G.J., and L.D. Jackel, 1977, Phys. Rev. Lett. 39, 1628.
Entin-Wohlman, O., and R. Orbach, 1979, Phys. Rev. B19, 4510.
Entin-Wohlman, O., and R. Orbach, 1981, Phys. Rev. B24, 1177.

Fickett, F.R., 1971, Cryogenics 11, 349.
Fjordbge, B.R., P.E. Lindelof and J. Clarke, 1981, J. Low Temp. Phys. 44, 535.
Gal'perin, Yu. M., V.L. Gurevich and V.I. Kozub, 19'74, Zh. Eksp. Teor. Fiz. 66, 1387 [Sov. Phys. JETP 39, 680].
Ginzburg, V.L., and L.D. Landau, 1950, Zh. Eksp. Teor. Fiz. 20, 1064.
Gordon, J.M., C.J. Lobb and M. Tinkham, 1983, Phys. Rev. B28, 4046.
Gray, K.E., 1981, in: Nonequilibrium Superconductivity, Phonons, and Kapitza Boundaries (Proc. NATO ASI) ed. K.E. Gray (Plenum, New York) ch. 5.
Gschneidner, K.A., 1964, Solid State Phys. 16, 275.
Harding, G.L., A.B. Pippard and J.R. Tomlinson, 1974, Proc. Roy. Soc. (London) A340, 1.
Heidel, D.F., and J.C. Garland, 1981, J. Low Temp. Phys. 44, 295.
Hsiang, T.Y., 1980, Phys. Rev. B21, 956.
Hsiang, T.Y., and J. Clarke, 1980, Phys. Rev. B21, 945.
Jillie, D.W., J.E. Lukens and Y.H. Kao, 1977, Phys. Rev. Lett. 38, 915.
Jillie, D.W., M.A.H. Nerenberg and J.A. Blackburn, 1980, Phys. Rev. 21B, 125.
Kadin, A.M., W.J. Skocpol and M. Tinkham, 1978, J. Low Temp. Phys. 33, 481.
Kadin, A.M., L.N. Smith and W.J. Skocpol, 1980, J. Low Temp. Phys. 33, 497.
Kaplan, S.B., 1979, J. Low Temp. Phys. 37, 343.
Kaplan, S.B., C.C. Chi, D.N. Langenberg, J.-J. Chang, S. Jafarey and D.J. Scalapino, 1976, Phys. Rev. B14, 4854.
Kaplan, S.B., J.R. Kirtley and D.N. Langenberg, 1977, Phys. Rev. Lett. 39, 291.
Kirtley, J.R., D.S. Kent, S.B. Kaplan and D.N. Langenberg, 1978, J. Physique Suppl. 39, C6-511.
Kittel, C., 1976, Introduction to Solid State Physics, 5th Ed. (Wiley, New York).
Klapwijk, T.M., and J.E. Mooij, 1976, Phys. Lett. 57A, 97.
Klapwijk, T.M., G.E. Blonder and M. Tinkham, 1982, Physica 109B, 1657.
Krhenbhl, Y., and R.J. Watts-Tobin, 1978, J. Physique 39, C6-677.
Krhenbhl, Y., and R.J. Watts-Tobin, 1979, J. Low Temp. Phys. 35, 569.
Lawrence, W.E., and A.B. Meador, 1978, Phys. Rev. B18, 1154.
Lemberger, T.R., 1981, Phys. Rev. B24, 4105.
Lemberger, T.R., and J. Clarke, 1981a, Phys. Rev. B23, 1088.
Lemberger, T.R., and J. Clarke, 1981b, Phys. Rev. B23, 1100.
Lindelof, P.E., and J. Bindslev Hansen, 1977, J. Low Temp. Phys. 29, 369.
Lindelof, P.E., and J. Bindslev Hansen, 1981, in: Nonequilibrium Superconductivity, Phonons, and Kapitza Boundaries (Proc. NATO ASI), ed. K.E. Gray (Plenum, New York) ch. 19.
Maki, K., 1969, in: Superconductivity, ed. R.D. Parks (Marcel Dekker, New York).
Mamin, H.J., J. Clarke and D.J. Van Harlingen, 1983, Phys. Rev. Lett. 51, 1480.
Mamin, H.J., J. Clarke and D.J. Van Harlingen, 1984, Phys. Rev. B29, 3881.
Markowitz, D., and L.P. Kadanoff, 1963, Phys. Rev. 131, 563.
Meservey, R., and B.B. Schwartz, 1969, in: Superconductivity, ed. R.D. Parks (Marcel Dekker, New York).
Meyer, J.D., 1973, Appl. Phys. 2, 303.
Meyer, J., and G. von Minnigerode, 1972, Phys. Lett. 38A, 529.
Moody, M.V., and J.L. Paterson, 1979, J. Low Temp. Phys. 34, 83.
Nyquist, H., 1928, Phys. Rev. 32, 110.
Octavio, M., M. Tinkham, G.E. Blonder and T.M. Klapwijk, 1983, Phys. Rev. B27, 6739.
Ovchinnikov, Yu.N., 1977, J. Low Temp. Phys. 28, 43.
Ovchinnikov, Yu.N., 1978, J. Low Temp. Phys. 31, 785.
Palmer, D.W., and J.E. Mercereau, 1977, Phys. Lett. 61A, 135.
Pethick, C.J., and H. Smith, 1979a, Ann. Phys. 119, 133.

Pethick, C.J., and H. Smith, 1979b, Phys. Rev. Lett. 43. 640.
Pethick, C.J., and H. Smith, 1981a, in: Nonequilibrium Superconductivity, Phonons, and Kapitza Boundaries (Proc. NATO ASI), ed. K.E. Gray (Plenum, New York) ch. 15.
Pethick, C.J., and H. Smith, 1981b, J. Phys. C13, 6313.
Pippard, A.B., 1965, The Dynamics of Conduction Electrons (Gordon and Breach, New York).
Pippard, A.B., 1981, in: Nonequilibrium Superconductivity, Phonons, and Kapitza Boundaries (Proc. NATO ASI), ed. K.E. Gray (Plenum, New York) ch. 12.
Pippard, A.B., J.G. Shepherd and D.A. Tindall, 1971, Proc. Roy. Soc. (London) A324, 17.
Rieger, T.J., D.J. Scalapino and J.E. Mercereau, 1971, Phys. Rev. Lett. 27, 1787.
Santhanam, P., and D.E. Prober, 1984, Phys. Rev. B29, 3733.
Schmid, A., and G. Schön, 1975, J. Low Temp. Phys. 20, 207.
Schmid, A., and G. Schön, 1979, Phys. Rev. Lett. 43, 793.
Schön, G., 1981a, in: Festkörperprobleme (Advances in Solid State Physics), Vol. 21, ed. J. Treusch (Vieweg, Braunschweig) p. 341.
Schön, G., 1981b, Physica 107B, 171.
Skocpol, W.J., 1981, in: Nonequilibrium Superconductivity, Phonons, and Kapitza Boundaries (Proc. NATO ASI), ed. K.E. Gray (Plenum, New York) ch. 18.
Skocpol, W.J., and L.D. Jackel, 1981, Physica 108B, 1021.
Skocpol, W.J., M.R. Beasley and M. Tinkham, 1974, J. Low Temp. Phys. 16, 145.
Stuivinga, M., J.E. Mooij and T.M. Klapwijk, 1981, Physica 108B, 1023.
Stuivinga, M., J.E. Mooij and T.M. Klapwijk, 1982, J. Low Temp. Phys. 46, 555.
Stuivinga, M., C.L.G. Ham, T.M. Klapwijk and J.E. Mooij, 1983a, J. Low Temp. Phys. 53, 633.
Stuivinga, M., T.M. Klapwijk, J.E. Mooij and A. Bezuijen, 1983b, J. Low Temp. Phys. 53, 673.
Tinkham, M., 1972, Phys. Rev. B6, 1747.
Tinkham, M., 1975, Introduction to Superconductivity (McGraw-Hill, New York).
Tinkham, M., 1979, Festkörperprobleme (Advances in Solid State Physics), Vol. 19, ed. J. Treusch (Vieweg, Braunschweig) p. 363.
Tinkham, M., and J. Clarke, 1972, Phys. Rev. Lett. 28, 1366.
Van Harlingen, D.J., 1981, J. Low Temp. Phys. 44, 163.
Van Harlingen, D.J., 1982, Physica 109&110B + C, 1710.
Waldram, J.R., 1975, Proc. Roy. Soc. (London) A345, 231.
Webb, W.W., and R.J. Warburton, 1968, Phys. Rev. Lett. 20, 461.
Yu, M.L., and J.E. Mercereau, 1972, Phys. Rev. Lett. 28, 1117.

Bibliography from Nonequilibrium phenomena in superconducting weak links by L.G. Aslamazov and A.F. Volkov

Ambegarkar, V., and A. Baratoff, 1963, Phys, Rev. Lett. 10, 486.
Andreev, A.F., 1964, Zh. Eksp. Teor. Fiz, 46, 1823.
Artemenko, S.N., and A.F. Volkov, 1979, Usp. Fiz. Nauk 128, 4.
Artemenko, S.N., A.F. Volkov and A.V. Zaitsev, 1979a, Zh. Eksp. Teor. Fiz. 76, 1816.
Artemenko, S.N., A.F. Volkov and A.V. Zaitsev, 1979b, Solid State Commun. 30, 771.
Artemenko, S.N., A.F. Volkov and A.V. Sergeev, 1981, J. Low Temp. Phys. 44. 405.
Astamazov, L.G., and A.I. Larkin, 1969, Zh. Eksp. Teor. Fiz, Pis'ma 2, 150.
Aslamazor, L.G., and A.I. Larkin, 1976, Zh. Eksp. Teor. Fiz. 70. 1341).
Aslamazov, L.G., and A.r. Larkin, 1978, Zh. Eksp. Teor. Fiz. 74, 2184.
Barone, A., and G. Paterno, 1981, Physics and Applications of the Josephson Effect (Wile), New York).
De Gennes, P.G., 1966. Superconductivity of Metals and Alloys (Benjamin, New York).

Divin, Yu.Ya., and F.Ya.N"ad", 1978, Fiz. Nizk. Temp. 4, 1115.
Dorozhkin, S.I., 198(). Zh. Eksp. Teor. Fiz. 79, 1025.
Ellenherger, G., 1968. Z. Phys. 214, 195.
Eliashberg, G.M., 1970, Zh. Eksp. Teor. Fiz. Pis'ma 11, 186.
Eliashberg, G.M. 1971, Zh. Eksp. Teor, Fiz, 61, 1254.
Goluh. A.A., 1976, Zh. Eksp. Teor. Fiz. 71, 341.
Gorkov, L.P., and G.M. Eliashberg, 1968, Zh. Eksp. Teor. Fiz. 54. 612: 55. 2431).
Gubankov, V.N., V.P. Koshelets and G.A. Ovsyannikov. 1977. Zh. Eksp. Teor. Fiz. 73. 1435.
Ivlev, B.I., and G.M. Eliashberg. 1971. Zh. Eksp. Teor. Fiz. Pis m 13. 464.
Josephson, B.D., 1962, Phys. Lett. 1, 251; Rev. Mod. Phys. 36. 216.
Jensen. H.H.. and P.E. Lindelof. 1976. J. Low Temp. Phys. 23. 469.
Klapwijk, T.M. J.N. Van den Bergh and J.E. Mooij. 1977. J. Low Temp. Phys. 26. 385.
Klapwijk. T.M.. G.E. Blonder and M. Tinkham. 1982. Physica 109-110B. 1657.
Kulik. I.O., and A.N. Omelyanchuk. 1975, Zh. Eksp. Teor. Fiz. Pisma 21. 216.
Kulik, I.O., and A.N. Omelyanchuk, 1977, Fiz. Nizk. Temp. 3. 945.
Kulik, I.O., A.N. Omelyanchuk and R.I. Shekhter, 1977, Zh. Eksp. Teor. Fiz. Pis ma 25. 465.
Likharev, K.K., 1979, Lisp. Fiz. Nauk 127, 185.
Likharev, K.K.. and L.A. Yakobson. 1975, Zh. Eksp. Teor. Fiz. 68. 1150.
Larkin. A.I., and Yu.N. Ovchinnikov. 1966. Zh. Eksp. Teor. Fiz. 51. 1535.
Larkin, A.I., and Yu.N. Ovchinnikov. 1977. Zh. Eksp. Teor. Fiz. 73. 299.
Larkin, A.I., and Yu.N. Ovchinnikov, 1975, Zh. Eksp. Teor. Fiz. 68, 1915.
Latyshev, Yu.I., and F.Ya.Nad', 1979, Zh. Eksp. Teor. Fiz. Pis'ma 29, 54.
Mitsay, Yu.N., 1976, Fiz. Nizk. Temp. 2, 189.
Octavio, M., W.J. Skocpol and M. Tinkham, 1978, Phys. Rev. B17, 159.
Pethik, C.I., and H. Smith, 1979, Ann. Phys. 119, 133.
Schmid, A., 1981, in: Nonequilibrium Superconductivity, Phonons and Kapitza Boundaries (Proc. NATO ASI), ed. K.E. Gray (Plenum, New York) p. 423.
Schmid, A., 1981, Kinetic Equations for Dirty Superconductors, preprint.
Schmid, A., and G. Schön, 1975, J. Low Temp. Phys. 20, 207.
Schmid, A., G. Schön and M. Tinkham, 1980, Phys. Rev. B21, 5076.
Tinkham, M., 1979, in: Festkörperprobleme, Advances in Solid State Physics XIX, ed. I. Treusch (Vieweg, Braunschweig) p. 363.
Werthammer, W.R., 1966, Phys. Rev. 147, 255.
Zaitsev, A.V., 1980, Zh. Eksp. Teor. Fiz., 78, 221; 79, 2015.

Bibliography from Time-dependent superconductivity in SNS bridges: an example of TDGL theory by A.L. De Lozanne and M.R. Beasley

Alfeev, V.N., A.V. Verbilo, D.P. Kolesnikov and V.A. Ryzhkov, 1979, Fiz. Tekh. Poluprovodn. 13, 164 [Sov. Phys. Semicond. 13, 93].
Aslamazov, L.G., and A.I. Larkin, 1968, Zh. Eksp. Teor. Fiz. Pis'ma 9, 150 [1969, JETP Lett, 9, 87].
de Lozanne, A.L., 1982, Ph.D. Thesis (Stanford Univ.).
de Lozanne, A.L., M.S. DiIorio and M.R. Beasley, 1983, Appl. Phys. Lett. 42, 541; see also Proc. XVI Low Temp. Conf., 1981, Physica 108B, 1027.
Dilorio, M.S., A.L. de Lozanne and M.R. Beasley, 1983, IEEE Trans. Magn. Mag-19, 308.
Fjordbge, B.R., and P.E. Lindelof, 1978, J. Low Temp. Phys. 31, 83.
Golub, A.A., 1980, Fiz. Nizk. Temp. 6, 979 [Sov. J. Low Temp. Phys. 6, 475].
Gor'kov, L.P., and G.M. Eliashberg, 1968, Zh. Eksp. Teor. Fiz. 54, 612 [Sov. Phys. JETP 27, 328]
Gudkov, A.L., K.K. Likharev, O.V. Snigirev, E.S. Soldatov, S.S. Tinchev and V.V. Khanin,

1979, Zh. Tekh. Fiz. Pis'ma 5, 1206 [Sov. Tech. Phys. Lett. 5, 506]
Hu, C.-R., and R.S. Thompson, 1972, Phys. Rev. B6, 110; see also Tinkham (1980) p. 273.
Ivanov, Z.G., O.V. Snigirev, E.S. Soldatov, Yu.V. Maslennikov, A.V. Chervyakov and V.L. Golubev, 1981, Fiz. Nizk. Temp. 7, 1245 [Sov. J. Low Temp. Phys. 7, 603].
Kadin, A.M., and A.M. Goldman, ch. 7, this volume.
Komarovskikh, N.I., G.M. Lapir, A.N. Samus', and V.K. Semenov, 1975, Zh. Tekh. Fiz. Pis'ma 1, 1002 [Sov. Tech. Phys. Lett. 1, 432].
Kramer, L., and A. Baratoff, 1977, Phys. Rev. Lett. 38, 518; Proc. Int. Conf. on Superconductors and Quantum Devices, Berlin, 1976, eds. H.-D. Hahlbohm and H. Lbbig (W. de Gruyter, Berlin).
Kramer, L., and R.J. Watts-Tobin, 1978, Phys. Rev. Lett. 40, 1041.
Kulik, I.O., and I.K. Yanson, 1972, The Josephson Effect in Superconducting Tunneling Structures (Keter, Jerusalem).
Liengme, O., P. Lerch, W. Liu and P. Martinoli, 1983, IEEE Trans. Magn. Mag-19, 995.
Likharev, K.K., 1979, Rev. Mod. Phys. 51, 101.
Likharev, K.K., and L.A. Yakobson, 1975, Zh. Eksp. Teor. Fiz. 68, 1150 [1976 Sov. Phys. JETP 41, 570].
Ruby, R.C., and T. van Duzer, 1981, IEEE Trans. Electron. Dev. ED-28, 1394.
Russer, P., 1972, J. Appl. Phys. 43, 2008.
Schön, G., and V. Ambegaokar, 1979, Phys. Rev. B19, 3515.
Tinkham, M., 1980, Introduction to Superconductivity (Krieger, New York) pp. 250-254.
van Dover, R.B., A.L. de Lozanne, R.E. Howard, W.L. McLean and M.R. Beasley, 1980, Appl. Phys. Lett. 37, 838.
van Dover, R.B., A.L. de Lozanne and M.R. Beasley, 1981, J. Appl. Phys. 52, 7327.
Warlaumont, J., J.C. Brown and R.A. Buhrman, 1979, Appl. Phys. Lett. 34, 415.

Bibliography from Pair breaking in nonequilibrium superconductors by J. Beyer, C.J. Pethick, J. Rammer and H. Smith

Eilenberger, G., 1968, Z. Phys. 214, 195.
Eliashberg, G.M., 1971, Zh. Eksp. Teor. Fiz. 61, 1254 [1972, Sov. Phys. JETP 34, 668].
Fjordbge, B.R., P.E. Lindelof and J. Clarke, 1981, J. Low Temp. Phys. 44, 535.
Gunault, A.M., 1961, Proc. Roy. Soc. (London) A204, 420.
Keldysh, L.V., 1964, Zh. Eksp. Teor. Fiz. 47, 1515 (1965, Sov. Phys. JETP 20, 1018].
Larkin, A.I., and Yu.N. Ovchinnikov, 1968, Zh. Eksp. Teor. Fiz. 55, 2262 [1969, Sov. Phys. JETP 28, 1200].
Larkin, A.I., and Yu.N. Ovchinnikov, 1977, Zh. Eksp. Teor. Fiz. 73, 299 [Sov. Phys. JETP

[0]Ambegaokar, V., and L. Tewordt, 1964, Phys. Rev. 134A, 805.
Ambegaokar, V., and J. Woo, 1965, Phys. Rev. 139A, 1818.
Aronov, A.G., 1974, Zh. Eksp. Teor. Fiz. 67, 178 [Sov. Phys. JETP 40, 90].
Aronov, A.G., and V.L. Gurevich, 1974, Fiz. Tverd. Tela 16, 2656 [Sov. Phys. Solid State 16, 1722].
Aronov, A.G., Yu.N. Gal'perin, V.L. Gurevich and V.J. Kozub, 1981, Adv. Phys. 30, 539.
Bardeen, J., G. Rickayzen and L. Tewordt, 1959, Phys. Rev. 113, 982.
Betbeder-Matibet, O., and P. Nozires, 1969, Ann. Phys. 51, 392.
Beyer Nielsen, J., and H. Smith, 1982, Phys. Rev. Lett. 49, 689.
Beyer Nielsen, J., and H. Smith, 1985, Phys. Rev. B31, 2831.
Beyer Nielsen, J., Y.A. Ono, C.J. Pethick and H. Smith, 1980, Solid State Commun. 33, 925.
Beyer Nielsen, J., C.J. Pethick, J. Rammer and H. Smith, 1981, Physica 107B+C, 161.
Beyer Nielsen, J., C.J. Pethick, J. Rammer and H. Smith, 1982, J. Low Temp. Phys. 46, 565.
Beyer Nielsen, J., H. Smith and S.R. Yang, 1985, J. Low Temp. Phys. 55, 33.
Clarke, J., 1972, Phys. Rev. Lett. 28, 1363.
Clarke, J., and M. Tinkham, 1980, Phys. Rev. Lett. 44, 106.
Clarke, J., B.R. Fjordbge and P.E. Lindelof, 1979, Phys. Rev. Lett. 43, 642.

46, 155].
Lemberger, T.R., and J. Clarke, 1981, Phys. Rev. B23, 1088, 1100.
Mezahov-Deglin, L.P., 1979, Zh. Eksp. Teor. Fiz. 77, 733 [Sov. Phys. JETP 50, 369].
Ovchinnikov, Yu.N., A. Schmid and G. Schön, 1981, Phys. Rev. Lett. 46, 1013.
Peters, R., and H. Meissner, 1973, Phys. Rev. Lett. 30, 965.
Pethick, C.J., and H. Smith, 1978, Physica 90B, 107.
Pethick, C.J., and H. Smith, 1979a, Ann. Phys. 119, 133.
Pethick, C.J., and H. Smith, 1979b, Phys. Rev. Lett. 43, 640.
Ritger, A.J., and H. Meissner, 1980, J. Low Temp. Phys. 40, 495.
Scalapino, D.J., 1969, in: Superconductivity, Vol. I, ed. R.D. Parks (Marcel Dekker, New York) p. 445.
Schmid, A., 1968, Phys. Kondens. Mater. 8, 129.
Schmid, A., 1969, Phys. Rev. 186, 420.
Schmid, A., 1981, in: Non-equilibrium Superconductivity, Phonons and Kapitza Boundaries (Proc. NATO ASI) ed. K.E. Gray (Plenum, New York) p. 423.
Schmid, A., and G. Schön, 1975, J. Low Temp. Phys. 20, 207.
Schmid, A., and G. Schön, 1979, Phys. Rev. Lett. 43, 793.
Shelankov, A.L., 1980, Zh. Eksp. Teor. Fiz. 78, 2359 [Sov. Phys. JETP 51, 1186].
Schön, G., 1981a, Physica 107B + C, 171.
Schön, G., 1981b, in: Festkörperprobleme (Advances in Solid State Physics), vol. XXI, ed. J. Treusch (Vieweg, Braunschweig) p. 341.
Tinkham, M., 1972, Phys. Rev. B6, 1747.
Tinkham, M., and J. Clarke, 1972, Phys. Rev. Lett. 28, 1366.
Vashishta, P., and J.P. Carbotte, 1972, Phys. Rev. B5, 1859.
Watson, J.H.P., and G.M. Graham, 1963, Can. J. Phys. 41, 1738.

Bibliography from Experimental study of enhanced superconductivity by V.M. Dmitriev, V.N. Gubankov and F.Ya. Nad'

Artemenko, S.N., A.F. Volkov and A.V. Zaitsev, 1979a, Zh. Eksp. Teor. Fiz. 76, 1816.
Artemenko, S.N., A.F. Volkov and A.V. Zaitsev, 1979b, Solid State Commun. 30, 771.
Aslamazov, L.G., 1978, Zh. Eksp. Teor. Fiz. 75, 1778.
Aslamazov, L.G., and V.I. Gavrilov, 1980, Fiz. Nizk. Temp. 6, 877.
Aslamazov, L.G., and A.I. Larkin, 1969, Zh. Eksp. Teor. Fiz. Pis'ma 9, 150.
Aslamazov, L.G., and A.I. Larkin, 1976, Zh. Eksp. Teor. Fiz. 70, 1340.
Aslamazov, L.G., and A.I. Larkin, 1978, Zh. Eksp. Teor. Fiz. 74, 2184.
Aslamazov, L.G., and A.F. Volkov, 1985, ch. 2, this volume.
Aslamazov, L.G., A.I. Larkin and Yu.N. Ovchinnikov, 1968, Zh. Eksp. Teor. Fiz. 55, 323.
Bar'yakhtar, V.G., and V.P. Seminozhenko, 1976, Fiz. Nizk. Temp. 2, 1516.
Bar'yakhtar, V.P., and V.P. Seminozhenko, 1977, Fiz. Nizk. Temp. 3, 272.
Bevza, Yu.G., G.G. Zah, V.M. Karamushko and I.M. Dmitrenko, 1976, Zh. Tekhn. Fiz. Pis'ma 2, 367.
Bevza, Yu.G., V.M. Karamushko and I.M. Dmitrenko, 1977, Zh. Tekhn. Fiz. 47, 646.
Bulyzhenkov, I.E., and B.I. Ivlev, 1976, Zh. Eksp. Teor. Fiz. 70, 1405; 71, 1172.
Chang, J.J., and D.J. Scalapino, 1977, J. Low Temp. Phys. 29, 477.

[0]Anderson, P.W., 1967, in: Progress in Low Temperature Physics V, ed. C.J. Gorter (NorthHolland, Amsterdam) p. 1.

Anderson, P.W., and A.H. Dayem, 1964, Phys. Rev. Lett. 13, 195.
Andratskii, V.P., L.M. Grundel, V.N. Gubankov and N.B. Pavlov, 1973, Zh. Eksp. Teor. Fiz. 65, 1591.
Andreev, A.F., 1964, Zh. Eksp. Teor. Fiz. 46, 1823.
Artemenko, S.N., A.F. Volkov and A.V. Zaitsev, 1978, Zh. Eksp. Teor. Fiz. Pis'ma 28, 637.

Chang, J.J., and D.J. Scalapino, 1978, J. Low Temp. Phys. 31, 2.
Chi, C.C., and J. Clarke, 1979, Phys. Rev. B19, 4465.
Chien, M.K., and D.E. Farrell, 1975, J. Low-Temp. Phys. 19, 75.
Christiansen, P.V., E.B. Hansen and C.J. Sjöström, 1971, J. Low-Temp. Phys. 4, 349.
Clarke, J., and J.L. Paterson, 1974, J. Low-Temp. Phys. 15, 491.
Dayem, A.H., and C.C. Grimes, 1966, Appl. Phys. Lett. 9, 47.
Dayem, A.H., and R.J. Martin, 1962, Phys. Rev. Lett. 8, 246.
Dayem, A.H., and J.J. Wiegand, 1967, Phys. Rev. 155, 418.
Deaver, B.S., and J.M. Pierce, 1972, Phys. Lett. 38 A, 81.
Divin, Yu.Ya., and F.Ya. Nad', 1978, Fiz. Nizk. Temp. 4, 1105.
Divin, Yu.Ya., and F.Ya. Nad', 1979, Zh. Eksp. Teor. Fiz., Pis'ma, 29, 567.
Dmitriev, V.M., and E.V. Khristenko, 1978, Fiz. Nizk. Temp. 4, 821.
Dmitriev, V.M., and E.V. Khristenko, 1979, J. Physique 40, L-85.
Dmitriev, V.M., E.V. Khristenko, A.V. Trubitsyn and F.F. Mende, 1970, Ukr. Fiz. Zh. 15, 1611.
Dmitriev et al. 73 from p. 55.
Dmitriev, V.M., E.V., Khristenko and L.V. Esichko, 1976, Microwave Enhanced Superconductivity in Thin Film Bridges, in: Proc. LT-19 Conference, Minsk, 1976, p. 393.
Dmitriev, V.M., N.I. Glushchuk and E.V. Khristenko, 1978, Nonequilibrium critical current of the superconducting channels in the microwave field, in: Proc. LT-20 Conference, Moscow, 1979, v. 3, p. 194.
Dmitriev, V.M.. E.V. Khristenko and S. Shapiro, 1973, Fiz. Kond. Sost., 28, 3.
Dorozhkin, S.I., 1980, Temperature Dependence of the S-N Point Contacts Conductivity, in: Proc. LT-21 Conference, Kharkov, 1980, v. 1, p. 221.
Eckern, U., A. Schmid, M. Schmutz and G. Schön, 1979, J. Low Temp. Phys. 36, 643.
Eliashberg, G.M., 1970, Zh. Eksp. Teor. Fiz. Pis'ma 11, 186.
Eliashberg, G.M., 1971, Zh. Eksp. Teor. Fiz. 61, 1254.
Eliashberg, G.M., and B.I. Ivlev, 1985, ch. 6, this volume.
Fil', V.D., V.I. Denisenko and P.A. Bezuglyi, 1975, Zh. Eksp. Teor. Fiz. Pis'ma 21, 693.
Fil', V.D., V.I. Denisenko, P.A. Bezuglyi and A.S. Pirogov, 1976, Fiz. Nizk. Temp. 2, 1506.
Fil', V.D., A.L. Gaiduk and V.I. Denisenko, 1980, Zh. Eksp. Teor. Fiz. 78, 1464.
Galaiko, V.P., V.S. Shumeiko and T. Kshishton', 1981, Zh. Eksp. Teor. Fiz., 80, 2078.
Gor'kov, L.P., 1959, Zh. Eksp. Teor. Fiz. 37, 1407.
Gor'kov, L.P., and G.M. Eliashberg, 1969, Zh. Eksp. Teor. Fiz. Pis'ma 8, 329; Zh. Eksp. Teor. Fiz. 56, 1297.
Gray, K.E., 1978, Solid State Commun. 26, 633.
Gregers-Hansen, P.E., and M.T. Levinsen, 1971, Phys. Rev. Lett. 27, 847.
Gubankov, V.N., and N.M. Margolin, 1979, Zh. Eksp. Teor. Fiz. Pis'ma 29, 733.
Gubankov, V.N., and N.M. Margolin, 1981, Zh. Eksp. Teor. Fiz. 79, 1419.
Gubankov, V.N., V.P. Koshelets, K.K. Likharev and G.A. Ovsyannikov, 1973, Zh. Eksp. Teor. Fiz. Pis'ma 18, 292.
Gubankov, V.N., V.P. Koshelets and G.A. Ovsyannikov, 1975, Zh. Eksp. Teor. Fiz. Pis'ma 21, 489.
Gubankov, V.N., V.P. Koshelets and G.A. Ovsyannikov, 1976, Zh. Eksp. Teor. Fiz. 71, 348.
Gubankov, V.N., V.P. Koshelets and G.A. Ovsyannikov, 1977, Zh. Eksp. Teor. Fiz. 73, 1435.
Gubankov, V.N., V.P. Koshelets and G.A. Ovsyannikov, 1978, J. Physique 39 (suppl. No 8) c. 6-535.
Gubankov, V.N., V.P. Koshelets and G.A. Ovsyannikov, 1979, Zh. Tekhn. Fiz. 49, 832.
Gubankov, V.N., V.P. Koshelets and G.A. Ovsyannikov, 1980, Fiz. Nizk. Temp. 6, 50.

Hall, J.T., L.B. Holdeman and R.J. Sonlen, 1980, Phys. Rev. Lett. 45, 1011.
Hansen, J.B., P. Jespersen and P.E. Lindelof, 1978, J. Physique 39 (suppl. No 8) c. 6-500.
Hunt, T.K., 1969, Phys. Rev. 177, 749.
Hunt, T.K., and J.E. Mercereau, 1967, Phys. Rev. Lett. 18, 551.
Ivlev, B.I., 1972, Zh. Eksp. Teor. Fiz. 72, 1197.
Ivlev, B.I., and G.M. Eliashberg, 1971, Zh. Eksp. Teor. Fiz. Pis'ma 13, 464.
Ivlev, B.I., S.G. Lisitsyn and G.M. Eliashberg, 1973, J. Low-Temp. Phys. 10, 449.
Jillie, D.W., J. Lukens and Y.H. Kao, 1975, IEEE Trans. Magn. MAG-11, 671.
Kirichenko, I.K., S.A. Peskovatskii and V.P. Seminozhenko, 1979, Solid State Commun. 26, 633.
Klapwijk, T.M., and J.E. Mooij, 1976, Physica 81B, 132.
Klapwijk, T.M., J.N. Van den Bergh and J.E. Mooij, 1977, J. Low-Temp. Phys. 26, 385.
Klapwijk, T.M., H.B. van Linden van den Heuvell and J.E. Mooij, 1978, J. Physique 39 (suppl. No 8) c. 6-525.
Kommers, T.M., and J. Clarke, 1977, Phys. Rev. Lett. 38, 1091.
Kulik, I.O., and A.N. Omelyanchuk, 1978, Fiz. Nizk. Temp. 4, 296.
Latyshev, Yu.I., and F.Ya. Nad', 1974, Zh. Eksp. Teor. Fiz. Pis'ma 19, 737.
Latyshev, Yu.I., and F.Ya. Nad', 1975, IEEE Trans. Magn. MAG-11, 877.
Latyshev, Yu.I., and F.Ya. Nad', 1976, Zh. Eksp. Teor. Fiz. 71, 2158.
Latyshev, Yu.I., and F.Ya Nad', 1977, Zh. Eksp. Teor. Fiz. Pis'ma 26, 488.
Latyshev, Yu.I., and F.Ya. Nad', 1978, J. Physique 39 (suppl. No. 8) c. 6-531.
Latyshev, Yu.I., and F.Ya. Nad', 1979, Zh. Eksp. Teor. Fiz. Pis'ma 29, 58.
Levinsen, M.T., 1974, Phys. Rev. Appl. 9, 135.
Likharev, K.K., and L.A. Yakobson, 1975, Zh. Eksp. Teor. Fiz. 68, 1150.
Likharev, K.K., and B.T. Ulrich, 1978, Systems with Josephson contacts (Moscow University, Moscow).
Lindelof, P.E., 1976, Solid State Commun. 18, 283.
McCumber, D.E., 1968, J. Appl. Phys. 39, 3113.
Mitsen, K.V., G.P. Motulevich, A.I. Golovashkin, O.M. Ivanchenko and M.V. Tihansky, 1980, Superconductivity Enhancement in Tin by Quasiparticle Tunneling, in: Proc. LT-21 Conference, Kharkov, USSR, 1980, (FTINT, Kharkov) v. 1, p. 173.
Mooij, J.E., N. Lambert and T.M. Klapwijk, 1980, Solid State Commun. 36, 585.
Nad', F.Ya., and O.Yu. Polanskii, 1973, Radiotekhn. Elektron. 18, 2448.
Octavio, M., 1978, Thesis (Harvard Univ.).
Octavio, M., M.J. Skocpol and M. Tinkham, 1977, IEEE Trans. Magn. MAG-13, 739.
Octavio, M., M.J. Skocpol and M. Tinkham, 1978, Phys. Rev. 17B, 159.
Ovchinnikov, Yu.A., 1973, Zh. Eksp. Teor. Fiz. 64, 719.
Pals, J.A., and J. Dobben, 1978, J. Physique 40, L-85.
Pals, J.A., and J. Dobben, 1979, Phys. Rev. 20B. 935.
Pankove, J.J., 1966, Phys. Lett. 21, 406.
Parmenter, R.H., 1961, Phys. Rev. Lett. 7, 274.
Peskovatskii, S.A., and V.P. Seminozhenko, 1976, Fiz. Nizk. Temp. 2, 943.
Peskovatskii, S.A., and L.P. Strizhko, 1979, Zh. Eksp. Teor. Fiz. Pis'ma 29, 68.
Rieger, T.J., D.J. Scalapino and J.E. Mercereau, 1972, Phys. Rev. B6, 1734.
Schmid, A., 1977, Phys. Rev. Lett. 38, 922.
Seminozhenko, V.P., and A.A. Yatsenko, 1980, Solid State Commun. 33, 753.
Shepard, K.W., 1971, Physica 55, 786.
Skocpol, W.J., M.R. Beasley and M. Tinkham, 1974, J. Low-Temp. Phys. 16, 145.
Stewart, W.S., 1968, Appl. Phys. Lett. 12, 277.
Tredwell, T.J., and E.H. Jakobson, 1975, Phys. Rev. Lett. 35, 244.

Volkov, A.F., N.V. Zavaritskii, and F.Ya Nad', 1978, Electronic Devices on the Base of the Weakly Coupled Superconductors, ed. N.V. Zavaritskii (Sov. Radio, Moscow).
Weitz, D.A., W.J. Skocpol and M. Tinkham, 1978, Phys. Rev. Lett. 40, 253.
Wyatt, A.F.G., V.M. Dmitriev, and W.S. Moore, 1966a, The Effect of Microwaves on Constricted Tin Films, in: Proc. LT-10 Int. Conference Moscow, v. 2-A, p. 242.
Wyatt, A.F.G., V.M. Dmitriev, W.S. Moore and F.W. Sheard, 1966b, Phys. Rev. Lett. 16, 1166.
Zaitsev, A.V., 1980a, To the Theory of the Variable Thickness Bridges, in: Proc LT-21 Conference, Kharkov, ed. N.V. Zavaritskii (FTINT, Kharkov) v. 1, p. 132.
Zaitsev, A.V., 1980b, Zh. Eksp. Teor. Fiz. 79, 1025.
Zhilinskii, S.K., Yu.I. Latyshev and F.Ya. Nad', 1980, Temperature Dependence of Excess Current in Short Superconducting Bridges, in: Proc. LT-21 Conference, Kharkov, ed. (FTINT, Kharkov) v. 1, p. 223.

Bibliography from Theory of superconductivity stimulation by G.M.Eliashberg and B. I. Ivlev

Aronov, A.G., and V. L. Gurevich, 1972, Zh. Eksp. Teor. Fiz. 63, 1809.
Artemenko, S.N., and A.F. Volkov, 1975, Zh. Eksp. Teor. Fiz. Pis'ma 21, 662.
Artemenko, S.N., A.F. Volkov and A.V. Zaitsev, 1978, J. Low Temp. Phys. 30, 487.
Aslamazov, L.G., and V.I. Gavrilov, 1980, Fiz. Nizk. Temp. 6, 877.
Aslamazov, L.G., and A.I. Larkin, 1978, Zh. Eksp. Teor. Fiz. 74, 2184.
Bulyzhenkov, I.E., and B.I. Ivlev, 1976a, Zh. Eksp. Teor. Fiz. 70, 1405.
Bulyzhenkov, I.E., and B.I. Ivlev, 1976b, Zh. Eksp. Teor. Fiz. 71, 1112.
Bulyzhenkov, I.E., and B.I. Ivlev, 1978, Zh. Eksp. Teor. Fiz. 74, 224.
Bulyzhenkov, I.E., and B.I. Ivlev, 1979, Fiz. Tverd. Tela 21, 2325.
Chang, J.J., 1978, Phys. Rev. B11, 20.
Chang, J.J., and D.J. Scalapino, 1977, J. Low Temp. Phys. 29, 477.
Chi, C.C., and J. Clarke, 1979, Phys. Rev. B11, 20.
Dayem, A.H., and J.J. Wiegand, 1967, Phys. Rev. 155, 419.
Dmitriev, V.M., and E.V. Khristenko, 1978, Fiz. Nizk. Temp. 4, 821.
Dmitriev, V.M., V.N. Gubankov and F. Nad', 1985, ch. 5, this volume.
Douglass, D., and L. Falicov, 1964, Energy gap in superconductors, in: Progress in Low Temperature Physics IV, ed. C. Gorter (North-Holland, Amsterdam) p. 97.
Eckern, U., A. Schmid, M. Schmutz and G. Schön, 1979, J. Low Temp. Phys. 36, 643.
Eliashberg, G.M., 1970, Zh. Eksp. Teor. Fiz. Pis'ma 11, 186.
Eliashberg, G.M., 1971, Zh. Eksp. Teor. Fiz. 61, 1254.
Galaiko, V.P., 1974, Zh. Eksp. Teor. Fiz. 66, 379.
Ginzburg, E.V., and B.Z. Spivak, 1981, Zh. Eksp. Teor. Fiz. 80, 2013.
Gor'kov, L.P., and G.M. Eliashberg, 1968, Zh. Eksp. Teor. Fiz. 56, 612.
Gor'kov, L.P., and N.B. Kopnin, 1973, Zh. Eksp. Teor. Fiz. 65, 396.
Gray, K.E., 1978, Solid State Commun. 26, 633.
Ivlev, B.I., and G.M. Eliashberg, 1971, Zh. Eksp. Teor. Fiz. Pis'ma 13, 464.
Ivlev, B.I., S.G. Lisitsyn and G.M. Eliashberg, 1973, J. Low Temp. Phys. 10, 449.
Ivlev, B.I.. 1978, Zh. Eksp. Teor. Fiz. 75, 1771.
Kaplan, S.B., J.R. Kirtley and D.N. Langenberg, 1977, Phys. Rev. Lett. 39, 291.
Keldysh, L.V., 1964, Zh. Eksp. Teor. Fiz. 47, 1515.
Kittel, G., 1963, Quantum theory of solids (Wiley, New York).
Klapwijk, T.M., and J.E. Mooij, 1976, Physica 81B + C, 132.
Kommers, T., and J. Clarke, 1977, Phys. Rev. Lett. 38, 1091.
Kozub, V.I., and B.Z. Spivak, 1981. J. Low Temp. Phys. 42, N5/6.

Larkin, A.I., and Yu.N. Ovchinnikov, 1977, Zh. Eksp. Teor. Fiz. 73, 299.
Latyshev, Yu.I., and F.Ya. Nad', 1974, Zh. Eksp. Teor. Fiz. Pis'ma 19, 737.
Latyshev, Yu.I., and F.Ya. Nad', 1976, Zh. Eksp. Teor. Fiz. 71, 2158.
Parmenter, R.H., 1961, Phys. Rev. Lett. 11, 274.
Peskovatski, S.A., and V.P. Seminozhenko, 1976, Fiz. Nizk. Temp. 2, 943.
Schmid, A., and G. Schön, 1975, J. Low Temp. Phys. 20, 207.
Tinkham, M., and J. Clarke, 1972, Phys. Rev. Lett. 28, 1366.
Tredwell, T.J., and E.H. Jacobsen, 1975, Phys. Rev. Lett. 35, 244.
Vardanyan, R.A., and B.1. Ivlev, 1973, Zh. Eksp. Teor. Fiz. 65, 2315.
Volkov, A.F., and A.V. Zaitsev, 1975, Zh. Eksp. Teor. Fiz. 69, 2222.
Wyatt, A.F., V.M. Dmitriev, W.S. Moore and F.W. Sheard, 1966, Phys. Rev. Lett. 16, 1166.

Bibliography from Dynamical effects in nonequilibrium superconductors: some experimental perspectives by A.M. Kadin and A.M. Goldman

Abraham, D.W., C.J. Lobb, M. Tinkham and T.M. Klapwijk, 1982, Phys. Rev. B26, 5268.
Anderson, J.T., and A.M. Goldman, 1970, Phys. Rev. Lett. 25, 743.
Anderson, J.T., R.V. Carlson and A.M. Goldman, 1972, J. Low Temp. Phys. 8, 29.
Anderson, P.W., 1958, Phys. Rev. 110, 827.
Andreev, A.F., 1964, Zh. Eksp. Teor. Fiz. 19, 1228 [Sov. Phys. JETP 19, 1228].
Aponte, J., and M. Tinkham, 1983, J. Low Temp. Phys. 51, 189.
Aronov, A.G., and B.Z. Spivak, 1978, Fiz. Nizk. Temp. 4, 1365 [Sov. J. Low Temp. Phys. 4, 641].
Artemenko, S.N., and A.F. Volkov, 1975, Zh. Eksp. Teor. Fiz. 69, 1764 [1976, Sov. Phys. JETP 42, 896].
Artemenko, S.N., and A.F. Volkov, 1979, Usp. Fiz. Nauk 128, 3 [1980, Sov. Phys. Usp. 22, 295].
Artemenko, S.N., A.F. Volkov and A.V. Zaitsev, 1978a, J. Physique 39, C6-588.
Artemenko, S.N., A.F. Volkov and A.V. Zaitsev, 1978b, Zh. Eksp. Teor. Fiz. Pis'ma 27, 122 [JETP Lett. 27, [13].
Artemenko, S.N., A.F. Volkov and A.V. Zaitsev, 1979, Zh. Eksp. Teor. Fiz. 76, 1816 [Sov. Phys. JETP 49, 924].
Aslamazov, L.G., and A.I. Larkin, 1976, Zh. Eksp. Teor. Fiz. 70, 1340 [Sov. Phys. JETP 43, 698].
Aslamazov, L.G., and A.F. Volkov, 1985, ch. 2, this volume.
Aspen, F.E., and A.M. Goldman, 1979, Phys. Rev. Lett. 43, 307.
Aspen, F.E., and A.M. Goldman, 1981a, J. Low Temp. Phys. 43, 559.
Aspen, F.E., and A.M. Goldman, 1981b, Phys. Rev. B22, 3508.
Baratoff, A., 1982a, Phys. Rev. Lett. 48, 434.
Baratoff, A., 1982b, Physica 109+110B, 2058.
Baru, V.G., and A.A. Sukhanov, 1975, Zh. Eksp. Teor. Fiz. Pis'ma 21, 209 [JETP Lett. 21, 93].
Bindslev Hansen, J., 1982, Phys. Scripta 25, 844.
Bindslev Hansen, J., and P.E. Lindelof, 1981, Nonequilibrium Phenomena in Josephson Junctions, in: Proc. 2nd IC-SQUID Conf., Berlin 1980, eds. H.-D. Hahlbohm and H. Lubbig (W. de Gruyter, Berlin), p. 29.
Bindslev Hansen, J., P.E. Lindelof and T.F. Finnegan, 1981, IEEE Trans. Magn. MAG-17, 95.
Blackburn, J.A., 1983, J. Low Temp. Phys. 50, 475.
Blonder, G.E., and M. Tinkham, 1983, Phys. Rev. B27, 6747.
Blonder, G.E., M. Tinkham and T.M. Klapwijk, 1982, Phys. Rev. B25, 4515.
Boone, B.G., C.A. Arrington, L.K. Wang and B.S. Deaver, 1977, IEEE Trans. Magn. MAG-13,

735.

Carlson, R.V., and A.M. Goldman, 1973, Phys. Rev. Lett. 31, 880.

Carlson, R.V., and A.M. Goldman, 1975, Phys. Rev. Lett. 34, 11.

Carlson, R.V., and A.M. Goldman, 1976, J. Low Temp. Phys. 27, 67.

Chang, J.-J., and D.J. Scalapino, 1974, Phys. Rev, B10, 4047.

Chang, J.-J., and D.J. Scalapino, 1978, J. Low Temp. Phys. 31, 1.

Chaudhari, P., A.N. Broers, C.C. Chi, R. Laibowitz, E. Spiller and J. Viggiano, 1980, Phys. Rev. Lett. 45, 930.

Chi, C.C., and J. Clarke, 1979, Phys. Rev. B20, 4465.

Chi, C.C., M.M.T. Loy and D.C. Cronemeyer, 1981, Phys. Rev. B23, 124.

Clarke, J., 1972, Phys. Rev. Lett. 28, 1363.

Clarke, J., 1985, ch. 1, this volume.

Clarke, J., and J.L. Paterson, 1974, J. Low Temp. Phys. 15, 491.

Cyrot, M., 1973, Rep. Prog. Phys. 36, 103.

Dahlberg, E.D., R.L. Orbach and I.K. Schuller, 1979, J. Low Temp. Phys. 36, 367.

Davidson A., 1981, IEEE Trans. Magn. MAG-17, 108.

de Lozanne, A., and M.R. Beasley, 1985, ch. 3, this volume.

Dinter, M., 1977, J. Low Temp. Phys. 26, 39.

Dinter, M., 1978, J. Low Temp. Phys. 32, 529.

Divin, Yu.Ya., and F.Ya. Nad', 1979, Zh. Eksp. Teor. Fiz. Pis'ma 29 [JETP Lett. 29, 516].

Dmitriev, V.M., and E.V. Khristenko, 1978, Fiz. Nizk. Temp. 4, 821 [Sov. J. Low Temp. Phys. 4, 387].

Dmitriev, V.M., V.N. Gubankov and F.Ya. Nad', 1985, ch. 5, this volume.

Dolan, G.J., and L.D. Jackel, 1977, Phys. Rev. Lett. 39, 1628.

Dynes, R.C., V. Narayanamurti and J.P. Garno, 1977, Phys. Rev. Lett. 39, 229.

Eckern, U., A. Schmid, M. Schmutz and G. Schön, 1979, J. Low Temp. Phys. 36, 643.

Elesin, V.F., 1974, Zh. Eksp. Teor. Fiz. 66, 1755 [Sov. Phys. JETP. 39, 862].

Elesin, V.F., 1976, Zh. Eksp. Teor. Fiz. 71, 1490 [Sov. Phys. JETP 44, 780].

Elesin, V.F., 1977a, Zh. Eksp. Teor. Fiz. 73, 355 [Sov. Phys. JETP 46, 185].

Elesin, V.F., 1977b, Fiz. Tverd. Tela 19, 2977 [Sov. Phys. Solid State 19, 1744].

Eliashberg, G.M., 1970, Zh. Eksp. Teor. Fiz. Pis'ma 11, 186 [JETP Lett. 11, 114].

Eliashberg, G.M., and B.I. Ivlev, 1985, ch. 6, this volume.

Entin-Wohlman, O., and R. Orbach, 1978, Ann. Phys. 116, 35.

Entin-Wohlman, O., and R. Orbach, 1979, Ann. Phys. 122, 64.

Faris, S.M., 1980, Appl. Phys. Lett. 36, 1005.

Faris, S.M., S.I. Raider, W.J. Gallagher and R.E. Drake, 1983, IEEE Trans. Magn. MAG-19, 1293.

Ferrell, R.A., 1969, J. Low Temp. Phys. 1, 423.

Frank, D.J., and M. Tinkham, 1983, Phys. Rev. B28, 5345.

Frank, D.J., M. Tinkham, A. Davidson and S.M. Faris, 1983, Phys. Rev. Lett. 50, 1611.

Galako, V.P., and N.B. Kopnin, 1985, ch. 12, this volume.

Geier, A., and G. Schön, 1982, J. Low Temp. Phys, 46, 151.

Goldman, A.M., 1981, Collective Modes of the Superconducting Order Parameter, in: Nonequilibrium Superconductivity, Phonons, and Kapitza Boundaries (Proc. NATO ASI), ed. K.E. Gray (Plenum, New York) ch. 17.

Golub, A.A., 1976, Zh. Eksp. Teor. Fiz. 71, 341 [Sov. Phys. JETP 44, 178].

Gordon, J.M., C.J. Lobb and M. Tinkham, 1983, Phys. Rev. B28, 4046.

Gor'kov, L.P., and G.M. Eliashberg, 1968, Zh. Eksp. Teor. Fiz. 54, 612 [Sov. Phys. JETP 27, 328].

Gorlach, A.F., and R.P. Huebner, 1983, J. Low Temp. Phys. 53, 619.

Gorter, C.J., and H.B.J. Casimir, 1934, Phys. Z. 35, 963.
Gray, K.E., 1978a, Solid State Commun. 26, 633.
Gray, K.E., 1978b, Appl. Phys. Lett. 32, 392.
Gray, K.E., ed., 1981a, Nonequilibrium Superconductivity, Phonons, and Kapitza Boundaries (Proc. NATO ASI) (Plenum, New York).
Gray, K.E., 1981b, Tunneling: A Probe of Nonequilibrium Superconductivity, in: Nonequilibrium Superconductivity, Phonons and Kapitza Boundaries (Proc. NATO ASI), ed. K.E. Gray (Plenum, New York) ch. 5.
Gray, K.E., and H.W. Willemsen, 1978, J. Low Temp. Phys. 31, 911.
Gubankov, V.N., V.P. Koshelets and G.A. Ovsyannikov, 1977, Zh. Eksp. Teor. Fiz. 73, 1435 [Sov. Phys. JETP 46, 755].
Gubankov, V.N., V.P. Koshelets and G.A. Ovsyannikov, 1980, Fiz. Nizk. Temp. 6, 50 [Sov. J. Low Temp. Phys. 6].
Hall, J.T., L.B. Holdeman and R.J. Soulen Jr, 1980, Phys. Rev. Lett. 45, 1011.
Hsiang, T.Y., and J. Clarke, 1980, Phys. Rev. B21, 945.
Hunt, B.D., and R.A. Buhrman, 1983, IEEE Trans. Magn. MAG-19, 1155.
Iguchi, I., 1978a, J. Low Temp. Phys. 31, 605.
Iguchi, I., 1978b, J. Low Temp. Phys. 33, 439.
Iguchi, I., and D.N. Langenberg, 1980, Phys. Rev. Lett. 44, 486.
Ivlev, B.I., and N.B. Kopnin, 1980, J. Low Temp. Phys. 39, 137.
Ivlev, B.I., and N.B. Kopnin, 1981, J. Low Temp. Phys. 44, 453.
Ivlev, B.I., and N.B. Kopnin, 1982, Solid State Commun. 41, 107.
Jain, A.K., P. Mankiewich, A.M. Kadin, R.H. Ono and J.E. Lukens, 1981, IEEE Trans. Magn. MAG-17, 99.
Jillie, D.W., 1976, Doctoral dissertation (State University of New York) unpublished.
Jillie, D.W., J. Lukens and Y.H. Kao, 1977, Phys. Rev. Lett. 38, 915.
Jillie, D.W., M.A.H. Nerenberg and J.A. Blackburn, 1980, Phys. Rev. B21, 125.
Kadin, A.M., and A.M. Goldman, 1982, Phys. Rev. B25, 6701.
Kadin, A.M., W.J. Skocpol and M. Tinkham, 1978, J. Low Temp. Phys. 33, 481.
Kadin, A.M., L.N. Smith and W.J. Skocpol, 1980, J. Low Temp. Phys. 38, 497.
Kadin, A.M., C. Varmazis and J.E. Lukens, 1981, Physica 107B + C, 159.
Kaplan, S.B., 1979, J. Low Temp. Phys. 37, 343.
Kaplan, S.B., C.C. Chi, D.N. Langenberg, J.-J. Chang, S. Jafarey and D.J. Scalapino, 1976, Phys. Rev. B14, 4854.
Klapwijk, T.M., and J.E. Mooij, 1975, IEEE Trans. Magn. MAG-11, 858.
Klapwijk, T.M., and J.E. Mooij, 1976a, Physica 81B, 132.
Klapwijk, T.M., and J.E. Mooij, 1976b, Phys. Lett. 57A, 97.
Klapwijk, T.M., J.N. van den Bergh and J.E. Mooij, 1977, J. Low Temp. Phys. 26, 385.
Klapwijk, T.M., G.E. Blonder and M. Tinkham, 1982, Physica 109+110B, 1657.
Kommers, T., and J. Clarke, 1977, Phys. Rev. Lett. 38, 1091.
Kramer, L., and R.J. Watts-Tobin, 1978, Phys. Rev. Lett. 40, 1041.
Kulik, I.O., 1980, Solid State Commun. 35. 383.
Langenberg, D.N., 1974, in: Festkörperprobleme XIV (Advances in Solid State Physics) ed. H.J. Queisser (Pergamon, Oxford) pp. 67-86.
Latyshev, Yu.I., and F.Ya. Nad', 1976, Zh. Eksp. Teor. Fiz. 71, 2158 [Sov. Phys. JETP 44, 1136].
Lemberger, T.R., 1981a, Phys. Rev. B24, 4105.
Lemberger, T.R., 1981b, Physica 107B + C, 163.
Lemberger, T.R., and J. Clarke, 1981a, Phys. Rev. B23, 1088.
Lemberger, T.R., and J. Clarke, 1981b, Phys. Rev. B23, 1100.

Likharev, K.K., 1979, Rev. Mod. Phys. 51, 101.
Likharev, K.K., and L.A. Yacobson, 1975, Zh. Tekh. Fiz. 20, 1950 [Sov. Phys. Tech. Phys. 20, 950].
Likharev, K.K., L.S. Kuzmin and G.A. Ovsyannikov, 1981, IEEE Trans. Magn. MAG-17, 111.
Lindelof, P.E., 1981, Rep. Prog. Phys. 44, 949.
Lindelof, P.E., and J. Bindslev Hansen, 1977, J. Low Temp. Phys. 29, 369.
Lindelof, P.E., and J. Bindslev Hansen, 1981, Short-range interaction between two superconduct-
ing weak links, in: Nonequilibrium Superconductivity, Phonons and Kapitza Boundaries (Proc. NATO ASI), ed. K.E. Gray (Plenum, New York) ch. 19.
Meyer, J., and G. von Minnigerode, 1972, Phys. Lett. 38A, 529.
Meyer, J.D., and R. Tidecks, 1976, Solid State Commun. 18, 305.
Mooij, J.E., N. Lambert and T.M. Klapwijk, 1980, Solid State Commun. 36, 585.
Mller, W.H.G., and F. Baumann, 1978, Thin Solid Films 48, 193.
Octavio, M., and W.J. Skocpol, 1981, Physica 107B + C, 173.
Octavio, M., W.J. Skocpol and M. Tinkham, 1977, IEEE Trans. Magn. MAG-13, 739.
Octavio, M., W.J. Skocpol and M. Tinkham, 1978, Phys. Rev. B17, 159.
Octavio, M., M. Tinkham, G.E. Blonder and T.M. Klapwijk, 1983, Phys. Rev. B27, 6739.
Owen, C.S., and D.J. Scalapino, 1972, Phys. Rev. Lett. 28, 1559.
Palmer, D.W., and J.E. Mercereau, 1974, Appl. Phys. Lett. 25, 467.
Palmer, D.W., and J.E. Mercereau, 1977, Phys. Lett. 61A, 135.
Pals, J.A., and J. Dobben, 1979, Phys. Rev. B20, 935.
Pals, J.A., and J. Dobben, 1980, Phys. Rev. Lett. 44, 1143.
Pals, J.A., and J. Wolter, 1979, Phys. Lett. 70A, 150.
Pals, J.A., K. Weiss, P.M. Van Attekum, R.E. Horstman and J. Wolter, 1982, Phys. Rep. 89, 323.
Parker, W.H., 1975, Phys. Rev. B12, 3667.
Paterson, J.L., 1978, J. Low Temp. Phys. 33, 285.
Pethick, C.J., and H. Smith, 1979, Ann. Phys. 119, 133.
Pethick, C.J., and H. Smith, 1980, J. Phys. C13, 6313.
Pippard, A.B., J.G. Shephard and D.A. Tindall, 1971, Proc. Roy. Soc. (London) A324, 17.
Resnick, D.J., T.C. Garland, J.T. Boyd, S. Shoemaker and R.S. Newrock, 1981, Phys. Rev. Lett. 47, 1542.
Riedel, E., 1964, Z. Naturforsch. 19, 1634.
Rieger, T.J., D.J. Scalapino and J.E. Mercereau, 1972, Phys. Rev. B6, 1734.
Sandell, R.D., C. Varmazis, A.K. Jain and J.E. Lukens, 1979, IEEE Trans. Magn. MAG-15, 462.
Santhanam, P., and D.E. Prober, 1984, Phys. Rev. B29, 3733.
Scalapino, D.J., 1970, Phys. Rev. Lett. 24, 1052.
Schmid, A., 1978, J. Physique 39, C6-1360.
Schmid, A., 1981, in:Nonequilibrium Superconductivity, Phonons, and Kapitza Boundaries (Proc. NATO ASI), ed. K.E. Gray (Plenum, New York) ch. 14.
Schmid, A., and G. Schön, 1975a, J. Low Temp. Phys. 20, 207.
Schmid, A., and G. Schön, 1975b, Phys. Rev. Lett. 34, 941.
Schmid, A., G. Schön and M. Tinkham, 1980, Phys. Rev. B11, 5076.
Schön, G., 1985, ch., this volume.
Schön, G., and V. Ambegaokar, 1979, Phys. Rev. B19, 3515.
Schrieffer, J.R., and J.W. Wilkins, 1963, Phys. Rev. Lett. 10, 17.
Schuller, I., and K.E. Gray, 1976, Phys. Rev. Lett. 36, 429.
Schuller, I., and K.E. Gray, 1977, Solid State Commun. 23, 337.

Seligson, D., and J. Clarke, 1983, Phys. Rev. B28, 6297.
Simanek, E., and J.C. Hayward, 1974, Physica 78, 199.
Skocpol, W.J., 1981, Nonequilibrium effects in 1-D superconductors, in: Nonequilibrium Superconductivity, Phonons, and Kapitza Boundaries (Proc. NATO ASI), ed. K.E. Gray (Plenum, New York) ch. 18.
Skocpol, W.J. and L.D. Jackel, 1981, Physica 108B + C, 1021.
Skocpol, W.J., and M. Tinkham, 1975, Rep. Prog. Phys. 38, 1049.
Skocpol, W.J., M.R. Beasley and M. Tinkham, 1974a, J. Low Temp. Phys. 16, 145.
Skocpol, W.J., M.R. Beasley and M. Tinkham, 1974b, J. Appl. Phys. 45, 4054.
Smith, A.D., W.J. Skocpol and M. Tinkham, 1980, Phys. Rev. B22, 4346.
Smith, L.N., 1977, J. Low Temp. Phys. 28, 519.
Smith, L.N., 1980, J. Low Temp. Phys. 38, 553.
Solymar, L., 1972, Superconductive Tunneling and Applications (Wiley, New York).
Stuivinga, M., J.E. Mooij and T.M. Klapwijk, 1982, J. Low Temp. Phys. 46, 555.
Stuivinga, M., C.L.G. Ham, T.M. Klapwijk and J.E. Mooij, 1983, J. Low Temp. Phys. 53, 633.
Thouless, D.J., and D.R. Tilley, 1961, Proc. Phys. Soc. (London) 77, 1175.
Tidecks, R., and J.D. Meyer, 1979, Z. Phys. B32, 363.
Tinkham, M., 1972, Phys. Rev. B6, 1747.
Tinkham, M., 1979, Nonequilibrium superconductivity, in: Advances in Solid State Physics XIX, ed. J. Treusch (Pergamon, Oxford) pp. 363-385.
Tinkham, M., 1981, Heating and dynamic enhancement in metallic weak links, in: Nonequilibrium Superconductivity, Phonons, and Kapitza Boundaries (Proc. NATO ASI), ed. K.E. Gray (Plenum, New York) ch. 8.
Tinkham, M., and J. Clarke, 1972, Phys. Rev. Lett. 28, 1366.
Tinkham, M., M. Octavio and W.J. Skocpol, 1977, J. Appl. Phys. 48, 1311.
Tredwell, T.J., and E.H. Jacobsen, 1975, Phys Rev. Lett. 35, 244.
Tredwell, T.J., and E.H. Jacobsen, 1976, Phys. Rev. B13, 293.
Van Attekum, P.M., and J.J. Ramekers, 1982, Solid State Commun. 43, 735.
Van Attekum, P.M., J.J. Ramekers, J.A. Pals and A.M. Hoeben, 1983, Phys. Rev. B27, 1623.
Volkov, A.F., and A.V. Zaitsev, 1975, Zh. Eksp. Teor. Fiz. 69, 222 [Sov. Phys. JETP 42, 1130].
Voss, R.F., and R.A. Webb, 1982, Phys. Rev. B25, 3446.
Waldram, J.R., 1975, Proc. Roy. Soc. (London) A345, 231.
Watts-Tobin, R.J., Y. Krhenbhl and L. Kramer, 1981, J. Low Temp. Phys. 42, 459.
Werthamer, N.R., 1966, Phys. Rev. 147, 255.
Wolter, J., P.M. Van Attekum, R.E. Horstman and M.C.H.M. Wouters, 1981a, Solid State Commun. 40, 433.
Wolter, J., P.M. Van Attekum, R.E. Horstman and M.C.H.M. Wouters, 1981b, Physica 108B, 781. Yoshihiro, K., and K. Kajimura, 1970, Phys. Lett. 32A, 269.
Yu, M.L., and J.E. Mercereau, 1972, Phys. Rev. Lett. 28, 1117.
Yu, M.L., and J.E. Mercereau, 1975, Phys Rev. B12, 4909.

Bibliography from Nonequilibrium properties of superconductors (transport equation approach) by A.G. Aronov, Yu.M. Gal'perin, V.L. Gurevich and V.I. Kozub

Akhieser, A.I., 1938, Zh. Eksp. Teor. Fiz. 8, 1900.
Akhieser, A.I., M.I. Kaganov and G.Ya. Ljubarskii, 1957, Zh. Eksp. Teor. Fiz. 32, 837.
Aronov, A.G., 1974, Zh. Eksp. Teor. Fiz. 67, 178 [1975, Sov. Phys. JETP 40, 908].
Aronov, A.G., 1976, Zh. Eksp. Teor. Fiz. 70, 1477 [Sov. Phys. JETP 43, 770].
Aronov, A.G., and V.L. Gurevich, 1974, Fiz. Tverd. Tela 16, 2656 [1975, Sov. Phys. Solid.

State 16. 1722].
Aronov, A.G., and V.L. Gurevich, 1976, Zh. Eksp. Teor. Fiz. 70, 955 [Sov. Phys. JETP 43, 498].
Aronov, A.G., and B.Z. Spivak, 1977, J. Low Temp. Phys. 29, 149.
Aronov, A.G., and B.Z. Spivak, 1978, Fiz. Nizk. Temp. 4, 1305.
Aronov, A.G., M.A. Zelikman and B.Z. Spivak, 1976, Fiz. Tverd. Tela 18, 2209.
Artemenko, S.N., and A.F. Volkov, 1975a, Zh. Eksp. Teor. Fiz. Pis'ma 21, 662.
Artemenko, S.N., and A.F. Volkov, 1975b, Zh. Eksp. Teor. Fiz. 69, 1764 [Sov. Phys. JETP 42, 896].
Artemenko, S.N., and A.F. Volkov, 1976, Zh. Eksp. Teor. Fiz. 70, 1061 [Sov. Phys. JETP 43, 548]. Artemenko, S.N., and A.F. Volkov, 1979, Usp. Fiz. Nauk 128, 3.
Azbel', M.Ya., 1970, Zh. Eksp. Teor. Fiz. 59, 295 [1971, Sov. Phys. JETP 32, 159].
Betbeder-Matibet, O., and P. Nozires, 1969, Ann. Phys. 51, 392.
Bulyzhenkov, I.E., and B.I. Ivlev, 1976a, Zh. Eksp. Teor. Fiz. 70, 1405.
Bulyzhenkov, I.E., and B.I. Ivlev, 1976b, Zh. Eksp. Teor. Fiz. 71, 1172.
Carlson, P.L., and A.M. Goldman, 1975, Phys. Rev. Lett. 34, 11.
Clarke, J., and M. Tinkham, 1972, Phys. Rev. Lett. 28, 1366.
Clarke, J., B.R. Fjordbge and P. E. Lindelof, 1979, Phys. Rev. Lett. 43, 642.
De Gennes, P., 1968, Superconductivity of Metals and Alloys (Benjamin, New York).
Eliashberg, G.M., 1970, Zh. Eksp. Teor. Fiz. Pis'ma 11, 186 [Sov. Phys. JETP. Lett. 11, 114].
Eliashberg, G.M., 1971, Zh. Eksp. Teor. Fiz. 61, 1254 [Sov. Phys. JETP 34, 668].
Eliashberg, G.M., and B.I. Ivlev, 1985, ch. 6, this volume.
Eilenberger, G., 1968, Z. Phys. 214, 195.
Galaiko, V.P., 1973, Zh. Eksp. Teor. Fiz. 64, 1824 [Sov. Phys. JETP 37, 922].
Galaiko, V.P., 1974, Zh. Eksp. Teor. Fiz. 66, 379 [Sov. Phys. JETP 39, 181].
Galaiko, V.P., 1975, Zh. Eksp. Teor. Fiz. 68, 223 [Sov. Phys. JETP 41, 108].
Galaiko, V.P., and N.B. Kopnin, 1985, ch. 12, this volume.
Galako, V.P., and V.S. Shumeiko, 1976, Zh. Eksp. Teor. Fiz. 71, 671 [Sov. Phys. JETP 44, 353].
Galako, V.P., V.S. Shumeko and T. Kshishton', 1981, Zh. Eksp. Teor. Fiz. 80. 2078.
Galitskii, V.M., V.F. Elesin and Yu.V. Kopaev, 1985, ch. 9, this volume.
Gal'perin, Yu.M., 1974, Zh.Eksp.Teor.Fiz. 67, 2195 [Sov. Phys. JETP 40, 1088].
Gal'perin, Yu.M., 1978, Zh. Eksp. Teor. Fiz. 74, 1126.
Gal'perin, Yu.M., and V.I. Kozub, 1977, Fiz. Nizk. Temp. 3, 1512.
Gal'perin, Yu.M., V.D. Kagan and V.I. Kozub, 1972, Zh. Eksp. Teor. Fiz. 62, 1521 [Sov. Phys. JETP. 35, 798].
Gal'perin, Yu.M., V.L. Gurevich and V.I. Kozub, 1973a, Zh. Eksp. Teor. Fiz. 65, 1045 [1974, Sov. Phys. JETP 38, 517].
Gal'perin, Yu.M., V.L. Gurevich and V.I. Kozub, 1973b, Zh. Eksp. Teor. Fiz. Pis'ma 17, 687.
Gal'perin, Yu.M., V.L. Gurevich and V.I. Kozub, 1974a, Zh. Eksp. Teor. Fiz. 66, 1387 [Sov. Phys. JETP, 39, 680].
Gal'perin, Yu.M., V.L. Gurevich and V.I. Kozub, 1974b, Fiz. Tverd. Tela 16, 1151.
Gal'perin, Yu.M., V.L. Gurevich and V.I. Kozub, 1978, Phys. Rev. B18, 5116.
Gantsevich, S.V., V.L. Gurevich and R. Katilius, 1974, Phys. Kond. Mater. 18, 165.
Garland, J.C., and D.J. Van Harlingen, 1974, Phys. Lett. A47, 423.
Gelikman, B.T., 1958, Zh. Eksp. Teor. Fiz. 34, 1042 [Sov. Phys. JETP 34, 721].
Geilikman, B.T., and M.Yu. Reizer, 1975, Fiz. Tverd. Tela 17, 2002 [Sov. Phys. Solid State 17, 1309].
Ginzburg, V.L., 1944, Zh. Eksp. Teor. Fiz. 14, 177.

Gor'kov, L.P., and G.M. Eliashberg, 1968, Zh. Eksp. Teor. Fiz. 54, 612 [Sov. Phys. JETP 27, 328].
Gor'kov, L.P., and G.M. Eliashberg, 1969, Zh. Eksp. Teor. Fiz. 56, 1297 [Sov. Phys. JETP 29, 698].
Gurevich, L.E., and E.T. Krylov, 1975, Zh. Eksp. Teor. Fiz. Pis'ma 22, 467 [Sov. Phys. JETP Lett. 22, 226].
Kagan, V.D., 1967, Fiz. Tverd. Tela 9, 3293.
Keldysh, L.V., 1964, Zh. Eksp. Teor. Fiz. 47, 1515 [1965, Sov. Phys. JETP 20, 1018].
Kemoklidze, M.P., and L.P. Pitaevskii, 1967, Zh. Eksp. Teor. Fiz. 52, 1556 [Sov. Phys. JETP 25, 1036].
Kon, L.Z., 1975, Fiz. Tverd. Tela 17, 1711 [Sov. Phys. Solid State 17, 1113].
Kon, L.Z., and Yu.N. Nika, 1976, Fiz. Tverd. Tela 18, 3474.
Kozub, V.I., 1978, Zh. Eksp. Teor. Fiz. 74, 344 [Sov. Phys. JETP 47, 178].
Kresin, V.Z., 1959, Zh. Eksp. Teor. Fiz. 36, 1947 [Sov. Phys. JETP 36, 1385].
Landau, L.D., 1946, Zh. Eksp. Teor. Fiz. 16, 574.
Larkin, A.I., and Yu.N. Ovchinnikov, 1973, J. Low Temp. Phys. 10, 407.
Larkin, A.I., and Yu.N. Ovchinnikov, 1977, Zh. Eksp. Teor. Fiz. 73, 299 [Sov. Phys. JETP 46. 155].
Larkin, A.I., and Yu.N. Ovchinnikov, 1985, ch. 11, this volume.
Luttinger, J.M., 1964, Phys. Rev. 136A. 1481.
Ovchinnikov, Yu.N., 1977, Zh. Eksp. Teor. Fiz. 72, 773 [Sov. Phys. JETP 45, 404].
Owen, T.S., and D.J. Scalapino, 1972, Phys. Rev. Lett. 28, 1559.
Pegrum, C.M., and A.M. Gunault, 1976, Solid State Commun. 25, 419.
Pegrum, C.M., A.M. Gunault and C.R. Picket, 1975, Proc. 14th Int. Conf. on Low Temperature Physics (Otaniemi, Finland) vol. 2, 513.
Prange, R.E., and L.P. Kadanoff, 1964, Phys. Rev. 134A, 566.
Privorotskii, I.A., 1962, Zh. Eksp. Teor. Fiz. 42, 450 [Sov. Phys. JETP 42, 315].
Rieger, T.J., D.J. Scalapino and J.E. Mercereau, 1971, Phys. Rev, Lett. 27, 1787.
Rothwarf, A., and B.M. Taylor, 1967, Phys. Rev. Lett. 19, 27.
Schmid, A., 1968, Phys. Kond. Mater. 8, 129.
Schmid, A., 1969, Phys. Rev. 186, 480.
Schmid, A., and G. Schön, 1975a, J. Low Temp. Phys. 20, 207.
Schmid, A., and G. Schön, 1975b, Phys. Rev. Lett. 34, 941.
Schmid, A., and G. Schön, 1979, Phys. Rev. Lett. 43, 793.
Schrieffer, J.R., and D.M. Ginsberg, 1962, Phys. Rev. Lett. 8, 207.
Selzer, P.M., and W.W. Fairbank, 1974, Phys. Lett. 48A, 279.
Shelankov, A.L., 1977, Fiz. Tverd. Tela 19, 3256.
Shelankov, A.L., 1980, Zh. Eksp. Teor. Fiz. 78, 2359.
Stephen, M.J., 1965, Phys. Rev. 139A, 197.
Tinkham, M., 1972, Phys. Rev. B6, 1747.
Van Harlingen, D.J., and J.C. Garland, 1978, Solid State Commun. 25, 419.
Vardanyan, R.A., and B.I. Ivlev, 1973, Zh. Eksp. Teor. Fiz. 65, 2315.
Volkov, A.F., 1974, Zh. Eksp. Teor. Fiz. 66, 758.
Weinreich, G., 1957, Phys. Rev. 107, 317.
Zavaritskii, N.V., 1974, Zh. Eksp. Teor. Fiz. Pis'ma 19, 205.

Bibliography from The kinetic theory of superconductors with excess quasiparticles by V.M. Galitskii, V.F. Elesin and Yu.V. Kopaev

Abrikosov, A.A., and L.P. Gor'kov, 1960, Zh. Eksp. Teor. Fiz. 39, 1781.
Abrikosov, A.A., and I.M. Khalatnikov, 1958, Usp. Fiz. Nauk 65, 551.

Abrikosov, A.A., L.P. Gor'kov and I.E. Dzyaloshinskii, 1962, Metody kvantovoi teorii polya v statisticheskoi fizike (Quantum Field Theoretical Methods in Statistical Physics), Fizmatgiz, Moscow (Engl. trans.: Pergamon Press, Oxford, 1965).
Aronov, A.G., and V.L. Gurevich, 1972, Zh. Eksp. Teor. Fiz. Pis'ma 13, 564.
Aronov, A.G., and V.L. Gurevich, 1973, Zh. Eksp. Teor. Fiz. 65, 1111.
Aronov, A.G., and B.Z. Spivak, 1976, Fiz. Tverd. Tela 18, 541.
Aronov, A.G., and B.Z. Spivak, 1978, Fiz. Nizk. Temp. 4, 1365.
Aronov, A.G., and B.Z. Spivak, 1979, Zh. Eksp. Teor. Fiz, 21, 2868.
Artemenko, S.N., and A.F. Volkov, 1979, Usp. Fiz. Nauk 128, 3.
Balkashin, O.P., I.K. Yanson and A.V. Khotkevich, 1977, Zh. Eksp. Teor. Fiz. 72, 1182.
Baru, V.G., and A.A. Sukhanov, 1975, Zh. Eksp. Teor. Fiz. Pis'ma 21, 209.
Blazhin, A.G., and A.S. Selivanenko, 1970, Fiz. Tekhn. Poluprovodn. 4, 239.
Buimistrov, V.M., 1968, Zh. Eksp. Teor. Fiz. Pis'ma 8, 274.
Buisson, R., R. Chicauft, F. Madeore and R. Romestain, 1978, Phys. Lett. 39, 130.
Chang, J.J., and D.J. Scalapino, 1974, Phys. Rev. B10, 4047.
Chang, J.J., and D.J. Scalapino, 1977, Phys. Rev. B15, 2651.
Chang, J.J., Y.L. Warren and D.J. Scalapino, 1979, Phys. Rev. B20, 2739.
Dmitriev, V.M., and E.V. Khristenko, 1978, Fiz. Nizk Temp. 4, 821.
Dynes, R.C., and V. Narayanamurti, 1972, Phys. Rev. B6, 143.
Dynes, R.C., V. Narayanamurti and J.P. Garno, 1977, Phys. Rev. Lett. 39, 229.
Eckern, V., A. Schmid, M. Schmutz and G. Schön, 1979, J. Low Temp. Phys. 36, 643.
Elesin, V.F., 1969, Fiz. Tverd. Tela 11, 1820.
Elesin, V.F., 1970a, Zh. Eksp. Teor. Fiz. 59, 602.
Elesin, V.F., 1970b, Fiz. Tekhn. Poluprovodn. 4, 1520.
Elesin, V.F., 1974, Zh. Eksp. Teor. Fiz. 66, 1755.
Elesin, V.F., 1975, Zh. Eksp. Teor. Fiz. 69, 572.
Elesin, V.F., 1976, Zh. Eksp. Teor. Fiz. 71, 1490.
Elesin, V.F., 1977a, Zh. Eksp. Teor. Fiz. 72, 365.
Elesin, V.F., 1977b, Fiz. Tverd. Tela 19, 2977.
Elesin, V.F., 1979a, Fiz. Tverd. Tela 21, 2868.
Elesin, V.F., 1979b, Zh. Eksp. Teor. Fiz. 76, 2218.
Elesin, V.F., 1980, Fiz. Tverd. Tela 22, 3097.
Elesin, V.F., 1981, Zh. Eksp. Teor. Fiz. 80, 293.
Elesin, V.F., and Yu.V. Kopaev, 1972, Fiz. Tverd. Tela 14, 669.
Elesin, V.F., and Yu.V. Kopaev, 1974, Fiz. Tverd. Tela 16, 840.
Elesin, V.F., and Yu.V. Kopaev, 1981, Usp. Fiz. Nauk 133, 259.
Elesin, V.F., and E.B. Levchenko, 1978, Fiz. Tverd. Tela 20, 2454.
Elesin, V.F., Yu.V. Kopaev and R.Kh. Timerov, 1973, Zh. Eksp. Teor. Fiz. 65, 2343.
Elesin, V.F., V.V. Kapaev and Yu.V. Kopaev, 1976a, Zh. Eksp. Teor. Fiz. 71, 714.
Elesin, V.F., V.E. Kondrashov and Yu.M. Sklyarov, 1976b, Fiz. Tverd. Tela 18, 3393.
Elesin, V.F., V.E. Kondrashov and B.N. Shamraev, 1977a, Fiz. Tverd. Tela 19, 1525.
Elesin, V.F., V.E. Kondrashov, B.N. Shamraev and A.S. Sukhikh, 1977b, Fiz. Tverd. Tela 19, 3702.
Elesin, V.F., V.E. Kondrashov and A.S. Sukhikh, 1979, Fiz. Tverd. Tela 21, 3225.
Elesin, V.F., V.E. Kondrashov, E.B. Levchenko and A.S. Sukhikh, 1980a, Fiz. Tverd. Tela 22, 1571.
Elesin, V.F., V.E. Kondrashov, E.B. Levchenko and A.S. Sukhikh, 1980b, VINITI, No 1862-80, UDK 537.312.62.
Eliashberg, G.M., 1970, Zh. Eksp. Teor. Fiz. Pis'ma 11, 186.
Eliashberg, G.M., 1971a, Zh. Eksp. Teor. Fiz. 61, 1274.

Eliashberg, G.M., 1971b, Thesis (Landau Inst. Teor. Fiz., Moskva-Chernogolovka).
Fush, J., P.W. Eppelrein, M. Welte and W. Eisenmenger, 1977, Phys. Rev. Lett. 38, 919.
Galitskii, V.M., and V.F. Elesin, 1973, Zh. Eksp. Teor. Fiz. 64, 691.
Galitskii, V.M., S.P. Goreslavskii and V.F. Elesin, 1969, Zh. Eksp. Teor. Fiz. 57, 207.
Galitskii, V.M., V.F. Elesin and Yu.V. Kopaev, 1973, Zh. Eksp. Teor. Fiz. Pis'ma 18, 50.
Galitskii, V.M., V.F. Elesin and V.E. Kondrashov, 1978, Preprint IAE, 3055.
Geilikman, B.T., and V.Z. Kresin, 1969, Usp. Fiz. Nauk 99, 51.
Golovashkin, A.I., K.V. Mitsen and G.P. Motulevich, 1975, Zh. Eksp. Teor. Fiz. 68, 1408.
Golovashkin, A.I., O.M. Ivanenko, K.V. Mitsen, G.P. Motulevich and A.L. Shubin, 1978, Zh. Eksp. Teor. Fiz. 75, 1515.
Golovashkin, A.I., O.M. Ivanenko, K.V. Mitsen, G.P. Motulevich and V.F. Elesin, 1979a, Proc. XX Conf. Fiz. Nizk Temp. (Moskva) ed. W.F. Gantmaher (Institute of Chemical Physics, Academy of Science, USSR) v.3, p. 210.
Golovashkin, A.I., O.M. Ivanenko, K.V. Mitsen and G.P. Motulevich, 1979b, Proc. XVIII Conf. Fiz. Nizk. Temp. (Dresden) p. 24.
Golovashkin, A.I., V.F. Elesin, O.M. Ivanenko, K.V. Mitsen and G.P. Motulevich, 1980, Fiz. Tverd. Tela 21, 105.
Gor'kov, L.P., and L.M. Eliashberg, 1968, Zh. Eksp. Teor. Fiz. 54, 612.
Gor'kov, L.P. and L.M. Eliashberg, 1969. Zh. Eksp. Teor. Fiz. 56, 1297.
Gray, K.E., and H.W. Willemsen, 1978, J. Low Temp. Phys. 31, 911.
Hida, K., 1978a, J. Low Temp. Phys. 32. 881.
Hida, K., 1978b, Phys. Lett. 68 A, 71.
Hu, P., R.C. Dynes and V. Narayanamurti, 1974, Phys. Rev. B10, 2786.
Iguchi, I., 1977. Phys. Rev. B16, 1954.
Iguchi, I., D. Kent, H. Gilmartin and D.N. Langenberg, 1981, Phys. Rev. 23, 3240.
Imai, S., 1980, J. Low Temp. Phys. 40, 595.
Janik, R., L. Morli, N.C. Cirillo, T.N. Lechevet, W.D. Gregory and W.L. Goodman, 1975, IEEE Trans. Magn. Mag-11, 687.
Jaworsky, F., and W.H. Parker, 1979, Phys. Rev. B20, 945.
Kaplan, S.B., J.R. Kirtley and D.N. Langenberg, 1977, Phys. Rev. Lett. 39, 291.
Keldysh, L.V., 1964, Zh. Eksp. Teor. Fiz. 47, 1515.
Keldysh, L.V., and Yu.V. Kopaev, 1964, Fiz. Tverd. Tela 6, 2791.
Kemoklidze, M.L., and L.P. Pitaevskii, 1967, Zh. Eksp. Teor. Fiz. 52, 1556.
Kirichenko, I.K., and V.P. Seminozhenko, 1977, Fiz. Nizk. Temp. 3, 987.
Kirichenko, I.K., S.A. Peskovatskii and V.P. Seminozhenko, 1976, Preprint, IAE Akad. Nauk, No 74. Kiev.
Kirzhnits, D.A., and Yu.V. Kopaev, 1973, Zh. Eksp. Teor. Fiz. Pis'ma 17, 379.
Kumar, N., and K.P. Sinha, 1968, Phys. Rev. 174, 482.
Lambert, D., D. Salin, and T. Joffin, 1977, J. Phys. Lett. 38, 368.
Langenberg, D.N., 1975, Proc. LT-14, 14th Int. Conf. on Low Temperature Physics (Otaniemi, Finland) eds. M. Krusius and M. Vuorio vol. 5, p. 223.
Mitsen, K.V., 1979, Fiz. Tverd. Tela 21, 3475.
Mitsen, K.V., 1981, Thesis (FIAN, Moskva).
Mitsen, K.V., G.P. Motulevich, A.I. Golovashkin and O.M. Ivanenko, 1981, Solid State Commun. 38. 6366.
Owen, C.S., and D.J. Scalapino, 1972, Phys. Rev. Lett. 28, 1559.
Pan, V.M., and E.M. Rudenko, 1981, Zh. Eksp. Teor. Fiz. Pis'ma 34, 57.
Parker, W.H., 1975, Phys. Rev. B12, 3667.
Ryvkin, S.M., 1963, Fotoelectricheskie Yavleniya v Poluprovodnikakh (Fizmatgiz, Moskva).
Sai-Halasz, C.A., C.C. Chi, A. Denstein and D.N. Langenberg, 1974, Phys. Rev. Lett. 33, 215.

Scalapino, D.N., and B.A. Huberman, 1977, Phys. Rev. Lett. 39, 1365.
Schön, A., and M. Tremblay, 1979, Phys. Rev. Lett. 42, 1086.
Smith, L.N., 1977, J. Low Temp. Phys. 28, 519.
Smith, L.N., 1980, J. Low Temp. Phys. 38, 553.
Testardi, L.R., 1971, Phys. Rev. B4, 2189.
Tremblay, A.-M.S., 1981, Stability of nonequilibrium superconductivity states, in: Nonequilibrium Superconductivity, Phonons, and Kapitza Boundaries (Proc. NATO ASI), ed. K.E. Gray (Plenum, New York) chs. 10 and 11.
Vardanyan, R.A., and B.I. Ivlev, 1973, Zh. Eksp. Teor. Fiz. 52, 1556.
Volkov, A.F., and Sh.M. Kogan, 1968, Usp. Fiz. Nauk 96, 633.
Willemsen, H.W. and K.E. Gray, 1978, Phys. Rev. Lett. 41, 812.

Bibliography from Kinetic equations in superconducting thin films by Jhy-Jiun Chang

Chang, Jhy-Jiun, and D.J. Scalapino, 1977c, Phys. Rev. B15, 2651.
Chang, Jhy-Jiun, and D.J. Scalapino, 1978, J. Low Temp. Phys. 31, 1.
Chang, Jhy-Jiun, W.Y. Lai and D.J. Scalapino, 1979, Phys. Rev. B20, 2739.
Chi, C.C., and J. Clarke, 1979a, Phys. Rev. B19, 4495.
Chi, C.C., and J. Clarke, 1979b, Phys. Rev. B20, 4465.
Clarke, J., 1972, Phys. Rev. Lett. 28, 1363.
Clarke, J., 1981, Charge imbalance, in: Nonequilibrium Superconductivity, Phonons and Kapitza Boundaries (Proc. NATO ASI), ed. K.E. Gray (Plenum, New York) ch. 13.
Cohen, M.G., L.N. Falicov and J.C. Phillips, 1962, Phys. Rev. Lett. 8, 316.
Dayem, A.H., and J.J. Wiegand, 1967, Phys. Rev. 155, 419.
Dayem, A.H., and J.J. Wiegand, 1972, Phys. Rev. B5, 4390.
Dynes, R.C., and V. Narayanamurti, 1972, Phys. Rev. B6, 143.
Dynes, R.C., V. Narayanamurti and M. Chin, 1971, Phys. Rev. Lett. 26, 181.
Eisenmenger, W., 1981, Nonequilibrium phonons, in: Nonequilibrium Superconductivity, Phonons, and Kapitza Boundaries (Proc. NATO ASI), ed. K.E. Gray (Plenum, New York) ch. 3.
Eisenmenger, W., and A.H. Dayem, 1967, Phys. Rev. Lett. 18, 125.
Elesin, V.F., 1979, Sov. Phys. JETP 49, 1121.
Eliashberg, G.M., 1970a, JETP Lett. 11, 696.
Eliashberg, G.M.. 1970b, JETP Lett. 11, 114.
Eliashberg, G.M., 1972, Sov. Phys. JETP 34, 668.

---

[0]Ambegaokar, V., and L. Tewordt 1964, Phys. Rev. A134, 805.
Bardeen, J., 1961, Phys. Rev. Lett. 6, 57.
Bardeen, J., 1962, Phys. Rev. Lett. 9, 147.
Bardeen, J., L.N. Cooper and J.R. Schrieffer, 1957, Phys. Rev. 108, 1175.
Bardeen, J., G. Rickayzen and L. Tewordt, 1959, Phys. Rev. 113, 982.
Chang, Jhy-Jiun, 1977, Phys. Rev. Lett. 39, 1352.
Chang, Jhy-Jiun, 1978, Phys. Rev. B17, 2137.
Chang, Jhy-Jiun, 1979, Phys. Rev. B19, 1420.
Chang, Jhy-Jiun, 1981, Properties of nonequilibrium superconductors: A kinctic equation approach, in: Nonequilibrium Superconductivity, Phonons, and Kapitza Boundaries (Proc. NATO ASI), ed. K.E. Gray (Plenum, New York) ch. 9.
Chang, Jhy-Jiun, and D.J. Scalapino, 1974, Phys. Rev. B10, 4047.
Chang, Jhy-Jiun, and D.J. Scalapino, 1976, Phys. Rev. Lett. 37, 522.
Chang, Jhy-Jiun, and D.J. Scalapino, 1977a, IEEE Trans. Magn. MAG-13, 747.
Chang, Jhy-Jiun, and D.J. Scalapino, 1977b, Hot superconductors- The physics and application of nonequilibrium superconductivity, in: Superconductor Applications: SQUIDS and Machines, eds. B.B. Schwartz and S. Foner (Plenum, New York).

Entin-Wohlman, O., and R. Orbach, 1979a, Ann. Phys. 122, 64.
Entin-Wohlman, O., and R. Orbach, 1979b, Phys. Rev. B19, 4510.
Gray, K.E., 1969, Quasiparticle lifetime in superconducting aluminium, Ph.D. Thesis (Cambridge Univ.).
Gray, K.E., 1978, Solid State Commun. 26, 633.
Hall, J.T., L.B. Holdeman and R.J. Soulen, 1980, Phys. Rev. Lett. 45, 1011.
Hall, J.T., L.B. Holdeman and R.J. Soulen, 1981, Physica 108 B + C, 827.
Hida, K., 1978, J. Low Temp. Phys. 32, 881.
Horstman, R.E., J. Wolter and E.J. Bartels, 1981, Physica B + C, 833.
Ivlev, B.I., and G.M. Eliashberg, 1971, JETP Lett. 13, 333.
Ivlev, B.I., S.G. Lisitsyn and G.M. Eliashberg, 1973, J. Low Temp. Phys. 10, 449.
Jaworski, F., and W.H. Parker, 1979, Phys. Rev. B20, 945.
Kaplan, S.B., C.C. Chi, D.N. Langenberg, Jhy-Jiun Chang, S. Jafarey and D.J. Scalapino, 1976, Phys. Rev. B14, 4854.
Kaplan, S.B., J.R., Kirtley and D.N. Langenberg, 1977, Phys. Rev. Lett. 39, 291.
Kirtley, J.R., D.S. Kent, D.N. Langenberg, S.B. Kaplan, Jhy-Jiun Chang and Chi-Chung Yang, 1980, Phys. Rev. B22, 1218.
Kommer, T., and J. Clarke, 1977, Phys. Rev. Lett. 38, 1091.
Lemberger, T.R., and J. Clarke. 1981, Phys. Rev. B23, 1088, 1100.
Little, W.A., 1959, Can. J. Phys. 37, 334.
Mattis, D.C., and J. Bardeen, 1958, Phys. Rev. 111, 412.
Moody, M.V., and J.L. Paterson, 1978 J. Low Temp. Phys. 34, 83.
Moody, M.V., and J.L. Paterson, 1981, Phys. Rev. B23, 133.
Mooij, J.E., 1981, Enhancement of superconductivity, in: Nonequilibrium Superconductivity, Phonons, and Kapitza Boundaries (Proc. NATO ASI), ed. K.E. Gray (Plenum, New York) ch. 7.
Narayanamurti, V., and R.C. Dynes, 1971, Phys. Rev. Lett. 27, 410.
Owen, C.S., and D.J. Scalapino, 1972, Phys. Rev. Lett. 28, 1559.
Parker, W.H., 1975, Phys. Rev. B12, 3667.
Parmenter, R.H., 1961, Phys. Rev. Lett. 7, 274.
Paterson, J.L., 1978, J. Low Temp. Phys. 33, 285.
Peskovatskii, S.A., and V.P. Seminozenko, 1976, Sov. J. Low Temp. Phys. 2, 464.
Pethick, C.J., and H. Smith, 1980, J. Phys. C13, 6313.
Prange, R.E., and L.P. Kadanoff, 1964, Phys. Rev. A134, 566.
Rothwarf, A., and B.N. Taylor, 1967, Phys. Rev. Lett. 19, 27.
Rutledge, J.R., R.C. Dynes and V. Narayanamurti, 1979, Bull. Am. Phys. Soc. 24, 330.
Scalapino, D.J., 1969, The electron-phonon coupling and strong superconductors, in: Superconductivity, ed. R.D. Parks (Marcel Dekker, New York) ch. 10.
Scalapino, D.J., and B.A. Huberman, 1977, Phys. Rev. Lett. 39, 1365.
Schmid, A., 1977, Phys. Rev. Lett. 38, 922.
Schmid, A., and G. Schön, 1975, J. Low Temp. Phys. 20, 207.
Schrieffer, J.R., 1964, Theory of superconductivity (Benjamin, New York) chs. 2 and 3.
Seligson, D., and J. Clarke, 1982, Bull. Am. Phys. Soc. 27, 252.
Smith, A.D., W.J. Skocpol, and M. Tinkham, 1980, Phys. Rev. B21, 3879.
Tinkham, M., 1972, Phys. Rev. B6, 1747.
Tinkham, M., and J. Clarke, 1972, Phys. Rev. Lett. 28, 1366.
Tremblay, A.-M.S., 1981, Stability of nonequilibrium superconducting states, in: Nonequilibrium Superconductivity, Phonons, and Kapitza Boundaries (Proc. NATO ASI), ed. K.E. Gray (Plenum, New York) chs. 10 and 11.
Willemsen, H.W., and K.E. Gray, 1978. Phys. Rev. Lett. 41, 812.

Wyatt, A.F.G., V.M. Dmitriev, W.S. Moore and R.W. Sheard, 1966, Phys. Rev. Lett. 16, 1166.

Bibliography from Vortex motion in superconductors by A.J. Larkin and Yu.N. Ovchinnikov

Abrikosov, A.A., 1957, On magnetic properties of type II superconductors, Zh. Eksp. Teor. Fiz. 32, 1442 [Sov. Phys. JETP 5, 1174].
Bardeen, J., and R.D. Sherman, 1975, Flux flow in nearly pure low- κ superconductors, Phys. Rev. B12, 2634.
Bardeen, J., and M.J. Stephen, 1965, Theory of the motion in superconductors, Phys. Rev. 140, A1197.
Brandt, E.H., 1976, On the shear modulus of the flux line lattice, Phys. Stat. Sol. (b) 77, 551.
Brandt, E.H., 1977, Elastic energy of the vortex state in type II superconductors. I. High Inductions, J. Low Temp. Phys. 26, 709; II. Low Induction, 735.
Borka, S., I.N. Goncharov, D. Frichevski and I.S. Khukhareva, 1977, Investigation of vortex pinning forces in superconducting $Nb - Zr$ alloys with low j_c, Fiz. Nizk. Temp. 3, 716.
Caroli, C., M. Cyrot and P.G. De Gennes, 1966, The magnetic behaviour of dirty superconductors, Solid State Commun. 4, 17.
Chang, C.C., and J.B. McKinnon, 1968, On the occurrence of the peak effect in type-II superconductors, Phys. Lett. 27 A, 414.
Chang, C.C., J.B. McKinnon and A.C. Rose-Innes, 1969, Peak effect in Type-II Superconductors: Yield point of the Fluxon lattice, Phys. Stat. Sol. 36, 205.
Danilov, V.V., M.Yu. Kupriyanov and K.K. Likharev, 1974, On resistance of superconductors in a dynamic mixed state, Fiz. Tverd. Tela 16, 935.
Eilenberger, G., 1968, Transformation of Gor'kov's equation for type II superconductors into transport-like equations, Z. Phys. 214, 195.
Eliashberg, G.M., 1971, Electron inelastic collisions and nonequilibrium stationary states in superconductors, Zh. Eksp. Teor. Fiz. 61, 1254.
Fiory, A.T., 1971, Quantum interference effects of a moving vortex lattice in Al films, Phys. Rev. Lett. 27, 501.
Gor'kov, L.P., 1958, On the energy spectrum of superconductors, Zh. Eksp. Teor. Fiz. 34, 735.
Gorkov, L.P., 1959, Theory of superconducting alloys in a strong magnetic field near the critical temperature, Zh. Eksp. Teor. Fiz. 37, 1407 [1960, Sov. Phys. JETP 10, 998].
Gor'kov, L.P., and N.B. Kopnin, 1973a, Some features of viscous flow of vortexes in superconducting alloys near the critical temperature, Zh. Eksp. Teor. Fiz. 64, 356 [Sov. Phys. JETP 37, 183].
Gor'kov, L.P., and N.B. Kopnin, 1973b, Viscous flow of vortexes in type II superconducting alloys, Zh. Eksp. Teor. Fiz. 65, 396 [1974, Sov. Phys. JETP 38, 195].
Ioffe, L., and A.I. Larkin, 1981, Properties of Superconductors with Smearing-out Transition Temperature, Zh. Eksp. Teor. Fiz. 81, 707 [Sov. Phys. JETP 54, 378].
Keldysh, L.V., 1964, Diagram technique for nonequilibrium processes, Zh. Eksp. Theor. Fiz. 47, 1515 [1965, Sov. Phys. JETP 20, 1018].
Kramer, E.J., 1978, Summation curves for flux pinning in superconductors, J. Appl. Phys. 49, 742.
Kramer, L., and W. Pesch, 1974, Core structure and low-energy spectrum of isolated vortex lines in clean superconductors as $T \ll T_c$, Z. Phys. 269, 59.
Kpfer, H., and A.A. Manuel, 1979, Summation and Saturation Behaviour of the Volume Pinning Force in Neutron Irradiated V_3Si, Phys. Stat. Sol. (a) 54, 153.
Labusch, R., 1967, Elastische Konstanten des Flussfadengitters in Supraleitern zweiter Art,

Phys. Stat. Sol. 19, 715.
Labusch, R., 1969a, Elastic constants of the fluxoid lattice near the upper critical field, Phys. Stat. Sol. 32, 493.
Labusch, R., 1969b, Calculation of the critical field gradient in type II superconductors, Cryst. Lattice Defects 1, 1.
Larkin, A.I., 1970, Effect of inhomogeneities on the structure of the mixed state of superconductors, Zh. Eksp. Teor. Fiz. 58, 1466 [Sov. Phys. JETP 31, 784].
Larkin, A.L., and Yu.N. Ovchinnikov, 1968, On the quasiclassical method in superconductivity theory, Zh. Eksp. Teor. Fiz. 55, 2262 [1969, Sov. Phys. JETP 28, 1200].
Larkin, A.L., and Yu.N. Ovchinnikov, 1973a, Fluctuation conductivity in the vicinity of the superconducting transition, J. Low Temp. Phys. 10, 407.
Larkin, A.I., and Yu.N. Ovchinnikov, 1973b, Resistance of superconductors near the critical field H_{C2}, Zh. Eksp. Teor. Fiz. 64, 1096 [Sov. Phys. JETP 37, 557].
Larkin, A.I., and Yu.N. Ovchinnikov, 1973c, Electrodynamics of inhomogeneous type II superconductors, Zh. Eksp. Teor. Fiz. 65, 1704 [1974, Sov. Phys. JETP 38, 854].
Larkin, A.I., and Yu.N. Ovchinnikov, 1975, Nonlinear conductivity of superconductors in the mixed state, Zh. Eksp. Teor. Fiz. 68, 1915 [1976, Sov. Phys. JETP 41, 960].
Larkin, A.I., and Yu.N. Ovchinnikov, 1976, Vortex viscosity in clean superconductors, Zh. Eksp. Teor. Fiz. Pis'ma 23, 210.
Larkin, A.I., and Yu.N. Ovchinnikov, 1977, Nonlinear effects during the motion of vortexes in superconductors, Zh. Eksp. Teor. Fiz. 73, 299 [Sov. Phys. JETP 46, 155].
Larkin, A.I., and Yu.N. Ovchinnikov, 1978, Peak-effect in the dependence of the superconductor critical current on the magnetic field, Zh. Eksp. Teor. Fiz. Pis'ma 27, 301.
Larkin, A.I., and Yu.N. Ovchinnikov, 1979, Pinning in type II superconductors, J. Low Temp. Phys. 34, 409.
Larkin, A.I., and Yu.N. Ovchinnikov, 1981, Volt-ampere characteristic of superconductors with large-size defects, Zh. Eksp. Teor. Fiz. 80, 2334 [Sov. Phys. JETP 53, 1221].
Maki, K., 1966, Electrodynamics of superconducting alloys in high magnetic fields, Phys. Rev. 141, 331.
Meier-Hirmer, R., M. David Maloney and M. Gey, 1976, Temperature dependence of the flux flow resistance near H_{C2} in $Pb-In$ alloys, Z . Phys. B23, 139.
Musienko, L.E., I.M. Dmitrenko and V.G. Volotskaya, 1980, On nonlinear conductivity of thin films in a mixed state, Zh. Eksp. Teor. Fiz. Pis'ma 31, 603.
Osborne, K.E., and E.J. Kramer, 1974, The influence of plastic deformation on the peak effect in a type II superconductor, Phil. Mag. 29, 685.
Ovchinnikov, Yu.N., 1974, Conductivity of type II superconductors near the critical field H_{C2} for arbitrary free paths, Zh. Eksp. Teor. Fiz. 66, 1100 [Sov. Phys. JETP 39, 538].
Ovchinnikov, Yu.N., 1980, Metastable states and one-particle pinning in type II superconductors near the critical field- H_{C2}, Zh. Eksp. Teor. Fiz. 79, 1825 [Sov. Phys. JETP 52, 923].
Ovchinnikov, Yu.N., and E.H. Brandt, 1975, Properties of type-II superconductors with arbitrary impurity concentration near H_{C2}, Phys. Stat. Sol. (b) 67, 301.
Reichert, T., R. Meier-Hirmer and H. Kpfer, 1981, Annealing behavior of the critical current density and the superconducting parameters T_c, κ, and H_{C2} in a neutron-irradiated V_3 Si single crystal, Phys. Stat. Sol. (a) 64, 585.
Schmid, A., 1981, Kinetic equations for dirty superconductors, in: Nonequilibrium Superconductivity, Phonons, and Kapitza Boundaries (Proc. NATO ASI), ed. K.E. Gray (Plenum, New York).
Schmid, A., and W. Hauger, 1973, On the theory of vortex motion in an inhomogeneous superconducting film, J. Low Temp. Phys. 11, 667.
Schmid, A., and G. Schön, 1975, Linearized kinetic equations and relaxation processes of a

superconductor near T_c, J. Low Temp. Phys. 20, 207.
Shelankov, A.L., 1980, Normal component drag by the condensate in nonequilibrium superconductors, Zh. Eksp. Teor. Fiz. 78, 2359 [Sov. Phys. JETP 51, 1186].
Shubnikov, L.V., V.I. Khotkevich, Yu.D. Shepelev and Yu.N. Ryabinin, 1937, Magnetic properties of superconducting metals and alloys, Zh. Eksp. Teor. Fiz. 7, 221.
Strnad, A.R., C.F. Hempstead and Y.B. Kim, 1964, Dissipative mechanism in type-II superconductors, Phys. Rev. Lett. 13, 794.
Thompson, R.S., 1970, Microwave, flux flow and fluctuation resistance of dirty type-II superconductors, Phys. Rev. B1, 327.
Tinkham, M., 1964, Viscous flow of flux in type-II superconductors, Phys. Rev. Lett. 13, 804.
Truble, H., and U. Essmann, 1968, Flux-line arrangement in superconductors as revealed by direct observation, J. Appl. Phys. 39, 4052.
Vinnikov, L.Ya., V.I. Grigoriev and O.V. Zharikov, 1976, The resistive state and pinning in deformed niobium single crystals, Zh. Eksp. Teor. Fiz. 71, 252 [Sov. Phys. JETP 44, 1976].
Watts-Tobin, R.J., Y. Krhenbhl and L. Kramer, 1981, Nonequilibrium theory of dirty current carrying superconductors: phase-slip oscillators in narrow filaments near T_c, J. Low Temp. Phys. 42, 459.

Bibliography from Theory of the resistive state in narrow superconducting channels by V.P. Galaiko and N.B. Kopnin

Galako, V.P., 1976a, Zh. Eksp. Teor. Fiz. 71, 273.
Galako, V.P., 1976b, Fiz. Nizk. Temp. 2, 807.
Galaiko, V.P., 1977, J. Low Temp. Phys. 26, 483.
Galaiko, V.P., and V.S. Shumeko, 1976, Zh. Eksp. Teor. Fiz. 71, 761.
Galako, V.P., V.M. Dmitriev and G. E. Churilov, 1973, Zh. Eksp. Teor. Fiz. Pis'ma 18, 362.
Galako, V.P., V.M. Dmitriev and G.E. Churilov, 1976, Fiz. Nizk. Temp. 2, 299.
De Gennes, P.G., 1966, Superconductivity of Metals and Alloys (Benjamin, New York).
Golub, A.A., 1976, Zh. Eksp. Teor. Fiz. 71, 341.
Gor'kov, L.P., 1970, Zh. Eksp. Teor. Fiz. Pis'ma 11, 52.
Gor'kov, L.P., and G.M. Eliashberg, 1968, Zh. Eksp. Teor. Fiz. 54, 612.
Gor'kov, L.P., and G.M. Eliashberg, 1969, Zh. Eksp. Teor. Fiz. 56, 1297.
Gor'kov, L.P., and N.B. Kopnin, 1975, Usp. Fiz. Nauk 116, 413.
Huebner, R.P., and D.E. Gallus, 1973, Phys. Rev. B7, 4089.
Ivlev, B.I., and N.B. Kopnin, 1978, Zh. Eksp. Teor. Fiz. Pis'ma 28, 640.
Ivlev, B.I., and N.B. Kopnin, 1980, Zh. Eksp. Teor. Fiz. 79, 672.
Ivlev, B.I., and N.B. Kopnin, 1981, J. Low Temp. Phys. 44, 453.
Ivlev, B.I., and N.B. Kopnin, 1982, Solid State Commun. 41, 107.
Ivlev, B.I., N.B. Kopnin and L.A. Maslova, 1980a, Fiz. Tverd. Tela 22, 252.
Ivlev, B.I., N.B. Kopnin and L.A. Maslova, 1980b, Zh. Eksp. Teor. Fiz. 78, 1963.
Ivlev, B.I., N.B. Kopnin and V.I. Mel'nikov, 1980c, Fiz. Tverd. Tela 22, 3386.
Ivlev, B.I., N.B. Kopnin and C.J. Pethick, 1980d, Zh. Eksp. Teor. Fiz. 79, 1017.
Ivlev, B.I., N.B. Kopnin and C.J. Pethick, 1980e, J. Low Temp. Phys. 41, 297.
Kadin, A.M., W.J. Skocpol and M. Tinkham, 1978, J. Low Temp. Phys. 33, 481.
Kramer, L., and A. Baratoff, 1977, Phys. Rev. Lett. 38, 518.
Kramer, L., and R.J. Watts-Tobin, 1978a, Phys. Rev. Lett. 40, 1041.
Kramer, L., and R.J. Watts-Tobin, 1978b, in: Proc. 15th Int. Conf. on Low Temperature Physics, J. Physique, Suppl. no. 8, tome 39, C6-554.
Kulik, I.O., 1970, Zh. Eksp. Teor. Fiz. 59, 584.
Landau, I.L., and Yu.V. Sharvin, 1969, Zh. Eksp. Teor. Fiz. Pis'ma 10, 192.
Landau, I.L., and Yu.V. Sharvin, 1972, Zh. Eksp. Teor. Fiz. Pis'ma 15, 88.

Langer, J.S., and V. Ambegaokar, 1967, Phys. Rev. 164, 498.
Larkin, A.I., and Yu.N. Ovchinnikov, 1985, ch. this volume.
Likharev, K.K., 1974, Zh. Eksp. Teor. Fiz. Pis'ma 20, 730.
Little, W.A., 1967, Phys. Rev. 156, 396.
Lukens J.E., R.J. Warburton and W.W. Webb, 1970, Phys. Rev. Lett. 25, 1180.
McCumber, D.E., and B.I. Halperin, 1970, Phys. Rev. B1, 1054.
Meyer, J., and G. von Minnigerode, 1972, Phys. Lett. 38 A, 529.
Newbower, R.S., M.R. Beasley and M. Tinkham, 1972, Phys. Rev. B6, 864.
Rieger, T.J., D.J. Scalapino and J.E. Mercereau, 1972, Phys. Rev. B6, 1734.
Schmid, A., 1966, Phys. Kondens. Mater. 5, 302.
Schmid, A., and G. Schön, 1975, J. Low Temp. Phys, 20, 207.
Schön, G., and V. Ambegaokar, 1979, Phys. Rev. B19, 3515.
Skocpol, W.J., M.R. Beasley and M. Tinkham, 1974, J. Low Temp. Phys. 16, 145.
Smith, L.N., 1980, J. Low Temp. Phys. 38, 553.
Tinkham, M., 1972, Phys. Rev. B6, 1747.
Tinkham, M., 1979, J. Low Temp. Phys. 35, 147.
Tinkham, M., and J. Clarke, 1972, Phys. Rev. Lett. 28, 1366.
Tucker, J.R., and B.I. Halperin, 1971, Phys. Rev. B3, 3768.
Volkov, A.F., and Sh. M. Kogan, 1974, JETP Lett. 19, 4.
Watts-Tobin, R.J., Y. Krhenbhl and L. Kramer, 1981, J. Low Temp. Phys. 42, 459.
Webb, W.W., and R.J. Warburton, 1968, Phys. Rev. Lett. 20, 461.

Bibliography from Collective modes in superconductors by G. Schon

Abrahams, E., and T. Tsuneto, 1966, Phys. Rev. 152, 416.
Ambegaokar, V., and L.P. Kadanoff, 1961, Nuovo Cimento 22, 914.
Anderson, J.T., R.V. Carlson and A.M. Goldman, 1972, J. Low Temp. Phys. 8, 29.
Anderson, P.W., 1958, Phys. Rev. 110, 827; 112, 1900.
Aronov, A.G., and V.L. Gurevich, 1974, Fiz. Tverd. Tela 16, 2656 [1975, Sov. Phys. Solid State 16, 1722].
Artemenko, S.A., and A.F. Volkov, 1975, Zh. Eksp. Teor. Fiz. 69, 1764 [Sov. Phys. JETP 42, 896].
Artemenko, S.A., and A.F. Volkov, 1979, Usp. Fiz. Nauk 128, 3 [1980, Sov. Phys. Usp. 22, 295].
Aspen, F.E., and A.M. Goldman, 1979, Phys. Rev. Lett. 43, 307.
Aspen, F.E., and A.M. Goldman, 1981, J. Low Temp. Phys. 43, 559.
Balseiro, C.A., and L.M. Falicov, 1980, Phys. Rev. Lett. 45, 662.
Baratoff, A., 1982, in: Proc. 16th Int. Conf. on Low Temperature Physics, Part III, Physica 109 & **110B** + **C**, 2058.
Bardeen, J., 1957, Nuovo Cimento 5, 1766.
Bardeen, J., 1958, Phys. Rev. Lett. 1, 399.
Bardeen, J., L.N. Cooper and J.R. Schrieffer, 1957, Phys. Rev. 108, 1175.
Bardeen, J., G. Rickayzen and L. Tewordt, 1959, Phys. Rev. 113, 982.
Baym, G., 1962, Phys. Rev. 127, 1391.
Baym, G., and L.P. Kadanoff, 1961, Phys. Rev. 124, 287.
Bezuglyi, E.V., and E.N. Bratus', 1981, Physica 107B, 167.
Bezuglyi, E.V., E.N. Bratus' and V.P. Galaiko, 1982, J. Low Temp. Phys. 47, 511.
Bogoliubov, N.N., V.V. Tolmachev and D.N. Shirkov, 1959, New Method in the Theory of Superconductivity (Consultants Bureau, New York).
Bray, A.J., and H. Schmidt, 1975a, J. Low Temp. Phys. 21, 669.
Bray, A.J., and H. Schmidt, 1975b, Solid State Commun. 17, 1175.

Brieskorn, G., M. Dinter and H. Schmidt, 1974, Solid State Commun. 15, 757.
Byrd, P.F., and M.D. Friedman, 1971, Handbook of Elliptic Integrals for Engineers and Scientists (Springer, Berlin).
Carlson, R.V., 1975, Thesis (Univ. of Minnesota).
Carlson, R.V., and A.M. Goldman, 1973, Phys. Rev. Lett. 31, 880.
Carlson, R.V., and A.M. Goldman, 1975, Phys. Rev. Lett. 34, 11.
Carlson, R.V., and A.M. Goldman, 1976, J. Low Temp. Phys. 27, 67.
Cheishvili, O.D., 1977, Fiz. Nizk. Temp. 3, 736 [Sov. J. Low Temp. Phys. 3, 357].
Cheishvili, O.D., 1982, J. Low Temp. Phys. 48, 445.
Chi, C.C., and J. Clarke, 1979, Phys. Rev. B19, 4495.
Clarke, J., 1972, Phys. Rev. Lett. 28, 1363.
Dinter, M., 1978a, Phys. Rev. B18, 3163.
Dinter, M., 1978b, J. Low Temp. Phys. 32, 529.
Eckern, U., and A. Schmid, 1981, J. Low Temp. Phys. 45, 137.
Eckern, U., and G. Schön, 1978, J. Low Temp. Phys. 32, 821.
Eilenberger, G., 1968, Z. Phys. 214, 195.
Eliashberg, G.M., 1971, Zh. Eksp. Teor. Fiz. 61, 1254 [1972, Sov. Phys. JETP 34, 668].
Entin-Wohlman, O., and R. Orbach, 1978, Ann. Phys. 116, 35.
Enz, C.P., 1974, Rev. Mod. Phys. 46, 705.
Ferrell, R.A., 1969, J. Low Temp. Phys. 1, 423.
Galako, V.P., N.I. Glushchik and V.S. Shumeko, 1978, Fiz. Nizk. Temp. 4, 289 [Sov. J. Low Temp. Phys. 4, 139].
Ginzburg, V.L., 1961, Zh. Eksp. Teor. Fiz. 41, 828 [1962, Sov. Phys. JETP 14, 594].
Goldman, A.M., 1981, in: Nonequilibrium Superconductivity, Phonons and Kapitza Boundaries (Proc. NATO ASI), ed. K.E. Gray, (Plenum, New York).
Gor'kov, L.P., and G.M. Eliashberg, 1970, J. Low Temp. Phys. 2, 161.
Hu, C.R., 1980, Phys. Rev. B21, 2775.
Jillie, D.W., J.E. Lukens and Y.H. Kao, 1977, IEEE Trans. Magn. Mag 13, 578.
Kadanoff, L.P.. and P.C. Martin, 1961, Phys. Rev: 124, 670.
Kadin, A.M., and A.M. Goldman, 1982, Phys. Rev. B25, 6701.
Kadin, A.M., L.N. Smith and W.J. Skocpol, 1980, J. Low Temp. Phys. 38, 497.
Kadin, A.M., C. Varmazis and J.E. Lukens, 1981, Physica 107B, 159.
Kaplan, S.B., C.C. Chi, D.N. Langenberg, J.-J. Chang, S. Jafarey and D.J. Scalapino, 1976, Phys. Rev. B14, 4854.
Keldysh, L.V., 1964, Zh. Eksp. Teor. Fiz. 47, 1515 [1965 Sov. Phys. JETP 20, 1018].
Khalatnikov, I.M., 1965, An Introduction to the Theory of Superfluidity (Benjamin, New York).
Khalatnikov, I.M., 1969, Zh. Eksp. Teor. Fiz. 57, 489 [Sov. Phys. JETP 30, 268].
Kulik, I.O., 1979, Fiz. Nizk. Temp. 5, 1391 [Sov. J. Low Temp. Phys. 5, 656].
Kulik, I.O., O. Entin-Wohlman and R. Orbach, 1981, J. Low Temp. Phys. 43, 591.
Landau, L.D., 1956, Zh. Eksp. Teor. Fiz. 30, 1058 [1957, Sov. Phys. JETP 3, 920].
Landau, L.D., 1957, Zh. Eksp. Teor. Fiz. 32, 59 [Sov. Phys. JETP 5, 101].
Landau, L.D., 1958, Zh. Eksp. Teor. Fiz. 35, 95 [1959, Sov. Phys. JETP 8, 70].
Landau, L.D., and E.M. Lifshitz, 1959, Fluid Mechanics (Addison-Wesley, Reading, MA), $78.
Larkin, A.I., and A.B. Migdal, 1963, Zh. Eksp. Teor. Fiz. 44, 1703 [Sov. Phys. JETP 17, 1146].
Larkin, A.I., and Yu.N. Ovchinnikov, 1968, Zh. Eksp. Teor. Fiz. 55, 2262 [1969, Sov. Phys. JETP 28, 1200].
Larkin, A.I., and Yu.N. Ovchinnikov, 1977, Zh. Eksp. Teor. Fiz. 73, 295 [Sov. Phys. JETP 46, 155].
Larkin, A.I., and Yu.N. Ovchinnikov, 1981, preprint; see their chapter in the present volume.

Leggett, A.J., 1965, Phys. Rev. A140, 1869.
Leggett, A.J., 1966, Phys. Rev. 147, 119.
Leggett, A.J., 1975, Rev. Mod. Phys. 47, 331.
Lemberger, T.R., and J. Clarke, 1981, Phys. Rev. B23, 1100.
Lindelof, P.E., and J. Bindslev Hansen, 1977, J. Low Temp. Phys. 29, 369.
Littlewood, P.B., and C.M. Varma, 1981, Phys. Rev. Lett. 47, 811.
Maki, K., and H. Sato, 1974, J. Low Temp. Phys. 16, 557.
Martin, P.C., 1969, in: Superconductivity, vol. 1, ed. R.D. Parks (Marcel Dekker, New York), ch. 7.
Mattis, D.C., and J. Bardeen, 1958, Phys. Rev. 111, 412.
Nambu, Y., 1960, Phys. Rev. 117, 648.
Ovchinnikov, Yu.N., 1970, Zh. Eksp. Teor. Fiz. 59, 128 [1971, Sov. Phys. JETP 32, 72].
Ovchinnikov, Yu.N., 1977, Zh. Eksp. Teor. Fiz. 72, 773 [Sov. Phys. JETP 45, 404].
Ovchinnikov, Yu.N., and G. Schön, 1981, preprint.
Ovchinnikov, Yu. N., A. Schmid and G. Schön, 1981, Phys. Rev. Lett. 46, 1013.
Palmer, D. W., and J.E. Mercereau, 1977, Phys. Lett. 61 A, 135.
Paulson, D.N., R.T. Johnson and J.C. Wheatley, 1973, Phys. Rev. Lett. 30, 829.
Pethick, C.J., and H. Smith, 1979, Ann. Phys. 119, 133.
Putterman, S.J., 1974, Superfluid Hydrodynamics (North-Holland, Amsterdam).
Putterman, S.J., 1977, J. Low Temp. Phys. 28, 339.
Scalapino, D.J., 1970, Phys. Rev. Lett. 24, 1052.
Schmid, A., 1966, Phys. Kondens. Mater. 5, 302.
Schmid, A., 1968, Phys. Kondens. Mater. 8, 129.
Schmid, A., 1980, J. Low Temp. Phys. 41, 37.
Schmid, A., 1981, in: Nonequilibrium Superconductivity, Phonons, and Kapitza Boundaries (Proc. NATO ASI), ed. K.E. Gray, (Plenum, New York).
Schmid, A., and G. Schön, 1975a, J. Low Temp. Phys. 20, 207.
Schmid, A., and G. Schön, 1975b, Phys. Rev. Lett. 34, 941.
Schmid, A., and G. Schön, 1975c, in: Proc. 14th Int. Conf. on Low Temperature Physics (Otaniemi, Finland), eds. M. Krusius and M. Vuorio (North-Holland, Amsterdam) vol. 5.
Schön, G., 1976, Thesis (Univ. of Dortmund).
Schön, G., and V. Ambegaokar, 1979, Phys. Rev. B19, 3515.
Shenoy, S.R., and P.A. Lee, 1974, Phys. Rev. B10, 2744.
Skocpol, W.J., M.R. Beasley and M. Tinkham, 1974, J. Low Temp. Phys. 16, 145.
Sooryakumar, R., and M.V. Klein, 1980, Phys. Rev. Lett. 45, 660.
Takayama, H., 1971, Prog. Teor. Phys. 46, 71.
Tinkham, M., 1972, Phys. Rev. B6, 1747.
Tinkham, M., and J. Clarke, 1972, Phys. Rev. Lett. 28, 1366.
Usadel, K.S., 1970, Phys. Rev. Lett. 25, 507.
Wölfle, P., 1973, Phys. Rev. Lett. 31, 1437.
Wölfle, P., 1977, Physica 90B, 96.
Wölfle, P., 1978, in: Progress in Low Temperature Physics VIII, ed. D.F. Brewer (North-Holland, Amsterdam).

Bibliography from resistive states of type-I superconductors by V.T. Dolgopolov and I.L. Landau

Alekseevskii, N.E., 1938, Zh. Eksp. Teor. Fiz. 8, 342.
Andreev, A.F., 1966, Zh. Eksp. Teor. Fiz. 51, 1510 [1967, Sov. Phys. JETP 24, 1019].
Andreev, A.F., 1967, Zh. Eksp. Teor. Fiz. 52, 1106 [Sov. Phys. JETP 25, 735].
Andreev, A.F., 1968, Zh. Eksp. Teor. Fiz. 54, 1510 [Sov. Phys. JETP 27, 809].

Andreev, A.F., 1972, private communication.
Andreev, A.F., and W. Bestgen, 1973, Zh. Eksp. Teor. Fiz. 64, 1865 [Sov. Phys. JETP 37, 942].
Andreev, A.F., and Yu.K. Dzhikaev, 1977, Zh. Eksp. Teor. Fiz. Pis'ma 26, 756, [JETP Lett. 26, 590].
Andreev, A.F., and Yu.V. Sharvin, 1967, Zh. Eksp. Teor. Fiz. 53, 1499 [1968, Sov. Phys. JETP 26, 865].
Andreev, A.F., and P. Tekel, 1972, Zh. Eksp. Teor. Fiz. 76, 1740 [Sov. Phys. JETP 35, 807].
Baird, D.C., and B.C. Mukherjee, 1968, Phys. Rev. Lett. 21, 996.
Balashova, V.M., and Yu.V. Sharvin, 1956, Zh. Eksp. Teor. Fiz. 31, 40 [1957, Sov. Phys. JETP 4, 54].
Bestgen, W., 1973, Zh. Eksp. Teor. Fiz. 65, 2097 [1974, Sov. Phys. JETP 38, 1048].
Bestgen, W., 1979, Zh. Eksp. Teor. Fiz. 76, 556 [Sov. Phys. JETP 49, 285].
Chandrasekhar, B.S., D.E. Farrel and S. Huang, 1967, Phys. Rev. Lett. 18, 43.
Chien, M.K., and D.E. Farrel, 1974, Phys. Rev. B9, 2092.
Dolgopolov, V.T., and S.I. Dorozhkin, 1978, Zh. Eksp. Teor. Fiz. Pis'ma 27, 459 [JETP Lett. 27. 430].
Dolgopolov, V.T., and S.S. Murzin, 1976, Zh. Eksp. Teor. Fiz. Pis'ma 24, 434 [1977, Sov. Phys. JETP Lett. 24, 397].
Dolgopolov, V.T., and S.S. Murzin, 1977, Zh. Eksp. Teor. Fiz. 73, 2281 [Sov. Phys. JETP 46, 1195].
Dolgopolov, V.T., and S.S. Murzin, 1979, Zh. Eksp. Teor. Fiz. 76, 1740 [Sov. Phys. JETP 49, 885].
Dorozhkin, S.I., and V.T. Dolgopolov, 1979a, Solid State Commun. 30, 205.

From The Behavior of a Superconductor in a Variable Field by Gor'kov, Eliashberg

[1] L. P. Gor'kov and G. M. Éliashberg, Zh. Eksp. Teor. Fiz. 54, 612 (1968) [Soviet Phys.-JETP 27, 328 (1968)].

[2] V. L. Ginzburg and L. D. Landau, Zh. Eksp. Teor. Fiz. 20, 1064 (1950).

[3] I. M. Lifshitz, Zh. Eksp. Teor. Fiz. 20, 834 (1950); Dokl. Akad. Nauk SSSR 90, 363 (1953).

[4] V. L. Ginzburg, Zh. Eksp. Teor. Fiz. 34, 113 (1958) [Soviet Phys.-JETP 7, 78 (1958)].

[5] G. E. Churilov, V. M. Dmitriev, F. F. Mende, E. V.

[6] Khristenko and I. M. Dmitrenko, ZhETF Pis. Red. 6, 752 (1967) [JETP Lett. 7, 222 (1967)].

[7] V. V. Golubev, Lektsii po analiticheskoĭ teorii differentsial'nykh uravnenii (Lectures on the Analytic Theory of Differential Equations), Gostekhizdat, 1950.

[8] D. Saint-James and P. G. de Gennes, Phys. Lett. 7, 306 (1963).

[9] P. G. de Gennes, Superconductivity of Metals and Alloys, Pt. 6, Benjamin, 1966.

From Inelastic Electron Collisions and Nonequilibrium Stationary States in Superconductors G. M. Eliashberg

[1] J. Bardeen, L. Cooper, and J. Schrieffer, Phys. Rev., 108, 1175 (1957).

[2] M. P. Kemoklidze and L. P. Pitaevskiĭ, Zh. Eksp. Teor. Fiz. 52, 1556 (1967) [Sov. Phys.-

JETP 25, 1036 (1967)].
[3] L. P. Gor 'kov and G. M. Éliashberg, ibid. 54, 612 (1968) [27, 328 (1968)].
[4] G. M. Eliashberg, ibid. 55, 2443 (1968) [28, 1298 (1969)].
[5] L. D. Landau and E. M. Lifshitz, Mekhanika sploshnykh sred (Fluid Mechanics), Gostekhizdat, 1953, Sec. 65.
[6] A. B. Migdal, Zh. Eksp. Teor. Fiz. 34, 1438 (1958) [Sov. Phys.-JETP 7, 996 (1958)].
[7] G. M. Éliashberg, ZhETF Pis. Red. 11, 186 (1970) [JETP Lett. 11, 114 (1970)].
[8] G. M. Éliashberg, Zh. Eksp. Teor. Fiz. 39, 1437 (1960) [Sov. Phys.-JETP 12, 1000 (1961)].
[9] L. V. Keldysh, ibid. 47, 1515 (1964) [20, 1018 (1965)].
[10] V. L. Pokrovskiĭ and S. K. Savvinykh, ibid. 43, 564 (1962) [16, 404 (1963)].
[11] G. Eilenberger, Zs. Phys., 214, 195 (1968).
[12] A. A. Abrikosov and L. P. Gor'kov, Zh. Eksp. Teor. Fiz. 39, 1781 (1960) [Sov. Phys.-JETP 12, 1243 (1961)].
[13] G. M. Éliashberg, ibid. 42, 1658 (1962) [15, 1151 (1962)].
[14] I. O. Kulik, ibid. 57, 600 (1969) [30, 329 (1970)].
[15] L. P. Gor'kov and G. M. Éliashberg, ibid. 56, 1297 (1969) [29, 698 (1969)].
Translated by J. G. Adashko 129

From A Time Dependent Ginzburg-Landau Equation and its Application to the Problem of Resistivity in the Mixed State by A. Schmid, 1966

[1] Ginzburg, V. L., and L. D. Landau: J. Exptl. Theoret. Phys. (U.S.S.R) 20, 1064 (1950).
[2] Abrikosov, A. A.: J. Exptl. Theoret. Phys. (U.S.S.R.) 32, 1442 (1957) [translation: Soviet Phys. - JETP 5, 1174 (1957)].
[3a] Gorkov, L. P.: J. Exptl. Theoret. Phys. (U.S.S.R.) 36, 1918 (1959) [translation: Soviet Phys. - JETP 9, 1364 (1959)].
[3b] - J. Exptl. Theoret. Phys. (U.S.S.R.) 37, 1407 (1959) [translation: Soviet Phys. JETP 10, 998 (1960)].
[4] Bardeen, J., L. N. Cooper, and J. R. Sohrieffer: Phys. Rev. 108, 1175 (1957).
[5a] Kim, Y. B., C. F. Hempstead, and A. R. Strnad: Phys. Rev. 139 A, 1163 (1965).
[5b] Strnad, A. R., C. F. Hempstead, and Y. B. Kim: Phys. Rev. Letters 13, 794 (1964).
[5c] Hempstead, C. F., and Y. B. Kım: Phys. Rev. Letters 12, 145 (1964). See for similar observations:
Druyvesteyn, W. F., and J. Volger: Philips Res. Repts 19, 359 (1964);
Farrell, D. E., I. Dinewitz, and B. S. Chandrasekhar: Phys. Rev. Letters 16, 91 (1966).
[6] Stephen, M. J., and J. Bardeen: Phys. Rev. Letters 14, 112 (1965). Bardeen, J., and M. J. Stephen: Phys. Rev. 140 A, 1197 (1965). A model with some similar features has been considered by van Vijfeijken, A. G. and A. K. Niessen: Philips Res. Repts 20, 505 (1965).
[7] Tinkham, M.: Phys. Rev. Letters 13, 804 (1964).
[8] Stefhen, M. J., and H. Suhl: Phys. Rev. Letters 13, 797 (1964).
[9] Anderson, P. W., N. R. Werthamer, and J. M. Luttinger: Phys. Rev. 138 A, 1157 (1965).
[10] Jakeman, E., and E. R. Pike: Phys. Letters 20, 593 (1966).
[11] Gorkov, L. P.: J. Exptl. Theoret. Phys. (U.S.S.R.) 34, 735 (1958) [translation: Soviet Phys. - JETP 8, 505 (1958)].
[12] Landau, L. D., and I. M. Khalatnikov: Dokl. Akad. Nauk SSSR, 96, 469 (1954) [translation: Collected Papers of L. D. Landau, edited by D. ter Haar. Oxford: Pergamon Press, pag. 626].
[13] Kadanoff, L. P., and G. Baym: Quantum Statistical Mechanics. New York: W. A. Benjamin, Inc. 1962, chap. 8-2.
[14] Maki, K.: Physics 1, 21 (1964).
[15] Bateman manuscript project. New York-Toronto-London: McGraw-Hill Book Company,

Inc. 1953; Higher transcendental functions II, chap. VIII.
[16] Jones, R. G., E. H. Rhoderick, and A. C. Rose-Innes: Phys. Letters 15, 214 (1965); Josephson, B. D.: Phys. Letters 16, 242 (1965).
[17] Kleiner, W. H., L. M. Roth, and S. H. Autler: Phys. Rev. 138 A, 1226 (1964).

From Stability of nonequilibrium Fermi distributions with respect to Cooper pairing by Aronov, Gurevich

Comments:

[2)] We have learned that D. A. Kirzhnits and Yu. V. Kopaev are also studying a similar problem.

[3)] A similar formalism has also been used by Elesin [[16]] in order to solve the problem of a semiconductor in the field of a strong electromagnetic wave.

[4)] In this representation the factors $\mathbf{u_p}$ and $\mathbf{v_p}$ are determined by other expressions (see [[11]]). We take this opportunity to mention that in [[11]] in expression (2.18) for the collision operator the last two terms were erroneously omitted. Taking these terms into account leads to a change of the numerical coefficients in the final formulas, namely, it leads to the replacement in formula (43) of the coefficient associated with Δ/kT by $1/2 + \pi/4$ and it also leads to the addition of the term $(\,1 - \ln 2)/2$ in the expression for $\ln C$.

[5)] This implies, as one can easily see, a "negative temperature" of the superconducting excitations.

[6)] This state has subsequently been studied in detail experimentally. [[20]]

[7)] Equation (4.3), which we have derived, differs slightly from the corresponding equation in [[12]].

Refs:

[1] V. M. Dmitriev, E. V. Khristenko, A. V. Trubitsyn, and F. F. Mende, UFZh 15, 1611 (1970).
[2] L. R. Testardi, Phys. Rev. B4, 2189 (1971).
[3] R. H. Parmenter, Phys. Rev. Letters 7, 274 (1961).
[4] É. G. Batyev, ZhETF Pis. Red. 5, 45 (1967) [JETP Lett. 5, 35 (1967)].
[5] G. M. Éliashberg, ZhETF Pis. Red. 11, 186 (1970) [JETP Lett. 11, 114 (1970)].
[6] G. M. Éliashberg, Zh. Eksp. Teor. Fiz. 61, 1254 (1971) [Sov. Phys.-JETP 34, 668 (1972)].
[7] B. I. Ivlev and G. M. Éliashberg, ZhETF Pis. Red. 13, 464 (1971) [JETP Lett. 13, 333 (1971)].
[8] A. G. Aronov and V. L. Gurevich, Fiz. Tverd. Tela 14, 1129 (1972) [Sov. Phys.-Solid State 14, 966 (1972)].
[9] A. G. Aronov and V. L. Gurevich, ZhETF Pis. Red. 15, 564 (1972) [JETP Lett. 15, 400 (1972)].
[10] A. G. Aronov and V. L. Gurevich, Fiz. Tverd. Tela 14, 2675 (1972) [Sov. Phys.-Solid State 14, 2309 (1973)].
[11] A. G. Aronov and V. L. Gurevich, Zh. Eksp. Teor. Fiz. 63, 1809 (1972) [Sov. Phys.-JETP 36, 957 (1973)].
[12] C. S. Owen and D. J. Scalapino, Phys. Rev. Lett. 28, 1559 (1972).
[13] a) A. A. Abrikosov, L. P. Gor'kov, and I. E. Dzyaloshinskiĭ, Metody kvantovoĭ teorii polya v statisticheskoĭ fizike (Quantum Field Theoretical Methods in Statistical Physics), Fizmatgiz, 1962, p. 367 (English Transl., Pergamon Press, 1965); b) V. L. Ginzburg, Usp. Fiz. Nauk 69, 537 (1959) [Sov. Phys.-Uspekhi 2, 874 (1960)].
[14] L. V. Keldysh, Zh. Eksp. Teor. Fiz. 47, 1515 (1964) [Sov. Phys.-JETP 20, 1018 (1965)].
[15] E. F. Gross, V. I. Perel', and R. I. Shekhmamet'ev, ZhETF Pis. Red. 13, 320 (1971) [JETP Lett. 13, 229 (1971)].
[16] V. F. Elesin, Zh. Eksp. Teor. Fiz. 59, 602 (1970) [Sov. Phys.-JETP 32, 328 (1971)].

[17] A. B. Migdal, Zh. Eksp. Teor. Fiz. 40, 684 (1961) [Sov. Phys.-JETP 13, 478 (1961)].
[18] N. N. Bogolyubov, V. V. Tolmachev, and D. V. Shirokov, Novyĭ metod v teorii sverkhprovodimosti (A New Method in the Theory of Superconductivity), 1958, p. 38 (English Transl., Consultants Bureau, 1959).
[19] P. W. Anderson, Phys. Rev. 112, 1900 (1958).
[20] W. H. Parker and W. D. Williams, Phys. Rev. Lett. 29, 924 (1972).

34.12 Bibliography from Well-known, Important Artiles

From Quantum quench phase diagrams of an s-wave BCS-BEC condensate by Yuzbashyan, Dzero, Gurarie, Foster

References

[Anderson(1958)] P. W. Anderson, Phys. Rev. **112**, 1900 (1958).

[Galaiko(1972)] V. P. Galaiko, Sov. Phys. JETP **34**, 203 (1972).

[Volkov and Kogan(1974)] A. F. Volkov and S. M. Kogan, Zh. Eksp. Teor. Fiz **65**, 2038 (1974), English translation: Sov. Phys. JETP, **38**, 1018 (1974).

[Galperin et al.(1981)] Y. M. Galperin, V. I. Kozub, and B. Z. Spivak, Sov. Phys. JETP **54**, 1126 (1981).

[Littlewood and Varma(1982)] P. B. Littlewood and C. M. Varma, Phys. Rev. B (1982).

[Shumeiko(1990)] V. S. Shumeiko, *Dynamics of electronic system with off-diagonal order parameter and non-linear resonant phenomena in superconductors* (Doctoral Thesis, Institute for Low Temperature Physics and Engineering, Kharkov, Ukraine, 1990).

[Barankov et al.(2004)] R. A. Barankov, L. S. Levitov, and B. Z. Spivak, Phys. Rev. Lett. **93**, 160401 (2004).

[Amin et al.(2004)] M. Amin, E. Bezuglyi, A. Kijko, and A. Omelyanchouk, Low Temp. Phys. **30**, 661 (2004).

[Andreev et al.(2004)] A. V. Andreev, V. Gurarie, and L. Radzihovsky, Phys. Rev. Lett. **93**, 130402 (2004).

[Barankov and Levitov(2004)] R. A. Barankov and L. S. Levitov, Phys. Rev. Lett. **93**, 130403 (2004).

[Szymanska et al.(2005)] M. H. Szymanska, B. D. Simons, and K. Burnett, Phys. Rev. Lett. **94**, 170402 (2005).

[Warner and Leggett(2005)] G. L. Warner and A. J. Leggett, Phys. Rev. B **71**, 034514 (2005).

[Yuzbashyan et al.(2005a)] E. A. Yuzbashyan, B. L. Altshuler, V. B. Kuznetsov, and V. Z. Enolskii, J. Phys. A **38**, 7831 (2005a).

[Yuzbashyan et al.(2005b)] E. A. Yuzbashyan, B. L. Altshuler, V. B. Kuznetsov, and V. Z. Enolskii, Phys. Rev. B **72**, 220503(R) (2005b).

[Yuzbashyan et al.(2005c)] E. A. Yuzbashyan, V. B. Kuznetsov, and B. L. Altshuler, Phys. Rev. B **72**, 144524 (2005c).

[Yuzbashyan et al.(2006)] E. A. Yuzbashyan, O. Tsyplyatyev, and B. L. Altshuler, Phys. Rev. Lett. **96**, 097005 (2006), erratum: Phys. Rev. Lett. **96**, 179905 (2006).

[Barankov and Levitov(2006)] R. A. Barankov and L. S. Levitov, Phys. Rev. Lett. **96**, 230403 (2006).

[Yuzbashyan and Dzero(2006)] E. A. Yuzbashyan and M. Dzero, Phys. Rev. Lett. **96**, 230404 (2006).

[Dzero et al.(2007)] M. Dzero, E. A. Yuzbashyan, B. L. Altshuler, and P. Coleman, Phys. Rev. Lett. **99**, 160402 (2007).

[Barankov and Levitov(2007)] R. A. Barankov and L. S. Levitov, arXiv:0704.1292 (2007).

[Tomadin et al.(2008)] A. Tomadin, M. Polini, M. P. Tosi, and R. Fazio, Phys. Rev. A **77**, 033605 (2008).

[Nahum and Bettelheim(2008)] A. Nahum and E. Bettelheim, Phys. Rev. B **78**, 184510 (2008).

[Gurarie(2009)] V. Gurarie, Phys. Rev. Lett. **103**, 075301 (2009).

[Faribault et al.(2009)] A. Faribault, P. Calabrese, and J.-S. Caux, J. Math. Phys. **50**, 095212 (2009).

[Matsunaga et al.(2013)] R. Matsunaga, Y. I. Hamada, K. Makise, Y. Uzawa, H. Terai, Z. Wang, and R. Shimano, Phys. Rev. Lett. **111**, 057002 (2013).

[Matsunaga et al.(2014)] R. Matsunaga, N. Tsuji, H. Fujita, A. Sugioka, K. Makise, Y. Uzawa, H. Terai, Z. Wang, H. Aoki, and R. Shimano, Science **345**, 1145 (2014).

[Papenkort et al.(2007)] T. Papenkort, V. M. Axt, and T. Kuhn, Physical Review B **76** (2007).

[Papenkort et al.(2009)] T. Papenkort, T. Kuhn, and V. M. Axt, Journal of Physics **193**, 012050 (2009).

[Krull et al.(2013)] H. Krull, D. Manske, G. S. Uhrig, and A. P. Schnyder, arXiv:1309.7318 (2013).

[Tsuji(2014)] H. Tsuji, Naoto; Aoki, arXiv:1404.2711 (2014).

[Matsunaga and Shimano(2012)] R. Matsunaga and R. Shimano, Phys. Rev. Lett. **109**, 187002 (2012).

[Beck et al.(2013)] M. Beck, I. Rousseau, M. Klammer, P. Leiderer, M. Mittendorff, S. Winnerl, M. Helm, G. N. Gol'tsman, and J. Demsar, Phys. Rev. Lett. **110**, 267003 (2013).

[Brierley et al.(2011)] R. T. Brierley, P. B. Littlewood, and P. R. Eastham, Phys. Rev. Lett. **107**, 040401 (2011).

[Pehlivan et al.(2011)] Y. Pehlivan, T. Balantekin, A. B.; Kajino, and T. Yoshida, Phys. Rev. D **84**, 065008 (2011).

[Raffelt et al.(2013)] G. Raffelt, S. Sarikas, and D. d. S. Seixas, Phys. Rev. Lett. **111** (2013).

[Foster et al.(2013)] M. S. Foster, M. Dzero, V. Gurarie, and E. A. Yuzbashyan, Phys. Rev. B **88**, 104511 (2013).

[Foster et al.(2014)] M. S. Foster, V. Gurarie, M. Dzero, and E. A. Yuzbashyan, Phys. Rev. Lett. **113**, 076403 (2014).

[Gaudin(1983)] M. Gaudin, *La fonction d'onde de Bethe* (Masson, Paris, 1983).

[Richardson(2002)] R. W. Richardson, arXiv:cond-mat/0203512 (unpublished) (2002).

[Ibanez et al.(2009)] M. Ibanez, J. Links, G. Sierra, and S.-Y. Zhao, Phys. Rev. B **79**, 180501(R) (2009).

[Dunning et al.(2010)] C. Dunning, M. Ibanez, J. Links, G. Sierra, and S.-Y. Zhao, J. Stat. Mech. p. P08025 (2010).

[Rombouts et al.(2010)] S. M. A. Rombouts, J. Dukelsky, and G. Ortiz, Phys. Rev. B **82**, 224510 (2010).

[Dukelsky et al.(2004)] J. Dukelsky, S. Pittel, and G. Sierra, Rev. Mod. Phys. **76**, 643 (2004).

[Ortiz et al.(2005)] G. Ortiz, R. Somma, J. Dukelsky, and S. Rombouts, Nucl.Phys. B **707**, 421 (2005).

[J. Dukelsky(2001)] P. S. J. Dukelsky, C. Esebbag, Phys. Rev. Lett. **87**, 066403 (2001).

[L. Amico(2001)] A. O. L. Amico, A. di Lorenzo, Phys. Rev. Lett. **86**, 5759 (2001).

[Regal et al.(2004)] A. Regal, M. Greiner, and D. S. Jin, Phys. Rev. Lett. **92**, 040403 (2004).

[Zwierlein et al.(2004)] M. W. Zwierlein, C. A. Stan, C. H. Schunck, S. M. F. Raupach, A. J. Kerman, and W. Ketterle, Phys. Rev. Lett. **92**, 120403 (2004).

[Calabrese and Cardy(2006)] P. Calabrese and J. Cardy, Phys. Rev. Lett. **96**, 136801 (2006).

[Kollath et al.(2007)] C. Kollath, A. M. Läuchli, and E. Altman, Phys. Rev. Lett. **98**, 180601 (2007).

[Leggett(1980)] A. Leggett, in *Modern Trends in the Theory of Condensed Matter* (Springer-Verlag, Berlin, 1980), pp. 13–27.

[Nozières and Schmitt-Rink(1985)] P. Nozières and S. Schmitt-Rink, J. Low Temp. Phys. **59**, 195 (1985).

[Gurarie and Radzihovsky(2007)] V. Gurarie and L. Radzihovsky, Ann. Phys. **322**, 2 (2007).

[Burovski et al.(2006)] E. Burovski, N. Prokof'ev, B. Svistunov, and M. Troyer, New J. Phys. **8**, 153 (2006).

[Bulgac and Yoon(2009)] A. Bulgac and S. Yoon, Phys. Rev. Lett. **102**, 085302 (2009).

[Levinsen and Gurarie(2006)] J. Levinsen and V. Gurarie, Phys. Rev. A **73**, 053607 (2006).

[Richardson(1977)] R. Richardson, J. Math. Phys. **18**, 1802 (1977).

[Sträter et al.(2012)] C. Sträter, O. Tsyplyatyev, and A. Faribault, Phys. Rev. B **86**, 195101 (2012).

[Pekker and Varma(2014)] D. Pekker and C. M. Varma, arXiv:1406.2968 (2014).

[Anderson(1959)] P. W. Anderson, J. Phys. Chem. Solids **11**, 26 (1959).

[Kurland et al.(2000)] I. L. Kurland, I. L. Aleiner, and B. L. Altshuler, Phys. Rev. B **62**, 14886 (2000).

[not(a)] The integrand in Eq. (5.37) generally has a nonvanishing zeroth Fourier mode, i.e. it contributes to both linear and periodic parts.

[Arnold(1978)] V. I. Arnold, *Mathematical Methods of Classical Mechanics* (Springer-Verlag, New York, 1978).

[Tabor(1989)] M. Tabor, *Chaos and Integrability in Nonlinear Dynamics* (Wiley, New York, 1989).

[H. Goldstein(2002)] J. S. H. Goldstein, C. Poole, *Classical Mechanics*, Ch. 10 (Addison Wesley, 2002), 3rd ed.

[Carlson and Gustafson(1994)] B. C. Carlson and J. L. Gustafson, SIAM J. Math. Anal., 25(2) p. 288 (1994).

[DLMF()] DLMF, *NIST Digital Library of Mathematical Functions*, Ch. 19, Release date 2014-04-25, URL `http://dlmf.nist.gov/`.

[Chin et al.(2004)] C. Chin, M. Bartenstein, A. Altmeyer, S. Riedl, S. Jochim, J. H. Denschlag, and R. Grimm, Science **305**, 1128 (2004).

[Zwierlein et al.(2005)] M. W. Zwierlein, A. S. J. R. Abo-Shaeer, C. H. Schunck, and W. Ketterle, Nature **435**, 1047 (2005).

[Schrieffer(1989)] R. Schrieffer, *Theory of Superconductivity* (Perseus Books Group, N.Y., 1989).

[Bardeen et al.(1957)] J. Bardeen, L. N. Cooper, and J. R. Schrieffer, Phys. Rev. **108**, 1175 (1957).

[not(b)] See Ref. [Foster et al.(2013)] for a detailed calculation of analogous Green's functions and expectation values.

[Törmä and Zoller(2000)] P. Törmä and P. Zoller, Phys. Rev. Lett. **85**, 487 (2000).

[Regal and Jin(2003)] C. A. Regal and D. S. Jin, Phys. Rev. Lett. **90**, 230404 (2003).

[et al.(2003)] S. G. et al., Science **300**, 1723 (2003).

[Kinnunen et al.(2004)] J. Kinnunen, M. Rodriguez, and P. Törmä, Science **305**, 1131 (2004).

[Schunk et al.(2008)] C. H. Schunk, Y. Shin, A. Schirotzek, and W. Ketterle, Nature **454**, 739 (2008).

[Basu and Mueller(2008)] S. Basu and E. J. Mueller, Phys. Rev. Lett. **101**, 060405 (2008).

[Schirotzek et al.(2008)] A. Schirotzek, Y. Shin, C. H. Schunck, and W. Ketterle, Phys. Rev. Lett. **101**, 140403 (2008).

[not(c)] We note that the contribution of stimulated emission processes is missing in Ref. [Dzero et al.(2007)]. This mistake is fixed in Ref. [Foster et al.(2013)]. Moreover, we computed the RF response for the two-channel model taking this term into account and we find that the absorbed intensity is not significantly affected by this term for quenches to both BCS and BEC final detunings at least for the values of the relevant parameters considered.

[Dong et al.(2014)] Y. Dong, L. Dong, M. Gong, and H. Pu, arXiv:1406.3821 (2014).

[Duyckaerts et al.(2013)] T. Duyckaerts, C. Keni, and F. Merle, Cambridge Journal of Mathematics **1**, 75 (2013).

[Phillips(2003)] P. Phillips, *Advanced Solid State Physics* (Westview Press, Boulder, CO, 2003).

From relaxation and persistent oscillations of the order parameter in the non-stationary BCS theory by A. Yuzbashyan, Tsyplyatyev, Altshuler

References

[1] P. W. Anderson: Phys. Rev. 112, 1900 (1958).

[2] V. P. Galaiko: Sov. Phys. JETP 34, 203 (1972).

[3] A. F. Volkov and Sh. M. Kogan: Sov. Phys. JETP 38, 1018 (1974).

[4] Yu. M. Gal'perin, V. I. Kozub, and B. Z. Spivak: Sov. Phys. JETP 54, 1126 (1981).

[5] R. A. Barankov, L. S. Levitov, and B. Z. Spivak: PRL 93, 160401 (2004); A. V. Andreev, V. Gurarie, and L. Radzihovsky: PRL 93, 130402 (2004); R. A. Barankov and L. S. Levitov: PRL 93, 130403 (2004).

[6] R. A. Barankov and L. S. Levitov: cond-mat/0508215 (2005).

[7] M.H.S. Amin, E.V. Bezuglyi, A.S. Kijko, A.N. Omelyanchouk: Low Temp. Phys. 30, 661 (2004).

[8] E. A. Yuzbashyan, B. L. Altshuler, V. B. Kuznetsov, V. Z. Enolskii: J. Phys. A 38, 7831, (2005); cond-mat/0505493 (2005).

[9] E. A. Yuzbashyan, V. B. Kuznetsov, B. L. Altshuler: Phys. Rev. B 72, 144524 (2005).

[10] M. H. Szymanska, B. D. Simons, and K. Burnett: PRL 94 , 170402 (2005).

[11] G.L. Warner and A. J. Leggett: Phys. Rev. B 71, 134514 (2005).

[12] N. B. Kopnin: Theory of Nonequilibrium Superconductivity, Clarendon Press, Oxford (2001).

[13] T. Loftus et. al.: PRL 88, 173201 (2002); J. L. Bohn: Phys. Rev. A 61, 053409 (2000); M. W. Zwierlein et. al.: PRL 92, 120403 (2004); C. Chin et. al.: Science 305, 1128 (2004).

[14] Y. Nakamura, Yu. A. Pashkin and J. S. Tsai: Nature 398, 786, (1999); O. Astafiev et. al.: PRL 93, 267007 (2004); D. Vion et. al.: Science, 296, 886 (2002).

[15] E. A. Yuzbashyan and M. Dzero, unpublished.

[16] An m-spin solution can be expressed in terms of a Riemann theta function of genus $m-1$[8]. In particular, 2-spin solutions are genus one – ordinary elliptic functions.

[17] If the initial state is particle-hole symmetric k is equal to the integer part of $m/2$. In this case the effective m-spin problem is also particle-hole symmetric, which reduces the number of independent degrees of freedom and therefore the number of incommensurate frequencies.

[18] Far from the Fermi level $s_z(\epsilon) = -\text{sgn}\epsilon$. Therefore, the total number of jumps in $s_z(\epsilon)$ for normal states is always odd. For anomalous stationary states the number of discontinuities in the spin distribution is even by the same argument.

[19] E. Abrahams and T. Tsuneto: Phys. Rev. 152, 416 (1966).

[20] A. Schmid: Phys. Kond. Mat. 5, 302 (1966).

[21] The two solutions merge for Δ_{in} comparable to the mean level spacing d. Here we consider the thermodynamic limit $d/\Delta_{in} \to 0$.

From Onset of superconductivity in a voltage-biased NSN microbridge by Serbyn, Skvortsov

References

[Kopnin(2001)] N. B. Kopnin, *Theory of Nonequilibrium Superconductivity* (Oxford University Press, New York, 2001).

[Gray(1981)] K. Gray, ed., *Nonequilibrium superconductivity, phonons, and Kapitza boundaries* (Plenum Press, New York, 1981).

[Gulian and Zharkov(1999)] A. Gulian and G. Zharkov, *Nonequilibrium Electrons and Phonons in Superconductors*, Selected Topics in Superconductivity (Springer, 1999).

[Langenberg and Larkin(1986)] D. Langenberg and A. Larkin, *Nonequilibrium superconductivity*, Modern problems in condensed matter sciences (North-Holland, 1986).

[Vodolazov *et al.*(2003)] D. Y. Vodolazov, F. M. Peeters, L. Piraux, S. Mátéfi-Tempfli, and S. Michotte, Phys. Rev. Lett. **91**, 157001 (2003).

[Xiong *et al.*(1997)] P. Xiong, A. V. Herzog, and R. C. Dynes, Phys. Rev. Lett. **78**, 927 (1997).

[Rogachev *et al.*(2006)] A. Rogachev, T.-C. Wei, D. Pekker, A. T. Bollinger, P. M. Goldbart, and A. Bezryadin, Phys. Rev. Lett. **97**, 137001 (2006).

[Li *et al.*(2011)] P. Li, P. M. Wu, Y. Bomze, I. V. Borzenets, G. Finkelstein, and A. M. Chang, Phys. Rev. B **84**, 184508 (2011).

[Astafiev *et al.*(2012)] O. V. Astafiev, L. B. Ioffe, S. Kafanov, Y. A. Pashkin, K. Y. Arutyunov, D. Shahar, O. Cohen, and J. S. Tsai, Nature **484**, 355 (2012).

[Ivlev and Kopnin(1984)] B. I. Ivlev and N. B. Kopnin, Adv. Phys. **33**, 47 (1984).

[Meyer and Minnigerode(1972)] J. Meyer and G. Minnigerode, Physics Letters A **38**, 529 (1972).

[Langer and Ambegaokar(1967)] J. S. Langer and V. Ambegaokar, Phys. Rev. **164**, 498 (1967).

[McCumber and Halperin(1970)] D. E. McCumber and B. I. Halperin, Phys. Rev. B **1**, 1054 (1970).

[Keizer *et al.*(2006)] R. S. Keizer, M. G. Flokstra, J. Aarts, and T. M. Klapwijk, Phys. Rev. Lett. **96**, 147002 (2006).

[Vercruyssen *et al.*(2012)] N. Vercruyssen, T. G. A. Verhagen, M. G. Flokstra, J. P. Pekola, and T. M. Klapwijk, Phys. Rev. B **85**, 224503 (2012).

[Snyman and Nazarov(2009)] I. Snyman and Y. V. Nazarov, Phys. Rev. B **79**, 014510 (2009).

[Gorkov and Eliashberg(1968)] L. P. Gorkov and G. M. Eliashberg, Sov. Phys. JETP **27**, 328 (1968).

[Kramer and Watts-Tobin(1978)] L. Kramer and R. J. Watts-Tobin, Phys. Rev. Lett. **40**, 1041 (1978).

[Michotte *et al.*(2004)] S. Michotte, S. Mátéfi-Tempfli, L. Piraux, D. Y. Vodolazov, and F. M. Peeters, Phys. Rev. B **69**, 094512 (2004).

[Vodolazov(2007)] D. Y. Vodolazov, Phys. Rev. B **75**, 184517 (2007).

[Elmurodov *et al.*(2008)] A. K. Elmurodov, F. M. Peeters, D. Y. Vodolazov, S. Michotte, S. Adam, F. d. M. de Horne, L. Piraux, D. Lucot, and D. Mailly, Phys. Rev. B **78**, 214519 (2008).

[Rubinstein *et al.*(2007)] J. Rubinstein, P. Sternberg, and Q. Ma, Phys. Rev. Lett. **99**, 167003 (2007).

[Chtchelkatchev and Vinokur(2009)] N. Chtchelkatchev and V. Vinokur, Europhys. Lett. **88**, 47001 (2009).

[Giazotto *et al.*(2006)] F. Giazotto, T. T. Heikkilä, A. Luukanen, A. M. Savin, and J. P. Pekola, Rev. Mod. Phys. **78**, 217 (2006).

[Chen *et al.*(2009)] Y. Chen, S. D. Snyder, and A. M. Goldman, Phys. Rev. Lett. **103**, 127002 (2009).

[Tian *et al.*(2005)] M. Tian, N. Kumar, S. Xu, J. Wang, J. S. Kurtz, and M. H. W. Chan, Phys. Rev. Lett. **95**, 076802 (2005).

[Boogaard *et al.*(2004)] G. R. Boogaard, A. H. Verbruggen, W. Belzig, and T. M. Klapwijk, Phys. Rev. B **69**, 220503 (2004).

[Larkin and Varlamov(2002)] A. I. Larkin and A. A. Varlamov, *Theory of Fluctuations in Superconductors* (Oxford University Press, New York, 2002).

[Levchenko and Kamenev(2007)] A. Levchenko and A. Kamenev, Phys. Rev. B **76**, 094518 (2007).

[Feigel'man *et al.*(2000)] M. V. Feigel'man, A. I. Larkin, and M. A. Skvortsov, Phys. Rev. B **61**, 12361 (2000).

[Kamenev(2011)] A. Kamenev, *Field Theory of Non-Equilibrium Systems* (Cambridge University Press, 2011).

[Nagaev(1995)] K. E. Nagaev, Phys. Rev. B **52**, 4740 (1995).

[Pothier *et al.*(1997)] H. Pothier, S. Guéron, N. O. Birge, D. Esteve, and M. H. Devoret, Phys. Rev. Lett. **79**, 3490 (1997).

[Bender and Boettcher(1998)] C. M. Bender and S. Boettcher, Phys. Rev. Lett. **80**, 5243 (1998).

[Bender(2007)] C. M. Bender, Rep. Prog. Phys. **70**, 947 (2007).

[Vodolazov and Peeters(2007)] D. Y. Vodolazov and F. M. Peeters, Phys. Rev. B **75**, 104515 (2007).

[Serbyn and Skvortsov()] M. Serbyn and M. A. Skvortsov, in preparation.

From Observing Dynamical Phases of BCS Superconductors in a Cavity QED Simulator by Young et al.

References

[Bardeen *et al.*(1957)] J. Bardeen, L. N. Cooper, and J. R. Schrieffer, Phys. Rev. **108**, 1175 (1957).

[Yuzbashyan *et al.*(2006)] E. A. Yuzbashyan, O. Tsyplyatyev, and B. L. Altshuler, Phys. Rev. Lett. **96**, 097005 (2006).

[Barankov and Levitov(2006)] R. A. Barankov and L. S. Levitov, Phys. Rev. Lett. **96**, 230403 (2006).

[Yuzbashyan and Dzero(2006)] E. A. Yuzbashyan and M. Dzero, Phys. Rev. Lett. **96**, 230404 (2006).

[Gurarie and Radzihovsky(2007)] V. Gurarie and L. Radzihovsky, Ann. Phys. **322**, 2 (2007), January Special Issue 2007.

[Gurarie(2009)] V. Gurarie, Phys. Rev. Lett. **103**, 075301 (2009).

[Foster *et al.*(2013)] M. S. Foster, M. Dzero, V. Gurarie, and E. A. Yuzbashyan, Phys. Rev. B **88**, 104511 (2013).

[Yuzbashyan *et al.*(2015)] E. A. Yuzbashyan, M. Dzero, V. Gurarie, and M. S. Foster, Phys. Rev. A **91**, 033628 (2015).

[Lewis-Swan *et al.*(2021)] R. J. Lewis-Swan, D. Barberena, J. R. Cline, D. J. Young, J. K. Thompson, and A. M. Rey, Phys. Rev. Lett. **126**, 173601 (2021).

[Kelly *et al.*(2022)] S. P. Kelly, J. K. Thompson, A. M. Rey, and J. Marino, Phys. Rev. Res. **4**, L042032 (2022).

[Stewart(2017)] G. R. Stewart, Adv. Phys. **66**, 75 (2017).

[Sato and Ando(2017)] M. Sato and Y. Ando, Rep. Prog. Phys. **80**, 076501 (2017).

[Zhou *et al.*(2021)] X. Zhou, W.-S. Lee, M. Imada, N. Trivedi, P. Phillips, H.-Y. Kee, P. Törmä, and M. Eremets, Nat. Rev. Phys. **3**, 462 (2021).

[Shuryak(2017)] E. Shuryak, Rev. Mod. Phys. **89**, 035001 (2017).

[Harlow(2016)] D. Harlow, Rev. Mod. Phys. **88**, 015002 (2016).

[Marino *et al.*(2022)] J. Marino, M. Eckstein, M. Foster, and A.-M. Rey, Rep. Prog. Phys. **85**, 116001 (2022).

[Volkov and Kogan(1974)] A. F. Volkov and S. M. Kogan, JETP **38**, 1018 (1974), [Russian original - Zh. Eksp. Teor. Fiz. **65**, 2038 (1973)].

[Yuzbashyan *et al.*(2005)] E. A. Yuzbashyan, B. L. Altshuler, V. B. Kuznetsov, and V. Z. Enolskii, J. Phys. A: Math. Gen. **38**, 7831 (2005).

[Barankov *et al.*(2004)] R. A. Barankov, L. S. Levitov, and B. Z. Spivak, Phys. Rev. Lett. **93**, 160401 (2004).

[Yuzbashyan(2008)] E. A. Yuzbashyan, Phys. Rev. B **78**, 184507 (2008).

[Foster *et al.*(2014)] M. S. Foster, V. Gurarie, M. Dzero, and E. A. Yuzbashyan, Phys. Rev. Lett. **113**, 076403 (2014).

[Collado *et al.*(2023)] H. P. O. Collado, N. Defenu, and J. Lorenzana, Phys. Rev. Res. **5**, 023011 (2023).

[Mansart *et al.*(2013)] B. Mansart, J. Lorenzana, A. Mann, A. Odeh, M. Scarongella, M. Chergui, and F. Carbone, Proc. Natl. Acad. Sci. U.S.A. **110**, 4539 (2013).

[Matsunaga *et al.*(2013)] R. Matsunaga, Y. I. Hamada, K. Makise, Y. Uzawa, H. Terai, Z. Wang, and R. Shimano, Phys. Rev. Lett. **111**, 057002 (2013).

[Matsunaga *et al.*(2014)] R. Matsunaga, N. Tsuji, H. Fujita, A. Sugioka, K. Makise, Y. Uzawa, H. Terai, Z. Wang, H. Aoki, and R. Shimano, Science **345**, 1145 (2014).

[Randeria and Taylor(2014)] M. Randeria and E. Taylor, Annu. Rev. Condens. Matter Phys. **5**, 209 (2014).

[Behrle *et al.*(2018)] A. Behrle, T. Harrison, J. Kombe, K. Gao, M. Link, J.-S. Bernier, C. Kollath, and M. Köhl, Nature Physics **14**, 781 (2018).

[Anderson(1958)] P. W. Anderson, Phys. Rev. **112**, 1900 (1958).

[Davis *et al.*(2020)] E. J. Davis, A. Periwal, E. S. Cooper, G. Bentsen, S. J. Evered, K. Van Kirk, and M. H. Schleier-Smith, Phys. Rev. Lett. **125**, 060402 (2020).

[Norcia *et al.*(2018a)] M. A. Norcia, R. J. Lewis-Swan, J. R. Cline, B. Zhu, A. M. Rey, and J. K. Thompson, Science **361**, 259 (2018a).

[Allred *et al.*(2002)] J. C. Allred, R. N. Lyman, T. W. Kornack, and M. V. Romalis, Phys. Rev. Lett. **89**, 130801 (2002).

[Kleine *et al.*(2008)] A. Kleine, C. Kollath, I. P. McCulloch, T. Giamarchi, and U. Schollwoeck, New J. Phys. **10**, 045025 (2008).

[Deutsch *et al.*(2010)] C. Deutsch, F. Ramirez-Martinez, C. Lacroûte, F. Reinhard, T. Schneider, J. N. Fuchs, F. Piéchon, F. Laloë, J. Reichel, and P. Rosenbusch, Phys. Rev. Lett. **105**, 020401 (2010).

[Smale *et al.*(2019)] S. Smale, P. He, B. A. Olsen, K. G. Jackson, H. Sharum, S. Trotzky, J. Marino, A. M. Rey, and J. H. Thywissen, Sci. Adv. **5**, eaax1568 (2019).

[Muniz *et al.*(2020)] J. A. Muniz, D. Barberena, R. J. Lewis-Swan, D. J. Young, J. R. Cline, A. M. Rey, and J. K. Thompson, Nature **580**, 602 (2020).

[Baghdad *et al.*(2023)] M. Baghdad, P.-A. Bourdel, S. Schwartz, F. Ferri, J. Reichel, and R. Long, Nat. Phys. **19**, 1104 (2023).

[Sauerwein *et al.*(2023)] N. Sauerwein, F. Orsi, P. Uhrich, S. Bandyopadhyay, F. Mattiotti, T. Cantat-Moltrecht, G. Pupillo, P. Hauke, and J.-P. Brantut, Nat. Phys. **19**, 1128 (2023).

[Richardson and Sherman(1964)] R. Richardson and N. Sherman, Nuclear Physics **52**, 221 (1964).

[Gaudin(1976)] M. Gaudin, J. Phys. (Paris) **37**, 1087 (1976).

[Weiner *et al.*(2012)] J. M. Weiner, K. C. Cox, J. G. Bohnet, Z. Chen, and J. K. Thompson, Appl. Phys. Lett. **101**, 261107 (2012).

[Bohnet *et al.*(2013)] J. G. Bohnet, Z. Chen, J. M. Weiner, K. C. Cox, and J. K. Thompson, Phys. Rev. A **88**, 013826 (2013).

[Norcia *et al.*(2016)] M. A. Norcia, M. N. Winchester, J. R. Cline, and J. K. Thompson, Sci. Adv. **2**, e1601231 (2016).

[Rey *et al.*(2008)] A. M. Rey, L. Jiang, M. Fleischhauer, E. Demler, and M. D. Lukin, Phys. Rev. A **77**, 052305 (2008).

[Black-Schaffer(2012)] A. M. Black-Schaffer, Phys. Rev. Lett. **109**, 197001 (2012).

[Nandkishore *et al.*(2012)] R. Nandkishore, L. S. Levitov, and A. V. Chubukov, Nat. Phys. **8**, 158 (2012).

[Kiesel *et al.*(2012)] M. L. Kiesel, C. Platt, W. Hanke, D. A. Abanin, and R. Thomale, Phys. Rev. B **86**, 020507 (2012).

[Kiesel *et al.*(2013)] M. L. Kiesel, C. Platt, W. Hanke, and R. Thomale, Phys. Rev. Lett. **111**, 097001 (2013).

[Fischer *et al.*(2014)] M. H. Fischer, T. Neupert, C. Platt, A. P. Schnyder, W. Hanke, J. Goryo, R. Thomale, and M. Sigrist, Phys. Rev. B **89**, 020509 (2014).

[Shankar *et al.*(2022)] A. Shankar, E. A. Yuzbashyan, V. Gurarie, P. Zoller, J. J. Bollinger, and A. M. Rey, PRX Quantum **3**, 040324 (2022).

[Laughlin(1998)] R. Laughlin, Phys. Rev. Lett. **80**, 5188 (1998).

[Balatsky *et al.*(2006)] A. V. Balatsky, I. Vekhter, and J.-X. Zhu, Rev. Mod. Phys. **78**, 373 (2006).

[Schäfer and Teaney(2009)] T. Schäfer and D. Teaney, Rep. Prog. Phys. **72**, 126001 (2009).

[Pehlivan *et al.*(2011)] Y. Pehlivan, A. Balantekin, T. Kajino, and T. Yoshida, Phys. Rev. D **84**, 065008 (2011).

[Norcia *et al.*(2018b)] M. A. Norcia, J. R. Cline, J. A. Muniz, J. M. Robinson, R. B. Hutson, A. Goban, G. E. Marti, J. Ye, and J. K. Thompson, Phys. Rev. X **8**, 021036 (2018b).

[Young *et al.*(2023)] D. J. Young, A. Chu, E. Y. Song, D. Barberena, D. Wellnitz, Z. Niu, V. Schäfer, R. J. Lewis-Swan, A. M. Rey, and J. K. Thompson, Data for: Observing dynamical phases of BCS superconductors in a cavity QED simulator (2023), dryad dataset.

[Reiter and Sørensen(2012)] F. Reiter and A. S. Sørensen, Phys. Rev. A **85**, 032111 (2012).

From Theory of Anderson pseudospin resonance with Higgs mode in SC

References

[Anderson(1958)] P. W. Anderson, Phys. Rev. **112**, 1900 (1958).

[Volkov,Kogan (1973)] A. F. Volkov and S. M. Kogan, Sov. Phys. JETP **38**, 1018 (1974).

[Littlewood (1981)] P. B. Littlewood and C. M. Varma, Phys. Rev. Lett. **47**, 811 (1981); Phys. Rev. B **26**, 4883 (1982).

[Varma(2002)] C. Varma, J. Low Temp. Phys. **126**, 901 (2002).

[Pekker and Varma(2015)] D. Pekker and C. Varma, Annual Review of Condensed Matter Physics **6**, 269 (2015).

[Eng()] F. Englert and R. Brout, Phys. Rev. Lett. **13** 321, (1964).

[Hig()] P. W. Higgs, Phys. Lett. **12**, 132 (1964); Phys. Rev. Lett. **13**, 508 (1964).

[Gur()] G. S. Guralnik, C. R. Hagen, and T. W. B. Kibble, Phys. Rev. Lett. **13**, 585 (1964).

[Nam(a)] Y. Nambu and G. Jona-Lasinio, Phys. Rev. **122**, 345 (1961).

[Anderson(1963)] P. W. Anderson, Phys. Rev. **130**, 439 (1963).

[Sooryakumar and Klein(1980)] R. Sooryakumar and M. V. Klein, Phys. Rev. Lett. **45**, 660 (1980).

[Méasson et al.(2014)] M.-A. Méasson, Y. Gallais, M. Cazayous, B. Clair, P. Rodière, L. Cario, and A. Sacuto, Phys. Rev. B **89**, 060503 (2014).

[Matsunaga et al.(2013)] R. Matsunaga, Y. I. Hamada, K. Makise, Y. Uzawa, H. Terai, Z. Wang, and R. Shimano, Phys. Rev. Lett. **111**, 057002 (2013).

[Mat()] R. Matsunaga, N. Tsuji, H. Fujita, A. Sugioka, K. Makise, Y. Uzawa, H. Terai, Z. Wang, H. Aoki, and R. Shimano, Science **345**, 1145 (2014).

[ATL()] ATLAS Collaboration, Phys. Lett. B **716**, 1 (2012).

[CMS()] CMS Collaboration, Phys. Lett. B **716**, 30 (2012).

[Gor()] L. P. Gor'kov, Sov. Phys. JETP **9**, 1364 (1959).

[Bogoliubov et al.(1958)] N. N. Bogoliubov, V. V. Tolmachev, and D. V. Shirkov, *A New Method in the Theory of Superconductivity* (Achademy of Sciences of USSR, Moscow, 1958).

[Nam(b)] Y. Nambu, Physica **15D**, 147 (1985).

[Vol(b)] G. E. Volovik and M. A. Zubkov, Phys. Rev. D **87**, 075016 (2013); J. Low Temp. Phys. **175**, 486 (2014).

[Barankov et al.(2004)] R. A. Barankov, L. S. Levitov, and B. Z. Spivak, Phys. Rev. Lett. **93**, 160401 (2004).

[Yuzbashyan et al.(2005)] E. A. Yuzbashyan, B. L. Altshuler, V. B. Kuznetsov, and V. Z. Enolskii, Phys. Rev. B **72**, 220503 (2005).

[Man()] B. Mansart, J. Lorenzana, A. Mann, A. Odeh, M. Scarongella, M. Chergui, and F. Carbone, Proc. Natl. Acad. Sci. **110**, 4539 (2013).

[Lor()] J. Lorenzana, B. Mansart, A. Mann, A. Odeh, M. Chergui, and F. Carbone, Eur. Phys. J. Special Topics **222**, 1223 (2013).

[Tsuji et al.(2009)] N. Tsuji, T. Oka, and H. Aoki, Phys. Rev. Lett. **103**, 047403 (2009).

[Barankov and Levitov(2006)] R. A. Barankov and L. S. Levitov, Phys. Rev. Lett. **96**, 230403 (2006).

[Yuzbashyan and Dzero(2006)] E. A. Yuzbashyan and M. Dzero, Phys. Rev. Lett. **96**, 230404 (2006).

[Zimmermann et al.(1991)] W. Zimmermann, E. Brandt, M. Bauer, E. Seider, and L. Genzel, Physica C: Supercond. **183**, 99 (1991).

[Freericks et al.(2006)] J. K. Freericks, V. M. Turkowski, and V. Zlatić, Phys. Rev. Lett. **97**, 266408 (2006).

[Aoki et al.(2014)] H. Aoki, N. Tsuji, M. Eckstein, M. Kollar, T. Oka, and P. Werner, Rev. Mod. Phys. **86**, 779 (2014).

[not()] Note that what essentially matters in the DMFT calculation here is the density of states near the Fermi energy and the α_1 parameter. Thus, one may take our model adopted here as a certain infinite-dimensional lattice model that has the corresponding density of states and α_1, to which DMFT can be applied.

[Tsuji and Werner(2013)] N. Tsuji and P. Werner, Phys. Rev. B **88**, 165115 (2013).

[Tsuji et al.(2013)] N. Tsuji, M. Eckstein, and P. Werner, Phys. Rev. Lett. **110**, 136404 (2013).

[Turkowski and Freericks(2005)] V. Turkowski and J. K. Freericks, Phys. Rev. B **71**, 085104 (2005).

From Dynamical vanishing of the order parameter in a fermionic condensate by Yuzbashyan, Dzero

References

[1] C. A. Regal, M. Greiner and D. S. Jin, Phys. Rev. Lett. **92**, 040403 (2004).

[2] M. W. Zwierlein *et.al.*, Phys. Rev. Lett. **92**, 120403 (2004).

[3] J. Kinast *et. al.* Phys. Rev. Lett. **92**, 150402 (2004).

[4] C. Chin *et.al.*, Science **305**, 1128 (2004).

[5] R. A. Barankov, L. S. Levitov, and B. Z. Spivak, Phys. Rev. Lett. **93**, 160401 (2004).

[6] E. A. Yuzbashyan, B. L. Altshuler, V. B. Kuznetsov, V. Z. Enolskii, J. Phys. A **38**, 7831,(2005); Phys. Rev. B **72**, 220503(R) (2005).

[7] M. H. Szymanska, B. D. Simons, and K. Burnett: Phys. Rev. Lett. **94**, 170402 (2005).

[8] G.L. Warner and A. J. Leggett, Phys. Rev. B **71**, 134514 (2005).

[9] E. A. Yuzbashyan, O. Tsyplyatyev, B. L. Altshuler, Phys. Rev. Lett. **96**, 097005 (2006).

[10] K. M. O'Hara *et. al.*, Science **298**, 2179 (2002).

[11] T. Loftus, C. A. Regal, C. Ticknor, J. L. Bohn, D. S. Jin, Phys. Rev. Lett. **88**, 173201 (2002).

[12] P. W. Anderson, Phys. Rev. **112**, 1900 (1958).

[13] A. F. Volkov and Sh. M. Kogan, Sov. Phys. JETP **38**, 1018 (1974).

[14] M. E. Fisher, M. N. Barber, and D. Jasnow, Phys. Rev. A **8**, 1111 (1973).

[15] J. R. Schrieffer, *Theory of superconductivity*, W. A. Benjamin, New York, 1964, Ch. 8.

[16] W. Kohn and D. Sherrington, Rev. Mod. Phys, **42**, 1 (1970).

[17] K. Maki, in *Superconductivity* (edited by R. D. Parks), Marcel Dekker, New York, 1969, v.2, p. 1035.

[18] R. B. Diener and T. L. Ho, cond-mat/0404517; E. Altman and A. Vishwanath, Phys. Rev. Lett. 95, 110404 (2005).

[19] R. A. Barankov and L. S. Levitov, cond-mat/0603317.

From Dynamical vanishing of the order parameter in a confined Bardeen-Cooper-Schrieffer Fermi gas after an interaction quench by Hannibal et al.

References

[Bloch et al.(2008)] I. Bloch, J. Dalibard, and W. Zwerger, Rev. Mod. Phys. **80**, 885 (2008).

[Goldman et al.(2016)] N. Goldman, J. Budich, and P. Zoller, Nature Physics **12**, 639 (2016).

[Galitski and Spielman(2013)] V. Galitski and I. B. Spielman, Nature **494**, 49 (2013).

[Wu et al.(2016)] Z. Wu, L. Zhang, W. Sun, X.-T. Xu, B.-Z. Wang, S.-C. Ji, Y. Deng, S. Chen, X.-J. Liu, and J.-W. Pan, Science **354**, 83 (2016).

[Liao et al.(2010)] Y.-a. Liao, A. S. C. Rittner, T. Paprotta, W. Li, G. B. Partridge, R. G. Hulet, S. K. Baur, and E. J. Mueller, Nature **467**, 567 (2010).

[Giorgini et al.(2008)] S. Giorgini, L. Pitaevskii, and S. Stringari, Rev. Mod. Phys. **80**, 1215 (2008).

[Chin et al.(2010)] C. Chin, R. Grimm, P. Julienne, and E. Tiesinga, Rev. Mod. Phys. **82**, 1225 (2010).

[Regal et al.(2004)] C. A. Regal, M. Greiner, and D. S. Jin, Phys. Rev. Lett. **92**, 040403 (2004).

[Zwerger(2011)] W. Zwerger, *The BCS-BEC crossover and the unitary Fermi gas*, vol. 836 (Springer, 2011).

[Grimm et al.(2000)] R. Grimm, M. Weidemüller, and Y. B. Ovchinnikov, Adv. At., Mol., Opt. Phys. **42**, 95 (2000).

[Shanenko et al.(2012)] A. A. Shanenko, M. D. Croitoru, A. V. Vagov, V. M. Axt, A. Perali, and F. M. Peeters, Phys. Rev. A **86**, 033612 (2012).

[Polkovnikov et al.(2011)] A. Polkovnikov, K. Sengupta, A. Silva, and M. Vengalattore, Rev. Mod. Phys. **83**, 863 (2011).

[Yin and Radzihovsky(2013)] X. Yin and L. Radzihovsky, Phys. Rev. A **88**, 063611 (2013).

[Yin and Radzihovsky(2016)] X. Yin and L. Radzihovsky, Phys. Rev. A **94**, 063637 (2016).

[Collaboration(2012)] C. Collaboration, Physics Letters B **716**, 30 (2012), ISSN 0370-2693.

[Sooryakumar and Klein(1980)] R. Sooryakumar and M. V. Klein, Phys. Rev. Lett. **45**, 660 (1980).

[Littlewood and Varma(1981)] P. B. Littlewood and C. M. Varma, Phys. Rev. Lett. **47**, 811 (1981).

[Endres et al.(2012)] M. Endres, T. Fukuhara, D. Pekker, M. Cheneau, P. Schauß, C. Gross, E. Demler, S. Kuhr, and I. Bloch, Nature **487**, 454 (2012).

[Papenkort et al.(2007)] T. Papenkort, V. M. Axt, and T. Kuhn, Phys. Rev. B **76**, 224522 (2007).

[Papenkort et al.(2008)] T. Papenkort, T. Kuhn, and V. M. Axt, Phys. Rev. B **78**, 132505 (2008).

[Matsunaga et al.(2014)] R. Matsunaga, N. Tsuji, H. Fujita, A. Sugioka, K. Makise, Y. Uzawa, H. Terai, Z. Wang, H. Aoki, and R. Shimano, Science **345**, 1145 (2014).

[Matsunaga et al.(2013)] R. Matsunaga, Y. I. Hamada, K. Makise, Y. Uzawa, H. Terai, Z. Wang, and R. Shimano, Phys. Rev. Lett. **111**, 057002 (2013).

[Matsunaga and Shimano(2012)] R. Matsunaga and R. Shimano, Phys. Rev. Lett. **109**, 187002 (2012).

[Fröhlich et al.(2011)] B. Fröhlich, M. Feld, E. Vogt, M. Koschorreck, W. Zwerger, and M. Köhl, Phys. Rev. Lett. **106**, 105301 (2011).

[Clark et al.(2015)] L. W. Clark, L.-C. Ha, C.-Y. Xu, and C. Chin, Phys. Rev. Lett. **115**, 155301 (2015).

[Yuzbashyan et al.(2015)] E. A. Yuzbashyan, M. Dzero, V. Gurarie, and M. S. Foster, Phys. Rev. A **91**, 033628 (2015).

[Yuzbashyan et al.(2006)] E. A. Yuzbashyan, O. Tsyplyatyev, and B. L. Altshuler, Phys. Rev. Lett. **96**, 097005 (2006).

[Yuzbashyan and Dzero(2006)] E. A. Yuzbashyan and M. Dzero, Phys. Rev. Lett. **96**, 230404 (2006).

[Yuzbashyan et al.(2005)] E. A. Yuzbashyan, B. L. Altshuler, V. B. Kuznetsov, and V. Z. Enolskii, Phys. Rev. B **72**, 220503 (2005).

[Barankov and Levitov(2006)] R. A. Barankov and L. S. Levitov, Phys. Rev. Lett. **96**, 230403 (2006).

[Bruun et al.(1999)] G. Bruun, Y. Castin, R. Dum, and K. Burnett, Eur. Phys. J. D **7** 433 (1999).

[Bruun(2014)] G. Bruun, Phys. Rev. A **90**, 023621 (2014).

[Scott et al.(2012)] R. G. Scott, F. Dalfovo, L. P. Pitaevskii, and S. Stringari, Phys. Rev. A **86**, 053604 (2012).

[Hannibal et al.(2015)] S. Hannibal, P. Kettmann, M. D. Croitoru, A. Vagov, V. M. Axt, and T. Kuhn, Phys. Rev. A **91**, 043630 (2015).

[Zachmann et al.(2013)] M. Zachmann, M. D. Croitoru, A. Vagov, V. M. Axt, T. Papenkort, and T. Kuhn, New J. Phys. **15**, 055016 (2013).

[Kettmann et al.(2017)] P. Kettmann, S. Hannibal, M. Croitoru, A. Vagov, V. Axt, and T. Kuhn, Physica C **533**, 133 (2017).

[Papenkort et al.(2009)] T. Papenkort, T. Kuhn, and V. M. Axt, Journal of Physics: Conference Series **193**, 012050 (2009).

[Chou et al.(2017)] Y.-Z. Chou, Y. Liao, and M. S. Foster, Phys. Rev. B **95**, 104507 (2017).

[Datta and Bagwell(1999)] S. Datta and P. F. Bagwell, Superlattices and Microstructures **25**, 1233 (1999).

[De Gennes(1989)] P. De Gennes, *Superconductivity of metals and alloys* (Addison-Wesley New York, 1989).

[Anderson(1959)] P. W. Anderson, J. Phys. Chem. Solids **11**, 26 (1959).

[Bruun and Heiselberg(2002)] G. M. Bruun and H. Heiselberg, Phys. Rev. A **65**, 053407 (2002).

[Leggett(2006)] A. J. Leggett, *Quantum liquids: Bose condensation and Cooper pairing in condensed-matter systems* (Oxford University Press, 2006).

From Pure Goldstone mode in the quench dynamics of a confined ultracold Fermi gas in the BCS-BEC crossover regime by Kettmann et al.

References

[Giorgini *et al.*(2008)] S. Giorgini, L. Pitaevskii, and S. Stringari, "Theory of ultracold atomic Fermi gases," Rev. Mod. Phys. **80**, 1215–1274 (2008).

[Bloch *et al.*(2008)] I. Bloch, J. Dalibard, and W. Zwerger, "Many-body physics with ultracold gases," Rev. Mod. Phys. **80**, 885 (2008).

[Weinberg(1996)] Steven Weinberg, *The quantum theory of fields*, Vol. 2 (Cambridge university press, 1996) pp. 332–352.

[Higgs(1964)] P. W. Higgs, "Broken symmetries and the masses of gauge bosons," Phys. Rev. Lett. **13**, 508–509 (1964).

[Burgess(2000)] C. P. Burgess, "Goldstone and pseudo-Goldstone bosons in nuclear, particle and condensed-matter physics," Phys. Reports **330**, 193–261 (2000).

[Paulson *et al.*(1973)] D. Paulson, R. Johnson, and J. Wheatley, "Propagation of collisionless sound in normal and extraordinary phases of liquid ^{3}He below 3 mK," Phys. Rev. Lett. **30**, 829 (1973).

[Lawson *et al.*(1973)] D. Lawson, W. Gully, S. Goldstein, R. Richardson, and D. Lee, "Attenuation of zero sound and the low-temperature transitions in liquid ^{3}He," Phys. Rev. Lett. **30**, 541 (1973).

[Anderson(1958)] P. W. Anderson, "Random-phase approximation in the theory of superconductivity," Phys. Rev. **112**, 1900 (1958).

[Pekker and Varma(2015)] David Pekker and CM Varma, "Amplitude/higgs modes in condensed matter physics," Annu. Rev. Condens. Matter Phys. **6**, 269–297 (2015).

[Bissbort *et al.*(2011)] U. Bissbort, S. Götze, Y. Li, J. Heinze, J. S Krauser, M. Weinberg, C. Becker, K. Sengstock, and W. Hofstetter, "Detecting the amplitude mode of strongly interacting lattice bosons by Bragg scattering," Phys. Rev. Lett. **106**, 205303 (2011).

[Endres *et al.*(2012)] M. Endres, T. Fukuhara, D. Pekker, M. Cheneau, P. Schauß, C. Gross, E. Demler, S. Kuhr, and I. Bloch, "The 'Higgs' amplitude mode at the two-dimensional superfluid/Mott insulator transition," Nature **487**, 454–458 (2012).

[Matsunaga *et al.*(2013)] R. Matsunaga, Y. I. Hamada, K. Makise, Y. Uzawa, H. Terai, Z. Wang, and R. Shimano, "Higgs amplitude mode in the BCS superconductors Nb 1-x Ti x n induced by terahertz pulse excitation," Phys. Rev. Lett. **111**, 057002 (2013).

[Matsunaga *et al.*(2014)] R. Matsunaga, N. Tsuji, H. Fujita, A. Sugioka, K. Makise, Y. Uzawa, H. Terai, Z. Wang, H. Aoki, and R. Shimano, "Light-induced collective pseudospin precession resonating with Higgs mode in a superconductor," Science **345**, 1145–1149 (2014).

[Barankov *et al.*(2004)] R.A. Barankov, L.S. Levitov, and B.Z. Spivak, "Collective Rabi oscillations and solitons in a time-dependent BCS pairing problem," Phys. Rev. Lett. **93**, 160401 (2004).

[Barankov and Levitov(2006)] R. A. Barankov and L. S. Levitov, "Synchronization in the BCS pairing dynamics as a critical phenomenon," Phys. Rev. Lett. **96**, 230403 (2006).

[Yuzbashyan *et al.*(2006)] E. A. Yuzbashyan, O. Tsyplyatyev, and B. L. Altshuler, "Relaxation and persistent oscillations of the order parameter in fermionic condensates," Phys. Rev. Lett. **96**, 097005 (2006).

[Dzero *et al.*(2007)] M. Dzero, E.A. Yuzbashyan, B.L. Altshuler, and P. Coleman, "Spectroscopic signatures of nonequilibrium pairing in atomic Fermi gases," Phys. Rev. Lett. **99**, 160402 (2007).

[Scott *et al.*(2012)] R.G. Scott, F. Dalfovo, L.P. Pitaevskii, and S. Stringari, "Rapid ramps across the BEC-BCS crossover: A route to measuring the superfluid gap," Phys. Rev. A **86**, 053604 (2012).

[Bruun(2014)] G. Bruun, "Long-lived Higgs mode in a two-dimensional confined Fermi system," Phys. Rev. A **90**, 023621 (2014).

[Hannibal *et al.*(2015)] S. Hannibal, P. Kettmann, M. D. Croitoru, A. Vagov, V. M. Axt, and T. Kuhn, "Quench dynamics of an ultracold Fermi gas in the BCS regime: Spectral properties and confinement-induced breakdown of the Higgs mode," Phys. Rev. A **91**, 043630 (2015).

[Kinast *et al.*(2004a)] J. Kinast, S.L. Hemmer, M.E. Gehm, A. Turlapov, and J.E. Thomas, "Evidence for superfluidity in a resonantly interacting Fermi gas," Phys. Rev. Lett. **92**, 150402 (2004a).

[Kinast *et al.*(2004b)] J. Kinast, A. Turlapov, and J.E. Thomas, "Breakdown of hydrodynamics in the radial breathing mode of a strongly interacting Fermi gas," Phys. Rev. A **70**, 051401 (2004b).

[Bartenstein *et al.*(2004)] M. Bartenstein, A. Altmeyer, S. Riedl, S. Jochim, C. Chin, J. H. Denschlag, and R. Grimm, "Collective excitations of a degenerate gas at the BEC-BCS crossover," Phys. Rev. Lett. **92**, 203201 (2004).

[Altmeyer *et al.*(2007a)] A. Altmeyer, S. Riedl, M. J. Wright, C. Kohstall, J. H. Denschlag, and R. Grimm, "Dynamics of a strongly interacting Fermi gas: The radial quadrupole mode," Phys. Rev. A **76**, 033610 (2007a).

[Altmeyer *et al.*(2007b)] A. Altmeyer, S. Riedl, C. Kohstall, M. J. Wright, R. Geursen, M. Bartenstein, C. Chin, J. H. Denschlag, and R. Grimm, "Precision measurements of collective oscillations in the BEC-BCS crossover," Phys. Rev. Lett. **98**, 040401 (2007b).

[Riedl *et al.*(2008)] S. Riedl, E. R. Sánchez Guajardo, C. Kohstall, A. Altmeyer, M. J. Wright, J. H. Denschlag, R. Grimm, G. M. Bruun, and H. Smith, "Collective oscillations of a Fermi gas in the unitarity limit: Temperature effects and the role of pair correlations," Phys. Rev. A **78**, 053609 (2008).

[Baranov and Petrov(2000)] M. A. Baranov and D. S. Petrov, "Low-energy collective excitations in a superfluid trapped Fermi gas," Phys. Rev. A **62**, 041601 (2000).

[Bruun and Mottelson(2001)] G. M. Bruun and B. R. Mottelson, "Low energy collective modes of a superfluid trapped atomic Fermi gas," Phys. Rev. Lett. **87**, 270403 (2001).

[Bruun(2002)] G. M. Bruun, "Low-energy monopole modes of a trapped atomic Fermi gas," Phys. Rev. Lett. **89**, 263002 (2002).

[Hu *et al.*(2004)] H. Hu, A. Minguzzi, X. J. Liu, and M. P. Tosi, "Collective modes and ballistic expansion of a Fermi gas in the BCS-BEC crossover," Phys. Rev. Lett. **93**, 190403 (2004).

[Heiselberg(2004)] H. Heiselberg, "Collective modes of trapped gases at the BEC-BCS crossover," Phys. Rev. Lett. **93**, 040402 (2004).

[Stringari(2004)] S. Stringari, "Collective oscillations of a trapped superfluid Fermi gas near a Feshbach resonance," Europhys. Lett. **65**, 749–752 (2004).

[Grasso *et al.*(2005)] M. Grasso, E. Khan, and M. Urban, "Temperature dependence and finite-size effects in collective modes of superfluid-trapped Fermi gases," Phys. Rev. A **72**, 043617 (2005).

[Korolyuk *et al.*(2011)] A. Korolyuk, J. J. Kinnunen, and P. Törmä, "Density response of a trapped Fermi gas: A crossover from the pair vibration mode to the Goldstone mode," Phys. Rev. A **84**, 033623 (2011).

[Clark *et al.*(2015)] L. W. Clark, L. C. Ha, C. Y. Xu, and C. Chin, "Quantum dynamics with spatiotemporal control of interactions in a stable Bose-Einstein condensate," Phys. Rev. Lett. **115**, 155301 (2015).

[De Gennes(1989)] P. De Gennes, *Superconductivity of metals and alloys* (Addison-Wesley New York, 1989).

[Datta and Bagwell(1999)] S. Datta and P. F. Bagwell, "Can the Bogoliubov-de Gennes equation be interpreted as a one-particle wave equation?" Superlattices and Microstruct. **25**, 1233–1250 (1999).

[Lord(1949)] R. D. Lord, "Some integrals involving Hermite polynomials," Journal of the London Mathematical Society **1**, 101–112 (1949).

[Shanenko *et al.*(2012)] A.A. Shanenko, M. D. Croitoru, A.V. Vagov, V.M. Axt, A. Perali, and F.M. Peeters, "Atypical BCS-BEC crossover induced by quantum-size effects," Phys. Rev. A **86**, 033612 (2012).

[Jain(2017)] Akash Jain, "Theory of non-abelian superfluid dynamics," Phys. Rev. D **95**, 121701 (2017).

[Yuzbashyan *et al.*(2015)] Emil A. Yuzbashyan, Maxim Dzero, Victor Gurarie, and Matthew S. Foster, "Quantum quench phase diagrams of an s-wave BCS-BEC condensate," Physical Review A **91**, 033628 (2015).

[Stewart *et al.*(2008)] J. Stewart, J. Gaebler, and D. Jin, "Using photoemission spectroscopy to probe a strongly interacting Fermi gas," Nature **454**, 744–747 (2008).

[Stewart *et al.*(2010)] J.T. Stewart, J.P. Gaebler, T.E. Drake, and D.S. Jin, "Verification of universal relations in a strongly interacting Fermi gas," Phys. Rev. Lett. **104**, 235301 (2010).

[Ketterle and Zwierlein(2008)] W. Ketterle and M. Zwierlein, "Making, probing and understanding ultracold Fermi gases," ArXiv (2008).

From Synchronization in the BCS Pairing Dynamics as a Critical Phenomenon by Barankov, Levitov

References

[1] C. A. Regal, M. Greiner, and D. S. Jin, Phys. Rev. Lett. **92**, 040403 (2004).

[2] M. W. Zwierlein, C. A. Stan, C. H. Schunck, S. M. F. Raupach, A. J. Kerman, and W. Ketterle, Phys. Rev. Lett. **92**, 120403 (2004).

[3] E. Timmermans, P. Tommasini, M. Hussein, and A. Kerman, Physics Reports **315**, 199 (1999).

[4] F. Dalfovo, S. Giorgini, L. P. Pitaesvkii, and S. Stringari, Rev. Mod. Phys. **71**, 463 (1999).

[5] H. J. Lewandowski, D. M. Harber, D. L. Whitaker, and E. A. Cornell, Phys. Rev. Lett. **88**, 070403 (2002); J. M. McGuirk, H. J. Lewandowski, D. M. Harber, T. Nikuni, J. E. Williams, and E. A. Cornell, Phys. Rev. Lett. **89**, 090402 (2002).

[6] C. Chin, M. Bartenstein, A. Altmeyer, S. Riedl, S. Jochim, J. H. Denschlag, and R. Grimm, Science, **305**, 1128 (2004).

[7] T. M. O'Neil, Phys. Fluids **8**, 2255 (1965).

[8] I. B. Bernstein, J. M. Green, and M. D. Kruskal, Phys. Rev. **108**, 546 (1957)

[9] J. R. Danielson, F. Anderegg, and C. F. Driscoll, Phys. Rev. Lett. **92**, 245003 (2004).

[10] M.Ö. Oktel and L. S. Levitov, Phys. Rev. Lett. **83**, 6 (1999).

[11] T. Nikuni and J. E. Williams, J. Low Temp. Phys. **133**, 323 (2003).

[12] R. J. Ragan, W. J. Mullin, and E. B. Wiita, cond-mat/0502189

[13] S. Tsuchiya and A. Griffin, Phys. Rev. A **72**, 053621 (2005).

[14] R. A. Barankov, L. S. Levitov, and B. Z. Spivak, Phys. Rev. Lett. **93**, 160401 (2004).

[15] A. V. Andreev, V. Gurarie, and L. Radzihovsky, Phys. Rev. Lett. **93**, 130402 (2004); R. A. Barankov and L. S. Levitov, Phys. Rev. Lett. **93**, 130403 (2004).

[16] M. H. Szymańska, B. D. Simons, and K. Burnett, Phys. Rev. Lett. **94**, 170402 (2005).

[17] G. L. Warner and A. J. Leggett, Phys. Rev. B **71**, 134514 (2005).

[18] A. F. Volkov and Sh. M. Kogan, Zh. Eksp. Teor. Fiz. **65**, 2038, (1973) [Sov. Phys. JETP **38**, 1018 (1974)].

[19] E. A. Yuzbashyan, O. Tsyplyatyev, and B. L. Altshuler, Phys. Rev. Lett. **96**, 097005 (2006).

[20] E. A. Yuzbashyan, B. L. Altshuler, V. B. Kuznetsov, and V. Z. Enolskii, Phys. Rev. B **72**, 220503 (2005).

[21] P. W. Anderson, Phys. Rev. **112**, 1900 (1958)

[22] M. H. S. Amin, E. V. Bezuglyi, A. S. Kijko, and A. N. Omelyanchouk, Low Temp. Phys. **30**, 661 (2004), cond-mat/0404401

[23] R. W. Richardson and N. Sherman, Nucl. Phys. **52**, 221 (1964).

[24] M. C. Cambiaggio, A. M. F. Rivas, and M. Saraceno, Nucl. Phys. A **424**, 157 (1997).

[25] L. P. Gor'kov and T. K. Melik-Barkhudarov, Zh. Eksp. Teor. Fiz. **40**, 1452, (1961) [Sov. Phys. JETP, **13**, 1018 (1961)].

From Higgs Mode in Superconductors by Shimano, Tsuji

References

[1] Nambu Y. 2011. *BCS: 50 Years*, edited by L. N. Cooper and D. Feldman (World Scientific, Singapore)

[2] Ginzburg VL, Landau LD. 1950. *Zh. Eksp. Teor. Fiz.* 20:1064

[3] Bogoliubov NN. 1958. *J. Exptl. Theoret. Phys.* 34:58 [1958. *Sov. Phys.* 34:41]

[4] Anderson PW. 1958. *Phys. Rev.* 110:827

[5] Anderson PW. 1958. *Phys. Rev.* 112:1900

[6] Nambu Y. 1960. *Phys. Rev.* 117:648

[7] Goldstone J. 1961. *Nuovo Cim.* 19:154

[8] Goldstone J, Salam A, Weinberg S. 1962. *Phys. Rev.* 127:965

[9] Anderson PW. 1963. *Phys. Rev.* 130:439

[10] Englert F, Brout R. 1964. *Phys. Rev. Lett.* 13:321.

[11] Higgs PW. 1964. *Phys. Lett.* 12:132

[12] Higgs PW. 1964. *Phys. Rev. Lett.* 13:508

[13] Guralnik GS, Hagen CR, Kibble TWB. 1964. *Phys. Rev. Lett.* 13:585

[14] Anderson PW. 2015. *Nat. Phys.* 11:93

[15] Bardeen J, Cooper LN, Schrieffer JR. 1957. *Phys. Rev.* 108:1175

[16] Volkov AF, Kogan SM. 1974. *Sov. Phys. JETP* 38:1018

[17] Kulik IO, Entin-Wohlman O, Orbach R. 1981. *J. Low Temp. Phys.* 43:591

[18] Littlewood PB, Varma CM. 1981. *Phys. Rev. Lett.* 47:811

[19] Littlewood PB, Varma CM. 1982. *Phys. Rev. B* 26:4883

[20] Nambu Y, Jona-Lasinio G. 1961. *Phys. Rev.* 122:345

[21] Nambu Y. 1985. *Physica* 15D:147

[22] Volovik GE, Zubkov MA. 2014. *J. Low Temp. Phys.* 175:486

[23] ATLAS Collaboration. 2012. *Phys. Lett. B* 716:1

[24] CMS Collaboration. 2012. *Phys. Lett. B* 716:30

[25] Sooryakumar R, Klein MV. 1980. *Phys. Rev. Lett.* 45:660

[26] Sooryakumar R, Klein MV. 1981. *Phys. Rev. B* 23:3213

[27] Varma C. 2002. *J. Low Temp. Phys.* 126:901

[28] Méasson MA, Gallais Y, Cazayous M, Clair B, Rodière P, Cario L, Sacuto A. 2014. *Phys. Rev. B* 89:060503(R)

[29] Cea T, Benfatto L. 2014. *Phys. Rev. B* 90:224515

[30] Grasset R, Cea T, Gallais Y, Cazayous M, Sacuto A, Cario L, Benfatto L, Méasson MA. 2018. *Phys. Rev. B* 97:094502

[31] Barankov RA, Levitov LS, Spivak BZ. 2004. *Phys. Rev. Lett.* 93:160401

[32] Yuzbashyan EA, Altshuler BL, Kuznetsov VB, Enolskii VZ. 2005. *Phys. Rev. B* 72:220503

[33] Barankov RA, Levitov LS. 2006. *Phys. Rev. Lett.* 96:230403

[34] Yuzbashyan EA, Tsyplyatyev O, Altshuler BL. 2006. *Phys. Rev. Lett.* 96:097005

[35] Yuzbashyan EA, Dzero M. 2006. *Phys. Rev. Lett.* 96:230404

[36] Gurarie V. 2009. *Phys. Rev. Lett.* 103:075301

[37] Tsuji N, Eckstein M, Werner P. 2013. *Phys. Rev. Lett.* 110:136404

[38] Papenkort T, Axt VM, Kuhn T. 2007. *Phys. Rev. B* 76:224522

[39] Papenkort T, Kuhn T, Axt VM. 2008. *Phys. Rev. B* 78:132505

[40] Schnyder AP, Manske D, Avella A. 2011. *Phys. Rev. B* 84:214513

[41] Krull H, Manske D, Uhrig GS, Schnyder AP. 2014. *Phys. Rev. B* 90:014515

[42] Tsuji N, Aoki H. 2015. *Phys. Rev. B* 92:064508

[43] Kemper AF, Sentef MA, Moritz B, Freericks JK, Devereaux TP. 2015. *Phys. Rev. B* 92:224517

[44] Chou Y-Z, Liao Y, Foster M. S. 2017. *Phys. Rev. B*95:104507

[45] Matsunaga R, Hamada YI, Makise K, Uzawa Y, Terai H, Wang Z, Shimano R. 2013. *Phys. Rev. Lett.* 111:057002

[46] Matsunaga R, Tsuji N, Fujita H, Sugioka A, Makise K, Uzawa Y, Terai H, Wang Z, Aoki H, Shimano R. 2014. *Science* 345:1145

[47] Cea T, Castellani C, Benfatto L. 2016. *Phys. Rev. B* 93:180507(R)

[48] Tsuji N, Murakami Y, Aoki H. 2016. *Phys. Rev. B* 94:224519

[49] Matsunaga R, Tsuji N, Makise K, Terai H, Aoki H, Shimano R. 2017 *Phys. Rev. B* 96:020505(R)

[50] Cea T, Barone P, Castellani C, Benfatto L. 2018. *Phys. Rev. B* 97:094516

[51] Jujo T. 2015. *J. Phys. Soc. Jpn.* 84:114711

[52] Jujo T. 2018. *J. Phys. Soc. Jpn.* 87:024704

[53] Murotani Y, Shimano R. 2019. arXiv:1902.01104

[54] Silaev M. 2019. arXiv:1902.01666

[55] Katsumi K, Tsuji N, Hamada YI, Matsunaga R, Schneeloch J, Zhong RD, Gu GD, Aoki H, Gallais Y, Shimano R. 2018. *Phys. Rev. Lett.* 120:117001

[56] Chu H, Kim M-J, Katsumi K, Kovalev S, Dawson RD, Schwarz L, Yoshikawa N, Kim G, Putzky D, Li ZZ, Raffy H, Germanskiy S, Deinert J-C, Awari N, Ilyakov I, Green B, Chen M, Bawatna M, Christiani G, Logvenov G, Gallais Y, Boris AV, Keimer B, Schnyder A, Manske D, Gensch M, Wang Z, Shimano R, Kaiser S. 2019. arXiv:1901.06675

[57] Moor A, Volkov AF, Efetov KB. 2017. *Phys. Rev. Lett.* 118:047001

[58] Nakamura S, Iida Y, Murotani Y, Matsunaga R, Terai H, Shimano R. 2018. arXiv:1809.10335

[59] Vollhardt D, Wölfle P. 1990. *The Superfluid Phases of Helium 3* (Taylor & Francis)

[60] Endres M, Fukuhara T, Pekker D, Cheneau M, Schauβ P, Gross C, Demler E, Kuhr S, Bloch I. 2012. *Nature* 487:454

[61] Behrle A, Harrison T, Kombe J, Gao K, Link M, Bernier J-S, Kollath C, Köhl M. 2018. *Nat. Phys.* 14:781

[62] Rüegg C, Normand B, Matsumoto M, Furrer A, McMorrow DF, et al. 2008. *Phys. Rev. Lett.* 100:205701

[63] Pekker D, Varma CM. 2015. *Annu. Rev. Condens. Matter Phys.* 6:269

[64] Abraham E, Tsuneto T. 1966. *Phys. Rev.* 152:416

[65] Schmid A. 1966. *Phys. Kond. Mater.* 5:302

[66] Caroli C, Maki K. 1967. *Phys. Rev.* 159:306

[67] Ebisawa H, Fukuyama H. 1971. *Prog. Theor. Phys.* 46:1042

[68] Sá de Melo CAR, Randeria M, Engelbrecht JR. 1993. *Phys. Rev. Lett.* 71:3202

[69] Tsuchiya S, Yamamoto D, Yoshii R, Nitta M. 2018. *Phys. Rev. B* 98:094503

[70] Gor'kov LP, Eliashberg GM. 1968. *Sov. Phys. JETP* 27:328

[71] Gulian AM, Zharkov GF. 1999. *Nonequilibrium electrons and phonons in superconductors* (Kluwer Academic/Plenum Publishers)

[72] Kopnin N. 2001. *Theory of Nonequilibrium Superconductivity* (Oxford University Press)

[73] Schrieffer JR. 1999. *Theory of Superconductivity* (Westview Press)

[74] Kihlstrom KE, Simon RW, Wolf SA. 1985. *Phys. Rev. B* 32:1843

[75] Brorson SD, Kazeroonian A, Moodera JS, Face DW, Cheng TK, Ippen EP, Dresselhaus MS, Dresselhaus G. 1990. *Phys. Rev. Lett.* 64:2172

[76] Chockalingam SP, Chand M, Jesudasan J, Tripathi V, Raychaudhuri P. 2008. *Phys. Rev. B* 77:214503

[77] Aoki H, Tsuji N, Eckstein M, Kollar M, Oka T, Werner P. 2014. *Rev. Mod. Phys.* 86:779

[78] Murakami Y, Werner P, Tsuji N, Aoki H. 2016. *Phys. Rev. B* 93:094509

[79] Murakami Y, Werner P, Tsuji N, Aoki H. 2016. *Phys. Rev. B* 94:115126

[80] Nosarzewski B, Moritz B, Freericks JK, Kemper AF, Devereaux TP. 2017. *Phys. Rev. B* 96:184518

[81] Kumar A, Kemper AF. 2019. arXiv:1902.09549

[82] Yu T, Wu MW. 2017. *Phys. Rev. B* 96:155311

[83] Yu T, Wu MW. 2017. *Phys. Rev. B* 96:155312

[84] Yang F, Wu MW. 2018. *Phys. Rev. B* 98:094507

[85] Yang F, Wu MW. 2018. arXiv:1812.06622

[86] Leggett AJ. 1966. *Prog. Theor. Phys.* 36:901

[87] Akbari A, Schnyder AP, Manske D, Eremin I. 2013. *Europhys. Lett.* 101:17002

[88] Krull H, Bittner N, Uhrig GS, Manske D, Schnyder AP. 2016. *Nat. Commun.* 7:11921

[89] Cea T, Benfatto L. 2016. *Phys. Rev. B* 94:064512

[90] Murotani Y, Tsuji N, Aoki H. 2017. *Phys. Rev. B* 95:104503

[91] Barlas Y, Varma CM. 2013. *Phys. Rev. B* 87:054503

[92] Peronaci F, Schiró M, Capone M. 2015. *Phys. Rev. Lett.* 115:257001

[93] Foster MS, Dzero M, Gurarie V, Yuzbashyan EA. 2013. *Phys. Rev. B* 88:104511

[94] Fauseweh B, Schwarz L, Tsuji N, Cheng N, Bittner N, Krull H, Berciu M, Uhrig GS, Schnyder AP, Kaiser S, Manske D. 2017. arXiv:1712.07989

[95] Grasset R, Gallais Y, Sacuto A, Cazayous M, Mañas-Valero S, Coronado E, Méasson MA. 2019. Phys. Rev. Lett. 122:127001

[96] Hebling J, Yeh KL, Hoffmann MC, Bartal B, Nelson KA. 2008. *J. Opt. Soc. Am. B* 25:B6

[97] Watanabe S, Minami N, Shimano R. 2011. *Optics Express* 19:1528

[98] Shimano R, Watanabe S, Matsunaga R. 2012. *J. Infrared Millim. Terahz Waves* 33:861

[99] Matsunaga R, Shimano R. 2012. *Phys. Rev. Lett.* 109:187002

[100] Matsunaga R, Shimano R. 2017. *Phys. Scr.* 92:024003

[101] Beck M, Klammer M, Lang S, Leiderer P, Kabanov VV, Gol'tsman GN, Demsar J. 2011. *Phys. Rev. Lett.* 107:177007

[102] Mansart B, Lorenzana J, Mann A, Odeh A, Scarongella M, Chergui M, Carbone F. 2013. *Proc. Natl. Acad. Sci. USA* 110:4539

[103] Gor'kov LP, Eliashberg GM. 1969. *Sov. Phys. JETP* 29:698

[104] Amato JC, McLean WL. 1976. *Phys. Rev. Lett.* 37:930

[105] Entin-Wohlman O. 1978. *Phys. Rev. B* 18:4762

[106] Bardasis A, Schrieffer JR. 1961. *Phys. Rev.* 121:1050

[107] Mattis DC, Bardeen J. 1958. *Phys. Rev.* 111:412

[108] Zimmermann W, Brandt EH, Bauer M, Seider E, Genzel L. 1991. *Physica C: Supercond.* 183:99

[109] Podolsky D, Auerbach A, Arovas DP. 2011. *Phys. Rev. B* 84:174522

[110] Gazit S, Podolsky D, Auerbach A. 2013. *Phys. Rev. Lett.* 110:140401

[111] Sachdev S. 1999. *Phys. Rev. B* 59:14054

[112] Zwerger W. 2004. *Phys. Rev. Lett.* 92:027203

[113] Sherman D, Pracht US, Gorshunov B, Poran S, Jesudasan J, Chand M, Raychaudhuri P, Swanson M, Trivedi N, Auerbach A, Scheffler M, Frydman A, Dressel M. 2015. *Nat. Phys.* 11:188

[114] Cea T, Bucheli D, Seibold G, Benfatto L, Lorenzana J, Castellani C. 2014. *Phys. Rev. B* 89:174506

[115] Cea T, Castellani C, Seibold G, Benfatto L. 2015. *Phys. Rev. Lett.* 115:157002

[116] Pracht US, Cea T, Bachar N, Deutscher G, Farber E, Dressel M, Scheffler M, Castellani C, García-García AM, Benfatto L. 2017. *Phys. Rev. B* 96:094514

[117] Seibold G, Benfatto L, Castellani C. 2017. *Phys. Rev. B* 96:144507

[118] Cheng B, Wu L, Laurita NJ, Singh H, Chand M, Raychaudhuri P, Armitage NP. 2016. *Phys. Rev. B* 93:180511

[119] Maiti S, Hirschfeld PJ. 2015. *Phys. Rev. B* 92:094506

[120] Müller MA, Shen P, Dzero M, Eremin I. 2018. *Phys. Rev. B* 98:024522

[121] Blumberg G, Mialitsin A, Dennis BS, Klein MV, Zhigadlo ND, Karpinski J. 2007. *Phys. Rev. Lett.* 99:227002

[122] Giorgianni F, Cea T, Vicario C, Hauri CP, Withanage WK, Xi X, Benfatto L. 2019. *Nat. Phys.* online publication

[123] Scott RG, Dalfovo F, Pitaevskii LP, Stringari S. 2012. *Phys. Rev. A* 86:053604

[124] Yuzbashyan EA, Dzero M, Gurarie V, Foster MS. 2015. *Phys. Rev. A* 91:033628

[125] Tokimoto J, Tsuchiya S, Nikuni T. 2019. *J. Phys. Soc. Jpn.* 88:023601

[126] Wölfle P. 1977. *Physica B* 90:96

[127] Fausti D, Tobey RI, Dean N, Kaiser S, Dienst A, Hoffmann MC, Pyon S, Takayama T, Takagi H, Cavalleri A. 2011. *Science* 331:189

[128] Kaiser S, Hunt CR, Nicoletti D, Hu W, Gierz I, Liu HY, Le Tacon M, Loew T, Haug D, Keimer B, Cavalleri A. 2014. *Phys. Rev. B* 89:184516

[129] Hu W, Kaiser S, Nicoletti D, Hunt CR, Gierz I, Hoffmann MC, Le Tacon M, Loew T, Keimer B, Cavalleri A. 2014. *Nat. Mater.* 13:705

[130] Mitrano M, Cantaluppi A, Nicoletti D, Kaiser S, Perucchi A, Lupi S, Di Pietro P, Pontiroli D, Riccò M, Clark SR, Jaksch D, Cavalleri A. 2016. *Nature* 530:461

34.13 Bibliography from Other Artiles

From Nonequilibrium Cooper pairing in the nonadiabatic Regime by Yuzbashyan et al.

References

[1] N. B. Kopnin: Theory of Nonequilibrium Superconductivity, Clarendon Press, Oxford (2001).

[2] E. Abrahams and T. Tsuneto: Phys. Rev. **152**, 416 (1966).

[3] A. Schmid: Phys. Kond. Mat. **5**, 302 (1966).

[4] L. P. Gor'kov and G. M. Eliashberg: Sov. Phys. JETP **27**, 328 (1968).

[5] O. Betbeder-Matibet and P. Nozieres: Ann. Phys. **51**, 392 (1969).

[6] A. G. Aronov et. al.: Adv. Phys. **30**, 539 (1981); In: Nonequilibrium Superconductivity (ed. D. N. Landenberg and A. I. Larkin), Elsevier (1986).

[7] M. W. Zwierlein et. al.: Phys. Rev. Lett. **92**, 120403 (2004). C. A. Regal, M. Greiner, and D. S. Jin: Phys. Rev. Lett. **92**, 040403 (2004).

[8] C. A. Regal, M. Greiner, and D. S. Jin: Phys. Rev. Lett. 92, 040403 (2004); M. W. Zwierlein et. al.: Phys. Rev. Lett. 92, 120403 (2004); J. Kinast et. al.: Phys. Rev. Lett. 92, 150402 (2004); M. W. Zwierlein et. al.: cond-mat/0412675.

[9] E. A. Yuzbashyan, V. B. Kuznetsov, B. L. Altshuler: unpublished.

[10] R. W. Richardson: J. Math. Phys. **18**, 1802 (1977).

[11] P. W. Anderson: Phys. Rev. **112**, 1900 (1958).

[12] A. F. Volkov and Sh. M. Kogan: Sov. Phys. JETP **38**, 1018 (1974).

[13] Yu. M. Gal'perin, V. I. Kozub, and B. Z. Spivak: Sov. Phys. JETP **54**, 1126 (1981).

[14] V. S. Shumeiko: Doctoral Thesis, Institute for Low Temperature Physics and Engineering, Kharkov, 1990.

[15] R. A. Barankov, L. S. Levitov, and B. Z. Spivak: Phys. Rev. Lett. 93, 160401 (2004).

[16] A. V. Andreev, V. Gurarie, and L. Radzihovsky: Phys. Rev. Lett. 93, 130402 (2004).

[17] R. A. Barankov and L. S. Levitov: Phys. Rev. Lett. 93, 130403 (2004).

[18] M. H. Szymanska, B. D. Simons, and K. Burnett: Phys. Rev. Lett. 94 , 170402 (2005).

[19] M.H.S. Amin, E.V. Bezuglyi, A.S. Kijko, A.N. Omelyanchouk: Low Temp. Phys. 30, 661 (2004).

[20] J. Bardeen, L.N. Cooper, and J.R. Schriefer: Phys. Rev. **108** 1175 (1957).

[21] P. W. Anderson: J. Phys. Chem. Solids **11**, 26 (1959).

[22] I. L. Kurland, I. L. Aleiner, and B. L. Altshuler: Phys. Rev. B **62**, 14886 (2000).

[23] In the presence of spatial symmetries additional quantum numbers are needed to distinguish states. For example, if there is translational invariance, time-reversed pairs of states are $|j\uparrow\rangle = |\mathbf{p}\uparrow\rangle$ and $|j\downarrow\rangle = |-\mathbf{p}\downarrow\rangle$.

[24] R. W. Richardson and N. Sherman: Nucl. Phys. **52**, 221 (1964); **52**, 253 (1964).

[25] M. Gaudin: La fonction d'onde de Bethe, Masson, Paris (1983).

[26] M. C. Cambiaggio, A. M. F. Rivas, and M. Saraceno: Nucl. Phys. A **424**, 157 (1997).

[27] Each of H_j can be viewed as a Hamiltonian of a system of classical spins, these Hamiltonians are known as classical Gaudin magnets[25].

[28] V. I. Arnold: Mathematical Methods of Classical Mechanics, Springer-Verlag, New York, (1978); M. Tabor, Chaos and Integrability in Nonlinear Dynamics, Wiley, New York, (1989).

[29] E. K. Sklyanin: J. Sov. Math. **47**, 2473 (1989); Progr. Theoret. Phys. Suppl. **118**, 35 (1995); V. B. Kuznetsov: J. Math. Phys. **33**, 3240, (1992).

[30] E. A. Yuzbashyan, B. L. Altshuler, V. B. Kuznetsov, V. Z. Enolskii: J. Phys. A **38**, 7831, (2005); cond-mat/0407501.

[31] E.D. Belokolos, A.I. Bobenko, V.Z. Enolskii, A.R. Its: *Algebro-geometric approach to nonlinear-integrable equations*, (Springer-Verlag, Berlin, 1994); D. Mumford: *Tata Lectures on Theta*, (Birkhauser, Boston, 1983, 1984) Vols. 1-2.

[32] J. C. Eilbeck, V. Z. Enolskii, and H. Holden: Proc. R. Soc. Lond. A **459**, 1581, (2003).

[33] R. Bonifacio and G. Preparata: Phys. Rev. A **2**, 336 (1970).

[34] A. Vardi, V. A. Yurovsky and J. R. Anglin: Phys. Rev. A **64**, 063611 (2001).

[35] For certain initial conditions the dynamics in the thermodynamic limit can reduce to that of a few spin solution *asymptotically* at long times. For example, we expect $m = 3, 5, \ldots$ spin solutions at long times if the coupling is changed abruptly while the condensate is in an excited state.

[36] G.L. Warner and A. J. Leggett: Phys. Rev. B **71**, 134514 (2005).

From Nonequilibrium dynamics of weakly and strongly paired superconductors by Gurarie

References

[Calabrese and Cardy(2006)] P. Calabrese and J. Cardy, Phys. Rev. Lett. **96**, 136801 (2006).

[Kollath et al.(2007)] C. Kollath, A. M. Läuchli, and E. Altman, Phys. Rev. Lett. **98**, 180601 (2007).

[Volkov and Kogan(1973)] A. F. Volkov and S. M. Kogan, Zh. Eksp. Teor. Fiz **65**, 2038 (1973), English translation: Sov. Phys. JETP, **38**, 1018 (1974).

[Barankov et al.(2004)] R. A. Barankov, L. S. Levitov, and B. Z. Spivak, Phys. Rev. Lett. **93**, 160401 (2004).

[Dukelsky et al.(2004)] J. Dukelsky, S. Pittel, and G. Sierra, Rev. Mod. Phys. **76**, 643 (2004).

[Barankov and Levitov(2006)] R. A. Barankov and L. S. Levitov, Phys. Rev. Lett. **96**, 230403 (2006).

[Yuzbashyan and Dzero(2006)] E. A. Yuzbashyan and M. Dzero, Phys. Rev. Lett. **96**, 230404 (2006).

[Eagles(1969)] D. M. Eagles, Phys. Rev. **186**, 456 (1969).

[Leggett(1980)] A. Leggett, in *Modern Trends in the Theory of Condensed Matter* (Springer-Verlag, Berlin, 1980), pp. 13–27.

[Nozières and Schmitt-Rink(1985)] P. Nozières and S. Schmitt-Rink, J. Low Temp. Phys. **59**, 195 (1985).

[Regal et al.(2004)] A. Regal, M. Greiner, and D. S. Jin, Phys. Rev. Lett. **92**, 040403 (2004).

[Zwierlein et al.(2004)] M. W. Zwierlein, C. A. Stan, C. H. Schunck, S. M. F. Raupach, A. J. Kerman, and W. Ketterle, Phys. Rev. Lett. **92**, 120403 (2004).

[Andreev et al.(2004)] A. V. Andreev, V. Gurarie, and L. Radzihovsky, Phys. Rev. Lett. **93**, 130402 (2004).

[Barankov and Levitov(2004)] R. A. Barankov and L. S. Levitov, Phys. Rev. Lett. **93**, 130403 (2004).

[Holland et al.(2001)] M. Holland, J. Park, and R. Walser, Phys. Rev. Lett. **86**, 1915 (2001).

[Giorgini et al.(2008)] S. Giorgini, L. P. Pitaevskii, and S. Stringari, Rev. Mod. Phys. **80**, 1215 (2008).

[Levinsen and Gurarie(2006)] J. Levinsen and V. Gurarie, Phys. Rev. A **73**, 053607 (2006).

[Bulgac and Yoon(2009)] A. Bulgac and S. Yoon, Phys. Rev. Lett. **102**, 085302 (2009).

[Timmermans et al.(1999)] E. Timmermans, P. Tommasini, M. Hussein, and A. Kerman, Physics Reports **315**, 199 (1999).

[Gurarie and Radzihovsky(2007)] V. Gurarie and L. Radzihovsky, Ann. Phys. **322**, 2 (2007).

From Solitons and Rabi Oscillations in a Time-Dependent BCS Pairing Problem by Barankov, Levitov, Spivak

References

[1] B. DeMarco, *et al.*, Phys. Rev. Lett. **82**, 4208 (1999); Science **285**, 1703 (1999); Phys. Rev. Lett. **86**, 5409 (2001); Phys. Rev. Lett. **88**, 040405 (2002); A. G. Truscott *et al.*, Science **291**, 2570 (2001); T. Loftus *et al.*, Phys. Rev. Lett. **88**, 173201 (2002); K. M. O'Hara, *et al.*, Science **298**, 2179 (2002); Phys. Rev. A **66**, 041401 (2002)

[2] H. T. C. Stoof, M. Houbiers, C. A. Sackett, and R. G. Hulet, Phys. Rev. Lett. **76**, 10 (1996)

[3] Tin-Lun Ho and S. Yip, Phys. Rev. Lett. **82**, 247 (1999)

[4] J. L. Bohn, Phys. Rev. A**61**, 053409 (2000)

[5] M. Holland, S. J. J. M. F. Kokkelmans, M. L. Chiofalo, and R. Walser, Phys. Rev. Lett. **87**, 120406 (2001)

[6] S. J. J. M. F. Kokkelmans, J. N. Milstein, M. L. Chiofalo, R. Walser, and M. J. Holland, Phys. Rev. A**65**, 053617 (2002)

[7] J. N. Milstein, S. J. J. M. F. Kokkelmans, and M. J. Holland, Phys. Rev. A**66**, 043604 (2002)

[8] Y. Ohashi, and A. Griffin, Phys. Rev. Lett. **89**, 130402 (2002); Phys. Rev. A**67**, 033603 (2003); Phys. Rev. A**67**, 063612 (2003)

[9] J. Stajic, J. N. Milstein, Q. Chen, M. L. Chiofalo, M. J. Holland, and K. Levin, cond-mat/0309329

[10] H. Heiselberg, C. J. Pethick, H. Smith, and L. Viverit, Phys. Rev. Lett. **85**, 2418 (2000)

[11] M. A. Baranov, M. S. Marenko, V. S. Rychkov, and G. V. Shlyapnikov, Phys. Rev. A **66**, 013606 (2002)

[12] H. Heiselberg and B. Mottelson, Phys. Rev. Lett. **88**, 190401 (2002)

[13] C. P. Search, H. Pu, W. Zhang, B. P. Anderson, and P. Meystre, Phys. Rev. A **65**, 063616 (2002)

[14] J. Carlson, S.-Y. Chang, V. R. Pandharipande, and K. E. Schmidt, Phys. Rev. Lett. **91**, 050401 (2003)

[15] H. Heiselberg, Phys. Rev. A **68**, 053616 (2003)

[16] M. Houbiers and H. T. C. Stoof, Phys. Rev. A**59**, 1556 (1999)

[17] M. Tinkham, *Introduction to Superconductivity*, (McGraw-Hill, 1996)

[18] A. Schmid, Phys. Kond. Mat. **5**, 302 (1966)

[19] E. Abrahams and T. Tsuneto, Phys. Rev. **152**, 416 (1966)

[20] L. P. Gor'kov, G. M. Eliashberg, Zh. Eksp. Teor. Fiz. **54**, 612 (1968) [Sov. Phys. JETP **27**, 328 (1968)]

[21] A. G. Aronov and V. L. Gurevich, Sov. Phys. Solid State, **16**, 1722, (1974); Sov. Phys. JETP, **38**, 550, (1974);

[22] A. I. Larkin, Yu. N. Ovchinnikov, Sov. Phys. JETP, **46**, 155, (1977)

[23] P. W. Anderson, Phys. Rev. **112**, 1900 (1958)

[24] A. F. Volkov and Sh. M. Kogan, Sov. Phys. JETP, **38**, 1018 (1974);

[25] Yu. M. Gal'perin, V. I. Kozub, and B. Z. Spivak, Sov. Phys. JETP, **54**, 1126 (1981)

[26] S. L. McCall and E. L. Hahn, Phys. Rev. Lett. **18**, 908 (1967); Phys. Rev. **183**, 457 (1968)

From Collisionless relaxation of the energy gap in superconductors by Volkov, Kogan, 1973

[1)] We note that the term $(2\pi)^4(\omega)\delta(\mathbf{k})$ in Eq. (13) of Éliashberg's paper [[5]] should be discarded.

[T] E. Abrahams and T. Tsuneto, Phys. Rev., 152, 416 (1966).

[2] L. P. Gor'kov and G. M. Éliashberg, Zh. Eksp. Teor. Fiz. 54, 612 (1968) [Sov. Phys.-JETP 27, 328 (1968)].

[3] G. M. Éliashberg, ibid. 55, 2443 (1968) [28, 1298 (1969)].

[4] B. I. Ivlev, ZhETF Pis. Red. 15, 441 (1972) [JETP Lett. 15, 313 (1972)].

[5] G. M. Eliashberg, Zh. Eksp. Teor. Fiz. 61, 1254 (1971) [Sov. Phys.-JETP 34, 668 (1972)]. .

[6] L. V. Keldysh, Zh. Eksp. Teor. Fiz. 47, 1515 (1964) [Sov. Phys.-JETP 20, 1018 (1965)].
[7] J. R. Schrieffer, Theory of Superconductivity, Benjamin, 1964.
[8] A. A. Abrikosov, L. P. Gor'kov, and I. E. Dzyaloshinskiĭ, Metody kvantovoĭ teorii polya v statisticheskoĭ fizike (Quantum Field-Theoretical Methods in Statistical Physics), Fizmatgiz, 1962 [Pergamon, 1965)]. [9] L. D. Landau, Zh. Eksp. Teor. Fiz. 16, 574 (1946).

From Higgs mode in a strongly interacting fermionic superfluid by Behrle, Harrison et al.

References

[1] Higgs, P. W. Broken symmetries and the masses of gauge bosons. *Phys. Rev. Lett.* **13**, 508–509 (1964). URL https://link.aps.org/doi/10.1103/PhysRevLett.13.508.

[2] Littlewood, P. B. & Varma, C. M. Gauge-invariant theory of the dynamical interaction of charge density waves and superconductivity. *Phys. Rev. Lett.* **47**, 811–814 (1981). URL http://link.aps.org/doi/10.1103/PhysRevLett.47.811.

[3] Sooryakumar, R. & Klein, M. V. Raman scattering by superconducting-gap excitations and their coupling to charge-density waves. *Phys. Rev. Lett.* **45**, 660–662 (1980). URL http://link.aps.org/doi/10.1103/PhysRevLett.45.660.

[4] Matsunaga, R. *et al.* Higgs amplitude mode in the BCS superconductors $Nb_{1-x}Ti_xN$ induced by terahertz pulse excitation. *Phys. Rev. Lett.* **111**, 057002 (2013). URL http://link.aps.org/doi/10.1103/PhysRevLett.111.057002.

[5] Sherman, D. *et al.* The Higgs mode in disordered superconductors close to a quantum phase transition. *Nature Physics* **11**, 188–192 (2015).

[6] Pekker, D. & Varma, C. Amplitude/Higgs modes in condensed matter physics. *Annual Review of Condensed Matter Physics* **6**, 269–297 (2015).

[7] Podolsky, D., Auerbach, A. & Arovas, D. P. Visibility of the amplitude (Higgs) mode in condensed matter. *Phys. Rev. B* **84**, 174522 (2011). URL http://link.aps.org/doi/10.1103/PhysRevB.84.174522.

[8] Scott, R. G., Dalfovo, F., Pitaevskii, L. P. & Stringari, S. Rapid ramps across the BEC-BCS crossover: A route to measuring the superfluid gap. *Phys. Rev. A* **86**, 053604 (2012). URL http://link.aps.org/doi/10.1103/PhysRevA.86.053604.

[9] Barlas, Y. & Varma, C. M. Amplitude or Higgs modes in *d*-wave superconductors. *Phys. Rev. B* **87**, 054503 (2013). URL https://link.aps.org/doi/10.1103/PhysRevB.87.054503.

[10] Liu, B., Zhai, H. & Zhang, S. Evolution of the Higgs mode in a fermion superfluid with tunable interactions. *Phys. Rev. A* **93**, 033641 (2016). URL http://link.aps.org/doi/10.1103/PhysRevA.93.033641.

[11] Han, X., Liu, B. & Hu, J. Observability of Higgs mode in a system without Lorentz invariance. *Phys. Rev. A* **94**, 033608 (2016). URL http://link.aps.org/doi/10.1103/PhysRevA.94.033608.

[12] Littlewood, P. B. & Varma, C. M. Amplitude collective modes in superconductors and their coupling to charge-density waves. *Phys. Rev. B* **26**, 4883–4893 (1982). URL http://link.aps.org/doi/10.1103/PhysRevB.26.4883.

[13] Rüegg, C. *et al.* Quantum magnets under pressure: Controlling elementary excitations in $TlCuCl_3$. *Phys. Rev. Lett.* **100**, 205701 (2008). URL https://link.aps.org/doi/10.1103/PhysRevLett.100.205701.

[14] Halperin, W. & Varoquax, E. Order-parameter collective modes in superfluid 3He. In Halperin, W. & Pitaevskii, L. (eds.) *Helium Three*, 353–522 (Elsevier Science Publishers, 1990).

[15] Bissbort, U. *et al.* Detecting the amplitude mode of strongly interacting lattice bosons by Bragg scattering. *Phys. Rev. Lett.* **106**, 205303 (2011). URL http://link.aps.org/doi/10.1103/PhysRevLett.106.205303.

[16] Endres, M. *et al.* The 'Higgs' amplitude mode at the two-dimensional superfluid/Mott insulator transition. *Nature* **487**, 454–458 (2012).

[17] Hoang, T. M. *et al.* Adiabatic quenches and characterization of amplitude excitations in a continuous quantum phase transition. *Proceedings of the National Academy of Sciences* **113**, 9475–9479 (2016). URL http://www.pnas.org/content/113/34/9475.abstract. http://www.pnas.org/content/113/34/9475.full.pdf.

[18] Leonard, J., Morales, A., Zupancic, P., Donner, T. & Esslinger, T. Monitoring and manipulating Higgs and Goldstone modes in a supersolid quantum gas. *Science* **358**, 1415–1418 (2017).

[19] Yuzbashyan, E. A. & Dzero, M. Dynamical vanishing of the order parameter in a fermionic condensate. *Phys. Rev. Lett.* **96**, 230404 (2006). URL http://link.aps.org/doi/10.1103/PhysRevLett.96.230404.

[20] Hannibal, S. *et al.* Quench dynamics of an ultracold Fermi gas in the BCS regime: Spectral properties and confinement-induced breakdown of the Higgs mode. *Phys. Rev. A* **91**, 043630 (2015). URL http://link.aps.org/doi/10.1103/PhysRevA.91.043630.

[21] Greiner, M., Regal, C. A. & Jin, D. S. Probing the excitation spectrum of a Fermi gas in the BCS-BEC crossover regime. *Phys. Rev. Lett.* **94**, 070403 (2005). URL https://link.aps.org/doi/10.1103/PhysRevLett.94.070403.

[22] Chin, C. *et al.* Observation of the pairing gap in a strongly interacting Fermi gas. *Science* **305**, 1128–1130 (2004).

[23] Ketterle, W. & Zwierlein, M. W. Making, probing and understanding ultracold Fermi gases. *Proceedings of the International School of Physics "Enrico Fermi"* **164**, 95–287 (2007).

[24] Stewart, J. T., Gaebler, J. P. & Jin, D. S. Using photoemission spectroscopy to probe a strongly interacting Fermi gas. *Nature* **454**, 744–747 (2008).

[25] Feld, M., Fröhlich, B., Vogt, E., Koschorreck, M. & Köhl, M. Observation of a pairing pseudogap in a two-dimensional Fermi gas. *Nature* **480**, 75–78 (2011).

[26] Bruun, G. M. Low-energy monopole modes of a trapped atomic Fermi gas. *Phys. Rev. Lett.* **89**, 263002 (2002). URL https://link.aps.org/doi/10.1103/PhysRevLett.89.263002.

[27] Korolyuk, A., Kinnunen, J. J. & Törmä, P. Density response of a trapped fermi gas: A crossover from the pair vibration mode to the goldstone mode. *Phys. Rev. A* **84**, 033623 (2011). URL https://link.aps.org/doi/10.1103/PhysRevA.84.033623.

[28] Korolyuk, A., Kinnunen, J. J. & Törmä, P. Collective excitations of a trapped fermi gas at finite temperature. *Phys. Rev. A* **89**, 013602 (2014). URL https://link.aps.org/doi/10.1103/PhysRevA.89.013602.

[29] Tokimoto, J., Tsuchiya, S. & Nikuni, T. Higgs mode in a trapped superfluid Fermi gas. *Journal of Low Temperature Physics* 1–6 (2017). URL http://dx.doi.org/10.1007/s10909-017-1766-2.

[30] Ries, M. G. *et al.* Observation of pair condensation in the quasi-2D BEC-BCS crossover. *Phys. Rev. Lett.* **114**, 230401 (2015). URL https://link.aps.org/doi/10.1103/PhysRevLett.114.230401.

[31] Schirotzek, A., Shin, Y.-i., Schunck, C. H. & Ketterle, W. Determination of the superfluid gap in atomic Fermi gases by quasiparticle spectroscopy. *Phys. Rev. Lett.* **101**, 140403 (2008). URL https://link.aps.org/doi/10.1103/PhysRevLett.101.140403.

[32] Hoinka, S. *et al.* Goldstone mode and pair-breaking excitations in atomic Fermi superfluids. *Nature Physics* **13**, 943—-946 (2017).

[33] Chang, S. Y., Pandharipande, V. R., Carlson, J. & Schmidt, K. E. Quantum Monte Carlo studies of superfluid Fermi gases. *Phys. Rev. A* **70**, 043602 (2004). URL https://link.aps.org/doi/10.1103/PhysRevA.70.043602.

[34] Gezerlis, A. & Carlson, J. Strongly paired fermions: Cold atoms and neutron matter. *Phys. Rev. C* **77**, 032801 (2008). URL https://link.aps.org/doi/10.1103/PhysRevC.77.032801.

[35] Bulgac, A., Drut, J. E. & Magierski, P. Quantum Monte Carlo simulations of the BCS-BEC crossover at finite temperature. *Phys. Rev. A* **78**, 023625 (2008). URL https://link.aps.org/doi/10.1103/PhysRevA.78.023625.

[36] Chen, Q. Effect of the particle-hole channel on BCS-–Bose–Einstein condensation crossover in atomic Fermi gases. *Scientific Reports* **6**, 25772 (2016).

[37] Haussmann, R., Rantner, W., Cerrito, S. & Zwerger, W. Thermodynamics of the BCS-BEC crossover. *Phys. Rev. A* **75**, 023610 (2007). URL https://link.aps.org/doi/10.1103/PhysRevA.75.023610.

[38] Pieri, P., Pisani, L. & Strinati, G. C. BCS-BEC crossover at finite temperature in the broken-symmetry phase. *Phys. Rev. B* **70**, 094508 (2004). URL https://link.aps.org/doi/10.1103/PhysRevB.70.094508.

[39] Ohashi, Y. & Griffin, A. Superfluidity and collective modes in a uniform gas of Fermi atoms with a Feshbach resonance. *Phys. Rev. A* **67**, 063612 (2003). URL https://link.aps.org/doi/10.1103/PhysRevA.67.063612.